USGS
science for a changing world

Field-Trip Guide to Continental Arc to Rift Volcanism of the Southern Rocky Mountains—Southern Rocky Mountain, Taos Plateau, and Jemez Mountains Volcanic Fields of Southern Colorado and Northern New Mexico

Scientific Investigations Report 2017–5022–R

U.S. Department of the Interior
U.S. Geological Survey

COVER

(top) Crest of the Bonanza resurgent dome. View is to the east from the west caldera rim, across Whale Hill toward the San Luis Valley segment of the Rio Grande rift zone. Photograph by P.W. Lipman, U.S. Geological Survey, 2014.

(bottom) View northeast from the summit of Cerro Chiflo. Photograph by K.J. Turner, U.S. Geological Survey.

Field-Trip Guide to Continental Arc to Rift Volcanism of the Southern Rocky Mountains—Southern Rocky Mountain, Taos Plateau, and Jemez Mountains Volcanic Fields of Southern Colorado and Northern New Mexico

By Ren A. Thompson, Kenzie J. Turner, Peter W. Lipman, John A. Wolff, and Michael A. Dungan

With sections on

A New Look at the Dacite Pumice Component in the Tshirege Member of the Bandelier Tuff

By Joseph R. Boro, John A. Wolff, and Owen K. Neill

The Evolution of Thought on the Embudo Fault—Putting Legendary Exposures in Hondo Canyon into a More Regional Context and a New Paradigm, Southern Taos Plateau, New Mexico

By V.J.S. Grauch, Keith I. Kelson, Paul W. Bauer, and Benjamin J. Drenth

Sanidine From the Fish Canyon Tuff and Its Use as a $^{40}Ar/^{39}Ar$ Geochronology Standard

By L.E. Morgan and M.A. Cosca

Scientific Investigations Report 2017–5022–R

U.S. Department of the Interior
U.S. Geological Survey

U.S. Geological Survey, Reston, Virginia: 2022

For more information on the USGS—the Federal source for science about the Earth, its natural and living resources, natural hazards, and the environment—visit https://www.usgs.gov or call 1–888–ASK–USGS.

For an overview of USGS information products, including maps, imagery, and publications, visit https://store.usgs.gov.

Suggested citation:
Thompson, R.A., Turner, K.J., Lipman, P.W., Wolff, J.A., and Dungan, M.A., 2022, Field-trip guide to continental arc to rift volcanism of the southern Rocky Mountains—Southern Rocky Mountain, Taos Plateau, and Jemez Mountains volcanic fields of southern Colorado and northern New Mexico: U.S. Geological Survey Scientific Investigations Report 2017-5022-R, 346 p., https://doi.org/10.3133/sir20175022r.

Associated data for this publication:
Turner, K.J., Thompson, R.A., and Cosca, M.A., 2022, Data release for geochronology and geochemistry of volcanic rocks in the Southern Rocky Mountains and Taos Plateau volcanic fields and other Oligocene to Pleistocene volcanic rocks within the southern San Luis Basin and San Juan Mountains, southern Colorado and northern New Mexico: U.S. Geological Survey data release, https://doi.org/10.5066/P9BKL3ZE.

ISSN 2328-0328 (online)

Preface

The North American Cordillera is home to a greater diversity of volcanic provinces than any comparably sized region in the world. The interplay between changing plate-margin interactions, tectonic complexity, intra-crustal magma differentiation, and mantle melting have resulted in a wealth of volcanic landscapes. Field trips in this series visit many of these landscapes, including (1) active subduction-related arc volcanoes in the Cascade Range; (2) flood basalts of the Columbia Plateau; (3) bimodal volcanism of the Snake River Plain-Yellowstone volcanic system; (4) some of the world's largest known ignimbrites from southern Utah, central Colorado, and northern Nevada; (5) extension-related volcanism in the Rio Grande Rift and Basin and Range Province; and (6) the spectacular eastern Sierra Nevada featuring Long Valley Caldera and the iconic Bishop Tuff. Some of the field trips focus on volcanic eruptive and emplacement processes, calling attention to the fact that the western United States provides opportunities to examine a wide range of volcanological phenomena at many scales.

The 2017 Scientific Assembly of the International Association of Volcanology and Chemistry of the Earth's Interior (IAVCEI) in Portland, Oregon, marks the first time that the U.S. volcanological community has hosted this quadrennial meeting since 1989, when it was held in Santa Fe, New Mexico. The 1989 field-trip guides are still widely used by students and professionals alike. This new set of field guides is similarly a legacy collection that summarizes decades of advances in our understanding of magmatic and tectonic processes of volcanic western North America.

The field of volcanology has flourished since the 1989 IAVCEI meeting, and it has profited from detailed field investigations coupled with emerging new analytical methods. Mapping has been enhanced by plentiful major- and trace-element whole-rock and mineral data, technical advances in radiometric dating and collection of isotopic data, GPS (Global Positioning System) advances, and the availability of lidar (light detection and ranging) imagery. Spectacularly effective microbeam instruments, geodetic and geophysical data collection and processing, paleomagnetic determinations, and modeling capabilities have combined with mapping to provide new information and insights over the past 30 years. The collective works of the international community have made it possible to prepare wholly new guides to areas across the western United States. These comprehensive field guides are available, in large part, because of enormous contributions from many experienced geologists who have devoted entire careers to their field areas. Early career scientists are carrying forward and refining their foundational work with impressive results.

Our hope is that future generations of scientists as well as the general public will use these field guides as introductions to these fascinating areas and will be enticed toward further exploration and field-based research.

Michael Dungan, University of Oregon
Judy Fierstein, U.S. Geological Survey
Cynthia Gardner, U.S. Geological Survey
Dennis Geist, National Science Foundation
Anita Grunder, Oregon State University
John Wolff, Washington State University

Field-trip committee, IAVCEI 2017

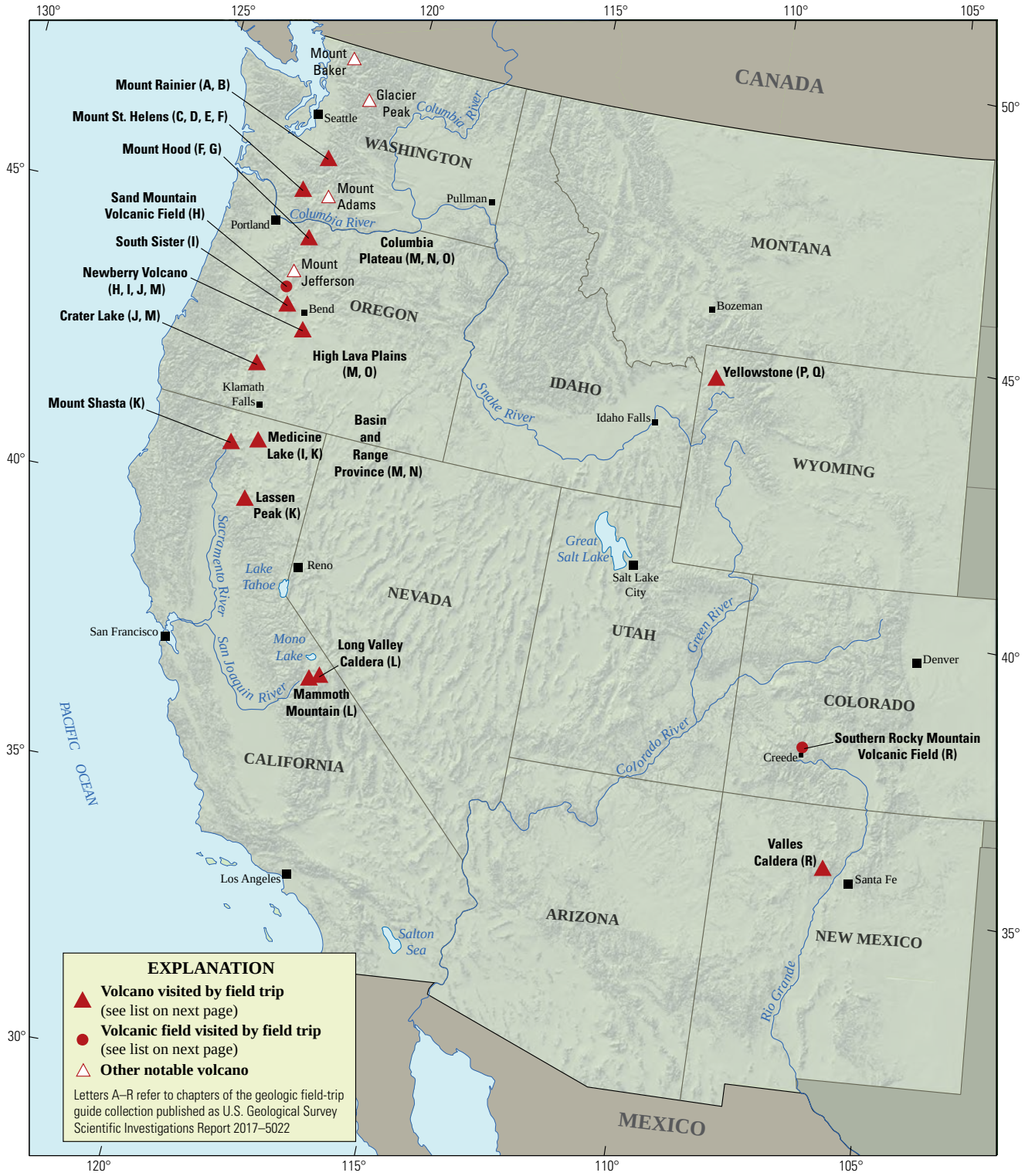

Shaded-relief base from U.S. Geological Survey National Elevation Dataset 30-meter digital elevation model data.

Map of the western United States showing volcanoes and volcanic fields visited by geologic field trips scheduled in conjunction with the 2017 meeting of the International Association of Volcanology and Chemistry of the Earth's Interior (IAVCEI) in Portland, Oregon, and available as chapters in U.S. Geological Survey Scientific Investigations Report 2017–5022.

Contributing Authors

Boise State University
Brittany D. Brand
Nicholas Pollock

Colgate University
Karen Harpp
Alison Koleszar

Durham University
Richard J. Brown

Eastern Oregon University
Mark L. Ferns

ETH Zurich
Olivier Bachmann

Georgia Institute of Technology
Josef Dufek

GNS Science, New Zealand
Natalia I. Deligne

Hamilton College
Richard M. Conrey

Massachusetts Institute of Technology
Timothy Grove

National Science Foundation
Dennis Geist (also with Colgate University and University of Idaho)

New Mexico Bureau of Geology and Mineral Resources
Paul W. Bauer
William C. McIntosh
Matthew J. Zimmerer

New Mexico State University
Emily R. Johnson

Northeastern University
Martin E. Ross

Oregon Department of Geology and Mineral Industries
William J. Burns
Lina Ma
Ian P. Madin
Jason D. McClaughry

Oregon State University
Adam J.R. Kent

Portland State University
Jonathan H. Fink (also with University of British Columbia)
Martin J. Streck
Ashley R. Streig

San Diego State University
Victor E. Camp

Smithsonian Institution
Lee Siebert

Universidad Nacional Autónoma de San Luis Potosi
Damiano Sarocchi

University of California, Davis
Kari M. Cooper

University of Liverpool
Peter B. Kokelaar

University of Northern Colorado
Steven W. Anderson

University of Oregon
Ilya N. Binderman
Michael A. Dungan
Daniele McKay (also with Oregon State University and Oregon State University, Cascades)

University of Portland
Kristin Sweeney

University of Tasmania
Martin Jutzeler
Jocelyn McPhie

University of Utah
Jamie Farrell

U.S. Army Corps of Engineers
Keith I. Kelson

U.S. Forest Service
Gordon E. Grant (also with Oregon State University
Robert A. Jensen

U.S. Geological Survey
Charles R. Bacon
Andrew T. Calvert
Christine F. Chan
Robert L. Christiansen
Michael A. Clynne
Michael A. Cosca
Julie M. Donnelly-Nolan
Benjamin J. Drenth
William C. Evans
Judy Fierstein
Cynthia A. Gardner
V.J.S. Grauch
Christopher J. Harpel
Wes Hildreth
Richard P. Hoblitt
Peter W. Lipman
Jacob B. Lowenstern
Jon J. Major
Seth C. Moran
Lisa A. Morgan
Leah E. Morgan
L.J. Patrick Muffler
James E. O'Connor
John S. Pallister
Thomas C. Pierson
Joel E. Robinson
Juliet Ryan-Davis
Kevin M. Scott
William E. Scott
Wayne (Pat) Shanks
David R. Sherrod
Thomas W. Sisson
Mark Evan Stelten
Weston Thelen
Ren A. Thompson
Kenzie J. Turner
James W. Vallance
Alexa R. Van Eaton
Jorge A. Vazquez
Richard B. Waitt
Heather M. Wright

U.S. Nuclear Regulatory Commission
Stephen Self (also with University of California, Berkeley)

Washington State University
Joseph R. Boro
Owen K. Neill
Stephen P. Reidel
John A. Wolff

Acknowledgments
Juliet Ryan-Davis and Kate Sullivan created the overview map, and Vivian Nguyen created the cover design for this collection of field-trip guide books. The field trip committee is grateful for their contributions.

Contents

Sections

Figures

Tables

Conversion Factors

Inch/Pound to SI

Multiply	By	To obtain
	Length	
inch (in.)	2.54	centimeter (cm)
inch (in.)	25.4	millimeter (mm)
foot (ft)	0.3048	meter (m)
mile (mi)	1.609	kilometer (km)
mile, nautical (nmi)	1.852	kilometer (km)
yard (yd)	0.9144	meter (m)
	Area	
square mile (mi^2)	2.590	square kilometer (km^2)
	Volume	
cubic foot (ft^3)	0.02832	cubic meter (m^3)
cubic yard (yd^3)	0.7646	cubic meter (m^3)
cubic mile (mi^3)	4.168	cubic kilometer (km^3)
acre-foot (acre-ft)	1,233	cubic meter (m^3)

Datum

Vertical coordinate information is referenced to the insert datum name (and abbreviation) here for instance, “North American Vertical Datum of 1988 (NAVD 88).”

Horizontal coordinate information is referenced to the insert datum name (and abbreviation) here for instance, “North American Datum of 1983 (NAD 83).”

Altitude, as used in this report, refers to distance above the vertical datum.

Acronyms and Abbreviations

CSDP	Continental Scientific Drilling Program
Ga	billion years ago
JMVF	Jemez Mountains volcanic field
Ma	million years ago
SRMVF	southern Rocky Mountain volcanic field
TPVF	Taos Plateau volcanic field

Field-Trip Guide to Continental Arc to Rift Volcanism of the Southern Rocky Mountains—Southern Rocky Mountain, Taos Plateau, and Jemez Mountains Volcanic Fields of Southern Colorado and Northern New Mexico

By Ren A. Thompson,[1] Kenzie J. Turner,[1] Peter W. Lipman,[1] John A. Wolff,[2] and Michael A. Dungan[3]

Introduction

The southern Rocky Mountains of northern New Mexico and southern Colorado preserve the Oligocene to Pleistocene record of North American continental arc to rift volcanism. The 35–23 million year old (Ma) southern Rocky Mountain volcanic field (SRMVF), spectacularly preserved in the San Juan Mountains of southern Colorado, records the evolution of large andesitic stratovolcanoes to complex caldera clusters, from which at least 22 major ignimbrite sheets (each 150–5,000 cubic kilometers) were erupted. Outflow deposits of the SRMVF preserved along the broadly uplifted northwest flank of the northern Rio Grande rift basin (the San Luis Valley) provide critical structural and temporal constraints on the inception of crustal extension. Coincident with waning stages of SRMVF caldera-forming volcanism (~25.4 Ma), extensional tectonism was accompanied by a transition from bimodal early Miocene to intermediate-composition late Miocene and dominantly basaltic Pliocene rift volcanism of the Taos Plateau in the southern San Luis Basin. Concomitant rift volcanism in the Española Basin and bordering Jemez Mountains of northern New Mexico records a similar Miocene eruptive history dominated by intermediate-composition volcanism that transitioned locally to Pliocene rift-related basaltic volcanism of the Cerros del Rio volcanic field and culminated in eruptions of the iconic rhyolitic Pleistocene Bandelier Tuff and formation of the Valles Caldera along the northwestern rift-basin margin.

This 6-day, 7-night field trip will focus, in broadly equal proportions, on rift-related extensional volcanism of the Jemez Mountains and Taos Plateau regions during the first half of the trip, and on caldera-forming volcanism of the southern Rocky Mountain volcanic field during the second half of the trip. The 35-million-year volcanic history of the region highlighted by new geologic mapping, high-resolution geochronology, petrologic, geochemical, and geophysical data facilitates discussion of (1) the magmatic response to the tectonic transition from subducted-slab arc to continental-rift volcanism; (2) the nature and temporal evolution of rift magmas; (3) fault controls on the spatial evolution of rift magmatism; (4) the diversity of continental-arc ignimbrite volcanism and associated lavas; (5) ignimbrite caldera structure and associated intrusions in three-dimension; (6) the role of recycled crystal mush and magmatic cumulates during growth of Cordilleran batholiths; and (7) high-precision geochronologic contributions to interpretation of relations between regional tectonic and volcanic processes. Most stops will be along roads, but there will be moderate hikes on trails of less than 1-hour duration covering 1–2 kilometers (0.6–1.2 miles) with modest elevation gain of <150 meters (<492 feet).

The route will progress in reverse stratigraphic order, starting in the Jemez Mountains of New Mexico and proceed northward to San Luis Basin and San Luis Hills before turning west to the southeast and central San Juan Mountains. Our last full day takes us to the little-visited and only recently mapped, Bonanza caldera of the northeastern San Juan Mountains and on the final day, we leave the San Luis Valley to briefly explore the Tertiary subvolcanic plutons of the Collegiate Range along the west side of the Arkansas Valley rift valley, en route to Denver.

The authors of all daily contributions acknowledge the helpful reviews by Amy Gilmer and Joe Colgan and thank Christine Chan and Jeremy Havens for assistance with figures, tables, and guidebook text.

[1]U.S. Geological Survey.

[2]Washington State University.

[3]University of Oregon.

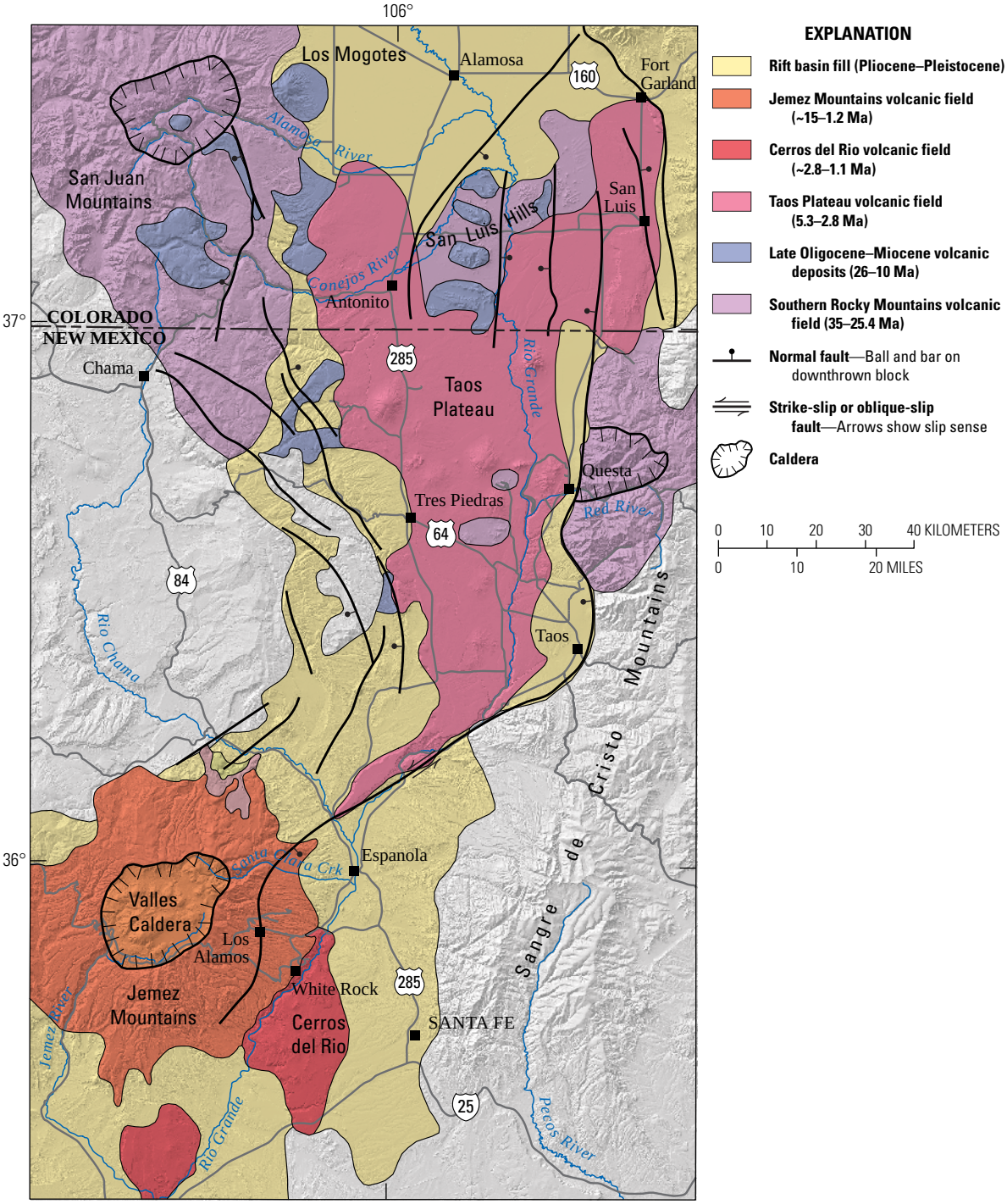

Shaded-relief base generated from U.S. Geological Survey 10-m Digital Elevation Model (DEM) data from the National Elevation Dataset, accessed November 2016 at http://ned.usgs.gov/. Horizontal: UTM projection, NAD 83 Datum, zone 13, Vertical Datum: NAVD 1988

Geology by K.J. Turner and R.A. Thompson, 2015

Figure 1. Regional shaded-relief map showing distribution of Cenozoic volcanic deposits discussed in the field guide. Preserved deposits record the transition from Oligocene subducted arc volcanism to Miocene to Pliocene extensional volcanism of the northern Rio Grande rift, and range in age from approximately 35 to 1 million years old.

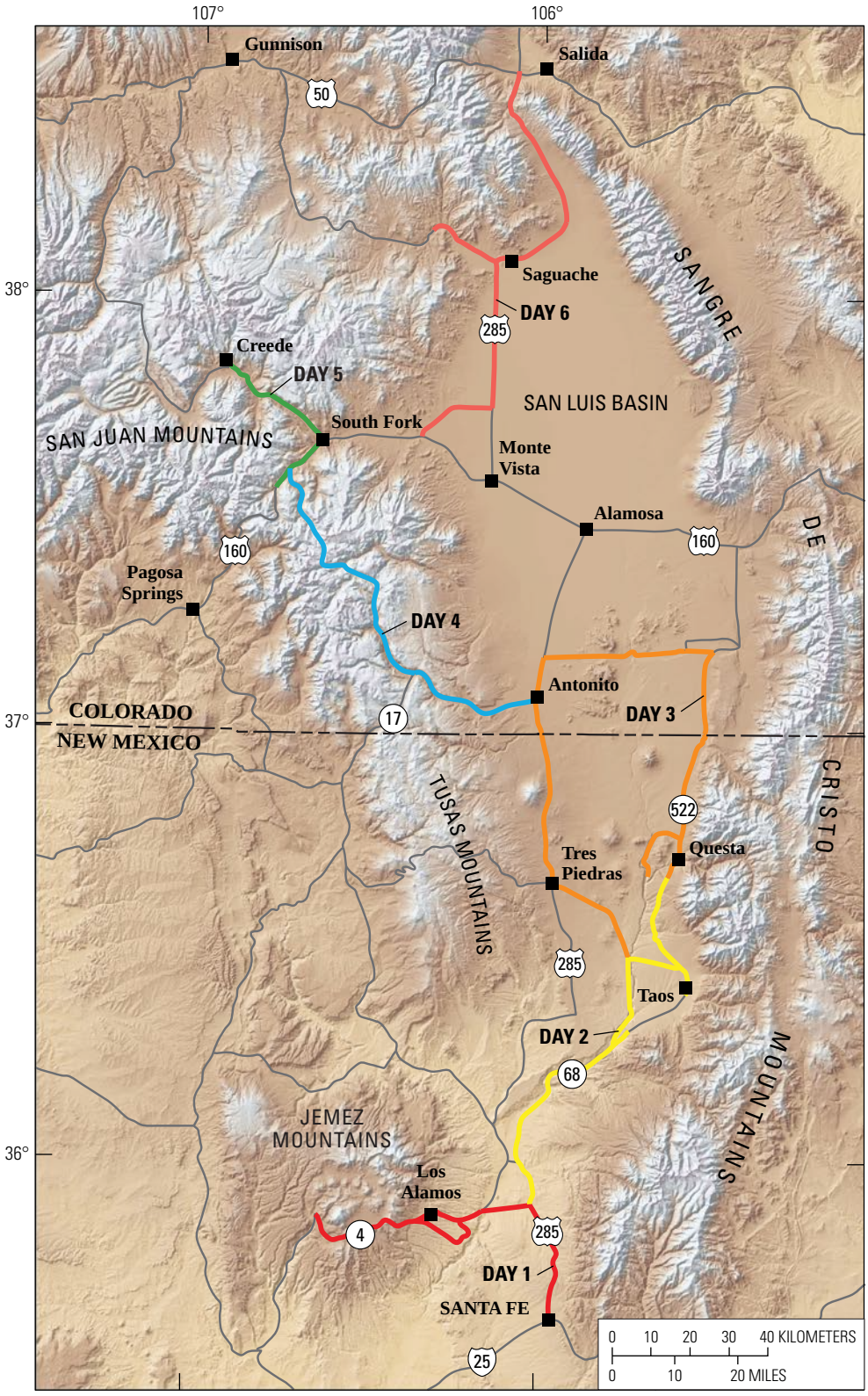

Shaded-relief base generated from U.S. Geological Survey 10-m Digital Elevation Model (DEM) data from the National Elevation Dataset, accessed November 2016 at http://ned.usgs.gov/. Horizontal: UTM projection, NAD 83 Datum, zone 13, Vertical Datum: NAVD 1988

Geology by K.J. Turner and R.A. Thompson, 2015

Figure 2. Physiographic map showing daily road log routes presented in the field guide. Only primary routes are indicated, optional routes presented in road logs are not shown.

Day 1—The Jemez Mountains Volcanic Field and Valles Caldera

By John A. Wolff[1] and Ren A. Thompson[2]

Introduction

The Jemez Mountains of New Mexico are a classic area to examine the interplay between extensional tectonism and volcanism in North America. Scientific investigations in the region began in the 19th century with early exploratory surveys, including John Wesley Powell's expeditions to the Colorado Plateau region (1869–1872) and J.P. Iddings' (1890) petrological study of the rocks collected by Powell. In his brief but colorful description of the so-called Tewan Plateau, Powell (1895) drew parallels between the volcanic rocks and landforms he had seen in New Mexico and the then recent events that produced similar rocks and landforms at Krakatau, Indonesia. Starting before World War II and extending into the 1970s, detailed mapping of the Valles Caldera and Bandelier Tuff by U.S. Geological Survey (USGS) scientists C.S. Ross, R.L. Smith, and R.A. Bailey spawned classic papers that, for several decades, provided a basic manual for the investigation and interpretation of ash-flow tuffs and their source calderas (Smith, 1960a,b; Ross and Smith, 1961; Smith and Bailey, 1968). In addition, these workers provided the first comprehensive scheme for the stratigraphy and development of the Jemez Mountains volcanic field (Bailey and others, 1969), and a 1:125,000 scale geological map (Smith and others, 1970). Subsequently, Goff and others (2011) published a new geologic map of the caldera based on revised geologic mapping, stratigraphic nomenclature and geochronology.

Since 1980, in addition to continuing work by the USGS, most investigations of the Valles Caldera and Jemez Mountains volcanic field (JMVF) have been conducted by scientists from the New Mexico Bureau of Geology and Mineral Resources, Los Alamos National Laboratory, and researchers at numerous American universities. The JMVF is now one of the most intensely studied volcanic fields in North America (for example, see the volumes edited by Heiken, 1986; Goff and Gardner, 1988; Goff and others, 1996; and Kues and others, 2007). This brief introduction to the geology, petrology, and geochemistry of the volcanic field and accompanying one-day road log, with a principal focus on the Valles Caldera and Bandelier Tuff, summarizes current knowledge and relies heavily on the following publications: Smith and others (1970), Gardner and others (1986, 2010), Self and others (1986, 1996), Goff and others (1989, 1990, 2011), Wolff and others (2005), Rowe and others (2007), and Kelley and others (2013). We use the revised stratigraphic nomenclature of Gardner and others (2010) and Kelley and others (2013).

Despite intense study, some questions remain unanswered. The problem of quartz-bearing basalts, raised by Iddings (1890) in the very first paper devoted to JMVF petrology, was still under investigation 100 years later (Duncker and others, 1991). Mechanisms of caldera collapse and eruption of ash-flow tuffs (ignimbrites) continue to be studied in the Valles Caldera (for example, Goff and others, 2014) and by volcanologists in other places all over the world, more than 50 years after the classic studies by Smith and coworkers. The JMVF and Valles Caldera endure as a superb natural laboratory for the study of continental volcanism.

Regional Setting and Pre-JMVF Geologic History

The JMVF sits on the western shoulder of the Española Basin, one of the north-south trending series of Cenozoic en echelon sedimentary basins that make up the Rio Grande Rift (fig. 3*A*). The rift here is intersected by the Jemez lineament, an alignment of late Cenozoic volcanic fields and fault zones which corresponds to the surface boundary of a south-dipping suture between the Proterozoic Yavapai (1.8–1.7 billion years old [Ga]) and Mazatzal (1.65 Ga) lithospheric provinces (Shaw and Karlstrom, 1999; Karlstrom and others, 2002; Magnani and others, 2004). The volcanic field is built on a substrate of Phanerozoic sedimentary rocks that rest on the Proterozoic basement, which consists of granitoids and metavolcanic amphibolites locally dated at 1.62–1.44 Ga (Eichelberger and Koch, 1979; Brookins and Laughlin, 1983; Laughlin and others, 1983). Upper Paleozoic strata, well exposed in the western Jemez Mountains, are associated with basin development during the ancestral Rocky Mountains orogeny (Pazzaglia and others, 1999). They are overlain by a veneer of Cenozoic sedimentary units, the uppermost of which is the rift-filling Santa Fe Group (Spiegel and Baldwin, 1963; Galusha and Blick, 1971). The Española Basin is a half-graben hinged on the east side, and the thickness of the Santa Fe Group sediments increases westward to a maximum of 2 kilometers (km) beneath the JMVF (Smith, 2004).

Proterozoic rocks exposed in uplifts around the borders of the Española and adjacent basins include a variety of metavolcanic, metasedimentary, and granitoid rocks. Those

[1]Washington State University.

[2]U.S. Geological Survey.

found in the immediate vicinity of the JMVF, and penetrated by geothermal wells and scientific drilling within the Valles Caldera are exclusively granitoid (Smith and others, 1970; Nielsen and Hulen, 1984, Hulen and Gardner, 1989), although metavolcanic rocks were penetrated by a well at Fenton Hill (Stop 1-10, fig. 3), and both amphibolite and granitoid are found as lithic fragments in the Bandelier Tuff (Eichelberger and Koch, 1979). The rocks are of mixed Mazatzal and Yavapai affinities (Magnani and others, 2004); this variability has contributed, through crustal assimilation, to geochemical and isotopic diversity of volcanic rocks in the JMVF.

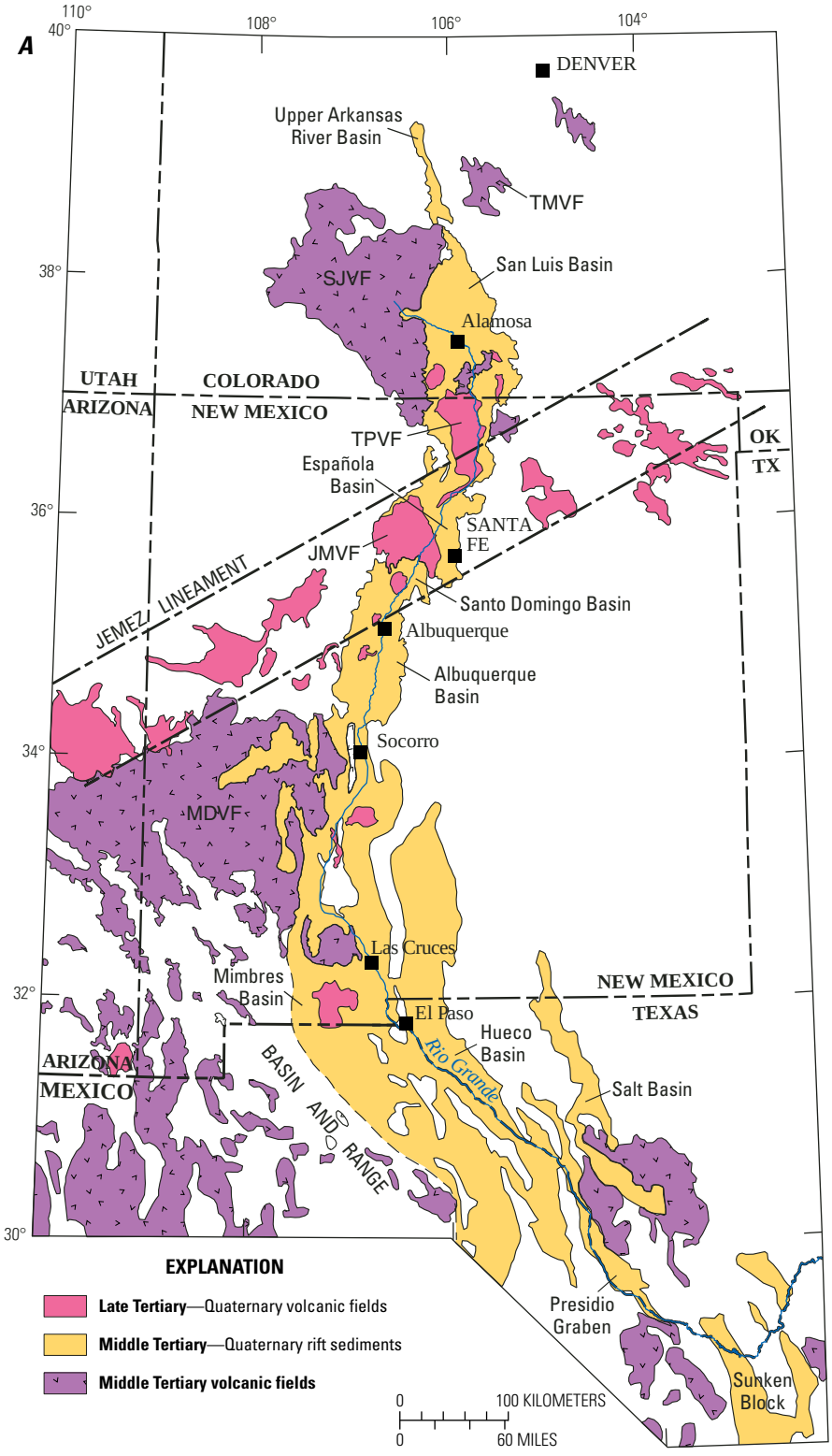

Figure 3. Geologic maps of the Rio Grande rift and parts of the Valles Caldera, Jemez Mountains volcanic field, and Day 1 route log and field-trip stops. *A*, Simplified geologic map of the Rio Grande Rift region in Colorado, New Mexico, and Texas indicating major prerift and synrift volcanic fields, geomorphic and structural basins, and course of the Rio Grande (modified from Hudson and Grauch [2013]). SJVF, San Juan locus of the southern Rocky Mountain volcanic field; TPVF, Taos Plateau volcanic field; JMVF, Jemez Mountains volcanic field (including the Cerros del Rio volcanic field); MDVF, Mogollon volcanic field. The northeast trending Jemez lineament is depicted as a zone defined by the aerial extent of dominantly basaltic Pliocene to Pleistocene volcanic rocks extending from Arizona to southern Colorado. Tx, Texas; OK, Oklahoma. *B*, Regional shaded-relief map of the Valles Caldera and Jemez Mountains volcanic field area indicating locations of Day 1 field-trip stops, denoted in red, and major geographic features discussed in guide. *C*, Simplified geologic map of the Valles Caldera area with stop locations indicated (modified from Goff and others [2011]). *D*, Simplified geologic map of parts of the Pajarito Plateau area with field-trip stops indicated in red.

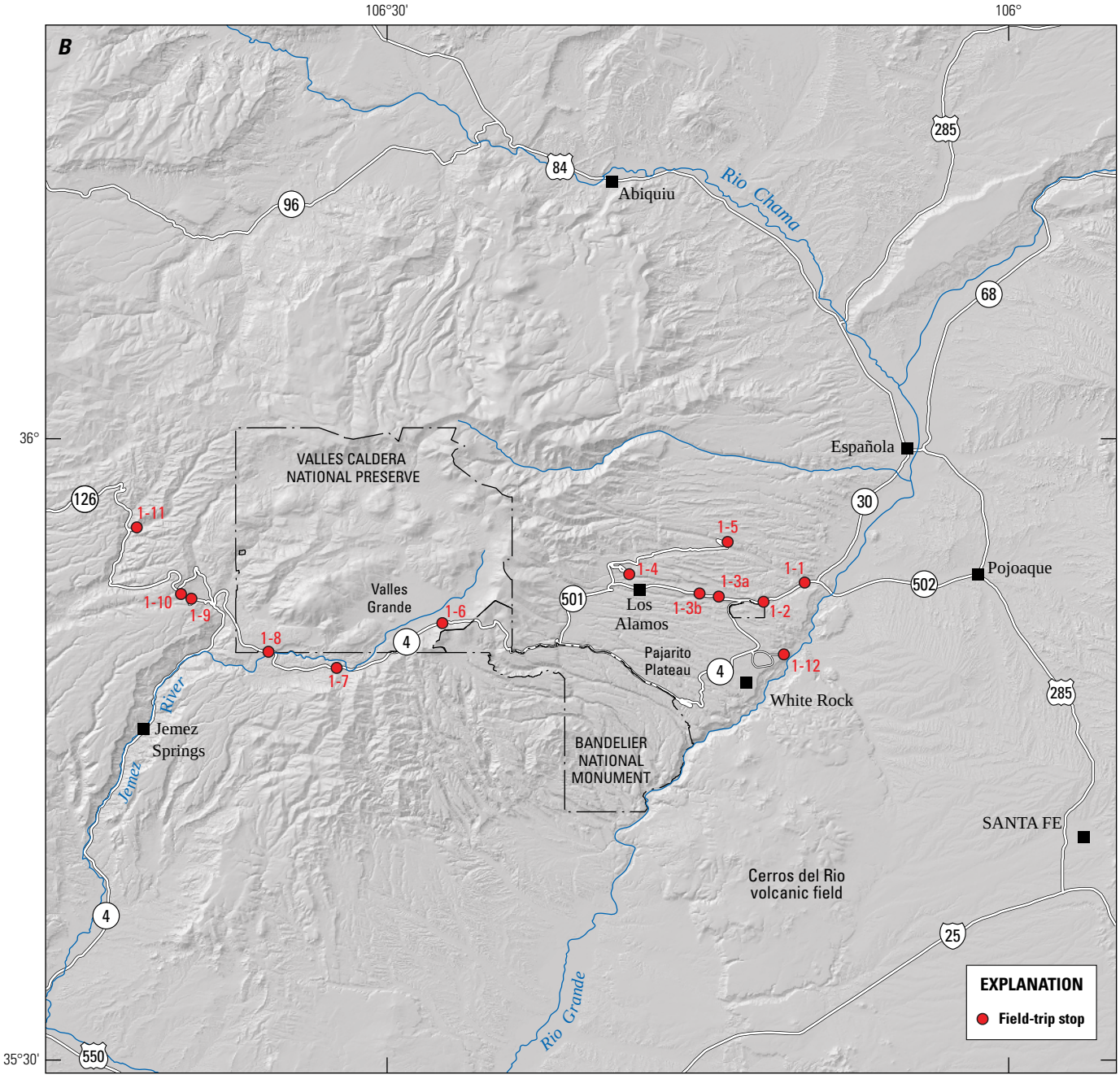

Shaded-relief base generated from U.S. Geological Survey 10-m Digital Elevation Model (DEM) data from the National Elevation Dataset, accessed November 2016, Projection UTM, NAD83 Horizontal Datum, zone 13N, NAVD 1988 Vertical Datum

Figure 3. Geologic maps of the Rio Grande rift and parts of the Valles Caldera, Jemez Mountains volcanic field, and Day 1 route log and field-trip stops. *B*, Regional shaded-relief map of the Valles Caldera and Jemez Mountains volcanic field area indicating locations of Day 1 field-trip stops, denoted in red, and major geographic features discussed in guide.—Continued

C

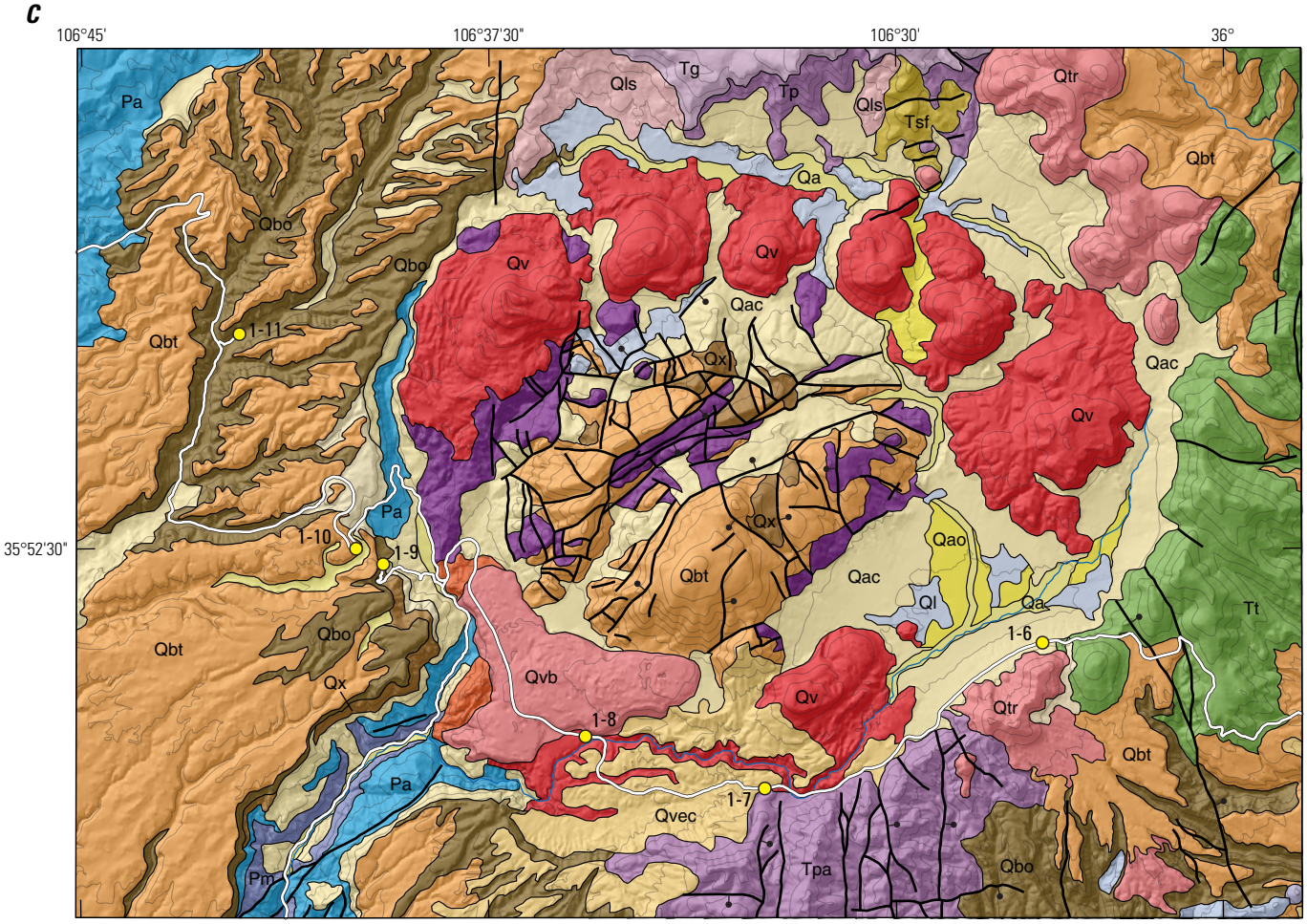

EXPLANATION

Surficial deposits

- Qa — Active alluvium (Holocene)
- Qao — Older alluvium (Holocene to late Pleistocene?)
- Qac — Colluvium, undivided (Holocene to late Pleistocene?)
- Qls — Landslide deposits (late Pleistocene?)
- Ql — Intracaldera lake deposits (Pleistocene)

Tewa Group—Caldera and postcaldera deposits

- Qvb — Valles Rhyolite, Banco Bonito Flow (Pleistocene)
- Qvbr — Valles Rhyolite, Battleship Rock Ignimbrite (Pleistocene)
- Qvec — Valles Rhyolite, El Cajete Pyroclastic Beds (Pleistocene)
- Qv — Valles Rhyolite, undivided (Pleistocene)
- Qrc — Valles Rhyolite, Redondo Creek and Deer Canyon Members (Pleistocene)
- Qbt — Bandelier Tuff, Tshirege Member (Pleistocene; 1.2 Ma)
- Qx — Bandelier Tuff, upper (Pleistocene)—Caldera collapse breccias
- Qtr — Rabbit Mountain rhyolite, Valle Toledo Member (Pleistocene)
- Qbo — Bandelier Tuff, Otowi Member (Pleistocene; 1.6 Ma)

Keres Group-precaldera volcanic rocks

- Tt — Tschicoma Formation, undivided (Pliocene)—Dominantly dacite
- Tg — La Grulla Formation, undivided (Miocene)—Andesite and dacite
- Tpa — Paliza Canyon Formation (Miocene)—Andesite to dacite

Regional basin-fill deposits

- Tsf — Santa Fe Group, undivided (Miocene)

Prevolcanic rocks

- Pa — Glorieta Sandstone, Yeso Formation, Abo Formation, undivided (Permian)
- Pm — Madera Group and older deposits, undivided (Pennsylvanian–Mississippian)

Contact

Fault—Ball and bar on downthrown block

1-6 **Field-trip stop**

Paved road

Figure 3. Geologic maps of the Rio Grande rift and parts of the Valles Caldera, Jemez Mountains volcanic field, and Day 1 route log and field-trip stops. *C*, Simplified geologic map of the Valles Caldera area with stop locations indicated (modified from Goff and others [2011]).—Continued

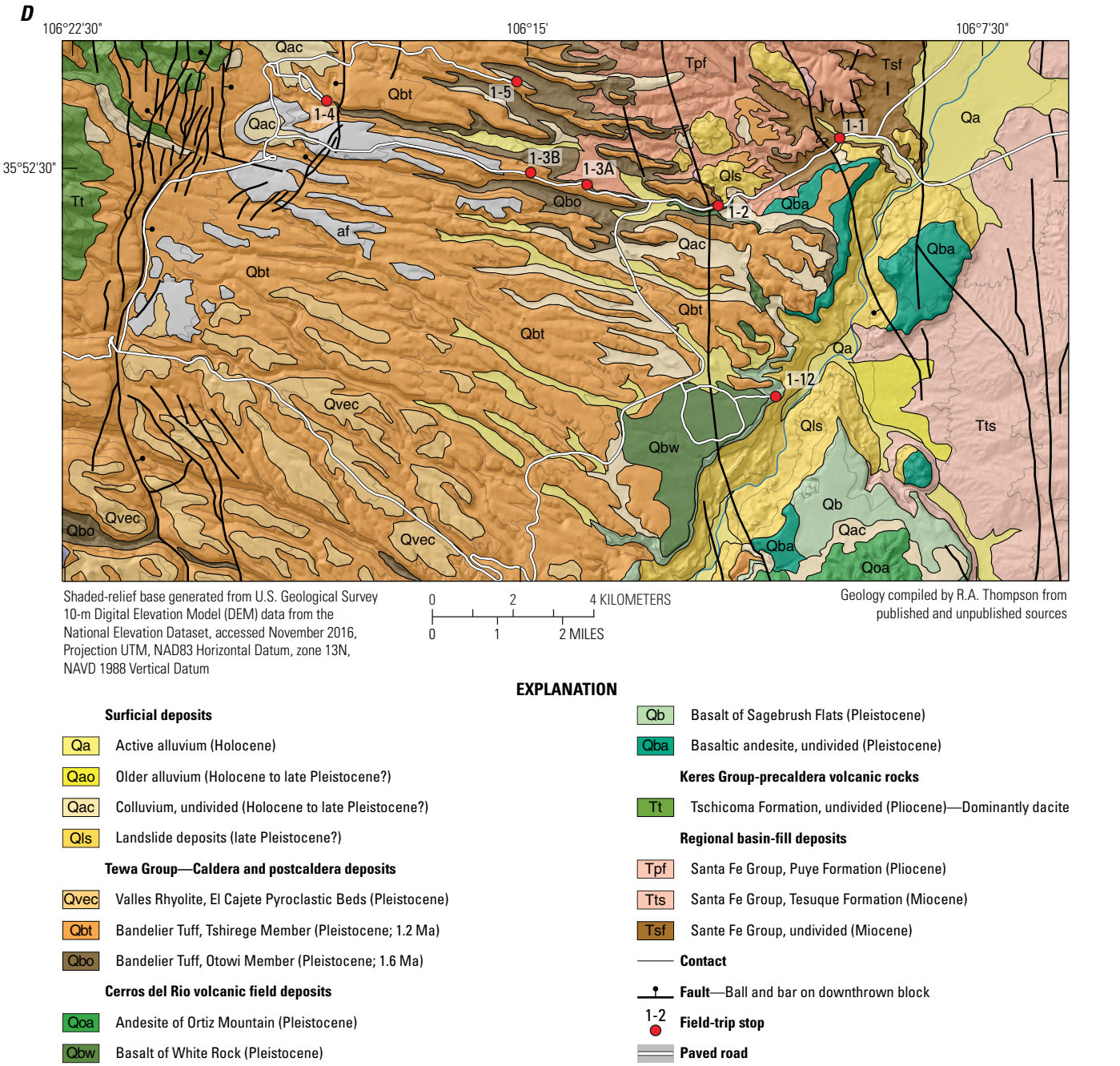

Figure 3. Geologic maps of the Rio Grande rift and parts of the Valles Caldera, Jemez Mountains volcanic field, and Day 1 route log and field-trip stops. *D*, Simplified geologic map of parts of the Pajarito Plateau area with field-trip stops indicated in red.—Continued

In the Española Basin, the Santa Fe Group west of the Rio Grande is divided into the pre-13 Ma Tesuque Formation and the overlying Chamita Formation (Koning and others, 2013). The Santa Fe Group is dominated by arkosic fluvial sands and gravels with lesser amounts of silt and clay. Overall the sediments coarsen upwards, with an increasing input from the growing JMVF after ~13.5 million years ago (Ma). The Tesuque Formation includes numerous ash beds with distant sources in the Yellowstone hotspot track and the southwest Nevada volcanic field (Galusha and Blick, 1971; Perkins and others, 1998; Slate and others, 2013). By contrast, pyroclastic and volcaniclastic beds in the Chamita Formation are dominated by early volcanic products of the JMVF (Koning and others, 2007; Slate and others, 2013). Scattered small interbedded mafic lavas and minor intrusions, ranging in silica saturation from nephelinite to tholeiite, are also found in Santa Fe Group sediments (Smith, 1938; Smith and others, 1970; May, 1984; Kelley and others, 2013). These range in age from late Oligocene to middle Miocene; the Oligocene lavas are 10

million years (m.y.) older than the onset of edifice construction in the JMVF and, although presumably erupted in response to early rifting, are not directly related to tectono-thermal events that produced large-scale Jemez Mountains volcanism. However, the lavas are probably derived from the same mantle sources as the more voluminous basalts of the Jemez Mountains proper (Wolff and others, 2000, 2005). Mafic lavas interbedded with Chamita Formation sediments, intersected in wells beneath the Pajarito Plateau, are more abundant (Woldegabriel and others, 2013), reflecting the transition to edifice construction; indeed, these basalts and basaltic andesites are assigned to the Lobato Formation by Kelley and others (2013).

Tectonic Setting

Extension in northern New Mexico began around 30 Ma and has continued episodically to the present (Aldrich, 1986; Morgan and others, 1986; Gardner and others, 1986). Following a period of quiescence from at least 18 to 13 Ma, spreading was reinitiated and continued for several million years, during which time much of the JMVF was constructed. A further lull in extensional activity between 7 and 5 Ma (Gardner and others, 1986; Kelley and others, 2013) ended with the development of the Pajarito fault zone, a series of north-trending, down-to-east extensional faults cutting the eastern part of the volcanic field.

The west boundary of the Española Basin is structurally complex, with lateral temporal shifts in faulting, long-lived faults indicated by declining offsets in progressively younger units, and reactivation of ancient Laramide structures (Kelley and others, 2013). The JMVF preserves a complex history of extensional faulting and a close spatial and temporal relation between faulting and volcanic episodes, with age patterns of volcanism reflecting the timing of motion on faults (Gardner and others, 1986; Kelley and others, 2013).

The Underlying Mantle

The Rio Grande Rift is starved of magma compared with the abundant volcanism along the Jemez lineament. Regional geophysical surveys shed light on this issue. Seismic reflection data across the lineament (CD-ROM Working Group, 2002) show a south-dipping mantle boundary, extending to >200 km depth, separating high-velocity mantle to the south from low-velocity mantle to the north; this is interpreted as the Yavapai–Mazatzal suture. The low-velocity mantle is internally layered and extends from ~45 to 120 km depth, suggesting that it resides within the lithosphere. Wolff and others (2005) argue that the primary basalt magmas for the JMVF are derived by variable degrees of partial melting of variably enriched, but overall fertile, lithospheric mantle associated with the Proterozoic suture. Extensional tectonism associated with the Rio Grande Rift, superposed on the mantle melting associated with the Jemez lineament, may result in the disproportionately large, erupted volumes of evolved lavas relative to other volcanic field of the northern Rio Grande Rift.

Low-velocity mantle extends to the base of the thinned crust beneath the rift axis, where the lithospheric mantle has either been thermally eroded or is geophysically indistinguishable from the asthenosphere owing to shearing and heating. A similar low-velocity zone exists at the base of the crust beneath the JMVF (Steck and others, 1998; Aprea and others, 1998). Temperatures may exceed 900 °C in the lower crust beneath the rift (Baldridge and others, 1984; Clarkson and Reiter, 1984; Morgan and Golombek, 1984), nearing solidus temperatures of crustal lithologies. The thermally weakened Proterozoic crust may then be susceptible to partial melting resulting from intrusions of mantle-derived primitive basaltic magma.

Precaldera Volcanic History

Intensive field investigations and remapping since 2000 have led to major revisions of the stratigraphy established by Bailey and others (1969) and modified by Gardner and others (1986). All pre-Bandelier Tuff volcanic and volcaniclastic rocks in the JMVF are now assigned to the Keres Group, and the Bandelier Tuff and later volcanic and volcaniclastic units are assigned to the Tewa Group (Gardner and others, 2010; Kelley and others, 2013). A simplified stratigraphy is shown in figure 4; see Gardner and others (2010) and Kelley and others (2013) for more detail. Geochemical data for Keres Group rocks are reported by Singer (1985), Gardner and others (1986), Goff and others (1989), Ellisor and others (1996), Justet and Spell (2001), Wolff and others (2005), Rowe and others (2007), and Kelley and others (2013).

Keres Group

The principal volcanic formations (fig. 4) of the Keres Group are the Paliza Canyon Formation (basaltic to dacitic) in the central and southern Jemez Mountains, the Lobato Formation (dominantly mafic) in the northeast, the La Grulla Formation (basaltic to dacitic) in the northwest, the Tschicoma Formation (dominantly dacitic) in the central and northeastern JMVF, and the Bearhead Rhyolite-Peralta Tuff in the south-central to north-central JMVF. Additional units of note are the basalt of Chamisa Mesa and Canovas Canyon Rhyolite, respectively at the base and interbedded with the Paliza Canyon Formation in the southern Jemez Mountains, and the basalt of El Alto and El Rechuelos Rhyolite, which overlie the Tschicoma Formation in the northeast. The volcanic formations are flanked and overlain by, and interbedded with, locally thick volcaniclastic alluvial deposits, most notably (for the purposes of this guide) the Puye Formation in the north and northeastern JMVF, derived from the Tschicoma Formation. The basaltic to benmoreite lavas of the Pliocene-Pleistocene Cerros del Rio Basalt occupy the central Española Basin, and overlie and interfinger with Puye Formation gravels and Tschicoma dacites beneath the Pajarito Plateau (Woldegabriel and others, 1996; Samuels and others, 2007). Over most of their extent west of the Rio Grande, Cerros del Rio basalts lie directly

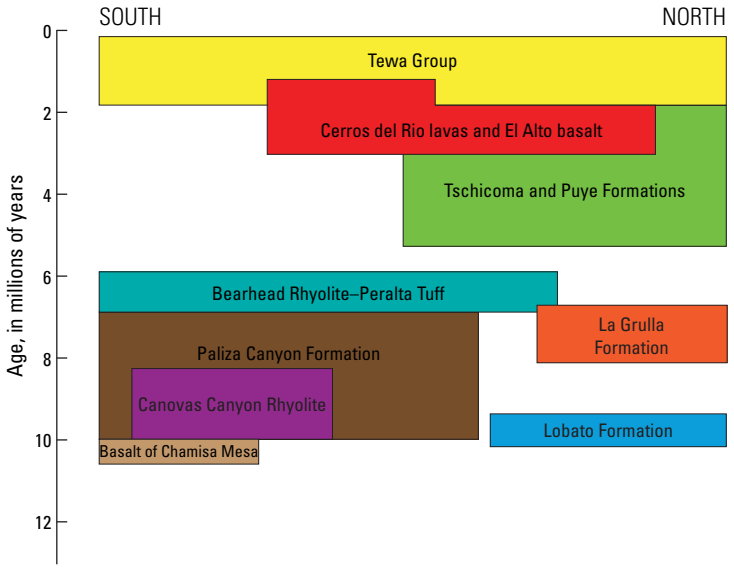

Figure 4. Simplified time-space stratigraphic chart of the primary volcanic formations within the Keres Group of the Jemez Mountains volcanic field, as well as the overlying Tewa Group, after Kelley and others (2013). See figure 8 for details of Tewa Group stratigraphy.

beneath Bandelier Tuff; however, the youngest Cerros del Rio lavas overlie Bandelier Tuff in the Cochiti area (Thompson and others, 2006).

Initiation and Tempo of Jemez Volcanism

The onset of JMVF volcanism construction is hard to identify. In the east to northeast Jemez Mountains area, early Lobato Formation basalts, interbedded with Chamita Formation sediments, record an increase in magmatic tempo at ≤13.5 Ma (Kelley and others, 2013; Woldegabriel and others, 2013), leading to edifice construction beginning with the building of the thick (>400 m) Lobato Mesa section, from which the oldest age determinations are 10.59±0.10 Ma and 10.45±0.05 Ma (Justet, 2003; Kelley and others, 2013). Evidence for older dacitic volcanism at 13–11 Ma in the northeastern JMVF is preserved in Chamita Formation volcaniclastic sediments (Koning and others, 2007). In the southern JMVF, although early K-Ar dating suggested ages older than 12 Ma (Gardner and Goff, 1984; Gardner and others, 1986), more recent $^{40}Ar/^{39}Ar$ age determinations on the oldest basalts and rhyolites are significantly younger, ~11 Ma (Justet, 2003). Most recently, Kelley and others (2013) determined that ages of the stratigraphically oldest basalts and rhyolites are between 10.0 and 9.5 Ma. In summary, edifice construction was certainly underway by 10.5 Ma, and probably before. At this time, the future JMVF may have been a cluster of small basaltic shields and silicic dome complexes with accompanying volcaniclastic deposits.

A histogram of the $^{40}Ar/^{39}Ar$ age determinations for precaldera JMVF volcanic rocks (Keres Group, precursor lavas interbedded with Chamita Formation, and flanking basalts, 14.0–1.5 Ma) determined and compiled by Kelley and others (2013) is shown in figure 5. No attempt has been made to weight the data in figure 5 by unit volume, and the Bearhead Rhyolite and Cerros del Rio volcanic field units are highly overrepresented, but the distribution of peaks and troughs is nonetheless instructive. Strong peaks occur at 9.5 and 9.0 Ma (Lobato and Paliza Canyon Formations), 7.8 Ma (La Grulla Formation), 6.8 Ma (Bearhead Rhyolite) and 2.5 Ma (flanking basalt fields), suggestive of individual magma systems with brief peak eruption rates. By contrast, Tschicoma Formation activity shows a more even tempo from ~5 to 2 Ma. Especially noteworthy is the apparent complete cessation of volcanic activity between 6.0 and 5.5 Ma, following emplacement of the Bearhead Rhyolite.

Overall magma production rates are low throughout the history of the JMVF compared with supervolcanoes and other

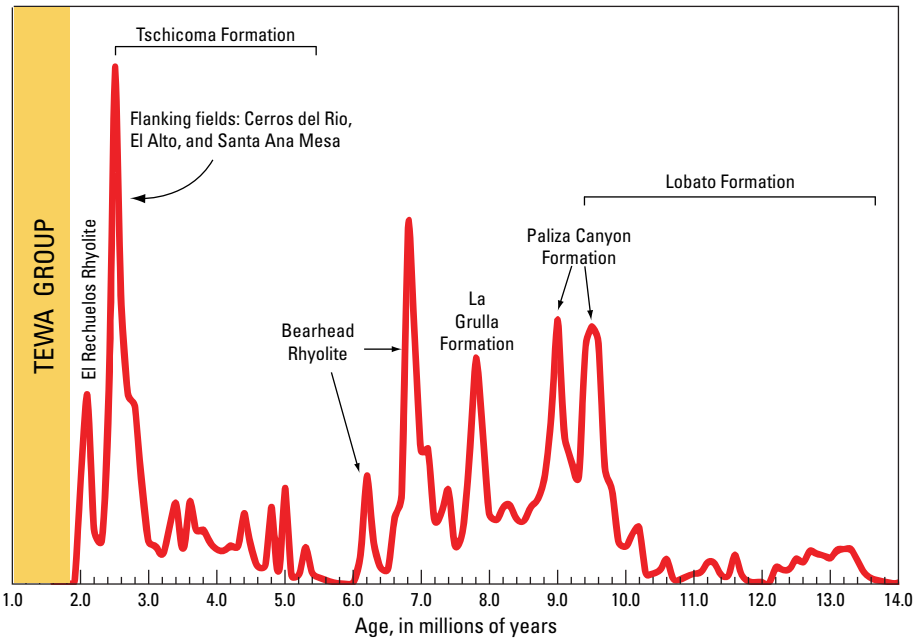

Figure 5. Probability density function histogram for all determined Keres Group $^{40}Ar/^{39}Ar$ ages presented and compiled by Kelley and others (2013). The principal contributors to major age spikes are identified, but those formations are not necessarily limited to the peaks. Thus, mafic to intermediate lavas erupted in the Cerros del Rio field over the period from ~5 to ~1.5 Ma, but most were emplaced between 3.0 and 2.4 Ma. Although lavas assigned to the Lobato Formation extend back in time to, and are interbedded with, Santa Fe Group sediments, most edifice-forming Lobato lavas erupted 10–9.5 Ma, overlapping with early Paliza Canyon activity in the southern Jemez Mountains volcanic field. The onset of Tewa Group activity is at 1.85 Ma.

large volcanic systems. The two most voluminous formations of the Keres Group, the Paliza Canyon and the Tschicoma Formations, have approximate volumes of 1,000 cubic kilometers (km^3) and 500 km^3, respectively (Gardner and others, 1986). Assuming that the bulk of the former was emplaced over a 2-million-year period yields an average eruption rate of 0.5 km^3 per thousand years (ka), similar to that of the Tewa Group at 0.6 km^3/ka (see below). These are maximum values; the total volume of the whole volcanic field is approximately 2,200 km^3, yielding an average eruption rate of ~0.2 km^3/ka. In a global context, these values are modest; for example, they are an order of magnitude lower than the estimated eruption rate for the Snake River Plain, Idaho (Ellis and others, 2013), and more than two orders of magnitude lower than the modern eruption rate at Hawaii.

Summary of Keres Group Petrology and Geochemistry

A range of alkalinity at all silica contents indicates complex petrogenesis in precaldera JMVF rocks, from basalts to high-silica rhyolites (fig. 6), indicating complex petrogenesis. Basalts of the Lobato and younger formations vary from ne- to hy-normative; the older Santa Fe Group basalts additionally include some very strongly silica-undersaturated basanites and nephelinites. The range in alkalinity is attributed by Wolff and others (2005) and Rowe and others (2007) to distinctly different parental basalts interacting to varying degrees with continental crust. These authors distinguish two categories of mafic lavas: type I and type II. Type I lavas may be ne- or hy-normative with overall alkaline affinity (dominantly hawaiites and mugearites) and have very distinctive trace element patterns (fig. 7) that do not conform to any globally common magma type. Type I lavas are derived from primitive nephelinites and basanites through assimilation-fractional crystallization (AFC) processes within the deep crust (Wolff and others, 2000, 2005). Type II lavas are tholeiites and basaltic andesites, generally less chemically enriched than type I (fig. 7) and also interpreted to have been affected by crustal contamination. Lobato Formation basalts are dominantly type II, whereas Paliza Canyon Formation lavas with <57 weight percent SiO_2 are mostly type I or transitional between types I and II. The two types are most clearly distinguished among Cerros del Rio lavas and scoria; most of the section in White Rock Canyon consists of type I hawaiites and mugearites, overlain by type II olivine tholeiites on the eastern Pajarito Plateau. Simple petrogenetic models allow for derivation of type I and type II magmas from the same mantle source by way of different degrees of partial melting (Wolff and others, 2005) prior to crustal contamination within each suite. The source mantle is thought to be ancient subducted oceanic lithosphere trapped in the regional Proterozoic suture beneath the JMVF; however, a contribution to type II basalts from a convecting asthenospheric mantle source, or to both types from subduction-related fluids during early Cenozoic flat-slab subduction beneath western North America (Rowe and others, 2015), cannot be ruled out.

Variable alkalinity persists among derivative lavas. Most Paliza Canyon Formation lavas in the range of 57–63 weight percent SiO_2 are weakly alkaline trachyandesites. Tschicoma Formation dacites are distinctively less alkaline than most JMVF intermediate rocks. Whereas most Paliza Canyon lavas with >57 weight percent SiO_2 can be modeled as the result of AFC and simple fractional crystallization from a type I mafic parent, Tschicoma dacites have, on average, more crustal isotopic signatures and may have been produced by crustal melting followed by mixing with type I mugearite/benmoreite. For example, the dacite of Pajarito Mountain may consist of as much as 80 percent crustal material (Rowe and others, 2007). Notably, several Tschicoma dacite lavas contain mafic

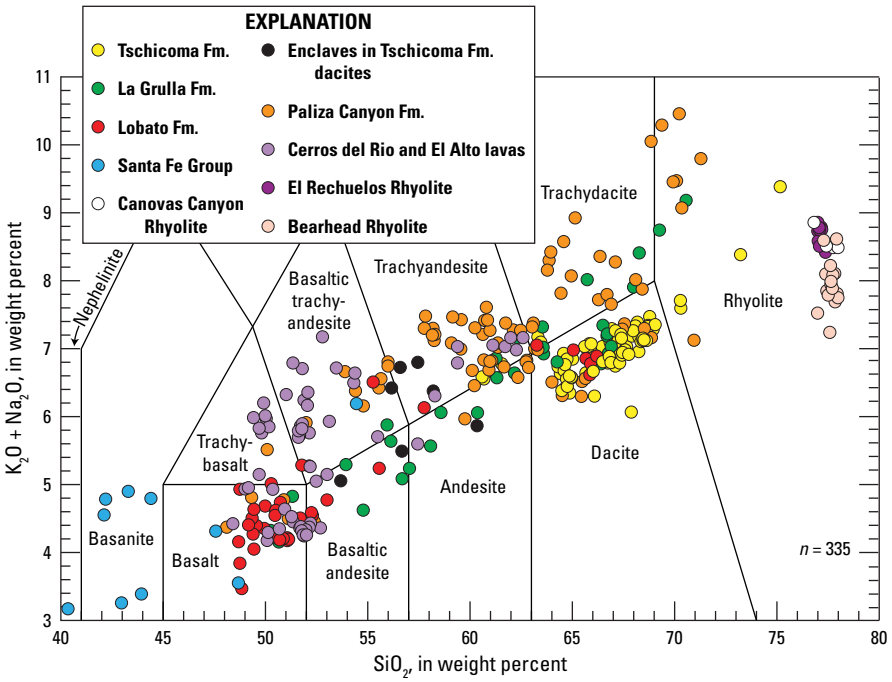

Figure 6. Total alkali-silica classification diagram for Santa Fe Group and Keres Group volcanic rocks. The Santa Fe Group includes lavas and scoria from the Española Basin outside the confines of the Jemez Mountains volcanic field (Gibson and others, 1993; Wolff and others, 2005). Note that the majority of trachybasalts, basaltic andesites, and many trachyandesites have weight percent $Na_2O>(K_2O+2)$; hence, they are hawaiites, mugearites, and benmoreites, respectively. The more generic terms have been retained because this does not apply to every sample in each field. See Kelley and others (2013) for additional data. Fm., formation.

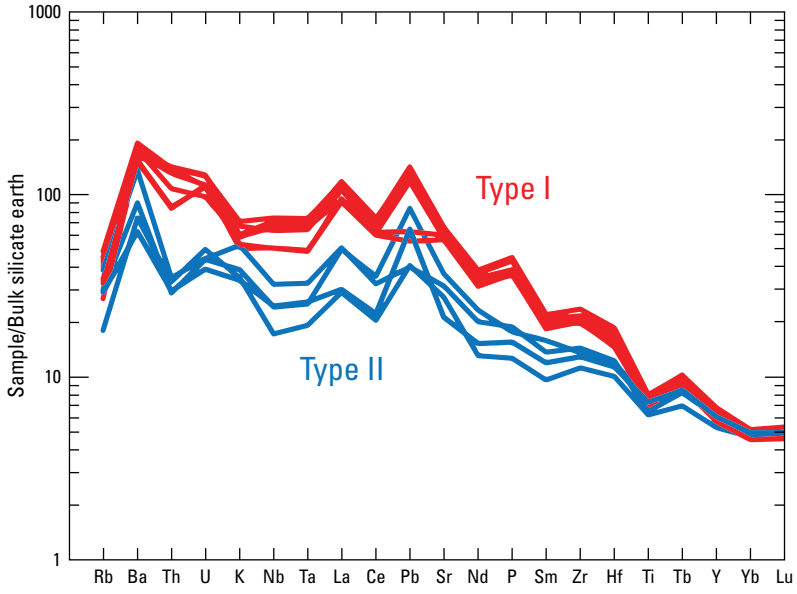

Figure 7. Normalized trace element diagrams of representative samples of Type I (red) and Type II (blue) Jemez Mountains volcanic field mafic lavas from the Paliza Canyon Formation, Lobato Basalt, Cerros del Rio and El Alto units. Type I lavas mostly have alkaline affinity, whereas Type II are mostly tholeiites. Bulk silicate earth of McDonough and Sun (1995). Note the distinctive depletion in potassium, as well as niobium and tantalum, of the Type I lavas. This is a consequence of mixing potassium-depleted nephelinite-basanite magma, derived from melting of lithospheric mantle with residual amphibole, with niobium/tantalum-depleted continental crust (Wolff and others, 2000, 2005); the resulting relative depletions in potassium, niobium, and tantalum are globally uncommon. Type II basalts are enriched in potassium with respect to niobium and tantalum, a feature that is generally more typical of continental basalts.

inclusions (fig. 6) with type I and transitional type I-type II trace element chemistry, a petrogenetic link with both earlier mafic magmatism and the contemporaneous mafic lavas of the Cerros del Rio volcanic field. Intermediate to silicic rocks of the La Grulla Plateau are slightly less alkaline than the Paliza Canyon Formation, but have a distinctive petrogenesis, indicated by higher $^{87}Sr/^{86}Sr$ ratios at equivalent values of neodymium and lead isotope ratios compared to both Paliza Canyon and Tschicoma rocks.

The Bearhead Rhyolite and associated Peralta Tuff consist of numerous domes and tuffs of crystal-poor, high-silica rhyolite (Justet and Spell, 2001); vent locations extend from the southern to northern JMVF and probably much of the Bearhead Rhyolite-Peralta Tuff was destroyed or buried during caldera formation. Most of the surviving volume was erupted between 7.1 and 6.6 Ma, with a few younger domes dated at 6.3–6.0 Ma. Chemical compositions are remarkably constant, with very modest variability of trace element contents compared to the later Tewa Group high-silica rhyolites (Justet and Spell, 2001). The ultimate petrogenesis of the Bearhead Rhyolite is not well constrained; the rhyolites have a different combination of lead and neodymium isotope ratios relative to most older Keres Group rocks, and therefore require a different mix of crustal components (Rowe and others, 2007). The Bearhead Rhyolite-Peralta Tuff footprint is similar in area to the Valles Caldera, suggesting a rhyolitic magma system comparable in size to that which produced the Bandelier Tuff, but which failed to produce a major caldera-forming eruption (Justet and Spell, 2001). Following emplacement of these units, the JMVF was apparently quiescent for ~0.5 m.y. prior to the onset of Tschicoma Formation activity (fig. 5).

Rowe and others (2007) point out that each major formation of the Keres Group has its own petrologic and chemical flavor and that successive formations are somewhat geographically distinct. Once initiated, the activity building each formation persisted for one to a few million years. These spatio-temporal-compositional patterns may relate to sites of melt lenses and maximum heat transport into the crust that act as focusing traps for later rising magma. Formation transitions result when the system is starved of mafic melt input, and is reinitiated, probably under tectonic control, at a new location.

Tewa Group and the Valles–Toledo Caldera Complex

The present Valles Caldera topographic feature is the result of two collapse events accompanying the eruptions of the Otowi and Tshirege Members of the Bandelier Tuff, at about 1.60 and 1.25 Ma, respectively. In the usage of the heading to this section, the term “Toledo” refers to the first (Otowi) collapse, and the term “Valles” to the later (Tshirege) collapse. The original Toledo structure was partly obliterated during the Tshirege eruption, but portions of it survive as the north and east walls of the present topographic caldera (Self and others, 1986; Goff and others, 2011). Through the work of Smith and Bailey (1968), the Valles Caldera is considered the type example of a structurally resurgent caldera; from most vantages the resurgent dome of Redondo Peak is the dominant topographic feature of the Jemez Mountains, standing higher than all but a single point on the caldera margin (fig. 3). It is noteworthy that resurgent doming was extremely rapid; $^{40}Ar/^{39}Ar$ dating of the Tshirege Member and syn- and postresurgent lava domes constrains the whole of the uplift to ≤54,000 years (Phillips and others, 2007a.)

The Tewa Group consists of the Bandelier Tuff, Cerro Toledo Formation, and Valles Rhyolite Formation, each of which is formally divided into members (fig. 8). The Bandelier Tuff is exclusively pyroclastic, the others have both effusive and explosive components. Most of the Tewa Group volume consists of Bandelier Tuff, but it must be understood that estimating the volumes of pyroclastic formations is fraught with difficulties and errors. Cook and others (2016) provide a dense-rock-equivalent (DRE) volume for the Otowi Member of 298+252/-82 km^3; the median of this range is 383 km^3. Goff and others (2014) give a

volume of 400 km³ for the Tshirege Member, but do not provide errors. Providing uncertainties is uncommon for the majority of studies that postulate volume estimates for large pyroclastic bodies, however, similar relative uncertainties to those estimated by Cook and others (2016) for the Otowi Member may apply to the estimate by Goff and others. The volumes of the Cerro del Medio and East Fork Members of the Valles Rhyolite have been estimated at ~5 km³ (Gardner and others, 2007) and ~15 km³ (Wolff and others, 2011), respectively. The volumes of other Tewa Group units are not well constrained, but the total for primary volcanic units other than the Bandelier Tuff may lie in the range of 50–100 km³. The total volume of the Tewa Group is therefore on the order of 900 km³ DRE, and the error associated with this estimate may be (very approximately) ±400 km³. It is worth noting that this volume was anticipated by Powell (1895), who estimated "more than 200 cubic miles of this [volcanic] dust, now compacted into somewhat coherent rocks" on the Tewan Plateau!

The Tewa Group consists almost exclusively of high-silica rhyolite, with compositions near the minimum in the system Q-Ab-Or (petrogeny's residua system). Exceptions to this are the presence of minor low-silica rhyolitic, dacitic, and andesitic components in the Tshirege Member (Bailey and others, 1969; Self and others, 1996; Goff and others, 2014), the rhyodacite Redondo Creek Member of the Valles Rhyolite (Goff and others, 2011), and the low-silica rhyolitic East Fork Member of the Valles Rhyolite (Wolff and Gardner, 1995). The dominant high-silica rhyolites, especially the two members of the Bandelier Tuff, exhibit wide variations in trace element content, as first noted by Smith and Bailey (1966).

Tewa Group units display systematic changes in neodymium isotope ratios, interpreted as a fluctuating relative contribution of mantle and crustal inputs to the rhyolitic system (fig. 9). Interestingly, there is no clear signal of increased crustal involvement consequent upon caldera collapse episodes; rather the neodymium signature becomes steadily more crustal from the inception of Tewa magmatism until just after 1.0 Ma (Cerros del Abrigo and Cerro Santa Rosa Members, fig. 8), and increases slightly thereafter to the most recent eruptions (East Fork Member).

La Cueva Member of the Bandelier Tuff

This unit, formerly referred to as the "San Diego Canyon ignimbrites" (Turbeville and Self, 1988), consists at its type locality of two rhyolitic ignimbrites that underlie the Otowi Member in the southwest caldera and in the walls of Cañon de San Diego. These correlate with the lower tuffs found in cores and well cuttings beneath the Otowi Member in the caldera (Hulen and others, 1991). Correlative fallout units have been identified at the north and south edges of the Pajarito Plateau, east of the caldera (fig. 3); they have been dated at 1.85±0.07 Ma (Spell and others, 1996). The total volume is unconstrained, but Turbeville and Self (1988) suggest 3–4 km³ excluding correlative units in, and east of, the caldera; it is possible that tens of cubic kilometers may be buried beneath the caldera (Cook and others, 2016). A conservative order-of-magnitude estimate is 10 km³.

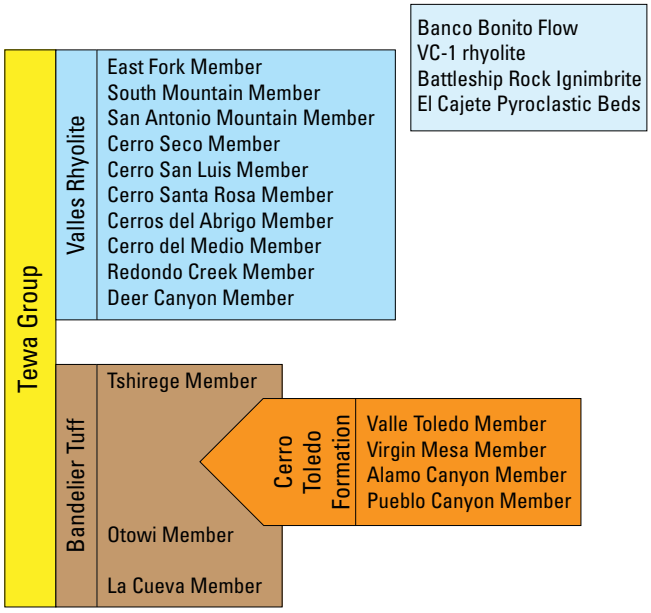

Figure 8. Diagram of Tewa Group stratigraphy modified from Gardner and others (2010).

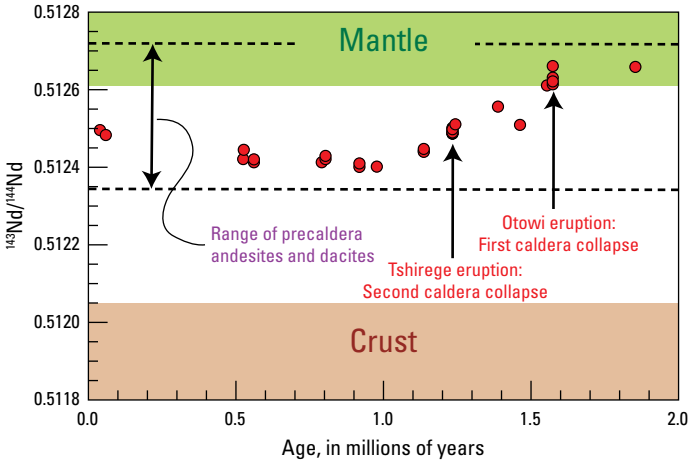

Figure 9. $^{143}Nd/^{144}Nd$ versus time for rhyolites of the Tewa Group. Regional Proterozoic crust varies widely in $^{143}Nd/^{144}Nd$; the range of values indicated by the tan field labeled "Crust" are thought to represent crustal rocks involved in Jemez Mountains volcanic field magmatism, whereas the green field labeled "Mantle" represents the regional lithospheric mantle source for mafic lavas of the JMVF (Wolff and others, 2005). Data sources include Loeffler and others (1988), Skuba (1990), Spell and others (1993, 1996), Justet and Spell (2001), Wolff and others (2005), and Rowe and others (2007).

The La Cueva ignimbrites are non- to incipiently welded and contain phenocrysts of sanidine and quartz with traces of magnetite and clinopyroxene. Trace element abundances are similar to those of late-erupted Otowi Member (see the section "Otowi Member of the Bandelier Tuff").

Otowi Member of the Bandelier Tuff

The Otowi Member of the Bandelier Tuff consists of a basal fallout unit, the Guaje Pumice Bed, best developed east of the caldera, overlain by and interbedded with voluminous ignimbrites (fig. 10). Wolff and Ramos (2014) reviewed the numerous earlier $^{40}Ar/^{39}Ar$ age determinations on the Otowi Member and presented some new U/Pb zircon ages; they concluded that the best estimate for the eruption age of the unit is 1.60±0.02 Ma. The Guaje Pumice has been divided into five units, A–E, by Self and others (1986, 1996). Unit A (3.3–4.4 km^3, Cook and others, 2016) consists of the first-erupted magma; units C–E, and perhaps unit B, were coerupted with the volumetrically dominant ignimbrite. Over most of its extent, the ignimbrite is lithic-rich and poorly to non-welded, but thick, densely welded canyon-filling sequences are found on the Jemez plateau west of the caldera. The ignimbrite is typically massive with few sedimentary structures, although pumice swarms locally occur at the base. In the southwest caldera wall and upper Cañon de San Diego, lithic breccia zones occur partway through the unit; they may record vent shifting and an increment of caldera collapse (Self and others, 1986, 1996). Additional evidence for a vent shift late in the eruption sequence is seen in changing lithic populations through the Otowi Member

The Otowi Member is petrographically, mineralogically, and compositionally zoned. Total phenocryst contents of pumice clasts vary from <5 percent in Guaje Pumice Unit A to ~20 percent in late-erupted ignimbrite. The phenocryst assemblage is sodic sanidine + quartz + hedenbergite + magnetite + zircon + allanite ± fayalite ± chevkinite ± britholite (a rare earth element silicophosphate mineral). Quartz and sanidine together account for ~95 percent of phenocrysts. Fayalite is prominent in heavy mineral separates prepared from Guaje Pumice Unit A, but scarce to absent otherwise. Late-erupted, porphyritic pumice clasts have abundant quartz-sanidine glomerocrysts as large as 1 centimeter (cm) in diameter, interpreted as fragments from a crystal-rich magmatic mush that was stratified below the crystal-poor rhyolite prior to eruption (Wolff and Ramos, 2014; Wolff and others, 2015). Little major-element compositional zoning is seen in feldspars, however sanidine and quartz grains from all except the first-erupted parts of the tuff exhibit zoning under cathodoluminescence (CL) with bright rims enriched in compatible trace elements including titanium, strontium, and barium; the enrichments are most strongly developed in glomerocryst feldspars (Wolff and Ramos, 2014).

Whole-pumice compositional variations are manifested in minor and trace elements. Incompatible trace elements (Cs, Rb, Nb, Ta, U, Th, Pb, and heavy-group rare earth elements [HREE]; fig. 11*A*) show as much as five-fold variation and are most

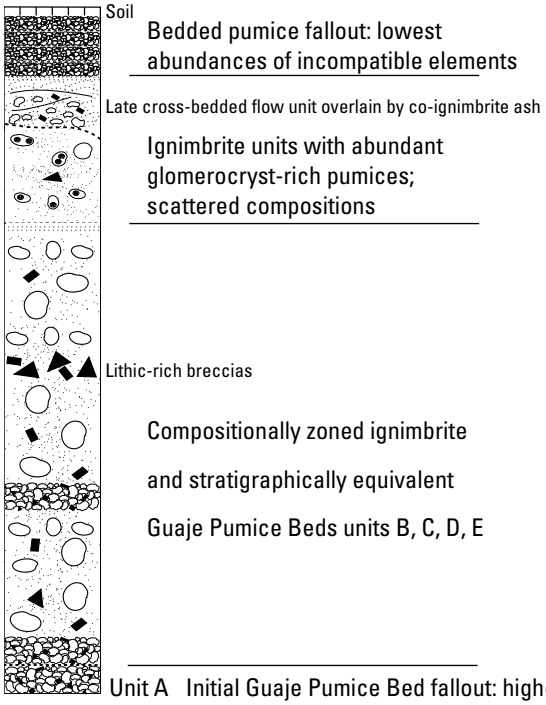

Figure 10. Schematic composite stratigraphy of the Otowi Member of the Bandelier Tuff.

abundant in the first-erupted tephra, whereas Sr, Ba, Eu, Ti, P, and light-group rare earth elements (LREE) show the opposite trend with eruption progress (fig. 11*B*).

The Otowi Member is also zoned in isotopic compositions. Strontium exhibits the widest range, a consequence of very low concentrations and hence great leverage exerted by any conceivable contaminant, as well as a possible contribution from in situ aging over timescales of 10^4–10^5 years, owing to extremely high Rb/Sr (Wolff and Ramos, 2014). Feldspars from early-erupted Guaje Pumice have $^{87}Sr/^{86}Sr = 0.7067$–0.7080, whereas those from late-erupted glomerocrysts are mostly in the range of 0.7052–0.7056. By contrast, lead isotope ratios exhibit very muted variation (Wolff and Ramos, 2003, 2014). The same isotopic variations are seen in the zoned feldspars, in which the compatible element-enriched rims have lower $^{87}Sr/^{86}Sr$ and more mantle-like lead isotope ratios (Wolff and Ramos, 2014).

The crystal-scale observations were explained by Wolff and Ramos (2014) in terms of a model similar to that first proposed by Wark and others (2007) for the Bishop Tuff in California, in which melting of the crystal-rich lower portion of the rhyolite chamber is induced by heating as a result of mafic recharge, followed by renewed crystallization to develop the zoned feldspar and quartz. The process was also invoked and developed by Wolff and others (2015) as a general model for compositional zoning in bodies of felsic magma (fig. 12). Briefly, the starting point is a cumulate bed of crystals beneath its cognate supernatant melt layer. Heating of the crystal bed by invading magma produces new melt with

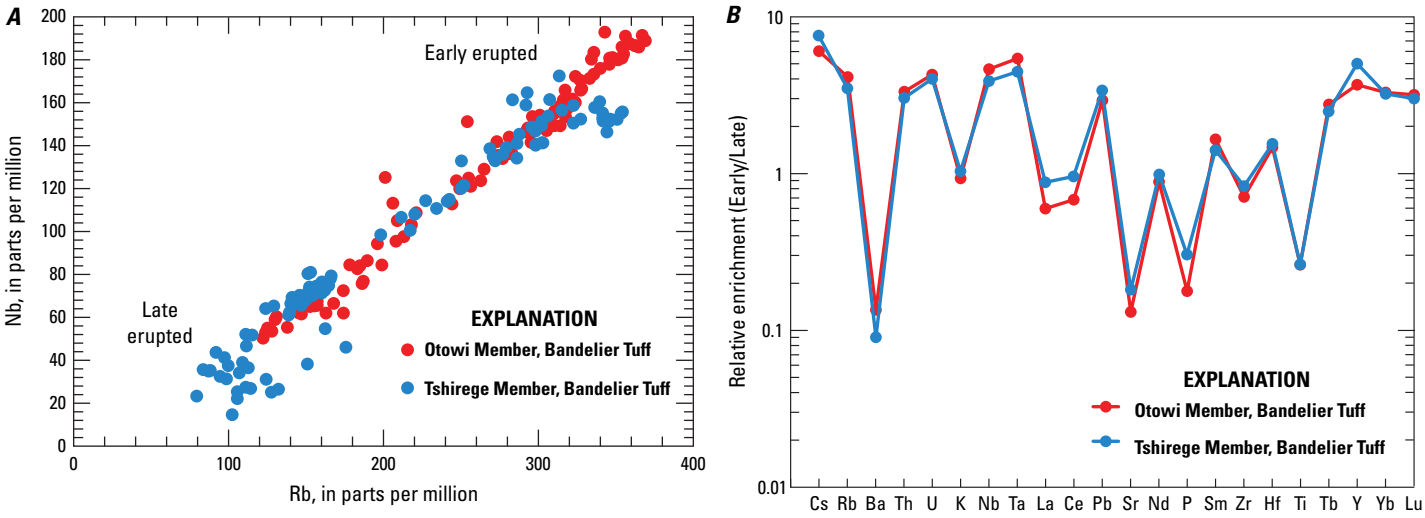

Figure 11. *A*, Covariation of concentrations of two strongly incompatible elements, rubidium and niobium, in whole pumice clasts from the Otowi and Tshirege Members of the Bandelier Tuff. Both units are continuously zoned. *B*, Enrichment diagram (Hildreth, 1979) for the Otowi and Tshirege Members of the Bandelier Tuff. Elements that plot above the 1.0 line are enriched upwards in the pre-eruption magma column; those that plot below the 1.0 line are depleted upwards. Depleted elements are compatible into the phenocryst assemblage: barium and strontium into feldspar, light rare earth elements into allanite and chevkinite, zirconium into zircon, phosphorous into apatite-group minerals, titanium into iron-titanium oxides. Note also that potassium is buffered at 1.0, as expected for crystallization at the granite minimum. The relative enrichments and depletions therefore require that crystal-liquid processes play the dominant role in zoning.

an accumulative composition, lower water content, and higher density than the overlying melt lens, thus forming a zoned melt column. Element variations within the melt column are consistent with fractionation of the observed assemblage, because the same mineral phases have been partly melted to make the new, denser melt. This model reconciles evidence for thermal rejuvenation of stagnant silicic magma bodies preserved in crystals with evidence for the production of zoning by crystal-liquid processes apparent in whole-rock chemistry.

Cerro Toledo Formation

This complex volcanic-sedimentary unit formed in the time between Otowi and Tshirege Members of the Bandelier Tuff (Jacobs and Kelley, 2007). As defined by Gardner and others (2010), it contains four members, of which one, the Valle Toledo Member, consists of three types of primary volcanic rocks: (1) rhyolite domes in the Toledo embayment, the northern moat of the caldera, and at Rabbit Mountain on the southeast rim (fig. 3*C*); (2) pyroclastic fallout deposits dispersed east and southeast of the Toledo embayment; and (3) block-and-ash flows derived from Rabbit Mountain. The pyroclastic fallout deposits are the most interesting for rhyolite petrogenesis because they provide the clearest stratigraphic control on the development of the Tewa magma system between eruptions of the Otowi and Tshirege Members (Smith, 1979; Stix and others, 1988; Spell and others, 1996).

At least five Valle Toledo Member fallout deposits are found on the Pajarito Plateau. The oldest of these is interpreted here as the last phase of the Otowi Member eruption (fig. 10). Its radiometric age is indistinguishable from that of the Otowi (Spell and others, 1996), and it shows chemical continuity with the last-erupted Otowi products. Most significantly, field relations support near-continuous emplacement. At Stops 1–3 of the field trip, Valle Toledo fallout pumice rests directly on a very fine coignimbrite fallout ash at the top of the Otowi Member, with clear evidence of pumice clasts sinking into fluffy ash (see Road Log). The preservation potential of the coignimbrite ash is extremely low, and it has been observed nowhere else in the JMVF, indicating preservation by rapid burial.

Overlying Valle Toledo fallout deposits exhibit progressively increasing incompatible element contents; the youngest, separated in the field from the overlying Tsankawi Pumice Bed by a weathering horizon, nonetheless has identical chemistry and age to the Tsankawi, the opening phase of the Tshirege eruption (Spell and others, 1996).

Tshirege Member

Over most of the extent of the Bandelier Tuff (fig. 3*C*), welded Tshirege Member tuff forms the capping plateau surface. The spectacular salmon-colored mesas of the Pajarito Plateau (fig. 13) and other sectors of the volcanic field are formed of variably indurated and partly recrystallized Tshirege ignimbrite. The volcanology and petrology of the Tshirege Member have been the subject of several studies (Smith and Bailey, 1966; Self and others, 1986, 1996; Balsley, 1988; Warshaw and Smith, 1988; Caress, 1996; Stimac, 1996; Wolff and others, 2002; Dethier and others, 2007; Warren and

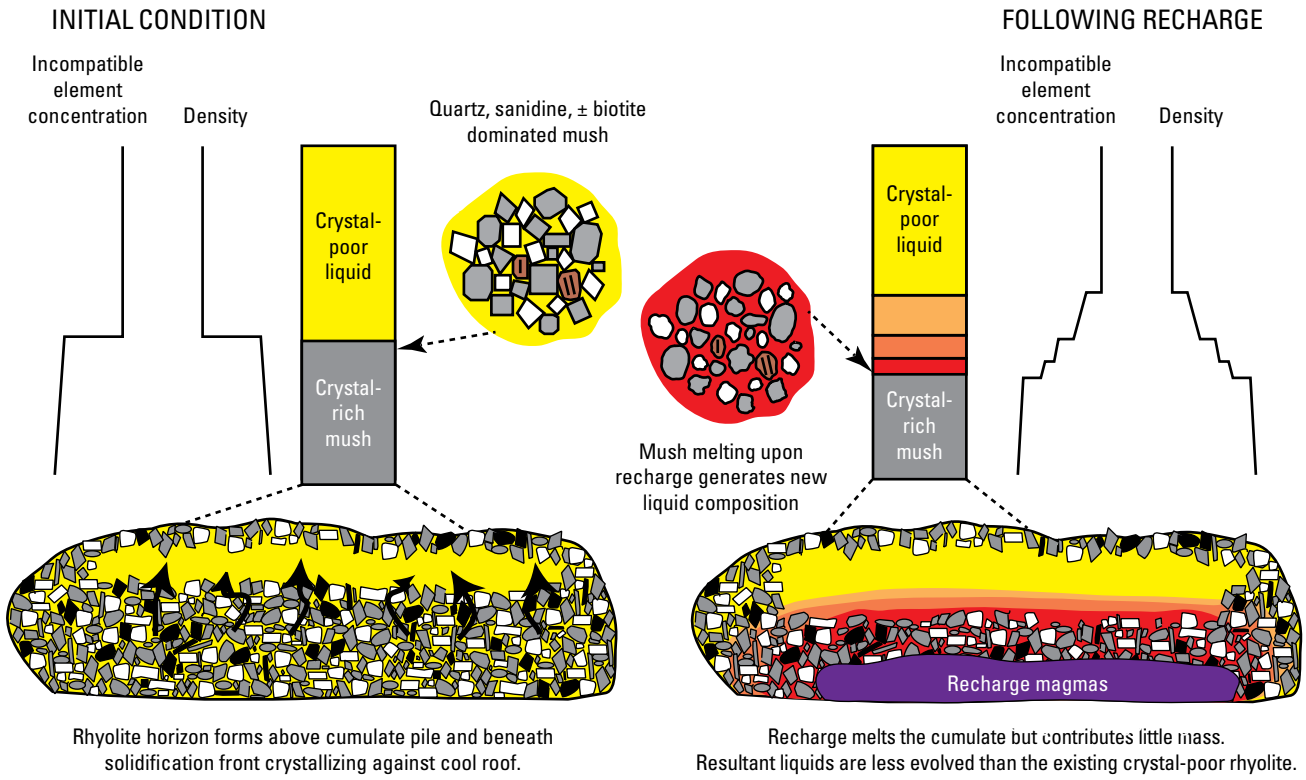

Figure 12. A model for the generation of compositional zoning in silicic magmas based on composition and mineral-melt relations in the Otowi Member and other zoned tuffs, from Wolff and others (2015). The initial condition is a melt lens sandwiched between cognate cumulate crystal mush and an upper solidification front (Bachmann and Bergantz, 2004), shown on the left. The interface between the melt lens (eruptible magma) and the cumulate is a large step in rheology, density, and trace element concentrations. The condition following an episode of recharge, heating, and melting is shown on the right. Melting of the fusible quartz + sanidine cumulate adds liquid of intermediate density and composition which pools at the interface, creating a column of zoned, eruptible magma. Escape of this liquid from the mush is enabled by the reduction in crystallinity due to melting. A single recharge melting episode will induce variable degrees of melting, and the new melt may also mix with the initial liquid lens, resulting in near-continuous zoning. Melting also results in partly resorbed crystals that, with time, may develop overgrowth rims (not shown) with enhanced concentrations of compatible elements grown from the new melt (Wolff and Ramos, 2014). Repeated recharge will tend to enhance these effects.

Figure 13. Mesas of Bandelier Tuff near Los Alamos, New Mexico. The skyline is dominated by Tschicoma Formation rocks. The variegated cliff-forming unit is the Tshirege Member; strata at the base of the nearest cliff are Valle Toledo pumice beds within the Cerro Toledo Formation and the Otowi Member forms the slopes. Photograph by John Wolff, Washington State University, 2016.

others, 2007; Brunstad, 2013; Wilcock and others, 2013; Goff and others, 2014), and only a brief summary is given here. The most recent $^{40}Ar/^{39}Ar$ eruption age determination of the Tshirege Member is 1.256±0.010 Ma (Phillips and others, 2007a).

The Tshirege Member is compositionally and mineralogically zoned and contains three distinct geochemical pumice types: high-silica rhyolite, dacite, and low-silica rhyolite. Phenocryst assemblages in the rhyolites are dominated by alkali feldspar, progressing from sanidine to anorthoclase upward through the unit. Similar to the Otowi Member, the high-silica rhyolite component shows systematic chemical and petrographic variation throughout the sequence, becoming less evolved and more porphyritic with eruption progress. It is also mineralogically similar to the Otowi Member, except that ilmenite and trace amounts of biotite are present, britholite has not yet been positively identified, and both allanite and zircon are more scarce. On the basis of oxygen isotopic disequilibrium, Wolff and others (2002) suggest that feldspar and quartz crystals in the earliest-erupted high-silica rhyolitic pumice were largely derived from a roofward crystalline carapace behind the upper solidification front of the magma body.

Dacite pumice becomes abundant about halfway above the base of the Tsankawi Pumice Bed but is present at low abundances throughout, mostly less than 1 percent but locally as much as 10 percent (Stimac, 1996). The dacite is typically found as monolithologic clasts. Sparse bomb- and block-shaped fragments and disaggregated streaks or bands of dacite pumice are observed as inclusions in high-silica rhyolite pumice. Dacite phenocrysts include plagioclase, hornblende, two pyroxenes, and biotite. Most groundmass displays a sugary texture owing to abundant plagioclase and hornblende microphenocrysts, although these are not ubiquitous. Xenocrysts of partly resorbed quartz and alkali feldspar derived from the host rhyolite are common. These observations are consistent with the dacite pumices being erupted enclaves, analogous to mafic inclusions found in granites and silicic lava domes (Stimac, 1996), that mingled with high-silica rhyolite shortly before or during eruption. The dispersal of the dacite through the Tshirege Member suggests that it formed a laterally restricted plume in the zoned, crystal-poor rhyolite magma layer sometime prior to eruption (Stimac, 1996) after punching through a mush zone where it entrained quartz and alkali feldspar xenocrysts. Zoning and textural relations among feldspars and other phenocrysts in the dacite record an earlier history of mixing and (or) crystal transfer involving more mafic magma (Boro and others, 2016). Previous workers have noted that the dacite pumice is mineralogically and chemically similar to the Tschicoma dacites (Smith and Bailey, 1966; Stix and others, 1988); however, lead isotope ratios of the dacite pumice ($^{206}Pb/^{204}Pb$ = 17.89) lie well outside the range of the Tschicoma rocks ($^{206}Pb/^{204}Pb$ = 17.12–17.64; Rowe and others, 2007) and instead resemble the Tshirege high-silica rhyolite ($^{206}Pb/^{204}Pb$ = 17.90–18.02; Skuba, 1990).

Low-silica rhyolite pumice is absent from Tsankawi Pumice Bed fallout and early-erupted Tshirege flow units but dominates in some of the upper flow units (Goff and others, 2014). Late-erupted glomerocrysts include some of syenitic composition, dominated by feldspar and lacking quartz. The low-silica rhyolite additionally contains plagioclase, hornblende, and biotite, and lacks REE-phases.

Goff and others (2014) provide a detailed study of field relations and mineralogical and compositional variations in the Tshirege Member within the caldera. They identify a vent breccia for a late-stage low-silica rhyolite unit on the resurgent dome, and show that the overlying, very last-erupted part of the Tshirege Member consists of high-silica rhyolite; hence, the upper Tshirege is reversely zoned. The low-silica rhyolite unit contains a minor, juvenile component of andesite, representing a recharge magma; its relation to the dacite is unclear. Goff and others (2014) also suggest that multiple vent transitions occurred between centrally located and ring-fracture-zone vents in the following sequence: (1) central (Tsankawi), (2) ring fracture, (3) central, (4) ring fracture.

Valles Rhyolite

This formation includes all of the rocks erupted from the caldera after the Tshirege Member. The earliest postcaldera lavas and tuffs, the Deer Canyon and Redondo Creek Members, are respectively high silica- and low-silica rhyolite, with some affinities to the respective pumice populations in the Tshirege Member (Phillips and others, 2007b). Both units were emplaced on and around the resurgent dome and are deformed; the Deer Canyon Member appears to have been emplaced before most of the structural resurgence, whereas the Redondo Creek Member was emplaced synresurgence. $^{40}Ar/^{39}Ar$ dates are statistically indistinguishable from the age of the Tshirege Member (Phillips and others, 2007a,b).

Subsequent high-silica rhyolite lavas and tuffs of the Valles Rhyolite are undeformed and were emplaced in the moat between the caldera wall and the resurgent dome (fig. 3*C*); this distribution has long been interpreted to trace the ring fracture of the caldera (Smith and others, 1970). The lavas consist of multiple extrusions and several have accompanying pyroclastic deposits (Goff and others, 2011). There is a rough, but not completely monotonic, temporal trend of counterclockwise emplacement of these lavas: Cerro del Medio Member, 1.23–1.17 Ma; Cerros del Abrigo, 0.97 Ma; Cerro Santa Rosa, 0.94–0.79 Ma; Cerro San Luis, 0.80 Ma; Cerro Seco, 0.80–0.77 Ma; San Antonio Mountain, 0.56 Ma; South Mountain, 0.53–0.52 Ma (Spell and Harrison, 1993; Phillips and others, 2007a; Kelley and others, 2013). Mineral assemblages are similar to that of the Bandelier Tuff, although the ubiquitous presence of hydrous pheno crysts (biotite and[or] hornblende) is notable. Trace element abundances are similar to, but differ in detail from the Bandelier high-silica rhyolites. The extreme enrichments in incompatible elements seen in the first-erupted parts of the Otowi and Tshirege Members have not been found in any high-silica Valles Rhyolite (Spell and Kyle, 1989); their

isotopic character is more crustal than that of the Bandelier Tuff (fig. 9).

Following a near half-million-year hiatus, East Fork Member eruptions from El Cajete crater in the south caldera moat produced a series of petrologically distinct, low-silica rhyolitic Plinian deposits, ignimbrites, and lava extrusions between 74 and 68 ka (Wolff and others, 2011; Zimmerer and others, 2016). The El Cajete Pyroclastic Beds, Battleship Rock Ignimbrite, Banco Bonito Flow, and VC-1 rhyolite that make up the East Fork Member (fig. 8) contain a complex crystal cargo (Wolff and Gardner, 1995). The mineral assemblage is dominated by strongly resorbed grains of plagioclase (An_{16}–An_{51}) as much as 3 millimeters (mm) in length, with lesser amounts of quartz, hornblende, biotite, hypersthene, augite, olivine, magnetite, ilmenite, and accessory apatite and zircon in high-silica rhyolite glass (76.0–77.8 weight percent SiO_2). Quartz grains are invariably resorbed and mafic minerals show complex overgrowth relations; commonly, biotite is overgrown by hornblende. Crystal aggregates containing plagioclase, biotite, and pyroxene ± quartz are also characterized by hornblende replacement of biotite to varying degrees. The resorption relations and the replacement of biotite by hornblende strongly suggest that much of the East Fork Member magma was being heated up until the time of eruption. Small euhedral grains of plagioclase and hornblende, lacking reaction or resorption textures, are scattered throughout the high-silica rhyolite matrix glass. Banded mingled pumices are a rare component of the East Fork pyroclastic deposits. The brown glass component in these is less silicic (72.5–76.0 weight percent SiO_2) than the prevalent colorless glass. Associated with this brown glass is a crystal population characterized by magnesium-rich pyroxenes (Mg#≤78), titanomagnetite with as much as 2.3 weight percent Cr_2O_3, and olivine (Fo_{74}). Wolff and Gardner (1995) interpreted these crystals and glass as representatives of a mafic magma of probable basaltic andesite composition. In summary, the East Fork Member rocks were generated by remobilization of crystalline, or near fully crystalline, granodiorite shortly before eruption resulting from heating by injection of mafic magma. Detailed U/Th dating of zircons indicates that generation of the magma body may have been initiated as early as 350 ka (Zimmerer and others, 2016).

Nonetheless, it is notable that the only comparable hiatus in the eruptive history of the entire JMVF appears to be the ~0.5 m.y. gap between the Bearhead Rhyolite and Tschicoma Formations (fig. 5). The long gap between South Mountain and East Fork Member eruptions led Wolff and Gardner (1995) to suggest that the latter may represent the onset of a new, long-term eruptive cycle at the Valles Caldera. In this context, geophysical investigations have detected the presence of a minimum of 10 percent melt within seismically anomalous crust between 5 and 15 km depth beneath the caldera (Steck and others, 1998). Consequently, the East Fork Member deposits have consequently been used to inform volcanic hazard prediction models of future comparable rhyolitic eruptions from the Valles Caldera (Alcorn and others, 2013).

Storage Temperatures and Pressures of Tewa Group Rhyolitic Magmas

Some attempts have been made to determine the depths and temperatures of the Tewa Group magma chambers using mineral thermometers (Warshaw and Smith, 1988; Wilcock and others, 2013) and structural models (Marsh, 1984; Nielson and Hulen, 1984). Here, we note that phase relations in the system Q–Ab–Or demand that high-silica rhyolites with quartz and alkali feldspar phenocrysts equilibrate at shallow crustal pressures (<300 megapascals [MPa]), because increasing pressure drives the minimum away from the Q corner of the ternary diagram (Tuttle and Bowen, 1958; Gualda and Ghiorso, 2013). Most Tewa Group high-silica rhyolites have compositions implying residence at 150–250 MPa, and temperatures corresponding to the minimum under water-saturated conditions (~700–750 °C). These pressure estimates are consistent with geophysical evidence for the depth of present-day melt beneath the caldera (Aprea and others, 2002). Mineral temperatures extracted from the less evolved rhyolites are as high as 850 °C (Warshaw and Smith, 1988; Phillips and others, 2007b). Titanium-in-quartz thermometry supports the existence of thermal gradients in the Tshirege Member magma body (Wilcock and others, 2013), although the strong dependence of quartz titanium contents on crystal growth rate means that results from this thermometer should be treated with great caution (Huang and Audétat, 2012). Thermal and chemical gradients in the two zoned members of the Bandelier Tuff are attributed to heat influx by recharging mafic magma and consequent melting of quartzofeldspathic cumulates (Wolff and Ramos, 2014; Wolff and others, 2015).

Hydrothermal Systems of the Valles Caldera and JMVF

The JMVF has a long history of hydrothermal activity associated with magmatism. Although earlier hydrothermal alteration has been partly overprinted and somewhat obscured by the modern (in other words, postcaldera) activity, there is evidence for a widespread event affecting rocks both north and south of the present caldera at about 8 Ma (Woldegabriel, 1990; Goff and others, 1992). Keres Group rocks near the Cochiti gold mining district display considerable argillic, phyllic, and propylitic alteration, dated to between 6.5 and 5.6 Ma (Woldegabriel and Goff, 1989), overlapping late Bearhead Rhyolite-Peralta Tuff activity. Oxygen isotope ratios decrease systematically from magmatic values as the rocks approach the zone of most intense alteration at Cochiti. The Bearhead magma system, which underlies an area similar to that of the Tewa Group magma chambers, was apparently the heat source for a major mineralizing meteoric-hydrothermal system.

The present-day system was initiated soon after eruption of the Tshirege Member, leading to widespread and intense alteration of prevolcanic and JMVF rock formations within and around the caldera. Fumaroles and acid springs

characterize surface outflow within the caldera in the area of Sulphur Springs. Subsurface activity in the caldera consists of a liquid-dominated, neutral-chloride geothermal reservoir. Several hot and warm springs and fumaroles are present in Cañon de San Diego southwards to Jemez Springs, the surface expression of a hydrothermal plume flowing out of the caldera along the Jemez fault zone (Goff and others, 1988). Travertine deposits near Jemez Springs have been dated between ~1 Ma and the present by ^{234}U and U/Th-series disequilibrium methods (Goff and Shevenell, 1987).

The hydrothermal systems and altered rocks of the Valles Caldera were the subject of intense investigations during the 1980s, including two Continental Scientific Drilling Project coreholes, VC-2A and VC-2B, drilled at Sulphur Springs. The results of these investigations have been ably summarized by Goff and others (1992) and Goff and Gardner (1994).

Day 1—Route Through the Jemez Mountains Volcanic Field and Valles Caldera

Mileage

0.0 *Trip begins (0 miles [mi]) at the intersection of New Mexico State Road (NM) 30 and NM 502. Coming from Santa Fe on NM 502, reset your trip odometer to 0 mi as you pass under the NM 30 bridge. To reach Stop 1-1, drive 0.6 mi (0.97 km) and pull over at the entrance to Guaje Canyon Road, in front of the locked gate by the water tank. Beyond the fence is Native American tribal land which is not accessible without permission—please do not leave parked cars blocking the gate.*

0.6 **Stop 1-1. Overview of Puye Formation and Cerros del Rio Basalt** (35°53.04' N., 106°9.83' W.; 5,692 feet [ft], 1,735 meters [m] elevation)

At this stop, Puye Formation conglomerates, gravels, and sands rest on Chamita Formation (upper Santa Fe Group) fluvial gravels (fig. 14). This location is several kilometers from the source area of the Tschicoma Formation highlands, and the Puye Formation here is dominated by fluvial and sheetflood deposits, with fewer debris flows than farther west. South of the road, a Cerros del Rio hawaiite flow caps Puye gravels.

To reach Stop 1-2, drive 2.5 mi (4.0 km) up the road and park on the broad shoulder. Do not step onto the busy road or attempt to cross the highway! Do not climb above the roadway-it is tribal land. The base of the Guaje Pumice Bed is seen here; to examine the upper bedded units of the Guaje, walk a few hundred meters up the road.

3.1 **Stop 1-2. Guaje Pumice Bed resting on Cerros del Rio lava** (35°52.07' N., 106°12.03 ' W.; 6,283 ft, 1,915 m elevation)

The road has climbed onto Cerros del Rio tholeiitic lava (basalt of White Rock) dated at 2.33 Ma. The lava is capped by a discontinuous soil containing basalt fragments overlain by fall unit A of the Guaje Pumice Bed. This was the first magma vented during the eruption of the Otowi Member of the Bandelier Tuff, and it is highly enriched in incompatible trace elements. The overlying bedded fall units, B through E (fig. 15), are compositionally zoned and emplaced coevally with ~400 km^3 of ignimbrite and fine ash distributed around the Jemez Mountains, Valles Caldera, and further afield. At this location the overlying Otowi ignimbrite units were emplaced later in the eruption; pumice fragments have a broad range of trace element abundances, but the flows are not systematically zoned. Further upslope, the Otowi Member is capped

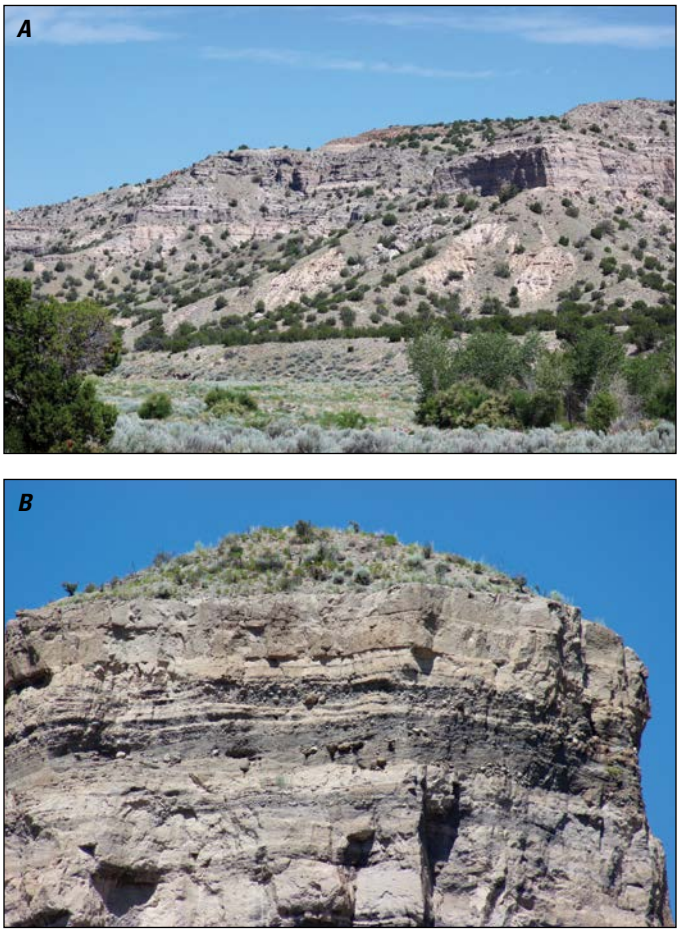

Figure 14. *A*, Puye Formation gravels and conglomerates (gray, coarser grained) resting on Chamita Formation sediments (pale pink, finer grained) on the north side of Guaje Canyon, viewed from Stop 1-1; the contact is about halfway up the slope. The sequence is capped by Bandelier Tuff. *B*, Closeup of Puye Formation gravels and conglomerates at Stop 1-1. Photographs by John Wolff, Washington State University, 2016.

Figure 15. The upper part of the Guaje Pumice Bed at Stop 1-2. The base of the hammer handle rests on the top of fall unit A; the hammer head rests on fall unit B. The stratified fallout pumice, deposited by eruptions of Plinian intensity (Self and others, 1986, 1996) consists of units B–E and is compositionally zoned. On the basis of chemical and petrographic similarity, it is equivalent to the bulk of the Otowi ignimbrites found around and within the Valles Caldera. In this area, the overlying nonwelded Otowi ignimbrites are the products of late eruptions from vents in the northeast part of the caldera. Photograph by John Wolff, Washington State University, 2016.

by the 1.24 Ma Tshirege Member of the Bandelier Tuff, including its basal fallout Tsankawi Pumice Bed.

To reach Stop 1-3a, continue on NM 502 and take the fork to Los Alamos. Proceed up the hill for 2.3 mi (3.7 km), noting the sequence in the roadcut to your left (south): pale tan Otowi ignimbrite overlain by Cerro Toledo and Tsankawi pumice beds and Tshirege ignimbrite, which grades upwards from white and nonwelded tuff through vitric orange tuff and gray sillar to more densely welded tuff forming the mesa top. Pass the large Clinton P. Anderson overlook pullout and park in the small pullout near the top of the grade, overlooking a small box canyon tributary to Pueblo Canyon.

5.4 **Stop 1-3a. Cerro Toledo Formation exposed between both Otowi and Tshirege Members of Bandelier Tuff** (35°52.37’ N., 106°14.34’ W.; 6,824 ft, 2,080 m elevation)

Look down into the head of the box canyon (fig. 16*A*). The Tshirege Member rests on a surface cut through the Cerro Toledo Formation and the Otowi Member. Thin discontinuous Tsankawi pumice partly coats the downcut surface. There are five Valle Toledo Member pumice fallout units, separated by orange bioturbated sediments and soils. The lowest of these is interpreted to represent the closing stage of the Otowi eruption. The Valle Toledo deposits may be seen in greater detail at optional stop 1-3b (fig. 16*B*).

To reach Stop 1-3b, proceed along NM 502 for 0.6 mi (0.9 km) and turn right onto Eastgate Drive into the small industrial park just east of the Los Alamos airport. Walk between the sheds at the east end of the park and about 0.2 mi (300 m) to the tip of the mesa, then follow the trail down to your right where it is cut into soft sillar of the Tshirege Member. When you reach the orange to white nonwelded vitric tuff at the base of the Tshirege Member, leave the trail and follow the contour around to the south until you are in the box canyon.

Figure 16. *A*, View from Stop 1-3a of the Otowi (white, slope-forming) and Tshirege Members (gray to salmon-colored, cliff-forming) of the Bandelier Tuff and the intervening Cerro Toledo Formation (stratified). Note downcutting of a canyon through the Cerro Toledo and Otowi prior to filling by emplacement of the Tshirege Member. Several zones of welding induration can be seen in the Tshirege; the lower pale gray to salmon-colored part is vitric; above that the tuff is largely recrystallized. *B*, Close-up of relations at Stop 1-3a. Note remnant lenses of the Tsankawi Pumice Bed mantling the slope cut into the Cerro Toledo Formation, largely removed by Tshirege pyroclastic density currents. Five pumice fallout beds make up the Valle Toledo Member of the Cerro Toledo. The lowest of these, in which small caves are developed, rests directly on the Otowi above a co-ignimbrite ash (thin white layer in shadow at left-center of photograph) and is interpreted as the final deposit from the Otowi eruption. Photographs by John Wolff, Washington State University, 2016.

6.0 Stop 1-3b. Outcrop examination of deposits seen from Stop 1-3a (35°52.53' N., 106°14.91' W.; 6,923 ft, 2,110 m elevation)

The top of the Otowi Member has been eroded away over nearly all of its extent. This is one of the few places where the depositional top may be seen. Typical ignimbrite consisting of coarse pumice and lithic clasts dispersed in a matrix of fine ash gives way in the uppermost 70 cm to a pyroclastic, surge-like facies with fine bedding and crossbedding, interpreted as the deposit from a dilute pyroclastic density current that was running out of material. This in turn is overlain by 7.5 cm of normally graded, very fine ash containing occasional millimeter-size pumice, interpreted as a coignimbrite ash. At the contact with the overlying crystal-rich pumice fallout deposit, loading of the fine ash and occasional sunken lithics are clearly seen, indicating that the ash was still uncompressed when the coarser material was deposited; the fallout is therefore interpreted as the closing event of the Otowi eruption. This interpretation is strengthened by the chemical continuity between the Otowi Member and the fallout pumice. The fallout is overlain by repeated alternations of thin (≤7 cm) crossbedded ashes with thicker (9–50 cm) fallout deposits. Some of the crossbedded ashes contain plant fragments and rootlets. The fallout deposits increase in crystal content upwards and are chemically continuous with Otowi pumice; hence, this sequence represents the very last expulsion of Otowi magma. The entire 1.9-m-thick sequence above the coignimbrite ash is capped by reworked pumice and a 40-cm-thick soil containing roots and burrows. Above the soil are at least four more Valle Toledo fallout deposits separated by reworked intervals and soils, frequently burrowed, with an aggregate thickness of ~6 m and capped by the Tsankawi Pumice Bed and Tshirege ignimbrite.

Continue mileage at the entrance to Eastgate Drive (6.0 mi [9.5 km]). Proceed 4.1 mi (6.6 km) past the airport through the town of Los Alamos, taking Trinity Drive, to the intersection with Diamond Drive (10.1 mi [16.1 km]). To reach optional Stops 1-4 and 1-5, turn right on Diamond Drive. To proceed to Stop 1-6, turn left on Diamond Drive.

To reach Optional Stop 1-4 from the Trinity Drive-Diamond Drive intersection, proceed north on Diamond Drive for 1.3 mi (2.1 km) to the intersection with Arkansas Avenue/38th Street, where there is a gas station. Turn right on 38th Street, then left on Villa Street and drive for 5 blocks. Turn left on 33rd Street, then right on Walnut Street Follow Walnut Street to its end at the playlot and park in front of the playlot (12.6 mi [20.2 km]). Walk past the playlot and through the gate at the far end, turn left, and follow the trail downhill. Turn left on the dirt road and walk for ~164 yd (150 m), then turn right onto the road running downhill through a gate. Walk ~87 yd (80 m) and turn left across the footbridge, following the "East Fork Trail." Follow this switchback trail to the canyon bottom and walk down canyon on the dirt road for ~219 yd (200 m). Halt and look up to your left. ***This may be impassable during flash flood conditions****.*

Optional Stop 1-4. Cerro Toledo Formation (35°53.46' N., 106°18.28' W.; 7,218 ft, 2,200 m elevation)

At this stop (fig. 17) a thick sequence of interbedded Cerro Toledo Formation sediments (Pueblo Canyon Member) and interbedded primary pumice fallout (Valle Toledo Member) deposits rests on Tschicoma Formation lava; the Otowi Member is absent but is exposed a short distance away. The Pueblo Canyon Member consists of deposits of fluvial systems that drained the Tschicoma Formation highlands in the ~360,000 year period between the eruption of the two members of the Bandelier Tuff. They represent a continuation of Puye-type sedimentation, and indeed the sandstones and conglomerates resemble those of the Puye Formation, but also contain significant components of reworked Otowi Member tuff and Valle Toledo tephra (Gardner and others, 2010). The proportion of sediment to primary tephras in the Cerro Toledo Formation varies greatly from place to place; contrast this location, in a paleocanyon bottom, with the mesa-top location of Stop 1-3b.

To reach Optional Stop 1-5, return to Diamond Drive (1.2 mi, 1.9 km from the playlot) and turn right. Proceed past the golf course and at the roundabout turn left onto San Ildefonso Road. Turn left onto Rendija Canyon Road (15.5 mi, 24.9 km). Follow Rendija Canyon down to the bottom where it joins Guaje Canyon (19.2 mi, 30.8 km); turn left on Guaje Canyon Road by the water tank.

Figure 17. Cerro Toledo Formation at Stop 1-4 , dominated by Pueblo Canyon Member sediments with interbedded Valle Toledo tephras. The section is capped by the Tshirege Member. Photograph by John Wolff, Washington State University, 2016.

Note that Rendija Canyon affords several opportunities to stop and examine the Puye Formation gravels and conglomerates (fig. 18*A*), and occasional primary pyroclastic deposits, more closely than was possible at Stop 1-1.

Guaje Canyon may be impassable during flash flood conditions. *Proceed up Guaje Canyon for 0.6 mi (0.9 km) and turn right over the water crossing and up the grade.* ***This road is only suitable for high-clearance or 4-wheel drive vehicles.*** *At the top of the grade, follow the road around to the left, drive for ~328 yd (300 m) to a broad pullout area and park. Follow the old road to your right, on foot through the fence to the pumice quarry areas.*

21.5 **Optional Stop 1-5. Guaje pumice mine** (35°55’ N., 106°13.53’ W.; 6,709 ft, 2,045 m elevation)

This is the type locality for the Guaje Pumice Bed, the opening phase of the Otowi eruption, as originally defined by Bailey and others (1969). The appearance and chemical zonation of the Guaje Pumice Bed is similar to that at Stop 1-2. Notable here, however, are prominent coarse pumice swarms and rare log molds at the base of the Otowi pyroclastic flow deposits (fig. 18*B*). The swarms yield occasional white-and-gray banded pumice clasts. The gray component contains a high proportion of country-rock granite, indicated by strongly elevated $^{87}Sr/^{86}Sr$ ratios, and fragments of microcline (Wolff and Ramos, 2014).

Return to Los Alamos. Mileage continues from the intersection of Trinity Drive and Diamond Drive, EXCLUDING optional stops 1-4 and 1-5.

To reach Stop 1-6, turn left onto Diamond Drive (if coming from Stop 1-3a or 1-3b), or continue on Diamond Drive (if coming from Stop 1-4 or 1-5). Follow the road across the bridge and through the security checkpoint (be prepared to show photo identification at the checkpoint). Continue onto West Jemez Road past Los Alamos National Laboratory to the T-junction at the old Back Gate (15.1 mi [24.2 km]) and turn right onto NM 4 up the hill.

The first tight hairpin turn is where the road crosses the basin-bounding Pajarito Fault, which here offsets the 1.24 Ma Tshirege Member of the Bandelier Tuff by >150 m. The road continues to climb the flanks of the Jemez Mountains; to the south the prominent hill of St. Peter’s Dome, a kipuka of Paliza Canyon Formation and older rocks surrounded by Bandelier Tuff can be seen. The road crosses a pass into the caldera between two forested hills of Tschicoma Formation dacite. *Park at the second pullout area (8.3 mi [13.3 km] from the Back Gate) that offers a view over Valle Grande and Redondo Peak.*

Figure 18. *A*, Boulder-capped tent rocks of Puye Formation conglomerates in Rendija Canyon. *B*, Guaje Pumice Bed and late-stage Otowi Member ash flows at the Guaje Pumice Mine. This is the same sequence as seen at Stop 1-2. Here, Guaje Unit A is >8-meters thick. Note the coarse pumice swarm at the base of the ignimbrite. Photographs by John Wolff, Washington State University, 2016.

23.4 **Stop 1-6. Valles Grande Overlook** (35°51.03’ N., 106°27.58’ W.; 8,711 ft, 2,655 m elevation)

From here the view to the northwest is dominated by the Redondo resurgent dome (fig. 3). The Valles Caldera is the type area for postcaldera structural resurgence. Here, the top of the resurgent dome stands 840 m above the present caldera floor. The dome consists of deformed Bandelier Tuff (both members), diverse caldera-collapse breccias, lava extrusions preceding and accompanying resurgence (Deer Canyon and Redondo Creek Members of the Valles Rhyolite), and tilted early lake sediments (Goff and others, 2011). Resurgence was complete within 27 ka of the Tshirege eruption (Phillips and others, 2007a). Also visible from here are several members of the Valles Rhyolite. To the north are the postresurgence lava flows, domes, and coulées of the Cerro del Medio, Cerros del Abrigo, and Cerro Santa Rosa Members, and in the foreground is the small dome of La Jara, a part of the South Mountain Member (fig. 3).

South Mountain itself is the sloping flat-topped mountain to the west; the main mass of South Mountain lava flows extend out of view several kilometers westward along the southern moat of the caldera to the head of Cañon San Diego. Several sectors of the caldera wall can also be seen; the immediate sector, to the southeast, is occupied by Rabbit Mountain, an obsidian dome of the Valle Toledo Member that was partly destroyed during the Tshirege eruption and Valles Caldera collapse.

To reach Stop 1-7, proceed on NM 4 along the edge of Valle Grande and into the southern moat area of the caldera. Park in the pullout area opposite the large roadcut through the El Cajete Pyroclastic Beds, which rest on South Mountain lava (5.5 mi [8.9 km] from Stop 1-6).

28.9 **Stop 1-7. Lower El Cajete Pyroclastic Beds** (35°48.91' N., 106°32.42' W.; 8,563 ft, 2,610 m elevation)

At this stop, products of the first phase of the East Fork Member eruptions, the last major activity of the Valles Caldera, are exposed about 3 km southeast of the vent area of El Cajete crater. Units A through D of the El Cajete Pyroclastic Beds (Wolff and others, 2011) rest on South Mountain rhyolite lava (fig. 19*A*). Log molds, some containing remnant charcoal, are prominent in pyroclastic surge bed C. The East Fork Member activity postdates the remainder of the Valles Rhyolite postcaldera lavas by 0.45 m.y. Like the remainder of the East Fork Member units (Battleship Rock Ignimbrite and Banco Bonito Flow), the El Cajete has a complex crystal cargo, with resorbed quartz and sodic plagioclase phenocrysts and biotite reacting to hornblende, accompanied by magnesian pyroxenes and ~Fo_{70} olivine. These relations have been interpreted as representing remobilization of pre-existing, solid or near-solid but still warm, plutonic rock beneath the caldera, perhaps signaling the onset of a new cycle of rhyolitic activity (Wolff and Gardner, 1995).

Proceed westwards on NM 4, passing several more roadcuts through the El Cajete Pyroclastic Beds. Drive 4.0 mi (6.5 km) and park in the pullout on the left of the road, just before the Jemez Falls Road turn-off. Walk back down the road to a point opposite the east end of the retaining wall, cross the roadcut and go through the narrow gap at the end of the wall. ***Caution, this is a very busy road. Please take care crossing the road!***

32.9 **Stop 1-8. Upper El Cajete Pyroclastic Beds and Banco Bonito Flow** (35°49.69' N., 106°35.71' W.; 8,022 ft, 2,445 m elevation)

Here, the Lower El Cajete Pyroclastic Beds are reworked but the exposure behind the wall offers a near-complete section through the upper El Cajete; the photograph in figure 19*B* was taken before the retaining wall was built. In contrast to Stop 1-7, the sequence here is dominated by nonwelded pyroclastic flow deposits, interpreted to be equivalent to Battleship Rock Ignimbrite (Wolff and others, 2011). The sequence can be seen pinching out against a steep surface caused by South Mountain lava at the east end of the exposure. These units are overlain by a conglomerate, followed by gravels related to emplacement of the Banco Bonito Flow, and finally vitrophyre and rhyolite blocks representing the marginal breccia of the lava itself. Approximately 6,000 years elapsed between the emplacement of the pyroclastic units and the lava (Zimmerer and others, 2016).

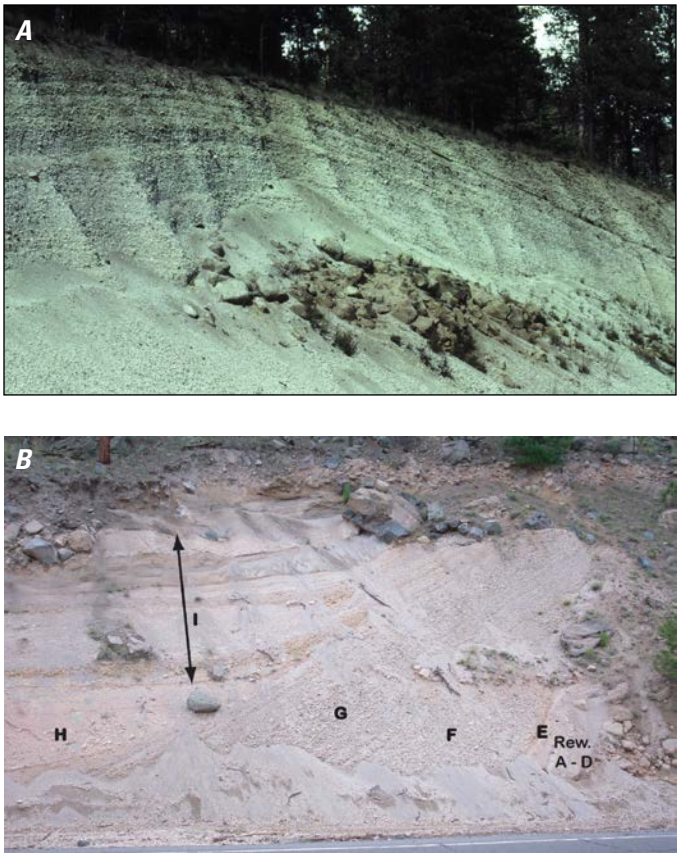

Figure 19. *A*, Units A, B, C, and D (Wolff and others, 2011) of the lower El Cajete Pyroclastic Beds resting on South Mountain Rhyolite lava at Stop 1-7. Unit C is the thin surge-like layer with log molds. *B*, Units of the upper El Cajete Pyroclastic Beds at Stop 1-8; letters are the unit designations of Wolff and others (2011). Note that fallout units F and G are draped over South Mountain Member lava to the right, whereas ignimbrite unit H pinches out against the slope. Rew., reworked. Photographs by John Wolff, Washington State University, 2016.

Continue along NM 4. The road passes a cut in Battleship Rock Ignimbrite containing coarse lithic breccias and then climbs onto the surface of the

Banco Bonito Flow for a few miles. Follow the highway just past the junction with NM 126 and turn right onto Mica Road (5.6 mi [9.0 km] from Stop 1-8). Proceed along Mica Road for 0.15 mi (0.24 km) and turn right onto Obsidian Road. Follow this for 0.4 mi (0.6 km) and make a sharp right onto Beryl Road. Follow Beryl Road 1.3 mi (2.1 km) to its end at a turnaround past the prominent tent rocks (7.5 mi [12.0 km] from Stop 1-8). Walk down the grade to the tent rocks. ***The last (~0.33 mi [600 m] of the road includes travel up a dirt grade and is not advisable for vehicles with poor ground clearance; park at the bottom by the tent rocks instead.***

40.4 **Stop 1-9. Section through the Bandelier Tuff including the La Cueva Member** (35°52.27' N., 106°39.43' W.; 8,317 ft, 2,535 m elevation)

Here, at the southwest margin of the caldera, a near-complete section through the Bandelier Tuff, redefined by Gardner and others (2010) to include the early La Cueva Member (formerly the San Diego Canyon ignimbrites), is well displayed in near-continuous roadcuts. La Cueva unit A is thick (>20 m, fig. 20); unit B is represented by a thin, partly reworked layer, but is observable in the tent rocks to the southwest of the section. Both the Guaje Pumice Bedand the Valle Toledo tephras, dispersed to the east of the caldera, are absent. The Otowi Member here is more than 13-m thick and is characteristically nonwelded and moderately lithic-rich, with a soil developed on the top surface.

The Tsankawi Pumice Bed is well-developed here; although the location is not on the dispersal axis, the Tsankawi is very broadly dispersed, the product of an exceptionally violent Plinian eruption (Self and others, 1986, 1996). This location lies approximately on the 3-m isopach (Self and others, 1996) indicating that about half the thickness was removed as a result of erosion by early Tshirege flows, a common feature on all sides of the caldera. The basal 20 cm of the Tsankawi is finer grained; it is in this interval that oxygen isotope disequilibrium between quartz and feldspar is most marked, leading Wolff and others (2002) to propose that the crystals in this earliest-vented magma of the Tshirege eruption were largely derived from a rigid crystal-rich cognate roof to the magma chamber. Early flow units are fine-grained and stratified with sedimentary structures, the products of relatively dilute (surge-like) pyroclastic density currents; again, this is a very typical feature of the Tshirege Member. Overlying massive, nonwelded pumice-rich ignimbrite grades into sillar (partly to wholly crystallized tuff lacking welding compaction).

Return to NM 4 and turn left, then left again onto NM 126. Follow the road as it ascends the west caldera wall through prevolcanic basement and precaldera Keres

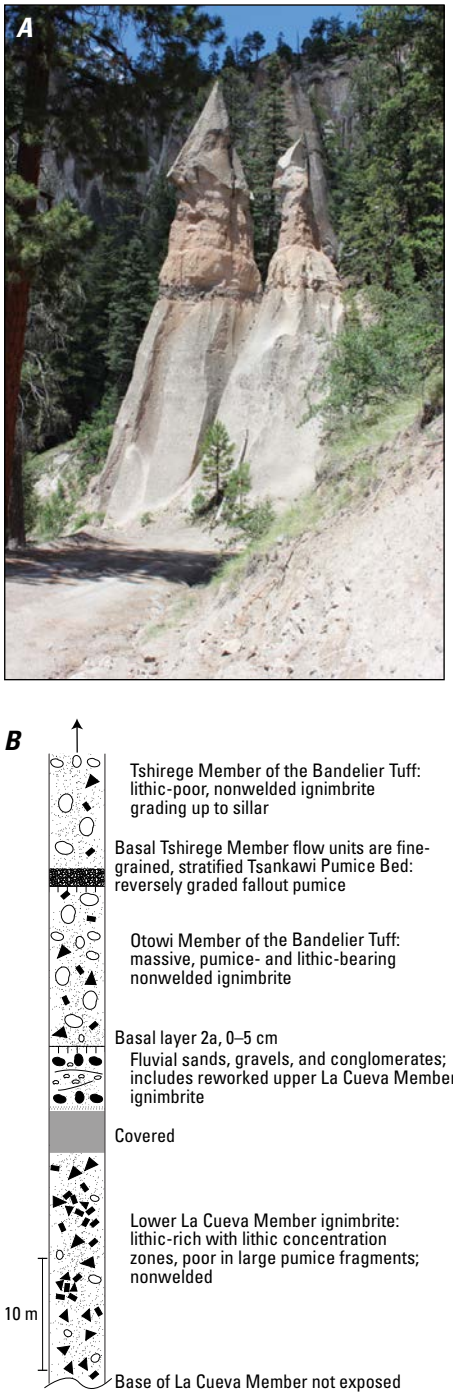

Figure 20. *A*, Tent rocks at the base of the section at Stop 1-9. The lower ~60 percent of the two prominent, sunlit tent rocks in the foreground consists of massive, lithic-rich ignimbrite—the lower of the two ignimbrite units in the La Cueva Member of the Bandelier Tuff. The upper of the two units is largely missing at this locality. Otowi Member ignimbrite forms the jutting caps of the two tent rocks, above the sedimentary interval. *B*, The section at Stop 1-9, showing all three members of the Bandelier Tuff. Cm, centimeters; m, meters. Photograph by John Wolff, Washington State University, 2016.

Group rocks (and much Quaternary colluvium) onto the Tshirege Member. Pull into the unmarked picnic area on the outside of the hairpin at the top of the grade (4.3 mi [7.0 km] from the junction of Mica Road and NM 4).

46.6 **Stop 1-10. Fenton Hill overlook** (35°52.5' N., 106°39.94' W.; 8,579 ft, 2,615 m elevation)

The viewpoint is on the lip of the east caldera wall, situated on Tshirege Member welded tuff. This vantage affords an overview of the southwestern part of the Valles Caldera. The high mountain to the east is Redondo Peak; the nearer ridge, not visible from Stop 1-6, is Redondo Border, the northwestern part of the resurgent dome. Separating the two is the apical graben of the dome. Almost the entire extent of the Banco Bonito rhyolite flow can be seen to the south of the resurgent dome; it forms a thick tongue filling the southern caldera moat, covering earlier East Fork Member units (Battleship Rock Ignimbrite and El Cajete Pyroclastic Beds) and South Mountain Member rhyolite. South Mountain itself is in the distance to the east-southeast. The peak in the southeast is Los Griegos, consisting of Paliza Canyon Formation andesite, although most of the caldera wall in that area has a coating of El Cajete fallout pumice. To the north-northeast is San Antonio Mountain, the youngest of the northern arc of Valles Rhyolite lavas; a coulée extends ~4 km south along the western moat from the vent area. The low ground between the nose of San Antonio Mountain and the Banco Bonito Flow consists of Redondo Creek Member rhyolite lava. The area of Sulphur Springs, the main surface expression of the active hydrothermal system within the caldera, lies in the western caldera moat between Redondo Border and San Antonio Mountain lava.

Continue on NM 126 past Fenton Lake. At 8.4 mi (13.5 km) from Stop 1-10, turn on to Forest Service Road (FS) 314 and drive just past the fish hatchery, parking at the pul-out at the base of the prominent pinnacle on the northwest side of the road.

55.4 **Stop 1-11. Densely welded Otowi Member at Seven Springs fish hatchery** (35°55.71' N., 106°42.08' W.; 7,940 ft, 2,420 m elevation)

Over most of its extent north, south, and east of the caldera, the Otowi Member is largely nonwelded. West of the caldera, on the Jemez plateau, it is densely welded for much of its preserved thickness. The prominent pinnacle varies from densely welded at the bottom to partly welded and vapor-phase altered (sillar) at the top. Fragments of densely welded Otowi Member may be collected from the talus adjacent to the parking area. The base is not exposed, but the Otowi in this area ponded in a paleocanyon and is in excess of 200 m thick. Possible reasons for the dense welding are rapid deposition and, perhaps, higher magmatic temperature; the Otowi here, although compositionally zoned, is not as strongly differentiated and enriched in incompatible elements as elsewhere.

Retrace by way of NM 126 and NM 4 through and out of the caldera towards Los Alamos. At the Back Gate, do not turn onto NM 501 (W. Jemez Road), but continue down the hill towards White Rock. In the town of White Rock, turn right onto Rover Boulevard and then left onto Meadow Lane, following the signs to Overlook Park. Turn left onto Overlook Road and follow the road to its end (43.3 mi [69.7 km] from Stop 1-10). Park and walk to the deck overlooking White Rock Canyon.

98.7 **Stop 1-12. White Rock overlook** (35°49.57' N., 106°10.83' W.; 6,234 ft, 1,900 m elevation)

This viewpoint (fig. 21) affords an overview of the western basin margin of the Española Basin where volcanic rocks of the JMVF are intercalated with sedimentary deposits of the Miocene to Quaternary rift basin (figs. 3*A*,*B*,*D*; 21*A*–*C*). Here, the Rio Grande carved a 275-m canyon through the overlying Pliocene to Pleistocene volcanic sequence exposing the Miocene to Pliocene sedimentary basin deposits beneath. Where volcanic deposits overlie largely unconsolidated sediments, landslide deposits are common and channel width increases, resulting in limited exposure of underlying sediments either high on colluvium covered slopes on canyon walls or low in the canyon between landslide lobes. Within the sedimentary basin-fill deposits the pink-orange, arkosic sandstones at river level are part of the Miocene Tesuque Formation and are overlying grey colored Chamita Formation sands and gravels; both formational units of the Santa Fe Group. At the base of the exposed section south of the overlook, Miocene basalts are exposed (Dethier, 1997) and are correlative with intercalated basaltic lava flows encountered in drill holes south and southwest of here on the Pajarito Plateau (see WoldeGabriel and others [2013] and references therein). These dated lavas provide the primary age constraints on sedimentary deposits underlying the plateau. Overlying sedimentary deposits in the canyon are basaltic to intermediate composition volcanic rocks of the Cerros del Rio volcanic field.

The Cerros del Rio volcanic field is a predominantly trachybasaltic to trachyandesitic volcanic plateau along the southeast flank of the Pajarito Plateau (fig. 3*D*). Locally, as observed at the overlook, tholeiitic basalts are also preserved but restricted to the northwest part of the field. Lavas and related pyroclastic deposits are exposed over 600 square kilometers (km^2) and reflect eruption of at least 180 km^3 of rift-related mafic magma, mainly between 2.7 and 1.1 Ma (Aubele, 1978; Dunker and others, 1991; Dethier, 1997; Sawyer and others, 2002; Thompson and others, 2006, 2011; Dethier and others, 2011). Most of the lava flows are of Pliocene and early Pleistocene age and predate the large-volume silicic caldera eruptions in the nearby Jemez volcanic system. However, late-stage eruptions from the Cerros del Rio volcanic field postdate eruption of the Tshirege Member of the Bandelier Tuff in the Jemez Mountains volcanic field and are preserved along the Rio Grande near the

south boundary of the Caja del Rio (Dethier and others, 2011). Most of the eruptive centers in the Cerros del Rio volcanic field are monogenetic central-vent volcanoes ranging from low-relief shield centers to remnants of steep-sided, breached cinder cones. These lavas have 49–64 weight percent SiO_2 and exhibit a strong correlation between landform and whole-rock chemistry. The low-silica, subalkaline basaltic lavas erupted from broad shield volcanoes and formed thin (<3–4 m) low-viscosity flows that traveled far; whereas transitional to mildly alkaline basalts and basaltic andesites formed thick (as much as 30 m) discontinuous lavas flows that erupted from high-relief, steep-sided vents. Dacitic lavas are related to late-stage dome growth and eruption of thick (as much as 50 m), even more viscous blocky lava flows that issued from one well-defined vent area at Tetilla Peak (Sawyer and others, 2002) and locally in tributary canyons of the Rio Grande, south of the overlook.

Volcanic deposits of the Cerros del Rio volcanic field are divided into a three-fold classification representing early, middle, and late phases of eruption that persisted from about 2.7 to 1.1 Ma. Volcanic units represent products of monogenetic eruptive centers of the early (>2.7–2.59 Ma), middle (2.59–2.1 Ma), and late (1.5–1.1 Ma) volcanic phases of Thompson and others (2006). These subdivisions are based on 1:24,000-scale geologic mapping, stratigraphic studies, $^{40}Ar/^{39}Ar$ geochronology, geochemistry, and paleomagnetic and aeromagnetic data.

West of the river, the sequence is unconformably overlain by the Bandelier Tuff, and Quaternary sediments that locally contain a component of Valles Rhyolite pumice. In the distance to the north is the isolated basaltic vent of Black Mesa, dated at 2.75 Ma. Closer to the observer is the Buckman Mesa vent, which consists of phreatomagmatic tephra, overlain by Strombolian-Hawaiian scoria and spatter, with a lava tongue extending southward. To the west, the skyline is dominated by the Tschicoma highlands and Redondo Peak in the Jemez Mountains.

End of route 1.

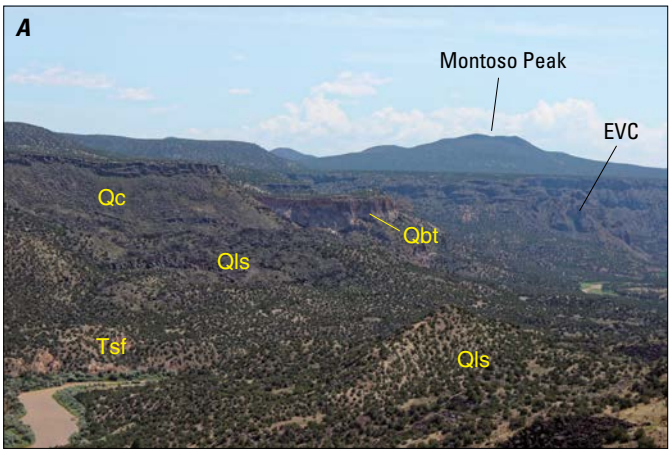

Figure 21. Views from White Rock overlook (Stop 1-12). *A*, View south along White Rock Canyon, to the northeastern part of the Pliocene to Pleistocene Cerros del Rio volcanic field. Here, the Rio Grande has incised a 275-meter-deep canyon through the west side of the volcanic field and underlying Santa Fe Group sediments. Flat lying lavas include trachybasalts and trachyandesites, likely derived from one of many deeply dissected volcanoes of the volcanic field, predominantly east of the Rio Grande (Thompson and others, 2006). The most prominent of these, Montoso Peak, rises 350 meters above the canyon rim. Abundant landslide deposits (Qls) flank both sides of the Rio Grande, although local deposits of Santa Fe Group sediments (Tsf) are observed in the lower left of the photograph. Colluvium-covered slopes beneath lava flows (Qc) typically overlie basin-fill sediments. Eroded near-vent deposits (EVC) are visible in the canyon wall in the middle-right of the image. Bandelier Tuff (Qbt) forms prominent cliffs in the middle of the image. *B*, View west from overlook toward tholeiite and basal pillow-palogonite delta carpet. Olivine tholeiites, characteristic of those exposed at the overlook, are preserved only on the west side of the river. Palagonite breccias, hyaloclastite, phreatomagmatic, and maar-like deposits are commonly found at the base of the basaltic section where lavas erupted through wet sediments and the high water table of an actively subsiding basin. *C*, View north, showing (youngest to oldest) Tshirege and Otowi Members of the Bandelier Tuff; Cerros del Rio lava; and colluvium covered slopes of the Santa Fe Group rift-basin sediments. Photographs by John Wolff, Washington State University, 2016.

Day 2—The Southern San Luis Basin and Taos Plateau Volcanic Field

By R.A. Thompson[1], K.J. Turner[1], M.A. Cosca[1], C.F. Chan[1], L.E. Morgan[1], M.A. Dungan[2], and B.J. Drenth[1]

Introduction

The San Luis Basin of the northern Rio Grande Rift has been the subject of multiple geologic excursions described in field guides published over more than three decades. Most notable among these are guides published by the New Mexico Geological Society in 1984 and 2004 in conjunction with the 35th and 55th annual field conferences (see Dungan and others, 1984; Read and others, 2004; and additional contributions within these volumes); the New Mexico Bureau of Mines and Mineral Resources (Dungan and others, 1989b), the United States Geological Survey (Machette and others, 2007) and the Geological Society of America (Ruleman and others, 2016). These guides all contain valuable information on the geology of the San Luis Basin not covered in this guide. The expansive guide by Dungan and others (1989b) focused on a 6-day excursion to the Taos Plateau, Ocate, and Clayton-Raton volcanic fields and was published in conjunction with the International Association of Volcanology and Geochemistry of the Earth's Interior meeting held in Santa Fe, New Mexico, in 1989. Day 2 and the first half of Day 3 of this guide offer a new perspective on the geology discussed in 1989, utilizing many of the stops originally presented on that trip.

In the intervening decades, considerable focus worldwide on the temporal evolution of rifts, rift magmatism, extensional tectonism, and the role of the lithosphere and asthenosphere in rift history provide expanded opportunities for revisiting this terrane. New data and interpretations bearing on the temporal evolution of faulting, basin development, range front uplift, and rift volcanism within the northern Rio Grande Rift provide the framework for the stops presented in the guide. The eruptive history of the Taos Plateau volcanic field, its tectonic evolution, and rift basin architecture is derived largely from new geologic mapping conducted by the United States Geological Survey (USGS) and the New Mexico Bureau of Geology and Mineral Resources funded by the USGS National Cooperative Geologic Mapping Program. Additional insights and constraints are provided by extensive new $^{40}Ar/^{39}Ar$ geochronology and high-resolution aeromagnetic and gravity surveys, accompanied by new geophysical modeling of basin geometry and fault history. This guide provides just a brief introduction to these topics, establishing the Pliocene framework as a starting point for moving further back in time in the days to follow.

Continental Rifting

Continental rifting is the dynamic process responsible for thinning of the subcontinental lithosphere, extension and rupture of the overlying crust, and eventual formation of a mid-ocean ridge and new plate boundaries. Lithospheric thinning may be passive, resulting from tectonic extension driven by far-field stresses related to plate boundary motion, or active, resulting from increased thermal flux at the base of the lithosphere, most likely related to mantle upwelling derived from plumes deeper in the lithosphere (Sengör and Burke; 1978; Condie, 1982; Sengör and Natal'in, 2001). Both mechanisms may be associated with rift magmatism but represent end-member scenarios relative to the timing of upper crustal extension and associated volcanism. Passive rifting likely results in coeval extension of both lithosphere and crust, facilitating the buoyant rise of underlying mantle, and may or may not be associated with extensional magmatism. Early extension of the entire crust and upper mantle column would likely be associated with early faulting and rift sedimentation prior to the onset of any rift volcanism. Active rifting is characteristically associated with upwelling mantle plumes and thermal erosion of the base of the lithosphere followed by buoyant crustal uplift and thinning. In active rifting, volcanism manifests early in the extension cycle owing to thinning and thermal weakening of the crustal column associated with decompression melting within the buoyant mantle plume. This distinction reflects important observable geologic characteristics of rifted terranes, such as the temporal evolution of volcanism and faulting or the nature of associated basin-fill deposits; it makes no allowance for the changing tectonic environment in which a rift may evolve over timescales of millions to tens of millions of years.

The inherent limitations of the end-member passive and active descriptors for rift characterization were recognized by Sengör (1995) and Sengör and Natal'in (2001) in the wake of vastly expanded research into the tectonic setting, timing, style, and causes of extensional deformation of rifts worldwide (Neuman and Ramberg, 1978; Illies, 1981; Buck, 1991; Ziegler, 1992; Brun, 1999; Corti and others, 2003). This early descriptive attempt at linking rift characteristics

[1]U.S. Geological Survey.

[2]University of Oregon.

to tectonic environments failed to adequately recognize that some rifts temporally evolve through a sequence of changing tectonic regimes and that individual rift basins within the same rift system may exhibit vastly different evolutionary histories, particularly with respect to timing and styles of associated faulting, as well as timescales and magnitudes of associated volcanism. In an attempt to greatly simplify rift classification, Merle (2011) proposed a descriptive scheme that relates rift evolution to four active tectonic environments: transfer zones, continental rifts, subduction zones, and hot spots; all of these tectonically link rifting to the end-member evolutionary stage of ocean-ridge inception (fig. 22). Inherent in this scheme is the recognition that rifts are often subject to variable rates and styles of extensional faulting, magmatism, and basin evolution, and may go through multiple, different phases of extension throughout the evolution of the rift. For example, extensional rift basins in back-arc settings may passively initiate as a result of plate collision and subduction, but evolve to active rift basins through subducting-plate foundering, slab induced melting, and buoyant rise of asthenospheric mantle plumes.

Most intracontinental rifts, as the name implies, become inactive long before plate boundary formation and preserve the time-integrated record of tectonic and magmatic components of rifting, often spanning tens of millions of years. The underlying process responsible for lithospheric thinning may, and often does, evolve over time, reflecting changes in plate boundary geometries, transient thermal anomalies within underlying mantle, and associated changes in far-field regional stress regimes. This is interpreted to be the case for much of the Basin and Range, including the Rio Grande Rift, as subduction of the Pacific and Farallon Plates beneath the North American continent was accompanied by the transition from Oligocene arc volcanism to Miocene and Pliocene rift volcanism and associated extensional faulting subsequent to subduction of the East Pacific Rise beneath the North American Plate (Christiansen and Lipman, 1972; Lipman, 1980; Verall, 1989; Ricketts and others, 2016). Foundering and (or) detachment of the subducting slab followed by sinking into the mantle may have generated asthenospheric and lithospheric melts associated with the dominantly basaltic rift deposits of the Pliocene Taos Plateau volcanic field. Consequently early-rift volcanism of the Rio Grande Rift may be associated with passive rifting, whereas Miocene to Pliocene magmatism reflects the transition to a more active phase.

The geologic record of rift evolution is incomplete, as progressive extension, associated basin formation, and erosional stripping of uplifted fault blocks progressively denude the terrane of critical outcrops that enable temporal correlation of magmatism and faulting—two of three primary proxies for models of rift evolution. Basin sedimentation—the third proxy in rift reconstruction—is critical to the evolutionary record of rifting, but inherently difficult to study,

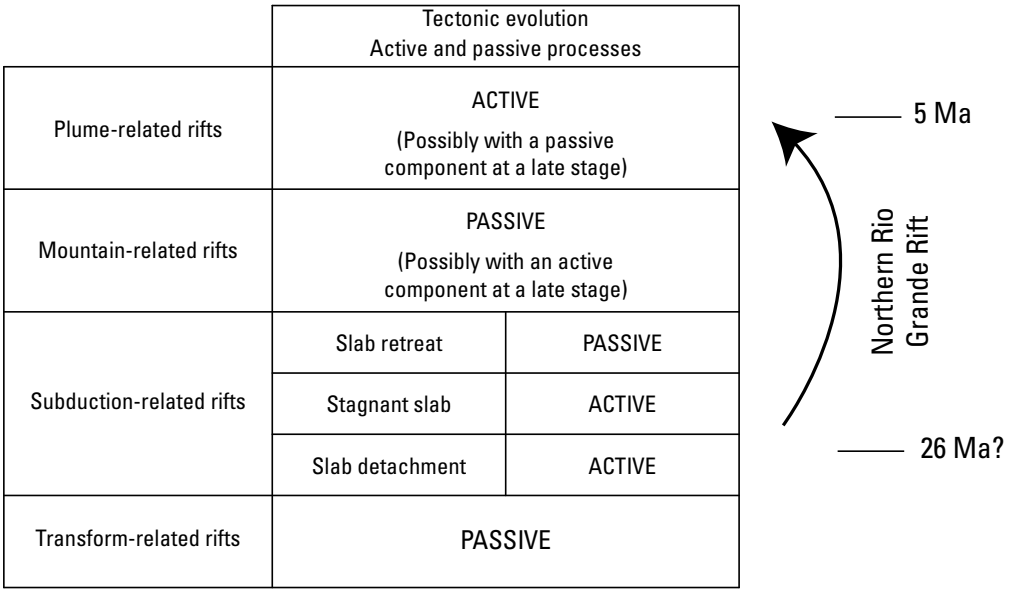

Figure 22. Rift classification scheme of Merle (2011) illustrating the major tectonic settings of rifts and associated active versus passive rifting processes. Temporal evolution of the Rio Grande Rift is illustrated to the right of the classification scheme (arrow) and illustrates the potential for transition from subduction related (passive) to plume-related (active) continental rifting during the transition from arc to rift volcanism.

as most deposits are buried within extensional rift basins and provenance studies are limited to correlation of clast lithologies with poorly exposed, deeply dissected source terranes. The San Luis Basin and adjacent mountain ranges preserve an exceptional combined record of extensional volcanism and sedimentation facilitating rift reconstruction.

Rio Grande Rift and the San Luis Basin

The Rio Grande Rift extends from Chihuahua, Mexico, to northern Colorado, structurally separating the North American craton to the east from the Colorado Plateau and Great Basin to the west (see fig. 3*A* of this guidebook, Day 1). The rift has long been considered the easternmost component of western North America's Basin and Range extensional terrane (Chapin, 1971; Christiansen and Lipman, 1972; Lipman, 1980; Keller and Cather, 1994; Baldridge and others, 1995). In its southernmost reaches, the rift is characterized by discontinuous, narrow basins with intervening ranges that are largely indistinguishable from the neighboring Basin and Range. Rift basins narrow northward and, by 34° N., well-established physiographic valleys occupy structurally defined basins extending from near Socorro, New Mexico, in the south to near Poncha Pass at the northern constriction of the San Luis Basin. The Arkansas Valley, north of the San Luis Valley, is the northernmost geomorphic expression of a modern rift basin, separated from the basins to the south by a strike-slip accommodation zone at Poncha Pass (Minor and others, 2016). North of the Arkansas Valley, expressions of rift extension are only preserved as discontinuous exposures of basin sediments, often along uplifted flanks of range fronts. Discontinuous and eroded remnants of small-volume basaltic fields as far north as Yampa, Colorado, are coeval with larger basaltic fields in basins to the south, and are attributed to lithospheric melting associated with rift extension (Cosca and others, 2014), albeit on a smaller scale.

From south to north, the Albuquerque, Santo Domingo, Española, and San Luis half-grabens are the primary structural basins of the northern rift, each characterized by a basin-bounding fault or fault zone bordering adjacent mountain ranges. The dominant sense of dip-slip displacement alternates from down-to-west in the southern Albuquerque-Santo Domingo and northern San Luis Basins, to down-to-east in the intervening Española Basin. Basins are structurally linked by accommodation zones characterized by northeast- or southwest-trending zones of strike-slip and oblique-slip fault deformation that are responsible for the distribution of strain across basins. Strike-slip fault zones merge, typically in complicated ways across many fault strands, with dip-slip basin bounding faults accommodating the inversion of dip-slip sense across the north-south elongate basins. The most notable of these, the Embudo Fault Zone, defines the north and south terminus of the Española and San Luis Basins, respectively, and will be discussed at the first stop of this guide as an introduction to the San Luis Basin.

The San Luis Basin is the largest high-altitude intermontane basin in North America. The physiographic extent is greater than 13,000 km^2, with an elevation that is everywhere above 7,546 ft (2,300 m). The elongate basin extends for nearly 250 km from Poncha Pass, Colorado, in the north to south of Pilar, New Mexico, (Stop 2-1) and almost 90 km east-west near the New Mexico-Colorado border. The Sangre de Cristo Mountains, which rise to elevations in excess of 13,944 ft (4,250 m), form the eastern margin of the basin and border the structurally deepest parts of the basin. The high elevations in the Sangre de Cristo Mountains are a result of the combined effects of Laramide contractional deformation and uplift, followed by extensional deformation during the late Oligocene to present day.

The western margin of the Sangre de Cristo Mountains is associated with the Sangre de Cristo Fault Zone, a major system of normal faults. These normal faults have variable slip rates and total displacements, but everywhere expose Proterozoic crystalline basement rocks or Pennsylvanian sedimentary deposits at valley level and elevate rocks as young as early Miocene to positions along the range crest (fig. 23). This structural juxtaposition of early-rift magmatic remnants against younger Pliocene to Pleistocene volcanic deposits of the valley provides an opportunity to assess evolving magmatic sources, differentiation paths, emplacement mechanisms, and eruption styles throughout rift history. Most notable in this regard is the contrast of Pliocene basaltic to intermediate composition volcanic deposits of the Taos Plateau volcanic field to the range-front exposures of the plutonic underpinnings of the Oligocene rhyolitic Questa caldera along the Red River drainage near the small community of Questa, New Mexico; an area of multiple stops during the second and third days of the field trip.

The western margin of the San Luis Valley is bordered by the San Juan Mountains along the northern two-thirds of its length. East-dipping ignimbrites from multiple calderas of the southern Rocky Mountains volcanic field are intercalated with basin-fill sediments of the Santa Fe Group (fig. 24) derived from both east and west within an asymmetric half-graben. In the southern third of the valley, the western rift margin is underlain by near-surface and surface exposures of Proterozoic crystalline basement rocks, distal exposures of ignimbrites from calderas of the San Juan Mountains and Sangre de Cristo Range, and intercalated sediments recording both proximal and distal sources; distal sources would require significant paleodrainage reorientation from those interpreted for the Pleistocene and present day (Turner and others, Day 3, this volume; Ruleman and others, 2016).

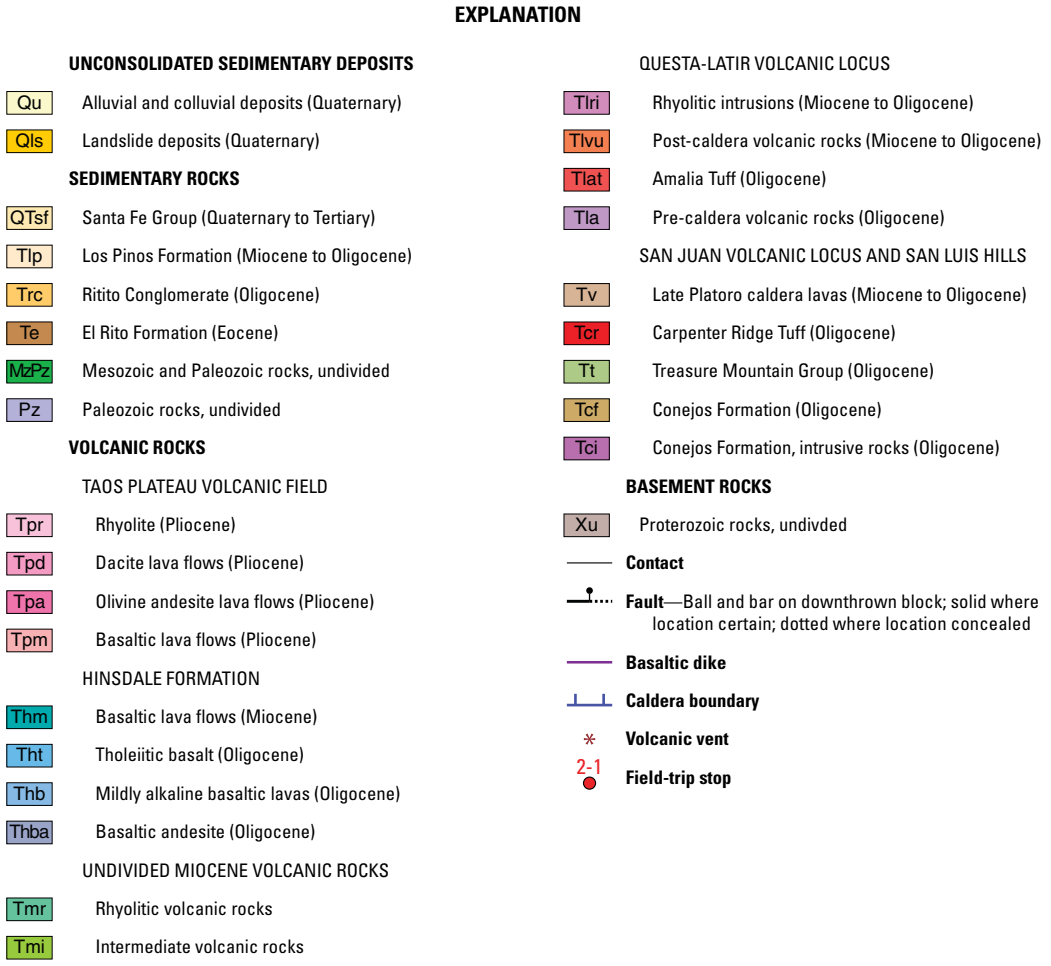

Figure 23. Generalized geologic map of the Taos Plateau area showing distribution of volcanic deposits of the Pliocene Taos Plateau volcanic field underlying the plateau surface of the southern San Luis Valley. Dominantly basaltic lavas form flat lying tablelands and are locally intercalated with more evolved andesitic and dacitic deposits preserved as eroded, moderate- to steep-sided volcanic edifices. Servilleta Basalt and related flows are locally uplifted along western basin- bounding faults of the Sangre de Cristo Fault Zone, most notably between Costilla, New Mexico, and San Luis, Colorado, and form gently east-tilted, uplifted surfaces northwest of Antonito, Colorado, in the northwestern part of the map area. Remnants of the Proterozoic-cored Sangre de Cristo Mountains are punctuated by deeply eroded postcaldera intrusions of the Questa-Latir locus of the southern Rocky Mountains volcanic field, marking the southeastern limit of this Oligocene volcanic arc province. The western basin margin of the San Luis Valley preserves distal outflow sheets of Treasure Mountain Group tuff deposits that overlie precaldera andesite of the Conejos Formation. Proterozoic rocks rim the southwestern, southern, and eastern basin margins except where Paleozoic rocks unconformably overlie crystalline basement in the southern Sangre de Cristo Mountains. Locally, late Oligocene to Miocene basaltic rocks of the Hinsdale Formation are coincident with early extension and temporally overlap caldera forming eruptions in the Questa area. Intermediate composition volcanic rocks of Miocene age are locally preserved throughout the region, but poor exposure precludes a definitive temporal association with active rift faulting.

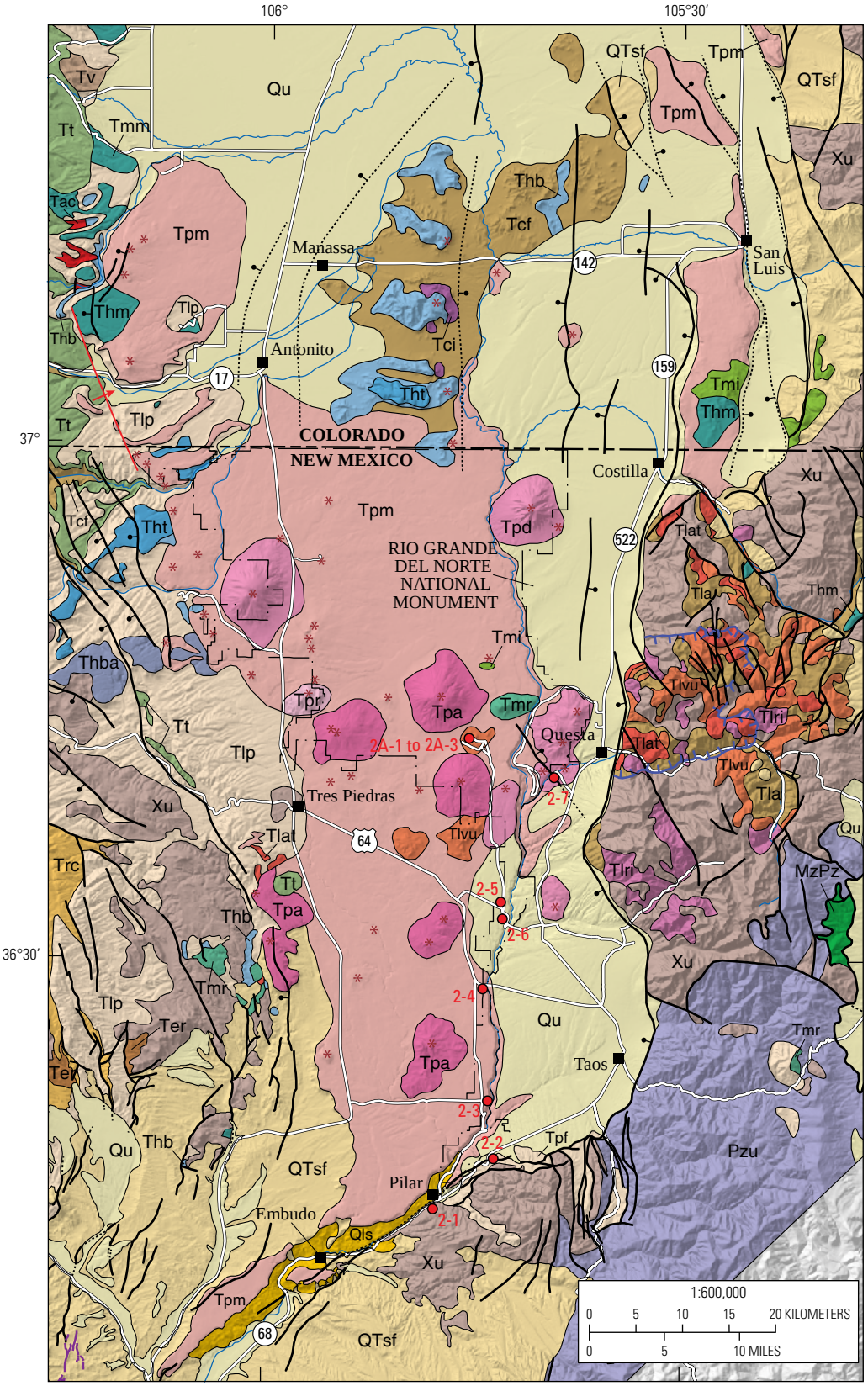

Projection UTM, NAD83 Horizontal Datum, zone 13N, NAVD 1988 Vertical Datum
Shaded-relief base generated from U.S. Geological Survey 10-m Digital Elevation Model (DEM) data from the National Elevation Dataset, accessed November 2016 at http://ned.usgs.gov/.

Geology compiled by K.J. Turner, 2016

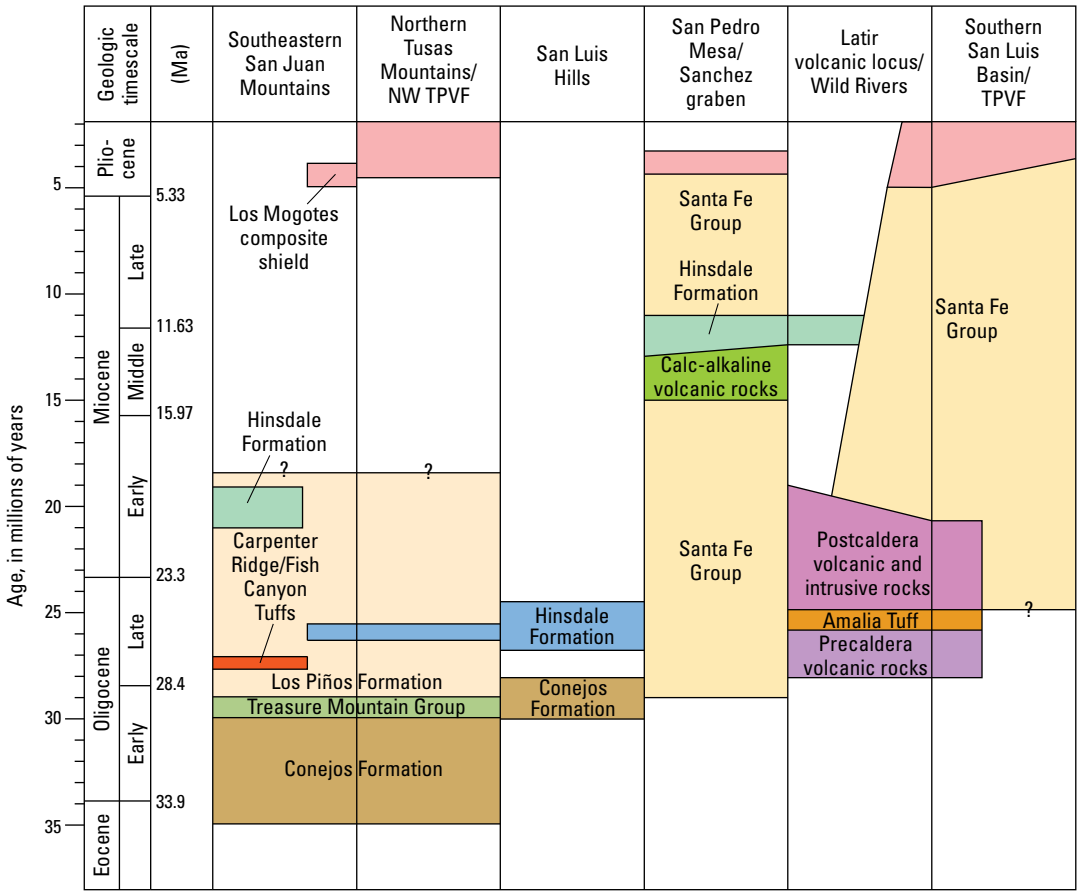

Figure 24. Simplified stratigraphic correlation diagram for regional bedrock and basin-fill deposits of the southern San Luis Valley. Ma, million years ago; TPVF, Taos Plateau volcanic field; NW, northwest.

The subsurface structural configuration of the San Luis Basin is interpreted from regional geologic mapping integrated with new regional gravity data and geophysical models constraining the geometry and depth of subbasins within the broader geomorphic San Luis Valley (Drenth and others, 2013, 2016). Gravity data collected across the length and width of the San Luis Valley (fig. 25*A*,*B*) reveal discontinuous, narrow, elongate gravity lows paralleling the Sangre de Cristo frontal fault, and less well-defined lows along the western margin of the valley. Separating the two are distinct, broad gravity highs correlative with surface exposures of Oligocene and Miocene volcanic rocks in the southern half of the valley (best exposed in the San Luis Hills, Timber Mountain, and Brushy Mountain) and subsurface Oligocene ignimbrites erupted from calderas in the San Juan Mountains encountered in deep exploration drill holes in the northern half of the valley (Brister and McIntosh, 2004).

Derivative gravity modeling (fig. 25*C*,*D*) estimates basin-fill thickness and structure elevation contours for subbasins within the broader San Luis Basin (Drenth and others, 2016). We infer that the basins are all likely fault bounded, although the temporal evolution of faulting associated with intrabasin faults likely is as temporally and spatially variable as that associated with the Sangre de Cristo Fault Zone (Ruleman and others, 2013). The gravity modeling suggests the largest subbasin occurs in the northern San Luis Valley, having dimensions approximately 40 km wide by 60 km in length, with a maximum basin-fill thickness of approximately 6 km. The southern two-thirds of the basin is characterized by discrete elongate subbasins that rarely exceed 20–25 km in length and 10–20 km in width. These smaller subbasins range in fill thickness from a maximum of 1.5 km near Taos, New Mexico, in the Taos subbasin, to only a kilometer or so near Questa, New Mexico, at the southern end of the Costilla-Sunshine subbasin; similar small subbasins exist along the western valley margins (Drenth and others, 2011). This model illustrates the broadly distributed subbasin characteristics of the eastern San Luis Valley, the large shallow platform of dominantly volcanic basement of the southern Rocky Mountains volcanic field (previously referred to as an intrarift horst within the basin [Lipman and Mehnert, 1979; Thompson and others, 1986; Dungan and others, 1989b]) and the significantly shallower nature of the southern subbasins than previously reported (Cordell, 1982). In the southernmost part of the San Luis Valley down-to-west faults extend into the Proterozoic rocks of the Tusas Mountains (figs. 25, 26). The Tusas Mountains broadly define the structurally uplifted western margin of the San Luis Basin.

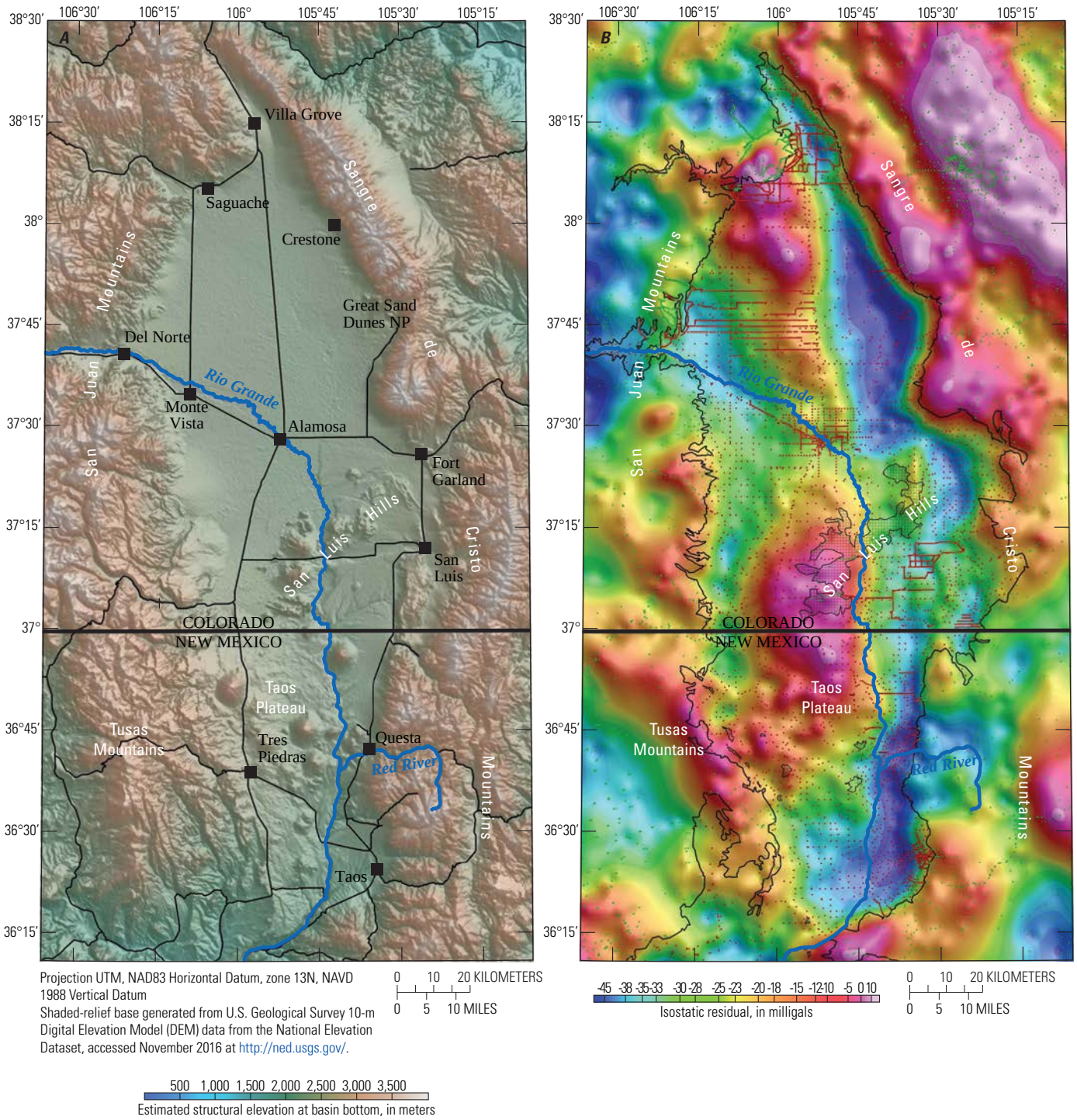

Figure 25. Results of geophysical modeling of the southern San Luis Valley, modified from Drenth and others (2016). *A*, Physiographic relief map of the San Luis Valley and bordering mountain ranges showing locations of the Rio Grande, major population centers, and highways. *B*, Isostatic residual gravity anomaly map of the San Luis Valley. Black line indicates basin boundary, hachured polygons indicate exposures of Miocene and older intrabasin volcanic deposits. Green and red dots are gravity station locations on pre-Pliocene and basin-fill sediments, respectively. *C*, Gravity model indicating estimated thickness of Santa Fe Group sediments and locations of major extensional depocenters. Limited seismic and borehole data, indicated by orange triangles, and wells, indicated by green circles, were used to constrain the geophysical model. *D*, Estimated structural elevation at the base of the rift basin derived by subtracting the known thickness of Pliocene volcanic cover from the surface elevation model.

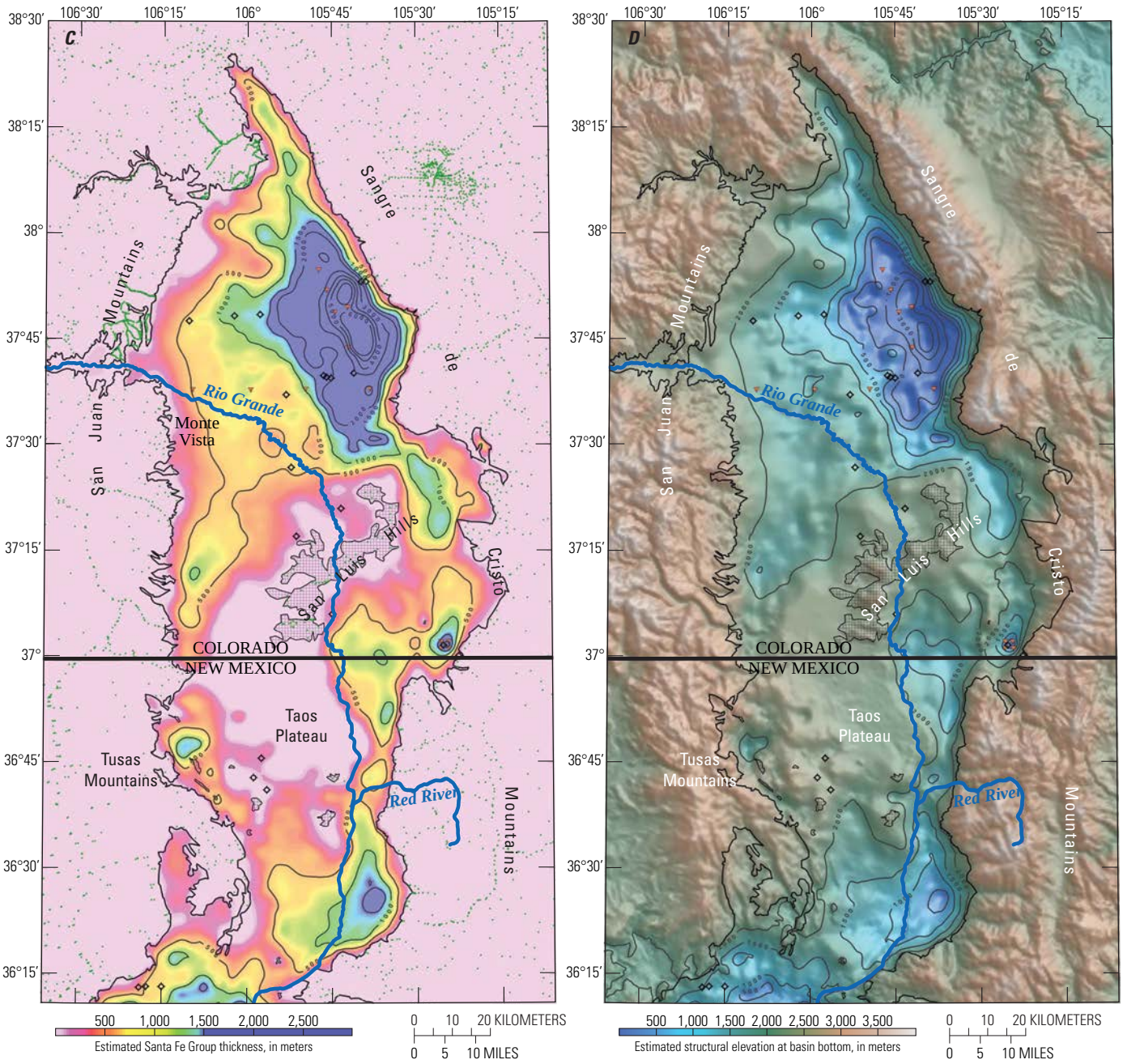

Figure 25. Results of geophysical modeling of the southern San Luis Valley, modified from Drenth and others (2016). *C*, Gravity model indicating estimated thickness of Santa Fe Group sediments and locations of major extensional depocenters. Limited seismic and borehole data, indicated by orange triangles, and wells, indicated by green circles, were used to constrain the geophysical model. *D*, Estimated structural elevation at the base of the rift basin derived by subtracting the known thickness of Pliocene volcanic cover from the surface elevation model.—Continued

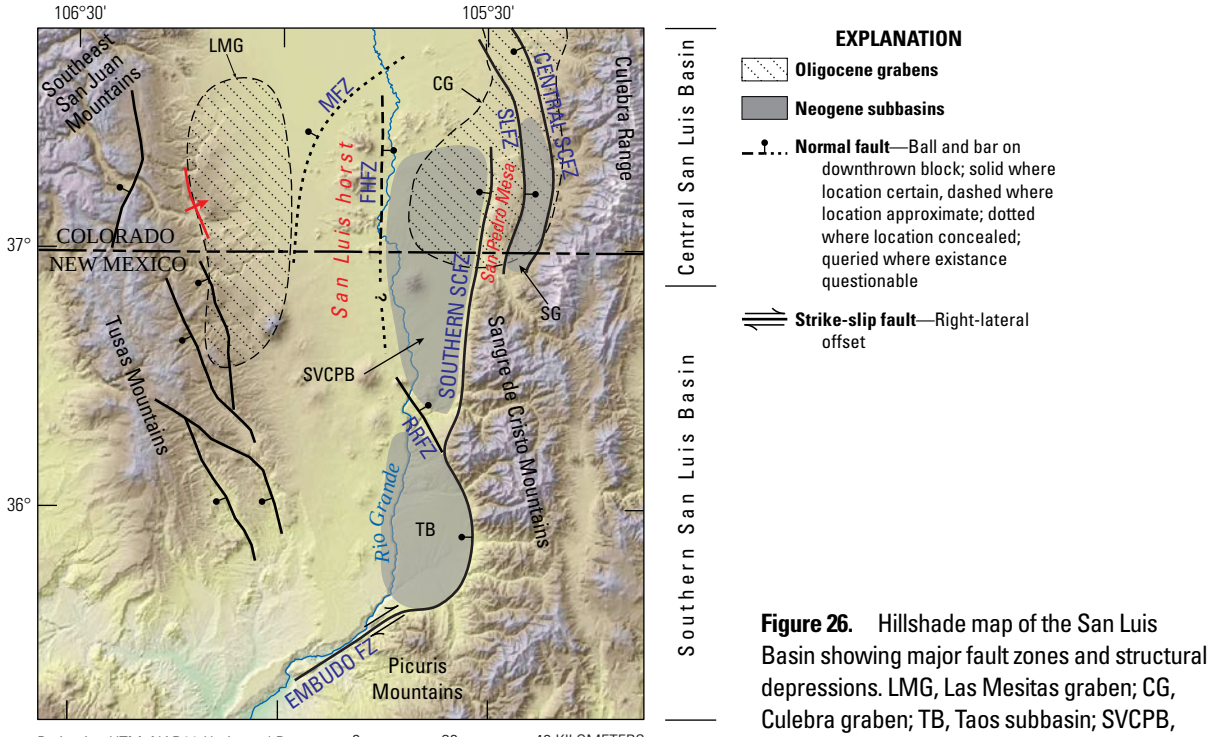

Figure 26. Hillshade map of the San Luis Basin showing major fault zones and structural depressions. LMG, Las Mesitas graben; CG, Culebra graben; TB, Taos subbasin; SVCPB, Sunshine Valley-Costilla Plain subbasin; SG, Sanchez graben; FHFZ, Fairy Hills Fault Zone; MFZ, Manassa Fault Zone; RRFZ, Red River Fault Zone; SLFZ, San Luis Fault Zone; SCFZ, Sangre de Cristo Fault Zone.

Taos Plateau Volcanic Field

The Taos Plateau volcanic field (TPVF) is the largest of the dominantly mafic volcanic fields of the Rio Grande Rift (fig. 3*A* of this volume, Day 1) and lies along the northern margin of the Jemez lineament, the northeast trending alignment of late Tertiary to Pleistocene basaltic volcanic fields extending from southeastern Colorado to central Arizona (Aldrich, 1986). The Jemez lineament is geophysically linked to a Proterozoic suture zone resulting from the accretion of the Mazatzal island arc to the southern margin of the Yavapai protocraton at 1.68–1.65 Ga (Karlstrom and Daniel, 1993; Karlstrom and Humphreys, 1998; CD-ROM Working Group, 2002; Magnani and others, 2005). Teleseismic data used to interpret the suture zone (Magnani and others, 2005) also suggest the presence of deep reflectors related to low velocity zones in the mantle spatially linking the crustal suture to the lithospheric mantle; this supports an interpretation of basaltic magma accumulation along the deep trace of the lineament (Dueker and others, 2001). Volumetrically, basaltic to intermediate composition volcanism of the Jemez lineament far exceeds that associated with the Rio Grande Rift; it is not clear how the suture zone is related to physical constraints on mantle melting or its extraction.

The correlation between Proterozoic suture zones and mantle-derived basaltic melts does not fully explain the connection between melt sources and middle- to upper-crustal controls on the geographic distribution of erupted magmas of the TPVF. However, basaltic lavas are more prevalent close to, or along, the lineament. The distribution of Pliocene to Pleistocene volcanic centers are largely limited to the southern San Luis Basin. These centers are tectonically related to the dominantly north-south trending extensional intrabasin faults that bound Pliocene subbasins, or major older structures inferred to parallel the dominantly north-trending fault zones, such as those exposed within the intrarift platform of Timber Mountain, Brushy Mountain, and the San

Luis Hills (see Stops 2-5 and 2A-1; Turner and others, Day 3, this volume). As these structures, or similarly oriented ones, extend well into the northern San Luis Valley, the loci of Pliocene volcanism in the southern part of the basin is more likely the result of geographic proximity to underlying deep sources of mantle derived magma than to different rates of extension or to fault density or geometry elsewhere in the basin.

Deposits of the TPVF are distributed across ~4,500 km^2 in the southern part of the ~12,000 km^2 San Luis Valley, dominantly in northern New Mexico but extending as far northeast in Colorado as Fort Garland (fig. 25). As such, primary volcanic deposits constitute a major component of the structural San Luis Basin fill (figs. 23, 24, and 27), ranging from a few meters thick near the distal termini of basaltic lava flows along western and northeastern basin margins to ~170 m in the Rio Grande gorge near Taos, New Mexico. Eastward along the thickening wedge of detritus shed from the Sangre de Cristo Mountains, lava flows pinch out against prograding alluvial fans, resulting in intercalated sediments and lava flows observed locally in the Rio Grande gorge, major tributary gorges, and encountered in drill holes or inferred from high resolution aeromagnetic data (Grauch and Keller, 2004). New geologic mapping and ~150 high-resolution $^{40}Ar/^{39}Ar$ age determinations reveal a complex distribution of more than 60 exposed eruptive centers ranging in composition from basalt to rhyolite. Total eruptive volume, estimated from geologic map relations, geophysical modeling of basin geometry, and subsurface distribution of basaltic deposits, is approximately 300 km^3 and consists of 66 percent Servilleta Basalt (tholeiite), 12 percent olivine andesite, 17 percent dacite, 3 percent mildly alkaline trachybasalt and trachyandesite, and <1 percent rhyolite. Representative age determinations and geochemical analyses of TPVF samples are presented in tables 1 and 2, respectively.

Servilleta Basalt is preserved throughout the TPVF, ranging in age from ~5.6 to ~3 Ma. The maximum exposed thickness of 172 m in the Rio Grande gorge is geographically and structurally associated with the largest Pliocene subbasin in the southern San Luis Valley, the Taos graben (fig. 26). Smaller basalt centers as young as 2.2 Ma are spatially associated with monogenetic trachybasalt and trachyandesite centers (~4.3 to ~2.8 Ma) along the uplifted footwall of a western fault-bounded subbasin, the Las Mesitas graben (fig. 26). The plateau surface, underlain primarily by Servilleta Basalt, is interspersed with large (~15 km^3 typical erupted volume) monogenetic to polygenetic andesitic shield volcanoes (~5–4.3 Ma). These are north-south aligned and distributed along the central axis of the San Luis Basin, parallel to major intrabasin faults (figs. 23 and 27). Large (as much as 21 km^3 erupted volume) zoned dacitic lava dome complexes (~5 Ma Guadalupe Mountain and Cerro Negro, ~3.95 Ma Ute Mountain, and ~3 Ma San Antonio Mountain) reach elevations of 10,827 ft (3,300 m), approximately 2,526 ft (770 m) above the valley floor. Each is spatially and temporally associated with fault-bounded subbasins superposed on the broader structural San Luis Basin.

Mesita cone is the youngest eruptive center of the TPVF. Located approximately 12 km north of the New Mexico-Colorado border, this small, ~1 Ma xenocrystic trachyandesite cinder cone

Figure 27. View northeast from the summit of Cerro Chiflo (8,976 feet [ft], 2,736 meters [m]). The Taos Plateau surface is underlain by Pliocene Servilleta Basalt that was incised by the Rio Grande. The thin mantle of eroded middle Pleistocene fluvial and reworked eolian deposits overlie basaltic lava flows and largely obscure fault scarps of the gorge fault zone that extend northward to the west flank of Ute Mountain (10,093 ft; 2,990 m), a 3.95-Ma trachyandesite volcano on the Colorado-New Mexico border. Incised north-trending fault scarps, visible as inflections in shadowed slopes on the west side of the Rio Grande, are visible in the middle ground of the photograph. The plateau surface at the approximate location of the Rio Grande and areas east are underlain by the Sunshine Valley-Costilla Plain subbasin, which is interpreted on the basis of gravity modeling to have a maximum depth of 1.5 kilometers (Ruleman and others, 2013; Drenth and others, 2016). The range front of the Sangre de Cristo Mountains is visible in the distance. Photograph by K.J. Turner, U.S. Geological Survey.

Table 1. Representative summary of $^{40}Ar/^{39}Ar$ geochronologic ages.

[Ma, million years ago; dms, degrees minutes seconds; SCLF, single crystal laser fusion; NA, not applicable]

Sample ID	Rock name or volcano	Material analyzed	Age (Ma) ± Error (2σ)	Age calculation method	Longitude (dms)	Lattitude (dms)
Taos Plateau volcanic field						
RGR-79	Ute Mountain-trachydacite	Whole rock	3.95 ± 0.12	Plateau	105° 42.269′	36° 56.941′
RGR-283	Cerro de la Olla-olivine andesite	Whole rock	4.33 ± 0.08	Integrated	105° 47.381′	36° 44.558′
RG-190[b]	Cerro Negro	Groundmass	4.84 ± 0.05	Integrated	NA[a]	NA[a]
RGR-513	Cerro de los Taoses-olivine andesite	Whole rock	4.86 ± 0.02	Plateau	105° 46.306′	36° 33.263′
RGR-127	Unnamed cerrito east of Montoso andesite	Whole rock	4.9 ± 0.09	Plateau	105° 44.200’	36° 38.650’
RGR-286	Cerro Montoso–olivine andesite	Whole rock	4.95 ± 0.04	Plateau	105° 45.129′	36° 41.140′
Dead Cholla area						
RGR-414	Servilleta Basalt-upper flow, upper sequence	Whole rock	3.3 ± 0.06	Plateau	105° 43.956′	36° 21.488′
RGR-412	Servilleta Basalt-upper flow, middle sequence	Whole rock	3.54 ± 0.09	Plateau	105° 43.938′	36° 21.486′
RGR-410	Servilleta Basalt-lowest exposed flow	Whole rock	3.79 ± 0.03	Plateau	105° 43.882′	36° 21.545′
High Bridge area						
RGR-123	Uppermost flow of Tsb3	Whole rock	3.71 ± 0.14	Plateau	105° 43.748′	36° 29.386′
RGR-122	Basal flow of Tsb3	Whole rock	3.67 ± 0.10	Plateau	105° 43.732′	36° 29.345′
RGR-121	Uppermost flow of Tsb2	Whole rock	4.07 ± 0.09	Plateau	105° 43.723′	36° 29.339′
RGR-119	Basal flow of Tsb2	Whole rock	4.17 ± 0.03	Plateau	105° 43.684′	36° 29.328′
RGR-117	Uppermost flow of Tsb1	Whole rock	4.55 ± 0.04	Plateau	105° 43.674′	36° 29.324′
RGR-115	Lowest exposed flow of Tsb1	Whole rock	4.81 ± 0.03	Plateau	105° 43.683′	36° 29.300′
Dunn Bridge area						
RGR-40	Uppermost Servilleta Basalt flow	Whole rock	3.52 ± 0.15	Plateau	105° 42.530′	36° 32.264′
RGR-41	Silicic alkalic basalt, river level	Whole rock	4.50 ± 0.06	Plateau	105° 42.576′	36° 32.101′
Red River Fish Hatchery area						
RGR-05	Upper Servilleta flow sequence - Red River	Whole rock	3.66 ± 0.11	Plateau	105° 41.201′	36° 39.344′
RT08GM12	Red River-dacite tailings pond	Whole rock	4.78 ± 0.11	Plateau	105° 38.198′	36° 41.514′
RGR-276	North Guadalupe Mountain flow	Whole rock	4.78 ± 0.01	Plateau	105° 38.439′	36° 45.845′
RGR-110	Hatchery volcano-olivine andesite	Whole rock	4.99 ± 0.07	Plateau	105° 39.602′	36° 40.946′
RGR-04	Lower Servilleta sequence - La Junta point	Whole rock	5.08 ± 0.09	Plateau	105° 41.252′	36° 39.321′
RGR-108	Guadalupe Mountain flow - base of section	Whole rock	5.35 ± 0.07	Plateau	105° 39.635′	36° 40.800′
Timber and Brushy Mountains						
RGR-311	Montoso dacite	Whole rock	21.57 ± 0.10	Plateau	105° 44.824′	36° 38.528′
RT08GM05	Erosional hill east of Brushy Mountain	Hornblende	22.4 ± 1.10	Plateau	105° 42.912′	36° 42.435′
RGR-308	Brushy Mountain andesite	Whole rock	22.48 ± 0.20	Integrated	105° 45.356′	36° 42.649′
RGR-316	Timber Mountain dacite	Whole rock	24.18 ± 0.06	Plateau	105° 45.807′	36° 36.333′
RGR-511	Brushy Mountain dacite	Hornblende	24.45 ± 0.57	Plateau	105° 45.030′	36° 43.076′
RTWP01	Amalia Tuff, east of Brushy Mountain	Sanidine	25.30 ± 0.05	SCLF	105° 44.146′	36° 43.137′
RGR-510	Amalia Tuff, Brushy Mountain	Sanidine	25.52 ± 0.07	SCLF	105° 45.206′	36° 42.960′
RGR-512	Rhyolite of Brushy Mountain	Sanidine	25.28 ± 0.05	SCLF	105° 45.252’	36° 42.574’
RGR-315	Timber Mountain rhyolite	Sanidine	25.35 ± 0.05	SCLF	105° 46.062′	36° 36.381′

[a]Coordinate data reported in Appelt (1998) do not correspond accurately to described locale.

[b]Data from Appelt (1998).

Table 2. Representative chemical analyses for Taos Plateau volcanic field samples.

[LOI, loss on ignition; DMS; degrees minutes seconds; SB, Servilleta Basalt; SAB, Silicic Alkalic Basalt; GM, Guadalupe Mountain; UCEM, Unnamed Cerito East of Montoso; ---, no data; n.r., not r

	Dead Chola Trail			High Bridge of the Rio Grande						Dunn Bridge		Red River Fish	
Sample number	**RGR-410**	**RGR-412**	**RGR-414**	**RGR-115**	**RGR-117**	**RGR-119**	**RGR-121**	**RGR-122**	**RGR-123**	**RGR-40**	**RGR-41**	**RGR-05**	**RGR-04**
Sample location	**SB**	**SB**	**SB**	**SB**	**SB**	**SB**	**SB**	**SB**	**SB**	**SB**	**SAB**	**SB**	**SB**
Sample location	**Lower**	**Middle**	**Upper**	**Base lower**	**Top lower**	**Base middle**	**Top middle**	**Base upper**	**Top upper**	**Upper**	**---**	**Upper**	**Lower**
Longitude (dms)	**105° 43.88′**	**105° 43.94′**	**105° 43.96′**	**105° 43.68′**	**105° 43.67′**	**105° 43.68′**	**105° 43.72′**	**105° 43.73′**	**105° 43.75′**	**105° 42.53′**	**105° 42.58′**	**105° 41.2′**	**105° 41.25′**
Latitude (dms)	**36° 21.55′**	**36° 21.49′**	**36° 21.49′**	**36° 29.3′**	**36° 29.32′**	**36° 29.33′**	**36° 29.34′**	**36° 29.35′**	**36° 29.39′**	**36° 32.26′**	**36° 32.1′**	**36° 39.34′**	**36° 39.32′**
													Weight
SiO_2	47.96	49.64	52.06	49.82	50.58	48.77	49.27	48.69	48.08	50.14	50.96	49.86	51.16
TiO_2	1.53	1.18	1.2	1.24	1.16	1.34	1.45	1.28	1.19	1.14	1.57	1.15	1.24
$Al2O_3$	15.99	16.06	15.6	15.49	16.43	15.74	15.51	15.48	16.56	15.87	16.82	15.9	16.54
Fe_2O_3	12.34	12.24	11.66	11.97	10.94	12.65	12.45	12.34	12.53	12.02	9.88	12.1	10.68
MgO	7.76	7.32	6.4	7.68	6.73	8.18	7.53	7.77	7.41	7.39	5.46	7.64	6.22
CaO	9.13	9.05	8.72	8.32	8.59	8.89	9.06	8.87	9.16	8.49	7.81	8.71	8.6
Na_2O	3.31	3.08	3.09	3.39	3.32	3.22	3.24	3.14	3.04	3.12	3.85	3.17	3.45
K_2O	0.78	0.39	0.54	0.83	0.81	0.48	0.48	0.63	0.24	0.72	1.66	0.61	0.88
P_2O_5	0.28	0.15	0.16	0.21	0.17	0.17	0.19	0.24	0.2	0.18	0.36	0.18	0.19
MnO	0.17	0.16	0.16	0.18	0.15	0.17	0.16	0.17	0.17	0.16	0.14	0.16	0.15
total	99.26	99.27	99.61	99.11	98.87	99.61	99.35	98.61	98.58	99.22	98.51	99.49	99.12
LOI	0	0	0.21	0.63	0.79	0.49	0.6	1	1.44	0.64	1.07	0.47	0.55
													Parts pe
Ba	375	229	333	377	313	195	240	376	342	346	588	330	284
Rb	8	5.1	7.3	13.7	11.4	6.5	5.9	9.6	1	8	25.7	9.3	20.2
Th	0.8	0.5	0.8	1	1.1	0.5	0.6	0.9	0.6	1.1	2.3	1.1	2
Nb	13	5	5	8	5	4	6	6	4	5	19	4	9
Ta	0.6	n.d	n.d.	n.d.	n.d.	n.d.	n.d.	n.d.	n.d.	n.d.	1.1	n.d.	0.6
La	14	8.1	9.6	12.6	13	8.4	9.3	12.9	11.6	12.1	22.8	11.3	16.8
Ce	31.8	16.8	21.1	27.2	27.2	18.7	20.7	28.1	25.6	25.7	51	24.4	36.8
Sr	451	284	284	390	430	333	374	364	362	333	628	353	437
Nd	18.6	10.3	12.1	15	14.9	11.8	13.1	15.4	14.5	14.1	23.4	13.6	20
Sm	4.2	2.7	3	3.5	3.5	3.1	3.5	3.7	3.4	3.3	4.8	3.3	4.4
Zr	120	79.8	85.8	102	100	86.5	87.8	92.1	83.2	79.5	164	90.7	142
Hf	3	2	2	2	2	1	1	2	1	3	4	1	3
Tb	0.78	0.63	0.69	0.59	0.62	0.61	0.63	0.64	0.6	0.61	0.73	0.62	0.82
Y	23.4	19.8	21	23.5	22.5	21.9	22.1	22.8	22	19.9	24.6	22.3	30.6
Tm	0.36	0.3	0.34	0.34	0.32	0.33	0.32	0.31	0.34	0.3	0.35	0.33	0.46
Yb	2.2	1.9	1.9	2.1	2	2	1.9	2	2.1	1.9	2.3	2	3

[a]Sample RG-61 compositional data reported from Thompson and others (1986); Fe_2O_3 reported here based on recalculating FeO and Fe_2O_3 originally reported.

reported]

Hatchery/Guadalupe Mountain			Other intermediate composition volcanoes					Brushy and Timber Mountains					
RGR-110	RGR-276	RGR-108	RGR-513	RGR-127	RGR-312	RGR-286	RGR-602	RGR-308	RGR-316	RGR-311	RGR-511	RG-61[a]	RGR-315
Hatchery volcano	GM	GM	Cerro de los Taoses	UCEM	UCEM	Cerro Motoso	Cerro Negro	Brushy Mountain	Timber Mountain: unit-Ttd	Timber Mountain: unit-Thdu	Brushy Mountain	Timber Mountain: unit-Tdl	Timber Mountain: unit-Trl
Olivine andesite	Dacite lava	Dacite lava	---	---	---	---	---	Olivine andesite	Pyroxene dacite	Upper dacite	Dacite lava	Dacite spatter	Low-Si rhyolite
105° 39.6′	105° 38.44′	105° 39.64′	105° 46.31′	105° 44.2′	105° 44.51′	105° 45.13′	105° 40.21′	105° 45.36′	105° 45.81′	105° 44.82′	105° 45.03′	105° 45.81′	105° 46.06′
36° 40.95′	36° 45.85′	36° 40.8′	36° 33.26′	36° 38.65′	36° 38.42′	36° 41.14′	36° 34.49′	36° 42.65′	36° 36.33′	36° 38.53′	36° 43.08′	36° 36.26′	36° 36.38′
percent													
55.29	61.43	63.23	56.1	59.59	61.1	57.8	63.1	57.6	63.3	64.6	64.7	65.02	70.5
1.1	0.85	0.7	1.06	0.82	0.8	1.09	0.76	1.25	0.92	0.67	0.65	0.94	0.44
16.27	15.63	15.49	16.3	14.78	14.8	15.81	15.7	15.7	15.2	15.1	14.9	15.46	14.5
7.95	5.45	5.45	8.21	7.46	7.2	7.45	5.56	7.68	4.97	5.09	4.94	4.8	2.56
4.9	2.26	2.2	4.6	4.55	4.33	4.16	2.53	4.09	1.42	2.36	2.24	1.88	0.52
6.66	4.17	3.98	6.64	5.58	5.83	6.03	4.87	5.98	3.32	4.22	4.03	3.41	1.4
4.3	4.69	4.02	4.05	3.51	3.38	4.12	4.25	4.06	3.7	3.74	3.87	3.34	4.4
2	3.32	3.17	2.14	1.97	2.43	2.47	2.7	2.53	4.09	3.15	2.94	4.27	5.23
0.3	0.7	0.3	0.34	0.09	0.08	0.54	0.42	0.53	0.32	0.25	0.21	0.28	0.12
0.12	0.08	0.08	0.12	0.12	0.1	0.11	0.07	0.08	0.1	0.05	0.06	0.11	0.06
98.88	98.57	98.62	99.2	98.47	100.05	99.57	99.96	99.5	97.34	99.23	98.54	99.51	99.73
0.98	0.2	1.3	0.83	1.89	1.51	0.31	0.32	1.13	3.05	2.18	1.62	2.72	1.27
r million													
861	3,360	1,320	890	312	368	1,020	1,161	1,350	1,330	1,350	1,150	1,302	722
35.8	43.9	67	34.3	50.5	53.9	36.2	45.1	38.8	81.4	57.1	61.5	83.6	83.1
2.7	2.9	5.7	2.6	4	4.3	4.2	4.7	4.8	11.3	6.1	5.9	10.2	11
18	7	18	20	12	14	11	21	21	26	14	12	24.4	25
1	n.d.	0.9	0.8	1	1.1	0.5	1.1	0.9	1.4	0.8	0	n.r.	1.5
31	40.4	52.4	29.5	9.9	10.7	49.8	45.3	49.3	60.8	40.7	33.8	55.3	97
64.6	75.6	102	64.1	22	21.8	91.9	88.5	93.6	119	76	66	118	192
904	1,520	629	697	224	223	980	761	1,100	559	675	616	558	144
29.7	34.4	43.1	27.4	10.3	10.9	40.3	37.2	42.7	56.2	32.1	26.3	n.r.	90
5.5	5.3	7.3	5.6	2.7	2.8	6.9	6.2	7	10.6	5.3	5	9.94	16.1
175	129	280	156	70.7	78.1	190	206	185	288	171	148	315	397
4	3	7	4	3	3	5	6	4	7	4	4	n.r.	8
0.61	0.5	0.68	0.71	0.49	0.52	0.86	0.66	0.63	1.16	0.52	0.51	1.06	1.84
21.8	11.4	23.1	19.6	18.2	16.6	22	20.2	14.8	33.2	12.9	14.1	41	44.9
0.29	0.16	0.33	0.31	0.27	0.29	0.34	0.25	0.24	0.61	0.22	0.21	n.r.	0.72
1.9	1	2.1	1.9	1.8	1.8	2.1	1.7	1.2	3.2	1.2	1.3	3.61	4.2

is cut by the Mesita Fault, a north-south oriented Pliocene to Pleistocene intrabasin fault midway between the San Luis Hills and San Pedro Mesa (Dungan and others, 1989b; Thompson and Machette, 1989; Thompson and others, 2007a,b, 2015; Turner and others, Day 3, this volume). Mapping of Rio Grande gorge stratigraphy (Dungan and others, 1984; Appelt, 1998), drilling near Taos (Bauer and Kelson, 2004a), and high-resolution aeromagnetic data east of the Rio Grande (Grauch and Keller, 2004) suggest that a number of buried vents may be additional source areas for Taos Plateau lavas.

The first comprehensive description of spatial distribution and compositional data for volcanic centers of the TPVF was presented in Lipman and Mehnert (1979). Subsequent detailed study of Rio Grande gorge stratigraphy, compositional variability, and petrogenesis of Taos Plateau volcanic field deposits is summarized in Dungan and others (1984, 1986, 1989b), Dungan (1987), and McMillan and Dungan (1986, 1988).

Lava flows and associated pyroclastic rocks span a compositional range from tholeiitic basalts to trachybasalts and basaltic trachyandesites to calc-alkaline andesites, dacites, and rhyolites. The geomorphic form of volcanic edifices is broadly correlative with composition; the more evolved dacites typically form steeper-sided volcanoes and lava domes like Ute Mountain (see figs. 27–30) and the least evolved tholeiites form broad low-relief shields (Lipman and Mehnert, 1979). Prominent vent locations for these tholeiites include a cluster of low shields west of Cerro Montoso, Pinabetoso Peaks, State line vent and unnamed vent areas northwest of San Antonio Mountain (fig. 30). In light of the geochemical complexity observed in the Taos Plateau lavas (Lipman and Mehnert, 1979; Dungan and others, 1986; McMillan and Dungan, 1986, 1988) the rock classification scheme adopted in the above studies and utilized on this trip is briefly described below.

Olivine tholeiites of the Servilleta Basalt are by far the dominant mafic composition of lavas erupted (>200 km^3) in the Taos Plateau volcanic field. These basalts contain olivine ($Fo_{80.5}$) + Cr-spinel ± plagioclase phenocrysts in an

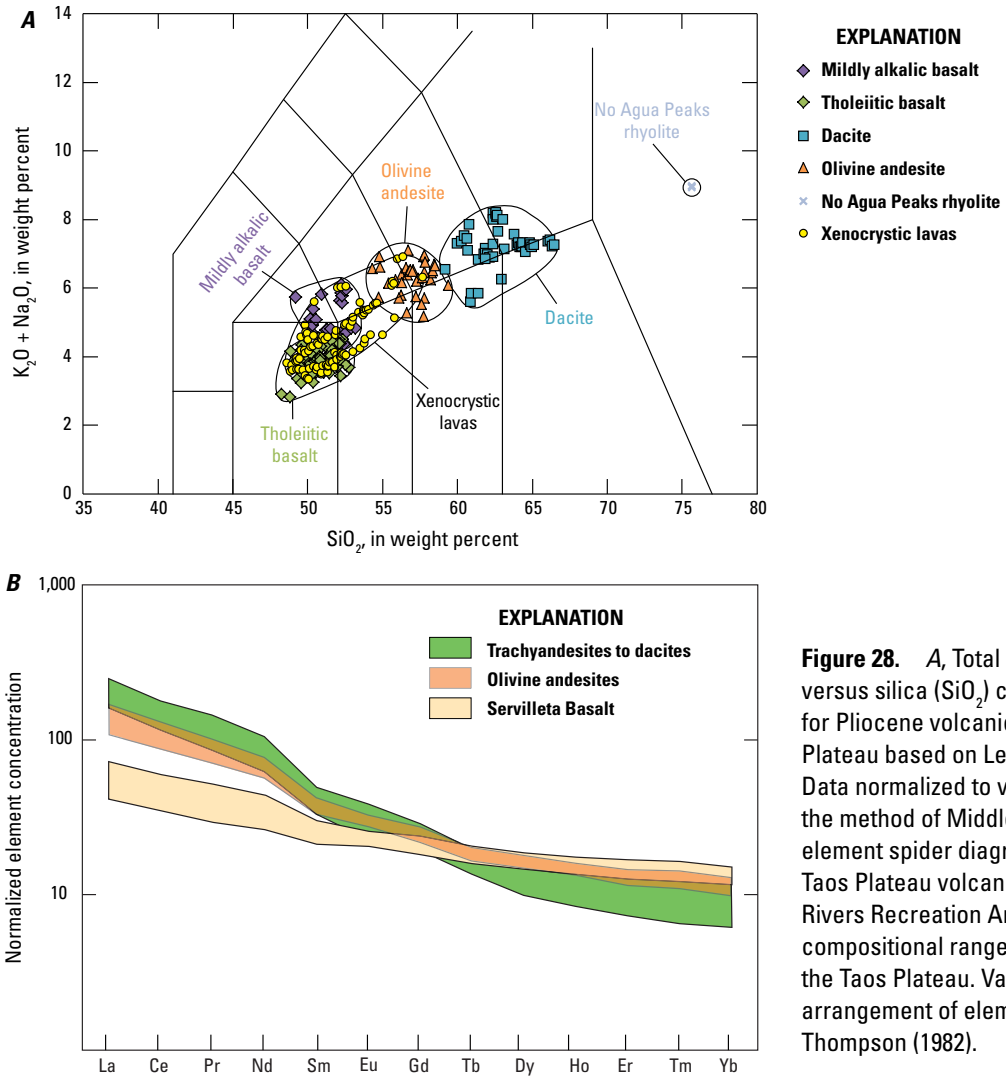

Figure 28. *A*, Total alkali (Na_2O+K_2O) versus silica (SiO_2) classification diagram for Pliocene volcanic rocks of the Taos Plateau based on LeBas and others (1986). Data normalized to volatile-free based on the method of Middlemost (1989). *B*, Trace element spider diagram of select samples of Taos Plateau volcanic field rocks in the Wild Rivers Recreation Area representative of the compositional range observed for most of the Taos Plateau. Values for chondrite and arrangement of elements follows discussion in Thompson (1982).

Figure 29. View north along the Rio Grande gorge. Cerro Chiflo and Ute Mountain are in the middle- and far-distance, respectively. Photograph by Ren A. Thompson, U.S. Geological Survey.

ophitic to diktytaxitic groundmass. The development of the diktytaxitic texture allowed the formation of extensive vesicular segregations as pipes and sheets during postemplacement in situ crystallization. These segregations are enriched in incompatible trace elements and depleted in nickel and chromium relative to massive interiors of the flows (Dungan and others, 1986), and are best developed in flows with the coarsest diktytaxitic groundmass textures.

Olivine andesites of the TPVF (26 km^3) are defined as the calc-alkaline, olivine-bearing intermediate volcanic rocks between 55–60 weight percent SiO_2 (McMillan and Dungan, 1988). The andesites occur as weakly to moderately vesicular ‘A‘ā flows and associated near-vent cinder, spatter, and agglutinate. The upper SiO_2 content of the olivine andesites is defined mineralogically by the reaction (olivine + melt = orthopyroxene) and volcanologically by the monolithologic character of the shield edifices. Andesites contain olivine ± plagioclase ± augite ± orthopyroxene in an intergranular groundmass. Olivine phenocrysts are euhedral to skeletal, weakly zoned, and in equilibrium with whole-rock compositions, indicating that olivine was the liquidus phase of these magmas. Andesites have magnesium-contents equivalent to, or only slightly lower than, the Servilleta Basalt, precluding fractional crystallization from the basalts as the major petrogenetic process. Incompatible trace elements are enriched in the andesites relative to the basalts and are comparable to those observed in many of the dacites. Olivine andesite volcanic centers include Cerro del Aire, Cerro de la Olla, Cerro Montoso, and Cerro de los Taoses (fig. 30).

Xenocrystic basaltic andesites erupted periodically throughout the Pliocene to Pleistocene on the Taos Plateau and are universally associated with short-lived, small volume eruptive centers. In places these eruptions predate major eruptions of more evolved compositions, such as the clustered centers of Los Cerritos de la Cruz and Red Hill southwest of San Antonio Mountain. However, they often appear to be late-stage eruptions such as those from the small vents of La Segita Peaks and a similar center on the northeast flank of San Antonio Mountain. These andesites are compositionally very similar to the olivine andesites, but carry numerous xenocrysts of sodic plagioclase and resorbed quartz.

Two-pyroxene dacites, referred to historically in the literature as rhyodacites (Dungan and others, 1986, 1989b; McMillan and Dungan, 1986, 1988; Dungan, 1987), form dark gray to black, nonvesicular lava flows containing augite + orthophyroxene + plagioclase in a typically glassy groundmass. Two-pyroxene dacites range in composition from low-silica (60.5 weight percent SiO_2) lava flows capping the Red River gorge sequence to high-silica (67.3 weight percent SiO_2) flows at Guadalupe Mountain. Other prominent two-pyroxene dacite volcanoes include San Antonio Mountain, Ute Mountain, Cerro Negro, the unnamed cerrito east of Montoso, and Tres Orejas.

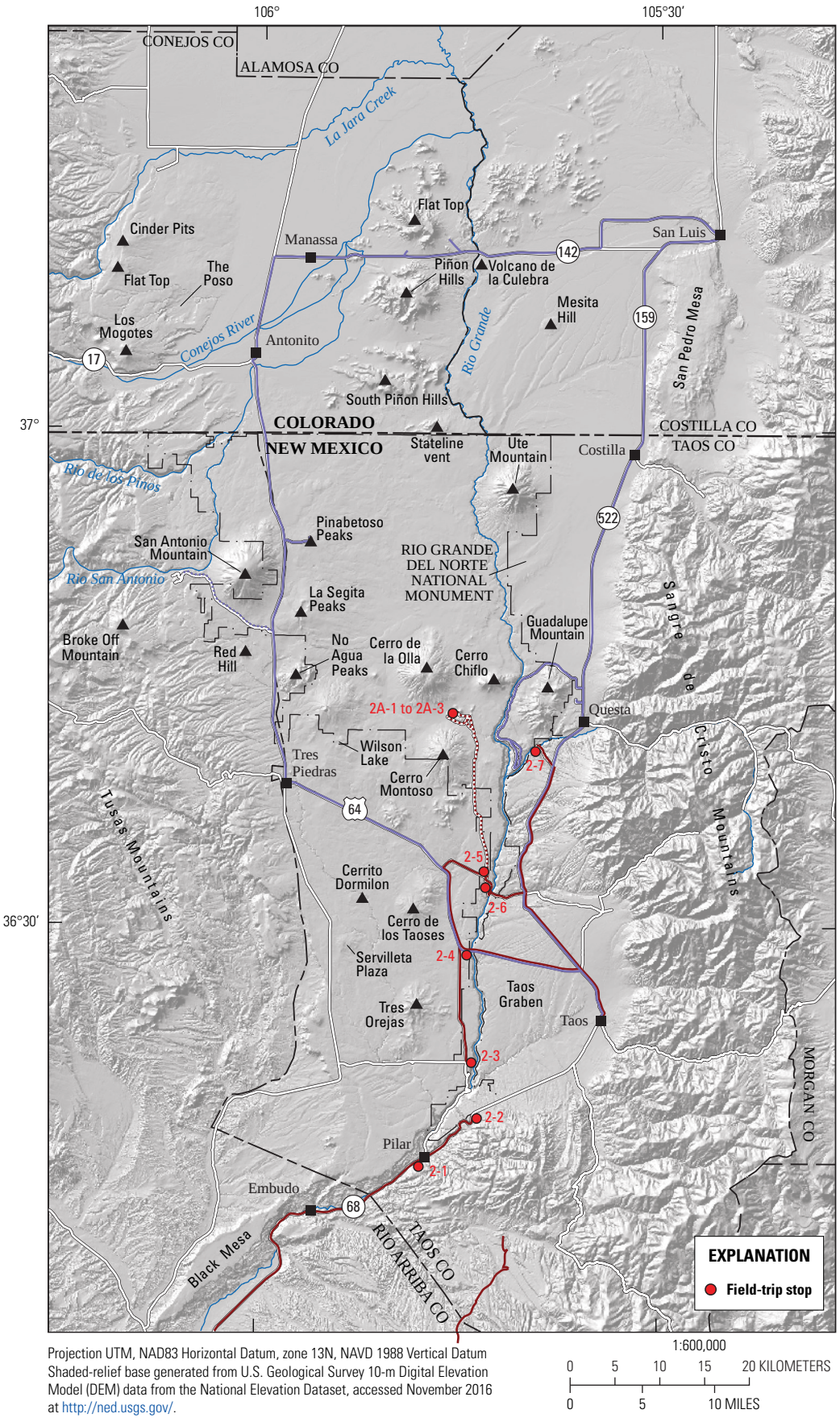

Figure 30. Regional shaded-relief map of the central and southern San Luis Valley area indicating the locations of Day 2 field-trip stops and major geographic features discussed in the guide. Solid red line and solid dots denote the planned route. An optional route to Brushy Mountain is shown by the dotted red line. The open red circle at Brushy Mountain indicates the general area of the three optional stops, which are shown in detail in the road log.

Projection UTM, NAD83 Horizontal Datum, zone 13N, NAVD 1988 Vertical Datum
Shaded-relief base generated from U.S. Geological Survey 10-m Digital Elevation Model (DEM) data from the National Elevation Dataset, accessed November 2016 at http://ned.usgs.gov/.

The Cerro Chiflo dacite, previously referred to as a quartz latite (Lipman and Mehnert, 1979), contains abundant plagioclase + biotite + hornblende phenocrysts and is unlike any other Pliocene dacites of the TPVF. The flow-banded dacite is light brown to gray, wholly devitrified, and contains xenoliths as much as 10 cm in diameter of Precambrian schist, gneiss, and granite (Lipman and Mehnert, 1979). Mineralogically and chemically similar dacites occur at Timber Mountain and Brushy Mountain as part of the Oligocene to Miocene volcanic section on the Taos Plateau.

The rhyolite lava domes at No Agua Peaks are the most evolved lavas of the TPVF (76.5 weight percent SiO_2; Lipman and Mehnert, 1979) and are nearly aphyric, containing less than 1 percent plagioclase + sanidine + quartz. The margins of the domes consist of hydrated perlitic glass with obsidian inclusions (often called apache tears). The interiors of the lava domes are flow laminated and mostly devitrified and contain xenocrystic sanidine derived from underlying deposits of the 25.4-Ma Amalia Tuff (Dickens, 2007).

Rio Grande Gorge

The Rio Grande is the fourth longest river in the United States, traversing 2,830 km (1,759 mi) from its headwaters northwest of Creede, Colorado, to the Gulf of Mexico near Brownsville, Texas (Kammerer, 1990). The river traverses all of the major basins of the Rio Grande Rift and carves a steep-sided 170-m gorge through the Pliocene volcanic cover of the Taos Plateau volcanic field in the southern half of the San Luis Basin. Locally, Rio Grande incision exposes underlying Oligocene to Miocene volcanic basement and distal alluvial fan deposits derived from the Sangre de Cristo Mountains to the east. Exceptional exposures in the canyon walls of the Rio Grande and the Red River tributary facilitate discussion of eruptive history, paleotopography, basin evolution, intrabasin faulting, and Rio Grande incision history. Incision history, though not a specific topic of discussion for this guide, is critical to the interpretation of basin integration attributed to fluvial response coupled to extensional tectonic and Pleistocene climatic change.

Two recent publications, Ruleman and others (2016) and Repasch and others (2017) present data supporting alternate interpretations of the temporal evolution of the Rio Grande during the Pliocene and Pleistocene, the hydrologic integration of the northern and southern segments of the San Luis Basin with basins to the south, the dominant forcing mechanisms (climate versus tectonics), and ultimately the age of the gorge itself. Both publications reference new geochronologic data collected from sites at or near field-trip stops described herein for Day 2 and Day 3 road logs of this guide. The reader is strongly encouraged to consider these publications and references therein as supplements to this guide for discussion of the Pliocene to Pleistocene fluvial history of the region. Given the opposing positions relative to the origins and timing of Rio Grande integration presented in these publications, a very brief summary is presented below and is intended as background for the discussion of Pliocene to Pleistocene volcanic history of the San Luis Basin and northern Rio Grande Rift.

Ruleman and others (2016) present ^{3}He exposure age determinations on scoured Servilleta Basalt surfaces along the course of the Rio Grande that constrain the ages of incised surfaces and inset terraces to between approximately 275 and 175 ka. Uranium-series disequilibrium dating of carbonate rinds contained within the overlying deposits suggest pregorge alluvial surfaces were all abandoned at about the same time. These ages are consistent with proposed middle Pleistocene breaching of a natural dam at the south end of Lake Alamosa in the San Luis Hills, subsequent to the glacial maxima that correlates to marine-oxygen isotope stages 11 (424–390 ka), 10 (390–337 ka), and 9 (337–300 ka). This correlation is consistent with ^{3}He exposure ages on basaltic clasts entrained in barrier spit deposits of the lake during the highstand of Lake Alamosa (Machette and others, 2013; Ruleman and others, 2016). Breaching of the lake and associated drawdown over 2–3 glacial cycles, expansion of the paleo-Rio Grande watershed to include the eastern San Juan Mountains, and lowering of the local base level of the river to that of the southern San Luis Valley facilitated accelerated incision of the Rio Grande gorge through dominantly Servilleta Basalt. In this interpretation, integration of the modern upper reaches of the Rio Grande with the paleodrainages in basins to the south is a middle Pleistocene event.

Repasch and others (2017) propose that a paleo-Rio Grande has occupied a geographic position largely coincident with the modern drainage system since the middle to late Miocene, with headwaters established in the San Juan Mountains by the Pliocene. This interpretation is based largely on ^{40}Ar/^{39}Ar sanidine ages determined from sedimentary grains collected from beneath lava flows and correlated on the basis of age with source areas in the San Juan Mountains and Questa-Latir area of the Sangre de Cristo Mountains. The authors infer similar paleodrainage locations to those observed in the present day and suggest that erosion of the gorge proceeded from south to north, integrating the San Luis Basin with the Española Basin. Repasch and others (2017) further point to small paleochannels incised in Servilleta lava flows on Black Mesa separating flow packages ranging from >5 Ma to approximately 3.5 Ma as evidence of the integrated paleo-Rio Grande drainage system reaching from the San Juan Mountains of Colorado to the Gulf of Mexico. In this model, incision of the Rio Grande was further enhanced by Pliocene uplift associated with Rio Grande Rift basaltic volcanism.

We adopt the former interpretation in this guidebook with the following caveat. Local drainage of the southern San Luis Basin likely was intermittently integrated with basins to the south throughout the Pliocene (Repasch and others, 2017). However, the northern San Luis Basin was closed and intermittently occupied by a large intermontane Pleistocene lake until the breach of a natural dam at the Fairy Hills area of the San Luis Hills (Machette and others, 2013). Consequently, the dramatic increase in the size of the watershed, combined with multiple glacial cycles affecting the carrying capacity of the system, facilitated rapid incision of the Rio Grande (Ruleman and others, 2016).

Day 2—Route Through the Southern Taos Plateau

The Day 2 route follows the course of the Rio Grande into the southern San Luis Basin of the Rio Grande Rift with seven primary and three optional stops designed to facilitate discussion of (1) Pliocene rift structures of the southern San Luis Basin, (2) volcanic stratigraphy and eruptive history of the Pliocene Taos Plateau volcanic field, and (3) pre- and early-rift volcanism of the Questa-Latir volcanic loci of the southern Rocky Mountains volcanic field (fig. 30). The route generally follows the course of the Rio Grande northward, starting at the Embudo Fault Zone, the strike-slip accommodation zone between the Española Basin and the right-stepping en echelon San Luis Basin to the north. Examination of the fault zone near Pilar, New Mexico, and a subsequent overview stop to the north provides the structural and stratigraphic framework for subsequent stops during the day that focus on the complex interplay of extensional rift volcanism and associated basin sedimentation. Two subsequent stops along the southern Rio Grande focus on Servilleta Basalt stratigraphy, petrology, geochemistry, and geochronology of these volumetrically dominant rift volcanic deposits culminating in a midday stop at the iconic "High Bridge" over the Rio Grande gorge. Afternoon stops include a distant view of erosional remnants of pre- and early-rift volcanic deposits preserved along an intrarift platform or horst within the broader extensional basin before descending into the Taos and Questa subbasins of the actively subsiding eastern margin of the San Luis Basin. The remainder of the day will focus on increasingly complex stratigraphic and structural relations between basin-bounding faults, spatially associated volcanic edifices, and prograding fan deposits exposed in gorges of the Rio Grande and major tributaries of Arroyo Hondo and the Red River.

Mileage

0.0 **Stop 2-1. Pilar mesa and Embudo Fault Zone** (36°16.08' N., 105°47.30' W.; 6,070 ft, 1,850 m elevation) *Park vehicles in the upper (east) parking lot of the Bureau of Land Management Rio Grande Gorge Visitor's Center near the junction of New Mexico State Road (NM) 68 and NM 567/570 at the village of Pilar. Public restrooms are available in the visitor's center. Proceed to the trail head at the southeast corner of the parking lot and walk approximately 160 ft uphill for view toward Pilar Mesa.*

The Embudo Fault Zone (fig. 26) is a structural accommodation zone approximately 64 km in length between the west-tilted Española Basin to the south and the east-tilted San Luis Basin to the north (fig. 3). The Embudo Fault Zone merges with the range-bounding Sangre de Cristo normal faults to the north (fig. 26) and the Pajarito Fault to the southwest, where it offsets Pleistocene ignimbrites erupted from the Valles Caldera on the Pajarito Plateau (Wolff and Thompson, Day 1, this volume). The sense of displacement along the Embudo Fault varies along strike, but the northern segment of the fault system typically displays west-down, high-angle displacement accompanied locally by sinistral oblique-slip deformation (Muehlberger, 1979; Leininger, 1982; Machette and Personius; 1984, Kelson and others, 1997, 2004, 2015; Grauch and others, 2017). Geologic mapping and geophysical modeling of aeromagnetic data (Kelson and Bauer, 1998; Kelson and others, 2004; Grauch and others, this volume) reveal the northeastern Embudo Fault Zone as an increasingly en echelon, segmented fault system of dominantly high-angle normal faults propagating toward a poorly defined stepover to the southern Sangre de Cristo Fault.

Approximately 1 km southwest of this stop along NM 68, the Embudo Fault is interpreted as a single northeast-trending fault trace, coincident with the course of the Rio Grande and largely buried by Pleistocene alluvium. At this locality, clastic basin deposits are juxtaposed against an erosional escarpment of Proterozoic metamorphic rocks exposed along the 500-m-high Pilar cliffs. Subordinate fault exposures in bedrock preserve gently west-plunging kinematic indicators documenting north-down, sinistral strike-slip component of deformation (Bauer and Kelson, 2004b). Approximately 11 km to the northeast of the Pilar cliff exposures, synthetic high-angle normal faults distribute extensional strain across a zone as much as 2-km wide near the junction with the southern end of the Taos embayment where it merges with the Sangre de Cristo Fault (Grauch and others, 2017) and are characterized by dominantly west-down, dip-slip displacement.

At this stop the Embudo Fault Zone is as much as 1.5-km wide and characterized by two subparallel fault strands (fig. 31), the southeastern strand buried in the Rito Cieneguilla valley immediately in the foreground between Pilar mesa and the Picuris Mountains, and the westernmost strand visibly displacing capping basaltic lava flows of Pilar mesa (figs. 31, 32). Eroded fault scarps in basaltic lava flows at Pilar mesa trend approximately N. 60° E. and preserve approximately 6 m of vertical offset in mesa-capping basalts. These lava flows are stratigraphically equivalent to the uppermost Servilleta Basalt flows observed at Stop 2-3, where a mesa-capping lava flow yielded an $^{40}Ar/^{39}Ar$ age determination of 3.30±0.06 Ma (sample RGR-414, table 1). This new age determination is within the error previously reported for Servilleta Basalt flows from near this locality (Appelt, 1998; Bauer and others, 2005). The Rito Cieneguilla trace of the Embudo Fault (approximately coincident with NM 68) offsets stratigraphically equivalent age Servilleta Basalt lava flows by approximately 105 m (Bauer and Kelson, 2004b), resulting in an order of magnitude greater post-3.3 Ma slip rate along the southeastern fault strand. The oblique-slip component of displacement

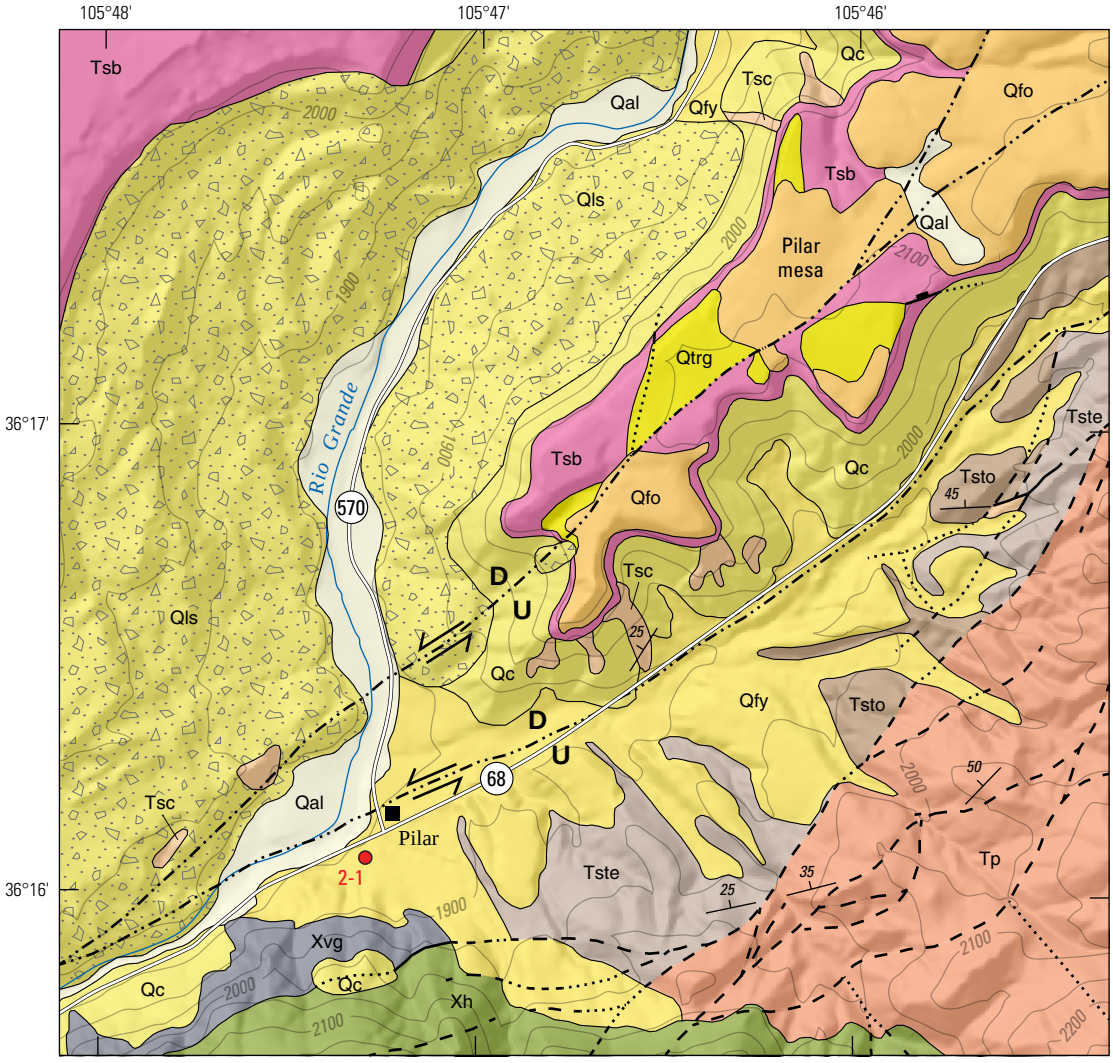

Projection UTM, NAD83 Horizontal Datum, zone 13N, NAVD 1988 Vertical Datum
Shaded-relief base generated from U.S. Geological Survey 10-m Digital Elevation Model (DEM) data from the National Elevation Dataset, accessed November 2016 at http://ned.usgs.gov/.

0 0.5 1 KILOMETER
0 0.25 0.5 MILES

Geology mapped by K.I. Kelson and P.W. Bauer in 1998 and P.W. Bauer and others in 2006

EXPLANATION

- Qal **Alluvium (Holocene)**
- Qc **Colluvium (Holocene to middle Pleistocene)**
- Qls **Landslide deposits (Holocene to late Pleistocene)**
- Qfy **Young alluvial fan and stream terrace deposits (Holocene to middle Pleistocene)**
- Qfo **Old alluvial fan and stream terrace deposits (middle to early Pleistocene)**
- Qtrg **Fluvial gravel of the Rio Grande (middle to early Pleistocene)**
- Tsb **Servilleta Basalt, upper sequence (Pliocene)**

Santa Fe Group

- Tsc Chamita Formation (Pliocene and Miocene)
- Tste Tesuque Formation, Chama-El Rito Member (Miocene)
- Tsto Tesuque Formation, Ojo Caliente Sandstone (middle Miocene)
- Tp Picuris Formation (Oligocene)
- Xh Hondo Group, Rinconada and Ortega Formations, undivided (Paleoproterozoic)
- Xvg Vadito Group, Glenwoody Formation (Paleoproterozoic)
- 2-1 **Field-trip stop**
- **Fault**—Solid where location certain; dashed where location approximate; dotted where location concealed
- D U **Embudo Fault**—Location inferred; arrows indicate inferred right-lateral strike-slip displacement; U, upthrown block; D, downthrown block
- **Reverse fault**—Solid where location certain; dotted where location concealed
- 25 **Strike and dip**—Approximate

Figure 31. Simplified geologic map of the southern Pilar mesa area, modified from Kelson and Bauer (1998) and Bauer and others (2005). The Embudo Fault in Pilar mesa consists of two subparallel strands characterized by left-lateral oblique, down-to-west displacement. Pliocene Servilleta Basalt is displaced to the west, as are underlying Santa Fe Group basin-fill sediments. Sedimentary deposits are increasingly displaced to the west such that the Picuris Mountains to the east preserve older remnants of basin-fill sediments than observed beneath Pilar mesa. Sedimentary deposits beneath flat-lying lava flows at Pilar mesa dominantly dip northwestward. East of this stop, along the flanks of the Picuris Mountains, older sedimentary deposits locally dip as much as 50–60 degrees westward (Kelson and Bauer, 1998; Bauer and others, 2005). Internal deformation and faulting are common along the fault zone, locally thrusting Quaternary deposits on Tertiary deposits. In the northeastern part of the map area, Servilleta lava flows are locally displaced along reverse faults, which are interpreted as local compression between splays of the Embudo Fault.

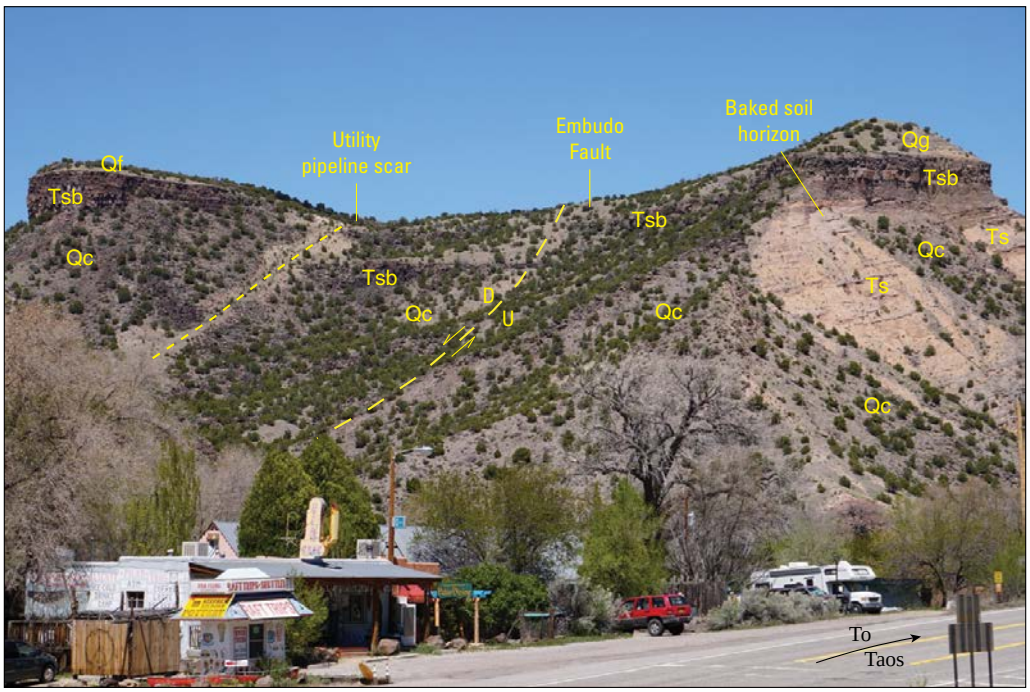

Figure 32. View northwest toward the south tip of Pilar mesa from the Stop 2-1 overlook. The flat lying Servilleta Basalt (Tsb) records approximately 4 meters of down-to-northwest dip-slip displacement along the northernmost strand of the Embudo Fault Zone. Note flat-lying lavas of Servilleta Basalt unconformably overlie northwest-dipping Tesuque Formation (Ts) basin-fill deposits of the Santa Fe Group. The lower slopes are largely covered by Quaternary colluvium (Qc), fan deposits (Qf), and lesser landslide deposits (not shown); locally, ancestral Rio Grande gravel deposits (Qg) are also offset (Kelson and Bauer, 1998; Bauer and others, 2005) but not visible from this vantage point. Photograph by Ren A. Thompson, U.S. Geological Survey.

along both strands of the Embudo Fault Zone at this stop is unknown, but tilted and deformed sediments beneath the lava flows suggest oblique-slip deformation predated eruption of the overlying basaltic lava flows. Bauer and Kelson (2004b) and Kelson and others (2015) suggest averaged values of post-3 Ma slip rates on this Embudo Fault segment of 35 meters per million years (m/m.y.) (vertical), 96 m/m.y. (horizontal), and 102 m/m.y. (net slip).

The view of the southern end of Pilar mesa to the northeast (figs. 32, 33) shows nearly flat-lying Servilleta Basalt lava flows unconformably overlying moderately northwestward dipping (approximately 25°) basin-fill sediments of the southern San Luis Valley. Late Oligocene to Pliocene basin fill within the San Luis Valley segment of the rift is principally assigned to the Santa Fe Group, a stratigraphically complex association of alluvial, fluvial, and mass-wasting sediments deposited in actively subsiding basins or subbasins. Discontinuous exposures of Santa Fe Group sediments in the basin are preserved in incised canyons or as sediment wedges along uplifted fault-bound range fronts. Both cases are represented here along the northeast segment of the Embudo Fault Zone, separating the actively subsiding San Luis Basin to the northwest from the uplifted Picuris Mountain segment of the Sangre de Cristo Mountains to the east.

The low slopes in the foreground of figure 32 largely covered in Pleistocene colluvium, are underlain by deposits of the Chamita and Tesuque Formations within the Santa Fe Group (Kelson and Bauer, 1998). Tesuque Formation deposits at Pilar mesa are dominantly late Miocene (10–5 Ma) but locally include early Pliocene deposits. Clast lithologies within the Chamita Formation grade upsection from mixed Proterozoic metamorphic and Tertiary volcanic clasts near the base to exclusively metamorphic clasts near the unconformity with the overlying Servilleta Basalt. Santa Fe Group sediments on the west side of NM 68 are locally mantled by middle Pleistocene fan deposits, but where exposed are dominantly middle Miocene (18–14 Ma; Steinpress, 1980) volcaniclastic deposits of the Tesuque Formation (Kelson and Bauer, 1998). These deposits lie unconformably on Proterozoic metamorphic rocks immediately to the east. The juxtaposition of late Miocene against middle Miocene deposits across the Embudo Fault supports an interpretation of significant Miocene and younger west-down dip-slip motion on the fault.

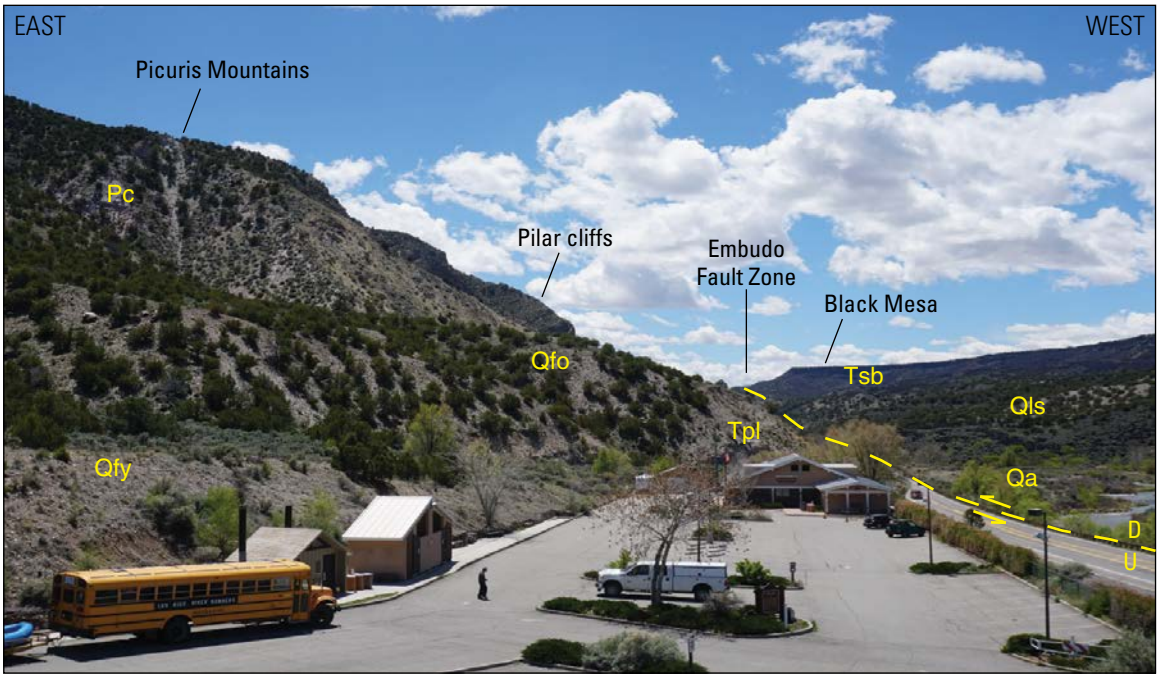

Figure 33. View southwest along New Mexico State Road (NM) 68. Proterozoic crystalline basement of the Picuris Mountains (Pc) forms prominent cliffs observed on the east side of highway. Local deposits of the Tertiary Picuris Formation (Tpl) are preserved in a fault block near the Bureau of Land Management visitors center. Early to middle Pleistocene (Qfo) sediments and middle Pleistocene to Holocene sediments(Qfy and Qa) are preserved east of the highway. Pleistocene landslide deposits (Qls) are preserved locally. Pliocene Servilleta Basalt (Tsb) caps Black Mesa, visible on the horizon, and preserves northwest-trending folds associated with the Embudo Fault Zone (Koning and others, 2013, plate 1). Northeast of this locale along NM 68, roadcut exposures preserve evidence of left-lateral slip (Kelson and others, 2004). Photograph by Ren A. Thompson, U.S. Geological Survey.

In the southern San Luis Basin these deposits are typically overlain by lava flows of the Servilleta Basalt; a formational name originally interpreted by Montgomery (1953) to include interbedded volcanic and sedimentary deposits of the Taos Plateau volcanic field but more recently restricted to Pliocene basaltic lavas of the volcanic field (Lipman and Mehnert, 1979; Thompson and Machette, 1989; Thompson and others, 2015).

0.0 *Route mileage (0 miles [mi]) begins at parking lot entrance intersection with NM 68. Turn right from the visitor's center parking lot onto NM 68 and proceed northeast. Beware of high-speed traffic on highway.*

0.25 Exposures in roadcuts on both sides of NM 68 are middle to late Pleistocene alluvial-fan and stream terrace deposits derived from drainages located to the east in the northern Picuris Mountains. Dominant lithologies are Proterozoic quartzite, schist, and slate (Kelson and Bauer, 1998).

1.5 Exposures in roadcuts on the west side of NM 68 are moderately to poorly sorted buff-colored sands containing clasts of Tertiary volcanic rock and Proterozoic metamorphic rocks; sediments assigned to the Tesuque Formation of the Santa Fe Group (Bauer and Kelson, 1998).

3.2 Basin-fill deposits exposed on the west side of the highway are overlain by Servilleta Basalt lava flows equivalent in age and stratigraphic position as those observed capping Pilar mesa at Stop 2-1.

4.7 Roadcut exposures (fig. 34) were first described by Muehlberger (1979) as a series of moderate- to low-angle strands of the Embudo Fault that cut Santa Fe Group sediments, reflecting transpression along this segment of an "intracontinental transform fault." Subsequent detailed mapping of the 1.5-km-wide Embudo Fault Zone and observations of fault kinematics (Kelson and others, 1997; Kelson and Bauer, 1998) reveal that the fault zone in this area is composed of three major strands. The northern and middle strands are exposed in this outcrop and the southern strand is located near the base of the Picuris Mountains to the southeast. The northern strand exposed in this outcrop juxtaposes Tertiary Ojo Caliente Sandstone deposits thrust over Quaternary alluvial fan deposits. Muehlberger

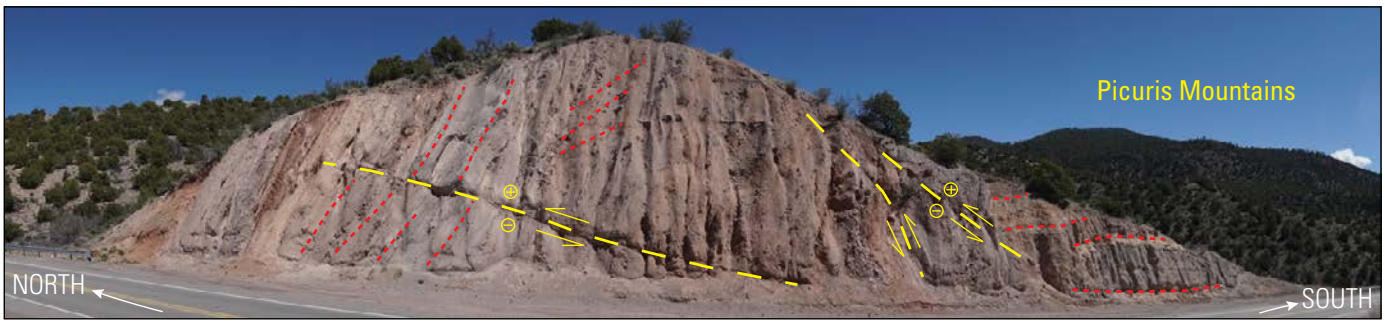

Figure 34. Roadcut exposures in faulted and deformed Santa Fe Group sediments, originally described by Muehlberger (1978, 1979) and Leininger (1982), identify the exposed faults as west-vergent thrusts that locally juxtapose Tertiary basin-fill over Pleistocene colluvium. Subsequently, Kelson and others (1996, 2004) interpreted the faults exposed in the New Mexico State Road 68 roadcuts as secondary thrust faults that merge down-dip with the primary, near-vertical Embudo Fault. Local thrusting is interpreted to reflect positive flower structures between major strands of the left-lateral Embudo Fault. Photograph by Ren A. Thompson, U.S. Geological Survey.

(1979) suggested this observation required that the Embudo Fault accommodated regional crustal shortening facilitated by north-vergent thrust faulting of the Picuris Mountain block over the obliquely extending southern San Luis Basin (Aldrich, 1986; Brown and Golembek, 1986). The middle fault strand, preserved in this outcrop, is associated with deformed and tilted basin-fill deposits. The northern and middle strands of the fault merge to the south (Kelson and others, 1997; Kelson and Bauer, 1998). Additional low-angle faults characterized by small displacement (<1–2 m) can also be observed in outcrop.

Based on detailed examination of this outcrop and associated 1:24,000 scale mapping of the northeastern section of the Embudo Fault Zone, Bauer and others (2004, p. 72–74) concluded that the observed low-angle faults and associated reverse displacement reflect positive flower structures on faults that merge with steeply dipping oblique-slip faults in the subsurface. See Grauch and others (2017) for a regional interpretation of the northeastern Embudo Fault Zone and cross section depicting the regional context of faults observed in this outcrop. Most significantly, these observations negate the need for any significant counterclockwise rotation of the southern San Luis Basin, requiring only oblique slip to accommodate the en echelon offset of the San Luis and Española Basins.

4.9 **Stop 2-2. Taos Plateau overview** (36°8.50’ N., 105°43.85’ W.; 7,077 ft, 2,157 m elevation) *Pull off on right shoulder of highway near sheltered picnic tables.*

The iconic view to the north across the Taos Plateau (fig. 35) extends from the southern end of the San Luis Valley to Ute Mountain (10,098 ft, 3,078 m summit elevation) near the Colorado-New Mexico border, a distance of nearly 70 km. Ute Mountain stands nearly 2,510 ft (765 m) above the surrounding plateau. The plateau surface is underlain by volcanic rocks of the Pliocene Taos Plateau volcanic field. The flat tablelands of Servilleta Basalt are punctuated by volcanic edifices ranging in composition from basaltic andesite to dacite; the gentle slopes of andesitic shield volcanoes such as Cerro de la Olla and Cerro Montoso stand in sharp

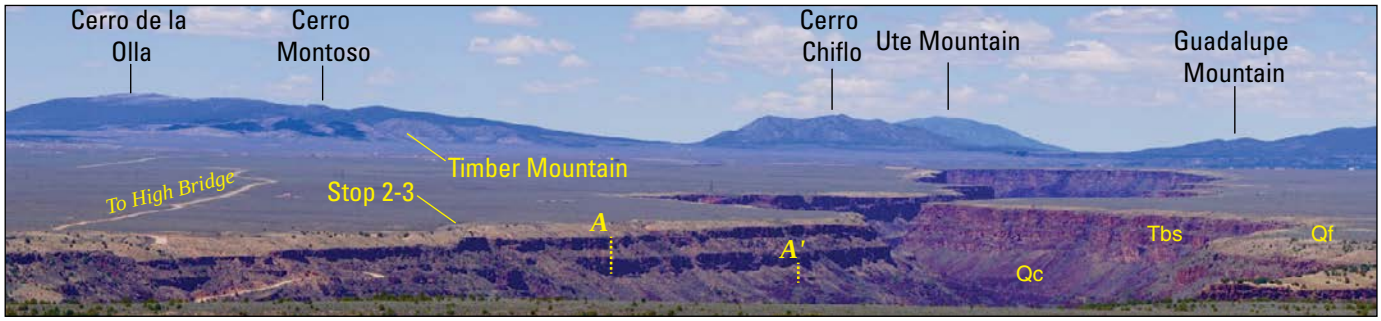

Figure 35. View north across the central Taos Plateau from Stop 2-2. From left to right are Cerro de la Olla (9,465 feet [ft], 2,885 meters [m]), a 4.33 million year old (Ma) olivine andesite, Cerro Montoso (8,655 ft, 2,638 m) a 4.95-Ma olivine andesite, Cerro Chiflo (8,976 ft, 2,736 m) a 10.99–9.64-Ma dacite, Ute Mountain (9,810 ft, 2,990 m) a 3.95-Ma trachyandesite volcano; and Guadalupe Mountain (8,763 ft, 2,671 m) an ~5.35-Ma trachyandesite to dacite volcano. Tbs, Servilleta Basalt; Qc, Quaternary colluvium; Qf, distal Quaternary fan, local fluvial, and reworked eolian deposits; *A* and *A*’ indicate sampled sections. Photograph by Ren A. Thompson, U.S. Geological Survey.

contrast to the steep-sided composite lava dome complex of Ute Mountain and the significantly smaller, though irregularly steep-sided form of Guadalupe Mountain in the near distance. Lipman and Mehnert (1979) noted the distinct geomorphic correlation of silica content and slope angle of volcanic edifice, suggesting that volcanic constructs have likely preserved a large component of their original geomorphic form. However, all volcanoes on the Taos Plateau have experienced substantial erosion, most likely driven by significantly wetter paleoclimate associated with repeated major glaciations during the Pleistocene that resulted in deeply incised canyons and valleys on the slopes of many volcanic edifices and removal of primary near-vent pyroclastic deposits. Since the middle Pleistocene the Rio Grande has carved the deep gorge observed on the Taos Plateau (Ruleman and others, 2016 and references therein) through intercalated basaltic to intermediate composition lava flows and underlying basin-fill sediments of the rift. This incision was coincident with the erosional degradation of the volcanic edifices on the plateau. In the foreground of figure 35, the Rio Grande gorge is approximately 185-m deep and cuts a sinuous path largely bordered on the west by Oligocene to Pliocene volcanic highlands and on the east by incised Pleistocene fan deposits from the Sangre de Cristo Mountains.

The gently east-dipping (<2–3 degrees) plateau surface forms the hanging wall of the basin-bounding Sangre de Cristo normal fault, juxtaposing the Sangre de Cristo Mountains on the east against the geomorphic San Luis Valley and the major extensional Pliocene subbasins therein. Intrabasin normal faults, both down-to-east and down-to-west, are superposed on paleotopography inherited from volcanic constructs of the Oligocene southern Rocky Mountains volcanic field (Days 4–6 and Stop 2-5 of this guide) and little known Miocene volcanic rocks observed at a distance from this stop and on Day 3 of this guide. Preserved remnants of these pre-extension and early-extension related volcanic rocks are exposed at Timber Mountain (Stop 2-5) and Cerro Chiflo (Stop 3-4), both visible from here. These remnants mark the western structural margin of a major intrarift platform, referred to as an intrarift horst (Lipman and Mehnert, 1979; Thompson and others, 1986; Dungan and others, 1989b), which extends nearly 80 km from Timber Mountain in the south to the north end of the San Luis Hills in Colorado, and is nearly 30-km wide at the latitude of Cerro Chiflo (fig. 30). This interpretation is based on recent acquisition of gravity measurements across the basin and into the bounding uplands, and new modeling techniques that remove the effect of high-density basaltic lavas from unconsolidated sediment fill (Drenth and others 2013, 2016). The area between this stop at the southern end of the Taos graben (fig. 30), the largest structurally bound subbasin in the southern San Luis Basin, and the northern end of the graben near Stop 2.7 attains a maximum basin-fill depth of 1.5 to 2 km.

Volcanoes of the Pliocene Taos Plateau volcanic field visible from this stop include (1) the basaltic andesite to andesitic edifices of Cerro de la Olla and Cerro Montoso (4.33 and 4.95 Ma, respectively; table 1), (2) the trachyandesite to dacitic edifices of Ute Mountain and Guadalupe Mountain (3.95 and 5.35 Ma, respectively; table 1), and (3) Servilleta Basalt lava flows exposed in the gorge, which range in age from 3.79 Ma near the base to 3.30 Ma at the rim (see Stop 2-2 for details). Intermediate to silicic volcanic remnants of the Questa-Latir volcanic locus formed significant paleotopographic barriers to basinward deposition of volcanic deposits during the Pliocene. This heavily influenced the relative thickness of eruptive packages within the Pliocene volcanic section observed in the Rio Grande gorge and gorges of major tributaries, particularly the Red River 33 km to the north. Likewise, large Pliocene andesitic to dacitic centers resulted in locally obstructed, dominantly east-directed flow of the plateau-forming lavas of the Servilleta Basalt.

Note historical signs at this stop referring to the complex cultural interactions of indigenous and immigrant populations of this valley during the late 18th and 19th centuries (fig. 36). Return southwest on NM 68 approximately 4.8 mi to intersection with County Road 570 at Pilar, New Mexico.

9.7 *Turn right at Pilar, New Mexico, onto County Road 570 and proceed north along the course of the Rio Grande approximately 6.1 mi to the low bridge crossing over the Rio Grande.*

10.8 *Entering Rio Grande del Norte National Monument, established in 2013* (https://www.blm.gov/publish/content/nm/en/prog/NLCS/RGDN_NM.html). *Please observe all monument regulations and watch for foot traffic and commercial shuttle buses during rafting season.*

15.8 *Junction of County Road 570 and County Road 567. Proceed west on County Road 567 and climb approximately 102 yd (93 m) from the Rio Grande (6,093 ft, 1,857 m elevation) to the west gorge rim (6,726 ft, 2,050 m elevation). Use caution, the narrow roadway contains switchback turns and limited visibility.*

15.83 The Rio Grande.

15.9 Exposures at right are rockslide debris at the southern end of a series of large Toreva blocks that choke the Rio Grande gorge for approximately 3.5 km north

Figure 36. Interpretive history signs at Stop 2-2 that document the cultural conflict and competition for resources and trade, including women and children, between indigenous populations and European immigrants to the Taos area during the 18th and 19th centuries. Photograph by Ren A. Thompson, U.S. Geological Survey.

of this locality. Toreva blocks are an end member of the rockslide family of mass-wasting deposits originally defined for the type locality on the flanks of Black Mesa on the Hopi Reservation near Toreva, Arizona (Reiche, 1937). Toreva blocks are generally characterized by unbroken tilted masses of stratified material backtilted toward the headwall of the breakaway zone.

16.0 Exposed in the Toreva block on the right are weakly developed pillow basalt structures in Servilleta Basalt interpreted to represent eruption of basaltic lava flows into standing water in the Pliocene San Luis Basin (fig. 37). These deposits are locally common at the base of Servilleta Basalt sections overlying Santa Fe Group basin-fill sediments or near sedimentary interbeds between eruptive packages of Servilleta Basalt. Pillows tend to form in the lower 2–3 m of flow sequences and are characterized by yellow palagonitized glassy rinds. Locally, steam injection pipes or cracks are filled with underlying sediment, likely the result of rapid boiling of local surface water.

To examine these deposits, please park in the small pulloff to the right 0.35 mi beyond the next switchback. These exposures are severely degraded owing to damage inflicted by geologists on previous field trips. Please do not repeat past transgressions. Remember, you are in a National Monument and these outcrops are protected!

16.13 *Parking area for pillow basalt locale.*

16.46 *Parking area to the right at trailhead for La Vista Verde Trail.* This trail traverses Toreva blocks along the canyon of the Rio Grande for approximately 1.75 km, providing excellent exposures of displaced Servilleta Basalt.

16.5 For the next mile the road climbs along the top of the Toreva block section near the headwall to the west. Elevation increases rapidly as the road climbs to the west gorge rim at 6,759 ft (2,060 m).

17.0 Note the distinctive vertical segregation pipes or tubes in the Servilleta Basalt in exposures to the right, a characteristic feature of olivine tholeiite lava flows on the Taos Plateau.

17.1 The road climbs onto middle Pleistocene distal fan deposits overlying Servilleta Basalt, which were deposited from streams discharging into a series of closed subbasins within the San Luis Basin (Ruleman and others, 2016) prior to incision of the Rio Grande.

17.46 *Turn right on the dirt road to the Dead Cholla Trailhead parking area.*

17.8 **Stop 2-3. Servilleta Basalt at Dead Cholla Trailhead** (36°21.41' N., 105°44.05' W.; 6,745 ft, 2,056 m elevation) *Park in the designated parking area and proceed on foot approximately 0.10 mi from the trailhead along Dead Cholla Trail to the southeast toward the Rio Grande gorge rim.*

The Rio Grande has cut a gorge approximately 185-m deep through Servilleta Basalt and underlying Santa Fe Group sediments at this locality (fig. 38). The exposed basalt thickness is approximately 40 m and the

Figure 37. Highly degraded roadcut in Servilleta Basalt pillow lavas included within a Toreva block. Pillow structures and locally preserved palagonite suggest eruption into water or underlying water-saturated sediments. In the Pliocene, this part of the San Luis Basin was intermittently closed to through flowing drainages (Ruleman and others, 2016), which often resulted in aerially restricted shallow playa deposits and seasonally saturated, fine-grained surficial deposits. Pillow lavas are restricted to the base of the eruptive packages, which indicate only early erupted flows experienced alteration through interaction with water. Photograph by Ren A. Thompson, U.S. Geological Survey.

underlying sedimentary deposits are inferred to be at least 120-m thick; the base is not exposed beneath the gravity slide deposits. The Toreva block morphology of the slides preserves the original stratigraphy exposed in the canyon walls and records multiple episodes of gravity sliding where less deformed, often smaller blocks are preserved above stratigraphically older blocks beneath. Downcutting of unstable, weakly consolidated sediments beneath basaltic lava flows may be the primary cause of collapse. However, it is likely that north-trending fractures prominent in the lava flows, parallel to small intrabasin Pleistocene extensional faults, also facilitate failure during earthquake shaking. The process may also have been exacerbated by wetter climates associated with interglacial cycles and significantly larger discharge of meltwater during the middle Pleistocene relative to the carrying capacity predicted for the Rio Grande throughout the Holocene.

Toreva blocks dominate the inner canyon morphology from Pilar, New Mexico, to a point 9 km north where intercanyon stratigraphy is dominated by vertical walls of Servilleta Basalt with relatively

Figure 38. View north across the Rio Grande gorge from the Dead Cholla trail head. Here the Rio Grande has carved a 185-meter-deep canyon through Servilleta Basalt and underlying basin-fill deposits of the Santa Fe Group. Toreva-block style landslide deposits fill the lower parts of the canyon and preserve stratigraphic relations of intact sections exposed in the canyon walls. Servilleta eruptive packages are interbedded with distal alluvial fan, fluvial, and eolian deposits, and record an eruptive record spanning approximately 250,000 years (see Stop 2-3). Middle Pleistocene surficial deposits cap the section. The Sangre de Cristo Mountains form the high country on the horizon. Photograph by Ren A. Thompson, U.S. Geological Survey.

thin intercalated deposits of fine-grained eolian sandstones. Basalt-dominated colluvial deposits are preserved as continuous cover along the lower reaches of the canyon or as truncated aprons perched on tops of basalt benches formed at the base of sedimentary interbeds. At this stop the gorge is 1.3-km wide but narrows to 350-m wide at the High Bridge (Stop 2-4) only 13.5 km to the north. Unconsolidated to weakly consolidated middle Pleistocene gravels and interbedded sandstones preserved above Servilleta Basalt at this stop (Kelson and Bauer, 1998) necessarily predate incision of the Rio Grande. Clast lithology is dominated by Proterozoic metamorphic rocks derived from the Picuris Mountains. Preliminary uranium-series disequilibrium dating of carbonate rinds on stratigraphically equivalent, incised deposits 19.5 km to the north (Ruleman and others, 2016) suggest canyon cutting may be as young as 250 ka.

Prograding alluvial fan deposits associated with Pliocene uplift along the down-to-west Sangre de Cristo Fault and northeasternmost Embudo Fault formed large fan complexes underlying most of the Servilleta Basalt in the east half of the San Luis Basin. Clast morphologies in the deposits suggest derivation from the Sangre de Cristo and Picuris Mountain blocks to the southeast and east. Fluvial systems associated with some of the clastic deposits underlying the Servilleta Basalt in the south half of the Taos Plateau may have been integrated with the Española Basin to the south (Koning and others, 2016). However, eruption of plateau-forming Servilleta Basalt, inferred to have largely erupted from vents to the west of this locality, infilled paleotopography established by the prograding fans from the east and eventually closed the basin at the constriction formed along the Embudo Fault Zone.

A composite 50-m vertical section approximately 0.2–0.3 km northeast of the parking lot on the west side of the gorge records three eruptive sequences of Servilleta Basalt. The lowermost exposure is a single lava flow mostly covered by colluvium, the middle and upper sequences are multiflow deposits equivalent to those observed on the east canyon wall (fig. 38). The upper two lava packages are underlain by thin sedimentary interbeds. Whole-rock $^{40}Ar/^{39}Ar$ determinations on the single lower flow yield a preferred age of 3.79±0.03 Ma; the upper flows of the overlying packages yield ages of 3.54±0.09 and 3.30±0.06 Ma, respectively (samples RGR-410, RGR-412, and RGR-414, table 1). The lavas are inferred to have been erupted from vents or fissures to the west or northwest. Preserved low-relief shield volcanoes of Servilleta Basalt to the northwest may be eruptive centers for some tholeiitic lava flows equivalent in stratigraphic position to the uppermost lavas preserved here.

All flows exposed in the gorge at the south end of the San Luis Valley are olivine tholeiites with characteristic diktytaxic texture characterized by void space within a framework lattice of plagioclase and interstitial olivine. Pahoehoe flow textures are common as are vertical vesicle pipes and horizontal vesicle partings (figs. 39–42). Coherent lava packages are often preserved over kilometers of exposure in the gorge, but distribution of individual lava flows is discontinuous over distances of meters to a hundred meters. The uppermost package of Servilleta lavas at this locality thins to single lava flow 8.5 km to the northeast in the Pueblo de Taos drainage, buttressed against Pliocene alluvial fan deposits.

Return to the parking area at Dead Cholla Trailhead, noting the dominantly metamorphic clasts in the middle Pleistocene deposits that overlie the Servilleta Basalt. This trail also affords an excellent view of the contact between deformed Pennsylvanian rocks that form the low divide in the Sangre de Cristo Mountains and the rugged peaks of the Proterozoic high country to the north of Taos, New Mexico (fig. 38).

Return to County Road 567.

18.1 *Intersection with County Road 567, turn right and proceed north.*

18.8 *Intersection with Taos County Road Cb-115. County Road 567 turns sharply west. Proceed north on County Road Cb-115 (Upper Rim Road).*

26.9 *Intersection with Sheep Herder Road. Turn right to intersection with NM 64.*

Figure 39. Pahoehoe flow structures commonly observed in Servilleta Basalt flows. Photograph by Ren A. Thompson, U.S. Geological Survey.

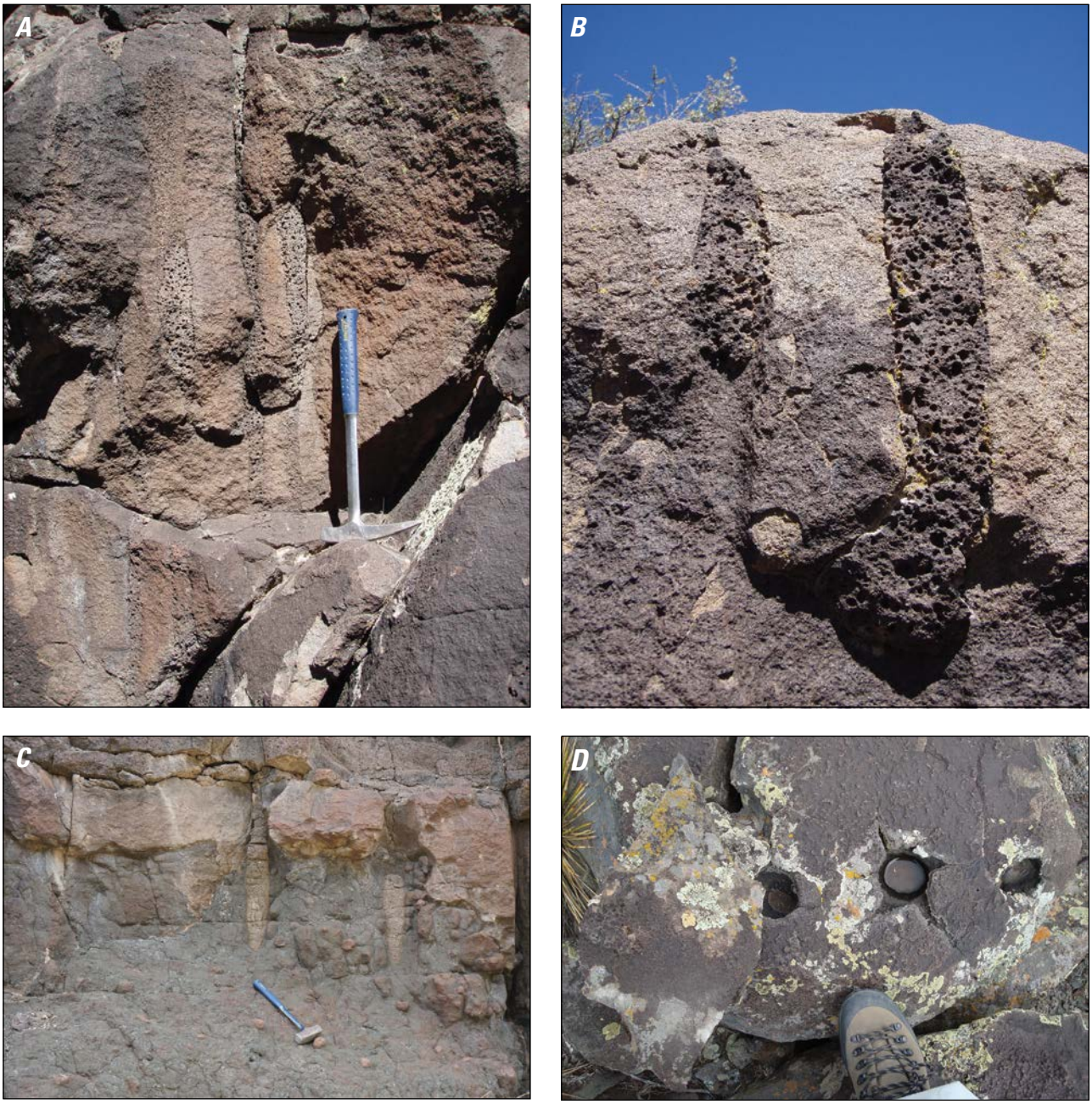

Figure 40. Vesicle segregations in Servilleta Basalt. *A*, Typical vesicle segregations relative to the scale of an 18-inch rock hammer handle. Vertical vesicle pipes often terminate in horizontal segregations or fractures along downward propagating cooling fronts. *B*, Cross sectional exposures of vesicle pipes that reach the exposed upper surface of lava flows typically indicate fluvial scouring of a basalt surface, often associated with the drainages in which these exposures are found. *C*, Vesicle pipes formed in pillow-palagonite breccias near the base of lava flows. *D*, Vesicle pipes in cross section preserve radial cooling fractures. This exposure is from near the current gorge rim and the upper part of the lava flow was removed by a paleo-Rio Grande system prior to entrenchment and formation of the gorge. Photographs by Ren A. Thompson, U.S. Geological Survey.

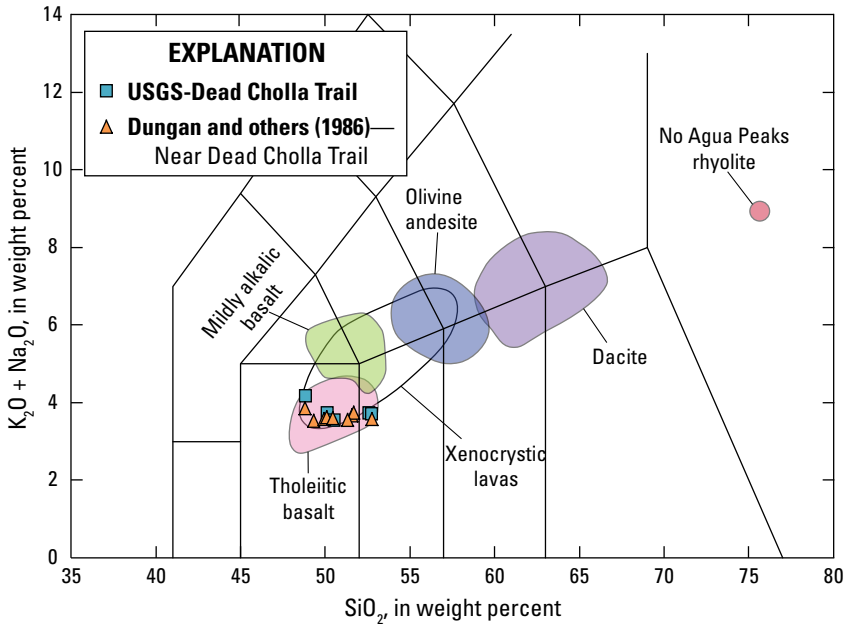

Figure 41. Total alkali (Na_2O+K_2O) versus silica (SiO_2) classification diagram for Pliocene volcanic rocks of the Taos Plateau based on Le Bas and others (1986) with Servilleta Basalt data from the Stop 2-3 locality superimposed. Data normalized to volatile-free based on the method of Middlemost (1989).

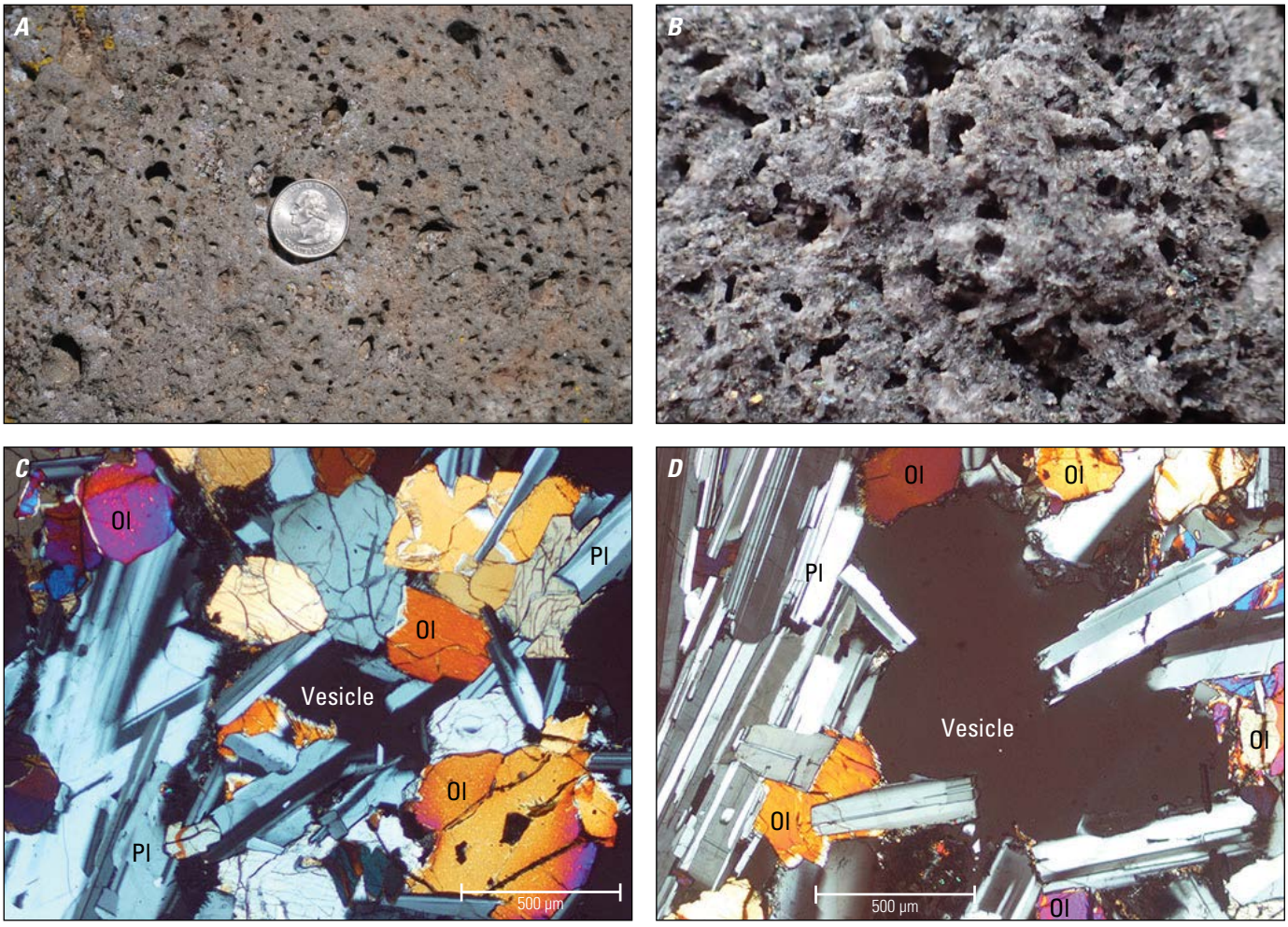

Figure 42. *A*, Field photograph of diktytaxitic texture and rounded vesicles characteristic of tholeiitic basalts of the Rio Grande Rift. *B*, Macroscopic photograph of diktytaxitic texture with angular void space bounded by plagioclase framework evident. Note the small iridescent olivine phenocrysts. *C*,*D*, Photomicrographs of resorbed-olivine textures. Pl, plagioclase, ol, olivine. Photographs by Christine Chan, U.S. Geological Survey.

26.9 *Intersection with NM 64. Watch for high-speed traffic. Turn right (southeast) towards the Rio Grande gorge parking area.*

27.6 *Turn right onto Rest Area Road and proceed to the east side of rest area parking lot. Walk to the bridge for an overview of the gorge.*

27.85 **Stop 2-4. Servilleta Basalt stratigraphy at High Bridge over Rio Grande gorge** (36°28.52' N., 105°44.14' W.; 6,995 ft, 2,132 m elevation) *Proceed to the parking area on the east side of the public restrooms at the rest area. Walk to the High Bridge over the Rio Grande for discussion. Please exercise caution while on the bridge and watch for traffic! Please do not throw anything off of the bridge, during the rafting season there is river traffic below.*

The High Bridge over the Rio Grande was completed in 1965. It is the tenth highest bridge in the United States, spanning 183 m at an elevation 172 m above the river (www.highestbridges.com). Prior to completion, traffic was routed across low-bridge crossings north of Pilar, New Mexico, en route to Stop 2-3, and the Dunn Bridge below Stop 2-6. At the time of completion the Rio Grande Gorge Bridge, also called the High Bridge, was the second highest bridge in the United States. The bridge was added to the National Register of Historic Places in 1997 and remains a highly visited tourist attraction in northern New Mexico.

At the High Bridge, the Rio Grande has cut an approximately 170-m gorge through a thick sequence of Servilleta Basalt (figs. 43–45). The base of the volcanic section is not exposed and is locally covered by basaltic colluvium at river level. Above the colluvium, three lava flow packages consist of multiple lava flows of variable individual thickness that are unconformably separated by sedimentary interbeds. The sedimentary beds are dominated here by fine-grained eolian sands and distal fluvial- and alluvial-gravel reworked from fan deposits sourced in the Sangre de Cristo Mountains. The lower sediment interval at this locality is typically less than 5 m in thickness but is visible across the canyon as buff colored breaks between the lower and middle packages of flows. The upper sedimentary interbed is more prominently inferred to underlie the colluvial slope separating the middle and uppermost lava packages. This upper sedimentary unit attains a local thickness of nearly 35 m at the bridge.

The three Servilleta Basalt packages are well characterized by $^{40}Ar/^{39}Ar$ dates from a section 1.5 km north of the High Bridge (fig. 44; table 1). The exposed basal and uppermost flows of the lower package yield ages of 4.81±0.03 Ma and 4.55±0.04 Ma, respectively. The ages for the base and top of the middle package are 4.17±0.03 Ma and 4.07±0.09 Ma, respectively; the ages for the base and top of the upper package are 3.71±0.14 Ma and 3.67±0.10 Ma, respectively. This defines an emplacement interval of approximately 260 ka for the lower package and <100 ka for both the middle and upper packages, separate by quiescent intervals on the order of 300–400 ka.

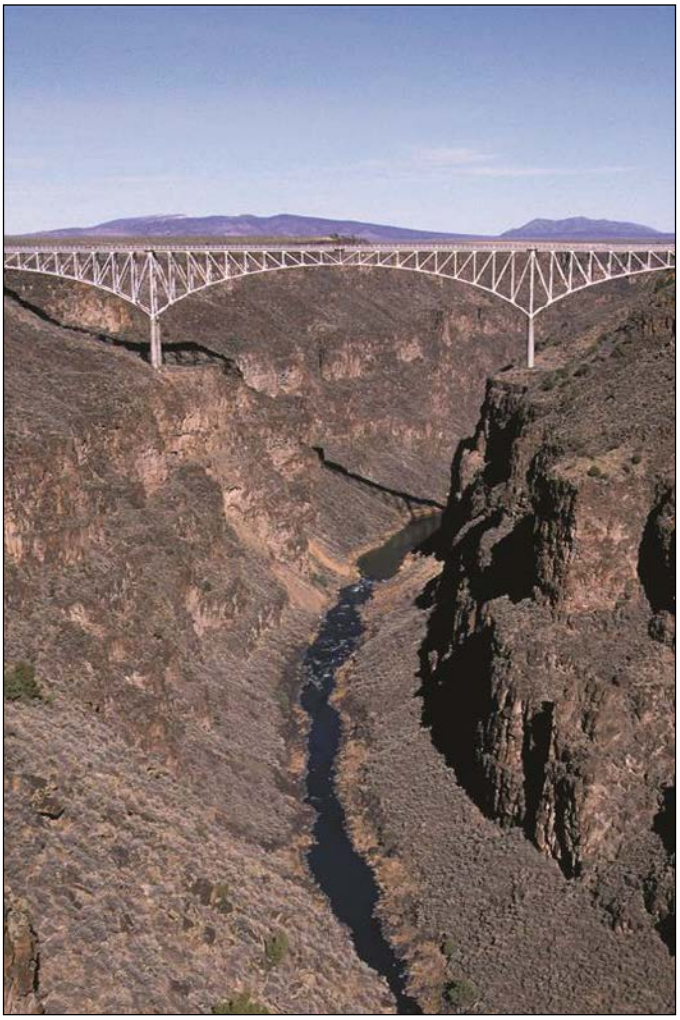

Figure 43. View north towards the High Bridge on New Mexico State Road 64 across the Rio Grande gorge. The bridge was completed in 1965 and the road platform is 172 meters above the river level. Three distinct eruptive packages of Servilleta Basalt are well exposed here, separated by sedimentary interbeds dominated by fine-grained reworked eolian and fluvial sands and lesser pebble gravels. Cerro Montoso, a Pliocene olivine andesite volcano of the Taos Plateau volcanic field and the eroded remnants of the Miocene trachydacite volcano at Cerro Chiflo are visible in the background. Photograph courtesy of the Bureau of Land Management.

Geologic mapping of gorge stratigraphy by Peterson (1981) and Leininger (1982) between Pilar, New Mexico, to the south and Red River to the north identified multiple intercalated volcanic and sedimentary deposits. Dungan and others (1984) described the geochemical character of Servilleta

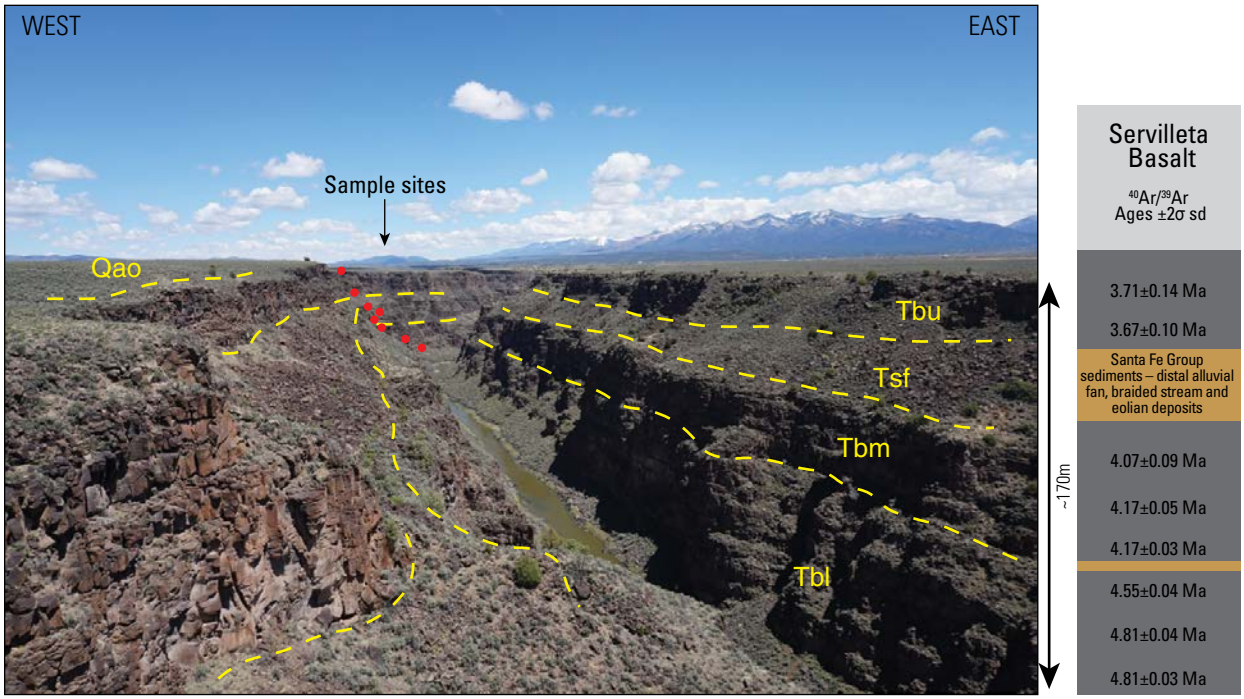

Figure 44. View north of the Rio Grande gorge from the High Bridge. Dashed lines indicate approximate contacts separating three major eruptive packages and red dots indicate sample sites for $^{40}Ar/^{39}Ar$ age determinations presented in column at right. Colluvium covered slopes between lava flow packages are underlain by sedimentary interbeds. Qao–middle Pleistocene surficial deposits; Tsf–Pliocene sedimentary deposits of the Santa Fe Group mantled by basalt colluvium; Tbl, Tbm, Tbu–lower, middle, and upper eruptive packages of Servilleta Basalt, respectively; Ma, million years ago; 2σ sd, 2-sigma standard deviation. Photograph by Ren Thompson, U.S. Geological Survey, 2016.

Figure 45. View south of the Rio Grande gorge from the High Bridge. Note the thickening sequence of sediments between the lower and middle eruptive packages to the south, relative to that observed looking north (fig. 44). At Stop 2-3, the lower eruptive package is absent, and the equivalent stratigraphic interval is replaced by a thick sequence of sedimentary deposits that underlie Toreva-block landslides. Photograph by Ren Thompson, U.S. Geological Survey, 2016.

Basalt at this section and others between Red River and Pilar and established a lower, middle, and upper lithostratigraphic nomenclature based on the stratigraphy at this type locality. Dungan and others (1984) correctly suggested that sedimentary interbeds represent time intervals in excess of those represented by the eruptive intervals, but incorrectly inferred that stratigraphic packages represent discrete eruptive events over short time periods. Results of new $^{40}Ar/^{39}Ar$ geochronology across the plateau, combined with new geologic mapping, suggest the Servilleta Basalt had a complex eruptive history and the original proposed stratigraphic nomenclature may have limited utility beyond this type locality. This is particularly relevant in the context of the time transgressive depositional history of alluvial fans and reworked eolian deposits distributed across the plateau. However, the stratigraphy observed at this stop does provide an excellent representation of geochemical variation within the most complete stratigraphic section exposed in the gorge.

Major element geochemical variation within the High Bridge section ranges from 49–52 weight percent SiO_2 with corresponding variation in total alkalis (Na_2O+K_2O) of 3.2–4.3 weight percent (fig. 46, table 2 Dungan and others, 1984). This represents approximately two-thirds of the variation observed within the Taos Plateau volcanic field. Increasing SiO_2 concentrations are accompanied by decreases in MgO (<1.7 weight percent), large-ion lithophile elements, and high-field strength elements. Variation in geochemistry within the lower, middle, and upper flow packages can be complex and varies with distribution along the gorge. Within the lower package, the most and least evolved lava flows occur at the base and top of the section, respectively. A similar progression is observed for the middle package and the opposite is observed for the upper package. By contrast, the least evolved Servilleta lava flows from the Dead Cholla section (Stop 2-3) occur at the base of the section and progress to more evolved compositions upward through the stratigraphic section. The stratigraphic equivalence of these two uppermost packages inferred by Dungan and others (1984) is not supported by the new $^{40}Ar/^{39}Ar$ age determinations (3.54–3.3 Ma at Stop 2-3; 4.17–3.17 Ma at Stop 2-4). However, the inversion of geochemical trends within these packages and discrete changes in eruption age within any given package preclude a direct petrogenetic link between lava flows of sediment-bound eruptive packages. This is particularly problematic as source areas for upper Servilleta lavas are poorly constrained, particularly north of this locality, and are largely unconstrained for deposits stratigraphically deeper in the section.

Return to NM 64.

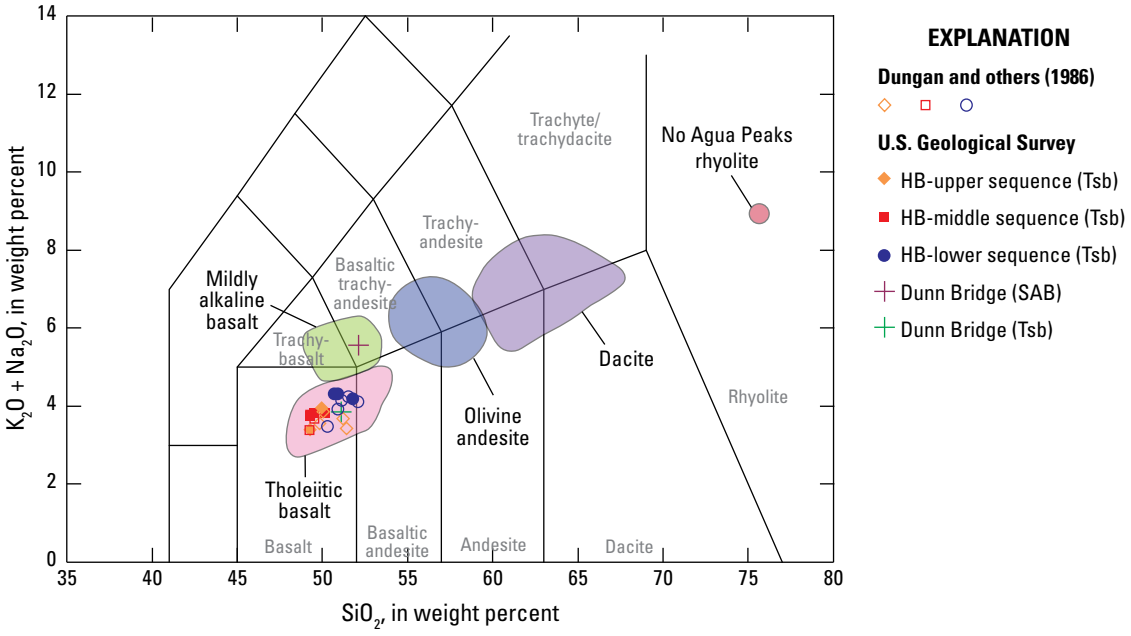

Figure 46. Total alkali (Na_2O+K_2O) versus silica (SiO_2) classification diagram for Pliocene volcanic rocks of the Taos Plateau based on LeBas and others (1986), with Servilleta Basalt data from Stop 2-4 superimposed on total range of compositions observed for Servilleta lavas. Data have been normalized to volatile-free based on the method of Middlemost (1989). Note the compositional range in SiO_2 for all lavas from this locality is representative of the average observed for all Servilleta Basalt. Mapped deposits identified as Servilleta Basalt (pink field on diagram) locally include basaltic andesite flows. HB, High Bridge; SAB, silicic alkalic basalt.

28.0 *Intersection with NM 64. Turn left and proceed west.*

28.5 View to the northwest (directly ahead) is of Cerro de los Taoses (fig. 47), a paired monogenetic basaltic trachyandesite volcanic complex (56.10 weight percent SiO_2 and 6.19 weight percent Na_2O+K_2O; sample RGR-513, table 2). A single $^{40}Ar/^{39}Ar$ whole-rock age of 4.86±0.02 Ma (sample RGR-513, table 1) was obtained for a lava flow on the north flank of the north cone. This is within the range of three ages (4.97–4.80 Ma) previously reported by Appelt (1998).

29.66 *Intersection with NM 64 and Lava Lane.* The Earthship community to the right (east) consists of homes described as "radically sustainable" and make extensive use of recycled building materials, solar energy, water catchment systems, and insulating properties of surficial deposits. These homes are underlain by middle Pleistocene alluvial and fluvial deposits likely discharged from a paleo-Red River drainage in the Sangre de Cristo Mountains approximately 25 km to the north. Gravel pits visible on the highest plateau surfaces 1.5 km to the northeast and others less visible to the southeast are dominated by Tertiary volcanic and intrusive clasts of the Questa magmatic system and Proterozoic metamorphic clasts of the Sangre de Cristo Mountains. Facing east, faint traces of scarps approximately 0.9 km distant, are cut into the underlying Servilleta Basalt beneath the surficial deposits marking the location of pre-Rio Grande gorge alluvial channels.

33.4 *Road crosses Servilleta Basalt lava flows.*

34.3 *Intersection of NM 64 and Montoso Road. Turn right on Montoso Road and proceed north. This road may become impassable during wet weather.*

35.2 *Turn right at dirt road T-intersection to stay on Montoso Road headed east.* View to the north is Timber Mountain, underlain by erosional remnants of late Oligocene volcanic rocks of the southern Rocky Mountains volcanic field. For approximately 4.5 mi the road traverses eroded middle Pleistocene alluvial and fluvial deposits and drainages incised into Servilleta Basalt lava flows.

38.1 **Stop 2-5. Timber Mountain and intrarift structure** (36°32.83' N., 105°42.92' W.; 7,083 ft, 2,159 m elevation) *Intersection of Montoso Road (B-007) and Camino de Lovato Road, pull onto parking area on northwest corner of road intersection.*

Timber Mountain consists of multiple low hills visible to the northwest, approximately 8 km distant. These exposures are the southernmost surface manifestation of a major intrarift horst or platform of Oligocene and Miocene volcanic rocks within the southern San Luis Basin of the Rio Grande Rift. Collectively, Timber Mountain and the smaller Brushy Mountain locality about 10 km to the north expose a compositionally diverse assemblage of Oligocene volcanic rocks of the Questa-Latir volcanic loci of the southern Rocky Mountains volcanic field. The Timber and Brushy Mountain deposits record pre- and postcaldera, calc-alkaline volcanism associated with the eruption of the 25.39-Ma Amalia Tuff from the Questa caldera approximately 17 km to the east (Lipman and others, 1986; Zimmerer and McIntosh, 2012b). Exposures mapped over approximately 25 km^2 (fig. 48; Thompson and Schilling, 1988) reflect only a small percentage of the geophysically imaged 2,400-km^2 extent of preserved Oligocene and volumetrically lesser Miocene volcanic deposits (fig. 25; Thompson and others, 2007a, 2014a,b, 2015; Kelson and others, 2008).

The magmatic roots of the Questa-Latir system are exposed in the footwall block of the Sangre de Cristo range-front bounding fault 25 km to the northeast. The north-dipping range block exposes a nearly 15 km north-south cross section through the Questa caldera and its plutonic underpinnings (Lipman and Reed, 1989).

Figure 47. View west toward the olivine andesite eruptive centers of Cerros de los Taoses volcanoes. Photograph by Ren Thompson, U.S. Geological Survey, 2016.

The erosional remnants of this system are dominated by intracaldera Amalia Tuff and postcaldera intrusions most prominent along the range front south of the southern caldera margin (Lipman and Mehnert, 1986; Lipman, 1988; Lipman and Reed, 1989). Most of the associated precaldera volcanic deposits and nearly all of the Oligocene postcaldera volcanic rocks were eroded from the Sangre de Cristo footwall block during late Oligocene to Pliocene uplift and extension. Based on $^{40}Ar/^{39}Ar$ determinations in the Sangre de Cristo Mountains, precaldera andesite to rhyolite lavas were erupted from 28.5 to 27.9 Ma, preceding collapse of the Questa caldera and eruption of the 25.4 Ma Amalia Tuff by 2.5 million years (Zimmerer and McIntosh, 2012b). Associated plutons, exposed along a north-south trend in the Sangre de Cristo Mountains, were emplaced over an approximately 4-million-year period from 25.4 to 21.5 Ma, decreasing in age with distance south of the Questa caldera (Tappa and others, 2011; Zimmerer and McIntosh, 2012b). The postcaldera Tertiary plutons were intruded into the approximately 1.75–1.65 Ga metamorphic basement rocks that form much of the high ranges visible to the east (Williams, 1987; Bauer and Williams, 1989; Karlstrom and Daniel, 1993).

Although postcaldera age deposits are largely eroded from the footwall block of the Sangre de Cristo Fault, gravity modeling of subbasins along the range front suggest the depth to Proterozoic basement may be as much as 1 km immediately east of the village of Questa, with the deepest parts of the Questa subbasin concealed beneath the Pliocene Guadalupe Mountain dacite volcano (Bauer and others, 2015; Grauch and others, 2015). Down-to-west and down-to-east intrabasin normal faults progressively step Proterozoic basement and Oligocene to Miocene volcanic rocks upward along the east-dipping basin floor of the underlying half-graben. The western margin of these structures underlies our position at this stop and trends northward near the eastern margin of Timber and Brushy Mountains for approximately 90 km, terminating near the north end of the San Luis Hills in Colorado. The preserved but eroded volcanic record of postcaldera volcanism of the Questa-Latir system is contemporaneous with the intrusive record of magmatism recorded by plutons in the Sangre de Cristo Mountains, reflecting protracted volcanism associated with the long-lived caldera forming magmatic system documented to the east.

Collectively, Timber and Brushy Mountains preserve postcaldera episodes of calc-alkaline volcanism that range compositionally from trachydacite lavas and basaltic trachyandesite to trachyandesite, a rhyolite dome, and rhyolite ash-flow tuffs. A low-silica rhyolite ash-flow tuff is preserved at the base of the exposed Timber Mountain section (fig. 48, unit Trl; sample RGR-315, tables 1 and 2); it yielded an $^{40}Ar/^{39}Ar$ sanidine age of 25.35±0.05 Ma, younger than the 25.4 Ma reported for the Amalia Tuff. This tuff is unconformably overlain by thin pyroxene dacite lava flows that yielded a $^{40}Ar/^{39}Ar$ whole rock age of 24.18±0.06 Ma (sample RGR-316, tables 1, 2). These are locally covered by a cogenetic cone of agglutinated dacite spatter (sample RG-61, table 2), grading vertically from a vitrophyric base to a devitrified top (unit Tdu, fig. 48). Remnants of a stratigraphically younger lava flow of glassy, low-silica rhyolite (unit Tru, fig. 48) and two olivine andesite flows (unit Tta, fig. 48) are preserved locally. The exposed thickness of this deeply eroded lower sequence is approximately 60 m. It is overlain by an upper sequence consisting of multiple dacite lava flows, divided into three units (Thdl, Thdm, Thdu, fig. 48; sample RG-61, table 2) on the basis of mineralogy. These flows extend northward beneath the southeast flank of the Pliocene Montoso andesite volcano. Hornblende separates from a sample low on the flanks of Montoso and interpreted to represent the upper part of the Timber Mountain section yielded an $^{40}Ar/^{39}Ar$ age of 21.57±0.10 Ma (sample RGR-311, table 1). The total exposed thickness of this upper sequence is approximately 150 m.

Low-silica rhyolites are dominated by phenocrysts of plagioclase, sanidine, quartz, and biotite, with subordinate amounts of iron-titanium oxides, and clinopyroxene ± orthopyroxene. Amphibole is present in a glassy to partly devitrified matrix. Lower sequence dacites contain a complex disequilibrium assemblage of phenocrysts, glomerocrysts, xenocrysts, and high-silica glass. Phenocrysts include plagioclase, clinopyroxene, orthopyroxene, iron-titanium oxides, and minor hornblende. Two texturally and compositionally distinct plagioclase populations are present. Euhedral plagioclase phenocrysts exhibiting oscillatory and normal zoning with core to rim compositions ranging from $An_{58–53}$ in lava flows and from $An_{52–47}$ in more silicic vitrophyric agglutinate. Less abundant sieve-textured plagioclase phenocrysts are relatively unzoned ($An_{45–48}$). Oligoclase ($An_{21}Ab_{73}0r_{6}$) and sanidine ($Ab_{55}An_{3}Or_{42}$) xenocrysts often have reaction rims in contact with the dacite host or are enclosed in or contain inclusions of high-silica rhyolite glass. Andesite micropillows as much as several millimeters in diameter are preserved in the glassy matrix of dacite spatter agglutinate and contain microphenocrysts of plagioclase, clinopyroxene, iron-titanium oxides and skeletal olivine (the same mineral assemblage found in the andesite lava flows). The micropillows are in various stages of disaggregation and fragmented debris trails are elongated parallel to the foliation in the glass matrix.

Thompson and others (1986) modeled the fractionation paths of andesitic parental magmas and concluded that major- and trace-element concentrations in lower sequence dacites can be approximated by fractionation of phenocryst phases, plus mixing with

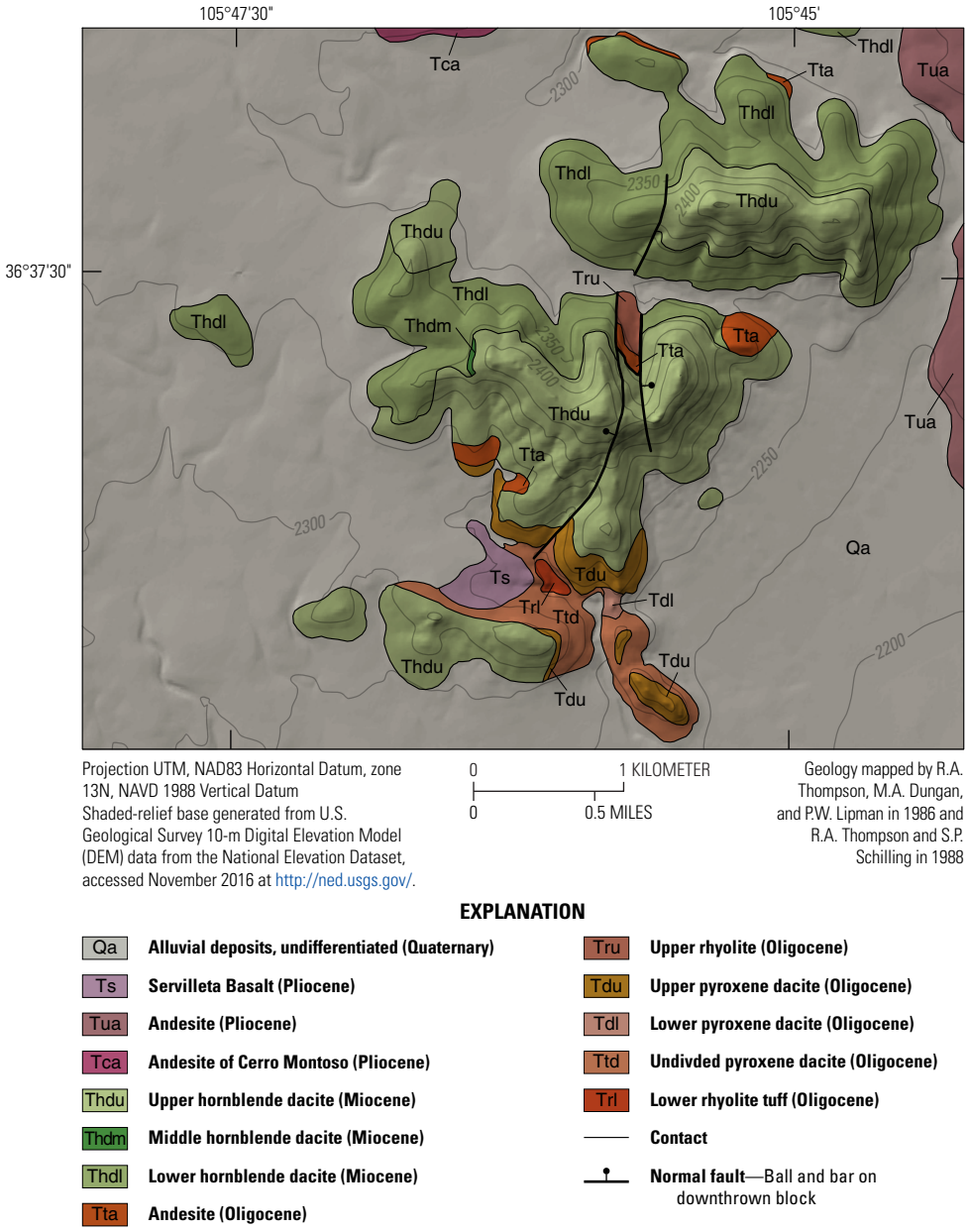

Figure 48. Simplified geologic map of the Timber Mountain area, an early Miocene erosional remnant of the southern Rocky Mountains volcanic field, modified from Thompson and others (1986) and Thompson and Schilling (1988). These deposits, similar ones to the north at Brushy Mountain, and Oligocene deposits in the San Luis Hills of southern Colorado are the surface expression of a fault- bound platform of late Oligocene to Miocene volcanic deposits preserved within the geomorphic San Luis Basin.

high-silica rhyolite similar in composition to the Amalia Tuff in a ratio close to 1:1. Lowsilica rhyolites may have been derived through fractionation of dacites plus mixing with the high-silica rhyolite. These differentiation models support a petrogenetic link—but not necessarily a cogenetic link—between the mildly peralkaline caldera-forming Amalia Tuff and early postcaldera lavas. Subsequent eruption of younger upper sequence volcanic rocks marks the return to more typical metaluminous magmas characteristic of both precaldera and postcaldera magmatism.

Continue south along Montoso Road (B-007). Use caution during the descent into the Rio Grande gorge. There are limited options for pulling off to accommodate large vehicles in the event of oncoming traffic. This is the starting point for optional route 2A of Day 2. See the end of the Day 2 road log for mileage, route, and descriptions of optional route 2A.

38.3 *Road starts the descent into the Rio Grande gorge.* Scarp on down-to-east Dunn Fault, one of many intrabasin normal faults. For the next kilometer, the road is underlain by Rio Grande fluvial terrace deposits and Servilleta Basalt lava flows in the hanging wall block of the Dunn Fault, a typical intrabasin fault active during Pliocene rift volcanism.

39.0 **Stop 2-6. John Dunn Bridge, growth faulting coeval with Servilleta Basalt volcanism** (36°32.20’ N., 105°42.645’ W.; 6,873 ft, 2,095 m elevation) *Pull vehicles onto dirt parking area on the east side of the*

road. Walk to the outcrop on the far east side of the parking lot for a view of the confluence of the Rio Grande and Arroyo Hondo.

Our location is approximately 7 km north of the High Bridge (Stop 2-4). Below this stop, the Dunn Bridge (also referred to as John Dunn Bridge) crosses the Rio Grande immediately north of the confluence with Arroyo Hondo, which flows west from its headwaters in the Sangre de Cristo Mountains. The bridge was built by John Dunn in 1908 and operated as a toll bridge for transportation of mail and travelers into Taos until it was sold to the Territory of New Mexico in 1912. It was likely one of many Rio Grande crossings used by local residents in the 18th and 19th centuries.

The parking area is located on middle Pleistocene gravels deposited on Servilleta lava flows that correlate to the lavas at the rim of the east side of the gorge (fig. 49). Below the upper Servilleta flows, a 58-m-thick sedimentary interbed overlies a 25-m-thick lava flow (fig. 50). In the east wall of the gorge this sedimentary interbed thins to the south and includes a single interbedded lava flow (fig. 51). Lateral correlation of gorge stratigraphy is complicated by colluvium-covered sections and laterally discontinuous sedimentary interbeds and lava flows; however, figure 52 is a schematic representation of the lateral changes in the stratigraphy between the Dunn and High Bridge areas based on detailed inspection of the gorge and $^{40}Ar/^{39}Ar$ geochronology.

Looking south into the gorge (fig. 50) three key observations include (1) lava flows at the rim of the gorge are higher on the west side than the east, (2) a much thicker section of basalts is exposed on the west side than on the east, and (3) from the bridge ~1.5 km south, the sedimentary interbed below the uppermost sequence of lavas is thicker on the east side. These stratigraphic differences are the result of growth faulting along the north-trending, down-to-east Dunn Fault (Peterson, 1981). The trace of the fault passes just west of our location, crosses Montoso Road at approximately the first switchback above river level, and follows the Rio Grande until it cross-cuts the east side of the gorge at the farthest point of the gorge visible from this location (fig. 51). Hot springs are located near the fault plane along the river north of the first switchback (Black Rock Hot Spring) and in the footwall about 300 m west of where the fault cuts the east wall of the gorge (Manby Hot Springs).

Multiple periods of displacement are identified for the Dunn Fault. The earliest demonstrable period of faulting occurred after emplacement of the silicic alkalic basalt (SAB) flow concurrent with sedimentation. The sedimentary interbed is ~58-m thick in the hanging wall of the fault but only ~27-m thick in the footwall. The SAB at the base of the sedimentary interbed is 4.50 Ma and the Servilleta Basalt flow that caps the sedimentary interbed is 3.52 Ma, indicating that about 31 m of down-to-east offset occurred along this segment of the fault over 1 m.y., which results in a slip rate of 0.03 mm/yr. This is the largest amount of displacement for this time period; the sedimentary interbed is nearly the same thickness on both sides of the fault to the south. A younger period of deformation offsets the upper sequence of Servilleta flows (3.52 Ma) 36-m down-to-east, as indicated by the higher elevation on the west gorge rim south of the Dunn Bridge. Kelson and Bauer (2006) indicate middle Pleistocene gravels are offset by the fault. However, fault scarps cutting the middle Pleistocene gravels are not apparent; rather, the difference in base of the gravels on either side of the fault may be entirely related to deposition over the pre-existing fault scarp.

The 25-m-thick lava flow at river level has a more alkaline composition than typical Servilleta tholeiitic basalt. Published references to this lava flow refer to it as a SAB (Lipman and Mehnert, 1975, 1979) based on a classification system derived from Hawaiian volcanic rock compositions (Macdonald and Katsura, 1964). SAB compositions throughout the TPVF, as defined by Lipman and Mehnert (1975), have 48–52 weight percent SiO_2, greater than 1 weight percent K_2O, and are neither quartz nor nepheline normative. Based on the classification system of Le Bas and others (1986), when renormalized to volatile free with ferric/ferrous iron ratios based on Middlemost (1989), the composition of the 25-m-thick lava flow at Dunn Bridge is a basaltic trachyandesite (fig. 46). This lava flow is representative of other mildly alkalic compositions that include alkaline basalt to basaltic trachyandesite that are volumetrically minor throughout the TPVF, but are ubiquitous throughout the southern Rocky Mountains (Lipman and Mehnert, 1975) including Oligocene to Miocene early-rift basaltic rocks in the San Luis Hills and southeast San Juan Mountains (Turner and others, Day 3, this volume; Lipman, 1975a,b; Thompson and others, 1991). Some of the better exposed shield volcanoes observed throughout the TPVF erupted alkalic compositions and include Wilson Lake, the State line vent, Cerrito Dormilon, and volcano de la Culebra (figs. 30, 46). *Continue the descent into the Rio Grande gorge on Montoso Road using caution on switchbacks. This route is subject to extreme runoff and hazardous driving conditions during thunderstorms.*

39.7 *Parking area for Black Hot Springs.* The trace of Dunn Fault projects through the parking lot. Depending on the state of road grading, fault gouge is often seen in Santa Fe Group deposits immediately uphill from the parking area.

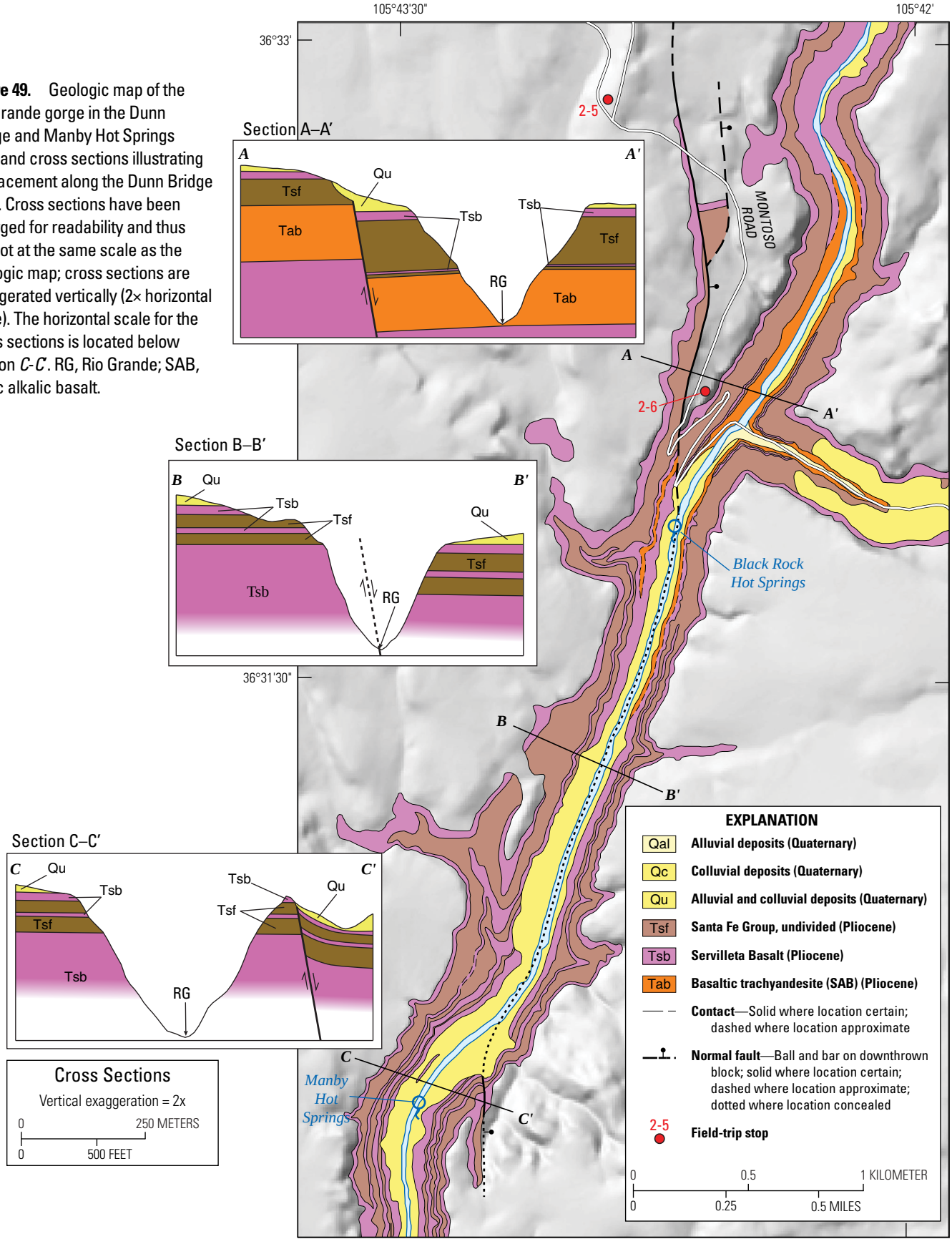

Figure 49. Geologic map of the Rio Grande gorge in the Dunn Bridge and Manby Hot Springs area and cross sections illustrating displacement along the Dunn Bridge Fault. Cross sections have been enlarged for readability and thus are not at the same scale as the geologic map; cross sections are exaggerated vertically (2× horizontal scale). The horizontal scale for the cross sections is located below section *C-C'*. RG, Rio Grande; SAB, silicic alkalic basalt.

Projection UTM, NAD83 Horizontal Datum, zone 13N, NAVD 1988 Vertical Datum
Shaded-relief base generated from U.S. Geological Survey 10-m Digital Elevation Model (DEM) data from the National Elevation Dataset, accessed November 2016 at http://ned.usgs.gov/.

Geology mapped by K. Kelson and P. Bauer in 2006 and K.J. Turner and R.A. Thompson in 2010–11

Figure 50. Photograph looking northeast at the Dunn Bridge and the confluence of the Rio Grande and Arroyo Hondo. Map units indicated on photograph correspond to units listed in figure 49. View is looking at the downthrown side of the Dunn Bridge Fault where interbedded sediments are as thick as 58 meters (m) between the uppermost Servilleta Basalt flows (Tsb) and the basaltic trachyandesite flow (Tab). Although not visible from this viewpoint, stratigraphically equivalent interbedded sediments below photo station on the upthrown side of fault are about 27-m thick. Tsf, undivided Santa Fe Group; Qu, alluvial and colluvial deposits. Photograph by Ren Thompson, U.S. Geological Survey, 2016.

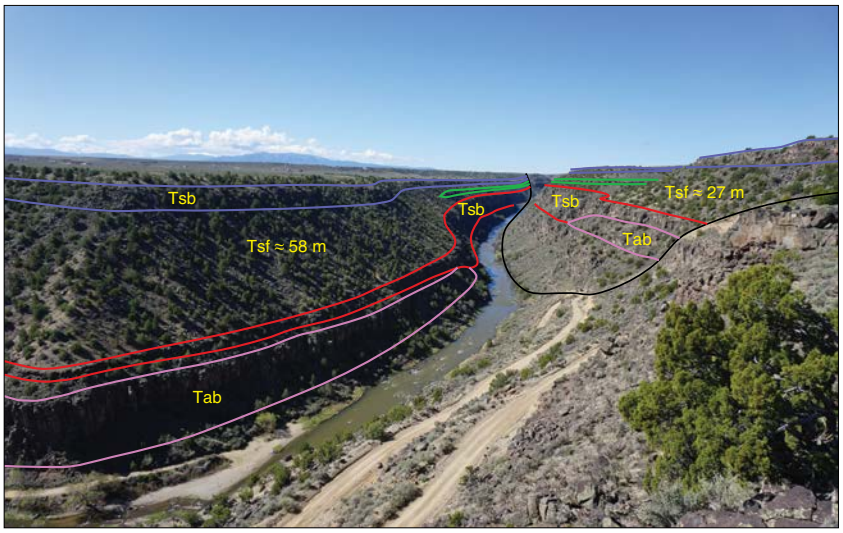

Figure 51. Photograph looking south into the Rio Grande gorge, approximately parallel to the trace of the Dunn Bridge Fault (black line). Pink lines highlight the basaltic trachyandesite lava flow (Tab). Red, green, and blue lines delineate distinct sequences of Servilleta Basalt flows that correlate across the fault. On the east, downthrown, side of the fault, interbedded sedimentary deposits are as thick as 58 meters (m), but stratigraphically equivalent sediments on the west, upthrown, side of the fault are only 27-m thick. The variable thickness is inferred to reflect growth faulting during deposition of sediments and prior to emplacement of the uppermost Servilleta Basalt flows (3.52 million years old). A younger period of offset displaces the entire section, including the upper Servilleta Basalt flows. Photograph by Ren Thompson, U.S. Geological Survey, 2016.

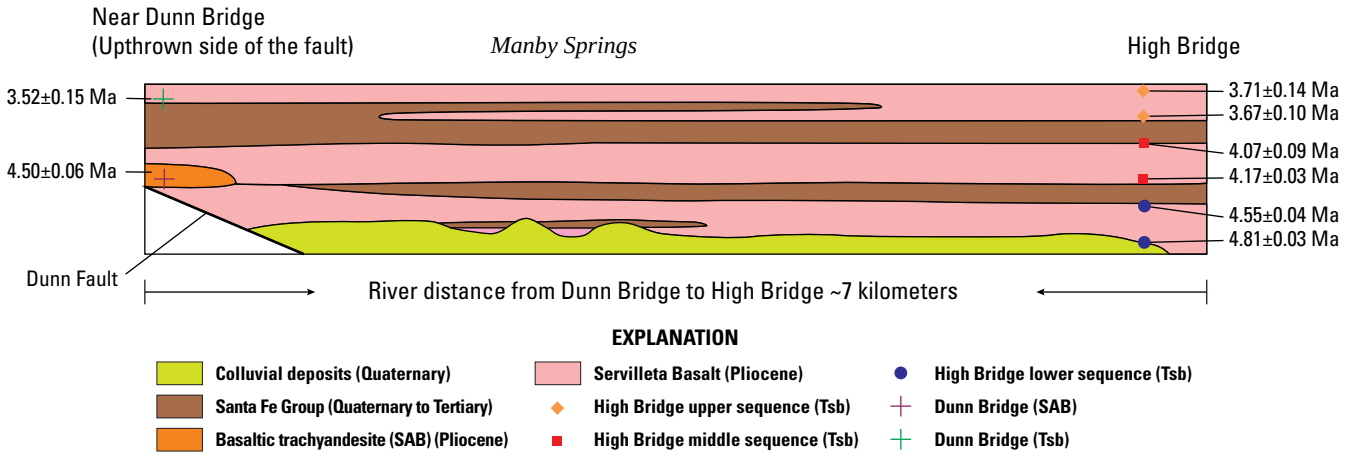

Figure 52. Schematic representation of lava flow sequences and interbedded sediments in the west wall of the Rio Grande gorge between the High Bridge of the Rio Grande and the Dunn Bridge. $^{40}Ar/^{39}Ar$ ages are also listed in table 1. Lava flow sequences at the High Bridge are easily separated into upper, middle, and lower sequences on the basis of intervening sedimentary deposits, but this stratigraphy becomes more complex to the north. Ma, million years ago.

39.9 *Turn right and cross John Dunn Bridge over the Rio Grande and continue up Arroyo Hondo on Montoso Road (B-007). There are seasonal restrooms available near the west and east ends of the Dunn Bridge.* The road climbs through Santa Fe Group sediments and volcanic section described at Stop 2-6.

41.0 *Intersection with Camida Del Medio, continue on Montoso Road (B-007).*

41.05 *Intersection with Lucero Road (B-006), turn left and continue on dirt road approximately 4.5 mi to intersection with NM 522.*

42.7 *Turn left (north) on NM 522 and proceed approximately 10.7 mi to the Red River State Fish Hatchery turn off.*

43.9 Outcrops of Cerro Negro dacite in the roadcut on the east side of road are blocky deposits of sparsely phyric to aphanitic, glassy dacite (63.1 weight percent SiO_2, 6.95 weight percent Na_2O+K_2O; sample RGR-602, table 2). This outcrop is typical of two-pyroxene dacites of the Taos Plateau. Sparse, but coarse orthopyroxene phenocrysts are characteristic and often contain resorbed olivine cores and plagioclase phenocrysts are characteristically lacking. Appelt (1998) reports an $^{40}Ar/^{39}Ar$ whole rock age from this outcrop of 4.90±0.05 Ma.

46.8 Outcrops of Cerro Negro dacite on east side of road (Kelson and Bauer, 2006).

47.7 NM 522 drops into the drainage of San Cristobal Creek, a small tributary to the Rio Grande. Excellent exposure of volcanic stratigraphy is preserved in the canyon on the west side of the highway. The erosional valley traversed by the highway for the next 5 mi is cut into Tertiary and Quaternary fan deposits derived from drainages in the Sangre de Cristo Mountains to the east. Tertiary gravels preserved in deeply dissected drainages stratigraphically overlie Servilleta Basalt flows that are temporally equivalent to the lowest flows observed at the High Bridge (Stop 2-4). Lava flows stratigraphically equivalent to the uppermost flows at the High Bridge, inferred to have erupted from vents west of the Rio Grande, thin and lap onto the western prograding terminus of the Tertiary alluvial fans. Younger Quaternary deposits, largely derived from reworking of Tertiary fan deposits in this area, locally overlie the uppermost Servilleta lava flows west of the Rio Grande. These are interpreted to reflect internal drainage into the large, closed drainage basin floored by lava flows of the TPVF.

53.4 *Intersection of NM 522 and NM 515 turnoff to Red River State Fish Hatchery. Turn left on NM 515 and proceed approximately 2 mi to the fish hatchery parking lot. Guadalupe Mountain is visible to the northwest.*

53.7 NM 515 follows the trace of the down-to-northeast Red River Fault, preserving olivine andesite lava flows in the footwall (cliffs and steep slopes to the west) and Pliocene to Pleistocene alluvial and fluvial deposits in the hanging wall to the east (Kelson and others, 2008). The road largely follows Holocene stream channel and valley floor alluvium.

55.4 **Stop 2-7. Red River State Fish Hatchery** (36°40.962' N., 105°39.222' W.; 7,096 ft, 2,163 m elevation) *Turn left into the parking lot before the bridge crossing the Red River. Park at the far west end of the parking area and proceed to the footbridge across the Red River for discussion of Red River Canyon stratigraphy visible to the southwest from the bridge. Public restrooms are available across the Red River at the fish hatchery visitors center. The visitor center parking lot is closed after normal visiting hours, plan your visit accordingly.*

This purpose of this stop is threefold. First, this stop provides an introduction to volcanic stratigraphy of the northern TPVF, which becomes stratigraphically more complex north of Stop 2-6, but is well exposed in the area of the Rio Grande and Red River drainages. Introducing the lower part of the volcanic section here also serves to clarify stratigraphic relations discussed during the first four stops of Day 3 and effectively closes a loop through the Wild Rivers Recreation Area of the Rio Grande del Norte National Monument ending at La Junta point near the confluence of the two rivers. Second, this stop provides an opportunity to discuss previous petrologic modeling of the magmatic evolution of the TPVF in light of new constraints provided by detailed geologic mapping and $^{40}Ar/^{39}Ar$ age determinations. This is intended to reconcile the general disconnect between published geochemical models for magma genesis and observed stratigraphic constraints on magma chamber evolution. Third, this stop lies at the southern end of the Questa subbasin of the southern San Luis Basin, where the Red River system of Pliocene faults marks the approximate location of the subsurface basement high that delineates the basin margin. Here, near the Red River State Fish Hatchery, down-to-west faults visibly offset Pliocene volcanic rocks along trends that parallel older basin bounding structures.

The Red River incises an 8.5-km long, 170-m-deep canyon through a Pliocene volcanic section ranging in composition from basalt near the base of the canyon to dacite at the canyon rim (fig. 53). The stratigraphic section representing most of the compositional suite is visible from this spot (fig. 54) and was sampled approximately 547 yd (0.5 km) downstream. A better view of this section is possible by walking downstream approximately 273 yd (250 m) along the fishing trail. Although not specifically part of the Day 2 field trip itinerary, field guide users are encouraged to explore the stratigraphy of the Red River gorge by the hiking/fishing

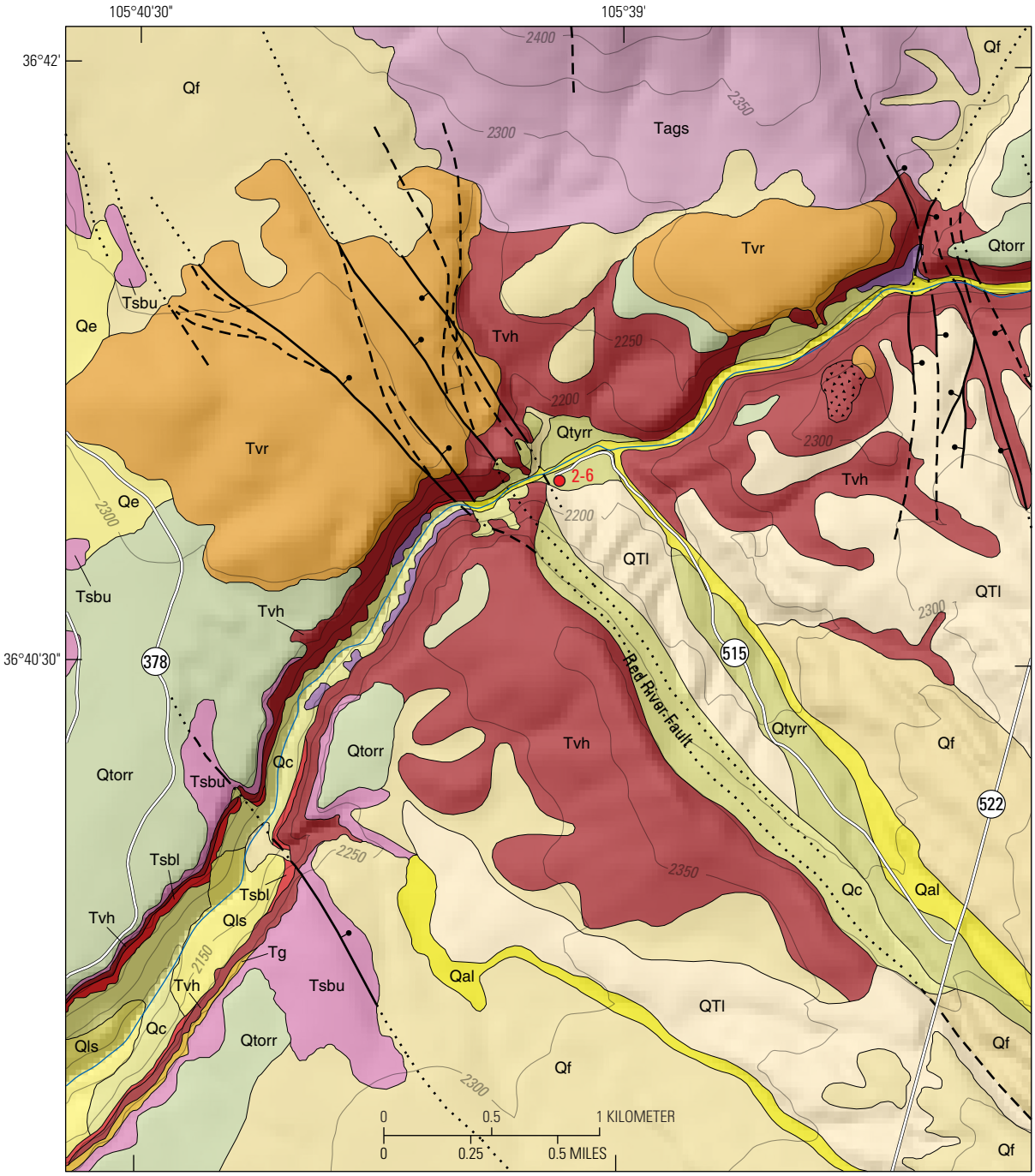

Projection UTM, NAD83 Horizontal Datum, zone 13N, NAVD 1988 Vertical Datum
Shaded-relief base generated from U.S. Geological Survey 10-m Digital Elevation Model (DEM) data from the National Elevation Dataset, accessed November 2016 at http://ned.usgs.gov/.

Modified from Kelson and others, 2008 by R.A. Thompson and K.J. Turner.

EXPLANATION

- Qal — **Alluvium (Holocene)**
- Qe — **Eolian deposits (Holocene to late Pleistocene)**
- Qls — **Landslide deposits (Holocene to late Pleistocene)**
- Qf — **Fan deposits (Holocene to middle Pleistocene)**
- Qc — **Colluvium (Holocene to middle Pleistocene)**
- Qtyrr — **Young Red River terrace deposits (Holocene to middle Pleistocene)**
- Qtorr — **Old Red River terrace deposites (late to middle Pleistocene)**
- QTl — **Lama formation (early Pleistocene to Pliocene)**
- Tsbu — **Servilleta Basalt, upper sequence (Pliocene)**
- Tg — **Older alluvial gravels (Pliocene)**
- Tvr — **Dacite of Red River volcanic complex (Pliocene)**
- Tvh — **Olivine andesite of Hatchery volcano (Pliocene)**
- Tsbl — **Servilleta Basalt, lower sequence (Pliocene)**
- Tags — **Dacitic lavas of south Guadalupe Mountain (Pliocene)**
- **Indicates near-vent pyroclastic deposits**
- **Normal fault**—Ball and bar on downthrown block; dashed where location approximate; dotted where location concealed
- 2-6 — **Field-trip stop**

Figure 53. Geologic map of the Red River State Fish Hatchery area. Modified from Kelson and others (2008) by R.A. Thompson and K.J. Turner.

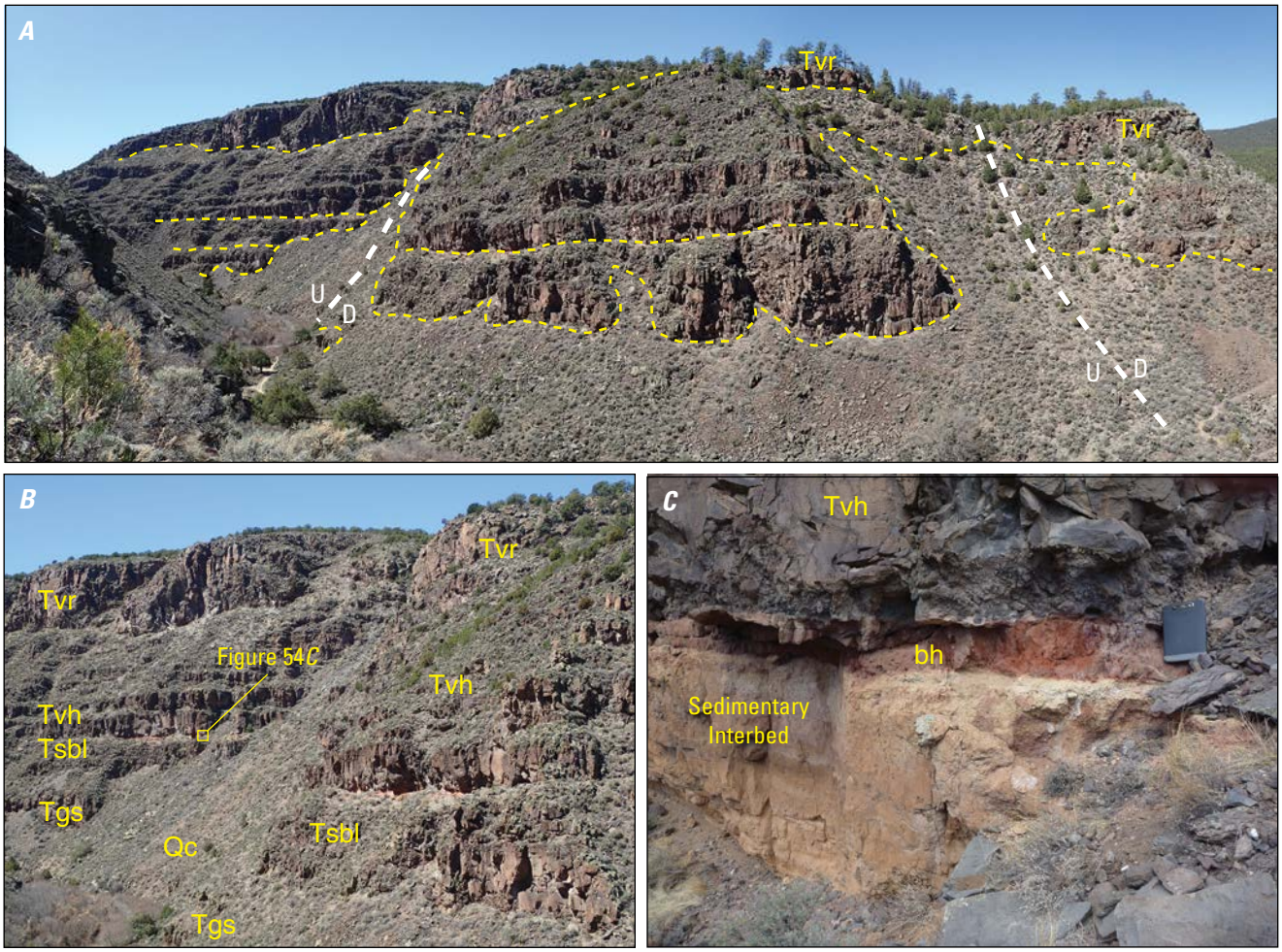

Figure 54. Photographs of the north wall of the Red River gorge, south of the fish hatchery. Unit symbols for all panels are the same as those used in figure 53. *A*, Geologic contacts between map units are designated by the dashed yellow lines for the mixed section described by McMillan and Dungan (1986). Down-to-east normal faults, splays of the Red River fault system, are indicated by the dashed white lines. *B*, Enlarged view of the stratigraphic section depicted in panel *A*. The map unit nomenclature reflects the different eruptive sources for the four temporally distinct eruptive sequences of the Red River gorge area. *C*, Note the prominent baked horizon (bh) at the base of olivine andesite section. Location of the figure detail is indicated by the inset square in figure 54*B*. Sedimentary interbeds between Guadalupe Mountain flows (Tgs), Servilleta Basalt (Tsbl), Hatchery olivine andesite (Tvh), and Red River trachyandesite (Tvr) mark erosional unconformities and at least a local hiatus in the magmatic activity between compositionally distinct eruptive events. Qc, colluvium; U, upthrown block; D, downthrown block. Photographs by Ren Thompson, U.S. Geological Survey, 2016.

trail on the north side of the river. Of particular interest is the dated stratigraphic section (fig. 54) in the context of the geologic map and cross sections presented in Bauer and others (2015), and the simplified geologic map in figure 53. Please note fault offsets are incorrectly depicted on the geologic map in Bauer and others (2015). Rotating the sense of displacement 180° corrects this problem.

If you intend to climb the talus slopes on the north gorge wall to access exposed lava flows, please be advised that loose rocks can present a potential fall hazard and be dangerous to trail users below. Use extreme caution. Climbing the southern walls of the Red River gorge is not advised. Note the bridge crossing at the fish hatchery is the only bridge crossing from the hatchery to the confluence of the Red River and the Rio Grande.

Another option for traversing the stratigraphy of the Red River gorge is to follow the trail that cuts northward from the fishing trail approximately 71 yd (65 m) west of the bridge (trail marker at intersection) and climbs through down-to-east sections of andesite lava flows offset by multiple strands of the Red River Fault. The trail eventually traverses the section through the capping dacitic lavas of the Red River volcano and ends at the Wild Rivers visitor center on the west flank of the Red River volcano.

Preserved lavas from four discrete volcanic edifices are preserved in the Red River gorge near the

fish hatchery. Each eruptive sequence is restricted in compositional range and separated by sedimentary interbeds deposited along erosional unconformities that separate flow packages. Sedimentary interbeds are dominantly reworked eolian deposits in the lower part of the section, but between the upper two flow packages deposits coarsen and contain Proterozoic and Tertiary pebbles and cobbles derived from the Sangre de Cristo Mountains.

Lobate lava flows of Guadalupe Mountain dacite exposed near river level are early eruptive products of the large twin-peaked eruptive center 2.5 km to the north. These flows are characteristically dacitic (approximately 62 weight percent SiO_2 and 6 weight percent Na_2O+K_2O) containing sparse, small phenocrysts of plagioclase, hypersthene, and augite in a pilotaxitic groundmass. Distal lava flows exposed in the gorge are laterally restricted, typically forming overlapping finger-like lobes characterized by radial cooling fractures and concentric brecciated carapaces where exposed in cross-section. Whole-rock $^{40}Ar/^{39}Ar$ age determinations from lava flows low in the section at river level and stratigraphically higher 9.3 km to the north range from a maximum of 5.35±0.07 Ma (sample RGR-108, table 1) to a minimum of 4.78±0.01 Ma (sample RGR-276, table 1) suggesting the possibility of a protracted dacitic system erupting from multiple events over approximately 0.5 million years. High-resolution aeromagnetic data of the area (Grauch and others, 2015) reveal the reversed and normal magnetic polarity of the northern and southern parts of Guadalupe Mountain, respectively, reflecting the magnetic reversal at the 5.01-Ma geochron boundary of the magnetically normal Thvera subchron of the Gilbert geochron.

Servilleta lava flows derived from unknown vents to the west of the Rio Grande thin eastward and pinch out against the lower flanks of Guadalupe Mountain. Servilleta Basalt lava flows are not present on either side of the gorge at the footbridge across the Red River, but two thin lava flows (<5 m total) are preserved in the sampled section 0.5 km to the southwest along the trail on the north side of the river. These lava flows dip gently to the east, reflecting a combination of regional eastward tilting of the Taos Plateau surface along the down-to-east Sangre de Cristo Fault and low-relief primary depositional topography. The flow package thickens eastward to a minimum of 30 m (base not exposed) at the confluence of the Red River and the Rio Grande. The base of the Servilleta section at La Junta point yields a whole-rock $^{40}Ar/^{39}Ar$ age determination of 5.08±0.09 Ma (sample RGR-04, table 1). Servilleta lavas are displaced beneath the surface east of the sampled section downstream by a series of down-to-east strands of the Red River Fault.

A sequence of andesitic lava flows erupted from a shield volcano informally named the “Hatchery volcano” overlie Servilleta lava flows in the gorge east of the footbridge. Downstream, andesite flows are exposed above a sedimentary interbed with a pronounced reddish baked horizon near the top. Lava flows and associated breccias form the gorge cliffs along most of the Red River gorge from the footbridge to a vent complex exposed approximately 1.5 km upstream in the gorge. The entire sequence is inferred to have been emplaced during a short-lived eruptive event, as there is no discernable age difference from the base to the top of the section and no erosional unconformities or sedimentary interbeds within the andesite. Many large blocks of andesite can be observed along the trail and have characteristically coarse (2–3 mm) olivine phenocrysts in a fine grained to microcrystalline groundmass of plagioclase, olivine, augite, and iron-titanium oxides. A whole-rock $^{40}Ar/^{39}Ar$ age determination of 4.99±0.07 Ma (sample RGR-110, table 1) was obtained from a lava flow near the top of the exposed section on the north side of the Red River.

Paleochannels or erosional depressions were cut into the upper surface of the Hatchery volcano flanks and locally preserve coarse conglomerates bearing clasts (as large as cobble size) derived from the Sangre de Cristo Mountains. These deposits suggest that cessation of eruption at the Hatchery volcano was followed by distal fan or braided stream deposition across the shield by fans emanating from the eastern Sangre de Cristo Mountains. Locally, dacitic lava flows fill shallow paleochannels along the north rim of the gorge and can be seen east and west of the footbridge. The south rim of the gorge is underlain by andesite and is inferred to represent the low-relief paleotopographic high against which dacite lava flows were subsequently emplaced.

Local eruptive centers for trachyandesite lavas that cap the section are observed in both the Red River and Rio Grande gorges. These range from single dike-fed lava flows to more disbursed lava dome complexes. The former is exposed approximately 1.5 km east of here, where a 2-m-wide dike cuts near-vent deposits of the Hatchery volcano and was the conduit for at least one low-relief dome shaped lava flow near the east end of the canyon. The larger dome complex of Red River volcano caps the section 250 km downstream, where domiform lava flows unconformably overlie Hatchery volcano andesite lava flows and scattered cobble conglomerate deposits. The Red River volcano only includes those lava dome and flow deposits preserved along the north gorge rim, unconformably overlying both Hatchery volcano andesites and dacites of Guadalupe Mountain as shown on the geologic map of Bauer and others (2015). These trachyandesites are characterized by as much as 5–10 percent phenocrysts of augite and bronzite, with common olivine xenocrysts in a fine grained to glassy groundmass of plagioclase, glass, pyroxenes, and titanomagnetite (McMillan and Dungan, 1986) and

typically do not exceed 61–62 weight percent SiO_2 and 7.3 weight percent Na_2O+K_2O.

McMillan and Dungan (1986) demonstrated that the Hatchery volcano andesite section was zoned from approximately 51.5 weight percent SiO_2 at the base to 56 weight percent SiO_2 near the top. They modeled the range of major and trace element compositions for the entire Red River gorge suite as the result of two-component mixing between Servilleta Basalt and Red River trachyandesite magmas (fig. 55). Shallow conduit mixing of basalt and dacite during eruption was inferred to generate the range of erupted lava compositions, although the model was inconsistent with isotopic data requiring nonunique, heterogeneous compositions for both basalt and trachyandesite end members (Dungan and others, 1989b). The small, erupted volume and local distribution of the Hatchery andesites relative to the large homogeneous andesitic centers to the west and the proximity to the coeval (within the limits of $^{40}Ar/^{39}Ar$ geochronology) and long-lived Servilleta Basalt eruptions supports mixing as a likely petrogenetic process in the evolution of at least some intermediate composition lavas. However, the disparate ages and observed unconformities between eruptive suites precludes a conduit-mixing model for the eruptive suites observed at this stop.

The Red River Fault (figs. 53, 56) is exposed near the fish hatchery (fig. 56) as a series of down-to-east normal faults that displace Hatchery andesite into the actively subsiding Questa subbasin between this stop and the western Sangre de Cristo range front (fig. 30). The fault trends southeast-northwest, coincident with NM 515, and merges with the Sangre de Cristo range front south of Questa, New Mexico. To the northwest, the fault merges with the north-south striking gorge fault zone (Ruleman and others, 2013), which parallels the Rio Grande gorge northward into Colorado. Gravity modeling (Drenth and others, 2016; fig. 2) suggests the trace of the Red River Fault is coincident with a buried Tertiary basement high delineating the western and southern margins of the broader San Luis Basin. Displacement of the exposed Hatchery andesite section suggests that extensional deformation was active during eruption of the andesites, as the hanging wall block of the Red River Fault in the Red River gorge is as much as 50-percent thicker than the section preserved in the footwall block. Posteruption displacement of stratigraphically overlying Servilleta Basalt flows as young as 3.66±0.11 Ma (sample RGR-05, table 1) is limited to approximately 25 m, suggesting a decrease in slip rate since eruptions ceased. Although difficult to quantitatively constrain, this allows for an interpretation of rapid magmatic emplacement, at least episodically and locally, during Pliocene extension.

End of route 2.

Optional Day 2 Road Log – Brushy Mountain

The primary destination of this road log is Brushy Mountain, approximately 12 mi north of Stop 2-5**.** The road network around Brushy Mountain affords easy access to postcaldera andesite, dacite, and rhyolite deposits on the preserved west flank of the Oligocene Questa-Latir magmatic system.

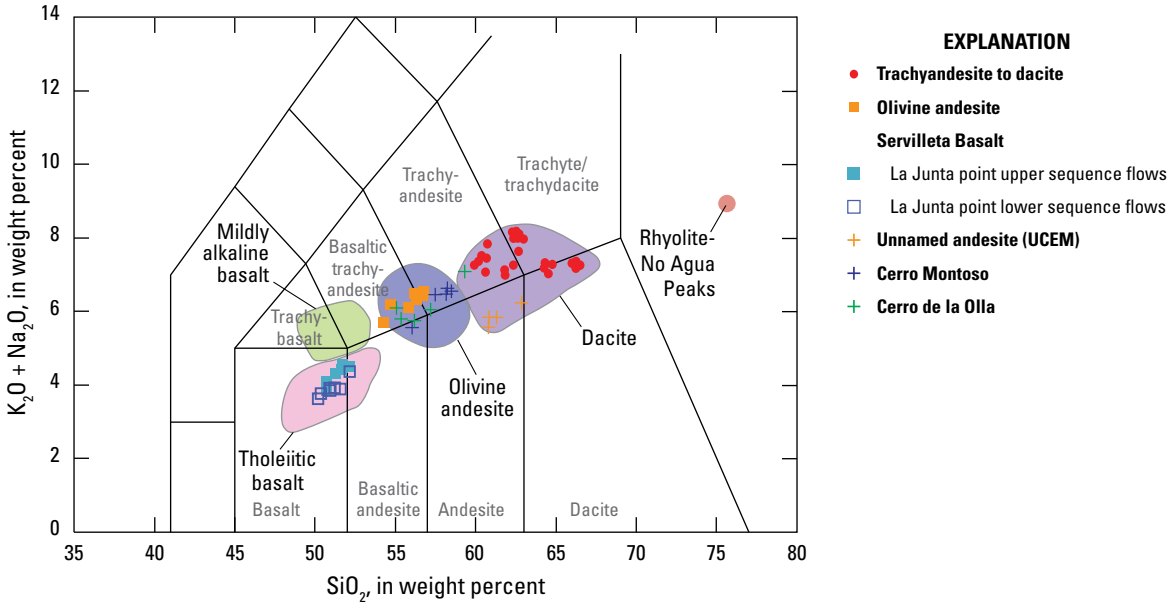

Figure 55. Total alkali (Na_2O+K_2O) versus silica (SiO_2) classification diagram for Pliocene volcanic rocks of the Taos Plateau based on LeBas and others (1986) with volcanic rock data (this study) from the Red River gorge and downstream areas near the confluence with the Rio Grande. Data normalized to volatile-free based on the method of Middlemost (1989). UCEM, unnamed cerrito east of Montoso.

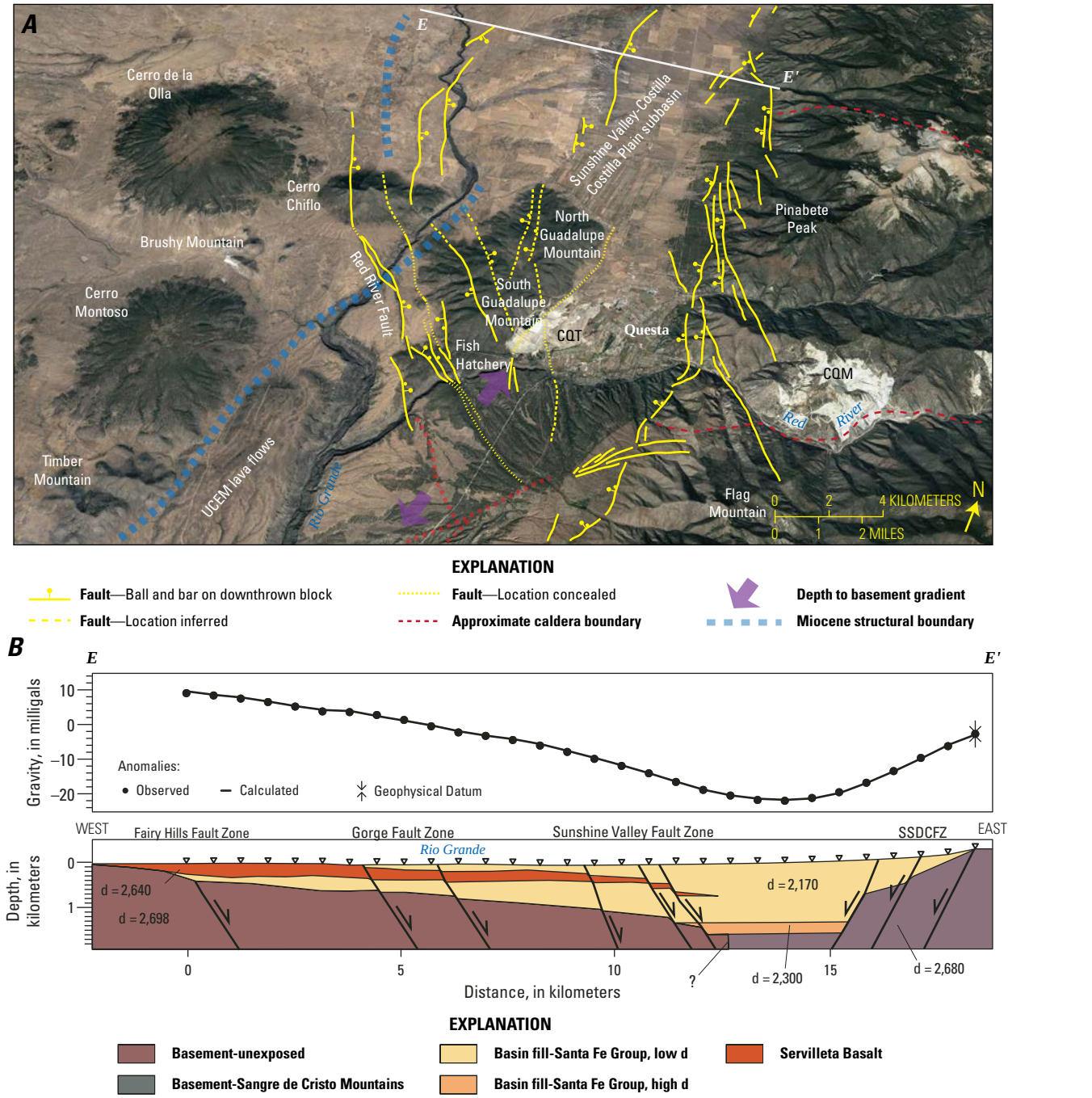

Figure 56. *A*, Oblique aerial view of the confluence area of the Red River and Rio Grande. Northwest trending faults of the Red River Fault Zone merge northward with older basin-bounding structures marked by the eastern limit of exposure of underlying Oligocene and Miocene volcanic deposits. The distribution of intrabasin bounding faults of the Sunshine Valley-Costilla Plain subbasin trend northwest to northward with increasing obliquity toward the subbasin bounding Red River Fault Zone. Geologic exposures of underlying Miocene deposits in the Rio Grande gorge at Stop 3-2 support a geophysical interpretation of a basement high running parallel to, but southwest of, the Pliocene Red River Fault Zone. Individual stands of the Red River Fault Zone converge south of the fish hatchery, but are inferred to exhibit decreasing amounts of displacement to the southeast where they are obliquely terminated by the fault segments of the Sangre de Cristo Fault Zone along the Sangre de Cristo range front. This relatively complex system of faults in the fish hatchery area is attributed to extension superposed on pre-Pliocene structures that define the southern margin of the Pliocene subbasin. The western third of the Questa caldera is buried beneath the deepest parts of the subbasin that directly underlies the eastern limits of north and south Guadalupe Mountain. The Chevron Questa tailings facilities (CQT) and molybdenum mine (CQM) east of the village of Questa are associated with postcaldera intrusions of the Questa caldera (indicated by red dashed line) and are now permanently closed; the tailings facilities upstream from the fish hatchery are a designated Environmental Protection Agency Superfund site. UCEM, unnamed Cerrito east of Montoso. *B*, Cross sections north of Guadalupe Mountain derived from geologic mapping and gravity model constraints assume a more typical structural style of inward-stepping subparallel intrabasin faults with the deepest parts of the basin being asymmetrically displaced toward the main basin-bounding Sangre de Cristo Fault Zone. Cross section *E-E'* modified from Ruleman and others (2013). SSDCFZ; Southern Sangre de Cristo Fault Zone; d, depth.

0.0 *Optional Day 2 route starts at the intersection of Montoso Road and Camino de Lovato Road. Proceed north on Camino de Lovato Road and follow the Bureau of Land Management road signs directed toward Brushy Mountain, Cerro Montoso, and Cerro de la Olla. This route is suitable for all-wheel drive and high-clearance vehicles only. Use of this road is not advised during inclement weather as it is prone to flash flooding.*

4.6 The road climbs onto lava flows of the unnamed cerrito east of Montoso (UCEM) volcano. These lava flows are typically dark gray, calc-alkaline andesite (59.59 weight percent SiO_2, 5.48 weight percent Na_2O+K_2O; sample RGR-127, table 2) containing sparse subhedral olivine and quartz xenocrysts in a microcrystalline to glassy groundmass.

4.7 View to the northeast is of Timber Mountain, exposing remnants of extensive Oligocene volcanic deposits associated with the Questa-Latir volcanic center (Thompson and others, 1986; Thompson and Schilling, 1988). *Please note, much of Timber Mountain is private property within the Rio Grande del Norte National Monument and can only be accessed with owner's permission.*

6.6 The low hill immediately west of the road is underlain by near-vent deposits of UCEM volcano and interpreted as the source of lava flows underlying the road for the past 2 mi (Kelson and others, 2008). An $^{40}Ar/^{39}Ar$ age determination on a whole-rock sample from these deposits yielded an interpreted age of 4.90±0.09 Ma (sample RGR-127, table 2). A northern vent area is visible is along the near tree-covered skyline to the northeast.

8.0 The large volcano directly to the west is Cerro Montoso, one of the largest petrologically uniform shield volcanoes of the TPVF. The summit of Cerro Montoso (8,402 ft, 2,561 m) rises approximately 260 m above the road elevation and the base spans more than 7 km in longest dimension. The summit crater preserves eroded near-vent pyroclastic deposits, cinder, spatter, abundant agglutinate, and interbedded lava flows and flow breccias that suggest multiple eruptive vents and a significant amount of summit erosion. The flanks of the Cerro Montoso are underlain by ubiquitous olivine-bearing lava flows and flow breccias. The lower slopes of Cerro Montoso are typically covered in blocky andesitic colluvium intermixed with fine-grained eolian sand and silt. Trachyandesite lava (59.59 weight percent SiO_2, 5.48 weight percent Na_2O+K_2O; sample RGR-127, table 2) contain 2–3 percent olivine phenocrysts in a microcrystalline groundmass of plagioclase, olivine, augite, and iron-titanium oxides. Three $^{40}Ar/^{39}Ar$ age determinations spatially distributed across the volcano yield identical ages, within 2σ error, of 4.95±0.04 (sample RGR-286, table 1).

10.0 Homestead turnoff to right. This part of the Taos Plateau was homesteaded by young families in the aftermath of World War I (1918–41) as returning military veterans filed claims under the Homestead Act (fig. 57). Remnants of small log homes and subsistence farms are common in the Cerro Montoso area.

10.5 Servilleta Basalt lava flows exposed in drainage a short distance east and west from the road.

10.9 *Road forks; take the left fork towards Brushy Mountain, the low hills to the northwest.*

11.7 *Road takes a sharp turn to the southwest. Do not take the right turn to the northeast!*

12.7 **Optional Stop 2A-1. Brushy Mountain south** (36°40.962' N., 105°39.222' W.; 7,096 ft, 2,163 m elevation)

The low ridges immediately north of the road are collectively referred to as Brushy Mountain. Brushy Mountain exposes Amalia Tuff at the base of the section, unconformably overlain by postcaldera andesite- to rhyolite-lava flows of the Questa-Latir magmatic system. Erosional remnants are stratigraphically discontinuous and variably faulted. Structural complexities are underrepresented on the schematic geologic map of figure 58 owing to limited exposure; however, stratigraphic relations are resolvable at map scale. $^{40}Ar/^{39}Ar$ geochronology was used to confirm stratigraphic relations and correlation of Amalia Tuff outcrops. Detailed geochemistry and petrology are discussed in Thompson and others (1986) and most deposits exposed here (except the Amalia Tuff) are similar to intermediate composition rocks at Timber Mountain. Unlike Timber Mountain, the Brushy Mountain deposits are entirely accessible on public land by way of an extensive four-wheel drive system of dirt roads and tracks formerly used for quarry excavation.

The quarry immediately north of the access road is cut into block-and-ash deposits of high-silica rhyolite, likely associated with local dome eruptions (fig. 59*A*, *B*). On the excavated floor of the abandoned quarry and lowermost quarry walls are reworked ash deposits, possibly remnants of air-fall and surge deposits similar in composition to the overlying block-and-ash deposits. Rhyolites in the quarry contain phenocrysts of sanidine, quartz, and minor biotite in a variably devitrified glass matrix. Blocks of hydrated rhyolite have as much as 4 weight percent water and when recalculated volatile-free, are similar in major element composition to Amalia Tuff

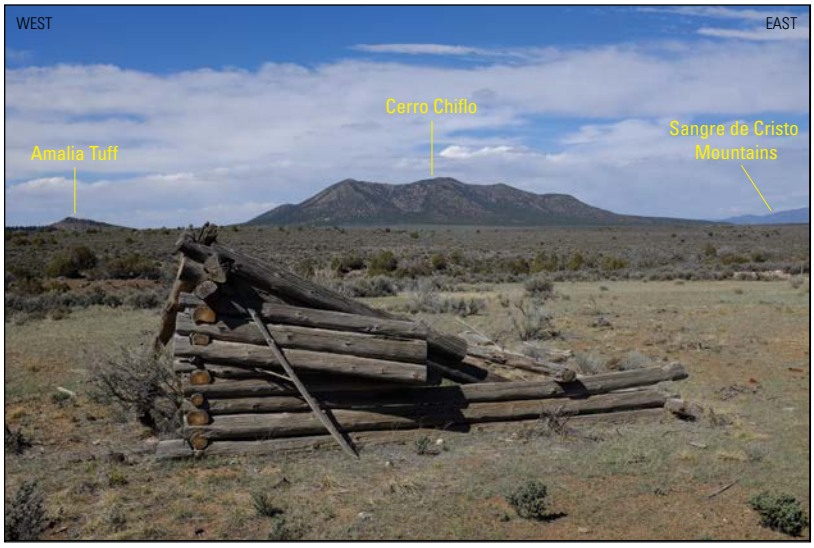

Figure 57. Homestead site en route to Brushy Mountain along Montoso Road. Amalia Tuff 1 kilometer east of Brushy Mountain is visible in in the distance to the left. Cerro Chiflo is visible in distant center and the Sangre de Cristo Mountains form the distant horizon in the far right of image. Photograph by Ren Thompson, U.S. Geological Survey, 2016.

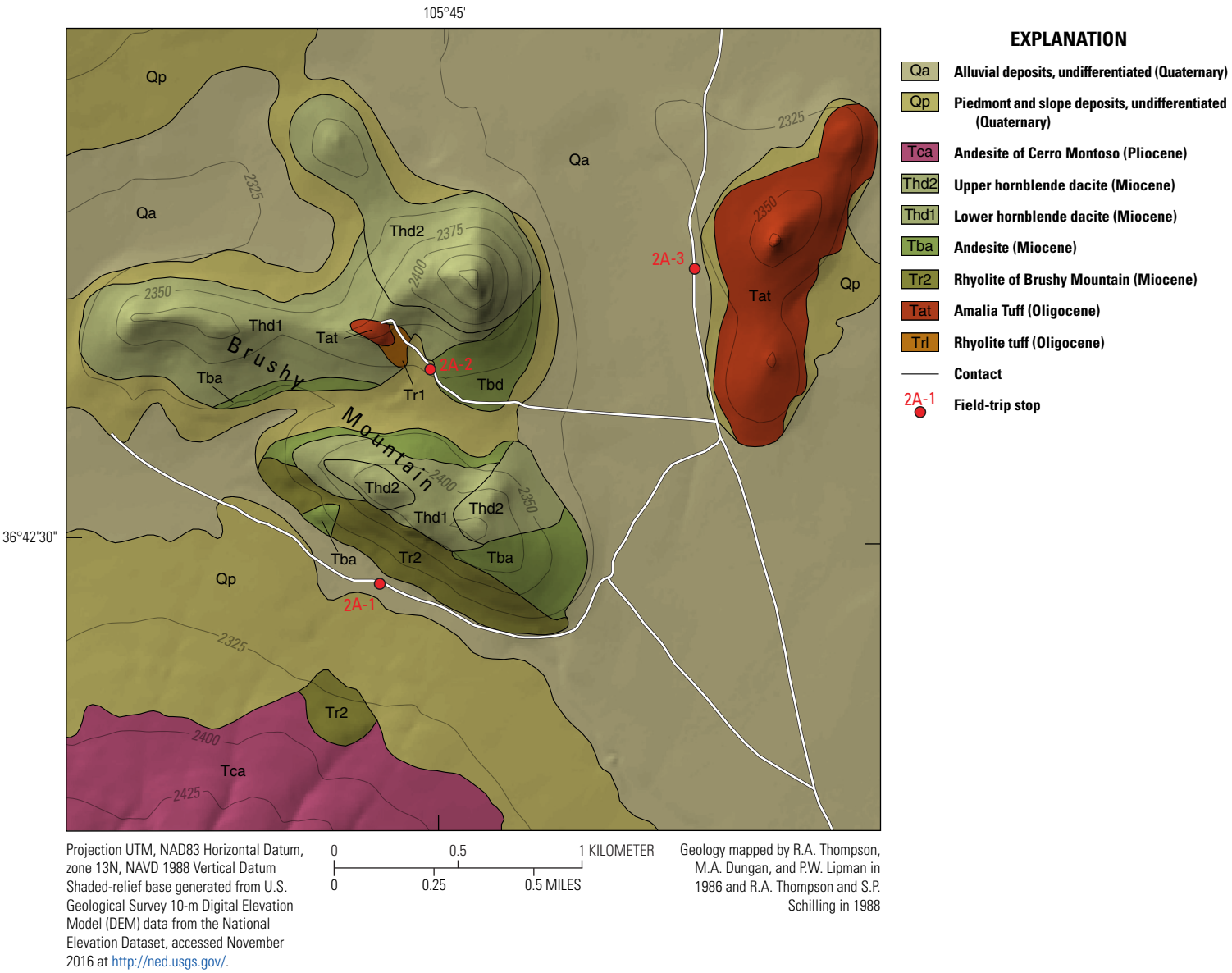

Figure 58. Simplified geologic map of the Brushy Mountain area modified from Thompson and others (1986) and Thompson and Schilling (1988).

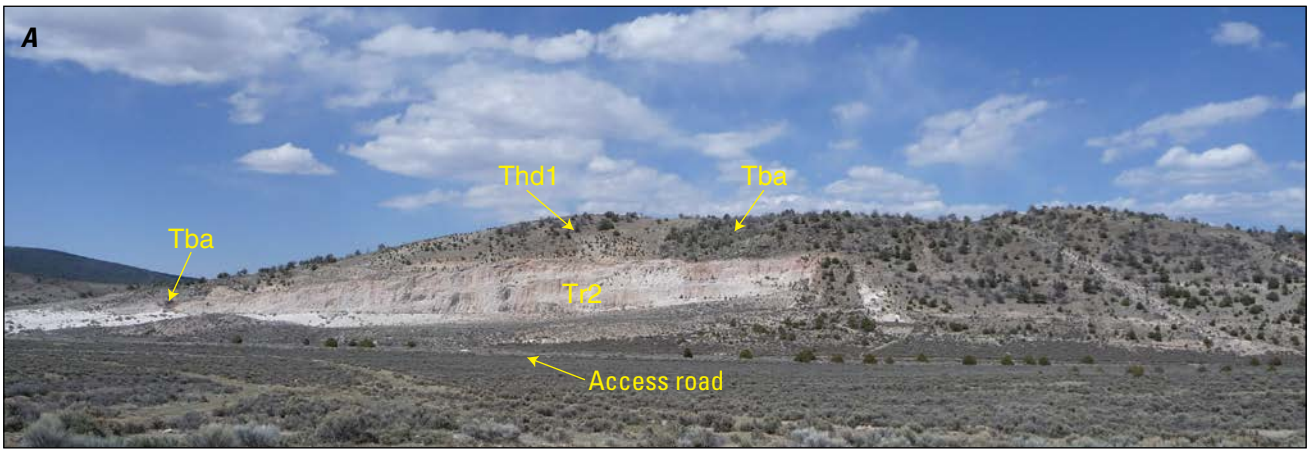

Figure 59. *A*, Abandoned Brushy Mountain perlite quarry on the south side of Brushy Mountain. Block- and ash-rhyolite (Tr2) is unconformably overlain by poorly exposed calc-alkaline dacite (Thd1) and andesite (Tba) lava flows. Map unit symbols are the same as those in figure 58. *B*, Quarry walls provide excellent exposures of glassy block- and ash-deposits. Photographs by Ren Thompson, U.S. Geological Survey, 2016.

(Thompson and others, 1986; Lipman, 1988). However, an $^{40}Ar/^{39}Ar$ age determination on sanidine yields an age of 25.28±0.05 Ma (sample RGR-512, table 1), possibly as much as 120 ka younger than the average accepted age of 25.4 Ma (Zimmerer and McIntosh, 2012b) for the Amalia Tuff.

Throughout the 1980s and early 1990s, rhyolite from the quarry was mined for perlite (hydrated volcanic glass), an important industrial additive in the production of ceramics, concrete, and insulation. When heated, volatiles in the rhyolite vaporize and escape, expanding the matrix volume to roughly 7–15 times that of the host rock. The low-density rhyolite has absorptive properties, allowing use as an agricultural and horticultural agent for distribution of supplements to plants and livestock. More recently, perlite is increasingly being used in filters of commercial beer brewing and bottling operations. Additional outcrops of the block-and-ash rhyolite flow are accessible in an abandoned quarry 0.6 km south of this locality beneath olivine andesite of Cerro Montoso.

Near the northeastern end of the quarry wall, stratigraphically above the rhyolite, is a single olivine andesite lava flow filling a small paleochannel cut into the block-and-ash deposits. The olivine-phyric lava flow contains olivine, clinopyroxene, plagioclase phenocrysts, plagioclase glomerocrysts, and orthopyroxene microphenocrysts in a fine- to medium-grained trachytic groundmass of plagioclase, clinopyroxene, and iron-titanium oxides, and is compositionally similar to precaldera andesites of the Questa-Latir system (54–59 weight percent SiO_2; >6.5 weight percent Na_2O+K_2O). An integrated whole-rock $^{40}Ar/^{39}Ar$ age determination of 22.48±0.2 Ma (sample RGR-308, table 1) was obtained from this locality.

Stratigraphically above the andesite are discontinuous remnants of dacite lava flows containing as much as 8 percent hornblende phenocrysts and lesser plagioclase, clinopyroxene, iron-titanium oxides, minor orthopyroxene, sanidine, sphene, and zircon. Biotite is only present in the most evolved flows. Dacites typically range in composition from 60 to 66 weight percent SiO_2 and are compositionally similar to those at Timber Mountain. Dacite lava flows are more easily observed at Stop 2A-2.

Return to intersection of mileage marker 11.7 at the east end of Brushy Mountain.

13.7 *Turn left onto the north fork at the intersection. Proceed northeastward to the intersection with Camino de Lovato Road.*

14.45 *Turn left onto Camino de Lovato Road and proceed north approximately 230 ft to the intersection with the dirt track headed west.*

15.15 *Intersection with dirt track that heads to Brushy Mountain north. Proceed west approximately 0.6 mi to intersection with dirt track headed uphill and to the northwest.*

16.18 *Intersection with dirt track headed northwest up lower flanks of Brushy Mountain north. Turn right, proceed approximately 200 ft and park near the trees on the right side of the track. Walk approximately 0.2 mi uphill along the dirt track to scraped exposures of Amalia Tuff on the left side of track.*

16.24 **Optional Stop 2A-2. Brushy Mountain north**
(36°42.828' N., 105°44.978' W., 7,703 ft, 2,348 m elevation)

Erosional remnants of Amalia Tuff are preserved in the low saddle at the crest of the ridge. The lithic rich, poorly welded Amalia Tuff contains relatively abundant andesite lithics and ubiquitous quartz and chatoyant sanidine phenocrysts. An $^{40}Ar/^{39}Ar$ sanidine age of 25.52±0.07 Ma (sample RGR-510, table 1) was obtained from this locality. Amalia Tuff is found on the west side of the San Luis Valley and in paleodrainages of the Tusas Mountains but is not preserved to the northwest or southwest. This pattern suggests that preservation of the ignimbrite was restricted to paleotopographic lows that likely corresponded to west-directed paleodrainage systems. Relatively steeply dipping contacts with overlying dacite lava flows suggest the Amalia Tuff at this locality was part of a paleotopographic high at the time of eruption of overlying dacite lava flows.

The overlying dacite lava flows are similar in composition and mineralogy to the dacites at the previous stop and those of Timber Mountain. At the crest of the hill to the northeast of this outcrop, an amphibole $^{40}Ar/^{39}Ar$ age determination of 24.45±0.57 Ma (sample RGR-511, table 1) supports the previous interpretation by Thompson and others (1986) that postcaldera volcanic activity associated with the Questa-Latir loci of the southern Rocky Mountains volcanic field was likely common, but limited in preservation, owing to extensional tectonism of the northern Rio Grande Rift and associated flank uplift.

Return to Camino de Lovato Road.

17.27 *Turn left at the intersection with Camino de Lovato Road and head north approximately 0.5 mi.*

17.77 **Optional Stop 2A-3. Brushy Mountain east**
(36°43.047' N., 105°44.317' W., 7,605 ft, 2,318 m elevation)
Park along the road as space permits. Do not block the road. Walk approximately 1,000 ft (305 m) northeast to outcrops exposed on the low hill east of the road.

The outcrops preserved here and on the smaller hill 1,312 ft (400 m) south are entirely underlain by silicified crystal-rich Amalia Tuff containing quartz, chatoyant sanidine, minor biotite phenocrysts, and traces of resorbed riebeckite amphibole. An $^{40}Ar/^{39}Ar$ determination on sanidine yields an age of 25.30±0.05 Ma (sample RTWP01, table 1), but distinct age peaks indicate a mixed population of sanidines with peaks near 25.43 and 25.25 Ma, possibly indicating that postcaldera Amalia Tuff was erupted from the Questa-Latir system for as long as 200 ka after caldera collapse.

Proceed south on Camino de Lovato Road approximately 12 mi to the intersection with Montoso Road and return to Taos by NM 64 (turn right) or NM 522 (turn left and proceed into Rio Grande gorge and across Dunn Bridge).

End of optional route 2A.

Day 3—The Taos Plateau Volcanic Field and Central San Luis Basin

By K.J. Turner[1], R.A. Thompson[1], C.F. Chan[1], M.A. Cosca[1], L.E. Morgan[1], and B.J. Drenth[1]

Introduction

The tectonic evolution of the San Luis Basin has been closely associated with multiple episodes of magmatism from the Oligocene through the Quaternary. Widespread Pliocene to Quaternary predominantly basaltic volcanism of the Taos Plateau volcanic field (TPVF) covers much of the southern and central San Luis Basin. Where exposed along uplifted portions of the Taos Plateau or in deeply incised gorges of the Rio Grande and Red River, TPVF deposits reveal the nature and timing of Pliocene and younger structural deformation related to development of compartmentalized subbasins within the Neogene San Luis Basin. However, characterization of extensional deformation that predates the Neogene basin depends on a fragmentary record of older basin-fill sedimentary and volcanic deposits exposed along structurally high areas in, and adjacent to, the central San Luis Basin. Oligocene deformation in the San Luis Basin area has not been well described, but previous mapping has established the stratigraphic and structural framework necessary for regional integration of the volcanic stratigraphy needed to decipher the structural evolution of the San Luis Basin area.

This field guide revisits areas (fig. 60) described by a previous International Association of Volcanology and Chemistry of the Earth's Interior field guide (Dungan and others, 1989b) but emphasizes results of recent studies largely focused on the relation between volcanism and tectonism. New $^{40}Ar/^{39}Ar$ age determinations as well as others from previous work are reported in table 3. This introduction and accompanying road log summarize the current understanding of the volcano-tectonic interactions in the San Luis Basin area from the Oligocene through the Pliocene and establish the geologic framework as the area transitioned from calc-alkaline volcanism associated with the southern Rocky Mountains volcanic field (SRMVF) to Rio Grande rifting.

Late Cretaceous to Early Tertiary Geologic Setting

The San Luis Basin is superposed on a broad uplift associated with Laramide compression in the Late Cretaceous to early Eocene that extended from the west side of the Tusas Mountains to the east side of the Sangre de Cristo Mountains (Tweto, 1975; Brister and Gries, 1994). On the western margin of the Tusas Mountains, Proterozoic rocks and overlying sedimentary rocks of Mesozoic and Paleozoic age dip as much as 75 degrees to the west (fig. 61; Muehlberger, 1968). Within the Tusas Mountains where Paleozoic and Mesozoic rocks are removed, considerable relief on the disconformable contact between Proterozoic rocks and mid-Tertiary volcanic and volcaniclastic rocks indicates an irregular topographic surface existed prior to the onset of Tertiary volcanism. The Sangre de Cristo Mountains on the east side of the uplift have been modified substantially by Cenozoic normal faulting and erosion, which has obscured the post-Laramide erosional surface. However, Questa-Latir volcanic locus deposits directly overlie Proterozoic rocks, erosional remnants of Paleozoic rocks, and Tertiary prevolcanic sedimentary deposits with irregular contacts as far north as the Culebra Range (Lipman and Reed, 1989; Fridrich and others, 2012).

Volcanism and Stratigraphy

Volcanic and volcaniclastic deposits on the margin of, and within, the San Luis Basin record late Oligocene through Quaternary volcanism and basin-filling sedimentation that overlap in time and space with formation of the Rio Grande Rift (fig. 24, Day 2, this volume). These volcanic and basin-filling episodes include (1) Oligocene to early Miocene, largely pre-extensional continental-arc volcanism of the SRMVF; (2) late Oligocene filling of subsiding extensional basins; (3) late Oligocene basaltic volcanism in the San Luis Hills; (4) early Miocene eruption of basaltic lavas and associated rhyolite in the southeast San Juan Mountains; (5) early to middle Miocene initial subsidence of the San Luis Basin; (6) middle Miocene calc-alkaline volcanism along the eastern margin of the basin; and (7) Pliocene to Quaternary, predominantly tholeiitic basaltic volcanism of the TPVF.

Southern Rocky Mountains Volcanic Field

Volcanic deposits in the San Juan Mountains, San Luis Hills, and Latir volcanic locus represent erosional remnants of the SRMVF, a composite middle Tertiary (38–23 Ma) volcanic field in Colorado and northern New Mexico (Steven, 1975; Lipman, 2007). Volcanic deposits associated with the field are characterized by volumetrically dominant

[1]U.S. Geological Survey.

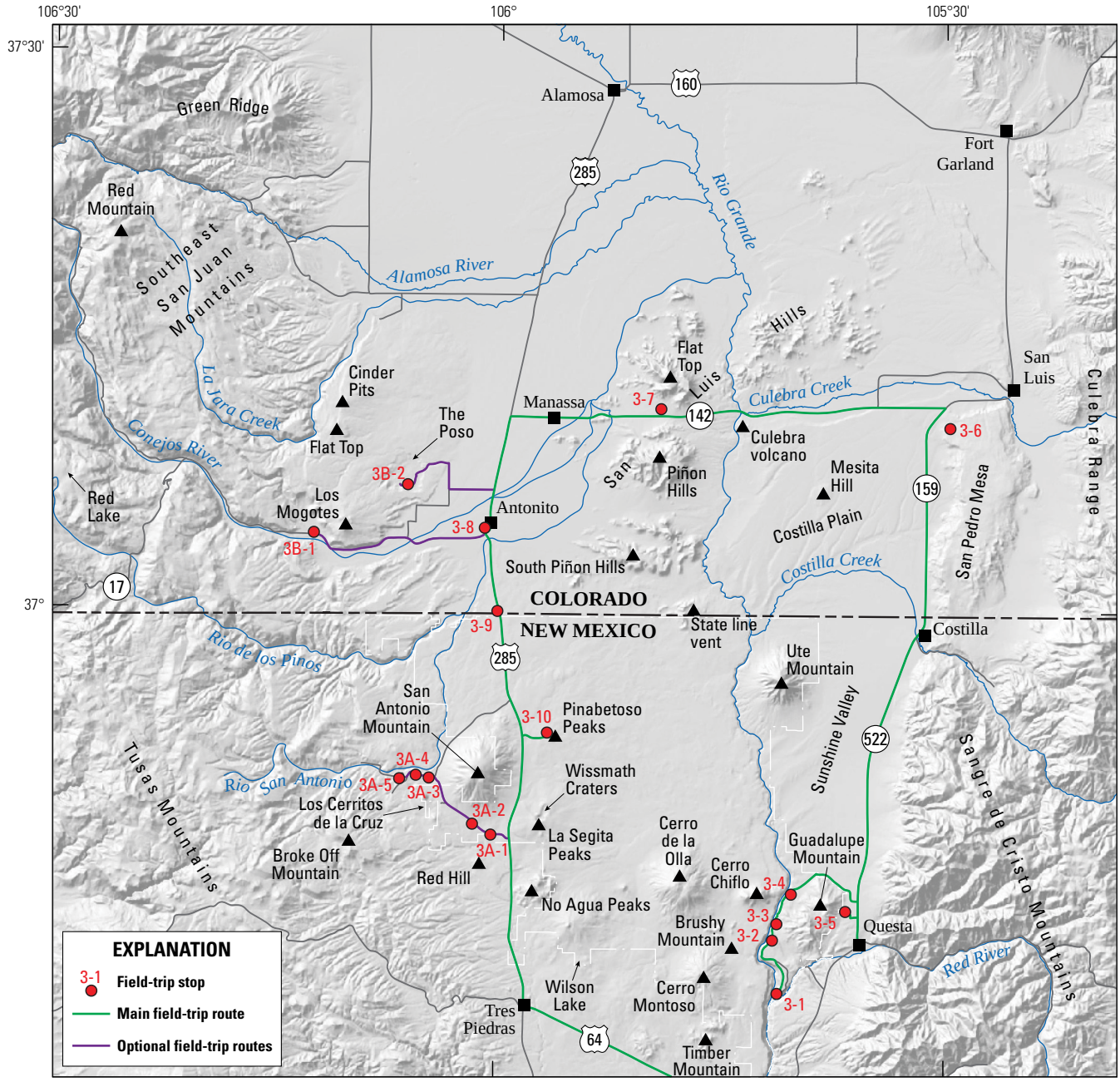

Projection UTM, NAD83 Horizontal Datum, zone 13N, NAVD 1988 Vertical Datum
Shaded-relief base generated from U.S. Geological Survey 10-m Digital Elevation Model (DEM) data from the National Elevation Dataset, accessed November 2016 at http://ned.usgs.gov/.

Figure 60. Hillshade map showing Day 3 route and stops. Geographic features referred to in the discussion and road log are indicated.

Table 3. Summary of $^{40}Ar/^{39}Ar$ and K-Ar geochronologic age determinations. All $^{40}Ar/^{39}Ar$ ages from published sources are reported here relative to a Fish Canyon Tuff neutron flux monitor age of 28.201 Ma (Kuiper and others, 2008).

[ID, identification; ---, no sample ID; Ma, million years ago; dms, degrees minutes seconds; N/A, not available; UCEM, unnamed cerrito east of Montoso; K, potassium; Ar, argon; SCLF, single crystal laser fusion; Fm, Formation]

Sample ID	Rock name or volcano	Material analyzed	Age (Ma) ± error (2σ)	Age calculation method	Source[a]	Longitude (dms)	Latitude (dms)
			Eastern Taos Plateau volcanic field				
RGR-03	Mesita Hill	Whole rock	1.13±0.03	Plateau	1	105°38.218′	37°6.475′
RGR-05	Servilleta Basalt–La Junta overlook	Whole rock	3.66±0.11	Plateau	1	105°41.202′	36°39.345′
RGR-79	Ute Mountain	Whole rock	3.95±0.12	Plateau	1	105°42.269′	36°56.941′
RGR-142	North UCEM	Whole rock	4.47±0.13	Plateau	1	105°41.951′	36°37.914′
RGR-283	Cerro de la Olla–olivine andesite	Whole rock	4.33±0.08	Integrated	1	105°47.382′	36°44.559′
RGR-127	South UCEM	Whole rock	4.9±0.09	Plateau	1	105°44.197′	36°38.654′
7MRG-2	San Pedro Mesa–Servilleta Basalt	Whole rock	4.61±0.07	Plateau	1	105°29.736’	37°1.026’
RGR-286	Cerro Montoso–olivine andesite	Whole rock	4.95±0.04	Plateau	1	105°45.130′	36°41.141′
SLH-501	Volcano de la Culebra–trachybasalt	Groundmass	5.19±0.11	Plateau	2	105°43.868′	36°9.493′
RGR-04	Servilleta Basalt–La Junta overlook	Whole rock	5.08±0.09	Plateau	1	105°41.252′	36°39.321′
RGR-108	Guadalupe Mountain–dacite to trachydacite	Whole rock	5.35±0.07	Plateau	1	105°39.636′	36°40.801′
			Northwestern Taos Plateau volcanic field				
TP505	Pinabetoso Peaks	Whole rock	2.18±0.15	Plateau	1	105°56.195′	36°53.221′
67L-30A	San Antonio Mountain trachydacite	Whole rock	3.12±0.17	K-Ar[b]	3	105°59′	36°52′
---	No Agua Peaks	Glass	3.88±0.06	Mean age-Ma[c]	4	N/A	N/A
---	No Agua Peaks	Glass/feldspar	4.1±0.03	Mean age-Ma[c]	4	N/A	N/A
68L-134I	Los Mogotes–south rim of shield	Whole rock	4.5±0.22	K-Ar[b]	5	106°9.851′	37°3.414′
67L-16	Los Mogotes–north rim of Los Mogotes crater	Plagioclase	4.8±1.4	K-Ar[b]	5	106°10.446′	37°4.885′
66L-36	Los Mogotes–north of Cinder Pits	Whole rock	4.8±0.26	K-Ar[b]	5	106°11.057′	37°12.594′
RGR-242	Los Mogotes–dike	Whole rock	4.85±0.02	Plateau	1	106°10.316′	37°4.566′
---	No Agua Peaks–xenocrystic	Alkali feldspar	25.35±0.13	SCLF	4	N/A	N/A
			Middle Miocene rocks				
RGR-143	Cerro Chiflo trachydacite	Amphibole	9.64±0.8	Integrated	1	105°43.636′	36°44.859′
RGR-143	Cerro Chiflo trachydacite	Biotite	10.99±0.09	Plateau	1	105°43.636′	36°44.859′
77L-RG19	Cerro Chiflo trachydacite	Biotite	10.15±0.53	K-Ar[b]	3	105°41′	36°45′
77L-RG19	Cerro Chiflo trachydacite	Plagioclase	10.28±0.57	K-Ar[b]	3	105°41′	36°45′
			Hinsdale Formation				
RGR-516	Trachybasalt–southeast San Juan Mountains	Whole rock	20.53±0.29	Integrated	1	106°22.720′	37°19.345′
RGR-379	Basaltic trachyandesite–West of Los Mogotes	Whole rock	20.62±0.07	Plateau	1	106°14.565′	37°7.726′
RGR-138	Basaltic trachyandesite–San Luis Hills	Whole rock	24.56±0.05	Plateau	1	105°40.784′	37°13.888′
RGR-490	Basalt–San Luis Hills	Whole rock	25.71±0.17	Plateau	1	105°49.219′	37°2.945′
RGR-456	Basalt–North Tusas Mountains	Whole rock	25.67±0.20	Plateau	1	106°14.907′	36°49.565′
13BP-23	Basaltic trachyandesite–San Luis Hills	Whole rock	25.90±0.07	Plateau	1	105°48.346′	37°12.118′
RGR-105	Trachybasalt–San Luis Hills	Whole rock	25.88±0.05	Plateau	1	105°48.431′	37°11.887′
RGR-33	Basaltic andesite–North Tusas Mountains	Whole rock	26.64±0.38	Plateau	1	106°10.552′	36°47.897′
RGR-380	Basalt–West of Los Mogotes	Whole rock	26.40±0.08	Plateau	1	106°14.973′	37°7.362′
RGR-104	Basaltic trachyandesite–San Luis Hills	Whole rock	26.96±0.26	Integrated	1	105°48.419′	37°11.758′
			Southern Rocky Mountains volcanic field				
---	Amalia Tuff	Alkali feldspar	25.39±0.04	Mean age-Ma[c]	6	N/A	N/A
---	Carpenter Ridge Tuff	Sanidine	27.73±0.05	SCLF	7	N/A	N/A
---	Fish Canyon Tuff	Sanidine	28.20±0.05	SCLF	8	N/A	N/A
SLH-512	Conejos Fm-dacite dike	Amphibole	29.34±0.55	Plateau	1	105°48.325′	37°11.381′
RGR-466	Chiquito Peak Tuff	Sanidine	28.94±0.31	SCLF	1	106°9.555′	36°57.823′
RGR-151	Alunite vein-San Luis Hills	Alunite	30.33±0.87	Plateau	1	105°45.668′	37°11.096′
SLH-507	Conejos Fm-andesite lava	Groundmass	30.33±0.06	Plateau	2	105°43.736′	37°10.848′
Brister90-6	Ignimbrite west of Fort Garland	Biotite	30.34±0.12	Plateau	9	105°20.1′	37°29.6′
SLH-514	Conejos Fm-andesite lava	Groundmass	30.45±0.09	Plateau	2	105°52.659′	37°10.533′

[a]Sources include: 1, this report; 2, Thompson and others (2015); 3, Lipman and Mehnert (1979); 4, Dickens (2007); 5, Hon and Mehnert (1983); 6, Zimmerer and McIntosh (2012b); 7, Lipman and McIntosh (2008); 8, Kuiper and others (2008); 9, Brister and McIntosh (2004).

[b]K-Ar ages originally reported in Lipman and others (1970) and Lipman and Mehnert (1975) were recalculated by Hon and Mehnert (1983) with IUGS decay constants (Steiger and Jager, 1977).

[c]Multiple analyses used in mean age calculation.

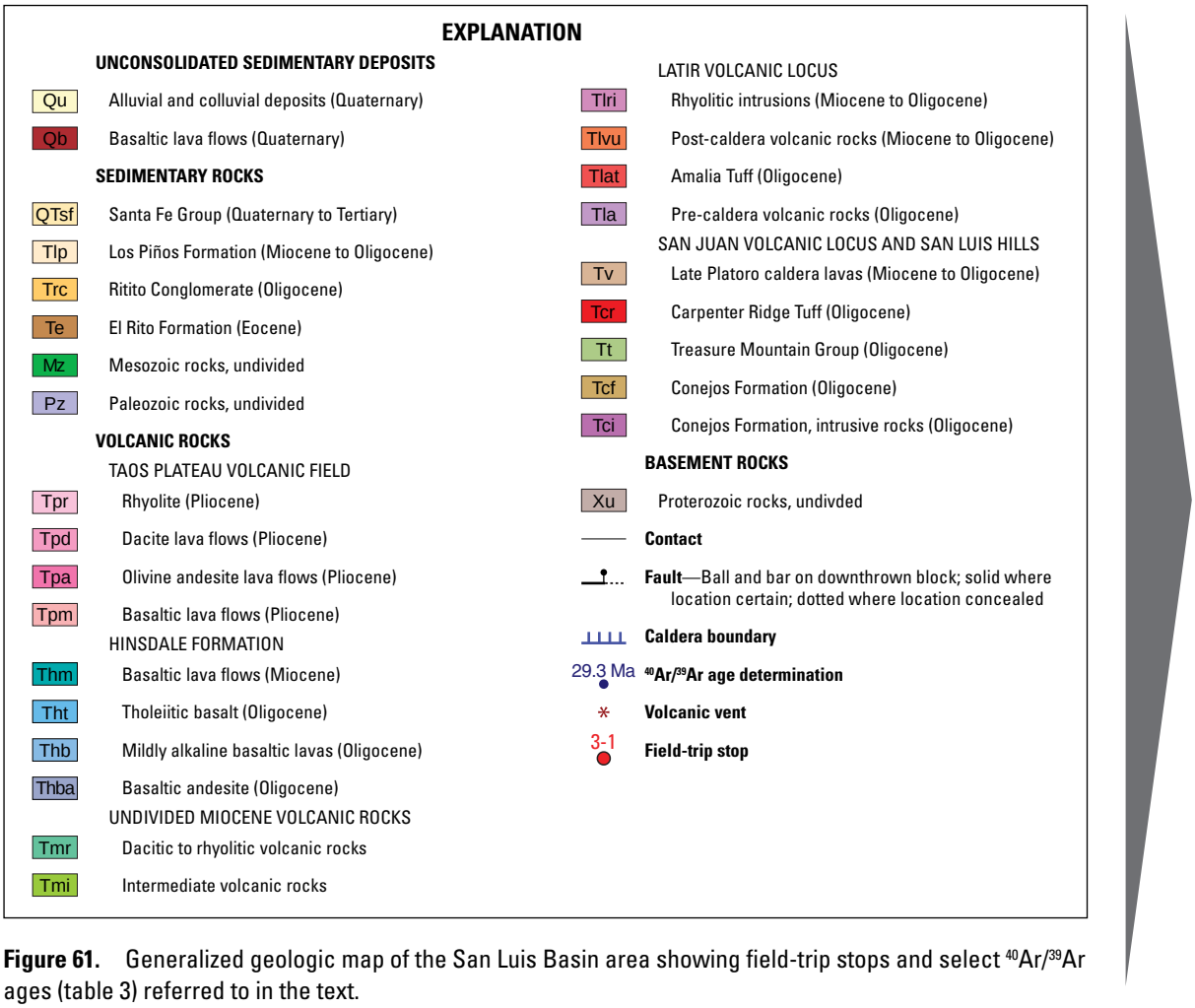

Figure 61. Generalized geologic map of the San Luis Basin area showing field-trip stops and select $^{40}Ar/^{39}Ar$ ages (table 3) referred to in the text.

intermediate-composition lavas and breccias erupted from scattered central volcanoes and volumetrically smaller but laterally extensive silicic ignimbrites sourced from large calderas (Lipman, 2007). From 33 Ma to about 25 Ma, the locus of volcanism migrated southeastward across the San Luis Basin region from the southeast San Juan Mountains, to the San Luis Hills, and finally to the southernmost portion of the SRMVF, the Latir volcanic locus. Volcanism and representative deposits in the southeastern San Juan Mountains are described here and in more detail in the Day 4 section of this field guide.

Intermediate-composition lavas and associated volcaniclastic deposits that preceded ignimbrite eruptions are collectively referred to as the Conejos Formation throughout the San Juan Mountains and San Luis Hills (Lipman and others, 1970; Lipman, 1974, 1975a,b; Thompson and Machette, 1989). The Conejos Formation dominantly consists of andesite to dacite lavas and breccias and associated volcaniclastic rocks that represent aprons around the large volcanoes. In the southeastern San Juan Mountains, development of volcanoes between 33–30 Ma (Lipman, 1975a; Colucci and others, 1991) was followed by multiple cycles of ignimbrite eruption and caldera collapse at the Platoro caldera complex (Lipman and others, 1996). Between ~30.5–29 Ma at least seven major ignimbrites (individual ignimbrite volumes were 75–1,000 km^3) were erupted as well as smaller ignimbrites and airfall tuffs that collectively represent the Treasure Mountain Group (Lipman, 1974, 1975a,b; Lipman and others, 1996). The last caldera-forming event erupted the Chiquito Peak Tuff at 28.94±0.31 Ma[2] (sample RGR-466, table 3). Ignimbrites erupted from the Platoro caldera flowed in all directions including extensively into the northern Tusas Mountains. Distal Treasure Mountain Group deposits are preserved more than 100 km away from the caldera rim in areas

[2]The age is determined from a sample of distal outflow in northern New Mexico, approximately 48 km southeast of the caldera boundary. The discussion in Day 4 uses an age of 28.6 Ma, but this is calculated based on a Fish Canyon Tuff age of 28.02 Ma. When corrected for the same Fish Canyon Tuff age, Chiquito Peak Tuff ages are within analytical uncertainty.

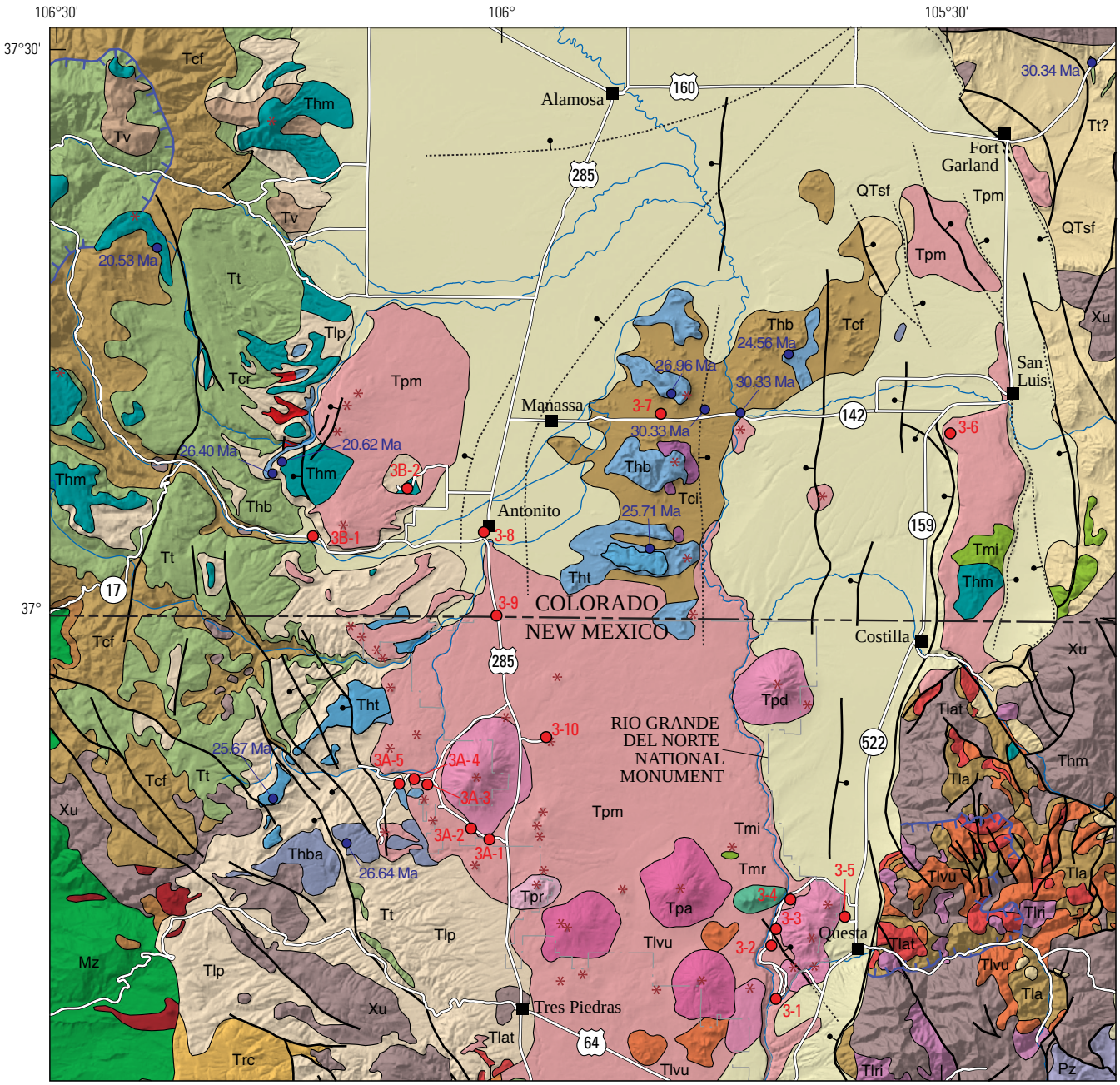

Projection UTM, NAD83 Horizontal Datum, zone 13N, NAVD 1988 Vertical Datum
Shaded-relief base generated from U.S. Geological Survey 10-m Digital Elevation Model (DEM) data from the National Elevation Dataset, accessed November 2016 at http://ned.usgs.gov/.

Geology by K.J. Turner and R.A. Thompson, 2015

south and west of Tres Piedras, New Mexico, and possibly on the east side of the San Luis Basin where a 30.34 Ma moderately welded ignimbrite is exposed northeast of Fort Garland (fig. 61; Kearney, 1983; Wallace, 1996; Brister and McIntosh, 2004).

Prior to caldera-forming eruptions in the southeastern San Juan Mountains, intermediate-composition magmatism began in the San Luis Hills. These deposits, also referred to as the Conejos Formation based on compositional similarities, record magmatism between 31 and 28 Ma (Thompson and Machette, 1989; Thompson and others, 2015). In contrast to the southeastern San Juan Mountains where eruption of voluminous ignimbrites and formation of multiple confocal calderas superseded Conejos volcanism, no calderas formed in the San Luis Hills. The absence of Treasure Mountain Group deposits in the San Luis Hills (Thompson and Machette, 1989) suggests that positive topography was established prior to ignimbrite eruptions at the Platoro caldera. Alternatively, a period of rapid erosion that deeply eroded Conejos deposits could have removed Treasure Mountain Group ignimbrites from the San Luis Hills (Thompson and Machette, 1989; Thompson and others, 1991).

Around 28 Ma, coincident with the waning of magmatism in the San Luis Hills, precaldera volcanism began in the Latir volcanic locus, the southernmost part of the SRMVF. As elsewhere in the field, compositions of precaldera volcanic rocks are predominantly intermediate (Steven, 1975; Lipman, 2006, 2007; Lipman and others, 2015), although basaltic andesite through rhyolite were erupted as lava flows, domes, and tuffs from 28.5 to 25.4 Ma (Lipman and Reed, 1989; Zimmerer and McIntosh, 2012b). Volcanism peaked at 25.4 Ma with the collapse of the Questa caldera during eruption of the greater than 500 km^3 Amalia Tuff, a high-silica (75–77 weight percent SiO_2) alkalic to peralkaline rhyolite (Lipman and others, 1986; Johnson and Lipman, 1988; Lipman and Reed, 1989; Zimmerer and McIntosh, 2012b). Resurgent plutons were emplaced immediately after caldera collapse and postcaldera intrusions are as young as 19 Ma south of the Questa caldera. Oligocene and Miocene volcanic deposits at Timber and Brushy Mountains, in the central San Luis Basin (Day 2 optional stop), are the best-preserved record of postcaldera volcanism (Thompson and others, 1986). Porphyry molybdenum deposits are associated with postcaldera intrusions along the south caldera boundary. Mineralization ages are approximately coincident with the host granitic rocks (24–21 Ma; Lipman and others, 1986) suggesting mineralization occurred shortly after pluton emplacement. These deposits were mined until recently.

Oligocene to Miocene Volcanism and Basin Filling

Los Piños Formation—Volcaniclastic deposits of the Los Piños Formation overlie the Treasure Mountain Group and consist primarily of weakly indurated sandstones and conglomerates with rounded to well-rounded volcanic clasts as much as 1.5 m in diameter (Atwood and Mather, 1932; Larsen and Cross, 1956; Lipman, 1975a,b; Manley, 1981). Relative to volcaniclastic deposits in the Conejos Formation, the Los Piños Formation has a lighter-colored tuffaceous matrix and a more diverse clast lithology. Two partly age-equivalent members of the Los Piños Formation are differentiated based on the dominant clast types that reflect distinct clast provenance. The Esquibel Member overlies the Chiquito Peak Tuff (28.94 Ma) and is composed of detritus eroded from the southeastern San Juan Mountains and the San Luis Hills. The Cordito Member is about 3.5 m.y younger than the Esquibel Member as the base of the unit is defined by the Amalia Tuff (25.4 Ma), which interfingers with the Los Piños Formation in the Tusas Mountains (Manley, 1981). Deposition of the Esquibel Member continued in areas closer to the San Juan Mountains and San Luis Hills concurrent with deposition of the Cordito Member in the central and southern Tusas Mountains (Manley, 1981). These deposits partly reflect coalescing alluvial fans that become more fluvially dominated away from volcanic highlands, but also represent early-rift basin-fill deposits, as their distribution and variations in thickness indicate areas of syndepositional subsidence in pre-San Luis Basin extensional basins. Exposed thicknesses are as much as 200 m in southern Colorado and 350 m in northern New Mexico, but gravity modeling suggests total thickness may be as much as 1,000 m (Drenth and others, 2011,2013).

Volcaniclastic deposits contemporaneous with the Los Piños Formation are preserved in the Culebra graben (figs. 24 and 26, Day 2, this volume), which is situated between the San Luis Hills and the Culebra Range on the east side of the San Luis Basin. These deposits, mapped as Santa Fe Group (for example, Wallace, 2004), are underlain by a 30.34±0.12 Ma ignimbrite, which provides a maximum age constraint for the deposits. A lower conglomerate bed within the volcaniclastic deposits contains clasts of 37–29 Ma volcanic rocks derived from the Thirty-nine Mile volcanic field located north of the San Luis Basin and east of the Sangre de Cristo Mountains (Armstrong and others, 2013). The presence of Thirty-nine Mile volcanic clasts is evidence that the Culebra graben formed prior to uplift of the Sangre de Cristo Mountains, as paleodrainages would have crossed the area now occupied by the range.

Hinsdale Formation—The Hinsdale Formation (fig. 24, Day 2, this volume) represents the earliest manifestation of Tertiary basaltic volcanism in the San Luis Basin region and was erupted during late Oligocene and Miocene deposition of the Los Piños Formation. Mildly alkaline compositions are most common in the Hinsdale Formation, but rare tholeiitic basalt and basaltic andesite are also preserved. By comparison, Quaternary to Pliocene basaltic lavas of the TPVF are dominantly tholeiitic basalt with subordinate mildly alkaline compositions.

The San Luis Hills preserve the greatest volume of Hinsdale Formation in the San Luis Basin region. Topographic highs at Flat Top, Piñon Hills, and South Piñon Hills are held up by thick sequences of Hinsdale lavas with maximum thicknesses of as much as 400 m (Thompson and Machette, 1989). The youngest Hinsdale lavas in the San Luis Hills occur east of the Rio Grande (fig. 61) where a lava near the base of a 180-m-thick sequence of lavas yielded a whole-rock $^{40}Ar/^{39}Ar$ age of 24.56±0.05 Ma (sample RGR-138, table 3). The oldest sampled lava flow is 26.96±0.26 Ma (sample RGR-104, table 3) from the basal flow of a 240-m-thick sequence of lavas on the south side of Flat Top (fig. 61). Although only three vents associated with lava sequences at Flat Top, Piñon Hills, and South Piñon Hills have been identified (Thompson and Machette, 1989), additional vents were likely active intermittently in the San Luis Hills to account for the volume and compositional diversity observed, but the vents are either concealed by overlying Hinsdale lavas or are eroded to a degree that they are no longer recognizable.

Along the margin of the southeastern San Juan Mountains and in the northern Tusas Mountains are late Oligocene flows of the Hinsdale Formation sourced from the San Luis Hills. Three alkaline basalt flows preserved along the margin of the southeastern San Juan Mountains (fig. 61; Lipman, 1975b) have major and trace element compositions overlapping least primitive compositions in the San Luis Hills (fig. 62) and a whole-rock $^{40}Ar/^{39}Ar$ age of 26.40±0.08 Ma (sample RGR-380, table 3) is within the range of documented Hinsdale ages in the San Luis Hills (table 3.1). In the northern Tusas Mountains, tholeiitic basalt (25.67±0.20 Ma; sample RGR-456, table 3) and basaltic andesite (26.64±0.38 Ma; sample RGR-33, table 3) hold up eastward-tilted

dip-slope surfaces (fig. 61; Butler, 1971; Manley, 1982a,b; Thompson and Lipman, 1994a,b). Tholeiitic basalts in the Hinsdale Formation are rare, but are also identified at South Piñon Hills in the San Luis Hills, where a 60-m-thick accumulation of tholeiitic basalts is indistinguishable in age (25.71±0.17 Ma; sample RGR-490, table 3) and composition (fig. 62) from the northern Tusas Mountains flows. Most known vent areas for late Oligocene lavas of the Hinsdale Formation are identified in the San Luis Hills and the thickest accumulation of tholeiitic basalts is in the South Piñon Hills; therefore, the South Piñon Hills are considered a likely source area. Basaltic andesite lavas in the Tusas Mountains erupted from an indeterminate source inferred to be northeast of the exposed lavas and concealed beneath volcanic rocks of the TPVF.

Exposures of early Miocene lavas of the Hinsdale Formation along the western margin of the San Luis Basin and in the southeastern San Juan Mountains consist of alkaline basalt to rhyolite (fig. 62*A*). Vent areas with eruptive sequences that include rhyolite are central to the Platoro caldera and along the northwestern caldera rim, whereas vent areas south and east of the Platoro caldera lack rhyolitic eruptive products (fig. 61; Lipman, 1974, 1975a; Thompson and Dungan, 1985). The westernmost early Miocene lavas along the western margin of the San Luis Basin are alkaline basalt to basaltic trachyandesite flows with an

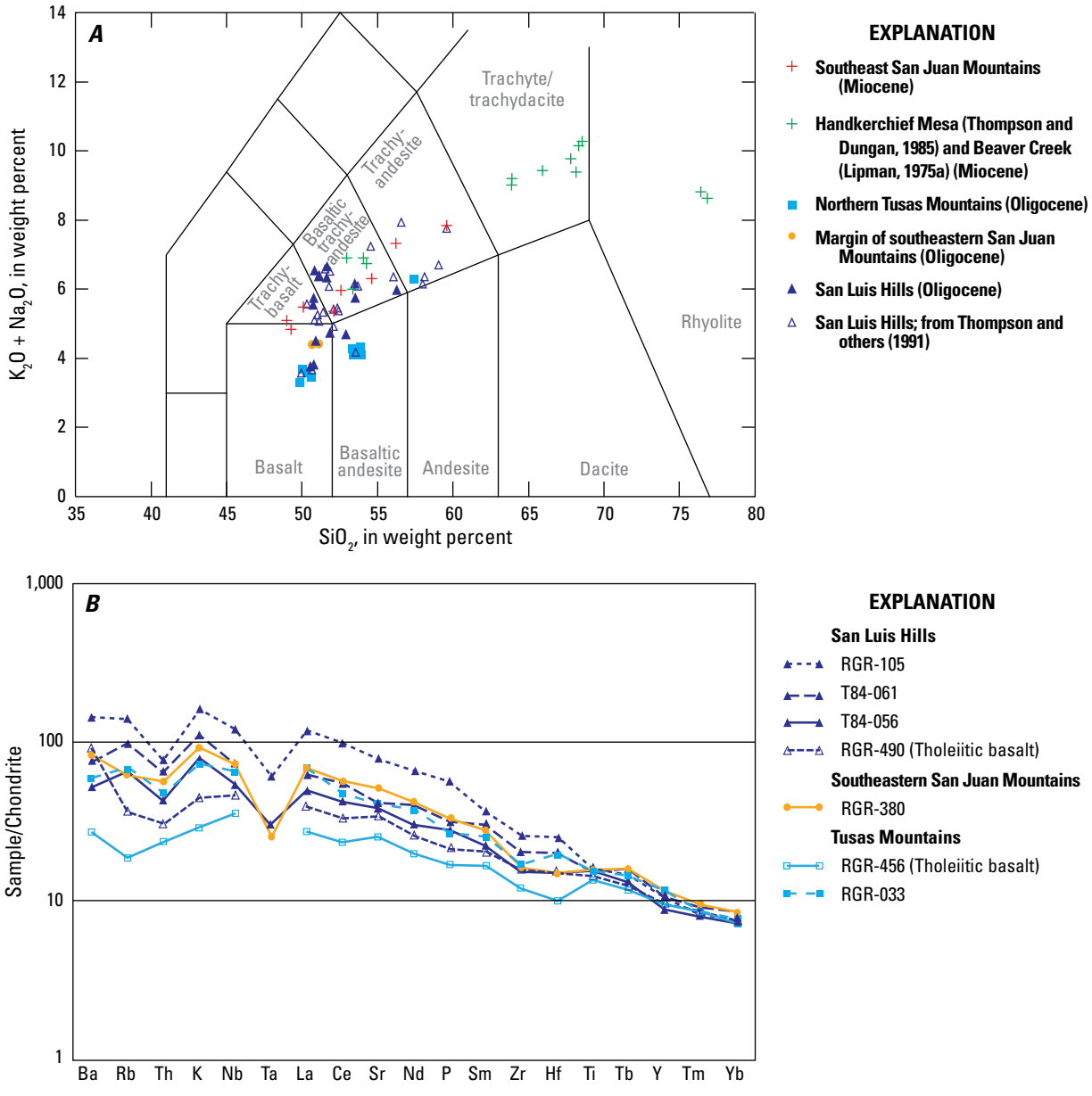

Figure 62. Geochemistry of the Hinsdale Formation. *A*, Alkali-silica classification diagram of Le Bas and others (1986). Data normalized to volatile-free based on method of Middlemost (1989). *B*, Chondrite-normalized trace element diagram for selected samples of Hinsdale Formation lavas. Values for the chondrite and the arrangement of elements follow the discussion in Thompson (1982).

$^{40}Ar/^{39}Ar$ age of 20.62±0.07 Ma (sample RGR-379, table 3). These basaltic lavas are tentatively correlated with a vent located on the southeast rim of the Platoro caldera where a compositionally similar trachybasalt flow proximal to the vent yielded a whole-rock $^{40}Ar/^{39}Ar$ age of 20.53±0.29 Ma (sample RGR-516, table 3).

Middle Miocene volcanic deposits preserved on the east side of the San Luis Basin at San Pedro Mesa and at the foot of the Culebra Range (fig. 61), consist of two compositionally distinct eruptive sequences that include hornblende- and biotite-bearing andesite and dacite overlain by basaltic lava flows of the Hinsdale Formation. At least 250 m of deeply dissected andesite and dacite is exposed in the southern part of San Pedro Mesa and overlying basaltic lavas are at least 220-m thick (Thompson and others, 2007a). At the foot of the Culebra Range east of San Pedro Mesa, volcanic deposits as much as 600-m thick with eruption ages that range from 15 to 11 Ma (Miggins, 2002; Miggins and others, 2002; Kirkham and others, 2004), are lithologically similar to middle Miocene volcanic rocks on San Pedro Mesa, but correlation between the two areas requires further investigation. Other middle Miocene volcanic remnants include basaltic lava flows in the northern part of the Latir volcanic locus (Lipman and Reed, 1989) and biotite dacite at Cerro Chiflo within the Wild Rivers Recreation Area (Stop 3-4; Lipman and Mehnert, 1975).

Deposits of the Taos Plateau Volcanic Field

Deposits of the TPVF record predominantly basaltic Pliocene to Quaternary volcanism. A detailed discussion of the TPVF is included in Day 2 of this field guide; therefore, only areas of the field pertaining to the Day 3 route will be discussed here. These areas include Wild Rivers Recreation Area and the northwestern portion of the TPVF.

Pliocene volcanic rocks associated with the TPVF in the Wild Rivers Recreation Area range from basalt to dacite (fig. 63) and were erupted from numerous vent areas between 5.35 and 3.1 Ma (table 3). The largest volume of dacitic lavas erupted from multiple vent areas at Guadalupe Mountain, identified by the presence of at least four spatially separated accumulations of highly oxidized near-vent pyroclastic deposits. Olivine andesite lavas are primarily exposed along the gorge of the Red River near known vent areas but are also found in at least two localities in the Rio Grande gorge. Lower and upper sequences of Servilleta Basalt at the La Junta point are temporally equivalent with the lower and upper sequences of Servilleta Basalt flows, respectively, observed at the High Bridge of the Rio Grande (Stop 2-4).

The northwestern portion of the TPVF, as discussed herein, covers the area from the rhyolite domes at No Agua Peaks in the southeast to the Los Mogotes composite shield in the northwest. The westernmost parts of this area are moderately elevated above the valley floor where the TPVF onlaps east-dipping dip-slope surfaces along the western basin margin. Eruption ages in the northwestern portion of the field range from an approximate 4.9-Ma dike in Los Mogotes composite shield to 2.18±0.15 Ma (sample TP505; table 3) for a near-vent lava at Pinabetoso Peaks, west of San Antonio Mountain. Although the range of compositions in the northwestern portion of the TPVF is similar to the rest of the field, mildly alkaline basaltic compositions are more common (fig. 64). Mildly alkaline basaltic lavas were erupted from vent areas associated with the Los Mogotes composite shield, Red Hill, Los Cerritos de la Cruz, and a vent on the northeast flank of San Antonio Mountain (fig. 61). Vent areas outside the northwestern portion of the Taos Plateau that erupted mildly alkaline basaltic compositions are less common and more spatially separated; examples include the State line vent, Wilson Lake, and Culebra volcano (figs. 60, 61). Eruptive centers in the northwestern portion of the field are more abundant than comparably sized areas elsewhere in the TPVF, and mafic centers are generally associated with small volume, aerially restricted lava flows (fig. 61). Approximately 20 vent areas consisting of cinder cones, small shields with central collapse, and a large-volume dacitic volcano at San Antonio Mountain are identified in the northwestern portion of the field. These vents account for nearly a third of the more than 60 vents currently identified throughout the entire field. Additionally, xenocrystic lavas, rarely observed throughout the majority of the TPVF, are more common in the northwestern portion of the field, with some lavas containing as much as 7 modal percent xenocrysts of predominantly quartz and plagioclase.

Extensional Tectonism

Two distinct phases of extensional tectonism are well established for the southern portions of the Rio Grande Rift, in southern and central New Mexico: (1) Oligocene development of broad and shallow basins followed by (2) Neogene development of narrow and deep basins accompanied by rapid uplift of basin-bounding blocks superposed on the older basins (Morgan and Golombeck, 1984; Seager and others, 1984; Morgan and others, 1986). Extensional tectonism in the San Luis Basin is broadly consistent with this two-stage history. Development of the San Luis Basin and rapid uplift of the Sangre de Cristo Mountains is consistent with the later, Neogene phase of extension in the central and southern rift. Erosional remnants of late Oligocene coarse-grained volcaniclastic deposits exposed along the uplifted rift margins adjacent to the central part of the San Luis Basin provide evidence for an earlier period of extension not well described previously.

Pre-San Luis Basin Extensional Deformation

Published estimates for the onset of Rio Grande rifting in the San Luis Basin are based on scattered structural and stratigraphic evidence that coincide temporally with compositional changes in volcanic rocks. Structural evidence includes the presence of a subtle angular unconformity along the eastern margin of the southeastern San Juan Mountains onlapped by Los Piños and Hinsdale Formations. Below the unconformity, progressively older Treasure Mountain Group ignimbrites and Conejos Formation

are exposed to the west, and units as young as the Fish Canyon and Carpenter Ridge Tuffs (28.2 Ma and 27.7 Ma, respectively) are truncated below the unconformity (Lipman, 1974,1975a,b; Lipman and Mehnert, 1975). Lipman and Mehnert (1975) suggest the erosional surface formed during eastward tilting associated with subsidence of the San Luis Basin sometime after emplacement of the Carpenter Ridge Tuff. In the Latir volcanic locus, some intrusions related to resurgent plutonism following caldera collapse at 25.4 Ma were emplaced along faults inferred to reflect regional extension, which suggests extensional faulting was underway around the time of caldera formation (Lipman and others, 1986). Petrologic evidence for the onset of extension includes eruption of predominantly basaltic lavas of the Hinsdale Formation, as early as 27 Ma, in contrast to the preceding calc-alkaline, intermediate- to silicic-magmatism associated with the SRMVF that lacked basalt (Lipman and Mehnert, 1975; Thompson and others, 1991). Recent investigations incorporating geologic mapping, reinterpretation of existing geologic mapping, $^{40}Ar/^{39}Ar$ geochronology, and geophysical studies in the central part of the San Luis Basin have established the structural evolution of early formed grabens that flank a north-trending horst beginning around 29 Ma.

The San Luis horst is a north-trending axial horst with surface expression where Oligocene and Miocene volcanic and

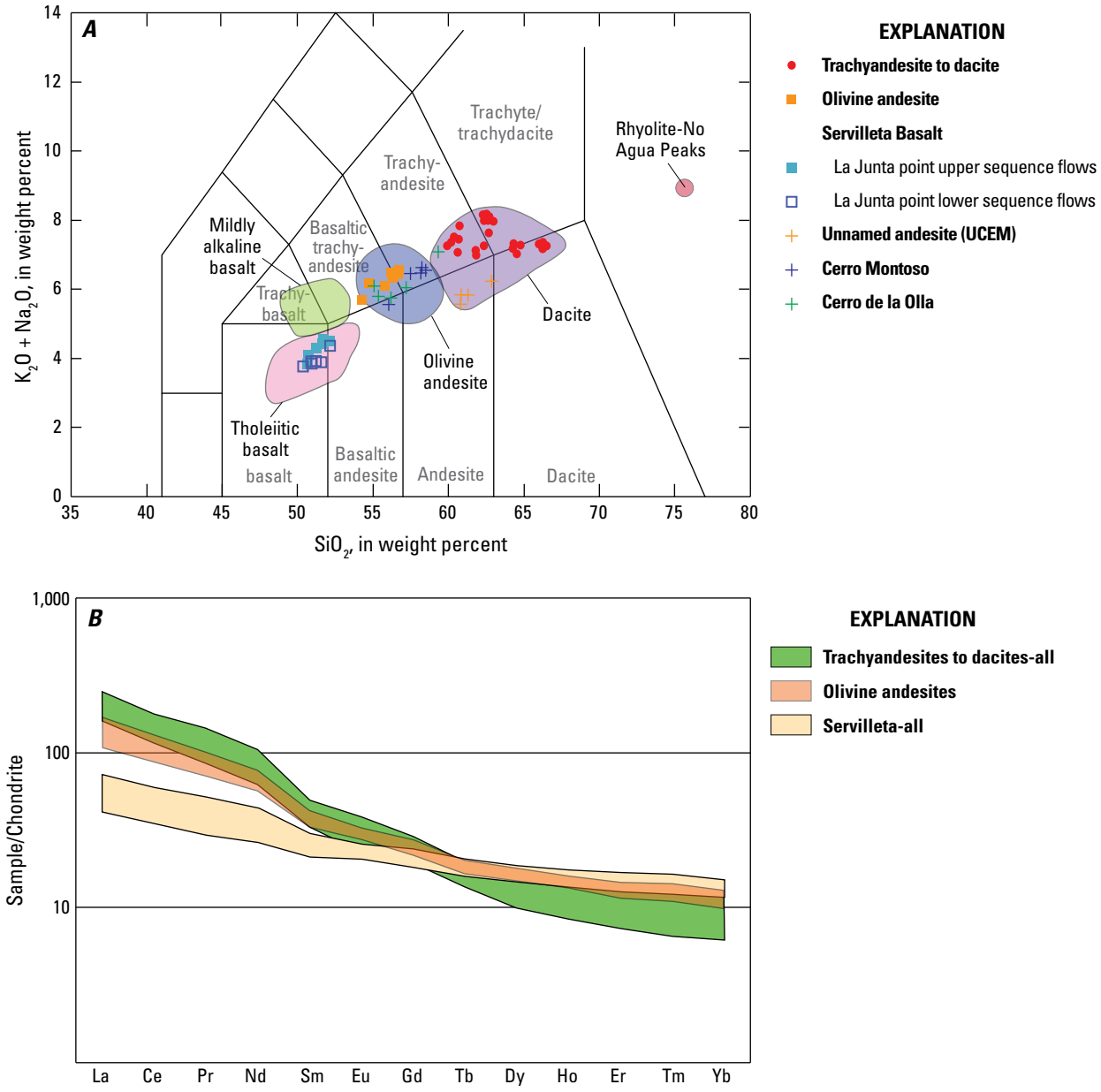

Figure 63. Geochemistry of Taos Plateau volcanic field rocks in the Wild Rivers Recreation Area. *A*, Alkali-silica classification diagram of Le Bas and others (1986). Data normalized to volatile-free based on the method of Middlemost (1989). *B*, Trace element spider diagram showing range of compositions within specific rock types in the Wild Rivers Recreation Area. Values for chondrite and arrangement of elements follows discussion in Thompson (1982).

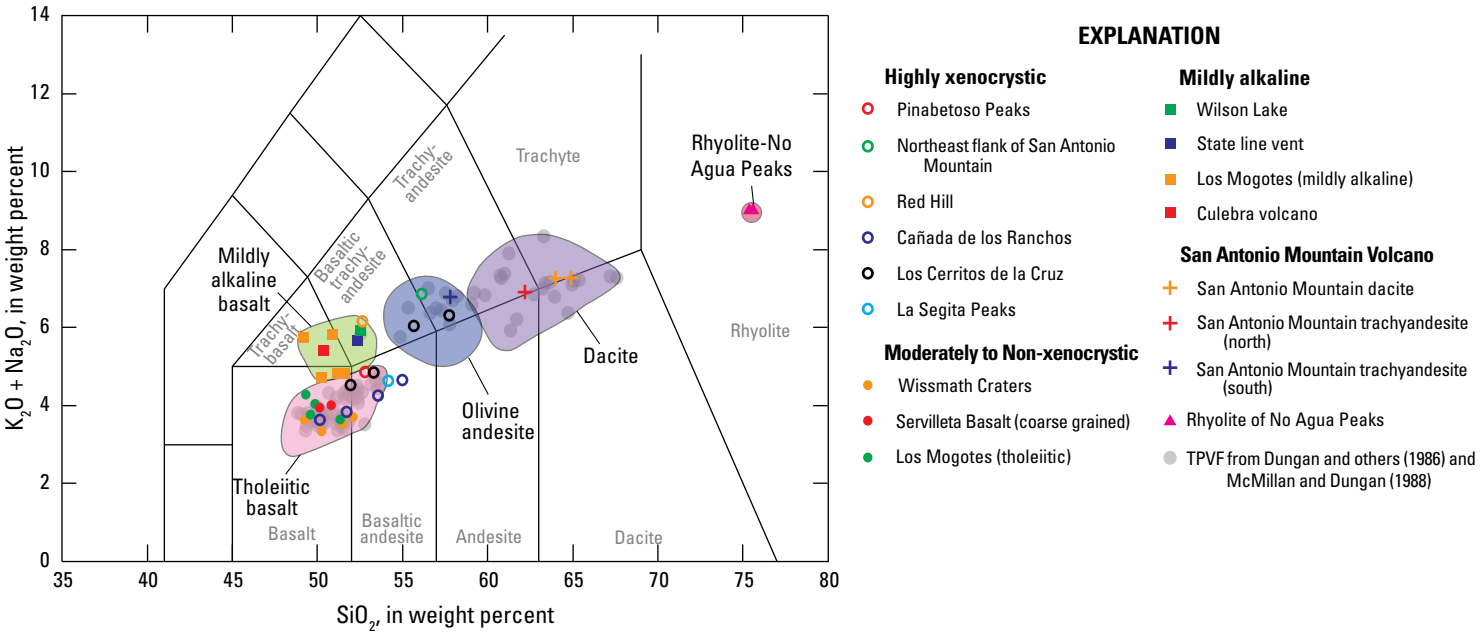

Figure 64. Geochemistry of Taos Plateau volcanic field rocks in the northwestern portion of the field. Alkali-silica classification diagram of Le Bas and others (1986). Data normalized to volatile-free based on the method of Middlemost (1989). TPVF, Taos Plateau volcanic field.

intrusive deposits are exposed at Timber and Brushy Mountains in the south and the San Luis Hills in the north (fig. 61). At the latitude of the San Luis Hills, the Manassa and Fairy Hills Fault Zones bound the horst (fig. 65). The Manassa Fault Zone bounds the horst to the west and northwest where it is concealed beneath younger alluvial basin-fill deposits. Although not exposed, down-to-west displacement is inferred based on the presence of aeromagnetic lineaments that coincide with a steeper gravity gradient (Drenth and others, 2013).

On the east side of the horst, and adjacent to the southern part of the San Luis Hills, the Fairy Hills Fault Zone (fig. 65) is concealed beneath Pliocene volcanic rocks, but cuts Conejos Formation deposits in the northern part of the San Luis Hills (fig. 61; Thompson and Machette, 1989). Although the Fairy Hills Fault Zone is poorly exposed, geologic relations and geophysical modeling support down-to-east displacement beginning in the late Oligocene (Thompson and Machette, 1989; Thompson and others, 2015). Gravity inversion modeling indicates a steep gravity gradient adjacent to the southern San Luis Hills, where the fault separates the San Luis horst from thick basin-fill deposits below the Costilla Plain, which suggests down-to-east displacement accommodating the sediment accumulation (Drenth and others, 2013; Ruleman and others, 2013). In the northern San Luis Hills, upper sequence Conejos Formation deposits on the east side of the fault are at equal or lower elevations than andesites at the base of the Conejos section at Flat Top, which suggests upper Conejos rocks have been eroded from the footwall. Hinsdale Formation lavas directly overlie subvolcanic intrusions west of the fault, which indicates erosion to deep levels. Hydrothermal alteration characterized by propylitic, argillic, and varying degrees of silicification is localized along the inferred trace of the Fairy Hills Fault Zone east of Piñon Hills and Flat Top. The area of alteration includes highly altered quartz monzonite in the east slopes of Piñon Hills, altered andesites at the King Turquoise Mine, and alunite veins north of the turquoise mine. An $^{40}Ar/^{39}Ar$ age of 30.33±0.87 Ma (sample RGR-151; table 3) on alunite provides a minimum age on fault formation.

Along the margin of the southeastern San Juan Mountains, stratigraphic and structural relations document inception of a north-trending graben, informally referred to as the Las Mesitas graben, situated between the southeastern San Juan Mountains and the San Luis Hills (fig. 65). The width of the graben is interpreted to extend from the Manassa Fault Zone on the east to the west side of the Los Mogotes composite shield. The northern structural boundary is poorly constrained but may coincide with an east-west oriented, down-to-north fault interpreted from seismic data (Brister and Gries, 1994) that is concealed below basin-fill deposits north of the Los Mogotes composite shield (fig. 60). The southern boundary of the graben may extend to Broke Off Mountain in the northern Tusas Mountains (fig. 60) where thick, age-equivalent basin-fill deposits are preserved below late Oligocene lava flows (fig. 61).

Structural and stratigraphic evidence that best constrains the inception of the Las Mesitas graben is observed along the western graben margin, west of Los Mogotes volcano. In this area, the Chiquito Peak Tuff forms an east-dipping monoclinal bend, and above the ignimbrite, Los Piños Formation thickens to the east. Hinsdale Formation basalt (26.4 Ma) overlies the Los Piños Formation and Chiquito Peak Tuff and is not deformed by the fold. A north-trending fault northwest of Los Mogotes (fig. 61), displaces Chiquito Peak Tuff, Carpenter Ridge Tuff, and

lower parts of the Los Piños Formation, but does not displace upper parts of the Los Piños or the overlying Hinsdale Formation basalt. These observations are consistent with subsidence of the graben, which started after emplacement of the Chiquito Peak Tuff (28.94 Ma) and ended prior to emplacement of the Hinsdale Formation basalt (26.40 Ma). Alternatively, the structural margin could have migrated basinward where evidence of continued subsidence after emplacement of the basalt is concealed. The subtle angular unconformity described by Lipman and Mehnert (1975) along the margin of the southeastern San Juan Mountains was formed by deformation associated with subsidence of the Las Mesitas graben.

Volcaniclastic deposits similar in age to Los Piños Formation in the Las Mesitas graben are preserved in the Culebra graben east of the San Luis horst (Wallace, 2004; Armstrong and others, 2013). The volcaniclastic sediments contain a basal conglomerate with intermediate-composition volcanic clasts that range in age from 37 to 29 Ma. These volcanic clasts have distinct mineral compositions characteristic of the Thirty-nine Mile volcanic locus of the SRMVF (Armstrong and others, 2013), which is located north and east of the San Luis Basin on the east side of the Sangre de Cristo Mountains. Stratigraphically below the volcaniclastic conglomerate is a suite of volcanic rocks that includes a 30.34±0.12 Ma welded ignimbrite (table 3) that provides a maximum age for the overlying deposits. High-angle normal faults observed throughout the Culebra graben generally crosscut the volcaniclastic deposits, indicating postdeposition displacement (Wallace, 2004). However, evidence of syndepositional faulting is preserved in the eastern part of the Culebra graben (Wallace, 2004), which may be related to a period of uplift in the Sangre de Cristo Mountains in the Oligocene (35–28 Ma) indicated by thermal history modelling of apatite fission track and apatite U-Th/He thermochronology (Kelley and others, 1992; Ricketts, 2014). These observations suggest subsidence of the Culebra graben may have been underway by 29 Ma, or earlier, approximately coeval with the Las Mesitas graben.

Structural Controls on Subsidence of the San Luis Basin

The generalized structure of the San Luis Basin is an east-tilted half graben bound by the west-dipping Sangre de Cristo Fault Zone at the base of the Sangre de Cristo Mountains. The Sangre de Cristo Fault Zone is divided into three segments: (1) the northern segment extends from Poncha Pass at the northern end of the San Luis Valley, 120 km north of Blanca Peak to Fort Garland, 10 km further south (fig. 60); (2) the central segment extends from Blanca Peak south to San Pedro Mesa (fig. 60); and (3) the southern segment extends from San Pedro Mesa to south of Taos, New Mexico (fig. 25), where it intersects with the Embudo Fault Zone (fig. 65). The southern and central segments of the Sangre de Cristo Fault Zone overlap in the San Pedro Mesa area and step eastward to the north (fig. 65). The east-dipping San Luis Fault Zone is situated between the central and southern segments of the Sangre de Cristo Fault Zone and bounds the east side of the San

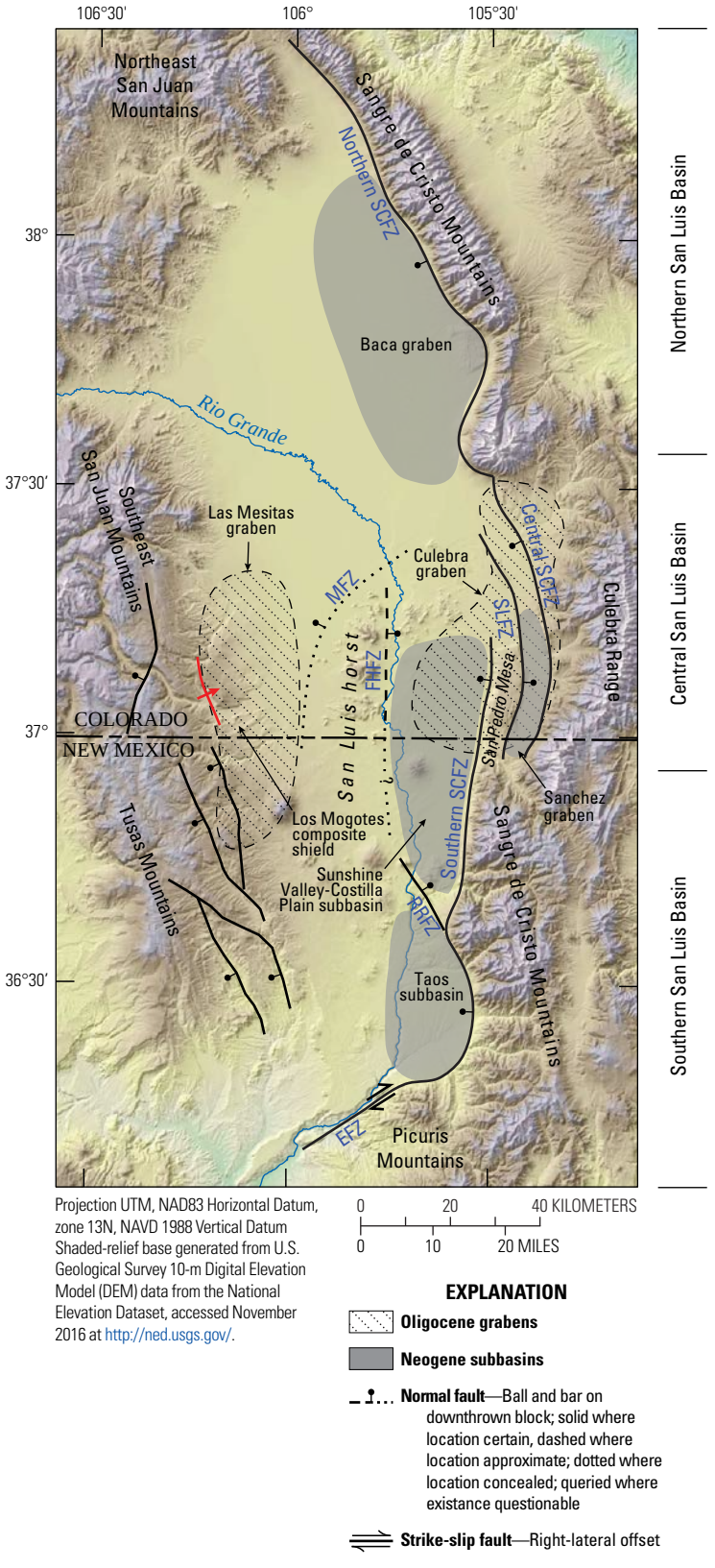

Figure 65. Hillshade map of the San Luis Basin showing major fault zones and structural depressions. Diagonal stippled pattern, Oligocene grabens; solid gray areas, Neogene subbasins. EFZ, Embudo Fault Zone; FHFZ, Fairy Hills Fault Zone; MFZ, Manassa Fault Zone; RRFZ, Red River Fault Zone; SCFZ, SLFZ, San Luis Fault Zone; Sangre de Cristo Fault Zone.

Pedro Mesa horst block. The San Luis Fault Zone is antithetic to the Sangre de Cristo Fault Zone, with down-to-east displacement, but is involved in the structurally complex transfer of strain between the southern and central segments of the Sangre de Cristo Fault Zone.

Miocene initiation of San Luis Basin subsidence is largely constrained by the uplift history of the Sangre de Cristo Mountains and associated initiation of the Sangre de Cristo Fault Zone based on apatite fission track and U-Th/He thermochronology. Thermochronologic results in the northern Sangre de Cristo Mountains, adjacent the northern segment of the Sangre de Cristo Fault Zone (fig. 65), suggests rapid exhumation and cooling beginning at ~20 Ma (Lindsey and others, 1986; Kelley and others, 1992). In the Culebra Range, adjacent to the central segment of the Sangre de Cristo Fault Zone (fig. 65), rapid cooling interpreted from thermal history modeling suggests isolated areas of uplift as old as ~35–28 Ma followed by rapid uplift from ~15 Ma to present (Ricketts, 2014). Initiation of slip on the southern segment of the Sangre de Cristo Fault Zone is not well constrained by thermochronologic data or offset stratigraphy but is inferred to be younger than the Questa caldera, which formed at 25.4 Ma.

Temporal and spatial variations in slip-rates since the inception of the Sangre de Cristo Fault Zone and the partitioning of strain between the main fault and intrabasin faults developed compartmentalized subbasins within the San Luis Basin (fig. 65). Subbasins adjacent to the Sangre de Cristo Fault Zone include the Sunshine Valley-Costilla Plain subbasin and the Sanchez graben, which are separated by the San Pedro Mesa horst. The Sunshine Valley-Costilla Plain subbasin is separated from the Taos subbasin to the south by a structural high approximately coincident with the Red River Fault Zone. Variations in slip rates associated with segments of the Sangre de Cristo Fault Zone and subbasin-bounding structures are well constrained as far back as the Pliocene as a result of the preservation of datable TPVF rocks. However, efforts to constrain slip rates prior to ~4 Ma are hampered by a fragmented stratigraphic record. Long-term slip rates (~4 million years [m.y.]) along the southern segment of the Sangre de Cristo Fault Zone, adjacent to San Pedro Mesa, range from 0.075–1 millimeter per year (mm/yr), but to the south, slip rates increase. Near the town of Costilla, displacement of Servilleta flows indicates slip rates of 0.14–0.16 mm/yr, and northwest of Taos, Menges (1990) reports slip rates of 0.12–0.23 mm/yr. Slip rates from late middle to late Pleistocene are lower by about a factor of two compared to long-term rates and range from 0.03 to 0.06 mm/yr throughout the southern segment of the Sangre de Cristo Fault Zone (Menges, 1987, 1990; Ruleman and Machette, 2007; Ruleman and others, 2013). In contrast, the slip rate on the central segment of the Sangre de Cristo Fault Zone since the late Pleistocene is 0.17 mm/yr (Ruleman and Machette, 2007), which is similar to long-term slip rates on the southern segment. Long-term slip rates along the central segment of the Sangre de Cristo Fault are not reported owing to the absence of TPVF volcanic deposits.

Intrabasin faults structurally linked to the Sangre de Cristo Fault Zone include the Red River, Fairy Hills, and Mesita Fault Zones (fig. 26). Variable displacement of lava flows along strands of the Red River Fault Zone indicates growth faulting coincident with Pliocene volcanism, and Bauer and others (2015) interpret displacement of colluvial deposits as old as middle Pleistocene where strands of the fault intersect the Rio Grande. The Sunshine Valley Fault Zone and the Mesita Fault displace middle to late Pleistocene alluvial deposits and the Mesita Hill cone (sample RGR-03; 1.13±0.03 Ma, table 3) by as much as 13 m. However, based on well data, the Mesita Fault displaces the 4 Ma Servilleta Basalt an estimated 42–53 m, indicating at least some slip between 4 Ma and the beginning of the Pleistocene (Machette and others, 2007).

Down-to-west faulting and intervening east-tilted dip-slopes on the passive western margin of the San Luis Basin are inferred to result from significant down-to-west offset along the Sangre de Cristo Fault Zone. New geologic mapping, reinterpretation of existing mapping, and geochronologic data for the west-central part of the basin presented here establish a maximum age of tilting along the western basin margin. Exposed stratigraphy in the Los Mogotes area and, to a lesser extent, the northern Tusas Mountains, records sediment and lava flow accumulation in a topographically low area into the early Miocene. Late Oligocene alkaline basalt (26.4 Ma) in the Los Mogotes area flowed from a source vent in the San Luis Hills into the Las Mesitas graben. South of the Los Mogotes area, tholeiitic basalt flowed from a source in the South Piñon Hills into the northern Tusas Mountains at 25.67 Ma (fig. 61), which indicates that the west-central portion of the San Luis Basin was topographically low relative to the San Luis Hills in the late Oligocene. Deposits that overlie the tholeiitic basalt in the northern Tusas Mountains are removed or concealed beneath Pliocene volcanic rocks. However, in the Los Mogotes area, stratigraphy above the late Oligocene alkaline basalt, in ascending order, includes 50–120 m of Los Piños Formation, early Miocene alkaline basalt (20.62 Ma), another interval of Los Piños Formation, and Pliocene volcanic rocks (fig. 61). The Miocene alkaline basalt is equivalent in age and composition to a lava flow proximal to a vent area near the rim of the Platoro caldera (fig. 61). Assuming that the alkaline basalt in the Los Mogotes area and along the Platoro caldera rim are correlative, the area of the Las Mesitas graben was a topographic low at the time of lava emplacement. Los Piños Formation preserved above the Miocene lava flows indicates the area persisted as a topographic low and that uplift of the western San Luis Basin margin did not commence until after emplacement of the Miocene lavas.

Quantitative estimates for relative vertical displacement between the San Luis Hills and the northern Tusas Mountains were calculated using late Oligocene tholeiitic basalt as a reflection of the paleotopographic surface. Hinsdale Formation tholeiitic lavas are inferred to have followed an existing paleochannel that sloped away from the San Luis Hills based on southwest-aligned outcrops in the northern Tusas Mountains that are more than 50 km from

the inferred source in the San Luis Hills. A primary emplacement dip for the lava flows inherited from the paleochannel slope was estimated based on fluvial systems draining other andesitic volcanic highlands. Paleochannel slopes of 2 percent (0–25 km from source) and 0.75 percent (25–50 km from source) result in an estimated 1.5-km displacement relative to the San Luis Hills over the length of the tholeiitic lavas. Additional stratigraphic offsets west of the tholeiitic lavas result in a total displacement of ~2 km. This estimate is comparable to displacement of ~2 km along the Sangre de Cristo Fault Zone in the Questa area (Ruleman and others, 2013), but is less than the estimated displacement of 5 km near the Colorado-New Mexico State line (Wallace, 2004) and as much as 9.2 km along the fault zone north of Blanca Peak (Kluth and Schaftenaar, 1994).

Evidence for deformation following emplacement of Pliocene lavas along the western margin of the San Luis Basin includes minor eastward tilting and displacement along north- to northwest-trending faults. Identification of faults in the northwestern portion of the TPVF is hindered by limited dissection, partial concealment of lavas by unconsolidated sheetwash and eolian deposits, and generally small offsets of 10 m or less. An exception is the series of north-trending faults that displace flows on the west side of the Los Mogotes composite shield. The faults generally display down-to-west offset with displacement of as much as 30 m, although at least one antithetic down-to-east fault is present (Lipman, 1975b). In the San Antonio Mountain area, the few confirmed faults displace Pliocene lavas 10 m or less with down-to-east and -west offset (Thompson and Lipman, 1994a,b). Similarly oriented faults are exposed west of the TPVF, but offset stratigraphy on these faults only indicate displacement after emplacement of early Miocene lavas west of Los Mogotes and Oligocene lavas in the northern Tusas Mountains (fig. 61).

Alignment of Pliocene vents in the San Antonio Mountain area suggests fault control on the location of some volcanic edifices, although no faults are observed directly displacing the vents. West of San Antonio Mountain, for example, vents with variable eruption ages and compositions are aligned northwest, and east of San Antonio Mountain, cinder cones are aligned north-south (fig. 61). Variable eruption ages and compositions indicate the aligned vents are not fed by a common fissure at depth, but their alignment is subparallel to faults west of the Pliocene volcanic rocks, which suggests prolonged control on placement of eruptive centers by fault or fracture systems.

Eastward tilting of Pliocene lava flows (~2–5° dips) in the northwestern portion of the TPVF is consistent with postemplacement tilting along the western margin of the San Luis Basin. The amount of tilting following emplacement of Pliocene lavas is not well constrained, however, as the flows likely inherited a primary emplacement dip from an east-sloping paleosurface. Northwest of San Antonio Mountain, for example, flows underlie linear to sinuous, east-tilted surfaces. Eruptive vents are preserved at the western extent of the lavas (fig. 61), which suggest the flows reflect inverted topography of lava-filled paleovalleys that flowed northeast off the uplifted western basin margin. Similarly, outflow distribution on the Los Mogotes composite shield is primarily east of vent areas, with only minor outflow to the west, which suggests paleotopography impeded westward flow.

Day 3—Route Through the San Luis Hills

The Day 3 route begins in the town of Questa, New Mexico, and heads north along the east side of the San Luis Basin. After heading west through the San Luis Hills, we turn to the south along the west side of the basin and northwestern part of the TPVF before heading back to Taos. Gorges incised by the Red River and Rio Grande in the Wild Rivers Recreation Area provide excellent exposures of Oligocene through Pliocene volcanic and volcaniclastic deposits and display their interaction with cross-cutting and coeval structures. The last stop in the Wild Rivers Area is an overview of the Questa caldera with a rare cross-sectional view of a caldera. Leaving the Wild Rivers Recreation Area, the trip heads north and explores Pliocene and younger basin-fill deposits but also allows for discussion of complex strain partitioning along segments of the Sangre de Cristo Fault Zone. The trip passes through late Oligocene to Miocene deposits heading west through the San Luis Hills and south along the west side of the basin, which allows for discussion of the extensional tectonism that preceded the San Luis Basin and how these factors relate to opposing views about the onset of regional extension versus onset of continental rifting. An optional route in the San Antonio Mountain area (optional route 3A) covers the large compositional and petrographic variation observed along the west side of the basin. An optional route in the Los Mogotes area (optional route 3B) presents additional details related to pre-San Luis Basin structures.

Mileage

0.0 *Begin mileage (0 miles [mi]) in Questa, New Mexico, at the intersection of State Road (NM) 522 and NM 38 heading north.*

2.6 *Intersection of NM 522 and Cerro Road (NM 378). Turn left and head west toward the Rio Grande del Norte National Monument entrance.* Guadalupe Mountain is prominent in the foreground and lies just west of the Monument boundary. Guadalupe Mountain is characterized by two prominent topographic edifices informally referred to as North and South. Deposits of North Guadalupe Mountain exhibit reverse magnetic polarity and those of South Guadalupe Mountain have normal polarity based on the interpretation of aeromagnetic data (Grauch and others, 2015). North and South Guadalupe Mountain lavas and near vent pyroclastic deposits are trachyandesite to dacite in composition (62–65 weight percent SiO_2; table 1) although the northern edifice is typically slightly less evolved.

4.8 Glassy lava flows of North Guadalupe Mountain trachyandesite containing sparse phenocrysts of plagioclase, pyroxene, and occasional olivine xenocrysts are exposed on both sides of the road.

5.0 **Rio Grande del Norte National Monument** (36°45.98' N., 105°41.12' W.; 7,530 ft, 2,295 m elevation). *The following four stops (3-1 through 3-4) are within the Wild Rivers Recreation Area in the Rio Grande del Norte National Monument. The use of rock hammers and sample collection is prohibited within the Monument.*

The small hill on north side of road is underlain by trachyandesite of North Guadalupe Mountain. This vantage point provides an excellent view of the northeastern Taos Plateau, Sangre de Cristo Mountains, southern San Luis Hills and southeastern San Juan Mountains. Counterclockwise relative to due north (12:00) are (1) the Sangre de Cristo Mountains, which expose post-Questa caldera intrusions emplaced into Proterozoic crystalline basement overlain by north-dipping Amalia Tuff outflow deposits at 2:00; (2) the flat lying Servilleta Basalt of San Pedro Mesa uplifted along the footwall of the Sangre de Cristo Fault (Thompson and others, 2015) at 1:00; (3) the Proterozoic Blanca Peak massif, the fourth highest summit in the Rocky Mountains of Colorado (14,351 ft; 4,374 m) at 12:30; (4) Ute Mountain (9,810 ft; 2,990 m), a 3.95-Ma trachyandesite volcano of the TPVF (sample RGR-79; table 3) at 12:00; (5) the San Luis Hills (9,193 ft; 2,802 m), flat-topped mesas of Hinsdale Formation basalt (26.96–25.67 Ma; table 3) that overlie Conejos Formation andesite of the southern Rocky Mountain volcanic field (31–28 Ma; table 3; Thompson and others, 2015) at 11:00; (6) San Antonio Mountain (10,804 ft; 3,293 m), the 3.12-Ma trachydacite of the TPVF (sample 67L-30A; table 3) at 10:00; (7) Cerro de la Olla (9,465 ft; 2,885 m), a 4.33-Ma olivine andesite of the TPVF (sample RGR-283; table 1) at 9:00; (8) Cerro Chiflo (8,976 ft; 2,736 m) a 10.99–9.64-Ma dacite (sample RGR-143; table 3) at 8:00; and (9) Cerro Montoso (8,655 ft; 2,638 m), a 4.95-Ma olivine andesite of the TPVF (sample RGR-286; tables 1 and 2) at 7:00. The flat-lying surfaces of the Taos Plateau are largely underlain by Servilleta Basalt and variably preserved Pleistocene alluvial fan, fluvial, colluvial, and eolian deposits.

Return to vehicles and proceed west on Cerro Road.

8.1 *Sheep Crossing trailhead.* Views of Miocene Cerro Chiflo trachydacite are afforded by walking to the west side of parking area. Note the erosional unconformity between the trachyandesite flows and the overlying Pliocene Servilleta Basalt to the north (Thompson and others, 2014a).

8.9 *Cerro Chiflo trailhead (see Stop 3-4).*

10.7 *Bear Crossing trailhead (see Stop 3-3).*

12.3 *Wild Rivers Recreation Area pay station (see Stop 3-2). This is a National Park Service pay area. It is recommended to pay the daily Monument fee at the self-serve kiosk before proceeding to La Junta campground, as this is a fee area. Please observe all posted regulations.*

13.8 *Intersection of NM 378 with NM 378 loop. Turn right and head south to La Junta campground.*

15.9 *Intersection with road to La Junta campground. Turn right and head to campground parking area.*

16.2 **Stop 3-1. La Junta campground** (36°39.44' N., 105°41.12' W.; 7,464 ft, 2,275 m elevation) *Park vehicles in the designated parking area and proceed south along the path ~650 ft (~200 m) to the scenic overlook.*

The La Junta viewpoint overlooks the confluence of the Rio Grande and Red River. The Red River is a major tributary of the Rio Grande, with headwaters in the upper reaches of the Sangre de Cristo Mountains to the east. The confluence is ~5.5 km downstream from the Red River State Fish Hatchery (Stop 2-7). Both drainage systems have incised 250-m-deep canyons through volcanic deposits of the Taos Plateau volcanic field and intercalated alluvial fan deposits of the paleo-Red River drainage system. Exposed gorge stratigraphy at this locality is relatively undisturbed by extensional faulting and provides important spatial and temporal constraints on the Pliocene eruptive history of multiple volcanic edifices. Stratigraphic relations discussed here build upon those introduced at the fish hatchery and are based on geologic mapping depicted in figure 66.

Exposures of volcanic flows in the west wall of the Rio Grande gorge include, from base to top, a lower package of Servilleta Basalt unconformably overlain by prominent cliff-forming lavas of the UCEM (unnamed cerrito east of Montoso) volcano, locally overlain by an upper package of Servilleta Basalt visible at the northern and southern margins of the UCEM flows (figs. 67, 68). The contact between the lower Servilleta lavas and the UCEM flow is marked by a prominent sedimentary interbed dominated by fine-grained, reworked eolian deposits that locally exhibit baked and oxidized textures where in contact with the overlying UCEM flow. The base of the lower Servilleta sequence is not exposed but is presumed to occur near the upper reaches of prominent colluvial aprons at the base of the cliffs. East of the active colluvium are incised Toreva landslide blocks that locally preserve river terraces of inferred late Pleistocene age.

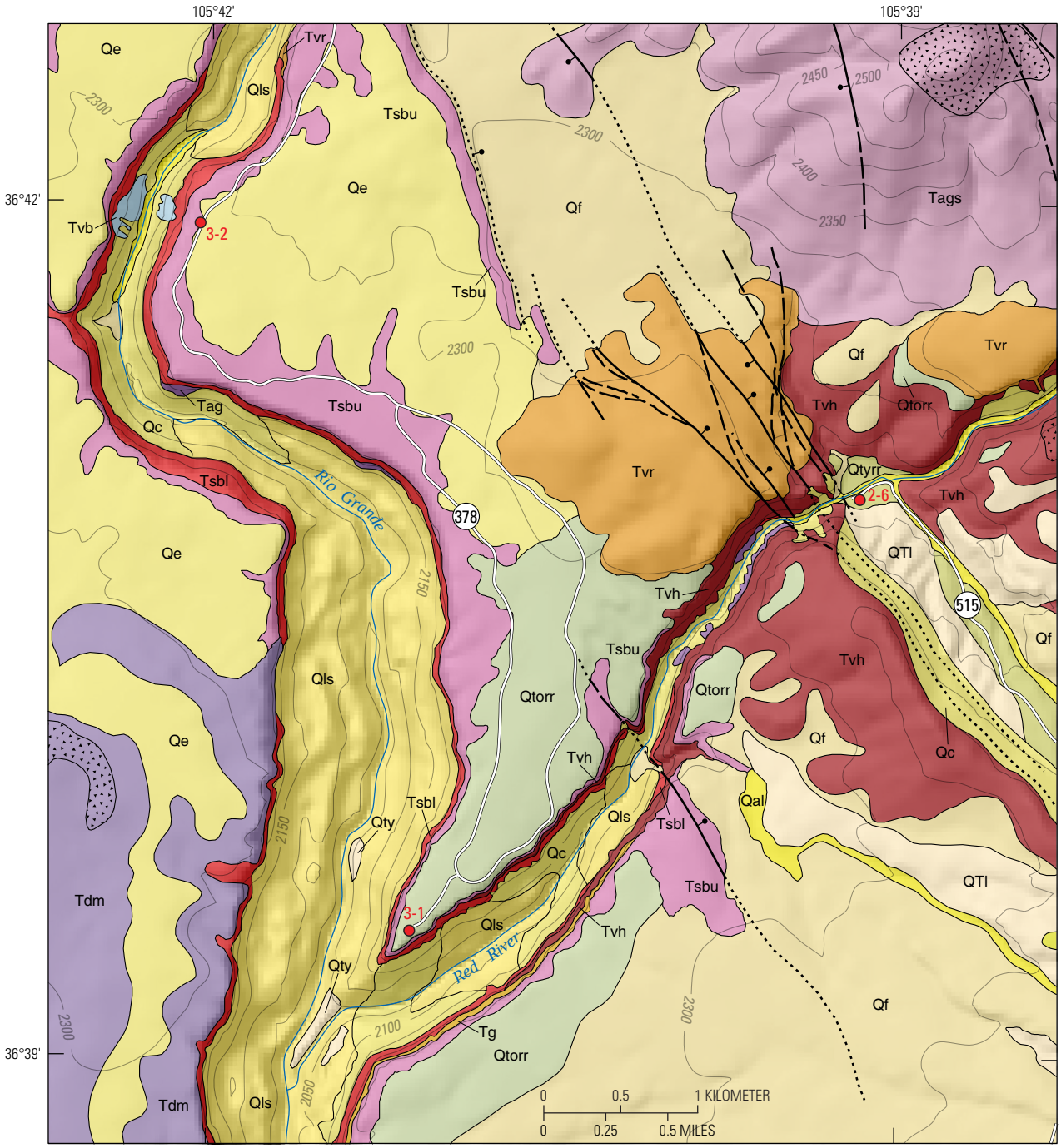

Base Projection UTM NAD83, Zone 13N, 1:40,000, Contour interval 50 m

Geology by Bauer and others, 2015 and new mapping by R.A. Thompson and K.J. Turner 2010–14

EXPLANATION

- Qal — Alluvium (Holocene)
- Qty — Young stream terrace deposits (Holocene to latest Pleistocene)
- Qe — Eolian deposits (Holocene to late Pleistocene)
- Qls — Landslide deposits (Holocene to late Pleistocene)
- Qf — Fan deposits (Holocene to middle Pleistocene)
- Qc — Colluvium (Holocene to middle Pleistocene)
- Qtyrr — Young Red River terrace deposits (Holocene to middle Pleistocene)
- Qtorr — Old Red River terrace deposites (late to middle Pleistocene)
- QTl — Lama formation (early Pleistocene to Pliocene)
- Tsbu — Servilleta Basalt, upper sequence (Pliocene)
- Tg — Older alluvial gravels (Pliocene)
- Tvr — Dacite of Red River volcanic complex (Pliocene)
- Tvh — Olivine andesite of Hatchery volcano (Pliocene)
- Tsbl — Servilleta Basalt, lower sequence (Pliocene)
- Tags — Dacitic lavas of south Guadalupe Mountain (Pliocene)
- Tdm — Unnamed cerrito east of Montoso (UCEM) trachyandesite (Pliocene)
- Tag — Dacitic lavas of Guadalupe Mountain, undivided (Pliocene)
- Tvb — Undivided volcanic rocks of the Latir volcanic locus (Miocene to Oligocene)
- Near-vent pyroclastic deposits
- Fault—Ball and bar on downthrown block; dashed where location approximately located; dotted where location concealed
- 2-6 — Field-trip stop

Figure 66. Geologic map of the southwestern part of the Wild Rivers Recreation Area.

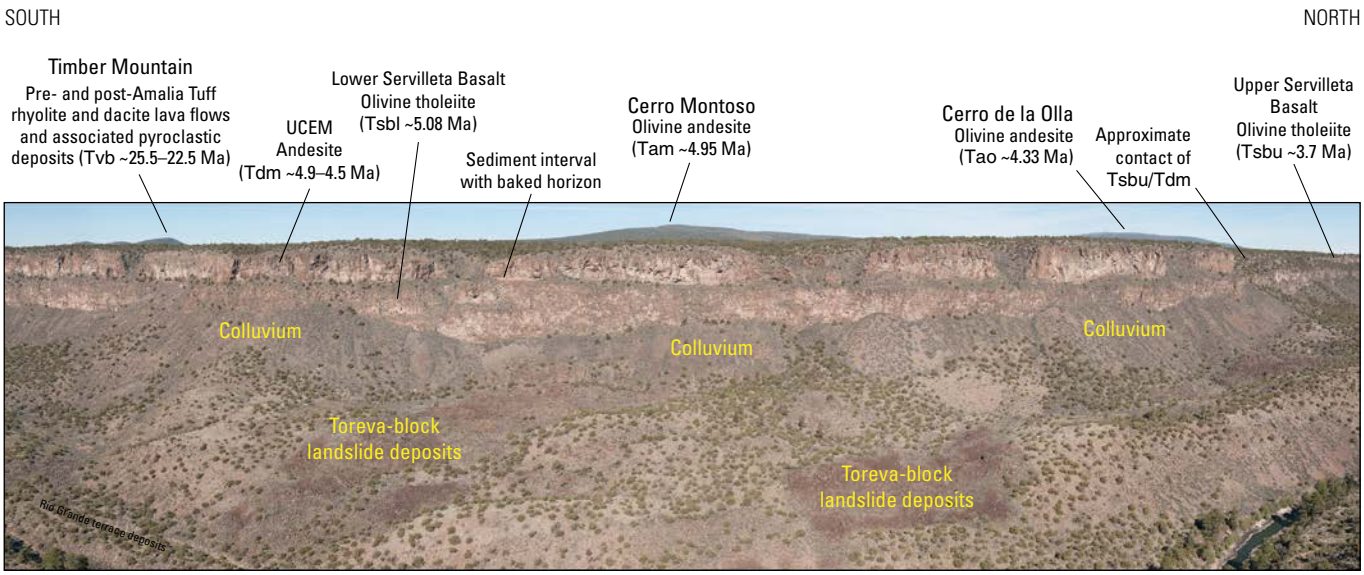

Figure 67. The view west from La Junta overlook across the Rio Grande gorge toward Cerro Montoso illustrates the stratigraphic relation between the lower sequence of Servilleta Basalt and intervening local deposits of the unnamed cerrito east of Montoso (UCEM) andesite flows. Toreva-block landslide deposits form prominent benches in the lower 90 meters of the gorge, and active colluvium obscures the base of the lower sequence of Servilleta Basalt. The overlook is underlain by the upper sequence flows of Servilleta Basalt (~3.7 million years ago [Ma]) overlain by a thin mantle of fluvial pebble to cobble gravels related to preincision Red River deposition and reworking of fan colluvium from the Sangre de Cristo Mountains. Map unit symbols refer to geologic map figure 66. Photograph by Dave Tewksbury, Hamilton College, 2014.

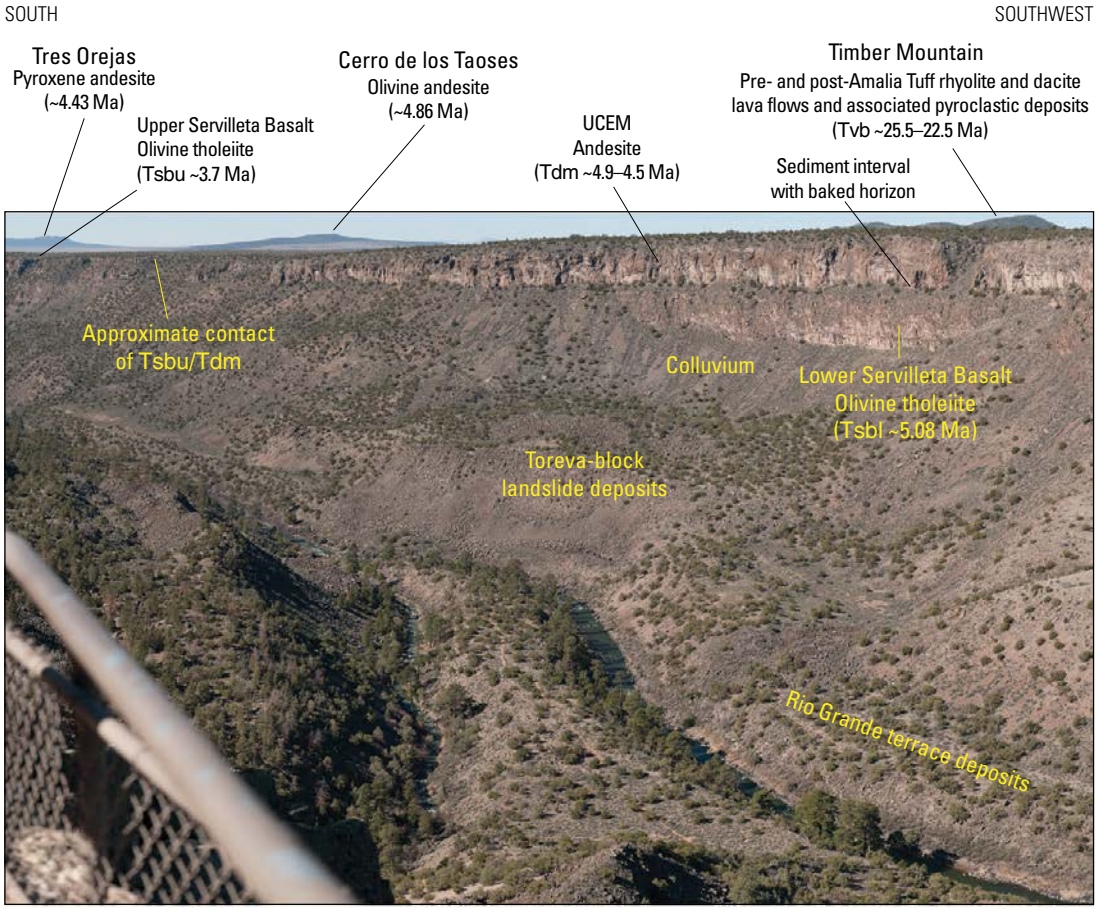

Figure 68. View southwest along Rio Grande gorge from La Junta overlook. The lower sequence flows of Servilleta Basalt disappear beneath active colluvium to the south but are observed at the far south end of photograph. Unnamed cerrito east of Montoso (UCEM) andesite flows thin to the south and pinch out beneath an onlapping sequence of upper Servilleta Basalt flows. Late Pleistocene river terrace deposits are locally preserved on incised Toreva blocks, visible in lower right foreground (fig. 66). The confluence of the Red River and Rio Grande is visible in the left central part of photograph. Map unit symbols refer to geologic map figure 66. Photograph by Dave Tewksbury, Hamilton College, 2014. Ma, million years ago.

Servilleta flows of the lower package are stratigraphically equivalent to the lower Servilleta flows exposed at the High Bridge (Stop 2-4) ~20 km to the south. A sample from near the base of the lower Servilleta section at this locality yields a whole-rock $^{40}Ar/^{39}Ar$ age of 5.08±0.09 Ma (sample RGR-04, table 3), one of the oldest ages reported for Servilleta Basalt. The ~20-m-thick section exposed in outcrop visible from here thins dramatically to the east to less than 3 m in exposures of the Red River gorge and terminates against down-to-east strands of the Red River Fault near the Red River State Fish Hatchery (Stop 2-7). Servilleta vents and near-vent deposits are not preserved in either the Rio Grande or Red River gorges. However, on the basis of stratigraphically younger vents mapped west of the Rio Grande, sources for the lower sequence of flows are inferred to have been largely to the west, where early Servilleta flows coursed across an eroded closed basin surface and lapped against alluvial fans prograding basinward in response to uplift of the Sangre de Cristo Mountains. Erosional remnants of late Oligocene and Miocene volcanic deposits preserved in elevated structural blocks to the west provided local topographic barriers to westward flowing Servilleta flows as did early erupted Pliocene andesite and dacite of Guadalupe Mountain. Preserved lava flows exposed here dip shallowly eastward, likely reflecting both tilting of the headwall block along the Sangre de Cristo Fault and shallowly dipping primary depositional surfaces. Visible in the distance beyond the west wall of the Rio Grande, from south to north, are late Oligocene volcanic rocks of Timber Mountain and the Pliocene olivine andesite eruptive centers of Cerro Montoso and Cerro de la Olla.

Deposits of the two mapped UCEM centers that overlie the lower Servilleta flows (fig. 66) range in age from 4.90±0.09 to 4.47±0.13 Ma (samples RGR-127 and RGR-142, respectively; table 3), reflecting a nearly 430 ka difference in age between southwestern and northeastern eruptive centers. Both centers erupted small volume lava flows, less than 0.05 km^3, and near-vent pyroclastic deposits and likely represent very short-lived events. UCEM lava flows range from 59.6 to 61.1 weight percent SiO_2 and 3.5–5.8 weight percent Na_2O+K_2O (samples RGR-127 and RGR-312; table 2) and are andesites on a TAS classification diagram (fig. 63*A*). Our sampling reflects a much narrower range of composition than previously reported by Dungan and others (1989b). UCEM flows are typically aphyric, containing rare quartz xenocrysts and sparse fine-grained crustal xenoliths. McMillan and Dungan (1988) interpreted these glassy rocks to reflect surprisingly efficient mixing of Servilleta magma and melted argillaceous metaquartzite while recognizing, but not accounting for, the concerns about the physical limitations that magma rheologies and solidi place on this model. Regardless, the geochemical model does account for the relatively incompatible-element depleted nature of these deposits (with the exception of rubidium and thorium) relative to other andesites of the Taos Plateau.

Upper Servilleta lavas locally overlie UCEM flows, just visible to the far north and south from this vantage point; they also form the upper sequence of lavas at the La Junta overlook. These lava flows are generally thin and discontinuous, and form flow packages less than half the thickness of the massive lower Servilleta sequence. The base of the upper Servilleta section at the La Junta overlook yields a whole-rock $^{40}Ar/^{39}Ar$ age of 3.66±0.11 Ma (sample RGR-05; table 3). Compositionally, Servilleta flows from the upper section are less alkalic than those from the lower section but otherwise are compositionally and petrographically similar. These flows are easily observed by walking the La Junta trail; the trailhead is located ~66 yd (60 m) east of the overlook. Well-exposed pahoehoe flow textures, vesicle segregations, flow terminations, as well as tops and bottoms of lava flows are easily observed from the trail.

The absence of UCEM flows is immediately evident in the view to the south across the Red River gorge. Between the lower and upper Servilleta sequences east of the Rio Grande—stratigraphically in place of UCEM flows—are fan deposits composed dominantly of alluvial gravels. These deposits contain imbricated, dominantly Proterozoic clasts derived from the Sangre de Cristo Mountains to the east that reflect deposition from a paleo-Red River drainage system prior to eruption of the uppermost Servilleta flows. These alluvial fan deposits would have impeded deposition of lava flows further east than the current location of the Rio Grande. These deposits are visible between the upper and lower Servilleta sequences along the trail. Note the repetition of lower Servilleta flows along landslide debris exposed in the trail. The lower part of the trail continues to river level through landslide deposits and colluvium.

The entire Pliocene volcanic sequence is underlain by, and locally intercalated with, alluvial fan deposits associated with paleo-Red River discharge into the closed Pliocene San Luis Basin. These deposits are not exposed along the trail but are locally exposed in cuts near river level in the Red River gorge. The lower reaches of both river gorges in this area are covered in colluvium and Toreva-block deposits. Limited exposures reveal coarse pebble to cobble conglomerates inferred to reflect fan deposits of the Pliocene Red River system. On the basis of $^{3}He/^{4}He$ dating of incised Servilleta flows within both the Rio Grande and Red River drainages (Ruleman and others, 2016), incision of both drainages was a middle Pleistocene event, related to overflow of Pleistocene Lake Alamosa. This contrasts with previous field guide interpretations of the diachronous evolution of the Rio

Grande and Red River drainage systems (Dungan and others, 1984, 1989; Repasch and others, 2017).

Return to vehicles and proceed to NM 378 loop.

16.5 *Turn left onto NM 378 loop and head to the intersection with NM 378.*

18.6 *Turn left onto NM 378 and head north to the pay station.*

20.1 **Stop 3-2. Pay station** (36°41.92' N., 105°42.05' W.; 7,530 ft, 2,295 m elevation) *Park vehicles in the pay station parking lot. Walk ~210 ft (~65 m) west to the gorge rim. Please note the incipient landslide blocks with potentially dangerous fractures at the gorge rim. Carefully proceed across the fractures at the narrowest point that requires no more than a wide step to safely reach the gorge rim for the best view of gorge stratigraphy. Do not attempt this if you are physically impaired or are fearful of heights.*

The west wall of the Rio Grande gorge at the pay station overlook preserves a 17 m.y. angular unconformity between postcaldera andesitic to dacitic volcanic rocks of the Questa-Latir system and Pliocene volcanic rocks of the Taos Plateau volcanic field (fig. 69). The prominent domiform outcrop that extends nearly 140 m above river level is composed of locally faulted intermediate composition pyroclastic deposits and flow deposits interpreted as an eastern extension of the Oligocene to Miocene volcanic rocks preserved at Brushy Mountain, the low, buff-colored hills visible above the gorge rim in the distant foreground. These Oligocene to Miocene deposits are unconformably overlain by (in stratigraphic order) (1) Servilleta Basalt of the lower sequence; (2) an intervening sequence of dominantly buff colored, reworked eolian sedimentary

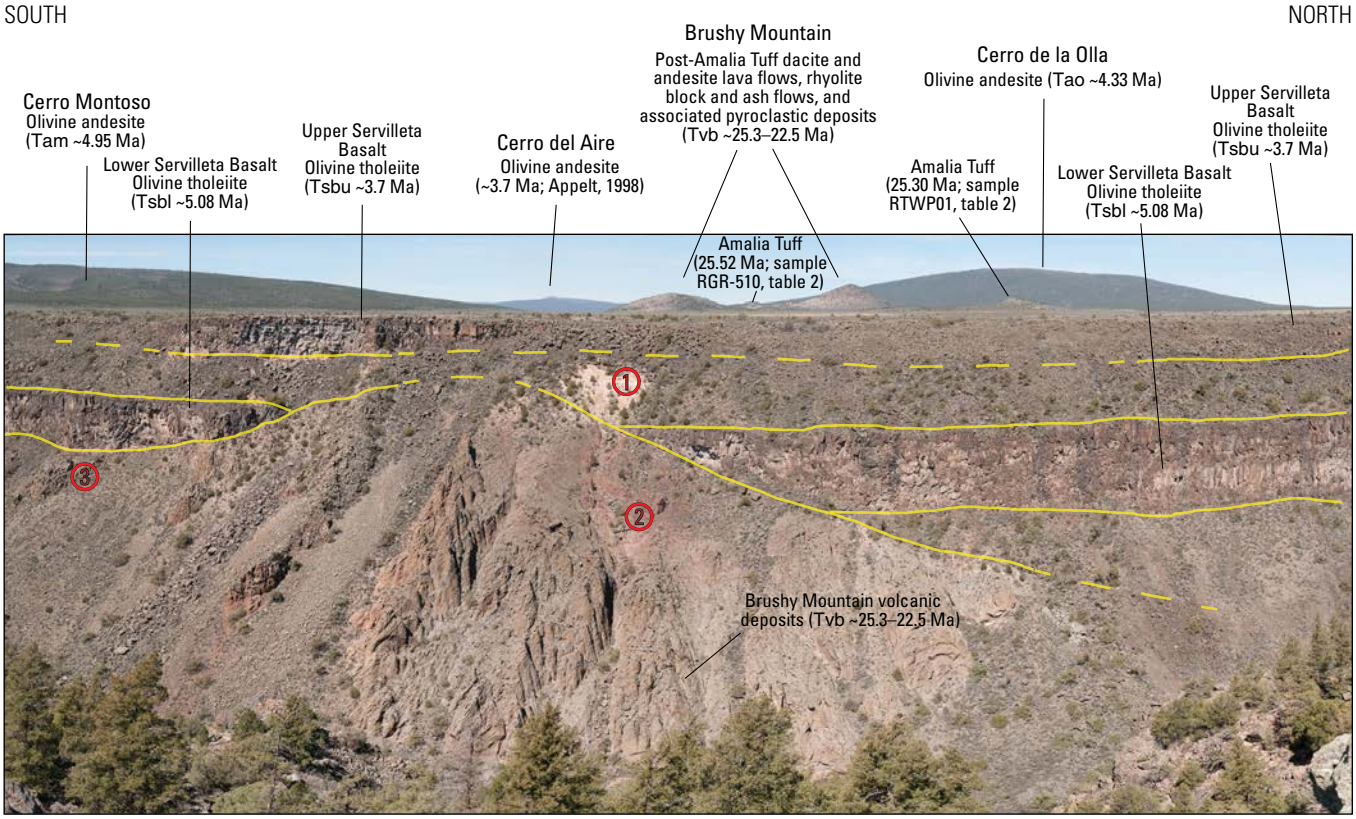

Figure 69. View west from pay station overlook. Locally faulted and tilted Miocene to Oligocene andesitic pyroclastic deposits are unconformably overlain by lower and upper sequences of Servilleta Basalt. Sedimentary interbeds separate the lower and upper units that occupy the same stratigraphic position as the unnamed cerrito east of Montoso (UCEM) flows viewed from Stop 3-1. The steeply dipping erosional flanks of the andesite exposures illustrate the influence of paleotopography on the distribution of Pliocene volcanic and sedimentary deposits. Pliocene sedimentary deposits between Servilleta flow sequences are dominantly eolian silty sands, sheetwash, and minor fluvial deposits related to closed basin sedimentation. Numbers indicate (1) light-colored deposits that are reworked ash, likely derived from Brushy Mountain in the distance and (or) No Agua Peaks rhyolite domes (4.1–3.9 million years ago [Ma]) 22 kilometers west of this locality; (2) steeply bedded Miocene to Oligocene volcanic deposits (25.3 to ~22.5 Ma) that exhibit local block rotation along high-angle normal faults demonstrated by strong discordance in bedding between deposits on the west and east sides of the Rio Grande; and (3) pyroclastic deposits that are overlain by less steeply dipping dacitic lava flows (hbld+bio+plag phenocrysts) similar to preserved dacites of Brushy Mountain. Map unit symbols refer to geologic map figures 66 and 70. Photograph by Dave Tewksbury, Hamilton College, 2014.

deposits; and (3) upper sequence Servilleta flows that underlie the plateau surface. The Servilleta stratigraphy can be traced from the La Junta overlook northward and is interpreted to be comparable in age to the $^{40}Ar/^{39}Ar$ ages discussed at Stop 3-1; 5.08 Ma and 3.66 Ma for the lower and upper Servilleta sequences, respectively.

The Oligocene to Miocene volcanic sequence visible beneath the cliffs of the western gorge rim is discontinuous across the Rio Grande gorge. On the east side of the gorge, andesitic pyroclastic deposits are displaced to lower topographic levels along inferred faults and biotite- and hornblende-bearing dacite lava flows are at the top of the section. These deposits are petrologically and mineralogically similar to the intermediate composition rocks of Brushy Mountain (fig. 61) and isolated small deposits of similar rocks 1.5 km to the northeast of the stop location. Based on the correlation of deposits between this locality and Brushy Mountain, it is likely that these eroded remnants are cut by pre-Pliocene extensional normal faults that progressively expose older parts of the Oligocene volcanic section westward. The oldest deposit, the Amalia Tuff (25.52±0.07 Ma; sample RGR-510, table 2), is exposed at the base of the section at Brushy Mountain. This northwest-trending series of exposures is the surface expression of a geophysical basement high evident in regional gravity modeling of the basin (fig. 25) and marks the southwestern basement boundary of the Sunshine Valley-Costilla Plain subbasin superposed on the broader San Luis Basin. The subbasin reaches a maximum depth of ~1 km beneath Guadalupe Mountain (Bauer and others, 2015).

The light tan to white deposits near the apex of the Oligocene andesitic rocks are reworked rhyolitic ash deposits likely derived from a combination of local sources including Oligocene to Miocene deposits at Brushy Mountain and Pliocene rhyolite (3.88±0.06 Ma and 4.1±0.03 Ma) of the No Agua Peaks domes (Dickens, 2007; table 3) ~22 km to the west. Mixed, reworked ash deposits observed in fan deposits along the Sangre de Cristo Mountains commonly have mixed Oligocene to Pliocene sanidine contributions, complicating correlations based on conventional geochemical tephrachronology.

Return to vehicles and head north on NM 378.

21.5 Top of the Red River Fault topographic scarp.

23.0 **Stop 3-3. Bear Crossing trailhead** (36°43.09' N., 105°41.42' W.; 7,464 ft, 2,275 m elevation) *Park vehicles in the parking pullout and proceed on foot to the gorge rim near the trailhead.*

The west wall of the Rio Grande gorge at Bear Crossing exposes en echelon strands of the northwest-trending Red River Fault Zone (fig. 70), which here displaces the entire exposed Pliocene volcanic section ~25 m to the northeast. From here, strands of the fault project northward and bifurcate likely juxtaposed dacite lava flows of the Cerro Chiflo dome complex in the saddles between prominent peaks observed in the distance. The Red River Fault exposed at this stop is interpreted as the southern structural margin of the Pliocene Sunshine Valley-Costilla Plain subbasin. This structural boundary has migrated ~1.5 km north of the basement structural high observed at Stop 3-2 and suggests extensional deformation associated with the preserved basement high likely pre-dates Pliocene faulting of the Red River system. North of Cerro Chiflo these north-trending, down-to-east faults (Thompson and others, 2014a,b) form the Gorge Fault Zone, which is the western margin of the Pliocene Sunshine Valley-Costilla Plain subbasin. This subbasin is bordered on the east by the southern segment of the Sangre de Cristo Fault Zone along the range front (Ruleman and others, 2013).

The exposed section at Bear Crossing preserves the lower and upper sequences of Servilleta Basalt observed at the previous two stops but also includes local intervening Red River trachyandesite flows (fig. 71). Red River flows at this locality are stratigraphically equivalent—and compositionally similar to—lava flows capping the fish hatchery section of Stop 2-7, 3.5 km to the southeast, but may have been erupted from local centers. Small volume, dike-fed flows exposed in the Red River gorge east of the state fish hatchery demonstrate the localization of vent areas for similar-composition deposits. Feeder dikes are observed in the east wall of the Rio Grande gorge ~0.6 km south of this location and appear to be the local source for at least one of the observed flows in the Red River sequence of flows. Similar vent areas likely exist to the east, buried beneath younger Servilleta flows.

Red River trachyandesite flows are typically discontinuous and lobate with radial fractures perpendicular to the dominant flow axis. These trachyandesites are characterized by containing as much as 5–10 percent augite and bronzite phenocrysts with common olivine xenocrysts in a fine grained to glassy groundmass of plagioclase, glass, pyroxenes, and titanomagnetite and typically do not exceed 61–62 weight percent SiO_2 and 7.3 weight percent Na_2O+K_2O (McMillan and Dungan, 1986).

Return to the vehicles and head north on NM 38 to the Cerro Chiflo trailhead.

24.8 **Stop 3-4. Cerro Chiflo trailhead** (36°44.48' N., 105°40.81' W.; 7,464 ft, 2,275 m elevation) *Park the vehicles and proceed to the sheltered picnic table at the first switchback along the Cerro Chiflo trail.*

Cerro Chiflo, the dominant landform exposed in the western Rio Grande gorge wall, is a strongly foliated

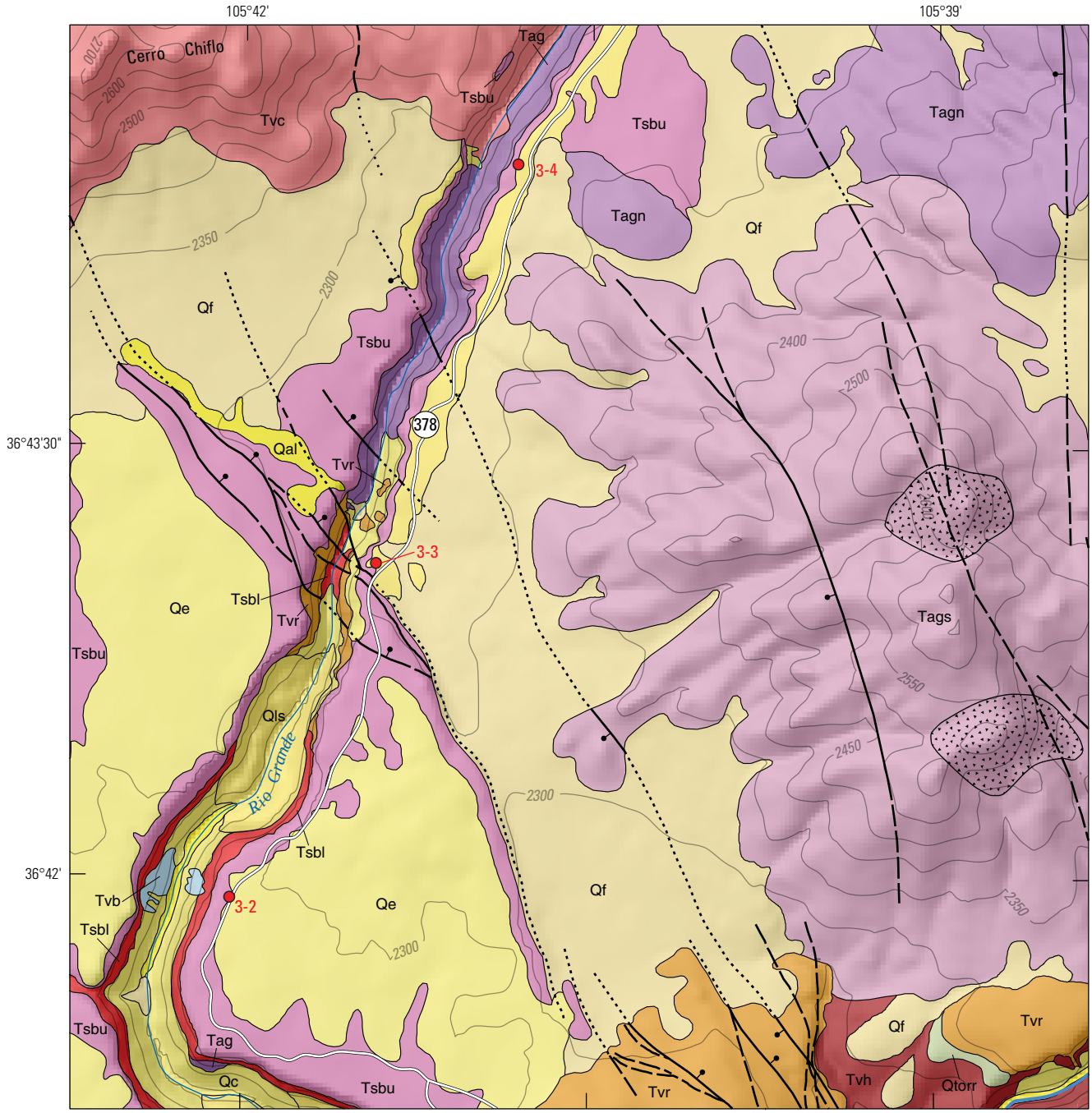

EXPLANATION

- Qal — **Alluvium (Holocene)**
- Qe — **Eolian deposits (Holocene to late Pleistocene)**
- Qf — **Fan deposits (Holocene to middle Pleistocene)**
- Qls — **Landslide deposits (Holocene to late Pleistocene)**
- Qc — **Colluvium (Holocene to middle Pleistocene)**
- Qtorr — **Old Red River terrace deposites (late to middle Pleistocene)**
- Qao3 — **Older alluvium (middle(?) Pleistocene)**
- Tsbu — **Servilleta Basalt, upper sequence (Pliocene)**
- Tvr — **Dacite of Red River volcanic complex (Pliocene)**
- Tvh — **Olivine andesite of Hatchery volcano (Pliocene)**
- Tsbl — **Servilleta Basalt, lower sequence (Pliocene)**
- Tags — **Dacitic lavas of south Guadalupe Mountain (Pliocene)**
- Tagm — **Dacitic lavas of north Guadalupe Mountain (Pliocene)**
- Tag — **Dacitic lavas of Guadalupe Mountain, undivided (Pliocene)**
- Tvc — **Dacite of Cerro Chiflo (Miocene)**
- Tvb — **Undivided volcanic rocks of the Latir volcanic locus (Miocene to Oligocene)**
- **Near-vent pyroclastic deposits**
- **Fault**—Ball and bar on downthrown block; dashed where location approximate; dotted where location concealed
- 3-2 — **Field-trip stop**

Figure 70. Geologic map of the northwestern part of Wild Rivers Recreation Area.

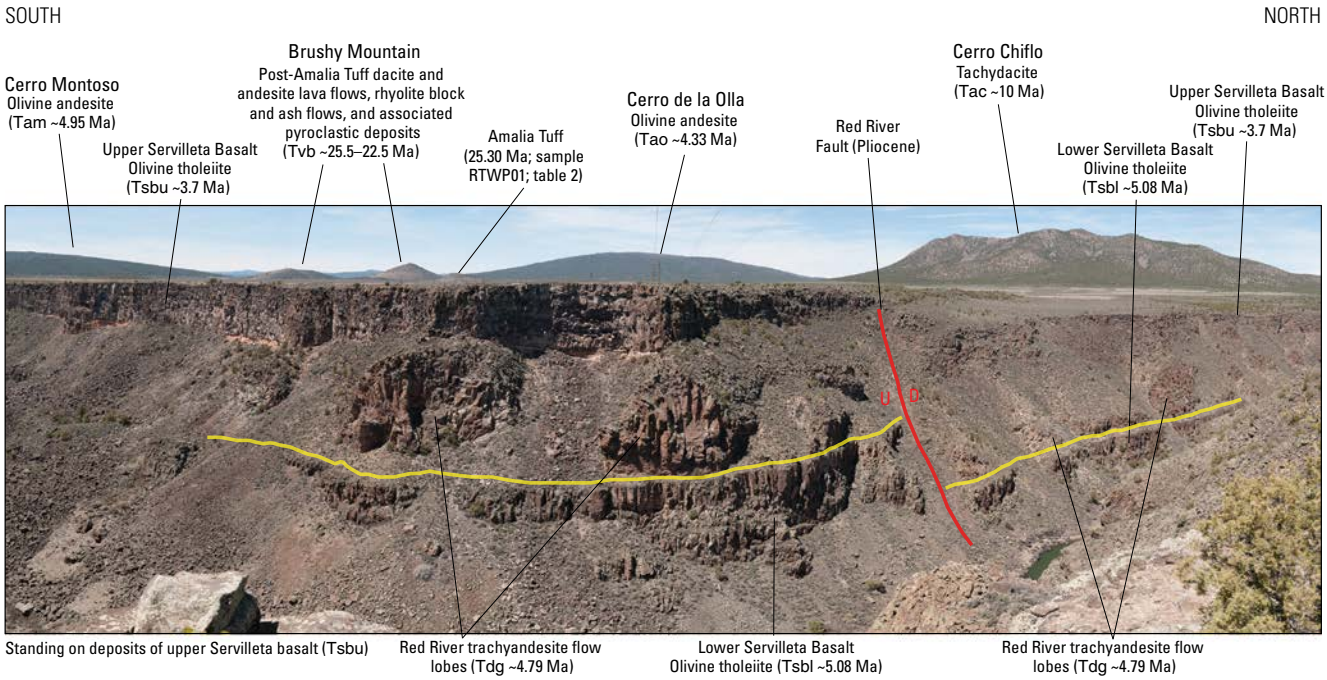

Figure 71. View northwest from point ~1,772 ft (~540 m) south of trailhead at the powerline crossing. The major northwest-trending strand of the down-to-north Red River Fault Zone is exposed in the foreground and projects along footwall exposures of the upper Servilleta Basalt sequence towards Cerro Chiflo in the distance. Cumulative offset at this locality is ~20–25 m. Lower sequence Servilleta Basalt is visible in the foreground and overlain (yellow line along contact) by lobate flows of Red River trachyandesite that exhibits characteristic radial fracture patterns and columnar jointing. Upper sequence flows of Servilleta Basalt cap a sedimentary interval characterized by baked upper contacts. No significant paleovalley fill of basalt is observed, which suggests topography developed on underlying Red River flows was largely leveled by eolian and sheetwash deposits. Map unit symbols refer to geologic map figure 70. Photograph by Dave Tewksbury, Hamilton College, 2014. Ma, million years ago.

and fractured eroded lava dome complex exposed at river level (2,175 m; 7,136 ft) extending to 8,978 ft (2,736 m) in elevation. The base of the complex is not exposed. This dacite to trachydacite complex is compositionally homogeneous (67–68 weight percent SiO_2; 7.5–7.7 weight percent Na_2O+K_2O; sample RGR-143, table 4), characterized by a glassy groundmass with feldspar microlites and elongate amphibole grains as much as 0.15 mm in length and 0.01 mm in width. Phenocrysts, locally as much as 25 percent of the rock, include (in order of abundance) amphibole, feldspar, biotite, and opaque minerals. Rare, conspicuous orthopyroxene grains are observed as are xenoliths of schist and gneiss. Lipman and Mehnert (1979) report K-Ar age determinations for biotite and plagioclase as 10.15±0.53 Ma and 10.28±0.57 Ma, respectively (sample 77L-RG19, table 3). Appelt (1998) reports a $^{40}Ar/^{39}Ar$ date of 5.31±0.31 Ma and 5.32±0.08 Ma from the west and east flanks of Cerro Chiflo, respectively, but with highly uncertain sample locations. Samples from this study yield $^{40}Ar/^{39}Ar$ ages on hornblende (9.64±0.08 Ma) and biotite (10.99±0.09 Ma) that are broadly consistent with previous determinations by Lipman and Mehnert (sample RGR-143, table 3).

The erosional unconformity between Cerro Chiflo dacite and the overlying flows of the Taos Plateau volcanic field are best exposed in the western gorge wall on the south side of the Cerro Chiflo dacite (fig. 72). Massive, highly fractured trachyandesite lava flows interpreted to be early erupted distal lava flows derived from the ~5 Ma Guadalupe Mountain center unconformably onlap the eroded, south-dipping upper surface of Cerro Chiflo dacites (left side of fig. 70). These flows are overlain by as much as 25 m of interbedded sedimentary deposits capped by Servilleta Basalt flows. This section is exposed along the Cerro Chiflo trail, but colluvial deposits partly obscure the section. After descending through the upper sequence of Servilleta flows to get to this spot, continue along the trail another 656 ft (200 m) to excellent exposures of Guadalupe Mountain trachyandesite flows that unconformably overlie Cerro Chiflo dacite. This contact is exposed at an elevation of ~7,316 ft (2,230 m). The relatively low elevation of Cerro Chiflo deposits on the east side of the gorge is broadly consistent with poorly exposed, down-to-east, Miocene to Pliocene north-trending faults that offset the section prior to the eruption of the Guadalupe Mountain and Servilleta Basalt flows.

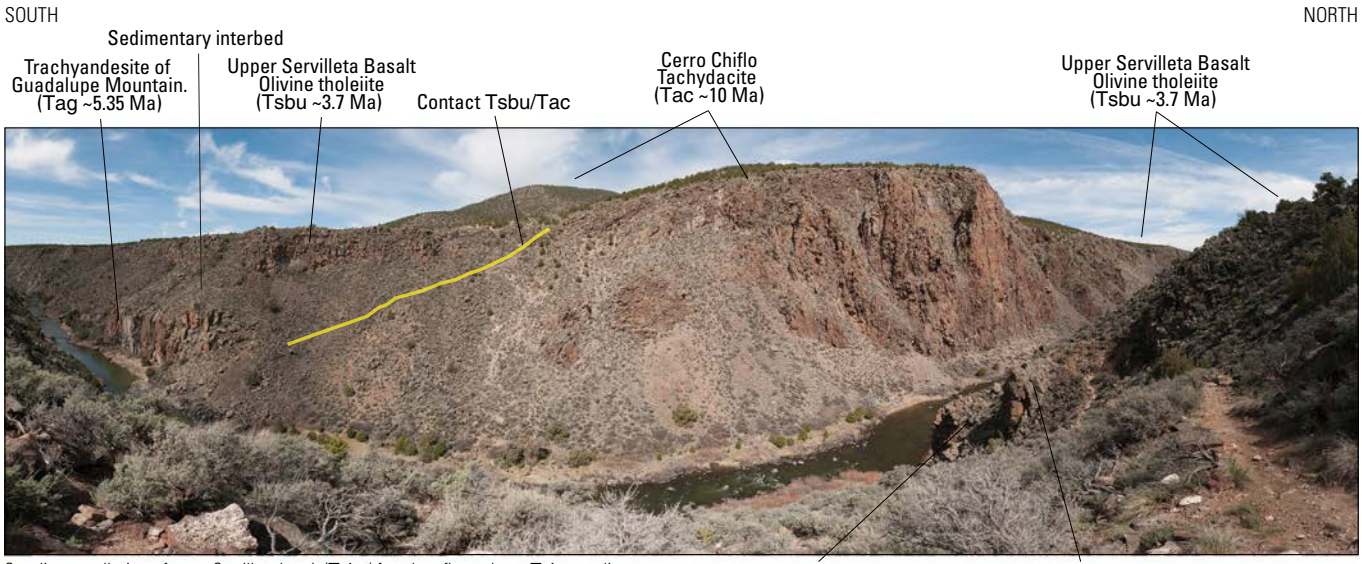

Figure 72. View northwest toward Cerro Chiflo along Chiflo Trail, below the plateau-capping Servilleta Basalt and north of the picnic shelter. Miocene trachydacite flow lobes of Cerro Chiflo overlain by distal Pliocene Guadalupe Mountain trachyandesite flows are visible in the foreground on the east side of the Rio Grande. Massive cliff-forming outcrops on the west side of the Rio Grande are fractured and faulted eroded remnants of the dacite lava dome complex; note the prominent columnar jointing and radial fracture patterns. The erosional unconformity is prominently visible along the south side of Cerro Chiflo, where Guadalupe Mountain trachyandesites abut the south flanks of Cerro Chiflo in the gorge. Distal trachyandesite lava flows of Guadalupe Mountain are visible at river level in the lower left part of the image. A thick sedimentary interbed, as much as 50 m, separates the basal Pliocene flows from overlying upper sequence flows of Servilleta Basalt. Lower sequence Servilleta lava flows are visibly missing from the section both here and in the gorge section to the north. The distal, lower flank deposits are more commonly flow deposits rather than fragmented dome deposits, which are preserved at higher stratigraphic levels. Map unit symbols refer to geologic map figure 70. Photograph by Dave Tewksbury, Hamilton College, 2014.

These faults, during a period of Miocene extensional deformation, were accompanied by dominantly andesitic to dacitic volcanism. Compositionally similar Miocene volcanic deposits crop out 40 km to the northeast at San Pedro Mesa where they are preserved as part of an intrarift horst block (Stop 3-7). Pliocene lava flows mapped north of Cerro Chiflo are offset by similarly oriented north-trending faults and are related to renewed extension in the Pliocene (Thompson and others, 2014a).

Return to the vehicles, proceed north on NM 378, and retrace the route through the village of Cerro back to the intersection with NM 522.

32.9 *Intersection of NM 378 and NM 522. Turn right and head south.*

33.9 *On the right (west) side of Don Martinez Road, turn right and head west.*

34.4 *T-intersection in the road. Turn right and head north.*

34.6 **Stop 3-5. Las Vistas de Questa trailhead and parking area. Overview of Questa caldera** (36°43.83' N., 105°36.27' W.; 7,644 ft, 2,330 m elevation)

The Las Vistas de Questa trail heads west into the saddle between North and South Guadalupe Mountains and can be followed to the visitor's center within the Wild Rivers Recreation Area. At this stop we focus our attention east for a rare cross-sectional view of the Questa caldera interior (fig. 73). Rift-related displacement along the Sangre de Cristo Fault Zone at the range front cut the Questa caldera and elevated the eastern part of the Latir volcanic locus. Northward tilting accompanied uplift along this segment of the Sangre de Cristo Mountain Fault Zone, which exposed deeper volcanic and intrusive levels to the south. Volcanic deposits are sparse south of the Questa caldera, but Proterozoic basement rocks and several postcaldera plutons are exposed at high elevations such as at Flag Mountain (11,942 ft, 3,640 m; fig. 73; Lipman and Reed, 1989).

Collapse of the Questa caldera accompanied eruption of the Amalia Tuff (25.39±0.04 Ma), an alkalic to peralkaline rhyolite ignimbrite that is compositionally unique in the SRMVF (Lipman, 2007). The Amalia Tuff is densely to moderately welded, with 10–20 percent phenocrysts of predominantly quartz and alkali feldspar, but with sparse sodic amphibole (Lipman and Reed, 1989).

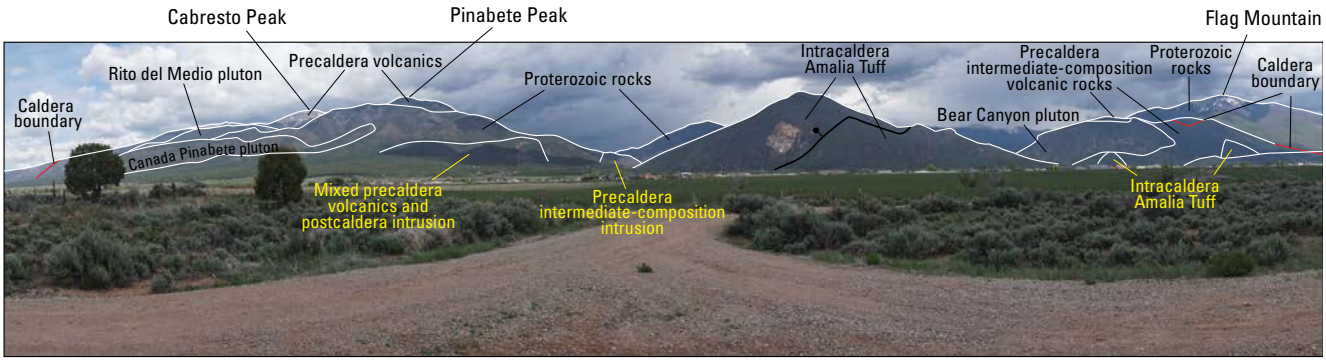

Figure 73. View of the Questa caldera looking east from the Vistas de Questa parking lot (Stop 3-5) with geologic units indicated based on mapping by Lipman and Reed (1989). The Sangre de Cristo Fault Zone trends north-south at the base of the range front. Although not highlighted in the photograph, intracaldera Amalia Tuff is observed directly on precaldera volcanic rocks and Proterozoic basement rocks, which indicates deep erosion that exposed parts of the caldera floor. The Rito del Medio and Canada Pinabete plutons are biotite granites interpreted as resurgent plutons. At the current level of erosion these plutons are not associated with mineralization. The Bear Creek pluton, emplaced along the south caldera boundary, is also biotite granite but is hydrothermally altered with extensive pyritic, argillic, and potassic alteration. The Bear Creek pluton and other compositionally similar and altered intrusions along the south caldera boundary were emplaced after the main phase of resurgence. The fresh scarp near the center of the photograph is a historical rockslide in intracaldera Amalia Tuff. Photograph by K.J. Turner, U.S. Geological Survey, 2016.

Where densely welded, the ignimbrite is typically devitrified and contains flattened pumice. Within the caldera, the Amalia Tuff accumulated to a thickness of >2 km (Lipman and others, 1986). Outflow Amalia Tuff is exposed below postcaldera volcanic deposits at Brushy Mountain (see Day 2 optional route; Thompson and others, 1986) and more than 45 km west of Questa caldera in the Tusas Mountains, south and west of Tres Piedras, New Mexico (fig. 61; Lipman and others, 1986; Koning and others, 2007; Aby and others, 2010).

The thick intracaldera Amalia Tuff overlies precaldera volcanic deposits and Proterozoic rocks (Lipman and Reed, 1989). Intracaldera ignimbrite contains megablocks, and megablock breccias are inferred to have slid into the caldera from an oversteepened caldera wall at the time of eruption of the Amalia Tuff (Lipman, 1983). The caldera fill is juxtaposed against Proterozoic basement rocks along the north and south caldera boundaries visible along the range front (fig. 73). In contrast, precaldera volcanic deposits are preserved outside the eastern caldera margin, 10–14 km east of the range front (Lipman and Reed, 1989).

Postcollapse resurgence of the caldera is associated with high-standing Proterozoic rocks and granitic intrusions, such as the Canada Pinabete and Rito del Medio plutons (fig. 73) exposed in the central and northern parts of the caldera interior (Lipman and others, 1986; Lipman and Reed, 1989). The structurally highest Virgin Canyon pluton intruded prevolcanic deposits northeast of Cabresto Peak (fig. 73); it is a biotite granite with a distinctive arfvedsonite-acmite peralkaline marginal phase (Lipman and others, 1986). The peralkaline phase is compositionally and isotopically similar to late-erupted peralkaline Amalia Tuff and is interpreted to represent quenched liquid from the Amalia Tuff magma (Lipman and others, 1986; Johnson and Lipman, 1988). Ring-dike intrusions along the southern margin of the caldera (for example, Bear Canyon pluton; fig. 73) were incrementally emplaced from ~25 to 24 Ma; however, reheating events have somewhat obscured $^{40}Ar/^{39}Ar$ results (Zimmerer and McIntosh, 2012b). Porphyry molybdenum deposits are primarily related to the ring-dike intrusions along the southern margin, as most interior resurgent intrusions have little hydrothermal alteration at the current levels of exposure (Lipman, 1983).

Postcaldera volcanic deposits of the Latir volcanic locus are best preserved at Brushy and Timber Mountains along a central horst in the southern San Luis Basin and include rhyolite, dacite, and andesite lava flows and tuffs (Thompson and others, 1986). $^{40}Ar/^{39}Ar$ geochronology indicates eruption ages from shortly after caldera collapse (~25 Ma) to about 22 Ma (Zimmerer and McIntosh, 2012b). The youngest magmatism (as young as 19 Ma) associated with the Latir system is represented by quartz monzonite to granitic intrusions south of the caldera (Lipman and others, 1986; Lipman and Reed, 1989; Zimmerer and McIntosh, 2012b). Isolated porphyry molybdenum mineralization is also associated with the late intrusions (Ludington, 1981).

Get back into the vehicles and return to NM 522, turn left and head north.

50.6 *Intersection with Taos County Road B-051.* Road heads west to Ute Mountain, a dacitic volcano similar in composition to Guadalupe Mountain. The upper parts of Ute Mountain are dacitic in composition but transition downward into olivine andesite lava flows. Unlike other large dacitic volcanoes in the TPVF (for example, Guadalupe Mountain and San Antonio Mountain), Ute Mountain has numerous radial dikes that suggest a slightly different eruptive style or deeper erosion.

52.6 *Town of Costilla and intersection with NM 196.* NM 196 heads east into the Sangre de Cristo Mountains along Costilla Creek and provides access to the northern part of the Latir volcanic locus. The type section for the Amalia Tuff is along NM 196 near the town of Amalia.

53.9 *Colorado-New Mexico State line.* Cross into Costilla County, Colorado. The road designation changes to CO 159. Continue heading north; on the right side of road (east) large Toreva blocks indicate mass wasting off the side of San Pedro Mesa. Similar to the gorge of the Rio Grande, capping Servilleta Basalt overlies thick deposits of sedimentary basin-fill.

65.8 *Stabilization reservoir on left side of road (west).* Prepare to turn right at the next dirt road.

66.0 *At mile marker 12, intersection of CO 159 and unmarked dirt road to right (east). Turn right onto dirt road and head east 0.6 mi to 90-degree bend in the road. Continue 0.1 mi and pull vehicles to the side of the road and exit the vehicles. The surrounding land is private property so please do not stray from the maintained road.*

66.7 **Stop 3-6. Road to radio tower; San Pedro Mesa** (37°10.12' N., 105°30.25' W.; 7,923 ft, 2,415 m elevation)

From this vantage point on San Pedro Mesa we gain a better understanding of the size of the San Luis Basin. This location is about 100 km north of Pilar, New Mexico, (Stop 2-1) at the southern end of the valley, whereas the northern topographic divide between the San Luis Basin and the Arkansas River valley at Poncha Pass (Day 6 route), is about 150 km north-northwest. The width of the basin at this latitude is more than 80 km. Day 3 stops around Guadalupe Mountain (Stops 3-1 to 3-5) are about 50 km to the south and the flat-topped mesas 25 km to the west are the San Luis Hills (Stop 3-7). The high peaks in the background, situated just west of the rift basin, are more than 90 km away in the southeast San Juan Mountains (fig. 74).

Servilleta Basalt underlies the surface of San Pedro Mesa (4.61±0.07 Ma; sample 7MRG-2, table 3), with the exception of the southern part of the mesa where Pliocene rocks onlap erosional remnants of middle Miocene volcanic rocks (fig. 61). Middle Miocene volcanic rocks include calc-alkaline andesite to dacite unconformably overlain by predominantly basaltic lavas of the Hinsdale Formation (Thompson and others, 2007a). Andesite to dacite lavas consist of porphyritic flows and breccias with phenocrysts of pyroxene, hornblende, plagioclase, with minor biotite, quartz, and Fe-Ti oxides. Compositionally similar rocks are identified at a depth of 1,280 m in the southern part of the Sanchez graben (Thompson and others, 2007a), and east of the graben where a 600-m-thick section ranges from 15 to 11 Ma ($^{39}Ar/^{40}Ar$ ages of Kirkham and others, 2004; fig. 61). The andesite and dacite are the youngest

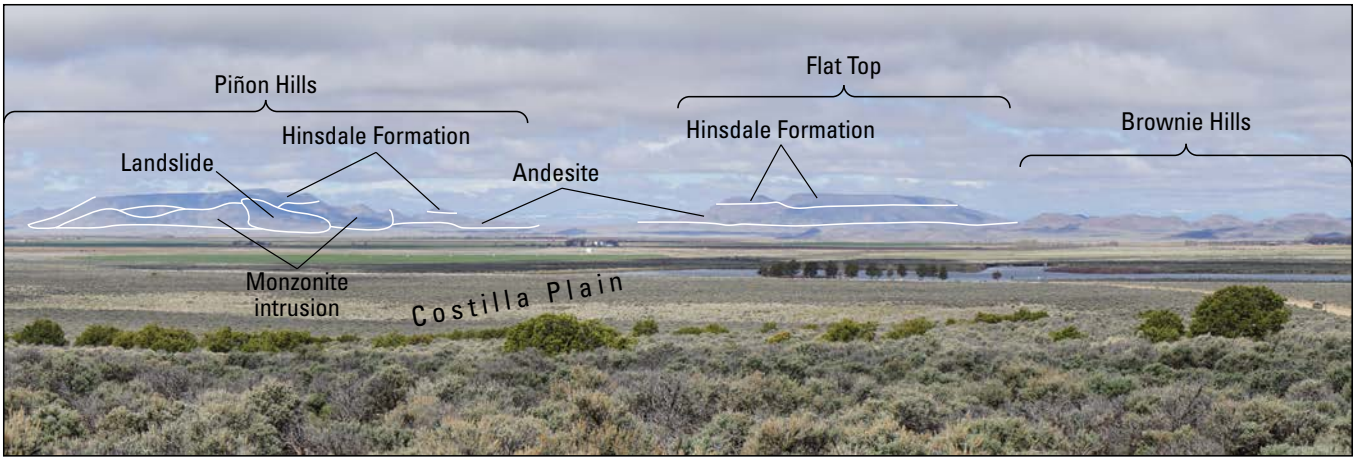

Figure 74. View from Stop 3-6 on San Pedro Mesa looking west across Costilla Plain to the flat-topped mesas of the San Luis Hills. Middle Pleistocene piedmont alluvium is at the surface of the Costilla Plain (Ruleman and others, 2013; Thompson and others, 2015) but south of the New Mexico-Colorado State line Holocene deposits are more widespread. At depth within the Costilla Plain-Sunshine subbasin is Pliocene and younger Santa Fe Group that likely overlies older Oligocene volcaniclastic deposits. The major landslide indicated on the left side of the image is developed in a highly altered monzonite intrusion. Photograph by K.J. Turner, U.S. Geological Survey, 2016.

manifestations of calc-alkaline volcanism in the region, which is more typical of volcanism associated with the SRMVF. The Hinsdale Formation here consists of olivine-bearing mildly alkaline basalt and basaltic andesite flows, breccias, and near-vent pyroclastic deposits. These rocks are inferred to correlate with basaltic flows on the east side of the Sanchez graben (~12–11 Ma; Miggins and others, 2002; Kirkham and others, 2004) and in the northern part of the Latir volcanic locus (~15–10 Ma; Lipman and others, 1986; Lipman and Reed, 1989). The Hinsdale Formation lava flows filled valleys eroded into the calc-alkaline volcanic sequence, indicating a hiatus in volcanism preceded basaltic volcanism.

San Pedro Mesa is a 6-km-wide north-trending horst that separates the Sunshine Valley-Costilla Plain subbasin to the west from the Sanchez graben to the east (fig. 65). This is a structurally complex area of strain partitioning between the southern and central segments of the Sangre de Cristo Fault Zone and the intervening San Luis Fault Zone (fig. 65). The southern segment of the Sangre de Cristo Fault Zone displaces Servilleta Basalt as much as 700 m down-to-west into the Sunshine Valley-Costilla Plain subbasin west of San Pedro Mesa (Ruleman and others, 2013). The San Luis Fault Zone separates San Pedro Mesa from the Sanchez graben to the east. Within the central and northern parts of the Sanchez graben, Servilleta Basalt is exposed at the surface, but in the southern part of the graben, the basalt is at a depth of 400 m (Thompson and others, 2007a). This is related to 500 m down-to-east displacement along the southern segment of the San Luis Fault Zone, which acts as a structural link between the central and southern segments of the Sangre de Cristo Fault Zone. The central segment of the Sangre de Cristo Fault Zone bounds the east side of the Sanchez graben with down-to-west displacement (Ruleman and Machette, 2007).

The Costilla Plain separates San Pedro Mesa and the San Luis Hills and is underlain by the northern part of the Sunshine Valley-Costilla Plain subbasin. Subbasin-bounding structures (fig. 65) include the Red River Fault Zone in the south and the southern segment of the Sangre de Cristo Fault Zone on the east. The west structural boundary is subparallel—and approximately coincident with—the Rio Grande on the east side of the San Luis Hills, where the boundary is superposed on the Fairy Hills Fault Zone. Servilleta Basalt conceals the west subbasin boundary south of the San Luis Hills. The north boundary of the subbasin coincides with the northeast-trending, eastern part of the San Luis Hills. Geophysical modeling by Drenth and others (2013) suggests the northern portion of the subbasin west of San Pedro Mesa may contain 400–600 m of low-density basin fill that thickens to as much as 900 m near the Colorado-New Mexico State line. Modeling by Ruleman and others (2013) estimates a depth of 1.6 km for the subbasin south of Ute Mountain in northern New Mexico. Estimates for low-density basin fill determined by gravity inversion modeling are unable to distinguish pre-San Luis Basin deposits (Oligocene) from San Luis Basin (Miocene and younger) deposits inasmuch as the sediments are similar in composition and density. Therefore, the above listed thickness estimates are cumulative amounts of low-density deposits.

Return to CO 159. Bathrooms are available for use at the stabilization reservoir. These are the last restroom facilities until the drive back to Taos at the end of the day.

67.4 *Head north on CO 159.*

68.7 *Turn left onto Costilla County Road P and head west.*

72.9 *Intersection of Costilla County Road P and CO 142. Continue heading west on CO 142.* The rounded hills north of the road make up the eastern part of the San Luis Hills, which are composed of Conejos Formation and minor Hinsdale Formation. The youngest documented Hinsdale Formation lava (24.56 Ma) in the San Luis Hills is located in this area (fig. 61).

80.9 South of the road, on the east side of Rio Grande, is Culebra volcano, a small Pliocene vent (5.19±0.11 Ma; sample SLH-501, table 3) that erupted olivine-bearing trachybasalt (49–50 weight percent SiO_2; sample RGR-150, table 4).

81.4 *Crossing the Rio Grande.* At river level are andesite lavas of lower sequence Conejos Formation. An $^{40}Ar/^{39}Ar$ age on groundmass concentrate from an andesite just north of the bridge yielded an age of 30.33±0.06 Ma (sample SLH-507, table 3).

83.4 South of the road is the privately owned King Turquoise Mine (fig. 75) intermittently operated as far back as 1100 C.E. Turquoise from the King Mine has been identified in ancestral Pueblo ruins in northwestern New Mexico (Hull and others, 2014). Hydrothermal alteration is primarily hosted by Conejos Formation andesite and dacite in close proximity to late stage intrusive rocks. Supergene alteration responsible for turquoise formation at the King Mine is underlain by hypogene alteration that indicates the lack of advanced argillic alteration in the immediate area surrounding the mine. More intense alteration formed in the low hills north of the turquoise mine, which produced coarse-grained alunite, high-temperature kaolin-group clays, hydrothermal breccia, and pebble dikes. Quartz alunite veins as much as 2-m wide are enveloped by an argillic zone in close proximity to a late intrusive stock north of the turquoise mine.

Table 4. Major and trace element data for representative samples of Quaternary to Oligocene volcanic rocks.

[LOI, loss on ignition]

Location	Culebra volcano	Servilleta	Pinabetoso Peaks	Wissmath craters	Red Hill	State line	No Agua Peaks	Los Mogotes composite sheild					San Antonio Mountain			
Sample ID	RGR-150	RGR-224	TP505	RGR-438	RGR-017	RGR-207	RGR-129	RGR-244	RGR-242	RGR-243	RGR-137	RGR-241	RGR-09	RGR-285	RGR-231	R
Rock type	Alkaline basalt	Tholeiitic basalt	Xeno-crystic basaltic andesite	Tholeiitic basalt	Xeno-crystic basaltic andesite	Alkaline basalt	Rhyolite	Alkaline basalt	Basaltic dike	Tholeiitic basalt	Cinder Pits alkaline basalt	Flat Top alkaline basalt	Xeno-crystic andesite	Dacite	North trachy-andesite	a
Longitude	105°43.3′	106°6.28′	105°56.19′	106° 0.01′	105°58.9′	105°46.67′	105°57.32′	106°7.59′	106°10.32′	106°7.7′	106°10.57′	106°10.93′	105°59.38′	106°0.55′	106°0.49′	1
Latitude	37°10.15′	36°54.41′	36°53.22′	36°48.12′	36°44.46′	37°0.04′	36°44.38′	37°7.27′	37°4.57′	37°7.13′	37°11.14′	37°9.59′	36°54.38′	36°51.04′	36°53.3′	3
																Weight
SiO_2	49.26	49.8	51.25	51.38	51.41	51.6	73.22	48.22	49.64	49.07	50.25	51.08	54.62	63.46	61.2	
TiO_2	1.4	1.19	1.25	1.2	1.79	1.58	0.06	1.8	1.63	1.39	1.51	1.54	1.64	0.72	0.78	
$Al2O_3$	15.63	17.1	15.62	15.95	16.44	16.5	13.26	16.39	16.05	16.22	16.16	16.4	15.91	15.86	15.8	
Fe_2O_3	10.37	11.4	10.74	11.53	10.53	10.5	0.7	10.2	12.02	12.07	10.61	10.5	9.16	5.38	6.03	
MgO	7.62	7.26	5.97	7.3	4.36	5.12	0.07	7.58	6.38	7.23	5.86	5.6	3.17	1.95	2.82	
CaO	8.49	9.31	7.81	8.99	7.17	7.57	0.75	8.5	8.95	9.56	9.25	9.66	5.93	4.41	4.98	
Na_2O	3.77	3.2	3.39	3.07	4.01	3.93	4.16	3.95	3.47	3.26	3.39	3.41	4.03	3.97	3.85	
K_2O	1.5	0.73	1.33	0.58	1.91	1.78	4.53	1.68	1.19	0.91	1.29	1.36	2.65	3.14	2.94	
P_2O_5	0.47	0.25	0.34	0.19	0.83	0.74	0.01	0.37	0.31	0.2	0.35	0.35	0.97	0.29	0.4	
MnO	0.15	0.17	0.14	0.15	0.14	0.15	0.08	0.16	0.18	0.18	0.16	0.16	0.13	0.09	0.09	
Total	98.66	100.41	97.84	100.36	98.59	99.47	96.84	98.85	99.82	100.09	98.82	100.06	98.21	99.27	98.89	
LOI	0.56	0	0	0	0.81	0.56	3.58	0.14	0	0.11	0.57	0	0.99	0.47	1.65	
																Parts pe
Ba	925	385	624	301	1,350	1,200	109	557	509	433	518	545	1,560	1,140	1,280	1
Rb	25.5	8.9	24.5	9.2	18.8	22.4	130	18.8	21.7	16.8	26.3	23.8	35.7	51.5	53.5	
Th	4.1	0.9	2.4	0.9	1.7	1.8	10.1	1.5	2	1.1	2	2	2.8	3.5	4.7	
Nb	23	9	10	8	24	25	33	19	10	8	17	14	28	6	19	
Ta	1.2	0.5	0.6	0	1.1	1.2	2.5	1.2	0.6	0	1	0.8	1.2	0	0.9	
La	30.8	15	20.7	11.2	45.8	48.5	11.6	21.3	18.7	12.4	22.6	22.7	60.6	40.6	50.3	
Ce	61.5	33.5	42.1	22.9	101	104	25.7	47	40.7	27	47.6	47.3	130	73.4	97.1	
Sr	930	416	384	327	1,100	898	35	1,020	470	440	635	670	1,100	570	714	
Nd	29.6	17.7	20.4	13.2	55.2	48.9	9.3	24	21.5	15.4	24.9	24.7	64.4	34.6	41.2	
Sm	5.7	4	4.4	3.1	9.8	9.1	2.3	5	4.9	3.6	4.9	5.1	11.3	5.8	7.3	
Zr	151	112	118	94.3	212	222	62	164	132	101	132	130	281	168	247	
Hf	3	2	4	2	5	5	3	4	3	3	3	3	6	4	6	
Tb	0.74	0.62	0.74	0.58	1.1	1.07	0.47	0.74	0.9	0.72	0.72	0.78	1.18	0.77	0.86	
Y	25.5	21.8	20.9	19.9	35.5	30.1	20	21.9	28.2	23	25.2	23.1	38.1	20.9	26.1	
Tm	0.37	0.3	0.34	0.29	0.46	0.4	0.32	0.35	0.46	0.39	0.38	0.38	0.49	0.31	0.33	
Yb	2.3	1.9	2.1	1.7	2.9	2.5	2.3	2.1	3	2.3	2.4	2.2	3.1	1.9	2.2	

	Canada de los Ranchos		Los Cerritos de la Cruz		Cerro Chiflo	Hinsdale Basalt (Miocene)			Hinsdale Basalt (Oligocene)						
RGR-133	RGR-434	RGR-495	RGR-229	89T019	RGR-143	RGR-245	RGR-516	RGR-379	RGR-105	RGR-456	RGR-490	T84056	RGR-380	T84061	RGR-033
South trachy-andesite	Xeno-crystic basalt	Xeno-crystic andesite	Xeno-crystic basaltic andesite	Xeno-crystic andesite	Dacite	South-eastern San Juan Mountains basalt	South-eastern San Juan Mountains basalt	South-eastern San Juan Mountains basalt	San Luis Hills basalt	Tusas Mountains basalt	San Luis Hills basalt	San Luis Hills basalt	South-eastern San Juan Mountains basalt	San Luis Hills basalt	Tusas Mountains basalt
106°0.14′	106°4.61′	106°3.47′	106°5.68′	106°4.23′	105°43.64′	106°6.28′	106°22.72′	106°14.56′	105°48.43′	106°14.91′	105°49.22′	105°48.73′	106°14.97′	105°48.03′	106°10.55′
36°48.11′	36°58.5′	36°54.07′	36°50.06′	36°48.95′	36°44.86′	37°6.72′	37°19.34′	37°7.73′	37°11.89′	36°49.56′	37°2.95′	37°2.2′	37°7.36′	37°4′	36°47.9′
percent															
56.57	49.58	53.77	51.4	57.07	66.32	48.07	48.3	51.7	49.08	49.36	49.89	50.01	50.4	50.84	52.41
1.26	1.15	1.14	1.42	1.13	0.51	1.74	1.98	1.6	1.69	1.41	1.47	1.6	1.65	1.57	1.59
15.89	16.25	15.57	16.2	15.8	15.12	14.6	15.1	15.6	13.76	14.57	15.02	15.58	14	14.65	13.92
8.06	12.15	9.98	11.1	8.56	3.99	11.97	11	11.3	10.91	14.02	12.68	11.86	13.2	12.35	11.11
3.36	7.7	5.76	6.84	4.35	1.42	7.61	6.92	5.9	7.39	7.95	7.05	6.46	6.96	6.43	6.08
5.92	9.17	7.45	8.07	5.9	2.88	9.46	8.04	8	8.33	9.33	9.21	8.9	8.62	8.13	9.16
4.03	3.05	3.09	3.47	3.66	3.92	3.35	3.06	3.8	3.25	2.84	3.1	3.31	3.1	3.06	2.96
2.6	0.55	1.44	1.12	2.59	3.81	1.61	2.23	1.53	2.33	0.42	0.65	1.15	1.35	1.61	1.09
0.68	0.2	0.2	0.29	0.38	0.19	0.41	0.5	0.37	0.6	0.18	0.23	0.29	0.35	0.33	0.28
0.12	0.16	0.14	0.15	0.13	0.06	0.16	0.15	0.14	0.16	0.18	0.16	0.15	0.17	0.16	0.15
98.49	99.96	98.54	100.06	99.57	98.22	98.98	97.28	99.94	97.5	100.26	99.46	99.31	99.8	99.13	98.75
1.11	0	0.38	0.22	0.96	0.6	0.86	3.25	0.47	1.99	0.01	0.19	0	0.5	0	1.32
er million															
,460	278	577	602	977	294	650	723	683	979	188	628	361	571	518	409
45	8	27	13.7	47.9	14.6	31	48.1	26.1	48.8	6.6	12.9	22.9	22	34.3	24.4
3.1	0.8	2.5	1.2	4.7	1.5	1.5	2.3	2.1	3.2	1	1.3	1.8	2.4	2.7	2
24	6	11	12	18	7	11	33	12	20	7	8	13	9	12	8
1	0	0.6	0.7	1.2	0	0.6	1.7	0.6	1.2	0	0	0.6	0.5	0	0
58.5	10.3	18.2	16.2	36.8	12.9	18.6	23.2	21	38.7	9	13	16.5	22.6	20.5	23.1
128	23.4	38.1	33.6	70.6	30.2	40.2	48.7	46.5	85.7	20.2	29	36.5	48.1	47.9	41.4
868	376	359	445	694	353	620	632	602	931	302	405	452	597	488	497
56.2	14.3	18.6	17.8	34.1	15.6	23.3	26.3	24.7	41.6	12.5	16.4	19.1	25.7	25.5	23.3
9.4	3.4	4.3	4.2	6.3	3.9	4.9	5.5	5.3	7.5	3.4	4.2	4.5	5.6	6.1	5.2
279	88.7	127	130	156	106	123	207	125	168	77.8	102	99.4	102	132	110
7	2	3	3	4	3	3	5	4	5	2	3	3	3	4	4
1.1	0.59	0.69	0.65	0.83	0.68	0.72	0.84	0.76	0.74	0.61	0.64	0.68	0.81	0.83	0.76
34.6	20.1	21.4	22.5	26.5	24.4	18.4	21.4	19.5	20.9	19	18.9	17.7	22.4	21.2	24
0.47	0.3	0.34	0.27	0.39	0.38	0.26	0.28	0.26	0.27	0.29	0.3	0.27	0.33	0.31	0.29
2.8	1.9	1.9	1.9	2.4	2.3	1.5	1.7	1.6	1.7	1.6	1.6	1.6	1.9	1.9	1.7

Figure 75. Turquoise mineralization at the King Turquoise mine developed in highly altered andesitic rocks of the Conejos Formation. This zone of highly altered rocks and alunite mineralization, immediately north of CO 142, are focused along the Fairy Hills Fault Zone. The landslide developed in highly altered monzonite identified in figure 74 is 4 kilometers southwest of the mine on the east slope of Piñon Hills (Thompson and Machette, 1989). The King Mine is privately owned, and permission should be obtained before entering. Photograph by R. Thompson, U.S. Geological Survey, 2015.

Continue west to an unmarked road on the right (north) side of the road, pull vehicles onto the dirt road and park. The dirt road is not maintained, so be cautious with low clearance vehicles. If vehicles are high clearance, continuing north on the dirt road provides a closer view of Flat Top, but spots wide enough to turn vehicles around are limited.

86.6 **Stop 3-7. Flat Top** (37°10.55' N., 105°49.3' W.; 7,858 ft, 2,395 m elevation)

Quaternary eolian deposits and piedmont-slope alluvium composed of volcanic debris mantle this broad valley (fig. 76). Flat Top (9,186 ft; 2,800 m) is north of the valley and south of the valley are the Piñon Hills (9,482 ft; 2,890 m). Calc-alkaline intermediate-composition volcanic and intrusive rocks of the Conejos Formation and predominantly basaltic rocks of the Hinsdale Formation underlie the San Luis Hills. Prominent flat-topped topographic highs west of the Rio Grande at Flat Top (fig. 77), Piñon Hills, and South Piñon Hills correspond to thick accumulations of Hinsdale Formation flows, in contrast to the generally rounded hills east of the Rio Grande where Hinsdale Formation is sparse.

Figure 76. Geologic map of the San Luis Hills modified from Thompson and Machette (1989). Thick dashed purple line is the approximate outline of a buried magnetic anomaly interpreted by Drenth and others (2013) as a buried intrusion. The exposed quartz monzonite intrusions are interpreted as cupolas associated with the larger, still buried intrusion.

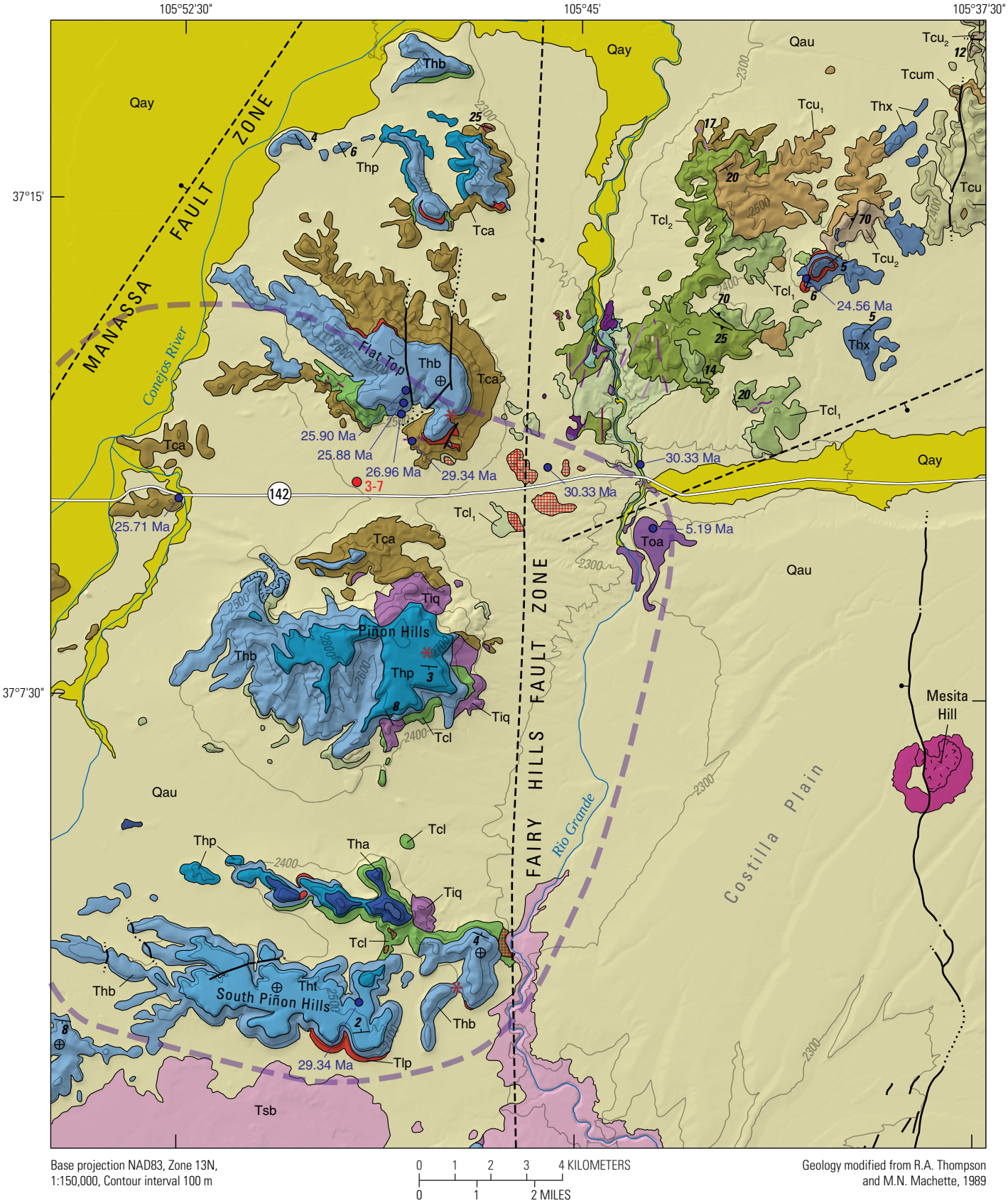
105°52'30"
105°45'
105°37'30"
37°15'
37°7'30"
MANASSA FAULT ZONE
FAIRY HILLS FAULT ZONE
Conejos River
Rio Grande
Flat Top
Piñon Hills
South Piñon Hills
Mesita Hill
Costilla Plain
Qay
Qau
Thb
Thp
Tca
Tcu2
Tcum
Tcu1
Thx
Tcl2
Tcl1
Tiq
Tcl
Tha
Tht
Tlp
Tsb
Toa
142
25.90 Ma
25.88 Ma
26.96 Ma
29.34 Ma
30.33 Ma
25.71 Ma
24.56 Ma
5.19 Ma
3-7
Base projection NAD83, Zone 13N,
1:150,000, Contour interval 100 m
0 1 2 3 4 KILOMETERS
0 1 2 MILES
Geology modified from R.A. Thompson
and M.N. Machette, 1989

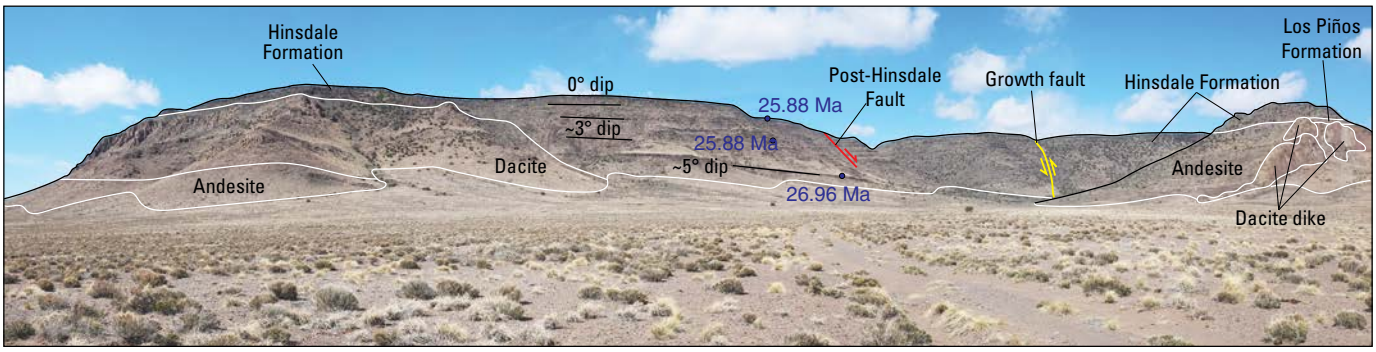

Figure 77. View looking north at the south side of Flat Top in the San Luis Hills. Geologic units based on mapping from Thompson and Machette (1989). Conejos Formation is represented by dacite lavas and andesite (left) and dacite dikes that intrude andesite (right). The upper part of the dacite dikes (29.34±0.55 million years ago [Ma]) are truncated and Los Piños Formation is deposited directly on the dikes, which indicates significant erosion occurred prior to emplacement of the overlying Hinsdale lava flows (27–25.9 Ma). The Hinsdale Formation thickens from about 30 meters (m) above the dacite lavas (left side of view) to more than 200 m (center of view). Lava flows appear to maintain fairly constant thickness from west to east, although more flows are present closer to the fault, which suggests the rapid change in thickness and increasing dips down section are at least partly a result of growth faulting (yellow line). Whole rock $^{40}Ar/^{39}Ar$ ages indicate that the upper ~100 m of Hinsdale Formation lava flows were emplaced rapidly at 25.9 Ma. The basal Hinsdale lava flow in the south face of Flat Top yields the oldest eruption age determined in the San Luis Hills (26.96±0.26 Ma). Photograph by R. Thompson, U.S. Geological Survey, 2014.

The Conejos Formation in the San Luis Hills includes andesite and dacite flows and breccias, comagmatic intrusions, and minor associated mudflow and volcaniclastic deposits emplaced between 31 and 28 Ma (Thompson and Machette, 1989; Thompson and others, 2015). Andesites are typically moderately to sparsely porphyritic with plagioclase, olivine, and clinopyroxene. Dacites are moderately to sparsely porphyritic with plagioclase, biotite, Fe-Ti oxides, ± clinopyroxene, orthopyroxene, and hornblende. Thompson and Machette (1989) divided the Conejos Formation in the San Luis Hills into lower and upper sequences. Lower sequence deposits are preserved throughout the San Luis Hills, but upper sequence deposits are restricted to the area east of the Rio Grande. Lower sequence andesite floors the valley between Flat Top and Piñon Hills and extends part way up the slopes of both topographic highs. In the slopes of Flat Top, immediately north of the stop, as much as 180 m of thick dacite flows overlie the andesite (fig. 77).

Comagmatic intrusions include dacite to andesite dikes and related quartz monzonite intrusions. Northeast of the stop, dacite dikes (29.34±0.55 Ma; sample SLH-512, table 3) protrude above the southeast slopes of Flat Top. The dikes are compositionally similar to a north- to northeast-trending dike-swarm intrusion east of Flat Top. Southeast of the stop, scattered outcrops of quartz monzonite stocks underlie the easternmost parts of Piñon Hills and South Piñon Hills (fig. 76). The intrusive stocks are compositionally and mineralogically similar, which suggests they may represent cupolas of a larger intrusion still mostly buried (Thompson and Machette, 1989). A buried intrusion may account for a ~16 × 20 km magnetic anomaly that underlies much of the San Luis Hills west of the Rio Grande (fig. 76; Drenth and others, 2013). Based on gravity and aeromagnetic interpretations, buried parts of the intrusive complex may be as shallow as 600 m below the valley surface north of South Piñon Hills (Drenth and others, 2013).

A period of erosion that followed Conejos Formation volcanism unroofed subvolcanic intrusions and formed an irregular surface onto which basaltic flows and breccias of the Hinsdale Formation were emplaced (Larsen and Cross, 1956; Thompson and Machette, 1989). Piñon Hills hosts the thickest sequence of Hinsdale Formation (exceeding 400 m); however, overall thickness varies dramatically due in part to the pre-Hinsdale erosion surface. Hinsdale Formation compositions are predominantly mildly alkaline (table 4), but volumetrically minor tholeiitic basalt (sample RGR-490, table 4) forms the upper flat surface at South Piñon Hills (fig. 76). Although Miocene rocks are included in the Hinsdale Formation elsewhere, whole-rock $^{40}Ar/^{39}Ar$ ages in the San Luis Hills are strictly late Oligocene and document almost 2.5 m.y. of intermittent volcanism between 26.96±0.26 Ma (sample RGR-104, table 3) and 24.56±0.05 Ma (sample RGR-138, table 3). Whole-rock $^{40}Ar/^{39}Ar$ ages for samples from the 200-m-thick section of Hinsdale flows at Flat Top (fig. 77) suggest rapid emplacement of individual lava sequences. Ages for three of the flows are (1) 26.96±0.26 Ma for the lowest exposed flow, (2) 25.88±0.05 Ma (sample RGR-105, table 3) for a flow ~100 m above the base, and (3) 25.90±0.07 Ma (sample 13BP-23, table 3) for the capping lava flow. Indistinguishable ages for the upper 100 m are consistent with rapid emplacement and correspondingly high eruption rates. In addition to rapid vertical accumulation of flows, high eruption rates

facilitated long travel distances for lavas. Distal flows 35–50 km from the San Luis Hills are indistinguishable in age and composition (fig. 62), and include alkaline basalt along the margin of the southeast San Juan Mountains (35 km to the west) and tholeiitic basalt in the northern Tusas Mountains (more than 50 km to the southwest).

The San Luis Hills are the northernmost surface expression of the north-trending San Luis horst. To the south, the horst becomes less well defined, but approximately 43 km south of the Colorado-New Mexico State line late Oligocene to Miocene volcanic deposits at Timber Mountain (Day 2 optional stops 2-1, 2-2, and 2-3) mark the southernmost exposure of the structural high where it forms the western structural margin of the Taos subbasin. At the latitude of the San Luis Hills, the Manassa Fault Zone bounds the west side of the horst, but younger alluvial deposits conceal the fault. Hydrothermal fluids that originated from late-stage Conejos Formation intrusions are focused along a broad, north-aligned zone on the east side of the San Luis Hills that may reflect localization of fluids along the Fairy Hills Fault Zone. Alunite mineralization at 30.33±0.87 Ma (sample RGR-151, table 3) provides a minimum age for fault formation that indicates tectonism was concurrent with Conejos magmatism (31–28 Ma). Continued faulting along the Fairy Hills and Manassa Fault Zones and associated uplift of the San Luis horst after Conejos volcanism most likely facilitated rapid erosion of Conejos Formation volcanic deposits, resulting in exposure of subvolcanic intrusions prior to, or overlapping with, Hinsdale Formation volcanism. The presence of a growth fault at Flat Top (fig. 77) that overthickens the stratigraphic section on the downthrown western side of the fault indicates continued tectonism coeval with Hinsdale volcanism.

Head west on CO 142 toward the town of Manassa.

89.6 Low hills on either side of road are andesite lavas and breccias of the Conejos Formation. An $^{40}Ar/^{39}Ar$ age on groundmass concentrate from an andesitic lava north of the road yields an age of 30.45±0.09 Ma (sample SLH-514, table 3).

95.8 *Intersection of CO 142 and U.S. Route (U.S) 285 on the west edge of the town of Romeo. Turn left onto U.S. 285 and head south to Antonito.*

103.1 **Optional Stop 3-8. Overview of Los Mogotes composite shield volcano and underlying stratigraphy** (37°4.27' N., 106°0.69' W.; 7,890 ft, 2,405 m elevation) *As road bends to west at south end of Antonito, pull into parking area on north side of road.*

The Los Mogotes composite shield (fig. 78) contains two lava suites erupted from at least four vent areas between 4.9 and 4.5 Ma (tables 3, 4; fig. 64): tholeiitic basalt (49–51 weight percent SiO_2; 0.4–0.9 weight percent K_2O) and alkaline basalt to trachybasalt (48–50 weight percent SiO_2; 1.2–1.8 weight percent K_2O). Preliminary investigations indicate a complex and possibly alternating stratigraphic relation between the two lava types (fig. 79), which suggests multiple pulses of at least tholeiitic lavas may be possible. The tholeiitic basalts

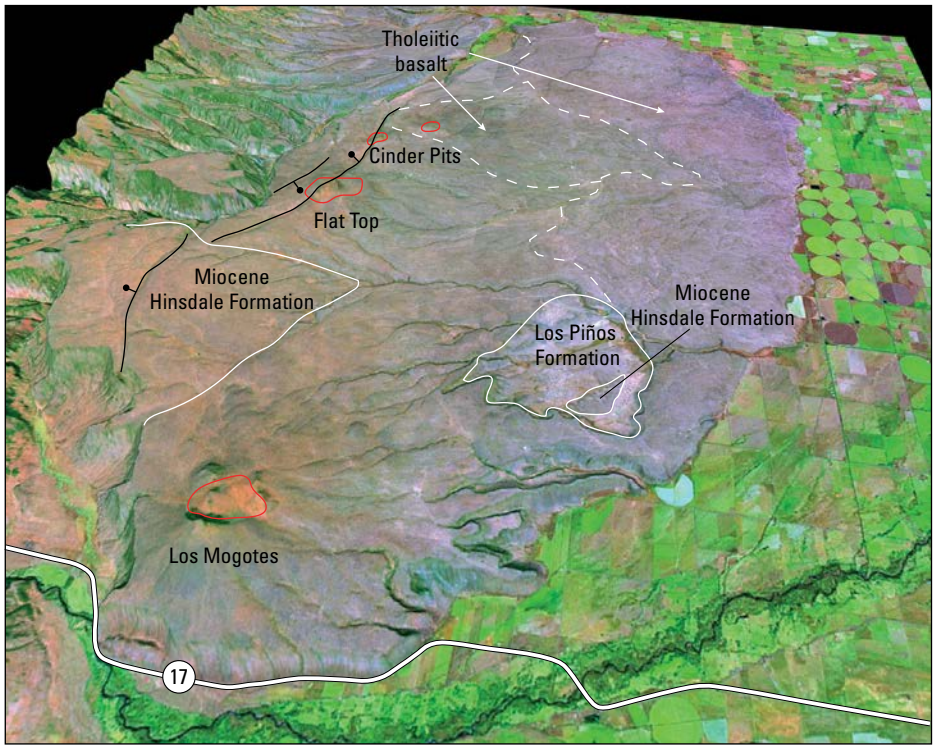

Figure 78. Oblique aerial view looking north-northwest at the Los Mogotes composite shield volcano. Image composed of Landsat 7 mosaic draped over 30-meter digital elevation data. Red lines indicate areas of highly oxidized near-vent pyroclastic deposits associated with Pliocene vents; at least four vent areas are identified, but additional vent(s) for the uppermost tholeiitic basalts are suspected. An angular unconformity separates the Pliocene composite shield from underlying Los Piños Formation and Miocene Hinsdale Formation. North-trending faults displace the Pliocene lava flows.

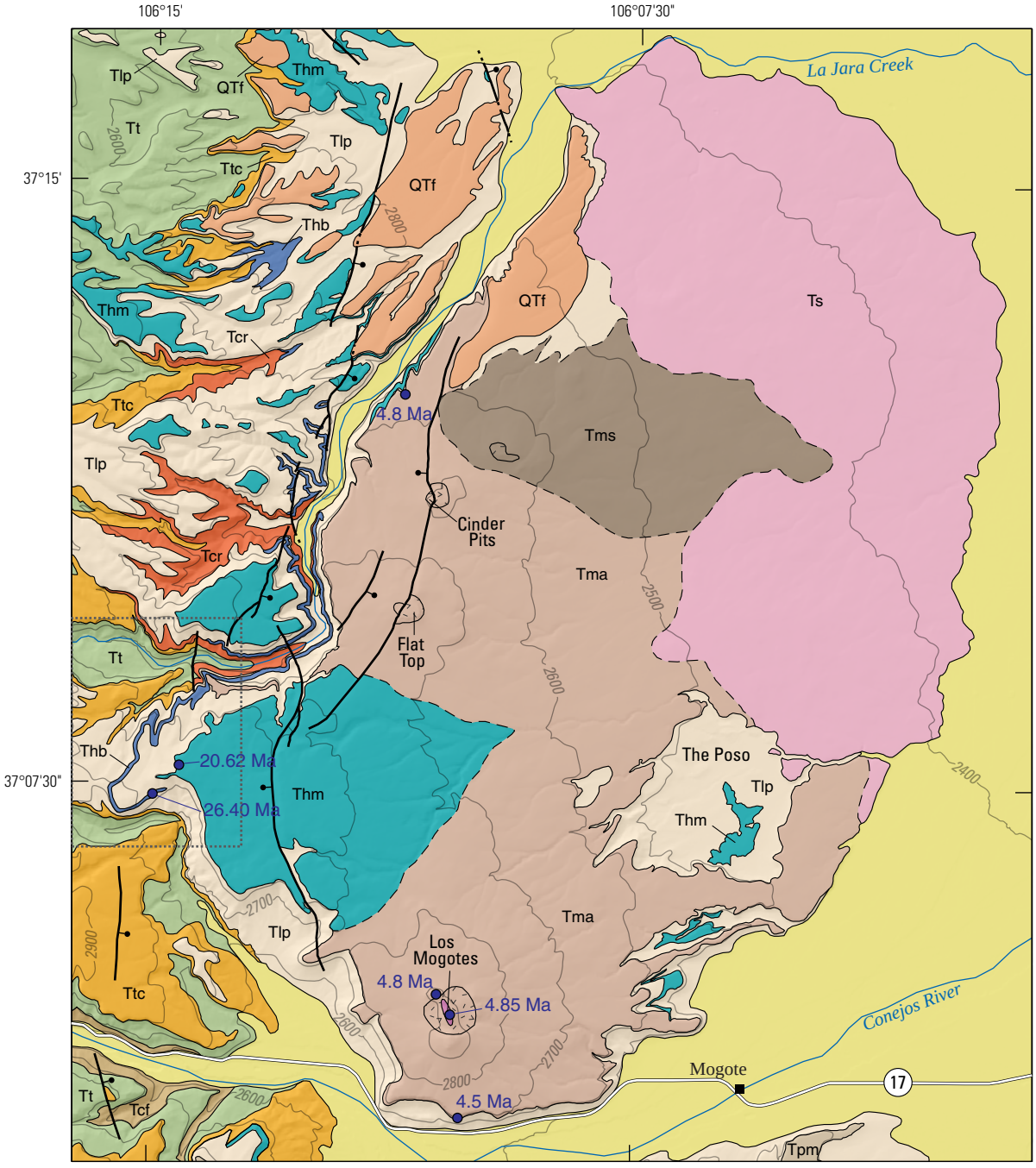

EXPLANATION

- Qu — Alluvial and colluvial deposits, undivided (Quaternary)
- QTf — Fan deposits (Quaternary to Tertiary(?))
- Tpm — Pliocene basalt, undivided
- Tms — Upper tholeiitic basalt [Servilleta Basalt(?)] (Pliocene)
- Mildly alkaline basalt, dike (Pliocene)
- Tma — Mildly alkaline basalt (Oligocene)
- Ts — Lower tholeiitic basalt [Servilleta Basalt(?)] (Pliocene)
- Thm — Hinsdale Formation (Miocene)
- Thb — Hinsdale Formation, mildly alkaline basalt (Oligocene)
- Tcr — Carpenter Ridge Tuff (Oligocene)
- Tlp — Los Piños Formation (Oligocene)
- Ttc — Chiquito Peak Tuff of Treasure Mountain Group (Oligocene)
- Tt — Treasure Mountain Group, undivided (Oligocene)
- Tcf — Conejos Formation (Oligocene)
- Cinder deposits
- Contact
- Fault—Ball and bar on downthrown block; solid where location certain; dotted where location concealed
- 4.5 Ma — Sample locality with $^{40}Ar/^{39}Ar$ or K-Ar age (table 3)

Figure 79. Geologic map of the Los Mogotes composite shield and surrounding area.

are tentatively identified as Servilleta Basalt of the TPVF based on compositional similarity, whereas alkaline basalt to trachybasalt of the Los Mogotes shield are compositionally similar to Culebra volcano (49.26 weight percent SiO_2; 1.5 weight percent K_2O; sample RGR-150, table 4), the State line vent (51.6 weight percent SiO_2; 1.78 weight percent K_2O; sample RGR-207, table 4), and the silicic alkalic basalt (50.14 weight percent SiO_2; 0.72 weight percent K_2O; sample RGR-40, table 1) observed at the Dunn Bridge along the Rio Grande (Stop 2-6).

The Los Mogotes composite shield is tilted eastward about 5 degrees and rift-related north-trending high-angle faults with dominantly down-to-west displacement offset in the western parts of the shield (fig. 79; Lipman, 1975b). Rift-related faulting indicates continued subsidence of the San Luis Basin following emplacement of Pliocene lavas. It is unclear how much of the currently observed dip in the Pliocene lavas is primary or the result of postemplacement tilting. The mapped distribution of Los Mogotes lavas is more extensive east of vent areas, which suggests a dominantly eastward flow direction. Additionally, Los Piños Formation sediments between the Miocene Hinsdale Formation lavas and overlying Pliocene lavas pinch out to the west, resulting in Pliocene lavas that directly overlie Miocene flows of the Hinsdale Formation. The apparent eastward flow direction of Los Mogotes lavas, and pinchout of the Los Piños Formation sediments, are consistent with an east-sloping paleotopographic surface formed prior to emplacement of Pliocene lavas.

Stratigraphy below the Pliocene lavas in the Los Mogotes area includes, from base to top; Conejos Formation, Treasure Mountain Group, discontinuous ignimbrites from the central San Juan caldera complex, and late Oligocene and Miocene Hinsdale Formation intercalated with Los Piños Formation (fig. 79). The Hinsdale and Los Piños Formations provide a record of Las Mesitas graben infilling concomitant with subsidence following emplacement of the Chiquito Peak Tuff (28.94 Ma). Subsidence of the Las Mesitas graben may have ended prior to emplacement of Hinsdale basalt flows (26.40±0.08 Ma; sample RGR-380, table 3) that erupted from a source in the San Luis Hills; however, the presence of Los Piños Formation above younger Miocene (20.62±0.07 Ma; sample RGR-379, table 3) basalts suggests the area remained a depositional low until after emplacement of the Miocene lavas (fig. 79; see also Stop 3B-2). Accordingly, tilting of the Las Mesitas graben along the western margin of the San Luis Basin did not commence until sometime after 20.62 Ma.

Continue west on CO 17 to the intersection with U.S. 285.

103.4 *Turn left onto U.S. 285 just past the railyard and head south to the Colorado-New Mexico State line.*

109.4 **Stop 3-9. New Mexico-Colorado State line** (36°59.7' N., 105°59.83' W.; 8,039 ft, 2,450 m elevation)

This stop at the New Mexico-Colorado State line provides an excellent view of the western margin of the San Luis Basin, structural high at San Luis Hills, and the northwestern part of the TPVF (fig. 61). The distribution of late Oligocene basaltic flows provides temporal constraints on the inception of tectonism associated with the San Luis Basin and provides paleogeographic control on relations between the San Luis horst and northern Tusas Mountains. The South Piñon Hills, to the northeast, are mantled by a 60-m-thick section of more than 20 thin tholeiitic basalt flows (Thompson and Machette, 1989) with an $^{40}Ar/^{39}Ar$ age of 25.71±0.17 Ma (sample RGR-490, table 3) for the basal flow. Tholeiitic basalts are rare in the Hinsdale Formation (Thompson and others, 1991), but basalts indistinguishable in age (25.67±0.20 Ma; sample RGR-456, table 3) and composition (fig. 62; table 4) are present in the northern Tusas Mountains (fig. 80; Thompson and Lipman, 1994b). In the Tusas Mountains, Hinsdale Formation tholeiitic basalt increases from 2 flows at its most distal location west of Broke Off Mountain, to as many as 10 flows where the unit dips below the surface along the Rio de los Piños (fig. 81). The northeastward increase in flow count suggests that the South Piñon Hills—more than 50 km from the most distal tholeiitic basalt in the Tusas Mountains—were the source area for these lavas at a time when the Tusas Mountains were topographically low relative to the San Luis Hills.

The Los Piños Formation that underlies Hinsdale Formation in the northern Tusas Mountains is of similar age and thickness to deposits filling the Las Mesitas graben north of the Colorado-New Mexico State line (fig. 81). In both areas, the Los Piños Formation is between the Chiquito Peak Tuff and late Oligocene lavas of the Hinsdale Formation (fig. 24). The thickest Los Piños Formation deposits in the northern Tusas Mountains align with the north-south-oriented Las Mesitas graben in southern Colorado. At least 350 m of Los Piños Formation is exposed beneath basaltic andesite lavas at Broke Off Mountain (fig. 81), and gravity inversion modeling suggests the total thickness may be 1,000–1,500 m (for example, Drenth and others, 2011). Models suggest a similar thickness of Los Piños Formation beneath the Los Mogotes volcano in southern Colorado (1,000 m; Drenth and other, 2013). Los Piños Formation deposits beneath Broke Off Mountain in the northern Tusas Mountains are inferred to represent basin-fill of the southern extent of the Las Mesitas graben based on similar thickness and stratigraphic position to Los Piños Formation beneath Los Mogotes in southern Colorado.

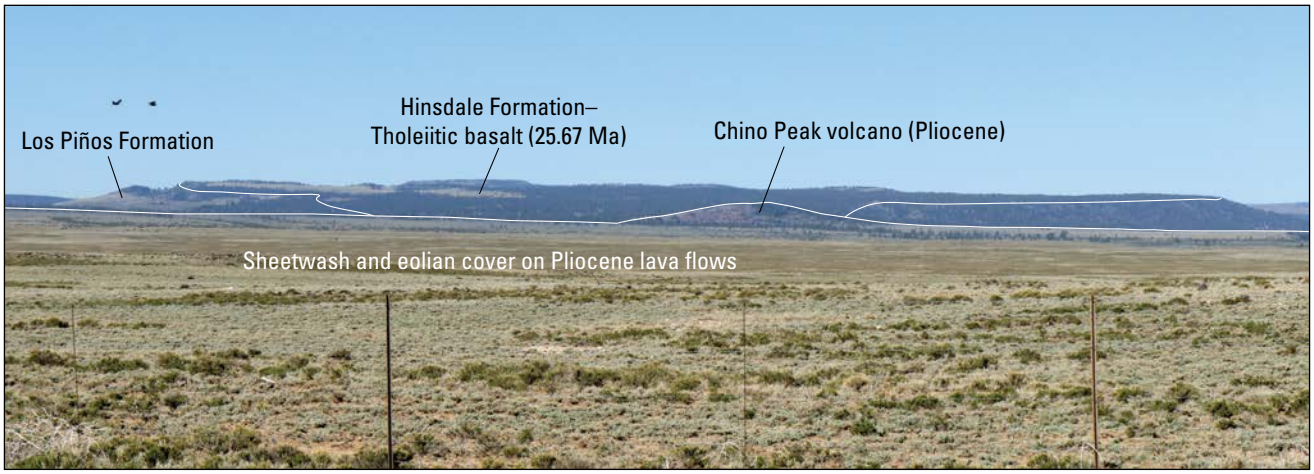

Figure 80. View looking west into the northern Tusas Mountains from U.S 285. Tholeiitic Hinsdale Formation lava flows cap the gently dipping dip-slope surface that rises to the west. Hinsdale lava flows dip about 5–7 degrees to the east and are overlain by Pliocene lava flows that dip about 1–3 degrees to the east. Photograph by K.J. Turner, U.S. Geological Survey, 2012.

The northern Tusas Mountains are thought to have remained a topographic low until after ~20.5 Ma based on an inferred tectonic history similar to that established in the Los Mogotes area. Eastward-tilting of the western basin margin after ~20.5 Ma accompanied subsidence of the San Luis Basin. Tholeiitic basalt in the northern Tusas Mountains, correlated to a San Luis Hills source area, provides a datum for quantitative assessment of subsidence along the western margin of the San Luis Basin. Assuming the tholeiitic basalt had a primary depositional dip to the southwest along a paleosurface (0.75 to 2 percent slope away from the San Luis Hills) and accounting for observed structural displacement, the San Luis Hills (San Luis horst) subsided ~2 km relative to the northern Tusas Mountains. Considering that the San Luis horst is uplifted relative to the rest of the basin interior, 2 km of displacement is considered a minimum.

Continue south on U.S. 285 to the turn off for Pinabetoso Peaks on the left side of the road.

117.1 *Turn left and head west to Pinabetoso Peaks.*

118.6 *Stay left at the fork in the road, continue due east. The road is not maintained after the fork, so use caution if it looks wet. The road forks two more times along route, stay left on both occasions and follow the road onto the north cone of Pinabetoso Peaks. Alternatively, if road conditions are wet, turn right at the first fork in the road and head toward the south cone. The road to the south cone is better maintained and the alternate stop provides an equally impressive view but requires a slightly longer walk from the road.*

119.4 **Stop 3-10. Pinabetoso Peaks** (36°53.42' N., 105°56.33' W.; 8,284 ft, 2,525 m elevation)

The vent complex at Pinabetoso Peaks includes two cinder cones that erupted xenocrystic basaltic andesite (51.25 weight percent SiO_2; 1.33 weight percent K_2O; sample TP505, table 4). Eruptions at Pinabetoso Peaks represent some of the youngest volcanism within the TPVF based on a whole rock $^{40}Ar/^{39}Ar$ age of 2.18±0.15 Ma (sample TP505, table 3) on a sample from the north cone. Although rare throughout most of the TPVF, xenocrystic lavas are common in the northwestern portion of the field. Plagioclase and quartz are the most common xenocrystic minerals and are determined based on grain characteristics, including highly skeletal plagioclase and embayed quartz. Within the area from No Agua Peaks in the south to the Colorado-New Mexico State line to the north, and the area west of Pinabetoso Peaks, at least 13 vent areas erupted lavas with xenocrysts of plagioclase and quartz. A cinder cone at the base of the north flank of San Antonio Mountain, directly west of this stop (fig. 82), erupted xenocrystic trachyandesite (54.62 weight percent SiO_2; 2.65 weight percent K_2O; sample RGR-09, table 4) that contains as much as 1 percent quartz and plagioclase xenocrysts with individual grains as large as 8 mm.

The summit of San Antonio Mountain volcano (3.12 Ma; Lipman and Mehnert, 1979) is 800 m above the elevation of this stop (fig. 82) and is largely composed of dacite to trachydacite lavas (63.46 weight percent SiO_2, 3.14 weight percent K_2O; sample RGR-285, table 4) that contain phenocrysts and glomerocrysts of plagioclase and orthopyroxene. The dacitic lavas flowed over a precursor volcano, or volcanoes,

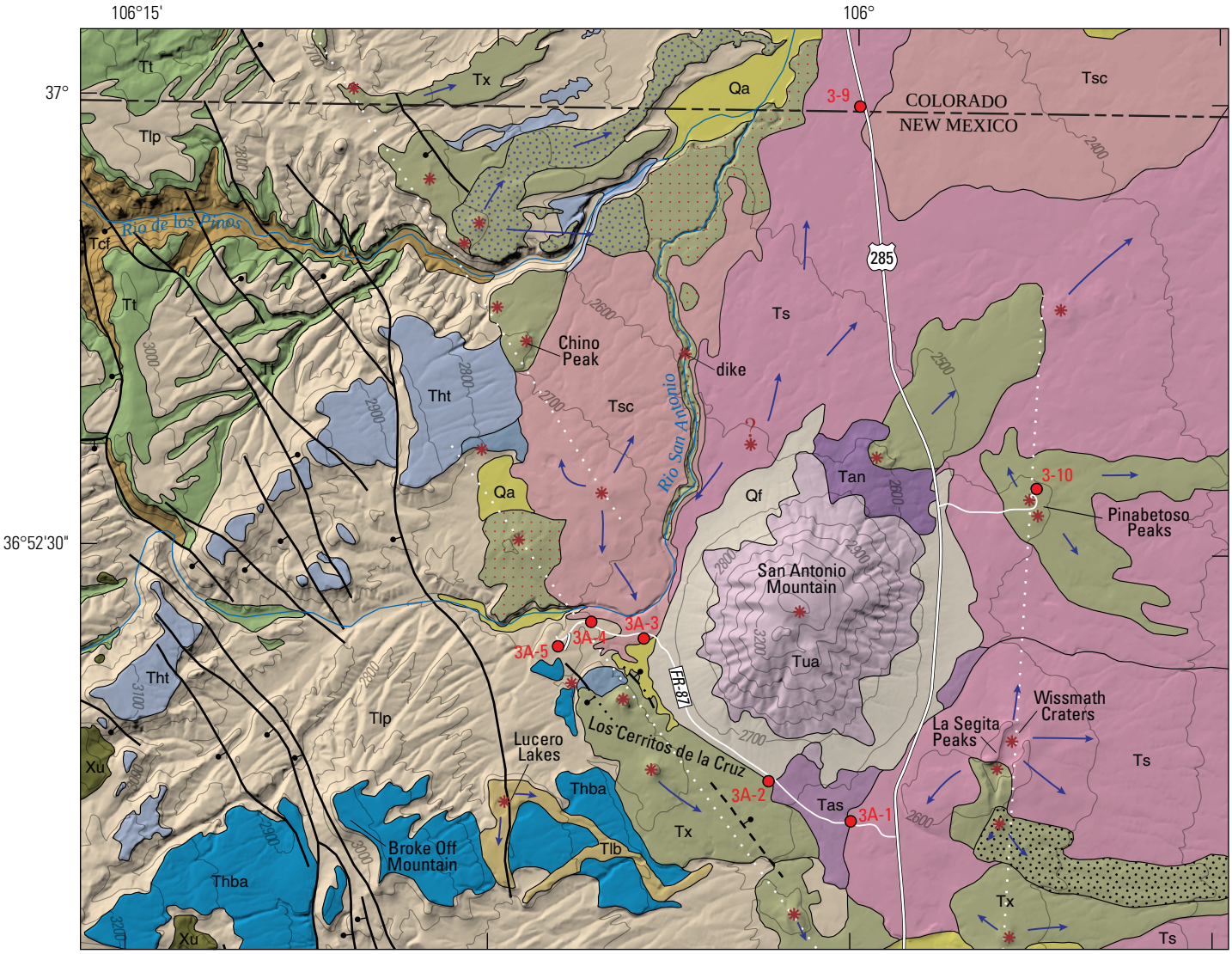

Projection UTM, NAD83 Horizontal Datum, zone 13N, NAVD 1988 Vertical Datum
Shaded-relief base generated from U.S. Geological Survey 10-m Digital Elevation Model (DEM) data from the National Elevation Dataset, accessed November 2016 at http://ned.usgs.gov/.

0 1 2 3 4 KILOMETERS
0 1 2 MILES

Geologic mapping by W.R. Muehlberger, 1968; P.W. Lipman, 1975b; K. Manley, 1982a,b; R.A. Thompson and P.W. Lipman, 1994a,b; and new geologic mapping by K.J. Turner and R.A. Thompson, 2015

EXPLANATION

- Qa — Alluvial and colluvial deposits, undivided (Quaternary)
- Qf — Fan deposits (Quaternary)
- Tua — Upper dacite of San Antonio Mountain (Pliocene)
- Tan — North andesite of San Antonio Mountain (Pliocene)
- Tas — South andesite of San Antonio Mountain (Pliocene)
- Ts — Servilleta Basalt (Pliocene)
- Tsc — Servilleta Basalt, coarse grained (Pliocene)
- Tlb — Basalt of Lucero Lakes (Pliocene)
- Tx — Xenocrystic basalts to trachyandesites, undivided (Pliocene) [patterns used only to correlate outflow to source area]
- Tht — Hinsdale Formation, tholeiitic basalt (Oligocene)
- Tha — Hinsdale Formation, aphyric trachyandesite (Oligocene)
- Thba — Hinsdale Formation, basaltic andesite (Oligocene)
- Tlp — Los Piños Formation (Oligocene)
- Tt — Treasure Mountain Group, undivided (Oligocene)
- Tcf — Conejos Formation (Oligocene)
- Xu — Proterozoic rocks, undivided
- Contact
- Fault—Ball and bar on downthrown block; solid where location certain; dashed where location inferred; dotted where location concealed
- Vent area—Queried where uncertain
- Direction of lava flow
- 3A-1 — Field-trip stop

Figure 81. Geologic map of the northern Tusas Mountains and San Antonio Mountain area. White dotted lines highlight Pliocene vent areas aligned north and northwest, subparallel to faults observed west of the Pliocene lava flows, which suggests buried faults may have been a controlling factor on the location of vent formation.

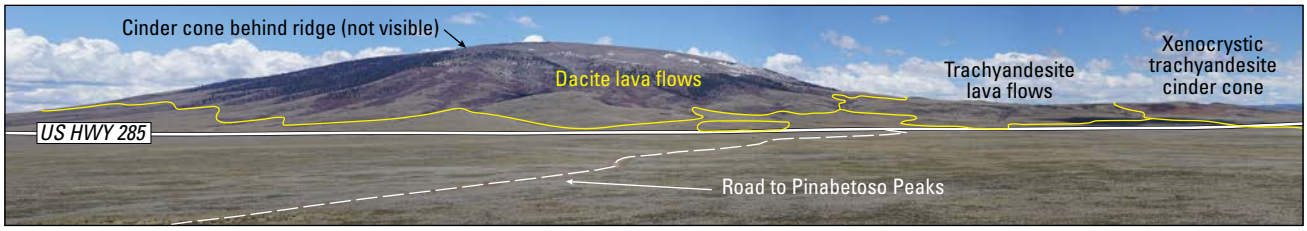

Figure 82. View looking west at San Antonio Mountain. Annotated geology based on geologic mapping by Thompson and Lipman (1994a,b). Dacite to trachydacite lava flows that form the main edifice (~3.1 million years ago [Ma]; Lipman and Mehnert, 1975) flowed over precursor trachyandesite lava flows on the north flank. A cinder cone that formed late in the development of San Antonio Mountain volcano is present near the summit (not visible in from this viewpoint). Eruption of the xenocrystic trachyandesite (2.8 Ma) occurred after formation of the San Antonio Mountain volcano based on geochronologic ages and stratigraphic relations. Photograph by K.J. Turner, U.S. Geological Survey, 2016.

composed of less evolved compositions. Trachyandesite (61.2 weight percent SiO_2; 2.94 weight percent K_2O; sample RGR-231, table 4) flows exposed low on the north flank of San Antonio Mountain (fig. 82) possess the same phenocryst assemblage as overlying dacitic lavas, whereas less evolved trachyandesite (56.57 weight percent SiO_2; 2.6 weight percent K_2O; sample RGR-133, table 4) lavas on the south flank contain plagioclase, olivine, and rare clinopyroxene. Ute Mountain, to the east, is similar to San Antonio Mountain in size, shape, and compositional evolution insomuch as olivine-bearing lava flows at the base of Ute Mountain transition upward to more evolved trachyandesite to trachyte lavas.

Vents in the northwestern portion of TPVF form north- and northwest-alignments parallel to observed faults (fig. 81). For example, as many as 10 vent areas are aligned in a northwest orientation from Red Hill volcano to the Colorado-New Mexico State line. Further, a north-trending alignment of vent areas extends from a xenocrystic vent on the northeast flank of the No Agua Peaks rhyolite domes to a vent north of Pinabetoso Peaks. At the intersection of the two trends are the No Agua Peaks rhyolite domes, the only rhyolite erupted as part of the TPVF. The similarity between faults exposed west of San Antonio Mountain and the north- and northwest-trending vent alignments suggests fault control on vent formation in this portion of the TPVF.

Return to U.S. 285.

121.7 *Intersection with U.S. 285. Turn left and head south.*

124.8 The gently north-sloping surface on the east side of the road is the north flank of the Wissmath Craters-La Segita Peaks composite volcano. The volcano formed from at least three eruptive episodes including, from oldest to youngest, highly xenocrystic basaltic andesite (quartz and plagioclase xenocrysts), sparsely xenocrystic tholeiitic basalt (plagioclase xenocrysts), and xenocrystic basaltic trachyandesite (quartz and plagioclase xenocrysts). Wissmath Craters is a depression at the summit of the tholeiitic basalt shield volcano. In the wall of the southern part of the crater, tholeiitic basalt onlaps flows and cinder deposits of basaltic andesite with abundant xenocrysts of quartz and plagioclase (fig. 83).

128.2 *Intersection with Forest Road (FR) 87. Optional route 3A starts at this intersection and heads west around San Antonio Mountain.*

129.1 To the west (right) of side of the road is the Red Hill cinder cone (fig. 84) that erupted basaltic trachyandesite (51.41 weight percent SiO_2, 1.91 weight percent K_2O; sample RGR-017, table 4). Phenocrysts include plagioclase, olivine, orthopyroxene, and clinopyroxene. Orthopyroxene grains have rims that are completely iddingsitized, which suggests olivine reaction rims may have been present at the time of eruption.

On the left side of the road are the No Agua Peaks rhyolites (73.22 weight percent SiO_2; 4.53 weight percent K_2O; sample RGR-129, table 4) that are the only Pliocene rhyolites erupted on the Taos Plateau (fig. 85). Based on composition and isotopic ratios Dungan (1987) suggest, the No Agua Peaks rhyolites are not cogenetic with other TPVF magmas but were instead derived from crustal melting above a zone of mafic magma accumulation. Dating of glass separates indicates two temporally distinct eruptive sequences at 4.1±0.03 Ma and 3.88±0.06 Ma, whereas single-grain laser-fusion of alkali feldspar grains yielded an age of 25.35±0.13 Ma, which suggests the rhyolites incorporated Amalia Tuff-related phenocrysts from buried outflow deposits (Dickens, 2007). Hydrated rhyolite glass has resulted in an economic deposit of perlite that is actively being quarried.

130.1 Lava flows in the roadcut are tholeiitic basalts that are compositionally similar to Wissmath Craters lava. Lavas above and below the thin sedimentary interbed are compositionally indistinguishable, suggesting the sedimentary interbed may represent a short hiatus between eruptions.

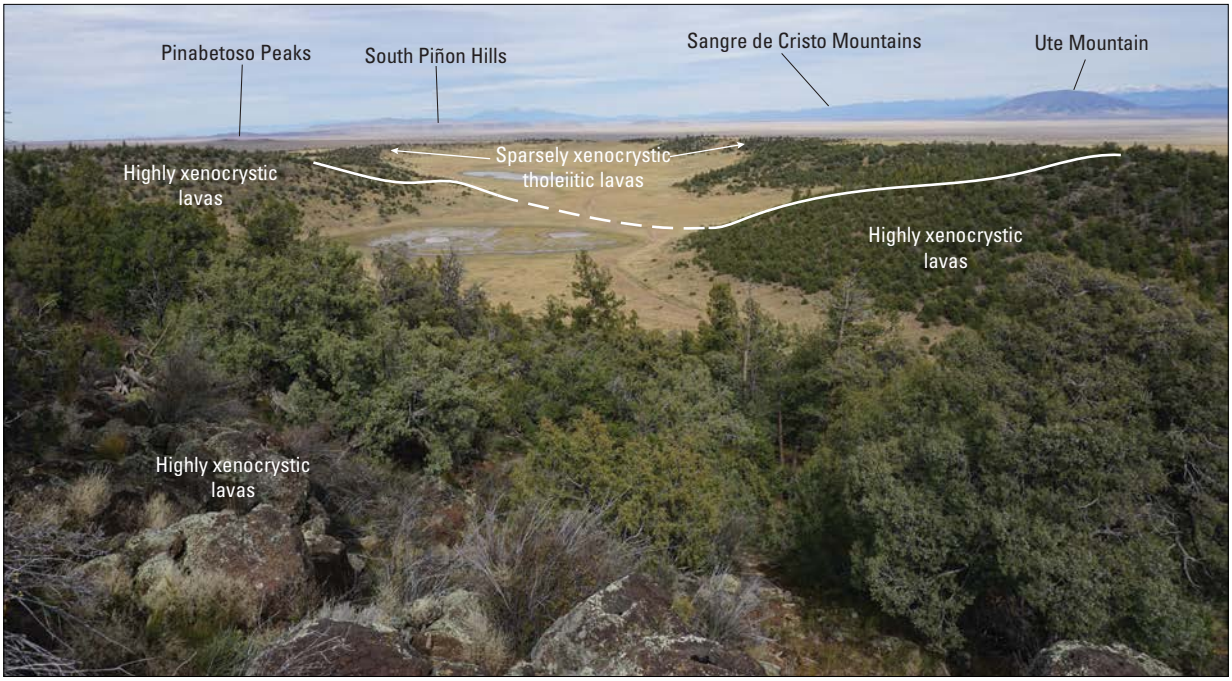

Figure 83. View from La Segita Peaks looking north into Wissmath Craters. The north rim of the crater is composed of sparsely plagioclase xenocrystic tholeiitic basalt. The southern part of the crater is composed of predominantly quartz and plagioclase xenocrystic lavas and cinder deposits that are stratigraphically lower than the tholeiitic lavas. The shield volcano that is the source of the tholeiitic lavas is inferred to have formed on the north flank of the volcano that erupted the highly xenocrystic lavas. Photograph by K.J. Turner, U.S. Geological Survey, 2014.

Figure 84. Red Hill volcano (pictured) is actively being quarried for scoria. Photograph by K.J. Turner, U.S. Geological Survey, 2016.

Figure 85. View looking southeast at No Agua Peaks rhyolites. Dickens (2007) reported compositional and age distinctions between the older north hills stage (4.1 million years ago [Ma]) and the younger west hills stage (3.88 Ma). Ages for the two stages are determined from obsidian, as attempts to date sanidine resulted in ages consistent with the Amalia Tuff (25.39 Ma). The disturbed ground is related to quarrying of perlite. A small cinder cone (left of view) erupted xenocrystic lavas that primarily flowed to the east (fig. 81). Photograph by K.J. Turner, U.S. Geological Survey, 2016.

132.0 The roadcut on the west side of the road exposes outflow from the Red Hill vent. Sediments below the vent include small Apache tears derived from No Agua Peaks rhyolite.

132.9 Cerro del Aire volcano. A flow from near the summit of the volcano is a trachyandesite with pyroxene and olivine phenocrysts and sparse xenocrystic quartz. Two cinder cones reside near the summit; the larger cinder cone is centered within the summit depression. The smaller cinder cone sits on the northeast rim of the central depression and is the source vent for a lava that flowed down the flank of the pre-existing volcano (Lipman and Mehnert, 1975).

135.6 View forward and to the right is of the Tres Piedras Granite (fig. 86), a fine- to medium-grained metagranite that consists of quartz, microcline, albite, muscovite, and biotite (Wobus and Hedge, 1982). U-Pb zircon geochronology indicates an emplacement age of 1.7–1.69 Ga (Davis and others, 2010). The Tres Piedras Granite and other Paleoproterozoic metasedimentary and intrusive rocks in the northern Tusas Mountains are characteristic of the Yavapai province. The Yavapai province and the Mazatzal province (south of the area) record progressive continental assembly by accretion of island arc terranes onto Laurentia between ~1.8–1.6 Ga (Bowring and Karlstrom, 1990; Williams and others, 1999). The boundary between the Yavapai and Mazatzal provinces, which corresponds broadly to the orientation of the Jemez lineament, is a broad transitional zone defined as the area between the northernmost 1.65-Ga deformation in the north and 1.7-Ga basement rocks in the south (Shaw and Karlstrom, 1999; Magnani and others, 2004). The shape of the granite outcrops reflects the paleotopographic surface at the end of the Laramide orogeny before burial by volcanic deposits from the SRMVF and volcaniclastic deposition of the Los Piños Formation.

138.7 *The town of Tres Piedras and the intersection of U.S. 285 and U.S. 64. Turn left onto U.S. 64 and head southeast toward Taos. Alternatively, bathroom facilities are available at the Carson National Forest Ranger Office; turn right and head west on U.S. 64 for 0.6 mi to the Ranger Office on the south side of the road.*

As a point of interest relevant to Day 4, ~8 km south of Tres Piedras, a highly welded ignimbrite with a phenocryst assemblage that includes plagioclase, clinopyroxene, highly altered biotite, and pink quartz is interpreted to have been erupted from the Platoro caldera complex. This distal outcrop is almost 100 km from the rim of the Platoro caldera. Although the ignimbrite has not been dated, given the lack of sanidine and the altered condition of biotite, it is unlike the younger Amalia Tuff from the Questa caldera (25.4 Ma). Incidentally, distal deposits of the Amalia Tuff are also located south and southwest of Tres Piedras. The distal Amalia Tuff—more than 30 km from the inferred, buried western rim of the Questa caldera—are only moderately welded, in contrast to outcrops more proximal to the caldera that are highly welded with highly compacted pumice.

Figure 86. View looking west from U.S. 285 of Tres Piedras granite (1.7–1.69 billion years old; Davis and others, 2010). The resistant granite outcrops rise above the valley floor as Los Piños Formation sediments are eroded. Photograph by K.J. Turner, U.S. Geological Survey, 2016.

End of route 3.

Optional Route 3A

Optional route 3A includes five stops principally focused on Pliocene volcanic rocks in the northwestern part of the TPVF that have characteristics less common throughout the main part of the volcanic field. The final stop west of San Antonio Mountain presents a view of the late Oligocene lavas of the Hinsdale Formation in the northern Tusas Mountains, which provides an opportunity for additional discussion on lava distribution and implications for the late Oligocene paleodrainages.

Mileage for optional route 3A will begin at the intersection of FR 87 and U.S. 285. Head west on FR 87.

1.0 **Stop 3A-1. Trachyandesite of south San Antonio Mountain and tholeiitic basalt of Wissmath Craters**
(36°48' N., 106°0.06' W.; 8,448 ft, 2,575 m elevation)
Park on the side of the road or pull into the small clearing north of the road.

The stop location is in a small gully that has formed along the contact between flow terminations. The high area east of the stop location is composed of tholeiitic basalt erupted from Wissmath Craters (51.38 weight percent SiO_2; 0.58 weight percent K_2O; sample RGR-438, table 4) and the topographically high area immediately west of the parking area (fig. 81) is composed of trachyandesite of south San Antonio Mountain (56.57 weight percent SiO_2; 2.6 weight percent K_2O; sample RGR-133, table 4). The basalt is medium

grained and composed of plagioclase, olivine, and subophitic clinopyroxene with intergranular and weakly diktytaxitic textures. By contrast, the trachyandesite contains a glassy to aphanitic groundmass that contains about 3 percent phenocrysts of plagioclase, olivine, and rare clinopyroxene. Outcrops of the trachyandesite are identified ~60 m up the south flank of San Antonio Mountain, which suggests that the trachyandesite lavas erupted from a volcano now mostly covered by dacitic lava erupted from San Antonio Mountain. The mapped distribution of trachyandesite outflow suggests a north to south flow direction that was confined between pre-existing topographic highs to the east and west (Thompson and Lipman, 1994b). Approximately 300 m north along the dirt road from where vehicles are parked, trachyandesite overlies basalt.

Continue west along FR 87 to small pullout on the southwest side of the road near an earthen dam.

1.7

Stop 3A-2. Trachyandesite of south San Antonio Mountain and outflow from Los Cerritos de la Cruz (36°48.7' N., 106°1.64' W.; 8,612 ft, 2,625 m elevation)

On the southwest side of FR 87 and southeast of the parking area is a knoll composed of trachyandesite of south San Antonio Mountain (fig. 87). Trachyandesite overlying basaltic trachyandesite of Los Cerritos de la Cruz is exposed in the ravine west of the knoll. The gentle slopes west of the ravine are underlain by flows from the south vent of Los Cerritos de la Cruz. Flows and near-vent pyroclastic deposits from the Los Cerritos de la Cruz volcanoes are highly xenocrystic in contrast to the nonxenocrystic trachyandesite. Los Cerritos de la Cruz lava flows are some of the most highly xenocrystic lava flows in the Taos Plateau, with as much as 7 percent xenocrysts that include quartz, plagioclase, alkali feldspar, orthopyroxene with reaction rims to clinopyroxene, and glomerocrysts of clinopyroxene. As much as 3 percent phenocrysts that

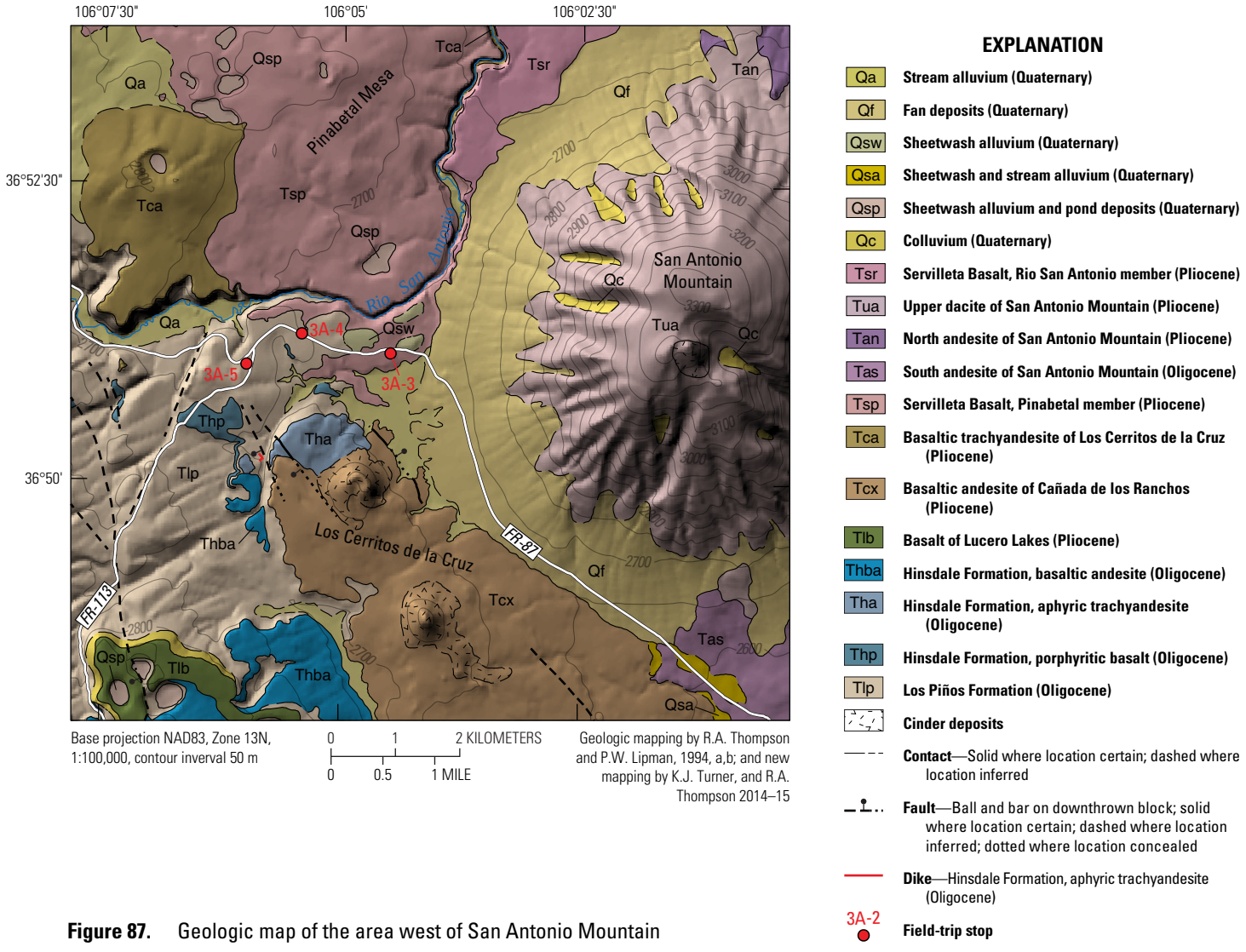

Figure 87. Geologic map of the area west of San Antonio Mountain

include plagioclase, olivine, and rare clinopyroxene are characterized by sharp grain boundaries and solid grain interiors in contrast to embayed or rounded grain boundaries and skeletal interiors in xenocrysts. Although basaltic trachyandesite compositions are most common, the compositional range from both vents includes basalt to trachyandesite (51.40–57.07 weight percent SiO_2, 1.12–2.59 weight percent K_2O; samples RGR-229 and 89T019, table 4). The north cone erupted generally more mafic compositions including basalt to basaltic trachyandesite, whereas the south cone erupted basaltic trachyandesite to trachyandesite. Despite the compositional difference between the two cones, the xenocryst and phenocryst assemblage and content are similar. It is unclear which vent may have erupted first or if the vents erupted simultaneously because stratigraphic relations for outflow from the two vents are difficult to establish. *Continue heading northwest on FR 87.*

4.6 *Intersection with FR 605 on the west side of FR 87.* View to the west is of the north and south cones of Los Cerritos de la Cruz.

6.4 *Intersection with FR 118 on the north side of FR 87. Continue on FR 87 as it curves due west.* As the road heads uphill, a particularly coarse-grained variety of Servilleta Basalt is present south of the road, and north of the road the basalts are draped by Quaternary sheetwash deposits composed almost entirely of remobilized Los Piños Formation volcaniclastic rocks. *Continue heading west on FR 87 for 0.7 mi to the large pullout on the south side of the road.*

7.1 **Stop 3A-3. Coarse-grained Servilleta Basalt** (36°51.07' N., 106°4.82' W.; 8,809 ft, 2,685 m elevation)

Servilleta Basalt is a tholeiitic basalt (49.8 weight percent SiO_2, 0.73 weight percent K_2O; sample RGR-224, table 4) with diktytaxitic to intergranular groundmass textures and a mineral assemblage that includes plagioclase, olivine, pyroxene, and Fe-Ti oxides. However, plagioclase grains are platy and average 4–6 mm (and can be as large as 8 mm) in contrast to more typical Servilleta Basalt in which plagioclase is typically less than 4 mm. This coarse-grained lava flow erupted from a shield volcano with central collapse about 4.4 km north of this site (fig. 87).

Continue heading west on FR 87 to small the pullouts along road. Another small pullout is about 0.1 mi (161 m) farther west if more space is needed.

7.7 **Stop 3A-4. Onlapping relation of coarse-grained Servilleta Basalt on Los Piños Formation** (36°51.21' N., 106°5.36' W.; 8,858 ft, 2,700 m elevation)

Exit vehicles and walk at a bearing of 350°, for about 525 ft (160 m). Surface will change from sediments to a lava flow-capped surface. This contact is the focus of the stop.

The walk from the vehicles to the start of the lava flow is along the weathered upper surface of the volcaniclastic Los Piños Formation (fig. 87). Clasts include andesitic to dacitic volcanic rocks of the Conejos Formation, ignimbrites from the southeast San Juan Mountains, and in some localities (not observed here), clasts of Oligocene lava flows of the Hinsdale Formation and Amalia Tuff. The lack of Amalia Tuff at this locality is consistent with the Esquibel Member, which is sourced from the southeast San Juan Mountains and San Luis Hills. To the south, the presence of Amalia Tuff clasts is diagnostic of the Cordito Member, which is sourced primarily from the Latir volcanic locus (Manley, 1981). Clasts are generally rounded to well-rounded and can range from pebbles to 1 m in diameter; clasts in this area are generally 10 cm or less. The interpretation that these are primary Los Piños deposits is based on bedded Los Piños Formation observed in roadcuts just west of our location and Oligocene pyroxene-bearing porphyritic lavas interbedded within the Los Piños Formation southwest of where the vehicles are parked. The Pliocene lava flows onlap this portion of Los Piños sediments on the north, east, and south sides, which suggests this was a paleotopographic high at the time the coarse-grained Servilleta Basalt was erupted. Due north of this locality, a shallow, steep-sided gorge has been carved by the Rio San Antonio, in which flows as thick as 20 m are exposed, which suggests lavas may have ponded in a topographic low adjacent to the paleotopographic high of Los Piños Formation.

Head back to the vehicles and continue heading west 0.6 mi to a cattle guard. Just past the cattleguard turn left onto FR 133, cattle pens will be on the right. At about the midpoint of the cattle pens turn right into the flat area and park.

8.4 **Stop 3A-5. Pliocene volcanoes and Oligocene paleodrainage in the northern Tusas Mountains** (36°51.02' N., 106°5.94' W.; 8,924 ft, 2,720 m elevation)

Walk 984 ft (300 m) to a high mound south-southwest of the vehicles (bearing of 220°). The walk traverses poorly exposed Los Piños Formation that, on sheetwash covered surfaces, is indicated by pebble- to cobble-sized, rounded volcanic clasts in a light-colored fine- to very fine-grained matrix.

To the north are the flanks of two shield volcanoes (fig. 87). The treeless, grass-covered slopes observed just

west of due north gently climb to the summit crater of the Canada de los Ranchos volcano. The shield volcano erupted basalt to basaltic andesite (49.58–53.77 weight percent SiO_2; 0.55–1.44 weight percent K_2O; samples RGR-434 and RGR-495, table 4) with sparse xenocrysts of quartz and plagioclase. Lava flows are fine grained with intergranular and intersertal textures resulting from pyroxene- or glass-filled areas between plagioclase and olivine grains. The lavas primarily flowed northeast, although some did flow south from the vent.

The second shield volcano holds up the high point just east of due north and is differentiated from the basaltic andesite shield by tree-covered slopes; this volcano is the source of the coarse-grained Servilleta Basalt observed at previous stops. The coarse-grained Servilleta Basalt is stratigraphically above the fine-grained basaltic andesite, which indicates eruption of the basaltic andesite ceased prior to eruption of the coarse-grained basalt. Similar to the basaltic andesite, the basalt flowed north and northeast from the vent, with only minor southward flow that was limited by paleotopographic highs of Los Piños Formation in this area.

To the southeast is the north cinder cone of Los Cerritos de la Cruz. Underlying the north flank of the cone is an aphyric trachyandesite flow of the Hinsdale Formation. This flow is downdropped ~30 m to the southwest across a series of northwest-trending faults. The inferred source of the aphyric lava flow is west of these faults, marked by a dike petrographically indistinguishable from the flow (fig. 87). This trachyandesite is not dated but is interpreted as Oligocene in age on the basis of stratigraphic position. West of the faults, the flow interfingers with Los Piños Formation ~20 m stratigraphically above basaltic andesite with a whole rock $^{40}Ar/^{39}Ar$ age of 26.64 Ma. Field relations suggest the down-to-southwest faults preceded Pliocene volcanism. A lava flow erupted from the north Los Cerritos de la Cruz vent onlaps the paleo-fault scarp and is mostly confined to the downthrown side of the fault but is not displaced. Typical fault displacement of Pliocene lavas in this portion of the Taos Plateau are generally as much as several meters.

End of optional route 3A. Return to the vehicles and follow the route along FR 87 back to U.S. 285.

Optional Route 3B

Optional route 3B is included to further discuss stratigraphic and structural observations related to the development of the Las Mesitas graben and eastward tilting along the western margin of the San Luis Basin, and to look at age and compositional trends on the Los Mogotes composite shield.

Overview of Los Mogotes and Las Mesitas Graben

0.0 *Start at the junction of CO 17 and U.S. 285. Proceed west on U.S. 285.*

5.2 *At the township of Mogote.* The forward view looking west is Los Mogotes volcano (the mounds, in Spanish), described in more detail at Stop 3-8. The high point is a central feeder dike (Lipman, 1975a) of mildly alkaline basalt (49.64 weight percent SiO_2, 1.19 weight percent K_2O; sample RGR-242, table 4), with a whole-rock age of 4.85±0.02 Ma (sample RGR-242, table 3).

8.9 In the cliffs to the right (north) are the thickest Los Mogotes lavas. At least 9 to 10 flows are present but the flow count and thickness changes over short distances, which indicates that paleotopography eroded into the underlying Los Piños Formation influenced emplacement of the earliest lavas.

10.0 The roadcut around the bend ahead exposes intact stratigraphy within a Toreva block in which Pliocene lavas have slid down to road level.

11.3 **Stop 3B-1. Overview of Las Mesitas graben** (37°4.02' N., 106°12.22' W.; 8,366 ft, 2,550 m elevation)

Park in the pullout on the right (north) side of the road.

The view north looks up the Fox Creek drainage, a tributary to the Conejos River that coincides with the western margin of the Las Mesitas graben (see additional discussion in Introduction). On the east side of Fox Creek, Pliocene lavas of Los Mogotes volcano cap the steep slope composed of Los Piños Formation (fig. 88), but farther north up the drainage, at bearing 330°, early Miocene trachybasalt to basaltic trachyandesite flows (51.70 weight percent SiO_2, 1.53 weight percent K_2O; sample RGR-379, table 4) of the Hinsdale Formation form the rim above Los Piños Formation (figs. 88, 89). A whole-rock $^{40}Ar/^{39}Ar$ age of the unit is 20.62±0.07 Ma (sample RGR-379, table 3). The Miocene flows dip 3–5 degrees east, in contrast to overlying Pliocene lavas that are nearly horizontal, which indicates tilting of originally west-dipping flows on this flank of Los Mogotes volcano (fig. 89).

Farther north up Fox Creek on a grass-covered slope (fig. 88), a flow of late Oligocene alkaline basalt (50.4 weight percent SiO_2, 1.35 weight percent K_2O; sample RGR-380, table 4) of the Hinsdale Formation interfingers with Los Piños Formation. The flow has a whole-rock $^{40}Ar/^{39}Ar$ age of 26.40±0.08 Ma (sample RGR-380, table 3) and is interpreted to have erupted from an undetermined source in the San Luis Hills. Late Oligocene basalts and stratigraphically higher Los Piños

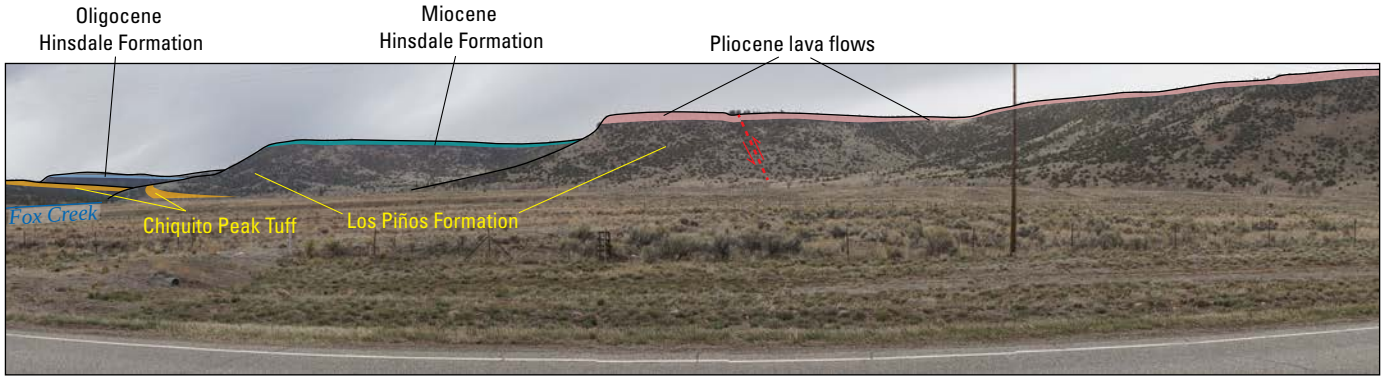

Figure 88. View looking north-northwest up Fox Creek drainage. Colored polygons used to indicate different volcanic units interbedded with Los Piños Formation: pink, Pliocene lava flows likely derived from Los Mogotes volcano; green, Miocene Hinsdale Formation basalt flows; light blue, late Oligocene Hinsdale Formation basalt flows; orange, Chiquito Peak Tuff. The view is subparallel to the axis of a monoclinal bend that brings Chiquito Peak Tuff (on left of view) down to the valley floor east of Fox Creek. Los Piños Formation thickens between the Chiquito Peak Tuff and the overlying late Oligocene Hinsdale Formation basalt flows. Photograph by K.J. Turner, U.S. Geological Survey, 2016.

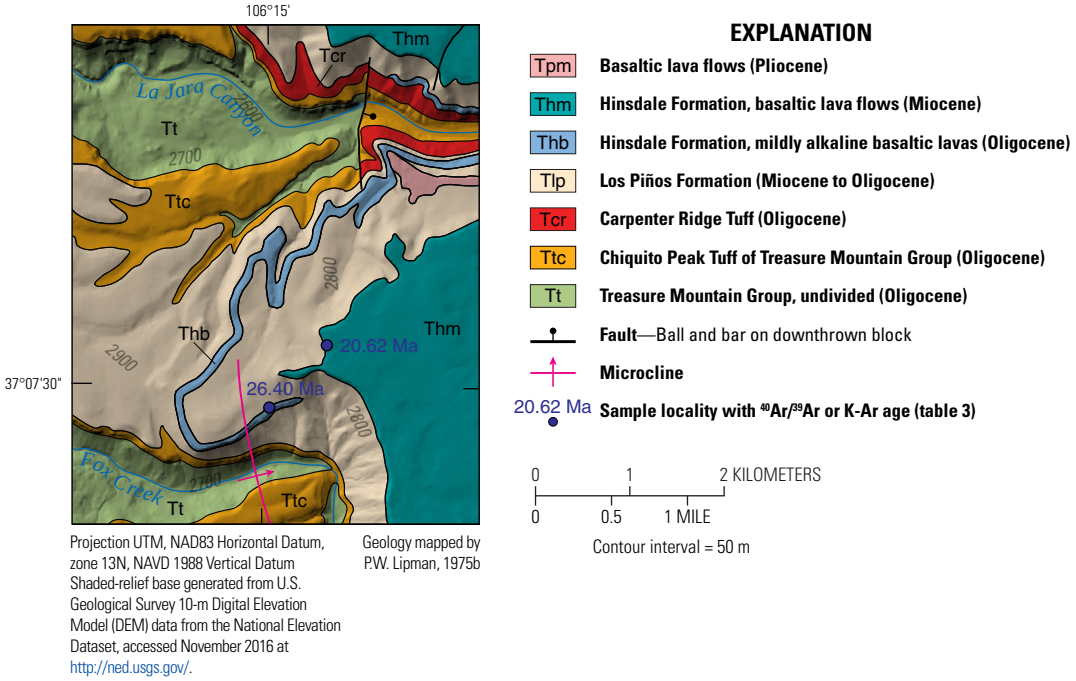

Figure 89. Geologic map of the area between La Jara Canyon (north) and Fox Creek (south) showing the stratigraphic and structural control on the formation of the Las Mesitas graben.

Formation and Miocene basalts consistently dip 5–7 degrees eastward.

Chiquito Peak Tuff, the last major ignimbrite erupted from the Platoro caldera (28.94 Ma), crops out beneath the Los Piños Formation topographically low along Fox Creek (fig. 88). Eastward dips in the Chiquito Peak Tuff increase from about 5–7 degrees to as much as 10 degrees across a monoclinal flexure along Fox Creek, whereas the ignimbrite maintains a constant thickness. Higher in the section, late Oligocene alkaline basalt extends above the monoclinal bend but is undeformed. The overlying Los Piños Formation thickens from 50 m west of the monocline to as much as 160 m on the east side. The monocline in the Chiquito Peak Tuff is interpreted as the western margin of the Las Mesitas graben (fig. 65) that began subsiding sometime after ignimbrite emplacement. Either basin subsidence ceased before emplacement of the Oligocene Hinsdale lavas or later subsidence was minor, because the Oligocene and Miocene flows have similar dips.

Return to the vehicles and head back to Antonito on CO 17.

22.6 *Junction of CO 17 and U.S 285. Continue heading north on U.S. 285 through the town of Antonito.*

26.5 *Intersection with Conejos County Road K on the left side of the road. Turn left and head west.*

29.5 *Intersection with County Road 11, turn right and head north.*

30.1 *Road takes a 90-degree turn to the left, continue on the main road and head west into the canyon. From this point on the road is poorly maintained and a high-clearance vehicle is advised. If it has recently rained, it is advised to abandon the route since roads can be impassible with very little water.*

30.7 *Property boundaries are poorly marked but a side drainage on the north side of the road is in public land managed by the Bureau of Land Management.* The lava flow capping the slope to the north is a medium-grained diktytaxitic to intersertal tholeiitic basalt with fresh green olivine phenocrysts.

31.4 *Y-intersection in the road. Veer left and head to the southwest.*

32.6 *Road climbs up onto Miocene Hinsdale alkaline basalt flow.*

33.1 *Road makes a sharp bend and intersects the unmaintained road at the apex of the turn. Stay on the main road as it bends around.*

33.8 **Stop 3B-2. The Poso; Miocene Hinsdale Formation basalt and Pliocene lava flow stratigraphy** (37°6.72' N., 106°6.31' W.; 8,104 ft, 2,470 m elevation) *Pull vehicles over to the side of the road as far as possible since the road does get ranching traffic that may include wide trailers.*

This topographic depression is called The Poso (the bowl, in Spanish). The Poso rim is formed by Pliocene lavas erupted from multiple vents on the Los Mogotes composite shield. Exposed on the floor of the topographic depression is a Miocene trachybasalt (48.07 weight percent SiO_2, 1.61 weight percent K_2O; sample RGR-245, table 4) stratigraphically equivalent and compositionally similar to the 20.62 Ma trachybasalt and basaltic trachyandesite lavas in Fox Creek at Stop 3B-1. No source is known for this lava but a flow proximal to a vent along the rim of the Platoro caldera near Red Mountain (fig. 61) is compositionally similar (48.30 weight percent SiO_2, 2.23 weight percent K_2O; sample RGR-516, table 4), and age equivalent, within analytical uncertainty (20.53±0.29 Ma; sample RGR-516, table 3).

The Miocene lava in The Poso is interbedded within the Los Piños Formation, in contrast to the area west of Los Mogotes volcano (fig. 79), where Los Piños Formation above the Miocene lavas is absent and Pliocene and Miocene lavas are in direct contact. Los Piños Formation stratigraphically above the Miocene lava flows at this location suggests the Las Mesitas graben remained an area of deposition after emplacement of 20.6–20.5 Ma lavas and places a maximum age on eastward tilting along the western margin related to subsidence of the San Luis Basin. The absence of Los Piños Formation to the west indicates tilting and erosion preceded emplacement Los Mogotes lavas.

West-northwest (bearing ~285°) of the stop location, Pliocene lava flow stratigraphy includes a tholeiitic basalt (49.07 weight percent SiO_2, 0.91 weight percent K_2O; sample RGR-243, table 4) with pahoehoe textures overlying a dense fine-grained intergranular olivine-rich trachybasalt (48.22 weight percent SiO_2, 1.68 weight percent K_2O; sample RGR-244, table 4). The tholeiitic basalt has well-developed diktytaxitic texture and is compositionally similar to Servilleta Basalt. The underlying trachybasalt is compositionally similar to the Los Mogotes feeder dike (49.64 weight percent SiO_2, 1.19 weight percent K_2O; sample RGR-242, table 4), lavas at Flat Top (51.08 weight percent SiO_2, 1.36 weight percent K_2O; sample RGR-241, table 4), and Cinder Pits (50.25 weight percent SiO_2, 1.29 weight percent K_2O; sample RGR-137, table 4). A whole-rock K-Ar age of 4.8±1.4 Ma (sample 67L-16, table 3) was determined for a lava flow on the north rim of the Los Mogotes vent complex and a whole rock $^{40}Ar/^{39}Ar$ age for the dike is 4.85±0.02 Ma (sample RGR-242, table 3). Further, a lava that flowed north from Cinder Pits is 4.8±0.26 Ma (sample 66L-36, table 3). The northward alignment of the vents and similar age and composition of lava flows and the dike suggests a common dike may have fed eruptions of alkaline compositions.

Return to the vehicles and retrace route back to the intersection with County Road K.

32.7 *Intersection with County Road K. Turn left and head east until the intersection with U.S. 285 north of Antonito.*

35.7 *Intersection with U.S. 285. End of optional route 3B.*

Days 4–6 Introductory Summary—The Southern Rocky Mountain Volcanic Field

By Peter W. Lipman[1]

The middle Cenozoic southern Rocky Mountain volcanic field (SRMVF) in Colorado and New Mexico is arguably the best preserved large-volume Cordilleran volcanic field in North America. The SRMVF contains widespread lavas, multiple super-eruption ignimbrites, and exposed subvolcanic granitoid intrusions, all minimally disrupted by subsequent extensional tectonics or obscured by younger sedimentary deposits (fig. 90). The SRMVF has long been studied as a site of middle Cenozoic silicic volcanism on especially voluminous scales (Cross and Larsen, 1935; Larsen and Cross, 1956; Lipman and others, 1970; Epis and Chapin, 1974; Steven and Lipman, 1976; Johnson and others, 1989; McIntosh and Chapin, 2004; Lipman, 2007), including at least 25 ignimbrite sheets (each 150–5,000 cubic kilometers [km^3]) and associated calderas active at 37–23 million years ago [Ma] (table 5). Small granitoid plutons, many spatially and temporally associated with ignimbrite calderas, are exposed at near-roof level; the geometry and composition of a vast, vertically extensive composite batholith beneath the volcanic locus can be constrained by geophysical and geochemical modeling.

The composite SRMVF, now widely erosionally dissected, is among several discontinuous sites of eastern Cordilleran magmatism of middle Cenozoic age, continuing southward through the Mogollon-Datil region in New Mexico (Elston, 1984; Ratté and others, 1984; McIntosh and others, 1992), into Trans-Pecos, Texas (Henry and Price, 1984), and the vast Sierra Madre Occidental of northern Mexico (McDowell and Clabaugh, 1979; Ferrari and others, 2007; McDowell and McIntosh, 2012). The SRMVF is also broadly similar in age, eruption volumes, caldera size, magma composition, and eruption duration to the ignimbrite flareup farther west in the Great Basin (Best and others, 2013, 2016; Henry and John, 2013). The SRMVF was originally comparable to large, young ignimbrite terranes such as the well-documented Altiplano-Puna volcanic complex (APVC) of the central Andes (de Silva, 1989; de Silva and Gosnold, 2007; Salisbury and others, 2011), although exposed more completely in the third dimension because of uplift and tilting along flanks of the Rio Grande Rift and the resulting deep erosional dissection. Based on regional structural setting and petrology of erupted rocks, the SRMV is interpreted as an eastern Cordilleran expression of continental-margin arc magmatism. The ignimbrite flareup coincides with the initial transition from a convergent to an extensional tectonic setting, whereas the Rio Grande Rift includes both basaltic lavas and silicic alkalic rhyolites consistent with its extensional structural environment.

Within the SRMVF, ignimbrite-caldera systems of the San Juan Mountains were the focus of a 1989 International Association of Volcanology and Chemistry of the Earth's Interior (IAVCEI) field excursion (Lipman, 1989) and have been a continuing laboratory for volcanologic and petrologic research, including the southeastern calderas (Platoro complex; Dungan and others, 1989a; Lipman and others, 1996; Tomek and others, 2019; Lipman and Zimmerer, 2019; Gilmer and others, 2021), western calderas (Uncompahgre-Silverton-Lake City; Hon and Lipman, 1989; Bove and others, 2001; Kennedy and others, 2016; Lubbers and others, 2020), and the central cluster (La Garita-Creede calderas; Lipman, 2000, 2006; Bachmann and others, 2002, 2007b, 2014; Streck, 2014; Sliwinski and others, 2017, 2019). Older eruptive centers for ignimbrite volcanism in the Sawatch Range to the north (Shannon, 1988; Toulmin and Hammarstrom, 1990; Johnson and Fridrich, 1990; Fridrich and others, 1991; Zimmerer and McIntosh, 2012a; Mills and Coleman, 2013) and the younger Questa-Latir locus to the south (Lipman, 1988; Tappa and others, 2011; Zimmerer and McIntosh, 2012b) also were sites for an IAVCEI excursion in 1989 (Johnson and others, 1989).

The original areal extent of the SRMVF appears to have exceeded 100,000 km^2, with a total volume of volcanic deposits greater than 60,000 km^3 (Lipman, 2007; Lipman and Bachmann, 2015). Peak magmatic volumes in the SRMVF, associated with ignimbrite eruptions, define a general (if imperfect) progression, from early eruptions along the trend of the Sawatch Range in central Colorado (37–34 Ma), southward into the San Juan region (33–27 Ma), and later to the 25-Ma Latir-Questa locus in northern New Mexico and the 23-Ma Lake City caldera in the western San Juan Mountains (fig. 91). Geophysical data document the presence of several composite subvolcanic batholiths that encompass most calderas of the SRMVF (Plouff and Pakiser, 1972; Cordell and others, 1985; Drenth and others, 2012; Lipman and Bachmann, 2015).

As summarized more fully in Lipman (2007) and references therein, dominantly intermediate-composition lavas and associated breccias (andesite, dacite) were voluminous precursors to most ignimbrite eruptions, and eruption of similar lavas continued concurrently with the major ignimbrites, commonly filling caldera depressions (Steven and Lipman, 1976). Basaltic lavas are virtually absent, despite repeated searches for mafic end-member compositions. Volcanic loci tended to migrate from north to south in the SRMVF, both for intermediate-composition lava eruptions and for ignimbrites (fig. 91, table 5; Lipman, 2007); the southward migration is parallel to that of eruptive centers in the Basin and Range region, probably related to disruption of the subducted Farallon Plate (Stewart and others, 1977; Lipman, 1980; Henry and John, 2013).

[1]U.S. Geological Survey.

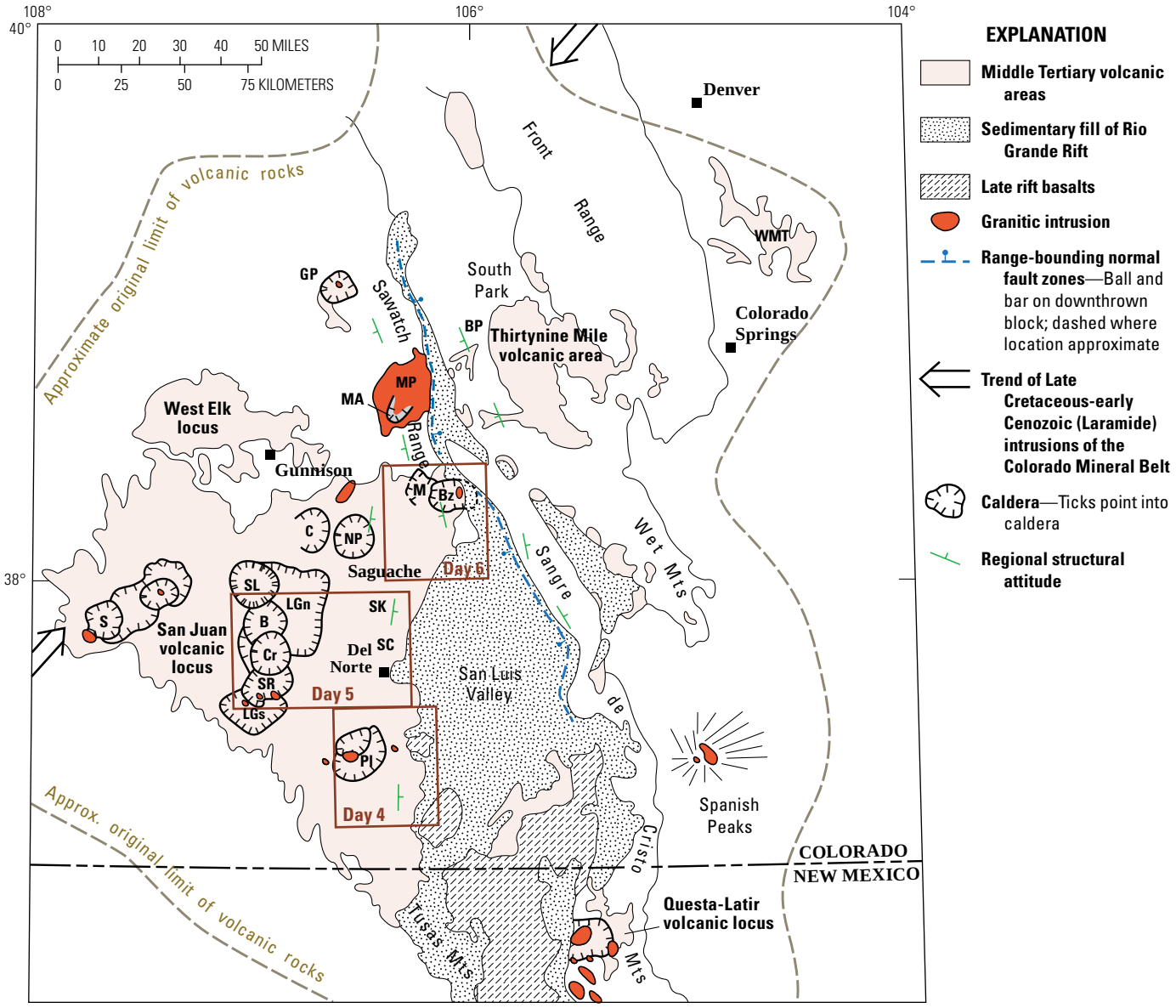

Figure 90. Map of the southern Rocky Mountain volcanic field (SRMVF) and Rio Grande Rift in southern Colorado and northern New Mexico. Also shown are ignimbrite calderas of the SRMVF, major erosional remnants, and inferred original extent of middle Cenozoic volcanic cover (Steven, 1974a), caldera-related granitic intrusions (Tweto, 1979; Lipman, 2007), and later sedimentary fill in asymmetric grabens of the Rio Grande Rift. Rift graben asymmetry and boundary-fault geometry reverse from east-dipping in the San Luis Valley segment to west-dipping in the Sawatch Range segment to the north. Blue-dashed lines, major bounding faults of asymmetrical rift grabens. Calderas: B, Bachelor; Bz, Bonanza; C, Cochetopa Park; Cr, Creede; GP, Grizzly Peak; LGn, La Garita, north segment; LGs, La Garita, south segment; M, Marshall; MA, Mount Aetna; NP, North Pass; Pl, Platoro; S, Silverton; SL, San Luis complex; SR, South River. Other features: BP, Buffalo Peak; SC, Summer Coon volcano; Mts, mountains. Modified from McIntosh and Chapin (2004).

The earliest well-documented regional ignimbrite, erupted from a caldera source in the SRMVF, was the far-traveled Wall Mountain Tuff at 37 Ma (Chapin and Lowell, 1979; Zimmerer and McIntosh, 2012a); the southernmost, and among the youngest ignimbrite eruptions, was the Amalia Tuff from the Questa caldera at 25.1 Ma (Lipman, 1988; Tappa and others, 2011; Zimmerer and McIntosh, 2012b). Structural unroofing associated with later extension along the Rio Grande Rift and deep erosion of this high-standing region, has exposed broadly synvolcanic batholithic intrusions associated with both ignimbrite centers. Geographically and temporally between these early and late centers, the San Juan region contains the largest erosional remnant of the composite Oligocene volcanic field (Larsen and Cross, 1956; Steven and others, 1974a).

Table 5. Summary of regional ignimbrites, caldera sources, and $^{40}Ar/^{39}Ar$ ages in the southern Rocky Mountain volcanic field. Updated and simplified from Lipman (2012, table 1).

[km, kilometers; Ma, million years ago; san, sanidine; bt, biotite; qtz, quartz; hbl, hornblende; Xl, crystal-rich; Xp, crystal-poor; --, no data]

Tuff	SiO_2 (percent)	Ignimbrite			Caldera	
		Rock and phenocrysts	Volume (km^3)	Age (Ma)[a]	Name	Area (km^2)
Latir Mountains, New Mexico						
Amalia	76–77	Peralkaline; qtz, sodic san	500	25.1	Questa	14 × >15
Central San Juan Mountains						
Nelson Mountain	Zoned, 63–74	Xp rhyolite; Xl dacite	>500	26.9	San Luis-Cochetopa	9 × 9, 20 × 25
Cebolla Creek	61–64	Xl dacite; hbl, no san	250	26.9	San Luis complex	14 × 16
Rat Creek	Zoned, 65–74	Xp rhyolite to Xl dacite	150	26.9	San Luis complex	9 × 12
Snowshoe Mountain	62–66	Xl dacite	>500	26.9	Creede	20 × 25
Wason Park	Zoned, 63–72	Xl rhyolite to dacite	>500	27.4	South River	20 × 20
Blue Creek	64–68	Xl dacite; no san	250	~27.45	Concealed	--
Carpenter Ridge	Zoned, 66–74	Xp rhyolite to Xl dacite	>1,000	27.55	Bachelor	25 × 30
Fish Canyon	66–68	Xl dacite; hbl, qtz	5,000	28.0	La Garita	35 × 75
Masonic Park	62–66	Xl dacite; no san	500	28.7	Concealed	--
West San Juan Mountains						
Sunshine Peak	Zoned, 68–76	Qtz, sodic san	200–500	23.0	Lake City	15 × 18
Crystal Lake	72–74	Xp rhyolite	50–100	27.6	Silverton	20 × 20
Sapinero Mesa	72–75	Xp rhyolite	>1,000	28.3	Uncompahgre-San Juan	20 × 45
Dillon Mesa	72–75	Xp rhyolite	50-100	28.5	Uncompahgre?	20 × 20
Blue Mesa	72–74	Xp rhyolite	200–500	28.5	Lost Lakes (buried)	10 × 10
Ute Ridge	66–68	Xl dacite, san	250–500	28.6	Ute Creek	8 × 8
Southeast San Juan Mountains (Treasure Mountain Group)						
Chiquito Peak	64–67	Xl dacite, san	500–1000	28.6	Platoro	18 × 22
South Fork	68–70	Xl dacite, san	50–100	28.8	Platoro/ Summitville?	8 × 12?
Ra Jadero	64–66	Xl dacite, san	150	28.9	Summitville?	8 × 12
Ojito Creek	67–70	Xl dacite, no san	100	~29.5	Summitville?	8 × 12
La Jara Canyon	66–68	Xl dacite, no san	500–1,000	30	Platoro	20 × 24
Black Mountain	67–69	Xl dacite, no san	200–500	30.1	Platoro	--
Northeast San Juan Mountains						
Saguache Creek	73–75	Alkali rhyolite, no bt	250–500	32.2	North Pass	15 × 17
Bonanza	Zoned, 60–76	Zoned: rhyolite-dacite-rhyolite-dacite	1,000	33.1	Bonanza	15 × 20
Thorn Ranch	77	Xl dacite; Xp rhyolite	250–500?	33.9	Marshall Creek	10 × 10?
North-South Sawatch Range trend						
Badger Creek	69–70	Xl dacite	250?	33.9	Mount Aetna	10 × 15
Grizzly Peak	Zoned, 57–77	Xl rhyolite-dacite-andesite	500?	34.3	Grizzly Peak	15 × 17
Wall Mountain	70–73	Xl rhyolite	~1,000	36.9	Mount Princeton	15 × 30?

[a] $^{40}Ar/^{39}Ar$ ages calibrated to Fish Canyon Tuff at 28.02 Ma.

San Juan Magmatic Locus

Preserved volcanic rocks occupy an area of more than 25,000 km^2 in the San Juan Mountains and have a volume of about 40,000 km^3. They cover a varied basement of Precambrian to early Cenozoic rocks along the uplifted and eroded western margin of the Late Cretaceous to early Cenozoic (Laramide) uplifts of the southern Rocky Mountains and adjoining eastern parts of Colorado Plateau (fig. 90). As middle Cenozoic volcanism migrated southward from the Sawatch Range (fig. 91), widely scattered intermediate-composition centers erupted lavas and flanking volcaniclastic breccias starting at 35–34 Ma (Lipman and others, 1970; Lipman and McIntosh, 2008). These rocks, which constitute about two-thirds the volume of the preserved volcanic assemblage, are widely overlain by large ignimbrites associated with calderas collapses (Steven and Lipman, 1976).

The San Juan locus is notable for the large number of large-volume compositionally diverse ignimbrites (cumulatively, ~15,000 km^3) and associated caldera collapses, at least 18 in only a 3-million year (m.y.) interval (30.2–26.9 Ma; table 5). Unzoned uniform crystal-poor rhyolite, crystal-rich dacite (monotonous intermediates), and ignimbrites that grade from initially erupted rhyolite upward into dacite are present is subequal numbers in the San Juan region and the overall SRMVF. Sizable precursor Plinian-fall deposits have not been recognized beneath any of these ignimbrite types.

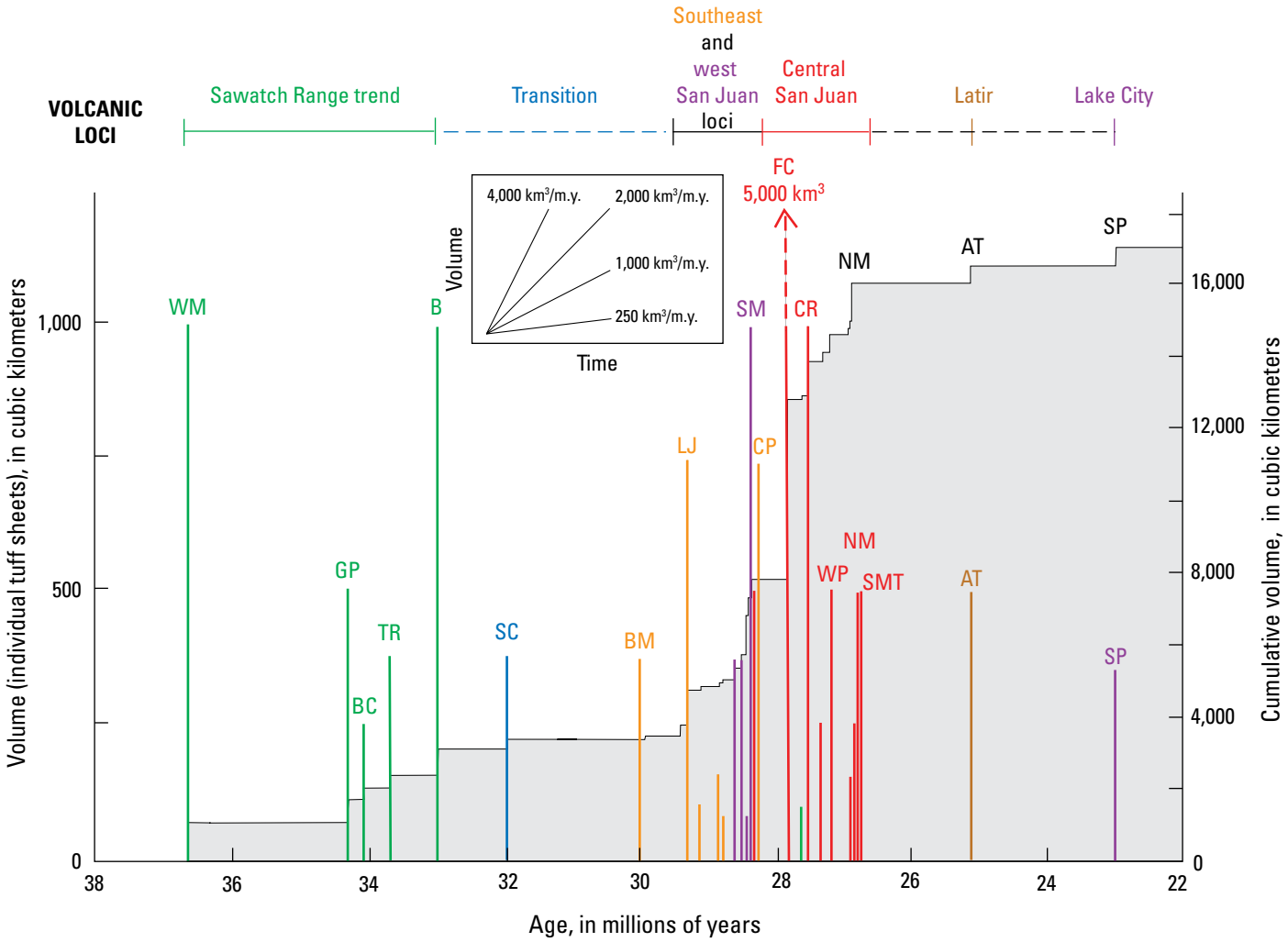

Figure 91. Age-volume plot for large southern Rocky Mountain volcanic field ignimbrites. Overall magma production for ignimbrite eruptions was ~1,000 cubic kilometers per million years (km³/m.y.) from 37 to 22 million years ago (Ma); peak production during eruptions from the central San Juan caldera complex exceeded 4,000 km³/m.y. (Lipman and others, 1996). Peak production, dominated by eruption of the Fish Canyon Tuff at 27.8 Ma, was near mid-stage in the evolution of the volcanic field, as is documented for several other volcanic regions dominated by ignimbrite eruptions. Ignimbrites: AT, Amalia; B, Bonanza; BC, Badger Creek; BM, Black Mountain; CP, Chiquito Peak; CR, Carpenter Ridge; FC, Fish Canyon; GP, Grizzly Peak; LJ, La Jara Canyon segment; NM, Nelson Mountain; SC, Saguache Creek; SM, Sapinero Mesa; SMT, Snowshoe Mountain; SP, Sunshine Peak; TR, Thorn Ranch; WM, Wall Mountain; WP, Wason Park.

After the initial eruptions from Marshall and Bonanza calderas at 33.9 and 33.1 Ma, respectively, in the northeastern San Juan Mountains (fig. 91, table 6), ignimbrite activity migrated southwest with eruption of the Saguache Creek Tuff from the North Pass caldera at 32.2 Ma (Lipman and McIntosh, 2008; Lipman, 2012), then to the Platoro caldera complex in the southeastern San Juan region at 30.1 Ma, followed shortly by eruptions mainly of crystal-poor rhyolitic ignimbrites from western calderas (Steven and Lipman, 1976). Ignimbrite activity became progressively focused in the central San Juan Mountains (table 5), leading to eruption of the enormous Fish Canyon Tuff (5,000 km³ of monotonously uniform crystal-rich dacite) and collapse of the 35 × 75 km La Garita caldera at 28.0 Ma (Lipman, 2000, 2006; Bachmann and others, 2002). In the central San Juan Mountains, seven more eruptions of compositionally diverse ignimbrite, with volumes of 100–1,000 km³, erupted during the 1.1-m.y. interval (28.0–26.9 Ma) from calderas nested within the La Garita caldera (figs. 90, 91). At about 26 Ma, magmatism shifted to a bimodal assemblage dominated by trachybasalt and silicic rhyolite, concurrent with the inception of regional extension along the Rio Grande Rift.

Within the SRMVF, the San Juan magmatic locus provides an exceptional natural laboratory for evaluating the geometry, composition, and emplacement history of intrusive bodies in relation to broadly associated surface volcanism:

- Volcanic rocks are widely preserved but eroded to depths that expose shallow parts of contemporaneous granitoid intrusions.

Table 6. Characteristic features of ignimbrite sheets in the central and northeastern San Juan region.

[Bold type indicates ignimbrite sheets of the Bonanza map area]

Ignimbrite sheet	SiO_2 composition	Textures and phenocrysts
Snowshoe Mountain Tuff	Mafic dacite	Phenocryst rich; densely welded within caldera, weakly welded outflow
Nelson Mountain Tuff	Low-silica rhyolite to dacite	Compositionally zoned; weakly welded crystal-poor to dense crystal-rich
Cebolla Creek Tuff	Mafic dacite	Typically weakly welded; abundant hornblende >> augite is distinctive
Rat Creek Tuff	Low-silica rhyolite to dacite	Compositionally zoned; weakly welded rhyolite to dense dacite
Wason Park Tuff	Rhyolite	Phenocryst-rich rhyolite; tabular sanidine phenocrysts
Blue Creek Tuff	Dacite	Phenocryst rich; sanidine is absent (contrast with Mammoth Mountain Member)
Carpenter Ridge Tuff Mammoth Mountain Member (upper)	Dacite	Phenocryst rich; sanidine is common (contrast with Blue Creek Tuff)
Carpenter Ridge Tuff - Outflow and lower intracaldera tuff	Low-silica rhyolite	Phenocryst poor; common basal vitrophyre, central lithophysal zone
Crystal Lake Tuff	Low-silica rhyolite	Similar to rhyolitic Carpenter Ridge Tuff, but less welded within map area
Fish Canyon Tuff	Dacite	Distinctive light-gray, phenocryst-rich; resorbed quartz, hornblende, absence of augite
Sapinero Mesa Tuff	Low-silica rhyolite	Similar to rhyolitic Carpenter Ridge Tuff, but generally less welded within map area
Dillon Mesa Tuff	Low-silica rhyolite	Similar to rhyolitic Carpenter Ridge Tuff, but generally less welded within map area
Blue Mesa Tuff	Low-silica rhyolite	Similar to rhyolitic Carpenter Ridge Tuff, but generally less welded within map area
Ute Ridge Tuff	Dacite	Phenocryst-rich; contains sparse sanidine (in contrast to Masonic Park Tuff)
Masonic Park Tuff	Dacite	Phenocrysts similar to Blue Creek Tuff; typically less welded
Tuff of Luders Creek	Low-silica rhyolite to dacite	Compositionally zoned; resembles Nelson Mountain Tuff
Saguache Creek Tuff	Low-silica rhyolite	Resembles Carpenter Ridge and Sapinero Mesa Tuffs, but lacks phenocrystic biotite
Bonanza Tuff	Complex zoning	Local basal crystal-poor rhyolite, lower crystal-rich dacite, upper rhyolite, local upper crystal-rich dacite
Thorn Ranch Tuff	Complex zoning	Intracaldera alternation of rhyolite and dacite; outflow mainly high-Si rhyolite
Badger Creek Tuff	Dacite	Crystal rich; resembles Fish Canyon Tuff
Wall Mountain Tuff	Rhyolite	Crystal-rich, large blocky sanidine; locally complexly rheomorphic

- Detailed regional volcanic stratigraphy and abundant petrologic, geochemical, and geochronologic data provide a comprehensive record of eruptive history.
- Rocks of the San Juan locus were emplaced mainly onto the structurally simple Colorado Plateau block that has been broadly stable since craton formation, thereby permitting well-constrained gravity and seismic modeling of subsurface intrusion geometry.
- Isotopic contrasts between the Proterozoic crust and underlying mantle provide robust geochemical tracers for evaluating magma-generation processes.

The SRMVF is currently well documented in terms of field mapping, petrology, geochemistry, geochronology, and geophysical framework, although the vast geographic scale and compositional diversity of its eruptive deposits offer many opportunities for additional studies. The numerous precursor

central volcanoes, compositionally diverse ignimbrites, source calderas, and exposed granitoid intrusions provide an outstanding framework for evaluating variations in magmatic evolution and eruptive behavior.

Many instructive comparisons and contrasts can be drawn with the Jemez Mountains volcanic field, the Bandelier ignimbrites, and Valles Caldera visited on Day 1. Voluminous lavas and volcaniclastic rocks of dominantly intermediate compositions (andesite-dacite) constructed clustered edifices that formed highlands in both volcanic fields, prior to inception of ignimbrite eruptions. In comparison to the Jemez Mountains volcanic field, SRMVF ignimbrites were erupted (1) more frequently, (2) from geographically disparate calderas, (3) in volumes to an order of magnitude larger, and (4) with a wider compositional range (crystal-rich dacites and crystal-poor rhyolites). Although most source calderas in the SRMVF were filled rapidly to overflow by postcollapse lavas and later-erupted ignimbrites, which obscured their constructional morphology, geologically recent excavation of weakly indurated volcaniclastic sediments within a few, such as Creede and Cochetopa Park, has restored present-day topographic expression to near-pristine morphology, comparable to that at the much younger Valles Caldera. Elsewhere in the SRMVF, deep erosional dissection, rugged topography, and structural tilting have also exposed ring faults, upper levels of subvolcanic granitoid intrusions, and other subsurface volcanic structures that can only be inferred from geophysical and other indirect evidence at younger systems such as Valles Caldera.

Some Themes for Discussion During the SRMVF Field Excursions

- The multi-dimensional relations (spatial, compositional, and temporal) between large-volume ignimbrites, their source calderas, and associated intrusions.
- The petrologic diversity of continental-arc ignimbrite volcanism and associated lavas; how do magmatic systems that produce large ignimbrites and calderas evolve with respect to sources, fractionation processes, and resulting eruptible compositions?
- The roles of recycled crystal mush and magmatic cumulates during generation of the erupted magmas.
- Relations between ignimbrites and spatially associated subvolcanic intrusions; do the caldera-associated intrusions record originally deeper nonerupted remnants of the ignimbrite magma bodies, do they represent unrelated younger magmatic pulses, or some combination of protracted mafic recharge, multilevel fractionations, and recurrent magma mixing?
- The contributions of high-precision geochronology to interpretation of relations between regional tectonic and volcanic processes.

Days 4–6 of the IAVCEI excursion will explore these topics, based mainly on field relations in the San Juan locus; on volcanologic, petrologic, geochronologic, and geophysical and thermal-model data obtained for the same region; and by comparisons with other Andean-type arc systems. Field stops will emphasize sites of recent research (since ~1995), especially

1. Polycyclic eruption (30.1–28.6 Ma) of five large-volume regional ignimbrites of the Treasure Mountain Group, caldera-filling lavas, and associated intrusions from the confocal Platoro caldera complex in the southeast San Juan Mountains (Day 4).
2. The enormous La Garita caldera, associated with eruption of the 28.0-Ma Fish Canyon Tuff and its lava-like precursor (Pagosa Peak Dacite), followed by seven successive ignimbrite eruptions (27.5–26.9 Ma) of the central San Juan caldera cluster (Day 5).
3. Older ignimbrites, lavas, granitoid intrusions, and diverse caldera structures exposed at deep levels related to the Bonanza and Marshall calderas (33.9–33.1 Ma) in the northeastern San Juan region (Day 6).
4. More briefly, the Princeton batholith and Aetna caldera, and their relation to the 37-Ma Wall Mountain Tuff and the 34-Ma Badger Creek Tuff erupted from Aetna caldera in the southern Sawatch Range.

Day 4—The Platoro Caldera Complex

By Peter W. Lipman[1], Michael A. Dungan[2], and Matthew J. Zimmerer[3]

Introduction

The Platoro caldera complex (fig. 92) was the initial site for major calc-alkaline ignimbrite eruptions from the arc-related San Juan magmatic locus of the southern Rocky Mountain volcanic field (SRMVF). It offers an exceptional example of focused recurrent eruption and subsidence at an areally restricted site (~20 × 25 kilometers [km]), comparable in size to the younger extension-associated Valles Caldera visited during Day 1. At Platoro, seven major ignimbrites with individual volumes of 75–1,000 km^3 erupted within a period of about 1.5 million years (m.y.; 30.2–28.8 million years ago [Ma]) (Lipman, 1974; Lipman and others, 1996). These ignimbrites are interbedded with roughly twice as many smaller tuff sheets (~5–10 km^3 each), and together are known as the Treasure Mountain Group. The existence of an ignimbrite caldera in the Platoro area was initially reported by Lipman and Steven (1970), then documented in more detail by a geologic map and interpretive report (Lipman, 1974, 1975a). Petrologic studies also provided compositional and isotopic characteristics in relation to changing magma-chamber processes and crustal interactions (Lipman and others, 1978; Dungan and others, 1989a, 1995), but further field, petrologic, paleomagnetic, and geochronologic studies have substantially modified the understanding of the eruptive history at Platoro (Lipman and others, 1996).

Most importantly, the unit depicted as Masonic Park Tuff on the 1970s-era Durango 2-degree and Platoro caldera maps (Steven and others, 1974a; Lipman, 1974) was reinterpreted as including two separate ignimbrites of similar crystal-rich dacite that overlap narrowly in areal extent (fig. 92) but erupted from geographically discrete sources (Lipman and others, 1996). All the tuff in the type area near South Fork, Colorado, and farther to the west, continue to be recognized as Masonic Park Tuff, the initial ignimbrite erupted from the central San Juan caldera cluster. In contrast, the tuff previously depicted as Masonic Park near Platoro caldera, and continuing southward to northern New Mexico, was identified as a slightly younger ignimbrite, the 28.8-Ma Chiquito Peak Tuff of the Treasure Mountain Group that represents the final large explosive eruption from the Platoro caldera complex. The Chiquito Peak and redefined Masonic Park Tuffs largely cover separate areas, but a narrow zone of overlap, a few kilometers wide, roughly coincides with the valley occupied by the South Fork of the Rio Grande (fig. 92; see the detailed geologic map by Lipman, 2006). Along this overlap zone, an abrupt contact can be mapped between the two tuffs on the basis of subtle lithologic contrasts. Intervening bedded tuffaceous sediment is exposed in a hillside excavation at one site, and andesitic lavas (andesite of Sheep Mountain) locally separate the two ignimbrite units at another areally restricted site. The distinction between these two similar-appearing crystal-rich dacitic ignimbrites is based on slight differences in phenocryst assemblages (especially the presence of sparse sanidine in the Chiquito Peak and the absence of this mineral in the Masonic Park), bulk compositions (slightly more silicic for Chiquito Peak), and paleomagnetic pole directions (Lipman and others, 1996).

The present field guide is an update of one prepared for a prior International Association of Volcanology and Chemistry of the Earth's Interior (IAVCEI) field excursion (Dungan and others, 1989a), modified mainly to reflect subsequent interpretive insights summarized by Lipman and others (1996) and more recent geochronologic studies (Lipman and Zimmerer, 2019; Gilmer and others, 2021). The emphasis for Day 4 (and similar themes for subsequent SRMVF days), in comparison with features seen on other days, include

- Clustered large stratovolcanoes that were precursors to ignimbrite eruptions (similar to the Valles and Bonanza caldera cycles).
- Complex stratigraphy and areal distributions of successive large ignimbrite eruptions associated with confocal caldera collapses at the Platoro locus, including five with volumes of 100–1,000 km^3 and many smaller ones with similar dacitic compositions and little or no compositional zoning. In contrast to the central San Juan cluster, the last ignimbrite of the Platoro complex is the most widespread.
- Mapping challenges for locating Oligocene calderas and their margins in comparison to the clear morphologic expression at Valles Caldera (and also Creede caldera).
- Comparisons between regional outflow sheets and thickly ponded intracaldera accumulations of the same ignimbrite deposit and challenges in establishing correlations (for example, Chiquito Peak Tuff) and the potential for confusion (for example, La Jara Canyon Tuff).
- Rapid postcollapse fill (to overflow) of the last Platoro subsidence basin by thickly ponded andesite lava (little to no dacite-rhyolite), with only minor intracaldera volcaniclastic rocks, in contrast to Valles and Creede calderas.
- Hinged trapdoor resurgent uplift of caldera floor, rather than a symmetrical dome (in contrast with Valles and Creede calderas).

[1]U.S. Geological Survey.

[2]University of Oregon.

[3]New Mexico Bureau of Geology & Mineral Resources, New Mexico Institute of Mining & Technology.

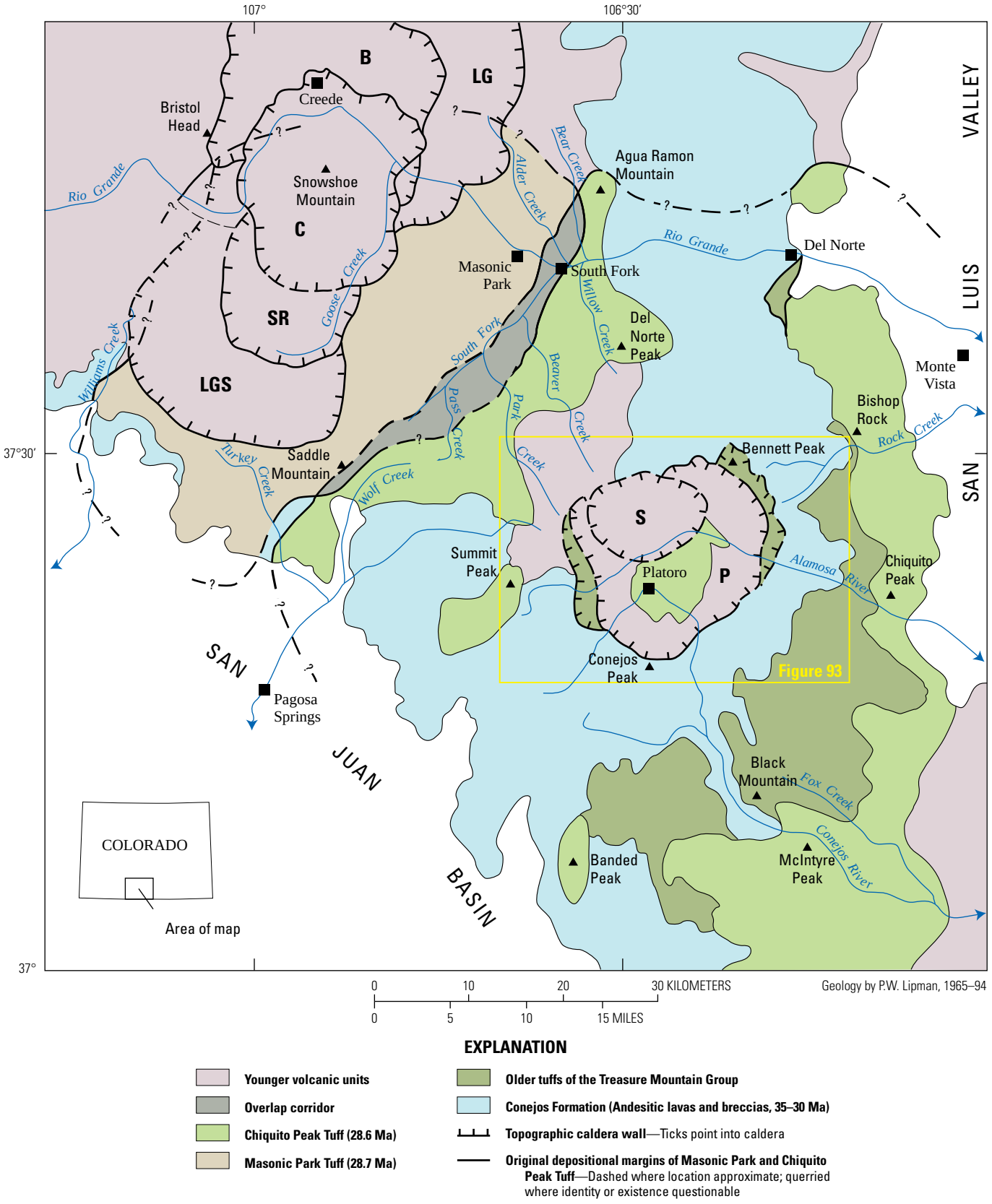

Figure 92. Generalized map of the eastern San Juan region, showing the distribution of the Chiquito Peak and Masonic Park Tuffs in relation to the Platoro caldera complex (P). Some units younger than the Chiquito Peak are not shown in certain locations or are highly generalized, in order to clarify the distributions of the Masonic Park and Chiquito Peak Tuffs. Other calderas include B, Bachelor; C, Creede; LG, La Garita, including its southern extension (LGS); S, Summitville; SR, South River. Modified from Lipman and others (1996).

- Exposure of large granitoid intrusions at high elevations; key evidence for existence of high-standing, postcaldera volcanic constructs and potential samples of batholithic-scale subvolcanic plutons at great depth.
- Multiple, spatially overlapping cycles of alteration and mineralization (~28 and 23 Ma), associated with the intrusive cores of postcaldera volcanoes.
- Prolonged, compositionally diverse postcollapse magmatism, both lavas and intrusions (28–20 Ma).
- A shift to a more-bimodal igneous suite (Hinsdale Formation), concurrent with the inception of regional extension along the Rio Grande Rift.
- Development of a regional dike swarm beyond the western caldera margin and its relation to the transition from an arc to a rift structural setting.
- Inferences about the growth and geometry of caldera-related subvolcanic batholiths.
- Implications of high-precision $^{40}Ar/^{39}Ar$ dating (all Day 4 ages calibrated to Fish Canyon Tuff at 28.201 Ma).
- Petrologic/magmatic evolution, including mantle and crustal components, the role of fractional crystallization, and the assembly and duration of a composite magma body.

Precaldera Volcanism—The Conejos Formation

All intermediate-composition lavas and breccias in the southeastern San Juan Mountains that predate ignimbrite eruptions have long been included in the Conejos Formation (Cross and Larsen, 1935; Lipman, 1975a; Dungan and others, 1989a; Colucci and others, 1991). Although petrographically diverse, compositions of these lavas are dominantly silicic andesite and mafic dacite. No basalts have been identified, despite a search for mafic end members. The cluster of Conejos-age stratovolcanoes in the area that became the Platoro caldera complex has been interpreted as recording the initial rise of intermediate-composition magma bodies to shallow crustal levels, a precursor to ignimbrite volcanism (Lipman and others, 1978). Andesitic and mafic dacitic Conejos lavas in the vicinity of the Platoro caldera complex have been subdivided locally into the Horseshoe Mountain, Rock Creek, and Willow Mountain types on the basis of differences in composition and phenocryst contents (Colucci and others, 1991).

The tuff of Rock Creek (Lipman, 1975a), a local ignimbrite sheet that interfingers with intermediate-composition lavas high on the northeast flank of the Platoro caldera complex (fig. 93), is petrologically similar to directly underlying lavas of the Rock Creek type; it has thus been considered part of the Conejos Formation. This tuff can also be regarded as the initial precursor to more voluminous and silicic ignimbrite magmatism at Platoro because its eruptive source appears to have been within the subsequent caldera complex.

In contrast to the efforts thus far devoted to caldera-related tuffs and lavas, most rocks of the Conejos Formation in the southeastern San Juan region remain crudely mapped, petrologically undocumented, and inadequately dated. For large areas, Conejos Formation rocks have been subdivided only into two broad groups: (1) lavas and proximal breccias that help define locations of primary volcanic constructs, versus more-distal laharic breccias, and (2) fluviatile conglomeratic rocks that form flanking volcaniclastic aprons (Stop 4-4). Sparse K-Ar and $^{40}Ar/^{39}Ar$ ages constrain Conejos activity to about 35–30 Ma. These volumetrically dominant components of the San Juan volcanic locus deserve more thorough study, especially more detailed mapping of the compositional units, definition of discrete volcanic centers, petrologic comparisons among centers, and improved geochronologic constraints on eruptive durations.

Platoro Caldera Complex and Ignimbrites of the Treasure Mountain Group

Multiple ignimbrites from the Platoro caldera complex that spread widely across the southeastern San Juan region were previously designated as members of the Treasure Mountain Tuff (Lipman, 1975a). This approach subdivided the tuff sheets, but only slightly modified the prior nomenclature (undivided Treasure Mountain Rhyolite of Larsen and Cross, 1956), in order to emphasize the pyroclastic nature of these distinctive large-volume units, as well as their eruption from a common caldera source. Several informally designated ignimbrite units were subsequently recognized to be as widespread and voluminous as the formally named members of the Treasure Mountain Tuff (fig. 94). Accordingly, each major named ignimbrite was raised to formational status within the revised Treasure Mountain Group (Lipman and others, 1996). Although all ignimbrites of the Treasure Mountain Group are unequivocally tied to eruptive sources within the Platoro caldera complex, exposed caldera-fill assemblages are associated with only the two largest eruptions, the La Jara Canyon and Chiquito Peak.

Initial Caldera(?) Eruptions—The Lower Rhyolite and Black Mountain Tuffs

The lower rhyolite tuff is a widespread, but discontinuously preserved, ignimbrite sheet of crystal-poor low-silica rhyolite (tables 7, 8). The lower rhyolite tuff is preserved mainly as paleovalley fills in the underlying Conejos Formation. As many as three lithologically similar rhyolite cooling units are present locally, for example near the geographic feature Treasure Mountain. Much of this unit is only weakly welded, but where thick, it can be densely welded (as at Treasure Mountain). The

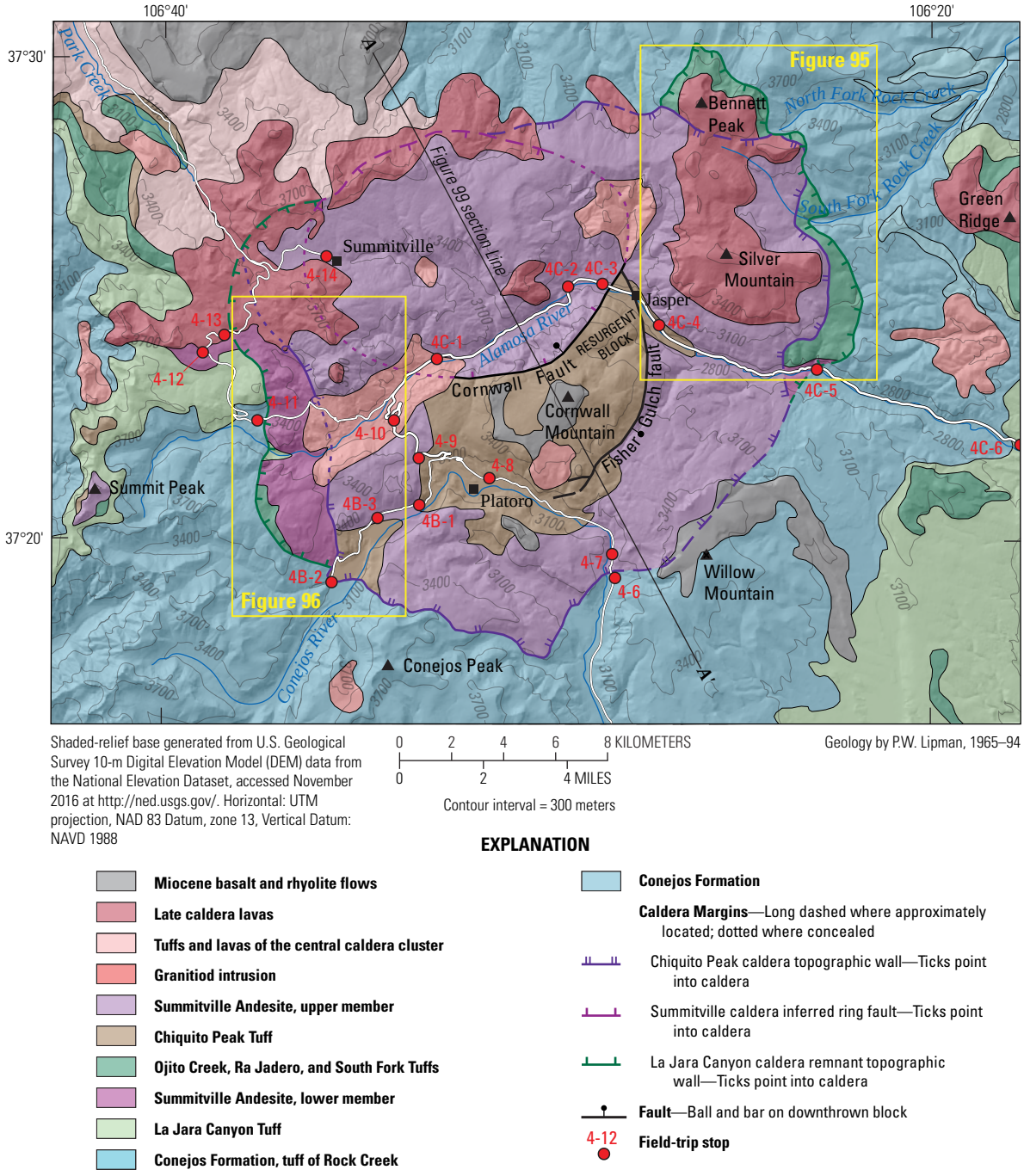

Figure 93. Generalized geologic map of the Platoro complex, showing preserved remnants of successive topographic walls related to eruptions of the La Jara Canyon and Chiquito Peak Tuffs. Surficial deposits and most faults omitted. Modified from Lipman and others (1996).

typical phenocryst assemblage is 5–10 percent plagioclase and sparse biotite; sanidine and quartz are absent (table 7).

The Black Mountain Tuff (Stop 4-1) is a densely welded silicic dacite (67–70 percent SiO_2; table 8) with 20–25 percent plagioclase, biotite, and augite; no sanidine is present. It is widely characterized by large pumice lenses, local lithophysal cavities, and both dacitic and hornblende-bearing andesitic pumice within an upper vitrophyre zone. In accord with the informal nomenclature of Dungan and others (1989a), this unit was named the Black Mountain Tuff for cliff exposures above the Conejos River canyon (Stop 4-3) along the southwest side of Black Mountain (Lipman and others, 1996). Although exposed only discontinuously because of cover by younger units, this ignimbrite sheet is almost as widespread to the south as the largest overlying tuffs. To the west, it is preserved on the south slope of Pagosa Peak, more than 40 km from the margins of Platoro caldera, and

Lipman (1975a)	Dungan and others (1989)	Lipman and others (1996)
Masonic Park Tuff	*Upper dacite of Masonic Park Tuff*	Chiquito Peak Tuff
	Lower dacite of Masonic Park Tuff	*Masonic Park Tuff*
Upper tuff	*Rhyolite unit of Masonic Park Tuff*	South Fork Tuff
Ra Jadero Member	Ra Jadero Member	Ra Jadero Tuff
Ojito Creek Member	Ojito Creek Member	
Middle tuff	Middle member	Middle tuff
	Fox Creek unit	Ojito Creek Tuff
	La Manga unit	
La Jara Canyon Member	La Jara Canyon Member	La Jara Canyon Tuff
Lower tuff	Lower member	
Upper unit	Black Mountain unit	Black Mountain Tuff
Lower unit	Lower unit	Lower rhyolite tuff

Figure 94. Ignimbrites of the Treasure Mountain Group and comparison with previously used geologic names. Italicized unit names not included within the Treasure Mountain Group; all other units considered part of Treasure Mountain.

Table 7. Summary of ignimbrite sheets, postcollapse lavas, and intrusions of the Platoro caldera complex. Modified mainly from Lipman (1975a), Dungan and others (1989a), Lipman and others (1996), and Lipman (2007).

[km^3, cubic kilometers; Ma, million years ago; bt, biotite; cpx, clinopyroxene; hbl, hornblende; pl, plagioclase; qtz, quartz; san, sanidine; n.d., not determined; N, normal polarity; R, reverse polarity]

Unit	Phenocrysts (percent and composition)	Rock composition	Volume (km^3)	Magnetic polarity	$^{40}Ar/^{39}Ar$ age[1] (Ma)
		Intrusions			
Dacite dike, North Mountain	20; pl>qtz, san>bt	Dacite	n.d.	n.d.	20.9
Rhyolite of Grayback Mountain	5–10; qtz,pl,san>bt	Rhyolite	n.d.	n.d.	21.3
Dacite dike, Schnitzel Meadow	20; p>san>bt	Dacite	n.d.	n.d.	26.1
Andesite dike, Rito Gato	15; pl>hbl	Andesite	n.d.	n.d.	27.4
Alamosa River stock	pl>cpx,bt	Granodiorite	n.d.	n.d.	(28)
		Lavas			
Rhyolite of Cropsy Mountain	15–25; pl,qtz,san>bt	Rhyolite	n.d.	n.d.	(20)
Dacite of South Mountain	20–25: pl>san,qtz,bt	Dacite	n.d.	n.d.	(23)
Dacite, Cat Creek volcano	15–25; pl>bt, cpx	Dacite	n.d.	n.d.	(28.5)
Dacite of Park Creek	15–25; pl>bt, cpx	Dacite	n.d.	n.d.	n.d.
Summitville Andesite, upper	0–15; pl>cpx	Andesite-dacite	n.d.	n.d.	n.d.
Summitville Andesite, lower	0–10; pl>cpx	Andesite	n.d.	n.d.	n.d.
Dacite of Fisher Gulch	20; pl>bt,cpx>san	Dacite	n.d.	n.d.	28.7
		Ignimbrite sheets			
Chiquito Peak Tuff	25–35; pl>bt>cpx, san	Dacite	1,000	R	28.8
South Fork Tuff	15–20; pl>bt>cpx, san	Low-silica rhyolite	50–100	R	28.9
Ra Jadero Tuff	20–25; pl>bt>cpx, san	Dacite	150–200	R	29.1
Ojito Creek Tuff	20–25; pl>bt>cpx	Dacite-rhyolite	100–150	N	n.d.
Middle tuff	5–10; pl>bt	Dacite	25–50	N/R	29.8
La Jara Canyon Tuff	25–35: pl>bt>cpx	Dacite	1,000	R	n.d.
Black Mountain Tuff	20–25; pl>bt>cpx(hbl)	Dacite	300–400	R	30.2
Lower rhyolite tuff	5–10; pl>bt	Low-silica rhyolite	25–50	n.d.	n.d.

[1]Some $^{40}Ar/^{39}Ar$ ages from Lipman and Zimmerer (2019); older K-Ar ages in parentheses.

Table 8. Representative chemical analyses of ignimbrite sheets, postcollapse lavas, and intrusions of the Platoro caldera complex.

[-, no data; Ma, million years ago; ppm, parts per million; LOI, loss on ignition; >, greater than; ages in parens based on stratigraphic sequence]

Sample	Unit	Sample location	Age (Ma)	Data source[1]	Major oxides normalized to 100 weight percent, without LOI										LOI	Total	Trace elements (ppm)							
					SiO_2	TiO_2	Al_2O_3	$FeTO_3$	MgO	CaO	Na_2O	K_2O	P_2O_5	MnO			Nb	Zr	La	Ce	Y	Ba	Rb	Sr
Postcaldera lavas																								
70L-115B	Rhyolite of Grayback Mountain	Northeast of Summitville	21.2	1	76.6	0.06	13.3	0.97	0.08	0.23	4.4	4.3	0.00	0.10	0.45	100.0	-	-	-	-	-	-	-	-
P 39	Rhyolite of Cropsy Mountain	Cropsy Mountain	21	2	70.73	0.51	14.64	1.78	0.85	2.36	4.29	4.66	0.18	0.00	2.51	100.0	-	-	-	-	-	-	-	-
SM 291	Dacite of South Mountain	South Mountain	23.0	3	68.4	0.53	15.1	3.6	0.7	2.8	4.0	4.3	0.41	0.12	2.9	100.0	-	-	-	-	-	-	-	-
SM 244	Dacite of Park Creek	Upper Park Creek	28–27.6	3	60.5	0.89	17.3	6.3	1.9	5.7	3.7	3.0	0.52	0.22	2.7	100.0	-	-	-	-	-	-	-	-
66L-48A	Andesite of Green Ridge	South slope, Jacobs Hill	~28	1	58.9	0.97	17.2	7.4	3.0	6.4	2.8	2.9	0.30	0.10	1.1	100.0	-	-	-	-	-	-	-	-
71J-1	Summitville Andesite	Saddle Creek road	(28)	1	56.6	1.1	17.9	8.2	3.2	6.4	3.4	2.8	0.41	0.15	1.4	100.0	-	-	-	-	-	-	-	-
71L-38	Dacite of Fisher Gulch	Platoro road	28.7	1	62.5	0.73	18.3	4.2	1.5	4.3	4.0	4.2	0.17	0.11	1.8	100.0	-	-	-	-	-	-	-	-
Postcaldera intrusions																								
66L-15	Sanidine-dacite plug	South of Jacobs Hill	26.5	1	67.6	0.40	16.4	3.2	1.1	3.6	3.9	3.5	0.22	0.04	0.49	100.0	-	-	-	-	-	-	-	-
SRM-24	Alamosa River granodiorite	North of Stunner Pass	28.0	4	60.29	0.94	15.86	6.45	3.50	5.38	3.40	3.75	0.31	0.12	1.49	100.0	14	243	39	84	26	783	103	601
SRM-23	Resurgent dacite	Robinson Gulch	(28.6)	4	64.63	0.58	16.41	4.06	1.37	4.56	3.96	4.07	0.22	0.13	3.23	100.0	13	214	36	66	20	986	85	573
Treasure Mountain Group																								
93L-14	Chiquito Peak Tuff	Platoro Reservoir (intracaldera)	28.6	5	63.99	0.61	17.24	4.61	1.06	4.04	4.34	3.73	0.26	0.10	3.01	100.0	10	225	31	64	22	1,050	79	700
93L-11B	Chiquito Peak Tuff	Beaver Creek (outflow)	28.6	5	64.36	0.59	16.67	4.35	1.38	4.06	3.69	4.53	0.26	0.12	3.43	100.0	12	215	42	65	24	1,000	93	570
MAD-139	South Fork Tuff	Willow Creek	28.7	6	72.5	0.35	15.27	0.71	0.16	0.81	4.1	5.94	0.10	0.02	-	100.0	18	373	51	102	30	825	175	229
MAD-1	Ra Jadero Tuff	Southwest of Chiquito Peak	28.8	6	65.5	0.72	17.26	3.78	0.99	2.40	3.3	5.80	0.19	0.09	-	100.0	20	423	53	107	37	1,062	181	435
MAD-148	Ojito Creek Tuff	Ojito Creek	-	6	67.1	0.62	16.56	2.98	0.82	2.07	4.2	5.42	0.14	0.11	-	100.0	13	303	43	86	34	1,137	121	403
MAD-57	La Jara Canyon Tuff	West of La Jara Reservoir	(29.9)	6	63.9	0.63	17.64	4.42	1.39	3.60	4.2	3.88	0.16	0.13	-	100.0	11	292	39	77	28	1,125	99	656
MAD-69	Black Mountain Tuff	Black Mountain	30.1	6	68.3	0.42	16.49	2.72	0.74	1.90	3.8	5.47	0.10	0.09	-	100.0	19	432	52	110	39	994	187	377
MAD-54	Lower tuff	South Fork Rock Creek	>30.1	6	73.8	0.24	14.15	1.44	0.29	0.88	2.9	6.17	0.03	0.07	-	100.0	18	221	56	107	32	412	187	162

[1]Data sources: 1, Lipman, 1975a; 2, Patton, 1917; 3, Steven and Ratte, 1960; 4, Lipman, unpub.; 5, Lipman and others, 1996; 6, Dungan, unpub.

farther than any overlying ignimbrite of the Treasure Mountain Group. An $^{40}Ar/^{39}Ar$ age of 30.19±0.16 Ma (table 9) on hornblende from the upper vitrophyre of this tuff documents the inception of major ignimbrite eruptions from the Platoro caldera complex after a pause of about 2 m.y. since the last ignimbrite erupted from the southern end of the broad Sawatch Range trend (the Saguache Creek Tuff at 32.2 Ma; Stop 6A-2).

Areal distributions, thickness changes, and distributions of proximal versus distal facies of the lower rhyolite tuff and the Black Mountain Tuff demonstrate that they were erupted from the Platoro caldera complex and deposited to their maximum thicknesses in broad valleys between Conejos Formation volcanic edifices (fig. 9 in Lipman, 1975a). Both of these tuff sheets have sufficiently large outflow volumes (lower rhyolite tuff, ~25–50 km^3; Black Mountain Tuff, ~300–400 km^3; table 7) to suggest that associated calderas formed. If the Black Mountain Tuff ponded thickly within its source subsidence depression, as is typical in more fully exposed calderas in the SRMVF and elsewhere, the total Black Mountain Tuff volume could have been >600 km^3.

La Jara Canyon Tuff and Evidence for Caldera Collapse

The La Jara Canyon Tuff (Stop 4C-6) is an exceptionally widespread and voluminous ignimbrite sheet of phenocryst-rich dacite (25–35 percent plagioclase, biotite, and augite), with an estimated original volume of 1,000 km^3 (table 7). The La Jara Canyon is the first major tuff sheet for which evidence of collapse is preserved at the Platoro complex. This ignimbrite cannot be dated precisely by $^{40}Ar/^{39}Ar$ methods because of the absence of sanidine, but its age is bracketed between 30.2 and 29.9 Ma by dates from underlying and overlying tuffs (Black Mountain Tuff and middle tuff, respectively, in table 9). Most exposed features within the caldera complex were initially interpreted as related to the La Jara Canyon eruption, including much of the preserved caldera wall and the resurgently uplifted block of thick intracaldera tuff (Lipman, 1975a). Further work demonstrated, however, that the tuff on the resurgent block is the younger Chiquito Peak Tuff and that most exposed features of the caldera complex resulted from this eruption (Lipman and others, 1996).

Table 9. $^{40}Ar/^{39}Ar$ age determinations for ignimbrite sheets, postcollapse lavas, and intrusions of the Platoro caldera complex. All ages calibrated to Fish Canyon Tuff at 28.201 Ma. Ages in italic are from Lipman and others (1996). All other ages from Lipman and Zimmerer (2019).

[-, not available; d dm, degrees and decimal minutes; Ma, million years ago]

Sample	Unit	Location	Latitude N (d dm)	Longitude W (d dm)	Mineral	Method	Age (Ma)
			Distal Platoro dikes				
15L-33	Dacite	Silver Creek	37°25.53	106°45.72	Sanidine	Isochron	26.44±0.06
15L-61	Dacite	Rio Blanco	37°16.40	106°44.52	Sanidine	Mean	26.49±0.06
15L-61	Dacite	Rio Blanco	37°16.40	106°44.52	Biotite	Isochron	26.78±0.03
			Proximal postcaldera intrusions				
11L-22	Dacite dike, South Mountain type	West slope, South Mountain	37°25.46	106°36.96	Sanidine	Mean	20.44±0.02
11L-23	Sanidine dacite dike	Schinzel Flats	37°23.88	106°33.94	Sanidine	Isochron	26.25±0.04
KF-132	*Sanidine dacite dike*	*Schinzel Flats*	*37°23.88*	*106°33.94*	*Sanidine*	*Mean*	*26.49±0.07*
SRM-33	Porphyritic granodiorite	Elwood Creek	37°24.99	106°42.59	Biotite	Isochron	26.61±0.01
			Postcaldera lavas				
11L-20	Rhyolite lava (Hinsdale)	Grayback Mountain	37°27.67	106°33.27	Sanidine	Mean	21.32±0.02
11L-19	Dacite of North Mountain	Park Creek	37°26.41	106°38.42	Sanidine	Mean	20.87±0.02
KF-58	*Intracaldera dacite of Fisher Gulch*	*Fisher Gulch*	*37°20.30*	*106°28.80*	*Sanidine*	*Mean*	*28.74±0.09*
			Treasure Mountain Group				
MD-8a	*Chiquito Peak Tuff, intracaldera*	*Platoro Reservoir*	*37°19.11*	*106°35.67*	*Sanidine*	*Mean*	*28.81±0.07*
11L-27	Chiquito Peak Tuff	The Canyon	37°23.14	106°15.55	Sanidine	Mean	28.77±0.03
MD-192	*Chiquito Peak Tuff, outflow*	*North of Bishop Rock*	*37°29.80*	*106°16.90*	*Sanidine*	*Mean*	*28.77±0.07*
05L-33	South Fork Tuff	Alder Creek	37°35.76	106°40.88	Sanidine	Mean	28.86±0.14
MD-167	*South Fork Tuff*	*East side, Bennett Peak*	*37°40.88*	*106°37.56*	*Sanidine*	*Mean*	*28.92±0.07*
11L-26	Ra Jadero Tuff	East of Terrace Reservoir	37°22.14	106°16.21	Sanidine	Mean	29.12±0.07
MD-165	*Ra Jadero Tuff*	*East side, Bennett Peak*	*37°24.60*	*106°29.20*	*Sanidine*	*Mean*	*29.12±0.07*
MD-43	*Ra Jadero Tuff*	*Dog Mountain*	*37°36.40*	*106°21.20*	*Sanidine*	*Mean*	*29.15±0.07*
MTM74	*Middle Tuff*	*Alamosa Creek*	*37°21.14*	*106°15.97*	*Sanidine*	*Mean*	*29.93±0.03*
11L-7B	Black Mountain Tuff	Rock Creek	37°28.50	106°18.79	Hornblende	Plateau	30.19±0.16
			Conejos Formation, southeast San Juan region				
15L-31	Cobble, upper conglomerate	Wolf Creek, Highway 160	37°28.08	106°52.51	Plagioclase	Isochron	30.59±0.09
15L-32	Basal dacitic breccia	Treasure Falls	37°26.63	106°52.66	Biotite	Isochron	35.43±0.09
15L-32	Basal dacitic breccia	Treasure Falls	37°26.63	106°52.66	Hornblende	Isochron	35.41±0.07

Remnants of the La Jara Canyon caldera that have escaped later burial include a lenticular scallop along the northeast caldera wall and three small tuff remnants deposited against the southwest wall (fig. 93). The northeast scallop, about 12 km long and 1 km wide, is marked by intracaldera lavas and overlying ignimbrites (Ojito Creek, Ra Jadero, and South Fork Tuffs) banked unconformably against an irregular southwest-concave slope that truncates the flanks of several Conejos-age volcanoes (fig. 95; Stop 4C-5). Small remnants of the La Jara Canyon caldera fill are also preserved along the western margin of the Platoro complex, specifically in Gold Creek, along the upper Alamosa River, and near Prospect Mountain (fig. 96; Stop 4-11).

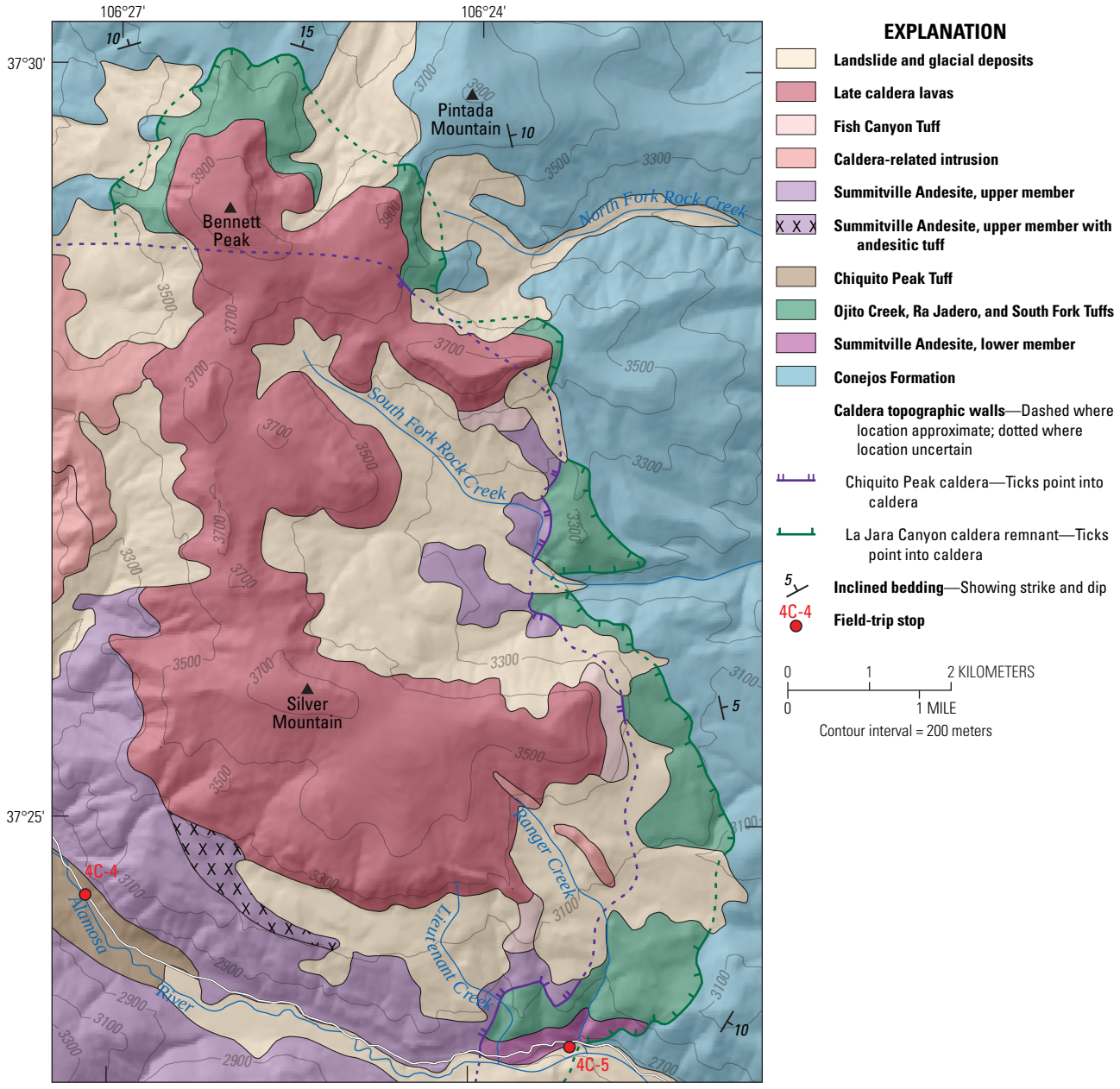

Shaded-relief base generated from U.S. Geological Survey 10-m Digital Elevation Model (DEM) data from the National Elevation Dataset, accessed November 2016 at http://ned.usgs.gov/. Horizontal: UTM projection, NAD 83 Datum, zone 13, Vertical Datum: NAVD 1988

Geology by P.W.Lipman, 1965–94

Figure 95. Geologic map of northeastern margin of the Platoro complex, showing preserved remnants of successive topographic walls related to eruption of the La Jara Canyon and Chiquito Peak Tuffs. Modified from Lipman and others (1996).

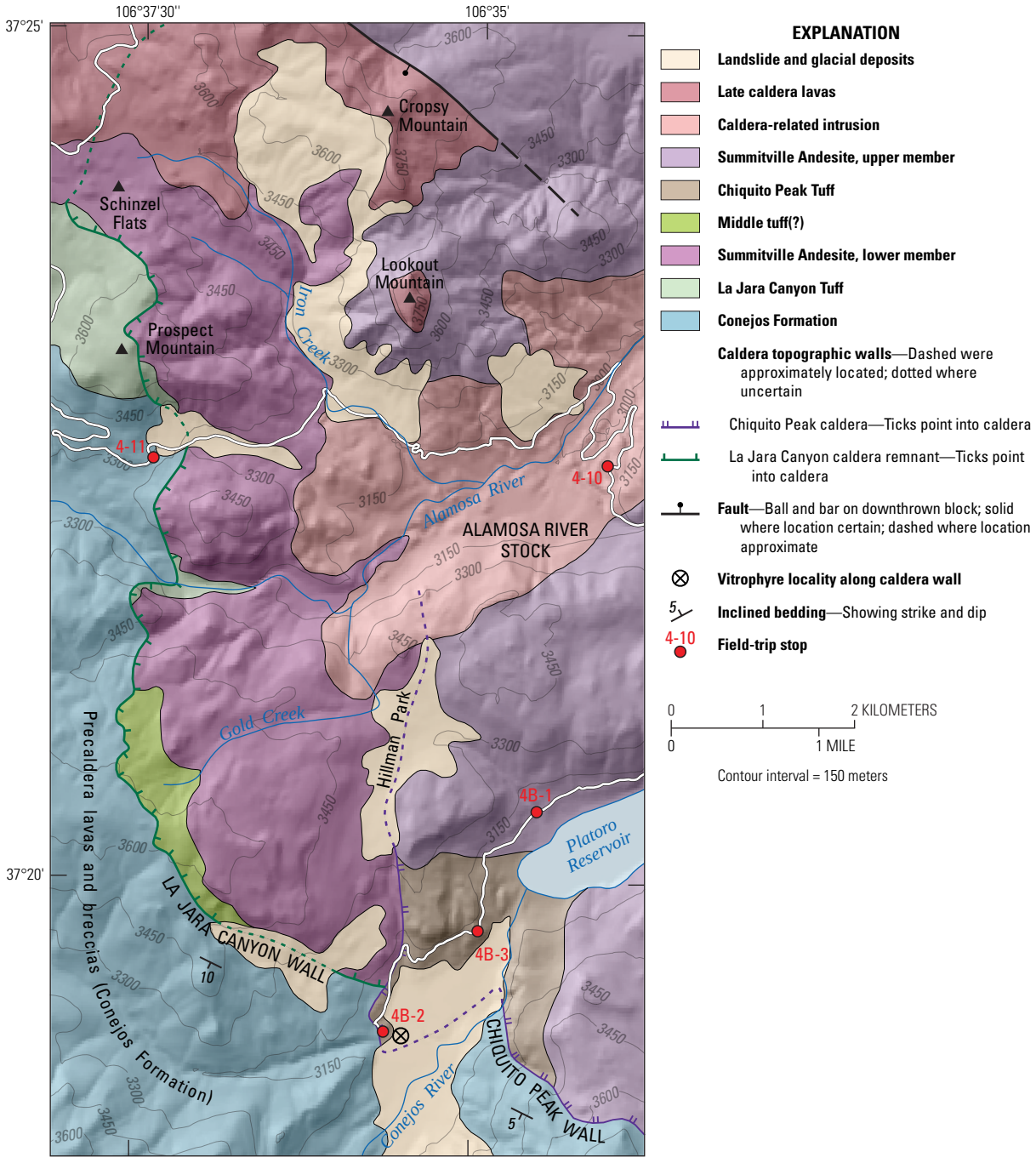

Figure 96. Geologic map of southwestern margin of the Platoro complex, showing preserved remnants of successive topographic walls related to eruption of the La Jara Canyon and Chiquito Peak Tuffs. Modified from Lipman and others (1996).

Later Caldera-Related Ignimbrite Deposits, Lacking Exposed Collapse Sources

After eruption of the La Jara Canyon Tuff, its caldera was at least partly filled by lower-member lavas of Summitville Andesite and several interlayered ignimbrites erupted from within the Platoro complex.

Middle Tuff

This unit consists of 10–15 separate ignimbrite sheets (Stops 4-2, 4C-7b), each with volumes that are smaller (5–10 km^3 each) than other tuffs of the Treasure Mountain Group. Most units of the middle tuff are phenocryst-poor (<5 percent) dacite to low-silica rhyolite, but no detailed chemical or petrologic data have been published. The overall distribution of the middle tuff documents sources from within the Platoro complex (Lipman, 1975a; Balsley, 1994), which provides further evidence for extraordinarily recurrent explosive volcanism from a single caldera complex. The ages and duration of these small-volume eruptions is directly bracketed between 30.2 and 28.9 Ma (ages for the Black Mountain and Ra Jadero Tuffs), and (detrital?) sanidine from a reworked tuff bed within the middle tuff yielded a $^{40}Ar/^{39}Ar$ age of 29.93±0.03 Ma (table 9).

Ojito Creek and Ra Jadero Tuffs

These two separate ignimbrites are relatively thin, but widespread sheets of densely welded silicic dacite contain sparse andesitic pumice lenses near their tops. Their distributions are similar to those of underlying tuffs, except that the Ojito Creek is absent on the north flank of the Platoro caldera complex (figs. 23 and 25 in Lipman, 1975a). The Ra Jadero Tuff is the earliest Treasure Mountain unit to contain sanidine phenocrysts; the weighted-mean $^{40}Ar/^{39}Ar$ age for three samples (11L-26, MD-165, and MD-43; table 9) is 28.93±0.02 Ma. Although both the Ojito Creek and Ra Jadero Tuffs are ponded within the outer topographic wall of the Platoro complex, which indicates proximal sources, neither is associated with exposed intracaldera tuff or other direct evidence of collapse. Lipman (1975a) initially inferred that both of these tuffs were erupted from the Summitville caldera, a paleodepression within the northwest Platoro caldera complex. As reinterpreted later (Lipman and others, 1996), most of the exposed Platoro complex, including the lavas of Summitville Andesite ponded within the inferred Summitville caldera, formed during eruption of the Chiquito Peak Tuff and later resurgence. Although several large arcuate faults associated with Chiquito Peak resurgence may be interpretable as reactivated ring faults associated with concealed Summitville caldera structures related to eruption of the Ojito Creek and Ra Jadero Tuffs (Lipman and others, 1996), no topographic or direct stratigraphic evidence remains for this inferred caldera.

South Fork Tuff

A petrologically distinctive rhyolitic tuff (upper tuff of Lipman, 1974, 1975a), which overlies the Ra Jadero Tuff on the north and northwest flanks of the Platoro caldera complex, was named the South Fork Tuff and included in the Treasure Mountain Group (Lipman and others, 1996) because (1) its distribution is similar to that of other Treasure Mountain units on the north and west flanks of the Platoro complex, (2) proximal-distal phenocryst size and abundance variations in outflow South Fork Tuff indicate that this unit was erupted from the Platoro area, and (3) $^{40}Ar/^{39}Ar$ determinations (table 9) indicate that the weighted-mean age of this tuff (28.86±0.08 Ma; sanidine) is indistinguishable, within analytical uncertainty, from the underlying Ra Jadero Tuff (28.93±0.02 Ma). The South Fork Tuff overlies Ra Jadero Tuff and is overlain by Chiquito Peak Tuff at its type locality east of the mouth of Willow Creek, 3 km east of South Fork (fig. 92). The South Fork Tuff consists of low-silica rhyolite (73 percent SiO_2; table 8), and typically contains 10–15 percent phenocrysts (plagioclase, sanidine, biotite, ±augite). Exposures in the South Fork area are a distal facies. This tuff sheet is thicker, more densely welded, and more phenocryst rich closer to the caldera complex. Bulk-sample phenocryst contents of only about 5 percent at the most distal exposures north of South Fork are interpreted to result from crystal sorting during emplacement. In contrast, proximal South Fork Tuff at Bennett Peak (fig. 95) is phenocryst rich (25 percent).

Eruption of the Chiquito Peak Tuff and Formation of the Main Platoro Caldera

The Chiquito Peak Tuff, as presently understood (fig. 94), is a major ignimbrite sheet of the San Juan volcanic locus, with an estimated volume of ~1,000 km^3. In early regional studies, Cross and Larsen (1935) included the currently recognized Masonic Park and Chiquito Peak Tuffs within their undivided Treasure Mountain Rhyolite. During 2° quadrangle mapping in the 1960s, the uppermost identified crystal-rich dacitic ignimbrite of the Treasure Mountain units was separated out as the Masonic Park Tuff (Steven and Lipman, 1973), because it was found to extend much farther west and north than earlier tuff sheets of the Treasure Mountain. Although puzzlement was expressed about the great southeasterly extent of the Masonic Park Tuff, this distribution was erroneously rationalized on the basis that underlying ignimbrites of the Treasure Mountain Group had provided a low-relief surface for transport of Masonic Park pyroclastic flows (Lipman, 1975a, p. 41–45).

The subtle distinction between Chiquito Peak and Masonic Park lithology was initially recognized by small differences in biotite chemistry (Dungan and Lipman, 1988) and sparse sanidine (5–10 percent of total feldspar) in the former. In most areas, only a single lithology is present, and the two ignimbrites units stratigraphically overlap only in a narrow zone along the

South Fork of the Rio Grande and Wolf Creek (fig. 92). The Chiquito Peak lithology is thus closely coextensive with other large tuff sheets of the Treasure Mountain Group. In the overlap corridor, a local lava and sparse float of bedded tuff and sandstone in a few places along the contact further document a break between two separate ignimbrite sheets, rather than possible alternative interpretation of compound cooling within a single compositionally zoned sheet.

Outflow Tuff Sheet

The Chiquito Peak Tuff is a petrologically uniform crystal-rich dacite with plagioclase, biotite, augite, and sanidine phenocrysts. The outflow tuff sheet is typically only partly welded and vapor-phase crystallized; it contains ubiquitous 1–2 centimeters (cm) lithic fragments, mainly brownish andesite. The Chiquito Peak Tuff is named for palisade exposures on the southwest flank of Chiquito Peak (Stop 4C-8b), where it overlies the South Fork, Ra Jadero, and older tuff sheets of the Treasure Mountain Group and is overlain by distal Fish Canyon Tuff. At Chiquito Peak, this tuff displays a weak compound cooling zonation but is only partly welded despite a thickness of about 100 meters (m) (near its outflow maximum). To the north, near South Fork, as many as three partly welded ledges are separated by less welded zones of vapor-phase crystallization (see Day 5, Stop 5-4). It is commonly light tan to gray-tan, in contrast to a more gray-green color for much of the Masonic Park Tuff.

The outflow Chiquito Peak Tuff is nowhere preserved within 5 km of the caldera margin. Around the south flank of the Platoro caldera, the closest Chiquito Peak is 10–20 km distant from the caldera rim. In contrast, the La Jara Canyon Tuff is present as a densely welded dark tuff unit along both eastern and western margins of the Platoro caldera complex. This difference in proximal distribution probably reflects preferential erosion of the stratigraphically higher and less welded Chiquito Peak Tuff, although both tuff sheets preserve evidence of local depositional wedge-outs in paleovalleys against Conejos volcanic highlands toward the caldera margins.

Intracaldera Tuff

The intracaldera Chiquito Peak ignimbrite is densely welded, dark gray, and intensely propylitically altered (Stops 4-8, 4B-3); its appearance differs strikingly from any outflow tuff in the Treasure Mountain Group (Lipman, 1975a, p. 27–29). Pumice and other pyroclastic textures have been widely obliterated, and phenocrysts are variably altered to epidote, calcite, chlorite, and other secondary minerals. On the Cornwall Mountain resurgent block, the intracaldera tuff is more than 800 m thick, although its top is eroded and its base is concealed.

A key locality is a locally exposed marginal vitrophyre along the southwest caldera wall, near Platoro Reservoir (fig. 96; Stop 4B-2). The vitrophyre and some adjacent devitrified tuff preserve unaltered sanidine phenocrysts, in contrast to the absence of this phenocryst phase in all outflow La Jara Canyon Tuff. This vitrophyre was originally interpreted as an evolved phase of the La Jara Canyon that was confined to the subsiding caldera (Lipman, 1975a; Dungan and others, 1989a), but partly argillized sanidine has since been identified in the least-altered tuff from several other intracaldera sites. Mineral chemistry from the vitrophyre also matches that of the outflow Chiquito Peak Tuff. Accordingly, the entire main mass of exposed intracaldera tuff is now interpreted as Chiquito Peak, excluding only the small exposures along the western margin that appear to represent a remnant of intracaldera La Jara Canyon Tuff (Stops 4-8, 4B-3).

Age

Intracaldera and outflow samples of the Chiquito Peak Tuff have yielded analytically indistinguishable ages by the laser-fusion $^{40}Ar/^{39}Ar$ technique (Lipman and others, 1996), with a weighted mean age of 28.77±0.03 Ma (table 9).

Paleomagnetic Evidence

Simple polarity data were originally used to test correlations among tuff sheets from the Platoro complex (Lipman and Steven, 1970). Both the Chiquito Peak and Masonic Park Tuffs are reversely polarized, but detailed laboratory paleomagnetic pole determinations define distinct populations at the 95-percent confidence level (Lipman and others, 1996, fig. 5), providing further support for interpretation of separate ignimbrite sheets.

Petrology

Despite the diagnostic presence of sanidine, bulk compositions of the Chiquito Peak Tuff are similar to the La Jara Canyon Tuff, except for slightly lower yttrium and heavy rare earth element contents in the Chiquito Peak (table 8; Dungan and others, 1995). Other than this subtle distinction, compositions vary more within each tuff sheet, mainly as a function of crystal-ash separation during emplacement, than between the tuff units. Also indistinguishable are phenocryst compositions (plagioclase, biotite, augite) from these two units despite erupting about 1 m.y. apart, supporting the interpretation that both erupted from the Platoro caldera complex. Sanidine phenocrysts in the Chiquito Peak are notably more potassic, as reflected in higher potassium feldspar concentrations than those in other late tuffs of the Treasure Mountain Group ($Or_{64–67}$; in contrast to Or_{54} for Ra Jadero Tuff, and $Or_{48–51}$ for South Fork Tuff). Such relatively potassic sanidine compositions are typical of later tuffs erupted from the central San Juan caldera cluster (Lipman, 1975a; Lipman and Weston, 2001), which suggests a petrologic progression at Platoro from inception toward more evolved later-erupted magma types. Samples from

low and high in sections of both Chiquito Peak and Masonic Park Tuffs have yielded no indication of chemical zoning or multiple magma compositions, in contrast to the Black Mountain, Ojito Creek, and Ra Jadero Tuffs (Dungan and others, 1995).

Lavas Associated with the Platoro Caldera Complex

Areally associated with the Platoro caldera complex, and intertongued between many of the ignimbrite sheets, are thick sequences of locally derived andesitic lavas. These lavas have previously been divided into the Summitville Andesite, the Sheep Mountain Andesite, and the andesite of Summit Peak (Steven and others, 1974a), but the reinterpreted relations among the Treasure Mountain ignimbrite sheets also have implications for correlation of the associated lavas, especially among members of the intracaldera Summitville Andesite. The Summitville Andesite, which is preserved largely as fill within the Platoro complex, contains two members: (1) areally widespread lower-member lavas emplaced after eruption of the La Jara Canyon Tuff, and (2) thick upper-member lavas that mainly ponded within the caldera.

Reinterpretation of most of the exposed Platoro caldera complex, as related to eruption of the Chiquito Peak Tuff, requires that the bulk of intracaldera lava belongs to the upper member of the Summitville Andesite. The upper-member lavas locally filled the caldera to overflow, and andesite lavas of similar stratigraphic position are present at scattered locations above outflow Chiquito Peak Tuff, such as at Summit Peak (Lipman, 1974). The only confirmed intracaldera lavas of lower-member Summitville Andesite are along the eastern caldera margin (fig. 95). Some lower-member andesite may also overlie intracaldera La Jara Canyon Tuff in the western remnant of the La Jara Canyon caldera (fig. 96), but criteria are currently inadequate to identify such rocks reliably.

In addition to the upper-member Summitville Andesite, an initial postcollapse lava, the dacite of Fisher Gulch, directly overlies the south flank of the resurgently uplifted intracaldera Chiquito Peak Tuff and forms a thick flow-layered mass banked against the southeast caldera wall (Stop 4-7). This lava, which locally displays spectacular textures indicative of magma mixing (fig. 37*A* in Lipman, 1975a), has yielded a $^{40}Ar/^{39}Ar$ age of 28.74±0.09 Ma, slightly younger but analytically indistinguishable from that for the Chiquito Peak Tuff (table 9).

Above the Summitville Andesite, especially along the northern caldera margin are compositionally diverse lavas of dacite and rhyolite, some as young as 20 Ma, that record a prolonged history of postcaldera magmatism (fig. 97). These include the relatively mafic dacites of Park Creek and Silver Mountain, the sanidine-megacrystic dacite of South Mountain, and the crystal-rich rhyolite of Cropsy Mountain (tables 7, 8). In addition to these late intracaldera lavas, a major eastern locus of postcaldera volcanism is marked by the andesite-dacite lavas of Green Ridge east of the caldera margin (fig. 93), interpreted as remnants of a separate high-standing volcanic construct.

Caldera-Related Intrusions

Intrusive rocks, which consist of numerous andesitic to rhyolitic dikes and scattered larger granitoid plutons, tend to cluster around, and radiate out from the Platoro caldera complex (Lipman, 1974; Lipman and Zimmerer, 2019; Gilmer and others, 2021). About 10 granitoid plutons, ranging from less than 0.5 to more than 5 km across, intrude the volcanic sequence near Platoro, and several large laccolithic granitoid bodies are localized along the boundary between the Conejos Formation and prevolcanic rocks along the southwestern margin of the San Juan Mountains and the underlying Cretaceous sedimentary strata in the San Juan Basin (fig. 98). These bodies consist mainly of texturally variable monzonite that, in places, transitions to diorite or granodiorite. Locally, the granitoid rocks are equigranular, but many are porphyritic, with plagioclase as the conspicuous phenocryst. Two pyroxenes are also typically present as early formed euhedral minerals; these tend to be variably altered with hypersthene to chlorite or serpentine, and augite to chlorite or tremolite.

The Alamosa River pluton, among the largest exposed Cenozoic granitoid intrusions (3 x 8 km) in the San Juan region (fig. 93), intrudes Summitville Andesite within the Platoro complex; its U-Pb zircon date (28.9±0.2 Ma; Gilmer and others, 2021) is indistinguishable within analytical uncertainty from the age of intracaldera Chiquita Peak Tuff that it intrudes. South of the Alamosa River, the pluton consists of little-altered fine- to medium-grained equigranular monzonite. It is fairly uniform in texture but varies in composition from ~57 to 62 percent SiO_2. Paleomagnetic study suggests pulsed emplacement of a vertically extensive pluton, as documented by three domains of concentric magnetic foliations (Tomek and others, 2019). In contrast, the northwestern part of the intrusion is texturally and compositionally complex and is also the locus of intense hydrothermal alteration (Stops 4-10, 4-11). In this area, a separately mappable porphyritic phase is younger (27.3±0.4 Ma; Gilmer and others, 2021) and more silicic (about 65 percent SiO_2). The composite pluton is interpreted as the intrusive core of a high-standing volcanic edifice, now largely eroded, the flanks of which are preserved as lavas of the Summitville Andesite.

The Cat Creek pluton, a large intrusive complex centered about 5 km east of the Platoro caldera rim (fig. 93), is thought to represent the core of a high-standing postcaldera volcano that erupted the volcanics of Green Ridge. This intrusion has a texturally uniform interior, about 3 km in diameter, consisting of fine-grained equigranular monzonite (60–63 percent SiO_2); a U-Pb zircon age is 28.0±0.2 Ma (Gilmer and others, 2021), distinctly younger than the caldera-forming events. The intrusion core is enclosed by a finer grained porphyritic margin around its south and east sides and is flanked in other directions by scattered satellitic laccolithic bodies of similar porphyry, including the Terrace laccolith.

In addition to the Alamosa River and Cat Creek plutons, sizable stocks of granodiorite and associated dikes that locally become fine grained and grade into andesite are present at Jasper and Crater Creek, define a broad east-west zone of subvolcanic intrusion that is continued westward by dikes of andesite and

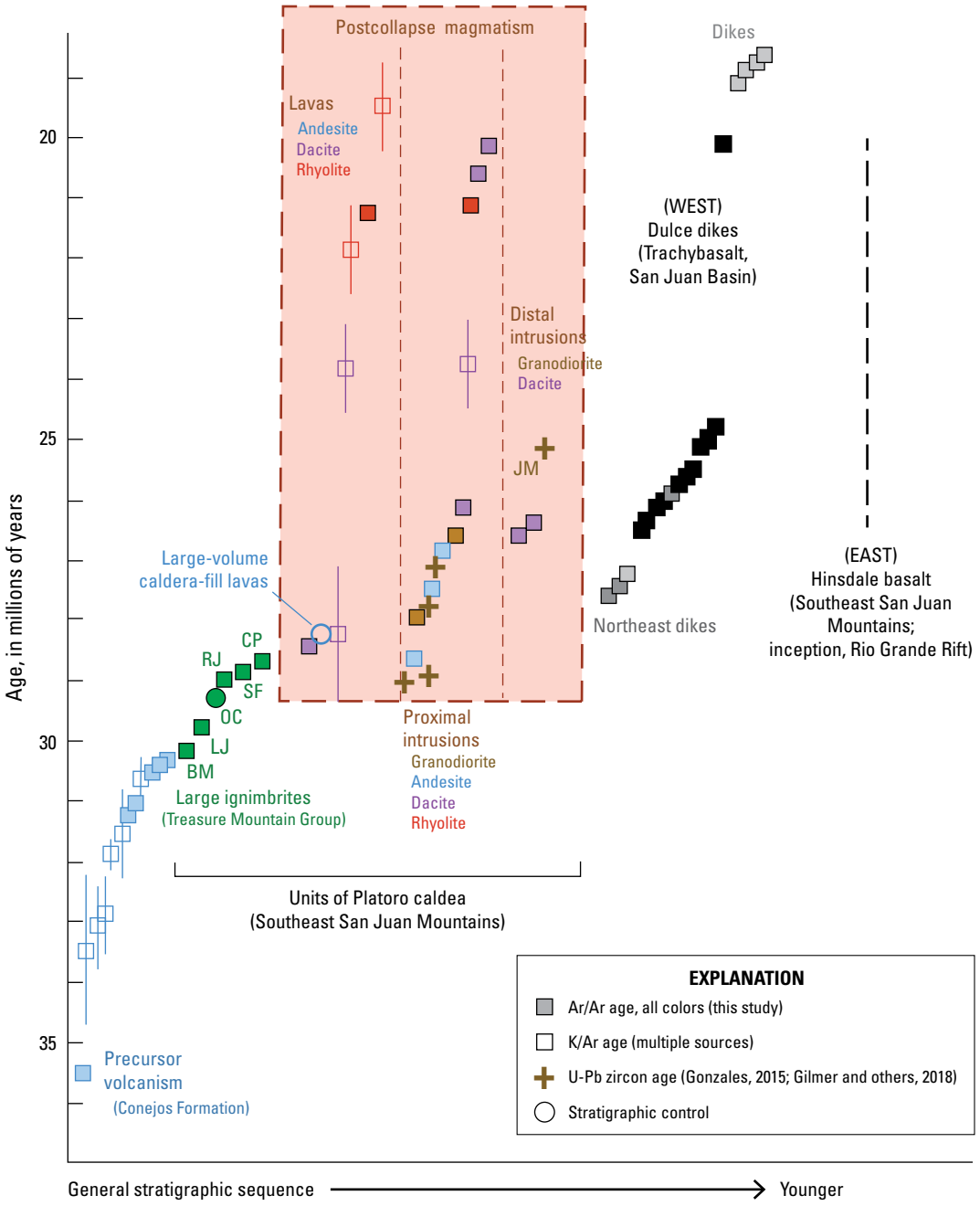

Figure 97. Summary of age determinations of volcanic and intrusive rocks associated with the Platoro caldera complex, post-ignimbrite rift-related basaltic lavas of the Hinsdale Formation to the east, and trachybasaltic dikes of the Dulce swarm (modified from Lipman and Zimmerer, 2019). The Dulce dikes are located along the margin of the San Juan Basin, beyond erosionally preserved volcanic rocks of the San Juan locus (fig. 98). For the Dulce swarm, proximal dikes are plotted as light-gray squares; more distal dikes are solid black. For Hinsdale basalts, vertical dashed line indicates age range for published determinations. For the Conejos Formation, dikes are solid-blue boxes, lavas are light blue. Recent and new $^{40}Ar/^{39}Ar$ determinations (square symbols with color fills) are from table 9 and Lipman and Zimmerer (2019). Previously published K-Ar ages are from Lipman and others, 1970, 1996; Mehnert and others, 1973; Lipman and Mehnert, 1975; Aldrich and others, 1986; Gibson and others, 1993; and Gonzales, 2015. Analytical uncertainty for K-Ar ages is indicated by a vertical line; uncertainties for $^{40}Ar/^{39}Ar$ and most U-Pb ages are smaller than the symbol size. BM, Black Mountain Tuff; CP, Chiquito Peak Tuff; Fm, Formation; JM, Jackson Mountain pluton; LJ, La Jara Canyon Tuff; Mtns, Mountains; OC, Ojito Creek Tuff; RJ, Ra Jadero Tuff; RG, Rio Grande rift; SF, South Fork Tuff; vol., volume.

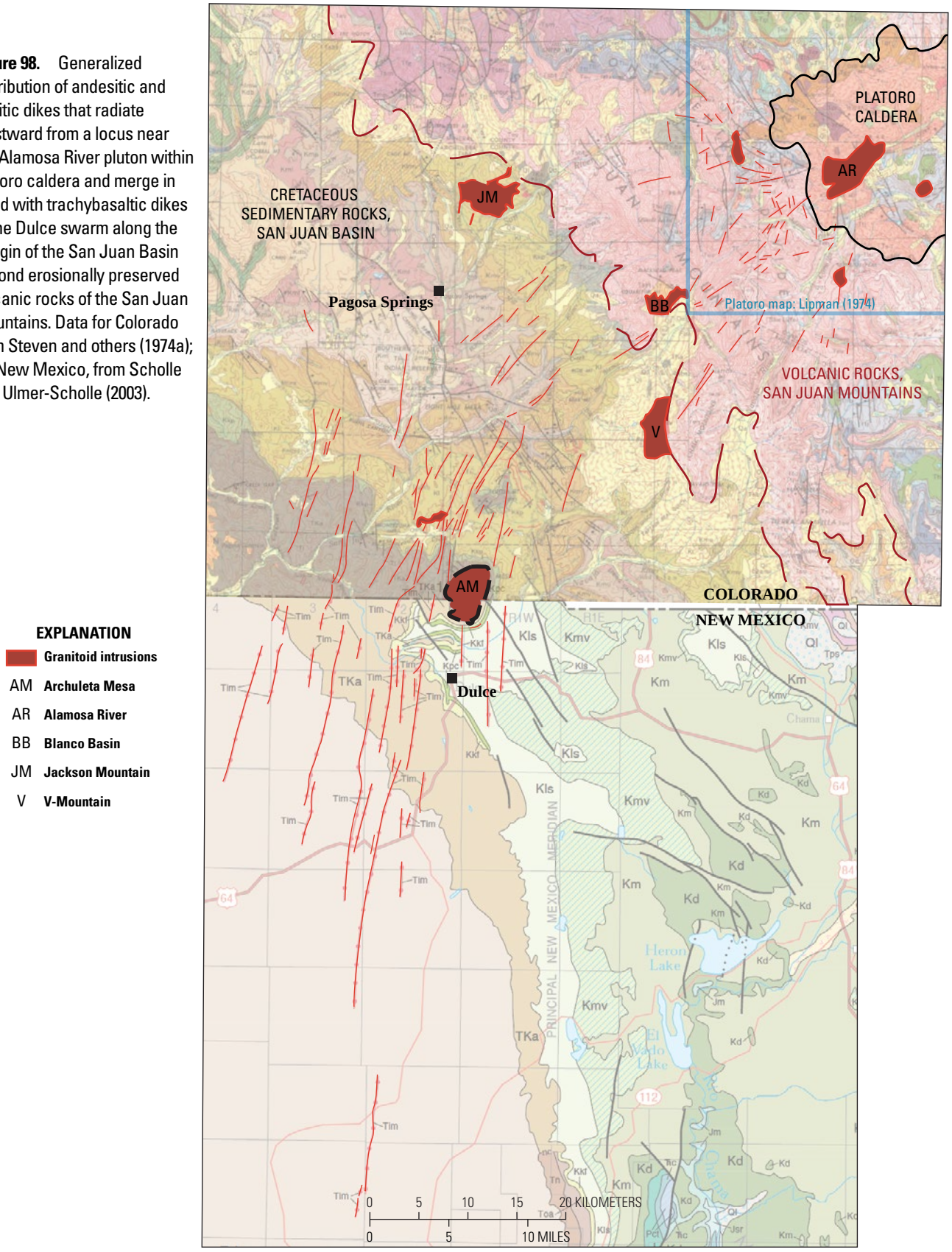

Figure 98. Generalized distribution of andesitic and dacitic dikes that radiate westward from a locus near the Alamosa River pluton within Platoro caldera and merge in trend with trachybasaltic dikes of the Dulce swarm along the margin of the San Juan Basin beyond erosionally preserved volcanic rocks of the San Juan Mountains. Data for Colorado from Steven and others (1974a); for New Mexico, from Scholle and Ulmer-Scholle (2003).

Geologic base maps from Steven and others, 1974a (CO) and Scholle and Ulmer-Scholler (2003) (NM)

dacite that radiate westward from a focus broadly within the Alamosa River pluton (fig. 98). This seemingly anomalous regional trend may be related to its location along the southern margin of the composite subvolcanic batholith that is inferred from gravity data to underlie much of the central San Juan region (Plouff and Pakiser, 1972; Drenth and others, 2012).

Ignimbrite Emplacement and Caldera Evolution

Diverse distributions of the major Treasure Mountain ignimbrites, along with recognition of the Chiquito Peak Tuff as a separate ignimbrite sheet erupted from the recurrently active Platoro caldera complex, have important implications for ignimbrite emplacement mechanisms, recurrent caldera subsidence, and magma generation in subcaldera continental crust.

Ignimbrite Emplacement

The nearly antithetic distributions of Chiquito Peak and Masonic Park Tuffs along the South Fork-Wolf Creek overlap corridor (fig. 92) document the impressive influence of even gentle depositional slopes on the emplacement of sluggish pyroclastic flows such as these crystal-rich dacites. The limited overlap between these two lithologically similar tuff sheets appears to be a primary depositional feature, only slightly modified by subsequent erosion. This interpretation is documented by lateral variations in the distal facies of both sheets, in which welding and crystallization zonations of cooling subunits thin and merge toward their depositional wedge-outs. The most plausible volcanologic interpretation is that both crystal-rich dacitic tuffs were characterized by low-energy emplacement in their distal regions, where they were too sluggish to override even low topographic barriers. The pyroclastic density flows from each eruption flowed down the gentle constructional aprons surrounding their source regions but could not cross the Oligocene valley between the two volcanic loci. The paleovalley system that marks the boundary between the two ignimbrites has persisted to the present, now approximated by the South Fork of the Rio Grande and by Wolf Creek (fig. 92). Similar pronounced effects of small topographic obstacles have been described for the 1912 Katmai eruption, where the distal pyroclastic flow had neither the momentum nor the degree of inflation necessary to surmount a glacial moraine, even though the moraine was only 5 m higher than the resulting ignimbrite deposit (Hildreth, 1983).

The persistence of Oligocene primary volcanic paleotopography has long been recognized in the San Juan region (Steven, 1968), but the influences of such paleotopography on subtle depositional features of ignimbrite emplacement are just becoming clear. Other aspects of tuff deposition and distribution, brought into focus by reinterpretation of the Platoro complex, include the influences of precaldera topography and changing patterns of caldera subsidence on extracaldera distribution, as well as ponding of tuff within subsiding areas. The discontinuous distributions and varied loci of maximum thickness of the lower rhyolite tuff and Black Mountain Tuff, in broad basins and paleovalleys at middle distances from the caldera complex, reflect the dominant influence of constructional topography on flanks of the clustered Conejos volcanoes in the area that became the Platoro complex. Major caldera collapse within the Platoro area almost certainly accompanied the early ignimbrite eruptions, based on their considerable volumes, but no evidence concerning the size or location of subsided areas is preserved.

The smoothing of topography by early ignimbrites allowed the large-volume La Jara Canyon Tuff to spread widely with less local variation in thickness. Eruption of the La Jara Canyon Tuff caused major subsidence, involving essentially the entire area of the Platoro caldera complex. Subsidence of the La Jara Canyon caldera appears to have generated a northeastern barrier, most likely a high caldera wall, which impeded spreading of the middle tuff sheets in this direction. Even the relatively small multiple eruptions of the middle tuff may have been associated with minor subsidence events. The typical size of these tuff units, at least 5–10 km^3, is comparable to deposits associated with small historical calderas such as Mount Pinatubo in 1991 (Wolfe, 1992). Emplacement of the Ojito Creek Tuff was blocked even more widely in the northeast to northwest sector, apparently overtopping the northern Platoro wall only in a narrow section along the present Park Creek (Lipman, 1975a, fig. 23). In contrast, the next ignimbrite, the Ra Jadero, was able to spread freely to the north as well as in all other directions, a change in eruptive behavior inferred to reflect breakdown of the northern barrier by caldera collapse (Summitville?) during Ojito Creek eruptions. The South Fork Tuff spread farther to the north than had any prior Treasure Mountain ignimbrite, yet it appears to have been blocked from deposition to the south, perhaps owing to further subsidence in the northern part of the Platoro complex in response to the Ra Jadero eruptions. These contrasting depositional patterns, seemingly in response to changing caldera-wall geometries, imply low eruption energy and sluggish emplacement even for the proximal dacitic ignimbrite tuffs at Platoro, in contrast with the mobility of some highly inflated pyroclastic flows (Aramaki and Ui, 1966; Miller and Smith, 1977; Wilson and Walker, 1985).

The large Chiquito Peak eruption, which generated virtually all exposed features of the caldera complex, produced pyroclastic flows that spread farther in most directions than earlier tuff sheets, as well as ponding to great thickness within the caldera. Intracaldera Chiquito Peak Tuff was resurgently uplifted after deposition, but as an asymmetrical trapdoor block rather than a simple structural dome. Finally, the widespread outflow distribution of multiple ignimbrite sheets in the southeastern San Juan region, without substantial erosion between successive eruptions, contrasts strikingly with the limited preservation of ignimbrites erupted from the Sawatch locus to the north where pre-eruption topography appears to have been more rugged (Day 6).

Recurrent Caldera Subsidence

The Platoro complex is an extreme example, for the San Juan region and elsewhere, in terms of successive voluminous ignimbrite eruptions that alternated with more quiescent lavas from an areally restricted source. Geologically recent multicyclic caldera complexes are relatively rare, and none records as many successive eruptions from a single source as the Platoro complex. Younger counterparts include Aso caldera in Japan, from which four major ignimbrite sheets erupted between about 300 and 29 thousand years ago (ka) interspersed with andesitic lavas (Ono and others, 1981; Machida and others, 1985); the Valles Caldera in New Mexico, where both ignimbrite members of the Bandelier Tuff (1.63–1.26 Ma; Spell and others, 1996b; Phillips and others, 2007) are recognized to have erupted from a common subsidence area (Nielson and Hulen, 1984; Self and others, 1986); and Santorini caldera in Greece where at least four instances of caldera subsidence since about 100 ka have accompanied ignimbrite eruptions with volumes of as much as 25 km^3 (Druitt and Francaviglia, 1992).

Although the evidence is clear for major subsidence accompanying the Chiquito Peak eruption, as indicated by the nearly 1 km exposed thickness of intracaldera tuff on the uplifted Cornwall Mountain block, the subsidence history during earlier eruptions is obscure. The wide areal extent and large outflow volume of the La Jara Canyon Tuff, the large east-west dimension of its caldera, and its fragmentary intracaldera exposure in the upper Alamosa drainage all suggest syneruptive caldera subsidence of a volume comparable to that of the Chiquito Peak. On the basis of their outflow volumes, eruptions of the Black Mountain, Ojito Creek, Ra Jadero, and South Fork Tuffs were also likely to have been accompanied by substantial caldera collapses, but the volumes of tuff ponded within their associated calderas can be inferred only by analogy with better-exposed systems. For many large calderas, on average, about half the total eruptive volume is deposited as the outflow tuff sheet, and about half ponds within the concurrently subsiding caldera (Lipman, 1984).

Recognition of a Platoro caldera source for the Chiquito Peak Tuff increases the estimated volume of volcanic products explosively erupted from this magmatic system by more than 50 percent, to at least 2,600 km^3 (table 7). Emplacement of the voluminous tuffs of the Treasure Mountain Group in the relatively brief interval between 30.2 and 28.8 Ma (fig. 97; table 9) indicates an integrated eruption rate of about 1,700 cubic kilometers per million years (km^3/m.y.). Such a rate is among the highest documented for sustained activity from a single continental volcanic center. A higher rate of about 4,000 km^3/m.y. characterizes the nine major ignimbrite sheets of the central San Juan caldera cluster (fig. 7 in Lipman, 2000), but this value is dominated by the unique Fish Canyon Tuff (5,000+ km^3) and the caldera sources are less confocal. The average magma supply for the early intermediate-composition lava sequence of the San Juan locus (Conejos Formation and equivalents) is also high, about 5,000 km^3/m.y., but these rocks were erupted from scattered central volcanoes distributed irregularly over much of the associated volcanic field. In contrast, the Platoro complex erupted a tuff volume that, if withdrawn solely from beneath the caldera area (about 300 km^2), would be equivalent to a cumulative vertical crustal section of 8–9 km.

Why other caldera complexes, such as that of the central San Juan region, develop overlapping but less confocal subsidence structures is unclear, but must ultimately be related to structural controls on upper-crustal accumulation of magma in subvolcanic chambers. The exceptional frequency of sizable pyroclastic eruptions at Platoro would perpetuate a thermally weak crustal locus, retard solidification of the subcaldera reservoir, and focus the subsequent rise and accumulation of additional magma. Another factor may have been the limited generation of silicic differentiates in the evolving subcaldera magma, as documented by the recurrent eruption of andesitic lavas between more-silicic explosive deposits, and by the absence of a postmagmatic Bouguer gravity low comparable to that associated with the central and western San Juan caldera clusters (Plouff and Pakiser, 1972; Steven and Lipman, 1976; Drenth and others, 2012) and other caldera systems characterized by silicic eruptive activity. Such a dominantly intermediate-composition system would tend to be hotter and less viscous, further augmenting a thermally weakened upper-crustal magmatic locus. Recurrent subsidence at varying loci within a caldera complex also provides a mechanism for generating a structurally disrupted caldera floor, even if individual collapse events are accommodated along ring faults. Many deeply eroded calderas expose well-defined ring faults that bound a relatively coherent plate-like floor (Lipman, 1984). Other caldera interiors that contain complexly fragmented floors have been interpreted as having been formed by piecemeal collapse within down-sagged margins, without bounding ring faults (Branney and Kokelaar, 1994). Such structural complexities in some calderas likely result from recurrent eruptions and accompanying subsidence, as exemplified by Platoro.

Prolonged History of Postcaldera Magmatism at Platoro

In contrast to other caldera loci in the San Juan region where postcollapse eruptions typically declined within ~10^5 years after the last ignimbrite, the Platoro complex had a lengthy history of postcollapse lava eruptions and associated intrusions (fig. 97). No other SRMVF caldera has comparably numerous associated intrusions, including both granitoid plutons and outward radiating dike swarms (fig. 98). After the voluminous caldera-filling eruptions of Summitville Andesite—complete by ~28.6 Ma (the minimum crystallization age for the Alamosa River and Jasper plutons; Gilmer and others, 2021), more-evolved dacitic-rhyolitic lavas erupted in the Platoro area for an additional 8 m.y. Poorly dated dacitic lavas of Park Creek on the northwest caldera flank are bracketed between the 28.2-Ma Fish Canyon Tuff and 27.7-Ma Carpenter Ridge Tuff. Similar age constraints bracket Los Piños Formation volcaniclastic deposits derived from dacite lavas at Green Ridge, part of the Cat Creek volcano east of Platoro caldera. Both the large 23-Ma sanidine-dacite lava dome and associated mineralization at South Mountain (Stop 4-14), and the crystal-rich

low-silica rhyolite lava of Cropsy Mountain (Stop 4-10), with K-Ar ages at ~20 Ma, are interpreted as postcaldera magmatism of the long-lived Platoro system.

Only a few of the compositionally diverse dikes and other intrusions within the Platoro caldera and radiating westward, had been dated by the time of the 2017 excursion; these had yielded varied K-Ar and $^{40}Ar/^{39}Ar$ ages between 28 and 21 Ma (table 9). Many more such intrusions have now been dated by U-Pb zircon methods, providing improved resolution for the postcollapse magmatism (Gilmer and others, 2021). These dikes and other intrusions appear to merge in structural trend, composition, and age with the spectacular Dulce dike swarm of trachybasalt (Lipman and Zimmerer, 2019) that trends southwest and south for 125 km along the northeastern margin of the Colorado Plateau (San Juan Basin) from southern Colorado into northern New Mexico (fig. 98). Individual Dulce dikes, though only 1–2-m thick, are traceable for 20 km or more. Subhorizontal grooves on some dike walls suggest rapid lateral injection, perhaps even originating from the Platoro locus. Mica $^{40}Ar/^{39}Ar$ ages (26–25 Ma) and published K-Ar dates (27–23 Ma) for Dulce dikes are within the range of $^{40}Ar/^{39}Ar$ ages from sanidine-dacite dikes (26.5–20.3 Ma) radial to Platoro (fig. 97). The Dulce dikes are also broadly similar in composition and age to trachybasalt and trachyandesite lavas of the Hinsdale Formation that are interpreted to be associated with initiation of the Rio Grande Rift along the east flank of the present-day San Juan Mountains. The radial Platoro intrusions and Dulce dikes may record the interrelated effects of uplift associated with prolonged solidification of an arc-related granitoid batholith beneath Platoro caldera, concurrent with the transition to crustal extension in the southern Rocky Mountain region (Lipman and Zimmerer, 2019). Weak extension along the northeastern margin of the Colorado Plateau, which localized intrusion of the Dulce dikes, was satellitic to the initial sustained extension and associated basaltic volcanism along the Rio Grande Rift farther east. The potential genetic link between the Platoro radial dikes and the Dulce swarm provides special opportunities to evaluate the role of transitional tectonics (convergent arc to continental rift) on mechanisms of magma emplacement and strain partitioning during the waning of a large caldera complex.

Magma-Generation Processes

Although no petrologic studies have been undertaken since the late 1980s, the available data (Lipman and others, 1978; Dungan and others, 1989a; Colucci and others, 1991) further constrain the evolution of the Platoro magmatic system and its eruptive output. Elemental and isotopic compositions document broad petrologic continuities among products of the Platoro complex, including similar mineral chemistry, involvement of multiple magma components in some ignimbrite sheets, and plausible generation of the silicic tuffs by crystal fractionation from andesitic parental magmas similar to those erupted from Conejos volcanoes prior to ignimbrite magmatism. The continued availability of such magma throughout the evolution of the caldera complex—but without the generation of a highly evolved batholith in the upper crust—is indicated by the sparse presence of hornblende-andesite pumice in late-erupted upper parts of some dacite ignimbrites, andesitic lavas interleaved at six horizons between the tuff sheets, and the absence of an associated Bouguer gravity low. Isotopic studies confirm major assimilation-crystallization-fractionation interactions between mantle-derived basaltic melts and lower continental crust to produce the dominant characteristics of the erupted volcanic deposits throughout the San Juan magmatic locus (Lipman and others, 1978; Dungan and others, 1989a, 1995; Riciputi and Johnson, 1990; Riciputi and others, 1995).

In addition to the large volume of erupted magma at caldera systems such as Platoro, even greater volumes of magma must have remained in the upper-crustal magma body into which the caldera complex subsided recurrently; the proportion of erupted magma in such caldera systems is estimated at 10 percent or less (Smith, 1979; Ward and others, 2014; Lipman and Bachmann, 2015). The subcaldera magma body at Platoro must have developed in the upper crust at an early stage, perhaps initially during the growth of the clustered Conejos volcanoes, because a large shallow magma reservoir must have existed to accommodate caldera subsidence during eruption of the La Jara Canyon Tuff or even earlier ignimbrites. The continuing presence of a shallow magma reservoir is documented by the Chiquito Peak collapse and subsequent resurgent uplift of the Cornwall Mountain block. Several covolcanic intrusions (including the Alamosa River and Jasper plutons, fig. 93) reached high structural levels, near the elevation of the regional land surface, and must have been capped by high-standing volcanoes. The overall effect of such magma-generation processes would have been to profoundly reconstruct the crustal column beneath the caldera system and associated upper-crustal magma chamber, as large volumes of mantle-derived basalt crystallized and hybridized with crustal rocks (Lipman and others, 1978; Hildreth, 1981; Johnson, 1991; Lipman and Bachmann, 2015).

A final complexity in the magmatic evolution of a multicyclic caldera system such as Platoro is the fate of the caldera floor and early emplaced caldera fill, as recurrent subsidence events cumulatively displace such material downward. At Platoro, the cumulative thickness of intracaldera fill likely reached 10 km or more (fig. 99), on the basis of the exposed thicknesses of intracaldera Chiquito Peak Tuff in the Cornwall Mountain block, analogy with observed thickness of caldera-fill assemblages in other San Juan calderas and elsewhere, and prorated thicknesses for horizons of Summitville Andesite (assumptions discussed more fully in the caption for fig. 99).

Complete sections through caldera fills, including the caldera floor, are rare, but syncollapse sections can be 3–5-km thick for deposits from individual ignimbrite eruptions that are comparable in size to larger events at the Platoro complex (Lipman, 1993; John, 1995; Lipman and others, 2015). Comparably thick intracaldera tuffs likely accumulated repeatedly within the Platoro complex during its multiple eruptive cycles, requiring much of the intracaldera section to have been recurrently stopped and (or) assimilated, in order to permit a subcaldera magma body to remain in the upper crust. Such a process provides a geologically rapid and efficient mechanism for cannibalizing and

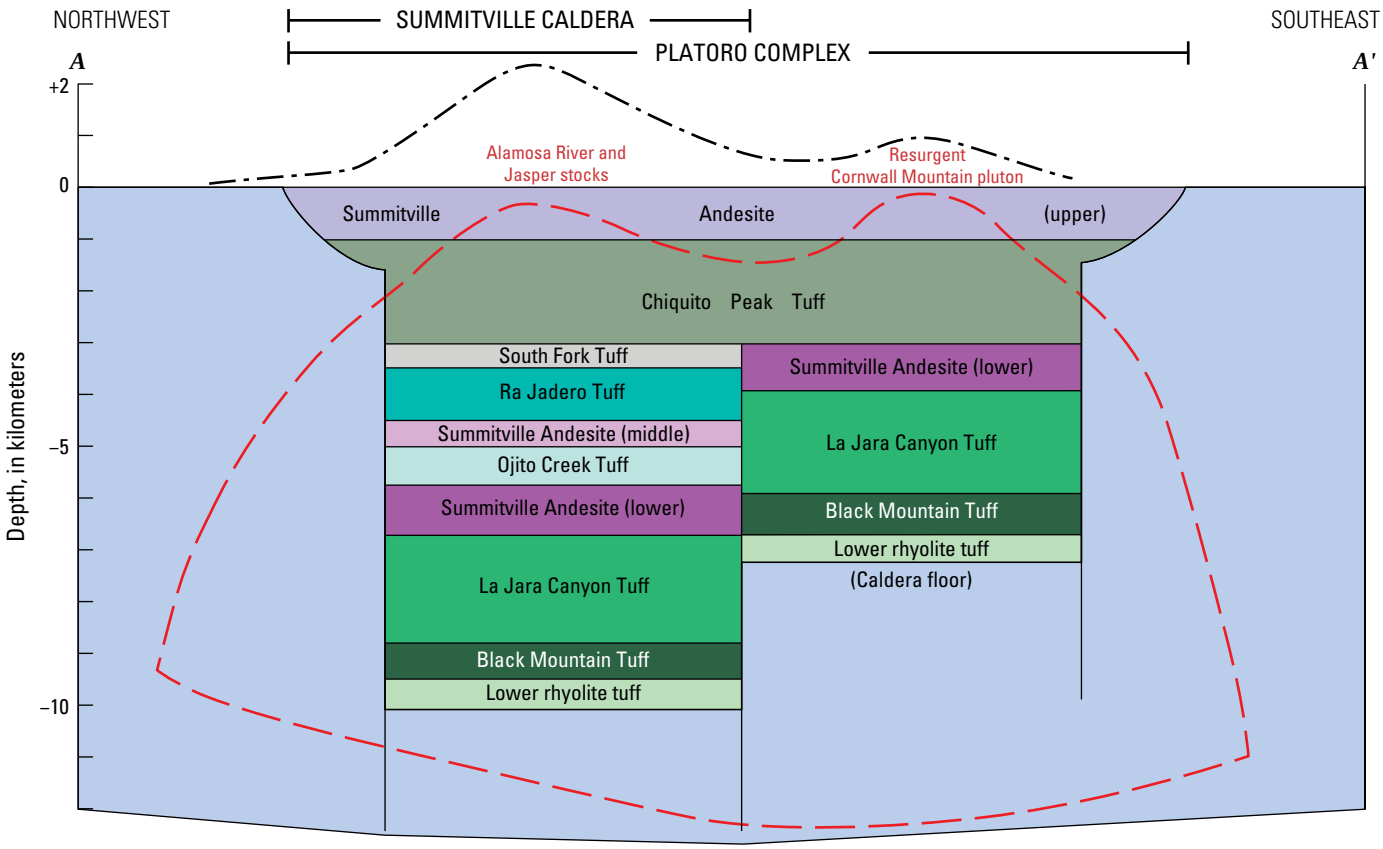

Figure 99. Schematic northwest-southeast section through the Platoro caldera complex, illustrating inferred cumulative thickness of ponded intracaldera fills associated with successive ignimbrite and lava eruptions. The location of the section is shown in figure 93. Thickness estimates for individual tuff units are based on volumes of their outflow sheet and analogies with more deeply exposed caldera systems in the San Juan region and elsewhere. No coeruptive subsidence is included for the multiple small eruptions recorded by the middle tuff, even though these tuffs are individually similar in size (5–10 square kilometers) to historical eruptions associated with small caldera collapses. Initial caldera subsidences (lower rhyolite tuff, Black Mountain Tuff) are arbitrarily assumed to have involved the entire caldera complex. Intracaldera lavas are inferred only for horizons where such lavas are exposed within the caldera or exist in proximal outflow sections; additional interleaved lavas are likely present at other horizons in the intracaldera section. Enlargement of topographic caldera walls by landslide slumping (which augments the volume and thickness of caldera fill that accumulates within the ring fault) is shown schematically, and only for the last (Chiquito Peak) eruption. For simplicity, present-day topography is omitted, post–Chiquito Peak resurgence of the Cornwall Mountain block is disregarded, and ring faults are arbitrarily shown as vertical. The former existence of large volcanic constructs above the Alamosa River and Jasper plutons (dot-dash line) is required to provide a roof for these high-level plutons, which are currently exposed at elevations approximating or exceeding the regional Oligocene land surface at the time of volcanic activity from the Platoro complex. The inferred size and shape of the overall subcaldera batholith in its final position (dashed line) are highly schematic, drawn to underlie the entire caldera complex, to connect with the exposed Alamosa River, Jasper, and Cornwall Mountain intrusions (adjacent to the line of section), and to indicate that much of the caldera-fill sequence must have been removed, probably by massive stopping, during upward rise of the batholith. Modified from Lipman and others (1996).

recycling upper-crustal volcanic products during the life span of a multicyclic caldera system. Similar geometric constraints concerning the fate of thick, ponded ignimbrites apply to other recurrently subsided nested caldera systems, such as the central San Juan caldera cluster (fig. 16 in Lipman, 2000), which is the focus of Day 5 of this field trip.

This apparent requirement for large-scale upper-crustal recycling of earlier-erupted volcanic material in the San Juan region adds yet another complexity to deciphering the sources of ignimbrite magmas. Analogous massive recycling of earlier-erupted volcanic deposits that were hydrothermally altered involving meteoric water is widely inferred as the origin of voluminous low-^{18}O magmas, such as have been documented for the rhyolitic caldera systems of the Snake River Plain-Yellowstone volcanic locus (Friedman and others, 1974; Bindeman and Valley, 2001). Late eruptions from polycyclic calderas such as Platoro, Creede, and other nested caldera complexes in the San Juan region, where intracaldera lake-bed sediments, travertine deposits, and sulfide mineralization attest to postsubsidence availability of water and hydrothermal activity. These seem to be ideal sites

for generation of low-^{18}O magmas, yet no substantially depleted tuff or lava magma compositions have been documented to date despite several detailed search efforts (Larson and Taylor, 1986; Balsley and Gregory, 1998). Continental-arc magmas that are relatively low-temperature and hydrous apparently interact differently with roof and wall rocks than the hot-dry rhyolitic magmas that characterize Yellowstone-type volcanism.

Day 4—Route Through the Platoro Caldera Complex

The following trip logs include a main route from Antonito to South Fork (route 4) that provides a southeast to northwest traverse though the Platoro caldera area, as well as three additional routes that provide opportunities to visit additional localities of potential interest. Route 4A diverges to the southwest, across La Manga Pass, to examine distal outflow ignimbrites from Platoro. Route 4B accesses the intracaldera Chiquito Peak ignimbrite, volcaniclastic sedimentary deposits, and caldera-filling lavas at the southwestern margin of the Platoro caldera complex along the upper Conejos River. Relations between the volcanic fills of the Chiquito Peak and the earlier La Jara Canyon calderas, caldera structures, and associated intrusions and mineralized areas along the lower Alamosa River are accessed by route 4C. These routes contain more stops than can be made during a single day trip but are included for completeness so that interested users can select the most appropriate stops for their purposes. Descriptions for some route stops are modified from the 1971 New Mexico Geological Society field guide (Lipman and Steven, 1971) and 1989 IAVCEI field guide (Dungan and others, 1989a). An additional route, through the proximal outflow geology in the Rock Creek area on the northeast flank of Platoro caldera, is available in the 1989 guide. Published U.S. Geological Survey (USGS) geologic maps especially pertinent to Day 4 of the field trip include the Platoro caldera area (Lipman, 1974) and the lower Conejos River Canyon area (Lipman, 1975b), although stratigraphic names for some ignimbrite units on these maps have been superseded (fig. 94).

Most latitude/longitude global positioning system (GPS) locations for this guide are based on North American Datum of 1927 (NAD27) coordinates, as used on USGS 7.5' topographic maps for the San Juan region; a few were determined by inspection from Google Earth images. Numbers at left in each route log are distances in miles from the starting point.

Route 4—Outflow Volcanic Stratigraphy, Caldera Structure, and Related Mineralization

This segment of the IAVCEI field trip follows the Conejos River canyon, providing a spectacularly exposed southeast-northwest cross section through outflow volcanic stratigraphy, the complex lava and ignimbrite fill of Platoro caldera, and associated intrusions and alteration/mineralization (fig. 100). Leaving the caldera at its northwest rim, the trip passes by the Superfund clean-up site at the Summitville gold-copper mine, then descends along tributaries of the Rio Grande to South Fork, where outcrops are mainly younger ignimbrite sheets from calderas located farther northwest in the central San Juan Mountains.

Mileage

0.0 *Begin the trip at the junction of U.S. Route (U.S.) 285 and Colorado State Highway (CO) 17, southwest of Antonito, Colorado (37°04.15', 106°00.89'; 7,907 ft, 2,410 m, elevation), in the lower Conejos River canyon map area (Lipman, 1975b). This is same location as the starting point for Day 3, route 3B. Drive west on CO 17.*

Basaltic lavas, from the 5-Ma Los Mogotes volcano to the north, dip gently eastward (fig. 100). Los Mogotes (the mounds, in Spanish) is a composite basaltic shield volcano. Three vent areas have been identified, including the main southern crater (on the skyline: 2,993 m elevation) and two smaller centers to the north (Flat Top and Cinder Pits). As many as 12 Los Mogotes lavas crop out in cliffs above CO 17, approximately 5 miles (mi) west of Antonito. These basaltic lavas have commonly been included in the Miocene Hinsdale Formation (Lipman, 1975b; Lipman and Mehnert, 1975; Dungan and others, 1989a), but they interfinger with tholeiitic basalts of the Servilleta Formation and could be interpreted as early eruptions of the Taos Plateau volcanic field (see Stop 3-8 in Day 3 for detailed discussion).

Covered slopes beneath these basalts along the lower Fox Creek valley are conglomeratic cobbles from the Los Piños Formation, a 26- to 5-Ma assemblage of poorly consolidated volcaniclastic sediments eroded from Oligocene strata of the San Juan region, which interleave with older basaltic lavas of the Hinsdale Formation. Exposed farther up Fox Creek are regional ignimbrites of the Treasure Mountain Group, erupted from the Platoro caldera complex.

Continue ahead to the junction with Fox Creek road on right (location of Stop 3B-1 in Day 3 guide).

12.0 **Optional Stop 4-O: Chiquito Peak Tuff** (37°04.52' N., 106°13.67' W.; 8,596 ft, 2,620 m elevation) An initial opportunity to examine outflow deposit of this ignimbrite before entering its source caldera.

Proceed north along the Fox Creek road, which provides views (to the east) of Los Mogotes volcano underlain by cliff-forming exposures of the uppermost Treasure Mountain ignimbrite, the 28.8-Ma Chiquito Peak Tuff (fig. 101). At 0.8 mi, a slightly slumped outcrop exposes partly welded crystal-rich dacite that is representative of this ignimbrite. Look for sparse sanidine (clear glass-like crystals with mirror cleavage reflections), in addition to abundant plagioclase, biotite, and green clinopyroxene. Perhaps take a sample, for

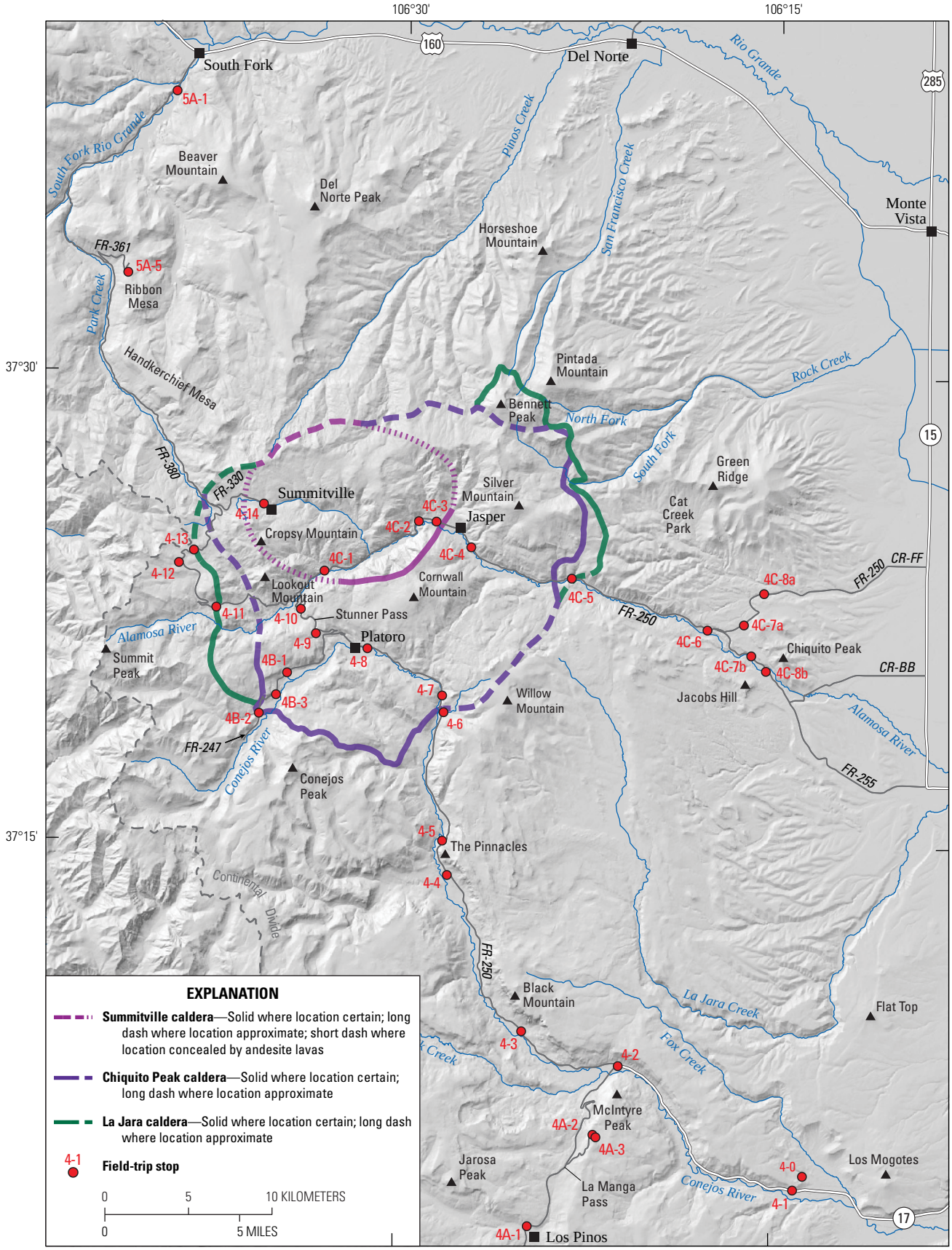

Shaded-relief base generated from U.S. Geological Survey 10-m Digital Elevation Model (DEM) data from the National Elevation Dataset, accessed November 2016 at http://ned.usgs.gov/. Horizontal: UTM projection, NAD 83 Datum, zone 13, Vertical Datum: NAVD 1988

Figure 100. Route map for Day 4.

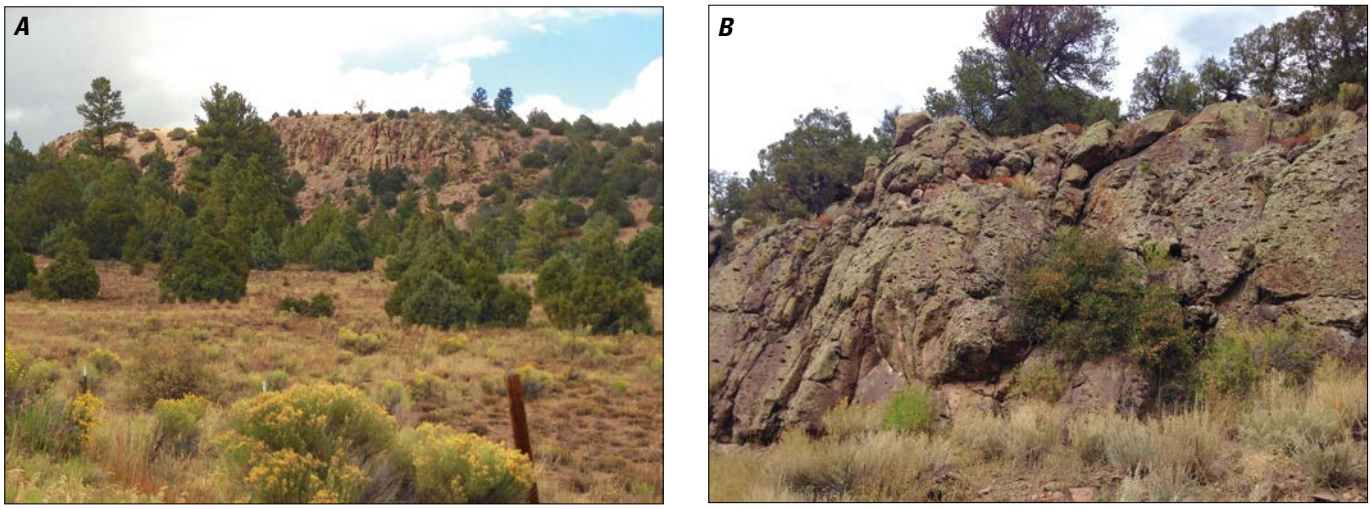

Figure 101. Outflow ignimbrites of the Treasure Mountain Group, along the lower Conejos River Valley. *A*, Cliffs of Chiquito Peak Tuff, east of lower Fox Creek. Photograph by P. Lipman, U.S. Geological Survey, 2016. *B*, Outcrop of Black Mountain Tuff, along CO 17 at the entrance to Mogote Campground (Stop 4-1). Lenticular cavities are weathered-out glassy pumice lenses, not gas cavities. Photograph by P. Lipman, U.S. Geological Survey, 2016.

comparison with the intracaldera equivalent (Stops 4-8, 4-B2, 4-B3, 4C-4). Return to CO 17.

From Fox Creek road, continue ahead on CO 17 to turnoff to Mogote campground. Park at campground entry (south side of road).

12.9 **Stop 4-1. Outflow ignimbrites at Mogote Campground** (37°04.07' N., 106°14.05' W.; 8,465 ft, 2,580 m elevation)

Exposed at road level to north is the Black Mountain Tuff, the first large regional ignimbrite of the Treasure Mountain Group (66–70 percent SiO_2; ~20 percent phenocrysts of plagioclase [pl]>biotite [bt]+clinopyroxene [cpx]). Lenticular cavities in these densely welded outcrops (fig. 102) are weathered-out glassy pumice lenses (fiamme). Although not exposed here, lower and upper black vitrophyre zones are characteristic of the Black Mountain Tuff. The upper vitrophyre contains sparse andesitic hornblende-bearing fiamme (a similar mafic component is present in late-erupted phases of the other large dacitic ignimbrites of the Treasure Mountain Group). Hornblende from the Black Mountain Tuff has yielded a recent $^{40}Ar/^{39}Ar$ age of 30.19±0.16 Ma (table 9, sample 11L-7B), which defines the initiation of major ignimbrite eruptions from the San Juan region.

In contrast to the substantial thickness of the Black Mountain Tuff in these outcrops, several overlying large ignimbrites of the Treasure Mountain Group are relatively thin in this area. The major upper

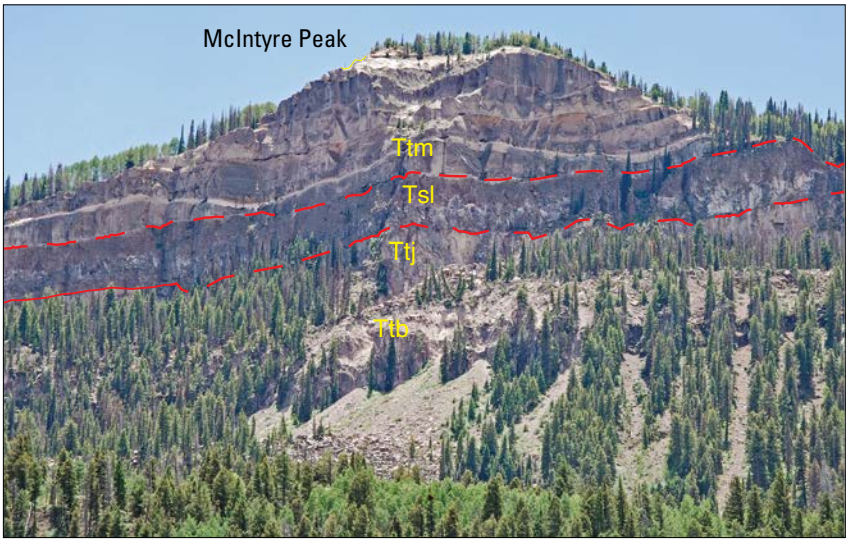

Figure 102. The north face of McIntyre Peak with ignimbrites of the Treasure Mountain Group exposed in a large Quaternary landslide scar (viewed from Stop 4-2). Lower slopes composed of lavas and breccias of the Conejos Formation are overlain by densely welded cliffs of the Black Mountain Tuff (Ttb) and the La Jara Canyon Tuff (Ttj), and a thick andesitic lava (red-dashed lines) correlated with lower Summitville Andesite (Tsl). Above this are eight units of the middle tuff (Ttm) separated by thin Plinian-fall deposits that are locally eroded by the passage of overlying pyroclastic flows. Contacts between units of the middle tuff are typically irregular; several of the units are compound. The base of the Ojito Creek Tuff is just out of sight to the south of the peak. Only the lowest middle-tuff unit is densely welded (near its base). Photograph by M. Dungan, University of Oregon, 2016.

ignimbrite, which generates abundant talus at road level, is the Chiquito Peak Tuff: a tan, partly welded crystal-rich dacite (62–68 percent SiO_2; ~35 percent phenocrysts of pl>bt+cpx>sanidine [san]) that records the youngest eruption from Platoro with a $^{40}Ar/^{39}Ar$ age of 28.77±0.03 Ma. Thus, this stop provides the opportunity to compare/contrast the first and last major ignimbrites erupted from the Platoro caldera complex over an interval of 1.5 m.y. (fig. 97). These can also be compared with the La Jara Canyon Tuff (65–68 percent SiO_2; 25–40 percent phenocrysts of pl>bt+cpx), the other largest ignimbrite erupted from Platoro caldera, exposed to the southwest at Stop 4A-1.

Ahead along CO 17, Conejos Formation lavas and volcaniclastic rocks are exposed along the lower slopes of the Conejos valley and its tributaries for the next 35 km, from this area to the Platoro caldera wall.

Continue to the junction with Platoro road (2,640 m elevation). Turn onto Platoro road (Forest Service Road [FS] 250), and immediately turn left into the parking area with mailboxes (2,640 m elevation). Route 4A continues south along CO 17, across Cumbres Pass, to permit the examination of more-distal facies of Treasure Mountain ignimbrites.

21.3 **Stop 4-2. Viewpoint for McIntyre Peak section and Cumbres Fault** (37°07.98' N., 106°21.08' W.; 8,661 ft, 2,640 m elevation)

Deep Pleistocene incision on the south flank of the Platoro caldera complex, particularly along the Conejos River valley and its tributaries, has created quasi-continuous exposures that reveal stratigraphic and geometric relations among the Conejos Formation and multiple ignimbrites of the Treasure Mountain Group. Sequential emplacement of these tuff sheets constructed an ignimbrite plateau, first by filling irregular topographic depressions on the flanks of Conejos volcanoes, and then by the dispersal of subsequent sheets across a surface with increasingly subdued relief. Precaldera topography, related to both erosion and construction, played contrasting roles in the local distributions, thicknesses, and degrees of welding of Treasure Mountain units in different sectors of the Platoro complex, but geologic relations in the southern sector are representative of the general impacts of preexisting topography and the progressive suppression of local relief created by the repeated emplacement of ignimbrite sheets. The south flank of the Platoro caldera complex preserves a thick and nearly complete record of Treasure Mountain volcanism, as only the South Fork Tuff is absent south of a divide broadly defined by the Alamosa River valley and the upper Conejos River.

The landslide scar on the north slope of McIntyre Peak (10,561 ft, 3,219 m) seen from this stop (fig. 103) offers the opportunity to establish a reference for comparing changes in thickness and degree of welding as a function of pre-eruptive paleotopography at more proximal and distal localities (Stops 4-3, 4-8, and 4A-1). The promontory of McIntyre Peak is underlain on its lower wooded slopes by lavas of the Conejos Formation and, discontinuously, by weakly welded lithic-rich lower rhyolite tuff of the Treasure Mountain Group. Upper ignimbrites of the Treasure Mountain Group are well exposed in the landslide breakaway scar higher on McIntyre Peak (fig. 102). The first cliff above the trees is the Black Mountain Tuff (already seen at Stop 4-1). The second cliff is the La Jara Canyon Tuff, and the dark overlying unit is an andesitic lava that is broadly equivalent to the lower member of the Summitville Andesite within Platoro caldera (lavas ponded after subsidence resulting from the La Jara Canyon eruption).

Above this lava are at least 10 densely to weakly welded ignimbrites, which constitute the middle tuff of the Treasure Mountain Group, with an aggregate thickness of ~175 m. The lower two tuffs, designated the La Manga units A and B (Dungan and others, 1989a; accessible at Stop 4A-1), are moderately to densely welded ignimbrite sheets of relatively modest thickness and volume; they have reversed magnetic polarities and phenocryst compositions similar to the La Jara Canyon Tuff. The La Manga units have been recognized south of the Platoro caldera in lower La Jara Creek and in the Conejos valley (including McIntyre Peak), the Los Pinõs area, and along the Continental Divide east of the upper Chama basin (Balsley, 1994). More than 80 percent of the volume of the middle tuff is represented by 12 or more upper ignimbrite sheets, most only slightly welded, that have petrologic affinities with both the Ojito Creek and Ra Jadero Tuffs. These ignimbrites, collectively designated the Fox Creek units of the middle tuff (a partial section is accessible at Stop 4C-7b), have the normal magnetic polarity of the overlying Ojito Creek Tuff, but paleomagnetic-pole positions vary substantially among successive units. Ignimbrites of the middle tuff accumulated to a substantial thickness by prograding laterally toward distal positions located beyond the thickest accumulations of the La Jara Canyon Tuff, thereby creating a broad plateau with minimal relief. As a result, the post-middle-tuff depositional surface surrounding Platoro caldera was much more subdued than the preignimbrite surface on the Conejos Formation.

Individual ignimbrites of the middle tuff are small in volume compared to other regional tuffs of the San Juan magmatic focus. No rigorously documented correlations between widely dispersed sections of the middle tuff have yet been established. Thus, little is known about the lateral extents of any individual ignimbrites; they may represent 10–15 widely distributed deposits or many more smaller ignimbrites that were

restricted in extent (probably some of both). Individual units appear to be too modest in volume to have been associated with caldera collapse events on the scale of other Treasure Mountain ignimbrites. However, the composite thickness of the middle tuff around the southeastern and southern peripheries of the Platoro complex commonly exceeds the combined thickness of the directly overlying Ojito Creek and Ra Jadero Tuffs.

Lipman (1975a) inferred that the entire middle tuff sequence postdated eruption of the intracaldera lower member of Summitville Andesite, based on the local presence of andesite lavas immediately above the La Jara Canyon Tuff, as at Mclntyre Peak, Black Mountain, and other outflow sites. The close petrologic affinities of the La Manga units to the La Jara Canyon, along with paleomagnetic evidence, suggest, however, that these ignimbrites represent continued eruptions from the La Jara Canyon magma body.

The Cumbres Fault runs through a side valley on the north wall of the Conejos canyon, 500 m northwest of this stop, and continues south along the west base of McIntyre Peak (Lipman, 1975b). This is the largest of several north-trending normal faults, related to development of the Rio Grande Rift, that cut the eastward-tilted dip slope of volcanic rocks as young as Hinsdale Formation lavas in the southeastern San Juan region. Most of the normal faults are antithetic to the Rio Grande Rift; they drop strata down to the west in opposition to the eastward dip of the volcanic rocks toward the rift. The Cumbres Fault has about 300 m of maximum displacement and is traceable for at least 40 km from the Alamosa River southward into New Mexico.

Continue northwest on Platoro road.

22.8 Proterozoic gneissic granite (~1.45 billion years old [Ga]), exposed on both sides of the road (2,660 m elevation), demonstrates significant paleorelief on the prevolcanic depositional surface resulting from Late Cretaceous-early Cenozoic (Laramide) uplift in the southern Rocky Mountains. In contrast, the oldest exposed rocks beneath the volcanic field west of the Continental Divide are upper Mesozoic sedimentary strata of the San Juan Basin.

Continue ahead (northwest); pull off into the wide spot on the right (east) side, by the Entering Restricted Area sign.

25.6 **Stop 4-3. Viewpoint for Black Mountain** (37°09.05' N., 106°24.96' W.; 8,760 ft, 2,670 m elevation)

Cliffs along this segment of the Conejos canyon expose a thick and relatively complete sequence of Treasure Mountain ignimbrites (fig. 103), although relations at this site are slightly complicated by three small normal faults that trend north-northeast, parallel to the Cumbres Fault to the east. The largest of these faults occupies the sharp reentrant in the cliff southeast of this stop. The high northwest-facing cliff of La Jara Canyon Tuff is upthrown on the southeast side of this fault (fig. 103*A*). The Treasure Mountain section to the northwest, above a lower slope of lavas and volcaniclastic rocks (Conejos Formation), provides informative comparisons with the ignimbrite sequence and thickness at McIntyre Peak, just 7 km to the southeast.

Large thickness changes over short distances, in discontinuous exposures of the weakly welded pinkish rhyolitic lower tuff (pl>bt±cpx) on this cliff (fig. 103*B*) and elsewhere around the Platoro system, reflect filling of preexisting valleys by the first caldera-related eruptions of pyroclastic density currents. In contrast, three densely welded ignimbrites of lower tuff are present at geographic Treasure Mountain (near Wolf Creek Pass, northwest of Platoro caldera). The lower tuff is preserved discontinuously because it was preferentially emplaced in post-Conejos valleys, where it locally ponded to variable thicknesses (generally not welded), then was substantially eroded prior to the emplacement of the Black Mountain Tuff.

The dark-gray densely welded dacitic Black Mountain Tuff (seen in outcrop at Stop 4-1) is more sheet-like in thickness than the lower tuff along these cliffs, but the basal contact and thickness reflect modest local topographic relief. Characteristic features, which are particularly clear from this vantage, are black vitrophyres at both the top and base of the densely welded and devitrified gray interior. Similar upper and lower vitrophyres are common in the younger Ojito Creek and Ra Jadero Tuffs. These three ignimbrites are comparable in bulk composition (67–69 percent SiO_2); modest contents of plagioclase, augite, and biotite (plus sanidine and relatively Or-rich sodic plagioclase in the Ra Jadero); mineral chemistry; and their dense welding at virtually all localities around the periphery of the Platoro caldera complex. The Black Mountain Tuff is exposed along the present-day Conejos valley from Black Mountain southward, at least as far southeast as Fox Creek (Lipman, 1975b), but in some areas both the lower rhyolite tuff and the Black Mountain Tuff are absent above the Conejos Formation. All of the subsequent Treasure Mountain ignimbrites are widely dispersed and semicontinuous from the geographic Chiquito Peak (Stop 4C-8b) southward into the Conejos River drainage (Stop 4-1), southwest toward the Rio Chama watershed (Stop 4A-1), and westward along the southern San Juan Mountain front. In this westward direction the Black Mountain Tuff extends at least as far as Pagosa Peak, ~40 km beyond the west rim of Platoro caldera (Lipman, 2006).

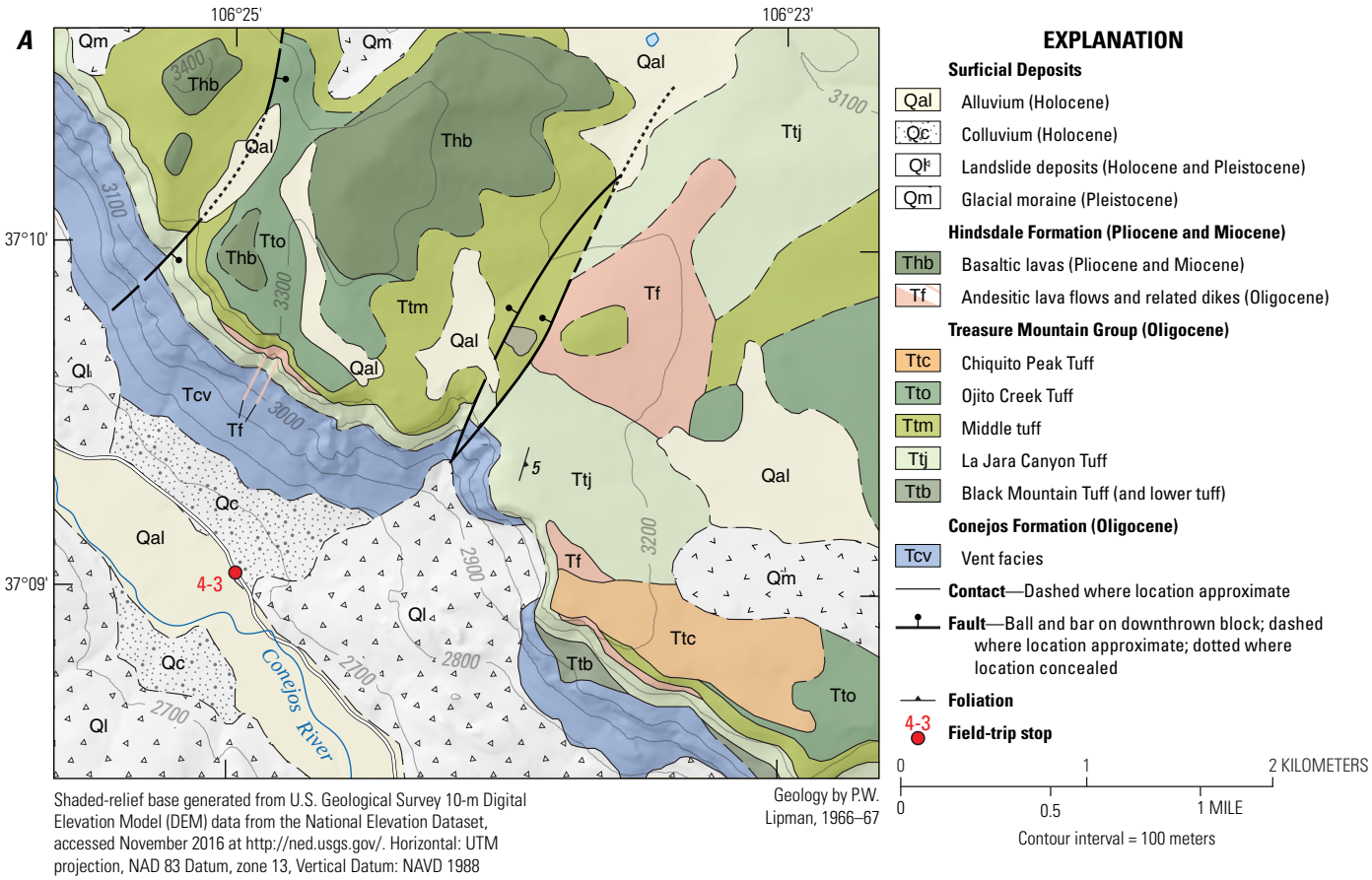

Figure 103. Treasure Mountain ignimbrites on cliffs southwest of Black Mountain, along the Conejos River canyon (Stop 4-3). A relatively complete section of ignimbrites from Platoro caldera is represented, overlying andesitic lavas, and volcaniclastic breccias and conglomerates of the Conejos Formation. *A*, Geologic map of the Black Mountain area modified from Lipman (1975b). This is the type locality of the densely welded Black Mountain Tuff (Ttb). This ignimbrite is similar in outcrop and petrographic features to exposures in the lower Conejos canyon (Stop 4-1), where it is locally even thicker and more uniform. The prominent dark upper vitrophyre is easily distinguished from the gray devitrified interior of the ignimbrite. The outflow La Jara Canyon Tuff (Ttj) attains its greatest thickness (200 meters) at this locality, owing to ponding in a broad depression south of the Conejos volcanoes that rim the south Platoro caldera. Geographic Black Mountain and adjacent hillcrests are capped by basaltic lavas (Thb) of the Hinsdale Formation, which overlies ignimbrites of the Treasure Mountain Group along an unconformity eroded during eastward tilting toward the early Rio Grande rift. *B*, Views of cliffs southeast of Black Mountain. Bedded andesitic conglomerates of Conejos type (Tcc) are interlayered between two ignimbrite units of the lower rhyolite tuff (Ttl-1,Ttl-2), which provide early documentation of the San Juan ignimbrite flare-up. Intermediate-composition lavas and volcaniclastic rocks interfinger locally between all the outflow tuff sheets and accumulated thickly within many of the associated calderas, demonstrating the continued, dominantly andesitic character of San Juan volcanism throughout the ignimbrite flare-up (30–27 million years ago [Ma]). Ttb, Black Mountain Tuff; Tcv, lavas of the Conejos Formation; Ttj, La Jara Canyon Tuff; Ql, Quaternary landslide deposits. Photographs by M. Dungan, University of Oregon, 2016.

The crystal-rich dacitic La Jara Canyon Tuff (Ttj; pl>bt+cpx) is as thick as 200 m in the cliffs above this stop (fig. 103*B*); it thins to the north, toward the caldera, as the elevation of the basal contact climbs (the current geometry is complicated by local normal faults). This exceptional section is interpreted as a result of the topographic inflection that marked the base of the steeper lava-dominated upper flanks of the Conejos volcano at Willow Mountain and the more subdued topography on volcaniclastic deposits around the southern margins of Conejos edifices. The white, weakly welded base of the La Jara Canyon Tuff at this outflow locality (no air-fall deposit is present) grades upward into densely welded and devitrified tuff, without the basal vitrophyre zone that is widely present elsewhere. Contacts between at least eight separate flow units are recognizable within the welded interior of this ignimbrite, based on subtle color changes and partings (fig. 103*B*).

The La Jara Canyon Tuff is separated from overlying densely welded ignimbrites by an andesitic lava (fig. 103*A*), which is interpreted as lower member of Summitville Andesite. Local andesite dikes, obscurely exposed in gullies cutting the cliff wall, may be feeders for these lavas. Lavas of similar dimensions and composition

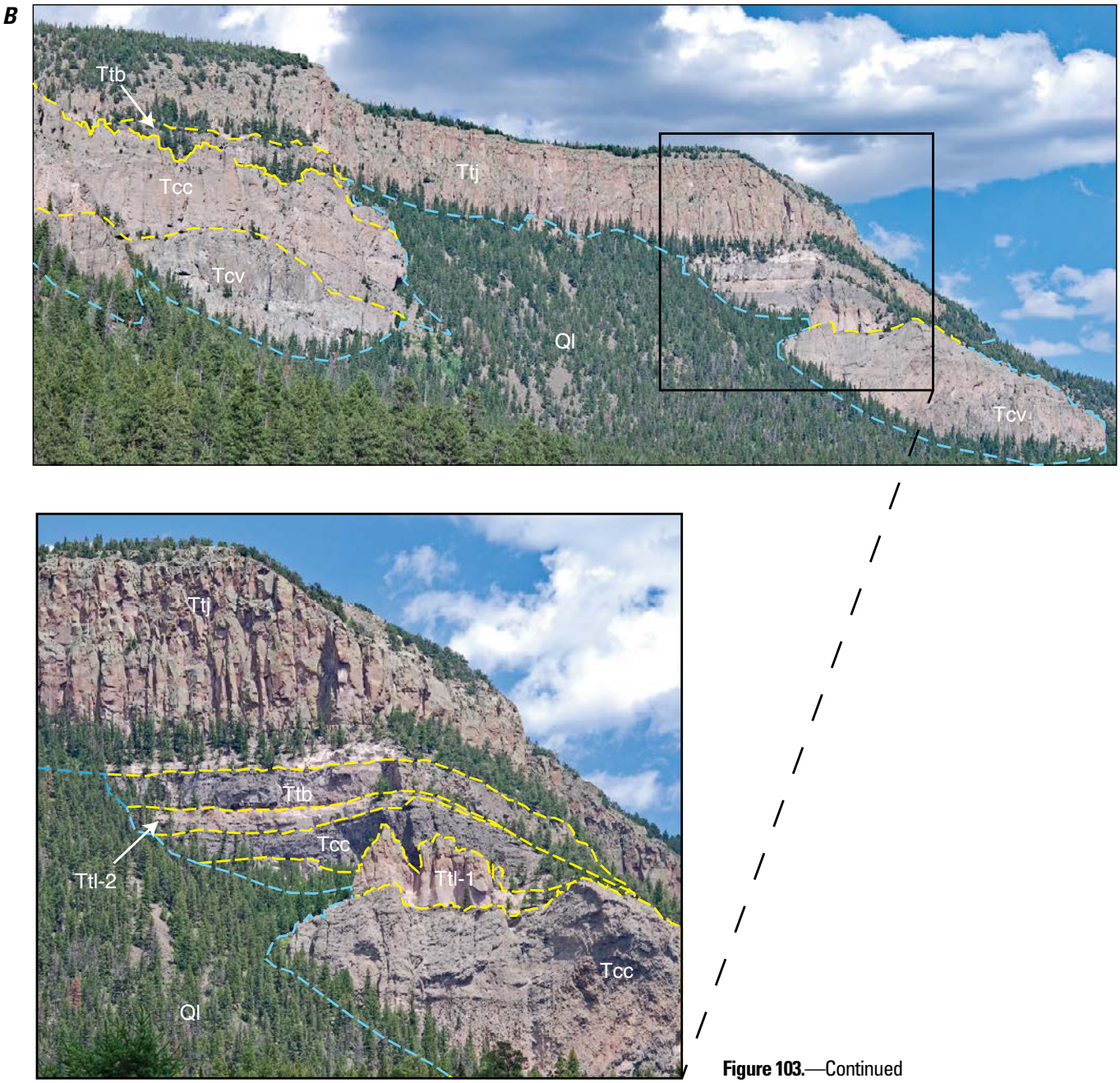

Figure 103.—Continued

form discontinuous cliff exposures at the same stratigraphic level elsewhere to the south; for example, at McIntyre Peak (Stop 4-2) and as far south as Spruce Hole, near La Manga Pass. These lavas affirm the importance of background andesitic magmatic input into the Platoro system during intervals between caldera-collapse events. The comparably large Chiquito Peak eruption, which signaled the termination of caldera-collapse activity at the Platoro complex, was also succeeded by voluminous intermediate-composition lavas.

The two welded ignimbrites directly above this andesitic lava are units of the middle tuff of the Treasure Mountain Group. As many as 10–12 ignimbrites of the middle tuff, which represent separate eruptions, are present at some distal localities where the middle tuff is as much as ~200-m thick (for example, at McIntyre Peak, Stop 4-2), but they are generally less welded. In contrast to the major ignimbrites of the Treasure Mountain Group, basal air-fall deposits are common beneath ignimbrite units of the middle tuff, and thin fluvial deposits (generally <5 m) are present between some units (for example, Stop 4C-7b). The large volume of the La Jara Canyon eruption (~500 km^3) may have led to a drastic reorganization of the magmatic system,

which in turn may have contributed to the anomalous character of middle tuff eruptions.

The caldera structure from which the La Jara Canyon magma erupted is now largely buried by younger volcanic rocks. Only along the northeastern and southwestern margins of the Platoro caldera complex are remnants of the La Jara Canyon subsidence structure preserved (fig. 93). At these sites, younger Treasure Mountain ignimbrites (middle, Ojito Creek, and Ra Jadero tuffs) are banked against early caldera-wall segments that postdate the La Jara Canyon Tuff. In the absence of more complete evidence concerning the nature and distribution of vents for the middle tuff, one could speculate that the La Jara Canyon caldera depression may have hosted dacitic postcaldera domes and cones, which could have been sources for some pyroclastic flows of the middle tuff. Origins such as this for the middle tuff would require that the abundant andesitic lithic fragments in many of these ignimbrites were derived from intracaldera lavas (lower member of Summitville Andesite) rather than from Conejos lavas, a hypothesis yet to be tested. Most pyroclastic-flow deposits with aerial distributions of 100–200 km^2 and volumes on the order of 10–50 km^3 are caldera-related, as seems likely for many ignimbrites of the middle tuff. Perhaps nested collapse-related eruptive centers developed recurrently within the caldera complex during this period.

This stop also highlights an inversion in the thickness of the La Jara Canyon and middle tuffs, in comparison to absolute and relative thickness at McIntyre Peak (Stop 4-2). The La Jara Canyon Tuff is ~200-m thick here, about double that at McIntyre Peak (~90 m). At McIntyre Peak, 10 or more ignimbrites of middle tuff have an aggregate thickness (~175 m) more than twice that of the underlying La Jara Canyon exposed there (fig. 102). In contrast, only two (densely welded) middle tuff units (~20–25 m) are present at Black Mountain. Ignimbrites of the middle tuff accumulated to a substantial thickness by prograding laterally toward distal positions located beyond the thickest accumulations of La Jara Canyon Tuff, thereby creating a broad plateau with minimal relief.

Observed differences from those predicted for ignimbrite emplacement across a surface with low relief include

- Patchy deposition on outwardly dipping proximal slopes of precaldera edifices, because pyroclastic density currents typically bypassed these areas. This is comparable to the east flank of Valles Caldera, where tuff outcrops are minimal on the upper east-facing slopes of the Sierra de los Valles.
- The tendency for poor representation of tuffs in near-vent areas of high relief, which is further augmented by enhanced postdepositional erosion in these areas.
- The earliest Treasure Mountain ignimbrites (lower rhyolite tuff), which are modest in volume, have highly irregular distributions that generally are confined to local paleodepressions (fig. 103*B*), and were subject to erosion prior to burial by the Black Mountain and La Jara Canyon Tuffs.
- The more voluminous overlying La Jara Canyon Tuff is a widespread densely welded sheet, locally >100-m thick, that varies in thickness as a function of first-order topographic gradients and distance from the caldera source.
- The thickness and welding intensity of late-erupted Treasure Mountain ignimbrites decrease with distance from the caldera source.

Continue up the Conejos valley, through lavas and clastics of the Conejos Formation at river level, with Treasure Mountain ignimbrites capping the canyon rims. Turn left onto a narrow road 0.3 mi beyond the sign, Lower South Fork Trailhead. Continue westward ~100 m to an unmarked parking and turnaround spot near the curve. The formal parking area at the trailhead provides the last easy opportunity for a bathroom break before Stunner U.S. Forest Service campground at mile 50.

32.1 **Stop 4-4. Conejos Formation stratigraphy—Interbedded lavas and volcaniclastic deposits** (37°14.02' N., 106°28.03' W.; 9,137 ft, 2,785 m elevation)

The lavas and interbedded clastic units seen from this locality (fig. 104) are part of the south flank of a Conejos volcano (marked by present-day Willow Mountain, fig. 93) that has been truncated along the southeastern topographic margin of the Platoro caldera and incised by the Conejos River. The precaldera Conejos Formation (35–30 Ma) represents about two-thirds of the magmatic output of the San Juan focus of the SRMVF. The andesitic average composition of the Conejos Formation, in the absence of erupted basaltic magma (basalt or basaltic andesite with <54 percent SiO_2 is rare), is consistent with the continental setting, magma evolution in thick crust, and the apparent lack of extensional stress during Oligocene San Juan volcanism. Platoro caldera is ringed by remnants of several large Conejos eruptive centers (for example, present-day Conejos, Willow, and Pintada Mountains) that were truncated during multiple collapse events. These still stand at high elevations along the outer, topographic margins of the composite caldera-collapse depression, despite the loss of their summit regions, and the original volcanic summits stood at substantially higher elevations, relative to the ultimate caldera-related depression, than do the present-day topographic highs

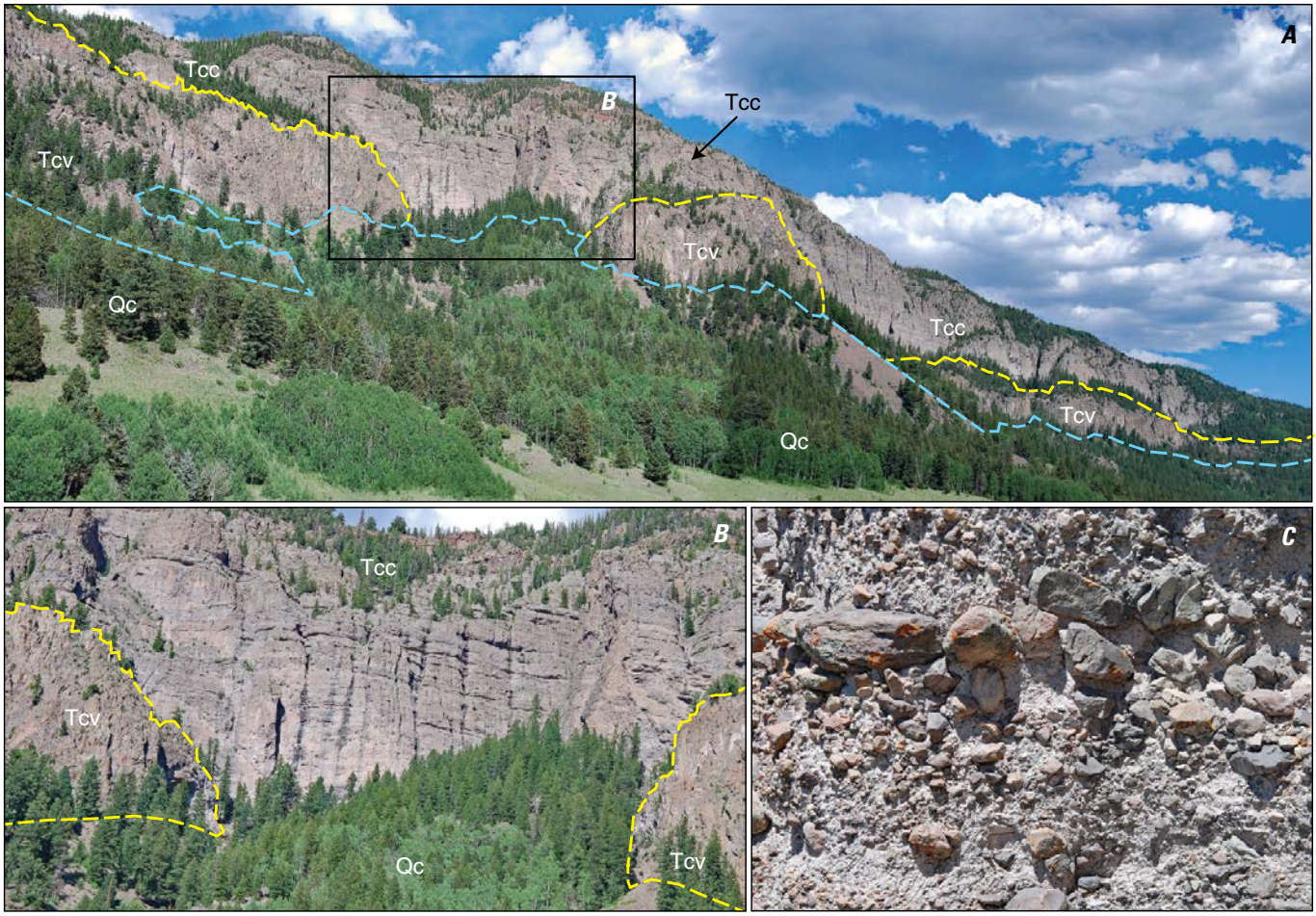

Figure 104. Interbedded lavas and volcaniclastic rocks of the Conejos Formation in cliffs on the east side of Conejos valley (Stop 4-4). Three successively more detailed views (*A*–*C*) of the volcaniclastic rocks deposited in a local paleovalley eroded into lavas of the Conejos Formation. Discontinuous lower cliffs (Tcv) are andesitic-dacitic lavas of the Willow Mountain compositional type. The overlying bedded clastic unit (Tcc) is a thick sequence of debris flows and fluviatile conglomerates containing clasts that locally exceed 2 meters. Coarse debris-flow deposits are widely characteristic of the clastic facies of the Conejos Formation south of the caldera. Qc, colluvium. Photographs by M. Dungan, University of Oregon, 2016.

(flank remnants). Among younger analogs to this annular arrangement of precaldera volcanic centers are the Pleistocene Crater Lake-Mazama system (Bacon, 1983, 2008) or the Jemez Mountains volcanic field (Valles Caldera, Day 1 of this trip).

Colucci and others (1991) refer to the one of three Conejos compositional types associated with the Platoro caldera as the Willow Mountain lava type on the basis of magma compositions from geographic Willow Mountain. These are intermediate in chemistry and mineralogy between the amphibole-bearing calc-alkaline Horseshoe Mountain type and the more alkali-rich Rock Creek type (anhydrous mineralogy).

A substantial volumetric fraction of the Conejos Formation associated with the Platoro caldera consists of coarse clastic deposits that represent posteruptive fragmentation, transport, and redeposition of primary eruptive products, as is strikingly exposed on the cliffs to the east (fig. 104). In contrast, the massive cliffs across the Conejos valley to the west consist largely of thick lavas that remain unstudied. The origins of precaldera volcaniclastic rocks pose important questions, as the cumulative volume of such deposits across the San Juan Mountains region totals several thousand cubic kilometers. Clastic strata interbedded with thick lava piles locally compose more than 50 percent of stratigraphic sections exposed in the valleys surrounding the Platoro caldera, and many units have fan-like geometries and thicknesses >100 m. In contrast, the volcaniclastic rocks at this stop fill deep paleovalleys. The proportion of clastic deposits relative to lavas tends to increase with distance from Platoro caldera. Nearly lava-free sections of Conejos volcaniclastic rocks are as much as ~725-m thick near the head of Rio Blanco southwest of Platoro caldera, and still ~350-m thick in the Rio Chama valley, 25 km

from the caldera rim (Steven and others, 1974a). Such volcaniclastic rocks compose lower proportions of Conejos volcanoes in the northeastern San Juan Mountains (Bonanza caldera), but higher proportions of the Conejos-equivalent volcanic centers associated with western San Juan calderas.

Most clasts in the Conejos deposits are fragments of dense lava; pumice and scoria are rare. Primary volcanic deposits were converted to fragments, then transported large distances. Initially angular clasts underwent rounding and fluvial reworking, particularly in more distal areas, but other processes may have been among the fragmentation steps that produced such large volumes of coarse, clastic material. These exposures pose several questions:

- Were eruptions directly involved in creating the volcaniclastic deposits?
- If so, were effusive or explosive eruptive dynamics involved?
- What were origins of the paleovalleys in which some Conejos volcaniclastic deposits are localized/confined?
- What processes were responsible for the creation, transport, and deposition of the clasts and matrix in these volcaniclastic units?
- If voluminous water was involved, how and where was it supplied, stored, and channeled in this system?
- To what degree does our limited knowledge of early Oligocene (~35–30 Ma) climatic conditions in this region influence our interpretations for emplacement of these deposits?

Return to Platoro road and continue northwest.

33.1 **Stop 4-5. Conejos-age ignimbrite at The Pinnacles**—Tuff of Rock Creek (?) **(**37°15.11’ N., 106°28.24’ W.; 9,514 ft, 2,900 m elevation)

At this locality, a densely welded ignimbrite of phenocryst-poor mafic trachydacite (3–5 percent potassic-pl>cpx>opx; ~64–65 percent SiO_2), characterized by high incompatible-element contents and large aphyric glassy fiamme, fills an erosional channel in older lavas and breccias of the Conejos Formation. This distinctive local tuff, with its conspicuous basal vitrophyre, can be traced for only a short distance laterally; it is overlain by lavas of Willow Mountain type higher on the south rim of Platoro caldera. Even local preservation of such welded tuff is rare within the Conejos, and this is the only such exposure known south of the Alamosa River. Northeast of Platoro caldera, the compositionally similar tuff of Rock Creek (Lipman, 1974, 1975a; Colucci and others, 1991) is a more widely preserved ignimbrite of similar composition that has been interpreted as a local precursor to more voluminous eruptions from Platoro caldera. It remains uncertain whether the tuff at the Pinnacles is an isolated southern lobe of the Rock Creek ignimbrite, or an unrelated tuff of similar composition.

Toward the southwest, along the South Fork of the Conejos River, distinctively thick lavas and domes of Willow Mountain type are as much as 300-m thick.

Continue north, entering the Platoro caldera area map (Lipman, 1974). **6.0**

39.1 **Stop 4-6. Southern margin of Platoro caldera at Beaver Creek (**37°19.22’ N., 106°28.27’ W.; 9,678 ft, 2,950 m elevation)

In contrast to the morphologically obvious Valles Caldera viewed on Day 1, most calderas of the SRMVF have obscure topographic expression, and their identification is dependent on interpretation of geologic features. Many of these calderas are recognized by the presence of thick caldera-fill deposits and by mappable unconformities between precaldera and intracaldera rocks along topographic margins. Only a few calderas, mainly in the western San Juan region (Lake City, Silverton), are eroded to levels sufficiently deep to expose ring faults.

Such an unconformity at the southern margin of Platoro caldera lies along Beaver Creek. Lower parts of the caldera-fill assemblage along Beaver Creek include laminated lake-bed strata exposed mainly as light-tan clay-rich float, in contrast to precaldera rocks of the Conejos Formation to the south that consist of intermediate-composition lavas and interleaved, poorly indurated coarse volcaniclastic rocks. Small outcrops of the lake-bed sediments can be reached by hiking about 1 km up the faint Beaver Creek trail (fig. 105).

Above these deposits of ancient Lake Platoro are thick intermediate-composition lavas that ponded within the southern caldera, including the dacite of Fisher Gulch (viewed at Stop 4-7) overlain by Summitville Andesite (Stops 4-10, 4C-2, 4C-5). Platoro was filled to overflow by such andesitic and dacitic lavas, and most of its caldera margins are marked only by obscure unconformities between precaldera and postcollapse lavas of similar intermediate-compositions, as at Beaver Creek. Locally preserved truncations of the regional Treasure Mountain ignimbrites (Stop 4-11) or margins of ponded intracaldera tuff (Stop 4B-2) along such unconformities, especially along the east and west sides of Platoro (figs. 95, 96), provide conclusive evidence that the mapped unconformities are caldera boundaries.

Figure 105. Intracaldera lake-bed sediments, abutting the southern caldera margin along Beaver Creek (Stop 4-6). The cutbank is along Beaver Creek, along the trail about 1 kilometer upstream from Platoro road. These sediments have yielded varied plant and pollen fossils indicative of a temperate climate similar to or milder than the present (Lipman, 1975a, p. 66; E. Leopold, University of Washington, written commun., 2015). Float of the lake-bed sediments can be examined in roadcuts along the Platoro road at Beaver Creek (Stop 4-6). Photograph by P. Lipman, U.S. Geological Survey, 1971.

Continue north toward the massive, dark outcrops of intracaldera lava (dacite of Fisher Gulch) that form cliffs ahead on both sides of the valley. Park along the side of the road.

39.6 **Stop 4-7. Caldera-filling dacite of Fisher Gulch** (37°19.76' N., 106°28.33' W.; 9,678 ft, 2,950 m elevation)

The dacite of Fisher Gulch, a single, thickly ponded lava that directly overlies intracaldera Chiquito Peak Tuff in exposures ahead, represents the first major postsubsidence eruption. This dacite is widely characterized by crude flow layering (fig. 106), and in the area of this stop, a northwest-trending zone of steeply dipping flow layering as much as a kilometer across has been interpreted as the vent area (Lipman, 1974, 1975a). The Fisher Gulch lava (62–64 percent SiO_2; ~30 percent pl>bt>cpx+san) is compositionally similar to the most mafic analyzed samples of Chiquito Peak Tuff. It is the only Oligocene caldera-filling lava that contains sanidine. Its $^{40}Ar/^{39}Ar$ age (28.74**±0.09 Ma**; table 9, sample KF-58) and U-Pb zircon age (28.9**±0.**3 Ma; Gilmer and others, 2021) are within analytical uncertainty of the underlying ignimbrite. High on this slope, the sanidine-bearing dacite of Fisher Gulch is overlain by less-evolved lavas of upper-member Summitville Andesite.

Dark-gray andesitic inclusions, a few centimeters to a meter across, are locally abundant. Most inclusions are angular to subrounded, and locally rimmed by

Figure 106. The dacite of Fisher Gulch (Stop 4-7). Obscure to well-developed flow foliation and layering are displayed in steeply dipping massive exposures of the porphyritic dacite. Photograph by P. Lipman, U.S. Geological Survey, 2016.

replacement carbonate (fig. 37 in Lipman, 1975a). In places, andesitic inclusions and the rhyodacitic matrix are intricately intermixed in a marble-cake style that suggests both components were mobile magmas at the time of mixing.

Continue ahead along more outcrops of dacite, crossing contact with intracaldera Chiquito Peak Tuff at Fisher Gulch 1.0 mi ahead, past Robinson Gulch at 2.0 mi, and passing several bold outcrops of intracaldera tuff. Pull off on the left side of the road, just past road sign (Speed Limit 25, on west side). Proceed on foot to examine blocks of intracaldera tuff along the right side of the road and the contact with porphyritic resurgent intrusion at road level in outcrops ahead.

43.2 **Stop 4-8. Intracaldera Chiquito Peak Tuff**
(37°21.22' N., 106°31.32' W.; 9,826 ft, 2,995 m elevation)

For the last 2 km (since the mouth of Fisher Gulch), the road has passed through the densely welded, propylitically altered crystal-rich facies of intracaldera Chiquito Peak Tuff. This stop highlights transformations that occur in deeply buried (more than several kilometers) intracaldera tuff relative to outflow of the same ignimbrite, such as that viewed at Stop 4-O in Fox Creek and in float at Stop 4-1. The impacts of deep burial, including low-grade metamorphism and deformation during resurgence, renders field correlations with the equivalent outflow ignimbrites challenging. The mismatches in outcrop-scale appearance and mineralogy were particularly challenging for workers who were attempting to understand San Juan volcanism during the mid-20th century, as many concepts and analytical tools that are in use today were not yet available. At Platoro, the intracaldera ignimbrite accumulation was initially miscorrelated with the widespread outflow La Jara Canyon Tuff (Lipman, 1974, 1975a), because the intense propylitic alteration widely obscured the diagnostic presence of sparse sanidine that distinguishes the Chiquito Peak lithology (Lipman and others, 1996; see further discussion for Stop 4B-3). We also call attention to the similarities between this locality and features that will be observed on Day 5 (Stop 5B-9 intracaldera Carpenter Ridge Tuff, near Creede, Colorado).

In the southern Platoro caldera, the tuff is strongly propylitized and therefore even difficult to recognize as pyroclastic rock, except for the scattered presence of small angular fragments of andesite. The intracaldera tuff exhibits distinctive slabby jointing that more closely resembles jointing in lavas than in outflow ignimbrite sheets (fig. 107); similar jointing is common deep within caldera-filling tuffs in the San Juan region and elsewhere, but not in outflow ignimbrites. The fractures are reminiscent of columnar jointing in some lavas, welded tuffs, and dikes, but these slabs lack the diagnostic hexagonal cross-sections of contraction-related columns. Instead, they result from intersections among multiple subvertical fracture sets, among which one direction is locally dominant. This configuration is likely to have resulted from contraction during cooling and devitrification, in combination with differential stress related to resurgence. This inference is supported by similar examples at Bachelor caldera, where comparably steep fracture surfaces postdate the development of rheomorphic flow structures in resurgently domed intracaldera Carpenter Ridge Tuff.

Chiquito Peak Tuff at this locality resembles the outflow ignimbrite (Stop 4-O), only in the sense that both have dacitic compositions and abundant small phenocrysts. Cursory examination does not immediately reveal that this is a pyroclastic rock. Early 20th century workers interpreted the tuff on Cornwall Mountain as thick andesitic lava (Patton, 1917; Cross and Larsen, 1935; Larsen and Cross, 1956). Propylitic alteration, equivalent to low-pressure greenschist-facies metamorphism, has converted primary minerals to

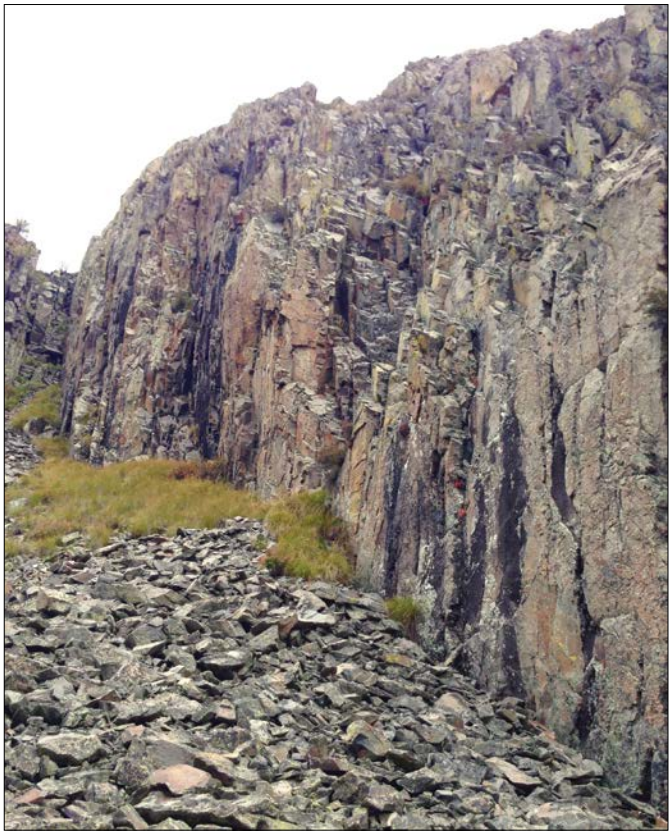

Figure 107. Jointing in intracaldera Chiquito Peak Tuff (Stop 4-8). Closely spaced slabby jointing is typical of densely welded and propylitized intracaldera Chiquito Peak Tuff deep in the Cornwall resurgent block (especially along the Platoro road between Fisher Gulch and Stunner Pass), and elsewhere within San Juan calderas. Photograph by P. Lipman, U.S. Geological Survey, 2016.

an assemblage of albite-chlorite-epidote-carbonate-magnetite-actinolite, hence the dark green color of freshly broken surfaces. Ghosts of pyroclastic textures are discernable in some thin sections, but mineral chemistry is not a viable tool for identification of this locality as Chiquito Peak Tuff.

In the roadcuts ahead, dacite porphyry (62–64 percent SiO_2) intrudes the intracaldera tuff along a gently dipping contact; larger masses of similar intrusive dacite are exposed over an area of several square kilometers along the south slopes of Cornwall Mountain. The small road-level exposure of the intrusion contains rounded inclusions of vesicular andesite in the dacitic matrix, indicative of mingling of compositionally diverse magmas. The exposed intrusion has been interpreted as the upper part of a larger body responsible for trapdoor resurgent uplift of the Platoro caldera floor. This resurgent intrusion has yielded a U-Pb zircon age of 28.0±0.3 Ma, insignificantly different from the $^{40}Ar/^{39}Ar$ age of 28.77±0.03 Ma for the Chiquita Peak Tuff, and indicating rapid postcollapse caldera magmatic and structural evolution (Gilmer and others, 2021). East of this locality, the uplifted block of intracaldera Chiquito Peak Tuff is bounded by an arcuate fault (see fig. 93) that is thought to be a reactivated segment of the caldera ring fault (structural boundary; Stop 4C-3). The intracaldera tuff is more than 800-m thick on this uplifted block, with its top eroded and no base exposed, and documents thick ponding of the tuff within the caldera during subsidence.

Continue west past Platoro, 0.3 mi ahead (last chance for gas for the next 50 mi).

The Mammoth Revenue mine, on the southwest side of the village, has been a gold producer intermittently over the past century (Patton, 1917; Bird, 1972). This mine follows veins along northwest-trending faults and fractures that are discontinuously traceable 25 km northwest to Wolf Creek Pass. Mineralization is most intense at three intersections of this regional fault zone with caldera structures, at the Platoro, Stunner, and Summitville districts.

45.2 *Intersection with Platoro Reservoir road (FS 242), on left (37°21.66' N., 106°32.84' W.; start of route 4A); continue uphill to right (north) to Stunner Pass*

45.9 **Stop 4-9. Stunner Pass overview** (37°21.68' N., 106°33.43' W.; 10,547 ft, 3,215 m elevation)

This southeastward panorama (fig. 108) provides an overview of the Conejos valley and southern Platoro caldera, including features observed at close hand during Stops 4-6 to 4-8, and displays relations among key units that manifest the late collapse and postcollapse history of the caldera, as well as precaldera lavas of the Conejos Formation. Stunner Pass lies along the zone of steep northeast-trending faults that have localized postresurgence hydrothermal alteration and ore mineralization in Platoro (Mammoth Revenue mine), north along the Alamosa River (Stop 4-10), to the Summitville mining district

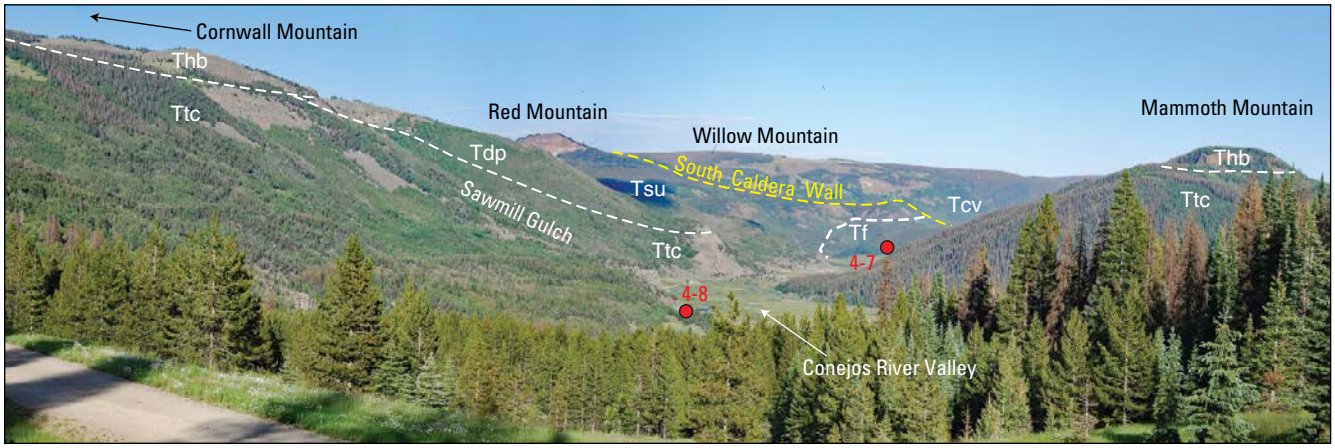

Figure 108. Platoro caldera view (Stop 4-9), from Stunner Pass looking south down the Conejos River valley. Thick intracaldera Chiquito Peak Tuff (Ttc), exposed on the Cornwall resurgent block, intruded by porphyritic dacite (Tdp) that crops out on the cliffs behind Sawmill Gulch. Cornwall Mountain (3,745 m elevation) and Mammoth Mountain (3,470 m elevation) are capped by trachybasalt lavas of the Hinsdale Formation (Thb). In the distance to the south, Willow Mountain (3,629 m elevation) is underlain by lavas and volcaniclastic rocks of the Conejos Formation (Tcv) at the southern wall of the Chiquito Peak caldera. Red Mountain (3,663 m elevation) to the east, exposes andesitic lavas and interbedded sedimentary strata of Summitville Andesite (Tsu) that overlie dacite of Fisher Gulch (Tf), the initial caldera-filling lava in this area (28.54±0.09 million years ago [Ma]), both banked against Conejos Formation at the southeastern caldera margin. Photograph by M. Dungan, University of Oregon, 2016.

at South Mountain (Stop 4-13) and beyond to Wolf Creek Pass (Lipman, 2006).

Cornwall Mountain is primarily an accumulation of densely welded, intracaldera Chiquito Peak Tuff more than 800-m thick, with its top eroded and no base exposed. The intracaldera tuff has been comprehensively transformed by propylitic alteration (Stop 4-8), in contrast to the outflow Chiquito Peak Tuff (Stops 4-1, 4C-8b), or to the wedge-edge of intracaldera vitrophyre and devitrified tuff exposed along the Platoro Reservoir road (Stops 4B-2, 4B-3). Mafic lavas of the Miocene Hinsdale Formation (~22 Ma?) cap Cornwall and Mammoth Mountains. The slope west of Sawmill Gulch is largely underlain by a resurgent intrusion of porphyritic dacite. This intrusion also lies at the southern end of an arcuate fault system that bounds the eastern margin of the trapdoor-like resurgent block of intracaldera Chiquito Peak Tuff. The fault continues northward, out of sight behind Cornwall Mountain, into the north-flowing California Gulch, and then through the village of Jasper and its abandoned mining district (Alamosa River drainage, Stop 4C-3).

Red Mountain (12,017 ft, 3,663 m elevation) is an erosional remnant of caldera-filling andesitic lavas and interbedded sediments, banked against the southeast topographic rim of the caldera with its north slope caved in by a Holocene landslide. Willow Mountain (11,906 ft, 3,629 m elevation), ~2 km to the south, is the eroded remnant of a late Conejos andesitic edifice, which gives its name to the youngest of three compositionally distinct suites of Conejos lavas in the Platoro area (Colucci and others, 1991). The postcollapse topographic depression between present-day Cornwall and Red Mountains (and also the southeast flank of Mammoth Mountain) is filled by the dacite of Fisher Gulch (Stop 4-7), the only sanidine-bearing lava fill of the Platoro caldera and overlain by more mafic lavas of Summitville Andesite. The upper slopes of the Conejos River valley that flank the Platoro Reservoir southwest of Stunner Pass consist dominantly of postcaldera Summitville Andesite, underlain by modest thicknesses of caldera-moat sediments (Stop 4B-1) and by intracaldera Chiquito Peak Tuff that wedges out against the high southwest caldera wall against Conejos Peak (Stop 4B-2).

Return to cars and continue north, down the road toward Stunner. Pull into the parking area on the left side of the road for overview.

47.9 **Stop 4-10. Potosi overview** (37°22.46' N., 106°34.05' W.; 10,170 ft, 3,100 m elevation)

The view north from this stop, across the Alamosa River, encompasses relations between postcollapse andesitic lavas, shallow caldera-related intrusions that were probably broadly coeval with the lavas they intrude, associated hydrothermal alteration and mineralization, and younger silicic lavas.

Directly ahead, the brightly colored lower slopes consist mainly of caldera-filling Summitville Andesite (fig. 109), which has been subjected to intense supergene alteration owing to weathering of disseminated pyrite. This alteration is concentrated within and adjacent to the northern margin of the elliptical Alamosa River pluton (2.5 × 8 km), among the largest Cenozoic granitoid intrusions in the San Juan region. The Alamosa River pluton consists of texturally and compositionally variable monzonite to granodiorite (56–65 percent SiO_2). Exploration drilling in the late 1970s encountered subeconomic porphyry molybdenum mineralization at a depth beneath Alum Creek (tributary drainage between Cropsy and Elephant Mountains). A zircon U-Pb date of 29.0±0.2 Ma for monzonite phase of this intrusion (Gilmer and others, 2021) is within analytical uncertainty of the Chiquito Peak Tuff, but biotite from a relatively silicic phase yielded an $^{40}Ar/^{39}Ar$ date of 27.98±0.11 Ma, about 0.8 m.y. younger. The porphyritic phase, at Alum

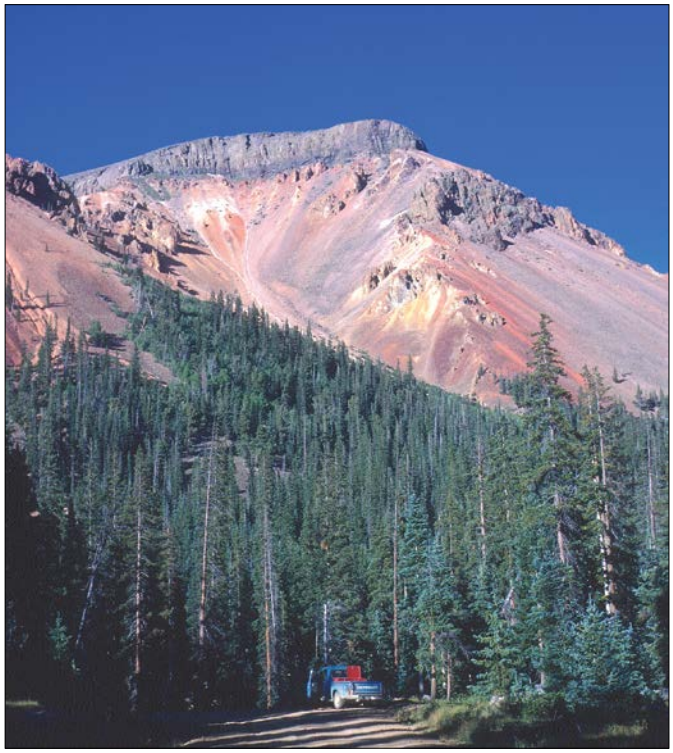

Figure 109. View of Lookout Mountain (3,794 m elevation), from east of Lake de Nolda. Lower slopes are composed of upper-member Summitville Andesite, intensely modified by supergene acid-sulfate alteration (weathering of disseminated pyrite). Unaltered capping lava is crystal-rich rhyolite of Cropsy Mountain. Early-determined K-Ar ages of phenocrysts from basal black vitrophyre are ~21 million years old (Steven and others, 1967. Photograph by P. Lipman, U.S. Geological Survey, 1970.

Creek has an even younger U-Pb date, 27.3±0.4 Ma (Gilmer and others, 2021). Modestly younger ages of granitoid intrusions that are spatially associated with ignimbrite calderas are common in the SRMVF and elsewhere; the younger ages have been inferred to record continued late magmatic recharge that delayed final crystallization of many subcaldera plutons until well after the associated ignimbrite eruption (Lipman, 2007; Lipman and Bachmann, 2015). In contrast, some U-Pb zircon determinations yield dates for volcanic and intrusive rocks that are older than permitted by stratigraphic constraints, suggesting a record of prolonged zircon crystallization during pluton assembly (Lipman and Bachmann, 2015).

In the far distance to the north is South Mountain (12,556 ft, 3,827 m elevation), a large lava dome of coarsely porphyritic dacite, characterized by sanidine megacrysts as much as 5 cm across (Steven and Ratté, 1960). The dacite of South Mountain was the locus of a second stage of supergene alteration, associated with gold-copper mineralization at the Summitville mining district (Stop 4-13), which spatially overlaps the earlier mineralization along the northern margin of the Alamosa River pluton. The South Mountain dome has a determined K/Ar age (sanidine) of 23.3±0.6 Ma, and coarse alunite yielded an analytically indistinguishable age of 22.9±0.5 Ma (Mehnert and others, 1973). Underground vein mining at Summitville was intermittently active from the late 19th into the mid-20th century. Open-pit heap leach extraction of gold later in the 20th century led to the escape of significant amounts of arsenic and heavy metals into the Alamosa River drainage, leading to designation as a Superfund cleanup site; remedial efforts have continued to the present.

The rhyolite of Cropsy Mountain, an unaltered crystal-rich silicic lava with a conspicuous basal vitrophyre, caps Lookout Mountain (3,794 m elevation) and overlies altered lavas of Summitville Andesite. The rhyolite of Cropsy Mountain (71–72 percent SiO_2; ~20 percent pl+quartz (qtz)+san>bt+hornblende (hbl) yielded K/Ar ages of 19.7±0.8 Ma (san) and 20.8±0.8 Ma (bt) [Steven and others, 1967]).

Hinsdale Formation lavas in the southeastern San Juan region are a broadly bimodal suite of silicic trachybasalt to mafic trachyandesite that form thin, widespread veneers above the Oligocene ignimbrites, accompanied by local plugs and lava domes of crystal-poor high-silica rhyolite. These differ notably from the andesitic to dacitic assemblages related to the Platoro caldera cycle and are inferred to represent regional Miocene magmatism that is broadly related to the Rio Grande Rift. No basaltic lavas are visible from this stop, but the light-gray unaltered rock on Elephant Mountain (3,605 m elevation) to the northeast has been interpreted as a Hinsdale rhyolite lava-dome. The rhyolite at Elephant Mountain contains about 5 percent phenocrysts (san+qtz). It has not been dated directly, but a petrographically similar rhyolite (76.6 percent SiO_2) at Grayback Mountain northeast of Summitville has a sanidine $^{40}Ar/^{39}Ar$ age of 21.32±0.02 Ma (table 9, sample 11L-20). Rhyolites assigned to the Hinsdale Formation in the Platoro area differ from the rhyolite of Cropsy Mountain in having higher SiO_2 and lower phenocryst contents. They also form local plugs or domes; in comparison, the rhyolite of Cropsy Mountain is preserved as a ridge-capping lava that extends more than 4 km north from Lookout Mountain toward Summitville and North Mountain.

Continue ahead downhill into the Alamosa River valley, cross the river, and proceed to the intersection with Alamosa and Summitville roads at Stunner townsite.

49.8 *Intersection with Summitville road (FS 380, left fork) and Alamosa River road (FS 250, right fork; start of route 4B). The Summitville road (this log) leads north, out of the Alamosa River, past Summitville, to Park Creek and South Fork.* This route provides access to the northwest wall of Platoro caldera, several units of postcollapse lavas, the Summitville mining district, and outflow tuff sheets from the central San Juan caldera cluster. Route 4B continues down the Alamosa River, focusing on intracaldera intrusions, stratigraphic and petrologic features of the Summitville Andesite, structural features of the Summitville and Platoro calderas, the eastern caldera margin, and outflow ignimbrite stratigraphy of the Treasure Mountain Group.

Turn left onto the Summitville road, past Stunner Cabin, and continue along the lower south slopes of Lookout Mountain (12,448 ft, 3,794 m elevation), which consists of intensely altered Summitville Andesite (fig. 109).

54.1 **Stop 4-11. Caldera wall at Prospect Mountain** (37°22.48’ N., 106°37.44’ W.; 10,827 ft, 3,300 m elevation)**.** *The road circles around the north side of Lake DeNolda (10,794 ft, 3,290 m elevation). Park vehicles at the pulloff near the Summitville junction (please respect private property).*

This view of the western topographic wall of Platoro caldera (fig. 110) on the south slope of Prospect Mountain (12,224 ft, 3,732 m elevation) is one of four localities where well-exposed caldera margins are observable from roads (also Stops 4-6, 4B-2, 4C-5). Volcaniclastic rocks and lavas of the Conejos Formation and lower tuffs of the Treasure Mountain Group are truncated at the caldera wall; outflow La Jara Canyon Tuff is draped over the wall, with compaction dips as steep as 60° to the east, continuous with the intracaldera tuff. Within 300 m of the caldera wall, the La Jara Canyon Tuff is onlapped by intracaldera tuffaceous sediments and Summitville Andesite. Based on the drape

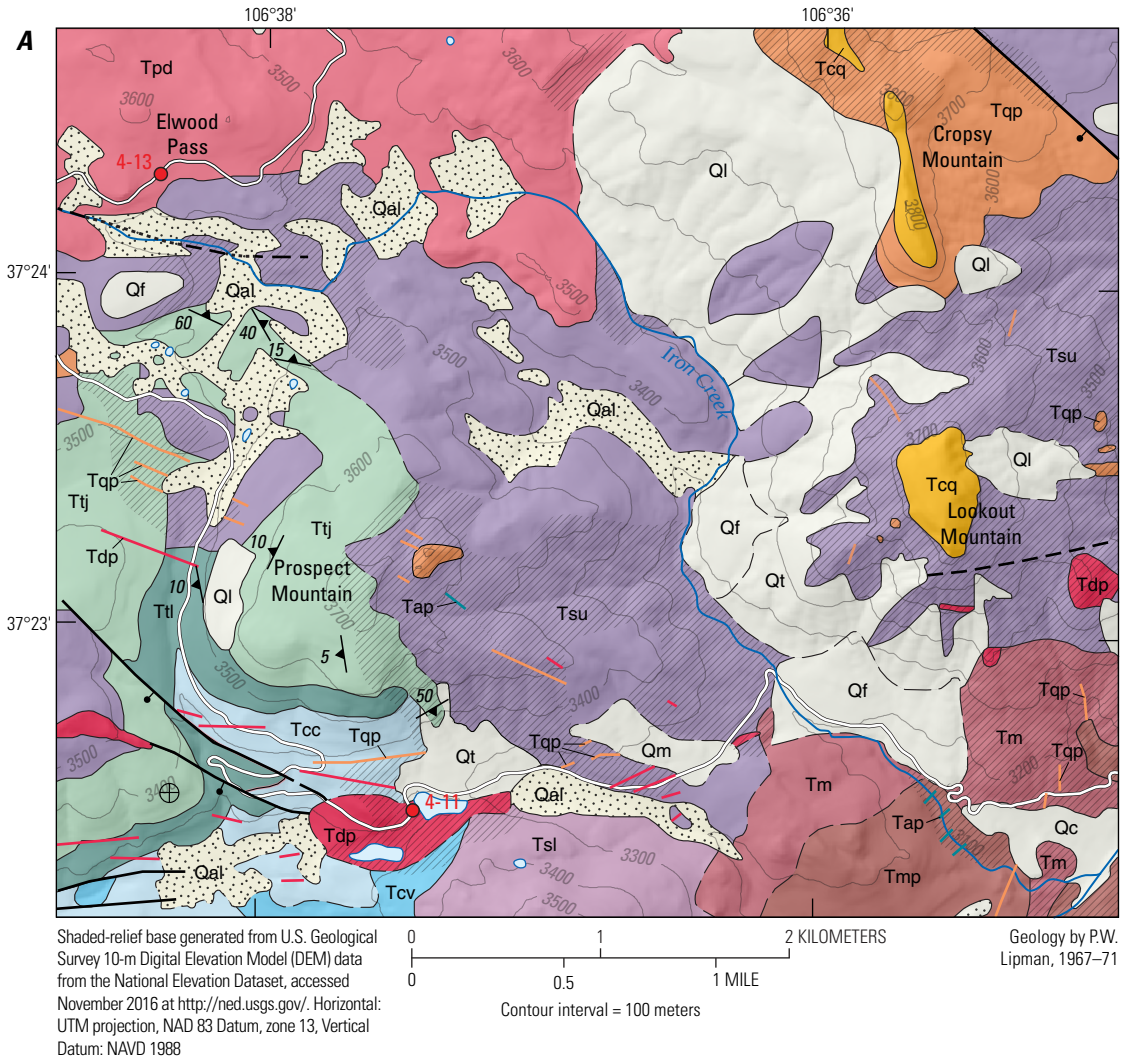

EXPLANATION

SURFICIAL DEPOSITS
- Qal — Alluvium (Holocene)
- Qf — Alluvium-fan deposits (Holocene)
- Qc — Colluvium (Holocene)
- Qt — Talus (Holocene)
- Ql — Landslide deposits (Holocene and Pleistocene)
- Qm — Glacial moraine (Pleistocene)

LAVAS AND INTRUSIVE ROCKS

Rocks of Platoro Caldera Complex

Intrusive rocks
- Tqp — Sanidine-dacite porphyry
- Tdp — Dacite porphyry
- Tap — Andesite porphyry
- Tmp — Monzonite porphyry
- Tm — Monzonite

Postcaldera lavas
- Tcq — Rhyolite of Cropsy Mountain
- Tpd — Dacite of Park Creek
- Tsu — Summitville Andesite, upper member
- Tsl — Summitville Andesite, lower member

Treasure Mountain Group
- Ttj — La Jara Canyon Tuff
- Ttl — Lower tuff

Conejos Formation
- Tcc — Volcaniclastic facies
- Tcv — Vent facies, mainly lavas

Hydrothermal alteration

Contact—Dashed where location approximate

Fault—Ball and bar on downthrown block; dashed where location approximate; dotted where location concealed

Horizontal bedding

5 **Foliation**

4-11 **Field-trip stop**

Figure 110. Depositional relations in the west wall of Platoro caldera at Prospect Mountain (3,732 m elevation) above Lake de Nolda (Stop 4-11). Subhorizontal volcaniclastic units of Conejos Formation (Tcv) and lower tuff (Ttl) of the Treasure Mountain Group are truncated at the topographic wall of the La Jara caldera, over which La Jara Canyon Tuff (Ttj) is draped. Compaction foliations in the La Jara Canyon are as much as 60° on the steepest slopes. Inside the caldera, subhorizontal dark lavas (variably altered) of the Summitville Andesite (Tsu) lap out against the dipping welded outcrops of the La Jara Canyon Tuff. More silicic postcollapse lavas, in upward sequence, include dacite of Park Creek (Tpd), dacite of South Mountain (Tsd), and rhyolite of Cropsy Mountain (Trc). Intrusive phases of the Alamosa River pluton include monzonite (Tm), monzonite porphyry (Tmp), and dacite porphyry (Tdp). *A*, Geologic map of Prospect Mountain area (modified from Lipman, 1974). The diagonal pattern indicates areas of supergene acid-sulfate alteration. *B*, View to north of the La Jara caldera margin. Volcaniclastic rocks and lavas of the Conejos Formation (Tcv) and lower tuffs of the Treasure Mountain Group are truncated at the caldera wall; outflow La Jara Canyon Tuff (Ttj) is draped over the wall and onlapped by intracaldera tuffaceous sediments and Summitville Andesite (Tsu). Photograph by P. Lipman, U.S. Geological Survey,1971 (compare with fig. 64 in Lipman, 1974).

Figure 110.—Continued

geometry, this exposure was interpreted by Lipman and others (1996) as a remnant of the western margin of the La Jara Canyon subsidence structure, which was undisturbed by subsequent collapse by the Chiquito Peak caldera; it can be traced for 8 km to the south, as far as Cat Creek (Stop 4B-1, fig. 95). The altered andesitic lavas on the east slopes of Prospect Mountain were tentatively interpreted to be the lower member of Summitville Andesite. The intense alteration obscures relations with upper member lavas; an unconformable contact is inferred to lie along the Iron Creek drainage to the east (fig. 95).

The view to the east, across Lake De Nolda, is toward Lookout Mountain (13,038 ft, 3,974 m elevation), where the unaltered capping rhyolite lava of Cropsy Mountain (~21 Ma) overlies highly altered Summitville Andesite (fig. 109).

Bear right. Follow Summitville road (FS 380).

The route climbs up-section through the Conejos Formation, lower tuff and La Jara Canyon Tuff of the Treasure Mountain Group, into Summitville Andesite just outside the western margin of the caldera complex.

57.7 **Stop 4-12. Porphyritic dike of silicic dacite** (37°23.88' N., 106°38.96' W.; 11,614 ft, 3,540 m elevation). *Park at the sharp bend in the road, at the northwestern margin of Schinzel Flats.*

This thick crystal-rich dike (fig. 111), dated at 26.25±0.04 Ma (table 9, sample 11L-23), is distinguished from older postcaldera dacite in this area by the presence of phenocrystic quartz and coarse (as large as 4 cm) mantled (rapakivi) sanidine. Although several million years older, it is broadly similar in texture and

Figure 111. Exposure of a large porphyritic dacite dike, about 40-meters thick (for scale, note the truck parked near the left contact of the dike). Poorly exposed wallrock is composed of upper-member Summitville Andesite. Biotite from this dike yielded a K-Ar age of 25.8±1.0 million years ago (Ma) (Lipman and others, 1970, table 4, no. 6). A recent sanidine $^{40}Ar/^{39}Ar$ age yielded 26.25±0.04 Ma (table 9). Photograph taken at Stunner-Summitville road, at the South Fork of Iron Creek in Schinzel Flats, by P. Lipman, U.S. Geological Survey, in 1971.

composition to the extrusive silicic dacite of South Mountain. None of the earlier-erupted Oligocene lavas related to the Platoro-Summitville magma system contains megacrystic sanidine or quartz. This dike trends west-northwest, parallel to dikes of similar composition exposed intermittently from Prospect Mountain to the Continental Divide and beyond. It represents a proximal silicic component of the compositionally diverse dikes that radiate westward from a focal point near the Alamosa River pluton and merge to the southwest with trachybasalts of the Dulce dike swarm (fig. 98).

Continue ahead to the roadcut, just beyond the trail to Elwood Pass Guard Station.

58.9 **Stop 4-13. Dacite of Park Creek** (37°24.29' N., 106°38.38' W.; 11,598 ft, 3,535 m elevation)

Postcaldera lavas of (lower?) Summitville Andesite, exposed downslope below the Elwood cabin, are overlain here by thick porphyritic lavas and domes of Park Creek dacite (60–67 percent SiO_2), characterized by phenocrysts of pl>bt>cpx±hbl. The dacite of Park Creek has not been dated directly, but its age is bracketed at 28.0–27.5 Ma by its stratigraphic position between the Fish Canyon and Carpenter Ridge Tuffs. Park Creek lavas are broadly correlative with the dacite of Green Ridge, at the Cat Creek volcano east of Platoro caldera (fig. 93), but they are less enriched in incompatible elements than many Green Ridge lavas. Most Park Creek lavas also lack the evidence for mixing that is common in Green Ridge lavas.

Continue ahead; roadcuts for next 3 mi are in dacite of Park Creek.

60.1 Pass at head of Park Creek, a tributary of the South Fork of the Rio Grande.

62.2 *Junction of Park Creek (FS 380) and Summitville Creek (FS 330) roads. Turn right.* Lavas of porphyritic silicic dacite exposed along the road are part of the ring-dome complex along the northwest rim of Platoro caldera.

63.0 Summitville Pass. To the east, the Wightman Fork drainage empties into Alamosa River east of Stunner. North Mountain (3,879 m elevation) at 12:00 and South Mountain (3,827 m elevation) at 3:30 are lava domes of porphyritic silicic dacite. The road crosses the northwest-trending Summitville Fault, which can be traced at least 20 km, as far as Wolf Creek Pass. Porphyritic dacite of Park Creek is dropped down on the west side of the fault, against intracaldera lavas of Summitville Andesite.

Continue ahead, to parking area at entry to Summitville mine.

64.9 **Stop 4-14. Summitville mining district** (37°25.80' N., 106°35.60' W.; 12,726 ft, 3,435 m elevation)

Summitville (fig. 112) is the site of one of the highest-altitude mining operations ever attempted in the United States (Bethke, 2011). Much of the northeast flank of the South Mountain dacite dome was removed during open-pit mining in the late 20th century; the tailings pond from this operation lies just east of the parking area.

Discovery of gold in the Summitville area in 1870 and in the Silverton area in the same year led to the first successful mining ventures in the San Juan Mountains. The gold-silver-copper ore at Summitville occurs at shallow levels within the South Mountain volcanic dome of coarsely porphyritic silicic dacite, located approximately on the northwest rim of the Platoro caldera. The shallow ore occurs in intensely altered pipes and irregular tabular masses of quartz-alunite-pyrite rocks that replaced the silicic dacite along northwest-trending fracture zones. Ore minerals, chiefly pyrite and enargite, fill irregular vugs that formed by local intense leaching of the quartz-alunite rock. The quartz-alunite masses are surrounded successively by soft argillically altered envelopes (illite-kaolinite zone) and by pervasively propylitized rocks (montmorillonite-chlorite zone). The alteration has been interpreted to have resulted from shallow solfataric activity (Steven and Ratté, 1960; Stoffregen, 1987; Gray and Coolbaugh, 1994). Several exploration programs in the 1960s and 1970s resulted in intermittent reopening of the mines. Total production prior to 1975, of about $7,500,000 in historical prices, was mostly from gold (Steven and Ratté, 1960; Lipman, 1975a). In 1985, a bulk-tonnage gold open-pit operation was started by Galactic Mining Company using cyanide-heap-leaching methods for recovery. Production in the late 1980s involved moving about 60,000 tons of ore (0.04 ounces per ton of gold [oz/T] of gold) per day, which yielded about 80,000 oz per year of gold (Gray and Coolbaugh, 1994).

The open pit was worked only in the summer months, but leaching operations continued year-round. Most of the gold mineralization (>0.05 oz/T) occurs in vuggy silica rocks, although the open-pit mining operation also recovered lower-grade ore from the enclosing alunitic and illitic alteration zones. The vuggy-silica rocks are best developed within 100–200 m of the surface and appear to grade downward into better defined but more restricted vein structures. Most of the ore mined at Summitville was from the oxidized zone, which extends to depths of 50–100 m. In this zone, native gold is intergrown with goethite, hematite, and local barite and jarosite. Beneath the oxidized zone, gold occurs with covellite, enargite, and luzonite. Sphalerite, galena, hinsdalite, marcasite, native sulfur, and chalcopyrite occur locally in the

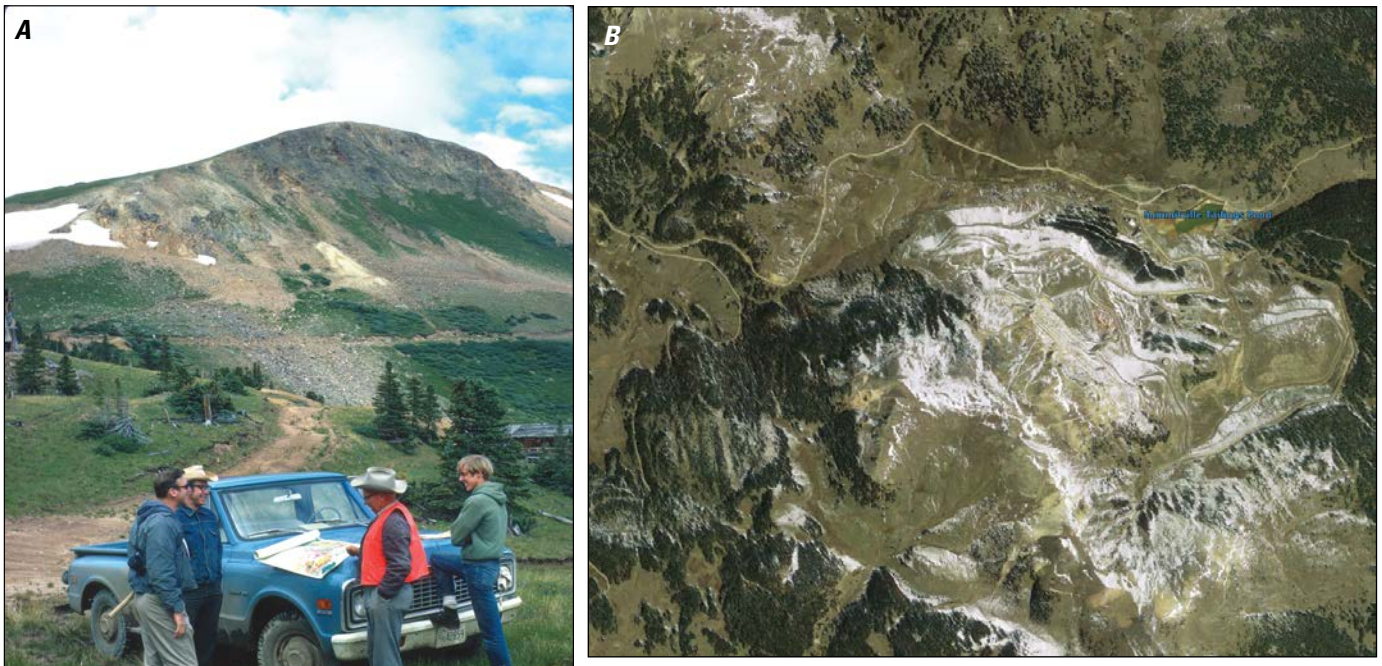

Base map data from Google, 2015

Figure 112. South Mountain dacite dome and Summitville mining district (Stop 4-13). *A*, The South Mountain dacite dome as viewed from the northeast, prior to commencement of an open-pit mine operation. In the foreground are U.S. Geological Survey scientists (left to right) Paul Barton, Phil Bethke, Tom Steven, and David Johnston. Photograph by P. Lipman, U.S. Geological Survey, 1971. *B*, Google Earth © image of present-day (2016) status of the stabilized open-pit mine and leaching field at Summitville.

assemblage. A deeper tennantite-chalcopyrite assemblage does not appear to contain appreciable gold (Perkins and Nieman, 1982). Both the geology and geochemistry of the Summitville deposit point to a close affinity with magmatic activity. Radiometric dating of alunite from the deposit indicates that it was contemporaneous with crystallization of the dacite lava dome (Mehnert and others, 1973). This temporal relation is consistent with the alteration patterns, which reflect acidic conditions probably produced by influx of magmatic SO_2. Ore deposition appears to postdate the acidleaching event, though, and was associated with less extreme chemical conditions.

The mining at Summitville, along with natural acidic drainage, has caused serious environmental damage downstream. Acidic runoff from waste dumps, leakage from the cyanide heap-leach pads, and discharge from mine tunnels have been the main problems (Gray and others, 1994). These deleterious fluids were generated by the exposure of sulfide minerals, particularly fine-grained pyrite, to atmospheric oxygen by mining operations. The oxidation of the sulfides produced sulfuric acid, which increased the dissolution of metal-bearing minerals; these processes have been greatly exacerbated by mining, particularly open-pit operations.

In December 1992, the Galactic Mining Company abandoned the Summitville property and declared bankruptcy. Following abandonment of the property, the state of Colorado asked for emergency assistance from the U.S. Environmental Protection Agency (EPA). In May 1994, Summitville was declared a Superfund site, and remediation was undertaken cooperatively by the State and EPA. Remedial actions included detoxifying and revegetating the heap-leach pad, removing material from waste dumps, backfilling open pits, and enlarging the water-runoff ponds (Bethke, 2011). As a result of these actions, metal concentrations in Wightman Fork and the Alamosa River have been significantly reduced, but remediation at Summitville is expected to be ongoing for the foreseeable future.

Retrace route to Summitville Pass.

66.8 The high peaks ahead to the west along the Continental Divide are Summit (13,270 ft, 4,045 m elevation) on left and Montezuma (13,150 ft, 4,008 m elevation) on right. These peaks consist of andesitic lavas that

overlie outflow Chiquito Peak Tuff. Though well beyond the western caldera margin, these andesites are stratigraphically and petrologically correlative with the intracaldera upper-member Summitville Andesite that filled the Platoro caldera and overflowed to the west.

Continue west to Park Creek Road.

67.7 *Junction with Park Creek Road; continue straight ahead.*

67.9 A roadcut exposes lavas of porphyritic silicic dacite on the northwest rim of Platoro caldera. At 10:00, the light green cliffs are a vent-cone complex that was a source for some of the late rim lavas. At 12:00 on the horizon, Mount Hope (12,831 ft, 3,911 m elevation) and Sawtooth Mountain (12,605 ft, 3,842 m elevation) are high points within the thick accumulation of Pagosa Peak Dacite (Bachmann and others, 2002), a large-volume precursor to the huge ignimbrite eruption of Fish Canyon Tuff (see Day 5, Stop 5A-4). Continue through deposits of porphyritic silicic dacite, moraine, and landslide for the next 5 mi. The rim on this side of the Platoro caldera is mostly covered by postcollapse lavas.

69.0 A quarry in sanidine-bearing silicic lava (intrusion?) is on the right. This fresh rock with large sanidine phenocrysts, previously correlated with the 23-Ma dacite of South Mountain (Lipman, 1975a, p. 73), yielded a $^{40}Ar/^{39}Ar$ age of 20.87±0.02 Ma (table 9, sample 11L-19). Accordingly, this site seems more appropriately interpreted as a lower unit of the lava sequence that caps North Mountain and previously interpreted as correlative with the rhyolite of Cropsy Mountain. The texturally complex silicic lavas on North Mountain and adjacent ridges (Lipman, 1975a, p. 75–76) would be attractive targets for more detailed petrologic and geochronologic study.

71.8 Ahead is Handkerchief Mesa, capped by basaltic lavas of Hinsdale Formation. The lavas are underlain by Fish Canyon and Carpenter Ridge Tuffs, erupted from La Garita and Bachelor calderas, respectively. These calderas are located to the northwest, in the central San Juan caldera cluster (see Day 5). The capping Hinsdale lava on Handkerchief Mesa is part of a mixed-lava complex (Lipman, 1975a; Thompson and Dungan, 1985).

73.1 The roadcut on the right is through a pinkish altered tuff, at the contact between nonwelded to partly welded Chiquito Peak Tuff and overlying partly welded basal Fish Canyon Tuff. The Fish Canyon (28.20 Ma) is a phenocryst-rich silicic dacite tuff (66–68 percent SiO_2) that is superficially similar to the Chiquito Peak Tuff, but the two are distinguished by phenocryst assemblages, high-precision age determinations, magnetic polarity, and xenoliths. Both contain plagioclase and biotite phenocrysts, but the Fish Canyon has sparse hornblende, quartz, sanidine, and sphene. In contrast, as seen at Stop 4-1, the Chiquito Peak Tuff has abundant clinopyroxene (where unaltered). The Fish Canyon Tuff has normal magnetic polarity; Chiquito Peak is reversed. Xenoliths are more abundant in the Chiquito Peak Tuff.

74.1 Roadcuts on the right expose Carpenter Ridge Tuff, a phenocryst-poor rhyolite (73 percent SiO_2) erupted from the Bachelor caldera at 27.55 Ma, which contains phenocrysts of sanidine, plagioclase, and biotite.

74.3 Porphyritic platy-plagioclase andesite lavas and breccias (Huerto Andesite), between Carpenter Ridge and Fish Canyon Tuffs. These andesite lavas petrographically resemble mafic lavas of the Rock Creek lava type in the older Conejos Formation, but this lithology was erupted recurrently in widely dispersed sites throughout evolution of the SRMVF. Huerto Andesite is the volumetrically dominant postcollapse lava associated with eruption of the Fish Canyon Tuff, having local thicknesses >750 m within and adjacent to the southern La Garita caldera (Lipman, 2006)

74.7 Entering area of the central San Juan geologic map (Lipman, 2006).

75.4 *Junction with Lost Mine Creek road; continue ahead.* Outcrops ahead are composed of Fish Canyon Tuff and glacial outwash.

75.9 The roadcut on the left exposes Chiquito Peak Tuff overlain by Fish Canyon Tuff.

79.0 The roadcut on the right exposes Fish Canyon Tuff.

80.2 Demijohn road (FS 361) on the right provides access to the upper part of the Fish Canyon Tuff, several andesitic lavas and flow breccias of the Huerto Andesite, and continues 2.4 mi to the exceptionally exposed base of the Carpenter Ridge Tuff (**Stop 5A-5**: 37°33.11' N., 106°41.27' W.; see Day 5, Stop 5A-5). *Otherwise, continue down valley.*

80.6 Fox Mountain road (FS 381) on left.

83.2 *Bridge over South Fork of Rio Grande and junction with U.S. 160. Turn right.* Continue through exposures of thick Fish Canyon Tuff. To the west along U.S. 160, exposures to the summit of Wolf Creek Pass are mostly Fish Canyon Tuff and the underlying Pagosa Peak Dacite; phenocryst mineralogy and chemistry of this large ignimbrite and precursor lava-like rock are indistinguishable (Bachmann and others, 2002).

84.8 Enter Rio Grande County; leave Mineral County.

86.6 Highway Spring Campground on the right, at the contact between the Masonic Park and Chiquito Peak Tuffs. Lower parts of Chiquito Peak Tuff are exposed along the road on the left, below higher cliffs of Fish Canyon Tuff, and the top of the Masonic Park Tuff crops out discontinuously within the campground area. These exposures are within the narrow overlap corridor, roughly along the South Fork of the Rio Grande to Wolf Creek Pass, where these two similar looking crystal-rich dacites are both present (fig. 92). The Masonic Park Tuff, a crystal-rich dacite that lacks sanidine in contrast to the Chiquito Peak Tuff (Sliwinski and others, 2017), was the initial ignimbrite erupted at ~28.7 Ma from a now completely concealed source within the central San Juan caldera cluster. Numerous northwesttrending faults between here and South Fork define a complex graben system.

89.2 **Stop 5A-1. Base of Fish Canyon Tuff** (37°39.03' N., 106°39.35' W.; see Day 5, Stop 5A-1). *At the curve to the left, park on the right (east side) of the road. Caution: high-speed traffic.*

89.5 Beaver Creek road on right. *Continue straight ahead.*

Entering South Fork, Colorado. Palisades to the west at 3:00 (up Rio Grande valley) are composed of Masonic Park and Fish Canyon ignimbrites (see Day 5, Stop 5A-4). In this area the Rio Grande follows the graben system previously mentioned. Fish Canyon Tuff on the south side of the river is dropped down against Masonic Park Tuff on the north. The low cliffs on the right across the South Fork are Conejos Formation breccias overlain by Chiquito Peak Tuff. The older ignimbrites of the Treasure Mountain Group that occur between these two units to the south and east are not present this far northwest.

End of route 4.

Route 4A—Distal Ignimbrites of the Treasure Mountain Group

[Modified from Dungan and others, 1989a]

This route diverges to the southwest, across La Manga Pass, to examine distal outflow ignimbrites erupted from the Platoro caldera complex.

0.0 *Start at the junction of CO 17 and Platoro road/ FS 250 (Stop 4-2; 37°07.98' N., 106°21.08' W.); proceed southwest on CO 17 toward La Manga Pass and Chama, New Mexico.*

Ascend the long grade toward La Manga Pass. Highway CO 17, between these two stops, closely follows the locus of the north-northeast-trending Cumbres Fault (down to the west), which extends from northern New Mexico to the Alamosa River. The block to the east of the Cumbres Fault dips eastward ~10° into the San Luis Valley, and records tilting in response to graben subsidence during the growth of the Rio Grande Rift. In contrast, rocks to the west, toward the Continental Divide, have a subhorizontal regional inclination.

6.0 Spruce Hole road (FS 108). Continue ahead, over La Manga Pass (10,252 ft, 3,125 m elevation). Past La Manga Pass, as the highway descends, a vista on the left looks across broad meadows on the Rio de los Pinõs valley floor. The CO 17 roadbed lies almost exclusively on landslides until Stop 4A-1. *Continue ahead to the bottom of the grade (at gravel road to Trujillo Meadows Reservoir, just before the paved highway turns to the south). At the sharp curve, pull off the paved road into a small quarry in La Jara Canyon Tuff (9,760 ft, 2,975 m elevation).*

9.2 **Stop 4A-1. Los Pinõs (abandoned townsite); La Jara Canyon Tuff, middle tuff** (37°02.82' N., 106°24.62' W.; 9,728 ft, 2,965 m elevation).

The La Jara Canyon Tuff here is a typical densely welded and devitrified outflow ignimbrite. The abundant but relatively small phenocrysts in the La Jara Canyon, and the typically low abundances of lithic fragments and large pumices, make this one of the more easily recognized Treasure Mountain ignimbrites. Minor hornblende is present in this outcrop, which is near the top of the tuff sheet (the base is not exposed at this locality). In contrast to the thick La Jara Canyon Tuff (200 m) at Black Mountain, 14 km to the north (Stop 4-3), this more distal facies is only ~12–15-m thick in the steep slope directly across the Rio de los Pinõs valley to the east (the west flank of Pinorealosa Mountain).

Directly overlying the La Jara Canyon is the type locality for two welded ignimbrite sheets of the middle tuff (the La Manga units of Dungan and others, 1989a). The lower ignimbrite (La Manga unit A) is a distinctive welded rhyolite (70 percent SiO_2) characterized by black, glassy fiamme as much as 60 cm long in an orange-brown lithic-rich matrix (fig. 113). Above this densely welded zone is a covered interval that lies beneath the densely welded interior of the overlying ignimbrite. This second ignimbrite (La Manga unit B) is markedly different; the fiamme are smaller and the lithics less abundant and smaller. These two units are also present at McIntyre Peak (Stop 4-2) and on the Continental Divide (western horizon, as viewed up Rio de los Pinõs).

To the east along Pinorealosa Mountain, across the Cumbres Fault, the ridge crest is underlain by relatively

Figure 113. Exceptionally welded vitrophyric zone in the lower ignimbrite, Manga Pass unit of the middle tuff (Stop 4A-1), in a roadcut along CO 17 at Los Piños townsite. Phenocryst and lithic contents are relatively high compared to overlying units of the middle tuff. Photograph by P. Lipman, U.S. Geological Survey, 2016.

thin and distal Ojito Creek, Ra Jadero, and Chiquito Peak Tuffs. This locality is 30 km south of the southern topographic wall of Platoro caldera, the eruptive source for these tuffs. The middle tuff (combined La Manga and Fox Creek units) reaches its maximum thickness, 150–200 m, at greater distances (25–30 km) than the La Jara Canyon Tuff from the south and southeast caldera rim. This outward shift in the axis of deposition (circumferential thickening) suggest that eruptions of the Treasure Mountain Group gradually built an ignimbrite plateau around the southeast side of the caldera complex. Cumulative filling of local topographic lows then allowed the Ojito Creek and Ra Jadero Tuffs, even though relatively small in volume, to travel long distances over lower-relief topography.

Return to Spruce Hole road by way of CO 17 over La Manga Pass.

12.4 *Turn right onto Spruce Hole road (FS 108). Continue uphill on gravel road.*

14.1 **Stop 4A-2. La Manga unit of the middle tuff and the Conejos Valley overlook** (37°05.77’ N., 106°22.05’ W.; 3,220 m elevation). *Park on the left side of the road, on the curve. Walk 328 ft (100 m) northeast, to the edge of a bench (3,200 m elevation) overlooking the Conejos valley.*

Several high points on the Platoro caldera rim can be seen from this vantage, including Conejos Peak (13,173 ft, 4,015 m elevation) on the south rim, Willow (11,906 ft, 3,629 m elevation) and Red (12,018 ft, 3,663 m elevation) Mountains on the southeast rim, and in the far distance Bennett (13,202 ft, 4,024 m elevation) and Pintada (12,841 ft, 3,914 m elevation) Peaks on the northeast rim (see fig. 2-2, in Dungan and others, 1989a). The bench is formed by the welded interior of La Manga ignimbrite unit A. Its lithic-rich basal vitrophyre is exposed 10 m below bench level.

Return to vehicles. Continue east.

14.4 **Stop 4A-3. Fox Creek units of the middle tuff** (37°05.70’ N., 106°21.94’ W.; 10,531 ft, 3,210 m elevation)**.** *Turn right onto the side road and park. Hike south through the forest to a small gully below steep exposures of nonwelded to partly welded tuffs (top of ridge 10,840 ft [3,304 m] elevation).*

The lowest exposed ignimbrite, La Manga unit B, has reversed magnetic polarity. The three overlying tuff sheets are Fox Creek units of the middle tuff, with normal magnetic polarities. These units correlate with only part of the sequence exposed at McIntyre Peak (Stop 4-2, fig. 102), and illustrate the limited lateral extent of some individual ignimbrites in the Fox Creek assemblage. The tuffs at this locality are typical of many Fox Creek units. Thin pumice-fall deposits separate the three overlying ignimbrites here; in other places, the fall deposits are missing and presumed to have been eroded during the passage of energetic pyroclastic flows. The dark-gray ignimbrite sheet midway up the slope contains mafic pumice clasts that are typical of many voluminous units of the middle tuff. Some mafic pumice clasts near the top of this ignimbrite approach 1 m in diameter. All of these deposits are lithic-rich and some units are heat-reddened at distances of more than 30 km from Platoro caldera

Return to CO 17.

16.4 *End of route 4A. Return to Platoro road by way of CO 17 over La Manga Pass.*

Route 4B—Southwestern Margin of the Platoro Caldera Complex Along the Upper Conejos River

This route accesses the intracaldera Chiquito Peak ignimbrite, volcaniclastic sedimentary deposits, caldera-filling lavas of Summitville Andesite, and associated andesitic dikes that radiate from a locus approximately concordant with the Alamosa River pluton.

0.0 *Start at the junction of Stunner Pass and Platoro Reservoir roads (route 4, mile 45.2: 37°21.66’ N., 106°32.84’ W.); drive southwest on FS 247 to Platoro Reservoir and then continue westward up the Conejos valley.* The road initially passes through faulted and hydrothermally altered intracaldera Chiquito Peak Tuff

near Mix Lake. About 1.4 mi from the intersection, shortly after turning southwest along the north shore of the reservoir, the road crosses a contact and passes into thick (~500 m) basal lavas of the overlying Summitville Andesite, ponded within the caldera along the south flank of Klondike Mountain. Continue 1.3 mi farther to Rito Gato. *Park along the road*, at an outcrop of sediments (overlain by upper Summitville Andesite).

2.6 **Stop 4B-1. Intracaldera moat sediments that contain plant fossils** (37°20.42' N., 106°34.56' W.; 10,121 ft, 3,085 m elevation).

Calderas tend to be closed depressions, occupied by lakes where the supply of water is sufficient. Many ancient calderas contain lacustrine sediments (for example, Creede caldera, Day 5), and the outcrops here (fig. 114) document the existence of a modest-scale Lake Platoro. The plant fossils at this locality suggest that climatic conditions at the time of the Chiquito Peak eruption may have been similar to present-day conditions (E. Leopold, University of Washington, written commun., 2014). The geometry of these deposits relative to the caldera margin, the resurgent dome (Cornwall Mountain), and the overlying Summitville Andesite all imply that these local sediments accumulated in a moat between the resurgent block on the east and the topographic caldera wall to the west. A small wedge of apparently correlative sedimentary rocks exposed ~2 km to the east (the eastern shore of Platoro Reservoir), dips ~15° SSW. This may indicate that sediments began accumulating prior to or during resurgence and then were tilted as the resurgent block rose; alternatively, this minor tilt could reflect local structural complexities related to northeast-trending postcaldera faults. Sedimentary deposits of Lake Platoro are also exposed at Beaver Creek along the southeastern caldera margin (Stop 4-6) and near Ranger Creek along the northeastern margin (Stop 4C-5). Sediments of Lake Platoro were volumetrically minor in the caldera, which was mostly filled (rapidly?) by thickly ponded lavas, in contrast to Creede caldera, where the dominant fill is sedimentary.

Also at this stop, a several-meter wide andesite dike (58.4 percent SiO_2, 27.4 Ma; table 7), well exposed on the north side of Rito Gato (more dikes in nearby roadcuts), is representative of the large swarm of andesitic and dacitic dikes that radiate westward from this side of the Platoro caldera complex (fig. 98). This and several other nearby andesitic dikes intrude caldera-fill sedimentary deposits, which documents their late-caldera emplacement (rather than an earlier Conejos age). The proximal dikes near Platoro vary in composition from andesite to dacite (for example, Stop 4-12). The proportion of dikes with mafic compositions increases with distance from the caldera and outward beyond the preserved San Juan volcanic accumulation, and dikes with Platoro compositional affinities merge in trend with trachybasaltic dikes intruded into Cretaceous sedimentary strata of the San Juan Basin (fig. 98). The overall dike swarm continues southward for about 125 km into northern New Mexico, and several dikes (both proximal and distal) have yielded $^{40}Ar/^{39}Ar$ ages in the range of 26–21 Ma, notably younger than the ignimbrite eruptions but within the span of prolonged postcollapse lava eruptions at Platoro (fig. 97; Lipman and Zimmerer, 2019).

Continue ahead to south on FS 24.

Figure 114. Finely bedded tuffaceous sediments at Rito Gato (Stop 4B-1). This local section contains lakebed and fluviatile strata that directly overlie intracaldera Chiquito Peak Tuff, and in turn are overlain by upper-member Summitville Andesite, near the southwestern margin of Platoro caldera. Photograph by K.J. Turner, U.S. Geological Survey, 2015.

3.0 The road re-enters intracaldera Chiquito Peak Tuff, close to its contact with the underlying Conejos Formation along the southwest caldera wall. These outcrops will be examined during the return (Stop 4B-3). *Proceed ahead past the junction with the Hillman Park road (FS 247) near the mouth of Cat Creek (which provides access to relatively fresh outcrops of characteristic Summitville Andesite, such as that viewed across the reservoir to the east). Continue left along the lake shore.*

Turn left into the wide parking and camping meadow area on the west bank of the Conejos River (the south end of Platoro Reservoir when full). A trail that starts at the campsite at the far southeast corner of this meadow leads down to the valley floor.

4.7 **Stop 4B-2. Intracaldera Chiquito Peak Tuff at the topographic caldera wall** (37°19.11' N., 106°35.67' W.; 10,089 ft, 3,075 m elevation).

The topographic wall of the Platoro caldera and the associated basal contact of the wedging intracaldera tuff run through the hill just east of the meadow. Before descending along the trail to outcrops of Chiquito Peak Tuff, look across the valley to the cliffs on the far side of the reservoir, where a north-dipping caldera-wall contact between andesitic lavas of the Conejos Formation and the intracaldera Chiquito Peak Tuff is well exposed on the north slope of Conejos Peak (fig. 115).

The same contact, with a shallow inclination, is also exposed along the trail. Abundant small angular fragments of Conejos Formation andesite along this contact have been interpreted as a landslide-breccia deposit that records syneruptive failure of the oversteepened wall of the Platoro caldera during subsidence along ring faults (Dungan and others, 1989a, p. 323–324). Alternatively, this small area of breccia resembles proximal volcaniclastic breccia elsewhere in the Conejos Formation and may just be an intact facies of caldera-wall rocks. Caldera-collapse landslide deposits are common within other San Juan calderas but are not exposed elsewhere within the Platoro caldera. On this basis, Lipman (1975a) proposed that the intracaldera Chiquito Peak Tuff exposed here accumulated late during the eruption, and that any slide breccias resulting from early stages of caldera collapse remain buried at greater depth within the caldera. Later, the preservation of sanidine in this vitrophyre, and in a few other intracaldera tuff samples, was among critical evidence for reinterpreting the thick ignimbrite fill at Platoro as correlative with outflow Chiquito Peak, rather than the La Jara Canyon Tuff (Lipman and others, 1996).

At the base of the trail, turn downstream (northeast) and walk 164 ft (50 m) to the first promontory, which consists of relatively lithic-poor vitrophyre. This is the only known vitrophyre exposure of intracaldera Chiquito Peak Tuff. Development of this thick glassy

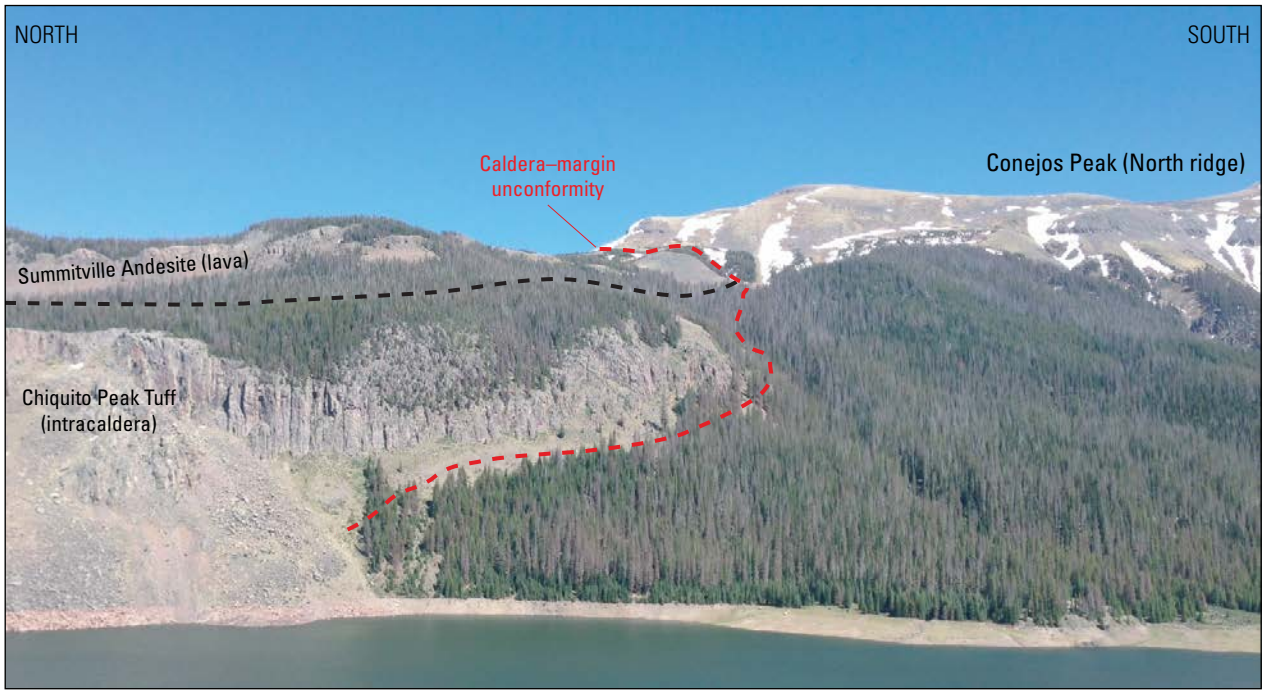

Figure 115. View of Conejos Peak from Hillman Park road, showing densely welded cliff-forming intracaldera Chiquito Peak Tuff within the caldera in depositional contact against the south caldera wall. All rocks at right side of photograph are precaldera lavas and breccias of Conejos Formation. Top rim, above Chiquito Peak Tuff within caldera, is intracaldera lava of upper-member Summitville Andesite. Photograph by P. Lipman, U.S. Geological Survey, 2016 (compare with fig. 2.7 in Dungan and others, 1989a).

zone is interpreted as a result of refrigeration against cold caldera-wall rocks, as also observed locally at other caldera margins (Lipman, 1976a).

Farther downstream, outcrops of overlying devitrified tuff are intruded by a large composite dike of fine-grained andesite that trends N. 15° E. and is a typical proximal representative of the large dike system that radiates from the western Platoro caldera (fig. 98). Three more previously unmapped dikes of similar trend and lithology, which intrude volcaniclastic rocks of the Conejos Formation, are well exposed along the north bank of lower Adams Fork, just south of the camp area. Several hornblende-phyric dikes with similar radial geometry, intrusive into the Conejos Formation in the reservoir area, have yielded precaldera ages (~31 Ma). Thus, the presence of both precaldera and postcollapse dikes with similar radial orientations along the west side of Platoro caldera documents a long-lived magmatic focus within the caldera area, but the relative proportions of radial dikes in relation to age (Conejos versus postcaldera) remains inadequately determined.

Return along the road to the east toward Platoro (past Cat Creek), then pull off to the right near pinkish outcrops to view the densely welded and devitrified Chiquito Peak Tuff that underlies moat-filling lavas of upper Summitville Andesite.

5.7 **Stop 4B-3. Uppermost intracaldera Chiquito Peak Tuff** (37°19.71' N., 106°34.98' W.; 10,269 ft, 3,130 m elevation).

This stop, at a devitrified but relatively nonpropylitic tuff just below overlying lavas of Summitville Andesite, provides intermediate comparisons between the pristine Chiquito Peak vitrophyre near the caldera-floor contact (Stop 4B-2) and the comprehensively reconstituted intracaldera tuff at the base of Cornwall Mountain (Stop 4-8). These stops provide a reminder that large-scale pyroclastic deposits (initially aggregates of particles) may undergo varied postdepositional changes, including compaction, welding, devitrification, and variable degrees of jointing, rheomorphic flow, and alteration that can change their appearance dramatically. Unlike the lithic-rich tuff immediately above the caldera floor at Stop 4B-2, lithic fragments are sparse at this outcrop. Flattened pumice (fiamme), which are obscure in most areas of intracaldera Chiquito Peak Tuff, define a conspicuous foliation, best discernable on moderately weathered outcrop surfaces (fig. 116). The pinkish groundmass color reflects oxidation, and biotite phenocrysts have the characteristic bronzy sheen that develops in response to mild alteration. Small tabular crystals of sanidine (chatoyant reflections from cleavage) confirm that these outcrops are the Chiquito Peak Tuff (Lipman and others, 1996), rather than the La Jara Canyon Tuff as previously interpreted (Lipman, 1974, 1975a).

End of route 4B. Continue eastward on this road, returning past Mix Lake to rejoin the intersection with the road to Platoro.

Figure 116. Densely welded upper part of intracaldera Chiquito Peak Tuff (Stop 4B-3), showing exceptionally conspicuous foliation defined by flattened pumice (fiamme). Specimen located along Platoro Reservoir road. Photograph by P. Lipman, U.S. Geological Survey, 2016.

Route 4C—Down the Alamosa River: Lavas and Intrusions Within the Northern Platoro Caldera, East Caldera Margin, and Adjacent Proximal Outflow Ignimbrites of the Treasure Mountain Group

This route, which connects with the main Day 4 route at Stunner, Colorado, examines relations between the volcanic fills of the Chiquito Peak and the earlier La Jara Canyon calderas, caldera structures, and associated intrusions and mineralization. This route also offers an option to tour the Platoro caldera in a counterclockwise direction, starting along the lower Alamosa River (end of route 4C), proceeding upstream and joining the main Day 4 route, and then continuing either to South Fork or proceeding counterclockwise across Stunner Pass and down the Conejos River to Antonito.

0.0 *Junction of Summitville and Stunner Pass roads (mile 49.8, field-guide main route 4); head downstream (east) on Alamosa River Road (FS 350).* For the next 2 mi, the road generally follows the variably altered northern margin of the 28-Ma Alamosa River pluton.

0.1 Bridge over Alum Creek. The area of intense hydrothermal alteration to the north is in Alum Creek porphyry, the late higher-silicic phase (64 percent SiO_2) of the Alamosa River intrusion. Kaolinite and quartz-sericite alteration of the Alamosa River pluton is evident along the road for the next mile.

1.2 **Stop 4C-1. Alamosa River pluton—Bridge over Bitter Creek** (37°23.70' N., 106°33.10' W.; 9,662 ft, 2,945 m elevation). *Pull off to the left, past the bridge.*

The first outcrop to the east of the bridge is a relatively unaltered coarse dioritic phase of the Alamosa River pluton (57 percent SiO_2). This pluton is thought to be the solidified top of the magma body that erupted lavas of the Summitville Andesite. Because the present topographic highs along the ridge crest to the south, such as Klondike and Telluride Mountains, consist of this intrusion, a large overlying volcanic edifice of Summitville Andesite and associated lavas is inferred to have been removed by erosion.

Blocks of glassy and devitrified high-silica rhyolite of the Hinsdale Formation, derived from the Elephant Mountain dome upstream, can be examined in the stream boulders. The Miocene Hinsdale Formation contains minor silicic rhyolite of this type in the Platoro area, in association with volumetrically dominant lavas of trachybasalt and trachybasaltic andesite. Hinsdale rhyolites (>76 percent SiO_2) characteristically contain only sparse phenocrysts of a single feldspar (sodic sanidine) and quartz. Continue east through variably altered Alamosa River pluton. At the east end of Government Park, the road enters Summitville Andesite (upper member) and remains in it for about 4 mi.

2.1 View of Lookout Mountain (12,448 ft, 3,794 m elevation) to the northwest. Caprock is unaltered 21-Ma rhyolite of Cropsy Mountain (71 percent SiO_2). This lava unconformably overlies solfatarically altered rocks of Summitville Andesite.

3.2 Canyon of Wightman Fork exposes thickly ponded intracaldera flows and breccias of dark nonporphyritic Summitville Andesite (upper member). Along the road ahead and low on the south side of Alamosa River are andesite lavas within the Summitville caldera. The upper slopes are intracaldera Chiquito Peak Tuff on the upthrown side of the Cornwall Fault (fig. 93). The arcuate Cornwall Fault is inferred to have initiated as a segment of the ring fault of the Summitville caldera, later occupied to the west by the Alamosa River pluton and to the east by the Jasper intrusive complex. This caldera is considered to be a possible source for the Ojito Creek and Ra Jadero Tuffs.

5.7 **Stop 4C-2. Summitville Andesite, Jasper mining district** (37°25.32' N., 106°29.37' W.; 9186 ft, 2,800 m elevation). *Park cars at small roadside borrow pit adjacent to meadow, 1 mi west of Jasper; walk up into meadow about 164 ft (50 m) for a better view.*

Directly to the south, Cornwalls Nose (11,647 ft, 3,550 m elevation) forms a promontory above steep cliffs of massive lavas and breccias of Summitville Andesite (upper member) within Summitville caldera. The Cornwall Fault, which passes through Cornwalls Nose, has juxtaposed the Summitville Andesite against intracaldera Chiquito Peak Tuff, accommodating late uplift of the trapdoor resurgent block within the Platoro caldera, and perhaps also some continued subsidence in the Summitville caldera during accumulation of the andesite sequence. The Summitville Fault curves northward and intersects the similarly reactivated southeast boundary fault of the Platoro caldera (California Gulch Fault) near the townsite of Jasper (fig. 93). This fault intersection localized a composite intrusion that produced the widespread intense alteration and local mineralization of the Jasper mining district (fig. 117). Alteration of the Summitville Andesite is prominent on the lower slopes of Silver Mountain (3,786 m elevation), due east of this viewpoint. Altered lavas below an unconformity are overlain by unaltered lavas on Silver Mountain (andesite of Green Ridge). The volcanics of Green Ridge were erupted from the Cat Creek volcano farther east and locally overlie the Fish Canyon Tuff. This area exemplifies the close association between zones of alteration (and mineralization) and fault intersections, particularly caldera-boundary faults, in the Platoro-Summitville area.

Continue ahead, down canyon.

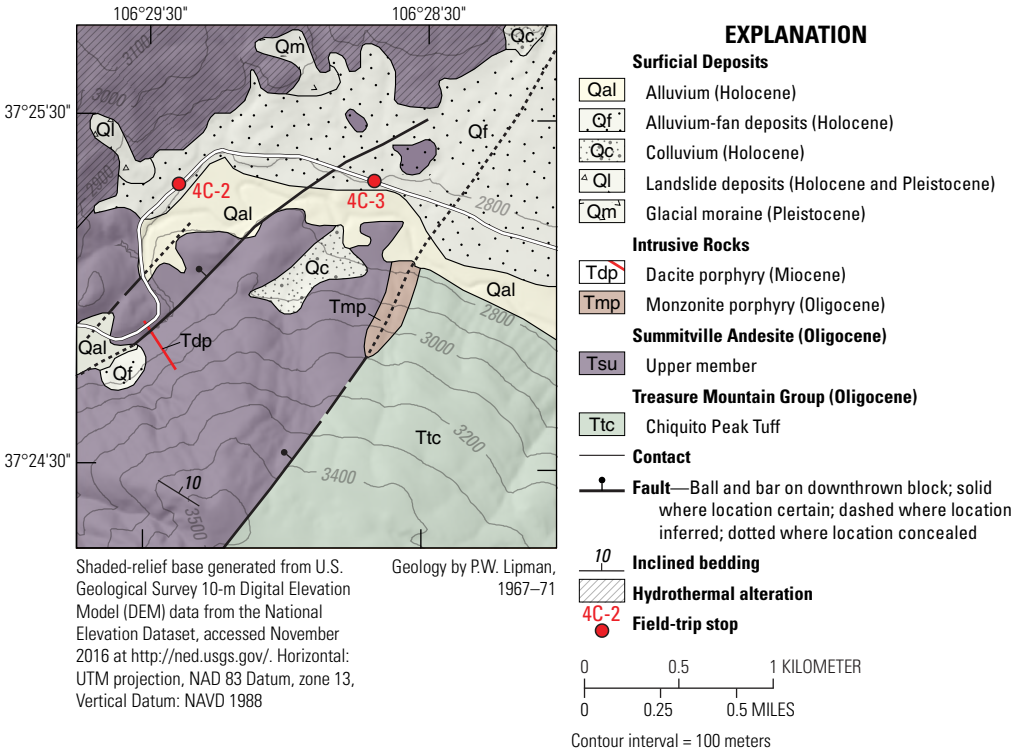

Figure 117. Geologic map of Jasper area (Stop 4C-3), modified from Lipman (1974). Porphyritic monzonite facies at the southern margin of the Jasper pluton (Tmp), intruded along the arcuate Cornwall Fault that juxtaposes upper-member Summitville Andesite (Tsu) against the resurgently uplifted block of intracaldera Chiquito Peak Tuff (Ttc).

1.8 **Stop 4C-3. Structural boundary of Summitville caldera** (37°25.31' N., 106°28.67' W.; 9,186 ft, 2,800 m elevation). *Leave cars on the road, pulling off to the right as far as possible. Take the jeep trail on the right (to the south). Go across Alamosa River bridge to the old workings of the Miser mine* (*request permission to cross private property, as needed*).

The Cornwall Fault, which follows the main gully ahead, is inferred to define the reactivated south structural boundary of the Summitville caldera (fig. 117). Southeast of the fault, propylitized Chiquito Peak Tuff extends from valley level (2,780 m elevation) nearly to the top of Cornwall Mountain (12,287 ft, 3,745 m elevation). Though the base of the Chiquito Peak is concealed, a typically thick intracaldera accumulation (>800 m) is exposed. On the northwest side of the fault, Summitville Andesite is preserved to the top of Cornwalls Nose.

The small adit and dumps across the river to the east, part of the workings of the Miser mine, are in monzonite porphyry intruded along the Cornwall fault zone. The monzonite is the coarsest facies of the highly altered Jasper pluton, much of which is so fine grained as to be best described as intrusive andesite. A U-Pb zircon date of 28.8±0.2 Ma from the monzonite at this locality (Gilmer and others, 2021) is similar to that for the Alamosa River pluton exposed 8 km to the southwest (Stop 4C-1), and both bodies may be high levels of a larger interconnected intrusion at greater depth. The Miser mine was opened and mostly developed during the 1880s. The main tunnel extends about 200 m directly into the mountainside and apparently intersected the Cornwall Fault, along which the richest ore was reportedly found (vein quartz with gold stringers).

Continue east.

7. 7 Town of Jasper. The town was founded and mining began about 1874–75. The largest mine workings were mainly along the south side of the Alamosa River, along the structures and alteration related to the southeastern margin of late collapse structures of the composite caldera. Small amounts of rich gold-silver ore were produced from quartz-pyrite veins, with associated sphalerite and galena (Patton, 1917). Production, mostly or entirely before the area was studied by Patton, was apparently small and complicated by acidic mine waters.

8.2 Fern Creek. Cliffs above the road on the right, just before the creek, are stratified tuffaceous sandstones between intracaldera Chiquito Peak Tuff (at road level) and overlying intracaldera andesitic lavas.

9.1 **Stop 4C-4. Top of the intracaldera Chiquito Peak Tuff** (37°24.51' N., 106°27.25' W.; 9,071 ft; 2,765 m elevation)**.**

Small outcrops of reddish-brown, densely welded tuff along the road are overlain by intracaldera andesite lavas that dip gently to the east, away from the resurgent core of the caldera. The reddish color here is characteristic of the upper 50–100 m of intracaldera Chiquito Peak Tuff (compare with that at Stop 4B-2),

and changes to grayish-green propylitic hues lower in the ignimbrite section. Small lithic fragments are present but collapsed pumice fiamme are obscure. Intracaldera tuff is exposed at higher elevations south of the river (to high on Cornwall Mountain), because of resurgent uplift along the fault near the base of the mountain.

Continue east, through caldera-filling lavas of lower Summitville Andesite.

10.2 Silver Creek. On the north side of the road, bedded tuffaceous sandstone, similar to that at Stop 4B-1, is interlayered with andesitic lavas. Across the river, the large mountain mass (Cornwall Mountain) is mainly Chiquito Peak Tuff in the structurally uplifted central part of the caldera.

12.6 Intracaldera lavas of Summitville Andesite on right. There is a large Holocene landslide across Alamosa River to the south.

12.8 **Stop 4C-5. Eastern margin of the Platoro caldera complex** (37°23.55' N., 106°23.20' W.; 8,875 ft, 2,705 m elevation)**.** *Park in the small pullout on the right side (south), just before the downhill grade.*

Volcaniclastic sediments and tuffs underlie and interfinger with thickly ponded dark andesitic lavas, as exposed in roadcuts along the decline to the east for 200 m toward Ranger Creek (fig. 118). Upslope to the northwest the Ojito Creek ignimbrite, here anomalously as much as 150-m thick, overlies the volcaniclastic and lava sequence, documenting that the road-level exposures are lower-member Summitville Andesite within the La Jara Canyon caldera (fig. 95). All of these units wedge out higher against the eastern topographic wall of the caldera, north-northeast of the vehicles. High along the caldera wall are well-bedded, welded ash-fall tuffs that agglutinated because of high-temperature emplacement (outcrops can be reached by hiking the U.S. Forest Service Ranger Creek trail). These tuffs must have erupted nearby to permit sorting but were deposited before cooling. In sedimentary intervals between lavas of Summitville Andesite within the caldera, angular blocks of andesite, as much as 1.5 m across, represent both ejected bombs showing breadcrust-jointed margins and other blocks that may have slid in from the caldera wall (Calkin and others, 1971, p. 5).

Here in the Alamosa River valley between Ranger Creek and the town of Jasper, and in the Platoro Reservoir area, both members of Summitville Andesite are preserved as thick lava sequences within the Platoro caldera complex. Both sequences consist of potassic basaltic andesite and andesite, typically with sparse phenocrysts of pl+augite (aug)+orthopyroxene (opx)±olivine (ol). Basal lavas of the upper andesite are similar to those in the lower member, but higher lavas are more porphyritic, and some contain phenocrysts of biotite. The lavas farther west in the Alamosa valley that overlie densely welded intracaldera Chiquito Peak Tuff and are intercalated with moat-filling sediments (Stop 4C-4) must be upper-member Summitville Andesite, but the inferred location near Lieutenant Creek of the boundary with the lower-member lavas at Ranger Creek (fig. 95) is not closely constrained.

Continue east, passing the Ranger Creek Guard Station.

13.5 Road to Silver Lakes, on right.

15.8 Alamosa Campground. Exposures along the road and in cliffs ahead are Conejos mudflows and capping lavas of andesitic composition.

16.5 Cabins on the right. On the left (north) is a large cliff that exposes a cross section through the Terrace Reservoir laccolith (fig. 119), a dacitic porphyry intrusion (64 percent SiO_2) peripheral to the Cat Creek volcano. Cliffs across the Alamosa River to the south are andesite lavas and breccias of the Conejos Formation, capped at the top of the hill by another remnant of the Terrace laccolith.

18.4 Dark-gray nonporphyritic Conejos andesitic lava underlies ignimbrites of the Treasure Mountain Group in outcrops ahead.

18.6 Prospect pit on the right in the altered nonwelded base of La Jara Canyon Tuff.

18.8 **Stop 4C-6. Roadcut in La Jara Canyon Tuff along the north bank of Terrace Reservoir** (37°21.95' N., 106°17.74' W.; 8,629 ft, 2,630 m elevation).

The ignimbrite interior is densely welded and weakly propylitized at this proximal location (fig. 120). Phenocrysts are abundant but relatively small and lithics are sparse in this crystal- rich dacite (65–68 percent SiO_2; 25–40 percent pl>bt+cpx), in comparison to younger major ignimbrites of the Treasure Mountain Group. Quartz and sanidine are absent despite high SiO_2 in rhyolite matrix glasses (>75 percent SiO_2). The La Jara Canyon Tuff lacks a precise age determination because of the absence of sanidine, but it was erupted at ~30.0 Ma, as bracketed by ages from the underlying Black Mountain Tuff and overlying middle tuff (table 9).

19.1 Road junction. Slabby-jointed upper parts of the La Jara Canyon ignimbrite are on the left (north).

There are two alternative routes to end route 4C. Both routes provide access to proximal outflow ignimbrites of the Treasure Mountain Group, and permit comparisons with more distal sections of these tuffs viewed during early stops of routes 4 and 4A.

Figure 118. Eastern margin of La Jara Canyon caldera (Stop 4C-5). *A*, Tuffaceous sandstones, which interfinger with dark nonporphyritic lavas of Summitville Andesite up the road to the west of the image, wedge eastward against lavas and volcaniclastic breccias of the Conejos Formation along a steep west-dipping unconformity that defines a remnant of the outer wall of the La Jara Canyon caldera (fig. 95). Above the tuffaceous sandstone, against the caldera wall to the east, is a cliff-forming exposure of well-bedded ash-fall tuffs that were welded and agglutinated because they were deposited while still hot. These units must have erupted nearby to permit sorting and then deposition before cooling. These beds may be equivalent to part of the middle tuff of the Treasure Mountain Group; they are overlain by west-dipping Ojito Creek Tuff that is densely welded and exceptionally thick (as much as 150 meters [m]) where ponded against the caldera wall in this area. *B*, Closer view of bedded sandstone of dominantly fluviatile origin, in roadcut. Note hammer (~0.4 m) for scale. Compare/contrast with more finely stratified lacustrine sediments in the southern and western caldera segments (figs. 105 and 114).

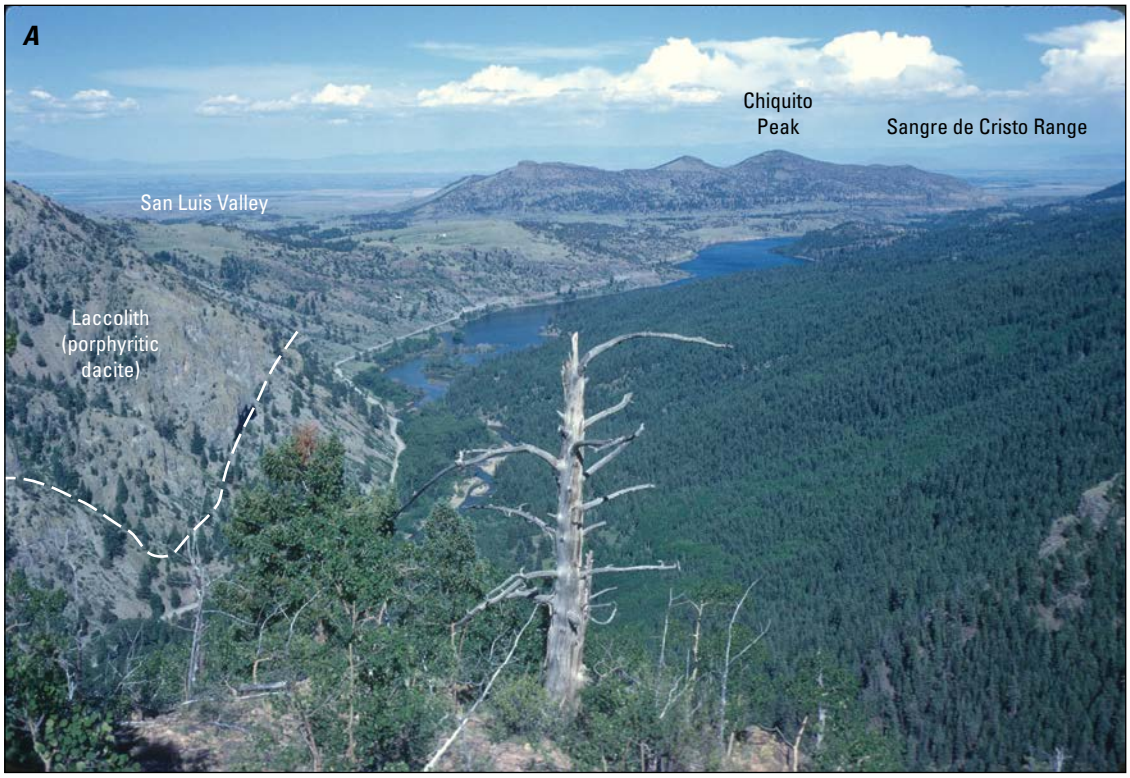

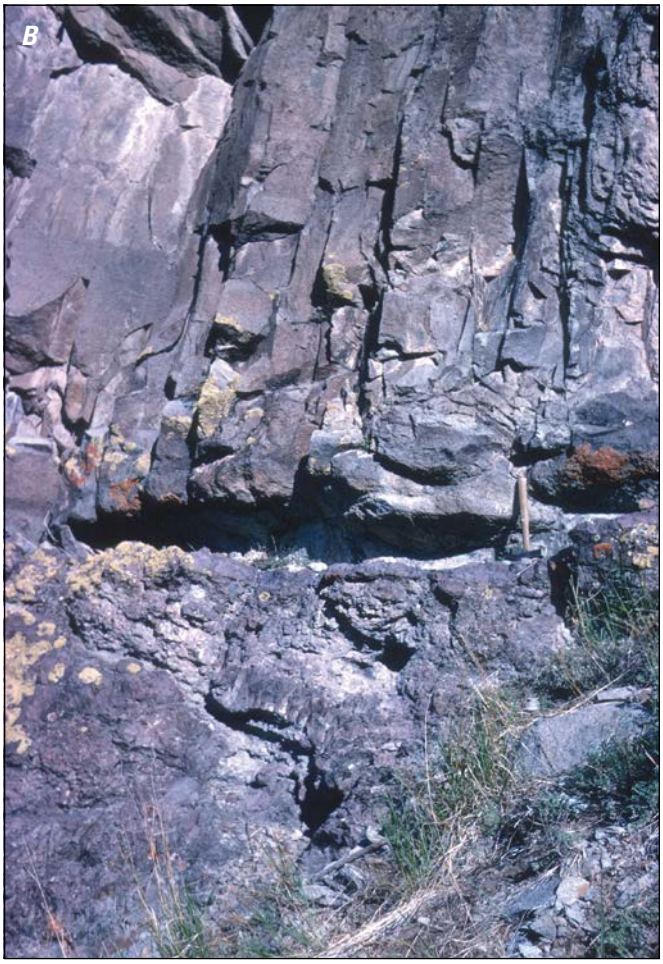

Figure 119. Lower Alamosa River valley and Terrace Reservoir laccolith. *A*, View east across Terrace Reservoir toward Chiquito Peak. The Terrace Reservoir laccolith is a southern offshoot from the intrusive complex that composes the core of Cat Creek volcano on the east side of Platoro caldera. In the distance to the east, the San Luis Valley segment of the Rio Grande Rift is bounded on its east side by the major faults against the uplifted Sangre de Cristo Range in the far distance. *B*, Gently dipping basal contact of Terrace Reservoir laccolith with the overlying laharic breccia of Conejos Formation on the slope north of Terrace Reservoir; note hammer for scale. Photographs by P. Lipman, U.S. Geological Survey, 1970.

- **Route 4C(a)** *Continue straight ahead (left) on FS 250* up section through the area known as The Canyon to Cat Creek, past upper ignimbrites of the Treasure Mountain Group, views of the postcaldera Cat Creek volcano, and into the Miocene sequence of Los Piños Formation overlain by basaltic lava of the Hinsdale Formation.
- **Route 4C(b)** *Alternatively, bear right on FS 255* and follow the Alamosa River for better exposures of Treasure Mountain ignimbrites (fig. 120).

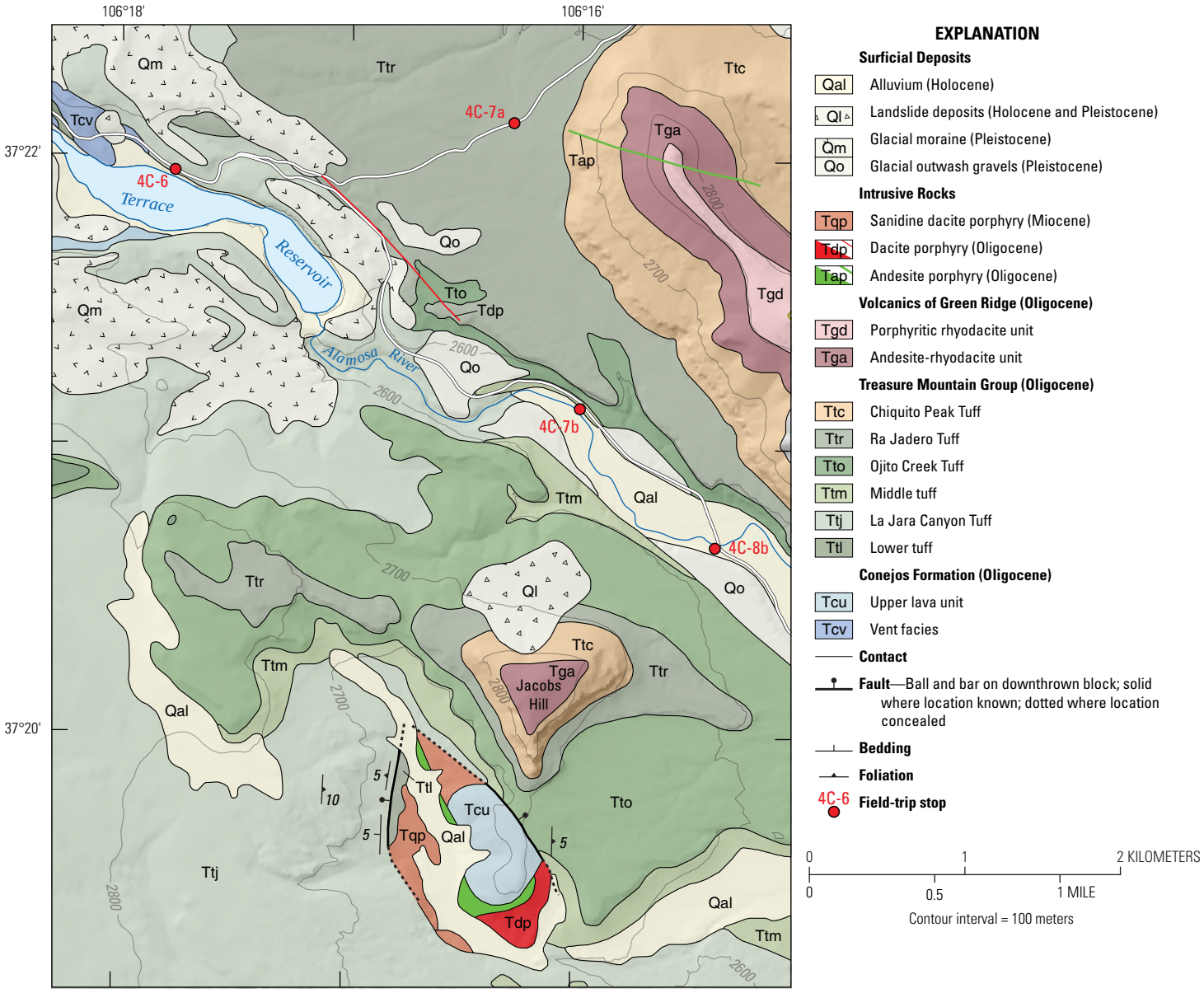

Shaded-relief base generated from U.S. Geological Survey 10-m Digital Elevation Model (DEM) data from the National Elevation Dataset, accessed November 2016 at http://ned.usgs.gov/. Horizontal: UTM projection, NAD 83 Datum, zone 13, Vertical Datum: NAVD 1988

Geology by P.W. Lipman, 1967–71

Figure 120. Geologic map of the lower Alamosa River valley (modified from Lipman, 1974), showing the stratigraphy of outflow Treasure Mountain ignimbrites on Jacobs Hill and the northwest ridge of Chiquito Peak: La Jara Canyon Tuff (Ttj), middle tuff (Ttm), Ojito Creek Tuff (Tto), Ra Jadero Tuff (Ttr), and Chiquito Peak Tuff (Ttc). Above the ignimbrites are andesitic (Tga) and dacitic (Tgd) lavas on the southeast flank of the postcaldera Cat Creek volcano. On the south side of Jacobs Hill, an elliptical fault-bounded intrusion of porphyritic dacite (Tdp) has uplifted its flat-lying roof, exposing pyroclastic rocks interpreted as lower tuff (Ttl) of the Treasure Mountain Group, overlain by andesitic lavas assigned to the upper unit of the Conejos Formation (Tcu).

Route 4C(a)

Continue ahead on FS 250 through poorly exposed upper parts of the La Jara Canyon Tuff and overlying tuffs of the Treasure Mountain Group.

10.5 **Stop 4C-7a. Near-vitrophyric top of the Ra Jadero Tuff; views of Cat Creek volcano** (37°23.13' N., 106°16.30' W.; 8,612 ft, 2,625 m elevation). Low, slabby exposures on the right side (south) of the road are typical of the upper parts of this ignimbrite. Abundant small angular fragments of intermediate-composition lavas help distinguish this ignimbrite from the underlying Ojito Creek Tuff (other distinctions are the presence of sparse sanidine and reverse magnetic polarity in the Ra Jadero, but not Ojito Creek Tuff, which had normal polarity). Sanidine from the Ra Jadero Tuff at this locality yielded an $^{40}Ar/^{39}Ar$ age of 29.12±0.07 Ma (table 9). Ahead to

the east, prominent light-tan cliffs above road level are Chiquito Peak Tuff along the elongate northwest ridge of the geographic Chiquito Peak, located just a few kilometers to the southeast.

Upper parts of the Chiquito Peak ridge are capped by andesitic lavas interpreted as erosional remnants of the southeast flank of the postcaldera Cat Creek volcano (fig. 120). The north end of this ridge is cut by a conspicuous andesitic dike that trends northwest, back toward the core of Cat Creek volcano. In the distance to the north is Green Ridge, a sequence of andesitic and dacitic lavas on the northeast flank of Cat Creek volcano. The east end of Green Ridge and Greenie Mountain are capped by basaltic-andesite lavas of the Hinsdale Formation, dated at about 22 Ma. Low hills in middle distance to the northwest are the intrusive core of Cat Creek volcano, and the more distant and higher skyline ridge, Silver Mountain, is a thick dacite lava within the eastern Platoro caldera that may be the west flank of Cat Creek volcano. Early K/Ar age determinations on biotite from lavas of Cat Creek volcano are in the range of 28–26 Ma (Lipman and others, 1970).

Significant petrologic differences exist between the Green Ridge lava and those within the caldera (Dungan and others, 1989a). Extracaldera lavas show a general progression from early andesite to late dacite, although andesite and dacite are intercalated on Green Ridge. Andesites have phenocrysts of pl+cpx±opx±ol+iron-titanium (fe-ti)-oxide in an intergranular groundmass; coarsely porphyritic dacites have pl+aug+bt±opx±hbl+fe-ti-oxide in a hyalopilitic groundmass. Chilled magmatic inclusions of basaltic andesite to andesite are abundant within the dacites, especially in upper parts of lavas. In contrast, the intracaldera lavas (mostly andesite) lack a compositional range or temporal progression comparable to the extracaldera lavas. They are less coarsely porphyritic than the extracaldera lavas, have hornblende instead of biotite (where a hydrous phase is present), have a microgranular groundmass, and generally lack evidence for mingling/mixing of compositionally diverse magmas.

The intracaldera lavas are enriched in incompatible elements relative to most extracaldera lavas of similar silica content (~60 percent SiO_2). This enrichment corresponds most closely to mixing models or models involving combined assimilation and fractional crystallization, in which the enriched end member has trace-element characteristics like the Rock Creek lavas of the Conejos Formation or the Ra Jadero Tuff of the Treasure Mountain Group. These characteristics, in conjunction with proximity to the vents for the Rock Creek lavas and to the Summitville caldera, suggest that magmas erupted late within the Platoro caldera incorporated some earlier products of the magmatic system or associated hybridized crust. Isotopic compositions of Cat Creek lavas are consistent with this model. Intracaldera lavas have isotopic ratios that become more radiogenic with increasing differentiation, shifting toward values similar to those of the Treasure Mountain ignimbrites, but extracaldera lavas have isotopic compositions that suggest extensive interaction with relatively nonradiogenic lower crust.

Continue ahead, entering the area known as The Canyon of Cat Creek.

12.3 **Stop 4C-8a. Chiquito Peak Tuff in The Canyon** (37°23.14' N., 106°15.48' W.; 8,349 ft, 2,545 m elevation).

This stop shows a typical proximal outflow section through this widespread ignimbrite of the Treasure Mountain Group. The tan, partly welded crystal-rich dacite (62–68 percent SiO_2; ~35 percent phenocrysts) records the youngest eruption from Platoro caldera, with an $^{40}Ar/^{39}Ar$ age of 28.77**±0.03 Ma** at this site (Lipman and Zimmerer, 2019). If the sun cooperates, look for sparse sanidine (clear glass-like crystals with mirror cleavage reflections), in addition to abundant plagioclase, biotite, and green clinopyroxene. Compare and contrast this ignimbrite with the La Jara Canyon Tuff (65–68 percent SiO_2; 25–40 percent phenocrysts of pl>bt +cpx) just viewed at Stop 4C-6, they are compositionally similar except for the presence of sanidine, but less welded and higher lithic content.

Continue down valley (up section) along FS 250, through nonindurated cobbles from the Los Piños Formation (volcaniclastic detritus probably eroded largely from the Cat Creek volcano) and overlying basaltic lava of the Hinsdale Formation, to the junction with Gunbarrel road (CO 15), which leads to Monte Vista and Alamosa.

End of route 4C(a).

Route 4C(b)

From road junction at mile 19.1, proceed ahead to right on FS 255 (fig. 120).

19.9 A dacite porphyry dike, striking nearly parallel to road and forming cliffs on the right, is radial from Cat Creek volcanic center. The Wisconsin terminal moraine of the Alamosa valley glacier is on the right.

20.2 Terrace Reservoir spillway. The dam is constructed around the Alamosa valley terminal moraine.

20.4 Cliffs of densely welded La Jara Canyon Tuff on both sides of Alamosa River. The La Jara Canyon (~30 Ma) is a crystal-rich dacite (65–69 percent SiO_2) with 20–35 percent phenocrysts of plagioclase, biotite, and clinopyroxene. It contains more phenocrysts, smaller

amounts of pumice, and fewer lithic fragments than upper ignimbrites of the Treasure Mountain Group. The road continues in glacial outwash.

21.4 **Stop 4C-7b. Middle tuff and overlying ignimbrites of the Treasure Mountain Group** (37°21.14' N., 106°15.97' W.; 8,382 ft, 2,555 m elevation).

The purpose of this stop is to examine non- to weakly welded ignimbrites of the middle tuff of the Treasure Mountain Group (previously seen in distant view at Mclntyre Peak [Stop 4-2] and in outcrop on route 4A), in comparison to the overlying densely welded Ojito Creek and Ra Jadero Tuffs (fig. 121). This locality is typical of the middle tuff, which elsewhere contains as many as 10–15 laterally extensive outflow ignimbrites of relatively modest volume, interbedded with air-fall and reworked tuffs. These units represent an anomalous period of repeated small eruptions during Treasure

Figure 121. Middle tuff and upper ignimbrites of the Treasure Mountain Group, overlain by the Ojito Creek (Tto) and Ra Jadero (Ttr) Tuffs (Stop 4C-7b) in Alamosa River canyon, west of Chiquito Peak. *A*, Partly welded ignimbrite within the middle tuff, underlain by bedded tephra-fall and fluviatile tuffaceous beds. Ojito Creek and Ra Jadero Tuffs form the upper cliffs along the skyline. *B*, Bedded tephra-fall, overlain by fluviatile tuffaceous beds. *C*, Ledge-forming Ojito Creek and Ra Jadero Tuffs above a bench mantled by glacial-outwash gravels. The dark upper part of the Ojito Creek is a near-vitrophyre zone, overlying the more completely devitrified interior of this ignimbrite. Photographs by K.J. Turner, U.S. Geological Survey, 2015 (*A*) and M. Dungan, University of Oregon, 2016 (*B*,*C*).

Mountain volcanism. Although many of the individual ignimbrites are limited in distribution and cannot be confidently traced laterally, several units are widely dispersed and locally exceed the overlying Ojito Creek or Ra Jadero Tuffs in thickness. The middle tuff shares petrologic and paleomagnetic affinities with the major Treasure Mountain ignimbrites. Many ignimbrites of the middle tuff also contain pumice clasts of mafic dacite as much as 30 cm in diameter.

Low along this exposure, gently dipping pumice-fall beds of the middle tuff drape the sides of a well-exposed paleovalley. Individual pumice-fall beds are 2 to 60-cm thick and contain varying proportions of pumice fragments, lithic clasts, and ashy matrix. Pumice is concentrated near the tops of a few layers, possibly indicating deposition in standing water. Cross-laminations and local channeling within some units result from reworking by water. The main ignimbrite sheet at this locality is 4 to 5-m thick, overlies the fall beds, and fills the paleovalley. It is lithic-rich (particularly near the base), nonwelded to weakly welded, and contains large mafic pumice clasts, especially in the upper part. Several rubbly lithic zones mark lag deposits at the bases of discrete flow pulses; these are overlain by tuff showing a well-preserved welding profile. Flattening of pumice fragments increases from the base to near the middle of the ignimbrite, then decreases upward.

A multibed fall deposit 0.5-m thick is sandwiched between this ignimbrite sheet and an overlying unit (2–3-m thick) that marks the top of the middle tuff. The middle tuff here is unusual in terms of the quantity of associated volcaniclastic sediment and its deposition in a fluvial channel. One of the fluvial reworked beds has yielded a sanidine $^{40}Ar/^{39}Ar$ age of 29.93±0.03 Ma (table 9).

Climb to a glacial-outwash terrace above the middle tuff, where the base of the Ojito Creek Tuff is well exposed to the west in cuts along the old Alamosa River road. A typically thick basal vitrophyre is overlain by a poorly developed lithophysal zone. Upward in the section, dark fiamme as much as 0.5-m long appear abruptly near the top of the main cliff, defining a flow-unit contact within the densely welded devitrified zone. Phenocryst and glass analyses document two discrete Ojito Creek magma compositions, in addition to the rare andesitic fiamme. Locally, compositions are more mafic at the base of the ignimbrite, forming a so-called reverse zonation. The distribution of these two compositions suggests that the Ojito Creek magma body was layered or zoned, but that these layers were tapped irregularly during eruption.

Walk eastward along the cliff to a small side canyon. Traverse up the far side of the canyon, to compare the Ojito Creek Tuff at the top of the bench with the basal vitrophyre of the Ra Jadero Tuff above the bench. Although superficially similar to the Ojito Creek, the Ra Jadero (1) generally has an upper vitrophyre; (2) has reverse remnant magnetic polarity, in contrast to the normal polarity of the Ojito Creek; (3) contains more abundant and larger phenocrysts, blocky rather than tabular plagioclase (commonly intergrown with augite and biotite); (4) more lithic fragments; (5) is the lowest member of the Treasure Mountain Group that contains sanidine phenocrysts (about 10 percent of total feldspar); and (6) has biotite phenocrysts that are distinctively high in iron, titanium, and barium. The high contents of incompatible trace elements closely resemble those of the Rock Creek lava type of the Conejos Formation. Two additional vitrophyre ledges of Ra Jadero Tuff crop out along the bench above the rim of the side canyon. The highest vitrophyre exposure (a small step, just below the main cliff of Chiquito Peak Tuff) contains abundant fiamme of hornblende andesite.

Traverse northwest below the cliff of Chiquito Peak Tuff, into the first canyon; bear to the right and upward, to the top of the thick compound-cooling unit Chiquito Peak Tuff. The covered slope above the Chiquito Peak is underlain by Los Piños Formation, a volcaniclastic conglomerate containing clasts of Green Ridge dacite in an ashy matrix. The triangular cliff face above is a dacitic lava, compositionally similar to lavas that crop out on Green Ridge, Greenie Mountain, and Chiquito Peak. These lavas are on the southeast flank of the Cat Creek volcano. The cliffs above the lava are monolithologic dacitic flow breccias.

Descend carefully down through the ignimbrite cliffs to road level.

22.1 **Stop 4C-8b. Bridge over Alamosa River** (37°20.66' N., 106°15.38' W.; 8,382 ft, 2,555 m elevation)**.** This stop provides good views of outflow layer-cake ignimbrite stratigraphy. To the left, exposed above the Alamosa River on geographic Chiquito Peak, are several ignimbrites of the Treasure Mountain Group (fig. 122*A*). Two welding zones of the Ojito Creek Tuff are visible upstream from this viewpoint, as just observed at Stop 4C-7b. A lower densely welded zone is overlain by a moderately welded and vapor-phase-altered zone that has an undulatory eroded contact with the overlying Ra Jadero Tuff. The lower orange-brown cliff directly across the river is the upper welding zone of the Ra Jadero Tuff. The Chiquito Peak Tuff overlies the variably eroded top of the Ra Jadero. The top of the Chiquito Peak is also eroded (fig. 122*B*), and a local valley-filling unit of fluvially reworked, weakly welded Fish Canyon Tuff (erupted at 28.20 Ma, from the central San Juan caldera cluster, Day 5) underlies nonindurated conglomerates of the Los Piños Formation. In one small exposure (fig. 122*C*), white weakly welded tuff grades upward into a dark bench of welded rhyolitic tuff beneath the Chiquito Peak cliff; this local exposure is interpreted as distal South Fork Tuff, an ignimbrite of the Treasure

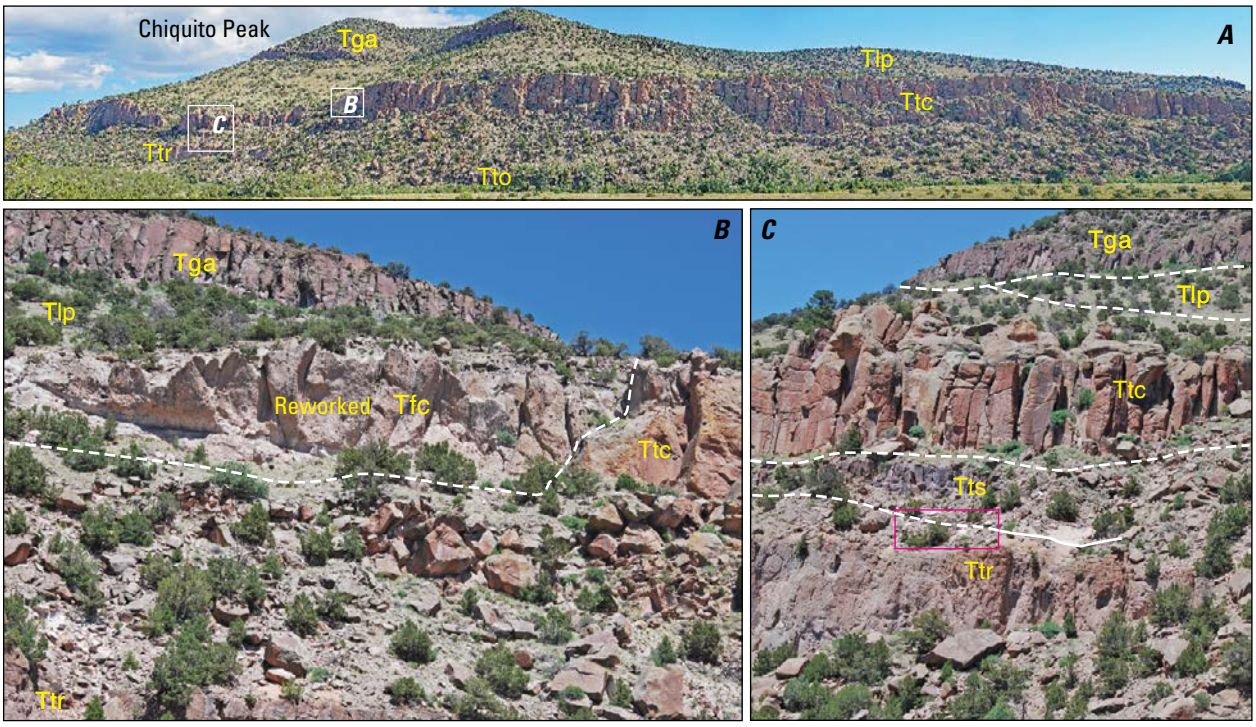

Figure 122. Outflow volcanic stratigraphy of eastern Chiquito Peak (Stop 4C-8b). *A*, Exceptional exposures of the major late-erupted ignimbrites of the Treasure Mountain Group: Ojito Creek Tuff (Tto), Ra Jadero Tuff (Ttr), and Chiquito Peak Tuff (Ttc). Nonindurated conglomerates of the Los Piños Formation (Tlp, covered slopes above the ignimbrite section) are a volcaniclastic apron shed from the nearby Cat Creek volcano. Andesitic and dacitic lavas of Green Ridge (Tga) that cap the hill are erosional remnants of the southeast flank of the Cat Creek volcano. *B*, Evidence for erosion between ignimbrite eruptions. The thick orange-brown upper cliff of Ra Jadero Tuff (Ttr) is only moderately welded in this area, and its upper weakly indurated zone was largely stripped by erosion prior to deposition of the Chiquito Peak Tuff (Ttc). The prominent light-colored deposit, filling a valley eroded into the top of the Chiquito Peak Tuff, is reworked material derived from distal weakly welded Fish Canyon Tuff (Tfc). Such erosion has commonly cut into the partly welded upper zones of San Juan ignimbrites, but not into densely welded interiors. *C*, Thin dark-brown rhyolitic outcrop of probable South Fork Tuff (Tts), beneath the Chiquito Peak (Ttc). This is the only known locality for the South Fork Tuff as far south as the Alamosa River valley. Outflow remnants of this ignimbrite are preserved mainly north of Platoro caldera. Photographs by M. Dungan, University of Oregon, 2016.

Mountain Group that is elsewhere preserved mainly on slopes north of Platoro caldera.

To the right is a view of Jacobs Hill, capped by andesitic lavas (fig. 120) and interlayered gravels of the Los Piños Formation, both derived from the postcaldera Cat Creek volcano to the northwest. The underlying cliffs are Chiquito Peak Tuff. Stratigraphic and structural relations are complicated in this area by faulting peripheral to a small intrusion of sanidine dacite (26.47±0.01 Ma; Lipman and Zimmerer, 2019) that has uplifted the Treasure Mountain section. A weakly welded tuff, beneath a capping andesitic lava, was interpreted as the lower rhyolite tuff of the Treasure Mountain Group (Lipman, 1974). This somewhat ambiguous locality is the only easily accessible field-trip site for the lower tuff. At this locality and to the south (Conejos valley), the lower tuff is a variably welded rhyolite that is lithic-rich and phenocryst-poor; phenocryst compositions resemble those in the La Jara Canyon Tuff.

Continue southeast along FS 255.

23.0 *Road junction; turn left (east), onto road CO Bb. Continue down valley (up section) along CO Bb, through poorly exposed conglomerates of the Los Piños Formation (volcaniclastic detritus largely eroded from the Cat Creek volcano), to the junction with Gunbarrel Road (C0 15), which leads to Monte Vista and Alamosa. End of route 4C(b).*

Acknowledgments

Summer-long assistance with fieldwork at Platoro, commonly under adverse conditions, by Russell Burmester, James Kirkpatrick, and David Johnston is much appreciated and fondly remembered. In addition to collaboration with numerous other geologists, as noted or referenced in this report, we also thank many friends in the southeastern San Juan region who provided diverse hospitality, logistical support, help with back-country and property access, and other assistance during fieldwork. We especially thank K.J. Turner for assistance in preparing publishable geologic map figures and other illustrations, Christine Chan for perceptive text editing, and Amy Gilbert and Joe Colgan for helpful technical reviews of this field guide segment.

Day 5—The Central San Juan Region

By Peter.W. Lipman[1], Olivier Bachmann[2], and Michael.A. Dungan[3]

Introduction

Andesitic to rhyolitic volcanic rocks of the central San Juan region, along with associated epithermal ores, have been studied intermittently since early in the 20th century (Emmons and Larsen, 1923; Cross and Larsen, 1935; Larsen and Cross, 1956), including detailed middle-century studies of the Creede mining district by Steven and Ratté (1965, 1973) and regional field and volcanological studies (Lipman and others, 1970; Steven and others, 1974a; Steven and Lipman, 1976). Although much was learned during these studies about the evolution of several complex caldera clusters within the San Juan locus of the southern Rocky Mountain volcanic field (SRMVF), which erupted at least 22 major ignimbrite sheets (each 150–5,000 cubic kilometers [km^3]) between 30 and 23 million years ago (Ma) (Lipman, 1989), mapping and other research in support of the Creede Scientific Drilling Project (Bethke and Lipman, 1987; Bethke and Hay, 2000) provided additional insights into stratigraphic sequence, duration of volcanism, eruptive processes, and structure in the central San Juan region (fig. 123). The ignimbrite tuffs and calderas of the central San Juan region have been widely recognized as exceptional sites for understanding (1) processes of pyroclastic eruption and emplacement, (2) interrelations between caldera subsidence and resurgence, (3) the petrologic diversity of sequential ignimbrite eruptions, (4) recurrent eruption of intermediate-composition lavas after caldera-forming events, (5) associated regional faulting, (6) volume relations between ignimbrite eruptions and associated calderas, (7) the emplacement subvolcanic batholiths, and (8) mantle contributions to magma generation at a continental arc.

The present field guide is an update of one prepared for a prior International Association of Volcanology and Chemistry of the Earth's Interior (IAVCEI) field excursion (Lipman and others, 1989). The emphasis is on three major ignimbrite-caldera cycles: Fish Canyon Tuff and La Garita caldera, Carpenter Ridge Tuff and Bachelor caldera, and Snowshoe Mountain Tuff and Creede caldera. Stratigraphic and volcanic-process observations are substantially based on an interpretive report (Lipman, 2000) and geologic map (Lipman, 2006), but new perspectives have resulted from high-resolution $^{40}Ar/^{39}Ar$ ages obtained in collaboration with William McIntosh and Matthew Zimmerer, geochronologists at New Mexico Tech (fig. 124), including important previously unpublished ages. Other recent volcanologic and petrologic studies, along with regional isotopic and geophysical surveys, have shed further light on eruptive processes, relations between volcanism and associated batholith growth, and magmatic evolution of the central San Juan locus (Riciputi and others, 1995; Bachmann and others, 2002, 2014; Bachmann and Bergantz, 2003; Parat and others, 2005; Drenth and others, 2012; Lipman and Bachmann, 2015). A separate field guide is available for the closely related Cochetopa Park caldera (fig. 125), just northeast of the central caldera complex (Lipman and others, 2013), as is a more-detailed guide to the Creede caldera (Larsen and Lipman, 2016).

Geologic Setting

In the central San Juan Mountains (fig. 123), the eruption of at least 8,800 km^3 of dacitic-rhyolitic magma as nine major ignimbrites (individually 150–5,000 km^3) was accompanied by recurrent caldera subsidence between 28.7 and 26.9 Ma (Steven and Lipman, 1976; Lipman and others, 1989; Lipman, 2000, 2007). Voluminous andesitic-dacitic lavas and breccias were erupted from central volcanoes prior to the ignimbrite eruptions, and similar lava continued to erupt within, and adjacent to, the calderas during the more silicic explosive volcanism (Lipman and others, 1978; Colucci and others, 1991; Parat and others, 2005). The seven exposed calderas vary in size from ~10 to at least 75 km in maximum dimension, and the largest calderas are associated with the most voluminous eruptions (table 10).

A caldera that likely accompanied the initial ignimbrite eruption (Masonic Park Tuff) is entirely concealed beneath younger rocks and structures in the central San Juan region. The giant La Garita caldera (35 × 75 km) collapsed in three or more successive northward-migrating segments during eruption of the Fish Canyon Tuff at 28.02 Ma[4] (fig. 125). After collapse of the La Garita caldera, seven additional eruptions of petrologically diverse ignimbrites (table 6) and associated calderas formed inside the La Garita depression within about 1 million years (m.y.) (fig. 125; table 10). Erosional dissection to depths of as much as 1.5 km has exposed diverse features of intracaldera ignimbrite tuff and interleaved landslide deposits that accumulated to multi-kilometer

[1]U.S. Geological Survey.

[2]ETH Zurich.

[3]University of Oregon.

[4]All $^{40}Ar/^{39}Ar$ dates for Day 5 are calibrated to Fish Canyon Tuff at 28.02 Ma, to provide consistency with published reports that list the analytical data (especially Lipman and McIntosh, 2008; Lipman, 2012; Lipman and others, 2015). This is in contrast to Day 4, where more-recently determined ages for Day 4 are based on a calibration of Fish Canyon Tuff at 28.201 Ma, which also permits more direct comparison with U-Pb dates.

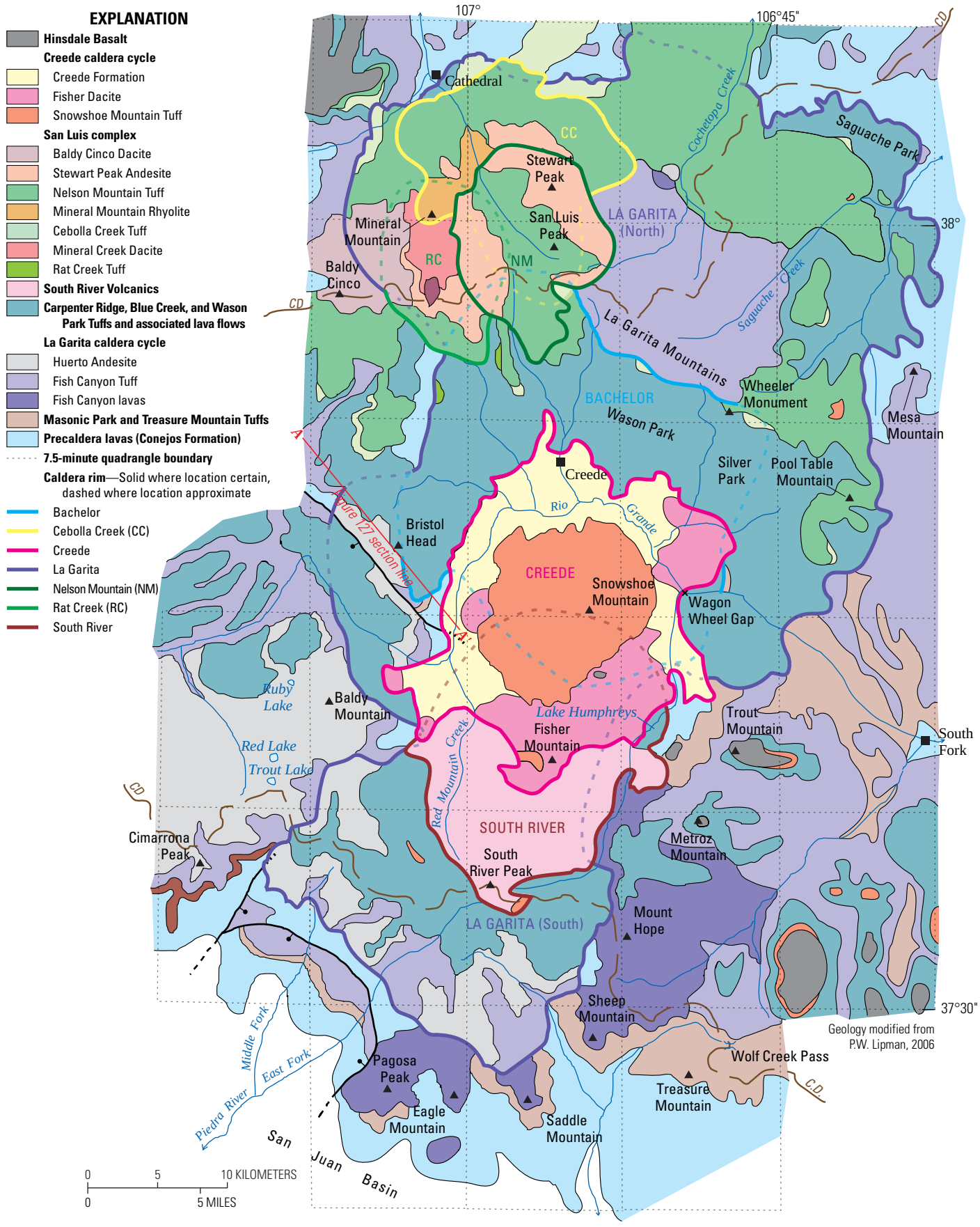

Figure 123. Geologic map of the central caldera cluster, San Juan volcanic region, Colorado, generalized from Lipman (2006). CD, continental divide.

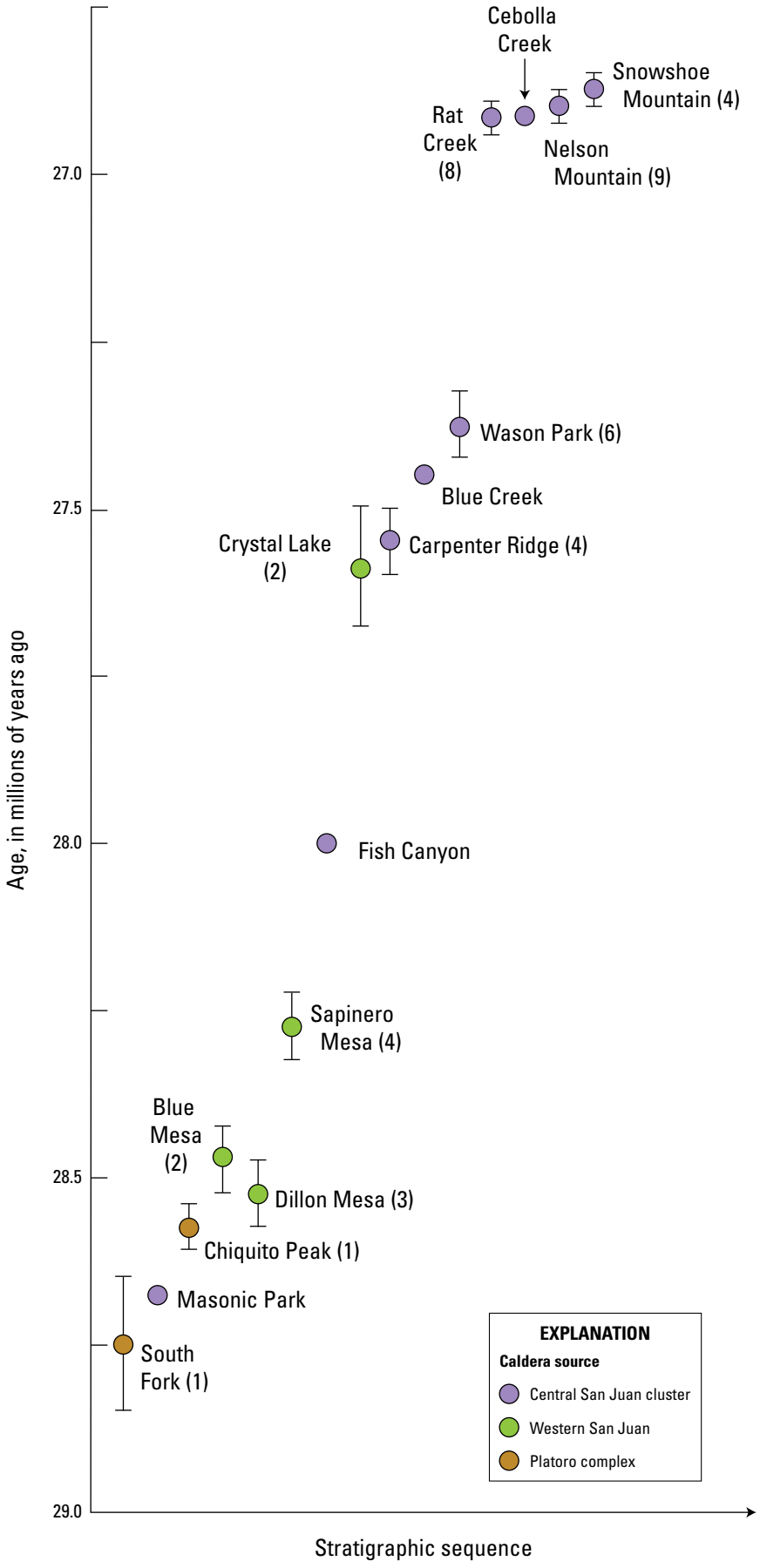

Figure 124. Summary of recent $^{40}Ar/^{39}Ar$ single-crystal sanidine age determinations for ignimbrites of the central San Juan caldera area, including interfingering tuff sheets from the Platoro caldera complex to the southeast and ones from western San Juan calderas (data from Lipman and McIntosh [2008] and table 9 of this report). The central San Juan ignimbrites erupted in four discrete episodes (28.7, 28.0, 27.55–27.38, and 26.9 Ma), separated by roughly 0.5 million year pauses. Numbers in parens represent the number of dated samples per unit. Circles indicate weighted-mean ages; vertical lines represent analytical uncertainties for individual ages (95-percent confidence, 2σ) or the standard error (Se) for weighted-mean ages. Determinations are calibrated relative to a Fish Canyon age of 28.02 Ma (Renne and others, 1998). Other ages without indicated uncertainty are less-precise biotite and hornblende determinations or ages constrained by stratigraphic sequence.

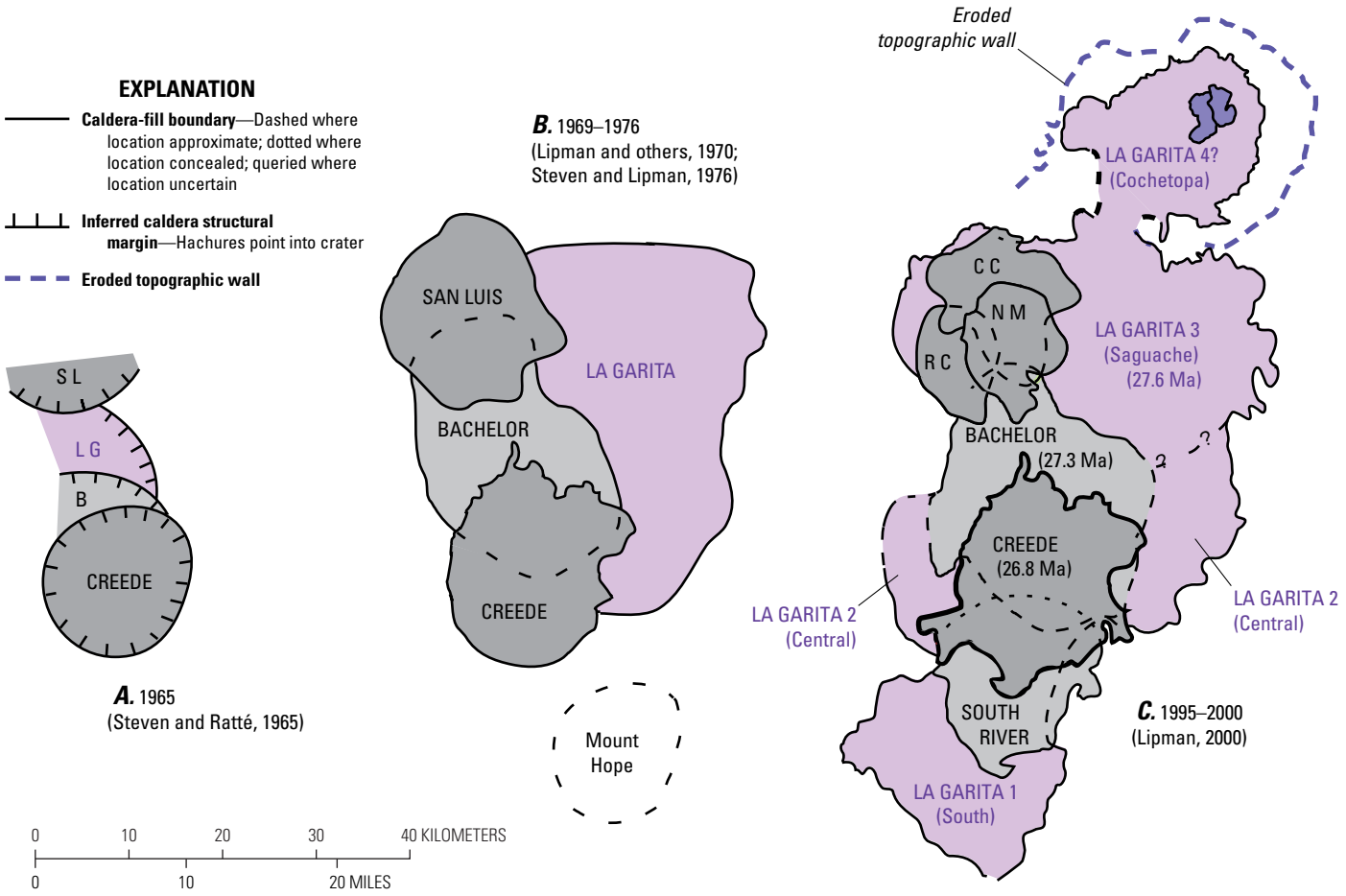

Figure 125. Successive interpretations of the central San Juan caldera geometry, 1965–2012. *A*, Initial caldera identifications (Steven and Ratté, 1965). Calderas: B, Bachelor; SL, San Luis; LG, La Garita. *B*, Revised geometries (Lipman and others, 1970; Steven and Lipman, 1976). *C*, Present interpretation (Lipman, 2000). Cochetopa caldera (Lipman, 2012) is depicted as having initially subsided as a northernmost segment of La Garita caldera, but major later subsidence accompanied the eruption of the Nelson Mountain Tuff. Calderas within the San Luis complex: RC, Rat Creek; CC, Cebolla Creek; NM, Nelson Mountain.

thickness within concurrently subsiding calderas. The calderas display a variety of postcollapse resurgent uplifts, and caldera-forming events produced complex fault geometries that localized late mineralization, including the epithermal base- and precious-metal veins of the much-studied Creede mining district (Steven and Ratté, 1965; Wetlaufer and others, 1979; Foley and others, 1993; Barton and others, 2000). Most of the central San Juan calderas have been variably disrupted by younger events and deeply eroded; as a result, their identification is dependent on detailed geologic mapping. In contrast, the primary morphology of the youngest ignimbrite center, the resurgent Creede caldera, has been exceptionally preserved because of rapid infilling by moat sediments of the Creede Formation that were preferentially eroded only during the past few million years.

The central caldera cluster offers exceptional opportunities to study the varied process of resurgent doming. La Garita, Bachelor, and Creede calderas all have fairly symmetrical and structurally simple resurgent domes. Dips on the flanks of the La Garita uplift are relatively gentle (mostly less than 15°). In contrast, the flanks of the resurgent dome within Creede caldera dip as steeply as 45°. The crest of the resurgent dome of the Bachelor caldera appears to be eccentrically located north of the center of this caldera. In addition, lineate and rheomorphic deformation of fiamme (flattened pumices) deep in the caldera-filling Carpenter Ridge Tuff on flanks of the resurgent dome suggests that definition of the domical structure began rapidly after the eruption, while the intracaldera ignimbrite remained sufficiently hot to deform viscously. The San Luis caldera resurged asymmetrically, as a structurally complex trapdoor uplift, somewhat similar to that at Platoro. Additionally, resurgence was eccentric to the subsidence basin, with the north margin of uplift marked by a hinge zone 2–5 km beyond caldera-fill deposits.

Compositions of tuffs and lavas associated with the central cluster (table 11) tend to be more silicic and evolved than those of the southeastern caldera complex (Platoro); even more evolved compositions are present in the western San Juan region. Several calderas, especially Bachelor and northern La Garita, contain only limited postsubsidence lavas prior to the next major ignimbrite. Nevertheless, the same general compositions prevailed, and

Table 10. Summary of the major ignimbrites, caldera sources, and $^{40}Ar/^{39}Ar$ ages in the central San Juan region.

[Bold type, major tuff sheets of the central caldera cluster. Age determinations from Lipman and McIntosh (2008) and this report. Ma, million years ago; m^3, cubic meters]

Ignimbrite sheet	Composition	Caldera source	Volume (m^3)	Magnetic polarity[1]	Age (Ma)
		West cluster			
Sunshine Peak	Silicic rhyolite-dacite	Lake City	200–500	R	23.1
Crystal Lake	Low-silica rhyolite	Silverton	50–100	R	27.61
Sapinero Mesa[2]	Low-silica rhyolite	San Juan	>1,000	R	28.28
Dillon Mesa[2]	Low-silica rhyolite	Uncompahgre?	25–100	R	28.52
Blue Mesa[2]	Low-silica rhyolite	Lost Lakes	100–500	R	28.48
		Central and northeast cluster			
Snowshoe Mountain	**Mafic dacite**	**Creede**	**>500**	**N**	**26.87**
Nelson Mountain	**Low-silica rhyolite to dacite**	**San Luis complex, Cochetopa Park**	**>500**	**N**	**26.90**
Cebolla Creek	**Mafic dacite**	**San Luis complex**	**250**	**N**	**~26.9**
Rat Creek	**Low-silica rhyolite to dacite**	**San Luis complex**	**150**	**N**	**26.91**
Wason Park	**Rhyolite**	**South River**	**>500**	**R**	**27.38**
Blue Creek	**Dacite**	**(concealed)**	**250**	**R**	**~27.45**
Carpenter Ridge	**Low-silica rhyolite to dacite**	**Bachelor**	**>1,000**	**R**	**27.55**
Fish Canyon	**Dacite**	**La Garita**	**>5,000**	**N**	**28.02**
Masonic Park	**Dacite**	**(concealed)**	**500**	**R**	**~28.7**
Luders Creek	Low-silica rhyolite to dacite	Cochetopa?	50?	n.d.	32.17
Saguache Creek	Rhyolite	North Pass	250–500	N	32.25
		Southeast complex			
Chiquito Peak	Dacite	Platoro	1,000	R	28.65
South Fork	Low-silica rhyolite	Platoro	50	R	28.75

[1]N, normal polarity; R, reverse polarity; n.d., not determined.

[2]Stratigraphic relation to southeast area is uncertain.

andesitic to dacitic lavas interleave locally between all major ignimbrite sheets of the central cluster, documenting the continued presence of mafic components during generation of the evolved ignimbrite magmas (Lipman and others, 1978; Riciputi and others, 1995; Lipman, 2000; Parat and others, 2005; Lipman and McIntosh, 2008).

Mineralization in the central cluster was mainly confined to the Creede district (Steven and Ratté, 1965). Ore deposits are localized by caldera structures (keystone graben faults of the resurgent Bachelor caldera and near walls of the San Luis and Creede calderas) but are about 1 m.y. younger than associated volcanic deposits (Bethke and others, 1976). No sizeable shallow intrusions are exposed in the mining district, but such bodies are likely present at shallow depth to provide heat sources for the hydrothermal systems responsible for the mineralization (Barton and others, 2000). Several small granitoid bodies exposed topographically low within the uplifted core of the San Luis caldera are interpreted as shallow parts of a larger, deeper intrusion.

Lavas, volcaniclastic sedimentary rocks, and intrusions emplaced concurrently with ignimbrites in the central San Juan Mountains have been interpreted as defining multiple caldera cycles, based on affinities of geographic distribution and stratigraphic sequence, isotopic age and paleomagnetic pole positions, and petrologic character (table 10). Interpretation of some units remains ambiguous, however, especially assignment of certain lavas to the late stages of one cycle versus the inception of the next. These interpretations of caldera geometry and regional volcanic history build upon earlier syntheses (Lipman and others, 1970, 1989; Steven and Lipman, 1976), utilizing concepts of caldera geometry and eruptive cycles summarized by Smith and Bailey (1968) and Lipman (1984, 1997) that may provide a useful framework for interpretation of features visited during the field excursion.

Precaldera Volcanism (Conejos Formation)

Precaldera lavas and breccias are exposed only locally within the trip area (fig. 123), mainly along caldera walls. Even the deepest erosion has cut through thick fills of ignimbrites and interleaved lavas in just a few places. The early lavas demonstrate that the central caldera cluster formed within a group of large volcanic constructs, similar to relations that are more clearly preserved elsewhere in the region (Lipman, 1975a; Colucci and others, 1991; Lipman and others, 2015).

The precaldera volcanoes, collectively designated as the Conejos Formation (Lipman and others, 1970) consist dominantly of andesite and dacite as lavas and proximal breccias, surrounded by voluminous aprons of volcaniclastic debris emplaced as mudflow and stream-fan deposits (Stop 5-3). Relatively distal Conejos volcaniclastic sedimentary rocks are 600–800-m thick

Table 11. Representative chemical analyses, central San Juan caldera cluster.

[Data from Lipman (2004). Major-oxide chemical analyses are calculated to reported totals, volatile-free. XRF, x-ray fluorescence; LOI, loss on ignition; intrac, intracaldera; xr, crystal rich; vitr, vitrophyre; rhy, rhyolite; --, no data]

Field number	Sample description	Major-oxides, in weight percent												XRF, in parts per million			
		SiO_2	TiO_2	Al_2O3	$FeTO_3$	MgO	CaO	Na_2O	K_2O	P_2O_5	MnO	LOI	Total	Rb	Sr	Zr	Ba
Creede caldera cycle																	
85L-39	Fisher Dacite, Wagon Wheel Gap lava	65.4	0.66	15.4	5.01	1.66	4.07	3.46	3.85	0.27	0.07	1.93	99.84	94	587	174	1,020
85S-129	Snowshoe Mountain Tuff, intrac, Point of Rocks	67.6	0.52	15.0	3.87	1.07	3.62	3.47	4.53	0.23	0.06	1.64	100.03	135	472	184	823
SJ-85-20	Snowshoe Mountain Tuff, outflow, Cattle Mountain	62.3	0.73	16.6	6.38	1.33	4.53	3.73	3.43	0.31	0.11	1.25	99.44	107	704	155	1,010
San Luis caldera complex																	
Nelson Mountain cycle																	
DS87-103	Resurgent intrusion	57.0	1.06	17.31	8.14	0.11	2.19	5.77	3.64	3.04	0.45	0.73	98.66	84	759	187	1,061
94L-19A	Volcanics of Baldy Cinco, dacite lava	64.4	0.64	15.90	4.51	1.11	3.41	3.78	4.31	0.37	0.09	0.70	98.52	144	580	210	1,100
85S-121	Volcanics of Stewart Peak, andesite lava	60.8	0.91	17.0	6.87	1.81	5.00	3.56	3.48	0.36	0.07	1.08	99.90	115	644	195	1,040
85S-110	Nelson Mountain Tuff, intrac dacite, San Luis Peak	62.8	0.69	16.4	5.76	1.94	4.52	3.80	3.61	0.31	0.10	1.77	99.96	107	671	183	--
85L-10	Nelson Mountain Tuff, intrac dacite, East Willow Creek	66.3	0.55	15.9	4.23	1.39	3.32	3.65	4.33	0.23	0.09	1.90	100.03	115	524	224	998
SD2-1064	Nelson Mountain Tuff, intrac rhy, SD-2 drillhole	70.7	0.33	14.8	2.25	0.57	1.84	3.72	4.77	0.08	0.08	4.80	99.21	118	313	226	1,070
85L-29C	Nelson Mountain Tuff, xr rhy vitr, Nelson Mountain	70.2	0.37	15.3	2.40	0.68	1.89	3.63	5.44	0.10	0.09	2.61	100.17	144	310	280	--
Cebolla Creek cycle																	
85S-139	Mineral Mountain Rhyolite, lava flow	73.8	0.23	13.7	1.64	0.38	1.37	3.39	4.87	0.05	0.08	5.74	99.57	182	169	161	513
88L-50	Dacite of East Willow Creek	65.5	0.58	15.4	4.21	1.33	3.43	3.56	4.11	0.28	0.09	0.44	99.0	106	532	203	1,003
85L-33D	Cebolla Creek Tuff	64.2	0.62	16.2	4.70	1.54	3.91	3.67	3.71	0.30	0.08	1.46	99.01	96	571	205	1,020
Rat Creek cycle																	
89L-161-B	Mineral Creek Dacite, lava	68.6	0.44	15.58	3.06	0.64	2.55	2.51	5.48	0.22	0.04	5.14	99.17	--	--	--	--
85L-29F	Rat Creek Tuff, dacite vitrophyre	65.8	0.57	16.6	3.87	1.37	3.22	3.89	4.17	0.21	0.09	2.03	99.82	97	622	337	1,910
85L-30	Dacite of Captive Inca, lava vitrophyre	69.7	0.42	15.0	3.20	1.03	2.89	3.20	4.34	0.16	0.10	4.45	100.04	162	400	167	658
SJ85-3	Dacite of McKenzie Mountain, near vitrophyre	63.7	0.68	15.9	5.79	1.93	4.43	3.49	3.65	0.30	0.09	2.29	99.93	116	628	170	870
South River caldera cycle																	
88L-36	South River Volcanics, intrusion	58.31	0.82	17.37	7.77	2.36	5.80	4.11	2.35	0.52	0.15	1.55	99.56	43	843	179	959
88L-62E	South River Volcanics, dacite lava	64.55	0.75	16.72	3.58	1.12	4.22	3.64	4.51	0.23	0.04	1.92	99.37	72	721	180	1,417
DS89-010	South River Volcanics, andesite lava	59.81	0.85	16.49	7.07	2.36	5.63	3.98	2.93	0.46	0.10	0.52	99.68	55	891	204	1,270
97L-5	Wason Park Tuff (intracaldera), Lake Humphreys	62.87	0.69	17.60	4.52	0.66	3.68	3.84	4.01	0.25	0.11	1.25	99.47	116	665	302	1,200
TW-32	Wason Park Tuff, Antelope Park	71.23	0.38	14.58	2.19	0.53	1.40	3.65	5.57	0.08	0.09	3.08	99.71	160	231	256	896

Table 11.—Continued

Field number	Sample description	Major-oxides, in weight percent												XRF, in parts per million			
		SiO_2	TiO_2	Al_2O3	$FeTO_3$	MgO	CaO	Na_2O	K_2O	P_2O_5	MnO	LOI	Total	Rb	Sr	Zr	Ba
Blue Creek cycle																	
88L-26	Volcanics of McClelland Mountain, dacite lava	66.80	0.44	15.10	2.62	0.78	2.28	3.16	5.25	0.15	0.09	0.44	97.11	--	--	--	--
LR88-634	Blue Creek Tuff, Palisades	63.50	0.67	16.40	4.43	1.69	3.71	3.46	4.07	0.23	0.10	1.70	99.91	115	541	279	1,175
89L-140	Volcanics of Beaver Creek, lava	67.87	0.32	16.53	3.00	0.61	3.36	3.67	3.71	0.14	0.11	2.59	99.31	71	539	183	1,043
Bachelor caldera cycle																	
88L-52	Rhyolite of Table Mountain, lava	72.91	0.28	14.16	1.60	0.35	1.37	3.03	5.62	0.07	0.05	2.87	99.44	--	--	--	--
89L-151	Dacite of Shallow Creek, lava	67.42	0.51	19.19	0.45	0.19	0.49	2.43	7.88	0.04	<0.01	3.61	98.61	--	--	--	--
99L-11	Mafic fiamme, upper outflow tuff	51.10	1.06	20.80	8.45	2.78	6.91	3.81	2.34	0.68	0.11	1.37	99.41	69	1,502	603	4,800
87-132	Mammoth Mountain Member, dacite, Palisades	64.30	0.71	16.50	3.86	1.90	4.47	3.51	4.13	0.29	0.07	1.58	100.92	124	525	254	1,187
85S-105	Bachelor Mountain Member, intracaldera, 1st fork	73.18	0.24	13.91	1.72	0.40	1.42	3.68	4.77	0.00	0.06	3.81	99.38	166	177	175	515
CR-24	Carpenter Ridge Tuff, outflow, Del Norte	72.07	0.27	14.69	1.76	0.39	1.51	3.75	5.17	0.00	0.07	3.25	99.68	164	250	75	1,180
85L-4	Rhyolite of Miners Creek, lava	74.96	0.19	13.33	1.28	0.21	0.90	3.40	5.17	0.06	0.00	4.94	99.51	178	74	158	--
La Garita caldera cycle																	
97L-8	Huerto Andesite, dacite lava Fern Creek	67.37	0.43	16.42	2.89	0.41	2.35	4.51	4.00	0.17	0.08	0.89	99.51	93	449	312	1,290
LR88-589	Huerto Andesite, platy-plagioclase lava, Ribbon Mesa	58.84	1.03	17.11	7.44	0.08	1.72	6.14	3.46	3.66	0.43	1.32	99.90	94	552	278	827
DY89-25	Huerto Andesite, aphanitic lava	60.83	0.64	17.21	6.66	2.13	6.05	3.49	2.43	0.33	0.15	1.20	99.92	53	661	171	760
90L-21	Nutras Creek Dacite, lava	66.00	0.53	15.70	4.65	1.09	3.34	3.71	3.98	0.23	0.09	0.51	99.34	111	399	154	861
DS88-081	Intracaldera La Garita Member, Cochetopa Creek	66.00	0.53	15.67	4.18	1.09	3.34	3.71	3.98	0.23	0.09	0.51	99.34	108	488	173	938
TFC-03	Fish Canyon Tuff, outflow, Goodrich Creek	66.47	0.54	15.95	4.71	1.38	3.64	3.74	3.63	0.20	0.09	1.67	100.35	--	--	--	--
94L-15	Pagosa Peak Dacite, Saddle Mountain	67.50	0.49	15.00	3.66	1.12	2.73	3.58	4.33	0.21	0.10	0.54	99.26	128	400	158	820
Masonic Park cycle																	
96L-5	Sheep Mountain Andesite, scoria, Pagosa Peak	57.93	0.71	15.26	5.77	2.72	5.25	2.18	1.29	0.31	0.15	8.36	99.92	116	665	302	1,200
93L-13-B	Masonic Park Tuff, Alder Creek	64.30	0.75	15.37	5.54	1.99	4.99	2.63	3.14	0.33	0.07	3.70	99.11	74	650	166	850

within about 5 km of the southern margins of the central caldera cluster, where exposed above Cretaceous sediments along the northeastern margin of the San Juan Basin. Basal Conejos lavas are also locally exposed about 10 km north of the central cluster, where these rocks wedge out against Proterozoic rocks along the flank of the Laramide Uncompahgre uplift. East of the central caldera cluster, petroleum exploration drilling has penetrated Conejos sequences 1.3–2.3-km thick (Gries, 1985; Brister and Gries, 1994).

The bulk of the Conejos lavas within the trip area are andesite and dacite (Lipman, 2006), similar to Conejos rocks elsewhere in the SRMVF. Small domes of flow-layered rhyolite (70–74 percent SiO_2; 3–5 percent plagioclase, biotite), present high in Conejos sequences in several areas near the margins of the subsequent calderas, may represent precursors of the silicic magma that later erupted explosively as ignimbrites. Such eruptive activity began about 34 Ma and produced roughly two-thirds of the total volume of the overall San Juan volcanic locus by about 30 Ma, before any sizable ignimbrites were erupted from the central caldera cluster. Intermediate-composition magmatism continued in essentially the same eruptive style during the ignimbrite eruptions and caldera formation, producing lavas and breccias that interleave locally between all the regional ignimbrite sheets and constitute much of the fill in calderas.

Masonic Park Tuff and its Source

The Masonic Park Tuff, the earliest ignimbrite erupted from the central San Juan region at 28.7 Ma, is transitional in age and petrology between tuffs of the Treasure Mountain Group erupted from the Platoro caldera complex 30.0–28.6 Ma and younger tuffs from the central cluster (Stops 5-4, 5B-1, 5B-2). It is a compositionally uniform, crystal-rich mafic dacite (62–65 percent SiO_2; 30–40 percent plagioclase, biotite, clinopyroxene: Sliwinski and others, 2017) that, except for the absence of sparse sanidine, petrologically resembles the areally adjacent Chiquito Peak Tuff from Platoro caldera (table 6), with which it was previously confused (Lipman and others, 1996). Stratigraphic complications among such petrologically similar ignimbrites of phenocryst-rich dacite have been a recurrent problem in San Juan work (table 12).

The Masonic Park Tuff is characterized by compound welding and numerous flow-unit partings (Stop 5B-1a). No vertical compositional zonation has thus far been documented, other than subtle effects of crystal elutriation during emplacement (Lipman and others, 1996). The most probable location for a Masonic Park Tuff caldera lies buried within the southern La Garita caldera (fig. 125). Such a location is supported by the overall distribution of Masonic Park Tuff and its exceptional thickness and dense welding where exposed along the southwestern margin of La Garita caldera. Wherever the source of the Masonic Park Tuff, this ignimbrite documents overlapping eruptive activity between calderas in the southeastern and central San Juan regions, comparable to that previously recognized between the western and central clusters.

La Garita Caldera Cycle (Fish Canyon Tuff)

The voluminous and seemingly homogeneous 28.0-Ma Fish Canyon Tuff, known as one of the world's largest ignimbrite sheets, is associated with formation of the 35 × 75-km La Garita caldera, the largest in the SRMVF (fig. 126). This tuff is an archetypal monotonous-intermediate eruption from a magma body that lacked compositional gradients (Hildreth, 1981), as are other phenocryst-rich dacite tuffs of the San Juan region that lack obvious magmatic compositional variation (Ute Ridge, Chiquito Peak, Blue Creek, Cebolla Creek, Snowshoe Mountain Tuffs; tables 5, 10). Compositionally similar tuff sheets with several thousand cubic kilometer volumes also dominate Oligocene volcanism in the Great Basin region of Utah and Nevada (Best and others, 1989, 2013).

Among the 22 large (100 to >1,000 km^3) Cenozoic ignimbrites erupted from the San Juan locus, the Fish Canyon Tuff is unique in its volume (~5,000 km^3), uniform high phenocryst content (35–50 percent), and near-solidus assemblage (plagioclase, sanidine, quartz, biotite, hornblende, titanite, apatite, zircon, iron-titanium [Fe-Ti] oxides). As the only San Juan ignimbrite that contains hornblende without augite, it is distinct from other voluminous sheets of uniform crystal-rich dacite that have been difficult to distinguish during field studies (table 12). The estimated Fish Canyon Tuff eruptive volume is derived from its areal extent (locally preserved >125 km from caldera rims), substantial outflow thickness (to 300 meters [m] in some proximal sections), thick intracaldera volume (>1.2-km thick in the La Garita Mountains, with no exposed base), large caldera area (about 2,000 km^2), and the generalization for large ignimbrites that outflow and intracaldera volumes tend to be subequal (Lipman, 1997).

Table 12. Evolving correlations of phenocryst-rich dacitic ignimbrites, central San Juan region.

[--, not recognized]

Steven and Ratté (1965)	Steven and others (1973)	Lipman and others (1989)	Lipman and others (1996)	Lipman (2000)
--	--	--	--	Blue Creek Tuff
Mammoth Mountain Rhyolite	Mammoth Mountain Tuff	Mammoth Mountain Member of Carpenter Ridge Tuff	Mammoth Mountain Member of Carpenter Ridge Tuff	Mammoth Mountain Member of Carpenter Ridge Tuff
--	--	--	Chiquito Peak Tuff	Chiquito Peak Tuff
--	Masonic Park Tuff	Masonic Park Tuff	Masonic Park Tuff	Masonic Park Tuff

Figure 126. Map showing the geometry of La Garita caldera and proximal eruptive deposits of this caldera cycle, generalized from Lipman (2006). Within the San Luis complex: RC, Rat Creek caldera; CC, Cebolla Creek caldera; NM, Nelson Mountain caldera; BC, Baldy Cinco. Abbreviated geographic names: BH, Bristol Head; CD, Cochetopa Dome; EM, Eagle Mountain; FM, Fisher Mountain; LH, Lake Humphreys; MM, Mineral Mountain; Me, Metroz Mountain; MeM, Mesa Mountain; MH, Mount Hope; NP, North Pass; PP, Pagosa Peak; PTM, Pool Table Mountain; RCD, Razor Creek Dome; SA, Saddle Mountain; SaP, Saguache Park; SL, San Luis Peak; SM, Sheep Mountain; SnM, Snowshoe Mountain; SP, Stewart Peak; SRP, South River Peak; STM, Sawtooth Mountain; TaM, Table Mountain; TM, Trout Mountain; TrM, Treasure Mountain; WCP, Wolf Creek Pass; WWG, Wagon Wheel Gap.

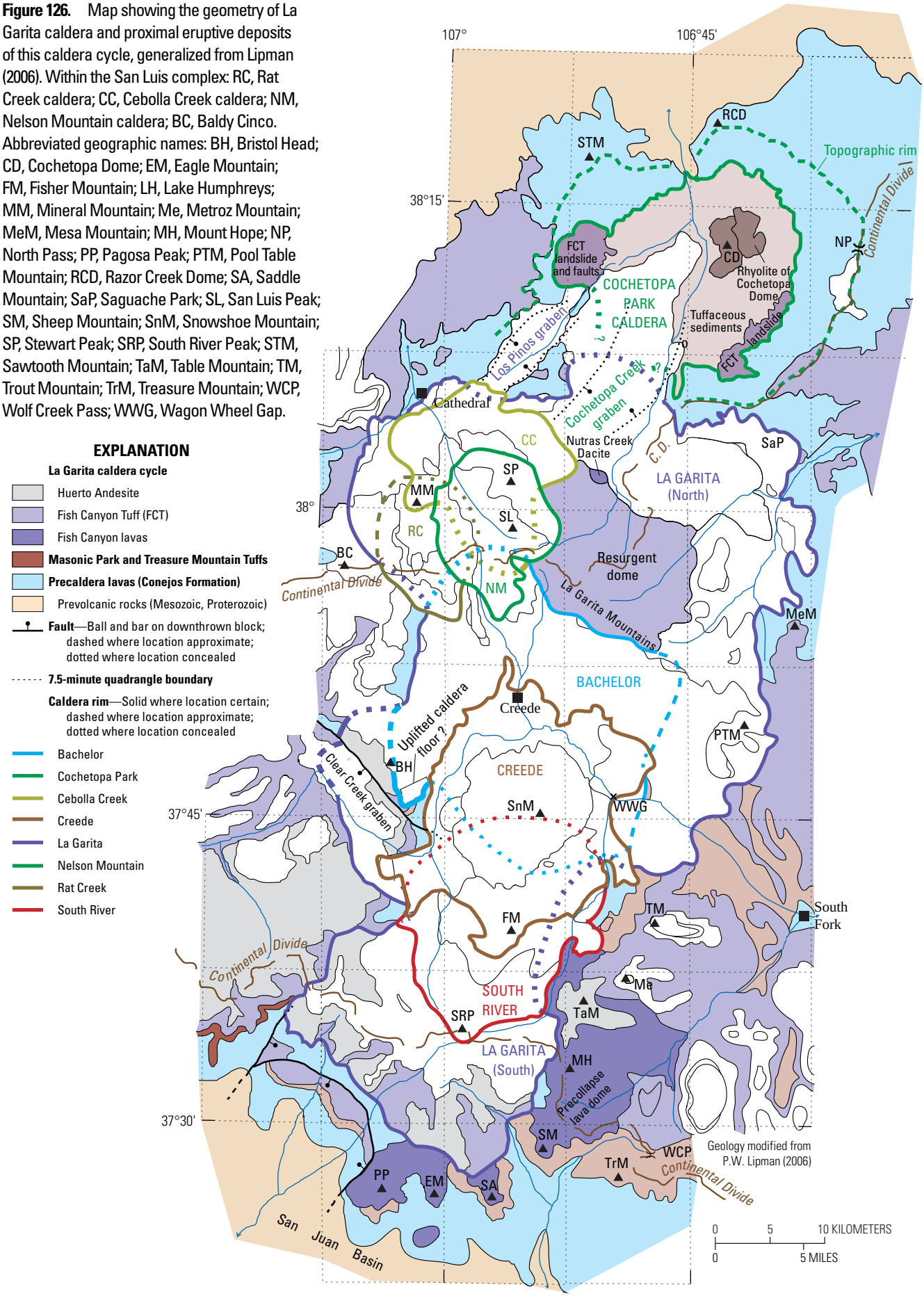

Despite its large volume, the Fish Canyon Tuff is a single ignimbrite sheet with a simple welding zonation (Stops 5-1, 5A-1, 5B-1). Its bulk composition is dacite because of high phenocryst content, but the matrix is silicic rhyolite (75–76 percent SiO_2) as determined by microprobe glass analyses. An $^{40}Ar/^{39}Ar$ eruption age of 28.02 Ma for the much-analyzed Fish Canyon Tuff is used in this field guide for consistency with most other publications on the SRMVF and San Juan region; calibrations by others have suggested ages as old as 28.20 Ma as a result of differing analytical methods and standardization schemes (Renne and others, 1998, 2010; Rivera and others, 2011; Wotzlaw and others, 2013). All the later ignimbrites of the central cluster were erupted within the next 1.1. m.y., from smaller calderas aligned north-south along the west side of La Garita caldera, almost as if these were postcollapse moat volcanoes analogous to the much-smaller moat-rhyolite domes viewed in Valles Caldera, on Day 1.

Precaldera Lava-Like Rocks (Pagosa Peak Dacite)

A large precaldera lava-like body (30 km across and locally more than 800-m thick, 200–300 km^3 in volume) along the southern margin of La Garita caldera (Stop 5A-3), and a small postcaldera lava in the northern moat (fig. 126), are compositionally indistinguishable from the main Fish Canyon Tuff; these deposits document variable eruptive processes from an enormous homogeneous magma body (Bachmann and others, 2000). The precaldera lava-like rocks, named the Pagosa Peak Dacite for a prominent 12,640 ft (3,853 m) peak in the southern San Juan Mountains (fig. 126), must have originally extended well to the north of present exposures, within the subsequently subsided interior of La Garita caldera, as thick dacite sections crop out along the south rim of this caldera.

The Pagosa Peak Dacite lacks lithic fragments and is locally flow layered in its massive interior (Bachmann and others, 2000). The dacite displays complex textures and structures that are transitional between typical silicic lavas and pyroclastic deposits. Initial eruptions were pumiceous, and the main dacite body contains widespread fragmental textures and distinctive, so-called blob breccias (rounded fragments to 2 m), which are suggestive of initial eruption as relatively dense spatter in a poorly sorted fragmental matrix (Stop 5A-4). Thick sections have devitrified as a single cooling unit, with commonly massive and structureless interiors. Lava-like carapace breccias are preserved at the tops of some thick sections, and gravitational spreading has locally generated large ramp structures (dips to 70°). In contrast, thin and distal sections are fragmental throughout and crudely bedded; they consist of glassy flow units a few meters to a few tens of meters thick. No evidence has been found to indicate nonexplosive eruption of fluid lava, although fragmental textures have been obliterated in the interiors of thick proximal sections. Consequently, the lava-like rocks are interpreted as rheomorphic products of low-energy pyroclastic fountaining. Although petrologically diverse lavas and tuffs were erupted widely before Fish Canyon eruptions, the Pagosa Peak Dacite is the only compositionally similar precursor to the voluminous Fish Canyon Tuff.

Caldera Geometry

The overall geometry of La Garita caldera, which subsided in response to the Fish Canyon Tuff eruption, has long been a challenge to decipher because of its size, concealment by later eruptive deposits and caldera subsidences, and the limitations of access, rugged terrain, and vegetative cover (Stop 5B-1). The north-south elongation of La Garita caldera differs from that of most calderas, which tend to be subequant. Contrasting eruptive activity, depths of subsidence, and postcollapse resurgence among three or more sectors defined by embayments in the caldera rim (Stop 5B-2) suggest a complex subsidence history (fig. 125). Even though the segmented caldera shape implies a multistage origin for La Garita caldera, the outflow Fish Canyon Tuff is a single ignimbrite sheet characterized by a simple to weakly compound welding zonation, which indicates deposition from a sustained eruption. In each geographic sector, outflow tuff is truncated along the caldera walls against which the intracaldera tuff wedges out depositionally (Stop 5D-7). Along with these stratigraphic constraints, intracaldera and outflow tuffs have the same crystal assemblage, mineral compositions, paleomagnetic polarity, isotopic ages, and elemental compositions.

The La Garita Mountains in the northern caldera sector (fig. 126, Stop 5C-2) are a resurgently uplifted block of densely welded intracaldera Fish Canyon Tuff more than 1,200-m thick without an exposed base (Steven and Lipman, 1976). The intracaldera tuff is strongly indurated and oxidized red-brown in comparison to the light-gray outflow, and it contains larger and more coarsely porphyritic pumice lenses (10–20 centimeters [cm]). Along the west side of the central sector, a tilted block on the east slope of Bristol Head (Stop 5D-5) may represent another locus of resurgence. Here, an incomplete section of intracaldera tuff (>350 m, with the top truncated by the younger Bachelor caldera) overlies older volcanic units of the caldera floor (fig. 127). Erosional levels in the southern sector, as in the northern sector, expose thick intracaldera tuff (>800 m) without reaching the caldera floor. No marked resurgence is evident in the southern sector; instead, linear northwest-trending faults disrupted the caldera fill, including the Huerto Andesite that flooded the southern sector after collapse (fig. 127).

The southern sector is thought to have been the first segment to subside, based on proximity to the accumulations of early erupted Pagosa Peak Dacite. This segment may have subsided initially in response to low-energy pyroclastic eruption of these unusual lava-like rocks, then filled, largely passively, with thick intracaldera tuff erupted from more northern segments. The northern segment is inferred to have been the last to subside or to complete its subsidence, based on the confinement of distinctive late-erupted granophyric fragments of Fish Canyon- magma type to this sector (Lipman and others, 1997). Despite such uncertainties, La Garita caldera dominates the volcanic structure of the central San Juan region, virtually completely enclosing the caldera sources for the seven major ignimbrite sheets erupted during the next 1.1 m.y.

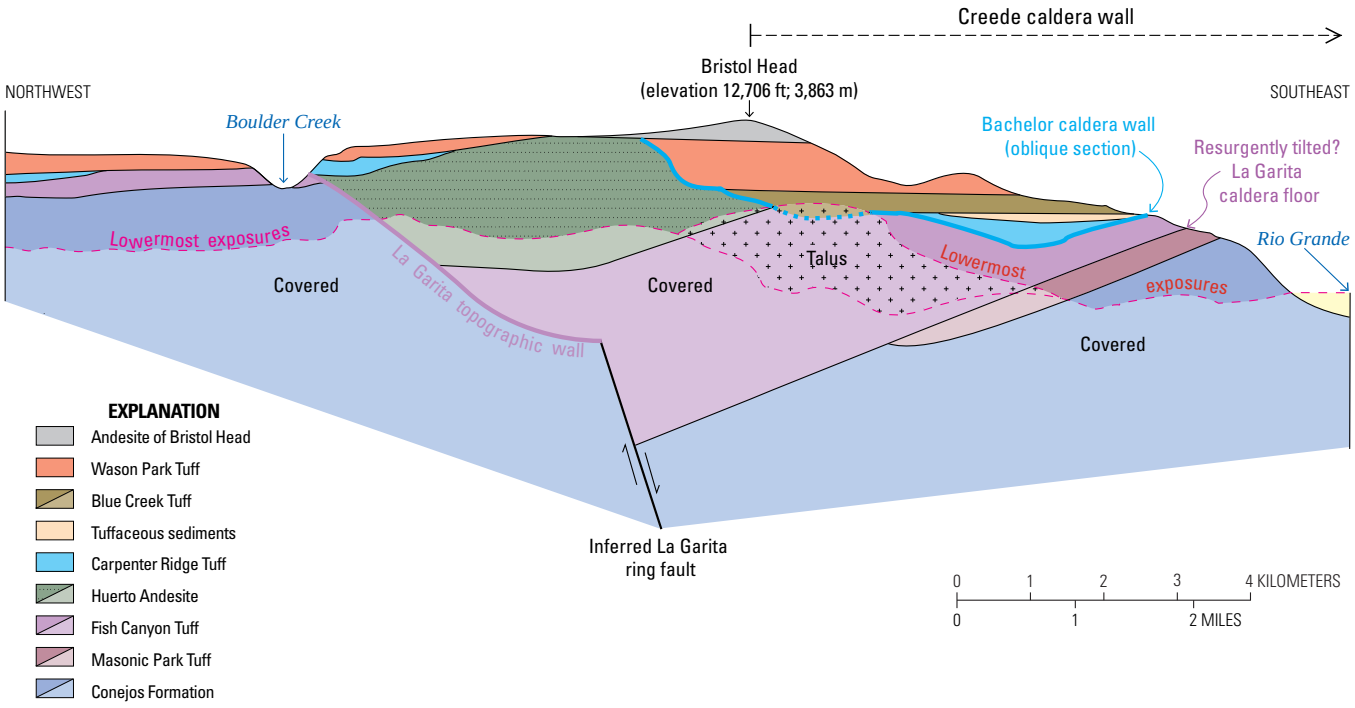

Figure 127. Interpretive cross-section of the south slopes of Bristol Head as viewed from the southwest, showing unconformities related to the La Garita and Bachelor caldera walls. The location of the section is shown on figure 123. The east slope of Bristol Head marks the eroded topographic wall of Creede caldera; it exposes a tilted section of Fish Canyon Tuff and older rocks that are interpreted as the flank of resurgent uplift within the central segment of La Garita caldera. This uplift predates thick lavas and mudflow conglomerates of Huerto Andesite, which are flat lying and confined to the caldera moat. The thick Huerto Andesite sequence on Bristol Head wedges out at Boulder Creek, along the west La Garita caldera wall. Bachelor caldera wall dips to the north, oblique to the cross section, resulting in a deceptively gentle and irregular unconformity. Darker colors represent present exposure levels; lighter colors represent interpreted relations at depth. Ft, feet; m, meters.

Postcaldera Fish Canyon Tuff-Like Lava (Nutras Creek Dacite)

The Nutras Creek Dacite, an erosional remnant of late-erupted flow-layered lava that is petrologically similar to Fish Canyon Tuff, crops out over an area of a few kilometers on the north flank of the resurgently uplifted La Garita Mountain block (fig. 126). In contrast to the precaldera Pagosa Creek Dacite, the Nutras Creek body lacks pyroclastic textures and is everywhere flow-layered or brecciated lava-like rock. South of Nutras Creek, the dacite is exposed vertically as much as 200 m, but the original thickness and extent of this body is uncertain owing to subsequent erosion and widespread cover by thick glacial deposits. Despite the small size of present-day exposures, the Nutras Creek Dacite also provides an important sample for understanding the state of the Fish Canyon magma chamber after the large-volume ignimbrite eruptions and attendant caldera collapse. Most $^{40}Ar/^{39}Ar$ and U-Pb ages from samples of Nutras Creek Dacite and earlier eruptive units (Fish Canyon Tuff, Pagosa Peak Dacite) of the La Garita cycle have been indistinguishable within analytical precision at 28.20 Ma (Bachmann and others, 2007b; Wotzlaw and others, 2013), but recent high-precision analyses suggest a duration of as much as 100 thousand years (k.y.) between eruption of the precursor Pagosa Peak Dacite and postcaldera Nutras Creek Dacite (Morgan and others, 2019).

Petrogenesis

Despite the uniform bulk-sample compositions (68–69 percent SiO_2), petrologic features are complex in both the Fish Canyon Tuff and associated lava-like rocks (Whitney and Stormer, 1985; Lipman and others, 1997; Bachmann and others, 2002; Charlier and others, 2007). Complicated disequilibrium features are present. Strikingly, resorbed quartz has long been recognized as a distinctive feature of the Fish Canyon Tuff, and feldspar-liquid disequilibria are comparably developed. The concurrent resorption of quartz, plagioclase, and sanidine must reflect a major thermal event (Bachmann and Dungan, 2002), not just a response to decreasing pressure during magma ascent (contraction of SiO_2 stability relative to feldspars). Large poikilitic sanidines enclose plagioclase, quartz, and other minerals; grain-boundary melting has occurred locally along contacts with these inclusions. Such features suggest that the eruptible Fish Canyon magma formed rapidly, by shallow

partial remelting of the solidified upper parts of a long-lived magma body (Bachman and others, 2002).

Despite the uniform bulk composition of the Fish Canyon Tuff and associated lava-like rocks, a mafic component was involved in generation of the magmas. Most of the precaldera dacite is homogeneous, but rare andesitic blebs (1–5 cm diameter, 58 percent SiO_2) and concentrations of finely porphyritic mafic minerals smeared along flow layers provide evidence for mingling with andesitic magma prior to eruption. Hornblende and biotite in the blebs have mineral chemistry similar to that of other San Juan andesites, in contrast to compositions of these minerals in the host Pagosa Peak Dacite and Fish Canyon Tuff. Postcollapse shield volcanoes around the southern and western margins of the caldera (Huerto Andesite) likely are additional larger-scale samples of mafic components in the La Garita caldera cycle.

Sparse small fragments of comagmatic granophyre in late-erupted intracaldera tuff and postcaldera lava, having mineral compositions indistinguishable from phenocrysts in the tuff and precaldera lava-like rocks, record complex events in the Fish Canyon chamber just prior to and during eruption (Lipman and others, 1997). Sanidine phenocrysts in the granophyre preserve zoning evidence of mingling with andesitic magma, then shattering by decompression and volatile loss accompanying early Fish Canyon eruptions (similar to processes described by Best and Christiansen [1997]), before overgrowth by granophyre.

Thus, these diverse petrologic features document multiple mineral components within the Fish Canyon magma body: (1) regular phenocrysts and megacrysts, (2) a disaggregated andesitic component, (3) mafic microphenocrystic aggregates depleted in interstitial matrix, and (4) granophyric crystallization products. Complex isotopic disequilibria among crystal and groundmass phases further document that this homogeneous body underwent a complex magmatic evolution (Charlier and others, 2007). Such textural and chemical disequilibria indicate that the eruption resulted from batholith-scale remobilization of a shallow subvolcanic chamber, triggered by mafic magma replenishment, and erupted before textural or chemical equilibrium were re-established.

Comparison with Masonic Park Tuff

Eruption of the Fish Canyon Tuff followed the Masonic Park Tuff by ~0.7 m.y.; with an erupted volume 10 times greater, it completely buried the Masonic Park Tuff source caldera. Although these two ignimbrites are both crystal-rich calc-alkaline dacites (table 6), they differ in mineral assemblages; the Fish Canyon Tuff contains abundant amphibole and titanite, has less biotite, lacks clinopyroxene, and is devoid of plagioclase microlites. The Fish Canyon Tuff is also slightly richer in SiO_2 and K_2O than the Masonic Park Tuff and evolved to a lower temperature ~710–760° C (Bachmann and Dungan, 2002) versus ~800–850 °C for the Masonic Park Tuff (Sliwinski and others, 2017). The presence of multiple hydrous phases in the Fish Canyon Tuff and its lower temperature suggest that the Fish Canyon Tuff magma evolved under more hydrous conditions and (or) slightly deeper, although pressure estimates are unreliable for the Masonic Park Tuff.

Despite their different volumes, mineralogy, and possibly water contents, the upper-crustal Fish Canyon and Masonic Park Tuff magma bodies or mush zones both underwent reheating and mechanical reactivation prior to eruption, as indicated by (1) highly resorbed (Fish Canyon Tuff) or totally dissolved (Masonic Park Tuff) sanidine and quartz; and (2) reverse zoning trends in phenocrysts, most obviously in plagioclase and amphibole crystals for the Fish Canyon Tuff (Bachmann and Dungan, 2002; Bachmann and others, 2002) but also detectible in Masonic Park Tuff pyroxene (Sliwinski and others, 2017). The scarce mafic enclaves in late-erupted Fish Canyon Tuff (and by inference in the Masonic Park Tuff) indicate that the rejuvenation event was likely triggered by mafic recharge that brought heat, volatiles, and melt (but no crystalline debris) to these upper-crustal crystal mushes (Bachmann and Bergantz, 2003, 2006).

Postcaldera Mafic Volcanism—Huerto Andesite

Overlying the intracaldera Fish Canyon deposits in the southern caldera segment are massive, thick chaotic breccias of Huerto Andesite, which contrast strikingly with the well-stratified thinner Huerto lavas outside the La Garita caldera. The Huerto Andesite has long been recognized as a petrologically distinctive assemblage of lavas and associated breccias (Cross and Larsen, 1935; Larsen and Cross, 1956), and was later defined as occupying the stratigraphic interval between the Fish Canyon and Carpenter Ridge Tuffs (Steven and others, 1974b). The thickest preserved accumulations of Huerto Andesite (more than 800 m) and largest areas of exposure are near the Continental Divide southwest of Creede (fig. 126), within La Garita caldera. This distribution within the southern caldera segment, along with involvement of the Huerto Andesite in faulting that predates the Carpenter Ridge Tuff, indicates that the unit represents a late-erupted andesitic component of the Fish Canyon magmatic system, comparable to postcaldera andesitic volcanism associated with several other San Juan ignimbrite calderas. In addition, caldera-wall landslide breccias dominated by Fish Canyon clasts locally interleave with Huerto lavas near the southern La Garita walls, providing further indication that Huerto lavas were erupted soon after caldera formation. Although the thick southern Huerto Andesite has not been dated directly, its age is bracketed by $^{40}Ar/^{39}Ar$ determinations on the overlying Crystal Lake Tuff (27.61 Ma); correlative northern Huerto lavas have yielded hornblende and groundmass ages of 28.0–27.6 Ma (table 10; Lipman and McIntosh, 2008).

Much of the Huerto Andesite consists of distinctive dark-gray coarsely porphyritic platy-plagioclase andesite (55–59 percent SiO_2), in which tabular plagioclase phenocrysts are commonly aligned to define a flow foliation, and sparsely porphyritic to aphanitic dark andesite (Larsen and Cross, 1956; Askren and others, 1991; Parat and others, 2005). In addition, lighter-colored hornblende-bearing Huerto lavas and breccias of silicic andesite and mafic dacite (60–66 percent SiO_2) are common within and along the southern margin of La Garita caldera, especially in the Turkey Creek and West Fork San Juan drainages and at Table Mountain (fig. 126). Distinctive light-tan biotite-bearing dacite (68.5 SiO_2) also forms a thick flow-layered

lava dome at Ruby Lake near the western margin of La Garita caldera (fig. 126). The newly recognized more silicic components of the Huerto assemblage, although volumetrically subordinate to the andesite, substantially extend its compositional range (Parat and others, 2005).

Bachelor Caldera Cycle (Carpenter Ridge Tuff)

Fish Canyon Tuff and Huerto Andesite are widely overlain by the 27.55-Ma Carpenter Ridge Tuff, the second largest ignimbrite (1,000 km^3) of the central caldera cluster. The Carpenter Ridge Tuff was erupted from Bachelor caldera along the west-central side of La Garita caldera (fig. 123). Thick intracaldera Carpenter Ridge Tuff forms the primary host for vein mineralization in the Creede district. The Carpenter Ridge Tuff is laterally and vertically complex, characterized by magmatic compositional gradients, intricate welding and crystallization zones, variably intense potassic alteration, and interleaved wedges of lithologically diverse landslide breccias (fig. 128) that have caused much interpretive confusion (Steven and Ratté, 1965; Lipman and others, 1989; Lipman, 2000).

Outflow Carpenter Ridge Tuff (Stops 5-2, 5A-5) correlates directly with a thick intracaldera accumulation of rhyolitic tuff, once thought to represent a separate eruptive deposit (Bachelor Mountain Rhyolite of Emmons and Larsen, 1923; Steven and Ratté, 1965), but now designated the Bachelor Mountain Member (Lipman, 2000). Interfingered with the Bachelor Mountain Member are multiple lithologically distinct lenses of caldera-collapse slide breccia that were previously assigned several separate formation names. The rhyolitic Bachelor Mountain units locally grade upward into silicic dacite (Mammoth Mountain Member). All these rocks are now interpreted as intracaldera equivalents of the outflow Carpenter Ridge Tuff (Lipman and others, 1989; Lipman, 2000, 2006). Current nomenclature for this complex pyroclastic deposit represents compromises between needs to (1) avoid confusion with long-existing stratigraphic names and concepts, (2) preserve detailed subdivisions of importance in the Creede mining district, (3) provide a reasonable framework to interpret the processes of pyroclastic volcanism responsible for the deposits, and (4) follow modern guidelines for stratigraphic nomenclature.

Welding and Compositional Variations

Outflow Carpenter Ridge Tuff consists largely of uniform, crystal-poor rhyolite (72–74 percent SiO_2; 3–5 percent sanidine, plagioclase, biotite), that locally grades upward into silicic dacite (66–68 percent SiO_2; 25–35 percent plagioclase, sanidine, biotite, clinopyroxene). In places, distinctive lenses of more mafic alkalic scoria (54–63 percent SiO_2) occur near the top of the rhyolite (Stop 5A-5) and along the transition from rhyolite upward into silicic dacite (Lipman, 1975a, p. 49–53; Whitney and others, 1988; Dorais and others, 1991; Bachmann and others, 2014). Within its source, Bachelor caldera, the Carpenter Ridge Tuff is a complex assemblage of variably welded, crystallized, and altered compositionally zoned tuff, interleaved with lithologically diverse landslide debris from the caldera walls (fig. 128). These intracaldera

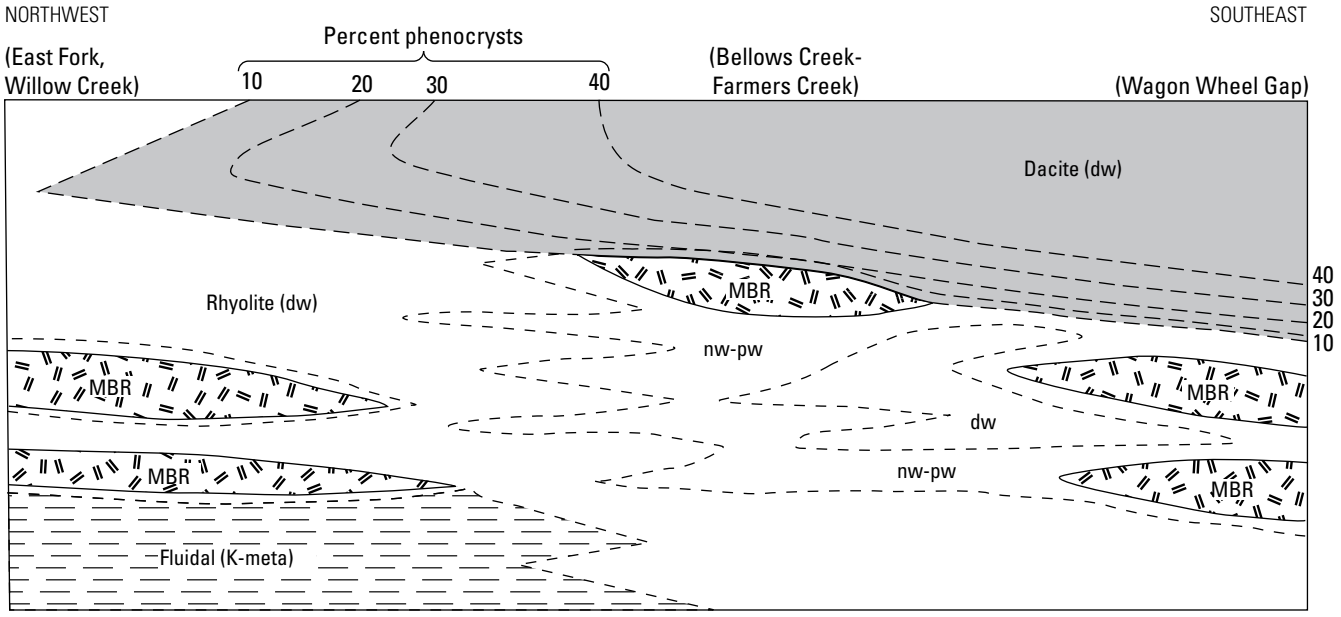

Figure 128. Diagrammatic section of intracaldera Carpenter Ridge Tuff along northeast side of Bachelor caldera showing complex depositional, compositional, and welding relations with interleaved landslide-megabreccia lenses. MBR, megabreccia; nw, nonwelded tuff; pw, partly welded tuff; dw, densely welded tuff; fluidal, fluidally welded Willow Creek zone; K-meta, areas affected by extreme potassium metasomatism. Long-dashed line contours show percent total phenocrysts, which increase upward and southeastward as the bulk chemical composition of tuff changes from rhyolite (Bachelor Mountain Member) to silicic dacite (Mammoth Mountain Member). Modified from Lipman (2000).

deposits ponded to a thickness of more than 1.1 km, with no base exposed. The fill of Bachelor caldera consists largely of variably welded rhyolitic tuff, divided into the Willow Creek (Stop 5B-8), Campbell Mountain (Stop 5C-3), and Windy Gulch welding zones. These zones define a general succession, becoming less welded upwards, but the zones alternate and interfinger complexly near caldera margins and adjacent to landslide-breccia lenses.

Previously, a compositionally zoned assemblage (66–74 percent SiO_2; 3–40 percent phenocrysts), mapped as the Mammoth Mountain Tuff of Ratté and Steven (1967), was interpreted to overlie the Bachelor Mountain Member as a discrete ignimbrite. However, the mapped contact between Mammoth Mountain and Bachelor Mountain rhyolites (Steven and Ratté, 1965, 1973) is an alteration boundary (Stop 5C-3), and all the intracaldera rhyolitic tuffs are now included as welding zones of the Bachelor Mountain Member (Lipman, 2000, 2006). The Mammoth Mountain Member has been restricted to the phenocryst-rich dacite high in the zoned Carpenter Ridge Tuff. Elsewhere in the central San Juan region, tuffs once correlated with the Mammoth Mountain are now recognized as parts of other regional ignimbrites (table 12). The eruptive significance of the distribution and large variations in thickness of the Mammoth Mountain Member is not fully understood. Several aspects of the Mammoth Mountain suggest that it was deposited against flanks of a central high area within the subsiding floor of the Bachelor caldera, permitting ponding of the dacite in an incipient moat between the central high and the topographic rim. Such an interpretation implies that the broad geometry of resurgent uplift within the Bachelor caldera may have been initiated during syneruptive subsidence.

Additional caldera-filling subunits of intracaldera Carpenter Ridge Tuff record repeated landslides from the adjacent walls of Bachelor caldera (Lipman and others, 1989; Lipman, 2000), similar to deposits recognized in other San Juan calderas (Lipman, 1976a). The slide breccias deposited within Bachelor caldera are divided into distinct geographic and lithologic units that mostly correlate closely with the rocks present on the adjacent caldera wall: for example, Fish Canyon Tuff fragments on the northeast side adjacent to the La Garita Mountains (Stop 5C-1), and andesitic lava fragments derived from Conejos volcanic constructs on the west side (Stop 5D-1). Such slide masses, enclosed by tuff of the Bachelor Mountain Member, have been confused at times with intrusions, especially in exploration drill core. Recognition of the caldera-landslide origin of these rocks eliminates the need for several previously inferred local volcanic and intrusive episodes in the Creede district.

Petrogenesis

Fe-Ti oxide thermometry for Carpenter Ridge Tuff samples yields temperatures of ~750–810° C in the rhyolite and ~850–1,000° C in trachytic fiamme (Whitney and others, 1988). Crystallization pressure was estimated at 100–200 megapascals (MPa) based on experimental phase equilibria, particularly the absence of quartz in this high-SiO_2 magma (Whitney and others, 1988). Results using amphibole thermometry for the trachytic fiamme yield temperatures in the range of 930–955 °C, higher than for coexisting Fe-Ti oxides (Bachmann and others, 2014). Similarly, amphiboles yield pressures from 280 to 320 MPa (10–12 km depth), which suggest that hornblende may have crystallized at greater depths than the rest of the mineral assemblage.

Much of the major and trace element variations in the Carpenter Ridge Tuff can be reproduced by way of in-situ differentiation by interstitial melt extraction from a crystal-rich upper-crustal mush zone, with the trachydacitic inclusions being the erupted crystal-cumulate complement to the high-SiO_2 rhyolite (Bachmann and others, 2014). The observed thermal and chemical zonation in the deposits formed by eruption of the crystal-poor cap of the magma body and a small portion of its cumulate counterpart, remobilized by a late recharge that reheated and partially melted the crystalline assemblage to the point that it was eruptible (less than ~50 volume-percent crystals). The recharge magma appears to be sampled by late-erupted mafic clasts, although some clasts also seem to show mineral accumulation (particularly biotite).

Caldera Geometry

Bachelor caldera is larger, especially in east-west dimension, than shown on maps before the 1990s (fig. 125). Southern remnants of the caldera walls are exposed in the Wagon Wheel Gap and Bristol Head areas (fig. 123), which indicates that the southern caldera projects beneath the younger Creede caldera. The northeast wall of Bachelor caldera is spectacularly defined north of Creede in East Willow Creek by talus and slide breccia, and consists of blocks of Fish Canyon Tuff with a local nonwelded matrix of Carpenter Ridge Tuff, banked against the southwest-facing paleoslope cut into the La Garita resurgent block. The caldera wall continues to the southeast, where Wason Park Tuff is banked against lower slopes of the La Garita Mountains.

A small east-wall segment of Bachelor caldera, exposed along Blue Creek just east of Wagon Wheel Gap, truncates fill of La Garita caldera and older rocks, and in turn is cut by the topographic wall of Creede caldera (Stop 5B-4). The lowermost cliffs along lower Blue Creek are composed of Masonic Park Tuff on the caldera wall, somewhat fractured and altered, but having coherent, gently dipping pumice-compaction foliations that indicate the absence of major structural disruption. On the slopes above and along roadcuts to the west, below the rugged cliffs of the Wagon Wheel Gap lava dome within Creede caldera, are brecciated landslide masses of Fish Canyon Tuff (some 100 m across) accompanied by large blocks of Masonic Park Tuff and andesitic lava, all lacking stratigraphic or structural coherence. These are interpreted as having slid down the east wall of Bachelor caldera. Nonwelded crystal-poor rhyolitic tuff that forms the matrix between the blocks is intracaldera Carpenter Ridge Tuff.

The western caldera margin is constrained along the west slopes of Miners Creek (location on fig. 129), where ponded Wason Park Tuff banks against Conejos Formation lavas. At least part of this contact may also follow the west wall of La Garita

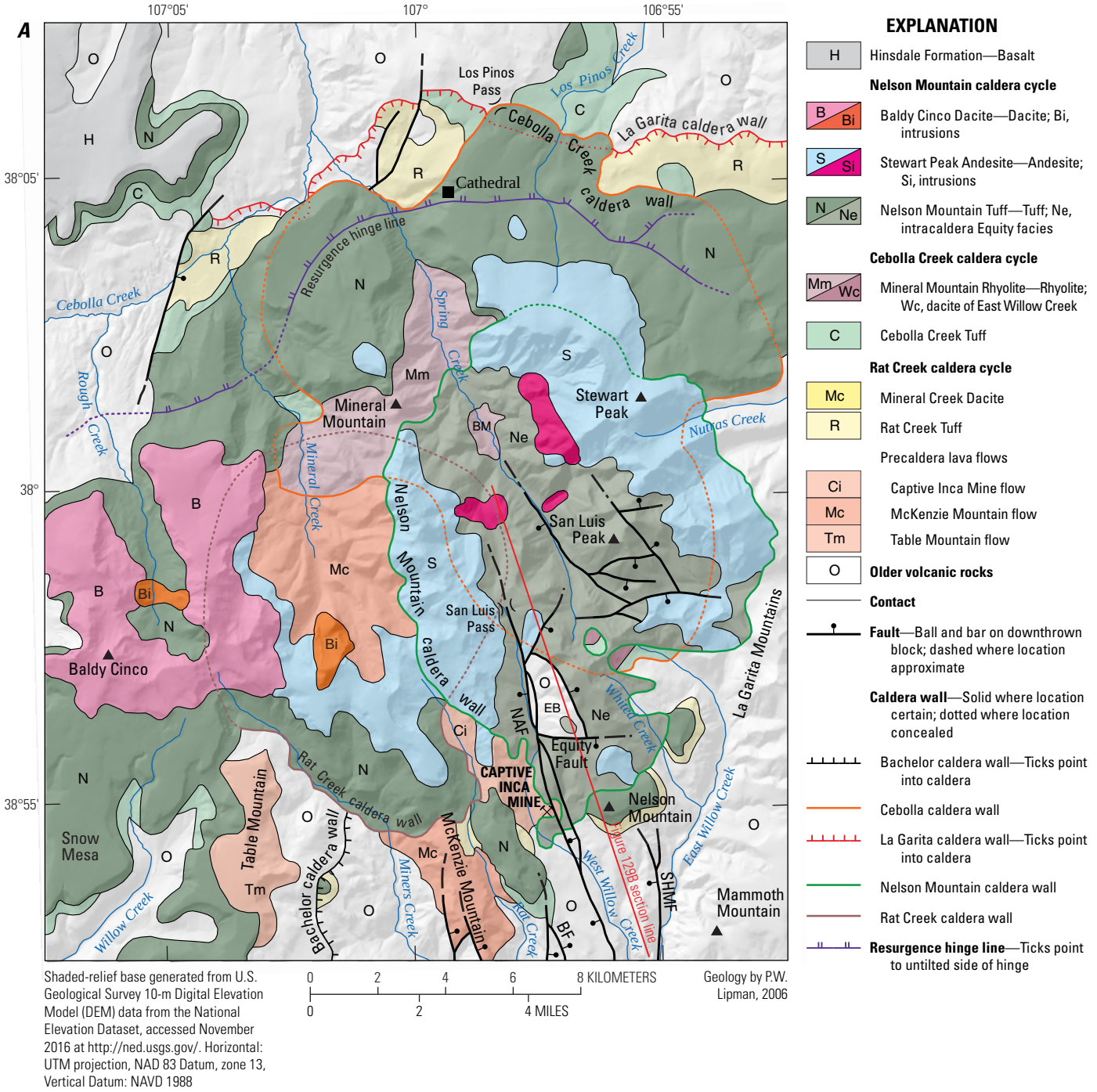

Figure 129. Major geologic features of the San Luis caldera complex (from Lipman, 2000). *A*, Geologic map. Abbreviated geographic names: BM, Bondholder Meadow; EB, Equity block. Faults of Creede graben: BF, Bulldog Mountain Fault; NAF, Northern Amethyst Fault; SHMF, Solomon-Holy Moses Faults. Generalized from Lipman (2006). *B*, Geologic section across the south side of the San Luis caldera complex, showing successive truncation of thick ignimbrite fill within Bachelor caldera by the southern margins of Cebolla Creek and Nelson Mountain calderas. Fault-bounded uplift and mineralization of the Equity block resulted from localized resurgence over a cupola of late granitic intrusion. A remnant of Cebolla Creek caldera fill is projected into the section from exposures in East Willow Creek; the position of the concealed northern caldera margin of Bachelor caldera and the margins of late intrusion(s) are only roughly constrained. Location of cross section shown in *A*. Ft, feet; m, meters.

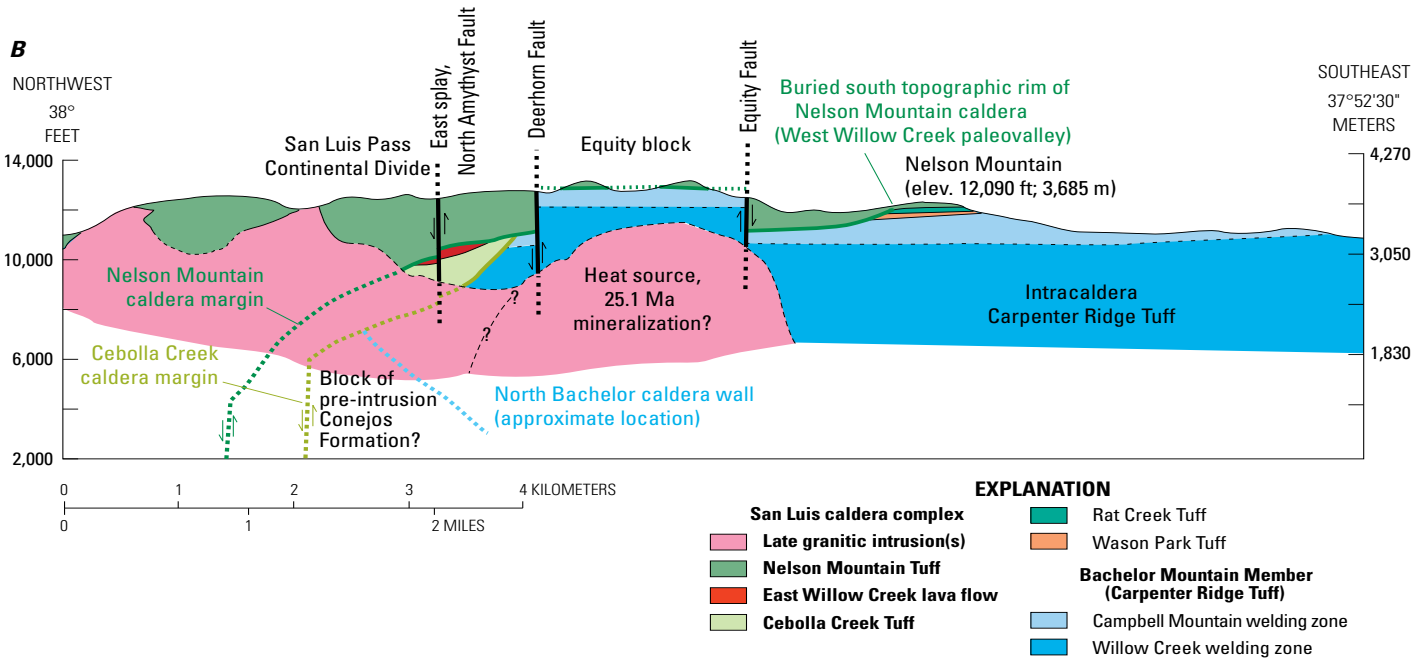

Figure 129.—Continued

caldera, as indicated by presence of the rhyolite of Miners Creek at high topographic levels, directly overlain by Wason Park Tuff, without intervening intracaldera Carpenter Ridge Tuff (Lipman, 2006). In this case, the contact between the rhyolite of Miners Creek and onlapping Carpenter Ridge Tuff just to the southeast is the margin of Bachelor caldera. The rhyolite of Miners Creek is a phenocryst-poor, flow-layered lava sequence (3–5 percent phenocrysts of plagioclase, sanidine, and biotite; 73–74 percent SiO_2). These lavas petrologically resemble the Carpenter Ridge Tuff and have recently yielded an essentially identical sanidine $^{40}Ar/^{39}Ar$ age (27.51±0.02 Ma: table 13), which suggests that they record precursor eruptions that ponded against the western margin of La Garita caldera prior to the collapse of Bachelor caldera during eruption of the Carpenter Ridge Tuff.

The southwest wall of Bachelor caldera is spectacularly exposed on the steep south face of Bristol Head (Stop 5D-6) and on down-dropped fault blocks to the southwest (fig. 127). Along this caldera-wall unconformity, thickly ponded Blue Creek (200 m) and Wason Park Tuffs (350 m), which overlie intracaldera sediments and the Bachelor Mountain Member, wedge out abruptly along a steep contact against Fish Canyon Tuff and overlying Huerto Andesite, as exposed in oblique section at Bristol Head.

The core of the Bachelor caldera was uplifted to form a broadly symmetrical resurgent dome. The crest of the dome appears to be eccentrically north of the center of subsidence, although detailed geometric interpretation of this dome is uncertain owing to truncation by the younger Creede and San Luis calderas and widespread cover by younger units. Faults along the crest of the Bachelor dome define a keystone graben that has had a complex history of recurrent later movement and provided the dominant structural control for subsequent Creede mineralization (fig. 16 in Steven and Lipman, 1976). Resurgent structures may have been inherited from a residual structural high within the subsided caldera floor. The high was apparently established late, during eruption of rhyolitic Carpenter Ridge Tuff, as suggested by distribution of the Mammoth Mountain Member, which appears to have accumulated to its greatest thickness in moat areas of the Bachelor caldera and to have wedged out against a central high. Local rheomorphic textures in the Willow Creek facies along the keystone graben (Stop 5B-8) also suggest early inception of these faults and growth of the resurgent dome while the intracaldera tuff remained hot and viscous. The bulk of Bachelor resurgence postdated emplacement of the Mammoth Mountain Member, however, as these dacitic tuffs are tilted on the flanks of the dome. The moat was further filled by Blue Creek and Wason Park Tuffs, and by local volcaniclastic sediments that thin against the apparent crest of the dome.

The crest of the Bachelor resurgent dome extends at least as far north as the fault-bounded Equity block (fig. 129) within a topographic embayment in fill of the younger San Luis caldera (Stop 5C-6), as indicated by wedge-outs of Wason Park Tuff and intracaldera sediments that are documented especially well in mineral-exploration drill cores. This large southerly, so-called Equity embayment of the Nelson Mountain caldera is a gently north-draining paleovalley. Its geometry was strongly influenced by paleotopography on the north flank of the Bachelor dome and its keystone graben structure (Stop 5C-4). The paleovalley was further enlarged by slumping into the Nelson caldera at the time of its collapse.

Table 13. Previously unpublished $^{40}Ar/^{39}Ar$ age determinations for lavas of the Bachelor caldera cycle. Analyzed in 2012 by Matthew Zimmerer and William McIntosh (New Mexico Bureau of Geology).

[n, number of samples, MSWD, mean square of weighted deviates; Ma, million years ago; --, not applicable]

Sample	Unit	Location	Latitude	Longitude	Lab no.	Mineral	Method	n	MSWD	K/Ca	±2σ	Age (Ma)	±2σ
Dacite of Shallow Creek													
10L-49	Intrusion	Shallow Creek	38°50.43'	107°00.90'	60864	Sanidine	Mean	10	2.9	43.0	±13.3	27.49	±0.02
11L-17	Basal flow-breccia	McKenzie stock trail	38°51.60'	107°00.19'	60858	Sanidine	Mean	13	9.7	45.3	±9.0	27.54	±0.02
Rhyolite of Table Mountain													
11L-16	Crystal-rich lava	Above Crystal Lake	38°52.91'	107°02.98'	60857	Sanidine	Mean	12	2.1	32.0	±7.3	27.52	±0.01
--	Carpenter Ridge Tuff (weighted mean of four samples; Lipman and McIntosh (2008)	--	--	--	--	--	--	4	--	--	--	27.55	±0.05
Rhyolite of Miners Creek													
10L-48	Crystal-poor lava	Miners Creek	38°52.43'	106°59.60'	60874	Sanidine	Mean	9	2.3	35.6	±16.5	27.51	±0.02

Postcaldera Volcanism

Only a few postcaldera lava eruptions appear related to the Bachelor caldera cycle. A distinctive phenocryst-rich lava of silicic dacite (68 percent SiO_2; 35 percent phenocrysts, abundant sanidine) overlies the Mammoth Mountain Member on the northwest side of the Bachelor caldera. It can be traced into a north-trending dike-like feeder (Steven, 1967) that is oriented appropriately to have risen along a caldera ring fault. This local unit, the dacite of Shallow Creek, has a sanidine $^{40}Ar/^{39}Ar$ age of 27.52±0.02 Ma (table 13) and thus likely was a late event of the Bachelor cycle. A porphyritic rhyolite lava that caps Table Mountain, only 3 km northwest, has a similar age (27.49±0.02 Ma) and probable caldera-cycle connection.

Blue Creek Tuff and its Source

Widespread tuff of crystal-rich dacite, once included as part of the Mammoth Mountain Tuff of Ratté and Steven (1967) and Steven and others (1974a), is now recognized as a separate major ignimbrite sheet, the Blue Creek Tuff (table 12). This tuff sheet is exceptionally exposed in its type locality, lower Blue Creek just east of Wagon Wheel Gap (Stop 5B-4), where its welding and petrographic features were carefully described by Ratté and Steven (1967). There, it is underlain by intracaldera Carpenter Ridge Tuff and associated megabreccias and overlain by the lavas of McClelland Mountain.

Like the Mammoth Mountain Member of the Carpenter Ridge Tuff, thick Blue Creek Tuff is largely ponded within the moat of Bachelor caldera and the central segment of La Garita caldera. Locally, the Blue Creek Tuff is as thick as 250 m at Blue Creek proper, in Bellows Creek, and along the Rio Grande southwest of Bristol Head. Eruption of the Blue Creek Tuff postdated resurgence of the intracaldera Carpenter Ridge Tuff, and near-horizontal Blue Creek Tuff wedges out against tilted Mammoth Mountain Member along the east and west sides of the resurgent dome. Although Blue Creek Tuff locally overlies the Mammoth Mountain, its distribution is mainly farther south. Obscure contacts between the Blue Creek and underlying similar-appearing dacite of the Mammoth Mountain Member are marked by a basal vitrophyre and local float of pebbly sediments that crop out only locally. The Blue Creek Tuff wedges out against domed intracaldera Carpenter Ridge Tuff to the north and is absent north of Creede.

Typical Blue Creek Tuff is densely welded, contains a basal vitrophyre, and has well developed flow-unit partings. The Blue Creek is a uniform phenocryst-rich dacite (65–68 percent SiO_2; 30–40 percent phenocrysts of plagioclase, biotite, and augite); in contrast to the Mammoth Mountain Member, it lacks even sparse sanidine. Although the absence of sanidine precludes high-precision $^{40}Ar/^{39}Ar$ dating, eruption of this ignimbrite is closely bracketed, between the 27.55-Ma Carpenter Ridge Tuff and the overlying 27.38-Ma Wason Park Tuff.

No remnants of a caldera source for the Blue Creek Tuff are exposed, but the widespread distribution (at least 1,000 km^2) and sizable outflow volume (estimated at 150 km^3) strongly suggest that caldera subsidence accompanied its eruption. A concealed source is inferred to lie beneath southern parts of the Creede caldera, based on the distribution of this ignimbrite.

Related(?) Lavas

Andesitic and dacitic lavas that overlie the Blue Creek Tuff near Wagon Wheel Gap (volcanics of McClelland Mountain) provide some suggestion that the source of this ignimbrite sheet is nearby to the west, within the younger Creede caldera. The lowest lava north of Wagon Wheel Gap is a sparsely porphyritic silicic

andesite (61–63 percent SiO_2); upper lavas are coarsely porphyritic plagioclase-biotite-augite dacite (65–69 percent SiO_2) that are petrologically similar to the Blue Creek Tuff.

South River Caldera Cycle (Wason Park Tuff)

Typical Wason Park Tuff is distinctive crystal-rich alkalic rhyolite and silicic dacite (68–72 percent SiO_2), erupted at 27.38 Ma, and characterized, where densely welded, by large light-gray vapor-phase-crystallized pumice and brick red-brown groundmass (Ratté and Steven, 1967). Bulk samples contain 15–25 percent phenocrysts of plagioclase, sanidine, and biotite. The outflow ignimbrite accumulated largely within La Garita and Bachelor calderas, where it ponded to as much as 300-m thick, forms rugged cliffs, and constitutes a distinctive marker along the walls of Creede caldera. The Wason Park Tuff also spread beyond these calderas, as far as the Continental Divide to the northwest, into the Saguache valley to the northeast, and beyond South Fork to the southeast. This tuff was erupted from South River caldera (fig. 123), which was filled to overflowing by younger andesitic and dacitic lavas (Lipman, 2000, 2006). South River no longer exists as a geographic name, having become Red Mountain Creek early in the 20th century, but South River Peak dominates the Continental Divide at the head of Red Mountain Creek.

Caldera Geometry

At exposed levels, exhumed margins of South River caldera are strikingly defined by unconformities along two arcuate drainages, Red Mountain Creek to the west and Goose Creek to the southeast (fig. 123), that expose parts of the original caldera walls. Along Red Mountain Creek, the caldera-filling South River Volcanics bank against Carpenter Ridge, Blue Creek, and proximal Wason Park Tuffs along inward-dipping contacts exposed vertically for as much as 700 m. Along the caldera margin in Goose Creek, the South River Volcanics lap out unconformably against diverse wall rocks that include Conejos Formation lavas, Masonic Park Tuff, Pagosa Peak Dacite, and Wason Park Tuff. The northern margin of South River caldera is covered by lavas and breccias of Fisher Dacite, which are related to Creede caldera. The Fisher Dacite overlaps in composition with the South River Volcanics; as a result, the boundary between the two caldera-filling lava assemblages is uncertain in places.

Along Goose Creek near Lake Humphreys, an erosional window of densely welded crystal-rich dacitic tuff (63–66 percent SiO_2; 30–40 percent phenocrysts), exposed beneath massive lavas of Fisher Dacite and South River Volcanics, has been interpreted as late-erupted intracaldera Wason Park Tuff (Lipman, 2000, 2006). This tuff was previously considered to be the Mammoth Mountain Tuff of Steven and others (1974a), but its sanidine phenocrysts are tabular and notably more sodic (Or_{55-60}) in comparison with other central San Juan ignimbrites, and are similar only to sanidine in the Wason Park Tuff. The tuff at Lake Humphreys dips 30–45 degrees eastward in an arcuate geometry and has an exposed thickness of at least 600–700 m, with no base exposed. The thickness and eastward dips of this undated tuff suggest that it constitutes the lower flank of an intracaldera resurgent uplift that predates emplacement of the overlying lavas, which are nearly flat lying. To the west, any higher parts of the resurgent interior of the South River caldera have caved into the younger Creede caldera; farther south, any uplifted rocks of the caldera floor have been completely buried by the South River Volcanics.

Postcaldera Magmatism

The South River Volcanics, which fill South River caldera, consist of fine-grained dark-gray andesite, hornblende andesite, and lighter-gray hornblende dacite as lava and mudflow deposits. At the type locality of South River Peak, the unit is underlain by Wason Park Tuff along the caldera wall and locally overlain by Snowshoe Mountain Tuff from Creede caldera. Andesitic rocks (56–61 percent SiO_2) are dominant in southern exposures, but more silicic hornblende-bearing lavas (60–63 percent SiO_2) are increasingly abundant northward in the caldera-fill sequence. The base of the intracaldera lavas is not exposed within southern parts of the caldera, but the section is at least 900-m thick at South River Peak.

Arcuate-trending intrusions of andesite to fine-grained granodiorite west and southwest of South River Peak and near Goose Creek are interpreted as discontinuous near-roof-level exposures of a ring intrusion along the southern margin of the South River caldera. Larger intrusions and adjacent wall rocks are variably propylitically altered, silicified, and pyritized. These intrusions are interpreted to be related to the South River caldera cycle, as indicated by local crosscutting relations with the Wason Park Tuff, by their distribution along the margins of the South River caldera, and by associated hydrothermal alteration that extends into the South River Volcanics. The intrusive rocks are likely to be feeders for the South River Volcanics, as indicated by similar mineralogy and chemistry, but they have not been dated directly by isotopic methods.

San Luis Cycle (Rat Creek, Cebolla Creek, Nelson Mountain Tuffs)

Three ignimbrites, Rat Creek, Cebolla Creek, and Nelson Mountain Tuffs, and compositionally diverse associated lavas of the San Luis caldera complex (fig. 129), nested along the northwest side of La Garita caldera (figs. 123, 126), are the youngest major eruptions from the central San Juan caldera cluster, other than the Snowshoe Mountain Tuff from Creede caldera farther south. The Rat Creek and Nelson Mountain Tuffs contain broadly similar phenocryst assemblages and are compositionally zoned from rhyolite to dacite (74–65 percent SiO_2), but the

intervening Cebolla Creek Tuff is a distinctively uniform mafic dacite (~62 percent SiO_2) that contains abundant hornblende but lacks sanidine (table 6). All three ignimbrites associated with the San Luis complex erupted within an interval too brief to distinguish within analytical uncertainty, between 26.91±0.02 and 26.90±0.02 Ma (Lipman and McIntosh, 2008). Eruption of the last-erupted Nelson Mountain Tuff was also close in time to the the Snowshoe Mountain Tuff and Creede caldera, leading to confusion about their relative eruption ages (Lipman, 2000; Lipman and McIntosh, 2008). Further complicating interpretation, eruption of the Nelson Mountain Tuff from a relatively small depression (~8 × 10 km) within the caldera complex was accompanied by concurrent subsidence at Cochetopa Park caldera 25 km to the northeast (Lipman and McIntosh, 2008). In part prompted by the large compositional variations among San Luis eruptions and tight age constraints on duration, several detailed petrologic studies have evaluated alternative processes of magma evolution and relation to reservoir geometry (Streck, 2014; Sliwinski and others, 2019; Curry and others, 2021).

Rat Creek Tuff

The initial ignimbrite erupted from the San Luis caldera complex, the Rat Creek Tuff is compositionally zoned (73–65 percent SiO_2) from weakly indurated light-tan crystal-poor rhyolite upward into welded crystal-rich dacite (table 6). The Rat Creek Tuff is the smallest of the San Luis ignimbrites in estimated volume (~150 km^3), the most restricted in known extent, and its source is the least understood (Lipman, 2000, p. 32–33). Eight samples from widespread sites have a weighted-mean laser-fusion sanidine age of 26.91±0.02 Ma.

Cebolla Creek Tuff

The Cebolla Creek Tuff is a distinctive uniform ignimbrite of gray to light-brown weakly vapor-phase-devitrified mafic dacite (62–66 percent SiO_2; 25–40 percent phenocrysts of plagioclase, biotite, hornblende, sparse clinopyroxene). In contrast to other dacitic tuffs of the San Luis caldera complex, the Cebolla Creek Tuff lacks sanidine and hornblende is abundant (table 6). Hornblende and biotite plateau ages for this unit (27.13–27.07 Ma) are about 0.2 m.y. older than the sanidine ages for the underlying Rat Creek Tuff (table 10). Such slightly older apparent ages for mafic minerals relative to sanidine are fairly common among dated volcanic rocks in the San Juan region (Lipman and McIntosh, 2008).

Like the underlying Rat Creek Tuff, preserved exposures of outflow Cebolla Creek Tuff deposits are weakly welded and are limited to ponded fill within the northern La Garita caldera and along the Los Pinos graben north of Cathedral, Colorado (fig. 126). These lower ignimbrite sheets were widely eroded prior to eruption of the overlying Nelson Mountain Tuff, which rests directly on older units in many places within the general distribution area of the Rat Creek and Cebolla Creek Tuffs. The source caldera for the Cebolla Creek Tuff, although now largely concealed beneath the Nelson Mountain caldera source and flanking postcollapse volcanoes, appears to be the largest among the three calderas of the San Luis complex, with dimensions of 12 × 17 km at present erosional levels (fig. 129). Small remnants of thick, densely welded intracaldera Cebolla Creek Tuff are exposed at the head of East Willow Creek, along the southeastern margin of the caldera complex.

Nelson Mountain Tuff

This unit includes a regional ignimbrite sheet and thick intracaldera fill; like the Rat Creek Tuff, it grades upward in composition (63–73 percent SiO_2) from crystal-poor rhyolite to densely welded dark crystal-rich dacite (table 6). The Nelson Mountain Tuff is the most densely welded and voluminous outflow deposit erupted from the San Luis caldera complex (estimated >500 km^3), and its eruption was followed by growth of large volcanoes on the east and west caldera flanks (Stewart Peak Volcanics, Baldy Cinco Dacite), roughly concurrent with resurgent uplift of the caldera interior (Steven and Lipman, 1976; Lipman, 2000, 2006). The Nelson Mountain Tuff and earlier tuffs from the San Luis complex may well have originally been deposited over sizable areas to the north, but as young and topographically high deposits, they have been widely eroded.

Exposed intracaldera Nelson Mountain Tuff is more than 800-m thick on San Luis Peak, and erosional remnants of the outflow sheet are preserved widely around southwest and southeast sides of the San Luis caldera complex (fig. 129), where this ignimbrite spread across northern parts of La Garita caldera (Lipman, 2006). A northeastern outflow lobe of the tuff was able to cross the La Garita caldera wall, following paleovalleys of the Cochetopa Creek and Los Pinos grabens into Cochetopa Park caldera (fig. 125; Lipman, 2012), and a weakly welded distal facies of this unit reached the southeast side of the caldera. No Nelson Mountain Tuff remains preserved north of Cochetopa Park caldera.

Single-crystal sanidine ages for the Nelson Mountain Tuff, both outflow and intracaldera (table 10; Lipman and McIntosh, 2008), have resolved some formerly enigmatic problems concerning this unit. Previously determined $^{40}Ar/^{39}Ar$ incremental-heating plateau ages on multiple-grain sanidine concentrates, although analytically reproducible, varied by as much as 1 m.y. among samples from different geographic localities and for intracaldera versus outflow parts of this ignimbrite unit (discussion in Lipman, 2000). In contrast, single-crystal sanidines from eight outflow samples yield a weighted mean age of 26.90±0.02 Ma, and two samples of intracaldera Nelson Mountain Tuff have a mean of 26.91±0.04 Ma (Lipman and McIntosh, 2008).

There is a sizable discrepancy between volume of the Nelson Mountain Tuff and the amount of subsidence at its eruptive source within the San Luis complex. The widespread outflow and thick intracaldera accumulation of the Nelson Mountain Tuff (estimated at 500 km^3) constitutes the largest of the three San Luis ignimbrites in eruptive volume (table 10). In contrast, the small subsidence basin at its eruptive source is

anomalous relative to the estimated eruptive volume. The basin defined by the unconformity between wall rocks and caldera fill is ~10 × 15 km (fig. 129), but the southern third of the basin is a truncated paleovalley (Stops 5C-4, 5C-5), as documented by mapping and mineral-exploration data (Lipman, 2000). The paleovalley is well outside of the structurally subsided block, which has estimated dimensions of only about 8 × 10 km and an area of about 65 km^2. About 8 km average caldera subsidence would thus be needed to accommodate the 500 km^3 erupted volume of the Nelson Mountain Tuff, but the asymmetric trapdoor subsidence geometry at this caldera (Lipman, 2000) permits only about 500 m of subsidence on the north side of the caldera and no more than 1.5–2 km at the more deeply subsided south side. The inconsistency between eruptive and subsidence volumes associated with eruption of the Nelson Mountain Tuff is interpreted as the result of concurrent subsidence at the larger Cochetopa Park caldera (fig. 125) 30 km to the northeast (Lipman and McIntosh, 2008).

Snowshoe Mountain Tuff and Creede Caldera

Creede caldera (fig. 130), which subsided during eruption of the Snowshoe Mountain Tuff at 26.87±0.02 Ma (Lipman and McIntosh, 2008), has spectacularly preserved constructional morphology for an Oligocene volcano (Stop 5B-9); many of its major features were initially well documented by Steven and Ratté (1965) and Steven and Lipman (1976). An updated summary is in a recent field guide (Larsen and Lipman, 2016).

The Snowshoe Mountain Tuff is another compositionally uniform phenocryst-rich dacite (62–66 percent SiO_2; 35–45 percent phenocrysts). It has some petrologic affinities to the Fish Canyon Tuff; the presence of sparse quartz and relatively potassic sanidine phenocrysts, despite the dacitic bulk composition, suggests relatively high-pressure crystallization (Lipman and others, 1978; Lipman and Weston, 2001). Intracaldera Snowshoe Mountain Tuff is densely welded and more than 1.8-km thick on the resurgent dome without any exposed base (Steven and Ratté, 1965, p. 59). In contrast, the sparsely preserved outflow sheet is only weakly welded, less than 100-m thick at maximum, and exposed mainly where capped by mafic lavas south of the South Fork area (Lipman, 2006) and along the Continental Divide near South River caldera.

Caldera Geometry

Creede is a symmetrically resurgent caldera (fig. 130) that has structural dips to as much as 45° on flanks of its domical uplift and a well-developed apical graben (Steven and Ratté, 1965). Its near-pristine constructional morphology is largely a result of erosional exhumation of its sedimentary moat fill by the Rio Grande during the past few million years (Steven and others, 1995; Rye and others, 2000). The well-preserved morphology and drilling in the caldera moat, for mineral exploration and by the U.S. Continental Scientific Drilling Program, provide special insights into the three-dimensional structure of this representative medium-size plate-subsidence caldera. Although not directly exposed, a ring fault about 16 km in diameter is inferred from arcuate trends of postcollapse lava vents and fossil warm-spring deposits (travertine), as well as from the resurgent doming along confocal boundaries (Steven and Lipman, 1976; Lipman, 1984). The much larger diameter of the topographic caldera rim provides evidence for large-scale enlargement of the caldera by gravitational landsliding during and after the eruption, forming a so-called collar volume between ring-fault structural boundary and topographic wall (fig. 131).

A minimum subsidence depth for Creede caldera is the combined >3.5 km vertical dimensions of the initially unfilled topographic caldera (1.7 km) and exposed intracaldera tuff (>1.8 km). Because only volumetrically minor landslide breccias interleave with tuff exposed on the resurgent dome near the center of the caldera, the large collar volume between ring fault and topographic wall indicates that much additional landslide debris must be concealed at depth near the ring faults.

Caldera-Collapse Landslide Deposits

Landslide deposits have long been recognized locally interleaved with upper parts of the intracaldera Snowshoe Mountain Tuff (Steven and Ratté, 1965), which demonstrates their emplacement prior to resurgence. On the west flank of the resurgent dome, north of McCall Creek, a few breccia lenses interfinger with upper parts of the Snowshoe Mountain Tuff, but most of the breccia overlies the uppermost weakly welded Snowshoe Mountain Tuff on outer flanks of the resurgent dome. The dominant clast type, especially in the lowermost breccia lenses, is dark gray andesite lava, probably derived from Bristol Head on the caldera wall to the west (Stop 5D-4).

The most spectacularly exposed rhyolitic landslide breccia is the rugged outcrop on the northwest flank of Snowshoe Mountain (Stop 5D-2), locally known as Point of Rocks (fig. 130), which was previously interpreted as a brecciated postcaldera rhyolitic lava dome (Steven and Ratté, 1965, p. 43). Further study showed, however, that these rocks are a resurgently tilted and slightly faulted layer of silicified monolithologic breccia, consisting solely of crystal-poor welded tuff derived from the Willow Creek welding zone of intracaldera Carpenter Ridge Tuff. Flattened pumice textures within breccia clasts are obscure in the most accessible exposures at Point of Rocks but are readily visible nearby. The rhyolite breccia layer conformably overlies several meter-scale beds of lithic-rich tuff that are interpreted to record the waning of Snowshoe Mountain eruptions.

Drilling in the caldera moat also penetrated thick breccias composed of fluidal Willow Creek clasts, which are likely correlative with the Point of Rocks deposit (Bethke and Hay, 2000). These breccias overlie flat-lying intracaldera tuff at depths of 1.5–1.7 km below the average elevations of high points on the preserved caldera topographic rim at 3,700–3,800 m

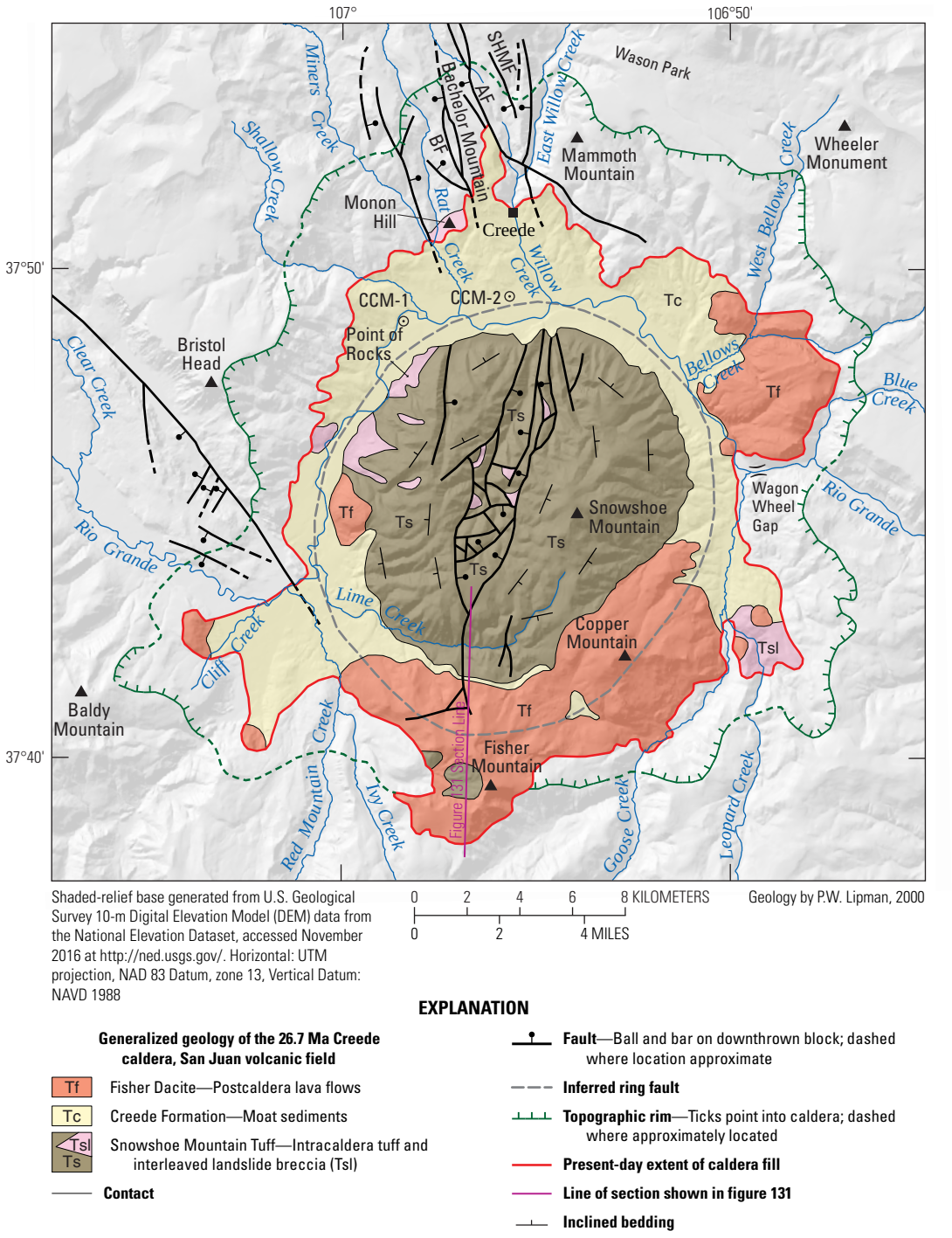

Figure 130. Generalized geologic map of Creede caldera, showing approximate location of eroded topographic caldera rim, present-day extent of caldera-fill deposits, inferred buried ring fault, and late normal faults during resurgent doming (Deep Creek graben) and mineralization (Creede graben). BF, Bulldog Mountain Fault; AF, Amethyst Fault; SHMF, Solomon-Holy Moses Faults; CCM-1 and CCM-2, drill-hole sites of the Continental Scientific Drilling Program Creede Scientific drilling Project. Modified from Lipman (2000).

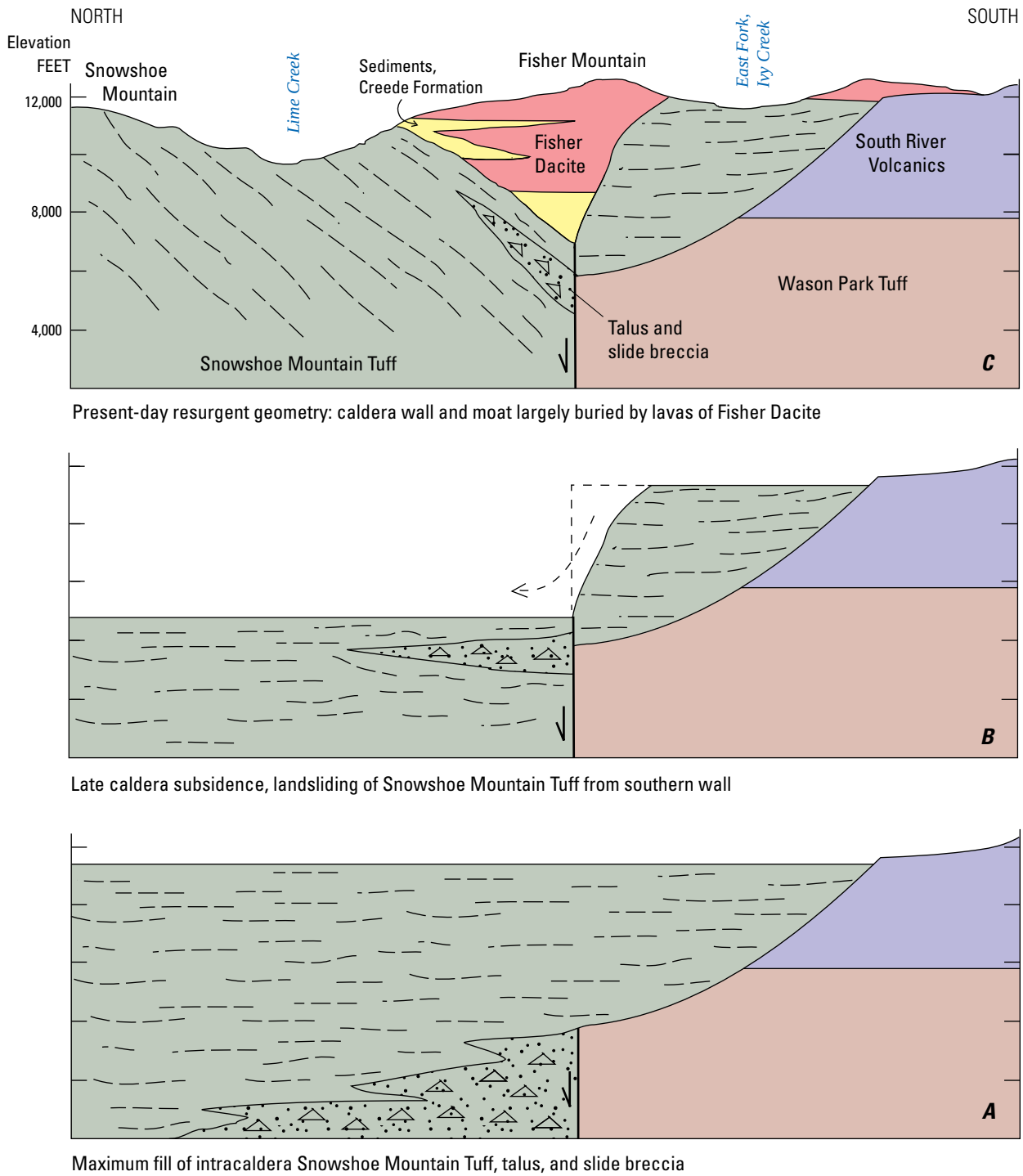

Figure 131. Simplified cross section through the southern margin of Creede caldera, and an interpretitive sequence of events during caldera subsidence and posteruption volcanism and sedimentation. *A*, Maximum height of the intracaldera Snowshoe Mountain Tuff, late during eruption, after the structurally bounded caldera had become enlarged by earlier landslide slumping. *B*, Further major subsidence near the end of the eruptions, causing additional landsliding of the highest intracaldera Snowshoe Mountain Tuff and adjacent wall rocks. *C*, Resurgent doming of the caldera floor, filling of the resulting moat by sediments of Creede Formation and lavas of Fisher Dacite, and subsequent erosion to the present-day land surface. Location of section shown in figure 130.

(12,200–12,500 feet [ft]), and provide tight constraints on the original postcollapse height of the unfilled caldera moat, now occupied by postcaldera sediments and lavas. Together with the outcrops of similar breccia at Point of Rocks and north of McCall Gulch, the drill holes provide evidence that a sheet of landslide breccia derived from the caldera wall spread over much of the northwest quadrant of the caldera floor, resting on uppermost Snowshoe Mountain Tuff. The most probable source for such a widespread breccia sheet would have been the high rugged caldera-wall cliffs near the mouth of Willow Creek, where the Creede caldera wall is embayed at the structurally weak intersection with keystone graben faults of the Bachelor caldera.

Willow Creek clasts from the landslide deposits, including Point of Rocks, have normal magmatic sodium-potassium ratios, similar to outflow Carpenter Ridge Tuff. In contrast, bedrock samples of Willow Creek type from the likely sources on the north caldera wall show large-scale alkali exchange (Ratté and Steven, 1967). These chemical data thus support interpretations that the potassic alteration in the Creede mining district was a precursor to the late faulting and major mineralization along the Creede graben (Sweetkind and others, 1993), rather than having occurred during the Bachelor caldera cycle.

Postcaldera Sedimentation and Volcanism

After the cessation of Snowshoe Mountain eruptions, Creede caldera was a steep-walled, flat-floored closed basin 20–25 km in rim diameter that filled rapidly with sediments, volcanic deposits, and water. Caldera-filling processes included (1) early mass wasting from unstable caldera walls, as documented by conglomerates and sedimentary breccias intertongued with lower fine-grained sediments of the Creede Formation; (2) emplacement of lavas of Fisher Dacite; (3) erosional recycling of caldera-fill deposits as the caldera floor resurged; and (4) gradual filling of the closed basin by surface waters (Barton and others, 2000).

Creede Formation.—Sedimentary deposits that accumulated within the caldera basin have been well described (Emmons and Larsen, 1923; Steven and Ratté, 1965; Larsen and Crossey, 1996, 2000; Finkelstein and others, 1999; Heiken and others, 2000; Larsen and Nelson, 2000; Larsen and Lipman, 2016). These deposits consist largely of finely laminated shale and sandstone that represent shallow- to deep-water deltaic and lake deposits in the central moat, and alluvial slope wash, fanglomerate, and stream conglomerates and sandstones along margins of the caldera and resurgently uplifted core. Travertine masses that are widely present within the moat sequence record activity of mineral springs during sedimentation.

Conglomeratic Creede Formation sediments lap unconformably onto resurgently domed Snowshoe Mountain Tuff in several places. Dips are locally as steep as 10–15° but are plausible as primary depositional attitudes. No resurgently tilted bedded deposits have been identified from stratigraphic levels above the Point of Rocks landslide deposit. Although sedimentation must have commenced before resurgence was complete, any such deposits have been stripped from the exposed dome.

Fisher Dacite.—Lavas and associated breccias of porphyritic dacite (62–66 percent SiO_2; 25–35 percent plagioclase, biotite, clinopyroxene, hornblende, sparse large sanidine in some lavas) completely fill the southern to southeastern moat of Creede caldera, and additional lavas are present in the eastern moat north of Wagon Wheel Gap, on the west flank of Snowshoe Mountain south of McCall Gulch (Stop 5D-3), and on the southwest caldera wall (fig. 130). In contrast to earlier calderas of the central cluster, postsubsidence eruptive activity was volumetrically subordinate to sedimentation as represented by the Creede Formation. Much of the southern area previously mapped as Fisher Dacite between Red Mountain and Goose Creeks (Steven and others, 1974a) is now recognized as older South River Volcanics. These lavas, which fill the South River caldera, overlap in composition with the Fisher Dacite, and contacts between the two assemblages are uncertain in places.

The McCall Gulch lava appears to have erupted early, on the caldera floor prior to major uplift on the flank of the resurgent dome, as indicated by the fairly uniform thickness of the lava, by downslope dips that are semiconformable with the tilted underlying Snowshoe Mountain Tuff, and by its unconformable onlap by untilted beds of the Creede Formation. This lava also yielded a relatively old $^{40}Ar/^{39}Ar$ age on sanidine, 26.82±0.05 Ma (Lipman and McIntosh, 2008). The Wagon Wheel Gap lava (Stop 5B-5), which is banked against the east topographic wall of Creede caldera, also erupted relatively early, as demonstrated by exposures down to the present-day valley, where it is onlapped by the Creede Formation. This lava could not be dated reliably because it lacks sanidine.

Lavas in the southern moat have not been subdivided, but several flows are present, with vents likely located beneath or near surviving topographic highs such as Fisher and Copper Mountains. East of Copper Mountain, multiple thick flows collectively are nearly 1-km thick as exposed down to Goose Creek, where dacite lavas rest directly on rocks older than Creede caldera. The variable elevations of these flows and the lack of exposed interbedded Creede Formation indicate recurrent lava eruptions as the caldera moat filled. In the large cirque on the southeast slopes of Fisher Mountain, two thick dacite lavas are separated by bedded laharic breccias. These lavas and breccias may be the youngest parts of the Fisher Dacite, based on their high topographic levels, above the highest known exposures of Creede Formation at about 10,900 ft (3,320 m) at the head of Lime Creek, and their relatively young $^{40}Ar/^{39}Ar$ age (26.77±0.04 Ma; Lipman and McIntosh, 2008).

Filling history of the caldera basin in relation to caldera resurgence.—Varied features of the Creede moat deposits indicate that early sedimentary filling was in shallow water, but the caldera lake later deepened (Steven and Ratté, 1965; Larsen and Crossey, 1996, 2000; Larsen and Lipman, 2016), perhaps in response to growth of the resurgent dome and attendant reduction in surface area of the lake. Both a smaller drainage basin than the present one and delayed caldera resurgence are required to permit water depth to have remained in balance with sedimentation rates during the initial shallow-water sedimentation (Barton and others, 2000).

Contrary to the prolonged interval (26.9–26.2 Ma) inferred for deposition of the Creede Formation (Lanphere, 2000), more rapid accumulation for the drill-core sediment section and resurgent doming is suggested by newer $^{40}Ar/^{39}Ar$ ages (Lipman and McIntosh, 2008). The preresurgence lava at McCall Gulch (26.82±0.05 Ma) is only about 0.05 m.y. older than the postresurgence Fisher Mountain lavas (26.77±0.04 Ma) that stratigraphically overlie the entire original thickness of the Creede Formation (4,396 ft; 1,340 m). Caldera resurgence was also insufficiently prolonged to permit erosion of the Point of Rocks landslide breccias prior to accumulation of Creede sediments to present-day river level, 350 m above the postcollapse caldera floor. Such rapid resurgence is consistent with well constrained rates for several young caldera systems that resurged within 100 k.y. or less after subsidence; these include Long Valley (Bailey and others, 1976), Yellowstone (Christiansen, 1984), Toba in Indonesia (de Silva and others, 2015), and Chegem in Russia (Lipman and others, 1993; Gazis and others, 1995).

Structure

Structural features of the central San Juan Mountains involve complex interactions between diverse localized faulting associated with volcanism (especially the calderas), concurrent assembly and consolidation of a large subvolcanic batholith, and effects of west-southwest-directed regional extension associated with inception of the Rio Grande rift zone (fig. 132). Many normal faults are exposed within the central caldera cluster, but erosion levels are insufficient to expose ring faults that might be inferred as directly related to caldera collapse, such as those well exposed within Lake City and Silverton calderas in the western San Juan Mountains (Steven and Lipman, 1976). A distinctive area of rectilinear faulting, within and adjacent to the southern segment of the enormous La Garita caldera (fig. 132), appears to have accommodated early large-scale piecemeal-style collapse, probably initiated during a precursor eruption of the Pagosa Peak Dacite (Lipman, 2000); some of these faults localized continued subsidence in the southern segment during subsequent eruptions of Fish Canyon Tuff.

Several fault clusters are related to resurgent uplift of caldera floors. Especially conspicuous is the Deep Creek graben along the keystone crest of the steep-sided Snowshoe Mountain dome within Creede caldera (Steven and Ratté, 1965). Other resurgent structures include (1) the graben faults of the Creede mining district that were also initiated as keystone faults on the elliptical resurgent uplift within Bachelor caldera (Steven and Lipman, 1976), (2) faults bounding trapdoor-style uplift of the San Luis Peak block within the caldera associated with eruption of the Nelson Mountain Tuff, and likely also (3) the faults that cut intracaldera Fish Canyon Tuff in the uplifted block of the La Garita Mountains.

Another group of structures includes linear graben and other faults adjacent to calderas that appear largely to have been established during segmented subsidence of the La Garita caldera, then passively buried by younger tuff sheets and lavas. These include the Los Pinos and Cochetopa grabens that connect the La Garita Mountain segment to Cochetopa Park caldera across the Continental Divide (fig. 125), some faults of the Clear Creek graben (Stop 5D-6) to the west of the central segment (fig. 132), and perhaps initial faulting along the Rio Grande graben to the southeast of the central segment (Stop 5-4). The southwestern bounding faults of the Clear Creek graben appear to have controlled a subparallel segment of the La Garita caldera-wall unconformity (fig. 126), along which Carpenter Ridge and younger tuffs bank depositionally against steep slopes without major subsequent faulting. In contrast, northeastern bounding faults from Bristol Head to Spring Creek Pass (Stops 5D-6, 5D-7) had continued later movement, after eruption of the Nelson Mountain Tuff. To the southeast, near Wolf Creek Pass, the Pass Creek Fault Zone bridges the area from the central caldera cluster to the Platoro caldera complex (Day 4), and involves displacements younger than Fish Canyon Tuff along with modest associated alteration (Lipman, 1975a, p. 110–111).

During late stages of San Juan volcanism, the Rio Grande Rift became active within the present-day San Luis Valley to the east of the San Juan Mountains (fig. 90), but only a few northwest-trending faults within the map area have the appropriate geometry and timing to reflect such regional tectonism (Lipman and Mehnert, 1975). Northwest-trending faults of the Rio Grande graben cut basaltic lavas of the Hinsdale Formation, dated at about 24 Ma south of South Fork, and the late movement along the Bristol Head Fault of the Clear Creek graben suggests that faults localized by and initially active during formation of La Garita caldera also were influenced by regional stresses associated with initial southwestward-directed extension along the Rio Grande Rift.

Day 5—Routes Through the Central San Juan Region

This trip segment (fig. 133) obliquely transects the central part of the San Juan volcanic locus, providing an east-west cross section through the giant La Garita caldera and several of the younger ignimbrite subsidence structures nested within it during the interval 28.02–26.87 Ma. Heading northwest from Del Norte, Colorado, at the western margin of the San Luis Valley segment of the Rio Grande Rift. The route 5 Introduction accesses respresentative exposures of two outflow ignimbrites, then follows an Oligocene paleovalley up the Rio Grande valley to South Fork, Colorado, between constructional highs of several precaldera volcanoes to the north (the ~33-Ma Summer Coon and Baughman Creek volcanoes) and those associated with the Platoro caldera complex to the south (as seen on Day 4). Route 5A is a side trip along the South Fork Rio Grande to view basal Fish Canyon Tuff, unusual lava-like pyroclastic deposits (Pagosa Peak Dacite) that were precursors to eruption of the Fish Canyon Tuff, and other proximal ignimbrites; Route 5B traverses the core of the central caldera cluster, following the Rio Grande graben, an extensional

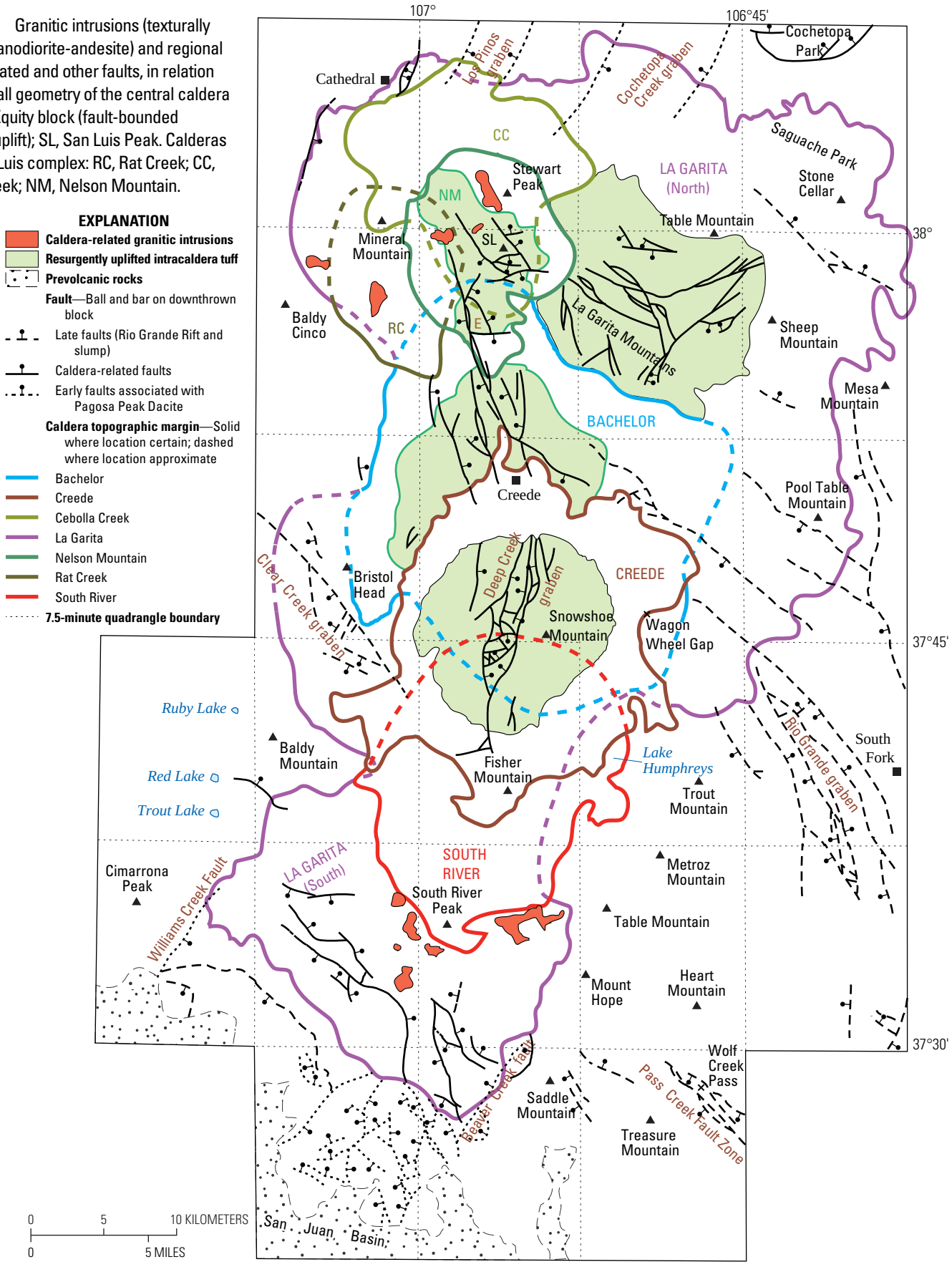

Figure 132. Granitic intrusions (texturally variable granodiorite-andesite) and regional caldera-related and other faults, in relation to the overall geometry of the central caldera cluster. E, Equity block (fault-bounded triangular uplift); SL, San Luis Peak. Calderas of the San Luis complex: RC, Rat Creek; CC, Cebolla Creek; NM, Nelson Mountain.

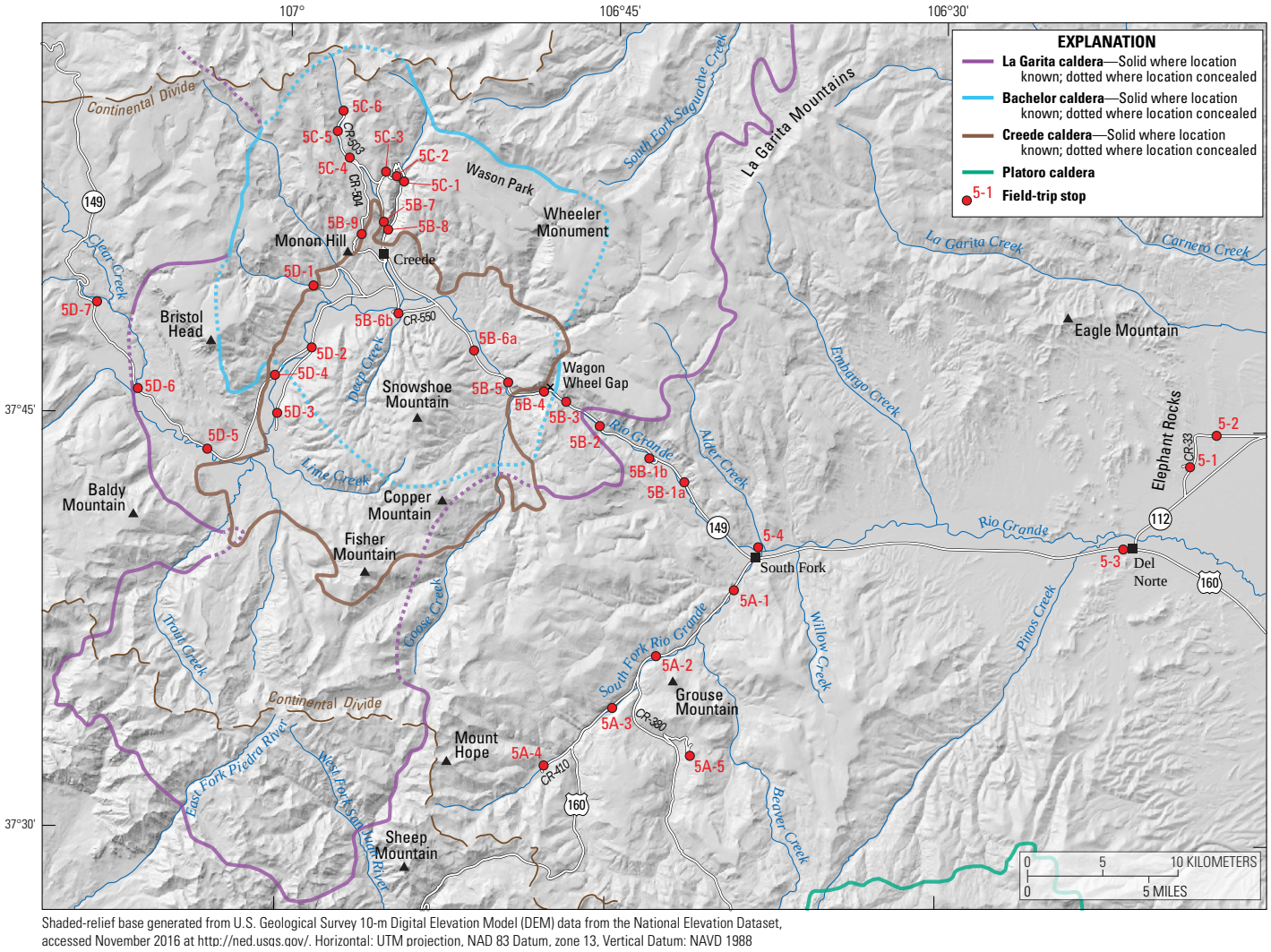

Shaded-relief base generated from U.S. Geological Survey 10-m Digital Elevation Model (DEM) data from the National Elevation Dataset, accessed November 2016 at http://ned.usgs.gov/. Horizontal: UTM projection, NAD 83 Datum, zone 13, Vertical Datum: NAVD 1988

Figure 133. Route map for Day 5.

structure likely related to regional uplift and emplacement of a composite batholith during growth of the volcanic field. The canyon of the Rio Grande cuts a spectacular section through the east wall of La Garita caldera, the source of the Fish Canyon Tuff. At Wagon Wheel Gap, after examining a southeastern remnant of Bachelor caldera (source of the 27.55-Ma Carpenter Ridge Tuff), we enter the resurgently domed Creede caldera, the best-preserved caldera in the San Juan region and source of the 26.87-Ma Snowshoe Mountain Tuff. The trip follows the caldera moat northwest to Creede, to examine complex fill deposits within the Bachelor caldera and structural features of the Creede mining district. Route 5C heads north from Creede (route 5C) to provide three-dimensional perspectives on depositional and welding complexities in thick intracaldera Carpenter Ridge Tuff, views of the northeast wall of Bachelor caldera where it truncates resurgently uplifted thick intracaldera Fish Canyon Tuff in the La Garita Mountains, access to the south side of the San Luis caldera complex, and a panoramic 180° view of Creede caldera. Route 5D then continues counterclockwise around the moat of the Creede caldera, into the northwest-trending Clear Creek graben, another distensional structure related to batholith-scale magmatic adjustments, to reach the western margins of Bachelor and La Garita calderas.

Published U.S. Geological Survey (USGS) geologic maps especially pertinent to Day 5 of the field trip include the Del Norte area (Lipman, 1976b) and the central San Juan caldera cluster (Lipman, 2006). Descriptions for some route stops are modified from the 1989 IAVCEI field guide (Lipman and others, 1989), from Lipman and others (2013), and from Larsen and Lipman (2016). Numbers at left in each route log are distances in miles from starting point. Latitude/longitude Global Positioning System (GPS) locations are based on NAD27 coordinates, as used on USGS 7.5-minute topographic maps for the San Juan region.

Route 5 Introduction—Outflow Ignimbrite Stratigraphy: Del Norte to South Fork, Colorado

This trip segment provides a brief introduction to the regional stratigraphy of the central San Juan region; well-stratified outflow ignimbrite sheets overlie thick accumulations of intermediate-composition lavas and breccias (Conejos Formation) that erupted from multiple stratovolcanoes. The initial focus is on the characteristic end-member types of San Juan ignimbrites: compositionally uniform crystal-rich dacite (Fish Canyon Tuff) and crystal-poor rhyolite (Carpenter Ridge Tuff). Both are underlain by Conejos andesitic lavas along the eastern margin of the San Juan Mountains. The route proceedes to the village of South Fork, where views provide perspectives on interfingering of ignimbrites from the Platoro caldera complex (Day 4) with those from the central caldera cluster.

Mileage

0.0 *The route begins in Del Norte, Colorado (fig. 134), 14 miles (mi) north of Monte Vista, by way of U.S. Route (US) 160. From the junction of US 160 and Colorado State Highway (CO) 112 in Del Norte (7,884 ft, 2,403 m elevation), proceed north 3.1 mi on CO 112 (Oak Street). Turn left (north) onto Rio Grande (RG) 33 and go 1.2 mi to gravel track (5203) on the left that leads to outcrops, proceed 0.1 mi to the fork in the road and park.*

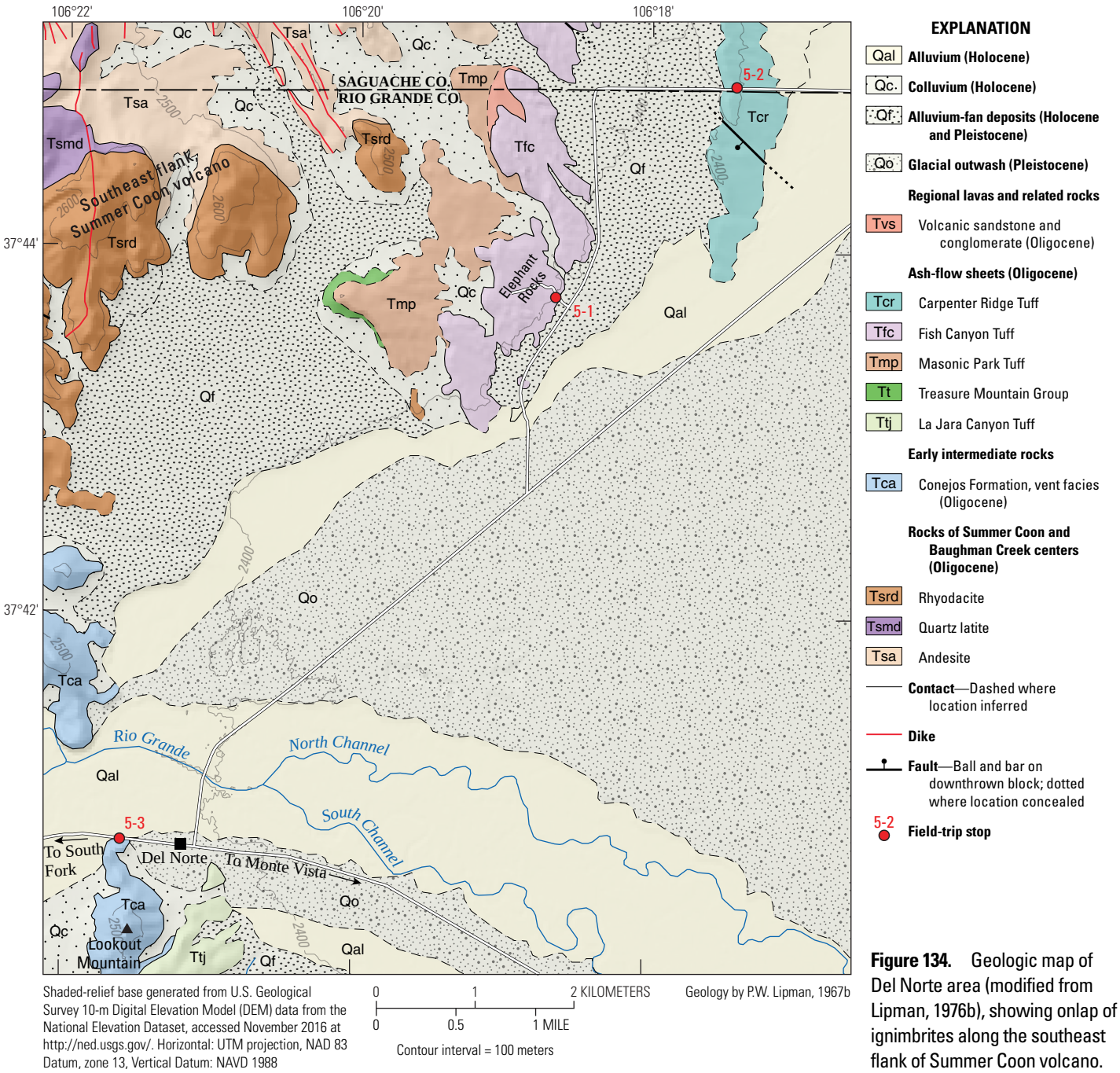

Figure 134. Geologic map of Del Norte area (modified from Lipman, 1976b), showing onlap of ignimbrites along the southeast flank of Summer Coon volcano.

4.4 **Stop 5-1. Fish Canyon Tuff at Elephant Rocks** (37°43.75' N., 106°18.64' W.; 7,874 ft, 2,400 m elevation).

Typical exposures of this large (~5,000 km^3), distinctive crystal-rich dacitic ignimbrite (fig. 135) that erupted at 28.02 Ma from La Garita caldera. The Fish Canyon Tuff is compositionally uniform in bulk-sample scale but contains an exceptionally mineralogically and chemically complex crystal cargo (Bachmann and others, 2002; Charlier and others, 2007). The outflow sheet is a single large cooling unit of light-gray to tan tuff, still preserved as much as 125 km beyond the rim of La Garita caldera. It is characterized by simple welding zonation except in thick proximal sections, especially in the South Fork area (Stop 5A-2), where compound welding zones are well developed and as many as six cooling subunits are mapped locally (Lipman, 2006). Pumice fragments are obscure in most exposures, and lithic fragments typically are sparse. Densely welded tuff is massive, and weathers to rounded granitoid-like outcrops, but upper less-welded parts commonly have slabby jointing parallel to obscure compaction foliation. Despite the enormous volume of this ignimbrite, its bulk composition is uniform crystal-rich silicic dacite (66–68 percent SiO_2; 40–50 percent plagioclase [pl]>>sanidine [san], biotite [bt]>hornblende [hbl]; Lipman, 1975a; Whitney and Stormer, 1985; Bachmann and others, 2002). The Fish Canyon Tuff at this locality is the most crystal-rich (55 percent) and least silicic (65.4 percent SiO_2) from anywhere in the San Juan Mountains where the unit has been well characterized (Bachmann and others, 2002, "Elep" sample). This implies ash elutriation at this relatively distal locality, perhaps related to control by paleotopography during transport and deposition.

The Fish Canyon Tuff phenocryst assemblage of sparse resorbed pinkish quartz, accessory titanite, and hornblende without augite is unique among ignimbrites erupted from the San Juan region. Sanidine phenocrysts (typically $Or_{72–74}Ab_{23–24}An_1Cn_{1.5}$) are relatively potassic and conspicuously zoned in barium, with cesium varying 1–4 mole percent. Other crystal-rich dacites erupted from San Juan calderas contain clinopyroxene with little or no hornblende, lack quartz or titanite, and most also lack sanidine (tables 5, 6). Among all ignimbrites in the SRMVF, only the much older Badger Creek Tuff (34.1 Ma) erupted from the Mount Aetna caldera in the Sawatch Range to the north (fig. 90) petrologically resembles the Fish Canyon Tuff.

Return to RG 33 and continue north 1.3 mi to the junction with RG-A; turn right and proceed 0.9 mi to Stop 5-2 at the gentle topographic rise; the best outcrops are north of the ridge crest.

6.6 **Stop 5-2. Basal vitrophyre of crystal-poor Carpenter Ridge Tuff at ridge crest of road** (37°44.89' N., 106°17.45' W.; 7,874 ft, 2,400 m elevation).

Stop 5-2 accesses a typical outflow exposure of this dominantly phenocryst-poor rhyolitic ignimbrite of large volume (~1,000 km^3), which was erupted from Bachelor caldera at 27.55 Ma. The Carpenter Ridge Tuff is typically densely welded; it is widely characterized by a conspicuous basal vitrophyre, and in places, by a central lithophysal zone, typical of many crystal-poor ignimbrites in the SRMVF. The moderately welded vitric zone at this relatively distal site is distinctive in that individual glass shards are readily discernable by hand lens. Much of the outflow ignimbrite sheet is uniform crystal-poor rhyolite, densely welded nearly to its base, but in places, it contains more complex welding and compositional zonations, especially within Bachelor caldera.

The volumetrically dominant rhyolite contains 3–5 percent phenocrysts (pl>san>>bt); in its caldera and locally elsewhere, it grades upward to silicic dacite and dacite (67–74 percent SiO_2) that contains as much as 30 percent phenocrysts (table 6). Locally, discrete scoria clasts have more mafic compositions

Figure 135. Fish Canyon Tuff at Elephant Rocks (Stop 5-1), view to the west. Rounded granitoid-like outcrops are typical of this ignimbrite with a moderately welded outflow tuff sheet. Photograph by K.J. Turner, U.S. Geological Survey, 2016.

(<55 to 65 percent SiO_2), and contain as much as 30–40 percent phenocrysts (table 6, Bachmann and others, 2014). Sanidine compositions are less potassic than in the Fish Canyon Tuff and somewhat variable, mostly $Or_{62–67}Ab_{35–31}An_{2–1}Cn_{1–4}$ (Whitney and others, 1988; Riciputi, 1991). The Carpenter Ridge Tuff is the only densely welded crystal-poor rhyolite of large volume erupted from the central caldera cluster, but in the field it can be difficult to distinguish from lithologically similar regional rhyolites that were erupted from western calderas (Blue Creek, Dillon Mesa, and Sapinero Mesa Tuffs) and northeastern calderas (Thorn Ranch, rhyolitic Bonanza, and Saguache Creek Tuffs). Outflow Carpenter Ridge rhyolite, as seen here, will be compared with its depositional equivalent deep within Bachelor caldera, at Stops 5B-8 and 5C-3.

Continue east on Rio Grande-A for 2.1 mi to intersection with CO 112. Turn right (west) on CO 112 and proceed west to Del Norte. Turn right (west) at the intersection with US 160 and proceed 0.4 mi west to the intersection with Pinos Rd (RG 14) at the west edge of town; turn left (south) into the Visitor Center parking area (east side of the road), near the base of a large cliff outcrop.

13.8 **Stop 5-3. Conejos Formation—Hornblende-andesite lava** (37°40.73' N., 106°21.65' W.; 7,940 ft, 2,420 m elevation).

The cliff exposure is a representative lava of the Conejos Formation, on the distal flank of a volcanic center near the northeast rim of the Platoro caldera complex to the south. The regional Conejos Formation consists dominantly of andesite and dacite as lavas and proximal breccias erupted from central volcanoes, surrounded by voluminous aprons of volcaniclastic debris emplaced as mudflow and stream-fan deposits (Lipman and others, 1970; Lipman, 1975a; Colucci and others, 1991). These thick accumulations of intermediate-composition lavas and breccias, which underlie the caldera-related ignimbrite sequence that dominates the central San Juan caldera area, constitute the volumetric bulk of the San Juan volcanic locus. Subsequently deeply eroded, these early eruptive deposits are now discontinuously exposed as surviving topographic highs along margins of the ignimbrite calderas. Compositional subunits among Conejos lavas have been subdivided in varying detail, depending on the degree of local diversity and quality of exposures, but they remain much less studied than the overlying ignimbrites. Proximal lavas tend to become more silicic upward, with biotite-bearing dacite and low-silica rhyolite especially abundant on northeast side of La Garita caldera. Northern units of the Conejos Formation, which underlie the Saguache Creek Tuff (32.20 Ma) and the Bonanza Tuff (33.12 Ma) northeast of the central caldera cluster, are mostly older than the widespread Conejos rocks to the south that are mainly 33–30 Ma (Lipman and others, 1970; Lipman and McIntosh, 2008). The maximum exposed thickness of Conejos rocks is 800 m along southern margins of the central caldera cluster; however, sections as thick as 2.3 km have been penetrated by petroleum exploration drilling in the San Luis Valley to the east (Gries, 1985; Brister and Gries, 1994).

Return to US 160. Turn left (west) and proceed west along the Rio Grande on US 160 to South Fork, Colorado.

The lower slopes on both sides of the Rio Grande valley consist of lavas and volcaniclastic rocks of the Conejos Formation. Higher on the heavily vegetated south side are ignimbrites of the Treasure Mountain Group, erupted from the Platoro caldera complex. To the north, most hills (Twin Peaks is especially conspicuous), are the south flanks of the Summer Coon and Embargo Creek volcanoes (~33–32 Ma: Lipman, 1968; Parker and others, 2005; Poland and others, 2008). Approaching South Fork, the prominent high mesa to the north (Agua Ramon Mountain) is capped by cliffs of Fish Canyon Tuff, above Chiquito Peak Tuff (from Platoro) and underlying Conejos lavas.

29.3 *At South Fork, bear right (northwest) 0.9 mi on CO 149 (Silver Thread Scenic Byway); just after crossing the Rio Grande bridge, turn right on Highway 25 (River Club Drive). Continue 0.9 mi to entry of River Club Condominiums to Stop 5-4.*

31.1 **Stop 5-4. South Fork overview** (37°40.59' N., 106°38.27' W.; 8,202 ft, 2,500 m elevation).

In this area (fig. 136), the outflow ignimbrites erupted from the Platoro caldera complex interfinger with those from the central San Juan caldera cluster along a southwest-trending overlap corridor (Day 4, fig. 92). The adjacent cliff outcrop is a brecciated flow of plagioclase andesite (Conejos Formation). Palisades to the northwest (up the Rio Grande Valley) consist of thick Masonic Park and Fish Canyon Tuffs. The Rio Grande follows faults of a northwest-trending graben system that drops Fish Canyon Tuff on the southwest side of the river down against Masonic Park Tuff to the north. The South Fork Rio Grande marks a narrow depositional corridor along which crystal-rich dacitic ignimbrites from Platoro caldera, as seen on Day 4, interfinger with and wedge out against Masonic Park Tuff, which, at ~28.7 Ma, was the initial dacitic ignimbrite erupted from the central caldera complex (Lipman and others, 1996). To the northeast and southeast of the town of South Fork, Chiquito Peak Tuff is the main ignimbrite beneath the Fish Canyon Tuff, but the Chiquito Peak wedges out depositionally against distal Masonic Park Tuff. The low cliffs to the

south across the mouth of the South Fork are Conejos breccias, overlain by a thin wedge of distal Masonic Park Tuff and then by Chiquito Peak Tuff. Older ignimbrites of the Treasure Mountain Group that occur beneath these two units to the south and east are absent this far northwest. The prominent ridge nose northeast of the town (point Baxter; 9,349 ft [2,850 m] elevation) contains an informative well-exposed section: several thick welding zones of Masonic Park Tuff are overlain by thin Chiquito Peak Tuff that completely wedges out only 1.5 km farther along the ridge, then capped by Fish Canyon Tuff (fig. 137).

Return to the intersection of CO 149 and US 160; turn right (southwest) and proceed along the South Fork Valley 1.2 mi to Stop 5A-1.

End of route 5; continue on to route 5A.

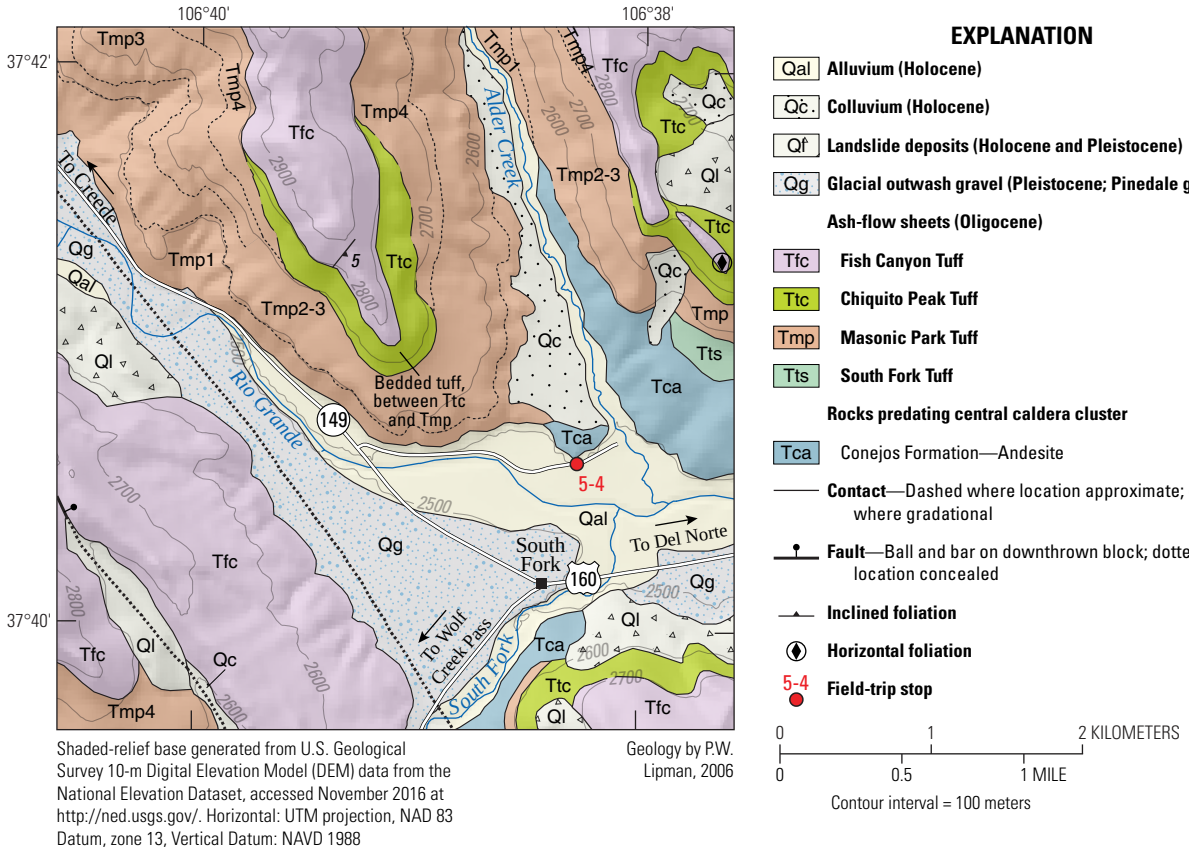

Shaded-relief base generated from U.S. Geological Survey 10-m Digital Elevation Model (DEM) data from the National Elevation Dataset, accessed November 2016 at http://ned.usgs.gov/. Horizontal: UTM projection, NAD 83 Datum, zone 13, Vertical Datum: NAVD 1988

Geology by P.W. Lipman, 2006

Figure 136. Geologic map of the South Fork area, showing interfingering between ignimbrites from the Platoro caldera complex and from calderas of the central cluster (modified from Lipman, 2006).

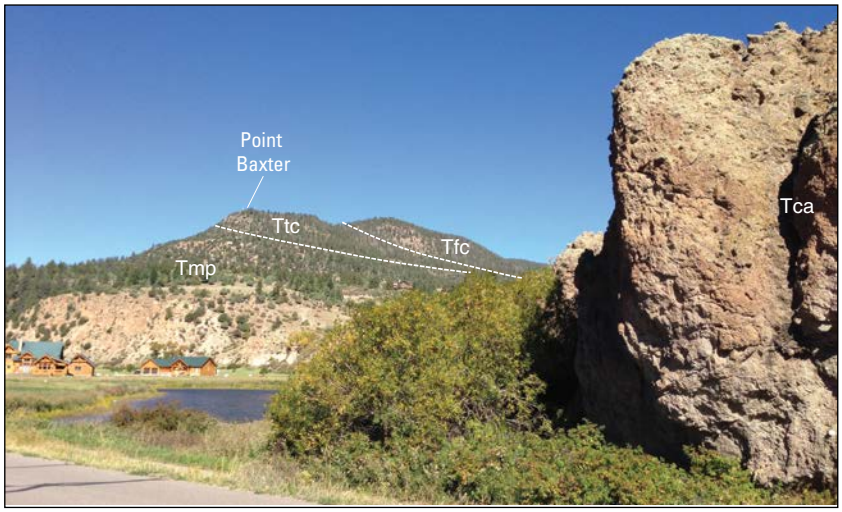

Figure 137. View of Point Baxter, a ridge northwest of South Fork village (Stop 5-4), showing the boundary zone between similar-appearing dacitic ignimbrites (Masonic Park, Chiquito Peak Tuffs). Along the ridge, thin Chiquito Peak Tuff (Ttc) wedges out just to the northwest, between thick underlying Masonic Park (Tmp) and overlying Fish Canyon (Tfc) Tuffs. In contrast, Masonic Park Tuff thins and ends abruptly southeast of South Fork, and these two ignimbrites overlap only along a narrow corridor a few kilometers wide wherever exposed all the way south beyond Wolf Creek Pass. Porphyritic plagioclase-andesite lava of the Conejos Formation (Tca), in foreground, directly underlies the Masonic Park Tuff at this site, but distal South Fork Tuff (from Platoro caldera) wedges between, just to the east across Alder Creek. Photograph by P.W. Lipman, U.S. Geological Survey, 2016.

Route 5A—South Fork of the Rio Grande: Proximal Ignimbrites and Eruptive Precursors Associated with the Two Largest Calderas of the Central Cluster (La Garita, Bachelor)

This trip segment explores depositional and textural features of the enormous Fish Canyon Tuff, eruption processes for the precursor Pagosa Peak Dacite, and the compositional variability in proximal outflow Carpenter Ridge Tuff.

0.0 *From the junction of US 160 and CO 149 at South Fork (8,170 ft, 2,490 m elevation), continue southwest on US 160, following the South Fork valley for 1.0 mi. Beaver Creek road is on the left (southeast). Continue ahead 0.3 mi to Stop 5A-1.*

1.3 **Stop 5A-1. Base of the Fish Canyon Tuff** (37°39.03' N., 106°39.35' W.; 8,268 ft, 2,520 m elevation).

At curve to right, park on the left (southeast side) of road. Caution: high-speed traffic. Large-scale crossbedded deposits (fig. 138), at the base of the Fish Canyon Tuff, overlie massive gray nonwelded ashy mudstone, containing small white pumice fragments in an outcrop only about 5 km from the rim of La Garita caldera. Self and Wright (1983) noted (1) the bedded units contain the same distinctive mineralogy as the Fish Canyon Tuff (pl-san-quartz[qtz]-bt-hbl-sphene[sph]), thereby linking them to the Fish Canyon magma body; (2) wavelengths of as much as 60 m in the bedding; and (3) an erosional interval between early- and late-deposited beds. They inferred that these beds are large-scale surge deposits, not draped tephra fall. The internal variability and geometric complexity of these tuff beds has led to vigorous discussion of their origins whenever scientists have visited this outcrop during the past 40 years. Despite decades of fieldwork on the Fish Canyon Tuff, which is exposed over an area of 15,000 km^3, no other similar outcrops have been found.

A possible alternative interpretation for these deposits is suggested by the work of Bachmann and others (2002), who showed that the eruption of several hundred cubic kilometers of Fish Canyon magma, as the lava-like volcaniclastic Pagosa Peak Dacite, preceded emplacement of the Fish Canyon ignimbrite (Stop 5A-3). Rather than a special case of volcanic-surge deposition, some observers infer that these units are volcaniclastic products derived from the Pagosa Peak Dacite, involving a combination of primary tephra-fall, fluvial, and lacustrine deposition.

Observations at this locality permit debate of questions such as (1) Are these units large-scale surge deposits related to initiation of La Garita caldera and eruption of the Fish Canyon Tuff? If so, why are they not seen elsewhere? Could they implicate phreatic explosions during subsidence of La Garita caldera? (2) Are the internal clast-size variations and three-dimensional bed geometries inconsistent with origin as

Figure 138. Crossbedded basal Fish Canyon Tuff of uncertain origin (see text discussion, Stop 5A-1). Photograph by K.J. Turner, U.S. Geological Survey, 2016.

draped tephra-fall deposits? (3) Are the small faults and other structures in this outcrop products of syneruptive seismicity, compaction and (or) slumping, or post-Fish Canyon Tuff faulting related to the Rio Grande graben? (4) If these units represent reworked ashy material, might they be distal Pagosa Peak ash mobilized within a local drainage? What might have been the relative roles of fluvial and lacustrine environments? Could the underlying ashy mudstone be a coignimbrite ash-cloud deposit at the top of the Chiquito Peak Tuff (an interpretation supported by the presence of sparse small fragments of sanidine and clinopyroxene, along with more abundant plagioclase and biotite)? Is there only one prominent erosion surface? Could these deposits be the distal facies of laharic-debris flows? Does the geometric complexity at outcrop-scale provide criteria for reconstruction of the depositional environment? This locality also provides the opportunity to examine the overlying nonwelded base of Fish Canyon ignimbrite for characteristic mineralogy, in comparison with Stop 5-1.

Proceed west on US 160 for 4.4 mi to Stop 5A-2.

4.0 Highway Spring Campground on left. Chiquito Peak Tuff is exposed along the road on the right, below cliffs of Fish Canyon Tuff. The contact at road level is with the underlying Masonic Park Tuff, which crops out in the campground. Numerous northwest-trending faults between South Fork and here are manifestations of the complex graben system followed by the main Rio Grande to the north.

5.0 Entry to Fun Valley Resort on left. The near-glassy Fish Canyon Tuff at the base of the roadcut and cliffs to the right has been extensively sampled and used as a geochronologic standard.

5.7 **Stop 5A-2. Moon valley** (37°36.59' N., 106°42.85' W.; 8,448 ft, 2,575 m elevation).

Park along the gap in the berm, opposite the entry to Moon Valley RV Park. Views of multiple cliff-forming welded zones within the single thick (to 300 m) ignimbrite sheet of proximal Fish Canyon Tuff (fig. 139). The top of the Fish Canyon and the contact with the overlying Carpenter Ridge Tuff is marked by the near-skyline change from conifers to aspen trees. Compound cooling in outflow Fish Canyon Tuff (as many as six mappable welded zones: Lipman, 2006) occurs only along the lower South Fork valley. Elsewhere, this widespread regional ignimbrite forms a simple cooling unit. The thick accumulation of Fish Canyon Tuff at Moon Valley and nearby appears to record ponding in the lee of the immediately preceding eruption of the Pagosa Peak Dacite (see Stops 5A-3 and 5A-4).

Continue southwest along Highway 160; all road-level outcrops are Fish Canyon Tuff.

7.0 *Park Creek road on left (south); this valley provides access to Stop 5A-5 later in the day. Continue on Highway 160 to Wolf Creek Ranch and Ski Lodge; pull off to the left, into the parking lot.*

Figure 139. Cliffs of thick, proximal outflow Fish Canyon Tuff (>450 meters, base not exposed), at Moon Valley (Stop 5A-2), showing multiple densely welded ledges separated by less-welded benches. Overlying unit is Carpenter Ridge Tuff (CRT). Photograph by K.J. Turner, U.S. Geological Survey, 2016.

8.5 **Stop 5A-3. Contact between** the **Pagosa Peak Dacite and Fish Canyon Tuff** (37°34.69' N., 106°44.80' W.; 8,579 ft, 2,615 m elevation).

Low rugged cliffs along the valley ahead are massive exposures of Pagosa Peak Dacite. The dacite appears homogeneous from a distance, but appropriately weathered surfaces locally display fragmental textures (more clearly visibile at Stop 5A-4). The break in slope that dips gently down valley toward us defines the abrupt depositional contact with the overlying Fish Canyon ignimbrite, which displays typical shard and pumice textures and is nonwelded at its base (only rarely exposed).

Continue southwestward on US 160 for 2.4 mi to U.S. Forest Service (FS) road 410 on the right to Big Meadows Campground/Reservoir. Proceed southwestward on FS 410 for 1.4 mi to the intersection with FS 430. Veer right at the intersection of FS 410 and FS 430 and proceed 0.1 mi; park on the road and climb to the glaciated outcrops on the north side of the road.

12.4 **Stop 5A-4. Pagosa Peak Dacite at Big Meadows Reservoir** (37°32.55' N., 106°47.86' W.; 9,170 ft, 2,795 m elevation).

The Pagosa Peak Dacite is an unusual pyroclastic deposit (perhaps globally unique) that immediately predated eruption of the enormous Fish Canyon Tuff (~5,000 km^3) from La Garita caldera at 28 Ma. The Pagosa Peak Dacite is thick (as much as 1 km), voluminous (~200 km^3), and has a high aspect ratio (1:50) similar to those of silicic lavas. It contains a large proportion (40–60 percent) of juvenile clasts (as large as 3–4 m) emplaced as viscous magma that was less vesiculated than typical pumice. Accidental lithic fragments are absent above the basal 5–10 percent of the unit. Thick densely welded proximal deposits flowed rheomorphically owing to gravitational spreading despite the high viscosity of the crystal-rich magma; this resulted in a macroscopic appearance similar to flow-layered silicic lava. Although a separate depositional unit, the Pagosa Peak Dacite is petrologically indistinguishable from the Fish Canyon Tuff and is interpreted as an eruption product from the same magma body.

The Pagosa Peak Dacite differs from other eruptive phases of the Fish Canyon magmatic system, and from other eruptive products of the San Juan volcanic field, by the presence of its unusual juvenile pyroclasts. These magmatic fragments are dense, low in vesicle fraction (commonly none), and subrounded to elliptical in shape. Fiamme-like interdigitations with the matrix are absent. The pyroclasts constitute a high proportion of the rock relative to matrix (~50 percent). The typical size range is 20–60 cm; many exceed 1 m, and some are 3–4 m in diameter. These parameters persist to distances greater than 5 km from the caldera margin (presumably even farther from their eruptive sources), and clasts <10 cm in diameter are a small minority. The Pagosa Peak Dacite fragments preserve primary magmatic textures, in contrast to the shattered crystal fragments and shard-pumice textures in the Fish Canyon Tuff.

We refer informally to these pyroclasts as magma blobs, to distinguish them from the rigid juvenile blocks characteristic of block-and-ash flows. The blobs are morphologically different from pumices in most silicic pyroclastic rocks, although similar lenticular fragments have been described in the Taylor Creek Rhyolite (Duffield, 1990). They have no relation to mafic enclaves resulting from magma mixing, for which the term "blob" is also sometimes applied. The Pagosa Peak blobs (fig. 140*A*) are fragments of dacitic Fish Canyon magma that are chemically indistinguishable from the matrix. Flattening ratios of less than 1:5 are rare for densely welded Pagosa Peak blobs, except where modified by rheomorphic flow. Even densely welded blobs commonly are subequant, although many are weakly elongate. Neither composite blobs nor evidence for incorporation of previously fragmented and welded material has been recognized. The subequant shapes of many blobs suggest limited compaction during welding, denoting relatively low vesicularity at the time of emplacement. The matrix (plus small blobs) does not compact differentially around larger blobs, even in densely welded units (fig. 140*B*), which indicates that primary porosity was comparable in both matrix and blobs. This is confirmed by microscopic observations that show mainly angular matrix fragments of dense glass and crystals, rather than bubble-wall shards. Matrix fragments are likely the products of mechanical abrasion during transport and (or) fracturing of high-viscosity magma in response to rapid magma acceleration in conduits. Weakly vesicular nonwelded Pagosa Peak Dacite deposits have been found at one basal locality, on Saddle Mountain, but the proportion of large dense magma clasts poses important questions about the mechanism of magma fragmentation during the Pagosa Peak Dacite eruption.

The unusual characteristics of this deposit have been interpreted as the consequences of eruption by low-column pyroclastic fountaining and lateral transport as dense, poorly inflated pyroclastic flows, possibly linked to concurrent and extremely rapid magma extrusion accompanied by explosions and gravitational collapse (Bachmann and others, 2000). The inferred eruptive style may be in part related to synchronous disruption of the southern margin of the Fish Canyon magma chamber by block faulting, with the creation of fissure-like vents (now lost to caldera collapse), but the lack of any other comparable unit in the modern or ancient record renders the modes of eruption and transport of Pagosa Peak Dacite magma a subject of speculation. Consider whether features of the Pagosa Peak Dacite could

Figure 140. Pagosa Peak Dacite at Big Meadow (Stop 5A-4). Outcrop textures of an indurated blob-and-ash-deposit that contains dense glassy magma blobs in a more finely comminuted matrix of similar composition. *A*, Blobs of dense nonfragmented dacite in a typical weathered, glaciated outcrop. Photograph by K.J. Turner, U.S. Geological Survey, 2016. *B*, Closer view of less-lichen-covered surface. Flattened pumice fiamme in matrix are not deflected around blobs, indicating uniform compaction deformation of both blobs and matrix. Outcrop located at the head of the valley, above Big Meadow. Photograph by P.W. Lipman, U.S. Geological Survey, ~1996.

indicate a different origin, perhaps exceptionally thick carapace breccia associated with a more conventional lava, or block-and-ash deposition resulting from flank failure of a growing lava dome? Any successful model for this system must explain numerous robust observations (Bachmann and others, 2002).

The Pagosa Peak Dacite is indistinguishable from the overlying Fish Canyon Tuff in bulk-rock chemistry, phenocryst compositions, and $^{40}Ar/^{39}Ar$ age, even though the eruptive mechanisms were different and the Pagosa Peak Dacite contrasts in many ways with the Fish Canyon Tuff. Although exposed growth faults that were active during emplacement of the Pagosa Peak Dacite are not associated with eruptive vents, vents may have been located along northern extensions of these faults, within the subsequent La Garita caldera, as erosional remnants of the Pagosa Peak Dacite are widely preserved along walls of the southern La Garita depression. We infer that collapse of La Garita caldera initiated at the southern end of the magma body, then propagated northward, as a resut of structural instability created by the withdrawal of the Pagosa Peak Dacite magma. The Fish Canyon Tuff was deposited without offset across growth faults that were active during the Pagosa Peak Dacite eruption. Existing observations are consistent with a short to negligible duration between the two eruptions (soils or sediments are absent at rarely exposed contacts), but no geologic or geochronologic constraints provide sufficient temporal resolution to quantify the time interval between them.

Petrologic summary.—The Fish Canyon magmatic system, including the Fish Canyon Tuff, the pre-caldera Pagosa Peak Dacite, and the post-caldera Nutras Creek Dacite, are interpreted to represent an erupted mush zone of dacitic/granodioritic composition (nearly identical to the bulk upper continental crust; Bachmann and others, 2002, 2007a). The mush zone was built by incremental recharge, likely over at least 0.5 m.y, as indicated by (1) zircon-crystallization histories (Bachmann and others, 2007b; Wotzlaw and others, 2013), and (2) the time gap since the previous caldera-forming event, the ~28.7-Ma Masonic Park Tuff, which occurred at the same area (its caldera is concealed by La Garita caldera, see discussion about type area in route 5B). The Fish Canyon Tuff magma reservoir clearly reached high crystallinity, but the warmest core likely remained above the solidus (with crystallinity perhaps as high as 70–75 percent; Wotzlaw and others, 2013), and was reactivated by hot recharge from below. The volcanic deposits that immediately followed the Fish Canyon Tuff are some of the most primitive of that eruptive cycle (Parat and others, 2005), and rare mafic enclaves, containing pyroxenes, occur in the late-erupted Fish Canyon Tuff (Bachmann and others, 2002). Although the mechanisms for mush reactivation that generate crystal-rich deposits are controversial (for example, Bachmann and Bergantz, 2003, 2006; Huber and others, 2009, 2010a,b, 2012; Gottsmann and others, 2009; Burgisser and Bergantz, 2011; Karlstrom and others, 2012), thermomechanical rejuvenation of a lock-up mush by heating, partial melting, and gas sparging following recharge seem the most likely processes to prepare the Fish Canyon magma reservoir for eruption (Parmigiani and others, 2014). This thermomechanical rejuvenation is thought to have occurred in the upper crust (~2–2.5 kilobars) and involved a reheating of a few tens of degrees, as recorded by multiple geothermobarometers (for example, Bachmann and Dungan, 2002).

Return toward South Fork by way of FS 410 to US 160. Turn left on US 160 and proceed northeast for 5.5 mi to the bridge over the South Fork Rio Grande and the junction with Park Creek road (FS 380). Turn right on Park Creek road and proceed up the valley. Fox Mountain road (FS 381) is on the right at 3.0 mi; at 3.8 mi is the intersection with Demijohn road (FS 361). Turn left on FS 361 and continue ~2.4 mi uphill to Stop 5-9. The road switchbacks through the upper part of the Fish Canyon Tuff, several andesitic lavas and flow breccias of the Huerto Andesite, then to the base of the Carpenter Ridge Tuff. Park along the road.

24.1 **Stop 5A-5. Welding and compositional variations in the Carpenter Ridge Tuff** (37°33.11' N., 106°41.27' W.; 9,908 ft, 3,020 m elevation).

Park vehicles and walk up the road through the section. The basal vitrophyre of the Carpenter Ridge Tuff, several meters thick here, is phenocryst-poor low-silica rhyolite (73 percent SiO_2, anhydrous); it grades downward, through partly welded gray tuff, to nonwelded white tuff (if not covered by slope wash). The abrupt contact between black vitrophyre and overlying tan devitrified rhyolitic tuff is a kinetic crystallization boundary. Gas cavities (lithophysae) several centimeters in diameter near the top of the glass zone were nuclei for devitrification that resulted in the growth of spherulites around the gas cavities. Outflow Carpenter Ridge Tuff commonly has a conspicuous lithophysal zone in the interior of the devitrified zone, but here they are developed atypically low in the section. Highly unusual complex gas cavities are present locally elsewhere in the Carpenter Ridge Tuff, especially where deposition in wet areas appears to have permitted interaction with external water (Lipman, 2018). The blotchy pale-tan exposures of devitrified Carpenter Ridge Tuff also are anomalously bleached and weakly argillically altered, in comparison to more typical light pinkish-brown rhyolitic Carpenter Ridge Tuff present nearby. The cause of alteration is unknown.

Either continue up the road on foot or drive 0.4 mi to the upper roadcuts of Carpenter Ridge Tuff (37°33.41' N., 106°41.13' W.). These exposures are more lithic and phenocryst-rich than previously observed lower in the section; they contain conspicuous dark scoriaceous fiamme (fig. 141), in addition to phenocryst-poor rhyolite pumices (Lipman, 1975a, p. 49–53; Whitney and others, 1988; Dorais and others, 1991). The scoriaceous fiamme have diverse andesitic compositions (54–63 percent $Si0_2$), are exceptionally high in barium (as much as 7,500 parts per million [ppm]), and are interpreted as documenting magma recharge and mobilization of a crystal-rich cumulate

Figure 141. A mafic alkalic scoria lens (Stop 5A-5), in the upper part of outflow Carpenter Ridge Tuff, Ribbon Mesa road. Photograph by P.W. Lipman, U.S. Geological Survey, 2016.

zone just prior to, or during, the Carpenter Ridge Tuff eruptions (Bachman and others, 2014).

Petrologic summary.—The Carpenter Ridge Tuff consists primarily of crystal-poor high-SiO_2 rhyolite, with a strong crystal fractionation signature (high Rb/Sr, low Ba, Zr, Eu), and is capped by a comparatively low-volume zone of crystal rich dacite (Mammoth Mountain Member). Upper parts of the Carpenter Ridge Tuff contain densely welded crystal-rich juvenile clasts of mostly trachydacitic composition (although more mafic clasts are present), with higher Fe-Ti oxide temperatures, and characterized by high Ba (as much as 5,000–7,000 ppm), Zr, Sr, and positive Eu anomalies.

The crystal-poor rhyolite (5–15 percent crystals), crystal-rich trachydacitic fiamme, and mafic clasts (~15–35 percent crystals) have the same mineral assemblage, and consist of plagioclase, sanidine, biotite, Fe-Ti oxides, and zircon. Some samples, particularly the crystal-rich fiamme, contain rare amphibole and pyroxene crystals. Quartz is absent in all samples (Whitney and others, 1988), although the magma is strongly quartz normative (as much as 20 percent). Crystals in the mafic clasts and trachydacitic fiamme are typically large and many have outlines of past resorption events.

Plagioclase is the dominant phase in all juvenile clasts; it is complexly zoned, and crystals vary from generally euhedral in the crystal-poor pumices and trachydacitic fiamme to more variable textures (including anhedral crystals) in the late-erupted mafic clasts. Plagioclase rims typically have low anorthite (An) content (An_{30} to An_{20}); interior zones are highly variable (from An_{30} to An_{70}), typically with anhedral shapes (Dorais and others, 1991; Bachmann and others, 2014). Similarly, strontium contents from plagioclase interiors in the rhyolitic pumices overlap with those in trachydacitic fiamme, but the rims of rhyolitic plagioclase tend to be lower in strontium for a given An-content compared to plagioclase from the fiamme. Some rims in the trachydacitic fiamme have high strontium, which indicates crystallization from a strontium-enriched melt. The broad overlap between plagioclase cores from trachydacite and rhyolite indicate that they both crystallized from a similar melt composition, but some mafic clasts are more anorthite-rich.

Sanidine crystals are present both as euhedral and highly embayed anhedral crystals (Whitney and others, 1988; Dorais and others, 1991), particularly in the trachydacite fiamme. The sanidines vary little in most major elements but are commonly strongly zoned in barium (both normal and reverse); sanidine is more enriched in barium in the trachydacitic fiamme than in the rhyolite (Whitney and others, 1988). Sanidines can be separated into three main groups (Bachmann and others, 2014): large crystals (>1.5 milimeters [mm]) that have low barium contents and can have both normal and reverse zoning; crystals intermediate in size (0.6–1.5 mm) that have moderate barium concentrations, are both normally and reversely zoned, and are present as both euhedral and resorbed crystals; and small crystals (<600 micrometers) that are rarely zoned and have the highest barium contents.

Biotite is the main ferromagnesian phase in the Carpenter Ridge Tuff and composes 1 to 2 percent of the modal assemblage. Crystals are typically euhedral; rare crystals are resorbed, particularly in the mafic clasts and trachydacitic fiamme. As with sanidine, biotite crystals are notably zoned in barium (Whitney and others, 1988; Dorais and others, 1991). BaO contents vary from below the detection limit to more than 4 percent (Bachmann and others, 2014). Magnetite and ilmenite occur as ubiquitous minor phases; rare amphibole (and clinopyroxene) are present in some trachydacitic fiamme. Magnetite exhibits a wide range of compositions (X_{Usp} = 0.2– >0.5), tending toward higher titanium contents in the trachydacitic fiamme than in rhyolitic pumices (Whitney and others, 1988). In contrast, ilmenite compositions are less variable (X_{Ilm} = 0.86–0.91; Whitney and others, 1988). Amphibole phenocrysts have higher Na_2O, K_2O, and concentrations than other trachydacites in the SRMVF; SiO_2 concentrations are distinctly lower (Dorais and others, 1991). The Carpenter Ridge amphiboles are, however, similar to pargasitic cores in magnesium-hornblende of the Fish Canyon Tuff (Bachmann and Dungan, 2002).

Fe-Ti oxide thermometry in Carpenter Ridge Tuff samples shows a range from ~750 to 810° C in the rhyolite and from ~850° to 1,000° C in trachytic fiamme (Whitney and others, 1988); pressures of crystallization were estimated at 100–200 MPa based on experimental phase equilibria (in particular, the absence of quartz in this high-SiO_2 magma; Whitney and others, 1988). New results using amphibole thermometry (from the trachyric fiamme), and the formulation of Ridolfi and others (2010), yield temperatures in the range of 930 to 955 °C, higher than most coexisting Fe-Ti oxides. Amphibole barometry (also using Ridolfi and others, 2010), yields pressures from 280 to 320 MPa (10–12 km depth, assuming an average density of 2,800 kilograms per cubic meter for the crust). This suggests that hornblende may have crystallized at greater depths than the rest of the mineral assemblage, although pressures from the Ridolfi and others (2010) calibration should be used with caution (Erdman and others, 2014).

Much of the major and trace-element variation in the Carpenter Ridge Tuff can be reproduced through in-situ differentiation by interstitial melt extraction from a crystal-rich upper-crustal mush zone, the trachydacitic inclusions being the erupted crystal-cumulate complement to the high-SiO_2 rhyolite. The

thermal and chemical zonation in the deposits resulted from eruption of the crystal-poor cap and a small portion of its cumulate counterpart, after remobilization by a late recharge event that reheated and partly melted the crystalline assemblage to the point where it was eruptible (less than ~50 percent crystals). The late recharge material appears to be sampled by late-erupted mafic clasts, although these clasts also show some mineral accumulation (Bachmann and others, 2014).

Return to Park Creek road (FS 380) and retrace the route to US 160. Turn right (east) and proceed 7.3 mi to South Fork. The intersection of US 160 and CO 149 in South Fork is the start of route 5B.

End of route 5A; continue on to route 5B.

Route 5B—Eastern La Garita, Bachelor, and Creede Calderas: South Fork to Creede

The main foci of this trip segment are the eastern topographic margins of several calderas of the central complex, the nature of the unconformities along caldera walls and contacts with intracaldera rocks, and the contrasts been proximal outflow and intracaldera ignimbrites.

0.0 *Junction of US 160 and CO 149 at South Fork (8,169 ft, 2,490 m elevation). Turn west on CO 149 and follow the main Rio Grande valley toward Creede* (figs. 142, 143). The valley follows several major faults of the Rio Grande graben system. As a result, the welded tuffs on the southwest side are entirely Fish Canyon Tuff, but on the northeast side the lower two-thirds of the slope is Masonic Park Tuff, capped by Fish Canyon Tuff. The Rio Grande graben is among several extensional fault systems that are peripheral to the central caldera complex and interpreted as responses to modest late uplift above a solidifying subvolcanic batholith centered beneath the calderas (Steven and Lipman, 1976).

3.0 Type locality of the Masonic Park Tuff. Compound cooling in the Masonic Park Tuff, on the right, is shown by alternating ledges and benches all within a single ignimbrite sheet. The Masonic Park Tuff is more than 250-m thick in this area, with no base exposed, yet it does not resemble a typical caldera-filling tuff in degree of welding or alteration. Some pre-existing depositional basin seems required, perhaps a topographically low area between older Conejos volcanic edifices. The Masonic Park Tuff, the first large ignimbrite erupted from the central San Juan caldera cluster, is present widely around the southern margin of La Garita caldera (see fig. 92); its caldera and a similarly obscure source for the younger Blue Creek Tuff are now concealed by younger subsidence structures, perhaps in the vicinity of South River caldera.

Petrologic summary.—The Masonic Park Tuff is a crystal-rich (~45 volume percent) dacitic ignimbrite that was erupted ~28.7 Ma (Lipman and others, 1996; Lipman, 2000, 2006). Bulk-rock compositions appear relatively homogeneous (mostly

Figure 142. Rio Grande valley between South Fork and Creede; San Juan travel can be time consuming! Photograph by P.W. Lipman, U.S. Geological Survey, 2011.

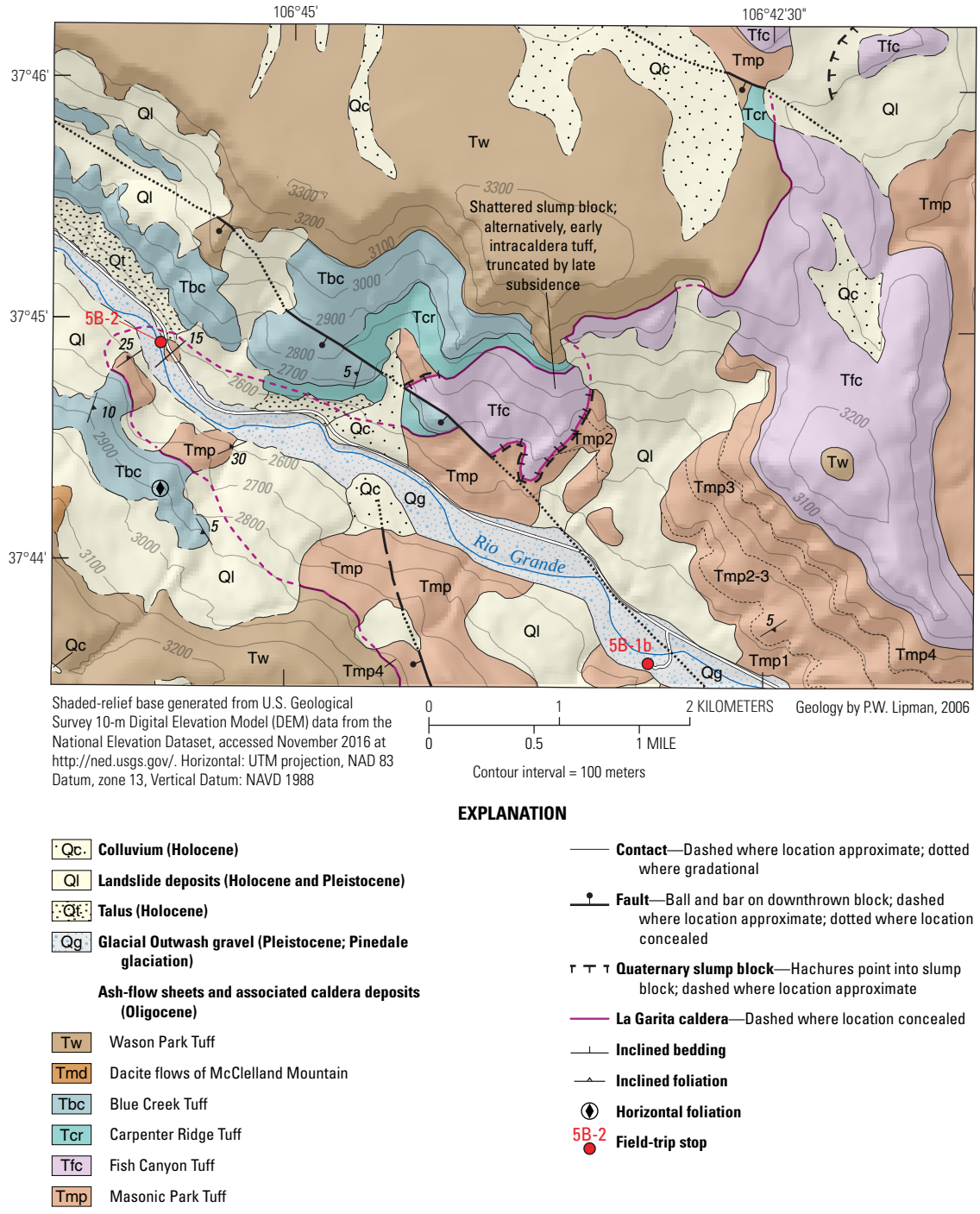

Figure 143. Geologic map of Rio Grande canyon, showing the eastern margin of La Garita caldera (modified from Lipman, 2006).

~62–65 percent SiO_2), but as pumice fragments are typically too small to analyze as whole-rock samples, some chemical variations are likely the result of eruption and emplacement processes. The Masonic Park Tuff crystal cargo includes plagioclase, pyroxene, biotite, Fe-Ti oxides, apatite, and zircon set in a high-SiO_2 (dominantly devitrified) rhyolitic shard matrix that contains plagioclase microlites and is characterized by significant variations in trace elements. Plagioclase is the most abundant mineral (~27–43 modal percent, present both as phenocrysts and microlites) and is characterized by pronounced An-rich spikes near rims. Biotite (5–9 modal percent) is the most abundant ferromagnesian phase, followed by clinopyroxene (<2–3 modal percent). As for plagioclase, clinopyroxene shows some reverse zoning (increase in MgO towards the rims).

The absence of quartz and sanidine, despite an evolved groundmass composition and the reverse zoning in plagioclase and clinopyroxene, suggest reheating of an upper-crustal mush (rejuvenation) in response to recharge from below (Sliwinski and

others, 2017). High strontium, barium, and titanium concentrations in plagioclase microlites and phenocryst rims require in situ melting of sanidine (plus quartz) and concurrent limited mass addition by the recharge, likely as a melt-gas mixture. Experimental phase diagrams for such dacitic compositions suggest that the pre-eruptive temperatures must have been above ~825 ºC for water-rich magma at upper-crustal conditions. However, to stabilize sanidine and quartz, the temperature must have dropped to ~750 °C, indicating pre-eruptive reheating of a few tens of degrees.

Comparison with Fish Canyon Tuff.— Eruption of the Fish Canyon Tuff followed the Masonic Park Tuff eruption by ~700,000 years. With an erupted volume 10 times greater, it completely buried the Masonic Park Tuff source caldera. Although these two ignimbrites are both crystal-rich calc-alkaline dacites, they differ in mineral assemblages; the Fish Canyon Tuff contains sanidine, quartz, amphibole and titanite, but lacks clinopyroxene, has less biotite, and is devoid of plagioclase microlites. The Fish Canyon Tuff is also slightly more silicic and potassic than the Masonic Park Tuff (average 68 percent SiO_2 and 4.1 percent K_2O versus 63 percent SiO_2 and 3.5 percent K_2O, respectively) and evolved to a lower temperature (~710–760 °C, Bachmann and Dungan, 2002) than the ~800–850 °C for the Masonic Park Tuff. Water contents in the magmas have not been estimated precisely, as glassy melt inclusions are unavailable in these densely welded devitrified tuffs, and the recent plagioclase hygrometer calibration (Waters and Lange, 2015) has not been applied to these rocks. The presence of multiple hydrous phases in the Fish Canyon Tuff and its lower temperature than the Masonic Park Tuff suggest that the Fish Canyon evolved under slightly more water-rich conditions. Alternatively, the Fish Canyon Tuff magma may have resided slightly deeper (higher water solubility), although total pressure estimates are insufficiently reliable for the Masonic Park Tuff to evaluate this.

Despite their different volumes, mineralogy, and possibly water contents, the upper-crustal Fish Canyon and Masonic Park Tuff magma bodies or mush zones both underwent reheating and mechanical reactivation prior to eruption as indicated by (1) highly resorbed (Fish Canyon Tuff) or totally dissolved (Masonic Park Tuff) sanidine and quartz; and (2) reverse zoning in phenocrysts, most obviously in plagioclase and amphibole for the Fish Canyon Tuff (Bachmann and Dungan, 2002; Bachmann and others, 2002; Sliwinski and others, 2017) but also detectible in pyroxene (Masonic Park Tuff). For both magma bodies, we infer that the rejuvenation event was triggered by a mafic recharge event that brought heat, volatiles, and some melt (but little to no crystalline debris) to these upper-crustal crystal mushes (Bachmann and Bergantz 2003, 2006).

The differences in plagioclase compositional profiles between the Masonic Park and Fish Canyon Tuffs (that is, the presence of ubiquitous sharp An-rich spikes at the rims of most plagioclase phenocrysts in the Masonic Park Tuff in comparison to the more gradual rimward An increase in the Fish Canyon Tuff plagioclase) suggest that the rejuvenation event was shorter and more intense for the Masonic Park Tuff. In comparison, the Fish Canyon Tuff underwent a progressive increase in temperature over an extended time interval, estimated to be as much as $>10^5$ years based on zircon geochronology and zircon trace-element chemistry (Wotzlaw and others, 2013). A more sudden reawakening of the Masonic Park Tuff is consistent with its smaller size, which allowed a typical lower-crustal recharge event to have more impact on temperature and crystal content of the dacitic mush than for the gigantic Fish Canyon Tuff. It is also possible that the highest crystallinity reached by the Masonic Park Tuff at the coldest point of its evolution was less than that of the Fish Canyon Tuff (estimated at ~75 percent crystals; Wotzlaw and others, 2013), making it energetically less costly to rejuvenate.

3.7 **Stop 5B-1a. Rio Grande canyon: La Garita and Creede caldera walls, Masonic Park Tuff** (37°42.91’ N., 106°41.69’ W.; 8,317 ft, 2,535 m elevation).

Pull off on right, by the Rio Grande National Forest entry sign, for a view of the eastern topographic wall of La Garita caldera and stratigraphic relations between ignimbrite sheets (fig. 143). The eastern topographic wall descends the broad side valley ahead to the northwest. On the caldera rim above, Fish Canyon Tuff forms the uppermost major columnar-jointed cliff and rests on thick Masonic Park Tuff that shows compound cooling of alternating welded ledges and less welded benches. To the west, three younger ignimbrite sheets are ponded within La Garita caldera (fig. 144*A*).

High along the distant ridge crest, thick columnar-jointed Wason Park Tuff that ponded within the caldera wedges out against the Fish Canyon Tuff, at about the same elevation as the similar columnar jointing in this tuff that caps the nearer ridge. Beneath the Wason Park Tuff, another thick dacitic ignimbrite sheet with multiple welding zones, the Blue Creek Tuff, wedges against the petrologically similar Masonic Park units. The Blue Creek is another phenocryst-rich silicic dacite that contains 25–45 percent phenocrysts of plagioclase, biotite, and augite—petrographically similar to the adjacent Masonic Park Tuff. Both ignimbrites are also characterized by crude layering, owing to the combined effects of compound cooling and subtle internal flow-unit discontinuities. At this site and farther northwest toward Creede, the Blue Creek Tuff was long confused with the dacitic Mammoth Mountain Member of the Carpenter Ridge Tuff (Ratté and Steven, 1967; Steven and others,

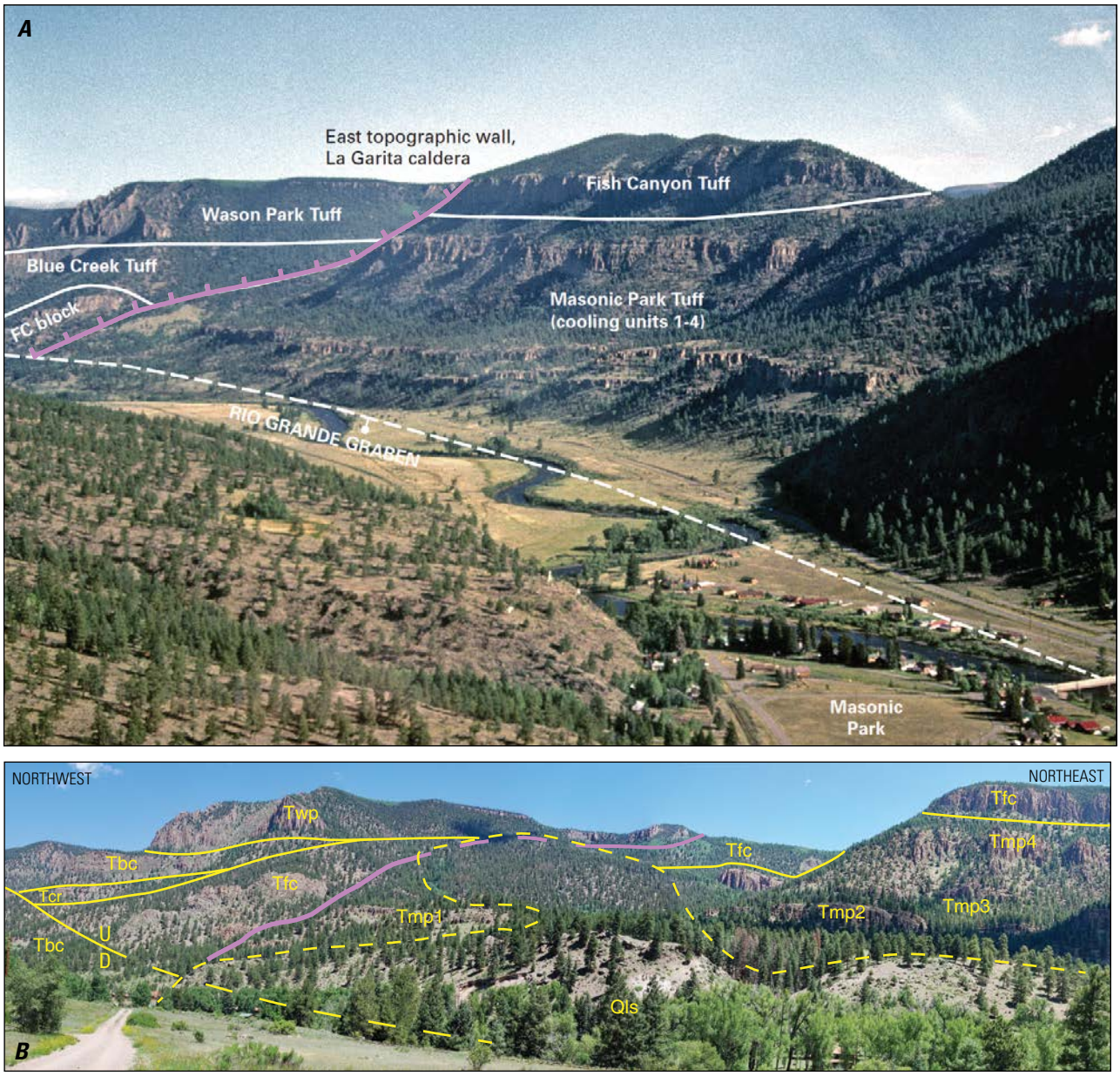

Figure 144. East topographic wall of La Garita caldera. *A*, Oblique aerial view, along Rio Grande canyon between South Fork and Creede. Multiple cooling units of flat-lying Masonic Park Tuff and proximal outflow of Fish Canyon (FC) Tuff are truncated by the caldera wall to the west (Stop 5B-1a). Caldera fill includes a slump block of Fish Canyon Tuff, and the depositionally overlying Blue Creek, Carpenter Ridge (not labeled), and Wason Park Tuffs that wedge out against the caldera wall. View to the northwest. Photograph by P.W. Lipman, U.S. Geological Survey, ~1995. *B*, Eastern margin of La Garita caldera, as viewed from Coller State Wildlife area (Stop 5B-1b). A side valley, north of the Rio Grande, exposes the La Garita caldera wall, which is defined by an unconformable contact (purple line). Precaldera rocks on the east rim include multiple welding zones within thick Masonic Park Tuff (Tmp1, Tmp2, Tmp3, Tmp4), overlain by columnar-jointed Fish Canyon Tuff (Tfc). Within La Garita caldera, younger ignimbrites are banked against the caldera-margin unconformity, which dips to the northwest oblique to the photo view. Thick columnar-jointed Wason Park Tuff (Twp) on the skyline, at the same elevation as Fish Canyon Tuff (Tfc) to the east, overlies Blue Creek Tuff (Tbc), a crystal-rich dacite that closely resembles the Masonic Park Tuff in megascopic appearance and in composition. A thin wedge of Carpenter Ridge Tuff (Tcr) underlies the Blue Creek Tuff and banks unconformably against a rib of shattered Fish Canyon Tuff that is interpreted as a slumped mass derived from the higher outcrops of this ignimbrite on the rim to the east. The Blue Creek Tuff is dropped down along a bounding fault of the Rio Grande graben. The distant perspective of Wason Park Tuff lapping against Fish Canyon Tuff, up the side valley to the north, is complicated by foreshortening, causing the Fish Canyon Tuff on the skyline at the valley head to misleadingly appear stratigraphically lower than the closer-in Fish Canyon Tuff cliff at the right side of the image. Much of the foreground along the caldera margin is occupied by landslide deposits (Qls). Panoramic photo montage by M.A. Dungan, University of Oregon, 2015.

1974b; Lipman and others, 1989), but the presence of a basal vitrophyre at this site and elsewhere, as well as the absence of sanidine phenocrysts, demonstrate that it is a discrete ignimbrite sheet (Lipman, 2000). Underlying the Blue Creek, though difficult to see from this vantage, is a thin lens of rhyolitic Carpenter Ridge Tuff, which provides tight age control on the timing of the caldera-wall unconformity in this side valley (post-Fish Canyon Tuff, before emplacement of Carpenter Ridge Tuff). Perched anomalously lower along the caldera wall, a shattered lens of outflow Fish Canyon Tuff, ~1 km across and interpreted to have slumped part way down the La Garita wall during collapse (figs. 143, 144), is an additional, critical piece of evidence of caldera-wall complexity.

In addition to La Garita caldera, the east wall of Creede caldera is visible up the canyon to the west. The large cliff-forming lava dome at Wagon Wheel Gap is within Creede caldera (Stop 5B-5), where it is draped across diverse rocks of the caldera wall, including Carpenter Ridge and Wason Park Tuffs and associated lavas that ponded within La Garita caldera. In addition, a small remnant of the southeast side of Bachelor caldera is preserved in this area (Stop 5B-4).

A short walk up the alluvial fan to the north provides access to the lowest outcrops of Masonic Park Tuff, including abrupt depositional breaks between variably sorted ignimbrite layers defined by changes in crystal content and pumice size. Do these layers record the deposits of successive distinct pyroclastic-flow units, or alternatively, are they a result of varied depositional dynamics during essentially continuous eruption and deposition?

Continue ahead, up canyon on CO 149 and proceed to Stop 5B-1b for an exceptional distant view of the La Garita caldera wall or proceed to Stop 5B-2 for a roadside contact of the caldera-wall unconformity. To reach Stop 5B-1b proceed 1.5 mi on CO 149 to the Coller State Wildlife Area; turn left onto NFS 430 and proceed across the bridge and railroad tracks for 0.5 mi up the valley to the "Y" road junction; park on the right.

5.7 **Stop 5B-1b (additional perspective). La Garita caldera wall, as viewed from Coller State Wildlife Area** (37°43.75' N., 106°43.31' W.; 8,333 ft, 2,540 m elevation).

Although lacking the up-canyon perspective of Creede caldera seen at Stop 5B-1a, this stop provides a closer cross-sectional view of the topographic margin of La Garita caldera along the side canyon to the north (fig. 144*B*). The caldera wall dips only moderately westward, as marked by the rib-like shattered block of Fish Canyon Tuff. Thick Blue Creek Tuff (dropped down and repeated as a lower cliff by a major fault of the Rio Grande graben) banks against the La Garita topographic wall but is nowhere preserved beyond it to the east. Exposures of the Blue Creek Tuff are confined within the La Garita and Bachelor calderas, a relation that captures the enormous scale of the central San Juan caldera complex. Caldera sources for the Carpenter Ridge Tuff, Blue Creek Tuff, and five younger large-volume ignimbrites of the central caldera cluster all lie entirely within La Garita caldera, essentially constituting postcollapse volcanoes within this enormous caldera. Contrast these volumetric relations with the scale of postcollapse domes and pyroclastic units in Valles Caldera.

Return to CO 149; turn left (northwest) and proceed 3.1 mi to Stop 5B-2.

8.8 **Stop 5B-2. La Garita caldera wall and Masonic Park Tuff** (37°44.88' N., 106°45.60' W.; 8,481 ft, 2,585 m elevation)**.** *The road-cut exposure at the prominent bend is Masonic Park Tuff within the reentrant on the La Garita caldera wall. Climb to the top of the road embankment to better see outcrop exposures to the north.*

An obscure bench about 75 m above road level marks the basal contact of the younger Blue Creek Tuff against Masonic Park Tuff that is interpreted as marking the La Garita caldera wall. The greenish-gray groundmass color of the Masonic Park, in contrast to the pinkish-brown groundmass of the Blue Creek, is locally distinctive, as is a somewhat higher augite content in Masonic Park Tuff. The contact is not exposed upslope, although blocks of Blue Creek vitrophyre are present as float and document the presence of a depositional unconformity and cooling break, as does the absence of any intervening Fish Canyon or Carpenter Ridge Tuff. The La Garita wall, along which Masonic Park Tuff is obliquely buried by caldera-filling Blue Creek Tuff, can also be followed along conspicuous topographic breaks on the north-facing canyon-wall slopes of McClelland Mountain, across the Rio Grande. This northwest-trending reentrant, which exposes Masonic Park Tuff, may mark the transition from central to northern segments along the east wall of the composite La Garita caldera (fig. 125).

Continue up canyon on CO 149 and pass the Palisade Campground turnoff. Watch for closer views of the Creede caldera wall and the Wagon Wheel Gap lava dome just inside this caldera (fig. 145). Proceed 1.7 mi to Stop 5B-3. Park carefully on the wide shoulder along the south side of the highway (eastbound lane); watch out for highway traffic!

10.5 **Stop 5B-3. Caldera moat lake-bed sediments** (37°45.74' N., 106°47.16' W.; 8,497 ft, 2,590 m elevation).

The tan to gray, finely laminated volcanic sediments exposed here beneath the Blue Creek Tuff have been interpreted as lacustrine beds (Lake La Garita) within the eastern La Garita caldera moat (Steven and Lipman, 1976; Lipman and others, 1989, p. 334). Alternatively, they may be younger deposits (Lake Bachelor) at a high level against the eastern topographic margin of Bachelor caldera, as perhaps indicated by the absence of any Carpenter Ridge Tuff beneath the directly overlying Blue Creek Tuff. At the westernmost exposures, the lake beds appear to be intruded by a texturally variable dacite, in which compositional boundaries and discontinuities in columnar jointing indicate several phases of emplacement. The intrusive dacite may have been a feeder for the thick lavas (volcanics of McClelland Mountain) that overlie Blue Creek Tuff higher on the canyon walls and were erupted prior to the ridge-capping Wason Park Tuff. These flows, and others in similar stratigraphic position, are candidates for postcaldera eruptions from the caldera source of the Blue Creek ignimbrite that is inferred to lie concealed beneath Creede caldera to the west.

Continue up canyon (northwest) for 0.7 mi on CO 149 to Blue Creek. (Entering the Creede 15-minute quadrangle). Park on the wide shoulder on the left (riverside); walk to the large roadcuts west of Blue Creek Lodge. Please don't block access to lodge!

11.2 **Stop 5B-4. Bachelor caldera wall at Blue Creek** (37°46.16' N., 106°47.85' W.; 8,415 ft, 2,565 m elevation).

To the northeast, across Blue Creek (fig. 145), is the thick type section of the Blue Creek Tuff, ponded in the La Garita caldera moat. Early in the era of modern ignimbrite studies, this section was the target of a detailed petrographic study by James Ratté, when it was still considered correlative with the dacitic Mammoth Mountain unit northeast of Creede (Ratté and Steven, 1967, p. 27–33). Ahead is the Wagon Wheel Gap lava dome, on the wall of the 26.87-Ma Creede caldera.

Low in Blue Creek valley and on poorly exposed slopes above to the west, are key volcanic deposits that document the presence of a segment of the Bachelor caldera wall. These units truncate older rocks, and in turn are cut off by the topographic wall of Creede caldera (fig. 145). The lowermost small cliffs along the west side of lower Blue Creek are Masonic Park Tuff, somewhat fractured and altered, but having coherent moderately dipping pumice-compaction foliations that indicate the absence of major structural disruption (*you must obtain permission from Blue Creek Lodge before going up Blue Creek road to examine outcrops*). The relation of these exposures to La Garita caldera is unclear. If they are in the original depositional location, the Masonic Park outcrops must also lie outside the embayed east wall of La Garita caldera, perhaps indicating an even more pronounced reentrant between the central and northern caldera segments than implied by the features noted at Stop 5B-2. The westward dips (15–25°) in the Masonic Park exposures, in contrast to near-flat attitudes in the Blue Creek and younger tuffs across the valley to the east, suggest a possible origin by down-slope slumping along the east wall of La Garita caldera.

In contrast, on the less well-exposed slopes above the outcrops of Masonic Park Tuff, but below the rugged cliffs of the Wagon Wheel Gap lava dome, brecciated masses of outflow Fish Canyon Tuff (as much as 100 m across) are accompanied by smaller blocks of Masonic Park Tuff and some andesitic lava, all lacking stratigraphic or structural coherence. These are interpreted as landslide megabreccia that slid down the wall of the Bachelor caldera. A diagnostic feature is the local presence of nonwelded crystal-poor rhyolitic tuff between blocks; this matrix is interpreted as intracaldera Carpenter Ridge Tuff (too crystal-poor to be from the Fish Canyon eruption).

The roadcuts immediately ahead along CO 149 (fig. 146) provide a limited sampling of relations among these caldera-fill landslide breccias. Despite mild alteration, the resorbed quartz phenocrysts in the Fish Canyon are distinctive and diagnostic in comparison with other phenocryst-rich silicic dacites, such as the Masonic Park Tuff, in this part of the volcanic section. The age of the deposit is bracketed as synchronous with eruption of Carpenter Ridge Tuff by the abundant blocks of Fish Canyon Tuff, the presence of crystal-poor rhyolitic tuff matrix, and the absence blocks of Wason Park Tuff despite its presence capping ridges east of Blue Creek.

11.8 Small road-cut exposures of tan crystal-poor ignimbrite ahead on the right (north), surrounded by talus from the overlying Wagon Wheel Gap lava dome, are typical densely welded rhyolite of the Carpenter Ridge Tuff that contains only sparse small lithic fragments within or near the megabreccia zone. Where voluminous tuff could accumulate distant from large adjacent cold blocks from the caldera wall, sufficient heat was retained to permit typical welding and devitrification textures. *Continue ahead on CO 149 toward River Springs Resort and Wagon Wheel Gap (8,448 ft, 2,575 m elevation).*

Ahead to the south is a view of the Bachelor caldera fill along the ridge crest that forms the divide between the Rio Grande and its Goose Creek tributary (fig. 145). Relations between several caldera-collapse megabreccia lithologies within the compositionally zoned intracaldera Carpenter Ridge Tuff are exceptionally exposed. A detailed guide to field relations is in Lipman and others (1989, Stop 5). *Access to this ridge is on private land*

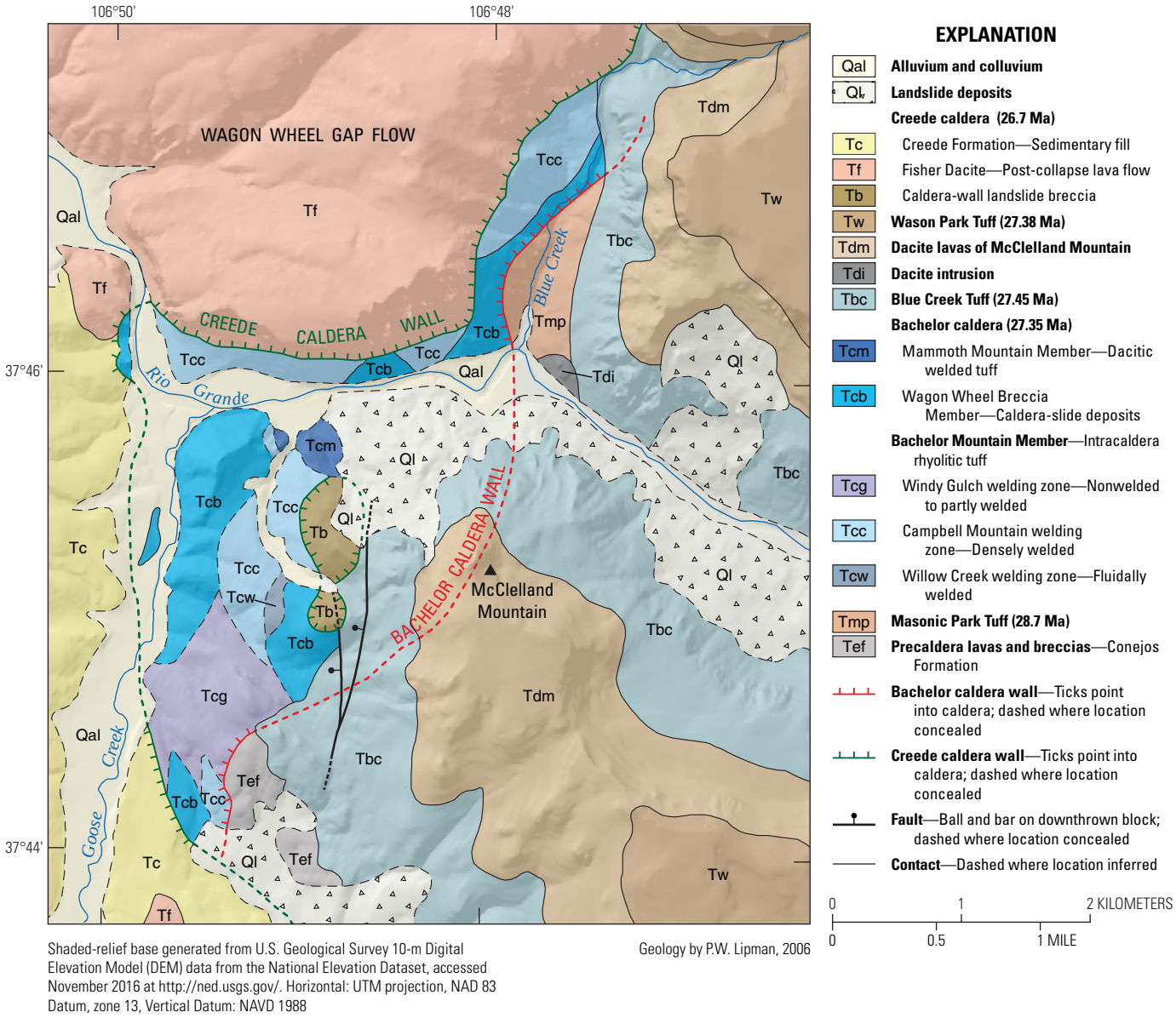

Shaded-relief base generated from U.S. Geological Survey 10-m Digital Elevation Model (DEM) data from the National Elevation Dataset, accessed November 2016 at http://ned.usgs.gov/. Horizontal: UTM projection, NAD 83 Datum, zone 13, Vertical Datum: NAVD 1988

Geology by P.W. Lipman, 2006

Figure 145. Generalized geologic map of Blue Creek area (Stop 5B-4), showing the margin of Bachelor caldera near Wagon Wheel Gap (Lipman, 2006). Complexly varying facies of intracaldera Carpenter Ridge Tuff (Bachelor Mountain Member) and interleaved landslide breccias (Wagon Wheel Breccia Member) lap out against this caldera wall and cut into precaldera lavas and breccias overlain by the Masonic Park and Fish Canyon Tuffs. Bachelor caldera and its fill were covered by younger units (Blue Creek and Wason Park Tuffs). All of these were then truncated by the Creede caldera wall and its fill of Snowshoe Mountain Tuff, landslide breccia, dacitic lava, and volcaniclastic sediments.

Figure 146. Bachelor caldera wall as seen at Blue Creek, view to the east. In the foreground, large chaotic shattered blocks of Masonic Park and Fish Canyon Tuffs, seamed by a nonwelded matrix of crystal-poor rhyolitic Carpenter Ridge Tuff, are interpreted as a landslide breccia deposit derived from east wall of Bachelor caldera. Distant cliffs, across the valley, are the type locality of the Blue Creek Tuff (here ~250-meters thick), overlain at the skyline by dacitic lava of McClelland Mountain. The Blue Creek Tuff, overlying lavas, and Wason Park Tuff (beyond view) are thickly ponded in the combined eastern moats of Bachelor and La Garita calderas. Photograph by K.J. Turner, U.S. Geological Survey, 2016.

and advance permission is required to examine these deposits.

Ahead, through Wagon Wheel Gap, is the resurgent dome of Snowshoe Mountain Tuff within Creede caldera. The Snowshoe Mountain Tuff is another fairly uniform phenocryst-rich dacite (monotonous intermediate), erupted at 26.87±0.02 Ma as indicated by multiple $^{40}Ar/^{39}Ar$ dates (Lipman and McIntosh, 2008).

Continue ahead to roadcut outcrops of dacite lava on the right.

13.6 **Stop 5B-5. Wagon Wheel Gap lava dome** (37°46.40' N., 106°49.81' W.; 8,743 ft, 2,665 m elevation). *Pull over at the National Forest viewpoint on the left.*

Ahead, the present valley defines the exhumed topographic moat of Creede caldera, where caldera-filling lacustrine sediments of the Creede Formation, deposited between the resurgent dome and the caldera wall, have been eroded by the Rio Grande (fig. 145). Farther upriver, the north-northwest wall of the Creede caldera forms the skyline. The Rio Grande has cut through the flank of the Wagon Wheel lava dome, a unit of the Fisher Dacite dated by $^{40}Ar/^{39}Ar$ at 26.85 Ma (biotite, Lanphere, 1988). Similar porphyritic silicic dacite makes up most of the postcollapse Fisher lavas that blanketed the southern margin of the Creede caldera. Note ramp structures in the Wagon Wheel Gap lava dome, where it rides up to the southwest on sediments of the Creede Formation (fig. 147).

Continue north on CO 149 toward Creede to Stop 5B-6a. Pull off to the left, into the parking area by the spring.

15.3 **Stop 5B-6a. East wall of Creede caldera, from the spring at the mouth of McKinney Gulch** (37°47.54' N.; 106°51.40' W.; 8,514 ft, 2,595 m elevation)**.**

Across the Rio Grande valley, the steep slopes to the northeast define the morphologically well-preserved inner wall and topographic rim of Creede caldera, as exhumed during the last few million years by erosion of the weakly indurated yellowish moat-fill sediments of the Creede Formation (fig. 148). The northeast wall, as dissected by Bellows and Farmers Creeks, exposes several ignimbrites erupted from the central caldera complex, mainly intracaldera facies of the zoned Carpenter Ridge Tuff (Bachelor Mountain Member, Mammoth Mountain Member, and intertongued landslide breccias) and then the Blue Creek and Wason Park Tuffs and interlayered lavas. Farther south is the northern margin of the large Wagon Wheel Gap flow

Figure 147. A spectacularly flow-layered dacite (Stop 5B-5), displaying upturned ramp structures, that possibly reflect cooling and increased viscosity as the lava flowed into Lake Creede along the caldera moat or in proximity to the resurgent dome across the valley. Photograph by P.W. Lipman, U.S. Geological Survey, ~1985.

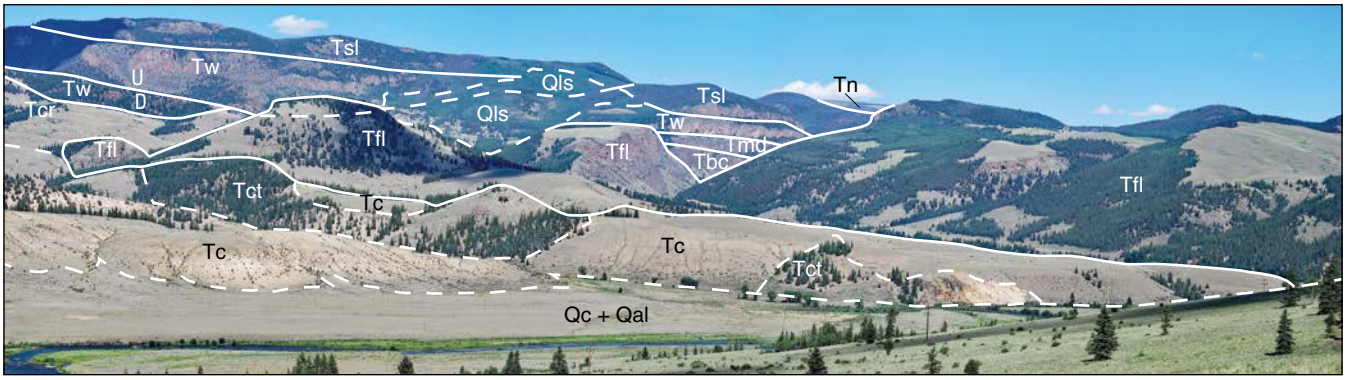

Figure 148. The eastern margin of Creede caldera (Stop 5B-6a), as viewed from low on the northeast flank of the Snowshoe Mountain resurgent dome (powerline access trail south of Deep Creek road). The large Wagon Wheel Gap flow of Fisher Dacite (Tfl) is banked against the Creede caldera wall, onlapped by caldera-moat lacustrine sediments (Tc) and warm-spring travertine deposits (Tct) of Creede Formation in the foreground. Diverse volcanic units on the distant cliffs (Tbc, Blue Creek Tuff; Tcr, Carpenter Ridge Tuff (intracaldera); Tmd, dacite lavas of McClelland Mountain; Tw, Wason Park Tuff; Tsl, dacite lavas of Silver Park; Tn, Nelson Mountain Tuff) define the Creede caldera wall, although they are repeated by a sizable longitudinal fault (largely covered beneath landslide deposits and roughly at the projection of the concealed southwest-trending margin of Bachelor caldera, not plotted on figure). Apparent unit thicknesses are somewhat deceptive, as a function of distance from the camera. The valley of the Rio Grande in the foreground is occupied by alluvium and colluvium (Qal, Qc); large landslide deposits (Qls) drape parts of the caldera wall. Panoramic photomontage by M.A. Dungan, Univ. Oregon, 2015.

of Fisher Dacite (Stop 5B-5) that spread down the east caldera wall.

Today's route has now traversed the exposed margins of La Garita, Bachelor, and Creede calderas. The latter two are nested within the middle of three subdepressions formed by collapse of La Garita caldera and eruption of the Fish Canyon Tuff. The northern margin of South River caldera (Wason Park Tuff) lies buried beneath Creede caldera, just south of Wagon Wheel Gap. Although nowhere exposed, the caldera sources for the Blue Creek and Masonic Park Tuffs are not far from our present position. A cumulative total of ~15 km of composite subsidence has been inferred beneath Creede caldera owing to repeated nested caldera formation that commenced with the Masonic Park eruption (fig. 16 in Lipman, 2000). The immensity of the central San Juan caldera complex is highlighted by the distant view of the La Garita Mountains to the north from this stop, even though only a small fraction of La Garita caldera is visible. With the resurgent dome of Creede caldera at our backs, we are near the core of the central complex, but are able to view less than 10 percent of the La Garita collapse depression. The skyline of the La Garita Mountains profiles the resurgent block of the northern La Garita caldera, which is truncated by the northeastern wall of Bachelor caldera, and against which multiple post-Carpenter Ridge units are banked. These include the Wason Park Tuff and younger ignimbrites from the San Luis caldera (Rat Creek, Cebolla Creek, and Nelson Mountain Tuffs).

Proceed northwest on CO 149 for 2.4 mi to the junction with Deep Creek road (FS 550). Turn left and proceed west on Deep Creek road for 2.1 mi to the intersection with an unnamed dirt road that heads southwest. Drive 0.1 mi up the hill and park near the frontier graveyard at the base of the trees for a panoramic view to the north.

19.9 **Stop 5B-6b. Overview of northern Creede caldera and the central San Juan caldera complex: Travertine knob at Deep Creek** (37°48.83' N., 106°54.88' W.; 8,743 ft, 2,665 m elevation). *View from the parking area. Continue on foot up the trail and climb to the top of the hill for an improved view to the north.*

This is one of many travertine knobs (fossil warm-spring deposits) that intertongue with the lake sediments of the Creede Formation that fill the caldera moat (fig. 130*A*). The bounding ring fault of the Creede caldera is inferred to lie concealed beneath the moat fill to the north. The resurgent dome of Creede caldera makes up most of Snowshoe Mountain to the south. The crest of the dome is broken by keystone graben faults that follow Deep Creek, the major north-south drainage that transects the caldera. The composite section of Snowshoe Mountain Tuff exposed on the resurgent dome is ~1.5-km thick, with no base exposed (Steven and Ratté, 1965). Most outflow Snowshoe Mountain Tuff has been eroded; the only sizeable preserved areas are weakly welded tuffs along hill crests south of South Fork and smaller remnants along the Continental Divide southwest of Creede caldera (Lipman, 2006).

From the travertine knob the view to the northeast includes the La Garita Mountains on the skyline. The La Garita Mountains, on the Continental Divide (high point: 13,710 ft, 4,179 m), are the resurgent core of the northern La Garita caldera, the earliest of the central San Juan caldera cluster, and expose more than 1.2 km of intracaldera Fish Canyon Tuff (La Garita Member), with the top eroded and the base concealed.

The view directly north, toward the town of Creede, is into the resurgent core of Bachelor caldera, the second collapse structure of the central caldera complex, here exposed in cross section on the north wall of the younger Creede caldera (fig. 149*A*) The fill of Bachelor caldera consists largely of variably welded rhyolitic tuff, long designated the Bachelor Mountain Rhyolite or tuff, but later recognized as the intracaldera equivalent to rhyolitic outflow Carpenter Ridge Tuff (Lipman and others, 1970; Steven and Lipman, 1976). For nearly a century, the Bachelor Mountain has been divided into the Willow Creek, Campbell Mountain, and Windy Gulch subunits (Emmons and Larsen, 1923). Once thought to constitute discrete eruptive deposits, they are welding zones within the thick rhyolitic fill of Bachelor caldera (Lipman and others, 1989; Lipman, 2000). In the center of Bachelor caldera, they define a crude stratigraphic succession, becoming less welded upward, but near the caldera margins the welding zones alternate and interfinger complexly (fig. 128). Welding reversals are also conspicuous near large landslide-breccia deposits from the caldera wall, which interfinger with the caldera-filling tuff. The Willow Creek zone, the lowermost exposed fill of Bachelor caldera, is an extremely welded, phenocryst-poor fluidal rhyolite that is generally purplish gray in color and shows evidence of secondary flowage during emplacement. The Campbell Mountain zone differs from the Willow Creek zone in that it has less intense welding, a reddish color, and generally contains more abundant lithic fragments. The Windy Gulch zone is a light-gray, non- to weakly welded porous rhyolitic tuff that is widely silicified and otherwise altered. All the welding zones were variably compositionally modified by later potassium metasomatism (Ratté and Steven, 1967; Sweetkind and others, 1993).

The structure of the Bachelor resurgent dome is well displayed from this vantage (fig. 149*B*). The Willow Creek drainage, directly ahead to the north, roughly follows the apical keystone graben (Creede graben) of Bachelor caldera. Structures of the Creede graben were reactivated recurrently following eruptions from Creede and San Luis calderas, and these faults localize the main epithermal mineralization of the Creede mining district.

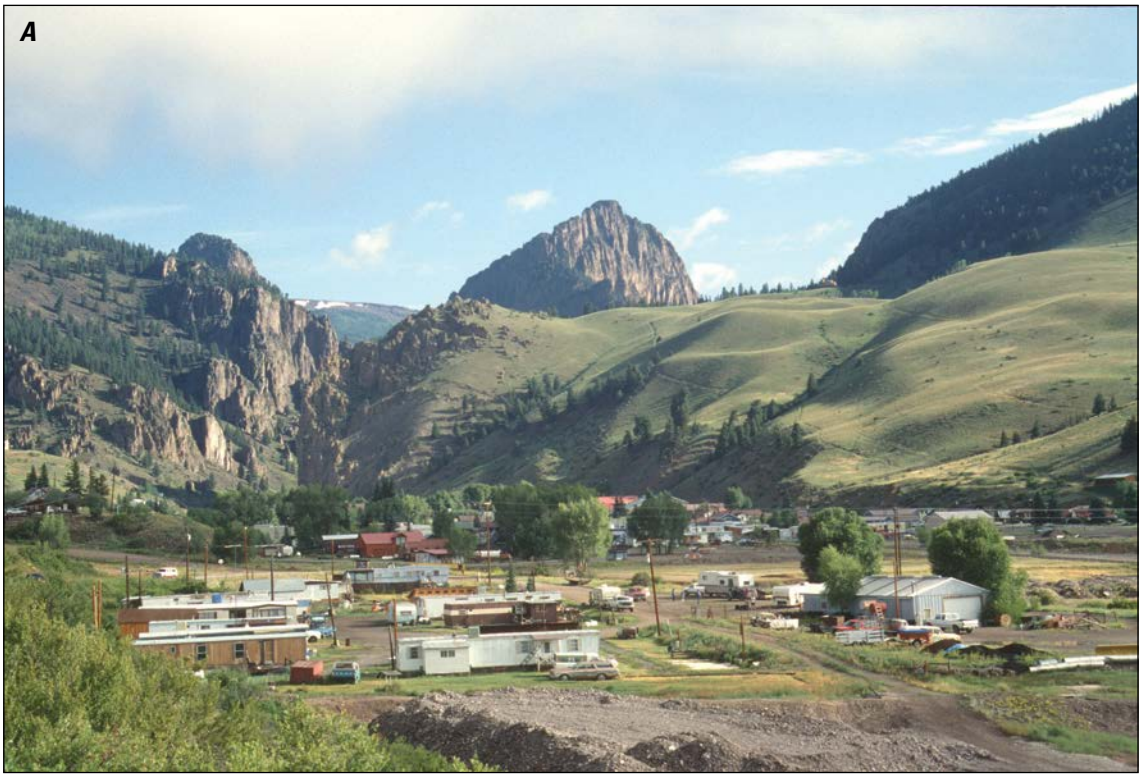

Figure 149. North wall and structures of Creede caldera. *A*, North topographic wall of Creede caldera, defined by cliffs of intracaldera Carpenter Ridge Tuff (Bachelor Mountain Member), viewed from south of the town of Creede. Geographic Nelson Mountain (snow patches) is on skyline, at the head of the valley. Photograph by Peter Lipman, U.S. Geological Survey, 2016. *B*, Map showing the major structures of the Creede district and sites of the 1991 drill holes for the Continental Scientific Drilling Program (modified from Bethke and Lipman, 1987).

The cliffs to the east of Willow Creek are fluidal rhyolite (Willow Creek welding zone) of the Bachelor Mountain Member; the unit grades upward abruptly into a thin Campbell Mountain zone, which is present above the cliffs as talus. The eastern vein-fault of the Creede graben, the Solomon-Holy Moses vein, runs along the east side of Campbell Mountain, the ridge between the forks of Willow Creek (fig. 149*B*). The Amethyst vein, which was most productive during early mining in the district, runs N. 20° W. along West Willow Creek, through Bachelor Mountain. The Amethyst Fault dips west and accommodates most of the normal displacement on the east side of the graben. West of the Amethyst Fault, Wason Park Tuff that ponded within the older Bachelor caldera is dropped against the Campbell Mountain and Willow Creek zones. The trace of the

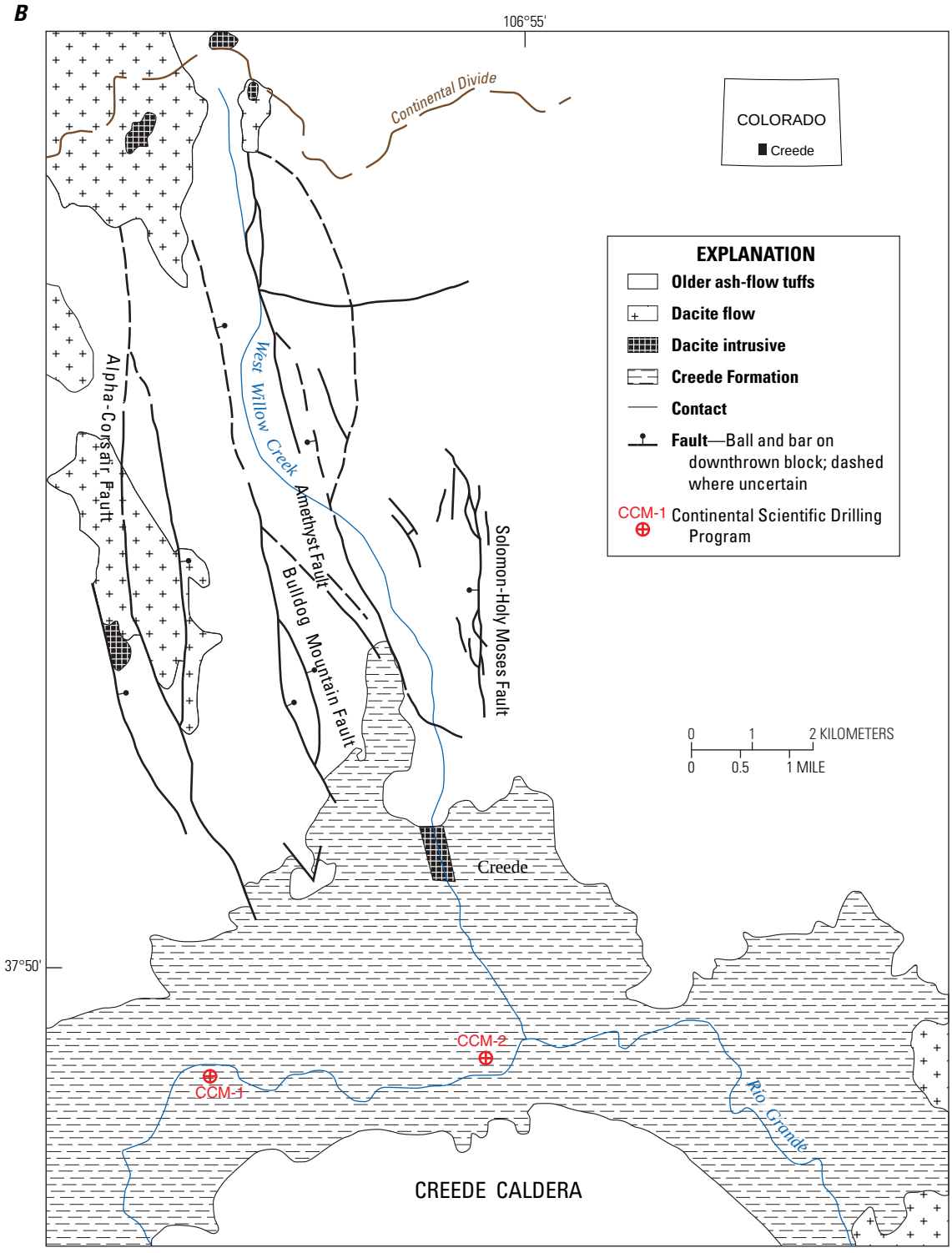

Figure 149.—Continued

east-dipping Bulldog Fault and vein, on the west side of the Creede graben, passes through Bulldog Mountain, the gently rounded hill just west of Windy Gulch. In the late 20th century the Bulldog Mine (Homestake Mining Corp.), located along this structure at the base of Windy Gulch, was especially productive. Farther west (east of Miners Creek), the Alpha-Corsair Fault and vein form the west boundary of the Creede graben.

The distant sawtooth-shaped peak just visible far to the north is San Luis Peak (14,012 ft, 4,271 m elevation), the high point on the resurgently uplifted trapdoor block within the San Luis caldera complex. Thus, parts of four calderas are in sight: La Garita, Bachelor, San Luis, and Creede. Two sites of the Continental Scientific Drilling Program (CSDP), for drilling 0.6–1 km through the Creede Formation in the moat of the caldera, are also within view (fig. 149*B*). One is near the airport, aligned with the Creede vein system; the other is several kilometers farther west. This drilling, undertaken in the fall of 1991, was intended to evaluate the connate-fluid environment of mineralization at depth in the Creede sediments (Bethke and Lipman, 1987; Bethke and Hay, 2000). The high salinities in fluid inclusions from the ores are a distinctive signature for the fluid component inferred to have been derived from the lake sediments and provide a basis for fluid-flow modeling not possible in mining districts where the fluid components are less distinct compositionally. In addition, the moat drill holes provide a record of postcaldera volcanic events; air-fall tuffs, late-erupted ignimbrite deposits, and caldera-collapse landslide deposits are interbedded with the moat sediments (Hulen, 1992; Heiken and others, 2000). At greatest depth, the caldera-moat drill holes penetrated into the top of the Snowshoe Mountain Tuff and provided critical controls on the geometry and history of caldera subsidence.

Return to Deep Creek road, turn right and proceed east. In 0.3 mi turn left on Airport road (FS 806) toward Creede. Cross the Rio Grande bridge and continue north, past the airport.

21.3 *Rejoin CO 149. Bear right to Creede.* Exposures on the left are lacustrine deposits of the Creede Formation that show soft-sediment deformation. The Emperius Mill site on the left processed ore from the Amethyst-OH vein, yielding the tailings ahead on the right. Much effort has been expended on stabilization and remediation in recent years. The newer Bulldog Mountain mine and Homestake mill site are up the hill to the left.

Entering Creede (8,839 ft, 2,694 m elevation). Continue on CO 149 westbound through town on South Main Street (fig. 150). Proceed through town where North Main Street intersects County Rd 503 (FS 503), to canyon of Willow Creek. At the canyon mouth, the portal on the left is the town firehouse! Rocks along the creek are part of the intracaldera Willow Creek welding zone of the Bachelor Mountain Member (fig. 150).

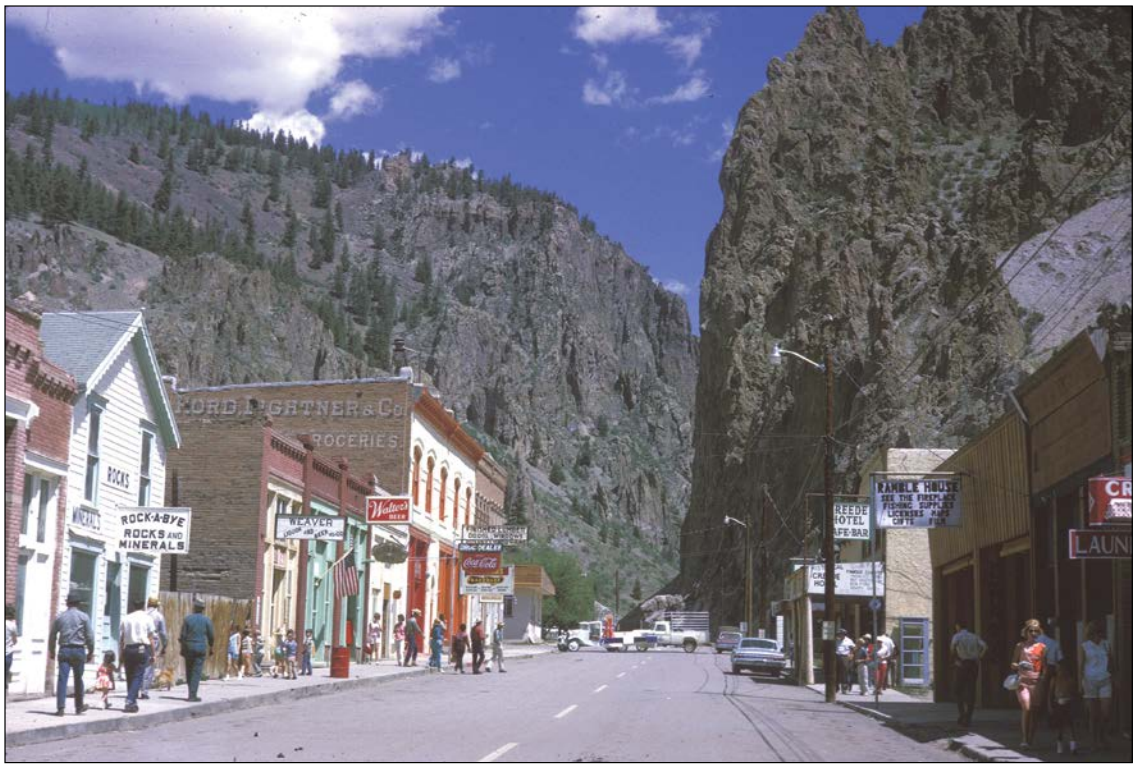

Figure 150. The town of Creede; cliffs in the background (intracaldera Carpenter Ridge Tuff, Willow Creek welding zone) form the north wall of Creede caldera. Photograph by P.W. Lipman, U.S. Geological Survey, ~1987.

22.4 *Junction of East and West Forks of Willow Creek. Bear left to stay in West Fork.* On the left are the foundations of the old Humphrey's Mill. Note strong brecciation and sheet jointing in outcrops of the Willow Creek welding zone.

Proceed 0.5 mi up hill; park along road shoulder.

22.9 **Stop 5B-7. Creede vein system: Commodore 5 level** (37°52.14' N., 106°55.64' W.; 9,203 ft, 2,805 m elevation).

The Commodore 5 level was the main haulage on the Amethyst-OH vein system (fig. 149*B*). The Commodore 4 and Commodore 3 levels are marked by buildings higher on the vein (fig. 151). The Amethyst vein is an epithermal silver-lead-zinc deposit that filled the Amethyst Fault at about 25 Ma (Steven and Eaton, 1975; Wetlaufer and others, 1979; Bethke and Rye, 1979; Barton and others, 2000). During caldera resurgence at about 27.5 Ma, rhyolitic tuffs of the Bachelor Mountain Member were faulted and brecciated while they were still hot and plastic along an ancestral Amethyst Fault Zone. The Creede graben was reactivated about 2.5 m.y. later, along the same general trends as the ancestral Amethyst, after eruptions from Creede and San Luis calderas (Steven and Ratté, 1965; Bethke and others, 1976). The Amethyst Fault strikes N. 15–20° W., as is typical of Creede graben structures, and dips 50–70° SW. The Willow Creek zone of the Bachelor Mountain Member foms most of the footwall; Campbell Mountain zone makes up higher parts of the hanging wall. Some major northwest-trending splays, such as the OH vein (fig. 149*B*), were also strongly mineralized. The Amethyst vein is bounded above by a clay cap and is little exposed at the surface, although sediments of the Creede Formation are mineralized near the Commodore 3 level.

Retrace the route south, to the forks of Willow Creek. Turn east over the bridge and park along the wide shoulder on the right.

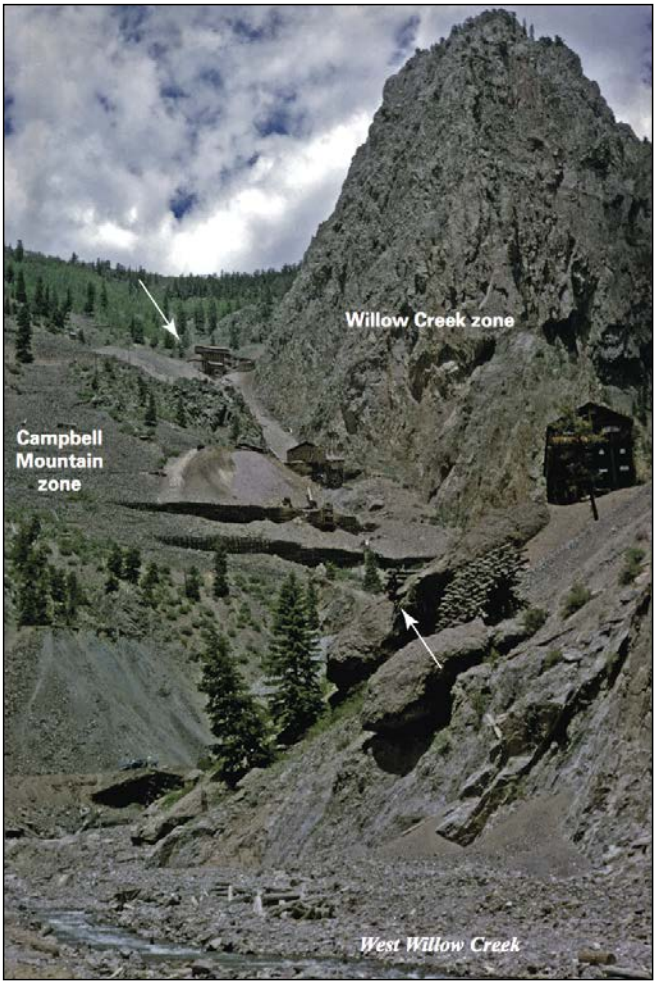

Figure 151. The Amethyst vein (Commodore 5 level) in the Creede mining district (Stop 5B-7). The vein follows a fault (arrows, mine workings) that downdrops Campbell Mountain zone of the intracaldera Carpenter Ridge Tuff (on west) against the Willow Creek zone. Fault control of the vein is inherited from the keystone graben of the resurgent dome within Bachelor caldera, but the mineralization is younger than Creede caldera. West Willow Creek, view northwest. Photograph by P.W. Lipman, U.S. Geological Survey, ~1997.

23.4 **Stop 5B-8. Willow Creek welding zone, junction of East and West Willow Creeks** (37°51.89' N., 106°55.48' W.; 8,973 ft, 2,735 m elevation).

The Willow Creek zone shows near-lava-like fluidal structures owing to extreme compaction and flowage of pumice. Pumice fiamme commonly have elongation ratios of 20–30:1; some exceed 100:l (figs. 4–7 in Ratté and Steven, 1967). In places, elongate pumices also define a flowage lineation in the plane of foliation. The foliation orientations are somewhat variable in attitude at this site but are typically steeper than 40°. Dips decrease up-section, and most are only 10–20° at the top of the cliffs east of East Willow Creek. Such decreases in dip up-section characterize all thick sections of the intracaldera Bachelor Mountain Member and indicate deformation during compaction, prior to completion of the intracaldera pyroclastic accumulation. The overall geometry of this deformation may be related to the inception of resurgent doming.

Locally, the pumice foliation of the Willow Creek zone is swirled and folded, and in places this fluidal rhyolite has been rheomorphically mobilized into discordant diapirs that penetrate the overlying Willow Creek and Campbell Mountain zones. These rocks were once mapped as intrusive rhyolite of the Bachelor Mountain Member (Steven and Ratté, 1965, 1973), but foliations grade from gently dipping to vertical and collapsed pumice textures are still locally discernible in the steeply dipping diapiric tuff. These relations

were exceptionally exposed in now-inaccessible workings of the Bulldog Mine. The rheomorphic tuff is spatially associated with faults of the Creede graben and indicate initial graben faulting at Bachelor caldera while the intracaldera tuff was still hot and plastic. Continued movement along the graben faults caused early brecciation of the tuff, especially along rheomorphic zones.

Return to FS 503 and continue north up East Willow Creek, following route 5C, or turn and retrace the route south for 1.4 miles, past town of Creede to Bachelor road (FS 504). Turn right (west) and proceed 2.5 miles up hill to the panoramic viewpoint just before crossing Windy Gulch.

27.3 **Stop 5B-9. Panoramic view of resurgent Creede caldera (**37°51.67' N., 106°56.63' W.; 9,908 ft, 3,020 m elevation).

At this stop, we are looking south toward Snowshoe Mountain (11,192 ft, 3,411 m elevation), the high point on the resurgent dome, surrounded by a topographically low moat followed by the Rio Grande, which has excavated tuffaceous sediments and lake beds of the Creede Formation (fig. 152). The flanks of Snowshoe Mountain are dip slopes of as much as 45° in the 26.87-Ma Snowshoe Mountain Tuff. Below is the town of Creede and the Bulldog Mountain mine. In the far distance is Fisher Mountain (12,858 ft, 3,919 m elevation), capped by late postcaldera lavas (27.77-Ma) of Fisher Dacite. The entire northern half of the Creede caldera wall is visible, extending from Bristol Head Mountain (12,706 ft, 3,873 m elevation) on the west (to right of fig. 152), through the north wall where we are standing, around to the east at Wagon Wheel Gap. The Wagon Wheel Gap lava dome is the site of Stop 5B-4. In the far distance southeast is North Mountain (12,723 ft, 3,411 m elevation; too distant to show clearly in fig. 152), at Summitville, which consists of thick dacite flows and shallow intrusions (as young as 20.7 Ma) adjacent to the northern margin of Platoro caldera (Day 4). In the far distance to the southwest is Baldy Mountain (12,488 ft, 2,806 m elevation), the top of a thick lava/breccia pile of Huerto Andesite that filled the southwest La Garita caldera. The drainage of Deep Creek on the north side of Snowshoe Mountain, too distant to show clearly in figure 152, follows the down-dropped keystone graben on the crest of the Snowshoe Mountain dome. The large outcrops on the Bachelor caldera wall, to the east, are the Willow Creek zone of the Bachelor Mountain Member, which represents a small part of the thick intracaldera accumulation of the Carpenter Ridge Tuff within Bachelor caldera.

Return downhill to the town of Creede.

End of route 5B.

Figure 152. Creede caldera, as viewed from its north wall (Stop 5B-9), along Bachelor road near Windy Gulch, looking south. Baldy Mountain (elevation 12,488 feet [ft], 3,806 meters [m]) is on southwest wall; Wagon Wheel Gap is at east wall. Fisher Mountain (elev. 12,865 ft, 3,921 m) is a sequence of postcaldera lavas (Fisher Dacite) on the south wall. Snowshoe Mountain is high point on the resurgently uplifted caldera floor, defining a symmetrical dome of intracaldera Snowshoe Mountain Tuff, with a keystone graben outlined by northward drainages and with flanks dipping as steeply as 45° (Steven and Ratté, 1965). The Rio Grande flows into the caldera moat from the west, arcs around the north side of the resurgent dome, and exits at Wagon Wheel Gap. The river has preferentially eroded weakly indurated moat-fill sediments of the Creede Formation, exhuming much of the Oligocene caldera morphology. The town of Creede is in the lower left of the image. Photograph by P.W. Lipman, U.S. Geological Survey, ~1997.

Route 5C—Interior of Bachelor Caldera, San Luis Caldera Complex: Willow Creek Loop

This northerly route provides three-dimensional perspectives of depositional and welding complexities in thick intracaldera Carpenter Ridge Tuff, views of the northeast wall of Bachelor caldera where it truncates resurgently uplifted intracaldera Fish Canyon Tuff in the La Garita Mountains, access to the south side of the San Luis caldera complex, and a panoramic 180° view of Creede caldera (connecting with Stop 5B-9).

0.0 *Starting at the forks of Willow Creek (Stop 5B-8), continue up East Willow Creek (FS 502).* Note the closely spaced sheet jointing in the Willow Creek zone. From the town of Creede to approximately 1 km north of the junction of East and West Willow Creeks, the Bachelor Mountain Member is strongly brecciated. This brecciated area is bounded on the north by an area of vertically sheet-jointed Willow Creek zone. The structural significance of the complex joint patterns in this area remains poorly understood; the joints probably reflect overlapping events, including compaction and cooling of the thick Bachelor caldera fill, resurgence of Bachelor caldera, truncation by Creede caldera, and subsequent continued movement and mineralization along the Creede graben.

0.7 Sheeted Willow Creek zone is distorted in a series of sigmoidal folds (fig. 5 in Steven and Ratté, 1965). Entering San Luis Peak 7.5-minute quadrangle.

1.7 South end of dump at Ridge mine; Solomon mine just above. The East Willow Creek drainage follows the Solomon-Holy Moses fault system, which defines the eastern margin of the Creede graben.

2.3 **Stop 5C-1. First Fork: Caldera slide breccia and Bachelor caldera fill** (37°53.60' N., 106°54.74' W.; 9,662 ft, 2,945 m elevation). *Pull off on the sidetrack to the right.*

The high cliffs directly ahead and on the right are intracaldera Carpenter Ridge Tuff and show a well-defined compositional zonation from phenocryst-poor rhyolite that has unaltered magmatic alkali ratios (formerly described as the rhyolitic Mammoth Mountain Tuff of Ratté and Steven, 1967) upward into more crystal-rich silicic dacite of the Mammoth Mountain Member (Lipman, 2000). The highest exposures are Wason Park Tuff (fig. 153). The general topics of this stop are the complex depositional, compositional, and welding variations in the intracaldera Carpenter Ridge Tuff between this area and Wagon Wheel Gap (fig. 128).

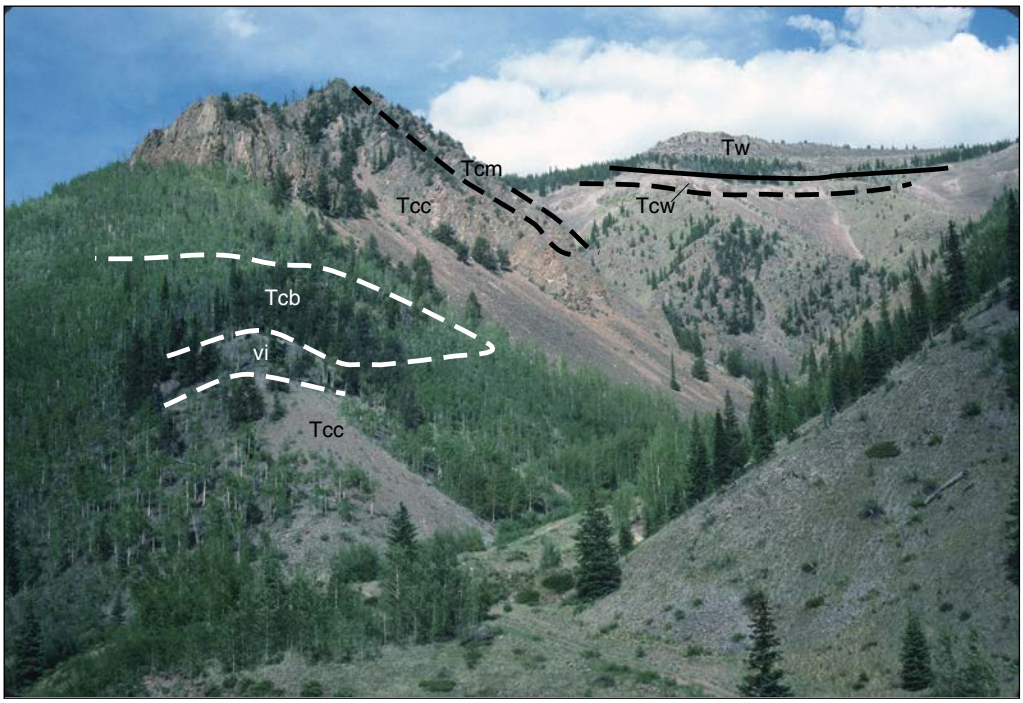

Figure 153. The First Fork section (Stop 5C-1), showing complex welding, crystallization, and compositional zonation of Carpenter Ridge Tuff within the Bachelor caldera. Units of the Carpenter Ridge Tuff: Tcc, rhyolitic Campbell Mountain zone; Tcb, Phoenix Park megabreccia unit (landslide blocks of intracaldera Fish Canyon Tuff derived from the La Garita Mountains on the northeast caldera wall); Tcm, dacitic Mammoth Mountain Member; Tcw, weakly welded rhyolitic Windy Gulch zone; vi, vitrophyric tuff where Campbell Mountain zone quenched against overlying landslide blocks of Phoenix Park unit; Tw, Wason Park Tuff. Photograph by P.W. Lipman, U.S. Geological Survey, 2016.

The lower slopes of the ridge north of First Fork that lead up to a conspicuous dark-gray outcrop are the main features that can readily be examined. Cross the stream and climb to the top of this outcrop, noting textural and compositional changes. Observe the gray to brown devitrified tuff of the Campbell Mountain zone that has undergone alkali exchange (potassium metasomatism) just across the stream. The dark-gray glassy outcrop and the overlying blocks of reddish-brown phenocryst-rich tuff were previously mapped as the Phoenix Park Member of the La Garita Tuff (Emmons and Larsen, 1923; Steven and Ratté, 1965, 1973). This unit was been interpreted as one of several late ash flows of Fish Canyon type from La Garita caldera that were thought to interfinger with and overlie the Bachelor Mountain Member in this area.

The Phoenix Park units, rather than being primary ignimbrite deposits, are now interpreted as landslide breccias derived from the northeast wall of Bachelor caldera (La Garita Mountains) during subsidence (Lipman and others, 1989; Lipman, 2000). Do you see the evidence for such an interpretation in these outcrops? Note the phenocryst types and abundance in the vitrophyre zone. Is the vitrophyre part of the Bachelor Mountain or the Phoenix Park unit? Keep in mind that upper vitrophyres are rare in ignimbrite sheets. How does the degree of welding change upward? Can you find matrix of crystal-poor rhyolitic tuff surrounding clasts of oxidized reddish crystal-rich tuff? These slide breccias are analogous to those at Stop 5B-4 (Wagon Wheel Gap megabreccia member), except that here the Fish Canyon blocks were derived from the thick intracaldera tuff on the resurgent dome rather than from the outflow sheet on the caldera rim. Cooling against the slide breccias caused the local reversal in welding and crystallization zones within the Bachelor Mountain Member. As a further challenging complexity for early studies of this area, before processes of ignimbrite emplacement and welding were well understood, the gray Campbell Mountain welding zone below this lid-breccia layer has undergone alkali exchange (increase in potassium, decrease in sodium), but the reddish-brown zone above the breccia retains near-magmatic alkali ratios.

Across valley to the west is the south end of the dump from the Outlet Tunnel mine. The cliffs on the left, above the mine, are Willow Creek zone; the juxtaposition with Campbell Mountain lithologies in First Fork is due mainly to the northeastward dip of these welded tuffs as a result of resurgence of Bachelor caldera. The Outlet Tunnel mine is the type locality for another named unit of Fish Canyon type, the Outlet Tunnel Member of the La Garita Tuff as mapped previously (Emmons and Larsen, 1923; Steven and Ratté, 1973). The rocks of Fish Canyon lithology are exposed there only in one small outcrop at creek level and in the now inaccessible mine workings. These previously were correlated with the main mass of intracaldera Fish Canyon Tuff in the resurgent dome of La Garita caldera to the northeast and were interpreted as part of the floor of the Bachelor caldera (Steven and Ratté, 1965). All the Outlet Tunnel rocks are now interpreted as landslide and talus breccia of Fish Canyon Tuff, similar to the mapped Phoenix Park breccia lenses higher in the caldera-fill section, and all derived from the Bachelor caldera wall during subsidence. The Outlet Tunnel unit, thus, has no stratigraphic significance, nor does any evidence exist for Bachelor caldera floor in this area. In addition, all previously mapped Fish Canyon (La Garita) Tuff, for 4 km up East Willow Creek from the Outlet Tunnel mine, is landslide and talus debris within Bachelor caldera, rather than in-place fill of La Garita caldera. Steven and Ratté noted the talus-breccia character of some of these rocks but did not recognize their relation to formation of Bachelor caldera nor map the boundary between the slide and talus breccias versus coherent intracaldera Fish Canyon Tuff.

Higher on this ridge, the Phoenix Park breccias are overlain at the base of the rugged cliffs by vitrophyric crystal-poor rhyolite, previously mapped as rhyolitic Mammoth Mountain Tuff (Steven and Ratté, 1965). Elsewhere within Bachelor caldera, where landslide-breccia units are absent, no vitrophyre or cooling break is present along mapped contacts between Bachelor Mountain Member and rhyolitic Mammoth Mountain lithology. Such contacts are marked only by a color change and decreased intensity of potassium metasomatic alteration (to be examined at Stop 5C-3). Accordingly, the term Mammoth Mountain Member is used only for the phenocryst-rich silicic dacitic upper part of the section. At First Fork, the silicic dacite unit is only about 25-m thick and is overlain by additional crystal-poor rhyolitic uppermost tuffs, but the thickness of the silicic dacite increases to the south, reaching 150–175 m along Farmers and Bellows Creeks. The silicic dacite wedges out northward, beyond First Fork, and the upper rhyolitic tuff wedges out southward (fig. 128); these lateral changes may reflect differing vent locations for rhyolite and dacite or changing depositional slopes within the caldera owing to differential subsidence.

The overall distribution of the Mammoth Mountain Member and the significance of large local variations in composition and thickness are not yet fully understood. Several aspects of this distribution, along with decreased amounts of tilt upward in the section, suggest that the Mammoth Mountain may have been deposited during initial phases of resurgent uplift, causing ponding of the silicic dacite in the moat between the resurgent dome and topographic wall of the caldera. Other features of the compositional gradients may be a result of fluctuations in discharge rate during the eruption, permitting varying drawdown and ephemeral cones of depression that crossed compositional boundaries in a layered or zoned body of eruptible magma.

Return to vehicles; continue up East Willow Creek.

2.9 Crossing East Willow Creek, in geographic Phoenix Park (9,705 ft, 2,958 m elevation). Follow the road up onto Campbell Mountain. Workings of the Phoenix Park mine are ahead on the right. *Park along road (37°53.78' N., 106°55.15' W.); walk ~328 ft (100 m) back (east) down the side trail to the overlook.*

4.1 **Stop 5C-2. View northeast, toward La Garita Mountains on skyline** (37°53.80' N.; 106°55.10' W.; 10,499 ft, 3,200 m elevation).

The La Garita Mountains consist entirely of intracaldera Fish Canyon Tuff on the resurgent dome of La Garita caldera (fig. 154). The southwestern third of this resurgent dome caved away during the collapse of Bachelor caldera, and the wedge-out of layered units on the gentle slopes at the base of the La Garita Mountains (geographic Wason Park; 11,730 ft, 3,575 m elevation) marks the top of the fill preserved within the moat of Bachelor caldera. Flat-topped cliffs, at the timberline to the north, are geographic Nelson Mountain (12,090 ft, 3,685 m elevation), the type locality for the Nelson Mountain Tuff. The section on the southeast shoulder of Nelson Mountain contains good exposures of compositionally zoned Nelson Mountain and Rat Creek Tuffs, erupted from the San Luis caldera complex to the north.

Continue up the road.

4.3 Road crosses a flat saddle underlain by Campbell Mountain member. Ahead to the left, jeep trail leads to Campbell Mountain, the type locality for the Campbell Mountain zone of the Bachelor Mountain Member. Continue ahead to Nelson Creek.

4.9 **Stop 5C-3. Nelson Creek crossing: Features of potassium metasomatism** (37°53.95' N., 106°55.58' W.; 10,466 ft, 3,190 m elevation).

The Campbell Mountain zone is intermittently exposed along roadcuts to the south for the next 0.2 mi, and the boundary with rocks formerly mapped as rhyolitic Mammoth Mountain Tuff (Steven and Ratté, 1973) crosses the road near this point. Collect a piece of Campbell Mountain zone for reference. Walk back uphill along the road, examining color and textural changes in welded rhyolitic tuff for about 150 m, to the first sharp curve east. The changes in color from purplish gray to tan, with accompanying textural changes, have previously been used to locate contacts between the Campbell Mountain and Mammoth Mountain units (Emmons and Larsen, 1923; Steven and Ratté, 1965). Despite the incomplete exposures, it should be clear that there is no significant decrease in welding or the development of a vitrophyre zone, such as characterize normal cooling-unit breaks between separate welded

Figure 154. View of La Garita Mountains (Stop 5C-2), as viewed to the northeast from the ridge between East Willow and Whited Creeks. These highlands, reaching 13,710 feet (ft) (4,180 meters [m]) at La Garita Peak the in center of the photograph, are the resurgently uplifted core of the north segment of La Garita caldera, associated with eruption of the Fish Canyon Tuff at 28.02 Ma. The resurgent La Garita block caved away on its south side by collapse of the Bachelor caldera at 27.55 Ma. The entire south slope of La Garita Peak, down to 10,200 ft (3,110 m) along East Willow Creek, consists of a single cooling unit of intracaldera Fish Canyon Tuff (La Garita Member) in an aggregate section more than 1-kilometer thick, with no base (caldera floor) exposed. Photograph by P.W. Lipman, U.S. Geological Survey, ~1974.

ignimbrite sheets or where the crystal-poor rhyolite overlies the Phoenix Park slide breccia (Stop 5C-1). Instead, the color change reflects decreased potassium metasomatism and other alteration in intracaldera rhyolite of the Carpenter Ridge Tuff. Indeed, interpretive problems with this contact were noted long ago (Emmons and Larsen, 1923, p. 43–44).

In places, altered intracaldera Carpenter Ridge (Bachelor Mountain Member) contains as much as 12 percent K_2O and less than 0.5 percent Na_2O (Ratté and Steven, 1967), in contrast with magmatic values of about 5.5 percent and 3.5 percent, respectively, in unaltered outflow tuffs. Here the degree of potassium-metasomatism is lower, but it decreases gradually across the previously mapped "contact" with tan (Mammoth Mountain-type) rhyolite. The tan rhyolite still shows modest alkali exchange (Na_2O increases from 0.62 to 1.90 percent along these roadcuts and K_2O decreases from 6.79 to 6.22 percent; Lipman, 2004). Such potassium metasomatism, first noted in this area (Ratté and Steven, 1967), now has been recognized widely in Cenozoic volcanic rocks in the western United States (Chapin and Lindley, 1986).

Return to the vehicles and continue down the road 0.5 mi to the portal and dump of the Midwest mine; 0.2 mi farther is the junction with West Willow Creek road (FS 503). Turn right, back toward the Midwest mine. Above a switchback at the Midwest mine, for the next 0.25 mi the rocks poorly exposed along road are Campbell Mountain zone. After 0.4 mi, the Amethyst mine is visible in views back through the aspen; continue ahead for 1.8 mi.

7.8 **Stop 5C-4. Southern margin of the San Luis caldera complex** (37°54.43' N., 106°57.26' W.; 10,564 ft, 3,220 m elevation). Junction with Equity mine road (FS 504), at West Willow Creek crossing.

Small exposures surrounded by glacial till in the road ahead are transitional rhyolite-silicic dacite of the Nelson Mountain Tuff, thinly plastered unconformably against a southern embayment of the Nelson caldera basin. Float exposures of andesitic lava just to the right of the road are andesite of Bristol Head, part of the caldera-wall sequence, but the intervening stratigraphic units that crop out below the Nelson Mountain Tuff on adjacent ridges (Rat Creek and Cebolla Creek Tuffs) have been truncated. Despite the sparse outcrops in this area, the caldera-margin truncation of the regional ignimbrite stratigraphic sequence is well documented by mineral-exploration drill-hole data. The southerly location of the caldera-wall unconformity is interpreted to be the reulst of a large north-trending paleovalley, far south of the structural caldera, and at least in part influenced by the keystone graben of the older Bachelor caldera (Lipman, 2000).

Small, mineralized structures related to the North Amethyst Fault probably are present in this poorly exposed area, but displacements are minor. Because of poor exposures, data are sparse on the Amethyst Fault and vein system between the Park Regent shaft and the Captive Inca mine.

Several other stratigraphic discontinuities in this area, previously inferred to result from sizeable offsets along faults of the Creede graben, have been reinterpreted as a result of unconformities along caldera walls (Lipman, 2000).

Continue up-valley on FS 504 (road crossing West Willow Creek at 1.1 mi).

9.4 **Stop 5C-5. San Luis caldera viewpoint** (37°55.38' N., 106°57.83' W.; 10,909 ft, 3,325 m elevation). This was the site of proposed CSDP Creede district drill hole (not completed). *Park along the right side of the built-up roadway, adjacent to a modest high point (Quaternary landslide slump block) near the beaver ponds.* Walk to the high point for the best view of caldera wall structures (fig. 155). We are within the large paleovalley reentrant in the southern margin of the Nelson caldera. Despite the heavy surficial cover, limited surface exposures and proprietary exploration drill-hole data permit confident reconstruction of the geometry of the caldera margin in this area.

On slopes to the northeast, across West Willow Creek, thick caldera-filling Nelson Mountain Tuff is compositionally zoned from weakly welded rhyolitic tuff (poorly exposed) upward into densely welded crystal-rich dacite (Equity phase). The Equity Fault is the reddish iron-stained structure to the northeast. Virtually all surface exposures south of the east-west-trending Equity Fault are of the dacitic tuff, which wedges southward on the caldera wall against the Captive Inca lava dome and associated flow breccias (silicic dacite; 69–70 percent SiO_2). The Captive Inca dome, which here overlies the Wason Park Tuff, is visible in the large exposure across the creek and through the trees to the southeast; the black glassy flow breccia is well exposed in basal outcrops. This is one of several lavas and domes emplaced around the southern margin of the San Luis caldera complex shortly before its initial pyroclastic eruptions (Rat Creek Tuff).

To the west, though obscured by Quaternary landsliding, thick intracaldera Nelson Mountain Tuff on the north transitions laterally southward across the topographic margin of the San Luis caldera into relatively thin sheet-like outflow ignimbrite, which rests on Rat Creek Tuff and older volcanic rocks southwest (fig. 155). Depositional truncation along the caldera margin is exposed in one place—a small set of cliffs to the northwest, where thick intracaldera dacitic tuff (on the east) wedges out against exposures of the

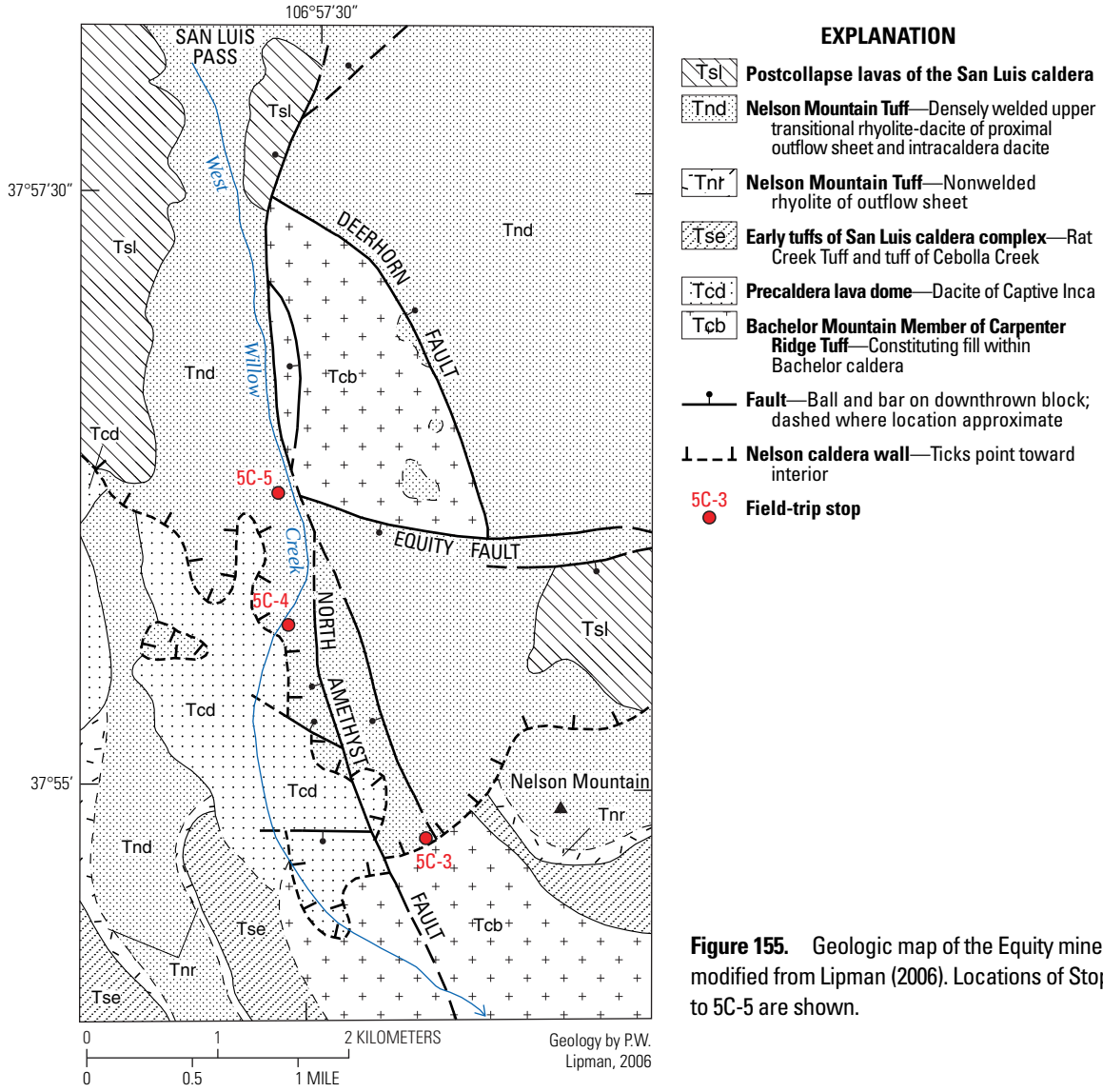

Figure 155. Geologic map of the Equity mine area, modified from Lipman (2006). Locations of Stops 5C-3 to 5C-5 are shown.

Captive Inca dome. Although previously mapped as a regional fault of potential economic significance, the northern continuation of the Bulldog Mountain Fault (Steven and Ratté, 1973), this contact is demonstrably steeply depositional. A vitrophyre along the base of the dacitic tuff demonstrates quenching along the contact, and primary compaction foliation in the tuff steepens from near horizontal to about 40° adjacent to this caldera-wall boundary.

The proposed 3–5 km CSDP Creede district drill hole in this area (Bethke and Lipman, 1987) would have provided a vertical section through the fossil geothermal system responsible for the Creede epithermal veins (fig. 156), permitting reconstruction of physical gradients with depth, testing for possible stacked concealed mineralization of porphyry copper-molybdenum type, and hopefully penetrating the causative intrusive heat source. In addition, the hole would have provided a deep section through fill of Bachelor caldera, the upper part of which is already well constrained by natural exposures.

Continue ahead to the Equity mine site.

10.3 **Stop 5C-6. Equity Fault and mine** (37°56.13’ N., 106°57.59’ W.; 11,073 ft, 3,375 m elevation).

The east-west Equity Fault bounds the southern end of a triangular uplifted block, presumably reflecting the presence of an intrusion at depth, that raises Carpenter Ridge Tuff (Willow Creek and Campbell Mountain zones) within northern Bachelor caldera several hundred meters upward against dacitic intracaldera Nelson Mountain Tuff to the south (figs. 155, 157). This fault trend is regionally anomalous in comparison with the dominant north-northwest trend of Creede graben structures; it appears to record localized late resurgent movement several kilometers south of the inferred

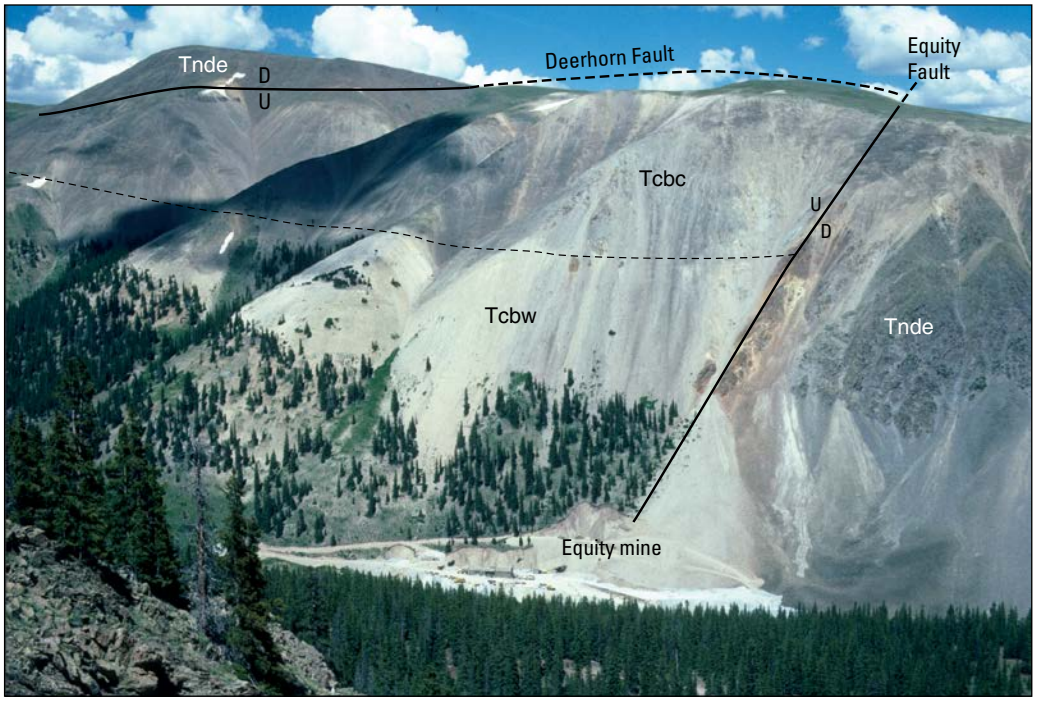

Figure 156. The Equity Fault and mine workings, as viewed from West Willow Creek (Stop 5C-6). The Equity Fault is an east-west reverse structure marked by the steeply dipping orange-brown oxidized zone, along which a triangular block of intracaldera rhyolitic Carpenter Ridge Tuff (welding zones Tcbw, Tcbc) was juxtaposed against densely welded gray-brown dacitic intracaldera Nelson Mountain Tuff (Tnde). The Equity block overlies a concealed dacitic intrusion (exposed in drill holes and mine workings). Photograph by P.W. Lipman, U.S. Geological Survey, ~2016.

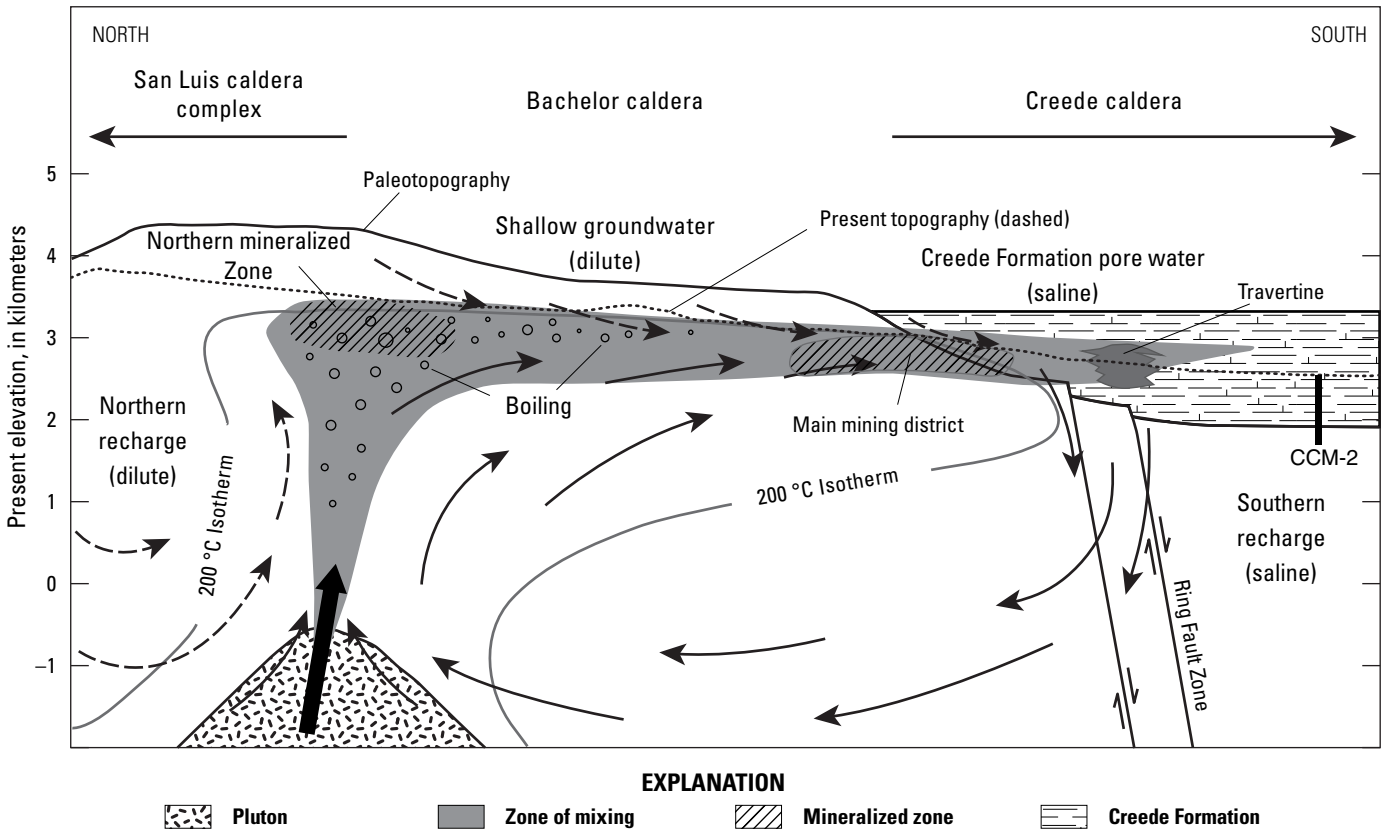

Figure 157. Model of the hydrothermal system responsible for the formation of epithermal silver and base-metal ores of the Creede mining district based on studies of veins and wall rocks (from Bethke and Hay, 2000). Solid arrows indicate deeply circulating waters; dashed arrows indicate surrounding waters mixing into the circulatiion system. Emplacement of unidentified small pluton in the northern part of the Creede mining district and concurrent fracturing initiated hydrothermal circulation (compare with fig. 129*B*). The hydrothermal system drew in moderately saline Creede Formation pore fluids and, possibly, residual lake waters from the south, and dilute meteoric waters from the north. These waters were heated by the pluton, joined by magmatic fluids (bold arrow), and mixed in the upwelling plume. Fluids boiled on ascent and moved laterally southward on nearing the surface. Along the top of the system, deeply circulating waters mixed with overlying groundwater. Through most of the district, overlying waters were dilute meteoric waters, but at the southern end, they were saline pore waters in the Creede Formation.

southern structural boundary of the Nelson Mountain subsidence (along the south side of San Luis Peak; fig. 129*B*).

Mineral exploration at the intersection of the Equity and north Amethyst Faults has been underway intermittently since early in the 20th century. Intensified exploration by the Homestake Mining Company in the late 1980s, which involved extensive core drilling, encountered promising intercepts, but a decline driven near the intersection of the Equity and north Amethyst Faults failed to encounter sufficient ore-grade mineralization. Studies in conjunction with the CSDP Creede Drilling Project (Hulen, 1992; Bethke and Hay, 2000) developed a detailed model for the mineralization of the Creede geothermal system. Available evidence indicates a single hydrothermal plume that rose in the general area along the northern Amethyst vein between the Captive Inca and Equity mines and flowed laterally as far as 8 km to the south, mineralizing the Amethyst and Bulldog vein systems (fig. 156). Two compositionally distinct fluid sources are required: (1) a saline brine thought to be derived from moat sediments of the Creede Formation, and (2) meteoric water derived from the north, near the present Continental Divide.

Turn the vehicles around and return the 2.5 mi to the Bachelor road junction (FS 504). Cross West Willow Creek and proceed 1.2 mi south. The dump on the left is the Park Regent shaft, the northwesternmost mine on the main Amethyst vein. Continue ahead 1.1 mi, past poorly exposed Wason Park Tuff in the aspen along the road, as well as in a Mineral County gravel pit on the right. Emerge out of the aspen into a meadow that was the site of the town of Bachelor in the late 1890s and early 1900s. Bachelor once had several thousand residents. Its location permitted easy access to the shafts along the Amethyst vein system. Proceed 0.8 mi, crossing Windy Gulch, where the Bulldog Mountain mine of the Homestake Company is visible down-valley, and continue 0.9 mi to Stop 5B-9 (location of the previously visited Stop 5B-9).

16.8 **Stop 5B-9. Panoramic view of resurgent Creede caldera** (37°51.67’ N., 106°56.63’ W.; 9,908 ft, 3,020 m elevation).

After stop, continue downhill 2.4 mi to the town of Creede and the junction with CO 149.

End of route 5C.

[Alternatively, to join route 5D at Stop 5D-1: At 1.0 mi downhill, make the sharp right turn, onto the less traveled road for 0.8 mi. At the fork in the road, bear left for 0.5 mi. At the junction with the road up Miners Creek, turn right. The Miners Creek drainage follows the Alpha-Corsair Fault, the westernmost fault system of the Creede graben (fig. 149B); continue for 0.5 mi to Shallow Creek road. Turn left, crossing Miners Creek in 0.2 mi. Bear left, through the stock gate, and again at the fork, to the road end at 1.7 mi and Stop 5D-1.]

Route 5D—Western Side of the Central Caldera Complex: Creede to South Clear Creek

This route segment continues to the northwest, counterclockwise along the Creede caldera moat, then follows the Clear Creek graben past the steep south face of Bristol Head (12,707 ft, 3,873 m elevation) that provides spectacular exposures of the western walls of Bachelor and La Garita calderas.

0.0 *From the town of Creede, follow CO 149 for 2.5 mi to the junction with Miners Creek road (FS 507). Turn right, and follow Miners Creek for 1.6 mi to Shallow Creek road (FS 508). Bear left, through the stock gate, and again at the fork 1.7 mi, to end of Shallow Creek road.*

6.0 **Stop 5D-1. Shallow Creek breccias, fill of Bachelor caldera** (37°49.77’ N., 106°58.80’ W.; 8,842 ft, 2,695 m elevation)**.** *The road becomes indistinct at the first Shallow Creek crossing; park vehicles in the clump of trees.*

Walk across the stream (log for crossing) to prospect in the gray Willow Creek zone. This mine adit is in the fluidal Willow Creek zone of the Bachelor Mountain Member. Note the large mafic fiamme that contain conspicuous biotite in rocks on the dump, and the strong flattening of the pumice foliation in the Willow Creek. Continue back across the stream and head west along the trail on the north side of Shallow Creek. The small quarry in Willow Creek lithology also contains the mafic pumice and shows stretched lineate pumice on the plane of compaction foliation. Continue about 0.25 mi west, to the first major drainage from the north.

Head up the ridge on the east side of the drainage, watching for lithologic variations in the Bachelor Mountain Member. Note the abundant andesitic lithic debris; at the top of the first small hill, clasts (as much as 2–3 m across) are andesite and dacite, enveloped by crystal-poor tuff. This mesobreccia (Shallow Creek breccia member of the Carpenter Ridge Tuff) is derived from precaldera (Conejos-age) early intermediate-composition stratovolcanoes on the west wall of the Bachelor caldera. Table Mountain, visible up Shallow Creek to the west, is one of these centers. Continue up the ridge to the next minor knob.

More mesobreccia of andesite clasts crops out on the way to, and at, this knob. Farther north, in a cliff exposure in the Bachelor Mountain fill, some house-sized andesite blocks are visible. Examine the texture and color of the rhyolitic tuff matrix. It passes from

typical purplish-gray Willow Creek zone below, through a mesobreccia-rich interval, into reddish-brown rhyolite (formerly grouped with the Mammoth Mountain Tuff) without evidence of a depositional break or intervening Campbell Mountain and Windy Gulch zones. Here the previously mapped Mammoth Mountain rhyolite (Steven and Ratté, 1973) located directly on top of fluidal rhyolite of the Willow Creek zone provides further evidence that the entire Bachelor-Mammoth sequence is part of a single caldera-fill sequence (as discussed in conjunction with Stop 5C-1).

Return to the vehicles and retrace the route 2.0 mi to Miners Creek road (FS 507). At the junction with Miners Creek road, turn right and go 1.6 mi toward the resurgent dome of Creede caldera. At the junction of Miners Creek road with CO 149, turn right and continue 1.7 mi toward Lake City.

11.3 Five-Mile bridge across the Rio Grande. A spectacular exposure of Creede Formation is visible (fig. 158). Ignimbrites on the caldera wall above are Mammoth Mountain Member of the Carpenter Ridge Tuff and Wason Park Tuff, capped by local andesitic-dacitic lavas of Bristol Head.

13.1 Seven-Mile bridge and the intersection with Middle Creek road. The rugged cliff on the left is Point of Rocks. *Turn left (south) onto Middle Creek road (FS 523). Park vehicles carefully along the road without blocking traffic.*

13.3 **Stop 5D-2. Top of the intracaldera Snowshoe Mountain Tuff at Point of Rocks (**37°47.53’ N., 106°58.82’ W.; 8,825 ft, 2,690 m elevation**).**

Outcrops along this road display partly to densely welded tuff at the top of the thick intracaldera accumulation of Snowshoe Mountain Tuff on the northwest flank of the resurgent dome; this stratigraphic level of the intracaldera ignimbrite is correlative with units penetrated at the bottoms of the two Creede moat scientific drill holes in 1991. The Snowshoe Mountain Tuff here displays crudely bedded meter-scale variations in lithic content and pumice abundance that probably result from fluctuating energetics during the waning of the ignimbrite eruption. Sparse sanidines from this dacitic tuff (67.6 percent SiO_2) at this site yielded a relatively low-precision single-crystal $^{40}Ar/^{39}Ar$ age (26.91±0.15 Ma; Lipman and McIntosh, 2008).

The rugged outcrops of white silicic rhyolite (76 percent SiO_2), locally known as Point of Rocks (fig. 159), were previously interpreted as a brecciated postcaldera rhyolitic lava dome (p. 43 in Steven and Ratté, 1965), but these rocks are a resurgently tilted and slightly faulted layer of silicified monolithologic breccia that consists solely of crystal-poor welded tuff derived from the Willow Creek welding zone of intracaldera Carpenter Ridge Tuff. This is the most spectacularly exposed landslide breccia in the Creede caldera. Flattened pumice textures within breccia clasts are obscure in the most accessible exposures at Point of Rocks but are readily visible nearby.

Figure 158. Laminated silts and fine sand of the Creede Formation (lacustrine facies), which constitute moat sediments of the Creede caldera, exposed in a cut-bank of the Rio Grande, just west of junction with Shallow Creek. Photograph by P.W. Lipman, U.S. Geological Survey, ~1965.

Figure 159. Intracaldera Snowshoe Mountain Tuff, at Point of Rocks (Stop 5D-2). The upper part of the intracaldera Snowshoe Mountain Tuff (Tsm) is in partial fault contact with caldera-landslide breccia (Tcbm) that consists of monolithologic clasts of intracaldera Carpenter Ridge Tuff (Willow Creek welding zone), on the northwest flank of the Creede resurgent dome at Point of Rocks. Photograph by P.W. Lipman, U.S. Geological Survey, 2015.

Willow Creek clasts from the landslide fill in Creede caldera, including Point of Rocks, have normal magmatic sodium-potassium ratios, similar to outflow Carpenter Ridge Tuff. Fragments of unaltered Willow Creek rhyolite are also abundant in adjacent exposures of the Creede Formation. In contrast, bedrock samples of Willow Creek type from the most likely sources on the north caldera wall show substantial alkali exchange (Ratté and Steven, 1967). There is no overlap in alkali contents between slide-block and caldera-wall samples. These chemical data thus support interpretations that the potassic alteration in the Creede mining district was a precursor to the late faulting and major mineralization along the Creede graben (Sweetkind and others, 1993), rather than during resurgence and early faulting associated with the Bachelor caldera cycle.

Between the Snowshoe Mountain Tuff and the overlying Point of Rocks breccia is a thin layer of brecciated crystal-rich silicic lava that contains sanidine phenocrysts. Although not dated directly, these breccia fragments closely resemble the 27.5-Ma post- Carpenter Ridge Tuff lavas in Shallow Creek and capping Table Mountain on the northwest wall of Creede caldera (table 13); this breccia layer is tentatively interpreted as a landslide deposit derived from one of these sources.

Continue south on Middle Creek road, past small outcrops of andesite breccia that are also interpreted as a late caldera-collapse landslide deposit.

16.4 **Stop 5D-3. McCall Creek flow of Fisher Dacite (**37°45.13’ N., 107°00.33’ W.; 8,940 ft, 2,725 m elevation**).** Talus slope beneath cliff outcrops above the road on the left (east) side.

The McCall Creek lava is sanidine-bearing and somewhat atypically silicic (67.3–70.0 percent SiO_2) for the Fisher Dacite; it has yielded a relatively old $^{40}Ar/^{39}Ar$ age of 26.82±0.05 Ma (Lipman and McIntosh, 2008). It appears to have erupted early, on the caldera floor prior to major uplift on the flank of the resurgent dome, as indicated by the fairly uniform thickness of the lava, downslope dips that are semiconformable with the tilted underlying Snowshoe Mountain Tuff, and unconformable onlap by untilted sedimentary beds of the Creede Formation. This is in contrast to the lavas on Fisher Mountain to the south, which interfinger with and overlie the Creede Formation, yield younger ages, and are inferred to have erupted largely after the completion of resurgence.

On the skyline to the south, several high peaks (with confusing geographic names) are within and adjacent to South River caldera, which is the source of the Wason Park Tuff. Closest is the steep termination of a north-trending ridge locally known as Red Mountain (12,587 ft, 3,837 m elevation; labeled point “Ivy” on USGS topographic maps); it exposes 850 m of intermediate-composition lavas that fill South River caldera. Although this so-called Red Mountain is not recognized as a formal geographic name, the drainage

along its west side, once known as South River, is now shown as Red Mountain Creek on USGS maps. The valley of Red Mountain Creek marks the western margin of South River caldera; the volcanic section on the west slope consists of multiple ignimbrite sheets (Fish Canyon, Carpenter Ridge, Blue Creek, Wason Park Tuffs), but the entire section to the east consists of intermediate-composition lavas within this caldera. And although South River no longer exists as a formal name, South River Peak (13,148 ft, 4,008 m elevation), which also consists of intracaldera lavas, is the high point along the local Continental Divide. Piedra Peak (12,238 ft, 3,730 m elevation), just to the west, is capped by thick, densely welded Wason Park Tuff on the southwest rim of its source caldera. Piedra Peak is also the type locality for the now-abandoned Piedra Rhyolite, the stratigraphic name applied to units dominated by crystal-poor rhyolite during the pioneering volcanic mapping in the San Juan Mountains by Cross and Larsen (1935).

Return north on Middle Creek road to CO 14.

19.7 *Continue northwest from Seven-mile bridge*. The lowest exposures in the caldera wall ahead and on the right are andesitic lavas of the Conejos Formation overlain by Masonic Park Tuff (figs. 127, 160), and are interpreted as a tilted fragment of the La Garita caldera floor within the western margin of the central San Juan caldera cluster (Lipman, 2000, 2006).

21.1 Entering the Bristol Head 15-minute quadrangle (Steven, 1967).

21.6 **Stop 5D-4. Caldera-margin breccia within the Snowshoe Mountain Tuff** (37°46.51' N., 107°00.46' W.; 8,891 ft, 2,710 m elevation). Roadcuts along tight curves in the road (*be alert for oncoming high-speed traffic; this stop is not suitable for large groups*).

These exposures were once mapped as intermediate-composition volcaniclastic facies of precaldera Conejos-age volcanics (Steven and Ratté, 1973). Indeed, andesite-dacite clasts as much as 1 m across are the dominant component, but several features indicate that clasts slid or washed into Creede caldera late during its formation: (l) though most clasts are of intermediate-composition lava, a few are distinctive Wason Park Tuff; (2) crude bedding dips 25–30° inward toward the core of the caldera; and (3) at the north end of the exposures, nonwelded phenocryst-rich dacitic tuff of Snowshoe Mountain type is present as poorly exposed matrix surrounding the clasts.

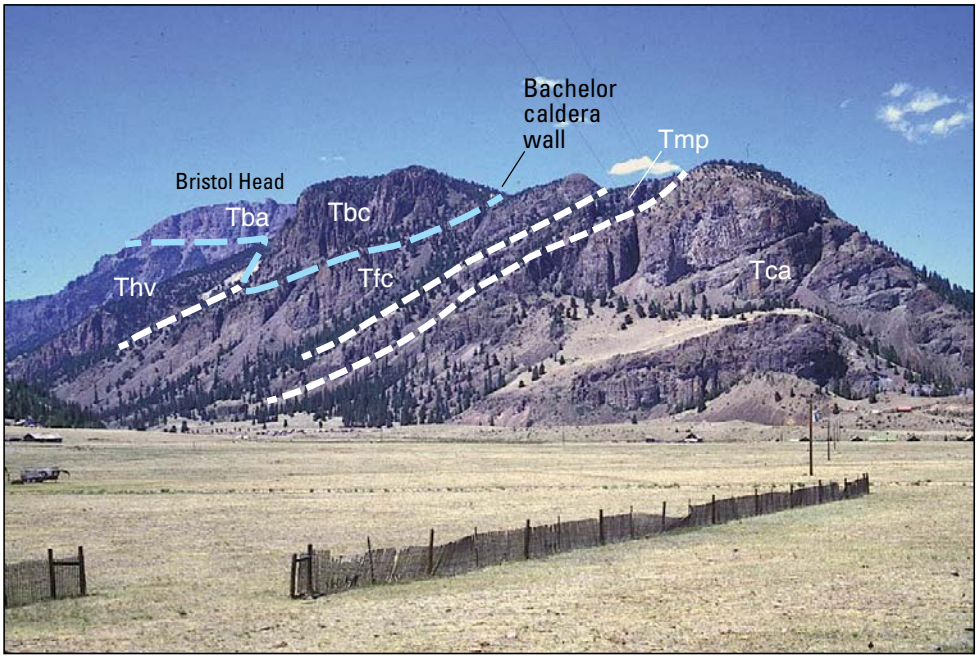

Figure 160. View of Bristol Head from the southeast along the Rio Grande, showing features of three calderas. Andesitic lavas of the Conejos Formation (Tca) and overlying Masonic Park Tuff (Tmp) are interpreted as the floor of La Garita caldera, which was filled by intracaldera Fish Canyon Tuff (Tfc), then tilted by postcollapse resurgent uplift. A thick sequence of laharic breccias of Huerto Andesite (Thv) that accumulated along the southwest side of La Garita caldera is truncated obliquely by the south wall of Bachelor caldera, against which Blue Creek Tuff (Tbc) was ponded. The overlying Wason Park Tuff (fig. 161) is not visible from this vantage because of foreshortening. Bristol Head (in distance) is capped by andesite of Bristol Head (Tba). The ridge profile on the right side is the topographic west wall of Creede caldera. Photograph by P.W. Lipman, U.S. Geological Survey, ~1987.

These deposits closely constrain the location of the Creede caldera wall in this area, as precaldera lavas of the Conejos Formation are exposed about 200 m up-slope. Many clasts are well rounded, in contrast with the angular fragments typical of landslide breccias interleaved with caldera-filling tuffs elsewhere in the San Juan region. Thus, these deposits are tentatively interpreted as emplaced by mudflows from the caldera walls, which scoured and incorporated nonwelded patches of Snowshoe Mountain Tuff during emplacement.

Continue southwest along CO 149.

23.4 Approaching the turn to the right, in the saddle between the caldera wall and the isolated hill of Conejos andesite flows that underlie Masonic Park Tuff. Prominent cliffs on the flank of Snowshoe Mountain, at 8:00, are the McCall Creek flow of Fisher Dacite (Stop 5D-3). High hills on the skyline at 10:00 are parts of Fisher Mountain. At 1:00 on the skyline, near the Continental Divide, is an ignimbrite sequence from the central San Juan calderas, mainly Carpenter Ridge and Fish Canyon Tuffs.

24.9 Climbing onto the terminal moraine of the late Wisconsinan glacier that came down the upper Rio Grande. Entering the Clear Creek graben, another of the northwest-striking extensional features that trend tangentially away from the central San Juan caldera cluster. These grabens are interpreted as related to broad regional extension over the roof of the large batholith that is inferred to underlie the calderas of the central and western San Juan region (Plouff and Pakiser, 1972; Steven and Lipman, 1976; Lipman, 2007; Drenth and other, 2012).

25.9 **Stop 5D-5. Remnant of the Bachelor caldera wall and fill (**37°43.77’ N., 107°03.47’ W.; 8,924 ft, 2,720 m elevation).

Roadcuts of Fish Canyon Tuff, on the right, are overlain by lavas and breccias of the Huerto Andesite, and then by transitional silicic dacitic-rhyolitic welded phases of Carpenter Ridge Tuff. These outcrops contain mafic alkalic fiamme, characteristic of upper parts of the Carpenter Ridge rhyolite unit (seen at Stop 5A-5), as well as a lag breccia of intermediate-composition lithic fragments. Similar relations are spectacularly exposed on the relatively inaccessible southeast slopes of Bristol Head.

The absence of rhyolitic Carpenter Ridge Tuff, which is as much as 200-m thick to the south and southwest, and the development of lag breccias are interpreted as a wedge-out of the intracaldera ignimbrite high on the southwest wall of Bachelor caldera (fig. 127). Despite the limited thickness of rhyolitic Carpenter Ridge Tuff, the overlying Blue Creek Tuff is as much as 200-m thick, reflecting ponding against yet higher levels of the caldera wall (or possibly growth of graben basins related to the inception of the Clear Creek fault system).

In the distance south of Creede caldera, hills south of the Continental Divide are composed of Fisher Dacite that onlaps earlier lavas (volcanics of South River Peak) that ponded within the largely filled South River caldera. Ridges to the west, along tributaries of Middle Creek, are underlain by Wason Park, Blue Creek, and Carpenter Ridge Tuffs that are truncated along the west wall of South River caldera, the source of the 27.38-Ma Wason Park Tuff.

27.1 Large cliffs of thick Blue Creek Tuff (200 m) to the right. Exposures across the Rio Grande, to the south, are also Blue Creek Tuff that ponded against the western margin of La Garita caldera.

28.3 Wright’s Lower Ranch. The massive outcrops on the right are thick Wason Park Tuff (~175 m), overlying dacitic Blue Creek Tuff; the exceptional thickness of these ignimbrite sheets again results from ponding in the western moat of La Garita caldera.

29.0 Wetherill Ranch. One of the famous old ranches of the Creede area. Low exposures on the right are Carpenter Ridge Tuff. Entering the southern margin of the Bristol Head quadrangle.

30.7 **Stop 5D-6. View of central Bristol Head and the margin of Bachelor caldera, from Freemon Ranch** (37°45.92’ N., 107°06.71’ W.; 8,990 ft, 2,740 m elevation). *Crossing Clear Creek. Park on the east side of the bridge.*

Exposures across the Rio Grande on the left (west) are mostly Fish Canyon Tuff. On the right, the lowest exposures just above the creek level are the younger Wason Park Tuff. If the weather cooperates, in the afternoon light at 3:00 direction there is a fine view of Bristol Head (12,707 ft, 3,873 m elevation), a prominent landmark that consists mostly of andesitic lavas, but of two distinct ages. The capping lavas are andesite of Bristol Head that postdates the 27.38-Ma Wason Park Tuff, both of which ponded against the southern margin of Bachelor caldera. The near-vertical dark cliff of Wason Park is nearly 300-m thick on the southeast side of Bristol Head but completely wedges out between andesites to the northwest (figs. 127, 161). The lower slopes are older andesitic lavas and laharic breccias of Huerto Andesite that ponded within the western La Garita caldera. The Bristol Head Fault, the major structure of the northwest-trending Clear Creek graben, lies along the base of the slope, and passes beneath Santa Maria Reservoir. This fault tilts and drops Carpenter Ridge and Wason Park Tuffs down about 350 m to the southwest along the base of Bristol Head.

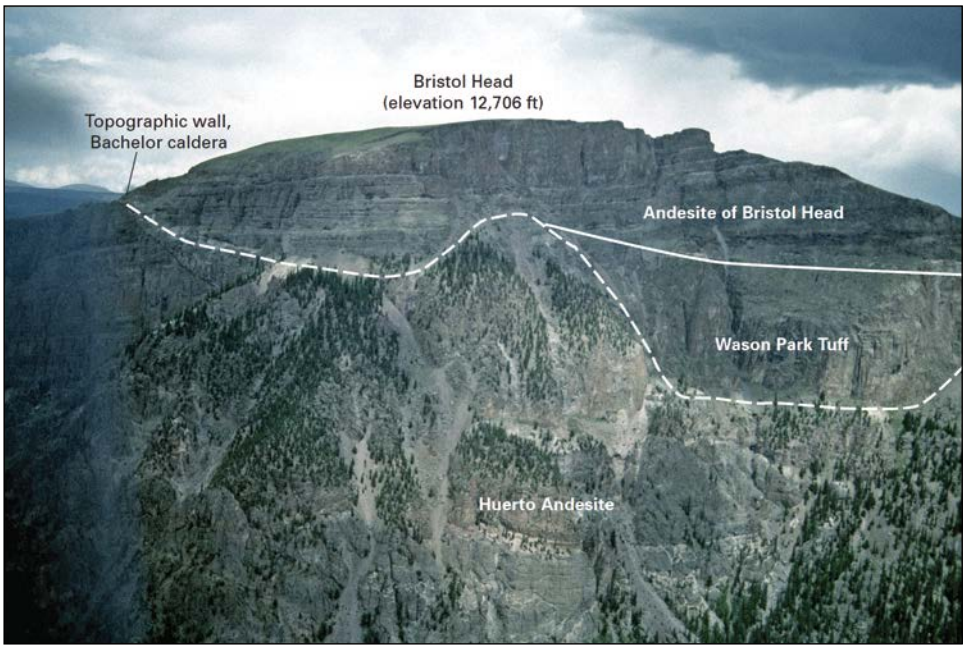

Figure 161. View to the northeast of the central part of Bristol Head and the margin of Bachelor caldera (Stop 5D-6), along the southwest wall of Bachelor caldera, as exposed on the south face of Bristol Head (compare with figs. 127, 160). Wason Park Tuff thins against the wall from a thickness of more than 300 meters (m) where ponded within Bachelor caldera, to ~1 m of ash-cloud tuff higher on the wall. Without the intervening presence of the Wason Park, the overlying andesite of Bristol Head would be lithologically nearly indistinguishable from the underlying precaldera Huerto Andesite. The camera view is oblique to the trend of the Bachelor caldera wall, which dips to the northeast. Aerial photograph by P.W. Lipman, U.S. Geological Survey, ~1985.

Continue ahead (west) on CO 149, where prominent light salmon-brown welded tuffs that cap the ridges ahead are rhyolitic Carpenter Ridge Tuff.

32.8 *Junction of Rio Grande Reservoir road with CO 149. Stay right on CO 149.* On the ridge between the two roads, the lowest, light-yellow exposures are partly welded Fish Canyon Tuff. The immediately overlying brown ledge is Crystal Lake Tuff, a phenocryst-poor low-silica rhyolite erupted from the Silverton caldera at 27.6 Ma. The upper large cliff exposures are lithologically similar rhyolite of the Carpenter Ridge Tuff from Bachelor caldera. In contrast with the caldera-wall environment of Stop 5D-5, here the rhyolitic Carpenter Ridge is thick and lag breccias are absent. Although exposures are less than ideal, both the Crystal Lake and Carpenter Ridge Tuffs appear to dip anomalously eastward and lap out against Fish Canyon Tuff to the west. Although perhaps in part a result of tilting by faults of the Clear Creek graben, this relatively gentle but unconformable contact has been interpreted as marking the western margin of La Garita caldera (Lipman, 2006).

33.3 Entering Hinsdale County.

34.9 **Stop 5D-7. View of western Bristol Head and margin of La Garita caldera (**37°49.03’ N., 107°08.66’ W.; 9,531 ft, 2,905 m elevation), at junction with South Clear Creek road (FS 510). *Pull off to the right.*

The highest slopes to the east are andesite of Bristol Head underlain by Wason Park Tuff. This tuff forms the broad mesa-capping ledge to the left (northwest) that is underlain along its west side by Fish Canyon Tuff and older andesite of the Conejos Formation (fig. 162). Both the Fish Canyon and Wason Park Tuffs wedge out against these early intermediate-composition lavas (fig. 163). Along a prominent north-trending side valley (Boulder Creek) that cuts into the Bristol Head cliffs, Huerto Andesite and Carpenter Ridge Tuff abruptly lap out against truncated units of the Conejos Formation and Fish Canyon Tuff. This relatively steep unconformity, which must postdate the Fish Canyon Tuff and predate the Carpenter Ridge Tuff, is another exposure of the western margin of La Garita caldera, more compelling than that viewed from the junction of Rio Grande Reservoir road with CO 149 (mile 32.8).

Several faults of the Clear Creek graben intervene between our vantage point and the cliffs of Bristol Head; at road level, poorly exposed beneath moraine is

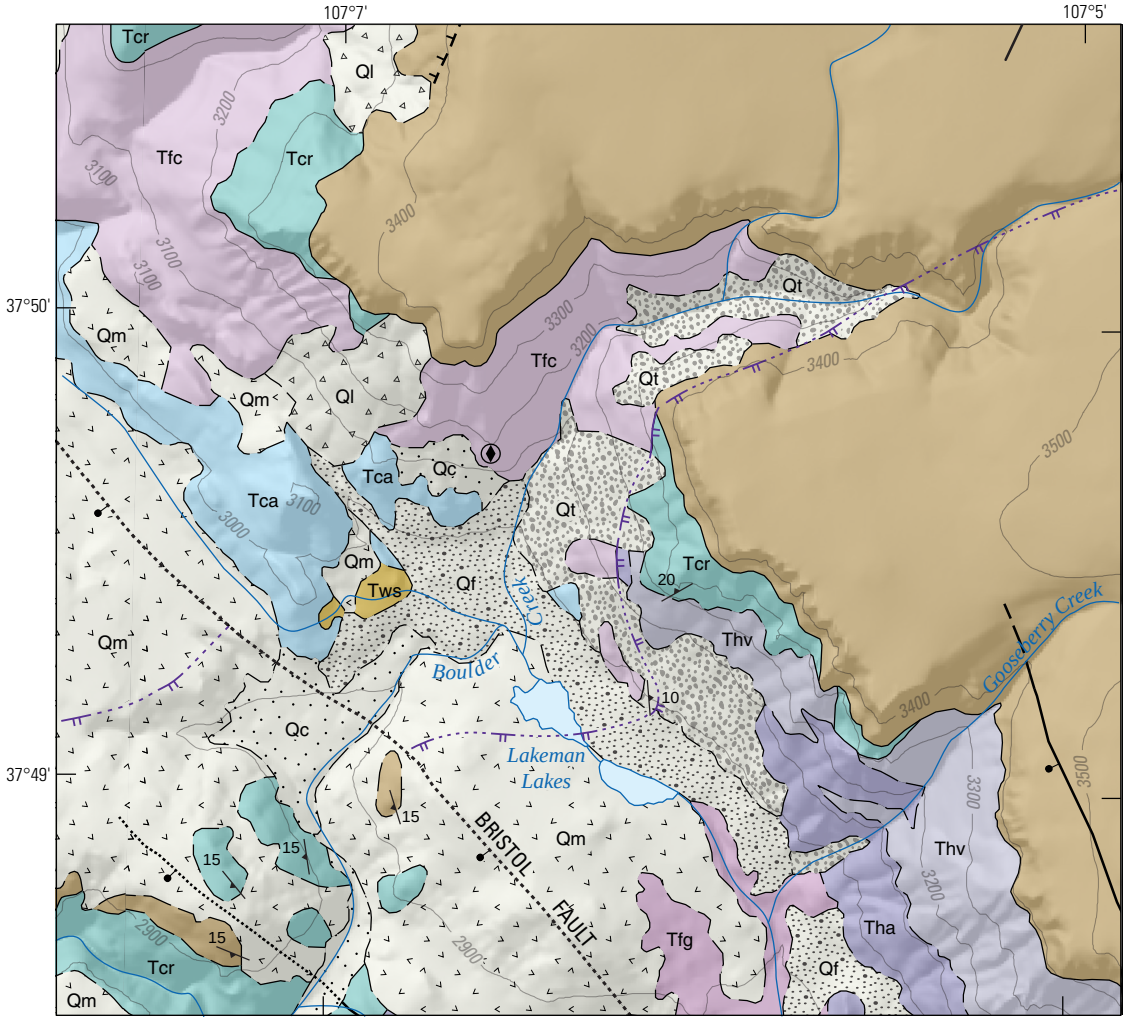

Figure 162. Geologic map of the western Bristol Head area (Stop 5D-7), showing the west topographic wall of La Garita caldera, as marked by the wedgeout of caldera-filling Huerto Andesite and Carpenter Ridge Tuff against thick proximal Fish Canyon Tuff on the caldera rim. Geology from Lipman (2006).

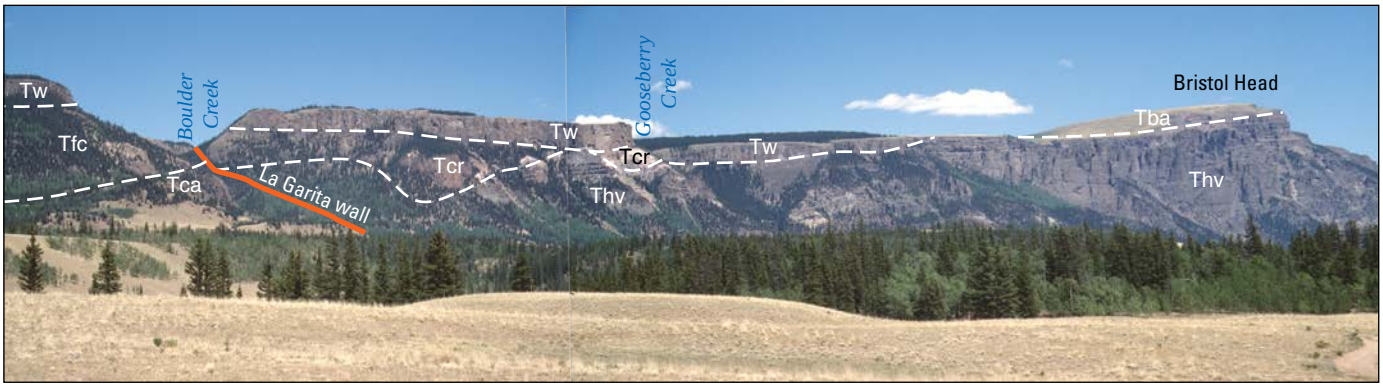

Figure 163. Northwest wall of La Garita caldera along Boulder Creek, as exposed along the Bristol Head fault scarp. Tca, andesitic lavas of the Conejos Formation; Tfc, Fish Canyon Tuff; Thv, lavas and volcaniclastic Huerto Andesite; Tcr, Carpenter Ridge Tuff; Tw, Wason Park Tuff; Tba, andesite of Bristol Head. Photograph by P.W. Lipman, U.S. Geological Survey, 2016.

26.90-Ma Nelson Mountain Tuff on the downthrown side of the Bristol Head Fault. On the upthrown side to the northeast, the Nelson Mountain Tuff widely overlies Wason Park Tuff near the treeline on high mesas northwest of Bristol Head. Light-colored roadcuts across the valley along South Clear Creek road expose the nonwelded rhyolitic base of the Nelson Mountain and underlying Cebolla Creek Tuffs.

End of route 5D: return to Creede.

Alternatively, continue to Lake City caldera along CO 149, following the field-trip guides prepared for the 1989 IAVCEI meeting. Start at mile 69.7 (Lipman and others, 1989); for Lake City and other western San Juan calderas see Hon and Lipman (1989). These guides remain largely current, except for improved $^{40}Ar/^{39}Ar$ geochronology (Bove and others, 2001).

Acknowledgments

Thomas Steven and Philip Bethke introduced Lipman to the spectacular geology of the central San Juan region starting in 1965, leading to many decades of productive joint research. Summer-long assistance with fieldwork, commonly under adverse conditions, by Pierre Christe, Chris Huber, Fleurice Parat, David Sawyer, and Doug Yager is much appreciated and fondly remembered. In addition to collaboration with numerous other geologists, as noted or referenced in this report, we also thank many friends in the San Juan Mountains who provided diverse hospitality, logistical support, help with back-country and property access, and other assistance during fieldwork. We especially thank K.J. Turner for assistance in preparing publishable geologic-map figures and other illustrations, Christine Chan for perceptive text editing, and Amy Gilbert and Joe Colgan who provided helpful technical review for this field-guide segment.

Day 6—Bonanza Caldera

By Peter W. Lipman[1], Matthew J. Zimmerer[2], and William C. McIntosh[2]

Introduction

Ignimbrite-caldera systems of the southeastern and central San Juan Mountains (Days 4–5), have been a laboratory for volcanologic and petrologic research since the middle of the 1950s, but calderas and associated ignimbrites in the northeastern San Juan region (fig. 164, table 14) have received less attention. These calderas define the transition from earlier southern Rocky Mountains volcanic field (SRMVF) volcanism in central Colorado to the larger-volume younger ignimbrite-caldera foci farther southwest (fig. 90). Besides mineral-resource studies of localized areas (for example, Scott and others, 1975; Van Alstine, 1975; Olson, 1988), most of the northeastern San Juan region, until recently, had been examined only in reconnaissance for the Colorado State geologic map (Tweto and others, 1976; Tweto, 1979).

One focus of recent ignimbrite studies in the northeast region (fig. 164) has been the enigmatic Cochetopa Park caldera and the previously unknown 32.2 million years ago (Ma) North Pass caldera and associated Saguache Creek Tuff (Lipman and McIntosh, 2008; Lipman, 2012). Farther to the northeast, the 33.1-Ma Bonanza caldera and the preceding 33.9-Ma Marshall caldera (Varga and Smith, 1984; McIntosh and Chapin, 2004) define an inflection point for the transition between volcanism along the north-south-trending Sawatch Range and the southwestward migration into the San Juan Mountains (fig. 90), as documented by field mapping, $^{40}Ar/^{39}Ar$ single-crystal age determinations[3], and petrologic studies (Lipman and others, 2013, 2015).

Existence of a caldera has long been inferred in the Bonanza area, based on gravity data (Karig, 1965) and regional studies (Steven and Lipman, 1976; Varga and Smith, 1984), but detailed geologic mapping, petrologic information, and geochronologic data have been sparse. The only previously published geologic maps for any part of Bonanza caldera were the pioneering report on the Bonanza mining district by Patton (1916) and a more detailed study of the district at a scale of 1:12,000 (Burbank, 1932). These studies distinguished the major local rock units for a relatively small area and provided important information on mine workings, but both were undertaken before development of modern concepts for ignimbrite volcanism and caldera subsidence. For example, the caldera-related ignimbrite was originally named Bonanza latite by Patton (1916), who carefully described the presence of abundant small fragments of andesite, puzzled over its so-called rhyoclastic texture, but interpreted the unit as a thick lava sequence. This unit was only identified as welded tuff a half century later (Bruns and others 1971).

Concurrently, a detailed stratigraphy for outflow ignimbrites (ash-flow tuffs) was developed in the Thirtynine Mile volcanic area farther to the northeast (fig. 90; Chapin and Epis, 1964; Epis and Chapin, 1968, 1974), but with insufficient regional control to locate eruptive sources unambiguously. Geochronologic and paleomagnetic studies of the distal ignimbrites in the Thirtynine Mile area, and comparisons with intracaldera ignimbrites and associated rocks along the Sawatch Range trend as far south as Bonanza caldera, subsequently demonstrated that one of the eastern ignimbrites, the Gribbles Park Tuff of Epis and Chapin (1974), is indistinguishable in age and paleomagnetic direction from proximal Bonanza Tuff (McIntosh and Chapin, 2004). Despite these discoveries, uncertainties have continued about the stratigraphic and structural relations in the Bonanza area and about the middle Cenozoic ignimbrite sources (for example, Grizzly Peak, Princeton, Aetna) that are aligned along the Sawatch Range to the north (fig. 90; Shannon, 1988; Fridrich and others, 1991; McIntosh and Chapin, 2004).

More-recent studies in the Bonanza area have evaluated eruptive and magmatic processes of silicic Cordilleran volcanism, based on new geologic mapping, high-precision $^{40}Ar/^{39}Ar$ age determinations, and chemical and petrographic data (Lipman and others, 2013, 2015; Lipman, 2020). The Bonanza caldera was initially interpreted as a relatively small trap-door structure that subsided in response to eruption of less than 50 cubic kilometers (km^3) of ignimbrite (Varga and Smith, 1984). The newer studies now document that Bonanza, the source of a compositionally complex regional ignimbrite sheet that erupted at 33.12±0.03 Ma, is a resurgently domed structure of much larger size (~15 × 20 km diameter), subsidence depth (>3 km), and eruptive volume (~1,000 km^3) than previously recognized. Although surface exposures are not ideal (heavy vegetation, widespread talus covers most slopes), the Bonanza center displays unusually complete and diverse features of a large ignimbrite caldera cycle. These features include (1) voluminous andesite and more silicic lavas erupted before the ignimbrite eruptions, (2) complex compositional zonations within both the outflow sheet and tuff that concurrently ponded within the caldera as a single ignimbrite unit, (3) extensive portions of the ring-fault system that accommodated caldera subsidence, (4) thick compositionally diverse lavas that filled the caldera after subsidence, (5) eroded remnants of the original topographic caldera rim, (6) widespread exhumation of

[1]U.S. Geological Survey.

[2]New Mexico Bureau of Mines and Geology.

[3]All $^{40}Ar/^{39}Ar$ dates for Day 6 are calibrated to Fish Canyon Tuff at 28.02 Ma, to provide consistency with published reports that list the analytical data (especially Lipman and McIntosh, 2008; Lipman and others, 2015). This is in contrast to Day 4, where more recently determined ages for Day 4 are based on a calibration of Fish Canyon Tuff at 28.201 Ma that also permits more direct comparison with U-Pb dates.

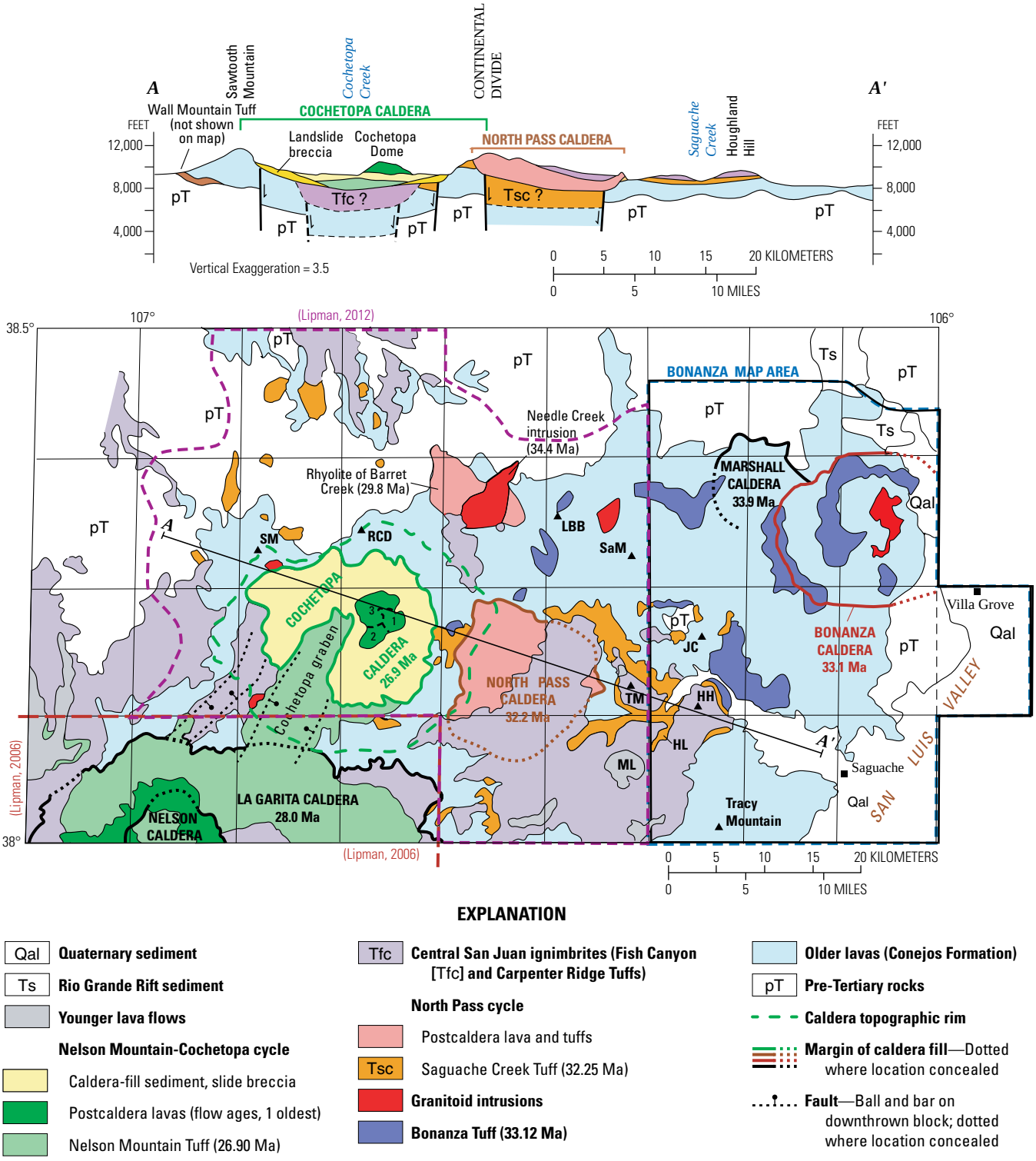

EXPLANATION

- Qal — **Quaternary sediment**
- Ts — **Rio Grande Rift sediment**
- **Younger lava flows**
- **Nelson Mountain-Cochetopa cycle**
  - Caldera-fill sediment, slide breccia
  - Postcaldera lavas (flow ages, 1 oldest)
  - Nelson Mountain Tuff (26.90 Ma)
- Tfc — **Central San Juan ignimbrites (Fish Canyon [Tfc] and Carpenter Ridge Tuffs)**
- **North Pass cycle**
  - Postcaldera lava and tuffs
  - Tsc — Saguache Creek Tuff (32.25 Ma)
- **Granitoid intrusions**
- **Bonanza Tuff (33.12 Ma)**
- **Older lavas (Conejos Formation)**
- pT — **Pre-Tertiary rocks**
- **Caldera topographic rim**
- **Margin of caldera fill**—Dotted where location concealed
- **Fault**—Ball and bar on downthrown block; dotted where location concealed

Figure 164. Generalized geologic map and cross section of the northeast San Juan region, modified from Lipman and others (2015). HH, Houghland Hill; HL, Houselog Creek; JC, Jacks Creek volcano; LBB, Long Branch Baldy; ML, Mount Lion; RCD, Razor Creek Dome; SaM, Sargents Mesa; SM, Sawtooth Mountain; Tsc, Saguache Creek Tuff; TM, Trickle Mountain. Black rectangular grid, boundaries of 7.5-minute quadrangle maps; purple-dashed line, area of Cochetopa-North Pass caldera map (Lipman, 2012); blue-dashed line, Bonanza map area (this field trip; Lipman, 2020); red-dashed line, corner of central San Juan map area (Lipman, 2006).

Table 14. Characteristic features of ignimbrite sheets in the central, western, and northeastern San Juan region and Sawatch Range.

[km, kilometers; Ma, million years ago; xl rich, crystal; xp, crystal poor; san, sanidine; qtz, quartz; bt, biotite; hbl, hornblende; --, no data]

Ignimbrite					Caldera		Postcaldera volcanism	
Tuff name	Percent SiO_2	Rock, phenocrysts	Volume, in km^2	Age, in Ma	Name	Area, in km	Unit, lithology	Age, in Ma
Central San Juan cluster								
Snowshoe Mountain	62–66	Xl dacite	>500	26.86	Creede	20 × 25	Fisher Dacite	26.8–26.2
Nelson Mountain	Zoned, 74–63	Xp rhyolite; xl dacite	>500	26.90	San Luis-Cochetopa	10 × 14, 20 × 25	Andesite lavas	26.9–25.9
Cebolla Creek	61–64	Xl dacite, hbl, no san	250	26.9	San Luis complex	14 × 16	Mineral Mountain Rhyolite	26.9
Rat Creek	Zoned, 74–65	Xp rhyolite to xl dacite	150	26.91	San Luis complex	9 × 12	Andesite-dacite	26.9
Wason Park	Zoned, 72–63	Xl rhyolite to dacite	>500	27.40	South River	20 × 20	Andesite-dacite	27.4–?
Carpenter Ridge	Zoned, 74–66	Xp rhyolite to xl dacite	>1,000	27.55	Bachelor	25 × 30	Dacite lavas	27.5–27.4
Fish Canyon	66–68	Xl dacite, hbl, qtz	>5,000	28.02	La Garita	35 × 75	Huerto Andesite	28.0–27.6
Western San Juan region								
Sapinero Mesa	72–75	Xp rhyolite	>1,000	28.35	Uncompahgre-San Juan	20 × 45	Andesite-rhyolite	28–27
Northeast San Juan region								
(Barret Creek)[1]	65–73	(Xl dacite to rhyolite lavas)	50?	29.8	(failed?)	--	Andesite lavas	--
Luders Creek Tuff	Zoned, 66–73	Xp rhyolite to xl dacite	50?	32.17	North Pass?	?	--	--
Saguache Creek	73–75	Alkali rhyolite, no bt	250–500	32.23	North Pass	15 × 17	Andesite-dacite	32.2
Bonanza	Zoned, 76–61	Zoned: dacite-rhyolite-dacite	500–1,000	33.12	Bonanza	20 × 25	Andesite-rhyolite	33.1–32.8
Thorn Ranch	76–66	Rhyolite outflow; dacite intracaldera	500	33.9	Marshall	15 × 18	Andesite-dacite	33.9–33.2
Sawatch Range								
Badger Creek	66–70	Xl dacite, hbl, qtz	500?	34.0	Mount Aetna	>10 × 15?	Subvolcanic intrusion	34–30
Wall Mountain	70–73	Xl rhyolite	±1,000	36.7	Mount Princeton	15 × 30?	Mount Aetna caldera	36.6–30

[1]Parens indicate failed caldera.

caldera-floor features, and (7) postcaldera intrusions that core a notably steep resurgent dome within the caldera (fig. 165). The tightly constrained chronology of the Bonanza caldera cycle (fig. 166, table 15) provides unique levels of caldera exposure (at least for the southern Rocky Mountain region), exemplifies an Andean-type association of intermediate-composition lavas with a complex ignimbrite sheet (Lipman and McIntosh, 2008), and offers special opportunities to explore relations between large-volume ignimbrite eruption, caldera structure, and magmatic evolution.

EXPLANATION

Erosionally modified remnants of Bonanza topographic caldera rim—Dashed where location approximate; dotted where location concealed

Crest of elliptical resurgent dome—Dashed where location approximate

Margin of Marshall caldera—Solid where location certain; dashed where location approximate

Caldera-subsidence ring fault—Ball and bar on downthrown block; solid where location certain; dashed where location approximate

Figure 165. Oblique view of Bonanza caldera area (modified from Google Earth), viewed from the south. Abbreviations: AP, Antora Peak; Bz, town of Bonanza; FM, Flagstaff Mountain; HP, Hayden Peak; MO, Mount Ouray; PP, Porphyry Peak; PoP, Poncha Pass; RM, Round Mountain; SaM, Sargents Mesa; SM, Sheep Mountain; SP, Saguache Peak; UP, Ute Pass; WH, Whale Hill.

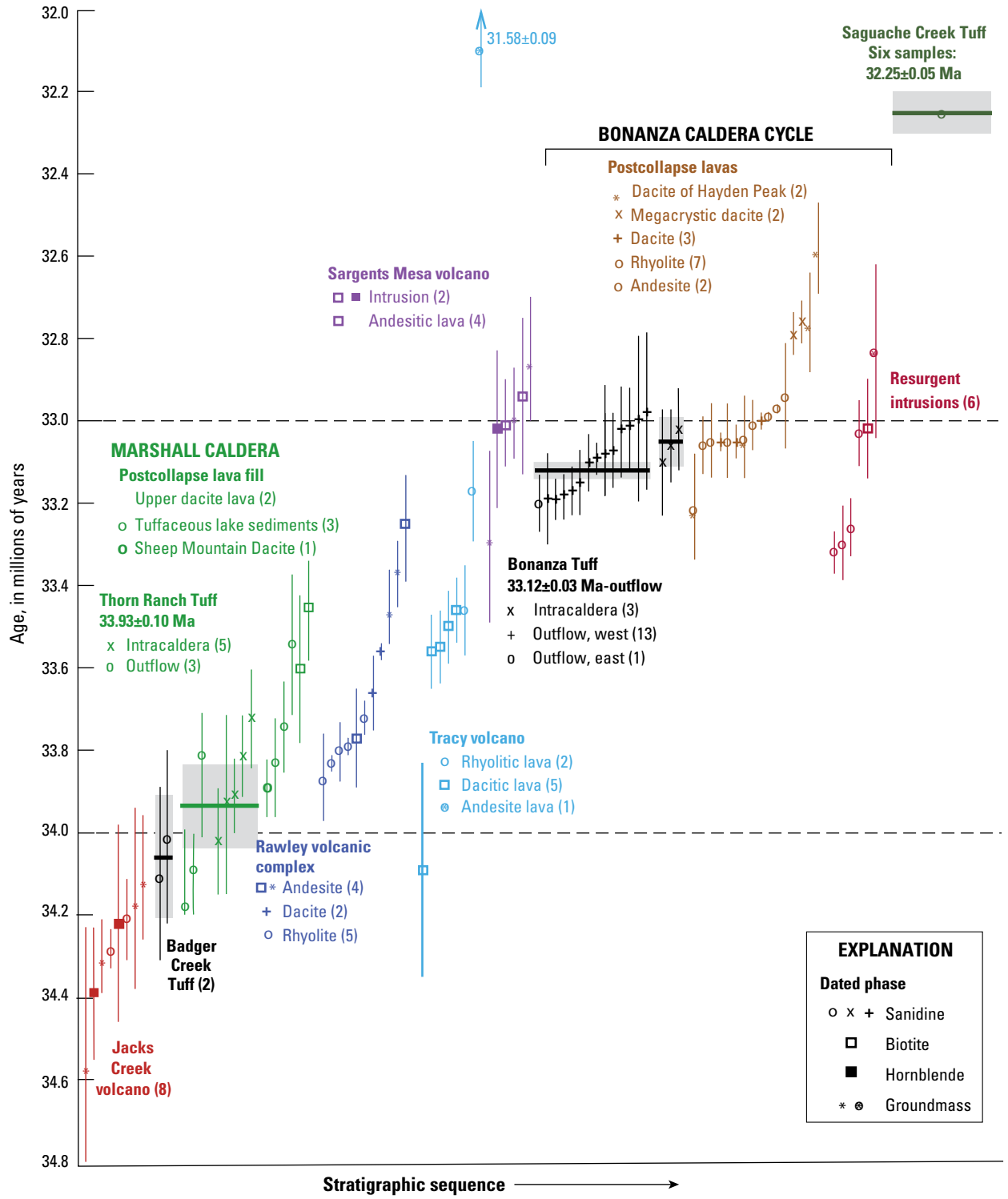

Figure 166. Summary of $^{40}Ar/^{39}Ar$ age-determinations for igneous rocks of the Bonanza-Marshall caldera area, illustrating the narrow ranges of ages obtained for multiple samples of individual ignimbrites, lavas, and intrusions of the Bonanza cycle and precursor eruptions. Data from Lipman and others (2015, supplemental table A). Precursors to the eruption of the Bonanza Tuff include several central volcanoes (Jacks Creek, Rawley, Tracy, Sargents Mesa) and Marshall caldera, source of the 33.9 Ma-Thorn Ranch Tuff. The number of dated samples per unit are shown in parens. Broad horizontal lines and gray rectangles represent weighted-mean ages and analytical uncertainties (95-percent confidence, 2 sigma) for major regional ignimbrites. Uncertainties are relatively large for biotite and groundmass determinations and much lower for recent sanidine ages, especially those determined with the Argus VI mass spectrometer (Lipman and others, 2015, supplemental table A).

Table 15. Summary of $^{40}Ar/^{39}Ar$ age determinations, Bonanza area and northeastern San Juan region (from Lipman and others, 2015).

[Ma, million years ago; --, no data]

Unit[1]	Material analyzed	Analysis type[2]	Sites	Age (Ma)[3]	Error[4] (±Se, 2σ)	Comments
Hinsdale Formation						
Basalt flow	Groundmass	Plateau	1	21.81	0.21	Overlies Carpenter Ridge Tuff
Conejos Formation, upper units						
Basalt of Point Benny	Groundmass	Plateau	5	30.22	0.10	Most mafic early lava in San Juan region
Andesite of Lone Tree Gulch	Groundmass	Plateau	1	30.21	0.17	--
Tuff of Big Dry Gulch	Biotite	Plateau	1	30.47	0.08	No sanidine, excess-argon biotite spectrum
Aphanitic andesite, hill 9519	Groundmass	Plateau	1	29.98	0.31	--
Hornblende andesite hill 9519	Hornblende	Plateau	1	30.41	0.79	Poor plateau
North Pass caldera cycle						
Luders Creek Tuff	Sanidine	SCLF	4	32.17	0.04	--
Volcanics of Cochetopa Hills						
Dacite of East Pass Creek	Biotite	Plateau	3	32.07–32.31	--	Main area of caldera-fill lavas
Rhyolite of Taylor Canyon	Sanidine	SCLF	1	32.15	0.10	--
Rhyolite breccia, Taylor Canyon	Sanidine	SCLF	1	32.44	0.08	Possibly landslide breccia from precursor lava
Saguache Creek Tuff	Sanidine	SCLF	6	32.25	0.05	--
Precursor? lava and intrusion	Sanidine	SCLF	2	32.18	0.07	At southeastern margin of North Pass caldera
Precursor? tuff of Spanish Creek	Sanidine	SCLF	4	32.50	0.03	--
Bonanza caldera cycle						
Resurgent intrusions						
Turquoise Mine	Groundmass	Plateau	1	32.83	0.21	Granodiorite and andesite
Alder Creek	Biotite	Plateau	1	33.02	0.12	Porphyritic granite
West side	Potassium feldspar	SCLF	2	33.02	0.08	Granodiorite
Spring Creek	Potassium feldspar	SCLF	2	33.28	0.06	Aplitic granite
Postcollapse lava flows and local tuffs						
Distal weakly welded tuffs	Sanidine	SCLF	2	32.7–32.8	--	May be distal facies of late caldera-fill lavas
Dacite of Hayden Peak	Groundmass	Plateau	2	32.66	0.18	On crest of resurgent dome
Megacrystic dacite	Sanidine	SCLF	3	32.76	0.02	Along north caldera wall
Caldera-fill lava flows						
Rhyolite cobbles (paleovalley fill)	Sanidine	SCLF	2	32.98	0.01	--
Dacite at Round Hill	Sanidine	SCLF	1	33.02	0.01	Against Proterozic rocks on northeast wall
Small-sanidine dacite	Sanidine	SCLF	4	33.03	0.03	--
Porphyry Peak Rhyolite	Sanidine	SCLF	5	33.03	0.04	--
Squirrel Gulch and other andesite	Biotite, groundmass	Plateau	3	33.0–33.3	--	West flank of resurgent uplift

Table 15.—Continued

Unit[1]	Material analyzed	Analysis type[2]	Sites	Age (Ma)[3]	Error[4] (±Se, 2σ)	Comments
Bonanza Tuff						
Intracaldera	Sanidine	SCLF	3	33.05	0.06	--
Outflow	Sanidine	SCLF	13	33.12	0.03	--
Precursor lavas						
Sargents Mesa volcano	Biotite, groundmass	Plateau	4	32.99	0.15	Age too young; lavas underlie Bonanza Tuff
Rawley volcano (dacite, rhyolite)	Sanidine	SCLF	7	33.73	0.09	--
Marshall caldera cycle						
Pitch-Pinnacle Formation	Sanidine	SCLF	4	33.5–33.9		Tuffaceous lake sediments
Caldera-fill lavas	Biotite	Plateau	2	33.4–33.6		--
Sheep Mountain Dacite	Sanidine	SCLF	1	33.89	0.07	--
Thorn Ranch Tuff; Bimodal population: 33.83 (n=4), 34.08 (n=4)						
Intracaldera	Sanidine	SCLF	5	33.87	0.11	--
Outflow	Sanidine	SCLF	3	34.01	0.17	--
Badger Creek Tuff						
Badger Creek Tuff	Sanidine	SCLF	2	34.06	0.15	McIntosh and Chapin, 2004
Conejos Formation, early (undivided)						
North side	Biotite, groundmass	Plateau	2	33.5–35.0	--	--
South side	Sanidine (dacite)	SCLF	1	32.72	0.09	--
Jacks Creek volcano						
Andesite to rhyolite lavas and dikes	Biotite, groundmass	Plateau	10	34.2–34.6	--	--
Central volcanoes south of Saguache paleovalley						
Tracy volcano	Sanidine, biotite, hornblende	SCLF, Plateau	8	31.6–33.7?		--
Beidell-Lime Creek volcano	Sanidine	SCLF	1	33.39	0.07	--

[1]Bold, regional ignimbrite sheets, major caldera units.

[2]Analysis type: SCLF, single-crystal laser fusion; Plateau, incremental-heating analysis. Calibrated to Fish Canyon Tuff, 28.02 Ma.

[3]Ages for multiple samples are weighted means or ranges.

[4]Error for SCLF, standard error of weighted mean (Se); error for plateau age, two standard deviations (2σ).

Among the broader topics examined during the Day 6 field trip (fig. 167) are some complexities of ignimbrite eruption and emplacement, geometric relations between caldera subsidence and resurgence, petrologic diversity during sequential eruptions that formed a single ignimbrite sheet, and volumes of outflow and intracaldera ignimbrite in relation to caldera size and the inception of subsidence. The Bonanza area also provides perspectives on recurrent eruption of intermediate-composition lavas after caldera-forming events, emplacement of subvolcanic plutons, magnitude and rates of caldera resurgence, relations to regional extensional faulting, involvement of mantle-derived mafic components in magma generation, time-space-volume-compositional progressions in the SRMVF, and comparisons with continental-margin volcanism elsewhere.

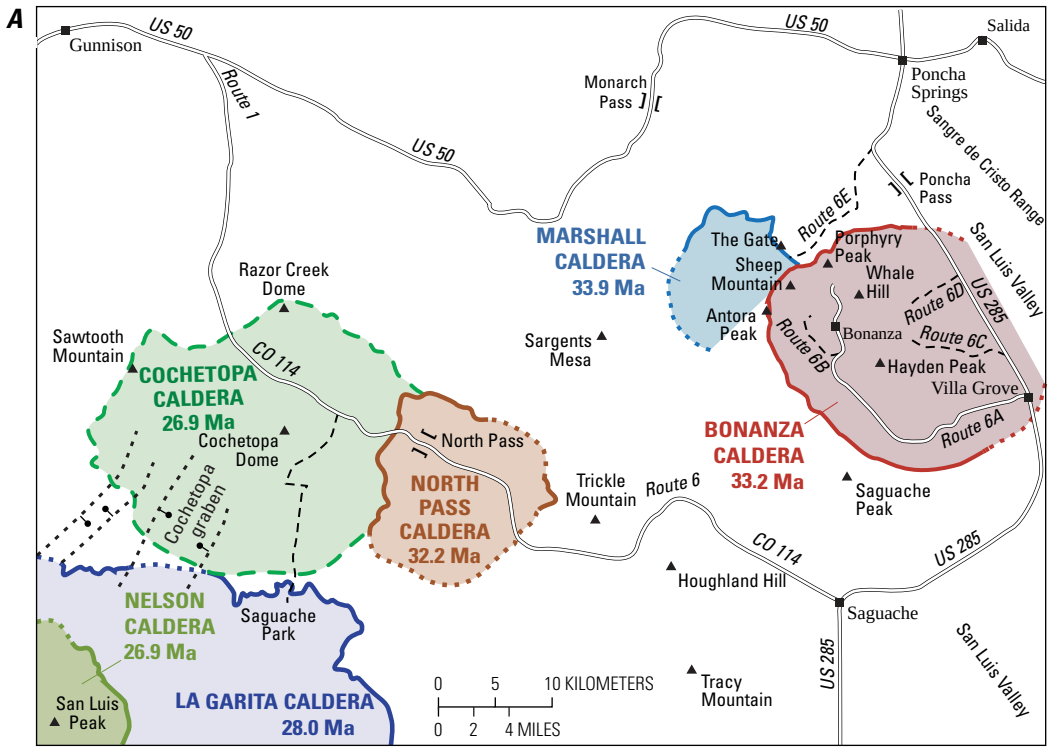

Figure 167. Field-trip location maps for Day 6. *A*, Road map for the northeastern San Juan region, showing trip routes between Saguache and Salida, Colorado, locations of ignimbrite calderas, and prominent geographic features. *B*, Map of Bonanza and Marshall caldera areas, showing locations of field-trip stops. Locations of some trip stops are shown in more detail on figures 168 and 173.

EXPLANATION

Caldera margins

Remnant of caldera topographic—Long dashed; Unconformable margins of caldera-fill lava and tuff—Solid where exposed, dotted where concealed

Normal fault—Ball and bar on downthrown block; dotted where location concealed

EXPLANATION

Caldera rim—Dotted where location concealed

Bonanza caldera

Marshall caldera

6-1 **Field-trip stop**

Shaded-relief base generated from U.S. Geological Survey 10-m Digital Elevation Model (DEM) data from the National Elevation Dataset, accessed November 2016 at http://ned.usgs.gov/. Horizontal: UTM projection, NAD 83 Datum, zone 13, Vertical Datum: NAVD 1988

Geologic Setting of the Bonanza Caldera

The Bonanza area is more complex than most other sectors of the San Juan Mountains because (1) deep erosion has exposed prevolcanic structures and paleotopography in Paleozoic and Proterozoic rocks beneath the thick Cenozoic volcanic cover of the SRMVF; (2) ring-fault-subsidence and uplift structures of the strongly resurgent Bonanza caldera are exposed at deep levels down to the floor of this geometrically complex caldera; (3) widespread alteration and vein mineralization obscures stratigraphy and structure within the Bonanza mining district; and (4) postvolcanic extension produced normal faults, tilted strata, and accommodation-zone structures at the junction between the San Luis Valley and Upper Arkansas segments of the Rio Grande rift zone (fig. 90). Recognition and interpretation of multiple episodes of faulting and other structures are further hindered by heavy vegetation and limited outcrops in many areas, a lack of well-defined stratigraphy within the massive ignimbrites that fill the Bonanza and Marshall calderas, uncertain distinctions among lava sequences of multiple ages that have similar lithologies, and difficulties in distinguishing effects of fault offsets from stratigraphic discontinuities resulting from nonplanar deposition of volcanic units in deep paleovalleys. Several unconformities along flanks of large paleovalleys in the Bonanza area previously have been represented on regional maps as large faults (for example, Tweto, 1979).

Pre-Cenozoic Rocks in the Bonanza Area

Proterozoic and Paleozoic rocks that crop out widely around the eastern and northern margins of the Bonanza caldera define a rugged paleosurface of highlands and valleys that were repeatedly partially buried and re-excavated during middle Cenozoic volcanism. The Proterozoic rocks include coarsely porphyritic granodiorite intruded into diverse metasedimentary and metavolcanic country rocks of quartzo-feldspathic gneiss, schist, and amphibolite.

Paleozoic sedimentary rocks preserved between Proterozoic basement and overlying Cenozoic volcanic rocks provide important evidence for pre- and synvolcanic structural events. Lower Paleozoic strata are dominantly marine carbonate deposits (Burbank, 1932; Cappa and Wallace, 2007); these have long been subdivided into several formations that provide high-resolution structural markers. Upper Paleozoic rocks are thick continental clastic deposits that record concurrent uplift (ancestral Rocky Mountains) and erosion; distinctive subunits are absent and detailed subdivision has not been possible.

The pre-Cenozoic rocks were further deformed, uplifted, and deeply eroded during Laramide compressional growth of the Rocky Mountains in the Late Cretaceous and early Cenozoic, and the middle Cenozoic volcanic rocks were deposited mainly on Proterozoic rocks with only locally surviving remnants of the Paleozoic sequence. The largest areas of exposed Paleozoic strata, on both sides of lower Kerber Creek, define a south-plunging anticline and an east-west-trending zone of faulting (fig. 168). These features have been interpreted as Laramide structures (Burbank, 1932, p. 37–42; Cappa and Wallace, 2007, p. 38, 45), but we infer that they largely resulted from the subsidence and subsequent resurgence of Bonanza caldera.

Early Lavas (35–33 Ma)

As elsewhere in the San Juan region, ignimbrite sheets and other rocks associated with calderas in the Bonanza region overlie thick lava sequences erupted from large central volcanoes (figs. 164, 168), and record the initial assembly of upper-crustal magma bodies prior to caldera-scale explosive eruptions. Sections of the early lavas as thick as 2.3 km have been penetrated by petroleum exploration drilling southeast of the Bonanza area (Gries, 1985; Brister and Gries, 1994). In comparison with the early-intermediate assemblages farther south and west in the San Juan Mountains, lava thicknesses in the northeastern area are more variable owing to the rugged prevolcanic paleotopography. The assemblage in the Bonanza region also contains greater proportions of proximal lavas and breccias relative to distal laharic conglomerates and other volcaniclastic rocks, and voluminous dacite and rhyolite components within the dominantly andesitic lava assemblage.

Rocks of the central volcanoes are broadly correlative with the regional Conejos Formation (Lipman and others, 1970; Colucci and others, 1991), but several early erupted tuff sheets from calderas along the Sawatch Range trend are interstratified with lavas that predate all ignimbrites from farther south and west in the San Juan Mountains (fig. 169). The ignimbrites and sparse sanidine-bearing lavas help define the eruptive history of early lavas in more detail than possible elsewhere in the region. The lavas that are interstratified with the early tuff sheets, as well as andesitic and dacitic lavas that ponded within ignimbrite calderas throughout the San Juan region, are compositionally indistinguishable from earlier-erupted lavas of the Conejos assemblage and document eruptive and compositional continuity during growth of the SRMVF.

On a regional scale, the total thickness and volume of the early lavas are far greater than for interstratified and overlying ignimbrite sheets. In the Bonanza area, lavas are locally exposed over a vertical range of more than 1,000 meters (m) from along Saguache Creek to the Continental Divide, but thickness tends to decrease northward toward the Gunnison valley and eastward toward the San Luis Valley segment of the Rio Grande rift zone. Paleohills of basement rocks project through the volcanic cover here more widely than farther to the south and west in the San Juan region. Within the Bonanza caldera area (fig. 168), the early lavas thin against prevolcanic paleohills, and some Bonanza Tuff was deposited directly against Proterozoic granite.

At least five major eruptive centers for pre-Bonanza lavas, all equivalent to rocks of the Conejos Formation farther to the southwest, lie within the Bonanza caldera area, and others are present farther west (Lipman, 2012). These centers probably include the earliest sizable eruptions in the San Juan region (table 15). Eruptions shifted west and south with time and include Jacks Creek volcano (34.6–34.2 Ma) and andesitic and dacitic lavas (33.9–33.4 Ma) that filled Marshall caldera (eruptive source of the Thorn Ranch Tuff). These eruptions were followed by the

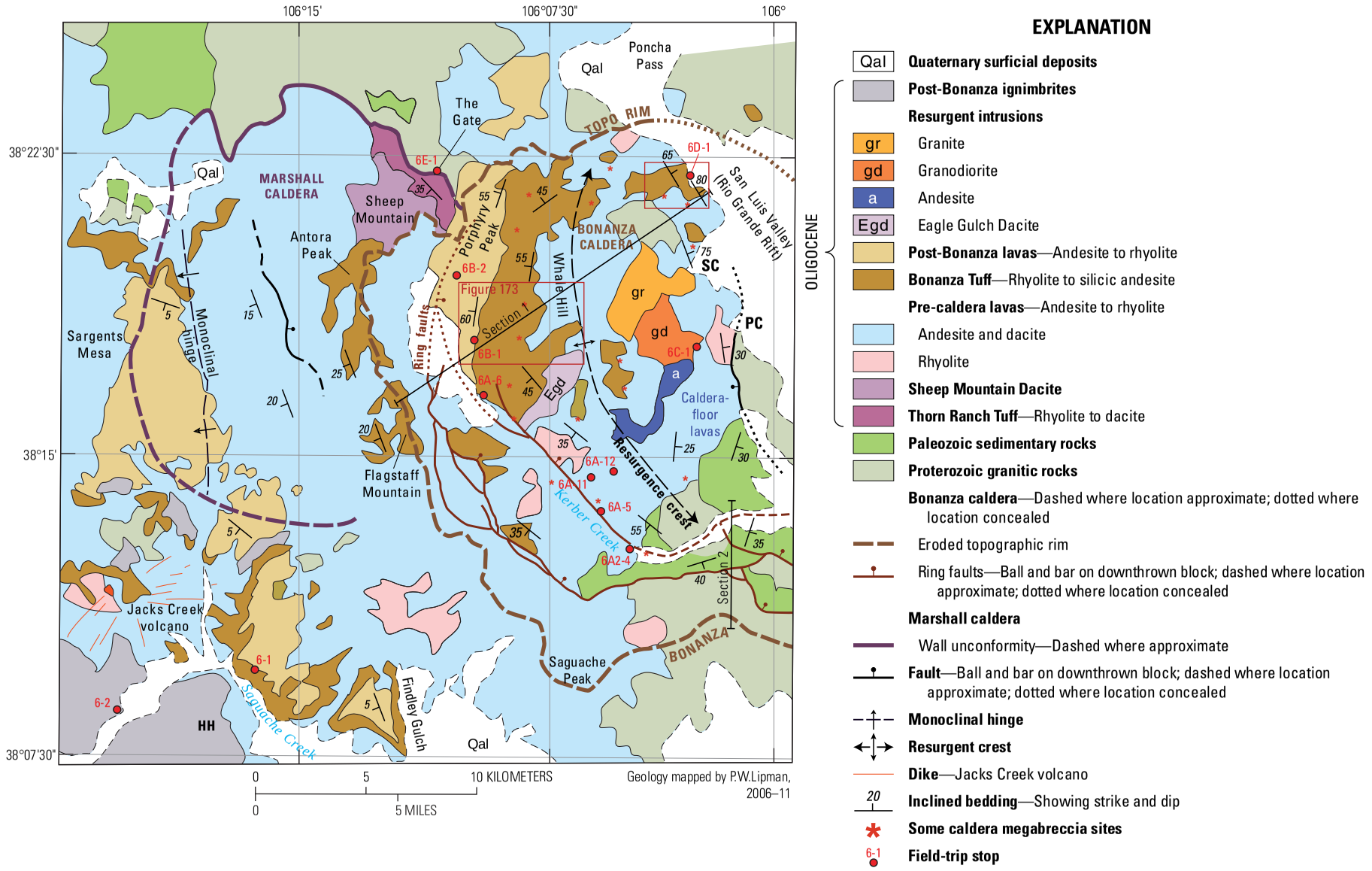

Figure 168. Generalized geologic map of Bonanza and Marshall calderas, showing major stratigraphic units, structural features, and locations of cross sections (fig. 175), modified from Lipman and others (2015). The margin of Marshall caldera is marked by an unconformity between caldera-fill and precaldera rocks. The approximate topographic rim of Bonanza caldera is inferred from the distribution of intracaldera rocks and from erosionally modified present-day morphology. Red rectangles indicate the location of detailed geologic maps (figs. 173, 204). Locations of Stops 6A-8 to 6A-10 and Stop 6B-1 shown on figure 173. Rectangular grid, boundaries of 7.5-minute quadrangle maps. HH, Houghland Hill; PC, Peterson Creek; SC, Spring Creek.

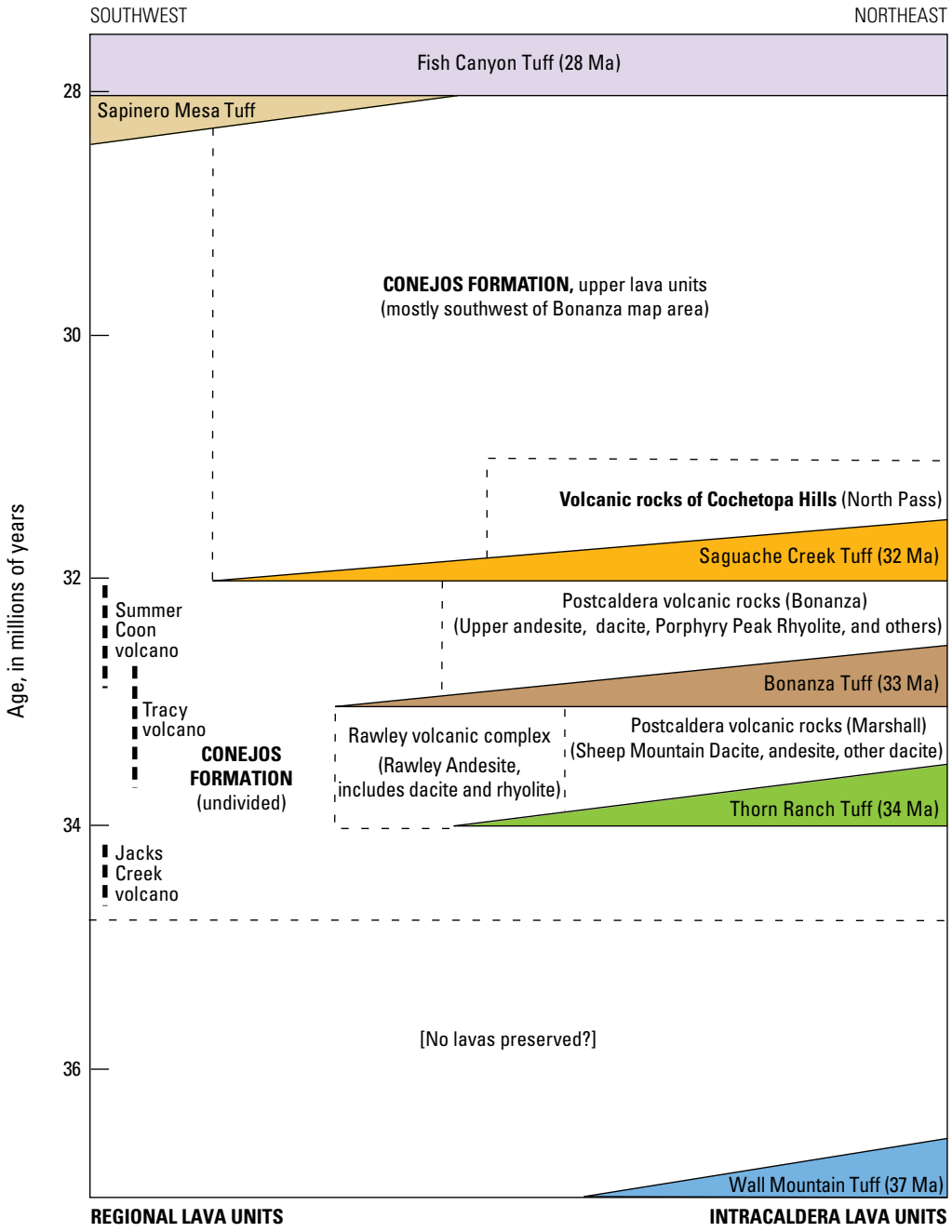

Figure 169. Diagram of stratigraphic relations between regional ignimbrites and early intermediate-composition lavas (Conejos Formation), northeast San Juan region. Thin-dashed lines delimit locally mapped lava units in relation to associated calderas. Thick vertical dashed lines, approximate age spans of mapped central volcanoes along the east flank of the San Juan Mountains.

Rawley cluster of volcanoes (33.7–33.3 Ma) that formed a volcanic highland within which Bonanza caldera is centered (fig. 168). A thick andesite pile of poorly constrained age (~33.2 Ma?) accumulated along Sargents Mesa along the Continental Divide west of Bonanza, and the large Tracy volcano south of the Saguache valley (~33.7–31.6 Ma) erupted intermediate-composition lavas both before and after the Bonanza Tuff.

Thorn Ranch Tuff and the Marshall Caldera Cycle (33.9 Ma)

Eruption of the Thorn Ranch Tuff, from the previously unmapped Marshall caldera (figs. 164, 165), was the closest in space and time to the ignimbrite from Bonanza 0.8 million years (m.y.) later, and features of this caldera provide the basic stratigraphic and morphologic framework for interpreting the younger volcanism at Bonanza. The thick sequence of intermediate-composition lavas that filled Marshall caldera merge with precursor lavas of the Bonanza cycle, and Bonanza caldera caved away the southeastern margin of the earlier caldera. Along with the slightly younger Saguache Creek Tuff (32.2 Ma; Lipman and McIntosh, 2008), these three major ignimbrite eruptions and associated calderas of the northeast San Juan Mountains bracket a major geographic transition, from earlier SRMVF activity along the Sawatch Range trend, into the locus of peak eruptive activity in the San Juan region (figs. 90, 91).

Although largely concealed beneath younger lavas and partly truncated by Bonanza caldera, Marshall caldera is the oldest ignimbrite source in the San Juan region. Along the previously unrecognized northeastern margin of this caldera, intracaldera Thorn Ranch Tuff, more than 400-m thick with no base exposed, banks spectacularly against Proterozoic wall rocks at a geographic feature known as The Gate (figs. 165, 168; Stop 6E-1), east of Marshall Pass. This steep unconformity has been depicted on regional maps as a contact of andesite lava against the Proterozoic basement (Tweto and others, 1976; Cappa and Wallace, 2007), but densely welded, lineated tuff dips parallel to caldera-wall contacts at The Gate and contains large fragments of Proterozoic rock derived from the wall.

The northern wall of Marshall caldera is exposed continuously from The Gate northwestward into upper Marshall Creek (figs. 165, 168), where it projects southward, as constrained by exposed Proterozoic and Paleozoic rocks farther west. Its southwestern margin is concealed beneath caldera-filling lavas and younger volcanic rocks (33.9–33.4 Ma), but an east-west alignment of paleohills composed of Proterozoic rocks and parallel exposures of the Bonanza and Saguache Creek Tuffs just to the north provide limits to the southern extent of Marshall caldera. The southeastern margins appear to have been deeply buried beneath younger lavas and clastic rocks of this caldera cycle and the Rawley volcanic complex, then truncated by Bonanza caldera. Based on these relations, Marshall caldera is estimated to be ~15 × 20 km, with a subsided area of ~250 km^2.

No postcollapse resurgence is evident at Marshall caldera, and much of its structure is concealed beneath lavas that overflowed the collapse area. The caldera is exposed at relatively shallow levels, revealing only the upper parts of the intracaldera ignimbrite, overlain by postcollapse lavas. Exposed landslide megabreccia in upper Marshall Creek is stratigraphically high in the intracaldera ignimbrite, and directly overlain by caldera-fill andesite. This geometry suggests abrupt subsidence late during the eruption, which followed sustained, slower subsidence at the time of accumulation of the thick ignimbrite exposed at The Gate. This ignimbrite contains abundant lithic fragments as much as 0.5-m across but lacks discrete interleaved megabreccia lenses.

The postcollapse lavas merge to the south and west with petrologically indistinguishable andesite and dacite of the Rawley volcanic complex (as old as 33.7 Ma) that form a constructional highland in the Bonanza area, a precursor to this caldera cycle. The postcollapse lavas of Marshall caldera also interfinger with lake-bed deposits of the Pitch-Pinnacle Formation of Olson (1983) and Gregory and McIntosh (1996). This sedimentary assemblage is thickest beyond the northwestern margin of Marshall caldera, in an embayment that appears to have been a broad paleovalley disrupted by caldera-forming events, then occupied by a lake concurrently with postcaldera lava eruptions.

Small remnants of partly welded dacite ignimbrite, preserved locally east and northeast of Marshall caldera, are interpreted as proximal Thorn Ranch Tuff on the basis of ages, compositions (tables 15, 16), and physical similarities to the intracaldera accumulation and widespread outflow east of the Rio Grande rift zone. Perplexingly, no outflow remnants of Thorn Ranch Tuff or any other ignimbrite sheet that could be related to Marshall caldera have been identified farther west or south in the San Juan Mountains, even though basal volcanic strata are exposed widely in contact with underlying Mesozoic and Proterozoic rocks (Lipman, 2012). Because of these limited exposures, the eruptive volume of the Thorn Ranch Tuff cannot be determined in detail, but the large area of Marshall caldera (>250 km^2), the presence of intracaldera tuff more than 400-m thick with no base exposed, and the preservation of outflow tuff at least 70 km east of the source caldera (McIntosh and Chapin, 2004, fig. 2D) indicate a major ignimbrite eruption, conservatively estimated as 250–500 km^3.

Marshall caldera is eroded less deeply than Bonanza, lacks exposed comagmatic intrusions, and exposes only the upper portions of the caldera-filling ignimbrite. This geometry is consistent with Rio Grande Rift-related regional westward tilting (~10–20°) of a large structural block that includes the Sawatch Range and continues south nearly to the valley of Saguache Creek (fig. 90).

Bonanza Caldera Cycle (33 Ma)

Bonanza caldera, source of the 33.12-Ma Bonanza Tuff (~1,000 km^3), is the southernmost and youngest of the ignimbrite centers aligned along the Sawatch Range trend (fig. 90). In contrast to the multicyclic, nested caldera loci for successive eruptions at many large-volume ignimbrite flare-ups elsewhere, Bonanza is an areally isolated collapse structure that formed in response to a single ignimbrite eruption. Although the western topographic rim of Bonanza impinges on Marshall caldera, projected structural boundaries of the two calderas appear to be largely or entirely separate.

Existence of a caldera in the Bonanza area was first inferred from a local gravity low (Karig, 1965), followed by recognition that the Bonanza latite of Patton (1916) and Burbank (1932) was a welded tuff that likely erupted from the Bonanza area (Bruns and others, 1971). As an outgrowth of exploration for porphyry copper-molybdenum deposits at depth below the mineralized veins at Bonanza, Varga and Smith (1984) synthesized available regional data, augmented by new chemical and isotopic analyses, as evidence for a trapdoor caldera of relatively modest size (~8 × 12 km), in which the subsided block was tilted westward and hinged on its east side. Details of this interpretation are problematic, however, because lavas that overlie the intracaldera ignimbrite are tilted steeply westward along with the underlying ignimbrite. Such a relation would require the caldera to have subsided after emplacement of the lavas, rather than accompanying the ignimbrite eruption.

Bonanza caldera is here reinterpreted as a much larger resurgent caldera, about 20 × 25 km across, in which the caldera floor was uplifted steeply after subsidence (figs. 165, 168). The previously inferred eastern hinge is now inferred to be the crest of a large elliptical resurgent uplift (Whale Hill dome). Small remnants of east-dipping Bonanza Tuff are preserved on the deeply eroded east flanks of the Whale Hill dome, but the eastern margin of the caldera lies concealed beneath the San Luis Valley segment of the Rio Grande rift zone. As a result of the larger

Table 16. Representative compositions, volcanic and intrusive rocks of Bonanza caldera area (from Lipman and others, 2015).

[Deg Min, degrees minutes; Ma, million years ago; LOI, loss on ignition; --, no data]

Sample number	Rock type	Location	$^{40}Ar/^{39}Ar$ Age (Ma)	Latitude (Deg Min)	Longitude (Deg Min)	Oxides, normalized to original totals, without LOI												Trace elements (parts per million)								
						SiO_2	TiO_2	Al_2O_3	Fe_2O_3	MgO	CaO	Na_2O	K_2O	P_2O_5	MnO	LOI	Total	Rb	Sr	Y	Zr	Nb	Ba	La	Ce	Nd
Hinsdale Formation																										
00L-1	Basaltic lava flow	Houghland Hill	21.81	38°7.35′	106°17.68′	50.14	1.86	14.83	11.53	7.30	8.03	2.99	2.68	0.49	0.14	2.87	99.99	53	653	21	160	21	686	23	54	26
Bonanza caldera cycle (33 Ma)																										
Late intrusions																										
11L-8	Interior granite	Spring Creek	--	38°19.22′	106°4.73′	72.84	0.29	13.92	1.74	0.38	0.64	4.15	4.69	0.09	0.08	0.76	98.83	178	164	22	220	35	465	66	107	33
06L-34	Sparsely porphyritic aplite	Spring Creek	33.26	38°19.43′	106°3.36′	77.60	0.17	12.60	0.74	<0.10	0.24	3.61	5.12	0.10	0.03	0.77	100.20	233	10	10	128	45	22	58	106	30
08L-4B	Granodiorite	Ridge, North of Kelly Creek	--	38°17.63′	106°3.71′	62.42	0.60	17.41	4.54	0.72	3.81	4.55	3.72	0.38	0.09	1.26	98.24	72	985	24	266	17	1,752	63	124	57
08L-41	Intrusive andesite	Ridge, North of Kelly Creek	33.06	38°17.62′	106°3.53′	54.14	1.61	15.62	9.20	4.29	6.12	3.35	3.46	0.67	0.15	0.18	98.61	120	836	38	472	43	1,227	89	192	81
06L-35	Coarse gabbro	Peterson Creek	--	38°17.89′	106°3.38′	55.17	1.49	15.91	8.71	3.68	5.57	3.30	4.11	0.72	0.14	1.92	98.81	161	751	35	530	46	1,350	110	223	115
Postcaldera lava flows																										
08L-17	Crystal-poor rhyolite	Porphyry Peak	--	38°21.35′	106°9.09′	74.67	0.23	13.73	0.80	0.20	0.41	3.19	5.55	0.03	0.01	1.26	98.83	198	37	16	203	39	106	41	67	23
07L-53	Dacite of Hayden Peak	Hayden Peak, east	32.64	38°16.47′	106°6.01′	69.73	0.45	15.42	1.99	0.31	0.86	4.52	5.77	0.06	0.06	1.03	99.18	144	261	31	378	28	1,825	57	116	50
08L-44	Large-sanidine dacite lava	Silver Creek	32.76	38°21.39′	106°10.24′	65.65	0.69	15.50	3.99	1.65	3.22	4.05	4.24	0.27	0.07	1.16	99.33	122	583	23	254	29	1,063	63	112	41
13L-4	Upper dacite lava	Slaughterhouse road	--	38°18.14′	106°10.39′	64.61	0.70	16.71	4.13	0.70	2.83	4.17	4.72	0.28	0.16	0.94	99.03	141	646	29	362	28	1,579	74	138	57
10L-19B	Malpais andesite	Bear Creek	--	38°14.84′	106°19.52′	58.69	1.10	17.18	6.66	2.47	5.30	3.66	3.49	0.45	0.12	0.92	99.11	72	931	26	215	16	1,465	43	97	47
07L-56	Squirrel Gulch Andesite	Kerber Creek	33.38	38°19.29′	106°9.58′	58.85	0.93	17.11	6.26	2.81	5.39	3.75	3.77	0.38	0.11	2.74	99.35	70	831	23	332	17	1,493	64	130	57
Bonanza Tuff (33.12 Ma)																										
09L-8A	Bonanza Tuff, upper dacite	Findley Ridge	--	38°7.88′	106°11.98′	61.76	0.82	17.64	4.98	1.21	3.64	4.03	5.14	0.44	0.07	1.15	99.73	119	680	37	446	25	1,362	94	186	82
09L-8B	Bonanza Tuff, upper rhyolite	Findley Ridge	33.07	38°7.85′	106°11.97′	74.14	0.22	13.06	1.35	0.26	1.09	4.02	5.14	0.05	0.07	0.96	99.41	241	53	29	208	43	126	56	112	30
09L-8D	Bonanza Tuff, mid lower dacite	Findley Ridge	33.41	38°7.78′	106°11.83′	63.49	0.81	17.27	3.82	1.06	4.24	3.98	4.96	0.25	0.04	1.60	99.91	196	710	30	431	35	1,175	80	156	61
09L-33B	Mafic scoria, resorbed potassium feldspar	Jacks Creek tributary	--	38°12.09′	106°21.07′	63.91	0.63	17.29	3.31	0.96	2.50	4.04	5.85	0.23	0.09	1.04	98.81	125	593	35	600	23	1,730	105	207	89
11L-10A	Mafic scoria, upper unit	Findley Ridge	--	38°7.84′	106°11.93′	59.72	0.95	17.77	5.35	1.94	4.33	3.91	4.61	0.43	0.13	0.84	99.14	103	825	32	530	21	1,809	92	178	82
08L-33A	Lower crystal-poor rhyolite	Two Creek section	33.09	38°36.49′	105°46.79′	74.57	0.28	13.07	1.23	0.26	0.75	3.80	5.09	0.08	0.04	1.29	99.16	238	84	29	209	47	201	68	111	35
Rawley volcanic complex (~33.8–33.3 Ma)																										
08L-26	Rhyolite lava	North of Kerber junction	33.81	38°13.09′	106°4.79′	71.23	0.31	14.74	1.34	0.09	0.41	4.12	6.46	0.03	0.04	0.54	98.78	137	111	31	355	31	1,158	66	126	51

Table 16.—Continued

Sample number	Rock type	Location	$^{40}Ar/^{39}Ar$ Age (Ma)	Latitude (Deg Min)	Longitude (Deg Min)	Oxides, normalized to original totals, without LOI										LOI	Total	Trace elements (parts per million)							
						SiO_2	TiO_2	Al_2O_3	Fe_2O_3	MgO	CaO	Na_2O	K_2O	P_2O_5	MnO			Rb	Sr	Y	Zr	Nb	Ba	La	Ce	Nd
						Marshall caldera cycle (34 Ma)																				
						Lava fill of Marshall caldera (partly correlative with Rawley volcanic complex)																				
10L-27	Rhyolite lava	Duncan Creek	--	38°21.38′	106°18.62′	76.12	0.11	12.89	0.73	0.09	0.68	3.56	5.24	0.02	0.05	0.64	99.48	195	63	10	97	24	109	32	49	19
08L-35	Sheep Mountain Dacite	Sheep Mountain	33.89	38°21.58′	106°11.68′	65.25	0.45	15.94	2.70	1.22	3.28	3.77	6.30	0.16	0.12	3.62	99.19	108	364	22	479	20	1,310	72	142	55
07L-22	Aphanitic andesite	Mill Gulch	33.61	38°12.56′	106°14.81′	56.58	0.99	17.63	7.04	2.66	5.70	4.37	3.63	0.61	0.13	0.65	99.35	73	1,150	28	350	19	1,712	80	162	69
						Thorn Ranch Tuff																				
09L-10C	Lower, partly welded	South Tallahassee Creek	33.90	38°31.18′	105°33.65′	74.82	0.19	13.27	1.22	0.45	0.71	2.33	5.82	0.03	0.05	4.52	98.89	233	45	32	162	33	116	47	92	38
08A-2	Crystal-poor rhyolite	Silver Creek	--	38°21.62′	106°10.79′	73.09	0.26	13.96	1.48	0.41	1.19	1.35	6.95	0.05	0.11	2.38	98.84	249	52	29	248	31	246	76	145	55
08L-39	Dacite, ridge crest	Starvation Creek	33.89	38°23.10′	106°12.89′	66.24	0.37	15.85	2.21	0.33	3.45	3.89	6.60	0.10	0.06	3.00	99.10	113	183	25	458	24	663	95	179	66

caldera size and revised correlation of the outflow ignimbrite, the combined intracaldera and outflow volume of Bonanza Tuff is estimated at about 1,000 km^3 (table 14), in contrast to the <50 km^3 proposed by Varga and Smith (1984).

Rocks of the Bonanza caldera cycle, along with other northeastern San Juan ignimbrites, are more alkalic than caldera-related rocks located farther southwest in the San Juan region. Total alkalis and incompatible traces elements such as zirconium and light rare earth elements, are higher than for counterpart rock units at calderas such as Creede, bulk compositions of intermediate-composition rocks plot well within trachytic fields, and alkali feldspars are more sodic and lower in barium (fig. 170).

Pre-Bonanza Caldera Volcanism

The composite volcanic highland in which the caldera formed is dominated by intermediate-composition to silicic lavas from several eruptive centers (table 16). Silicic lavas (dacite and rhyolite) high in the precaldera assemblage are more abundant at Bonanza than most other sites of ignimbrite eruptions in the San Juan region and appear to record a prolonged history (33.7–33.2 Ma) of magma assembly and evolution toward evolved compositions. Volcaniclastic deposits interlayered with the lava sequence are less abundant than in similar younger assemblages elsewhere in the San Juan Mountains, consistent with the inference of a precaldera constructional highland.

The presence of a central highland at Bonanza, prior to eruption of the Bonanza Tuff is confirmed by deposition of the ignimbrite in broad radial paleovalleys, as especially preserved on the west and south flanks of the caldera (Varga and Smith, 1984). Much of the highland constitutes fill of the earlier Marshall caldera, and many dated lavas are closer in age (33.7–33.5 Ma) to that caldera than to Bonanza. Only on Sargents Mesa and along the south flank of Bonanza caldera, near Saguache Peak, do relatively low-precision whole-rock dates on andesitic lavas (~33.3–33.2 Ma; Lipman and others, 2015) approach the age of the Bonanza cycle.

Bonanza Tuff

In contrast to the one-sided easterly distribution of preserved Thorn Ranch Tuff in relation its source from Marshall caldera, the Bonanza Tuff is preserved widely both to the east and west of its caldera (fig. 171). Any deposition of this ignimbrite in the vicinity of the Sawatch Range to the north has been completely eroded, however, and it has been covered by younger volcanic deposits or eroded south and west of the Saguache paleovalley.

The Bonanza Tuff is characterized by large and complex lateral and vertical variations in chemical and phenocryst compositions (tables 14, 16), from dark crystal-rich silicic andesite and dacite (25–35 percent; plagioclase, biotite, augite; 60–66 percent SiO_2) to light-colored crystal-poor rhyolite (~5 percent; sanidine, plagioclase, biotite; 73–76 percent SiO_2). A distinctive feature of the dacitic tuff, in both intracaldera and outflow deposits, is the presence of small angular lithics (typically several centimeters [cm] or less), dominantly fragments of andesitic lava (Stop 6A-6). Flattened pumice

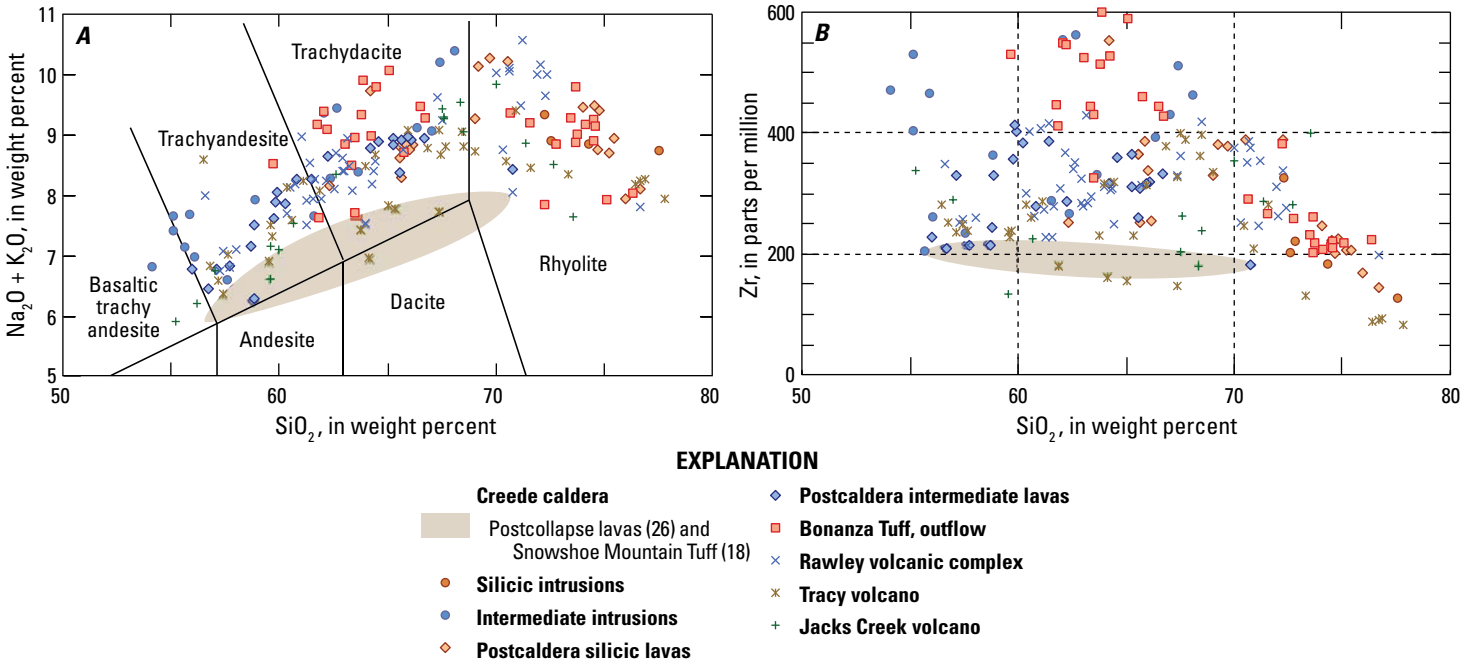

Figure 170. Plots of bulk-rock analyses for the Bonanza area (data from Lipman and others, 2015), compared to data fields for the 27-Ma Creede caldera (numbers of analyses in parentheses). *A*, Total alkali-silica diagram. *B*, Zirconium-silica diagram. Much of the considerable scatter among the Bonanza samples is a result of varying magma compositions, as reflected by the diverse assemblages and compositions, but some scatter also results from deep burial and widespread weak alteration. Overall, the Bonanza Tuff and closely associated postcollapse lavas and intrusions of the caldera cycle are more alkalic and enriched in incompatible elements such as zirconium, in comparison to earlier nearby Conejos volcanoes such as Jacks Creek and Tracy (figs. 164, 168). Lavas of the Rawley volcanic complex, which constitute the most direct precursors to the Bonanza ignimbrite eruption, tend to be transitional between the earlier volcanoes and rocks of the Bonanza cycle. All the volcanic rocks of the Bonanza area are more alkalic and enriched in incompatible elements in comparison to the Creede caldera and other ignimbrite systems farther southwest in the San Juan region (Creede data from Lipman, 2006).

fiamme are conspicuous in the dacite, commonly 5 cm or more long (fig. 172*B*,*C*). In contrast, lithic fragments are rare in the outflow rhyolite, and fiamme are small. Uniquely among rocks of the SRMVF, even mafic dacite (62–64 percent SiO_2) has phenocrysts of sanidine, and some rhyolite contains trace hornblende and titanite.

Prior studies had distinguished a lower dacite (latite) and upper rhyolite, starting with Burbank (1932), but the eruptive significance of the compositional change remained uncertain. From work on the southwest flank of the Bonanza center, Bruns and others (1971, p. 187) concluded that the "Bonanza Tuff consists of two cooling units" but did not describe the contact. Varga and Smith (1984) later described the Bonanza Tuff as consisting of two sheets, each a single cooling unit, not compositionally comagmatic, and erupted from geographically separate vents. Neither of these studies specifically discussed the presence or absence of evidence for a time break, such as bedded tuff or other sedimentary units, between the two Bonanza cooling units, but the implied interpretation was the existence of two separate ignimbrites, an interpretation that has been continued by others (for example, McIntosh and Chapin, 2004). In contrast, our work shows that all compositional variations in both intracaldera and outflow Bonanza Tuff occur within a single ignimbrite sheet characterized by compound welding zonations.

West and south of Bonanza caldera, the outflow ignimbrite sheet is dominantly dark brown crystal-rich dacite, but some proximal sections contain gradational transitions from densely welded lower crystal-poor rhyolite to a thick central zone of dacite, a somewhat less welded upper rhyolite, and, locally to an upper welded dacite (fig. 172). The compositional transitions correspond imperfectly with welding breaks. For example, the change from the main dacite to the upper rhyolite is associated with a bench-forming zone of weaker welding between cliffs of densely welded tuff where well exposed along lower Saguache Creek (Stop 6-1), but the upward gradational decrease in crystal content and increase in silica mainly occurs high in the lower cliff rather than coincident with the zone of least welding. Rare partings, defined by abrupt changes in pumice or lithic size or abundance within the ignimbrite (fig. 172*A*), are interpreted as recording pulsation of eruption intensity or ignimbrite-emplacement dynamics during essentially continuous ignimbrite deposition. No evidence was observed for the existence of significant time breaks during deposition, such as interlayered bedded-surge, tephra-fall, or fluviatile ash deposits in either the outflow ignimbrite or in the thick intracaldera accumulation.

In contrast, outflow Bonanza Tuff, which is preserved 80 km beyond the caldera to the east (fig. 171, was described until recently as a separate rhyolitic ignimbrite, the Gribbles Park Tuff (Epis and Chapin, 1974; McIntosh and Chapin, 2004). The eastern outflow sheet consists dominantly of light-colored, crystal-poor rhyolite but contains a thin internal zone of red-brown dacite, at least at the well exposed sequence at Two Creek (38°36.6' N., 105°46.7' W.) that has been used as a reference section (Epis and Chapin, 1974; McIntosh and Chapin, 2004). The eastern outflow ignimbrite is compositionally zoned similarly to the tuff in the Bonanza area and to the west , but with a much higher proportion of rhyolite to dacite. The total original volume of the eastern outflow must have been large, at least several hundred cubic kilometers.

The thick intracaldera Bonanza Tuff contains even more complex compositional and welding variations within a single ignimbrite unit (fig. 172). Where a complete ignimbrite section (2.5-km thick) from caldera-floor rocks to postcollapse lavas is exposed on the west flank of the resurgent dome (fig. 173), rhyolite and dacite compositional zones interfinger as many as 13 times. As identified by variations in crystal content and groundmass color, dacitic tuff is volumetrically dominant,

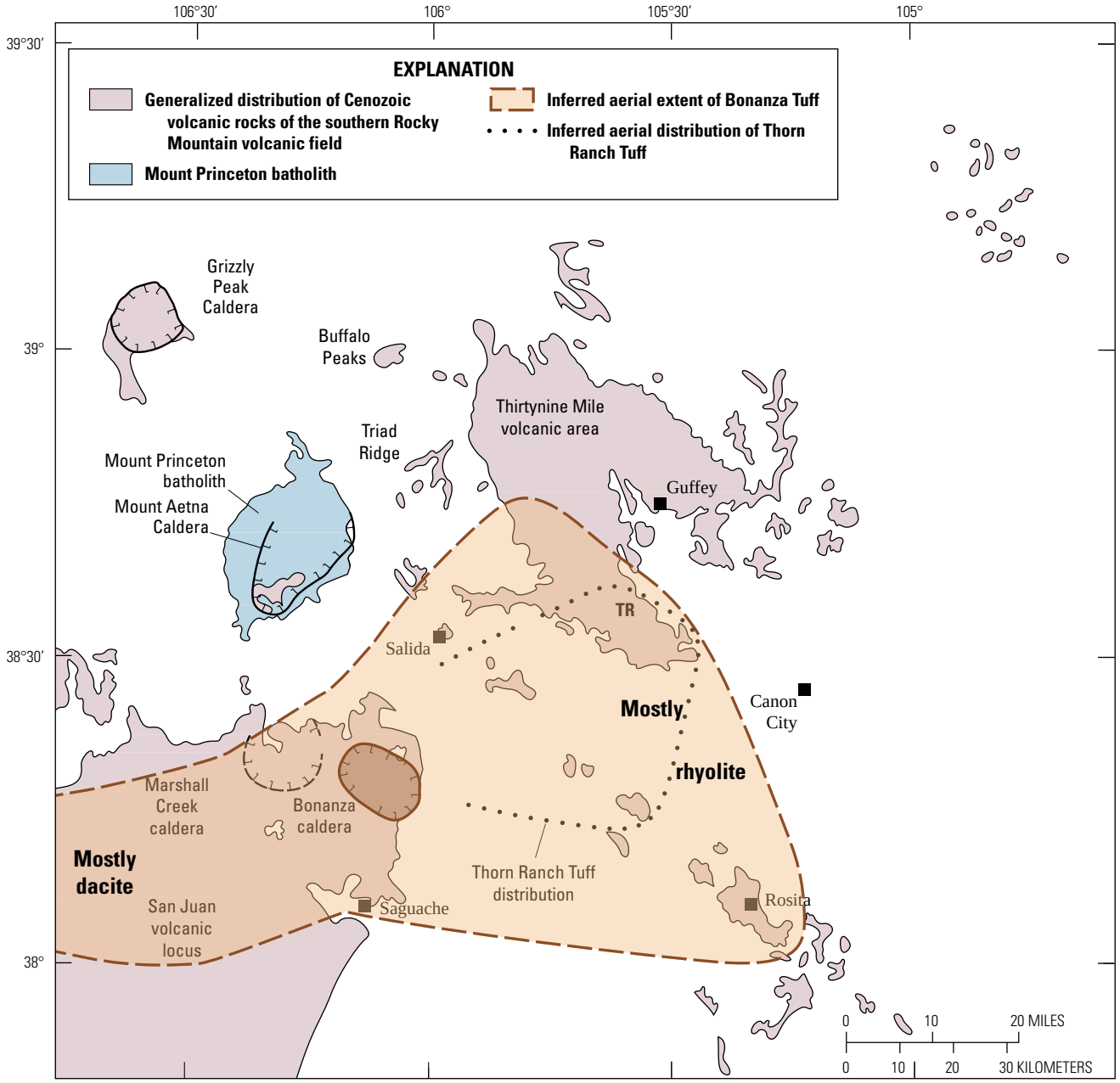

Figure 171. Map showing the approximate areal extent of the Bonanza and Thorn Ranch Tuffs, in relation to preserved erosional remnants (lavender) of middle Cenozoic volcanic rocks (modified from McIntosh and Chapin, 2004). Preserved Bonanza Tuff (tan) east of its source caldera is, dominated by crystal-poor rhyolite; western areas consist mainly of crystal-rich dacite. Numbers in red: distance from the caldera rim. The figure also shows the inferred distribution of the eastern outflow Thorn Ranch Tuff (dotted line). Numbered localities reference samples dated by McIntosh and Chapin (2004).

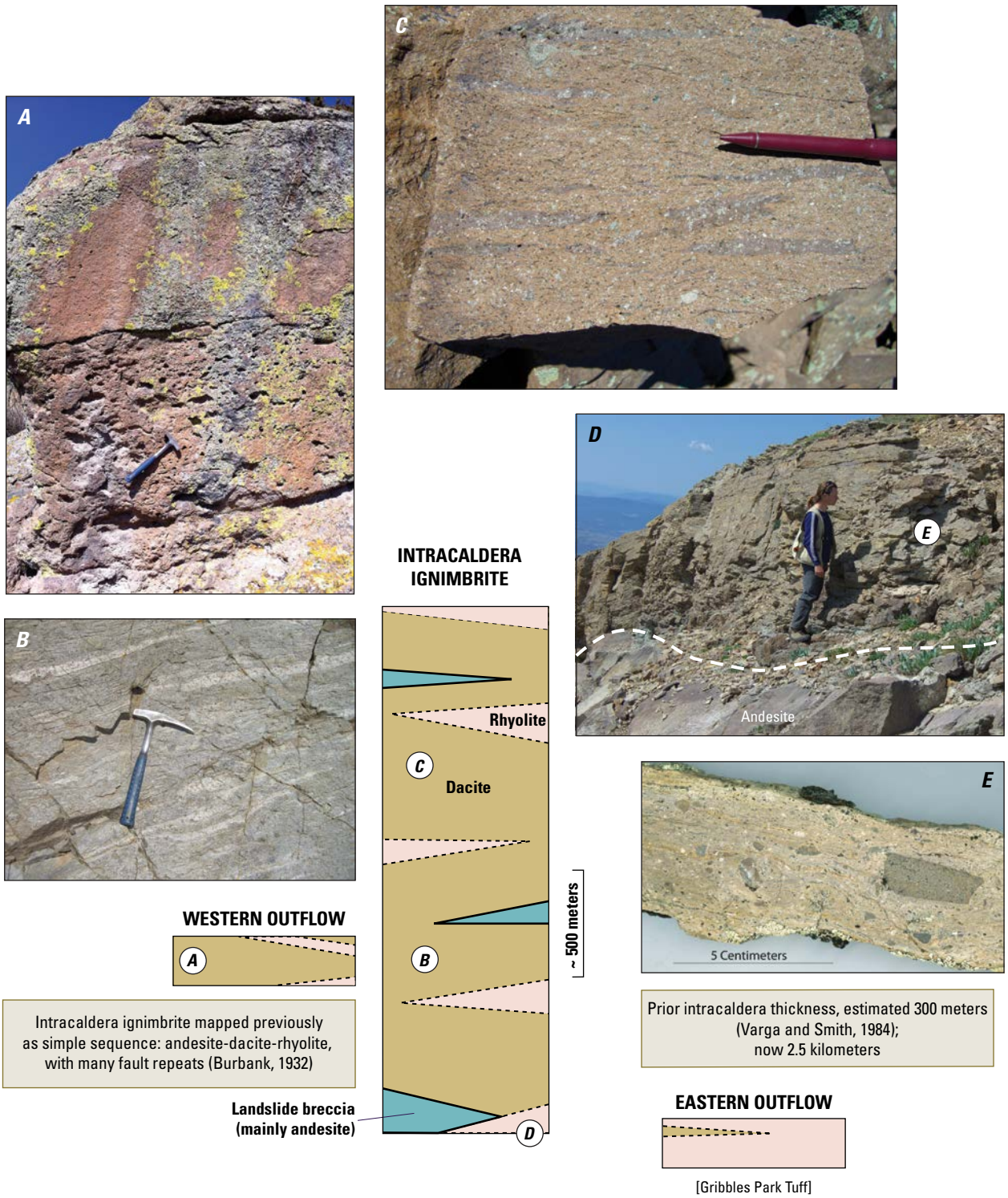

Figure 172. Regional thickness, compositional and textural variations in the Bonanza Tuff. The outflow ignimbrite consists mainly of early erupted rhyolite to the east, and later-erupted dacite to the west. The intracaldera tuff contains multiple compositional zones, ponded to thickness of at least 2.5 km, as exposed on the west flank of the resurgent dome. *A*, Parting within the welded dacite, between relatively pumice-poor tuff and the underlying tuff that contains larger flattened pumice blocks (weathered-out cavities) at the Findley Ridge section (at site of sample 08L-8C; fig. 176). The boundary is inferred to record a pulsating instability in eruptive discharge or fluctuations in emplacement kinematics. *B*, Densely welded intracaldera dacite, with elongate pumice lenses (as long as 0.5 m) that define a down-dip lineation, east of the road above Squirrel Creek. *C*, Typical densely welded dacite on Antora Peak. Flattened pumice lenses are 5–15 centimeters long. *D*, The lower rhyolite unit, densely welded to its base without intervening tephra deposits, deposited against caldera-wall andesite at Windy Point. *E*, The lower rhyolite unit, with a weakly weathered surface on hand sample, shows fluidal welding despite containing abundant andesite fragments. Same location as in *D*. Photographs by P.W. Lipman, U.S. Geological Survey, 2010.

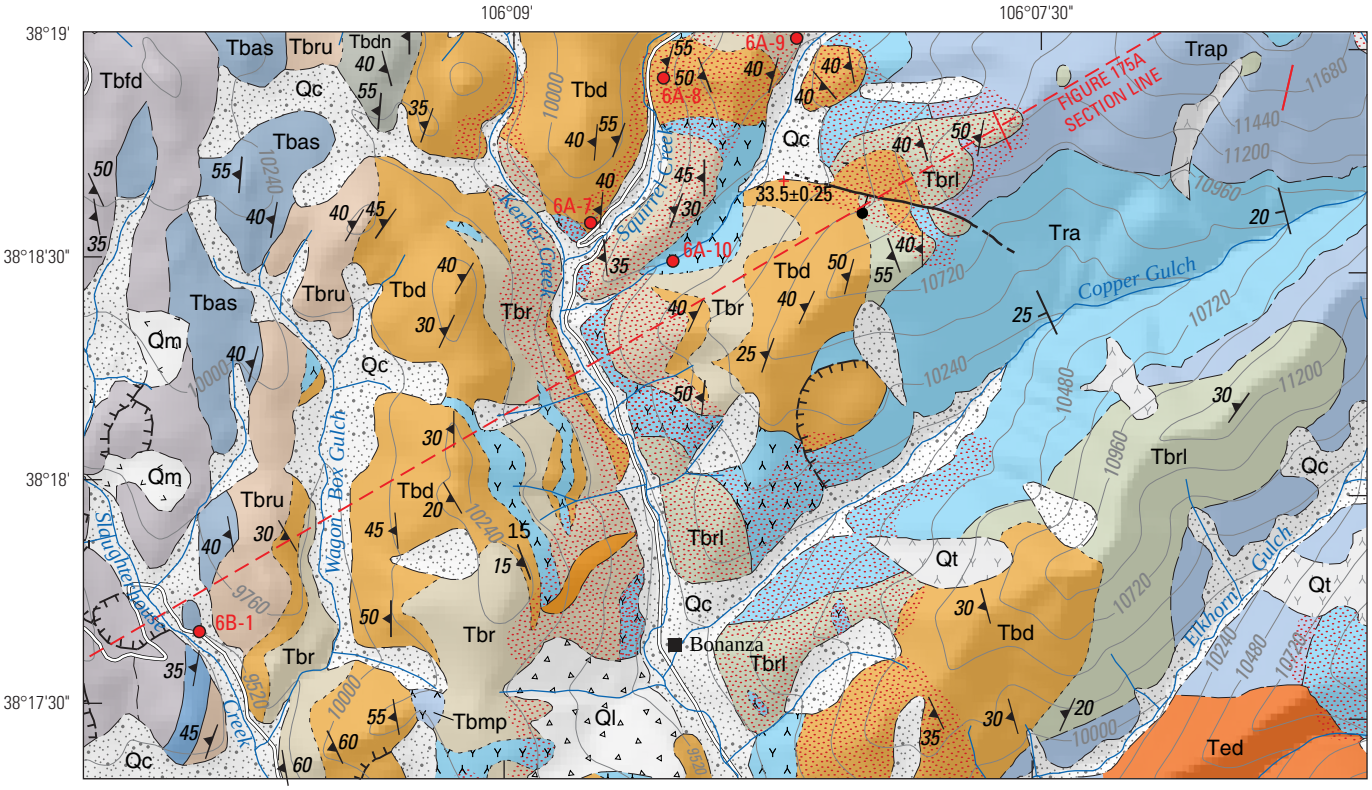

CORRELATION OF MAP UNITS

Quaternary surficial deposits

Qc Qt Ql Qm

Postcollapse lavas and intrusions

Tbfd
Tbap
Tbas
Ted

Bonanza Tuff

Tbru
Tbd Tbr Tbma Tbmp Tbdn
Tbrl

Caldera-floor lavas (Rawley volcanic complex)

Trap
Tra

EXPLANATION

- Qc — **Colluvium (Holocene)**
- Qt — **Talus (Holocene)**
- Ql — **Landslide deposits (Holocene and Pleistocene)**
- Qm — **Moraine and till (Pleistocene; Pinedale glaciation)**

BONANZA CALDERA CYCLE (OLIGOCENE)

Postcollapse lavas and intrusions

- Tbfd — Dacite lavas
- Tbap — Plagioclase andesite lavas
- Tbas — Squirrel Gulch Andesite
- Ted — Eagle Gulch Dacite (intrusion)

Bonanza Tuff

- Tbru — Upper rhyolite
- Tbd — Main dacite
- Tbdn — Nonwelded dacite
- Tbr — Rhyolite
- Tbrl — Lower rhyolite

Intracaldera landslide breccia

- Tbma — Andesite and dacite clasts
- Tbmp — Plagioclase-andesite clasts

RAWLEY VOLCANIC COMPLEX (OLIGOCENE)

- Trap — Plagioclase andesite
- Tra — Andesite

Altered rock—Bleached and oxidized rocks resulting from supergene weathering of pyrite

Contact—Dashed where location approximate; dotted where location gradational

Dike

Fault—Ball and bar on downthrown block; dashed where location concealed

Quaternary slump scarp—Hatchures on downthrown block

30 **Inclined bedding**

30 **Inclined foliation**

6A-10 **Field-trip stop**

Figure 173. Geologic map of the Kerber Creek valley near the town of Bonanza, Colorado, showing part of the west flank of the Whale Hill resurgent dome. The west-dipping section of intracaldera Bonanza Tuff (~2.5-kilometers thick) is overlain conformably by tilted postcollapse lavas, indicating that much of the resurgence postdated eruption of the lava fill. Within the thick intracaldera Bonanza Tuff, multiple compositional and welding zones interfinger with landslide-breccia lenses. Only one small mapped fault disrupts the tilted intracaldera ignimbrite and lava sequence. Location of figure is shown by large rectangle on figure 168. Red-dashed line indicates the position of the central part of the Line-1 cross section (fig. 175*A*).

but the eruptive sequence began and ended with rhyolite. The incomplete caldera-fill section on the steeply dipping northeast flank also contains multiple rhyolite-dacite alternations and is at least 1.5–2-km thick, including thick interleaved landslide-breccia deposits (Stop 6D-1). Besides contacts with landslide breccias, all compositional and welding variations are gradational. The multiple zones of dacitic tuff are typically densely welded (fig. 172*B*,*C*); many of the rhyolite zones appear to be less welded, although the degree of welding is more difficult to evaluate because of common absence of large pumice/fiamme lenses and widespread intense alteration.

The initially erupted lower rhyolite is relatively thin and small in volume within the caldera, varying greatly in thickness within short distances laterally and probably reflecting pre-eruption volcanic topography. This zone is as much as ~100-m thick locally on the southwest flank of the resurgent dome, but it is absent in other nearby exposures and almost the entire exposed north flank. The dacitic tuff is typically densely welded (fig. 172*B*,*C*); in places where it is propylitically altered, the intracaldera dacite is identifiable as welded tuff only by the typical presence of abundant small angular fragments of andesitic lava (Stop 6A-6). Much of the rhyolite is only moderately welded, but some deep intracaldera zones are densely welded to fluidal, and locally rheomorphic (Stop 6A-12). The lower rhyolite is especially fluidal and lava-like on the west caldera rim (fig. 172*D*,*E*) and along the steeply dipping northeast flank of the resurgent dome. Pumice lenses, where distinguishable in fluidal and rheomorphic zones (both rhyolitic and dacitic), commonly define a prominent lineation with prolate elongation ratios of as much as 20:1. Lineations are especially well developed low in the thick ignimbrite section that are well preserved on the west flank of the resurgent dome, typically plunging nearly directly down dip.

The weighted-mean age for sanidine from intracaldera Bonanza Tuff (33.05±0.06 Ma) is marginally younger than that for the outflow ignimbrite 33.12±0.03 Ma; table 15). Although within analytical uncertainty, this difference might reflect prolonged cooling of the multi-kilometer thick intracaldera accumulation or possible effects of later alteration.

Postcollapse Lavas and Intrusions

After the ignimbrite eruption, compositionally diverse lavas ranging from andesite to high-silica rhyolite (table 16) filled the caldera (Route 6B) and spread across adjacent slopes to the northwest and southwest. Postcollapse lavas are not preserved on the more-eroded eastern side of the caldera, but a distinctive thick lava sequence of crystal-poor silicic dacite (69–70 percent SiO_2) on Hayden Peak (figs. 165, 168) appears to have accumulated in a paleovalley carved deeply through intracaldera Bonanza Tuff. The ages of the upper lava sequence of the Bonanza center, including caldera-filling lavas, are broadly bracketed at 33.12–32.25 Ma by the underlying Bonanza Tuff and overlying Saguache Creek Tuff, but the ~1-km-thick intracaldera sequence capped by Porphyry Peak Rhyolite on the west flank of the Whale Hill dome was emplaced rapidly, by 33.03 Ma (mean of five samples; fig. 166, table 15). The lowermost postcollapse lavas (Squirrel Gulch Andesite) directly overlie upper-rhyolitic ignimbrite of the Bonanza Tuff and were tilted steeply along with the underlying tuff during later resurgent uplift. In contrast, some late caldera-filling lavas (Porphyry Peak Rhyolite and sanidine-bearing dacite) may be tilted somewhat less, based on contact geometry (primary depositional attitudes are difficult to constrain precisely in these massive viscous lavas that commonly form widespread talus on steep, vegetated slopes).

In contrast to many other large ignimbrite calderas, only small deposits of lake sediments or small late pyroclastic eruptions are preserved in the postcollapse fill at Bonanza. The rarity of intracaldera volcaniclastic rocks at Bonanza is consistent with rapid accumulation of the lavas, largely or entirely prior to major resurgent uplift The time span between the Bonanza ignimbrite eruption at 33.12±0.03 Ma and that of Porphyry Peak Rhyolite that overflowed the northern caldera margin by 33.03±0.04 Ma (table 15) indicates that at least 1 km of lava accumulated in the northwestern caldera area within as little as 20 thousand years (k.y.) and no more than 160 k.y., based on the 2-sigma uncertainties for the weighted-mean ages.

Compositionally and texturally diverse intrusions varying from gabbroic to silicic granitoid rocks intruded the caldera floor and lowest ignimbrite fill, and formed widely scattered exposures that are inferred to represent an irregular roof zone of a more continuous composite body at slightly greater depth (fig. 168). The largest intrusions crop out on the deeply eroded eastern side of the Whale Hill resurgent dome. Texturally diverse areas of granodiorite (56–62 percent SiO_2) and intergradational finer-grained phases, which form the 3 × 7 km exposed area of the Turquoise Mine intrusion on the eastern side of the dome (Route 6C), are compositionally similar to postcollapse andesite and dacite preserved on the west flank. Fine-grained intrusive phases, which cover areas as much as several hundred meters across, form bold outcrops of dense dark andesite (55–56 percent SiO_2), characterized by rectilinear jointing unlike the hackly fractures that characterize most andesite lavas in the Bonanza area. Some larger areas of the finer-grained phases are composites, and contain internal contacts between subunits that differ in phenocryst abundance, size, and (or) mode. The areal abundance of intrusive andesite, comingled with coarser granodiorite, is interpreted as representing the roof zone of a large intermediate-composition intrusion that would likely be less heterogeneous at greater depth. Several small exposures of similar granodiorite to andesite crop out farther west, along tributaries of Kerber Creek (Stop 6A-9), and mineral-exploration drilling on Mount Manitou (north end of Whale Hill, fig. 168) penetrated granitoid rocks at depths of about 1 km (Cook, 1960; Gordon Gumble, Union Molycorp, written commun., 2006).

A pluton of aplitic to porphyritic granite exposed at near-roof levels in an ~3 × 4 km area of upper Spring Creek (fig. 168) is compositionally similar to postcaldera lavas of the Porphyry Peak Rhyolite. The roof zone and margins of the Spring Creek intrusion are composed of aplitic porphyry (74–77 percent SiO_2) that contains 5–15 percent euhedral potassium feldspar; the deeper interior portions of the exposed intrusion are also porphyritic but have a medium-grained matrix that is modestly

less silicic (72–73 percent SiO_2). Microperthitic and weakly argillized potassium feldspar from the granitoid intrusions have not been datable with precision comparable to volcanic sanidine, but the somewhat varied cooling ages (33.3–32.8 Ma; table 15) overlap with those from the Bonanza Tuff and postcaldera lavas. These cooling ages, together with field relations, indicate emplacement of the resurgent plutons shortly after caldera eruption. Numerous other caldera systems display similarly rapid timing (for example, review by Lipman and Bachmann, 2015).

A roughly concordant sill-like body of uniform dacite (67–68 percent SiO_2), the Eagle Gulch Dacite (latite of Burbank, 1932), was intruded between caldera-floor andesitic lavas and basal intracaldera Bonanza Tuff along a northeast-trending belt about 8-km long from Kerber Creek to the north slope of Elkhorn Peak. The irregular sill-like shape and uniform texture and composition of the Eagle Gulch Dacite differ from the more diverse granitoid intrusions, which are interpreted as the uppermost levels of a vertically extensive composite intrusion within the Whale Hill resurgent dome.

Caldera Evolution and Structure

Despite detailed complexities, the overall evolution of Bonanza caldera has the simplifying attribute of involving only a single large ignimbrite eruption and attendant caldera formation. The diverse exposure levels provide special insights concerning the timing of caldera subsidence, distribution of subsidence faults, caldera-floor structures, geometry of resurgent uplift, and ignimbrite and subsidence volume estimates.

Inception of Caldera Subsidence

The asymmetric areal distributions of the outflow rhyolite and dacite tuffs from Bonanza caldera provide key information on the paleotopography and timing of the initial caldera collapse (fig. 174). At the inception of the eruption, some barrier on the west side, either prevolcanic structural highlands or earlier volcanic constructs, must have impeded ignimbrite flow; early erupted rhyolitic ash spread mainly to the east. The beginning of caldera collapse late during the eruption of the lower rhyolite appears to have disrupted the western barrier, accompanied by increased eruptive draw-down and (or) tapping of a new sector of a compositionally complex reservoir that led to the initial discharge of voluminous dacite. Dacite was then able to spread widely to the west while accumulating thickly within the subsiding caldera, concurrent with additional, intermittent eruptions of rhyolitic tuff.

The relatively modest thicknesses and limited areal extent of the lower-rhyolite zone within the Bonanza caldera provide the primary documentation that caldera collapse began relatively late during this phase of the ignimbrite eruption. If subsidence had accompanied the inception of the eruption, or even triggered initial magma expulsion as proposed in some models for large ignimbrite calderas (for example, Sparks and others, 1985), a much greater thickness and volume of the early rhyolitic ignimbrite should have ponded within Bonanza caldera. If a volume of early rhyolite tuff comparable to that of that in the eastern outflow sheet (estimated at 200–300 km^3) had accumulated concurrently within Bonanza caldera, the thickness of intracaldera early rhyolite would have been greater than 1 km. Even though later stages of the Bonanza eruption

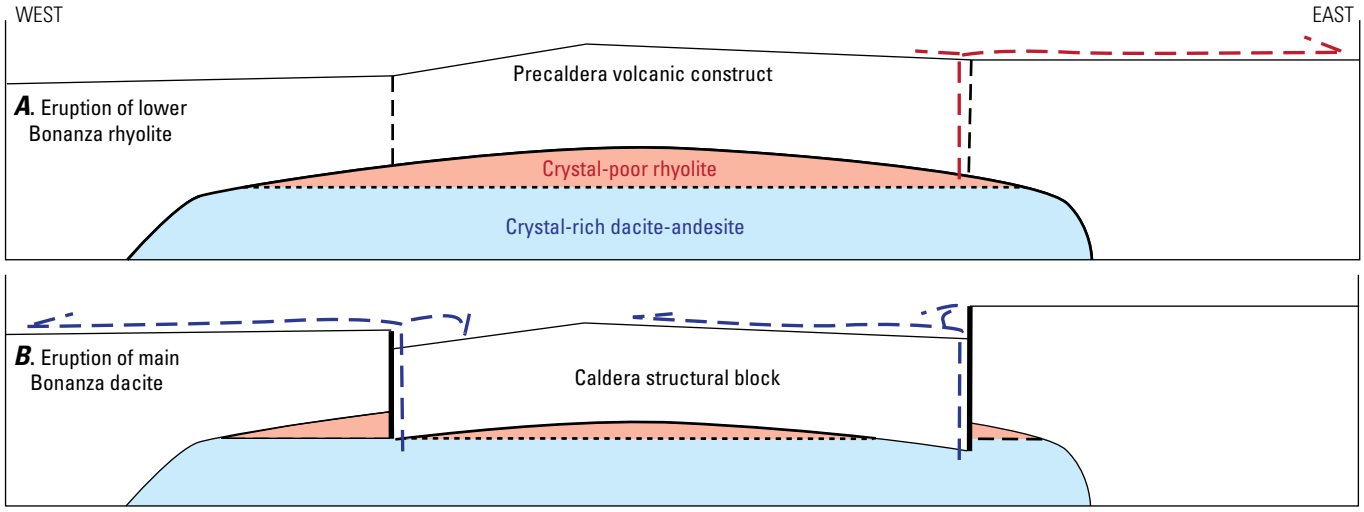

Figure 174. Schematic caldera-collapse model, indicating possible paleotopographic controls on contrasting distributions of outflow Bonanza Tuff, even though the tuff erupted from a laterally extensive layered or zoned magma body. *A*, Initial eruptions of rhyolite (from vents on the east side of the future caldera?) spread widely to the east, perhaps blocked from westward flow by the precaldera construct of the composite Rawley volcano complex and similar accumulations of intermediate-composition lava that filled the earlier Marshall caldera. The lower Bonanza rhyolite is thin and discontinuous within the caldera area, indicating that subsidence began only late during eruption of this phase. *B*, Dacitic phases of the Bonanza ignimbrite eruption ponded thickly within the subsiding caldera and spread far to the west but are largely absent in the eastern outflow sheet. A possible interpretation is that inception of caldera subsidence and perhaps shifting vent locations provided access for pyroclastic flows to cross the western flanks of the Bonanza center. An alternative could be the presence of separate rhyolite and dacite magma bodies in close proximity beneath the caldera.

were accompanied by concurrent caldera subsidence, the outflow volume of lower rhyolite alone is comparable to that of several uniform dacite ignimbrites in the SRMVF (table 9) and elsewhere, suggesting that no simple correlations exist between eruptive volumes or magma compositions and inception of caldera subsidence.

Interfingered with the alternating zones of rhyolite and dacite ignimbrite within Bonanza caldera are many irregular lenses of brecciated precaldera rocks (figs. 172, 173), both mesobreccia and much larger masses of little-broken massive lava, which are interpreted as landslide debris derived from caldera walls that had become oversteepened during subsidence. Individual blocks in some lenses are larger than outcrops and are termed megabreccia (Lipman, 1976b). Some breccias are heterolithologic at outcrop scale, but other large areas of blocks are composed of compositionally uniform lava. The most voluminous breccia, locally as much as several hundred meters thick, is low in the caldera fill, close to or in direct contact with caldera-floor rocks. Boundaries between breccia and floor can be obscure and difficult to map with precision. The deep breccia is well-preserved along the southwestern and northern margins of the central resurgent uplift, in proximity to caldera ring faults and the inner wall. Exposures are especially good on the dry, southwest-facing slopes of Kerber Creek valley (Stop 6A-12). Much less breccia appears to have reached central areas of the caldera floor as exposed along the crest of the resurgent dome, and the landslides appear to have thinned with distance from the inner caldera walls. The voluminous deep breccias, in places deposited directly on caldera-floor rocks, are interpreted to record catastrophic initial caldera collapse late during the eruption of the lower rhyolite. Thus, intracaldera landslide breccia at the base of an intracaldera ignimbrite sequence need not necessarily document caldera collapse (or vent enlargement) concurrent with eruption inception.

Smaller lenses of meso- and megabreccia interfinger at higher horizons of the intracaldera Bonanza Tuff (Stops 6A-7, 6A-10), indicating that caldera walls became oversteepened intermittently during subsidence, but not as severely as during the initial collapse. Most breccia consists of andesite and dacite fragments from the Rawley complex, but Proterozoic debris is also present, especially within northern sectors of the caldera fill. A Proterozoic source for landslides along this sector would have required deep, early subsidence (>1 km), cutting down below the volcanic fill of Marshall caldera. Another major subsidence event that occurred late during the eruption is recorded by the ~1,000-m difference in elevation between high remnants of Bonanza Tuff, plastered against the west caldera wall between Antora Peak and Windy Point, and the uppermost intracaldera tuff within the caldera structural block that subsided along the Kerber Creek ring fault (fig. 175*A*).

Varied thickness and lateral extent among the multiple interfingering zones of rhyolite and dacite in the intracaldera ignimbrite probably reflect diverse factors, including surface irregularities on the pre-eruption lava assemblage, depositional slopes generated by caldera-wall landslide deposits, and mildly asymmetric caldera subsidence. Caldera-floor morphology probably mainly affected distribution and thickness of the lower rhyolite. The varied thickness and extent of many compositional zones higher in the intracaldera accumulation are spatially unrelated to breccia lenses. These variations suggest that the ignimbrite depositional surface became weakly tilted in several directions during the course of caldera subsidence, and tuff accumulated more thickly down slope. Weakly asymmetrical subsidence at Bonanza is also suggested by rheomorphic structures in rhyolitic tuff deep in the caldera fill and by strongly prolate compaction and elongation of large pumice lenses in dacitic tuff (fig. 172*B*). Such flowage structures seem likely in calc-alkaline ignimbrites only when deposited on a slope (for example, Chapin and Lowell, 1979; John and others, 2008), especially in a dynamic environment of increasing steepness as could occur during caldera collapse.

Despite evidence for modest intermittent asymmetry during subsidence at Bonanza, the overall geometry is broadly coherent subsidence of a structural block about 15 × 20 km across, accommodated along peripheral ring faults. Dips of foliation defined by pumice fiamme (most 35–55°) do not vary significantly or systematically upward through the 2.5-km section of the intracaldera ignimbrite section exposed on the west flank of the resurgent dome (fig. 173), indicating that the overall subsidence did not involve sustained progressive tilting. No major fault offsets have been recognized within caldera-floor lavas of the main subsided block; subsidence was dominantly piston-style, not piecemeal.

Caldera-Collapse Faults

Caldera collapse during eruption of the Bonanza Tuff was primarily accommodated along ring faults that are well constrained but largely concealed beneath surficial deposits along Kerber Creek and its tributaries (fig. 168). Fault strands as much as several kilometers outboard of the major ring faults accommodated additional subsidence, slumping of large blocks along the southern and western caldera margins, and modest inward rotation. As much as 4 km of stratigraphic offset occurs along the concealed ring faults on the west side of the caldera, as indicated by a cross section from Whale Hill to Flagstaff Mountain (fig. 175*A*). Net offset along the Kerber Creek Fault diminishes farther to the south, approaching zero at the junction with Little Kerber Creek and the intersection with the anticlinal crest of the Whale Hill dome (figs. 165, 175*B*); the decreased net displacement along this southern fault segment is interpreted to result from uplift during resurgence. To the north, caldera faults are largely concealed beneath collapse-related megabreccia and later lavas of the Bonanza eruptive cycle; it remains unclear whether subsidence was as deep as to the south and west. The few other SRMVF calderas that are sufficiently deeply eroded to expose bounding ring faults display varied structural patterns. The multiple interconnected fault strands associated with the single ignimbrite eruption at Bonanza (fig. 168) differ from the predominantly single ring-fault strand that is well exposed at Lake City (Lipman, 1976a), or from the nested ring faults at Grizzly Peak and probably at Mount Aetna (Fridrich and others, 1991; Shannon, 1988).

Andesitic and dacitic lavas of the caldera floor that are adjacent to ring faults along Kerber Creek and to the south are locally severely shattered, and involve textures and structures

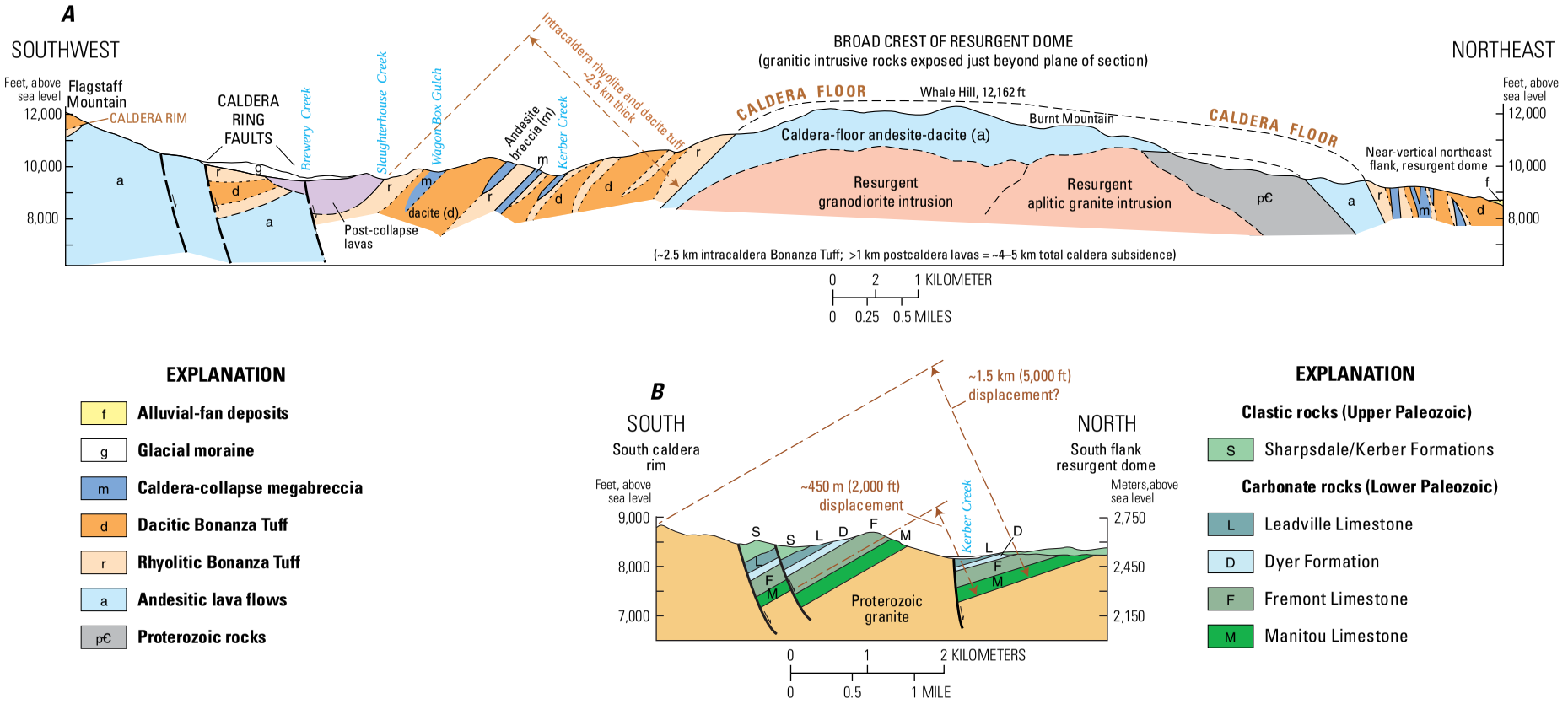

Figure 175. Cross sections showing structures and stratigraphic relations across Bonanza caldera; locations are on generalized map (fig. 168), but much more stratigraphic detail is illustrated by the sections. *A*, Line 1: Southwest topographic rim, across the crest of the resurgent dome (Whale Hill), to the western margin of San Luis Valley (segment of the Rio Grande Rift). This cross section shows large ring-fault displacements, a great thickness of intracaldera Bonanza Tuff, steep dips on flanks of resurgent dome, and the inferred location of subcaldera granitoid intrusions. *B*, Line 2: Southern caldera margin, showing displacements across ring-faults. The tilting of units reflects some combination of rotational block faulting during caldera subsidence, as well as possible uplift at the southern margin of the resurgent dome. Km, kilometer; ft, feet.

that have not been widely recognized at calderas elsewhere (Stop 6A-5). Angular blocks mostly less than 0.5 m across are juxtaposed, with only a minor matrix of comminuted lava. In many exposures, finely shattered fragments fit together without large-scale rotation or other movement, and such rocks grade into more massive lavas of the caldera floor within 100–200 m away from mapped ring faults. In some zones, breccias with angular and rounded clasts are matrix supported, but despite areal proximity to the megabreccia at the base of the intracaldera Bonanza Tuff, no tuffaceous component is present in the shatter breccia. Although fault planes, slickensides, or other evidence of offset are sparse, the close proximity of the shatter breccias to the main caldera-collapse faults suggest that they formed during subsidence (or resurgence), perhaps due in part to hydraulic fracturing. Alternatively, and perhaps more likely, shattering of the floor rocks may have resulted from compression and crushing of the subsiding structural caldera block in proximity to steeply inward-dipping ring faults.

Several east-trending arcuate faults south of Kerber Creek, which juxtapose Paleozoic sedimentary formations against Proterozoic rocks, are also interpreted as related to caldera subsidence (fig. 168). These were described by Burbank (1932, p. 39–40, Pl. 3) as low-angle thrust faults of prevolcanic age, but no specific evidence was cited for a thrust interpretation, other than the presence of Proterozoic granite on high ridges south of the southward-dipping Paleozoic strata exposed low along Kerber Creek. Detailed tracing of faults across ridges and gullies, with better base-map and Global Positioning System (GPS) control than was possible for Burbank, documents generally steep dips, at least 45–60°, although vertical relief is insufficient to quantify fault dip precisely. Accordingly, rather than low-angle thrusts active during Laramide compression, these faults are here interpreted as large-scale block slumps of middle Cenozoic age, related to peripheral subsidence and failure along oversteepened walls along the southern margin of Bonanza caldera (fig. 175*B*). Rotation during slumping could have produced the southward dips of the Paleozoic strata that crop out at low elevations. Additionally, at least some component of the southward dips in the prevolcanic rocks likely resulted from tilting along the lower south flank of the large resurgent dome within the caldera.

Caldera-Floor Structure

Particularly revealing within Bonanza caldera are the areally widespread exposures of structurally coherent caldera-floor lavas and basal deposits associated with the ignimbrite eruption and caldera collapse. Other than the thick, dipping section of Bonanza Tuff on the lower west flank, virtually the entire resurgently domed caldera floor has been erosionally exhumed at stratigraphic levels close to original contacts with the basal intracaldera ignimbrite, over an area about 10 × 15 km across in the ring-fault-bounded caldera structural block (fig. 168).

At Bonanza, stratigraphic levels close to the original caldera floor are exposed for about two-thirds of the area of the ring-fault bounded structural core (the little-broken thick sequence of overlying intracaldera ignimbrite covers only about 15 percent of the west flank of the resurgent dome, although surficial deposits on the east side of the San Luis Valley conceal an additional 15–20 percent). Exposures of the stratigraphic transition from caldera-floor lavas to ignimbrite fill at Bonanza are especially good on the relatively dry and weakly vegetated south-facing slopes above Kerber Creek. In this area, fractured but seemingly coherent, thick sequences of andesite and dacite lavas merge imperceptibly upward into shattered outcrops of similar lava, between which irregular crack-fills and pockets of dacitic and rhyolitic tuff form a matrix between megabreccia blocks (Stop 6A-12). Within the near-floor megabreccia, most good outcrops consist of erosion-resistant intermediate-composition lavas. Much of the matrix tuff is weakly welded, lithic rich, and exposed only as fragments on slopes. As a result, contacts between caldera floor and caldera-fill megabreccia can be broadly gradational and only approximately located in many places. Such deep levels of caldera structure have rarely been observed on such a comparable areal scale elsewhere, where floor rocks are seen mainly in oblique cross-sections through structurally disrupted and tilted caldera remnants, as in the Great Basin (for example, Henry and John, 2013; Best and others, 2013).

Ignimbrite Fracture Fills

Where well exposed, the tuff matrix in much of the caldera-collapse breccia is only weakly welded and distributed as highly irregular seams, but in some outcrops tuffaceous crack-fills have dike-like shapes, are strongly welded, and contain steeply dipping pumice fiamme (Stop 6A-11). The crack-fills are relatively thin (typically <1–2 m), discontinuous (commonly traceable only for a few tens of meters), and irregular in shape and trend. In places, fiamme-rich welded tuff grades along strike into flow-laminated rhyolite that lacks obvious fragmental textures; a few parallel dike-like bodies consist entirely of such rhyolite without lithic fragments or other surviving pyroclastic textures.

The best exposed fracture fills of highly welded and rheomorphic rhyolitic tuff, on slopes north of Kerber Creek, tend to be parallel to adjacent caldera ring faults, but all identified fracture fills are located near the transition from caldera floor upward into caldera-fill megabreccia and matrix tuff. No comparable fracture-fill tuff has been found at deeper exposed levels of caldera-floor lavas or in underlying Paleozoic and Proterozoic rocks. The highly welded to fluidal rhyolite in the dike-like fracture fills merges in places with areas of less welded tuffaceous matrix in the megabreccia and with larger pockets and lenses of more uniform intracaldera Bonanza Tuff that dip conformably with the flanks of the resurgent dome. Most fracture fills with identified pyroclastic textures consist of crystal-poor rhyolite (only one fracture fill of dacite tuff is well exposed), similar to that of the early erupted lower rhyolite phase of the ignimbrite sheet, as would be anticipated if caldera subsidence began during this stage of the eruption. Similar local pods of pumiceous to fluidal rhyolite are present elsewhere on flanks of the resurgent dome, especially within the large northern areas interpreted as megabreccia, but these areas are more vegetated and exposures are limited. Most of the crack-fill tuffs appear originally

to have been glassy, even where most are welded and fluidal, as suggested by well-preserved relict pumice and shard textures and by extreme alkali exchange (K_2O/Na_2O ratios, commonly 3–10) compared to analyzed samples of the outflow and intracaldera ignimbrite (typical ratios of 1.3–1.5).

Some of the ignimbrite crack-fills at Bonanza could be intrusive dikes of fluidal rhyolite or vent fissures for ignimbrite eruptions, but their stratigraphic distribution, lateral textural variations, and compositions suggest that they are best interpreted as surficial fills between blocks of early caldera-collapse megabreccia, injected down into dilatant cracks that opened during caldera subsidence. Dike-like pyroclastic bodies at several ignimbrite and caldera settings elsewhere have been similarly interpreted as dilatant crack-fills (Lipman, 1964; Branney and Kokelaar, 1994, p. 525; Best and others, 2013, p. 920).

Resurgent Uplift

After the ignimbrite eruption and emplacement of most of the caldera-filling lavas, the caldera floor was arched into a spectacularly large and steep-sided resurgent dome that is gently arcuate to the east (figs. 165, 168, 175*A*). Erosion has stripped most intracaldera Bonanza Tuff from the floor lavas along the crest of the dome, which is well defined at present by the gentle upland surface on Whale Hill (Stop 6A-1). Small remnants of subhorizontal Bonanza Tuff preserved along the crest of the resurgent structure at Round Mountain and Elkhorn Peak provide critical constraints on caldera-floor geometry and structure along highest parts of the dome. Notably, caldera-floor lavas are at elevations above 3,700 m on the crest of the resurgent dome, as high as comparable units on the west topographic rim (fig. 175*A*). This relation indicates ~3.5 km of resurgent uplift, equal to the subsidence documented by the thick caldera-fill section of ignimbrite and preresurgent lavas on the west flank of the dome. If the thickness of the caldera fill in the center of the caldera had been similar to the west-flank section, the original dome crest would have had an elevation of ~7,000 m above present-day sea level.

Bedding and foliation dips on flanks of the Whale Hill dome are uniquely steep and variable compared to resurgent uplifts at other well-documented ignimbrite calderas: 40–60° on the west side of the dome where widespread preservation of intracaldera tuff provides robust structural control, nearly vertical along parts of the northeast and southwest flanks (figs. 168, 175*A*), but typically only 20–30° on the southeast flank. This asymmetry may result in part from variable tilting of the Bonanza region, within a zone of structural transfer between segments of the Rio Grande rift zone. The dome appears to have been largely bounded and partly accommodated by ring faults that initially formed during caldera subsidence. Resurgence is inferred to have been caused by emplacement of multiple intrusions centrally within the caldera, including the granodiorite to granite bodies that are exposed on the east flank of the dome.

The southern margin of the resurgent dome is especially well constrained by the southeast-plunging Proterozoic-cored anticline and flanking Paleozoic sedimentary strata (figs. 168, 175*B*) that are stratigraphically much more precisely defined than the precaldera lava succession. The southern anticline has been previously interpreted as a prevolcanic (Laramide) structure (Burbank, 1932; Tweto and others, 1976; Cappa and Wallace, 2007). Although they are less widely measurable, dips of the immediately overlying volcanic strata, including the Bonanza Tuff, are locally nearly as steep on the fold flanks and have a similar asymmetry as the well-stratified Paleozoic sedimentary strata (Stop 6A-3). This requires that much of the tilting occurred after caldera formation. Accordingly, the main development of the fold must be Cenozoic in age; it is here interpreted as the southern continuation of the elongate Whale Hill dome. Because the Proterozoic rocks in the core of the anticline are directly overlain by Cenozoic lavas, without intervening Paleozoic sedimentary strata, this area must have also been a prevolcanic high. Perhaps a more open fold in the prevolcanic rocks influenced the location of postcaldera resurgence, or alternatively this area was simply a paleo-highland along a northwestward erosional truncation of Paleozoic strata.

Only a few faults with documentable displacement have been identified confidently within the resurgent dome. Evidence for sizable fault displacements has been elusive on heavily vegetated slopes where talus is widespread, outcrops rare, reliable stratigraphic-marker horizons sparse, and underground mines are no longer accessible. More faults than have been mapped are likely within the resurgent block, but major fault repetitions seem unlikely. Prior mapping depicted a highly intricate mosaic of rectilinear faults in the mining district (Burbank, 1932, Pl. 1), but many of the depicted faults were required to accommodate an overly simplified stratigraphic sequence, without adequate available concepts of ignimbrite-eruption and caldera-filling processes. In contrast to the work by Burbank, and with access to more of the underground mine workings in the Bonanza district, Patton (1916, p. 63) noted that, “While minor faults involving a movement of a few inches or, at most, a few feet are of common occurrence, no evidence of faulting on a large scale has been discovered.” Beyond the mining district, relatively coherent subsidence and subsequent resurgence of the caldera floor are well documented in the southern caldera area, where detailed structural control is provided by the high-resolution stratigraphy of the regional lower-Paleozoic formations. These strata dip steeply on flanks of the resurgent dome, but are traceable continuously across the nose of its south-plunging anticlinal termination without sizable fault displacements other than by the major caldera ring faults.

Despite the scarcity of mapped faults on the resurgent dome at Bonanza, some displacement likely accompanied uplift, as at other well-studied resurgent calderas that are characterized by keystone grabens and other uplift-related faults (for example, Valles and Creede calderas; Smith and Bailey, 1968; Steven and Ratté, 1973). In contrast to Valles and Creede, no large-scale keystone faults have been identified at Bonanza, despite the steep flank dips and the widespread exposure of caldera-floor rocks along the crest of the uplift. More limited fault disruption of the caldera floor and resurgent dome at Bonanza may be related to formation of this caldera in response to a single ignimbrite eruption. In contrast, the other resurgent calderas just noted are

nested within earlier ignimbrite subsidence structures, and prior disruption of the subsided areas may have contributed to more complex fracturing and larger displacements during resurgence. The relatively limited faulting at Bonanza may also partly account for the modest mineralization there, in comparison to otherwise analogous epithermal vein systems in SRMVF caldera settings such as Creede and Silverton.

Uplift of the Whale Hill dome was geologically rapid: 3.5 km at caldera-floor level in less than 100 k.y. (table 15), as bracketed by the ages of the tilted caldera-filling Bonanza Tuff (33.12 Ma) and Porphyry Peak Rhyolite (33.03 Ma). The average resurgence rate (3.5 cm/yr) at Bonanza is roughly similar to the well-constrained uplift of the Samosir Island resurgent dome at Toba caldera for the interval since ~34 ka, with a suggested long-term average of 2–3 cm/yr (de Silva and others, 2015).

Several tantalizing features suggest that resurgence at Bonanza may have been rapid, while deep parts of the caldera fill ignimbrite remained hot and ductile: (1) extreme fluidal welding and lava-like flowage of the lower rhyolite unit at the base of the thick intracaldera ignimbrite accumulation (fig. 172*D*,*E*); (2) down-dip trends of prolate fiamme lineations in fluidally welded ignimbrite on flanks of the dome; (3) apparently limited brittle-fault disruption of caldera-floor levels in the Whale Hill dome, in comparison to complex keystone and other faults in resurgently domed calderas elsewhere; (4) lower dips in upper lavas of the caldera fill than in initially erupted lavas and underlying Bonanza Tuff, suggesting rapid resurgence concurrent with the accumulation of these lavas as documented by geochronology; and (5) marginally younger sanidine ages from intracaldera Bonanza Tuff than from outflow portions (fig. 166), compatible with prolonged slow cooling deep in the intracaldera ignimbrite. Analogous rheomorphic textures for intracaldera Carpenter Ridge Tuff and decreasing dips of successive caldera-filling units hint at similarly rapid postcollapse resurgence, while the intracaldera tuff remained hot and plastic, as discussed briefly for Bachelor caldera in conjunction with the Day 5 excursion (see Stop 5B-8).

Day 6—Routes Through the Northeastern San Juan Region

The general route for Day 6 is northward by way of U.S. Route (US) 285, up the San Luis Valley from Monte Vista past the villages of Saguache, Villa Grove, and Bonanza; then crossing into the Upper Arkansas segment of the Rio Grande Rift (fig. 167). The route 6 Introduction involves a side trip to the west along Saguache Creek by way of Colorado State Highway (CO) 114, where diverse ignimbrite sheets accumulated in a broad Oligocene paleovalley. Initial stops examine outflow of the 33.12-Ma Bonanza and 32.25-Ma Saguache Creek Tuffs. Then, US 285 leads north to Villa Grove. The main route 6A follows Saguache County road LL56 up Kerber Creek to the village of Bonanza and provides access to many unusual structural and stratigraphic features of this extreme caldera. These include widely exposed caldera-floor volcanics and underlying Paleozoic and Proterozoic rocks, an ~3.5 km section through caldera-filling ignimbrite and overlying intracaldera lavas, steeply dipping flanks of a large elliptical resurgent uplift, intense shatter breccia adjacent to ring faults, vertically dipping ignimbrite interpreted as crack-fills high in the caldera-floor, and small exposures of granitoid intrusions associated with caldera resurgence.

After leaving the Kerber Creek valley at the end of route 6A, the trip route continues counterclockwise across Poncha Pass, which marks the accommodation zone between the San Luis and Upper Arkansas segments of the Rio Grande Rift. For Day 6 stops in Bonanza caldera, access could be equally efficient from a starting point in Saguache, Poncha Springs, or Salida.

Route 6B, up a side road within the western moat area of Bonanza caldera, traverses obliquely through gradational alternations of dacitic and rhyolitic Bonanza Tuff into a kilometer-thick sequence of andesitic to rhyolitic caldera-filling lavas. Additional routes up side roads from US 285 on the west side of the San Luis Valley provide access to large resurgent intrusions of texturally and compositionally diverse granodiorite-andesite (Turquoise Mine pluton) and aplitic-granite (Spring Creek pluton) (route 6C), and to the steeply dipping northeast flank of the resurgently domed caldera floor and fill (route 6D). Another route (6E), from Poncha Pass to a geographic site known as The Gate, provides access to the spectacularly exposed wall and intracaldera ignimbrite of the Marshall caldera, source of the 33.9-Ma Thorn Ranch Tuff.

The trip stops and geologic interpretation in this guide are largely based on a recent interpretive paper and geologic map for the Bonanza caldera area (Lipman and others, 2015; Lipman, 2020). A complementary field guide is available for the adjacent North Pass and Cochetopa Park calderas (Lipman and others, 2013), and a broader regional framework is provided by the geologic map of Saguache County (Cappa and Wallace, 2007). Latitude and longitude GPS locations for this guide are based on NAD27 coordinates, as used on USGS 7.5' topographic maps for the San Juan region. Numbers at left in each route log are distances in miles from starting point.

Route 6 Introduction—Outflow Ignimbrite Stratigraphy of the Saguache Valley

From Monte Vista, follow US 285 for 35 miles (mi) north to the town of Saguache (last available gas and toilet access); turn left (west) onto CO 114. Reset the odometer and proceed to Stop 6-1, noting the general stratigraphy in the Saguache valley en route.

Mileage

0.0 The Oligocene Saguache paleovalley was the locus for deposition of multiple outflow ignimbrite sheets along an east-west-trending lowland between Tracy volcano to the south and the Jacks Creek and Rawley edifices to the north. These include the Bonanza and Saguache Creek Tuffs (focus of Day 6 stops) erupted from northeastern

San Juan calderas, the Sapinero Mesa Tuff from farther west, and the Fish Canyon and Carpenter Ridge Tuffs from the central caldera complex, as visited on Day 5.

0.6 At the west edge of Saguache is the Public Lands Office of the U.S. Forest Service and Bureau of Land Management (no option for a toilet stop). To the northeast, the southwest flank of the Saguache Peak stratovolcano consists of ~33.4–33.2-Ma andesite and dacite lavas that are precursors to the Bonanza caldera cycle. These are among the youngest known rocks prior to eruption of the Bonanza Tuff and the formation of its caldera.

The timbered high terrain to the south is the north flank of the ~33.5–33.0-Ma Tracy volcano, underlain by finely porphyritic mafic dacite; the sparsely vegetated, rugged low ridge in the distance to the east is a well exposed, northeast-dipping sequence of lavas and breccias on the northeast flank of this volcano.

2.9 Findley Gulch road (Forest Service [FS] road 880, County road 43BB) on right. As viewed from this point, the striking exposure of the Bonanza Tuff, informally known as the Findley Ridge section (fig. 176), has been used as the primary reference for the proximal western facies of this ignimbrite. Despite complex welding and compositional zonations (table 16), the entire section is a single ignimbrite sheet, without any prolonged depositional breaks marked by nonwelded glass zones, interbedded tephra falls, or sediments. The apparent disconformity in dip between lower and upper welding zones resulted from depositional banking and differential welding compaction against the western margin of a large paleovalley. The basal welded zones of the section are mafic dacite that, atypically for this ignimbrite, lack sanidine phenocrysts (fig. 176, sites 8D, 8E; 63 percent SiO_2), but sanidine is present higher in the main dacite (8C); the upper rhyolite (8B; 74 percent SiO_2) is overlain by an upper dacite (8A; 62 percent SiO_2) present only locally in proximal sections. This superbly exposed section can be accessed by driving 1.0 mi up the Findley Gulch road (43BB, just before milepost 49); then turning left (west) on an obscure track (Klondike Mine quadrangle: 38°07.29’ N., 106°11.18’ W.); this requires a high-clearance vehicle (*use caution when crossing washes*).

All rocks to the south of Saguache Valley are on the northwest flank of Tracy volcano (fig. 177). The Bonanza Tuff wedges out against lower andesites of this edifice at the western end of the long low ridge,

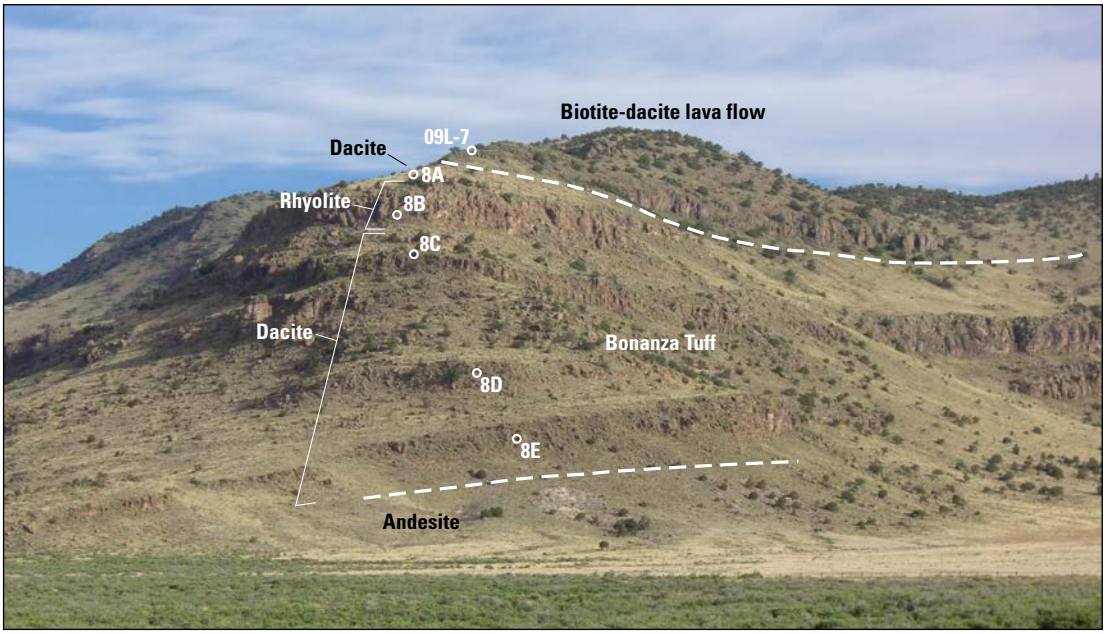

Figure 176. Findley Ridge reference section. Outflow Bonanza Tuff that contains several alternating layers of rhyolite and dacite and multiple partial welding/cooling breaks is well exposed along the ridge on west side of Findley Gulch (fig. 168). The section is exceptionally thick (~175 meters) because it is banked against the flank of a large paleovalley. Circles indicate the locations of analyzed samples. Variable dips in cliff-forming zones of densely welded tuff reflect differential compaction in proximity to the margin of the paleovalley. The lower rhyolite of the Bonanza Tuff is absent in this paleovalley section but crops out below the main dacite in exposures 6 kilometers to the southwest. The ridge is capped by a dacite lava (09L-7). This proximal site has been cited and sampled repeatedly as a reference section for the Bonanza Tuff (Bruns and others, 1971; Varga and Smith, 1984; McIntosh and Chapin, 2004). Photograph by P.W. Lipman, U.S. Geological Survey, 2013.

and the ignimbrite is overlain by massive upper dacite lavas. From this vantage there are good views of the paleovalley stratigraphic sequence on Houghland Hill to the west, where a thick section of major ignimbrite sheets (Bonanza, Saguache Creek, Fish Canyon, and Carpenter Ridge Tuffs) that ponded within the paleo-Saguache valley are capped by basaltic lavas (50.1 percent SiO_2, 21.81±0.21 Ma) of the Miocene Hinsdale Formation.

6.8 Continue west on Hwy 114, passing roadcuts in Proterozoic metamorphic rocks on the right (north). Basement rocks are exposed widely to the north, and the thickness of the pre-ignimbrite lava sequence varies greatly owing to rugged paleotopography on these Laramide-age uplifts.

7.7 At milepost 54, County road CC40 is on the left (south). On the right is a crystal-rich dacitic Bonanza Tuff, underlain by andesite lava. A partial compound welding break with the upper crystal-poor rhyolitic Bonanza Tuff is well exposed.

7.8 Continue past the ranch-entry road on the left (38°08.65' N., 106°16.02' W.). The slope on the right (north) is an alternate stop for the western outflow Bonanza Tuff, but less suitable for large groups. Compositional and welding gradations from dacite upward into rhyolite are especially well exposed along nose of ridge and contact with the underlying andesite is tightly constrained on the east side.

8.7 **Stop 6-1. Typical western outflow facies of Bonanza Tuff** (Lake Mountain northeast quadrangle: 38°09.24' N., 106°16.49' W.; 8,005 ft, 2,440 m elevation). Short, steep hike. *Caution: be alert for high-speed vehicle traffic.*

On the right, just after milepost 53 (at the Speed Limit 65 sign), a small roadcut outcrop exposes a basal vitrophyre of crystal-rich dacite, overlain by brown devitrified dacite (~30 percent plagioclase [pl]>>sanidine [san], biotite [bt], clinopyroxene [cpx]; 64–65 percent SiO_2) and crystal-poor rhyolite (~5 percent san>pl>>bt; 73–74 percent SiO_2) that form double cliffs of welded ignimbrite with less-indurated intervening tuff (fig. 178). The ignimbrite section is capped by andesite lavas. Ascend through the ignimbrite section, examining the welding break between the dacite and the upper crystal-poor rhyolitic Bonanza Tuff for evidence that

Figure 178. Close-up of compaction foliation in a densely welded dacitic tuff (Stop 6-1). In addition to near-glassy, dark-gray, crystal-rich pumice fiamme, sparse light-gray, crystal-poor pumice (not analyzed) appears to record minor intermixed rhyolite. Photograph by P.W. Lipman, U.S. Geological Survey, 2013.

Figure 177. Saguache Valley panorama of the northwest flank of Tracy volcano, view to the southwest from Saguache Valley. The northwest flank of Tracy volcano, at left and center, contains a well-stratified thick sequence of mafic dacite lavas (Tydu) that overlie lavas of andesite (Tya) and plagioclase andesite (Tyap). Dacitic Bonanza Tuff (Tbd) interfingers and wedges out between the andesite and overlying dacite of the Tracy edifice just east of Laughlin Gulch, and the southern (inferred) continuation of the horizon delimiting the Bonanza eruption is indicated by the black-dashed line. A low conical hill at Campo Santo (CS), is an early rhyolite lava dome. The present-day Saguache Valley coincides closely with an Oligocene paleovalley between Tracy volcano to the south and the composite highland of the Rawley volcanic complex to the north, within which the Bonanza caldera formed. Fill of the paleovalley, well displayed on Houghland Hill (Lipman, 2020), includes dacitic Bonanza Tuff (Tbd); an overlying complex succession (too thin to distinguish on the photo) of local andesite and rhyolite lavas, Saguache Creek Tuff, and interleaved river deposits; then Fish Canyon (Tfc) and Carpenter Ridge (Tcr) Tuffs from the central San Juan caldera cluster, and capping basalt lavas (21.81 Ma) of the Hinsdale Formation (Thb). Photograph by P.W. Lipman, U.S. Geological Survey, 2013.

no geologically significant depositional pause is present (hint: at what outcrop level does the phenocryst content begin to decrease?). Thus, the Bonanza Tuff here is a rare example of an eruption that in part was reversely compositionally zoned—mafic upward into silicic. At other sites, multiple compositional alternations of dacite and rhyolite are present, especially in intracaldera Bonanza Tuff (figs. 172, 173). The Bonanza Tuff in this area covers rugged paleotopography on Conejos lavas and breccias, resulting in patchy outcrops, irregular distribution, and varied primary dips of welding foliation. Several $^{40}Ar/^{39}Ar$ age determinations and paleomagnetic pole measurements for the Bonanza Tuff at this site are reported by McIntosh and Chapin (2004).

Continue ahead, west on CO 114.

9.4 Dacitic Bonanza Tuff at the prominent knob of Castle Rock, along CO 114. The upper rhyolitic facies of this ignimbrite are not present anywhere to the west up the Saguache valley, even though the dacitic Bonanza Tuff is preserved discontinuously for at least 30 km, farther northwest (fig. 164).

9.9 At the side road (Saguache 39EE) to Ford Creek, andesitic lavas on the southeast flank of the Jacks Creek volcano (~34.5 Ma) are exposed beneath dacitic Bonanza Tuff; similar lavas form the irregular hills ahead and to the north (fig. 179). These lavas are older but otherwise broadly correlative with the Conejos Formation to the south and west (seen during Days 4–5).

10.5 At milepost 50, the road to Jacks and Middle Creeks (FS 870, Saguache EE38) is on the right. Ragged low outcrops ahead are composed of dacitic Bonanza Tuff (with black basal vitrophyre), and lap against the south flanks of the Jacks Creek volcano.

12.7 *Continue west on CO 114; Trickle Mountain road (5255) is on right (north).* Farther ahead on the north side of the road, back-rotated Toreva slump blocks of Fish Canyon Tuff are morphologically complex. The high point on the south side is the grass-covered back side of Houghland Hill.

13.3 **Stop 6-2. Base of Saguache Creek Tuff** (Lake Mountain Northeast quadrangle: 38°08.69’ N., 106°20.50’ W.; 8,153 ft, 2,484 m elevation). *Caution: be alert for high-speed vehicle traffic.*

At the roadcut (fig. 180), the basal vitrophyre of Saguache Creek Tuff is underlain by crossbedded tuffaceous sediments of uncertain source and origin. The ignimbrite is densely welded almost to its base; the lower dark zone of vitrophyre about 2-m thick is abruptly overlain by red-brown devitrified tuff. Compare the overall appearance and phenocrysts of this crystal-poor rhyolite with rhyolitic Bonanza Tuff seen at Stop 6-1; both are relatively alkalic, with higher zirconium, lower barium, and more sodic sanidine compositions than megascopically similar appearing crystal-poor rhyolitic ignimbrites from central and western San Juan calderas (for example Carpenter Ridge Tuff, seen at Stop 5A-5). The Saguache Creek

Figure 179. Jacks Creek volcano, with outward-dipping andesitic lavas and interleaved laharic breccias on the east flank. View to the north from Middle Creek access road. Photograph by P.W. Lipman, U.S. Geological Survey, 2014.

Figure 180. Base of the Saguache Creek Tuff (Stop 6-2). The Saguache Creek Tuff is a crystal-poor rhyolitic ignimbrite erupted from the North Pass caldera 32.2 million years ago. The tuff, here welded nearly to its base, has a dark, lower zone of vitrophyre about 2-meters thick, overlain by red-brown devitrified tuff that grades upward into less welded tuff. This ignimbrite is underlain by weakly indurated cross-bedded ash of uncertain origin. Possible alternatives include wind-blown dune structures, water-transported fluviatile deposits, or large-scale initial surge deposits associated with proximal eruption of the Saguache Creek Tuff along the axis of the Saguache paleovalley. Photograph by P.W. Lipman, U.S. Geological Survey, 2014.

Tuff was erupted from the North Pass caldera, centered along the Continental Divide and the upper Saguache valley (Lipman and McIntosh, 2008; Lipman, 2012). This site yielded a slightly young and relatively imprecise $^{40}Ar/^{39}Ar$ sanidine age of 31.95±0.18 Ma; the weighted mean age for the Saguache Creek Tuff is 32.25±0.05 Ma (table 15).

Several hundred meters upstream from the stop, a slide scar exposes nonwelded upper Saguache Creek Tuff, overlain by densely welded Fish Canyon Tuff (best seen from near the highway bridge). Here and elsewhere, the Saguache Creek Tuff is separated from the overlying Fish Canyon Tuff by only a few meters of volcaniclastic sediments, which nevertheless represent a time interval of 4 m.y., bracketing the period of peak volcanic activity in southeastern and western parts of the San Juan Mountains.

The origin of the large-scale cross bedding in the ash beneath the welded Saguache Creek Tuff has been controversial (compare with the discussion of basal Fish Canyon Tuff, Stop 5A-1). Possibilities suggested during prior field excursions (Lipman and others, 2013) have included (1) reworking of ash from older SRMVF eruptions such as the Bonanza ignimbrite, (2) as wind-reworked dune structures, or (3) water-transported fluviatile deposits in in the Saguache paleovalley. An additional alternative could be a basal surge deposit associated directly with emplacement of the Saguache Creek Tuff, perhaps recording flowage instability at the toe of the ignimbrite related to local paleotopography. What outcrop evidence can be observed to help evaluate such possibilities?

Sanidine grains in the bedded ash have a restricted age range, with a weighted mean of 32.24±0.02 Ma (table 15), indistinguishable from the Saguache Creek Tuff (weighted mean: 32.25±0.05 Ma). The low K/Ca ratios for sanidine from the ash (~10–18) are also similar to those for the Saguache Creek Tuff (uniquely low among major SRMVF ignimbrites, because of its exceptionally sodic sanidine/anorthoclase composition: $Or_{50\text{-}51}Ab_{45\text{-}47}An_{2.6\text{-}2.8}Cs_{0.5}$ (Lipman, 2012). No deposits of rhyolite ash that could be counterpart precursors to the Saguache Creek Tuff are exposed nearby in the region; the units closest in age are the tuff of Spanish Creek, 15 km to the northwest (32.50±0.03 Ma; Lipman and McIntosh, 2008), and nonwelded ash on Sargents Mesa a similar distance to the north (32.79±0.03 Ma; Lipman and others, 2015). The only known sanidine-bearing unit close in time to the Saguache Creek Tuff is a local rhyolite lava dome (table 15) that yielded an age of 32.17±0.06 Ma (Lipman, 2012); however, this dome is ~25 km to the west (near the southwestern margin of North Pass caldera), no deposits of associated ash are exposed, and the sanidine K/Ca ratios are about double those for the bedded ash along CO 114 in the Saguache valley. Accordingly, interpretation of the bedded ash as an initial surge deposit of the Saguache Creek ignimbrite seems plausible.

South of the Saguache valley in lower Houselog Creek, distal partly welded Sapinero Mesa Tuff, here more than 80 km distant from its source caldera in the western San Juan Mountains, crops out discontinuously beneath mesa-capping cliffs of Fish Canyon Tuff. The 28.20±0.06-Ma Sapinero Mesa Tuff is yet another crystal-poor rhyolitic ignimbrite, but contains sparse biotite and relatively potassic and barium-rich sanidine that distinguishes it from the Saguache Creek Tuff with which it was previously miscorrelated in this area (Bruns and others, 1971).

South-dipping intermediate-composition lavas, visible downvalley to the east, compose the south flank of the Jacks Creek volcano, at ~34.5 Ma among the oldest rocks in the Saguache-Bonanza area.

End of route 6. Return 13.3 mi to Saguache by way of CO 114, then head north on US 285 for 19 mi to the north side of Villa Grove, for the start of route 6A.

Main Route 6A—Intracaldera Stratigraphy and Structure, Kerber Creek to Bonanza

Route 6A follows Kerber Creek from Villa Grove to north of Bonanza village, and progresses clockwise close to the southern and western structural margins of the caldera-collapse area to the north of Rawley Gulch (fig. 167). Stratigraphic units that can be examined include precaldera lavas of the Rawley volcanic complex, alternating dacitic and rhyolitic zones of the intracaldera Bonanza Tuff and interleaved caldera-collapse megabreccia, overlying andesitic to rhyolitic caldera-fill lavas, and postcollapse granitoid intrusions associated with extreme resurgent uplift of the caldera floor. Structural features include ring faults that accommodated caldera subsidence, extreme brecciation of rocks adjacent to the ring faults, the southwest flank of the spectacularly steep-sided resurgent dome cored by Proterozoic and Paleozoic rocks, and structurally coherent caldera-floor lavas, in places hosting dike-like crack-fills of Bonanza Tuff.

Field-trip stops are listed in order, progressing up Kerber Creek, but for a more logical interpretive sequence it may be preferable to defer Stops 6A-3 to 6A-5 until after Stops 6A-11 and 6A-12, during the return trip down Kerber valley.

0.0 *Start at the north side of Villa Grove, turning onto the Bonanza road (Saguache LL56) to the top of the small rise for Stop 6A-1.*

0.3 **Stop 6A-1. Panoramic view of southeast side Bonanza caldera** (Bushnell Peak quadrangle: 38°15.05' N., 105°57.43' W.; 8,061 ft, 2,457 m elevation).

This vantage provides a broad perspective on the geographic scale of Bonanza caldera and its major structural elements**.** Looking clockwise, on the skyline are (1) the south rim of the caldera, (2) a faulted fragment of Proterozoic granite on the southeast wall at Clayton Cone, (3) the valley of Kerber Creek containing the caldera ring fault, and (4) the elongate resurgent dome with its crest from Hayden Peak across to Whale Hill (fig. 181). Low grassy sage-covered slopes in the near distance are dissected old rift-fill fan deposits, perhaps as old as the Cenozoic Dry Union Formation (equivalent to Santa Fe Group in New Mexico). Mount Princeton (14,196 ft; 4,327 m elevation), across Poncha Pass to the north, is the high point in a batholith of Cenozoic granodiorite that is inferred to underlie the source of the 37-Ma Wall Mountain Tuff (fig. 90).

Silhouetted below the profile of Mount Princeton, at the north end of San Luis Valley, is the small knob of Round Hill just to the left of the powerline. At Round Hill, onlap of dacitic lava against Proterozoic basement is interpreted to define the northeastern margin of Bonanza caldera (see Stop 6D-2).

Continue on the Bonanza road up Kerber Creek, following the valley eroded along the major ring fault on the south and southwest sides of the Bonanza caldera.

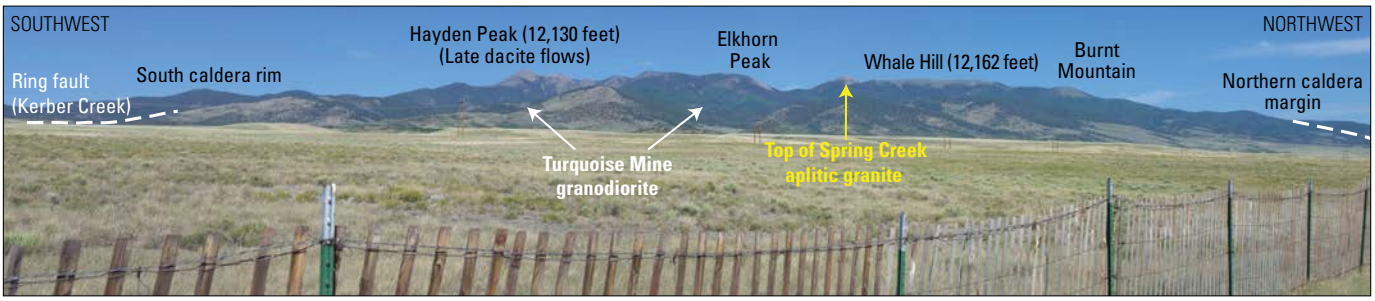

Figure 181. Bonanza caldera, from the San Luis Valley. The skyline profile is the crest of an elliptical resurgent dome, eroded approximately to the stratigraphic level of the caldera-floor andesite within Bonanza caldera. Broad, flat-topped Whale Hill and northeast-sloping Burnt Mountain are stripped upper surfaces of the caldera floor, locally capped by small erosional remnants of intracaldera tuff. The eastern hillside slopes from this vantage approximate the outward-dipping flanks of the resurgent dome. Hayden Peak is capped by thick lavas of crystal-poor dacite (69–70 percent SiO_2, 32.8–32.7 million years ago [Ma]), which appear to have filled a deep valley or graben (erosional, structural?) high on the resurgent dome. The Turquoise Mine granodiorite (54–67 percent SiO_2; 33.06±0.21 Ma) and aplitic granite of Spring Creek (73–77 percent SiO_2; 33.26±0.07 Ma) are compositionally contrasting shallow plutons exposed at roof level. Within analytical uncertainties, they are essentially indistinguishable in age from the Bonanza Tuff and are inferred to be upper parts of a much more extensive composite resurgent intrusive complex, having a broad compositional range comparable to that of the postcollapse andesite to rhyolite lavas of the Bonanza cycle (fig. 170). Photograph by P.W. Lipman, U.S. Geological Survey, 2012.

3.4 Small outcrops of upper Paleozoic sandstone (Sharpsdale Formation) dip to the east on east flank of the resurgent dome. Above the alluvial fan, a northwest-trending fault, probably related to development of the Rio Grande rift zone, raises Proterozoic granitic rocks up to the east. The pyramid-shaped hill ahead to the southwest is a south-dipping block containing lower Paleozoic carbonate strata above Proterozoic rocks, interpreted as a large back-rotated caldera-collapse slump.

4.1 Turn-off to Rafiki Ranch (base for Bonanza and regional geologic fieldwork by authors 2006–11, 2014–15) is on the right. Alluvial-fan deposits overlie upper Paleozoic sandstone and shale (Sharpsdale Formation) at the ranch.

4.9 On the right (north) is a roadcut of flat-lying Dyer Formation (Devonian). The small hilltop above is capped by Leadville Limestone (Mississippian), and just ahead on the west side of this hill (mouth of Cody Gulch: 38°13.62' N., 106°02.12' W.), the Leadville is silicified and brecciated, forming rugged outcrops of secondary black chert. These formations also cap the south side of the prominent pyramid-profile hill (9,532 ft, 2,905 m elevation; fig. 182) across Kerber Creek to the south (above the Ordovician Manitou and Fremont Limestones that form conspicuous cliffs). A cross-section documents about 1 km of net displacement along the Kerber Creek ring fault at this location (fig. 175*B*). Subsidence along this sector of the ring fault would likely have been greater during caldera collapse but has been partly counterbalanced by later resurgent uplift.

5.6 Pavement ends (in 2019). Higher ridges of lightly timbered hills directly ahead near the skyline are Proterozoic granitic rocks in the core of the plunging anticline that is interpreted to define the southern end of the Bonanza resurgent dome. Heavily timbered distant ridges across Kerber Creek to the southwest are precaldera andesitic and dacitic lavas that form eroded remnants of the original topographic caldera rim.

7.1 Lower Soda Spring Gulch roughly follows the contact between southwest-dipping Paleozoic strata on the west side of the resurgent dome and the overlying volcanic rocks (fig. 183*A*). The east slope of Soda Spring Gulch is an oblique dip slope on lower Paleozoic carbonate strata. At base of this slope, Kerber Formation (lowermost upper Paleozoic unit that records the initial erosion from the ancestral Rocky Mountain uplifts) is distinguishable from the overlying Sharpsdale Formation by the near-absence of muscovite (Burbank, 1932; Cappa and Wallace, 2007). On the prominent valley-bottom hill (8,826 ft; 2,690 m, elevation), ahead, intracaldera dacitic Bonanza Tuff overlies the Paleozoic strata on west flank of the resurgent dome. Skyline ridges to the south are composed of Proterozoic granitoid rocks and mark the eroded topographic rim of the caldera, as do distant ridges of precaldera lavas farther to southwest. The main caldera ring fault underlies Kerber Creek.

7.3 **Stop 6A-2. Intracaldera dacitic Bonanza Tuff at Soda Spring Gulch, containing large fragments of andesite** (Graveyard Gulch quadrangle: 38°12.80' N., 106°04.28' W.; 8,537 ft, 2,602 m elevation)

Outcrop is on the right (*park on the road shoulder*). The dacite at this site is crystal-rich, containing large flakes of chloritized biotite (fig. 183*B*). How does it compare with the dacitic Bonanza Tuff at Stop 6-1? How can one distinguish between interpretation as an ignimbrite with large lava fragments versus mingled andesite magmatic inclusions in a dacitic lava? At this site, pumice fiamme and the orientation of compaction foliations are obscure in the highly fractured propylitic rock, but these textures are better displayed higher along the ridge crest. The tuff dips about 60° to the southwest, semiconcordantly with the tilt of the Paleozoic sequence,

Figure 182. Lower Paleozoic carbonate section on the north slope of hill, elevation 9,532 feet (2,905 meters [m]), viewed from Kerber Creek (Graveyard Gulch quadrangle). The upper cliff is Fremont Limestone (Of, Upper Ordovician), capped by Dyer Formation (Dc, Devonian); the lower cliff is Manitou Limestone (Om, Lower Ordovician), with talus of Harding Quartzite on the bench above. The underlying slope consists of disaggregated Proterozoic granitoid rocks (pCg). Photograph by P.W. Lipman, U.S. Geological Survey, 2014.

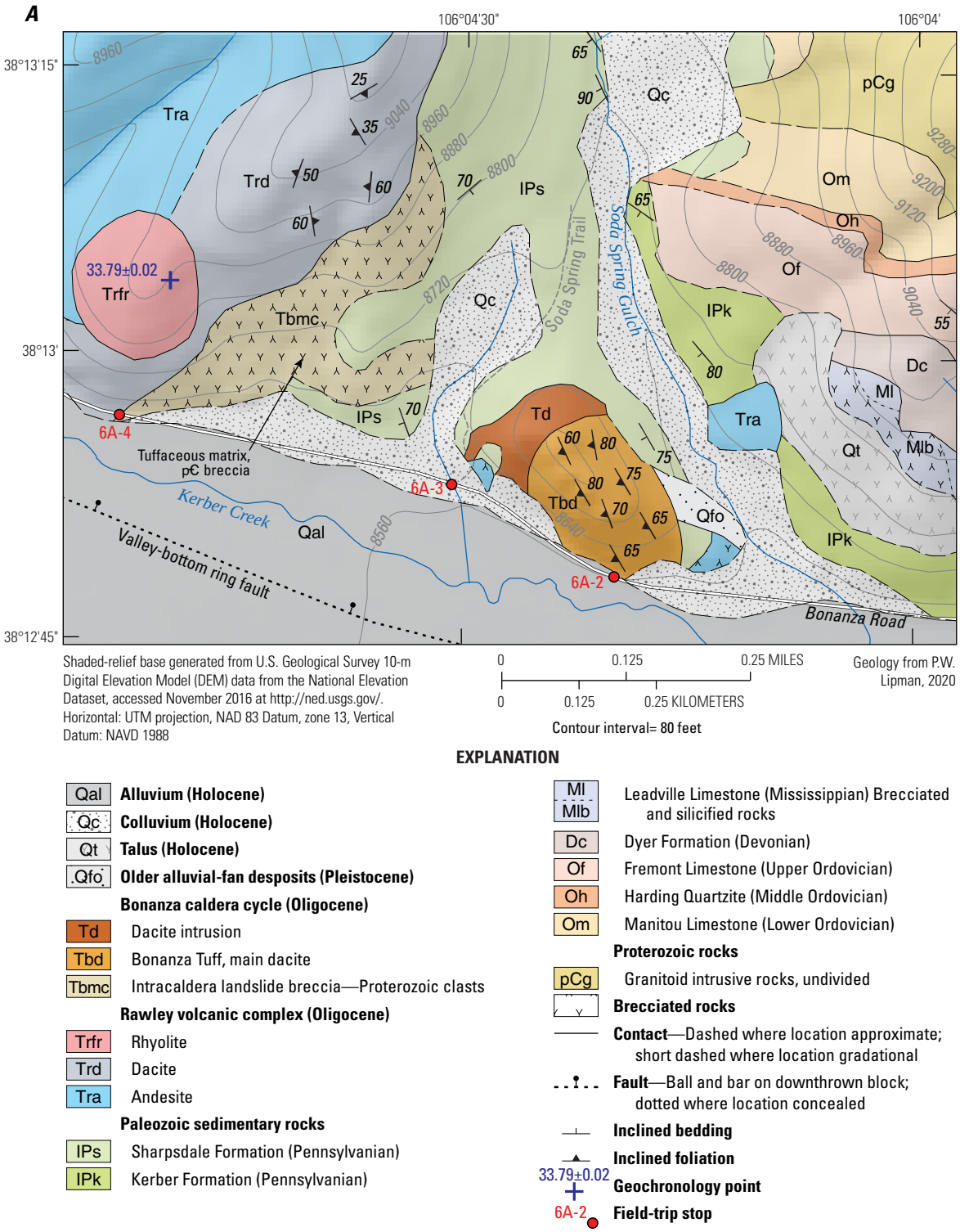

Figure 183. Lithic-rich intracaldera Bonanza Tuff at Soda Spring Gulch (Stop 6A-2). *A*, Geologic map of the Soda Spring area, showing features viewed at Stops 6A-2 to 6A-4. Modified from Lipman (2000). *B*, Abundant large andesite clasts (as large as 50 centimeters at this location) in densely welded intracaldera dacitic tuff, on a scale not present in the outflow ignimbrite. Photograph taken at Kerber Creek road, just west of the mouth of Soda Spring Gulch (Stop 6A-2). Photograph by P.W. Lipman, U.S. Geological Survey, 2014.

Figure 183.—Continued

and demonstrates that the south-plunging anticline is Cenozoic in age and caldera related, rather than a feature of Laramide deformation as inferred previously (Burbank, 1932; Cappa and Wallace, 2007).

Continue ahead along Bonanza road to Stop 6A-3.

7.5 **Stop 6A-3. Soda Spring Trailhead** (Graveyard Gulch quadrangle: 38°12.88' N., 106°04.47' W.; 8,570 ft, 2,612 m elevation). Steeply dipping intracaldera Bonanza Tuff, access to caldera views.

It is a short hike (~547 yds; ~0.5 km) to the crest of the isolated valley-bottom hill (8,826 ft; 2,690 m, elevation), which consists mainly of steeply tilted intracaldera Bonanza Tuff (dacite) on the southwest flank of the resurgent dome. To the east, across Soda Spring Gulch, Paleozoic strata overlie Proterozoic granitic rocks and also dip to the southwest, semiconformably beneath the Bonanza Tuff (fig. 184*A*). At base of the hill, several large isolated blocks of brecciated andesite (fig. 184*B*)

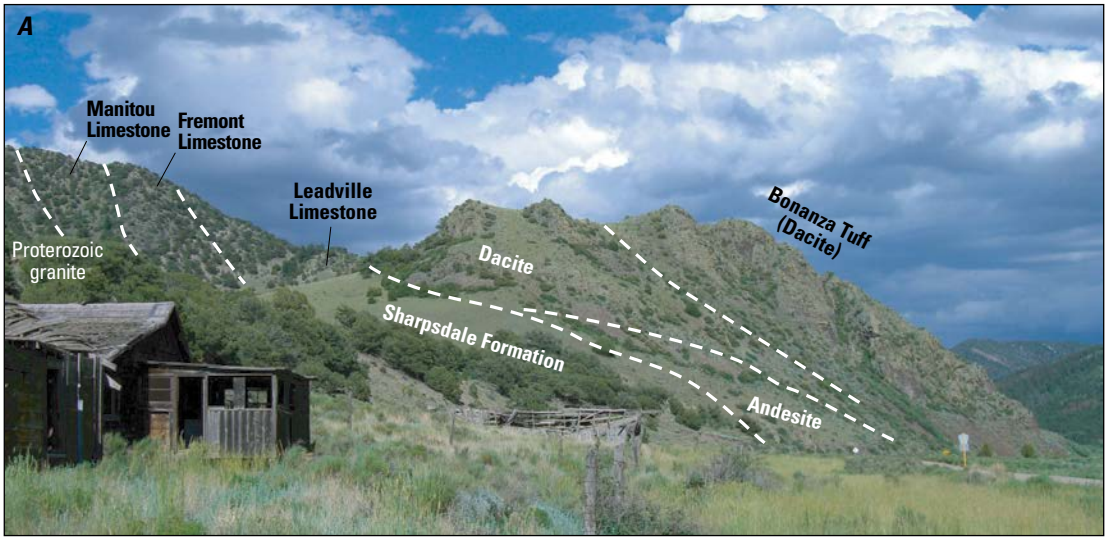

Figure 184. Stratigraphy and structure in the Soda Spring area, along the southwest flank of the resurgent dome (Stop 6A-3). *A*, Steeply dipping intracaldera Bonanza Tuff on hill, elevation 8,826 feet (2,690 meters [m]). Dips are conformable with the underlying Paleozoic strata that are exposed on the ridge at the left of the image. Andesite between the Pennsylvanian Sharpsdale Formation and the dacite is interpreted to be caldera-collapse landslide breccia (fig. 184*B*). The dacite may be an irregular sill-like intrusion (alternatively, a monolithologic landside megabreccia?). *B*, Andesite megablocks (as large as 10 m) on a slope mantled with small sandstone fragments derived from the Sharpsdale Formation, which is inferred to form the matrix between the andesite blocks. In the absence of large-displacement faults (for which evidence is lacking), the entire breccia complex, including andesite, Paleozoic sandstone, and Proterozoic gneiss, projects to lie above the Bonanza Tuff (at right of photo) that dips steeply on the southwest flank of the resurgent dome (fig. 184*A*). View to the north, from the Soda Spring trailhead. *C*, Smaller clasts of brecciated andesite, surrounded by fragmented sandstone of the Sharpsdale Formation, form small outcrops along the Soda Spring trail just upslope from the image in *A*. Higher portions of slope consist entirely of disaggregated blocks of Sharpsdale Formation and a few intermixed clasts of Proterozoic gneiss; no source is available for the andesite clasts, other than an essentially in-place origin. Photographs by P.W. Lipman, U.S. Geological Survey, 2014.

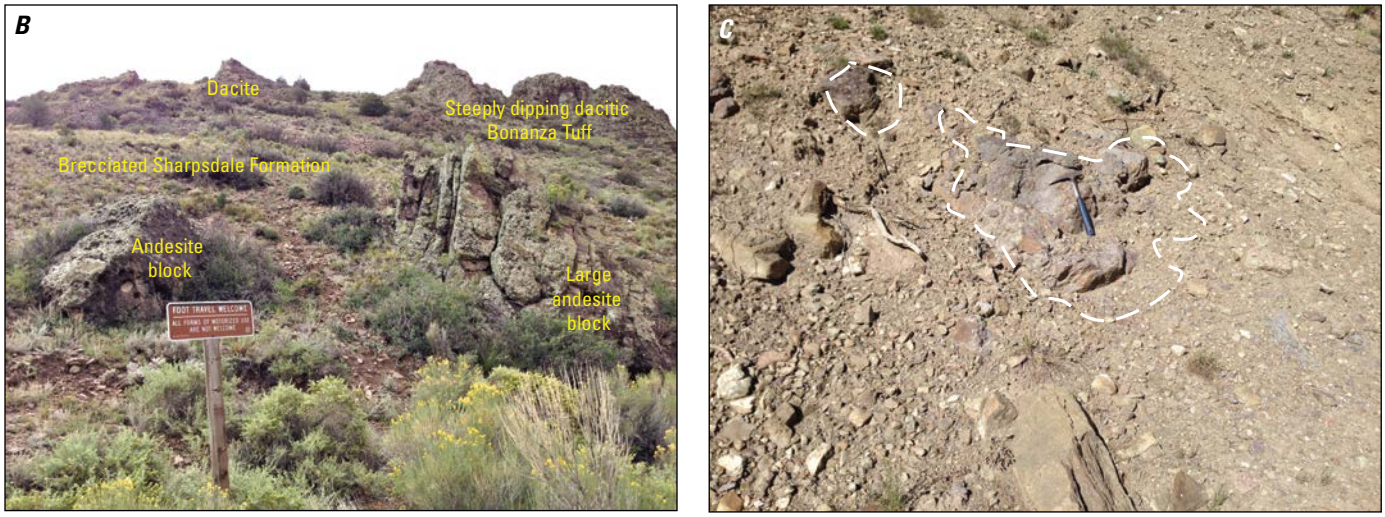

Figure 184.—Continued

are adjacent to the trail head. Hike up the trail through poorly exposed upper Paleozoic subaerial sandstone and shale (Sharpsdale Formation). Additional small outcrops of brecciated andesite and sparse Proterozoic granodiorite (fig. 184*C*) crop out low along the Soda Spring trail (38°12.92' N., 106°4.51' W.), closely confined within an area of chaotically mixed blocks of Sharpsdale Formation sandstone (fig. 184*C*), but again without precisely exposed contacts. What alternative interpretations could account for the presence of these diverse lithologies? Leave the trail to reach the saddle on the north side of the hill, then scramble through brush and talus to the hilltop. Look for eutaxitic foliation and lithic fragments in the massive dacitic Bonanza Tuff, petrographic distinctions, and the contact between the tuff and massive porphyritic dacite (63.7 percent SiO_2). What are some alternative interpretations for the dacite: an irregular intrusion; an eroded fragment of lava on the caldera floor, overlying the Sharpsdale Formation and predating intracaldera Bonanza Tuff; or perhaps a mass of intracaldera landslide megablocks (as can be discussed further in conjunction with Stop 6A-4)? The top of the hill provides great caldera views and a good lunch spot.

Return to vehicle; then continue by vehicle or on foot 0.3 mi to Stop 6A-4, at roadcuts near the junction with FS 852 (County HH50) to the left (south), which goes up Little Kerber Creek to Ute Pass.

7.8 **Stop 6A-4. Brecciated Proterozoic granite—An interpretive complexity** (Graveyard Gulch quadrangle: 38°12.95' N., 106°04.89' W.; 8,605 ft, 2,623 m elevation). Time permitting, a foot traverse can lead through diverse problematic outcrops, back to the parking area for Stop 6A-3.

On the right and in roadcuts ahead are large outcrops of shattered Proterozoic granodiorite, adjacent to a middle Cenozoic dacitic lava (fig. 185*A*). The origin of this distinctive breccia and its relations to adjacent Paleozoic and Cenozoic rocks has continued to perplex workers, and this stop provides access to many intriguing outcrops that provide a basis for exploring alternative interpretations. Close to the road, rotated Proterozoic blocks as much as several meters across are juxtaposed, some are finely shattered (fig. 185*B*) but with only a minor matrix of pulverized granodiorite. On slopes north of Kerber Creek, outcrops of granodiorite breccia in several zones are intermixed with upper Paleozoic Sharpsdale Formation, which contains coherent blocks of sandstone with chaotically divergent bedding orientations. This area is also complicated by the presence of a structural inflection from steep dips (to near vertical) in both Paleozoic and Cenozoic volcanic rocks to the east, on the southwest flank of the Sand Gulch anticline, to gentler attitudes in volcanic rocks west of the breccias. Alternative interpretations might include (1) thrust-fault breccias, (2) late Paleozoic talus deposits, (3) shatter breccias associated with caldera-ring faults, and perhaps most plausible as inferred here, (4) caldera-collapse landslide deposits.

1. The brecciated Proterozoic granodiorite was previously interpreted as overlying upper Paleozoic sandstone, within a zone of prevolcanic (Laramide) thrusting (Burbank, 1932, p. 40–41, Pl. 3), but no obvious evidence exists for a thrust contact. Inverted stratigraphy, fault planes, slickensides, discrete shear zones of finely comminuted microbrecciated rock, or other evidence of low-angle faulting are absent. Higher on the slope, most

Figure 185. Brecciated Proterozoic granite, an interpretive complexity (Stop 6A-4). Rotated blocks of foliated gneiss as much as several meters across are juxtaposed, many with only minor matrix of pulverized granodiorite. *A*, Road-cut outcrops of brecciated granodiorite gneiss, adjacent to dacite lava of the Rawley volcanic complex. In the center of image, a large weather-rounded block of gneiss several meters across is surrounded by more finely brecciated granodiorite. At first view, the dacite appears to overlie the breccia, but alternatively the breccia may have been deposited against the dacite along a paleovalley slope or may be in fault contact. *B*, Finely shattered coarse angular fragments of Proterozoic granodiorite gneiss is underlain by a zone of smaller fragments with a higher proportion of green-gray pulverized matrix. Hiking pole is ~0.9 meters in length. *C*, Large rounded blocks of granodiorite gneiss, with divergent foliation orientations, in a sandy matrix of more finely shattered gneiss. *D*, White, nonwelded tuff (Tbr, rhyolitic Bonanza Tuff?; 73.8 percent SiO_2) forming an indurated matrix to blocks of granodiorite gneiss (pCg) in a small, rare outcrop surrounded by surficial debris. The tuff also encloses centimeter-size fragments derived from the gneiss. Float of the tuff in adjacent areas suggests that the volcanic matrix is much more extensive than suggested by this small contact outcrop. Pen is 13 centimeters long. (Please do not hammer on or attempt to sample this minuscule outcrop; it provides critical interpretive evidence!) Photographs by P.W. Lipman, U.S. Geological Survey, 2013.

float debris consists of the sandstone, in places complexly intermixed with brecciated granodiorite.

2. Near the margins of the main breccia mass (for example: 38°12.94' N., 106°4.58' W.; 38°12.92' N., 106°4.57' W.), matrix-supported granodiorite clasts are surrounded by arkosic sand (fig. 185*C*), rather similar in appearance to some beds in the upper Paleozoic Sharpsdale Formation. These textures might suggest an origin as paleo-talus adjacent to steep slopes formed during the ancestral Rocky Mountain deformation (Pennsylvanian), but petrographic and chemical data show that the matrix is mainly derived directly from crushed granodiorite. Modestly higher SiO_2, FeO, MgO, and related trace elements in the breccia matrix suggest that quartz and mafic minerals have been concentrated relative to feldspar, compared to the protolith, but compositions remain distinct from quartz-rich sandstones of the Sharpsdale Formation. Additionally, no coherent beds of Sharpsdale-type sediment onlap or interleave with the granodiorite breccia. Instead, broad zones contain sizable blocks (as large as 2 m) of Sharpsdale sedimentary rocks with divergent orientations, unlike typical exposures of the Sharpsdale Formation elsewhere, which crop out boldly on steep slopes or break down readily into small fragments of scree where outcrops are lacking. Measurable attitudes on outcrop-size blocks of the Sharpsdale scatter widely but tend preferentially to strike northwesterly with steep dips, perhaps reflecting an influence from the nondisrupted southwest flank of the Sand Gulch anticline just to the east. Exposures are inadequate however, to define a mappable boundary between coherent versus brecciated Sharpsdale Formation.

3. The location of the brecciated Proterozoic rocks, immediately adjacent to the main caldera-collapse ring fault that occupies the valley of Kerber Creek, could suggest a possible origin as highly shattered wall rocks, analogous in origin to that inferred for brecciated andesite and dacite lavas that occur discontinuously adjacent to caldera ring faults farther up the valley in Kerber Creek (Stop 6A-5; fig. 186) and in Columbia Gulch to the south. The style of fragmentation here somewhat resembles shatter breccias in the andesite to the west, but the blocks of granodiorite tend to be larger, more rotated, are separated by more matrix—especially in the more easterly outcrops, and are locally mixed with other rock types. In places, the breccia is matrix supported, grading into sandstone that contains angular clasts of granodiorite (fig. 185*C*). Some shattering may be related to the Kerber Creek fault zone, but other features seem inadequately explained.

4. At least some of the breccia must be volcanic-related (fig. 185*D*), and probably caldera-associated, as indicated by locally exposed tuff matrix that encloses small blocks of the Proterozoic granodiorite (38°12.95' N., 106°4.59' W.). The tuff is only weakly indurated and has a composition similar to rhyolitic Bonanza Tuff (*Please do not hammer on or attempt to sample this minuscule outcrop; it provides critical interpretive evidence!*). A prominent outcrop (~3 m) of brecciated andesite is immediately adjacent to this exposure of rhyolite tuff, although contacts between the andesite and adjacent rocks are not exposed. Even larger blocks (as large as 10 m) of brecciated andesite, as viewed near the Soda Spring trailhead (Stop 6A-3), also make conspicuous outcrops surrounded by talus of Sharpsdale Formation (fig. 184*B*). No present-day source exists to have generated these large andesite blocks by Quaternary mass wasting; lavas of biotite dacite (rather than andesitic lava) cap the west slopes of lower Soda Spring Gulch. Shattered andesite masses of this type elsewhere disaggregate into talus downslope, rather than surviving as intact large blocks during surficial downhill transport. Thus, can a reasonable interpretation be made that the andesite blocks and rhyolitic tuff resulted from landslide processes during the Bonanza eruption and caldera collapse, similar to other megabreccia deposits that are better exposed farther up valley?

Textural and sedimentary features within the granodiorite/sandstone breccia also seem plausibly interpreted as caldera-landslide deposits, especially the variation from massively shattered granodiorite to intermixing of granodiorite clasts in a pulverized matrix (fig. 185*C*), and some hints of a stratigraphic sequence. Along lower slopes near the old ranch buildings (fig. 184*A*), abundant blocks of lithologically diverse Sharpsdale Formation sandstone (as large as 1 m) lie below massively brecciated granodiorite that is more erosion-resistant and holds up the prominent bench. Higher on this slope, sandstone is again the main lithology but as only small talus fragments (mostly <10 cm). The larger blocks of sandstone low on the slope, below the steep outcrops of granodiorite breccia, thus seem unlikely to have been derived by recent mass wasting from higher on this slope. Despite the absence of large sandstone outcrops, the distribution of sandstone clasts suggests the presence of at least two sandstone horizons, with massive granodiorite breccia making bold outcrops in between. Limited areas dominated by granodiorite breccia versus areas of sandstone higher on the slope hint at additional stratigraphic alternations, although these

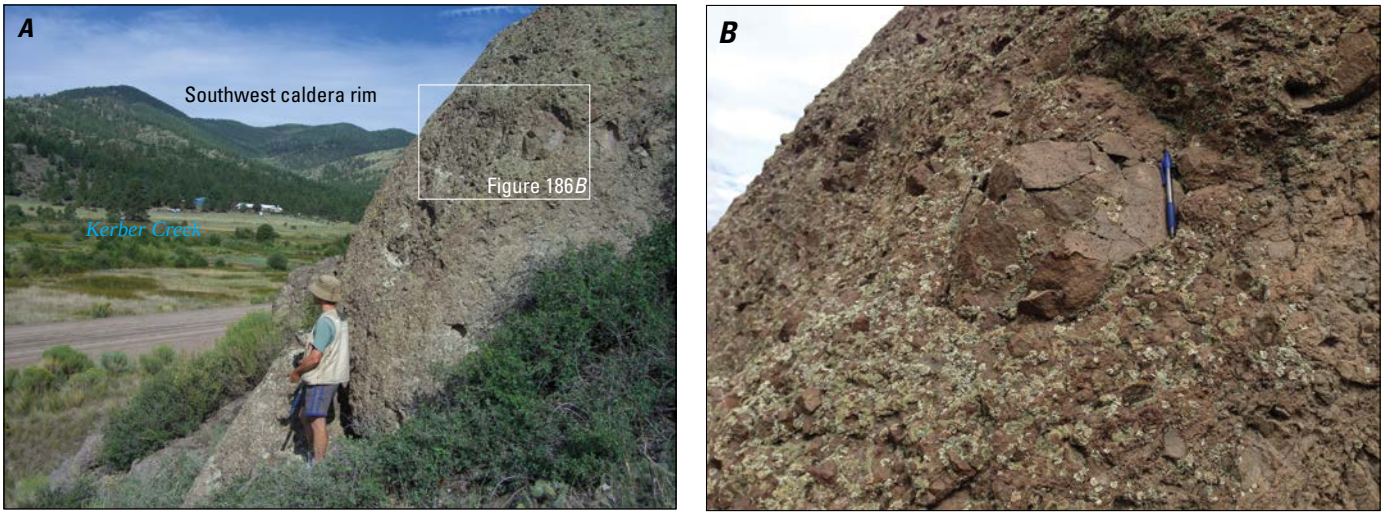

Figure 186. Highly shattered andesite at Stop 6A-5. Andesitic and dacitic lavas of the caldera floor are locally severely shattered adjacent to inferred ring faults along Kerber Creek and Columbia Gulch to the south. *A*, Brecciated caldera-floor andesite along the margin of the resurgent dome, adjacent to the valley of Kerber Creek (location of an inferred concealed ring fault); distant ridges form the eroded topographic rim of caldera (upper left). The white rectangle shows location of photograph *B*. *B*, Crushed fragments fit closely together, without abundant fine-grained matrix or evidence for major shearing. Photographs by P.W. Lipman, U.S. Geological Survey, 2013.

might otherwise result from an irregular upper surface on a single slide mass cored by granodiorite fragments.

Outcrops are lacking higher on the slope north of the Kerber Creek junction, but float is entirely Paleozoic sandstone without large clasts of granodiorite, and is thus consistent with a largely in-place stratigraphic sequence on the west limb of the Sand Gulch resurgent anticline. A granodiorite-dominated landslide at this site may have formed early during caldera collapse, probably before emplacement of the dacitic Bonanza Tuff that caps the hill (8,825 ft, 2,690 m elevation) just to the east (Stop 6A-3; fig. 184*A*). The landslide may have plowed into upper Paleozoic sedimentary rocks that floored the subsiding caldera in this area, ripping up and brecciating them; the absence of lower Paleozoic carbonates in the breccia suggests that sandstone of the Sharpsdale Formation was not transported long distances to the depositional site as part of the landslide mass.

Farther east, along the low ridge immediately west of lower Soda Spring Gulch (fig. 183*A*), small outcrops of even more diverse lithologies (andesite, upper Paleozoic sandstone, and lower Paleozoic limestone) are chaotically intermingled, but without exposed tuffaceous matrix. Without artificial exposures, however, tuff matrix to caldera megabreccia is rarely exposed in the Bonanza area; only the erosion-resistant blocks crop out. A megabreccia interpretation for the Soda Spring-Kerber Junction area would provide important information on caldera-wall geology of this sector. The dominance of Proterozoic debris accompanied by only volumetrically minor clasts of upper Paleozoic sediments and Cenozoic lavas suggests that the paleohills of Proterozoic basement stood high in the prevolcanic landscape and that volcanic cover was thin prior to eruption of the Bonanza ignimbrite. The inference of granitic caldera-collapse megabreccia in this area would also be consistent with the presence of another small area of granitic-clast megabreccia intermixed with andesite on the flank of the Bonanza resurgent dome, about 2 km farther northwest on the ridge east of Sawmill Gulch (38°13.72’ N., 106°5.64’ W.).

A problem with any caldera-breccia interpretation is the map pattern suggestive of a west-dipping depositional contact, along which Cenozoic volcanic rocks (dacitic to rhyolitic lavas) onlaps the brecciated Proterozoic assemblage (fig. 183*A*). An interpretation that the mixed granodiorite-sandstone breccia low on this slope is caldera-collapse breccia requires either that this contact be steeply depositional or a fault against the lavas along the ridge to the west. Across upper Soda Spring Gulch to the northeast, a steep contact between Paleozoic strata and Cenozoic lavas could also be a candidate for a fault, but the displacement would be down to the northwest, opposite that required to account for a fault contact between the lavas and inferred caldera-landslide deposit. Thus, steep depositional contacts resulting from paleotopography seem more plausible.

Nevertheless, the origin and structural significance of the brecciated granodiorite and its relation to adjacent Paleozoic and volcanic rocks remain in part unresolved. As a further puzzle, in contrast to the kilometer and greater displacements to east and west along the Kerber ring fault, the Proterozoic granite here crops out at near the creek level on both sides of the Kerber valley. The absence of significant net displacement is interpreted as a result of counterbalanced subsidence followed by

large-scale uplift in this sector along the crest of the south-plunging resurgent dome.

The hill across Kerber Creek to the south is capped by crystal-poor sanidine-bearing rhyolite, dated at 33.83±0.02 Ma, demonstrating its origin as a precaldera lava rather than as a rheomorphic rhyolitic facies of intracaldera Bonanza Tuff. An old jeep trail, 0.3 mi ahead on the right, climbs to a prominent shoulder on the ridge above the dacite, which is capped by another erosional remnant of rhyolite lava (table 15), similarly dated at 33.81±0.03 Ma.

Continue ahead 0.7 mi to Stop 6A-5, again parking along the road shoulder.

8.5 **Stop 6A-5. Highly shattered andesite** (Graveyard Gulch quadrangle: 38°13.40' N., 106°05.55' W.; 8,678 ft, 2,645 m elevation). *Park on the road shoulder; hike across the gully bottom to reach the outcrop to the north.*

The prominent outcrops of andesite and dacite lavas along the Bonanza road are intensely brecciated adjacent to the inferred ring fault along Kerber Creek. Angular blocks, mostly less than 0.5 m across, are juxtaposed, with only a minor matrix of comminuted lava (fig. 186). In many exposures, finely shattered fragments fit together without large-scale rotation or other movement (fig. 186*A*), and such rocks grade into more massive lavas of the caldera floor 100–200 m away from the mapped ring faults. In some zones, breccias with angular and rounded clasts are matrix supported (fig. 186*B*), but despite areal proximity to megabreccia at the base of the intracaldera Bonanza Tuff, no tuffaceous component is present in the shatter breccia. How do these textures in the andesite breccias compare with those of the brecciated Proterozoic granodiorite at Stop 6A-4? Chemical compositions of the andesite breccia matrix differ little from bulk andesite compositions, other than modestly variable alkali ratios and higher loss-on- ignition values. Although fault planes, slickensides, or other evidence of offset are sparse, the close proximity of the shatter breccias to the main caldera-collapse faults suggest that the shatter breccia formed during subsidence (or resurgence), perhaps due in part to hydraulic fracturing. Alternatively, and perhaps more likely, shattering of the floor rocks may have resulted from compression and crushing of the subsiding structural caldera block in proximity to steeply inward-dipping ring faults. Similar brecciation is developed in lavas adjacent to a satellitic arcuate fault along Columbia Gulch a few kilometers to the southwest. This style of brecciation has not been previously described for other Cenozoic ignimbrite calderas in the western United States, probably because comparably extensive exposures of caldera floor are rare.

Continue up the valley to the northwest on Bonanza road.

9.0 Turnoff to Bonanza Inn (not open in 2017). Up valley, the entire ridge on the skyline to the west is interpreted to represent eroded (but impressively preserved) morphologic remnants of the original topographic caldera rim (fig. 187*A*). The high point on the ridge is Antora Peak (13,269 ft, 4,044 m elevation), which is capped by Bonanza Tuff; the tuff is draped across the crest of the topographic rim. Lower slopes are pre-Bonanza lavas that dip gently westward on the inner caldera wall (fig. 187*B*).

Slopes on the right ahead contain large outcrops of brecciated andesite and dacite that lack obvious stratigraphic continuity; sparse float of less-indurated, partly welded Bonanza Tuff is present as sparse scree between outcrops. The slope is interpreted as consisting mainly of caldera-collapse megabreccia; a few small scabs of coherent Bonanza Tuff are present as well. The distinction between brecciated, but largely in place caldera-floor lavas, versus deposits of massive landslide breccia is difficult in much of this area. In addition, unusual dike-like ribs contain vertically dipping eutaxitic Bonanza Tuff (fig. 187*D*; also see Stop 6A-11), but access here requires crossing a fence onto private land. Although many of the ribs are subparallel to the caldera ring fault along Kerber Creek, these distinctive features are tentatively interpreted as dilatant crack-fills injected from above, as the caldera-floor rocks became fractured during subsidence (rather than true intrusive pyroclastic dikes), because of their confinement to upper levels of the caldera floor and overlying megabreccia. Although fragmental textures are well preserved, much of the tuff in these ribs has undergone alkali exchange (as much as 7.5 percent K_2O, 0.25 percent Na_2O). Across the valley to the south such features are absent, and the lavas exposed there are interpreted as lower slopes of the caldera wall.

9.4 Elk Horn Ranch subdivision is on the right (see Stop 6A-11, 6A-12). From here up-valley to the west, exposures north of the road (on the southwest flank of the resurgent dome) are more coherent andesite to rhyolite lavas that are interpreted as less-disrupted caldera floor. The view ahead is toward the morphologically well-preserved west rim of the caldera (fig. 188*A*). Northeast-facing slopes south of Kerber Creek are interpreted as lower parts of the inner caldera wall. Stratigraphically coherent andesitic lavas are well exposed in cirque headwalls higher along the valley of Kerber Creek (fig. 188*B*).

11.0 Greenback Gulch (fig. 189), on the right (north) farther up the valley, provides a view of Hayden Peak (12,130 ft, 3,697 m elevation). Lower slopes consist of caldera-floor lavas; high talus-mantled slopes are

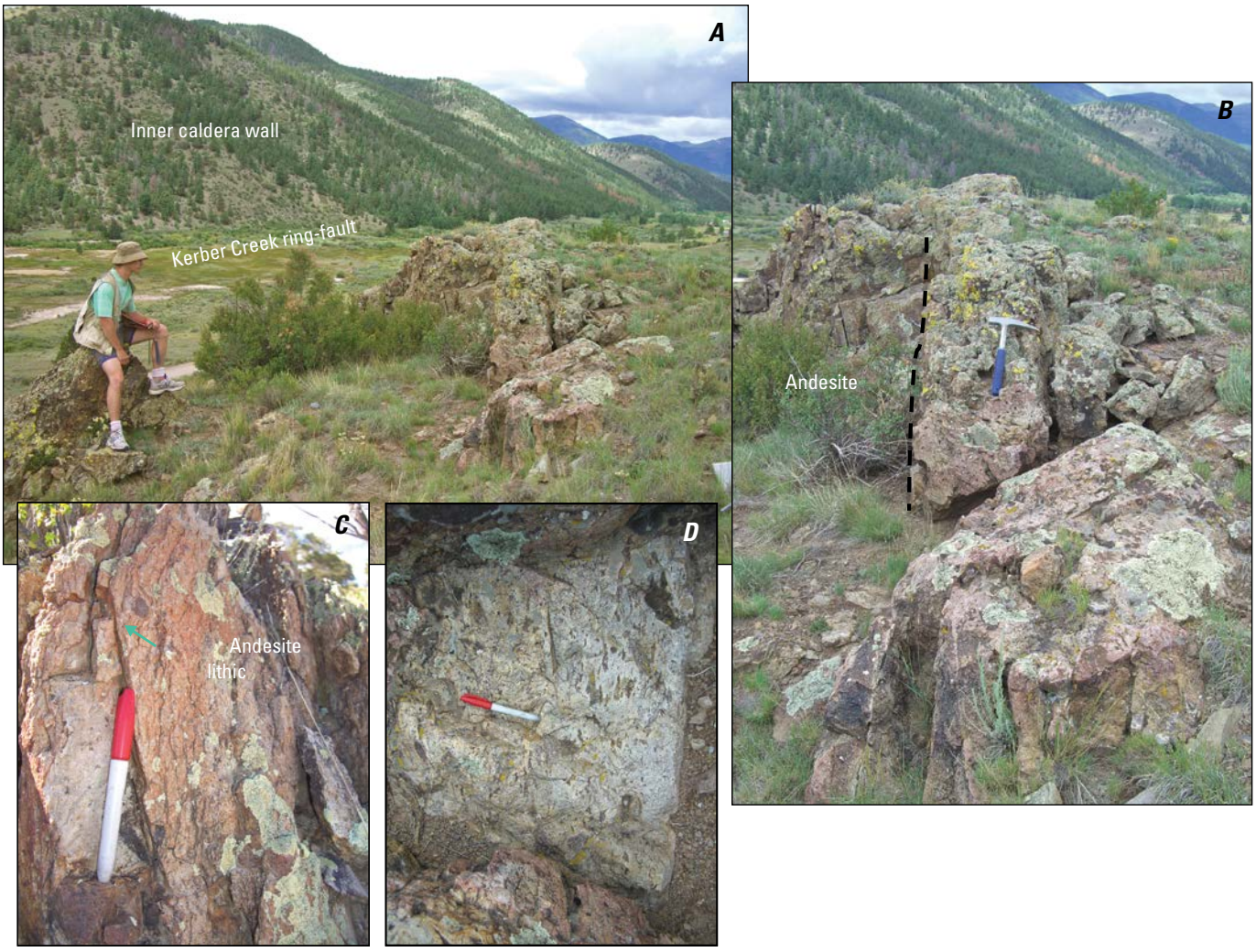

Figure 187. Discontinuous dike-like bodies of steeply dipping Bonanza Tuff, interpreted as filling dilatant fractures in the upper part of the caldera-floor lava and megabreccia sequence. All photographs show the lower slopes between Sawmill and Big Tree Gulches. *A*, View to southwest, up the valley of Kerber Creek, which follows the main caldera ring fault. Crack-fill is a rib of densely welded rhyolitic tuff, with near-vertical contact between fracture-filling tuff and country rock of andesitic lava, on the lower flank of the resurgent dome; high distant ridges are the eroded topographic rim of the caldera. This and some nearby crack-fills are semiparallel to the northwest-trend of the adjacent Kerber Creek ring fault, but others are at high angles 38°13.95′ N., 106°06.94′ W. *B*, Detail of fluidal-textured rhyolitic rib; the contact with the andesite and flattened pumice-foliation in the rib are near vertical. *C*, Sparse andesitic lithics document the fragmental nature of the tuff, even where it is strongly altered or fluidal in texture. *D*, At another rib, steeply dipping foliation is well defined by flattened-pumice fiamme in the rhyolitic tuff. Photographs by P.W. Lipman, U.S. Geological Survey, 2013.

crystal-poor silicic dacite (table 16), dated at about 32.8 Ma (several groundmass samples), and considered to be a postcaldera lava sequence. Small exposures and abundant scree of light-colored crystal-poor rhyolitic tuff that is highly altered, discontinuously present below the Hayden Peak lavas, are interpreted as intracaldera Bonanza Tuff. In contrast, the rugged light-colored outcrops on lower hills ahead at 2:00 consist of silicified and otherwise altered crystal-poor rhyolite lava that represents an uppermost unit of the caldera floor in this area.

Continue to the junction with Brewery Creek road (FS 880, County NN46).

13.5 **Stop 6A-6. Intracaldera dacitic Bonanza Tuff** (Bonanza quadrangle: 38°16.58’ N., 106°08.93’ W.; 9,199 ft, 2,804 m elevation)

The roadcut exposure is typical of intracaldera dacite tuff and is so propylitically altered that its initial pyroclastic nature is evident mainly from the abundant small fragments of andesite (try to discern flattened pumice or shard textures). Compare with

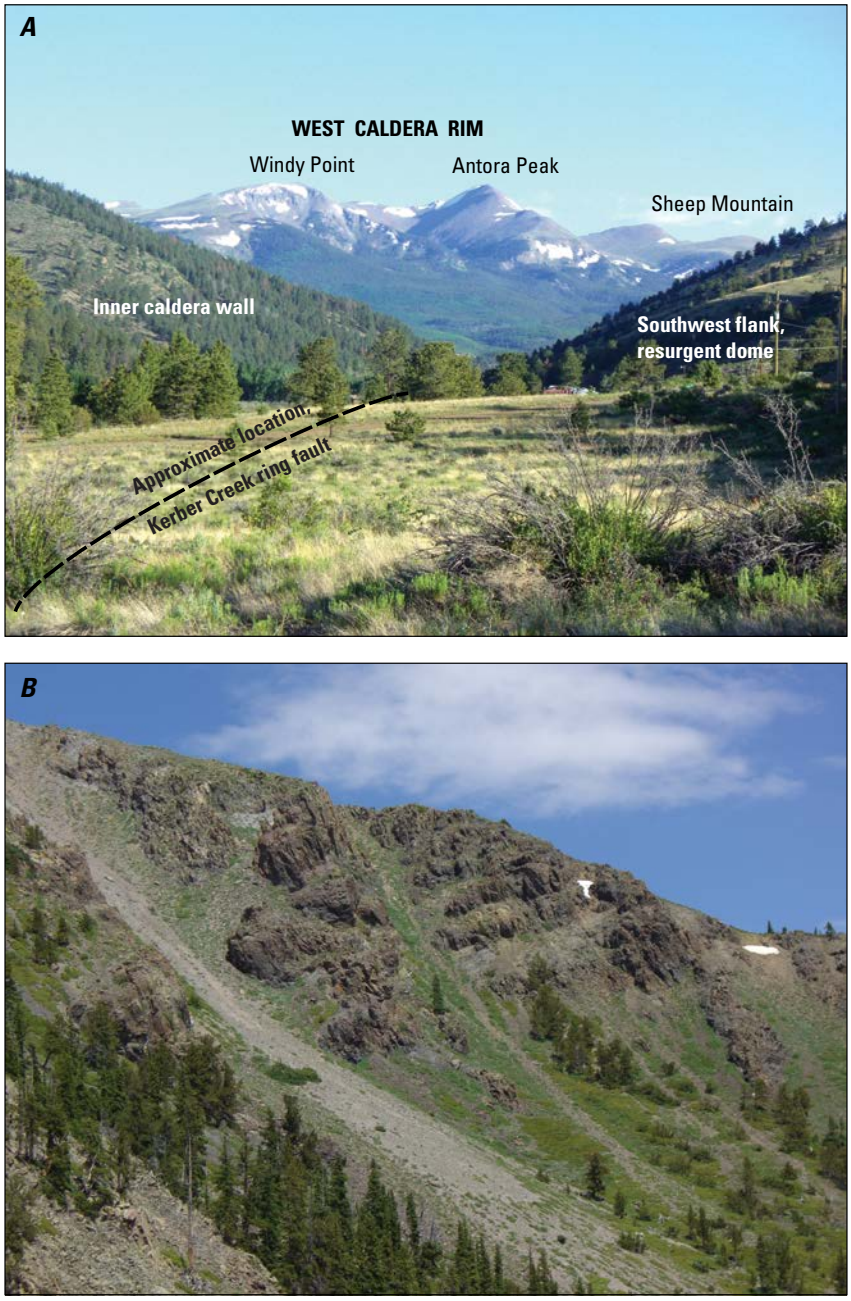

Figure 188. West rim of Bonanza caldera. The high arcuate ridge from Flagstaff Mountain north to Antora Peak and beyond is capped by discontinuous erosional remnants of thick Bonanza Tuff (mainly dacite). These areas of densely welded tuff bank thickly against older andesite on the caldera wall, where they are interpreted mainly to constitute high remnants of ponded intracaldera ignimbrite. In places, the ignimbrite is continuous across the present-day topographic ridge, into more widespread proximal outflow outcrops of the tuff to the west, suggesting that the ridge approximates the erosionally modified location of the original topographic rim of Bonanza caldera. *A*, West rim as viewed to the northwest, up valley of Kerber Creek. In the distance, Antora Peak (center, 13,269 feet [ft], 4,044 meters [m]) is capped by densely welded dacitic Bonanza Tuff (33.12 million years ago [Ma]), but Windy Point (left, 12,800 ft, 3,901 m) exposes a thin layer of basal rhyolitic Bonanza Tuff that has undergone local rheomorphic flowage. Lower slopes of both high points are a west-dipping sequence of interlayered andesitic lavas and volcaniclastic rocks that make up the erosionally modified inner wall of Bonanza caldera (see fig. 188*B*). Sheep Mountain (right distant skyline, 12,228 ft, 3,727 m) is a pre-Bonanza dacitic lava dome (33.89 Ma) that partly fills the older Marshall caldera, source of the 33.93-Ma Thorn Ranch Tuff. On the left (southwest) side of Kerber Creek, timbered slopes are the lower portions of the southwest caldera wall; the right side of the creek is a dip slope on the flanks of the postcollapse resurgent dome. The valley of Kerber Creek coincides with the main ring fault, along which more than 3 kilometers of subsidence was accommodated during eruption of the Bonanza Tuff and concurrent caldera collapse. *B*, Andesite lavas on the inner west caldera wall. Coherent stratigraphic sequences of west-dipping precaldera andesitic lavas of the Rawley volcanic complex along the east ridge of Windy Point, as viewed from the south. Photographs by P.W. Lipman, U.S. Geological Survey, 2013.

the outflow dacite tuff, as viewed at Stop 6-1; such contrasts are typical for intracaldera versus outflow ignimbrite deposits. The outcrop is near the top of the steeply tilted intracaldera tuff on the west flank of the resurgent dome, which in this area and just up the valley ahead interfingers multiple times with rhyolitic tuff and has a thickness of about 2.5 km (figs. 172, 175*A*).

Poorly exposed above this outcrop and in better outcrops along the ridge just to the south are basal biotite-andesite lavas (Squirrel Gulch Andesite; Stop 6B-1) of the postcollapse caldera fill. This distinctive porphyritic andesite (59.8 percent SiO_2) is characterized by unusually large and abundant biotite phenocrysts (table 16).

13.7 *Continue ahead, past the junction with Slaughterhouse Creek road (FS 861, Saguache 46PP) on left*, which provides access to upper units of the caldera-filling lava sequence (see route 6B). Just beyond are views up Elkhorn Gulch. Large, rugged outcrops low near the mouth of the gulch are dacitic Bonanza Tuff. Bare talus-covered slopes up valley on the right side are Eagle Gulch Dacite, a massive, fine-grained intrusion that has an irregular-sill geometry and roughly occupies the contact between the caldera-floor lavas and intracaldera Bonanza Tuff.

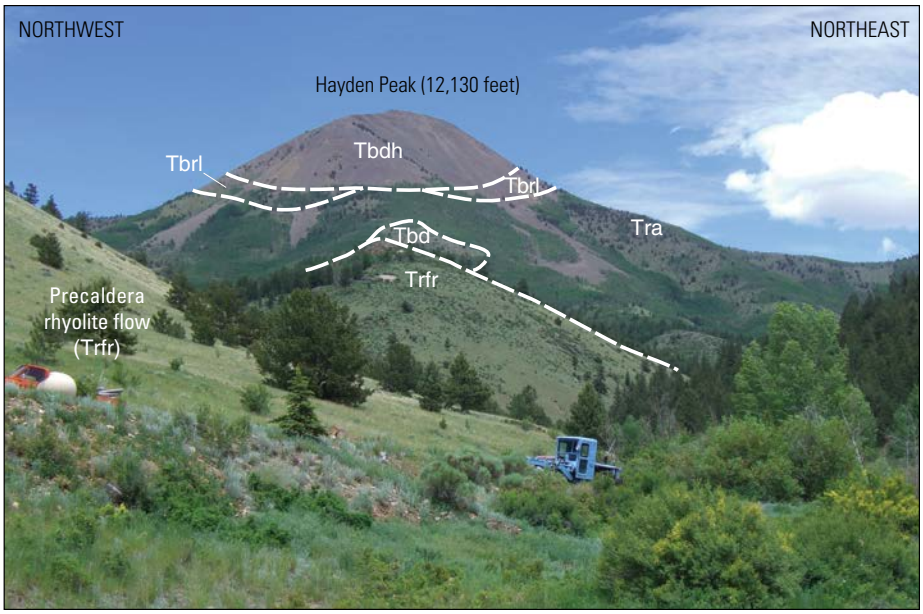

Figure 189. Hayden Peak, viewed from the south up Greenback Gulch. Areally restricted erosional remnants of distinctive massive gray lavas (Tbdh) of sparsely porphyritic silicic dacite (69.2–70.5 percent SiO_2) occupy the upper slopes of Hayden Peak and extend along the ridge to the north, and are exposed largely as talus on steep slopes (Lipman, 2020). The dacite lavas were deposited on lower rhyolitic Bonanza Tuff (Tbrl) and caldera-floor lavas of the Rawley volcanic complex, mainly andesite (Tra), in a deep paleovalley or possibly along an obscure fault-bounded keystone graben of the caldera resurgent dome. On the lower south slope of Hayden Peak, a thick rhyolite lava complex (Trfr) caps the caldera-floor andesite lavas on the southwest-dipping flank of the resurgent dome; these lavas are locally overlain by small erosional remnants of dacitic Bonanza Tuff (Tbd). Photograph by P.W. Lipman, U.S. Geological Survey, 2014.

14.6 Enter the town of Bonanza (fig. 190*A*); foundation of an old mill is on the left. All slopes in sight are thick intracaldera tuff. The downtown area is half a mile farther (fig. 190*B*).

16.1 A mile north of Bonanza, just beyond U.S. National Forest boundary, a prominent outcrop of andesite on the right is part of a large lenticular mass interleaved with intracaldera tuff and interpreted as landslide megabreccia derived from the caldera walls.

Continue past the Exchequer town site, at the mouth of Rawley Gulch, to the junction of Kerber Creek (FS 862) and Squirrel Gulch roads; stay right on Squirrel Gulch road (FS 869) for 0.3 mi farther to Stop 6A-7 at a prominent switchback.

16.5 **Stop 6A-7. Megablock in Bonanza Tuff** (Bonanza quadrangle: 38°18.55' N., 106°08.77' W.; 9,715 ft, 2,961 m elevation)

Exposed in a roadcut is a 4-m-diameter boulder of shattered andesite lava, floating in altered Bonanza Tuff (fig. 191). When was the andesite brecciated, during emplacement as lava, or shattered during caldera subsidence and incorporation in the caldera-filling ignimbrite (compare with brecciated andesite blocks viewed at Stop 6A-3)? Highly altered outcrops ahead are all Bonanza Tuff, dipping 40–60° to the west. These exposures are a small part of the 2.5-km-thick section of intracaldera ignimbrite that is preserved on the tilted west flank of the resurgent dome (fig. 173).

16.9 Passing the Rawley mine-drainage tunnel (possible lunch/toilet stop). This was the most productive mine in the district and operated intermittently from 1880 to 1969

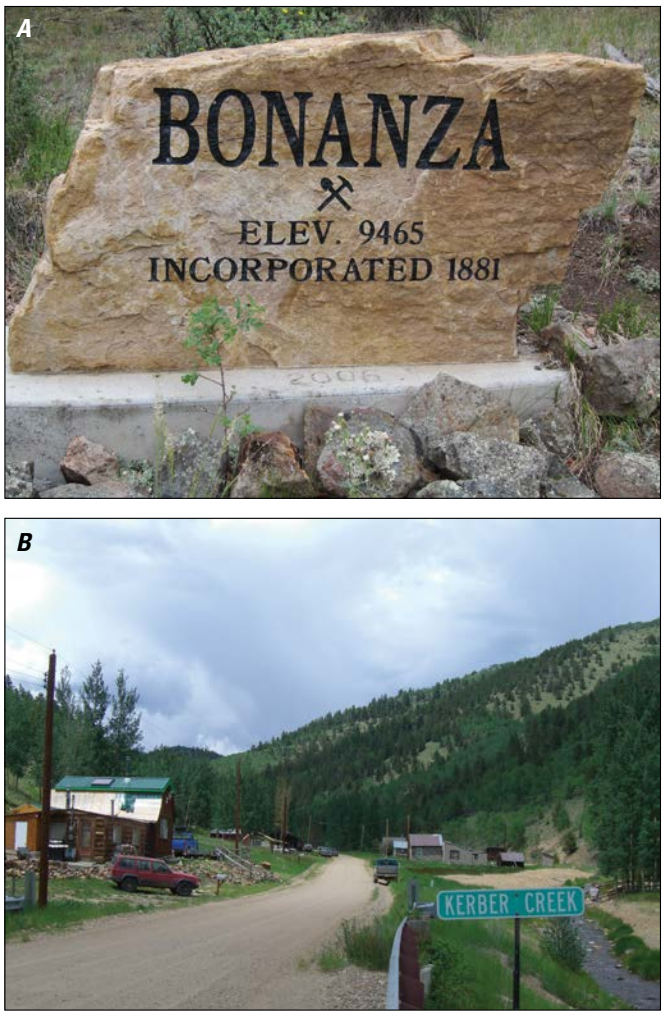

Figure 190. The town of Bonanza, the only settlement within exposed parts of the Bonanza caldera was a thriving boomtown in the 1880s, but at present has only a few year-round residents. *A*, Entry sign to the town of Bonanza, along Bonanza Road. *B*, Central Bonanza, population of two (in 2014). Photographs by P.W. Lipman, U.S. Geological Survey, 2014.

Figure 191. An isolated large block (3–4 meters) of brecciated andesite (Stop 6A-7), floating in partly welded Bonanza Tuff, all variably bleached by supergene alteration. The exposure, along lower Squirrel Creek, is within the 2.5-kilometer-thick section of intracaldera ignimbrite that is preserved on the tilted west flank of the resurgent dome. Photograph by P.W. Lipman, U.S. Geological Survey, 2014.

(Cappa and Wallace, 2007). The tunnel was plugged as part of a major mine-lands remediation effort, which was sufficiently effective that trout could be successfully reintroduced to the Kerber Creek drainage.

17.1 *Proceed for 0.2 mi, make a sharp turn to the right, onto FS 890 (a high-clearance vehicle recommended past this point), to Stop 6A-8 along the steep incline.*

17.3 **Stop 6A-8. Fluidally welded Bonanza Tuff** (Bonanza quadrangle: 38°18.91' N., 106°08.52' W.; 9,954 ft, 3,034 m elevation)

Light-gray, meter-long fiamme define a down-dip lineation in the matrix of somewhat altered dacite welded tuff (fig. 192). Similar lineations can be recognized in scattered exposures elsewhere on flanks of the resurgent uplift and are probably more widespread than mapped. Rheomorphic flow structures are so well developed in the lower intracaldera rhyolite that interpretation of some localities remains uncertain as to whether they represent the lower tuff or caldera-floor rhyolite lava (Stop 6A-12). Such extreme rheomorphic flowage is rare in calc-alkaline ignimbrites, although the Bonanza Tuff is somewhat more alkalic (for example, higher zirconium, light rare earth elements) than other regional tuff sheets farther west and south in the San Juan region (fig. 170). Development of lineations and rheomorphic flow is commonly interpreted to indicate deposition on a slope or in a confined paleovalley (for example, Chapin and Lowell, 1979). Could the widespread down-dip direction of the lineation on flanks of the resurgent dome suggest that uplift may have already been underway before the intracaldera tuff cooled to full rigidity?

Continue up the ramp to the junction with Rawley road (FS 892); stay right (into the valley).

17.6 The road intersection is in altered massive Bonanza Tuff, just above a large lens of andesitic megabreccia that is discontinuously exposed along the descending road. Dark andesite makes prominent outcrops; breccia matrix of light-colored weakly welded tuff (quenched against megablocks) is less well exposed.

Continue to the switchback in the bottom of the gulch; take the side road up the valley to the stream crossing, where the walk to Stop 6A-9 starts.

17.8 **Stop 6A-9. Granodiorite in Rawley Gulch** (Bonanza quadrangle: 38°18.88' N., 106°08.17' W.; 10,351 ft, 3,155 m elevation)

Figure 192. Large light-gray pumice lenses (upper limit >1 meter) in dacitic Bonanza Tuff (Stop 6A-8) along the mining road that traverses from Squirrel Creek into Rawley Gulch. In addition to extreme flattening, the pumice lenses are elongate in the foliation plane, defining a down-dip lineation. Photograph by P.W. Lipman, U.S. Geological Survey, 2014.

Walk up the valley ~219 yds (~200 m), to an obscure small exposure of medium-grain resurgent granodiorite (55.7 percent SiO_2; table 16) above an abandoned trail on the north side of Rawley Gulch (38°19.04' N., 106°08.06' W.). Despite its relatively mafic bulk composition, the granodiorite contains interstitial potassium feldspar dated at 33.02±0.08 Ma. This small, obscure exposure was the first granitic intrusion recognized in the Bonanza area, by Patton (1916, p. 54). Without the prior description, what would be the odds of finding such a locality along this now-heavily vegetated side hill? Similar small masses of granodiorite that intrude caldera-floor andesite and lower levels of Bonanza Tuff have been found in several other places on the west flank of the resurgent dome, and larger granitoid intrusions are exposed along the more deeply dissected east flank (see route 6D). Ages from six widely distributed sites are all similar to that of the Bonanza Tuff, and together are interpreted as documenting the irregular roof of a large, composite resurgent intrusion that underlies central parts of the caldera.

Return to the vehicle and continue down Rawley Gulch. In ~0.3 mi, the road begins to cross through more andesitic megabreccia in a tuffaceous matrix.

18.3 **Stop 6A-10. Andesitic landslide breccia within Bonanza Tuff** (Bonanza quadrangle: 38°18.51' N., 106°08.52' W.; 9,810 ft, 2,990 m elevation)

Exceptionally good roadcut exposures of meso- and megabreccia, in which variably welded light-colored tuffaceous matrix surrounds dark blocks of texturally diverse andesite (fig. 193). Without artificial exposures, slopes above display only small outcrops of andesite, with sparse scattered fragments of tuff in the adjacent soil. As is common in other caldera-collapse breccias, the lack of welding in much of the tuff matrix is attributed to chilling by the enclosed andesite blocks.

Continue down the Rawley Gulch road, rejoining Bonanza road at the Exchequer town site. Rhyolitic Bonanza Tuff is present as float above the graveyard.

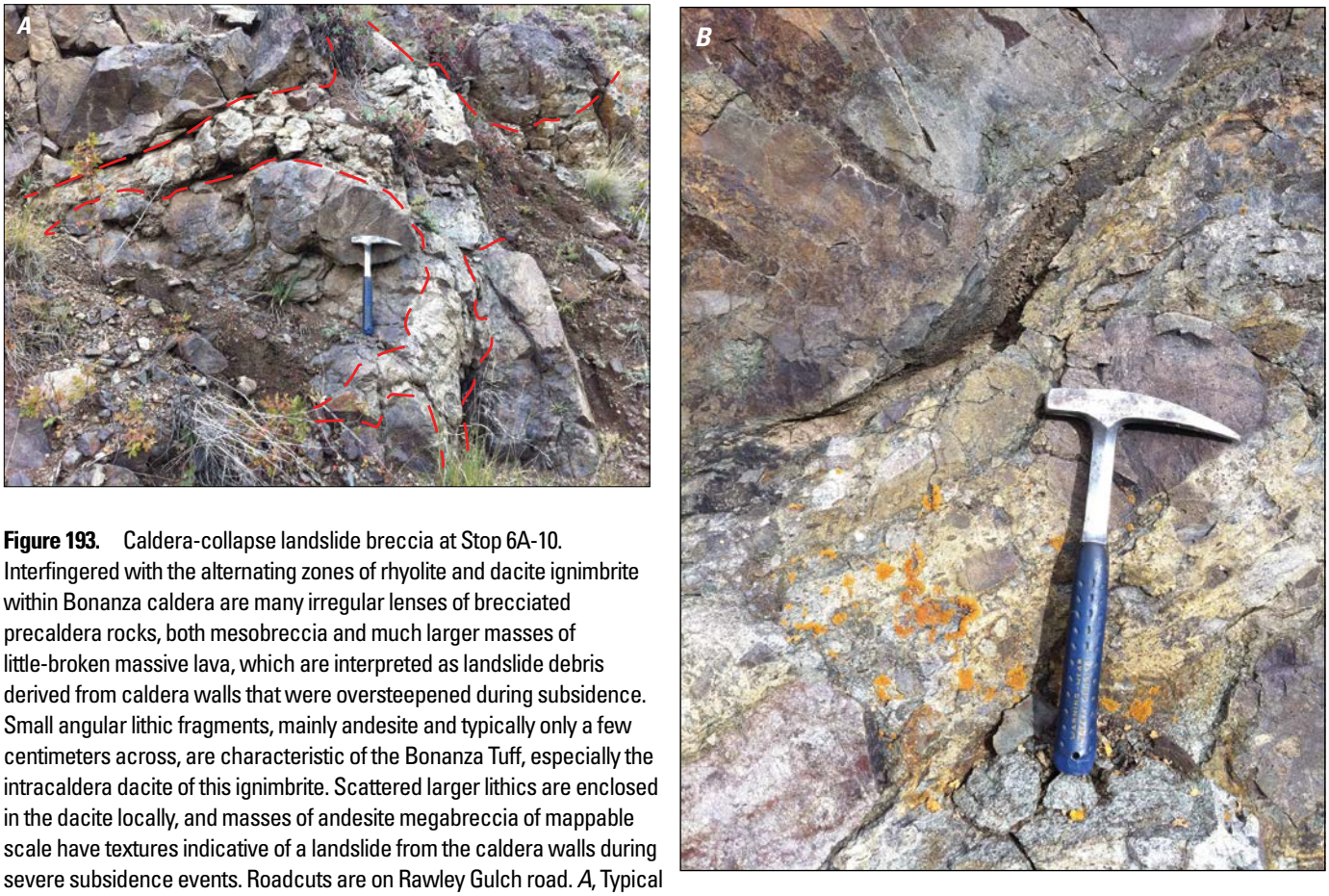

Figure 193. Caldera-collapse landslide breccia at Stop 6A-10. Interfingered with the alternating zones of rhyolite and dacite ignimbrite within Bonanza caldera are many irregular lenses of brecciated precaldera rocks, both mesobreccia and much larger masses of little-broken massive lava, which are interpreted as landslide debris derived from caldera walls that were oversteepened during subsidence. Small angular lithic fragments, mainly andesite and typically only a few centimeters across, are characteristic of the Bonanza Tuff, especially the intracaldera dacite of this ignimbrite. Scattered larger lithics are enclosed in the dacite locally, and masses of andesite megabreccia of mappable scale have textures indicative of a landslide from the caldera walls during severe subsidence events. Roadcuts are on Rawley Gulch road. *A*, Typical caldera-collapse mesobreccia. Equant rounded block of andesite, about 0.7 meters in diameter, surrounded by light-gray matrix of rhyolitic Bonanza Tuff and additional andesite fragments. The light color of the tuff indicates that it was originally only weakly welded and probably glassy, owing to quenching against the abundant clasts of wall-rock andesite. *B*, Closer view of the mesobreccia texture (same location as *A*), showing a wide range of andesite-clast sizes dispersed in lighter-colored tuffaceous matrix. Photographs by P.W. Lipman, U.S. Geological Survey, 2015.

18.6 *Retrace the route, through the town of Bonanza and down Kerber Creek valley, to the entry gate for the Elk Horn Ranch subdivision (38°13.98' N., 106°06.21' W.). Enter through the motorized gate (permission and the access code must be obtained!)*

25.0 Ascend the main switch-backed ranch road (Tree Gulch Lane), passing roadside outcrops of diverse lavas that appear to lack stratigraphic coherence. Small rare lenses and irregular patches of nonwelded rhyolitic tuff, seen only in artificial exposures, suggest that these rocks are massive landslide-megabreccia deposits deep within the caldera-fill, which grade downward into a more coherent caldera-floor volcanic assemblage. Aspects of this interpretation are focus of the next two stops.

27.1 **Stop 6A-11. Fracture fill of rhyolitic welded tuff with near-vertical fiamme** (Tree Gulch Lane, Graveyard Gulch quadrangle: 38°14.59' N., 106°05.73' W.; 9,554 ft, 2,912 m elevation)

Within the near-floor megabreccia, much of the matrix tuff is weakly welded, lithic rich, and exposed only as fragments on slopes, but some outcrops of tuffaceous crack-fills are strongly welded and have steeply dipping fiamme (fig. 194). The rhyolitic crack-fills are relatively thin (typically <1–2 m), discontinuous (commonly traceable for a few tens of meters or less), and irregular in shape and trend. In places, obviously welded tuff grades along strike into flow-laminated rhyolite that lacks obvious fragmental textures; a few parallel dike-like bodies appear to consist entirely of rhyolite without lithic fragments or other surviving pyroclastic textures.

Could some of these be intrusive dikes of fluidal rhyolite or vent fissures for ignimbrite eruptions? Available evidence suggests that they are better interpreted as surficial fills between blocks of early caldera-collapse megabreccia, injected down into dilatant cracks that opened during caldera subsidence. Well-exposed fracture fills of highly welded and rheomorphic rhyolitic tuff, on the slopes north of Kerber Creek between Express and Schoolhouse Gulches, tend to be parallel to adjacent caldera ring faults (fig. 187), but all identified fracture fills of highly welded and rheomorphic rhyolitic tuff are located near the transition from caldera floor upward into caldera-fill megabreccia and matrix tuff. No comparable fracture-fill tuff has been found at deeper exposed levels of caldera-floor lavas or in underlying Paleozoic and Proterozoic rocks. Most fracture fills with identified pyroclastic textures consist of crystal-poor rhyolite (only one fracture fill of dacite tuff is well exposed), similar to that of the early erupted lower rhyolite phase of the ignimbrite sheet, as would

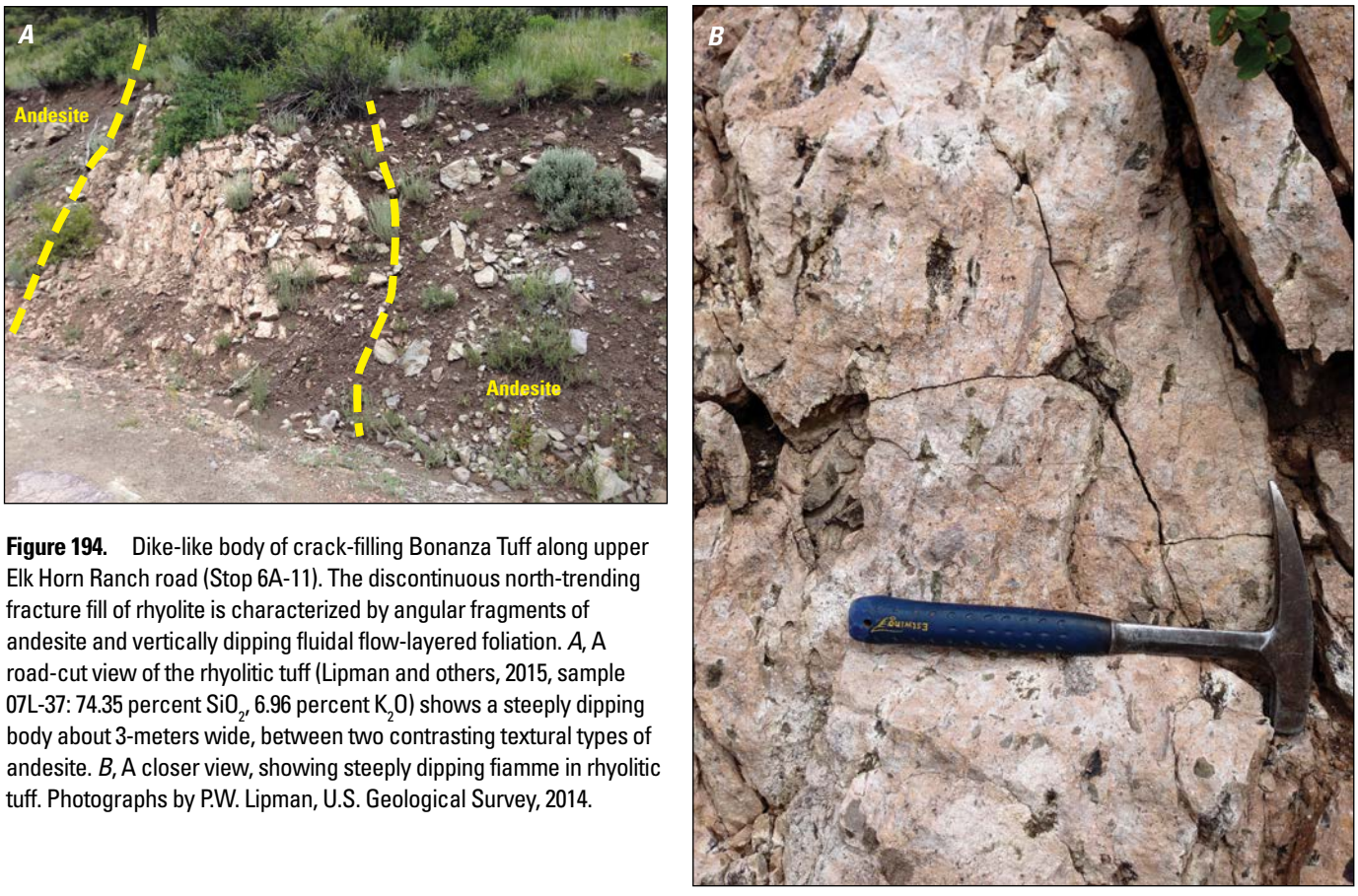

Figure 194. Dike-like body of crack-filling Bonanza Tuff along upper Elk Horn Ranch road (Stop 6A-11). The discontinuous north-trending fracture fill of rhyolite is characterized by angular fragments of andesite and vertically dipping fluidal flow-layered foliation. *A*, A road-cut view of the rhyolitic tuff (Lipman and others, 2015, sample 07L-37: 74.35 percent SiO_2, 6.96 percent K_2O) shows a steeply dipping body about 3-meters wide, between two contrasting textural types of andesite. *B*, A closer view, showing steeply dipping fiamme in rhyolitic tuff. Photographs by P.W. Lipman, U.S. Geological Survey, 2014.

be anticipated if caldera subsidence began during this phase of the eruption. Similar local pods of eutaxitic to fluidal rhyolite are present elsewhere on flanks of the resurgent dome, especially within large northern areas interpreted as megabreccia on both sides of Clover Creek (on the north side of the caldera), but these areas are heavily vegetated and exposures are limited.

Continue east for 0.5 mi to the fork in the subdivision road at the saddle; bear left (north) following Tree Gulch Lane for 0.3 mi to roadcuts.

27.9 **Stop 6A-12. Lava-like Bonanza Tuff and megabreccia** (Schoolhouse Gulch, Graveyard Gulch quadrangle: 38°14.58' N., 106°05.27' W.; 9,600 ft, 2,926 m elevation)

The highly welded to fluidal rhyolite in some dike-like fracture fills merges, in places, with areas of less-welded tuffaceous matrix in the megabreccia and with larger pockets and lenses of more uniformly welded intracaldera Bonanza Tuff that dip conformably with the flanks of the resurgent dome. In contrast, at this site high along the ridge west of Schoolhouse Gulch (fig. 195*A*), scattered steep lenses of rhyolitic Bonanza Tuff are spatially associated with a sheet-like erosional remnant of flow-layered rhyolite interpreted as rheomorphic lower Bonanza Tuff despite its fluidal lava-like fabric (fig. 195*B*).

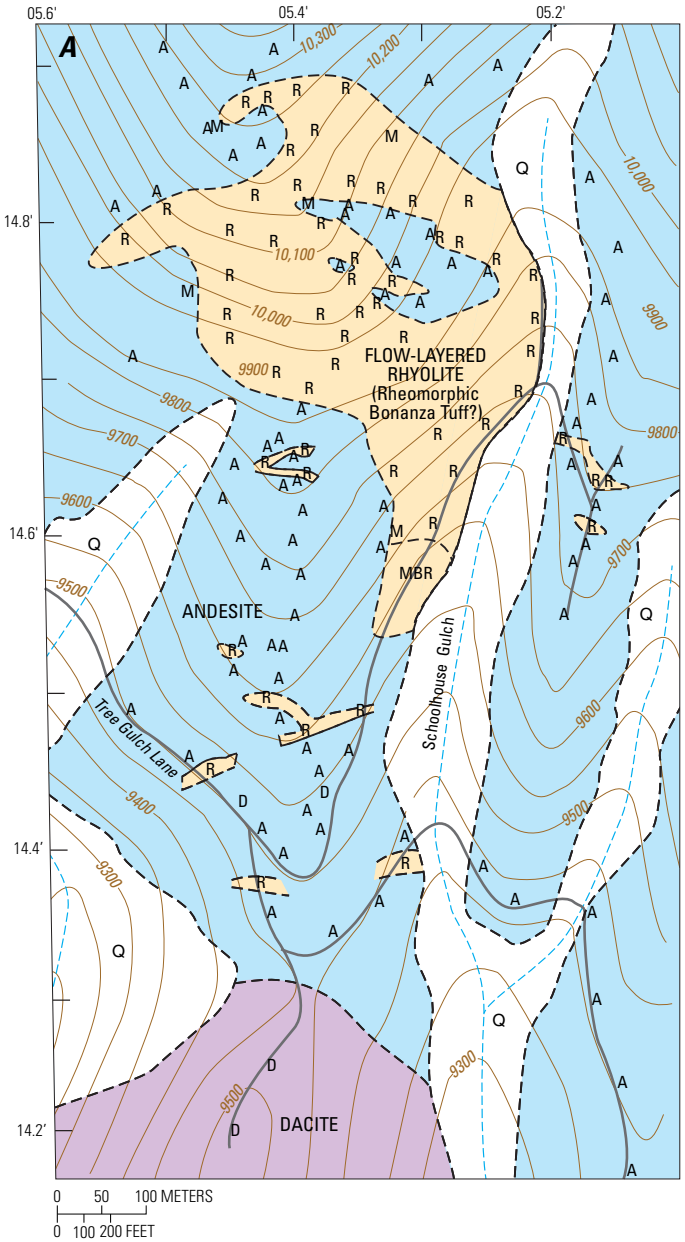

Figure 195. Rheomorphic lower Bonanza Tuff encloses diverse masses of precaldera andesite on the ridge west of upper Schoolhouse Gulch along Big Tree Lane (Stop 6A-12). In road-cut exposures, scattered steep lenses of rhyolitic Bonanza Tuff are spatially associated with a sheet-like erosional remnant of flow-layered rhyolite, interpreted as rheomorphic lower Bonanza Tuff despite its fluidal lava-like fabric. Where contacts with adjacent caldera-floor andesite are well exposed, especially at the southern end of the main body, masses of andesite ranging in size from several meters across down to centimeter-size chips are enclosed by fluidal rhyolite that is locally flow folded. In striking contrast to the weakly welded matrix tuff associated with most caldera-collapse breccias at Bonanza (fig. 193) and elsewhere (Lipman, 1976b), the texture of the rhyolite along Schoolhouse Gulch is strikingly lamellar and fluidal adjacent to andesite clasts, even in thin-section scale. *A*, Geologic map of the sheet-like mass of flow-layered rhyolite, interpreted as rheomorphic lower Bonanza Tuff along upper Schoolhouse Gulch. Letter symbols mark locations of Global Positioning System (GPS)-located outcrops and areas of monolithologic float inferred to reflect immediately underlying bedrock. A, andesite; D, dacite; MBR, mega- and mesobreccia of andesite blocks surrounded by rhyolite matrix; R, flow-layered rhyolite; Q, Quaternary surficial deposits. Topographic contour interval, 50 feet; gray lines, graded gravel roads of the Elk Horn Ranch subdivision. *B*, Highly irregular blocks of andesite laharic breccia, enclosed within flow-laminated rheomorphic rhyolite tuff. Although flow laminated, the rhyolite contains centimeter-size angular andesite fragments (hiking pole, ~0.9 meters). Roadcut along Tree Gulch Lane. Photograph by P.W. Lipman, U.S. Geological Survey, 2014.

Where contacts with adjacent caldera-floor andesite are well exposed, especially at the southern end of the main body, masses of andesite ranging in size from several meters across to centimeter-size chips are enclosed by fluidal rhyolite that is locally flow folded. In contrast to the weakly welded matrix tuff associated with most caldera-collapse breccias at Bonanza (fig. 193) and elsewhere (Lipman, 1976b), the texture of the rhyolite along Schoolhouse Gulch is strikingly lamellar adjacent to andesite clasts, even in thin-section scale; only in strain shadows adjacent to phenocrysts and to lithic fragments are local areas of shard texture preserved. The extreme welded and rheomorphic flowage of rhyolitic Bonanza Tuff along this basal contact with caldera-floor lavas is tentatively interpreted as related to thermally efficient emplacement followed by rapid deep burial beneath the thick intracaldera ignimbrite accumulation that is projected to have overlain it. An alternative interpretation of this unusual body as a large irregular ignimbrite vent fill seems less likely, because of the overall sheet-like geometry of the rhyolite.

Retrace the route to Kerber Creek, possibly stopping at Stops 6A-6 and 6A-5, which display features related to caldera subsidence and resurgence, as you head down valley (this sequence of stops progresses more logically toward greater interpretive complexity and uncertainty).

End of route 6A. Return to US 285 and continue north to Poncha Springs (21 mi), and then to Salida via US 50 (5 mi).

Additional Routes

Four additional routes provide access to the top of the intracaldera Bonanza Tuff and overlying caldera-filling lavas along Slaughterhouse Creek on the west flank of the resurgent dome (route 6B), to large resurgent granitoid intrusions on the east flank (route 6C), to the northeast flank of the Bonanza resurgent dome (route 6D), and to the margin of Marshall caldera (source of the 33.9-Ma Thorn Ranch Tuff) where it is truncated by the Bonanza subsidence (route 6E).

Route 6B—Top of the Intracaldera Bonanza Tuff and Overlying Caldera-Filling Lavas Along Slaughterhouse Creek

After the ignimbrite eruption and concurrent caldera subsidence, compositionally diverse lavas ranging from andesite to high-silica rhyolite filled the caldera to overflowing and spread across adjacent slopes. This side valley from Kerber Creek (figs. 167, 173) crosses obliquely through interfingering rhyolite and dacite zones in upper parts of the thick intracaldera Bonanza Tuff, which is overlain by as much as a kilometer of intermediate-composition and silicic caldera-filling lavas (fig. 196).

Take the Slaughterhouse Creek side road, from Kerber Creek (FS 861; see route 6A, mile 13.1; Bonanza quadrangle: 38°16.79' N., 106°8.79' W.). The upper part may require a high-clearance vehicle.

0.8 Dacitic Bonanza Tuff on the right; grades upward into rhyolitic tuff. Ahead 0.3 mi, rhyolitic Bonanza Tuff is exposed in a right-side roadcut. Another 0.2 mi, and back into dacitic tuff just beyond entry to Wagon Box Gulch. Gradational alternations of dacitic and rhyolitic tuff are well exposed along the ridge just above.

1.6 **Stop 6B-1. Basal caldera-fill lavas** (Bonanza quadrangle: 38°17.61' N., 106°9.89' W.; 9,531 ft, 2,905 m elevation)

Uppermost Bonanza rhyolite (poorly exposed at road level) is overlain by the basal postcaldera lava sequence, a dark biotite-hornblende andesite (Squirrel Gulch Andesite; here 59.8 percent SiO_2). The abundance of hydrous mafic minerals is distinctive. This andesite and other caldera-filling lavas are notably less propylitically altered than older lavas exposed on the caldera floor and inner walls, but they are tilted along with the underlying Bonanza Tuff on the west flank of the resurgent dome.

1.8 Low outcrops above the road are light-colored biotite dacite (no sanidine). Slaughterhouse Creek is just ahead. Ahead 0.2 mi up the grade, the road curves at the ridge crest (38°17.68' N., 106°9.89' W.) in mafic gray to reddish biotite dacite that transitions to plagioclase andesite, but is mapped as dacite because of light color and abundant biotite, despite low SiO_2 (60.2–61.4 percent) content. Ahead is a large area of hummocky landslide and slump material, which consists solely of similar sanidine-free dacite; it is distinguished from a morphologically similar moraine by the absence of andesite (and by the rough road!). Intermittently ahead, views to the east through the trees are of the profile of the Whale Hill resurgent dome (fig. 197).

3.2 Contact along the road, from slumped dacite into valley-filling moraine (38°18.23' N., 106°10.51' W.), that contains abundant boulders of green-gray propylitic andesite, derived from the caldera wall to the west.

3.7 **Stop 6B-2. Porphyry Peak Rhyolite, dacite, and andesite caldera-fill lavas** (Bonanza quadrangle: 38°18.63' N., 106°10.58' W.; 10,335 ft, 3,150 m elevation) Obscure small knob in the trees on the right side of the road.

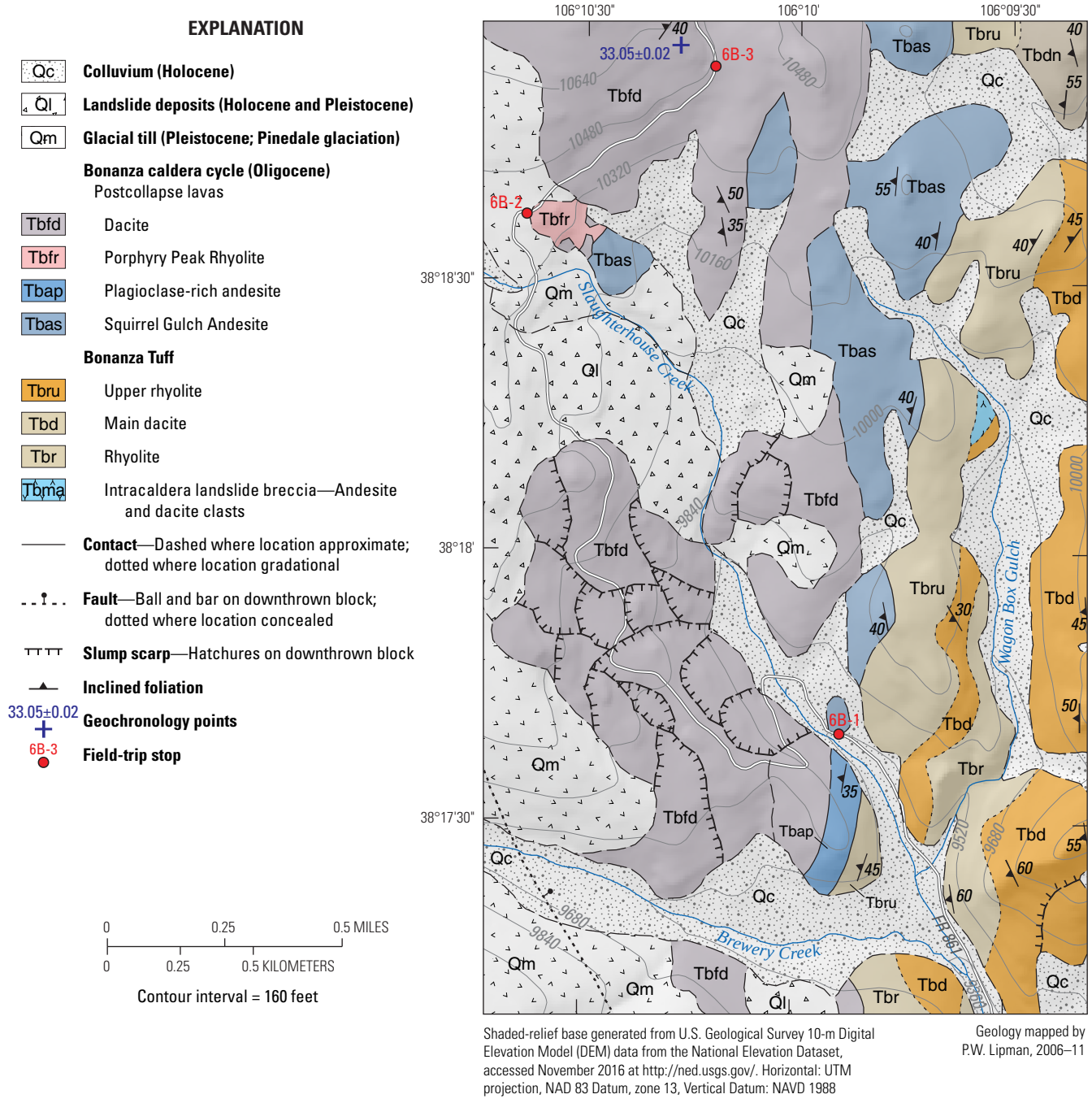

Shaded-relief base generated from U.S. Geological Survey 10-m Digital Elevation Model (DEM) data from the National Elevation Dataset, accessed November 2016 at http://ned.usgs.gov/. Horizontal: UTM projection, NAD 83 Datum, zone 13, Vertical Datum: NAVD 1988

Geology mapped by P.W. Lipman, 2006–11

Figure 196. Geologic map of Slaughterhouse Creek area, showing features viewed from Stops 6B-1 to 6B-3.

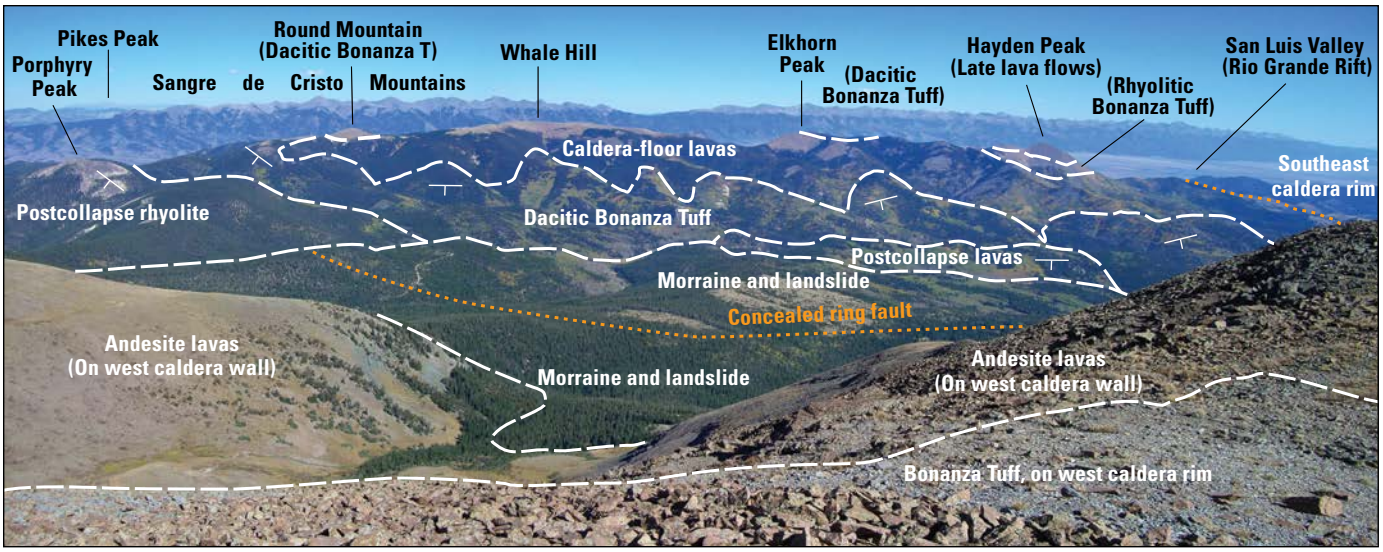

Figure 197. Crest of the Bonanza resurgent dome. View is to the east from the west caldera rim, across Whale Hill toward the San Luis Valley segment of the Rio Grande rift zone (compare with fig. 181). West-dipping intracaldera Bonanza Tuff, on the timbered slopes on the west flank of the dome, is a 2.5-kilometer (km)-thick sequence of interfingering dacite, rhyolite, and interleaved landslide breccia overlain by ~1 km of caldera-filling lavas (figs. 173, 175*A*). Photograph by P.W. Lipman, U.S. Geological Survey, 2014.

This small hill, now surrounded by moraine, was a residual paleohill of Porphyry Peak Rhyolite (table 16) against which small exposures of younger sanidine-bearing dacite lava (65.2–66.0 percent SiO_2) lap out on the downhill side. Underlying both the rhyolite and dacite down the ridge is Squirrel Gulch Andesite (table 16), offering a compact, accessible section of the compositionally variable caldera-fill lava sequence.

Ahead along road for the next 0.5 mi is float of the sanidine dacite. There are no outcrops but it is basically in place, and not glacial till because deposits lack andesite debris from the caldera wall.

4.3 **Stop 6B-3. Sanidine dacite, uppermost caldera-fill lavas** (Bonanza quad: 38°18.95' N., 106°10.18' W.; 10,531 ft, 3,210 m elevation). At cattle guard along Slaughterhouse Creek road.

Talus of tan to gray porphyritic dacite contains sparse small sanidine crystals (~15 percent plag>>bt,>san). On the crest of the nose just upslope (38°18.96' N., 106°10.27' W.), the dacite (table 16) has yielded a single-crystal sanidine date of 33.06±0.03 Ma, indistinguishably younger than the underlying rhyolite. Through the trees are distant views of the crest of the Whale Hill resurgent dome, and beyond that, the San Luis Valley segment of the Rio Grande Rift, bounded to the east by the down-to-west Sangre de Cristo range-front fault (fig. 196).

End of route 6B. Return to Bonanza back down Slaughterhouse Creek road or continue ahead to make a clockwise loop into upper Kerber Creek (rough 4-wheel road; no route log).

Route 6C—Peterson Creek to the Turquoise Mine and Spring Creek Resurgent Intrusions (Whale Hill Quadrangle)

High-clearance vehicle advised.

Resurgent intrusions of the Bonanza caldera are most widely exposed on the deeply eroded east flank of the domed caldera floor (fig. 168, 198). The Turquoise Mine intrusion is texturally and compositionally variable granodiorite-andesite, similar in composition and age to the small body of granodiorite in Rawley Gulch on the west flank of the resurgent dome at Stop 6A-9. The silicic Spring Creek intrusion is aplitic at the margins, porphyritic granite in the interior, and overlaps in composition and age with the caldera-filling lavas of Porphyry Peak Rhyolite.

From US 285 at 2.5 mi north of the Bonanza road junction at Villa Grove, take Peterson Creek road (FS 874, Saguache NN56) up the large dissected alluvial fan (may include some Cenozoic Dry Union [?] Formation).

3.0 Enter Rio Grande National Forest at 3.0 mi, passing by outcrops of Proterozoic granitic gneiss. Just after entering the National Forest, iron-stained rocks across the drainage to the north mark a large-displacement north-south fault, probably a Rio Grande rift structure, which drops pyritized and altered brown andesite and overlying light-gray rhyolite of the caldera-floor assemblage down to the west against yellowish Proterozoic granitic gneiss. Ahead along the road, volcanic rocks are intensely altered in proximity to the Turquoise Mine intrusion.

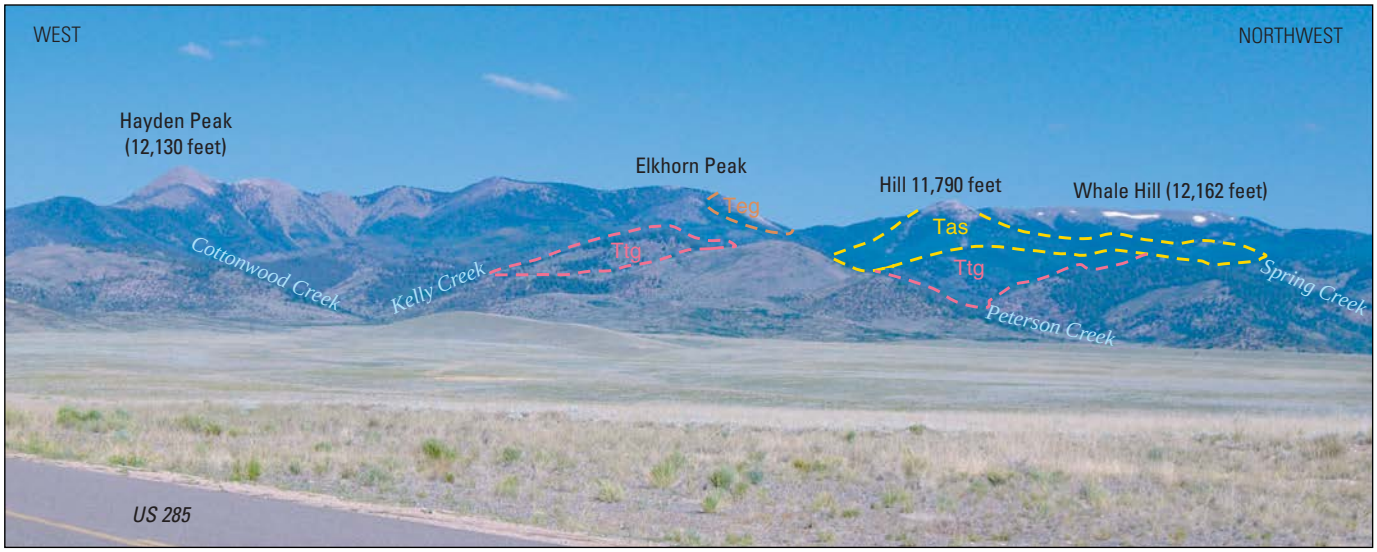

Figure 198. Intrusions on the east flank of the Bonanza resurgent dome. Panorama of the resurgently uplifted caldera floor from US 285. Valleys on the east flank of the Bonanza resurgent dome have eroded down into several compositionally diverse intrusions that are exposed at near-roof levels. These include the granodiorite to intrusive andesite of the Turquoise Mine pluton (Ttg) and aplitic and porphyritic granite of the Spring Creek intrusion (Tas). A sill-like body of Eagle Gulch Dacite (Teg) is exposed at its northeast termination on the north slope of Elkhorn Peak. The compositional range of these intrusions is comparable to that of the postcollapse andesite to rhyolite lavas of the Bonanza cycle. Wall rocks for the intrusions are precaldera andesite and dacite lavas of the Rawley volcanic complex, which form the floor of Bonanza caldera. The nearly flat crests of Whale Hill and Elkhorn Peak are close to the surface on which intracaldera Bonanza Tuff accumulated. The outward dipping slopes viewed from this vantage approximate tilts on flanks of the resurgent dome. Hayden Peak is underlain by a thick sequence of postcollapse dacitic lavas, probably filling a paleovalley. Photograph by P.W. Lipman, U.S. Geological Survey, 2012.

Continue to the junction on the left (southwest), with a side road that leads to a clearing and informal camp area, just before the access road to the Villa Grove Turquoise Mine (inactive).

4.7 **Stop 6C-1. Turquoise Mine intrusion** (Whale Hill quadrangle: 38°17.63' N., 106°3.18' W.; 9,311 ft, 2,838 m elevation). From the upper campsite, hike southwest up an informal but obvious trail to outcrops of intermediate-composition resurgent Turquoise Mine intrusion along the ridge crest (fig. 199).

Approaching the ridge, a prominent outcrop to the southeast (38°17.63' N., 106°3.71' W.; 9,970 ft, 3,039 m elevation) is a fine-grained andesitic facies of the Turquoise Mine intrusion (fig. 200*A*; table 16, 54.1 percent SiO_2; whole-rock age of 33.06±0.21 Ma). Along the ridge are typically varied textural and compositional facies of the intrusion (fig. 200*B*, *C*). At the crest of the 10,056 ft, hill (3,065 m elevation), fine-grain granodiorite (62.4 percent SiO_2) is veined by a more aplitic facies (table 16, 67.0 percent SiO_2). The compositional variability within the Turquoise Mine intrusion brackets the range for andesite-dacite postcollapse lavas of the caldera fill.

From this stop it is possible (*4-wheel drive only*) to proceed up Peterson Creek across a saddle into Spring Creek (FS 875), passing through additional texturally diverse exposures of the Turquoise Mine intrusion and then into aplitic granite of the Spring Creek intrusion (fig. 199; table 16, 74.4–76.7 percent SiO_2; potassium feldspar age 33.26±0.07 Ma). Then rejoin US 285 by continuing down Spring Creek. The Spring Creek intrusion is similar in age and composition to the caldera-filling lavas of the Porphyry Peak Rhyolite (Stop 6B-2).

End of route 6C.

Route 6D—Alder Creek Road to the Near-Vertical Northeast Flank of the Bonanza Resurgent Dome (Whale Hill Quadrangle).

High-clearance vehicle advised.

Bonanza caldera has an exceptionally large and steep-sided resurgent dome, perhaps uniquely eroded to levels that exhume intermediate-composition lavas of the caldera floor over large areas. Typical dips are 50–60° W. on the west side (fig. 173) and as much as 70–90° NE. on the northeast flank (fig. 201). Alder Creek road (fig.167, route D) provides access to outcrops of diverse rock types with near-vertical dips that exemplify the extraordinarily steeply dipping northeast flank of the Bonanza resurgence; however, the exposures are discontinuous, on timbered slopes, and considerable hiking is required to evaluate the proposed stratigraphic and structural correlations in any detail.

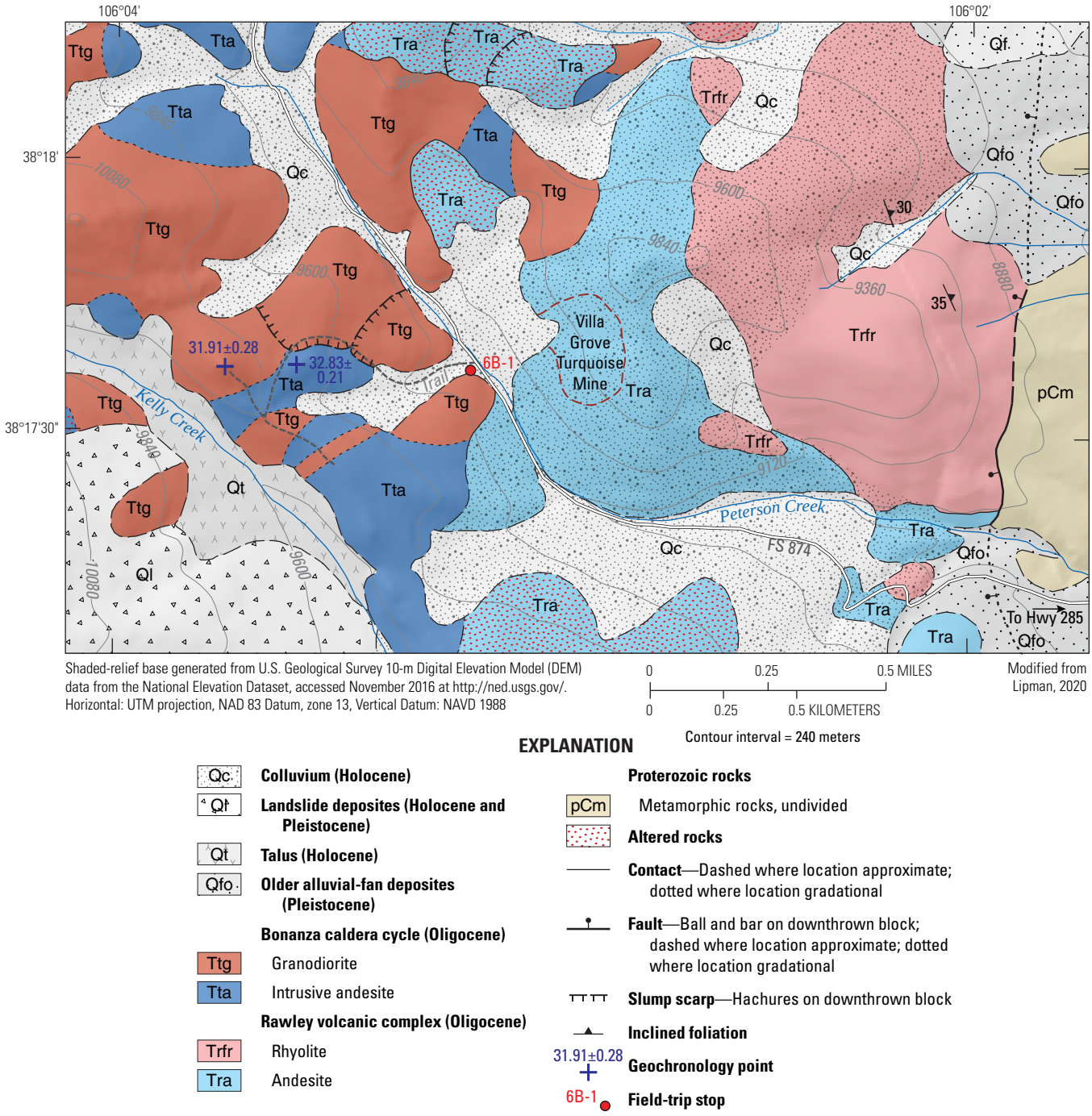

Figure 199. Geologic map of part of the Turquoise Mine intrusion (~33.0 million years old?). Texturally variable light-gray granodiorite and darker intrusive andesite form a composite intrusion about 3 × 7 kilometers across, extending from the head of Peterson Creek, across several drainages to the southwest, at least as far as the southeast ridge of Hayden Peak.

As an additional complexity, consistent westward dips of volcanic strata all the way to a north-trending monoclinal hinge 10 km west of Bonanza caldera (fig. 168) suggest that the opening of the Rio Grande rift zone has tilted the overall Bonanza block 10–15° westward, in continuity with the Sawatch Range (fig. 90). In this case, parts of the northeast flank could have originally been overturned. As a possible alternative, could broad resurgence, above batholithic intrusions more widespread than the caldera, have been responsible for the monoclinal tilting and uplift in the large area to the west?

From U.S. 285, 4.0 mi south of Poncha Pass just south of milepost 115 (or 7.4 mi north of the turnoff to route 6C), turn left onto Alder Creek road (FS 890, Saguache County road UU52).

1.4 **Stop 6D-1. Steeply dipping Bonanza Tuff and interlayered andesitic megabreccia** (38°22.85' N., 106°5.07' W.; 9,039 ft, 2,755 m elevation). Just past the Rio Grande National Forest boundary, limited parking is possible next to a gated fence. Alternatively, larger parking areas are available at informal campsites along the creek, below the road.

Figure 200. Textural and compositional variations within the Turquoise Mine intrusion. *A*, Intrusive andesite phases (Tta; fig. 199) are relatively unaltered dense dark-gray rocks that form prominent outcrops, characterized by closely spaced rectilinear joints. In places, the andesite is in sharp contact with granodiorite; elsewhere, contacts appear to be gradational. $^{40}Ar/^{39}Ar$ ages (whole-rock) of 33.06±0.21 Ma (plateau) and 32.83±0.21 Ma (isochron) at this site, on the ridge between Peterson and Kelly Creeks (38°17.62′ N., 106°03.52′ W.). *B*, The medium-grain granodiorite that forms much of the intrusion varies from equigranular to finely porphyritic (62.4 percent SiO_2), and consists mainly of plagioclase, biotite, chloritized pyroxene, and small interstices of quartz and alkali feldspar. From the ridge between Peterson and Kelly Creeks, hill 10,056 feet (ft) (38°17.63′ N., 106°03.71′ W.). *C*, Aplitic granodiorite (67.0 percent SiO_2) is a relatively minor phase, forming irregular pods as much as a few meters across within dominant volumes of the coarser granodiorite (Ttg; fig. 199). Sample from the ridge between Peterson and Kelly Creeks, hill 10,056 ft (38°17.63′ N., 106°03.71′ W.). Photographs by P.W. Lipman, U.S. Geological Survey, 2015.

From this point and extending back to the east of the U.S. Forest Service boundary, the timbered slope, from just above road level to the ridge crest, contains scattered prominent outcrops displaying diverse lithologies of densely welded dacitic and rheomorphic rhyolitic Bonanza Tuff interleaved with ribs of andesite interpreted as landslide megabreccia (fig. 201). Fiamme in the dacite (where discernable through propylitic alteration and lichen cover), flowage structures in the rhyolite, and alignment of outcrops all define near-vertical fabric and structure on this flank of the uplifted core of the Bonanza caldera. Exposures are even better on less accessible ridges southeast of Alder Creek, especially across the 9,812 ft hill (2,990 m). In this area,

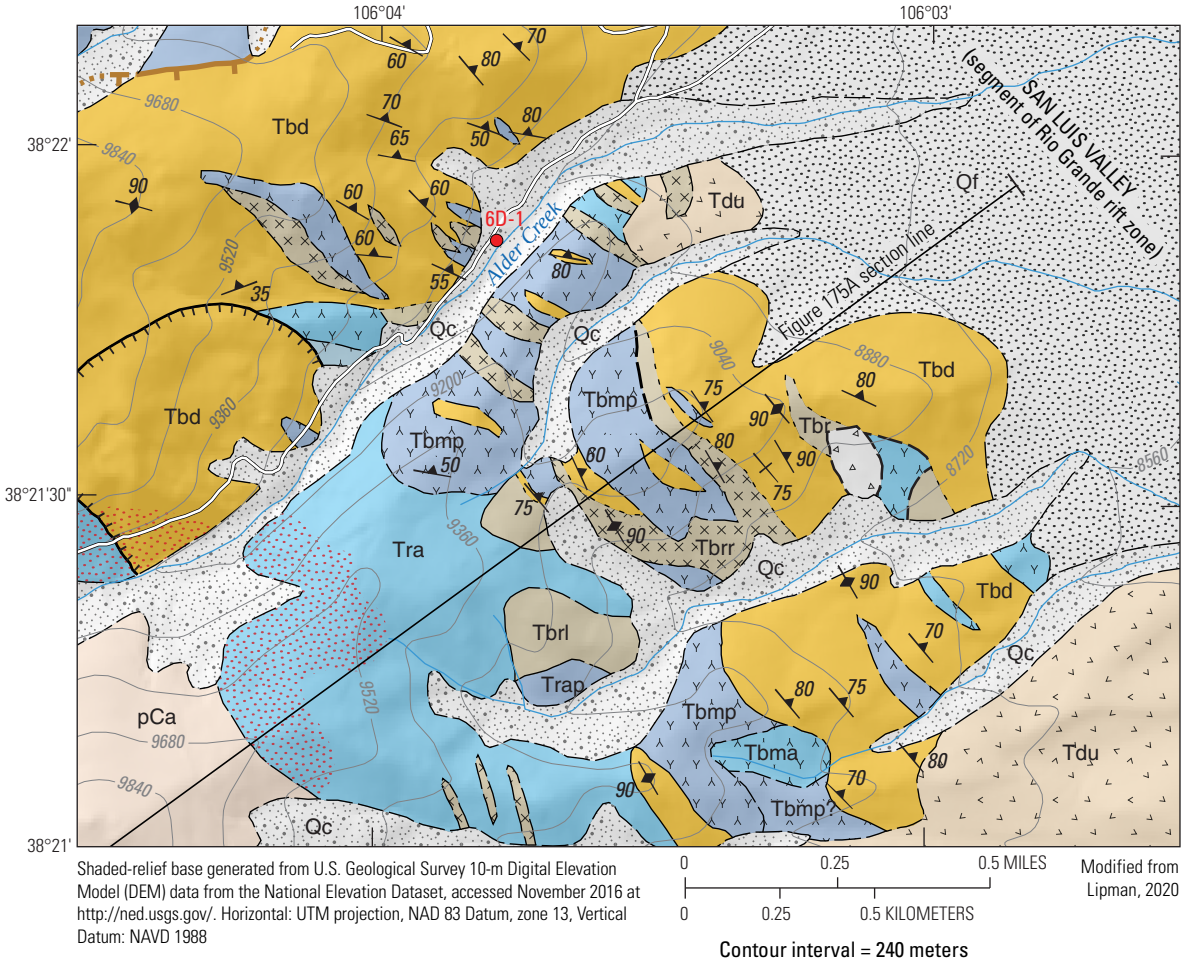

EXPLANATION

- Qf **Alluvium-fan deposits (Holocene)**
- Qc **Colluvium (Holocene)**
- Ql **Landslide deposits (Holocene and Pleistocene)**

RIO GRANDE RIFT FILL

- Dry Union Formation (Miocene)

BONANZA CALDERA CYCLE (OLIGOCENE)

Bonanza Tuff

- Main dacite
- Lower rhyolite
- Lower rhyolite, rheomorphic

Intracaldera landslide breccia

- Tbmu Mixed clasts or undivided
- Tbma Andesite and dacite clasts
- Tbmp Plagioclase-andesite clasts
- Tbmc Proterozoic clasts

RAWLEY VOLCANIC COMPLEX (OLIGOCENE)

- Andesite

PROTEROZOIC ROCKS

- Aplite of Alder Creek
- **Altered rock**
- **Bonanza caldera rim**—Hatchures on downthrown block; dotted where location concealed
- **Contact**—Dashed where location approximate; dotted where location gradational
- **Fault**—Dashed where location approximate
- **Slump scarp**—Hachures on downthrown block
- **Vertical bedding**
- **Inclined foliation**
- **Vertical foliation**
- 6D-1 **Field-trip stop**

Figure 201. Geologic map of the northeast flank of the steep-sided resurgent dome of Bonanza caldera (Alder Creek area; fig. 167). The caldera-filling ignimbrite (Bonanza Tuff) and interleaved landslide breccias consistently dip 60–80° to the northeast, and the exposed partial section of the ignimbrite (no top preserved) is as much as 1.8-kilometers thick. The location of the map is shown by the rectangle on figure 168. The red-dashed line indicates the position of eastern part of the Line-1 cross section (fig. 175*A*).

large masses of coarsely porphyritic plagioclase andesite interfinger in near-vertical contacts with eutaxitic dacite (fig. 202) and more fluidal rhyolite; both locally become less welded in proximity to the andesite.

Return to US 285 and continue north 1 mi, park on the right shoulder just beyond milepost 116, near a small lake.

3.8 **Stop 6D-2. View of Round Hill** (38°23.48 N., 106°3.35' W.; 8,724 ft, 2,659 m elevation), in the middle of the northern San Luis Valley. On this prominent knob (fig. 203), the westward-dipping contact between dacite lava and Proterozoic metamorphic rocks to the east, is interpreted as marking an isolated exposure of the depositional unconformity along the northeastern margin of Bonanza caldera. The contact appears too gentle and arcuate to permit alternative interpretation as a fault. The dacite of Round Hill contains sparse sanidine, unlike dacite lavas of the Conejos Formation to the northwest, and has yielded an $^{40}Ar/^{39}Ar$ age of 33.024±0.012 Ma. This age is distinctly younger than the weighted mean age of outflow Bonanza Tuff (33.12±0.03 Ma) but indistinguishable from ages from several of the lower postcaldera lavas on the west flank of the resurgent dome within Bonanza caldera (33.03 Ma, table 15).

Figure 202. Schistose-like fabric in rhyolitic Bonanza Tuff defines a steeply east-dipping foliation. View north, along the western slope of hill 9,812 feet (2,990 meters), south of Alder Creek. Photograph by P.W. Lipman, U.S. Geological Survey, 2012.

Figure 203. View of Round Hill (9,171 feet, 2,795 meters), showing the contact between dacite lava and Proterozoic metamorphic rocks that is interpreted as an unconformity along the northeastern margin of Bonanza caldera. The dacite of Round Hill contains sparse sanidine, unlike dacite lavas of the Conejos Formation to the northwest and has yielded an $^{40}Ar/^{39}Ar$ age of 33.024±0.012 million years ago (Ma). This age is analytically distinct from the weighted mean age of outflow Bonanza Tuff (33.12±0.03 Ma) but indistinguishable from ages from several of the lower postcaldera lavas on the west flank of the resurgent dome within Bonanza caldera (33.03±0.02 Ma). The dip of the contact between the dacite and Proterozoic rocks (~20–25° to the west) appears too gentle for a rift-related fault, especially if adjusted for regional westward tilt of rocks to the northwest, near Poncha Pass. Float of botryoidal travertine along the contact is interpreted as a fossil hot-spring deposit, concentrated along the caldera-wall contact between dacite and Proterozoic rocks. View to northeast from US 285. Photograph by P.W. Lipman, U.S. Geological Survey, 2012.

The field and age relations at Round Hill, along with a small exposure 2 km farther east, where Bonanza Tuff depositionally laps out against Proterozoic rocks, are interpreted to partly define the largely buried eastern margin of Bonanza caldera.

End of route 6D. Continue across Poncha Pass to Mears Junction, for route 6E.

Route 6E—Poncha and Silver Creek Roads to the Margin of Marshall Caldera at The Gate (Mount Ouray and Bonanza Quadrangles)

Marshall caldera is the source of the oldest regional ignimbrite erupted from within the San Juan Mountains, the 33.9-Ma Thorn Ranch Tuff (table 14). This tuff and source caldera were the last major explosive eruptions prior to Bonanza, but Marshall was filled to overflow and still largely concealed by postcollapse lava eruptions. Much of this caldera was further concealed by subsequent subsidence at Bonanza caldera. Intracaldera Thorn Ranch Tuff is exposed only along the northeastern margin of Marshall caldera, but the geographic feature known as The Gate in upper Silver Creek (fig. 167, Stop 6E-1) provides one of the most spectacularly exposed caldera walls anywhere in the SRMVF. Adjacent to these exposures, the fill of Marshall caldera is truncated by the northwestern margin of Bonanza caldera.

From US 285 at Mears Junction, proceed 2.3 mi down the north side of Poncha Pass, then take Marshall Pass road (Chafee County road 200).

2.4 Junction with Silver Creek at Shirley townsite. The large above-treeline peak upvalley is Sheep Mountain (12,228 ft, 3,727 m elevation), a huge postcollapse dacite lava dome that overlies thick Thorn Ranch Tuff within the Marshall caldera. Andesite lavas exposed along the road to Shirley are probably older than the Thorn Ranch Tuff. Marshall Pass road closely follows the grade of a former narrow-gage rail line from Salida to Gunnison. In the early- to middle-20th century, an aerial tram carried ore 12 km from the Rawley mine at Bonanza to Shirley, where it was transported to a smelter by the narrow-gage railway.

6.0 *Proceed up Silver Creek (road 201), past the Silver Creek Lakes and vacation homes at 4.0 mi from US 285 (after which high-clearance vehicles are needed), and continue about 2 mi farther to the Silver Creek trailhead* (fig. 204), at the point where the historic Otto Mears Toll road climbs out of valley.

The geology along Silver Creek road is complex, because the present drainage closely coincides with a paleovalley that was recurrently filled and erosionally excavated during Oligocene volcanism. Most road-level outcrops along Silver Creek Lakes and up-valley are sanidine-bearing dacite and crystal-poor rhyolite that are similar in composition and age to postcollapse lava fill of Bonanza caldera. A small remnant exposure of vitrophyric Bonanza Tuff, surrounded by andesitic landslide debris, is exposed at creek level just downstream of the outlet from the lakes.

12.0 **Stop 6E-1. Silver Creek trail to The Gate** (38°21.81' N., 106°10.58' W; 9,534 ft, 2,906 m elevation). *Walk up Silver Creek trail about 0.3 mi*, passing a spectacularly exposed contact between Proterozoic granitic gneiss and intracaldera Thorn Ranch Tuff on the west side of the prominent rib that forms The Gate (fig. 205). The rugged cliffs of Thorn Ranch Tuff are >300-m thick here, with no base exposed. The tuff contains abundant small fragments of diverse volcanic and Proterozoic rocks but no coarse megabreccia, in contrast to isolated exposures west of Marshall Pass (Olson, 1983; Gregory and McIntosh, 1996). As with many other ignimbrites in the SRMVF, intracaldera Thorn Ranch Tuff is more mafic and compositionally diverse (66.2–73.4 percent SiO_2) than its outflow sheet of silicic rhyolite (74.8–76.9 percent SiO_2).

Across Silver Creek to the south (and at the trail level ahead), the lava dome of caldera-filling dacite that overlies intracaldera Thorn Ranch Tuff is >675-m thick on Sheep Mountain, with its top eroded. An $^{40}Ar/^{39}Ar$ age of 33.89±0.07 Ma on this enormous body of dacite is indistinguishable from that of the underlying caldera-forming Thorn Ranch Tuff.

End of route 6E. If desired, you can return from the Shirley townsite to Gunnison by way of the old railway grade across Marshall Pass, which marks the north wall of the Marshall caldera.

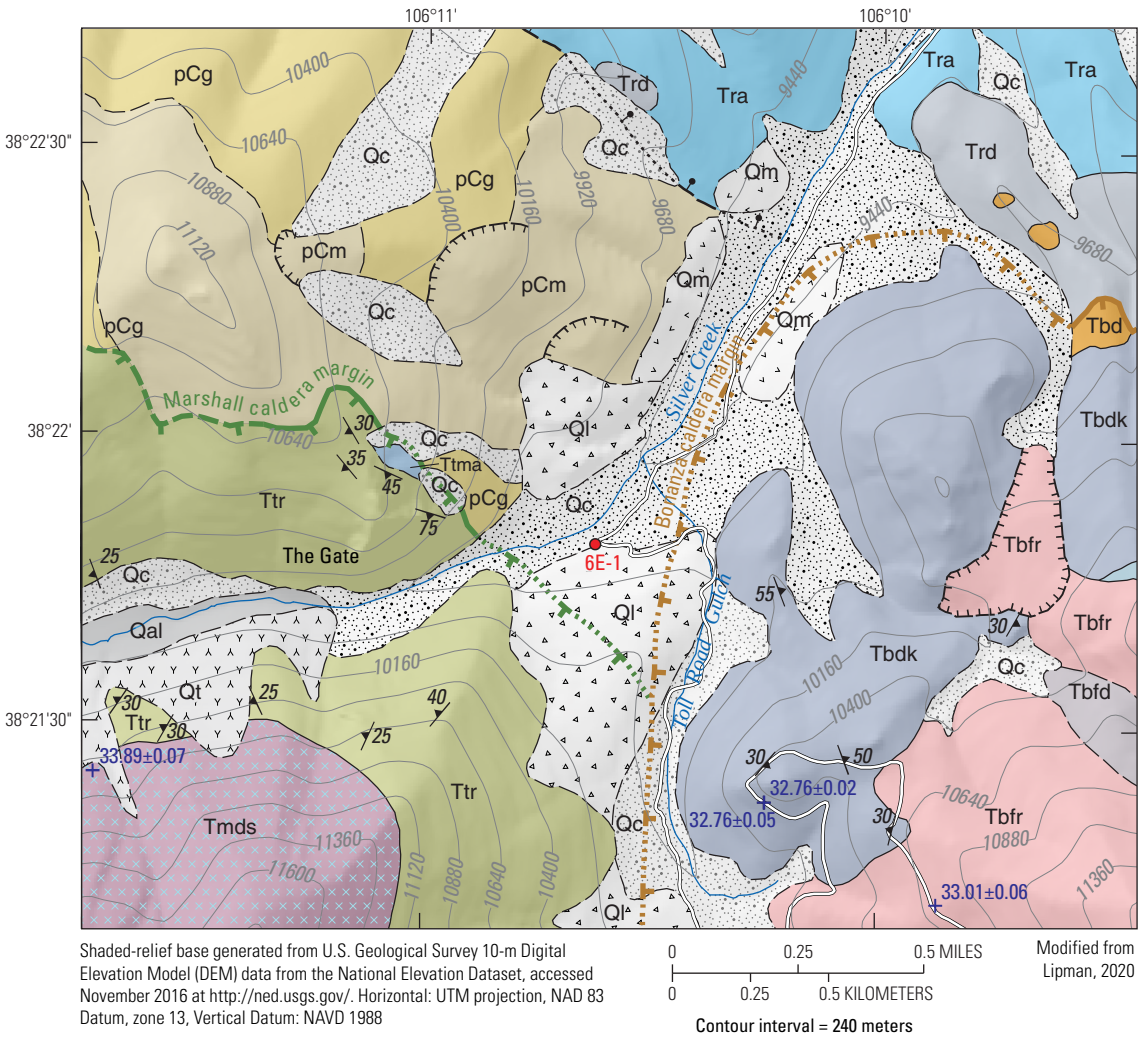

EXPLANATION

- Qal — **Alluvium (Holocene)**
- Qc — **Colluvium (Holocene)**
- Ql — **Landslide deposits (Holocene and Pleistocene)**
- Qt — **Talus (Holocene)**
- Qm — **Glacial till (Pleistocene; Pinedale glaciation)**

Bonanza caldera cycle (Oligocene)

- Tbdk — Potassium-feldspar dacite
- Tbfd — Dacite lava flows
- Tbfr — Porphyry Peak Rhyolite
- Tba — Andesite flows, sparsely porphyritic
- Tbd — Bonanza Tuff, main dacite

Rawley volcanic complex (Oligocene)

- Trd — Dacite
- Tra — Andesite

Marshall volcanic complex (Oligocene)

- Tmds — Sheep Mountain Dacite
- Ttr — Thorn Ranch Tuff
- Ttma — Megabreccia, andesite clasts dominant

Proterozoic rocks

- pCg — Granitoid intrusive rocks, undivided
- pCm — Metamorphic rocks, undivided

- **Contact**—Dashed where location approximate
- **Normal fault**—Ball and bar on downthrown block; dashed where location approximate; dotted where location concealed
- **Scarp**—Hachures on downthrown block
- **Bonanza caldera**—Dotted where location concealed
- **Marshall caldera**—Dashed where location approximate; dotted where location concealed
- **Inclined foliation**
- 33.01±0.06 **Geochronology point**
- 6E-1 **Field-trip stop**

Figure 204. Geologic map of the northeast boundary of Marshall caldera (Stop 6E-1), where it is truncated by the northwestern margin of Bonanza caldera.

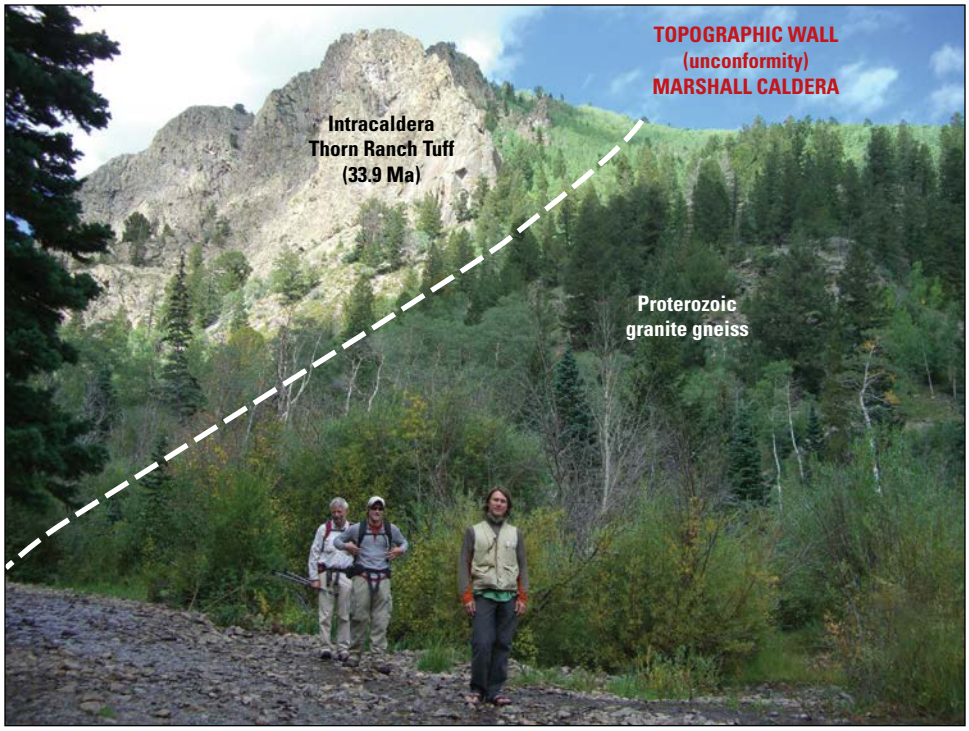

Figure 205. Topographic wall of Marshall caldera at The Gate. Densely welded Thorn Ranch Tuff, more than 300-meters thick with no base exposed, is depositionally banked against Proterozoic granite gneiss at this prominent topographic feature in upper Silver Creek. Photograph by P.W. Lipman, U.S. Geological Survey, 2014.

Acknowledgments

Special thanks go to Andrea Sibisa (University of Trieste, Italy), who provided outstanding mapping assistance during many long and difficult field days in the summers of 2009–11. We also thank K.J. Turner (U.S. Geological Survey [USGS]) for assistance in preparing publishable geologic -map figures and other illustrations, Christine Chan (USGS) for perceptive text editing, and Amy Gilmer (USGS) and Joe Colgan (USGS) for helpful technical reviews of this field guide segment. In addition to collaboration with numerous other geologists, as noted or referenced in this report, we also thank many friends in the northeastern San Juan region who provided diverse hospitality, logistical support, help with back-country and property access, and other assistance during work in the area. For the Bonanza studies, these especially include Pip and Aaron Conrad of the Rafiki Ranch near Villa Grove, who have created a virtual Rafiki Geologic Research Station and hosted many visiting earth scientists.

References

Aby, S., Karlstrom, K., Koning, D., and Kempter, K., 2010, Preliminary geologic map of the Las Tablas quadrangle, Rio Arriba County, New Mexico: New Mexico Bureau of Geology and Mineral Resources Open-File Geologic Map 200, scale 1:24,000.

Alcorn, R., Panter, K.S., and Gorsevski, P.V., 2013, A GIS-based volcanic hazard and risk assessment of eruptions sourced within Valles caldera, New Mexico: Journal of Volcanology and Geothermal Research, v. 267, p. 1–14, https://doi.org/10.1016/j.jvolgeores.2013.09.005.

Aldrich, M.J., Jr., 1986, Tectonics of the Jemez lineament in the Jemez Mountains and Rio Grande Rift: Journal of Geophysical Research, v. 91, B2, p. 1753–1762, https://doi.org/10.1029/JB091iB02p01753.

Aldrich, M.J., Jr., Chapin, C.E., and Laughlin, A.W., 1986, Stress history and tectonic development of the Rio Grande rift, New Mexico: Journal of Geophysical Research, v. 91, B6, p. 6199–6211, https://doi.org/10.1029/JB091iB06p06199.

Appelt, R.M., 1998, $^{40}Ar/^{39}Ar$ geochronology and volcanic evolution of the Taos Plateau volcanic field, northern New Mexico and southern Colorado: Socorro, New Mexico Institute of Mining and Technology, M.S. thesis, 149 p.

Aprea, C.M., Hildebrand, S., Fehler, M., Steck, L., Baldridge, W.S., Roberts, P., Thurber, C.H., and Lutter, W.J., 2002, Three-dimensional Kirchhoff migration—Imaging of the Jemez Mountains volcanic field using teleseismic data: Journal of Geophysical Research, v. 107, no. B10, 15 p.

Aramaki, S., and Ui, T., 1966, The aira and ata pyroclastic flows and related caldera depressions in southern Kyushu, Japan: Bulletin of Volcanology, v. 29, no. 1, p. 29–47, https://doi.org/10.1007/BF02597139.

Armstrong, C., Dutrow, B.L., Henry, D.J., and Thompson, R.A., 2013, Provenance of volcanic clasts from the Santa Fe Group, Culebra graben of the San Luis Basin, Colorado—A guide to tectonic evolution, in Hudson, M.R., and Grauch, V.J.S., eds., New perspectives on Rio Grande rift basins—From tectonics to groundwater: Geological Society of America Special Paper 494, p. 21–45, https://doi.org/10.1130/2013.2494(02).

Askren, D.R.R., Whitney, J.A., and Roden, M.F., 1991, Petrology and geochemistry of the Huerto Andesite, San Juan volcanic field, Colorado: Contributions to Mineralogy and Petrology, v. 107, no. 3, p. 373–386, https://doi.org/10.1007/BF00325105.

Atwood, W.W., and Mather, K.F., 1932, Physiography and Quaternary geology of the San Juan Mountains, Colorado: U.S. Geological Survey Professional Paper 166, 212 p., https://doi.org/10.3133/pp166.

Aubele, J.C., 1978, Geology of the Cerros del Rio volcanic field, Santa Fe, Sandoval, and Los Alamos Counties, New Mexico: Albuquerque, University of New Mexico, M.S. thesis, 136 p.

Bachmann, O., and Bergantz, G.W., 2003, Rejuvenation of the Fish Canyon magma body—A window into the evolution of large-volume silicic magma systems: Geology, v. 31, no. 9, p. 789–792, https://doi.org/10.1130/G19764.1.

Bachmann, O., and Bergantz, G.W., 2006, Gas percolation in upper-crustal silicic crystal mushes as a mechanism for upward heat advection and rejuvenation of near-solidus magma bodies: Journal of Volcanology and Geothermal Research, v. 149, no. 1–2, p. 85–102, https://doi.org/10.1016/j.jvolgeores.2005.06.002.

Bachmann, O., Deering, C.D., Lipman, P.W., and Plummer, C., 2014, Building zoned ignimbrites and recycling silicic cumulates—Insight from the 1,000 km^3 Carpenter Ridge Tuff, CO: Contributions to Mineralogy and Petrology, v. 167, no. 6, p. 1–13, https://doi.org/10.1007/s00410-014-1025-3.

Bachmann, O., and Dungan, M.A., 2002, Temperature-induced Al-zoning in hornblendes of the Fish Canyon magma, Colorado: The American Mineralogist, v. 87, no. 8–9, p. 1062–1076, https://doi.org/10.2138/am-2002-8-903.

Bachmann, O., Dungan, M.A., and Lipman, P.W., 2000, Voluminous lava-like precursor to a major ash-flow tuff—Low-column pyroclastic eruption of the Pagosa Peak Dacite, San Juan volcanic field, Colorado: Journal of Volcanology and Geothermal Research, v. 98, no. 1–4, p. 153–171, https://doi.org/10.1016/S0377-0273(99)00185-7.

Bachmann, O., Dungan, M.A., and Lipman, P.W., 2002, The Fish Canyon magma body, San Juan volcanic field, Colorado—Rejuvenation and eruption of an upper-crustal batholith: Journal of Petrology, v. 43, no. 8, p. 1469–1503, https://doi.org/10.1093/petrology/43.8.1469.

Bachmann, O., Miller, C.F., and de Silva, S.L., 2007a, The volcanic-plutonic connection as a stage for understanding crustal magmatism: Journal of Volcanology and Geothermal Research, v. 167, no. 1–4, p. 1–23, https://doi.org/10.1016/j.jvolgeores.2007.08.002.

Bachmann, O., Oberli, F., Dungan, M.A., Meier, M., Mundil, R., and Fischer, H., 2007b, $^{40}Ar/^{39}Ar$ and U-Pb dating of the Fish Canyon magmatic system, San Juan volcanic field, Colorado—Evidence of an extended crystallization history: Chemical Geology, v. 236, no. 1–2, p. 134–166, https://doi.org/10.1016/j.chemgeo.2006.09.005.

Bacon, C.R., 1983, Eruptive history of Mount Mazama and Crater Lake Caldera, Cascade Range, U.S.A: Journal of Volcanology and Geothermal Research, v. 18, no. 1–4, p. 57–115, https://doi.org/10.1016/0377-0273(83)90004-5.

Bacon, C.R., 2008, Geologic map of Mount Mazama and Crater Lake Caldera, Oregon: U.S. Geological Survey Scientific Investigations Map 2832, scale 1:24,000.

Bailey, R.A., Dalrymple, G.B., and Lanphere, M.A., 1976, Volcanism, structure, and geochronology of Long Valley caldera, Mono County, California: Journal of Geophysical Research, v. 81, no. 5, p. 725–744, https://doi.org/10.1029/JB081i005p00725.

Bailey, R.A., Smith, R.L., and Ross, C.S., 1969, Stratigraphic nomenclature of volcanic rocks in the Jemez Mountains, New Mexico: U.S. Geological Survey Bulletin 1274-P, 19 p.

Baldridge, W.S., Keller, G.R., Haak, V., Wendlandt, E., Jiracek, G.R., and Olsen, K.H., 1995, The Rio Grande rift, *in* Olsen, K.H., ed., Continental rifts—Evolution, structure, and tectonics: Amsterdam, Elsevier Publishing, p. 233–275.

Baldridge, W.S., Olsen, K.H., and Callender, J.F., 1984, Rio Grande rift—Problems and perspectives, *in* Baldridge, W.S., Dickerson, P.W., Riecker, R.E., and Zidek, J., eds., Rio Grande rift—Northern New Mexico: New Mexico Geological Society, 35th Fall Field Conference Guidebook, p. 1–12.

Balsley, S.D., 1988, The petrology and geochemistry of the Tshirege Member of the Bandelier Tuff, Jemez Mountains volcanic field, New Mexico, U.S.A: University of Texas at Arlington, M.S. thesis, 188 p.

Balsley, S.D., 1994, A combined stratigraphic, chronologic, and petrologic study of an Oligocene post-collapse pyroclastic sequence, southeastern San Juan Mountains, Colorado—The middle tuff member of the Treasure Mountain Tuff: Dallas, Southern Methodist University, Ph.D. dissertation, 197 p.

Balsley, S.D., and Gregory, R.T., 1998, Low-^{18}O silicic magmas—Why are they so rare?: Earth and Planetary Science Letters, v. 162, no. 1–4, p. 123–136, https://doi.org/10.1016/S0012-821X(98)00161-7.

Barton, P.B., Rye, R.O., and Bethke, P.B., 2000, Evolution of the Creede caldera and its relation to mineralization in the Creede mining district, Colorado, *in* Bethke, P.M., and Hay, R.L., eds., Ancient Lake Creede—Its volcano-tectonic setting, history of sedimentation, and relation to mineralization in the Creede mining district: Geological Society of America Special Paper 346, p. 301–326, https://doi.org/10.1130/0-8137-2346-9.301.

Bauer, P.W., Grauch, V.J.S., Johnson, P.S., Thompson, R.A., Drenth, B.J., and Kelson, K.I., 2015, Geologic cross sections and preliminary geologic map of the Questa area, Taos county, New Mexico: New Mexico Bureau of Geology and Mineral Resources Open-File Report 578, 15 p., 4 pls.

Bauer, P.W., Helper, M.A., and Aby, S., 2005, Geologic map of the Trampas quadrangle, Rio Arriba, Taos Counties, New Mexico: New Mexico Bureau of Geology and Mineral Resources Open-File Digital Geologic Map 104, scale 1:24,000.

Bauer, P.W., and Kelson, K.I., 1998, Preliminary geologic map of the Taos SW quadrangle, Taos County, New Mexico: New Mexico Bureau of Mines and Mineral Resources Open-File Geologic Map 12, scale 1:24,000.

Bauer, P.W., and Kelson, K.I., 2004a, Cenozoic structural development of the Taos area, New Mexico, *in* Brister, B.S., Bauer, P.W., Read, A.S., and Lueth, V.W., eds., Geology of the Taos region: New Mexico Geological Society, 55th Fall Field Conference Guidebook, p. 129–146.

Bauer, P.W., and Kelson, K.I., 2004b, Rift extension and fault slip rates in the southern San Luis Basin, New Mexico, *in* Brister, B.S., Bauer, P.W., Read, A.S., and Lueth, V.W., eds., Geology of the Taos region: New Mexico Geological Society, 55th Fall Field Conference Guidebook, p. 172–180.

Bauer, P.W., Read, A.S., Kelson, K.I., Muehlberger, W.R., and Koning, D.J., 2004, The flanks of the rift—Second-day road log from Taos to Taos Pueblo, Llano Quemado, Pilar, and return to Taos, *in* Brister, B.S., Bauer, P.W., Read, A.S., and Lueth, V.W., eds., Geology of the Taos region: New Mexico Geological Society 55th Annual Fall Field Conference Guidebook, p. 37–74.

Bauer, P.W., and Williams, M.L., 1989, Stratigraphic nomenclature of Proterozoic rocks, northern New Mexico—Revisions, redefinitions, and formalization: New Mexico Geology, v. 11, no. 3, p. 45–52.

Best, M.G., and Christiansen, E.H., 1997, Origin of broken phenocrysts in ash-flow tuffs: Geological Society of America Bulletin, v. 109, no. 1, p. 63–73, https://doi.org/10.1130/0016-7606(1997)109<0063:OOBPIA>2.3.CO;2.

Best, M.G., Christiansen, E.H., and Blank, R.H., Jr., 1989, Oligocene caldera complex and calc-alkaline tuffs and lavas of the Indian Peak volcanic field, Nevada and Utah: Geological Society of America Bulletin, v. 101, no. 8, p. 1076–1090, https://doi.org/10.1130/0016-7606(1989)101<1076:OCCACA>2.3.CO;2.

Best, M.G., Christiansen, E.H., Deino, A.L., Gromme, S., Hart, L.G., and Tingey, D.G., 2013, The 36–18 Ma Indian Peak–Caliente ignimbrite field and calderas, southeastern Great Basin, USA—Multicyclic super-eruptions: Geosphere, v. 9, no. 4, p. 864–950, https://doi.org/10.1130/GES00902.1.

Best, M.G., Christiansen, E.H., de Silva, S., and Lipman, P.W., 2016, Slab-rollback ignimbrite flareups in the southern Great Basin and other Cenozoic American arcs—A distinct style of volcanism: Geosphere, v. 12, no. 4, p. 1097–1135, https://doi.org/10.1130/GES01285.1.

Bethke, P.M., 2011, Mineralization in the eastern San Juan Mountains, chap. 3, *of* Blair, R., and Bracksiek, G., eds, The eastern San Juan Mountains—Geology, ecology, and human history: University of Colorado Press, p. 38–59.

Bethke, P.M., Barton, P.B., Jr., Lanphere, M.A., and Steven, T.A., 1976, Environment of ore deposition in the Creede mining district, San Juan Mountains, Colorado—II. Age of mineralization: Economic Geology and the Bulletin of the Society of Economic Geologists, v. 71, no. 6, p. 1006–1011, https://doi.org/10.2113/gsecongeo.71.6.1006.

Bethke, P.M., and Hay, R.L., eds., 2000, Ancient Lake Creede—Its volcano-tectonic setting, history of sedimentation, and relation to mineralization in the Creede mining district: Geological Society of America Special Paper 346, 332 p.

Bethke, P.M., and Lipman, P.W., 1987, Deep environment of volcanogenic epithermal mineralization—Proposed research drilling at Creede, Colorado: Eos, v. 68, no. 13, p. 177–189, https://doi.org/10.1029/EO068i013p00177.

Bethke, P.M., and Rye, R.O., 1979, Environment of ore deposition in the Creede mining district, San Juan Mountains, Colorado—Part IV. Source of fluids from oxygen, hydrogen and carbon isotope studies: Economic Geology and the Bulletin of the Society of Economic Geologists, v. 74, no. 8, p. 1832–1851, https://doi.org/10.2113/gsecongeo.74.8.1832.

Bindeman, I.N., and Valley, J.W., 2001, Low-$\delta^{18}O$ rhyolites from Yellowstone—Magmatic evolution based on analyses of zircons and individual phenocrysts: Journal of Petrology, v. 42, no. 8, p. 1491–1517, https://doi.org/10.1093/petrology/42.8.1491.

Bird, W.H., 1972, Mineral deposits of the southern portion of the Platoro Caldera Complex, southeast San Juan Mountains, Colorado: The Mountain Geologist, v. 9, p. 379–387.

Boro, J., Wolff, J.A., and Neill, O.K., 2016, Anatomy of a recharge magma—Dacite pumice blocks in the Tshirege Member of the Bandelier Tuff, Valles caldera, New Mexico [abs.]: Geological Society of America with Programs, v. 48, no.7, https://gsa.confex.com/gsa/2016AM/webprogram/Paper287073.html.

Bove, D.J., Hon, K., Budding, K.E., Slack, J.F., Snee, L.W., and Yeoman, R.A., 2001, Geochronology and geology of late Oligocene through Miocene volcanism and mineralization in the western San Juan Mountains, Colorado, with special emphasis on the Lake City caldera area: U.S. Geological Survey Professional Paper 1642, 30 p.

Bowring, S.A., and Karlstrom, K.E., 1990, Growth, stabilization, and reactivation of Proterozoic lithosphere in the southwestern United States: Geology, v. 18, no. 12, p. 1203–1206, https://doi.org/10.1130/0091-7613(1990)018<1203:GSAROP>2.3.CO;2.

Branney, M.J., and Kokelaar, P., 1994, Volcanotectonic faulting, soft-state deformation, and rheomorphism of tuffs during development of a piecemeal caldera, English Lake District: Geological Society of America Bulletin, v. 106, no. 4, p. 507–530, https://doi.org/10.1130/0016-7606(1994)106<0507:VFSSDA>2.3.CO;2.

Brister, B.S., and Gries, R.R., 1994, Tertiary stratigraphy and tectonic development of the Alamosa basin (northern San Luis Basin), Rio Grande rift, south-central Colorado, *in* Keller, G.R., and Cather, S.M., eds., Basins of the Rio Grande rift—Structure, stratigraphy, and tectonic setting: Geological Society of America Special Paper 291, p. 39–58, https://doi.org/10.1130/SPE291.

Brister, B.S., and McIntosh, W.C., 2004, Identification and correlation of Oligocene ignimbrites in well bores, Alamosa Basin (northern San Luis Basin), Colorado, by single-crystal laser-fusion $^{40}Ar/^{39}Ar$ geochronology of well cuttings: New Mexico Bureau of Geology and Mineral Resources Bulletin 160, p. 281–296.

Brookins, D., and Laughlin, A.W., 1983, Rb-Sr geochronological investigation of Precambrian samples from deep geothermal drill holes, Fenton Hill, New Mexico: Journal of Volcanology and Geothermal Research, v. 15, no. 1–3, p. 43–58, https://doi.org/10.1016/0377-0273(83)90095-1.

Brown, L.L., and Golombek, M.P., 1986, Block rotations in the Rio Grande Rift, New Mexico: Tectonics, v. 5, no. 3, p. 423–438, https://doi.org/10.1029/TC005i003p00423.

Brun, J.-P., 1999, Narrow rifts versus wide rifts—Inferences for the mechanics of rifting from laboratory experiments: Philosophical Transactions of the Royal Society of London, Series A, Mathematical and Physical Sciences, v. 357, no. 1753, p. 695–712, https://doi.org/10.1098/rsta.1999.0349.

Bruns, D.L., Epis, R.C., Weimer, R.J., and Steven, T.A., 1971, Stratigraphic relations between Bonanza center and adjacent parts of the San Juan volcanic field, southcentral Colorado, *in* James, H.L., ed., San Luis Basin: New Mexico Geological Society, 22nd Fall Field Conference Guidebook, p. 183–190.

Brunstad, K.A., 2013, Origin and evolution of a large silicic caldera complex—Valles caldera and the associated upper Bandelier Tuff: Pullman, Washington State University, Ph.D. dissertation, 274 p.

Buck, W.R., 1991, Modes of continental lithospheric extension: Journal of Geophysical Research, v. 96, B12, p. 20161–20178, https://doi.org/10.1029/91JB01485.

Burbank, W.S., and Henderson, C.W., 1932, Geology and ore deposits of the Bonanza mining district, Colorado, with a section on history and production: U.S. Geological Survey Professional Paper 169, 166 p.

Burgisser, A., and Bergantz, G.W., 2011, A rapid mechanism to remobilize and homogenize highly crystalline magma bodies: Nature, v. 471, no. 7337, p. 212–215, https://doi.org/10.1038/nature09799.

Butler, A.P., Jr., 1971, Tertiary volcanic stratigraphy of the eastern Tusas Mountains, southwest of the San Luis Valley, Colorado-New Mexico, *in* James, H.L., ed., San Luis Basin: New Mexico Geological Society, 22nd Fall Field Conference Guidebook, p. 289–300.

Calkin, W.S., Kendall, R., and Lipman, P.W., 1971, Road log from Alamosa to the eastern San Juan Mountains, via Alamosa River, Jasper, Summitville, South Fork, and return, *in* James, H.L., ed., San Luis Basin: New Mexico Geological Society, 22nd Fall Field Conference Guidebook, p. 1–13.

Cappa, J.A., and Wallace, C.A., 2007, Geology and mineral resources of Saguache County, Colorado: Colorado Geological Survey Resource Series 44, CD-ROM.

Caress, M.E., 1996, Zonation of alkali feldspar compositions in the Tshirege Member of the Bandelier Tuff in Pueblo Canyon, near Los Alamos, New Mexico, *in* Goff, F., Kues, B.S., Rogers, M.A., McFadden, L.S., and Gardner, J.N., eds., Jemez Mountains region: New Mexico Geological Society, 47th Fall Field Conference Guidebook, p. 275–283.

Cashman, K.V., and Giordano, G., 2014, Calderas and magma reservoirs: Journal of Volcanology and Geothermal Research, v. 288, p. 28–45, https://doi.org/10.1016/j.jvolgeores.2014.09.007.

CD-ROM Working Group, 2002, Structure and evolution of the lithosphere beneath the Rocky Mountains—Initial results from the CD-ROM experiment: GSA Today, v. 12, no. 3, p. 4–10, https://doi.org/10.1130/1052-5173(2002)012<0004:SAEOTL>2.0.CO;2.

Chan, C.F., Thompson, R.A., Zimmerer, M.J., Premo, W.R., and Shroba, R.R., 2016, Insight into small volume volcanic fields in Central Rio Grande Rift—Albuquerque Volcanoes [abs.]: New Mexico, Geological Society of America Abstracts with Programs, p. 173–174, https://doi.org/10.1130/abs/2016AM-286572.

Chapin, C.E., 1971, The Rio Grande rift, Part 1—Modifications and additions, *in* James, H.L., ed., San Luis Basin: New Mexico Geological Society, 22nd Fall Field Conference Guidebook, p. 191–202.

Chapin, C.E., and Epis, R.C., 1964, Some stratigraphic and structural features of the Thirtynine Mile volcanic field, central Colorado: The Mountain Geologist, v. 1, no. 3, p. 145–160.

Chapin, C.E., and Lindley, J.F., 1986, Potassium metasomatism of igneous and sedimentary rocks in detachment terranes and other sedimentary basins—Economic implications, *in* Frontiers in geology and ore deposits of Arizona and the Southwest: Arizona Geological Society Digest, v. 16, p. 118–126.

Chapin, C.E., and Lowell, G.R., 1979, Primary and secondary flow structures in ash-flow tuffs of the Gribbles Run paleovalley, central Colorado, *in* Chapin, C.E., and Elston, W.E. eds., Ash-flow tuffs: Geological Society of America Special Paper 180, p. 137–154.

Charlier, B.L.A., Bachmann, O., Davidson, J.P., Dungan, M.A., and Morgan, D., 2007, The upper crustal evolution of a large silicic magma body—Evidence from crystal-scale Rb-Sr isotopic heterogeneities in the Fish Canyon magmatic system, Colorado: Journal of Petrology, v. 48, no. 10, p. 1875–1894, https://doi.org/10.1093/petrology/egm043.

Christiansen, R.L., 1984, Yellowstone magmatic evolution—Its bearing on understanding large-volume explosive volcanism, *in* Explosive Volcanism—Inception, evolution, and hazards: Washington, D.C., National Academy Press, p. 84–95.

Christiansen, R.L., and Lipman, P.W., 1972, Cenozoic volcanism and plate-tectonic evolution of the western United States; Part 2, late Cenozoic: Proceedings of the Royal Society of London, v. 271, p. 249–284.

Clarkson, G., and Reiter, M., 1984, Analysis of terrestrial heat-flow profiles across the Rio Grande rift and southern Rocky Mountains in northern New Mexico, *in* Baldridge, W.S., Dickerson, P.W., Riecker, R.E., and Zidek, J., eds., Rio Grande rift—Northern New Mexico: New Mexico Geological Society, 35th Fall Field Conference Guidebook, p. 39–44.

Colucci, M.T., Dungan, M.T., Ferguson, K.M., Lipman, P.W., and Moorbath, S., 1991, Precaldera lavas of the southeast San Juan volcanic field—Parent magmas and crustal interactions: Journal of Geophysical Research, v. 96, B8, p. 13413–13434, https://doi.org/10.1029/91JB00282.

Condie, K.C., 1982, Plate tectonics and continental drifts, chap. 8 *of* Plate tectonics and crustal evolution: Oxford, Pergamon Press, p. 151–187, https://doi.org/10.1016/B978-0-08-028076-9.50013-8.

Cook, D.R., 1960, Bonanza project–Bear Creek Mining Company: American Institute of Mining, Metallurgy, and Petroleum Engineers Transactions, v. 217, p. 285–295.

Cook, G.W., Wolff, J.A., and Self, S., 2016, Estimating the eruptive volume of a large pyroclastic body—The Otowi member of the Bandelier Tuff, Valles caldera, New Mexico: Bulletin of Volcanology, v. 78, no. 10, 11 p., https://doi.org/10.1007/s00445-016-1000-0.

Cordell, L., 1982, Extension in the Rio Grande Rift: Journal of Geophysical Research, v. 87, no. B10, p. 8561–8569, https://doi.org/10.1029/JB087iB10p08561.

Cordell, L., Long, C.L., and Jones, D.W., 1985, Geophysical expression of the batholith beneath Questa caldera, New Mexico: Journal of Geophysical Research, v. 90, B13, p. 11263–11274, https://doi.org/10.1029/JB090iB13p11263.

Corti, G., Bonini, M., Conticelli, S., Innocenti, F., Manetti, P., and Sokoutis, D., 2003, Analogue modelling of continental extension—A review focused on the relations between the patterns of deformation and the presence of magma: Earth-Science Reviews, v. 63, no. 3–4, p. 169–247, https://doi.org/10.1016/S0012-8252(03)00035-7.

Cosca, M.A., Thompson, R.A., Lee, J.P., Turner, K.J., Neymark, L.A., and Premo, W.R., 2014, $^{40}Ar/^{39}Ar$ geochronology, isotope geochemistry (Sr, Nd, Pb), and petrology of alkaline lavas near Yampa, Colorado—Migration of alkaline volcanism and evolution of the northern Rio Grande rift: Geosphere, v. 10, no. 2, p. 374–400, https://doi.org/10.1130/GES00921.1.

Cross, W., and Larsen, E.S., Jr., 1935, A brief review of the geology of the San Juan region of southwestern Colorado: U.S. Geological Survey Bulletin 843, 138 p.

Curry, A, Caricchi, L., and Lipman, P.W., 2021, Magmatic evolution of zoned and unzoned ignimbrites—Evidence for a complex crustal architecture feeding four rapid-sequence, caldera-forming eruptions in the San Juan Mountains, Colorado: Journal of Petrology, v. 62, no. 5, 37 p., https://doi.org/10.1093/petrology/egab006.

Davis, P., Byerly, A., and Sparks, K., 2010, New insight into 1.7-1.65 Yavapai-Mazatzal aged tectonism in the Tusas Mountains of northern New Mexico [abs.]: Geological Society of America Abstracts with Programs, v. 42, p. 414.

de Silva, S., 1989, Altiplano-Puna volcanic complex of the central Andes: Geology, v. 17, no. 12, p. 1102–1106, https://doi.org/10.1130/0091-7613(1989)017<1102:APVCOT>2.3.CO;2.

de Silva, S., and Gosnold, W.D., 2007, Episodic construction of batholiths—Insights from the spatiotemporal development of an ignimbrite flare-up: Journal of Volcanology and Geothermal Research, v. 167, no. 1–4, p. 320–335, https://doi.org/10.1016/j.jvolgeores.2007.07.015.

de Silva, S.L., Mucek, A.E., Gregg, P.M., and Pratomo, I., 2015, Resurgent Toba—Field, chronologic, and model constraints on time scale and mechanism of resurgence at large calderas: Frontiers of Earth Science, v. 3, https://doi.org/10.3389/feart.2015.00025.

Dethier, D.P., 1997, Geology of the White Rock quadrangle, Los Alamos and Santa Fe Counties, New Mexico: New Mexico Bureau of Geology and Mineral Resources Geologic Map 73, scale 1:24,000.

Dethier, D.P., Kampf, S.K., Sawyer, D.A., and Budahn, J.R., 2007, Chemical zonation in the upper Bandelier Tuff—Evidence from the chemistry of distal outcrops, Puye quadrangle, *in* Kues, B.S., Kelley, S.A., Lueth, V.W., eds., Geology of the Jemez region II: New Mexico Geological Society, 58th Fall Field Conference Guidebook, p. 333–343.

Dethier, D.P., Thompson, R.A., Hudson, M.R., Minor, S.A., and Sawyer, D.A., 2011, Geologic map of the Cochiti Dam quadrangle, Sandoval County, New Mexico: U.S. Geological Survey Scientific Investigations Map 3194, 1 sheet, scale 1:24,000.

Dickens, A.K., 2007, Obsidian hydration and its consequences for the Ar-Ar dating method: Socorro, New Mexico Institute of Mining and Technology, M.S. Thesis,182 p.

Dorais, M.J., Whitney, J.A., and Stormer, J.C., Jr., 1991, Mineralogical constraints on the petrogenesis of trachytic inclusions, Carpenter Ridge Tuff, central San Juan volcanic field, Colorado: Contributions to Mineralogy and Petrology, v. 107, no. 2, p. 219–230, https://doi.org/10.1007/BF00310708.

Drenth, B.J., Grauch, V.J.S., and Rodriguez, B.D., 2013, Geophysical constraints on Rio Grande rift structure in the central San Luis Basin, Colorado and New Mexico, *in* Hudson, M.R., and Grauch, V.J.S., eds., New perspectives on Rio Grande rift basins—From tectonics to groundwater: Geological Society of America Special Paper 494, p. 75–99, https://doi.org/10.1130/2013.2494(04).

Drenth, B.J., Grauch, V.J.S., Thompson, R.A., Rodriguez, B.D., Bauer, P.W., and Turner, K.J., 2016, Preliminary 3D model of the San Luis Basin, northern Rio Grande rift, Colorado and New Mexico [abs.]: Geological Society of America Abstracts with Programs, v. 48, no. 7, https://doi.org/10.1130/abs/2016AM-281204.

Drenth, B.J., Keller, G.R., and Thompson, R.A., 2012, Geophysical study of the San Juan Mountains batholith complex, southwestern Colorado: Geosphere, v. 8, no. 3, p. 669–684, https://doi.org/10.1130/GES00723.1.

Drenth, B.J., Turner, K.J., Thompson, R.A., Grauch, V.J.S., Cosca, M.A., and Lee, J.P., 2011, Geophysical expression of elements of the Rio Grande rift in the northeast Tusas Mountains—Preliminary interpretations, *in* Koning, D.J., Karlstrom, K.E., Kelley, S.A., Lueth, V.W., and Aby, S.B., eds., Geology of the Tusas Mountains and Ojo Caliente: New Mexico Geological Society, 62nd Fall Field Conference Guidebook, p. 165–176.

Druitt, T., and Francaviglia, V., 1992, Caldera formation on Santorini and the physiography of the islands in the late Bronze Age: Bulletin of Volcanology, v. 54, no. 6, p. 484–493, https://doi.org/10.1007/BF00301394.

Dueker, K., Yuan, H., and Zurek, B., 2001, Thick-structured Proterozoic lithosphere of the Rocky Mountain region: GSA Today, v. 11, no. 12, p. 4–9, https://doi.org/10.1130/1052-5173(2001)011<0004:TSPLOT>2.0.CO;2.

Duffield, W.A., 1990, Eruptive fountains of silicic magmas and their possible effects on the Tin content of fountain-fed lavas, Taylor Creek Rhyolite, New Mexico, *in* Stein, H.J., and Hannah, J.L., eds., Ore-bearing granite systems; petrogenesis and mineralizing processes: Geological Society of America Special Paper 246, p. 251–262.

Duncker, K.E., Wolff, J.A., Harmon, R.S., Leat, P.T., Dickin, A.P., and Thompson, R.N., 1991, Diverse mantle and crustal components in lavas of the NW Cerros del Rio volcanic field, Rio Grande rift, New Mexico: Contributions to Mineralogy and Petrology, v. 108, no. 3, p. 331–345, https://doi.org/10.1007/BF00285941.

Dungan, M.A., 1987, Open system magmatic evolution of the Taos Plateau volcanic field, northern New Mexico—II. The genesis of cryptic hybrids: Journal of Petrology, v. 28, no. 5, p. 955–977, https://doi.org/10.1093/petrology/28.5.955.

Dungan, M.A., Lindstrom, M.M., McMillan, N.J., Moorbath, S., Hoefs, J., and Haskin, L.A., 1986, Open system magmatic evolution of the Taos Plateau volcanic field, northern New Mexico—1. The petrology and geochemistry of the Servilleta Basalt: Journal of Geophysical Research, v. 91, B6, p. 5999–6028, https://doi.org/10.1029/JB091iB06p05999.

Dungan, M.A., and Lipman, P.W., 1988, The Masonic Park Tuff and Mt Hope caldera, Oligocene San Juan volcanic field (SJVF), southwestern Colorado [abs.]: Eos, v. 69, p. 1487.

Dungan, M.A., Lipman, P.W., Colucci, M.T., Ferguson, K.M., and Balsley, S.D., 1989a, Southeastern (Platoro) caldera complex, *in* Lipman, P.W., comp., IAVCEI fieldtrip guide—Oligocene-Miocene San Juan volcanic field, Colorado: New Mexico Bureau of Mines and Mineral Resources Memoir 46, p. 305–329.

Dungan, M.A., Moorbath, S., Colucci, M.T., Balsley, S.D., and Ferguson, K.M., 1995, The origin and differentiation of magmas of the Oligocene SE San Juan volcanic field (Platoro caldera complex), Colorado, USA [abs.]: International Union of Geology and Geophysics, Abstract Volume, p. A444.

Dungan, M.A., Muehlberger, W.R., Leininger, L., Peterson, C., McMillan, N.J., Gunn, G., Lindstrom, M., and Haskin, L., 1984, Volcanic and sedimentary stratigraphy of the Rio Grande gorge and the late Cenozoic geologic evolution of the southern San Luis Valley, *in* Baldridge, W.S., Dickerson, P.W., Riecker, R.E., and Zidek, J., eds., Rio Grande rift (northern New Mexico): New Mexico Geological Society, 35th Fall Field Conference Guidebook, p. 157–170.

Dungan, M.A., Thompson, R.A., Stormer, J.S., and O'Neill, J.M., 1989b, Rio Grande rift volcanism—Northeastern Jemez zone, New Mexico, *in* Chapin, C.E., and Zidek, J., eds., Field excursions to volcanic terranes in the western United States, Volume I—Southern Rocky Mountains region: New Mexico Bureau of Mines and Mineral Resources Memoir 46, p. 435–486.

Eichelberger, J.C., and Koch, F.G., 1979, Lithic fragments in the Bandelier Tuff, Jemez Mountains, New Mexico: Journal of Volcanology and Geothermal Research, v. 5, no. 1–2, p. 115–134, https://doi.org/10.1016/0377-0273(79)90036-2.

Ellis, B.S., Wolff, J.A., Boroughs, S., Mark, D.F., Starkel, W.A., and Bonnichsen, B., 2013, Rhyolitic volcanism of the central Snake River Plain—A review: Bulletin of Volcanology, v. 75, no. 8, 19 p.

Ellisor, R., Wolff, J.A., and Gardner, J.N., 1996, Outline of the petrology and geochemistry of the Keres Group lavas and tuffs, *in* Goff, F., Kues, B.S., Rogers, M.A., McFadden, L.D., and Gardner, J.N., eds., The Jemez Mountains region: New Mexico Geological Society, 47th Fall Field Conference Guidebook, p. 237–242.

Elston, W.E., 1984, Mid-Tertiary ash-flow tuff cauldrons, southwestern New Mexico: Journal of Geophysical Research, v. 89, B10, p. 8733–8750, https://doi.org/10.1029/JB089iB10p08733.

Emmons, W.H., and Larsen, E.S., 1923, Geology and ore deposits of the Creede district, Colorado: U.S. Geological Survey Bulletin 718, 198 p.

Epis, R.C., and Chapin, C.E., 1968, Geologic history of the Thirtynine Mile volcanic field, central Colorado, *in* Epis, R.C., ed., Cenozoic volcanism in the Southern Rocky Mountains: Colorado School Mines Quarterly, v. 63, no. 3, p. 51–85.

Epis, R.C., and Chapin, C.E., 1974, Stratigraphic nomenclature of the Thirtynine Mile volcanic field: U.S. Geological Survey Bulletin 1395-C, 23 p.

Erdmann, S., Martel, C., Pichavant, M., and Kushnir, A., 2014, Amphibole as an archivist of magmatic crystallization conditions—Problems, potential, and implications for inferring magma storage prior to the paroxysmal 2010 eruption of Mount Merapi, Indonesia: Contributions to Mineralogy and Petrology, v. 167, no. 6, 23 p., article 1016.

Ferrari, L., Valencia-Moreno, M., and Bryan, S., 2007, Magmatism and tectonics of the Sierra Madre Occidental and its relation with the evolution of the western margin of North America, *in* Alaniz-Álvarez, S.A., and Nieto-Samaniego, A.F., eds., Geology of México—Celebrating the centenary of the Geological Society of México: Geological Society of America Special Paper 422, p. 1–39, https://doi.org/10.1130/2007.2422(01).

Finkelstein, D.B., Hay, R.L., and Altaner, S.P., 1999, Origin and diagenesis of lacustrine sediments in the Late Oligocene Creede Formation, southwestern Colorado: Geological Society of America Bulletin, v. 111, no. 8, p. 1175–1191, https://doi.org/10.1130/0016-7606(1999)111<1175:OADOLS>2.3.CO;2.

Foley, N.K., Caddey, S.W., Byington, C.B., and Vardiman, D.M., 1993, Mineralogy, mineral chemistry, and paragenesis of gold, silver, and base-metal ores of the North Amethyst vein system, San Juan Mountains, Mineral County, Colorado: U.S. Geological Survey Professional Paper 1537, 39 p., https://doi.org/10.3133/pp1537.

Fridrich, C.J., Shroba, R.R., and Hudson, A.M., 2012, Preliminary geologic map of the Big Costilla Peak area, Taos County, New Mexico, and Costilla County, Colorado: U.S. Geological Survey Open-File Report 2012–1041, scale 1:24,000, https://doi.org/10.3133/ofr20121041.

Fridrich, C.J., Smith, R.P., DeWitt, E., and McKee, E.H., 1991, Structural, eruptive, and intrusive evolution of the Grizzly Peak caldera, Sawatch Range, Colorado: Geological Society of America Bulletin, v. 103, no. 9, p. 1160–1177, https://doi.org/10.1130/0016-7606(1991)103<1160:SEAIEO>2.3.CO;2.

Friedman, I., Lipman, P.W., Obradovich, J.D., Gleason, J.D., and Christiansen, R.L., 1974, Meteoric water in magmas: Science, v. 184, no. 4141, p. 1069–1072, https://doi.org/10.1126/science.184.4141.1069.

Galusha, T., and Blick, J.C., 1971, Stratigraphy of the Santa Fe Group, New Mexico: Bulletin of the American Museum of Natural History, v. 44, p. 1–128.

Gardner, J.N., and Goff, F., 1984, Potassium-argon dates from the Jemez volcanic field—Implications for tectonic activity in the north-central Rio Grande rift, *in* Baldridge, W.S., Dickerson, P.W., Riecker, R.E., and Zidek, J., eds., Rio Grande rift—Northern New Mexico: New Mexico Geological Society, 35th Fall Field Conference Guidebook, p. 237–242.

Gardner, J.N., Goff, F., Garcia, S., and Hagan, R.C., 1986, Stratigraphic relations and lithologic variations in the Jemez volcanic field, New Mexico: Journal of Geophysical Research, v. 91, B2, p. 1763–1778, https://doi.org/10.1029/JB091iB02p01763.

Gardner, J.N., Goff, F., Kelley, S.A., and Jacobs, E., 2010, Rhyolites and associated deposits of the Valles-Toledo caldera complex, New Mexico: Geology, v. 32, p. 3–18.

Gardner, J.N., Sandoval, M.M., Goff, F., Phillips, E., and Dickens, A., 2007, Geology of the Cerro de Medio moat rhyolite center, Valles caldera, New Mexico, *in* Kues, B.S., Kelley, S.A., and Lueth, V.W., eds., Geology of the Jemez Mountains region II: New Mexico Geological Society, 58th Fall Field Conference Guidebook p. 367–372.

Gazis, C.A., Lanphere, M.A., Taylor, H.P., Jr., and Gurbanov, A., 1995, $^{40}Ar/^{39}Ar$ and $^{18}O/^{16}O$ studies of the Chegem ash-flow caldera and Eldjurta Granite—Cooling of two late Pliocene igneous bodies in the Greater Caucasus Mountains, Russia: Earth and Planetary Science Letters, v. 134, no. 3–4, p. 377–391, https://doi.org/10.1016/0012-821X(95)00141-X.

Gibson, S.A., Thompson, R.N., Leat, P.T., Morrison, M.A., Hendry, G.L., Dicken, A.P., and Mitchell, J.G., 1993, Ultrapotassic magmas along the flanks of the Oligo-Miocene Rio Grande rift, USA—Monitors of the zone of lithospheric mantle extension and thinning beneath a continental rift: Journal of Petrology, v. 34, no. 1, p. 187–228, https://doi.org/10.1093/petrology/34.1.187.

Gilmer, A.K., Thompson, R.A., Lipman, P.W., Vazquez, J.A., and Souders, A.K., 2021, Postcaldera intrusive magmatism at the Platoro caldera complex, southern Rocky Mountain volcanic field, Colorado, USA: Geosphere, v. 17, no. 3, p. 898–931, https://doi.org/10.1130/GES02242.1.

Goff, F., and Gardner, J.N., 1988, Valles caldera region, New Mexico, and the emerging continental scientific drilling program: Journal of Geophysical Research, v. 93, B6, p. 5997–5999, https://doi.org/10.1029/JB093iB06p05997.

Goff, F., and Gardner, J.N., 1994, Evolution of a mineralized geothermal system, Valles caldera, New Mexico: Economic Geology, v. 89, no. 8, p. 1803–1832, https://doi.org/10.2113/gsecongeo.89.8.1803.

Goff, F., Gardner, J.N., Baldridge, W.S., Hulen, J.B., Nielson, D.L., Vaniman, D., Heiken, G., Dungan, M.A., and Broxton, D., 1989, Excursion 17B—Volcanic and hydrothermal evolution of Valles caldera and Jemez volcanic field, *in* Chapin, C.E., and Zidek, J., eds., Field excursions in the western United States, Volume I—Southern Rocky Mountain region: New Mexico Bureau of Mines and Mineral Resources Memoir 46, p. 381–431.

Goff, F., Gardner, J.N., Hulen, J.B., Nielson, D.L., Charles, R., Woldegrabriel, G., Vuataz, F.D., Musgrave, J.A., Shevenell, L., and Kennedy, B.M., 1992, The Valles caldera hydrothermal system, past and present, New Mexico, USA: Scientific Drilling, v. 3, p. 181–204.

Goff, F., Gardner, J.N., Reneau, S.L., Kelley, S.A., Kempter, K.A., and Lawrence, J.R., 2011, Geologic map of the Valles caldera, Jemez Mountains, New Mexico: New Mexico Bureau of Geology and Mineral Resources Geologic Map 79, scale 1:50,000.

Goff, F., Gardner, J.N., and Valentine, G., 1990, Geology of St. Peter's Dome area, Jemez Mountains, New Mexico: New Mexico Bureau of Mines and Mineral Resources Geologic Map 69, scale 1:24,000.

Goff, F., Kues, B., Rogers, M.A., McFadden, L., and Gardner, J., 1996, Jemez Mountains region: New Mexico Geological Society, 47th Fall Field Conference Guidebook, 484 p.

Goff, F., and Shevenell, L., 1987, Travertine deposits of the Soda dam, New Mexico, and their implications for the age and evolution of the Valles caldera hydrothermal system: Geological Society of America Bulletin, v. 99, no. 2, p. 292–302, https://doi.org/10.1130/0016-7606(1987)99<292:TDOSDN>2.0.CO;2.

Goff, F., Shevenell, L., Gardner, J.N., Vuataz, F.D., and Grigsby, C.O., 1988, The hydrothermal outflow plume of Valles caldera, New Mexico and a comparison with other outflow plumes: Journal of Geophysical Research, v. 93, B6, p. 6041–6058, https://doi.org/10.1029/JB093iB06p06041.

Goff, F., Warren, R.G., Goff, C.J., and Dunbar, N., 2014, Eruption of reverse-zoned upper Tshirege Member, Bandelier Tuff from centralized vents within Valles caldera, New Mexico: Journal of Volcanology and Geothermal Research, v. 276, p. 82–104, https://doi.org/10.1016/j.jvolgeores.2014.02.018.

Grauch, V.J.S., Bauer, P.W., Drenth, B.J., and Kelson, K.I., 2017, A shifting rift—Geophysical insights into the evolution of Rio Grande rift margins and the Embudo transfer zone near Taos, New Mexico: Geosphere, v. 13, no. 3, p. 870–910, https://doi.org/10.1130/GES01425.1.

Grauch, V.J.S., Drenth, B.J., Thompson, R.A., and Bauer, P.W., 2015, Preliminary geophysical interpretations of regional subsurface geology near the Questa Mine Tailing Facility and Guadalupe Mountain, Taos County, New Mexico: U.S. Geological Survey Open-File Report 2015–1129, 35 p., https://doi.org/10.3133/ofr20151129.

Grauch, V.J.S., and Keller, G.R., 2004, Gravity and aeromagnetic expression of tectonic and volcanic elements of the southern San Luis Basin, New Mexico and Colorado, New Mexico, *in* Brister, B.S., Bauer, P.W., Read, A.S., and Lueth, V.W., eds., Geology of the Taos region: New Mexico Geological Society Guidebook, 55th Fall Field Conference Guidebook, p. 129–146.

Gray, J.E., and Coolbaugh, M.F., 1994, Geology and geochemistry of Summitville, Colorado—An epithermal acid-sulphate deposit in a volcanic dome: Economic Geology, v. 89, no. 8, p. 1906–1923, https://doi.org/10.2113/gsecongeo.89.8.1906.

Gray, J.E., Coolbaugh, M.F., Plumlee, G.S., and Atkinson, W.W., 1994, Environmental geology of the Summitville mine: Economic Geology and the Bulletin of the Society of Economic Geology, v. 89, no. 8, p. 2006–2014, https://doi.org/10.2113/gsecongeo.89.8.2006.

Gregg, P.M., de Silva, S.L., Grosfils, E.B., and Parmigiani, J.P., 2012, Catastrophic caldera-forming eruptions—Thermomechanics and implications for eruption triggering and maximum caldera dimensions on Earth: Journal of Volcanology and Geothermal Research, v. 241–242, p. 1–12 , https://doi.org/10.1016/j.jvolgeores.2012.06.009.

Gregory, K.M., and McIntosh, W.C., 1996, Paleoclimate and paleo-elevation of the Oligocene Pitch-Pinnacle flora, Sawatch Range, Colorado: Geological Society of America Bulletin, v. 108, no. 5, p. 545–561, https://doi.org/10.1130/0016-7606(1996)108<0545:PAPOTO>2.3.CO;2.

Gries, R.R., 1985, San Juan sag—Cretaceous rocks in a volcanic-covered basin, south-central Colorado: The Mountain Geologist, v. 22, p. 167–179.

Gonzales, D.A., 2015, New U-Pb zircon and $^{40}Ar/^{39}Ar$ age constraints on the late Mesozoic to Cenozoic plutonic record in the western San Juan Mountains: The Mountain Geologist, v. 52, p. 5–42.

Gottsmann, J., Lavallee, Y., Marti, J., and Aguirre-Diaz, G., 2009, Magma-tectonic interaction and the eruption of silicic batholiths: Earth and Planetary Science Letters, v. 284, no. 3–4, p. 426–434, https://doi.org/10.1016/j.epsl.2009.05.008.

Gualda, G.A.R., and Ghiorso, M.S., 2013, Low-pressure origin of high-silica rhyolites and granites: The Journal of Geology, v. 121, no. 5, p. 537–545, https://doi.org/10.1086/671395.

Heiken, G., 1986, Introduction to the special section on the Valles caldera and the Jemez Mountains volcanic field: Journal of Geophysical Research, v. 91, B2, p. 1741, https://doi.org/10.1029/JB091iB02p01741.

Heiken, G., Krier, D., McCormick, T., and Snow, M.G., 2000, Intracaldera volcanism and sedimentation—Creede caldera, Colorado, *in* Bethke, P.M., and Hay, R.L., eds., Ancient Lake Creede—Its volcano-tectonic setting, history of sedimentation, and relation to mineralization in the Creede mining district: Geological Society of America Special Paper 346, p. 127–158.

Henry, C.D., and John, D.A., 2013, Magmatism, ash-flow tuffs, and calderas of the ignimbrite flareup in the western Nevada volcanic field, Great Basin, USA: Geosphere, v. 9, no. 4, p. 951–1008, https://doi.org/10.1130/GES00867.1.

Henry, C.D., and Price, J.G., 1984, Variations in caldera development in the Tertiary volcanic field of Trans-Pecos, Texas: Journal of Geophysical Research, v. 89, B10, p. 8765–8786, https://doi.org/10.1029/JB089iB10p08765.

Hildreth, W., 1979, The Bishop Tuff—Evidence for the origin of compositional zonation in silicic magma chambers: Geological Society of America Special Paper, v. 180, p. 43–75.

Hildreth, W., 1981, Gradients in silicic magma chambers—Implications for lithospheric magmatism: Journal of Geophysical Research, v. 86, B11, p. 10153–10192, https://doi.org/10.1029/JB086iB11p10153.

Hildreth, W., 1983, The compositionally zoned eruption of 1912 in the Valley of Ten Thousand Smokes, Katmai National Park, Alaska: Journal of Volcanology and Geothermal Research, v. 18, no. 1–4, p. 1–56, https://doi.org/10.1016/0377-0273(83)90003-3.

Hon, K., and Lipman, P.W., 1989, Western San Juan caldera complex, *in* Chapin, C.E., and Zidek, J., eds., Field excursions to volcanic terranes in the western United States, Volume I— Southern Rocky Mountain region: New Mexico Bureau of Mines and Mineral Resources Memoir 46, p. 350–380.

Hon, K., and Mehnert, H.H., 1983, Compilation of revised ages of volcanic units in the San Juan Mountains, Colorado—Recalculated K-Ar age determinations using IUGS constants: U.S. Geological Survey Open-File Report 83-668, 14 p., https://doi.org/10.3133/ofr83668.

Huang, R., and Audétat, A., 2012, The titanium-in-quartz (TitaniQ) thermobarometer—A critical examination and re-calibration: Geochimica et Cosmochimica Acta, v. 84, p. 75–89, https://doi.org/10.1016/j.gca.2012.01.009.

Huber, C., Bachmann, O., and Dufek, J., 2010a, The limitations of melting on the reactivation of silicic mushes: Journal of Volcanology and Geothermal Research, v. 195, no. 2–4, p. 97–105, https://doi.org/10.1016/j.jvolgeores.2010.06.006.

Huber, C., Bachmann, O., and Dufek, J., 2012, Crystal-poor versus crystal-rich ignimbrites—A competition between stirring and reactivation: Geology, v. 40, no. 2, p. 115–118, https://doi.org/10.1130/G32425.1.

Huber, C., Bachmann, O., and Manga, M., 2009, Homogenization processes in silicic magma chambers by stirring and mushification (latent heat buffering): Earth and Planetary Science Letters, v. 283, no. 1–4, p. 38–47, https://doi.org/10.1016/j.epsl.2009.03.029.

Huber, C., Bachmann, O., and Manga, M., 2010b, Two competing effects of volatiles on heat transfer in crystal-rich magmas—Thermal insulation vs defrosting: Journal of Petrology, v. 51, no. 4, p. 847–867, https://doi.org/10.1093/petrology/egq003.

Hudson, M.R., and Grauch, V.J.S., 2013, Introduction, *in* Hudson, M.R., and Grauch, V.J.S., eds., New perspectives on Rio Grande rift basins—From tectonics to groundwater: Geological Society of America Special Paper 494, p. v–xii, https://doi.org/10.1130/2013.2494(00).

Hulen, J.B., 1992, Field geologic summaries for core holes CCM-2 (Airport 1-6) and CCM-1 (Hosselkus 1-10): Creede Scientific Drilling Project Report ESL-920111-TR, 38 p.

Hulen, J.B., Nielson, D.L., and Little, T.M., 1991, Evolution of the western Valles Caldera complex, New Mexico—Evidence from intracaldera sandstones, breccias and surge deposits: Journal of Geophysical Research, v. 96, B5, p. 8127–8142, https://doi.org/10.1029/91JB00374.

Hull, S., Fayek, M., Mathien, F.J., and Roberts, H., 2014, Turquoise trade of the ancestral Puebloan—Chaco and beyond: Journal of Archaeological Science, v. 45, p. 187–195, https://doi.org/10.1016/j.jas.2014.02.016.

Iddings, J.P., 1890, On a group of volcanic rocks from the Tewan Mountains, New Mexico, and on the occurrence of primary quartz in certain basalts: U.S. Geological Survey Bulletin 66, 34 p.

Illies, J.H., 1981, Mechanism of graben formation: Tectonophysics, v. 73, no. 1–3, p. 249–266, https://doi.org/10.1016/0040-1951(81)90186-4.

Jacobs, E.P., and Kelley, S.A., 2007, The time between the tuffs—Deposits of the Cerro Toledo interval in Bandelier National Monument, New Mexico, *in* Kues, B.S., Kelley, S.A., and Lueth, V.W., eds., Geology of the Jemez region II: New Mexico Geological Society, 58th Fall Field Conference Guidebook, p. 308–315.

Jacobs, E.P., WoldeGabriel, G., Kelley, S.A., Broxton, D., and Ridley, J., 2016, Volcanism and sedimentation along the western margin of the Rio Grande rift between caldera-forming eruptions of the Jemez Mountains volcanic field, north-central New Mexico: Journal of Volcanology and Geothermal Research, v. 327, p. 416–435, https://doi.org/10.1016/j.jvolgeores.2016.09.012.

John, D.A., 1995, Tilted middle Tertiary ash-flow calderas and subjacent granitic plutons, southern Stillwater Range, Nevada—Cross-sections of an Oligocene igneous center: Geological Society of America Bulletin, v. 107, no. 2, p. 180–200, https://doi.org/10.1130/0016-7606(1995)107<0180:TMTAFC>2.3.CO;2.

John, D.A., Henry, C., and Colgan, J., 2008, Magmatic and tectonic evolution of the Caetano caldera, north-central Nevada—A tilted mid-Tertiary eruptive center and source of the Caetano Tuff: Geosphere, v. 4, no. 1, p. 75–106, https://doi.org/10.1130/GES00116.1.

Johnson, C.M., 1991, Large-scale crust formation and lithosphere modification beneath middle to late Cenozoic calderas and volcanic fields, western North America: Journal of Geophysical Research, v. 96, B8, p. 13485–13507, https://doi.org/10.1029/91JB00304.

Johnson, C.M., and Fridrich, C.J., 1990, Non-monotonic chemical and O, Sr, Nd, and Pb isotope zonations and heterogeneity in the mafic-to-silicic-composition magma chamber of the Grizzly Peak Tuff, Colorado: Contributions to Mineralogy and Petrology, v. 105, no. 6, p. 677–690, https://doi.org/10.1007/BF00306533.

Johnson, C.M., and Lipman, P.W., 1988, Origin of metaluminous and alkaline volcanic rocks of the Latir volcanic field, northern Rio Grande rift, New Mexico: Contributions to Mineralogy and Petrology, v. 100, no. 1, p. 107–128, https://doi.org/10.1007/BF00399442.

Johnson, C.M., Shannon, J.R., and Fridrich, C.J., 1989, Roots of ignimbrite calderas—Batholithic plutonism, volcanism, and mineralization in the southern Rocky Mountains, Colorado and New Mexico, *in* Chapin, C.E., and Zidek, J., eds., Field excursions to volcanic terranes in the western United States, Volume I—Southern Rocky Mountain region: New Mexico Bureau of Mines and Mineral Resources Memoir 46, p. 275–302.

Justet, L., 2003, Effects of basalt intrusion on the multi-phase evolution of the Jemez volcanic field, NM: Las Vegas, University of Nevada, Ph.D. dissertation, 248 p.

Justet, L., and Spell, T.L., 2001, Effusive eruptions from a large silicic magma chamber—The Bearhead Rhyolite, Jemez volcanic field, NM: Journal of Volcanology and Geothermal Research, v. 107, no. 4, p. 241–264, https://doi.org/10.1016/S0377-0273(00)00296-1.

Kammerer, J.C., 1990, Largest rivers in the United States: U.S. Geological Survey Open-File Report 87-242, 2 p.

Karig, D.E., 1965, Geophysical evidence of a caldera at Bonanza, Colorado: U.S. Geological Survey Professional Paper 525-B, p. B9–B12.

Karlstrom, K.E., and Daniel, C.G., 1993, Restoration of Laramide right-lateral strike slip in northern New Mexico by using Proterozoic piercing points—Tectonic implications from the Proterozoic to the Cenozoic: Geology, v. 21, no. 12, p. 1139–1142, https://doi.org/10.1130/0091-7613(1993)021<1139:ROLRLS>2.3.CO;2.

Karlstrom, K.E., and Humphreys, E.D., 1998, Persistent influence of Proterozoic accretionary boundaries in the tectonic evolution of southwestern North America—Interaction of cratonic grain and mantle modification events: Rocky Mountain Geology, v. 33, no. 2, p. 161–179, https://doi.org/10.2113/33.2.161.

Karlstrom, L., Rudolph, M.L., and Manga, M., 2012, Caldera size modulated by the yield stress within a crystal-rich magma reservoir: Nature Geoscience, v. 5, no. 6, p. 402–405, https://doi.org/10.1038/ngeo1453.

Kearney, B.C., 1983, Volcanic stratigraphy and structure of the La Veta Pass area, northern Sangre de Cristo Mountains, south-central Colorado: Dallas, Southern Methodist University, M.S. Thesis, 67 p.

Keller, G.R., and Cather, S.M., 1994, Introduction, *in* Keller, G.R., and Cather, S.M., eds., Basins of the Rio Grande rift—Structure, stratigraphy, and tectonic setting: Geological Society of America Special Paper 291, p. 1–3, https://doi.org/10.1130/SPE291-p1.

Kelley, S.A., Chapin, C.E., and Corrigan, J., 1992, Late Mesozoic to Cenozoic cooling histories of flanks of the northern and central Rio Grande rift, Colorado and New Mexico: New Mexico Bureau of Geology and Mineral Resources Bulletin 145, 39 p.

Kelley, S.A., McIntosh, W.C., Goff, F., Kempter, K.A., Wolff, J.A., Esser, R., Braschayko, S., Love, D., and Gardner, J.N., 2013, Spatial and temporal trends in pre-caldera Jemez Mountains volcanic and fault activity: Geosphere, v. 9, no. 3, p. 614–646, https://doi.org/10.1130/GES00897.1.

Kelson, K., and Bauer, P., 2006, Preliminary geologic map of the Arroyo Hondo quadrangle, Taos County, New Mexico: New Mexico Bureau of Geology and Mineral Resources Open-File Digital Geologic Map 116, scale 1:24,000.

Kelson, K.I., and Bauer, P.W., 1998, Geologic map of the Carson quadrangle, Taos County, New Mexico: New Mexico Bureau of Geology and Mineral Resources Open-File Geologic Map 22, scale 1:24,000.

Kelson, K.I., Bauer, P.W., Unruh, J.R., and Bott, D.J., 2004, Late Quaternary characteristics of the northern Embudo fault, Taos County, New Mexico, *in* Brister, B.S., Bauer, P.W., Read, A.S., and Lueth, V.W., eds., Geology of the Taos region: New Mexico Geological Society, 55th Fall Field Conference Guidebook, p. 147–157.

Kelson, K.I., Haller, K.M., and Koning, D.J., compilers, 2015, Fault number 2007—Embudo fault, *in* Quaternary fault and fold database of the United States: U.S. Geological Survey database, https://earthquakes.usgs.gov/hazards/qfaults.

Kelson, K.I., Thompson, R.A., and Bauer, P.W., 2008, Geologic map of the Guadalupe Mountain quadrangle, Taos County, New Mexico: New Mexico Bureau of Geology and Mineral Resources Open-File Map 168, scale 1:24,000.

Kelson, K.I., Unruh, J.R., and Bott, J.D.J., 1996, Evidence for active rift extension along the Embudo fault, Rio Grande rift, northern New Mexico [abs.]: Geological Society of America Abstracts with Programs, v. 28, no. 7, p. A-377.

Kelson, K.I., Unruh, J.R., and Bott, J.D.J., 1997, Field characterization, kinematic analysis, and initial paleoseismologic assessment of the Embudo fault, northern New Mexico: 32nd Technical Report to U.S. Geological Survey, under Contract 1434-96-G-02739, 48 p.

Kennedy, B., Stix, J., Hon, K., Deering, C., and Gelman, S., 2016, Magma storage, differentiation, and interaction at Lake City caldera, Colorado, USA: Geological Society of America Bulletin, v. 128, no. 5–6, p. 764–776, https://doi.org/10.1130/B31305.1.

Kirkham, R.M., Lufkin, J.L., Lindsay, N.R., and Dickens, K.E., 2004, Geologic map of the La Valley Quadrangle, Costilla County, Colorado: Colorado Geological Survey Open-File Report 04-08, 37 p., 1:24,000 scale.

Kluth, C.F., and Schaftenaar, C.H., 1994, Depth and geometry of the northern Rio Grande rift in the San Luis Basin, south-central Colorado, *in* Keller, G.R., and Cather, S.M., eds., Basins of the Rio Grande rift—Structure, stratigraphy, and tectonic setting: Geological Society of America Special Paper 291, p. 27–38, https://doi.org/10.1130/SPE291-p27.

Koning, D.J., Aby, S., Grauch, V.J.S., and Zimmerer, M.J., 2016, Latest Miocene-earliest Pliocene evolution of the ancestral Rio Grande at the Española-San Luis Basin boundary, northern New Mexico: New Mexico Geology, v. 38, no. 2, p. 24–49.

Koning, D.J., Grauch, V.J.S., Connell, S.D., Ferguson, J., McIntosh, W., Slate, J.L., Wan, E., and Baldridge, W.S., 2013, Structure and tectonic evolution of the eastern Española Basin, Rio Grande rift, north-central New Mexico, *in* Hudson, M.R., and Grauch, V.J.S., eds., New perspectives on Rio Grande rift basins—From tectonics to groundwater: Geological Society of America Special Paper 494, p. 185–219, https://doi.org/10.1130/2013.2494(08).

Koning, D.J., Karlstrom, K., Salem, A., and Lombardi, C., 2007, Preliminary geologic map of the La Madera quadrangle, Rio Arriba County, New Mexico: New Mexico Bureau of Geology and Mineral Resources Open-File Geologic Map 141, scale 1:24,000.

Koning, D.J., Peters, L., Kelley, S., and McIntosh, W.C., 2007, Evidence for rhyodacitic volcanism in the northern Jemez Mountains at 11-13 Ma, *in* Kues, B.S., Kelley, S.A., and Lueth, V.W., eds., Geology of the Jemez region II: New Mexico Geological Society Guidebook, 58th Fall Field Conference Guidebook, p. 39–41.

Kues, B.S., Kelley, S.A., and Lueth, V.W., 2007, Geology of the Jemez region II: New Mexico Geological Society, 58th Fall Field Conference Guidebook, 499 p.

Kuiper, K.F., Deino, A., Hilgen, F.J., Krijgsman, W., Renne, P.R., and Wijbrans, J.R., 2008, Synchronizing rock clocks of Earth history: Science, v. 320, no. 5875, p. 500–504, https://doi.org/10.1126/science.1154339.

Lanphere, M.A., 1988, High resolution $^{40}Ar/^{39}Ar$ chronology of Oligocene volcanic rocks, San Juan Mountains, Colorado: Geochimica et Cosmochimica Acta, v. 52, no. 6, p. 1425–1434, https://doi.org/10.1016/0016-7037(88)90212-8.

Lanphere, M.A., 2000, Duration of sedimentation of the Creede Formation from $^{40}Ar/^{39}Ar$ ages, *in* Bethke, P.M., and Hay, R.L., eds., Ancient Lake Creede—Its volcano-tectonic setting, history of sedimentation, and relation to mineralization in the Creede mining district: Geological Society of America Special Paper 346, p. 71–76, https://doi.org/10.1130/0-8137-2346-9.71.

Larsen, D., and Crossey, L.J., 1996, Depositional environments and paleolimnology of an ancient caldera lake—Oligocene Creede Formation, Colorado: Geological Society of America Bulletin, v. 108, no. 5, p. 526–544, https://doi.org/10.1130/0016-7606(1996)108<0526:DEAPOA>2.3.CO;2.

Larsen, D., and Crossey, L.J., 2000, Sedimentary petrology and authigenic mineral distributions in the Oligocene Creede Formation, Colorado, U.S.A, *in* Bethke, P.M., and Hay, R.L., eds., Ancient Lake Creede—Its volcano-tectonic setting, history of sedimentation and relation to mineralization in the Creede Mining District: Geological Society of America Special Paper 346, p. 179–208, https://doi.org/10.1130/0-8137-2346-9.179.

Larsen, D., and Lipman, P.W., 2016, Exploring the ancient volcanic and lacustrine environments of the Oligocene Creede Caldera and environs, San Juan Mountains, Colorado: Geological Society of America Field Guide 44, p. 1–40.

Larsen, D., and Nelson, P.H., 2000, Stratigraphy, correlation, depositional setting, and geophysical characteristics of the Oligocene Snowshoe Mountain Tuff and Creede Formation in two cored boreholes, *in* Bethke, P.M., and Hay, R.L., eds., Ancient Lake Creede—Its volcano-tectonic setting, history of sedimentation and relation to mineralization in the Creede Mining District: Geological Society of America Special Paper 346, p. 159–178, https://doi.org/10.1130/0-8137-2346-9.159.

Larsen, E.S., Jr., and Cross, C.W., 1956, Geology and petrology of the San Juan region, southwestern Colorado: U.S. Geological Survey Professional Paper 258, 303 p., https://doi.org/10.3133/pp258.

Larson, P.B., and Taylor, H.P., Jr., 1986, $^{18}O/^{16}O$ ratios in ash-flow tuffs and lavas erupted from the central Nevada caldera complex and the central San Juan caldera complex, Colorado: Contributions to Mineralogy and Petrology, v. 92, no. 2, p. 146–156, https://doi.org/10.1007/BF00375290.

Laughlin, A.W., Eddy, A.C., Laney, R., and Aldrich, M.J., Jr., 1983, Geology of the Fenton Hill, New Mexico, hot dry rock site: Journal of Volcanology and Geothermal Research, v. 15, no. 1–3, p. 21–41, https://doi.org/10.1016/0377-0273(83)90094-X.

Le Bas, M.J., Le Maitre, R.W., Streckeisen, A., and Zanettin, B., 1986, A chemical classification of volcanic rocks based on the total alkali-silica diagram: Journal of Petrology, v. 27, no. 3, p. 745–750, https://doi.org/10.1093/petrology/27.3.745.

Leininger, R.L., 1982, Cenozoic evolution of the southernmost Taos Plateau, New Mexico: Austin, University of Texas, M.S. thesis, 110 p.

Lindsey, D.A., Andriessen, P.A.M., and Wardlaw, B.R., 1986, Heating, cooling, and uplift during Tertiary time, northern Sangre de Cristo Range, Colorado: Geological Society of America Bulletin, v. 97, no. 9, p. 1133–1143, https://doi.org/10.1130/0016-7606(1986)97<1133:HCAUDT>2.0.CO;2.

Lipman, P.W., 1964, A welded tuff dike in southern Nevada: U.S. Geological Survey Professional Paper 501-B, p. B79–B81.

Lipman, P.W., 1968, Geology of Summer Coon volcanic center, eastern San Juan Mountains, Colorado: Colorado School of Mines Quarterly, v. 63, no. 3, p. 211–236.

Lipman, P.W., 1974, Geologic map of the Platoro caldera area, southeastern San Juan Mountains, Colorado: U.S. Geological Survey Miscellaneous Investigations Series Map I-828, scale 1:48,000.

Lipman, P.W., 1975a, Evolution of the Platoro caldera complex and related volcanic rocks, southeastern San Juan Mountains, Colorado: U.S. Geological Survey Professional Paper 852, 128 p., https://doi.org/10.3133/pp852.

Lipman, P.W., 1975b, Geologic map of the lower Conejos River Canyon area, southeastern San Juan Mountains, Colorado: U.S. Geological Survey Miscellaneous Investigations Series Map I-901, scale 1:48,000.

Lipman, P.W., 1976a, Caldera-collapse breccias in the western San Juan Mountains, Colorado: Geological Society of America Bulletin, v. 87, no. 10, p. 1397–1410, https://doi.org/10.1130/0016-7606(1976)87<1397:CBITWS>2.0.CO;2.

Lipman, P.W., 1976b, Geologic map of the Del Norte area, eastern San Juan Mountains, Colorado: U.S. Geological Survey Miscellaneous Investigations Series Map I-952, scale 1:48,000.

Lipman, P.W., 1980, Cenozoic volcanism in the western United States—Implications for continental tectonics, *in* Burchfiel, B.C., Oliver, J.E., and Silver, L.T., eds., Continental tectonics: National Academy of Sciences, p. 161–174.

Lipman, P.W., 1983, The Miocene Questa caldera, northern New Mexico—Relation to batholith emplacement and associated molybdenum mineralization, *in* The genesis of Rocky Mountain ore deposits—Changes with time and tectonics: Proceedings of the Denver Region Exploration Geologists Society Symposium, Denver, Colo., p. 133–147.

Lipman, P.W., 1984, The roots of ash flow calderas in North America—Windows into the tops of granitic batholiths: Journal of Geophysical Research, v. 89, B10, p. 8801–8841, https://doi.org/10.1029/JB089iB10p08801.

Lipman, P.W., 1988, Evolution of silicic magma in the upper crust—The mid-Tertiary Latir volcanic field and its cogenetic granitic batholith, northern New Mexico, USA: Transactions of the Royal Society of Edinburgh, v. 79, no. 2–3, p. 265–288, https://doi.org/10.1017/S0263593300014279.

Lipman, P.W., comp., 1989, Oligocene-Miocene San Juan volcanic field, Colorado, *in* Chapin, C.E., and Zidek, J., eds., Field excursions to volcanic terranes in the western United States, Volume I—Southern Rocky Mountain region: New Mexico Bureau of Mines and Mineral Resources Memoir 46, p. 303–380.

Lipman, P.W., 1993, Geologic map of the Tucson Mountains caldera, southern Arizona: U.S. Geological Survey Map I-2205, scale 1:50,000.

Lipman, P.W., 1997, Subsidence of ash-flow calderas—Relation to caldera size and magma-chamber geometry: Bulletin of Volcanology, v. 59, no. 3, p. 198–218, https://doi.org/10.1007/s004450050186.

Lipman, P.W., 2000, Central San Juan caldera cluster—Regional volcanic framework, *in* Bethke, P.M., and Hay, R.L., eds., Ancient Lake Creede—Its volcano-tectonic setting, history of sedimentation, and relation of mineralization in the Creede Mining District: Geological Society of America Special Paper 346, p. 9–69, https://doi.org/10.1130/0-8137-2346-9.9.

Lipman, P.W., 2004, Chemical analyses of Tertiary volcanic rocks, central San Juan caldera complex, southwestern Colorado: U.S. Geological Survey Open-File Report 2004–1194, 6 p. and Excel file, http://pubs.usgs.gov/of/2004/1194/.

Lipman, P.W., 2006, Geologic map of the central San Juan caldera cluster, southwestern Colorado: U.S. Geological Survey Miscellaneous Investigations Map I-2799, 1:50,000, 4 sheets, pamphlet.

Lipman, P.W., 2007, Incremental assembly and prolonged consolidation of Cordilleran magma chambers—Evidence from the southern Rocky Mountain volcanic field: Geosphere, v. 3, no. 1, p. 42–70, https://doi.org/10.1130/GES00061.1.

Lipman, P.W., 2012, Geologic map of the Cochetopa Park and North Pass Calderas, northeastern San Juan Mountains, Colorado: U.S. Geological Survey Scientific Investigations Map 3123, scale 1:50,000, 2 sheets, pamphlet.

Lipman, P.W., 2018, When ignimbrite meets water—Megascale gas-escape structures formed during welding: Geology, v. 47, p. 63–66, https://doi.org/10.1130/G45772.1.

Lipman, P.W., 2020, Geologic map of the Bonanza caldera area, northeast San Juan Mountains, Colorado: U.S. Geological Survey Scientific Investigations Map 3394, 73 p., 2 sheets, scale 1:50,000, https://doi.org/10.3133/sim3394.

Lipman, P.W., and Bachmann, O., 2015, Ignimbrites to batholiths—Integrated perspectives from geological, geophysical, and geochronological data: Geosphere, v. 11, no. 3, p. 705–743, https://doi.org/10.1130/GES01091.1.

Lipman, P.W., Bogatikov, O.A., Tsvetkov, A.A., Gazis, C., Gurbanov, A.G., Hon, K., Koronovsky, N.V., Kovalenko, V.I., and Marchev, P., 1993, 2.8-Ma ash-flow caldera at Chegem River in the northern Caucasus Mountains (Russia), contemporaneous granites, and associated ore deposits: Journal of Volcanology and Geothermal Research, v. 57, no. 1–2, p. 85–124, https://doi.org/10.1016/0377-0273(93)90033-N.

Lipman, P.W., Doe, B.R., Hedge, C.E., and Steven, T.A., 1978, Petrologic evolution of the San Juan volcanic field, southwestern Colorado—Pb and Sr isotope evidence: Geological Society of America Bulletin, v. 89, no. 1, p. 59–82, https://doi.org/10.1130/0016-7606(1978)89<59:PEOTSJ>2.0.CO;2.

Lipman, P.W., Dungan, M.A., and Bachman, O., 1997, Comagmatic granophyric granite in the Fish Canyon Tuff, Colorado: Implications for magma-chamber processes during a large ash-flow eruption: Geology, v. 25, no. 10, p. 915–918, https://doi.org/10.1130/0091-7613(1997)025<0915:CGGITF>2.3.CO;2.

Lipman, P.W., Dungan, M.A., Brown, L.D., and Deino, A., 1996, Recurrent eruption and subsidence at the Platoro caldera complex, southeastern San Juan volcanic field, Colorado—New tales from old tuffs: Geological Society of America Bulletin, v. 108, no. 8, p. 1039–1055, https://doi.org/10.1130/0016-7606(1996)108<1039:REASAT>2.3.CO;2.

Lipman, P.W., and McIntosh, W.C., 2008, Eruptive and non-eruptive calderas, northeastern San Juan Mountains, Colorado—Where did the ignimbrites come from?: Geological Society of America Bulletin, v. 120, no.7-8, p. 771–795, https://doi.org/10.1130/B26330.1.

Lipman, P.W., McIntosh, W.C., and Zimmerer, M., 2013, From ignimbrite to batholith, northeastern San Juan Mountains, Colorado—Bonanza, Cochetopa Park, and North Pass calderas, *in* Abbott, L.D., and Hancock, G.S., eds., Classic concepts and new directions—Exploring 125 years of GSA discoveries in the Rocky Mountain region: Geological Society of America Field Guide, v. 33, p. 357–388, https://doi.org/10.1130/2013.0033(14).

Lipman, P.W., and Mehnert, H.H., 1975, Late Cenozoic basaltic volcanism and development of the Rio Grande depression in the southern Rocky Mountains: Geological Society of America, v. 144, p. 119–154, https://doi.org/10.1130/MEM144-p119.

Lipman, P.W., and Mehnert, H.H., 1979, The Taos Plateau volcanic field, northern Rio Grande Rift, New Mexico, *in* Riecker, R.W., ed., Rio Grande rift—Tectonics and magmatism: American Geophysical Union, International Symposium on the Rio Grande Rift, p. 289–312.

Lipman, P.W., Mehnert, H.H., and Naeser, C.W., 1986, Evolution of the Latir volcanic field, northern New Mexico, and its relation to the Rio Grande rift, as indicated by potassium-argon and fission track dating: Journal of Geophysical Research, v. 91, no. B6, p. 6329–6345, https://doi.org/10.1029/JB091iB06p06329.

Lipman, P.W., and Reed, J.C., 1989, Geologic map of the Latir volcanic field and adjacent areas, northern New Mexico: U.S. Geological Survey Miscellaneous Investigations Series Map I-1907, scale 1:48,000.

Lipman, P.W., Sawyer, D.A., and Hon, K., 1989, Central San Juan caldera cluster, *in* Chapin, C.E., and Zidek, J., eds., Field excursions to volcanic terranes in the western United States, Volume I—Southern Rocky Mountain region: New Mexico Bureau of Mines and Mineral Resources Memoir 46, p. 330–350.

Lipman, P.W., and Steven, T.A., 1970, Reconnaissance geology and economic significance of the Platoro caldera, southeastern San Juan Mountains, Colorado: U.S. Geological Survey Professional Paper 700-C, p. C19–C29.

Lipman, P.W., and Steven, T.A., 1971, Reconnaissance geology and economic significance of Platoro caldera, San Juan Mountains, Colorado: New Mexico Geological Society Guidebook, 22nd Fall Field Conference Guidebook, San Luis Basin, Colorado, p. 221–230.

Lipman, P.W., Steven, T.A., and Mehnert, H.A., 1970, Volcanic history of the San Juan Mountains, Colorado, as indicated by potassium-argon dating: Geological Society of America Bulletin, v. 81, no. 8, p. 2329–2352, https://doi.org/10.1130/0016-7606(1970)81[2329:VHOTSJ]2.0.CO;2.

Lipman, P.W., and Weston, P.E., 2001, Phenocryst compositions of late ash-flow tuffs from the central San Juan caldera cluster—Results from Creede drill-hole samples and implications for regional stratigraphy, *in* Bethke, P.M., ed., Preliminary scientific results of the Creede caldera continental scientific drilling program: U.S. Geological Survey Open-File Report 94-260-B, 43 p., https://doi.org/10.3133/ofr94260B.

Lipman, P.W., and Zimmerer, M.J., 2019, Magmato-tectonic links—Ignimbrite calderas, regional dike swarms, and the transition from arc to rift in the southern Rocky Mountains: Geosphere, v. 15, no. 6, p.1893–1926, https://doi.org/10.1130/GES02068.1.

Lipman, P.W., Zimmerer, M.J., and McIntosh, W.C., 2015, An ignimbrite caldera from the bottom up—Exhumed floor and fill of the resurgent Bonanza caldera, southern Rocky Mountain volcanic field, Colorado: Geosphere, v. 11, no. 6, p. 1902–1947, https://doi.org/10.1130/GES01184.1.

Lubbers, J., Deering, C., and Bachmann, O., 2020, Genesis of rhyolitic melts in the upper crust—Fractionation and remobilization of an intermediate cumulate at Lake City caldera, Colorado, USA: Journal of Volcanology and Geothermal Research, v. 392, 106750, https://doi.org/10.1016/j.jvolgeores.2019.106750.

Ludington, S., 1981, Quartz-pyrite-molybdenite stockwork near South Fork Peak, Taos County, New Mexico: U.S. Geological Survey Open-File Report 81-1080, 8 p., https://doi.org/10.3133/ofr811080.

MacDonald, G.A., and Katsura, I., 1964, Chemical composition of Hawaiian lavas: Journal of Petrology, v. 5, p. 82–133, http://dx.doi.org/10.1093/petrology/5.1.82.

Machette, M.N., Thompson, R.A., Marchetti, D.W., and Kirkham, R.M., 2007, Field trip day 2—Quaternary geology of Lake Alamosa and the Costilla Plain, southern Colorado, chap. B *of* Machette, M.N., Coates, M.-M., and Johnson, M.J., eds., 2007 Rocky Mountain section friends of the Pleistocene field trip—Quaternary geology of the San Luis basin of Colorado and New Mexico, September 7–9, 2007: U.S. Geological Survey Open-File Report 2007–1193, p. 53–109.

Machette, M.N., and Personius, S.F., 1984, Quaternary and Pliocene faults in the eastern part of the Aztec quadrangle and the western part of the Raton quadrangle, northern New Mexico: U.S. Geological Survey Miscellaneous Field Studies Map 1465-B, scale 1:250,000.

Machette, M.N., Thompson, R.A., Marchetti, D.W., and Smith, R.S., 2013, Evolution of ancient Lake Alamosa and integration of the Rio Grande during the Pliocene and Pleistocene, *in* Hudson, M.R., and Grauch, V.J.S., eds., New perspectives on Rio Grande rift basins—From tectonics to groundwater: Geological Society of America Special Paper 494, p. 1–20, https://doi.org/10.1130/2013.2494(01).

Machida, H., Arai, F., and Momose, M., 1985, Aso-4 ash—A widespread tephra and its implications to the events of late Pleistocene in and around Japan: Volcanological Society of Japan Bulletin, v. 30, p. 49–70.

Magnani, M.B., Levander, A., Miller, K.C., Eshete, T., and Karlstrom, K.E., 2005, Seismic investigation of the Yavapai-Mazatzal transition zone and the Jemez lineament in northeastern New Mexico, *in* Karlstrom, K.E., and Keller, G.R., eds., The Rocky Mountain region—An evolving lithosphere tectonics, geochemistry and geophysics: American Geophysical Union Monograph, v. 154, p. 227–238, https://doi.org/10.1029/154GM16.

Magnani, M.B., Miller, K.C., Levander, A., and Karlstrom, K., 2004, The Yavapai-Mazatzal boundary—A long-lived tectonic element in the lithosphere of southwestern North America: Geological Society of America Bulletin, v. 116, no. 9, p. 1137–1142, https://doi.org/10.1130/B25414.1.

Manley, K., 1981, Redefinition and description of the Los Piños Formation of north-central New Mexico: Geological Society of America Bulletin, v. 92, no. 12, p. 984–989, https://doi.org/10.1130/0016-7606(1981)92<984:RADOTL>2.0.CO;2.

Manley, K., 1982a, Geologic map of the Bighorn Peak quadrangle, Rio Arriba County, New Mexico and Conejos County, Colorado: U.S. Geological Survey Miscellaneous Field Studies Map 1451, scale 1:24,000.

Manley, K., 1982b, Geologic map of the Broke Off Mountain quadrangle, Rio Arriba County, New Mexico: U.S. Geological Survey Miscellaneous Field Studies Map 1450, scale 1:24,000.

Marsh, B.D., 1984, On the mechanics of caldera resurgence: Journal of Geophysical Research, v. 89, B10, p. 8245–8251, https://doi.org/10.1029/JB089iB10p08245.

May, S.J., 1984, Exhumed mid-Miocene volcanic field in the Tesuque Formation, northern Española basin, New Mexico, *in* Baldridge, W.S., Dickerson, P.W., Riecker, R.E., and Zidek, J., eds., Rio Grande rift—Northern New Mexico: New Mexico Geological Society, 35th Fall Field Conference Guidebook, p. 171–178.

McDowell, F.W., and Clabaugh, S.E., 1979, Ignimbrites of the Sierra Madre Occidental and their relation to the tectonic history of western Mexico, *in* Chapin, C.E., and Elston, W.E., eds., Ash-flow tuffs: Geological Society of America Special Paper 180, p. 113–124, https://doi.org/10.1130/SPE180-p113.

McDowell, F.W., and McIntosh, W.C., 2012, Timing of intense magmatic episodes in the northern and central Sierra Madre Occidental, western Mexico: Geosphere, v. 8, no. 6, p. 1505–1526, https://doi.org/10.1130/GES00792.1.

McIntosh, W.C., and Chapin, C.E., 2004, Geochronology of the central Colorado volcanic field, *in* Cather, S.M., McIntosh, W.C., and Shari A. Kelley, S.A., eds., Tectonics, geochronology, and volcanism in the southern Rocky Mountains and Rio Grande rift**:** New Mexico Bureau of Geology and Mineral Resources Bulletin 160, p. 205–238.

McIntosh, W.C., Chapin, C.E., Ratté, J.C., and Sutter, J.F., 1992, Time-stratigraphic framework for the Eocene-Oligocene Mogollon Datil volcanic field, southwest New Mexico: Geological Society of America Bulletin, v. 104, no. 7, p. 851–871, https://doi.org/10.1130/0016-7606(1992)104<0851:TSFFTE>2.3.CO;2.

McMillan, N.J., and Dungan, M.A., 1986, Magma mixing as a petrogenetic process in the development of the Taos Plateau volcanic field, New Mexico: Journal of Geophysical Research, v. 91, B6, p. 6029–6045, https://doi.org/10.1029/JB091iB06p06029.

McMillan, N.J., and Dungan, M.A., 1988, Open system magmatic evolution of the Taos Plateau volcanic field, northern New Mexico—3.Petrology and geochemistry of andesite and dacite: Journal of Petrology, v. 29, no. 3, p. 527–557, https://doi.org/10.1093/petrology/29.3.527.

Mehnert, H.H., Lipman, P.W., and Steven, T.A., 1973, Age of mineralization at Summitville, Colorado, as indicated by K-Ar dating of alunite: Economic Geology, v. 68, no. 3, p. 399–401, https://doi.org/10.2113/gsecongeo.68.3.399.

Menges, C.M., 1987, Temporal and spatial segmentation of Pliocene-Quaternary fault rupture along the western Sangre de Cristo mountain front, northern New Mexico, *in* Crone, A.J., and Omdahl, E.M., eds., Proceedings of Conference XXXIX—Directions in Palaeoseismology: U.S. Geological Survey Open-File Report 87-673, p. 203–222, https://pubs.usgs.gov/of/1987/0673/report.pdf.

Menges, C.M., 1990, Late Cenozoic rift tectonics and mountain-front landforms of the Sangre de Cristo Mountains near Taos, northern New Mexico, *in* Bauer, P.W., Lucas, S.G., Mawer, C.K., and McIntosh, W.C., eds., Tectonic development of the southern Sangre de Cristo Mountains, New Mexico: New Mexico Geological Society, 41st Fall Field Conference Guidebook, p. 113–122.

Merle, O., 2011, A simple continental rift classification: Tectonophysics, v. 513, no. 1–4, p. 88–95, https://doi.org/10.1016/j.tecto.2011.10.004.

Middlemost, E.A.K., 1989, Iron oxidation ratios, norms and the classification of volcanic rocks: Chemical Geology, v. 77, no. 1, p. 19–26, https://doi.org/10.1016/0009-2541(89)90011-9.

Miggins, D.P., 2002, Chronologic, geochemical, and isotopic framework of igneous rocks within the Raton Basin and adjacent Rio Grande Rift, south-central Colorado and northern New Mexico: Boulder, University of Colorado, M.S. Thesis, 417 p.

Miggins, D.P., Thompson, R.A., Pillmore, C.L., Snee, L.W., and Stern, C.R., 2002, Extension and uplift of the northern Rio Grande rift—Evidence from $^{40}Ar/^{39}Ar$ geochronology from the Sangre de Cristo Mountains, south-central Colorado and northern New Mexico, *in* Menzies, M.A., Klemperer, S.L., Ebinger, C.J., and Baker, J., eds., Volcanic rifted margins: Geological Society of America Special Paper 362, p. 47–64, https://doi.org/10.1130/0-8137-2362-0.47.

Miller, T.P., and Smith, R.L., 1977, Spectacular mobility of ash flows around Aniakchak and Fisher calderas, Alaska: Geology, v. 5, no. 3, p. 173–176, https://doi.org/10.1130/0091-7613(1977)5<173:SMOAFA>2.0.CO;2.

Mills, R.D., and Coleman, D.S., 2013, Temporal and chemical connections between plutons and ignimbrites from the Mount Princeton magmatic center: Contributions to Mineralogy and Petrology, v. 165, no. 5, p. 961–980, https://doi.org/10.1007/s00410-012-0843-4.

Minor, S.A., Caine, J.S., Hudson, M.R., Fridrich, C.J., and Ruleman, C.A., 2016, An enigmatic mountain-block extensional transfer zone within the central Colorado Rio Grande rift [abs.]: Geological Society of America Abstracts with Programs, v. 48, no. 7, https://doi.org/10.1130/abs/2016AM-283840.

Montgomery, A., 1953, Pre-Cambrian geology of the Picuris Range, north-central New Mexico: New Mexico Bureau of Mines and Mineral Resources Bulletin 30, 89 p.

Morgan, L.E., Johnstone, S.A., Gilmer, A.K, Cosca, M.A., and Thompson, R.A., 2019, A supervolcano and its sidekicks—A 100 ka eruptive chronology of the Fish Canyon Tuff and associated units of the La Garita magmatic system, Colorado, USA: Geology, v. 5, p. 453–456, https://doi.org/10.1130/G45898.1.

Morgan, P., and Golombek, M.P., 1984, Factors controlling the phases and styles of extension in the northern Rio Grande rift, *in* Baldridge, W.S., Dickerson, P.W., Riecker, R.E., and Zidek, J., eds., Rio Grande rift—Northern New Mexico: New Mexico Geological Society, 35th Fall Field Conference Guidebook, p. 13–19.

Morgan, P., Seager, W.R., and Golombek, M.P., 1986, Cenozoic thermal, mechanical and tectonic evolution of the Rio Grande rift: Journal of Geophysical Research, v. 91, B6, p. 6263–6276, https://doi.org/10.1029/JB091iB06p06263.

Muehlberger, W.R., 1968, Geologic map of the Brazos Peak fifteen-minute quadrangle, New Mexico and Colorado: New Mexico Bureau of Geology and Mineral Resources Geologic Map 22, scale 1:48,000.

Muehlberger, W.R., 1978, Frontal fault zone of northern Picuris Range, *in* Hawley, J.W., Guidebook to Rio Grande rift in New Mexico and Colorado: New Mexico Bureau of Mines and Mineral Resources Circular 163, p. 44–45.

Muehlberger, W.R., 1979, The Embudo fault between Pilar and Arroyo Hondo, New Mexico— An active intracontinental transform fault, *in* Ingersoll, R.V., Woodward, L.A., and James, H.L., eds., Guidebook of Santa Fe Country: New Mexico Geological Society, 30th Fall Field Conference Guidebook, p. 77–82.

Nielson, D.L., and Hulen, J.B., 1984, Internal geology and evolution of the Redondo Dome, Valles caldera, New Mexico: Journal of Geophysical Research, v. 89, B10, p. 8695–8712, https://doi.org/10.1029/JB089iB10p08695.

Neumann, E.-R., and Ramberg, I.B., eds., 1978, Petrology and geochemistry of continental rifts: Dordrecht, Reidel, 296 p., https://doi.org/10.1007/978-94-009-9803-2.

Olson, J.C., 1983, Geologic and structural maps and sections of the Marshall Pass Mining District, Saguache, Gunnison, and Chafee Counties, Colorado: U.S. Geological Survey Miscellaneous Investigations Series Map I-1425, scale 1:24,000.

Olson, J.C., 1988, Geology and ore deposits of the Cochetopa and Marshall Pass districts, Saguache and Gunnison Counties, Colorado: U.S. Geological Survey Professional Paper 1457, 44 p.

Ono, K., Kubotera, A., and Ota, K., 1981, Aso Volcano, *in* Kubotera, A., ed., Field excursion guide to Sakurajima, Kirishima, and Aso Volcanoes: Tokyo, Volcanological Society of Japan, p. 33–52.

Parat, F., Dungan, M.A., and Lipman, P.W., 2005, Contemporaneous trachyandesitic and calc-alkaline volcanism of the Huerto Andesite, San Juan volcanic field, Colorado, U.S.A.: Journal of Petrology, v. 46, no. 5, p. 859–891, https://doi.org/10.1093/petrology/egi003.

Parker, D.F., Ghosh, A., Price, C.W., Rinard, B.D., Cullers, R.L., and Ren, M., 2005, Origin of rhyolite by crustal melting and the nature of parental magmas in the Oligocene Conejos Formation, San Juan Mountains, Colorado, USA: Journal of Volcanology and Geothermal Research, v. 139, no. 3–4, p. 185–210, https://doi.org/10.1016/j.jvolgeores.2004.08.015.

Parmigiani, A., Huber, C., and Bachmann, O., 2014, Mush microphysics and the reactivation of crystal-rich magma reservoirs: Journal of Geophysical Research,, v. 119, no. 8, p. 6308–6322, https://doi.org/10.1002/2014JB011124.

Patton, H.B., 1916, Geology and ore deposits of the Bonanza District, Saguache County, Colorado: Colorado State Geological Survey Bulletin 9, 136 p.

Patton, H.B., 1917, Geology and ore deposits of the Platoro-Summitville mining district, Colorado: Colorado Geological Survey Bulletin 13, 122 p.

Pazzaglia, F.J., Woodward, L.A., Lucas, S.G., Anderson, O.J., Wegmann, K.W., and Estep, J.W., 1999, Phanerozoic geologic evolution of the Albuquerque area, *in* Pazzaglia, F.J., and Lucas, S.G., eds., Albuquerque geology: New Mexico Geological Society, 50th Fall Field Conference Guidebook, p. 97–114.

Perkins, M.E., Brown, F.H., Nash, W.P., Williams, S.K., and McIntosh, W., 1998, Sequence, age, and source of silicic fallout tuffs in middle to late Miocene basins of the northern Basin and Range province: Geological Society of America Bulletin, v. 110, no. 3, p. 344–360, https://doi.org/10.1130/0016-7606(1998)110<0344:SAASOS>2.3.CO;2.

Perkins, R.M., and Nieman, G.W., 1982, Epithermal gold mineralization in the South Mountain volcanic dome, Summitville, Colorado *in* The genesis of Rocky Mountain ore deposits—Changes with time and tectonics: Society of Exploration Geologists, Denver Region, November 4–5, Symposium Proceedings, p. 165–172.

Peterson, C.M., 1981, Late Cenozoic stratigraphy and structure of the Taos Plateau, northern New Mexico: Austin, University of Texas, M.S. thesis, 57 p.

Phillips, E.H., Goff, F., and Kyle, P.R., 2006, The Deer Canyon and Redondo Creek Members of the Valles Rhyolite Formation—Field relationships, mineral chemistry, and magnetite/ilmenite temperature of formation for the Redondo Creek Rhyolite, *in* Kues, B.S., Kelley, S.A., and Lueth, V.W., eds., Geology of the Jemez region II: New Mexico Geological Society, 58th Fall Field Conference Guidebook, p. 90–91.

Phillips, E.H., Goff, F., Kyle, P.R., McIntosh, W.C., Dunbar, N.W., and Gardner, J.N., 2007, The $^{40}Ar/^{39}Ar$ age constraints on the duration of resurgence at the Valles caldera, New Mexico: Journal of Geophysical Research, v. 112, B8, B08201, https://doi.org/10.1029/2006JB004511.

Plouff, D., and Pakiser, L.C., 1972, Gravity study of the San Juan Mountains, Colorado: U.S. Geological Survey Professional Paper 800-B, p. B183–B190.

Poland, M.P., Moats, W.P., and Fink, J.H., 2008, A model for radial dike emplacement in composite cones based on observations from Summer Coon volcano, Colorado, USA: Bulletin of Volcanology, v. 70, no. 7, p. 861–875, https://doi.org/10.1007/s00445-007-0175-9.

Powell, J.W., 1895, Canyons of the Colorado: Meadville, Pa., The Chatauqua-Century Press, 428 p.

Ratté, J.C., Marvin, R.F., Naeser, C.W., and Bikerman, M., 1984, Calderas and ash flow tuffs of the Mogollon Mountains, southwestern New Mexico: Journal of Geophysical Research, v. 89, B10, p. 8713–8732, https://doi.org/10.1029/JB089iB10p08713.

Ratté, J.C., and Steven, T.A., 1967, Ash flows and related volcanic rocks associated with the Creede caldera, San Juan Mountains, Colorado: U.S. Geological Survey Professional Paper 524-H, 58 p., https://doi.org/10.3133/pp524H.

Read, A.S., Bauer, P.W., Thompson, R.A., Kelson, K.I., and Muehlberger, W.R., 2004, The Taos Plateau and the Rio Grande gorge—First day road log from Taos to Questa, the Wild Rivers Recreation area, Arroyo Hondo, the Dunn Bridge, the Rio Grande gorge bridge, and return to Taos, *in* Brister, B., Bauer, P.W., Read, A.S., and Lueth, V.W., eds., Geology of the Taos region: New Mexico Geological Society, 55th Fall Field Conference Guidebook, p. 1–7.

Reiche, P., 1937, The toreva-block—A distinctive landslide type: Journal of Geology, v. 45, no. 5, p. 538–548, https://doi.org/10.1086/624563.

Renne, P.R., Mundil, R., Balco, G., Min, K., and Ludwig, K.R., 2010, Joint determination of ^{40}K decay constants and $^{40}Ar^*/^{40}K$ for the Fish Canyon sanidine standard, and improved accuracy for $^{40}Ar/^{39}Ar$ geochronology: Geochimica et Cosmochimica Acta, v. 74, no. 18, p. 5349–5367, https://doi.org/10.1016/j.gca.2010.06.017.

Renne, P.R., Swisher, C.C., Deino, A.L., Karner, D.B., Owens, T.L., and DePaolo, D.J., 1998, Intercalibration of standards, absolute ages and uncertainties in $^{40}Ar/^{39}Ar$ dating: Chemical Geology, v. 145, no. 1–2, p. 117–152, https://doi.org/10.1016/S0009-2541(97)00159-9.

Repasch, M., Karlstrom, K., Heizler, M., and Pecha, M., 2017, Birth and evolution of the Rio Grande fluvial system in the past 8 Ma—Progressive downward integration and the influence of tectonics, volcanism, and climate: Earth-Science Reviews, v. 168, p. 113–164, https://doi.org/10.1016/j.earscirev.2017.03.003.

Riciputi, L.R., 1991, Petrology and Nd, Sr, and Pb isotopes of the central San Juan caldera cluster, Colorado: University of Wisconsin, Madison, Ph.D. thesis, 2 volumes.

Riciputi, L.R., and Johnson, C.M., 1990, Nd and Pb isotope variations in the multicyclic central caldera cluster of the San Juan volcanic field, Colorado, and implications for crustal hybridization: Geology, v. 18, no. 10, p. 975–978, https://doi.org/10.1130/0091-7613(1990)018<0975:NAPIVI>2.3.CO;2.

Riciputi, L.R., Johnson, C.M., Sawyer, D.A., and Lipman, P.W., 1995, Crustal and magmatic evolution in a large multicyclic caldera complex—Isotopic evidence from the central San Juan volcanic field: Journal of Volcanology and Geothermal Research, v. 67, no. 1–3, p. 1–28, https://doi.org/10.1016/0377-0273(94)00097-Z.

Ricketts, J.W., 2014, Structural evolution of the Rio Grande rift—Synchronous exhumation of rift flanks from 20-10 Ma, embryonic core complexes, and fluid-enhanced Quaternary extension: Albuquerque, University of New Mexico, Ph.D. dissertation, 222 p.

Ricketts, J.W., Kelley, S.A., Karlstrom, K.E., Schmandt, B., Donahue, M.S., and van Wijk, J., 2016, Synchronous of the Rio Grande rift along its entire length at 25-10 Ma supported by apatite (U–Th)/He and fission-track thermochronology, and evaluation of possible driving mechanisms: Geological Society of America Bulletin, v. 128, no. 3-4, p. 397–424.

Ridolfi, F., Renzulli, A., and Puerini, M., 2010, Stability and chemical equilibrium of amphibole in calc-alkaline magmas—An overview, new thermobarometric formulations and application to subduction-related volcanoes: Contributions to Mineralogy and Petrology, v. 160, no. 1, p. 45–66.

Rivera, T.A., Storey, M., Zeeden, C., Hilgen, F.J., and Kuiper, K., 2011, A refined astronomical calibrated $^{40}Ar/^{39}Ar$ age for Fish Canyon sanidine: Earth and Planetary Science Letters, v. 311, no. 3–4, p. 420–426, https://doi.org/10.1016/j.epsl.2011.09.017.

Ross, C.S., and Smith, R.L., 1961, Ash-flow tuffs—Their origin, geologic relations, and identification: U.S. Geological Survey Professional Paper 366, 80 p.

Rowe, M.C., Lassiter, J.C., and Goff, K., 2015, Basalt volatile fluctuations during continental rifting—An example from the Rio Grande rift, USA: Geochemistry Geophysics Geosystems, v. 16, no. 5, p. 1254–1273, https://doi.org/10.1002/2014GC005649.

Rowe, M.C., Wolff, J.A., Gardner, J.N., Ramos, F.C., Teasdale, R., and Heikoop, C.E., 2007, Development of a continental volcanic field—Petrogenesis of pre-caldera intermediate and silicic rocks and origin of the Bandelier magmas, Jemez Mountains (New Mexico, USA): Journal of Petrology, v. 48, no. 11, p. 2063–2091, https://doi.org/10.1093/petrology/egm050.

Ruleman, C., and Machette, M., 2007, An overview of the Sangre de Cristo fault system and new insights to interactions between Quaternary faults in the northern Rio Grande rift, chap. J *of* Machette, M.N., Coates, M.M., and Johnson, M.L., eds., 2007 Rocky Mountain section friends of the Pleistocene field trip—Quaternary geology of the San Luis basin of Colorado and New Mexico, September 7–9, 2007: U.S. Geological Survey Open-File Report 2007–1193, p. 187–197.

Ruleman, C.A., Machette, M.N., Thompson, R.A., Miggins, D.P., Goehring, B.M., and Paces, J.B., 2016, Geomorphic evolution of the San Luis Basin and Rio Grande in southern Colorado and northern New Mexico, *in* Keller, S.M., and Morgan, M.L., eds., Unfolding the geology of the West: Geological Society of America Field Guide 44, p. 291–333, https://doi.org/10.1130/2016.0044(13).

Ruleman, C.A., Thompson, R.A., Shroba, R.R., Anderson, M.L., Drenth, B.J., Rotzien, J., and Lyon, J., 2013, Late Miocene-Pleistocene evolution of a Rio Grande rift subbasin, Sunshine Valley-Costilla Plain, San Luis Basin, New Mexico and Colorado, *in* Hudson, M.R., and Grauch, V.J.S., eds., New perspectives on Rio Grande rift basins—From tectonics to groundwater: Geological Society of America Special Paper 494, p. 47–73, https://doi.org/10.1130/2013.2494(03).

Rye, R.O., Bethke, P.M., and Finkelstein, D.B., 2000, Stable isotope evolution and paleolimnology of ancient Lake Creede, *in* Bethke, P.M., and Hay, R.L., eds., Ancient Lake Creede—Its volcano-tectonic setting, history of sedimentation and relation to mineralization in the Creede Mining District: Geological Society of America Special Paper 346, p. 233–265, https://doi.org/10.1130/0-8137-2346-9.233.

Salisbury, M.J., Jicha, B.R., de Silva, S.L., Singer, B.S., Jimenez, N.C., and Ort, M.H., 2011, $^{40}Ar/^{39}Ar$ chronostratigraphy of Altiplano-Puna volcanic complex ignimbrites reveals the development of a major magmatic province: Geological Society of America Bulletin, v. 123, no. 5–6, p. 821–840., https://doi.org/10.1130/B30280.1.

Samuels, K.E., Broxton, D.E., Vaniman, D.T., Woldegabriel, G., Wolff, J.A., Hickmott, D.D., Kluk, E.C, and Fittipaldo, M.M., 2007, Distribution of dacite lavas beneath the Pajarito Plateau, Jemez Mountains, New Mexico, in Kues, B.S., Kelley, S.A., and Lueth, V.W., eds., Geology of the Jemez region II: New Mexico Geological Society, 58th Fall Field Conference Guidebook, p. 296–307.

Sawyer, D.A., Shroba, R.R., Minor, S.A., and Thompson, R.A., 2002, Geologic map of the Tetilla Peak quadrangle, Santa Fe and Sandoval Counties, New Mexico: U.S. Geological Survey Miscellaneous Field Studies Map 2352, scale 1:24,000.

Scholle, P.A., and Ulmer-Scholle, D.S., 2003, A color guide to the petrography of carbonate rocks—Grains, textures, porosity, diagenesis: Tulsa, Okla., American Association of Petroleum Geologists, 474 p.

Scott, G.R., Van Alstine, R.E., and Sharp, W.N., 1975, Geologic map of the Poncha Springs quadrangle, Chaffee County, Colorado: U.S. Geological Survey Miscellaneous Field Studies Map 658, scale 1:62,500.

Seager, W.R., Shafiqullah, M., Hawley, J.W., and Marvin, R.F., 1984, New K-Ar dates from basalts and the evolution of the southern Rio Grande rift: Geological Society of America Bulletin, v. 95, no. 1, p. 87–99, https://doi.org/10.1130/0016-7606(1984)95<87:NKDFBA>2.0.CO;2.

Self, S., Goff, F., Gardner, J.N., Wright, J.V., and Kite, W.M., 1986, Explosive rhyolitic volcanism in the Jemez Mountains—Vent locations, caldera development, and relations to regional structure: Journal of Geophysical Research, v. 91, B2, p. 1779–1798, https://doi.org/10.1029/JB091iB02p01779.

Self, S., Heiken, G., Sykes, M.L., Wohletz, K., Fisher, R.V., and Dethier, D.P., 1996, Field excursions to the Jemez Mountains, New Mexico: New Mexico Bureau of Geology and Mineral Resources Bulletin 134, 72 p.

Self, S., and Wright, J.V., 1983, Large wave forms from the Fish Canyon Tuff, Colorado: Geology, v. 11, no. 8, p. 443–446, https://doi.org/10.1130/0091-7613(1983)11<443:LWFFTF>2.0.CO;2.

Sengör, A.M.C., 1995, Sedimentation and tectonics of fossil rifts, *in* Busby, C.J., and Ingersoll, R.V., eds., Tectonics of sedimentary basins: Oxford, Blackwell Science, p. 53–117, http://dx.doi.org/10.1016/j.earscirev.2017.03.003 0012-8252.

Sengör, A.M.C., and Burke, K., 1978, Relative timing of rifting and volcanism on earth and its tectonic implications: Geophysical Research Letters, v. 5, no. 6, p. 419–421, https://doi.org/10.1029/GL005i006p00419.

Sengör, A.M.C., and Natal'in, B.A., 2001, Rifts of the world, *in* Ernst, R.E., and Buchan, K.L., eds., Mantle plumes—Their identification through time: Geological Society of America Special Paper 352, p. 389–482, https://doi.org/10.1130/0-8137-2352-3.389.

Shannon, J.R., 1988, Geology of the Mount Aetna Cauldron Complex: Golden, Colorado School of Mines, Ph.D. dissertation, 434 p.

Shaw, C.A., and Karlstrom, K.E., 1999, The Yavapai-Mazatzal crustal boundary in the southern Rocky Mountains: Rocky Mountain Geology, v. 34, no. 1, p. 37–52, https://doi.org/10.2113/34.1.37.

Shroba, R.R., Thompson, R.A., Schmidt, D.L., and Personius, S.F., Maldonado, F., and Brandt, T.R., 2011, Geologic map of the La Mesita Negra SE quadrangle, Bernalillo County, New Mexico: U.S. Geological Survey Miscellaneous Field Studies Map 2416, scale 1:24,000.

Singer, B.S., 1985, Petrology and geochemistry of Polvadera Group rocks of La Grulla Plateau, northwestern Jemez volcanic field, New Mexico—Evidence favoring evolution by assimilation-fractional crystallization (AFC): Albuquerque, University of New Mexico, M.S. thesis, 148 p.

Skuba, C.E., 1990, Sr, Nd, Pb and O isotopic constraints on the genesis and evolution of the Bandelier Tuff: University of Texas at Arlington, M.S. thesis, 98 p.

Slate, J.L., Sarna-Wojcicki, A.M., Koning, D.J., Wan, E., Wahl, D.B., Connell, S.D., and Perkins, M.E., 2013, Upper Neogene tephrochronologic correlations of the Española Basin and Jemez Mountains volcanic field, northern Rio Grande rift, north-central New Mexico, *in* Hudson, M.R., and Grauch, V.J.S., eds., New perspectives on Rio Grande rift basins—From tectonics to groundwater: Geological Society of America Special Paper 494, p. 303–322, https://doi.org/10.1130/2012.2494(12).

Sliwinski, J.T., Bachmann, O., Dungan, M.A., Huber, C., Deering, C.D., Lipman, P.W., Martin, L.H., and Liebske, C., 2017, Rapid pre-eruptive thermal rejuvenation in a large silicic magma body—The case of the Masonic Park Tuff, southern Rocky Mountain volcanic field, CO, USA: Contributions to Mineralogy and Petrology, v. 172, no. 5, 20 p., https://doi.org/10.1007/s00410-017-1351-3.

Sliwinski, J., Farsky, D., Lipman, P.W., Guillong, M., and Bachmann, O., 2019, Rapid magma generation or shared magmatic reservoir? Petrology and geochronology of the Rat Creek and Nelson Mountain Tuffs, CO, USA: Frontiers in Earth Science, v. 7, p.271, https://doi.org/10.3389/feart.2019.00271.

Smith, G.A., 2004, Middle to late Cenozoic development of the Rio Grande rift and adjacent regions in northern New Mexico, *in* Mack, G.H., and Giles, K.A., eds., The geology of New Mexico—A geologic history: New Mexico Geological Society Special Publication 11, p. 331–358.

Smith, H.T.U., 1938, Tertiary geology of the Abiquiu quadrangle, New Mexico: Journal of Geology, v. 46, no. 7, p. 933–965, https://doi.org/10.1086/624710.

Smith, R.L., 1960a, Ash flows: Geological Society of America Bulletin, v. 71, no. 6, p. 795–842, https://doi.org/10.1130/0016-7606(1960)71[795:AF]2.0.CO;2.

Smith, R.L., 1960b, Zones and zonal variations in welded ash flows: U.S. Geological Survey Professional Paper 354-F, p. 149–159.

Smith, R.L., 1979, Ash-flow magmatism, *in* Chapin, C.E., and Elston, W.E., eds., Ash-flow tuffs: Geological Society of America Special Paper 180, p. 5–28, https://doi.org/10.1130/SPE180-p5.

Smith, R.L., and Bailey, R.A., 1966, The Bandelier Tuff—A study of zoned ash-flow eruption cycles from zoned magma chambers: Bulletin Volcanologique, v. 29, no. 1, p. 83–103, https://doi.org/10.1007/BF02597146.

Smith, R.L., and Bailey, R.A., 1968, Resurgent cauldrons, *in* Coates, R.R., Hay, R.L., and Anderson, C.A., eds., Studies in volcanology: Geological Society of America Memoir 116, p. 613–662, https://doi.org/10.1130/MEM116-p613.

Smith, R.L., Bailey, R.A., and Ross, C.S., 1970, Geologic map of the Jemez Mountains, New Mexico: U.S. Geological Survey Miscellaneous Geological Investigations Map I-571, scale 1:125,000.

Sparks, R.S.J., Francis, P.W., Hamer, R.D., Pankhurst, R.J., O'Callaghan, L.O., Thorpe, R.S., and Page, R., 1985, Ignimbrites of the Cerro Galan Caldera, NW Argentina: Journal of Volcanology and Geothermal Research, v. 24, no. 3–4, p. 205–248, https://doi.org/10.1016/0377-0273(85)90071-X.

Spell, T.L., and Harrison, T.M., 1993, $^{40}Ar/^{39}Ar$ geochronology of post-Valles caldera rhyolites, Jemez volcanic field, New Mexico: Journal of Geophysical Research, v. 98, B5, p. 8031–8051, https://doi.org/10.1029/92JB01786.

Spell, T.L., and Kyle, P.R., 1989, Petrogenesis of Valles Grande Member rhyolites, Valles Caldera, New Mexico—Implications for evolution of the Jemez Mountains magmatic system: Journal of Geophysical Research, v. 94, no. B8, p. 10379–10396.

Spell, T.L., Kyle, P.R., and Baker, J., 1996a Geochronology and geochemistry of the Cerro Toledo Rhyolite, *in* Goff, F., Kues, B.S., Rogers, M.A., McFadden, L.D., and Gardner, J.N., eds., The Jemez Mountains region: New Mexico Geological Society, 47th Fall Field Conference Guidebook, p. 263–268.

Spell, T.L., McDougall, I., and Doulgeris, A.P., 1996b, Cerro Toldedo Rhyolite, Jemez Volcanic Field, New Mexico—$^{40}Ar/^{39}Ar$ geochronology of eruptions between two caldera-forming events: Geological Society of America Bulletin, v. 108, no. 12, p. 1549–1566, https://doi.org/10.1130/0016-7606(1996)108<1549:CTRJVF>2.3.CO;2.

Spiegel, Z., and Baldwin, B., 1963, Geology and water resources of the Santa Fe area, New Mexico: U.S. Geological Survey Water-Supply Paper 1525, 258 p.

Steck, L.K., Thurber, C.H., Fehler, M.C., Lutter, W.J., Roberts, P.M., Baldridge, W.S., Stafford, D.G., and Sessions, R.K., 1998, Crust and upper mantle P wave velocity structure beneath Valles caldera, New Mexico—Results from the Jemez teleseismic tomography experiment: Journal of Geophysical Research, v. 103, B10, p. 24301–24320, https://doi.org/10.1029/98JB00750.

Steiger, R.H., and Jäger, E., 1977, Subcommission on geochronology—Convention on use of decay constants in geochronology and cosmochronology: Earth and Planetary Science Letters, v. 36, no. 3, p. 359–362, https://doi.org/10.1016/0012-821X(77)90060-7.

Steinpress, M.G., 1980, Neogene stratigraphy and structure of the Dixon area, Española basin, north-central New Mexico: Albuquerque, University of New Mexico, M.S. thesis, 127 p.

Steven, T.A., 1967, Geologic map of the Bristol Head quadrangle, Mineral and Hinsdale Counties, Colorado: U.S. Geological Survey Map GQ-631, scale 1:62,500.

Steven, T.A., 1968, Critical review of the San Juan peneplain, southwestern Colorado: U.S. Geological Survey Professional Paper 594-I, 19 p., https://doi.org/10.3133/pp594I.

Steven, T.A., 1975, Middle Tertiary volcanic field in the southern Rocky Mountains, *in* Curtis, B.F., ed., Cenozoic history of the southern Rocky Mountains: GSA Memoir 144, p. 75–94, https://doi.org/10.1130/MEM144-p75.

Steven, T.A., and Eaton, G.P., 1975, Environment of ore deposition in the Creede mining district, San Juan Mountains, Colorado; I. Geologic, hydrologic, and geophysical setting: Economic Geology, v. 70, no. 6, p. 1023–1037, https://doi.org/10.2113/gsecongeo.70.6.1023.

Steven, T.A., Hon, K., and Lanphere, M.A., 1995, Neogene geomorphic evolution of the central San Juan Mountains near Creede, Colorado: U.S. Geological Survey Miscellaneous Investigations Series Map I-2504, scale 1:100,000.

Steven, T.A., and Lipman, P.W., 1973, Geologic map of the Spar City quadrangle, Mineral County, Colorado: U.S. Geological Survey Map GQ-1052, scale 1:62,500.

Steven, T.A., and Lipman, P.W., 1976, Calderas of the San Juan volcanic field, southwestern Colorado: U.S. Geological Survey Professional Paper 958, 35 p.

Steven, T.A., Lipman, P.W., Hail, W.J., Jr., Barker, F., and Luedke, R.G., 1974a, Geologic map of the Durango quadrangle, southwestern Colorado: U.S. Geological Survey Miscellaneous Geologic Investigations Map I-764, scale 1:250,000.

Steven, T.A., Lipman, P.W., and Olson, J.C., 1974b, Ash-flow stratigraphy and caldera structures in the San Juan volcanic field, southwestern Colorado, *in* Cohee, G.V., and Wright, W.B., eds., Changes in the stratigraphic nomenclature by the U.S. Geological Survey, 1972: U.S. Geological Survey Bulletin 1349-A, p. 75–82.

Steven, T.A., Mehnert, H.H., and Obradovich, J.D., 1967, Age of volcanic activity in the San Juan Mountains, Colorado, *in* Geological Survey research 1967: U.S. Geological Survey Professional Paper 575-D, p. D47–D55.

Steven, T.A., and Ratté, J.C., 1960, Geology and ore deposits of the Summitville district, San Juan Mountains, Colorado: U.S. Geological Survey Professional Paper 343, 70 p., https://doi.org/10.3133/pp343.

Steven, T.A., and Ratté, J.C., 1965, Geology and structural control of ore deposition in the Creede district, San Juan Mountains, Colorado: U.S. Geological Survey Professional Paper 487, 90 p., https://doi.org/10.3133/pp487.

Steven, T.A., and Ratté, J.C., 1973, Geologic map of the Creede quadrangle, Mineral and Saguache Counties, Colorado: U.S. Geological Survey Map GQ-1053, scale 1:62,500.

Stewart, J.H., Moore, W.J., and Zietz, I., 1977, East-west pattern of Cenozoic igneous rocks, aeromagnetic anomalies, and mineral deposits, Nevada and Utah: Geological Society of America Bulletin, v. 88, no. 1, p. 67–77, https://doi.org/10.1130/0016-7606(1977)88<67:EPOCIR>2.0.CO;2.

Stimac, J.A., 1996, Hornblende-dacite pumice in the Tshirege Member of the Bandelier Tuff: Implications for magma chamber and eruptive processes, *in* Goff, F., Kues, B.S., Rogers, M.A., McFadden, L.D., and Gardner, J.N., eds., Jemez Mountains region: New Mexico Geological Society, 47th Fall Field Conference Guidebook, p. 269–274.

Stix, J., Goff, F., Gorton, M.P., Heiken, G., and Garcia, S.R., 1988, Restoration of compositional zonation in the Bandelier silicic magma chamber between two caldera-forming eruptions—Geochemistry and origin of the Cerro Toledo Rhyolite, Jemez Mountains, New Mexico: Journal of Geophysical Research, v. 93, B6, p. 6129–6147, https://doi.org/10.1029/JB093iB06p06129.

Stoffregen, R.E., 1987, Genesis of acid-sulphate alteration and Cu-Au-Ag mineralization at Summitville, Colorado: Economic Geology, v. 82, no. 6, p. 1575–1591, https://doi.org/10.2113/gsecongeo.82.6.1575.

Streck, M.J., 2014. Evaluation of crystal mush extraction models to explain crystal-poor rhyolites: Journal of Volcanology and Geothermal Research, v. 284, p. 79–94, https://doi.org/10.1016/j.jvolgeores.2014.07.005.

Sweetkind, D.S., Reynolds, R.L., Sawyer, D.A., and Rosenbaum, J.G., 1993, Effects of hydrothermal alteration on the magnetization of the Oligocene Carpenter Ridge Tuff, Bachelor caldera, San Juan Mountains, Colorado: Journal of Geophysical Research, v. 98, B4, p. 6255–6266, https://doi.org/10.1029/93JB00014.

Tappa, M.J., Coleman, D.S., Mills, R.D., and Samperton, K.M., 2011, The plutonic record of a silicic ignimbrite from the Latir volcanic field, New Mexico: Geochemistry Geophysics Geosystems, v. 12, no. 10, Q10011, https://doi.org/10.1029/2011GC003700.

Thompson, R., and Dungan, M.A., 1985, The petrology and geochemistry of the Handkerchief Mesa mixed magma complex, San Juan Mountains, Colorado: Journal of Volcanology and Geothermal Research, v. 26, no. 3–4, p. 251–274, https://doi.org/10.1016/0377-0273(85)90059-9.

Thompson, R.A., Dungan, M.A., and Lipman, P.W., 1986, Multiple differentiation processes in early-rift calc-alkaline volcanics, northern Rio Grande Rift, New Mexico: Journal of Geophysical Research, v. 91, B6, p. 6046–6058, https://doi.org/10.1029/JB091iB06p06046.

Thompson, R.A., Hudson, M.R., Shroba, R.R., Minor, S.A., and Sawyer, D.A., 2011, Geologic map of the Montoso Peak quadrangle, Santa Fe and Sandoval Counties, New Mexico: U.S. Geological Survey Scientific Investigations Map 3179, 20 p. pamphlet, 1 sheet, scale 1:24,000.

Thompson, R.A., Johnson, C.M., and Mehnert, H.H., 1991, Oligocene basaltic volcanism of the Northern Rio Grande Rift—San Luis Hills, Colorado: Journal of Geophysical Research, v. 96, B8, p. 13577–13592, https://doi.org/10.1029/91JB00068.

Thompson, R.A., and Lipman, P.W., 1994a, Geologic map of the San Antonio Mountain quadrangle, Rio Arriba County, New Mexico: U.S. Geological Survey Geologic Quadrangle Map GQ-1750, scale 1:24,000.

Thompson, R.A., and Lipman, P.W., 1994b, Geologic map of the Los Pinos quadrangle, Rio Arriba and Taos Counties, New Mexico, and Conejos County, Colorado: U.S. Geological Survey Geologic Quadrangle Map GQ-1749, scale 1:24,000.

Thompson, R.A., and Machette, M.N., 1989, Geologic map of the San Luis Hills area, Conejos and Costilla Counties, Colorado: U.S. Geological Survey Miscellaneous Investigation Series Map I-1906, scale 1:50,000.

Thompson, R.A., Machette, M.N., and Drenth, B.J., 2007a, Preliminary geologic map of the Sanchez Reservoir quadrangle and eastern part of the Garcia quadrangle, Costilla County, Colorado: U.S. Geological Survey Open-File Report 2007–1074, 10 p., scale 1:24,000.

Thompson, R.A., Machette, M.N., Shroba, R.R., and Ruleman, C.R., 2007b, Geology of Mesita Volcano, Colorado—Eruptive history and implications for basin sedimentation during the Quaternary, chap. H *of* Machette, M.N., Coates, M.-M., and Johnson, M.L., eds., 2007 Rocky Mountain section friends of the Pleistocene field trip—Quaternary geology of the San Luis basin of Colorado and New Mexico, September 7–9, 2007: U.S. Geological Survey Open-File Report 2007–1193, p. 169–179.

Thompson, R.A., Sawyer, D.A., Hudson, M.R., Grauch, V.J.S., and McIntosh, W.C., 2006, Cenozoic volcanism of the La Bajada constriction area, New Mexico, chap. C *of* Minor, S.A., The Cerrillos uplift, the La Bajada constriction, and hydrogeologic framework of the Santo Domingo basin, Rio Grande rift, New Mexico: U.S. Geological Survey Professional Paper 1720-C, p. 43–60.

Thompson, R.A., and Schilling, S.P., 1988, Generalized geologic maps of Brushy Mountain and Timber Mountain areas, Taos County, New Mexico: U.S. Geological Survey Open-File Report 88-561, 2 maps on one sheet.

Thompson, R.A., Shroba, R.R., Machette, M.N., Fridrich, C.J., Brandt, T.R., and Cosca, M.A., 2015, Geologic map of the Alamosa 30' × 60' quadrangle, south-central Colorado: U.S. Geological Survey Scientific Investigations Map 3342, 23 p., scale 1:100,000, http://dx.doi.org/10.3133/sim3342.

Thompson, R.A., Shroba, R.R., Menges, C., Schmidt, D.L., Personius, S.F., and Brandt, T.R., 2009, Geologic map of the Volcanoes quadrangle, Bernalillo and Sandoval Counties, New Mexico: U.S. Geological Survey Scientific Investigations Report 3083, 1 sheet, scale1:24,000.

Thompson, R.A., Turner, K.J., Shroba, R.R., Cosca, M.A., Ruleman, C.A., Lee, J.P., and Brandt, T.R., 2014a, Geologic map of the Sunshine 7.5' quadrangle, Taos County, New Mexico: U.S. Geological Survey Scientific Investigations Map 3283, scale 1:24,000, http://dx.doi.org/10.3133/sim3283.

Thompson, R.A., Turner, K.J., Shroba, R.R., Cosca, M.A., Ruleman, C.A., Lee, J.P., and Brandt, T.R., 2014b, Geologic map of the Ute Mountain 7.5' quadrangle, Taos County, New Mexico, and Conejos and Costilla Counties, Colorado: U.S. Geological Survey Scientific Investigations Map 3284, scale 1:24,000, http://dx.doi.org/10.3133/sim3284.

Thompson, R.N., 1982, Magmatism of the British Tertiary volcanic province: Scottish Journal of Geology, v. 18, p. 49–107, https://doi.org/10.1144/sjg18010049.

Tomek, F., Gilmer, A.K., Petronis, M.S., Lipman, P.W., and Foucher, M.S., 2019, Protracted multipulse emplacement of a post-resurgent pluton—The case of Platoro caldera complex (southern Rocky Mountain volcanic field, Colorado): Geochemistry, Geophysics, Geosystems, v. 20, no. 11, p. 5225–5250, https://doi.org/10.1029/2019GC008477.

Toulmin, P., and Hammarstrom, J.M., 1990, Geology of the Mount Aetna Volcanic Center, Chaffee and Gunnison Counties, Colorado: U.S. Geological Survey Bulletin 1864, 44 p.

Turbeville, B., and Self, S., 1988, San Diego Canyon ignimbrites—Pre-Bandelier Tuff explosive rhyolitic volcanism in the Jemez Mountains, New Mexico: Journal of Geophysical Research, v. 93, B6, p. 6148–6156, https://doi.org/10.1029/JB093iB06p06148.

Turner, K.J., Thompson, R.A., Cosca, M.A., Shroba, R.R., Chan, C.F., and Morgan, L.E., 2018, Geologic map of the San Antonio Mountain area, northern New Mexico and southern Colorado: U.S. Geological Survey Scientific Investigations Map 3417, scale 1:50,000, https://doi.org/10.3133/sim3417.

Tuttle, O.F., and Bowen, N.L., 1958, Origin of granite in the light of experimental studies in the system $NaAlSi_3O_8$-$KalSi_3O_8$-SiO_2-H_2O: Geological Society of America Memoir 74, 153 p.

Tweto, O., 1975, Laramide (Late Cretaceous-early Tertiary) orogeny in the southern Rocky Mountains, *in* Curtis, B.F., ed., Cenozoic history of the southern Rocky Mountains: Geological Society of America Memoir 144, p. 1–44, https://doi.org/10.1130/MEM144-p1.

Tweto, O., 1979, Geologic map of Colorado: U.S. Geological Survey Special Map, scale 1:500,000.

Tweto, O., Steven, T.A., Hail, W.J., Jr., and Moench, R.H., 1976, Preliminary geologic map of the Montrose 1x2° quadrangle, southwestern Colorado: U.S. Geological Survey Miscellaneous Field Studies Map 761, scale 1:250,000.

U.S. Geological Survey and New Mexico Bureau of Geology and Mineral Resources, 2015, Fault number 2007—Embudo fault, *in* Quaternary fault and fold database of the United States: U.S. Geological Survey database, https://earthquakes.usgs.gov/hazards/qfaults.

Van Alstine, R.E., 1975, Geologic map of the Bonanza NE quadrangle, Chafee and Saguache counties, Colorado: U.S. Geological Survey Open-File Report 75–53, scale 1:62,500.

Varga, R.J., and Smith, B.M., 1984, Evolution of the early Oligocene Bonanza caldera, northeast San Juan volcanic field, Colorado: Journal of Geophysical Research, v. 89, B10, p. 8679–8694, https://doi.org/10.1029/JB089iB10p08679.

Verrall, P., 1989, Speculations on the Mesozoic-Cenozoic tectonic history of the western United States, *in* Tankard, A.J., and Balkwill, H.R., eds., Extensional tectonics and stratigraphy of the North Atlantic margins: American Association of Petroleum Geologists Memoir 46, p. 615–631.

Wallace, A.R., 1996, Geologic map of the Trinchera Ranch quadrangle, Costilla County, Colorado: U.S. Geological Survey Miscellaneous Field Studies Map 2312-C, scale 1:24,000.

Wallace, A.R., 2004, Evolution of the southeastern San Luis Basin margin and the Culebra embayment, Rio Grande rift, southern Colorado, *in* Brister, B., Bauer, P.W., Read, A.S., and Lueth, V.W., eds., Geology of the Taos region: New Mexico Geological Society, 55th Fall Field Conference Guidebook, p. 181–192.

Ward, K.M., Zandt, G., Beck, S.L., Christensen, D.H., and McFarlin, H., 2014, Seismic imaging of the magmatic underpinnings beneath the Altiplano-Puna volcanic complex from the joint inversion of surface wave dispersion and receiver functions: Earth and Planetary Science Letters, v. 404, p. 43–53, https://doi.org/10.1016/j.epsl.2014.07.022.

Wark, D.A., Hildreth, W., Spear, F.S., Cherniak, D.J., and Watson, E.B., 2007, Pre-eruption recharge of the Bishop magma system: Geology, v. 35, no. 3, p. 235–238, https://doi.org/10.1130/G23316A.1.

Waters, L.E., and Lange R.A., 2015, An updated calibration of the plagioclase-liquid hygrometer-thermometer applicable to basalts through rhyolites: American Mineralogist, v. 100, no. 10, p. 2172–2184.

Wetlaufer, P.H., Bethke, P.M., Barton, P.B., Jr., and Rye, R.O., 1979, The Creede Ag-Pb-Zn-Cu-Au district, central San Juan Mountains, Colorado—A fossil geothermal system: The International Association on the Genesis of Ore Deposits, 5th Quadrennial Symposium Proceedings, v. 2, Nevada Bureau of Mines and Geology Report 33, p. 159–164.

Whitney, J.A., Dorais, M.J., Stormer, J.C., Jr., Kline, S.W., and Matty, D.J., 1988, Magmatic conditions and development of chemical zonation in the Carpenter Ridge Tuff, central San Juan volcanic field, Colorado: American Journal of Science, v. 288-A, p. 16–44.

Whitney, J.A., and Stormer, J.C., Jr., 1985, Mineralogy, petrology, and magmatic conditions from the Fish Canyon Tuff, central San Juan volcanic field, Colorado: Journal of Petrology, v. 26, no. 3, p. 726–762, https://doi.org/10.1093/petrology/26.3.726.

Williams, M.L., 1987, Stratigraphic, structural, and metamorphic relationships in Proterozoic rocks from northern New Mexico: Albuquerque, University of New Mexico, Ph.D. Thesis, 138 p.

Williams, M.L., Karlstrom, K.E., Lanzirotti, A., Read, A.S., Bishop, J.L., Lombardi, C.E., Pedrick, J.N., and Wingsted, M.B., 1999, New Mexico middle-crustal cross sections—1.65-Ga macroscopic geometry, 1.4-Ga thermal structure, and continued problems in understanding crustal evolution: Rocky Mountain Geology, v. 34, no. 1, p. 53–66, https://doi.org/10.2113/34.1.53.

Wilson, C.J.N., and Walker, G.P.L., 1985, The Taupo eruption, New Zealand. I. General aspects: Royal Society of London Philosophical Transactions, v. 314, no. 1529, p. 199–228, https://doi.org/10.1098/rsta.1985.0019.

Wobus, R.A., and Hedge, C.E., 1982, Redefinition of the Precambrian Tusas Mountain and Tres Piedras Granites, north-central New Mexico: The Mountain Geologist, v. 19, p. 105–114.

WoldeGabriel, G., Koning, D.J., Broxton, D., and Warren, R.G., 2013, Chronology of volcanism, tectonics, and sedimentation near the western boundary fault of the Española Basin, Rio Grande rift, New Mexico, *in* Hudson, M.R., and Grauch, V.J.S., eds., New perspectives on Rio Grande rift basins—From tectonics to groundwater: Geological Society of America Special Paper 494, p. 221–238, https://doi.org/10.1130/2013.2494(09).

Wolfe, E.W., 1992, The 1991 eruptions of Mount Pinatubo, Philippines: Earthquakes & Volcanoes, v. 23, p. 5–37.

Wolff, J.A., Balsley, S.D., and Gregory, R.T., 2002, Oxygen isotope disequilibrium between quartz and sanidine from the Bandelier Tuff, New Mexico, consistent with a short residence time of phenocrysts in rhyolitic magma: Journal of Volcanology and Geothermal Research, v. 116, no. 1–2, p. 119–135, https://doi.org/10.1016/S0377-0273(02)00214-7.

Wolff, J.A., Brunstad, K.A., and Gardner, J.N., 2011, Reconstruction of the most recent volcanic eruptions from the Valles caldera, New Mexico: Journal of Volcanology and Geothermal Research, v. 199, no. 1–2, p. 53–68, https://doi.org/10.1016/j.jvolgeores.2010.10.008.

Wolff, J.A., Ellis, B.S., Ramos, F.C., Starkel, W.A., Boroughs, S., Olin, P.H., and Bachmann, O., 2015, Remelting of cumulates as a process for producing chemical zoning in felsic tuffs—A comparison of cool, wet and hot, dry rhyolitic magma systems: Lithos, v. 236–237, p. 275–286, https://doi.org/10.1016/j.lithos.2015.09.002.

Wolff, J.A., and Gardner, J.N., 1995, Is the Valles Caldera entering a new cycle of activity?: Geology, v. 23, no. 5, p. 411–414, https://doi.org/10.1130/0091-7613(1995)023<0411:ITVCEA>2.3.CO;2.

Wolff, J.A., Heikoop, C.E., and Ellisor, R., 2000, Hybrid origin of Rio Grande rift hawaiites: Geology, v. 28, no. 3, p. 203–206, https://doi.org/10.1130/0091-7613(2000)28<203:HOORGR>2.0.CO;2.

Wolff, J.A., and Ramos, F.C., 2003, Pb isotope variations among Bandelier Tuff feldspars—No evidence for a long-lived silicic magma chamber: Geology, v. 31, p. 533–536.

Wolff, J.A., and Ramos, F.C., 2014, Pre-eruptive processes in caldera-forming high-silica rhyolite magma—Rb-Sr and Pb isotope systematics of the Otowi Member of the Bandelier Tuff, Valles Caldera, New Mexico, USA: Journal of Petrology, v. 55, no. 2, p. 345–375, https://doi.org/10.1093/petrology/egt070.

Wolff, J.A., Rowe, M.C., Teasdale, R., Gardner, J.N., Ramos, F.C., and Heikoop, C.E., 2004, Petrogenesis of pre-caldera mafic lavas, Jemez Mountains volcanic field (New Mexico, USA): Journal of Petrology, v. 46, no. 2, p. 407–439, https://doi.org/10.1093/petrology/egh082.

Wotzlaw, J.-F., Schaltegger, U., Frick, D.A., Dungan, M.A., Gerdes, A., and Günther, D., 2013, Tracking the evolution of large-volume silicic magma reservoirs from assembly to supereruption: Geology, v. 41, no. 8, p. 867–870, https://doi.org/10.1130/G34366.1.

Ziegler, P.A., 1992, Plate tectonics, plate moving mechanisms and rifting: Tectonophysics, v. 215, no. 1–2, p. 9–34, https://doi.org/10.1016/0040-1951(92)90072-E.

Zimmerer, M.J., and McIntosh, W.C., 2012a, An investigation of caldera-forming magma chambers using the timing of ignimbrite eruptions and pluton emplacement at the Mt. Aetna caldera complex: Journal of Volcanology and Geothermal Research, v. 245–246, p. 128–148, https://doi.org/10.1016/j.jvolgeores.2012.08.007.

Zimmerer, M.J., and McIntosh, W.C., 2012b, The geochronology of volcanic and plutonic rocks at the Questa caldera—Constraints on the origin of caldera-related silicic magmas: Geological Society of America Bulletin, v. 124, no. 7–8, p. 1394–1408, https://doi.org/10.1130/B30544.1.

A New Look at the Dacite Pumice Component in the Tshirege Member of the Bandelier Tuff

By Joseph R. Boro, John A. Wolff, and Owen K. Neill

A New Look at the Dacite Pumice Component in the Tshirege Member of the Bandelier Tuff

By Joseph R. Boro[1], John A. Wolff[1], and Owen K. Neill[1]

Silicic ignimbrites often contain a minor, more mafic magmatic component which, on textural grounds, is usually interpreted as having mingled with the dominant rhyolitic magma shortly before eruption. The recharge event is therefore assigned a role as the trigger for the eruption. The Tshirege Member of the Bandelier Tuff (see Wolff and Thompson, Day 1, this volume) contains two such mafic magmatic components: a long-recognized fraction of dacite pumice distributed throughout most of the unit (Bailey and others, 1969), and recently reported trace amounts of andesite inclusions in late-erupted tuff (Goff and others, 2014).

Prior to our study, the only work devoted to the dacite pumices was that of Stimac (1996), who noted their similarity to enclaves in silicic lavas and plutonic rocks, reported whole-rock and mineral chemistry, and offered some speculations on the dynamics of dacite-rhyolite interaction and the role of the dacite in triggering the Tshirege eruption. Here, we summarize results of a new petrologic investigation of the dacite pumice and present selected data; full details, and the entire data set, can be found in Boro and others (2020).

The Tshirege Member of the Bandelier Tuff

The Tshirege eruption began with emplacement of a basal Plinian fallout deposit, the Tsankawi Pumice Bed, Qbts (fig. 1), with an estimated volume of about 15 cubic kilometers (dense rock equivalent; Self and others, 1996). It mostly consists of a single fallout unit that lacks internal partings. Above the fallout, early thin Tshirege flow units are overlain by massive, structureless nonwelded ignimbrite. The ignimbrite becomes thermally lithified upwards and passes into sintered vitric and vapor-phase altered tuff near the top of Qbt1 (fig. 1). Stratigraphically higher levels of the Tshirege Member (Qbt2–5) consist of a complex succession of variably welded and vapor-phase altered ignimbrite and surge deposit units, but fresh, vitric pumice can be obtained from locations where successive emplacement units lap onto, and were quenched by, steep paleocanyon walls. The tuff is compositionally zoned from early erupted, crystal-poor high-silica rhyolite that is strongly enriched in trace elements to late-erupted, porphyritic, dominantly low-silica rhyolite, although zoning reversals are found at the highest stratigraphic levels (Self and others, 1996; Goff and others, 2014). The phenocryst assemblage of the rhyolite is dominated by quartz and sanidine, and relevant to this study, includes the accessory rare earth element (REE)-mineral chevkinite. Dacite pumice samples in this study come from the Tsankawi Pumice Bed and ignimbrite units Qbt1–3 (fig. 1).

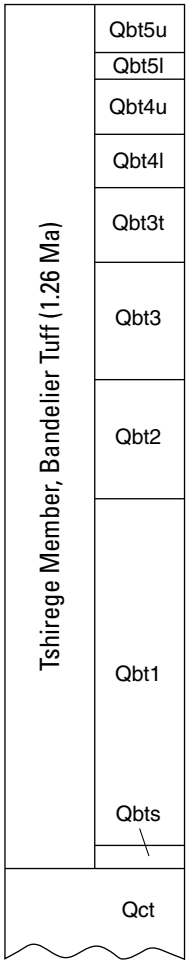

Figure 1. Schematic section of the Tshirege Member (modified from Goff and others, 2014). Samples in this study were collected from the Qbts, Qbt1, Qbt2, and Qbt3 units. Ma, million years ago.

Dacite Pumice

Dacite pumice is found above approximately one-quarter of the thickness above the base of the bed in the Tsankawi Pumice Bed and throughout the Tshirege ignimbrite, typically as discrete pumice clasts regarded as erupted enclaves by Stimac (1996). Some fragments bear a remnant carapace of rhyolitic pumice, whereas clasts of dacite mingled with high- or low-silica rhyolite also occur.

[1]Washington State University.

Dacite pumices are various shades of grey to grey-green and typically contain very fine (<1 millimeter [mm]) vesicles. Phenocrysts consist of plagioclase, hornblende, iron-titanium (Fe-Ti) oxide and sparse biotite; Stimac (1996) reports large (several millimeters long) clino- and orthopyroxene, but we have not found these in our set of 25 samples. Phenocrysts are set in a matrix of glass with abundant microlites and microphenocrysts (10–50 micrometers [µm]) of plagioclase and hornblende. Mingled samples contain alkali feldspar and quartz crystals, presumably derived from the host rhyolite. Especially prominent in some dacites are large (≥1 centimeter [cm]), heavily fritted (sieve-textured) feldspars of dominantly sodic plagioclase to ternary compositions (fig. 2).

Whole Rock Geochemistry

Dacite pumice samples fall into two compositional groups distinguished by contrasting REE concentrations (table 1; figs. 3, 4). Both groups are distributed throughout the sampled interval Qbts-Qbt3. Group 1 samples exhibit lower concentrations of light to middle REEs than do Group 2. Group 1 samples have light-REE abundances typical of precaldera dacites in the Jemez Mountains volcanic field (Rowe and others, 2007), whereas Group 2 are strongly enriched in these elements. Most dacite samples that exhibit magma mingling textures in hand sample fall into Group 2.

Stimac (1996) gives REE concentrations for four dacite pumices from the Tshirege Member, originally reported by Balsley (1988) and Stix and others (1988). All of these pumices have low light-REE. One of these samples is from unit Qbts, the Tsankawi Pumice Bed (sample F82-95; Stix and others, 1988) and the other three are all from the nonwelded portion of unit Qbt1 (samples 22-69a, 22-70, 27-26i; Balsley, 1988). We did not find any strongly light REE-enriched Group 2 samples (>200 parts per million Ce) in Qbts, thus, on average the degree of light REE enrichment seems to increase upwards from Qbts to Qbt3.

Dacite Pumice Petrography

Dacite pumices show a wide range of petrographic features, interpreted as a result of different degrees of interaction and mingling with rhyolite. The least affected pumices have euhedral phenocrysts of plagioclase, hornblende, and oxides. In dacites affected by rapid cooling on mingling with rhyolite, the feldspars often have irregular crystal rims and may be mantled

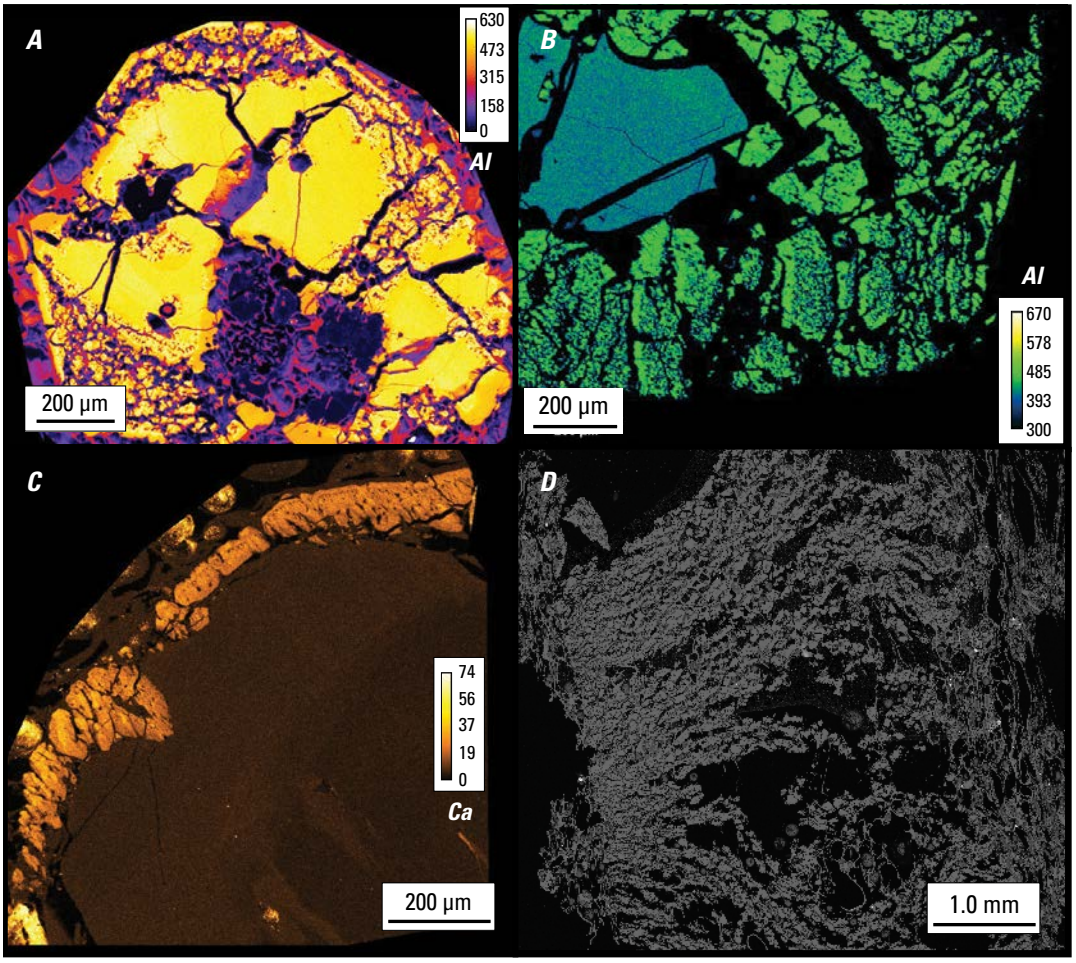

Figure 2. Images of fritted feldspars. *A*, *B*, and *C* are false-color composite photographs representing x-ray intensity maps of large, fritted feldspars. Color scales represent x-ray count rates, in counts per second, which increase in proportion with concentration. *A*, Aluminum map of feldspar from mingled sample with sanidine core. *B*, Aluminum map of feldspar from mingled sample showing ternary fritted feldspar mantling an orthoclase-rich core. *C*, Calcium map of sanidine crystal from mingled sample. Perforated calcium-enriched rim is a result of overgrowth of ternary feldspar. *D*, Back-scatter electron image of fritted feldspar showing dendritic morphology.

Table 1. Major and trace element analyses of representative whole-pumice samples. For details of sample preparation and analytical methods, see https://environment.wsu.edu/facilities/geoanalytical-lab/technical-notes/.

[XRF, x-ray fluorescence; ICP-MS, inductively coupled plasma-mass spectrometry; *Total Fe reported as FeO. All oxides reported in weight percent; all trace elements reported in parts per million]

Sample number	09JM-60	09JM-73	09JM-144	09JM-147	09JM-149	09JM-161
Geologic unit	Qbts	Qbts	Qbt2	Qbt2	Qbt2	Qbt3
SiO_2	68.05	67.48	67.89	69.68	70.61	68.96
TiO_2	0.448	0.438	0.480	0.465	0.425	0.486
Al_2O_3	15.74	16.04	15.84	15.55	15.63	16.05
FeO*	3.31	3.38	3.41	2.79	2.70	2.77
MnO	0.072	0.077	0.051	0.040	0.044	0.038
MgO	1.35	1.26	1.31	0.91	0.82	1.11
CaO	3.10	2.90	3.39	3.15	2.25	3.37
Na_2O	4.31	4.62	4.35	4.08	3.86	3.78
K_2O	3.46	3.64	3.11	3.22	3.59	3.34
P_2O_5	0.163	0.162	0.177	0.114	0.070	0.094
Trace elements by XRF						
Ni	14	13	14	9	10	10
Cr	22	22	24	21	20	23
Sc	6	6	8	6	6	8
V	48	46	51	42	39	43
Ba	895	860	1,106	884	782	952
Rb	209	175	104	122	110	106
Sr	435	440	537	447	370	472
Zr	212	227	181	228	239	189
Y	88	57	27	48	38	40
Nb	35	46	15	31	27	22
Ga	23	23	20	20	21	19
Cu	7	7	11	7	9	21
Zn	110	143	260	76	76	73
Pb	27	32	59	75	103	39
La	44	48	41	160	119	141
Ce	73	83	69	290	225	235
Nd	39	34	31	117	93	108
Trace elements by ICP-MS						
La	44.6	48.8	41.8	172	128	131
Ce	81.3	83.9	71.5	312	242	243
Pr	10.5	10.4	8.55	36.1	27.3	33.2
Nd	40.3	36.0	31.3	124.1	92.7	115
Sm	10.1	8.44	6.62	20.9	16.1	20.2
Eu	1.01	1.00	1.23	1.27	1.10	1.35
Gd	10.5	8.16	6.22	14.7	11.31	14.3
Tb	1.94	1.68	1.00	2.10	1.67	1.99
Dy	12.6	10.7	5.95	11.0	8.91	10.2
Ho	2.63	2.14	1.15	1.97	1.59	1.73
Er	7.06	5.81	3.10	4.96	3.98	4.10
Tm	0.94	0.85	0.44	0.70	0.58	0.56
Yb	5.43	5.26	2.70	4.21	3.61	3.49
Lu	0.78	0.75	0.42	0.64	0.57	0.52
Ba	895	889	1126	916	800	981
Th	10.7	14.1	5.99	12.1	11.5	11.8
Nb	34.9	46.2	14.7	31.2	27.6	22.2
Y	88.0	55.0	26.0	47.1	37.3	39.1
Hf	6.65	7.35	4.86	6.62	6.60	5.54

Table 1.—Continued

Sample number	09JM-60	09JM-73	09JM-144	09JM-147	09JM-149	09JM-161
Geologic unit	Qbts	Qbts	Qbt2	Qbt2	Qbt2	Qbt3
Ta	2.31	2.62	0.98	2.16	1.91	1.52
U	3.09	3.30	1.69	3.13	2.62	2.52
Pb	27.6	30.6	58.0	71.0	103	38.9
Rb	212	176	102	124	111	106
Cs	71.5	17.9	2.05	2.55	2.25	2.68
Sr	452	449	542	463	382	475
Zr	220	229	179	229	245	192

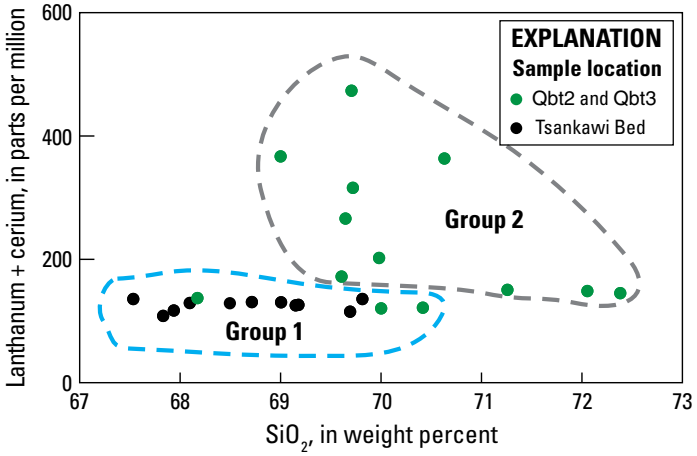

Figure 3. Lanthanum + cerium versus SiO_2 in whole-pumice samples. Groups 1 and 2 are outlined.

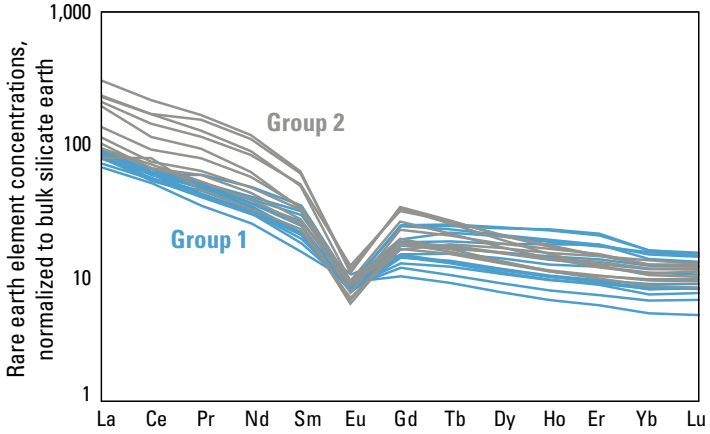

Figure 4. Rare earth element (REE) plots for whole-pumice samples. Groups 1 and 2 are distinct in their abundances of light REE. Rare earth element concentrations are normalized to bulk silicate earth values of McDonough and Sun (1995).

by alkali feldpsar. Other samples contain quartz and sanidine scavenged from rhyolite, large fritted albite-rich feldspars formed by rapid growth, and may exhibit visible banding owing to mixing with rhyolite.

Feldspars

Feldspars in the dacite include three main populations:

- Large, zoned plagioclase phenocrysts ~1–5 mm of anorthite $(An)_{34}$-An_{60} compositions (fig. 5). These feldspars may have melt inclusions, but lack heavily pitted zones resulting from resorption or rapid growth. They appear to be restricted to Group 1 pumice. Some plagioclase phenocrysts show pronounced oscillating concentrations of FeO and MgO from core to rim (fig. 5*B*).
- Small, groundmass (<50 μm) microlites and microphenocrysts with compositions of An_{30}-An_{55}. Some samples also have small quantities (<1 percent modal abundance) of groundmass sanidine.
- Large (≥1 cm) fritted feldspars (figs. 2*A*,*B*,*D*, 5*C*) occur in both chemical groups of dacite pumice. These feldspars have dominantly ternary compositions, defined for our purposes as albite (Ab)-rich feldspars with >5 percent of both anorthite (An) and orthoclase (Or) end members. Fine-scale fritting (or sieving) is shown in figure 5*C*. Micrometer-scale disequilibrium textures can be seen in figure 5*D*, where glass and feldspar can be discerned with darker and lighter shades of gray. The fritted feldspar in some cases shows apparent dendritic morphology (fig. 2*D*).

Amphiboles

Amphiboles range in size from >1 to <10 mm and are 5–10 percent modal abundance. Their dark green color gives the pumices a greenish appearance in hand sample. They are usually pargasite—magnesio-hornblende in the classification scheme of Hawthorne and others (2015); the tschermakite component increases towards the rims of some larger zoned crystals and small (<50 micrometers) groundmass crystals are also tschermakite-rich.

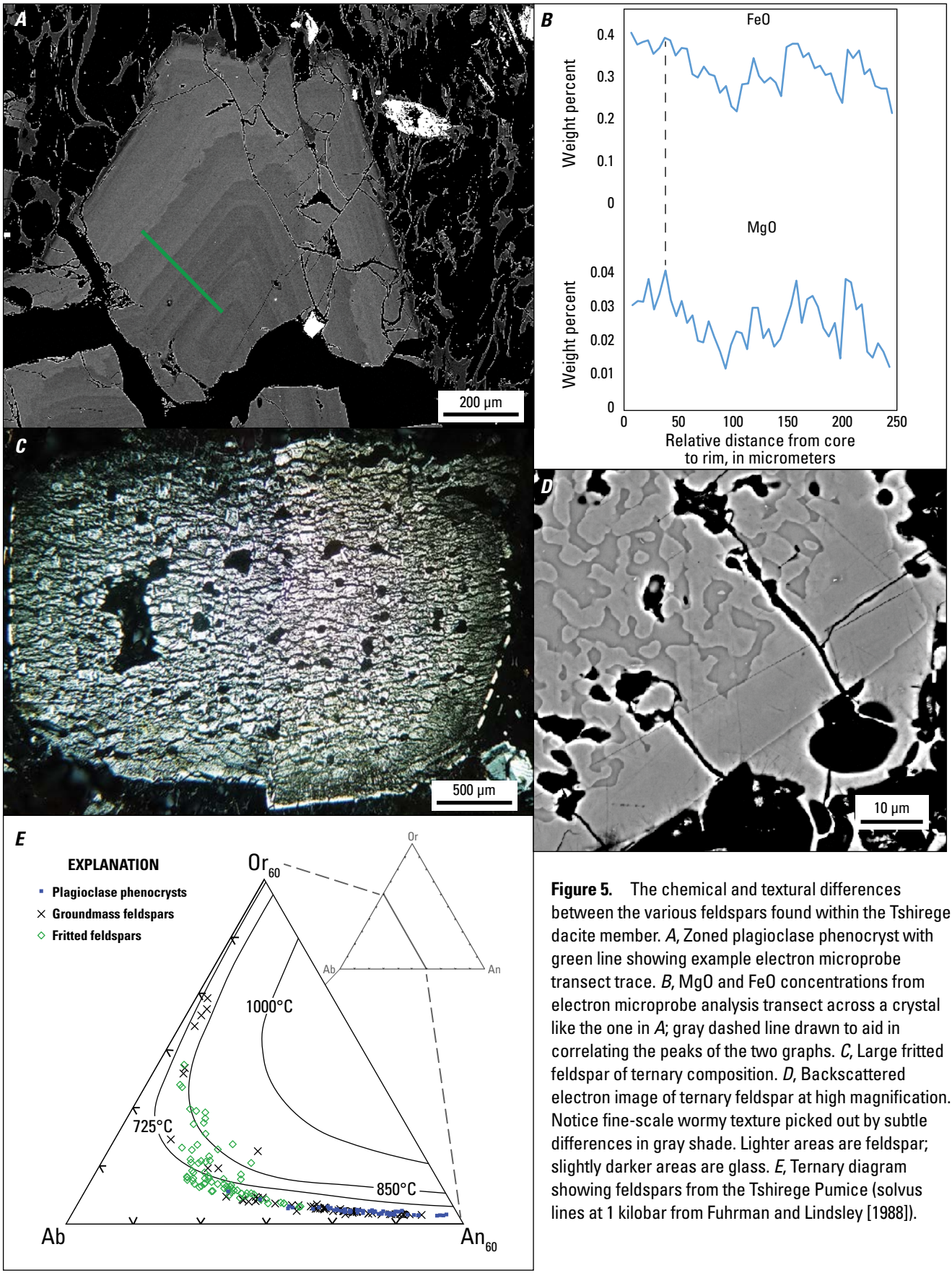

Figure 5. The chemical and textural differences between the various feldspars found within the Tshirege dacite member. *A*, Zoned plagioclase phenocryst with green line showing example electron microprobe transect trace. *B*, MgO and FeO concentrations from electron microprobe analysis transect across a crystal like the one in *A*; gray dashed line drawn to aid in correlating the peaks of the two graphs. *C*, Large fritted feldspar of ternary composition. *D*, Backscattered electron image of ternary feldspar at high magnification. Notice fine-scale wormy texture picked out by subtle differences in gray shade. Lighter areas are feldspar; slightly darker areas are glass. *E*, Ternary diagram showing feldspars from the Tshirege Pumice (solvus lines at 1 kilobar from Fuhrman and Lindsley [1988]).

Discussion

Feldspar Textures and Compositions

Core-to-rim concentrations of iron and magnesium in zoned plagioclase phenocrysts are variable and correlated (fig. 5*B*). These elements are incompatible in feldspar but are present at lower abundances in dacites than in more mafic magmas, hence the zoning pattern indicates feldspar growth from melts of variable mafic character. This could arise from periodic recharge of dacite by more mafic magma, or transfer between coexisting melts; in either case, a complex history for the dacite prior to mingling with rhyolite is indicated.

The fritted feldspars are interpreted as the products of rapid growth rather than resorption as proposed by Stimac (1996). Some sections show splayed dendritic textures (fig. 2*D*). No glass enriched in feldspar components has been found, even in very intimate association with feldspar, and texturally similar fritted zones are found enclosing both plagioclase and sanidine cores (fig. 2*A*,*B*; see also Boro and others, 2020). None of these features are consistent with resorption. Also, different stages of the fritted ternary feldspar overgrowth on sanidine are preserved within pumice (compare fig. 2 *A*–*C*).

Hence, the fritted feldspars are interpreted to have formed from rapid crystallization of compositions enriched in albite owing to a drop in pH_2O (Lange and others, 2009), as portions of dacite magma encountered H_2O-poor magma formed by partial melting of rhyolitic quartz-feldspar crystal mush (Boro and others, 2020).

Thermobarometry

Several geothermometers and geobarometers were applied to the compositions of feldspars, amphiboles, Fe-Ti oxides, glasses, and whole pumices to determine conditions of magma storage: amphibole thermobarometry (Putirka, 2016), plagioclase hygrometry (Waters and Lange, 2015), Fe-Ti oxide thermometry (Ghiorso and Evans, 2008), glass compositions (Blundy and Cashman, 2001), and rhyolite-MELTS simulations (Gualda and others, 2012). Results are summarized in table 2; full details of the data treatment and calculations are given by Boro and others (2020). The dacite began to crystallize at a pressure (*P*) of ~0.46 gigapascals (GPa) and temperature (*T*) of ~900 °C, with a water content of 5 weight percent. Most crystallization occurred following uprise and injection into crystal-rich rhyolite at *P* ~0.3 GPa and *T* ~800 °C. Glass and oxide compositions continued to evolve in response to further cooling associated with uprise and eruption.

Preliminary Model

Dacite pumices exhibit a range of textures; some have experienced little interaction with the dominant rhyolite, whereas others appear to have cooled against, and mixed with, rhyolite magma. Consistent with this observation, Fe-Ti oxides equilibrated at a range of temperatures from the dacite liquidus at 900 °C down to <700 °C (Boro and others, 2020). Oxides react rapidly, within a matter of hours to days (Venezky and Rutherford, 1999), so the preservation of a range of temperatures indicates re-equilibration of oxides over such a timescale, which in turn suggests that dacite recharge of the Tshirege magma body may have been the trigger for eruption (compare with Stimac [1996] and Goff and others [2014]). Group 2 dacites have mingled with rhyolite and experienced textural modification, so there is an increasing degree of interaction between dacite magma and crystal-rich rhyolite up-section in the Tshirege Member. The zoning in crystal content and composition of the dominant rhyolite are consistent with the presence of a cumulate mush pile beneath crystal-poor rhyolitic magma (Bachmann and Bergantz, 2004; Wolff and others, 2015). Enrichment of light REE in Group 2 dacites may therefore be a result of assimilation of crystal mush containing chevkinite or another REE-rich mineral. A conceptual model for recharge and triggering of the Tshirege eruption by dacite magma is shown in figure 6.

Conclusions

1. Dacite pumice clasts in the Tshirege Member of the Bandelier Tuff fall into two compositional groups with a broad range of textures. Many early erupted dacite pumices have light REE abundances similar to precaldera dacite lavas and typically show little evidence for mingling with rhyolite; however, later-erupted dacite pumices are strongly light REE-enriched and show abundant disequilibrium features.
2. Plagioclase phenocrysts record a complex prior history for the dacite magma, involving recharge by more mafic magma (the mafic kick in fig. 6).
3. Large, fritted feldspars formed by rapid growth owing to partial quenching consequent on mixing.
4. Thermobarometry records initial crystallization of dacite, uprise and mingling with crystal-rich rhyolite, followed by further uprise leading to eruption.
5. Variations in dacite pumice chemistry, mineralogy, and mineral textures are explained by a model in which dacite magma invades, and experiences progressively greater interaction with, crystal-rich rhyolite (fig. 6).

Acknowledgments

We thank Steve Self and Ren Thompson for discussion, and Suzanne Krahn and Charles Knaack for assistance in the laboratory. This research was funded by NSF EAR-0810306.

Table 2. Thermobarometry and hygrometry results from Boro and others (2020).

[Eqn., equation; °C, degrees Celsius; Gpa, gigpascal; wt. %, weight percent; H_2O, water]

Type	Author	Range	Average	Standard deviation
		Thermometer		
Two-oxide	Ghiorso and Evans (2008)	607–1,033 °C	764 °C	90 °C
Amphibole	Putirka (2016) Eqn. 7a	764–814 °C	797 °C	17 °C
		Barometer		
Amphibole	Putirka (2016) Eqn. 4a; 4b avg.	0.16–0.58 GPa	0.31; 0.46 GPa	0.048; 0.086 GPa
		Hygrometer		
Feldspar-liquid	Waters and Lange (2015)	2.5–5.5 wt. % H_2O	4.85 wt. % H_2O	0.43 wt. % H_2O

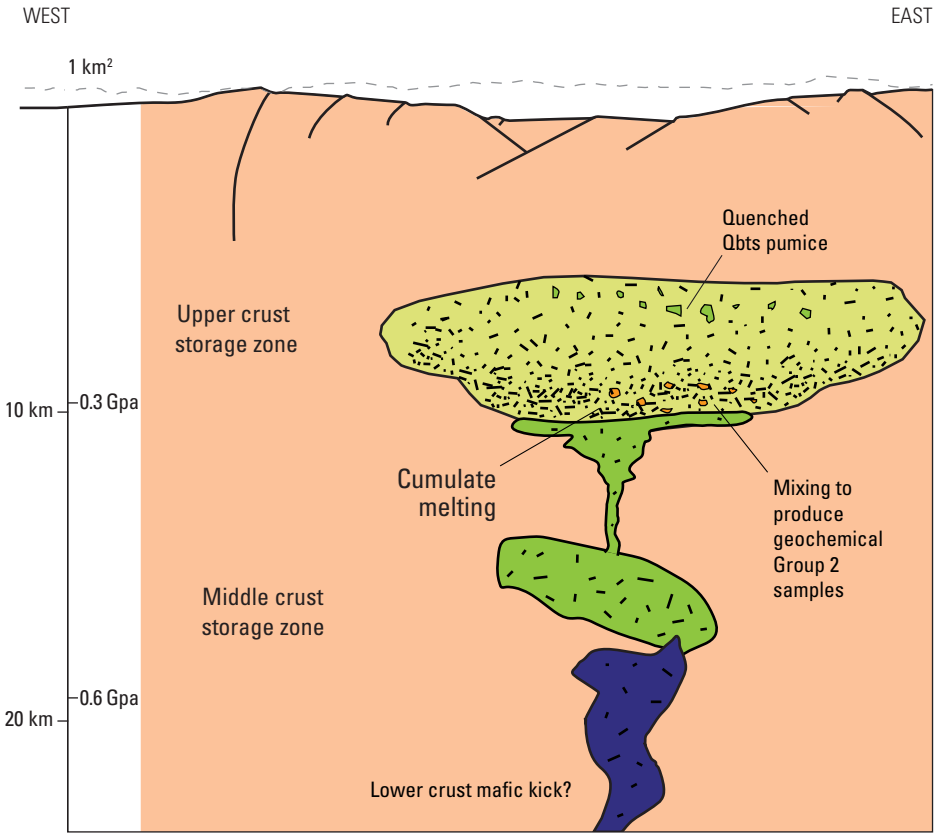

Figure 6. Conceptual model for the Tshirege eruption, that assigns a triggering role to the dacite. Initial condition is a body of dacite magma (green) beneath the Tshirege rhyolite magma chamber. The latter consists of chemically zoned rhyolite (yellow) with a crystal cumulate mush lower portion. A tentative depth scale, based on amphibole barometry, is given on the left side of the panel. Dacite is intruded into the mush pile; some of it quenches and buoyantly rises to the top of the chamber. Continued intrusion and heat transfer are accompanied by melting and remobilization of mush and mingling with dacite, growth of dendritic feldspar, and growth of hornblende rims (orange polygons), and primes the caldera for eruption.

References

Bachmann, O., and Bergantz, G.W., 2004, On the origin of crystal-poor rhyolites—Extracted from batholithic crystal mushes: Journal of Petrology, v. 45, no. 8, p. 1565–1582.

Bailey, R.A., Smith, R.L., and Ross, C.S., 1969, Stratigraphic nomenclature of volcanic rocks in the Jemez Mountains, New Mexico: U.S. Geological Survey Bulletin 1274-P, 19 p.

Balsley, S.D., 1988, The petrology and geochemistry of the Tshirege Member of the Bandelier Tuff, Jemez Mountains volcanic field, New Mexico, U.S.A.: University of Texas at Arlington, M.S. thesis, 188 p.

Blundy, J., and Cashman, K., 2001, Ascent-driven crystallization of dacite magmas at Mount St. Helens, 1980-1986: Contributions to Mineralogy and Petrology, v. 140, no. 6, p. 631–650.

Boro, J.R., Wolff, J.A., and Neill, O.K., 2020, Anatomy of a recharge magma– Hornblende dacite pumice from the rhyolitic Tshirege Member of the Bandelier Tuff, Valles Caldera, New Mexico, USA: Contributions to Mineralogy and Petrology, v. 175, 96, 26 p.

Ghiorso, M.S., and Evans, B.W., 2008, Thermodynamics of rhombohedral oxide solid solutions and a revision of the Fe-Ti two-oxide geothermometer and oxygen barometer: American Journal of Science, v. 308, p. 957–1039.

Goff, F., Warren, R.G., Goff, C.J., and Dunbar, N., 2014, Eruption of reverse-zoned upper Tshirege Member, Bandelier Tuff from centralized vents within Valles caldera, New Mexico: Journal of Volcanology and Geothermal Research, v. 276, p. 82–104.

Gualda, G.A.R., Ghiorso, M.S., Lemons, R.V., and Carley, T.L., 2012, Rhyolite-MELTS—A modified calibration of MELTS optimized for silica-rich, fluid-bearing magmatic systems: Journal of Petrology, v. 53, p. 875–890.

Hawthorne, F.C., Oberti, R., Harlow, G.E., Maresch, W.V., Martin, R.F., Schumacher, J.C., and Welch, M.D., 2012, Nomenclature of the amphibole supergroup: American Mineralogist, v. 97, p. 2031–2048.

McDonough, W.F., and Sun, S.-s., 1995, The composition of the Earth: Chemical Geology, v. 120, no. 3-4, p. 223–253.

Putirka, K., 2016, Amphibole thermometers and barometers for igneous systems and some implications for eruption mechanisms of felsic magmas at arc volcanoes: American Mineralogist, v. 101, no. 4, p. 841–858.

Rowe, M.C., Wolff, J.A., Gardner, J.N., Ramos, F.C., Teasdale, R., and Heikoop, C.E., 2007, Development of a continental volcanic field—Petrogenesis of pre-caldera intermediate and silicic rocks and origin of the Bandelier magmas, Jemez Mountains (New Mexico, USA): Journal of Petrology, v. 48, no. 11, p. 2063–2091.

Self, S., Heiken, G., Sykes, M.L., Wohletz, K., Fisher, R.V., and Dethier, D.P., 1996, Field excursions to the Jemez Mountains, New Mexico: New Mexico Bureau of Geology and Mineral Resources Bulletin 134, 72 p.

Stimac, J.A., 1996, Hornblende-dacite pumice in the Tshirege Member of the Bandelier Tuff—Implications for magma chamber and eruptive processes, in Goff, F., Kues, B.S., Rogers, M.A., McFadden, L.D., and Gardner, J.N., eds., Jemez Mountains region: New Mexico Geological Society, 47th Fall Field Conference Guidebook, p. 269–274.

Stix, J., Goff, F., Gorton, M.P., Heiken, G., and Garcia, S.R., 1988, Restoration of compositional zonation in the Bandelier silicic magma chamber between two caldera-forming eruptions—Geochemistry and origin of the Cerro Toledo Rhyolite, Jemez Mountains, New Mexico: Journal of Geophysical Research, v. 93, no. B6, p. 6129–6147.

Venezky, D.Y., and Rutherford, M.J., 1999, Petrology and Fe–Ti oxide reequilibration of the 1991 Mount Unzen mixed magma: Journal of Volcanology and Geothermal Research, v. 89, p. 213–230.

Waters, L.E., and Lange, R.A., 2015, An updated calibration of the plagioclase-liquid hygrometer-thermometer applicable to basalts through rhyolites: American Mineralogist, v. 100, p. 2172–2184.

Wolff, J.A., Ellis, B.S., Ramos, F.C., Starkel, W.A., Boroughs, S., Olin, P.H., and Bachmann, O., 2015, Remelting of cumulates as a process for producing chemical zoning in silicic tuffs—A comparison of cool, wet and hot, dry rhyolitic magma systems: Lithos, v. 236-237, p. 275–286.

The Evolution of Thought on the Embudo Fault— Putting Legendary Exposures in Hondo Canyon into a More Regional Context and a New Paradigm, Southern Taos Plateau, New Mexico

By V.J.S. Grauch, Keith I. Kelson, Paul W. Bauer, and Benjamin J. Drenth

The Evolution of Thought on the Embudo Fault— Putting Legendary Exposures in Hondo Canyon into a More Regional Context and a New Paradigm, Southern Taos Plateau, New Mexico

By V.J.S. Grauch[1], Keith I. Kelson[2], Paul W. Bauer[3], and Benjamin J. Drenth[1]

Numerous field trips to the Rio Grande Rift, including an International Association of Volcanology and Chemistry of the Earth's Interior (IAVCEI) field trip in 1989 (Dungan and others, 1989), have stopped along the horseshoe bend of New Mexico State Road (NM) 68 as it winds down into and across Hondo Canyon about 19 kilometers (km) southwest of Taos (fig. 1). Several roadcuts expose strands of the Embudo Fault, a 64-km-long rift transfer zone that links the west-dipping Sangre de Cristo Fault in the southern San Luis Basin to the southeast-dipping Pajarito Fault in the northern Española Basin. The coincidence of the Embudo fault system with the Jemez lineament, a more regional alignment of structural zones and Pliocene volcanism, suggests that its development may have been controlled, at least in part, by a pre-existing crustal structure (Aldrich, 1986).

Despite the extensional regime of the Rio Grande Rift, several of the roadcuts along NM 68 show south-dipping, reverse-fault relations in rift-age strata (fig. 1). Muehlberger (1979) noted these shortening features in his original paper on the Embudo Fault, which he attributed to regional-scale vertical-axis rotation that had thrust the Picuris Mountains northward over the Taos Plateau. Cross sections from his paper also depicted flows of Servilleta Basalt truncated by a reverse fault farther downstream in Hondo Canyon, north of the highway (fig. 1). Thoughts about the significance of the thrust relations and the faulted basalt have evolved with additional geologic, geomorphic, and geophysical evidence; the evidence puts these features into a more regional context with a different paradigm about the nature and evolution of the Embudo Fault Zone.

Almost two decades after Muehlberger's 1979 publication, detailed geologic mapping, geomorphic analysis, and kinematic measurements along the length of the Embudo Fault Zone placed the relations observed in the roadcuts into a broader perspective and new paradigm (Kelson and others, 1997, 2004). The reverse faults were recognized as secondary features within a complex zone of left-oblique deformation, consistent with a regional-scale accommodation or transfer zone. There are three major fault strands within this zone in the vicinity of the horseshoe bend (fig. 1). The southern strand lies within Proterozoic rocks at the range front, south of NM 68. The northern and middle strands cross the highway at roadcuts 1 and 2, respectively, then merge southwest of Arroyo Hondo. Kelson and others (1997) found that field relations and kinematic indicators in the vicinity of Arroyo Hondo were consistent with left-oblique slip on a high-angle fault with northwest-down vertical separation. The low-angle reverse faults at roadcuts 1 and 2 likely splay upward from a primary, left-oblique shear zone partly exposed at the southern end of roadcut 2 to form a positive flower structure. Such a structure is consistent with local shortening at a bend in the fault zone, indicated by a change in strike from northeast to east (fig. 1). Geologic mapping also shows that the fault truncates Servilleta Basalt in Hondo Canyon (Bauer and others, 1997). However, the fault has no geomorphic expression in the overlying middle to late Quaternary alluvium, so its total length and structural significance were not apparent.

Data from a high-resolution aeromagnetic survey flown in 2006 (Bankey and others, 2007) began to reveal the significance and regional extent of the faulted Servilleta Basalt in Hondo Canyon. The mapped fault aligns with a prominent, northeast-trending aeromagnetic lineament (the shaded gradient between the two bold arrows on fig. 2). Northwest of the lineament, the aeromagnetic map has a rough texture with large variations in values. Southeast of the lineament, there is little aeromagnetic expression and the map looks fairly smooth. Grauch and others (2004) ascertained that a similar rough texture in aeromagnetic data flown over the town of Taos, New Mexico, to the northeast is an expression of Servilleta Basalt, whereas the smooth texture indicates thicker sedimentary rocks. Moreover, the patterns and commonly low aeromagnetic values within the triangular area bounded by the lineament and the Rio Grande gorge indicate that the multiple flows of Servilleta Basalt in this area predominantly formed during a time when the Earth's magnetic field was reversed. This inference is supported by paleomagnetic measurements from the Rio Grande gorge to the north (Brown and others, 1993) and the inverse correlation of aeromagnetic anomalies over topographic shapes. For example, a strong linear aeromagnetic high corresponds to the deep topographic low of the gorge and a small narrow aeromagnetic high follows the narrow topographic low of Hondo Canyon.

[1]U.S. Geological Survey.

[2]U.S. Army Corps of Engineers.

[3]New Mexico Bureau of Geology and Mineral Resources.

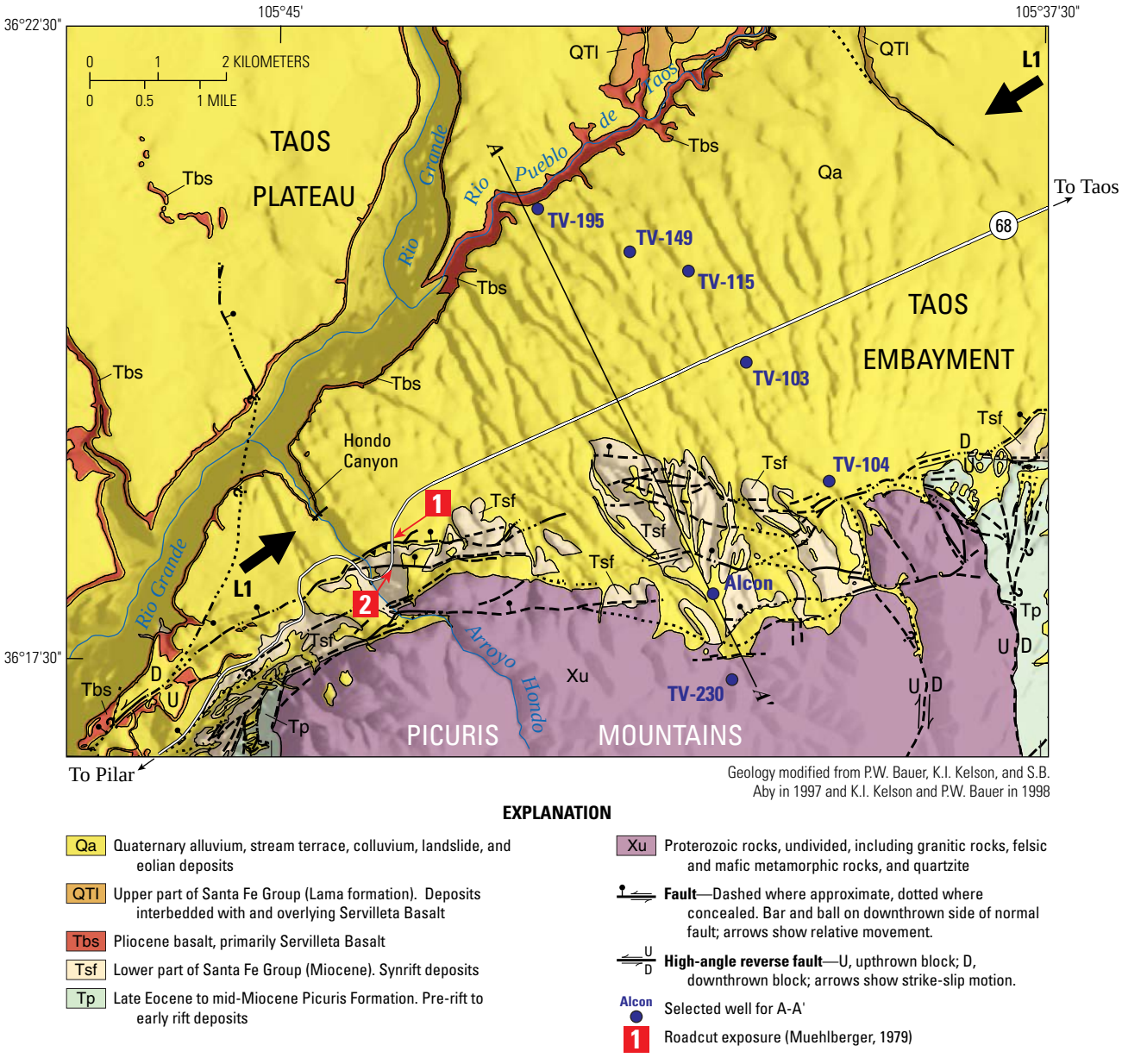

Geology modified from P.W. Bauer, K.I. Kelson, and S.B. Aby in 1997 and K.I. Kelson and P.W. Bauer in 1998

EXPLANATION

- Qa — Quaternary alluvium, stream terrace, colluvium, landslide, and eolian deposits
- QTl — Upper part of Santa Fe Group (Lama formation). Deposits interbedded with and overlying Servilleta Basalt
- Tbs — Pliocene basalt, primarily Servilleta Basalt
- Tsf — Lower part of Santa Fe Group (Miocene). Synrift deposits
- Tp — Late Eocene to mid-Miocene Picuris Formation. Pre-rift to early rift deposits
- Xu — Proterozoic rocks, undivided, including granitic rocks, felsic and mafic metamorphic rocks, and quartzite
- **Fault**—Dashed where approximate, dotted where concealed. Bar and ball on downthrown side of normal fault; arrows show relative movement.
- U/D — **High-angle reverse fault**—U, upthrown block; D, downthrown block; arrows show strike-slip motion.
- Alcon — Selected well for A-A'
- 1 — Roadcut exposure (Muehlberger, 1979)

Figure 1. Geologic map of the Embudo Fault Zone near Hondo Canyon and vicinity, modified and generalized from Bauer and others (1997) and Kelson and Bauer (1998). Legendary roadcuts #1 and #2 along State Road 68 (Muehlberger, 1979) are popular field trip stops because of the dramatic outcrops of reverse faulting. Bold black arrows point out the lineament from the aeromagnetic map (fig. 2) that aligns with the fault that terminates in basalt in Hondo Canyon. Cross section A-A' is shown in figure 3.

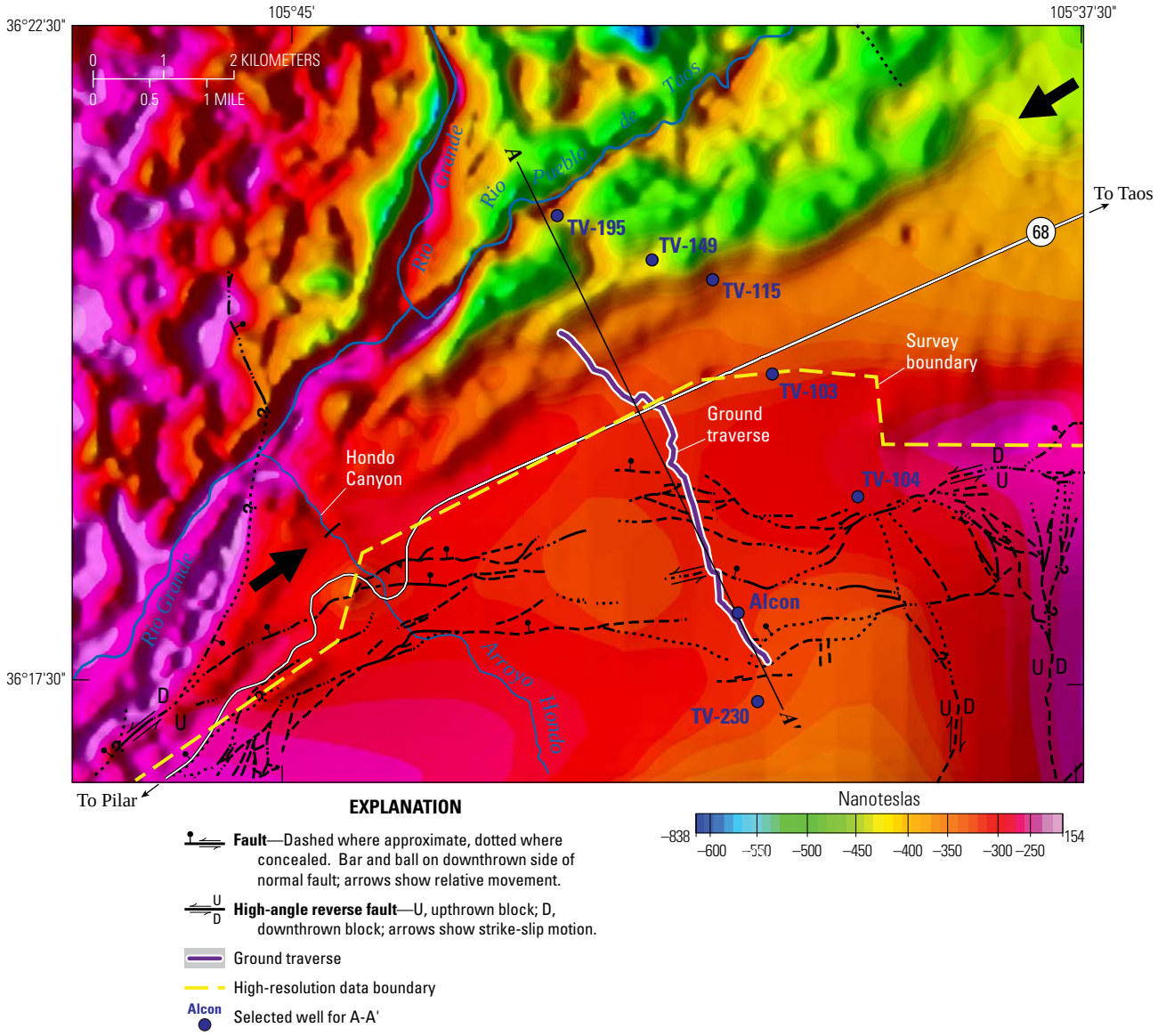

Figure 2. Aeromagnetic map for the area of figure 1. An aeromagnetic lineament interpreted as fault-terminated Servilleta Basalt is indicated by bold black arrows. Mapped faults are from figure 1. The aeromagnetic data are reduced-to-pole and shown as a color-shaded relief image (illuminated from the southeast) to enhance the expression of the lineament. Yellow dashed line delineates the boundary where high-resolution data (Bankey and others, 2007) on the north were merged with regional data (Kucks and others, 2001) on the south. Profile A-A' was located to generally follow a geophysical ground traverse (blue line).

The northeast-trending aeromagnetic lineament is remarkably straight for almost 11 km, suggesting the mapped fault at Hondo Canyon extends that far to the northeast under alluvial cover and truncates flows of Servilleta Basalt along the entire length of the feature. The location and northeast orientation, which directly aligns with the regional Jemez lineament, suggests an association with the Embudo Fault Zone. Additional northeasterly trends in the aeromagnetic data between the main lineament and the Rio Pueblo de Taos suggest a wide zone of buried, fault-disrupted basalt that extends as much as 7 km away from the mapped faults at the range front (fig. 2). If these interpreted faults are evidence of past activity on the Embudo Fault Zone, we can infer they were active during or shortly after eruption of Servilleta Basalt at 5.5–3.0 million years ago (Ma) (Appelt, 1998; Cosca and others, 2014) and were inactive by the middle Pleistocene, the age of the oldest overlying surficial deposits (Bauer and others, 1997).

A geologic cross section across the extended Embudo Fault Zone (fig. 3) puts the relations between basalt flows and the varied styles of faulting into the regional context of the Rio Grande rift margin. The cross section is constrained by well data, geologic mapping, and geophysical modeling of gravity and magnetic data. The mapped fault zone and associated flower structures span a width of about 2 km north of the range front. A number of inferred, buried, left-oblique faults are distributed within a zone that extends approximately 5 km farther north, to the Rio Pueblo de Taos. Servilleta Basalt flows variably extend over, or are truncated by, these faults, with the southernmost truncated flow marked by the aeromagnetic lineament.

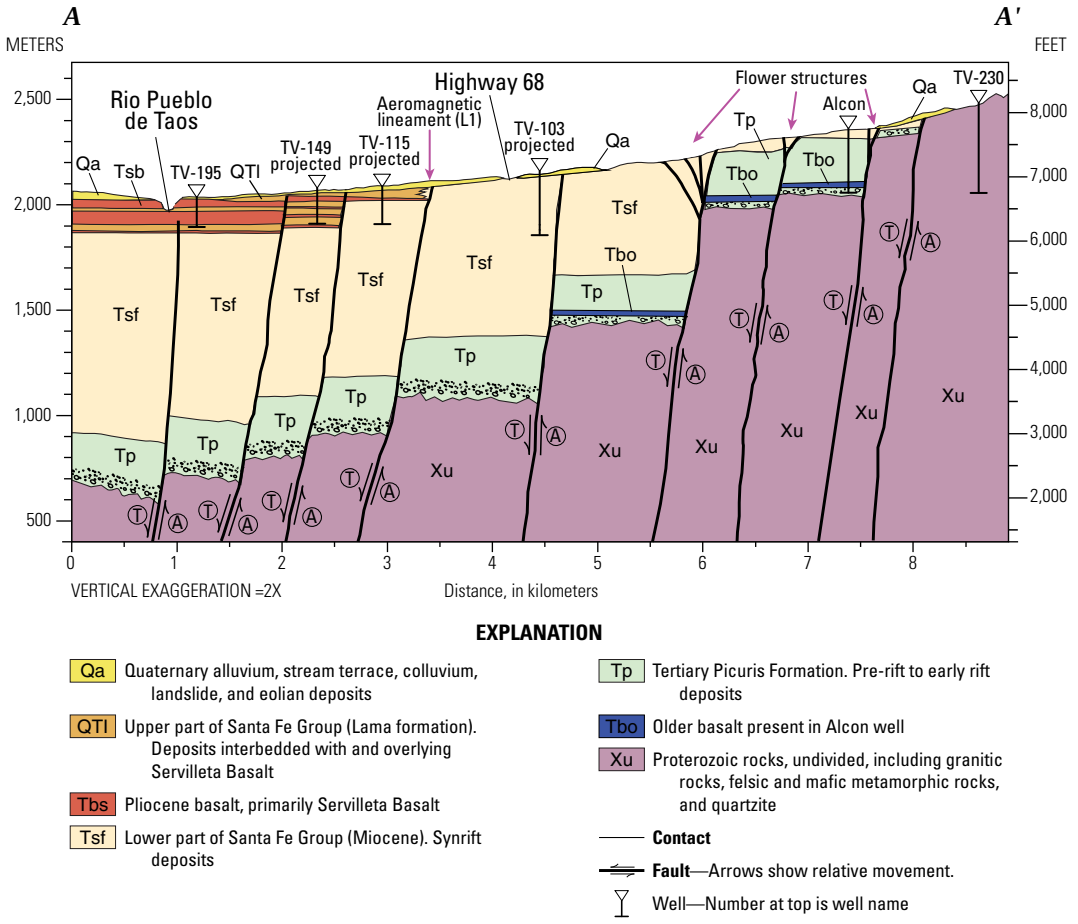

Figure 3. Geologic cross section for profile *A*-*A*′ constrained by geologic mapping, well data, and geophysical modeling. This section represents the updated understanding of the relations sketched for Hondo Canyon by Muehlberger (1979). Note the flower structures and the fault-bounded basalt indicated by the aeromagnetic lineament. Geologic units are the same as in figure 1, with the addition of an older basalt (Tbo) that is present only in the Alcon well, and Picuris Formation (Tp), a late Eocene to middle Miocene mainly volcaniclastic unit described by Aby and others (2004). The older basalt may also be present at greater depths but is not modeled. Modified from Grauch and others (2016) and Johnson and others (2016).

The cross section demonstrates several aspects of the Rio Grande rift margin associated with the Embudo Fault Zone. First, at least 1.8 km of normal displacement is accommodated across the width of the rift margin, which is surprising for fault strands considered to have dominantly left-lateral slip. To attain 1.8 km of vertical displacement since rift initiation (at approximately 25 Ma), an average vertical-slip rate of 72 meters per million years (m/m.y.) is required. This is much greater than the 35 m/m.y. of average vertical slip estimated for the last 3 m.y. (Bauer and Kelson, 2004); possible explanations include (1) vertical slip rates were considerably greater before 3 Ma, (2) the Embudo Fault has been active for much longer than 25 m.y., (3) the estimates of vertical-slip rates since 3 Ma are too low, or (4) some combination of these.

Second, cross section A-A' shows the variable thicknesses of Servilleta Basalt flows and inconsistent correlation of flows across faults. These relations are observed in well data all along Rio Pueblo de Taos (Johnson and others, 2016) and are consistent with the predominance of left-lateral offset. The increased number and thickness of basalt flows to the north of the fault at the aeromagnetic lineament L1 suggest that faulting and Servilleta volcanism were at least partly coeval.

Finally, basaltic rocks penetrated in the Alcon well near the range front, combined with modeling of magnetic data from a ground traverse, suggest the presence of a basaltic flow at depth. The rocks occur near the base of the Picuris Formation, which contains or underlies a 34.5 Ma ash (Aby and others, 2004). Although we have not tried to depict its presence deeper than 1,200-m elevation on figure 3, the discovery of likely late Eocene lava flows at the southern part of this profile suggests that pre-rift volcanic rocks may exist elsewhere, deeper within the subbasin.

In summary, geologic, geomorphic, and geophysical evidence gathered during the last several decades has progressively placed the legendary exposures in Hondo Canyon into a more regional context that presents new paradigms for the Embudo Fault (Grauch and others, 2017). The current paradigm involves a complex zone of left-oblique slip and shifts in the locus of fault activity along a wide rift margin. We speculate that the Embudo Fault developed in the early Miocene to the southwest of Hondo Canyon, aligned with the Jemez lineament. To explain the large amount of vertical displacement observed on the rift margin today, we suggest that normal-oblique slip on these early fault strands transitioned in space and time to dominantly left-lateral slip as the Embudo Fault propagated to the northeast. During and shortly after eruption of Servilleta Basalt, proto-Embudo Fault strands were active along and parallel to the modern, northeast-aligned Rio Pueblo de Taos, about 4–7 km basinward of the modern, mapped Embudo Fault Zone. By middle Pleistocene time, fault activity had shifted to the modern range front, attaining a concave curvature around the Taos embayment and developing flower structures where the strikes of fault strands bend from northeast to east.

References Cited

Aby, S.B., Bauer, P.W., and Kelson, K.I., 2004, The Picuris Formation—A late Eocene to Miocene sedimentary sequence in northern New Mexico, *in* Brister, B.S., Bauer, P.W., Read, A.S., and Lueth, V.W., eds., Geology of the Taos region: New Mexico Geological Society Guidebook, 55th Fall Field Conference Guidebook, p. 335–350.

Aldrich, M.J., Jr., 1986, Tectonics of the Jemez lineament in the Jemez Mountains and Rio Grande Rift: Journal of Geophysical Research, v. 91, no. B2, p. 1753–1762.

Appelt, R.M., 1998, $^{40}Ar/^{39}Ar$ geochronology and volcanic evolution of the Taos Plateau volcanic field, northern New Mexico and southern Colorado: Socorro, New Mexico Institute of Mining and Technology, M.S. thesis, 149 p.

Bankey, V., Grauch, V.J.S., Drenth, B.J., and EDCON-PRJ Inc., 2007, Digital data from the Taos West aeromagnetic survey in Taos County, New Mexico: U.S. Geological Survey Open-File Report 2007-1248, accessed October 2016 at http://pubs.usgs.gov/of/2007/1248/.

Bauer, P.W., and Kelson, K.I., 2004, Rift extension and fault slip rates in the southern San Luis Basin, New Mexico, *in* Brister, B.S., Bauer, P.W., Read, A.S., and Lueth, V.W., eds., Geology of the Taos region: New Mexico Geological Society, 55th Fall Field Conference Guidebook, p. 172–180.

Bauer, P.W., Kelson, K.I., and Aby, S.B., 1997, Geologic map of the Taos SW 7.5-minute quadrangle, Taos County, New Mexico (last modified March 13, 2006): New Mexico Bureau of Geology and Mineral Resources Open-File Geologic Map OF-GM 12, scale 1:24,000, accessed October 2016 https://geoinfo.nmt.edu/publications/maps/geologic/ofgm/downloads/12/TaosSW.pdf.

Brown, L.L., Caffall, N.M., and Golombek, M.P., 1993, Paleomagnetism and tectonic interpretations of the Taos Plateau volcanic field, Rio Grande rift, New Mexico: Journal of Geophysical Research, v. 98, no. B12, p. 22,401–22,413.

Cosca, M.A, Thompson, R.A, and Turner, K.J., 2014, High precision $^{40}Ar/^{39}Ar$ geochronology of Servilleta Basalts of the Rio Grande gorge, New Mexico [abs.]: American Geophysical Union, 2014 Fall Meeting, San Francisco, Calif., Dec. 15–19, 2014, abstract V51A–4728.

Dungan, M.A., Thompson, R.A., Stormer, J.S., and O'Neill, J.M., 1989, Rio Grande rift volcanism—Northeastern Jemez zone, New Mexico, *in* Chapin, C.E., and Zidek, J., eds., Field excursions to volcanic terranes in the western United States, Volume I—Southern Rocky Mountains region: New Mexico Bureau of Mines and Mineral Resources Memoir, v. 46, p. 435–486.

Grauch, V.J.S., Bauer, P.W., Drenth, B.J., and Kelson, K.I., 2016, A revised history of the Rio Grande rift in the Taos region, New Mexico—Integration of geophysical, geological, and borehole information [abs.]: Geological Society of America Abstracts with Programs, v. 48, no. 7.

Grauch, V.J.S., Bauer, P.W., Drenth, B.J., and Kelson, K.I., 2017, A shifting rift—Geophysical insights into the evolution of Rio Grande rift margins and the Embudo transfer zone near Taos, New Mexico: Geosphere, v. 13, no. 2, p. 870–910, accessed October 2016 at https://doi:10.1130/GES01425.1.

Grauch, V.J.S., Bauer, P.W., and Kelson, K.I., 2004, Preliminary interpretation of high-resolution aeromagnetic data collected near Taos, New Mexico, *in* Brister, B.S., Bauer, P.W., Read, A.S., and Lueth, V.W., eds., Geology of the Taos region: New Mexico Geological Society, 55th Fall Field Conference Guidebook, p. 244–256.

Johnson, P.S., Bauer, P.W., and Felix, B., 2016, Hydrogeologic investigation of the southern Taos Valley, Taos County, New Mexico: New Mexico Bureau of Geology and Mineral Resources Open-File Report 581, 96 p. plus 2 plates and appendices.

Kelson, K.I., and Bauer, P.W., 1998, Geologic map of the Carson quadrangle, Taos County, New Mexico (last modified March 9, 2006): New Mexico Bureau of Geology and Mineral Resources Open-File Geologic Map OF-GM 22, scale 1:24,000, accessed October 2016 at https://geoinfo.nmt.edu/publications/maps/geologic/ofgm/downloads/22/Carson.pdf.

Kelson, K.I., Bauer, P.W., Unruh, J.R., and Bott, D.J., 2004, Late Quaternary characteristics of the northern Embudo fault, Taos County, New Mexico, *in* Brister, B.S., Bauer, P.W., Read, A.S., and Lueth, V.W., eds., Geology of the Taos region: New Mexico Geological Society, 55th Fall Field Conference Guidebook, p. 147–157.

Kelson, K.I., Unruh, J.R., and Bott, J.D.J., 1997, Field characterization, kinematic analysis, and initial paleoseismologic assessment of the Embudo fault, northern New Mexico: 32nd Technical Report to U.S. Geological Survey, Reston, Virginia, under Contract 1434-96-G-02739, 48 p.

Kucks, R.P., Hill, P.L., and Heywood, C.E., 2001, New Mexico aeromagnetic and gravity maps and data—A web site for distribution of data (ver. 1.0): U.S. Geological Survey Open-File Report 01–0061, accessed October 2016 at http://pubs.usgs.gov/of/2001/ofr-01-0061/.

Muehlberger, W.R., 1979, The Embudo fault between Pilar and Arroyo Hondo, New Mexico—An active intracontinental transform fault, *in* Ingersoll, R.V., Woodward, L.A., and James, H.L., eds., Santa Fe country: New Mexico Geological Society, 30th Fall Field Conference Guidebook, p. 77–82.

Sanidine From the Fish Canyon Tuff and Its Use as a $^{40}Ar/^{39}Ar$ Geochronology Standard

By L.E. Morgan and M.A. Cosca

Sanidine From the Fish Canyon Tuff and Its Use as a $^{40}Ar/^{39}Ar$ Geochronology Standard

By L.E. Morgan[1] and M.A. Cosca[1]

$^{40}Ar/^{39}Ar$ Geochronology

$^{40}Ar/^{39}Ar$ geochronology is the most widely applied isotope-based method for determining time in the Earth sciences. The natural abundance of potassium (K) in the crust and its wide distribution in common minerals (for example, amphibole, mica, K-feldspar), and the long half-life of its naturally occurring radioactive isotope (^{40}K) are all factors in its usefulness as a reliable method for determining geologic time. The chronometer is based on the potassium-argon (K-Ar) method, which relies on the decay of ^{40}K to ^{40}Ar (see for example, Dalrymple and Lanphere, 1969); however, the $^{40}Ar/^{39}Ar$ method requires coirradiating samples with mineral standards, or neutron flux monitors, prior to isotopic analysis. Neutron irradiation (typically in a uranium [^{235}U] research reactor) converts some ^{39}K (approximately 93 percent of total K) in the sample into ^{39}Ar by way of the $^{39}K(n,p)^{39}Ar$ reaction (for example, Dalrymple and others, 1981). Isotopic determination of ^{39}Ar can therefore be used as a proxy for ^{39}K, and by assuming a constant $^{40}K/^{39}K$ ratio between sample and standard, the measurement of ^{39}Ar is also an effective measurement of ^{40}K (the radioactive parent isotope of $^{40}Ar^*$). In most volcanic environments, $^{40}Ar^*$ (the * denotes argon that is radiogenic) begins accumulating and is quantitatively retained in minerals almost immediately after rock emplacement. If rocks remain at temperatures below that which diffusive loss of argon occurs, the age of the mineral or rock is a reliable measurement of the timing of the volcanic event.

Neutron Flux Monitors

The $^{40}Ar/^{39}Ar$ method requires a mineral standard, or neutron flux monitor, which is coirradiated with samples of interest. The age of a mineral standard can be determined in several ways, including first-principles measurements (Lanphere and Dalrymple, 1966, 2000; McDougall and Roksandic, 1974; McDougall and Wellman, 2011), intercalibration with primary standards (Renne and others, 1998; Dazé and others, 2003; Spell and McDougall, 2003; Jourdan and Renne, 2007), astronomical calibrations (for example, Kuiper and others, 2008), and optimizations involving intercalibration with the uranium-lead (U-Pb) system (Renne and others, 2010, 2011).

The most direct of these options is first principles measurements, which require accurately calibrated laboratory equipment to make concentration measurements of both ^{40}K and $^{40}Ar^*$. Given the difficulty in quantitatively extracting all $^{40}Ar^*$ from highly viscous K-feldspar melts, these concentration measurements have proven most reliable when applied to phases such as biotite and hornblende. Thus, many commonly used neutron flux monitors, such as Fish Canyon sanidine, are considered secondary standards, in that they have been intercalibrated with primary standards that have reliable first principles data.

Fish Canyon Tuff Sanidine

Among the most commonly used mineral standards in $^{40}Ar/^{39}Ar$ geochronology is Fish Canyon sanidine (FCs). FCs has been separated from the Fish Canyon Tuff (FCT), which erupted from the La Garita caldera in the San Juan Mountains of southern Colorado. Minerals from the FCT were first dated by K-Ar by Steven and others (1967). Within the uncertainties attainable at the time (approximately ±1–3 million years ago [Ma]), results indicated that ages for all dated minerals (sanidine, biotite, hornblende, and plagioclase) from FCT were indistinguishable. The sample measured by Steven and others (1967) was collected at the summit of Agua Ramon Mountain, north of South Fork, Colorado.

Additional measurements were made by Hurford and Hammerschmidt (1985) on a sample collected along U.S. Route 160 about 9 kilometers southwest of South Fork, Colorado, by Naeser and others (1981). This locality is near what is now the Fun Valley Family Resort. A number of other early K-Ar measurements on FCT phases are summarized by McDougall and Harrison (1999).

In what became the most used calibration for a decade, Renne and others (1998) published an age of 28.02±0.16 Ma (1σ) for FCs, based on decay constants tabulated in Steiger and Jäger (1977), new isotope dilution K measurements of primary biotite standard GA-1550, previous Ar concentration measurements of GA-1550 (McDougall and Roksandic, 1974), and extensive intercalibration measurements between GA-1550 and FCs. Subsequent characterization and calibrations of the Fish Canyon sanidine ranged from an age of approximately 27.5 Ma (Lanphere and Baadsgaard, 2001) to an age of approximately 28.5 Ma (Schmitz and Bowring, 2001). More congruent results included 27.98±0.08 Ma (1σ) (Villeneuve and others, 2000) and 28.10±0.04 Ma (1σ) (Spell and McDougall, 2003).

[1]U.S. Geological Survey.

Recent Developments in the Ages of FCs and Other Standards

In 2008, Kuiper and others published an astronomical calibration of the age of FCs. This was accomplished using tephra from the astronomically tuned Messâdit section in the Melilla-Nador Basin of Morocco. The astronomical ages of tephra horizons allowed for these tephra to be used as $^{40}Ar/^{39}Ar$ standards when they were coirradiated with FCs. The age for FCs determined in this way is 28.201±0.023 Ma (1σ), which is based on (and must be used with) decay constants as compiled and calculated by Min and others (2000) that have significantly larger and more reasonable uncertainties than those tabulated by Steiger and Jäger (1977). The youngest U-Pb zircon age from Wotzlaw and others (2013) is indistinguishable from the Kuiper age, at 28.196±0.019 Ma.

More recently, a statistical optimization model (Renne and others, 2010, 2011) allowed for the simultaneous determination of an age for FCs and the ^{40}K decay constants. The model utilizes several existing constraints on the $^{40}Ar/^{39}Ar$ system, including $^{40}Ar/^{40}K$ values for FCs, activity data for ^{40}K decay, and results from data pairs, where the same samples were dated with both the $^{40}Ar/^{39}Ar$ and the ^{238}U-^{206}Pb systems. The model yields most likely values (and uncertainties) for ^{40}K decay constants and the $^{40}Ar^*/^{40}K$ ratio for FCs; combined, these indicate an age for FCs of 28.294±0.036 Ma (1σ) (Renne and others, 2011).

How Does a Revised Age of Fish Canyon Sanidine Affect Previous Age Calculations?

The effect of using different calibrations over much of geological history is shown in figure 1. There are three combinations of FCs age and decay constants shown, relative

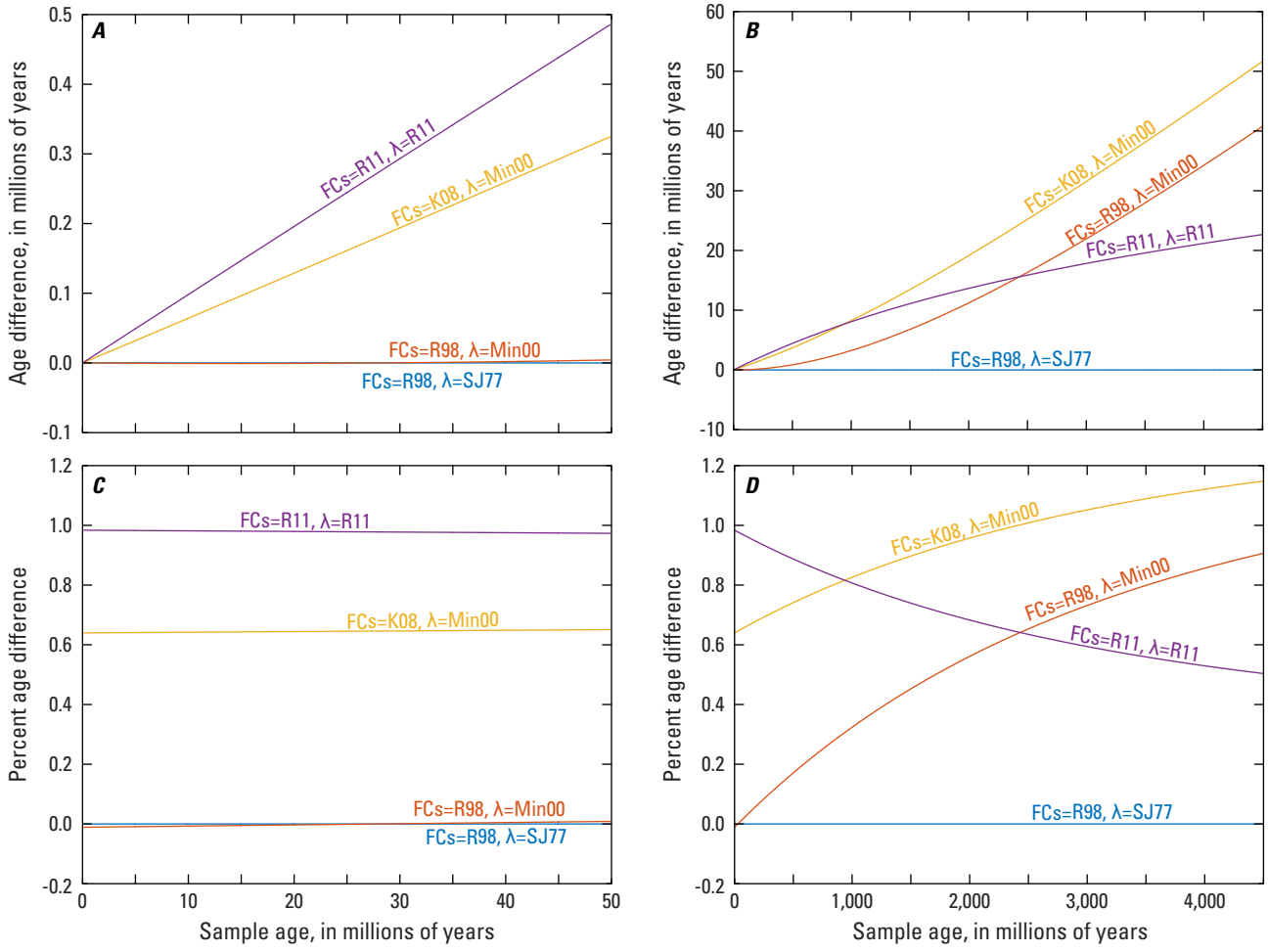

Figure 1. The effects of different calibrations of the 40Ar/39Ar system on calculated ages. (*A*) and (*B*) show the absolute age effect; (*C*) and (*D*) show the relative age effect. Note the different scales between (*A*,*C*) and (*B*,*D*). The four calibrations highlighted here are shown relative to the FCs (Fish Canyon sanidine standard) age of 28.02 million years ago (Ma) (Renne and others, 1998) and decay constants of Steiger and Jäger (1977), which thus plot at zero on these graphs. R98, Renne and others (1998); SJ77, Steiger and Jäger (1977); Min00, Min and others (2000); K08, Kuiper and others (2008); R11, Renne and others (2011).

to the reference calibration of FCs = Renne and others (1998) and λ = Steiger and Jäger (1977): (1) FCs = Renne and others (1998), λ=Min and others (2000); (2) FCs = Kuiper and others (2008), λ = Min and others (2000); and (3) FCs = Renne and others (2011), λ = Renne and others (2011). Over the last 50 Ma, the calculated difference in age between the four calibrations (including the reference calibration) is always <1 percent. For example, at 30 Ma, the Renne and others (2011) calibration differs from the reference by approximately 0.3 Ma, and the Kuiper and others (2008) calibration by approximately 0.2 Ma.

Most geochronologists now use either the Kuiper and others (2008) or Renne and others (2011) age for FCs and the associated decay constants (Min and others [2000] and Renne and others [2011], respectively). Recalculating previously determined ages to use the Kuiper and others (2008) age is relatively straightforward, but the Renne and others (2011) calibration requires the incorporation of error correlations.

Given the dwindling supply of high purity FCs, Morgan and others (2014) published data from a new sample, taken from County Road 433, south of South Fork, Colorado.

Future Work

Although it is no doubt frustrating for geologists to have continually updated parameters, updates to standard ages and decay constants will continue. One possibility is an iteration of the statistical optimization model (Renne and others, 2010, 2011), with updated input parameters. Towards this, work is in progress on a determination of ^{40}Ar concentrations in primary mineral standards (Morgan and others, 2011; Morgan and Davidheiser-Kroll, 2015). Future primary measurements of decay constants will also be integral to further improvements of the $^{40}Ar/^{39}Ar$ geochronometer.

References

Dalrymple, G.B., Alexander, E.C., Jr., Lanphere, M.A., and Kraker, G.P., 1981, Irradiation of samples for $^{40}Ar/^{39}Ar$ dating using the geological survey TRIGA reactor: U.S. Geological Survey Professional Paper 1176, 55 p.

Dalrymple, G.B., and Lanphere, M.A., 1969, Potassium-argon dating: Principles, techniques, and applications to geochronology: San Francisco, W.H. Freeman, 258 p.

Dazé, A., Lee, J.K.W., and Villeneuve, M., 2003, An intercalibration study of the Fish Canyon sanidine and biotite $^{40}Ar/^{39}Ar$ standards and some comments on the age of the Fish Canyon Tuff: Chemical Geology, v. 199, no. 1-2, p. 111–127.

Hurford, A.J., and Hammerschmidt, K., 1985, $^{40}Ar^{39}Ar$ and K/Ar dating of the Bishop and Fish Canyon Tuffs—Calibration ages for fission-track dating standards: Chemical Geology-Isotope Geoscience section, v. 58, no. 1-2, p. 23–32.

Jourdan, F., and Renne, P.R., 2007, Age calibration of the Fish Canyon sanidine $^{40}Ar/^{39}Ar$ dating standard using primary K–Ar standards: Geochimica et Cosmochimica Acta, v. 71, no. 2, p. 387–402.

Kuiper, K.F., Deino, A., Hilgen, F.J., Krijgsman, W., Renne, P.R., and Wijbrans, J.R., 2008, Synchronizing rock clocks of Earth history: Science, v. 320, no. 5875, p. 500–504.

Lanphere, M.A., and Baadsgaard, H., 2001, Precise K–Ar, $^{40}Ar/^{39}Ar$, Rb–Sr and U/Pb mineral ages from the 27.5 Ma Fish Canyon Tuff reference standard: Chemical Geology, v. 175, no. 3-4, p. 653–671.

Lanphere, M.A., and Dalrymple, G.B., 1966, Simplified bulb tracer system for argon analyses: Nature, v. 209, no. 5026, p. 902–903.

Lanphere, M.A., and Dalrymple, G.B., 2000, First-principles calibration of ^{38}Ar tracers—Implications for the ages of $^{40}Ar/^{38}Ar$ fluence monitors: U.S. Geological Survey Professional Paper 1621, 10 p.

McDougall, I., and Harrison, T.M., 1999, Geochronology and thermochronology by the $^{40}Ar/^{39}Ar$ method: New York, Oxford University Press, Inc., 269 p.

McDougall, I., and Roksandic, Z., 1974, Total fusion $^{40}Ar/^{39}Ar$ ages using Hifar reactor: Australian Journal of Earth Sciences, v. 21, no. 1, p. 81–89.

McDougall, I., and Wellman, P., 2011, Calibration of GA1550 biotite standard for K/Ar and $^{40}Ar/^{39}Ar$ dating: Chemical Geology, v. 280, no. 1-2, p. 19–25.

Min, K.W., Mundil, R., Renne, P.R., and Ludwig, K.R., 2000, A test for systematic errors in $^{40}Ar/^{39}Ar$ geochronology through comparison with U/Pb analysis of a 1.1-Ga rhyolite: Geochimica et Cosmochimica Acta, v. 64, no. 1, p. 73–98.

Morgan, L.E., and Davidheiser-Kroll, B., 2015, Pressure disequilibria induced by rapid valve closure in noble gas extraction lines: Geochemistry, Geophysics, Geosystems, v. 16, p. 1923–1931.

Morgan, L.E., Mark, D.F., Imlach, J., Barfod, D., and Dymock, R., 2014, FCs-EK—A new sampling of the Fish Canyon Tuff $^{40}Ar/^{39}Ar$ neutron flux monitor: Geological Society, London, Special Publications, v. 378, no. 1, p. 63–67.

Morgan, L.E., Postma, O., Kuiper, K.F., Mark, D.F., van der Plas, W., Davidson, S., Perkin, M., Villa, I.M., and Wijbrans, J.R., 2011, A metrological approach to measuring $^{40}Ar^*$ concentrations in K-Ar and $^{40}Ar/^{39}Ar$ mineral standards: Geochemistry, Geophysics, Geosystems, v. 12, no. 10, 17 p.

Naeser, C.W., Zimmermann, R., and Cebula, G., 1981, Fission-track dating of apatite and zircon—An interlaboratory comparison: Nuclear Tracks, v. 5, no. 1-2, p. 65–72.

Renne, P.R., Balco, G., Ludwig, K., Mundil, R., and Min, K., 2011, Response to the comment by W.H. Schwarz et al. on "Joint determination of ^{40}K decay constants and ^{40}Ar*/^{39}K for the Fish Canyon sanidine standard, and improved accuracy for ^{40}Ar/^{39}Ar geochronology" by P.R. Renne et al. (2010): Geochimica et Cosmochimica Acta, v. 75, no. 17, p. 5097–5100.

Renne, P.R., Mundil, R., Balco, G., Min, K., and Ludwig, K.R., 2010, Joint determination of ^{40}K decay constants and ^{40}Ar*/^{40}K for the Fish Canyon sanidine standard, and improved accuracy for ^{40}Ar/^{39}Ar geochronology: Geochimica et Cosmochimica Acta, v. 74, no. 18, p. 5349–5367.

Renne, P.R., Swisher, C.C., Deino, A.L., Karner, D.B., Owens, T.L., and DePaolo, D.J., 1998, Intercalibration of standards, absolute ages and uncertainties in ^{40}Ar/^{39}Ar dating: Chemical Geology, v. 145, no. 1-2, p. 117–152.

Schmitz, M.D., and Bowring, S.A., 2001, U-Pb zircon and titanite systematics of the Fish Canyon Tuff—An assessment of high-precision U-Pb geochronology and its application to young volcanic rocks: Geochimica et Cosmochimica Acta, v. 65, no. 15, p. 2571–2587.

Spell, T.L., and McDougall, I., 2003, Characterization and calibration of ^{40}Ar/^{39}Ar dating standards: Chemical Geology, v. 198, no. 3-4, p. 189–211.

Steiger, R.H., and Jäger, E., 1977, Subcommission on geochronology—Convention on use of decay constants in geochronology and cosmochronology: Earth and Planetary Science Letters, v. 36, no. 3, p. 359–362.

Steven, T.A., Mehnert, H.H., and Obradovich, J.D., 1967, Age of volcanic activity in the San Juan Mountains, Colorado, in Geological Survey research 1967: U.S. Geological Survey Professional Paper 575-D, p. 47–55.

Villeneuve, M., Sandeman, H.A., and Davis, W.J., 2000, A method for intercalibration of U-Th-Pb and ^{40}Ar-^{39}Ar ages in the Phanerozoic: Geochimica et Cosmochimica Acta, v. 64, no. 23, p. 4017–4030.

Wotzlaw, J.-F., Schaltegger, U., Frick, D.A., Dungan, M.A., Gerdes, A., and Günther, D., 2013, Tracking the evolution of large-volume silicic magma reservoirs from assembly to supereruption: Geology, v. 41, no. 8, p. 867–870.

Moffett Field Publishing Service Center
Manuscript approved February 28, 2022
Edited by Katherine Jacques
Illustration support by Katie Sullivan
Layout by Cory Hurd

ISSN 2328-0328 (online)
https://doi.org/10.3133/sir20175022r